Advanced direct injection combustion engine technologies and development

Related titles:

The science and technology of materials in automotive engines
(ISBN 978-1-85573-742-6)
This authoritative book provides an introductory text on the science and technology of materials used in automotive engines. It focuses on reciprocating engines, both four- and two-stroke, with particular emphasis on their characteristics and the types of materials used in their construction. The book considers the engine in terms of each specific part: the cylinder, piston, camshaft, valves, crankshaft, connecting rod and catalytic converter. The materials used in automotive engines are required to fulfil a multitude of functions. It is a subtle balance between material properties, essential design and high performance characteristics. The intention here is to describe the metallurgy, surface modification, wear resistance, and chemical composition of these materials. It also includes supplementary notes that support the core text.

HCCI and CAI engines for the automotive industry
(ISBN 978-1-84569-128-8)
HCCI/CAI has emerged as one of the most promising engine technologies with the potential to combine fuel efficiency and improved emissions performance. Despite the considerable advantages, its operational range is rather limited and controlling the combustion (timing of ignition and rate of energy release) is still an area of ongoing research. However, commercial applications are close to reality. This book reviews the key international research on optimising its use, including gasoline HCCI/CAI engines; diesel HCCI engines; HCCI/CAI engines with alternative fuels; and advanced modelling and experimental techniques.

Tribology and dynamics of engine and powertrain: Fundamentals, applications and future trends
(ISBN 978-1-84569-361-9)
Tribology is one element of many interacting within a vehicle engine and powertrain. In adopting a detailed, theoretical, component approach to solving tribological problems, the minutiae can be overwhelmingly complex, and practical solutions become elusive and uneconomic. The system perspective generally adopted in industry, however, can lead to shortcuts and oversimplifications, industrial projects are subject to *ad hoc* trial and error, and subsequent 'fire-fighting' activity is required. This book seeks to bridge this divide, using a multi-physics approach to provide sufficient fundamental grounding and understanding of both detailed and approximate analyses – thereby making 'first time right' design solutions possible. Tribological issues and solutions in piston systems, valve train systems, engine bearings and drivetrain systems are addressed. New developments in materials, micro-engineering, nano-technology and MEMS are also included.

Details of these and other Woodhead Publishing books can be obtained by:

- visiting our web site at www.woodheadpublishing.com
- contacting Customer Services (e-mail: sales@woodheadpublishing.com; fax: +44 (0) 1223 893694; tel.: +44 (0) 1223 891358 ext. 130; address: Woodhead Publishing Limited, Abington Hall, Granta Park, Great Abington, Cambridge CB21 6AH, UK)

If you would like to receive information on forthcoming titles, please send your address details to: Francis Dodds (address, tel. and fax as above; e-mail: francis.dodds@woodheadpublishing.com). Please confirm which subject areas you are interested in.

Advanced direct injection combustion engine technologies and development

Volume 2: Diesel engines

Edited by

Hua Zhao





CRC Press
Boca Raton Boston New York Washington, DC

WOODHEAD PUBLISHING LIMITED
Oxford Cambridge New Delhi

Published by Woodhead Publishing Limited, Abington Hall, Granta Park,
Great Abington, Cambridge CB21 6AH, UK
www.woodheadpublishing.com

Woodhead Publishing India Private Limited, G-2, Vardaan House, 7/28 Ansari Road, Daryaganj,
New Delhi – 110002, India
www.woodheadpublishingindia.com

Published in North America by CRC Press LLC, 6000 Broken Sound Parkway, NW,
Suite 300, Boca Raton, FL 33487, USA

First published 2010, Woodhead Publishing Limited and CRC Press LLC
© 2010, Woodhead Publishing Limited; Ch 17 © United States Government
The authors have asserted their moral rights.

This book contains information obtained from authentic and highly regarded sources. Reprinted material is quoted with permission, and sources are indicated. Reasonable efforts have been made to publish reliable data and information, but the authors and the publishers cannot assume responsibility for the validity of all materials. Neither the authors nor the publishers, nor anyone else associated with this publication, shall be liable for any loss, damage or liability directly or indirectly caused or alleged to be caused by this book.

Neither this book nor any part may be reproduced or transmitted in any form or by any means, electronic or mechanical, including photocopying, microfilming and recording, or by any information storage or retrieval system, without permission in writing from Woodhead Publishing Limited.

The consent of Woodhead Publishing Limited does not extend to copying for general distribution, for promotion, for creating new works, or for resale. Specific permission must be obtained in writing from Woodhead Publishing Limited for such copying.

Trademark notice: Product or corporate names may be trademarks or registered trademarks, and are used only for identification and explanation, without intent to infringe.

British Library Cataloguing in Publication Data
A catalogue record for this book is available from the British Library.

Library of Congress Cataloging in Publication Data
A catalog record for this book is available from the Library of Congress.

Woodhead Publishing ISBN 978-1-84569-744-0 (book)
Woodhead Publishing ISBN 978-1-84569-745-7 (e-book)
CRC Press ISBN 978-1-4398-2475-7
CRC Press order number: N10132

The publishers' policy is to use permanent paper from mills that operate a sustainable forestry policy, and which has been manufactured from pulp which is processed using acid-free and elemental chlorine-free practices. Furthermore, the publishers ensure that the text paper and cover board used have met acceptable environmental accreditation standards.

Typeset by Replika Press Pvt Ltd, India
Printed by TJ International Limited, Padstow, Cornwall, UK

Contents

Contributor contact details *xiii*

Preface *xvii*

Part I Light-duty direct injection diesel engines

1 Overview of high-speed direct injection diesel engines 3
R. W. Horrocks, Ford Motor Company Limited, UK

1.1 Background 3
1.2 Early development of the high-speed direct injection (HSDI) diesel engine 4
1.3 Recent trends in high-speed direct injection (HSDI) diesel engine design 10
1.4 A survey of some of today's engines 31
1.5 Future trends 48
1.6 Sources of further information and advice 55
1.7 References 56

2 Fuel injection systems for high-speed direct injection diesel engines 61
R. W. Horrocks, R. Lawther and L. Hatfield, Ford Motor Company Limited, UK

2.1 Introduction 61
2.2 Early high-speed direct injection (HSDI) diesel fuel systems 63
2.3 Common rail fuel injection systems 66
2.4 Common rail systems 74
2.5 Nozzle technology 86
2.6 High pressure (HP) pump technology 88
2.7 Diesel fuel injection equipment heat rejection 92
2.8 Electronic control of fuel systems 96

2.9 Future trends 102
2.10 References 103

3 Mixture formation, combustion and pollutant emissions in high-speed direct injection diesel engines 105
A. Velji, M. Lüft and S. Merkel, Universität Karlsruhe (TH), Germany

3.1 Mixture preparation 105
3.2 Combustion 120
3.3 Pollutant emissions 132
3.4 Future trends 151
3.5 References and further reading 153

4 Multiple injection diesel combustion process in the high-speed direct injection diesel engine 155
B. M. Vaglieco, Istituto Motori-CNR, Italy

4.1 Introduction 155
4.2 Double injection or pilot + main 158
4.3 Multiple injection technology 163
4.4 Other diesel combustion technologies 168
4.5 Conclusions 171
4.6 Acknowledgements 172
4.7 References 172

5 Turbocharging and air-path management for light-duty diesel engines 175
K. Tufail, Ford Motor Company Limited, UK

5.1 Introduction: air-path challenges and acceptance criteria 175
5.2 Air-path technologies, part 1: exhaust gas recirculation (EGR) 178
5.3 Air-path technologies, part 2: boosting systems 184
5.4 Air-path management 197
5.5 Future trends 206
5.6 Acknowledgements 207
5.7 References 208
5.8 Appendix: Acronyms 213

6 Advanced concepts for future light-duty diesel engines 215
I. Denbratt, Chalmers University of Technology, Sweden

6.1 Introduction 215

6.2 Legislative exhaust emission standards 216
6.3 Current developments 220
6.4 Low emissions concepts: key aspects 221
6.5 Combustion systems 227
6.6 Fuel injection 230
6.7 Charge induction 233
6.8 Combustion chamber shape 237
6.9 Exhaust gas after-treatment 237
6.10 Heat recovery 241
6.11 Engine control 242
6.12 Future fuels 242
6.13 References and further reading 243

7 Advanced control and engine management for future light-duty diesel engines 246
L. Guzzella, Swiss Federal Institute of Technology (ETH), Switzerland

7.1 Main control objectives 246
7.2 Standard control loops 248
7.3 System modelling 252
7.4 Advanced control systems 259
7.5 References 265

Part II Heavy-duty direct injection diesel engines

8 Overview of heavy-duty diesel engines 269
Z. Liu, Navistar, Inc., USA

8.1 Introduction 269
8.2 A survey of current heavy-duty diesel engines 273
8.3 Approaches to meet future emissions legislation and CO_2 targets 281
8.4 Summary 287
8.5 References 287

9 Fuel injection systems for heavy-duty diesel engines 289
P. J. G. Dingle, Delphi Diesel Systems, USA

9.1 Introduction 289
9.2 History of heavy-duty fuel injection equipment (FIE) 290
9.3 Current choices of fuel injection equipment (FIE) 290
9.4 Detailed fuel injection equipment (FIE) descriptions 293
9.5 Nozzle developments 306
9.6 Synergies with light-duty fuel injection equipment (FIE) 308

9.7 Future trends 309
9.8 References 316

10 Turbocharging technologies for heavy-duty diesel engines 318
J. Carter, N. K. Sharp and H. Tennant, Cummins Turbo Technologies, UK

10.1 Scope 318
10.2 Turbocharger technology state of the art 319
10.3 Engine performance requirements and operating characteristics 321
10.4 Turbocharger architectures and aerodynamic design considerations 328
10.5 Durability 343
10.6 Actuation 349
10.7 Future trends 356
10.8 Sources of further information and advice 357
10.9 References 357

11 Alternative combustion system for heavy-duty diesel engines 358
W. Su, Tianjin University, China

11.1 Introduction 358
11.2 Premixed charge compression ignition (PCCI) combustion organized by early direct injection 361
11.3 Lean diffusion combustion 367
11.4 Summary 373
11.5 References 373

12 Heavy-duty diesel engine system design 376
Q. Xin, Navistar, Inc., USA

12.1 Overview of analytical engine design process and system simulation approach 376
12.2 Fundamentals of in-cylinder cycle computation and air system steady-state performance 385
12.3 Engine–vehicle matching analysis for powertrain system design in engine firing and braking 415
12.4 Emissions calibration optimization development and engine performance design target 441
12.5 Diesel aftertreatment integration and matching 458
12.6 Engine heat rejection and base engine characteristics 467
12.7 Pumping loss theory and the principle of engine air system design 479

12.8 Transient powertrain performance modeling and engine electronic controls 499
12.9 Engine system specification design and subsystem interaction optimization 511
12.10 Analytical design of mechanical components for system performance improvement 520
12.11 Future trends 534
12.12 References 537

Part III Exhaust emission abatement, diesel combustion diagnostics and modelling

13 Fuel reforming for diesel engines 543
A. Megaritis, Brunel University, UK, A. Tsolakis and M. L. Wyszynski, University of Birmingham, UK, and S. E. Golunski, Johnson Matthey Technology Centre, UK
13.1 Why fuel reforming in diesel engines? 543
13.2 Diesel fuel reforming theory 546
13.3 Diesel fuel reforming process parameters and catalyst screening 553
13.4 Diesel fuel reforming applications: trends 555
13.5 Summary 558
13.6 References 558

14 Exhaust gas aftertreatment for light-duty diesel engines 562
P. Eastwood, Ford Motor Company Limited, UK
14.1 Introduction 562
14.2 Emissions legislation 563
14.3 Oxidation catalysts 568
14.4 Particulate filters 568
14.5 Selective catalytic reduction 572
14.6 Lean NO_x traps (LNT) 576
14.7 Integrated systems 581
14.8 Summary 585
14.9 Future trends 587
14.10 References 589
14.11 Appendix: Acronyms 594

15 Overview of diesel emissions and control for heavy-duty diesel engines 595
T. Johnson, Corning Incorporated, USA
15.1 Introduction 595

15.2 Heavy-duty regulatory developments 596
15.3 NO_x control technologies 599
15.4 Particulate matter (PM) control technologies 604
15.5 Integrated NO_x/PM systems 611
15.6 Future trends 612
15.7 Sources of further information and advice 613
15.8 References 613

16 Optical diagnostics in diesel combustion engines 617
C. Schulz, University of Duisburg-Essen, Germany

16.1 Introduction 617
16.2 Liquid spray diagnostics 619
16.3 Vapour-phase fuel distribution 620
16.4 Two-phase flows 623
16.5 Ignition and combustion 624
16.6 Pollutant measurements 626
16.7 Soot volume fraction laser-induced incandescence (LII) 630
16.8 Temperature 631
16.9 Future trends 634
16.10 Conclusions 634
16.11 References 635

17 In-cylinder spray, mixing, combustion, and pollutant-formation processes in conventional and low-temperature-combustion diesel engines 644
M. P. B. Musculus and L. M. Pickett , Sandia National Laboratories, USA

17.1 Introduction 644
17.2 Conventional diesel combustion 645
17.3 Positive ignition-dwell low-temperature diesel combustion 657
17.4 Quasi-steady low-temperature diesel combustion 664
17.5 Closing remarks on low-temperature combustion (LTC) diesel research needs 669
17.6 References 670

18 Advanced computational fluid dynamics modeling of direct injection engines 676
R. D. Reitz, University of Wisconsin-Madison, USA, and Y. Sun, General Motors Company, USA

18.1 Introduction 676
18.2 Basic approach 677
18.3 Turbulence modeling 678
18.4 Spray modeling 680

18.5 Combustion modeling 680
18.6 Emission modeling 693
18.7 Other models 695
18.8 Computational fluid dynamics (CFD) codes for engine simulations 697
18.9 Application of engine computational fluid dynamics (CFD) modeling 699
18.10 Future trends 701
18.11 References 703

Index *708*

Contributor contact details

(*= main contact)

Chapter 1

Dr Roy W. Horrocks*
Ford Motor Company Limited
Dunton Technical Centre
Laindon
Basildon
Essex SS15 6EE
UK

E-mail: rhorrock@ford.com

Chapter 2

Dr Roy W. Horrocks*, R. Lawther and Laurence Hatfield
Ford Motor Company Limited
Dunton Technical Centre
Laindon
Basildon
Essex SS15 6EE
UK

E-mail: rhorrock@ford.com

Chapter 3

Dr Amin Velji, Markus Lüft* and Sascha Merkel
Institut für Kolbenmaschinen
Universität Karlsruhe (TH)
PO Box 6980
76128 Karlsruhe
Germany

E-mail:
amin.velji@ifkm.uni-karlsruhe.de
markus.lueft@ifkm.uni-karlsruhe.de
sascha.merkel@ifkm.uni-karlsruhe.de

Chapter 4

Bianca Maria Vaglieco
Istituto Motori-CNR
Via G. Marconi, 8
80125 Naples
Italy

E-mail: b.m.vaglieco@im.cnr.it

Chapter 5

Khizer Tufail
Diesel Powertrain Development and Integration Group
Room GB-15/2A-C07-B
Dunton Technical Centre
Ford Motor Company Limited
Dunton Technical Centre
Laindon
Basildon
Essex SS15 6EE
UK

E-mail: ktufail@ford.com

Chapter 6

Professor Ingemar Denbratt
Division of Combustion
Chalmers University of Technology
Göteberg
Sweden

E-mail: denbratt@chalmers.se

Chapter 7

Professor Lino Guzzella
Department of Mechanical and Process Engineering
Swiss Federal Institute of Technology (ETH)
Sonneggstrasse 3
8092 Zurich
Switzerland

E-mail: lguzzella@ethz.ch

Chapter 8

Dr Zhengbai (Mike) Liu
Future Technology
Navistar, Inc.
10400 West North Avenue
Melrose Park, IL 60160
USA

E-mail: mike.liu@navistar.com

Chapter 9

Philip J. G. Dingle
Diesel Systems Division
Delphi Diesel Systems
1624 Meijer Drive
Troy, MI 48084
USA

E-mail: Philip.J.Dingle@delphi.com

Chapter 10

Jeffrey Carter, Nick K. Sharp* and Henry Tennant
Cummins Turbo Technologies
Huddersfield HD1 6RA
UK

E-mail: nick.k.sharp@cummins.com

Chapter 11

Professor Wanhua Su
State Key Laboratory of Engines
Tianjin University
Tianjin 300072
China

E-mail: whsu@tju.edu.cn

Chapter 12

Dr Qianfan (Harry) Xin
Advanced Analysis and Simulation Department
Navistar, Inc.
10400 West North Avenue
Melrose Park, IL 60160
USA

E-mail: Harry.Xin@navistar.com
QianfanHarryXin@yahoo.com

Chapter 13

Dr Thanos Megaritis*
Mechanical Engineering
School of Engineering and Design
Brunel University West London
Uxbridge UB8 3PH
UK

E-mail: thanos.megaritis@brunel.ac.uk

A. Tsolakis and M. L. Wyszynski
University of Birmingham
UK

S. E. Golunski
Johnson Matthey Technology Centre
UK

Chapter 14

Peter Eastwood
Diesel Engine Aftertreatment
Room GB-15/2A-D05
Ford Motor Company Limited
Dunton Technical Centre
Laindon
Basildon
Essex SS15 6EE
UK

E-mail: peastwo1@ford.com

Chapter 15

Timothy Johnson
HP-CB-2-4
Corning Incorporated
Corning, NY 14831
USA

E-mail: JohnsonTV@Corning.com

Chapter 16

Professor Dr Christof Schulz
Institute for Combustion and Gasdynamics, IVG
University of Duisburg-Essen
Lotharstr. 1
47057 Duisburg
Germany

E-mail: Christof.schulz@uni-du.de

Chapter 17

Dr Mark P. B. Musculus* and Dr Lyle M. Pickett
Combustion Research Facility
Sandia National Laboratories
PO box 969
Livermore, CA 94551-0969
USA

E-mail: mpmuscu@sandia.gov
lmpicke@sandia.gov

Chapter 18

Professor Rolf D. Reitz*
Engine Research Center
University of Wisconsin-Madison
1500 Engineering Drive
Madison, WI 53706
USA

E-mail: reitz@engr.wisc.edu

Dr Yong Sun
General Motors Company
GM R&D and Planning
Mail Code 480-106-252
30500 Mound Road
Warren, MI 48090-9055
USA

E-mail: yongsun00@gmail.com
yong.sun@gm.com

Preface

Over the last decade, significant progress has been made in the development of direct injection internal combustion engines. It may have been by coincidence that direct injection technology was developed and applied almost simultaneously to spark ignition (SI) gasoline engines and light-duty diesel engines in the mid-1990s, but the direct injection technology had been adopted in both engines for the same reason – to increase the efficiency of internal combustion (IC) engines for automotive applications while improving their performance. However, the route to growth and market penetration has proved more haphazard in the case of direct injection SI engines, owing to relatively high cost, lower than expected gains in fuel economy and full-load performance, their complexity and the requirement for a lean NO_x aftertreatment system. In comparison, the high-speed direct injection (HSDI) diesel engine has achieved remarkable commercial success due to its excellent fuel economy and good performance characteristics.

With heightened concern over the greenhouse gas effect, imminent CO_2 emission targets in Europe and Japan, and new fleet vehicle fuel consumption requirements in the US, direct injection gasoline engines are staging a comeback, mainly through downsized boosted operations in the short term and stratified charge and/or controlled autoignited combustion in the medium term. In the meantime, HSDI and heavy-duty (HD) diesel engines are facing the challenge of meeting ever more stringent emission legislation across the globe, but without deteriorating fuel economy. It is therefore timely that the state of the art with respect to current direct injection combustion engines and their development needs should be presented and discussed in a single volume so that researchers and practising engineers can 'stand on the giants' shoulders' in developing future high-efficiency and low-emission combustion engines. One particular strength of this book is its wide-ranging but balanced

coverage of the fundamental understanding and applied technologies involved in DI combustion engines and the complementary contributions by both practising engineers and academic researchers.

This book is divided into two volumes, the first dealing with gasoline and gas engines, and the second discussing diesel engines. In Volume 1, following an overview of the history and principles of high-efficiency direct injection gasoline engines, approaches to achieving better fuel economy from such engines are presented. These include a discussion on the stratified charge combustion for part-load operations in Chapter 2, downsized engines through turbocharging in Chapter 3, lean-boost and exhaust gas recirculation (EGR) boost for further engine downsizing in Chapters 4 and 5, and autoignition combustion for simultaneous reduction in NO and fuel consumption in Chapter 6. Chapter 7 illustrates the use of computational fluid dynamics (CFD) in the design and optimisation of direct injection gasoline engines. Chapter 8 reviews direct injection compressed natural gas (CNG) engines that have been developed for commercial vehicles. Chapter 9 has been written to reflect the experience of the world's most successful bio-fuel market in Brazil. Finally Chapter 10 provides an up-to-date summary of advanced optical techniques and their applications to the development of gasoline engines.

Volume 2 starts with a survey of HSDI diesel engines developed over the last decade, which sets the scene for the following chapters. Chapter 2 provides an overview of state-of-the-art fuel injection systems for light-duty diesel engines. The fundamentals of mixture formation, combustion and emissions from HSDI diesel engines are presented in Chapter 3. This is complemented by a detailed discussion on the effect of multiple injections on diesel combustion and emissions in Chapter 4. Air management and turbocharging technologies are crucial to the diesel engine's performance and emissions, and they are the subject of Chapter 5. Chapter 6 presents and discusses some advanced concepts for future light-duty HSDI diesel engines. With the incorporation of a more sophisticated fuel injection system, turbocharging, EGR, and regenerative and active aftertreatment systems in modern diesel engines, Chapter 7 introduces the concept and example of a model-based control and engine management approach to illustrate how such a complex system can be controlled and optimised.

In the second part of Volume 2, following an overview of current heavy-duty diesel engines in Chapter 8, the evolution and development in the fuel injection system for heavy-duty diesel engines is described in Chapter 9. Chapter 10 gives an excellent presentation on the turbocharging technologies for heavy-duty diesel engines by one of the major turbocharger manufacturers. Chapter 11 presents results of a series of experimental and CFD studies carried out on a single-cylinder heavy-duty diesel engine using multiple injections and combustion chamber designs. Part II concludes with a detailed description of the systematic process in the design of heavy-duty diesel engines in Chapter 12.

Part III discusses exhaust emission abatement, diesel combustion diagnostics and modelling. Fuel reforming is an interesting topic in that it offers the potential to generate on-board hydrogen for not only better combustion but also the opportunity for improving the performance of aftertreatment systems, which is the topic of Chapter 13. Aftertreatment systems are now an integral part of a diesel powertrain system. Chapters 14 and 15 provide a summary of current practice and future development needs in light-duty and heavy-duty diesel engine aftertreatment systems.

Advanced modelling and in-cylinder optical techniques have made significant contributions to the research and development of direct injection gasoline and diesel engines. Chapter 16 provides an up-to-date summary of advanced optical techniques and their applications to the development of diesel engines. Chapter 17 presents the latest research results on low-temperature diesel combustion through the application of advanced in-cylinder optical diagnostics. Finally, the latest developments in the CFD modelling of internal combustion engines are described in Chapter 18.

This book has been made possible by the dedication of contributing authors to complete their works to the agreed publication schedule, for which I am grateful. In particular, I would like to express my gratitude to the authors who had to endure the extracurricular activities imposed on them. I would also like to thank Sheril Leich and Diana Gill (née Leusenrink) of Woodhead Publishing for commissioning the project and their professional support in preparing this book. Finally, I would like to thank my wife and daughter, who put up with my absence during homework and playtimes.

Professor Hua Zhao
School of Engineering and Design
Brunel University West London
UK



SUPERIOR DOWNSIZING

OUR COMPETENCE FOR YOUR SUCCESS

Turbocharged engines, in conjunction with innovative technologies, provide the optimum solution for improved fuel economy and lower emissions. Our downsizing engine with a displacement of 1.2 liters, which we developed as a technology demonstrator, offers the performance of a conventional engine twice the size. More importantly, it reduces fuel consumption, and consequently CO_2 emissions by up to 30 percent. Our numerous high-performance projects and systems contribute to this achievement. As a result of this extensive systems expertise, MAHLE is the leading development partner for the international automotive and engine industry. **www.mahle-powertrain.com**

Contact: daren.mottershead@gb.mahle.com

MAHLE
Powertrain

1

Overview of high-speed direct injection diesel engines

R. W. HORROCKS, Ford Motor Company Limited, UK

Abstract: This chapter traces the historical development of the high-speed direct injection (HSDI) diesel engine and reviews some of today's engines. The European passenger car diesel market share rose rapidly over the last decade to reach above 50% at present. This has been due to significant improvements in performance and refinement, demonstrated by premium luxury manufacturers offering diesel engines for their top of the range models. Performance has been increased by higher fuel injection pressures, improvements in turbocharger design and efficiency, and more sophisticated electronic controls. Complex exhaust gas recirculation (EGR) systems and exhaust after-treatment have facilitated keeping pace with emissions legislation. Greater flexibility of injection timing and number of injections have greatly improved noise levels. HSDI engine designs and development are reviewed from the first production eight-valve four-cylinder engines with pump-line-nozzle fuel systems in the mid-1980s to the typical 16-valve four-cylinder common rail engines of the present day. A survey of some of today's notable engines is covered, including a 48-valve 12-cylinder engine with a 2000 bar common rail fuel system producing 368 kW and 1000 Nm torque. The chapter concludes with a contemplation of the future.

Key words: direct-injection, high-speed, diesel, engine, perfomance, fuel-injection, turbocharger, power, torque, emissions, exhaust, gas, recirculation.

1.1 Background

The diesel engine has been a true alternative power unit for European passenger cars for about a decade, not just the economy low-performance variant of years gone by, but a high-performance, fuel-efficient competitor to the gasoline engine. Today's diesel passenger cars range from small fuel-efficient 'sub-B cars' such as the Fiat 500 with its 1.3 litre 55 kW in-line four-cylinder engine, or the VW Fox with the 1.4 litre 51 kW three-cylinder diesel engine, to large luxury cars like the Mercedes-Benz S class with a 235 kW, 4 litre V8 diesel or the BMW 745 with its 4.4 litre 242 kW V8 engine, and most recently the new Audi 368 kW 6.0 litre V12. Looking back to the first half of 2000, BMW stepped up its production of diesel engines by an impressive 54%. During 2007 and 2008, BMW invested a further 14 million euros on its diesel development centre at the Steyr engine plant in Austria, where all the company's diesel research and development is conducted. In 2005 diesel cars accounted for 64% of BMW European sales

(*Automotive Engineer*, 2007). The total share of diesel-powered cars sold by Volkswagen in Europe was 47% in 2000 (Love, 2002); this grew to 62% in 2005. In France it was already a staggering 56% in 2001 and this rose further to 69% in 2005 and over 70% in 2007. In the mid-sized family car segment, typified by the Ford Mondeo, the diesel share throughout Europe was 44% in 2000; this grew to 67% in 2005. The overall market share of diesel passenger cars in Europe was 36% in 2001 and this grew to 49.8% in 2005. In 2007 more than 50% of all passenger vehicles sold in Europe were diesel powered, amounting to roughly 15 million sales according to the European Automobile Manufacturers' Association (ACEA).

This increase in diesel proportion is due in part to the improvements in specific power and torque over the past eight to ten years, seeing specific power reaching 75 kW/litre for modern high-speed direct injection (DI) diesel engines. In addition, the recent achievements in refinement, with new sophisticated fuel injection systems reducing combustion noise, are giving gasoline-like in-vehicle noise and vibration levels. This is demonstrated by the premium luxury manufacturers, the likes of Audi, BMW and Mercedes-Benz offering V8 diesel engines for their top of the range models. In 2002 VW announced a 5.0 litre 230 kW V10 diesel engine for its new large luxury Phaeton car (Birch, 2002). More recently, in 2008, Audi presented its 6.0 litre 368 kW V12 TDI for the Q7 vehicle (Bauder *et al.*, 2008).

This increase in performance has been made possible by three key engine component system developments. Firstly, there have been significant increases in fuel injection system operating pressure, together with greater flexibility of timing and the number of injection events per cycle, which has been enabled by the development of common rail fuel injection systems with electronic control. Secondly, there have been improvements in turbocharger efficiency with volume production of variable geometry turbochargers. Thirdly, more sophisticated electronic controls have been developed for greater flexibility and refinement of the engine systems to provide superior power and response and more acceptable noise levels. In parallel with these developments, exhaust gas recirculation (EGR) systems have become more sophisticated with more efficient coolers and bypass valves, and exhaust after-treatments in the form of oxidation catalysts and particulate traps have been developed and put into mass production to keep pace with more stringent emissions legislation.

1.2 Early development of the high-speed direct injection (HSDI) diesel engine

The Ford 2.5 DI naturally aspirated diesel engine was introduced in 1984 for the Ford Transit, as the world's first production high-speed DI diesel engine. The engine was a four-cylinder in-line unit, with bore and stroke of 93.67 mm and 90.54 mm respectively, giving a stroke to bore ratio of 0.97

and a capacity of 2.496 litres. Fuel was injected by Lucas DPS or Bosch VE rotary distributor fuel injection pumps through 17/21 mm Lucas or Bosch injectors. These were inclined at 23° from the vertical with the nozzle located 9.5 mm from the bore axis, giving a 10% offset. The bowl-in-piston was a conventional straight-sided toroidal design giving a 19:1 compression ratio. In-cylinder swirl, to support combustion, was generated by a helical intake port. The nominal power and torque were 52 kW at 4000 rpm and 145 Nm at 2700 rpm. In combination with revised drive ratios, this new engine gave improvements in vehicle fuel consumption of 20–24% for the Ford Transit (Bird, 1985). This was a major milestone in the development of small high-speed diesels, which demonstrated that DI technology could be used for light-duty vehicles. It was the first of a new concept of fuel-efficient prime movers for cars and light trucks. The introduction of more two-valve-per-cylinder high-speed DI diesels from Isuzu, Iveco (Sofim), Fiat, Perkins, Audi, Land Rover, VW and Mercedes-Benz followed.

The Isuzu 'J' series engines replaced the earlier 'C' series IDI engines, with 2.5 and 2.8 litre capacities, in 1985. The 2.5 litre engine was very similar to the Ford unit, but having a square combustion chamber in the piston with a small squish lip. The 2.5 litre produced 50 kW at 3600 rpm and 152 Nm at 2000 rpm, the larger version giving 57 kW and 172 Nm (Takeuchi *et al.*, 1985).

The Iveco DI diesel engine 8140.21 was developed from the 8100 engine family and manufactured in volume production from 1985 for light-duty truck application. The 2.45 litre turbocharged engine produced 68 kW at 3800 rpm and 215 Nm at 2200 rpm. The stroke was also increased from 90 to 92 mm which increased the capacity to 2.5 litres. This enabled an increase in power and torque to 76 kW and 225 Nm, respectively. This engine was subsequently used in passenger cars (Knecht *et al.*, 1988, 1991).

Fiat is credited with producing the world's first DI diesel for passenger cars with the launch of the 1.9 litre TCI for the Croma in mid-1988. This engine delivered 68 kW at 4200 rpm and 182 Nm at 2500 rpm (*Ward's Engine Update*, 1988). In 1991, this engine was upgraded by installing a Garrett VNT 25 variable geometry turbocharger; the power was increased to 69 kW and the torque to 200 Nm at the lower speed of 2000 rpm. Although constant-speed fuel consumption was unaffected, mixed driving consumption was reported to be 7–8% lower (*High Speed Diesels and Drives*, 1991).

The Perkins Prima 2.0 litre DI diesel, in naturally aspirated form, was available in the Maestro van in late 1986, but it was not introduced in the Maestro car until 1990. A turbocharged and intercooled version was installed in the Montego at the beginning of 1989; this engine produced 60 kW at 4500 rpm and set a new standard for fuel economy, for this size of car, of 5.8 litres per 100 km on the urban cycle (Stephenson and Hood, 1988).

Audi introduced their new five-cylinder turbo diesel engine with 'Second Generation Direct Injection' at the 1989 Frankfurt Motor Show for the

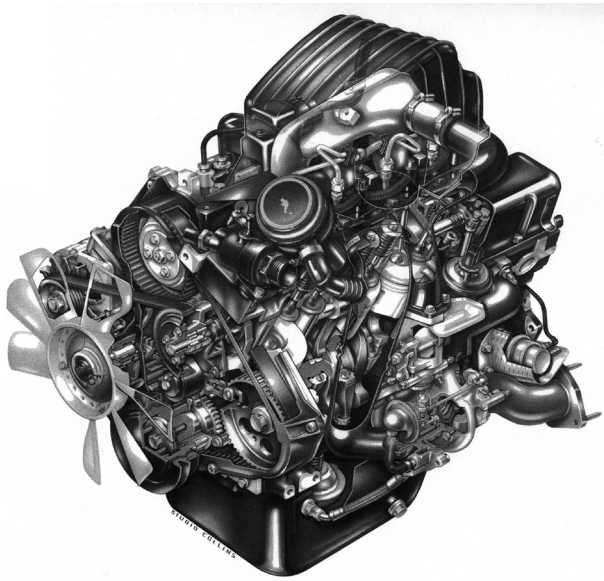
Audi 100. This engine featured pistons with a re-entrant combustion bowl incorporating a 'Mexican sombrero' raised centre portion, five-hole two-spring injectors, an electronically controlled Bosch VP-34 fuel injection pump and an electronic engine management system which provided improved driveability. Installation features for further refinement included electronically controlled engine mounts with variable damping and a fully enclosed engine compartment, with an automatically operated blind for the intercooler to reduce external noise at idle. Producing 88 kW at 4250 rpm and 265 Nm at 2250 rpm, the Audi 100 TDi established a high standard for DI passenger car diesels (Basshuysen *et al.*, 1989; Stock and Bauder, 1990). Peak power was subsequently reduced to 85 kW for the next Audi 100 car.

In 1989, to meet tightening European emissions legislation and to improve the NVH refinement, Ford introduced an improved 2.5 litre naturally aspirated engine. The major changes were Stanadyne 'slim-tip' injectors which facilitated locating the injector closer to the cylinder centre-line to reduce the nozzle offset to 5.5 mm (6% of the bore), a new re-entrant combustion bowl with an increased compression ratio of 20.7:1, and a novel Ford-patented mechanically controlled modulating EGR system for reduction of NO_x emissions. This engine met 88/76 EEC (5th Amendment) passenger car, 88/436 EEC (particulates) and 1984 US Federal Light Truck emissions standards. Power remained at 52 kW at 4000 rpm with the peak torque of 146 Nm at the slightly slower speed of 2500 rpm (Bird *et al.*, 1989). At the rated power, the Bosch VE rotary distributor pump developed 800 bar fuel pressure at the injector.

Land Rover introduced their 2.5 litre in-line four-cylinder 82 kW DI TCI for the Discovery at the end of 1989 (*High Speed Diesels and Drives*, 1989). Following this, in January 1995, Rover launched a 2.0 litre DI passenger car for the 620 models. This engine, known as the 'L' series, developed a maximum power of 77 kW at 4200 rpm and 210 Nm at 2000 rpm. It had a conventional aluminium cylinder head with two valves per cylinder (*Rover External Affairs*, 1995).

Ford introduced a turbocharged version of the 2.5 DI diesel for the Transit in 1992 with the Lucas EPIC electronic fuel injection pump and engine management system; this was the first European light truck to use drive-by-wire controls. The turbocharged version of this engine had a lower compression ratio of 18.3:1. Fuel was injected through Stanadyne 'slim-tip' injectors and with a fixed geometry KKK K04 turbocharger the engine developed 75 kW peak power at 4000 rpm and peak torque of 224 Nm at 2100 rpm. To meet the emissions legislation, the engine management system controlled a throttle valve in the boost air path and an EGR valve on the exhaust manifold to modulate recirculation of exhaust gas to the intake manifold (Bostock and Cooper, 1992). The Ford 2.5 litre turbocharged engine is shown in Fig. 1.1.

In 1992 VW-Audi installed a 1.9 litre TDI diesel in the Audi 80. The engine

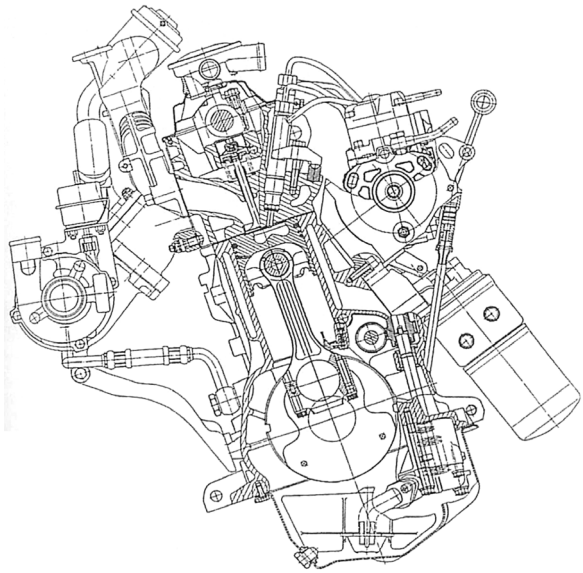


1.1 Ford 2.5 litre turbocharged diesel engine introduced in 1992 (courtesy of Ford Motor Company).

had a rating of 66 kW at 4000 rpm and a torque of 182 Nm at 2300 rpm. This engine used the Bosch VP34 electronic rotary distributor fuel injection pump, with the Bosch MSA6 electronic controller (Rhode *et al*., 1991). In the autumn of 1993, this engine was introduced in the VW Golf and Passat with revised turbocharger and fuel injection equipment, to give an increased peak torque of 202 Nm and exhaust emissions to Euro II standards.

In 1995 VW extended their DI diesel range by offering the TDI in the Golf Convertible and introducing a naturally aspirated version of the 1.9 DI in the Golf, Golf Estate and Vento. This engine produced 47 kW at 4200 rpm and 124 Nm at 2000 rpm and had a minimum full load BSFC of 222 g/kWh. At that time, the company also reported plans to introduce an 81 kW version of the 1.9 litre engine to give GTI-type performance with good fuel economy (Jelden and Willman, 1995). This engine was available a year later for the Golf, Vento and Passat. With a variable geometry turbocharger it provided 235 Nm at 1900 rpm and 81 kW at 4150 rpm (Volkswagen Press Information, 1996). Figure 1.2 shows the VW 1.9 litre 81 kW diesel.

Mercedes-Benz was a more recent entrant into DI passenger cars with the introduction of its 2.9 litre turbocharged intercooled DI diesel for the E-Class in 1995. This five-cylinder engine produced 95 kW at 4000 rpm and 300 Nm from 1900 to 2400 rpm. Like all the newer engines of that time, it had a re-entrant combustion bowl and used the Bosch VP37 fuel injection pump with two-spring injectors. (Krause and Saltzer, 1995; Peters and Pütz, 1995).



1.2 VW 1.9 litre 81 kW TDI diesel engine (courtesy of *MTZ*).

It is interesting to note that Mercedes-Benz reverted back to two vertical valves per cylinder for the DI engine, from the previous final developments of their IDI engine with four valves per cylinder.

Opel/Vauxhall led the industry with four valves per cylinder by introducting the Ecotec 16-valve 2.0 litre DI diesel engine in the autumn of 1996. This engine was introduced in turbocharged form, producing 60 kW for the Vectra car. The four vertical valves per cylinder were operated by a single camshaft, which was driven with a simplex chain from the injection pump. Bridge pieces actuated each pair of intake and exhaust valves. Bosch's then new radial piston, high-pressure distributor injection pump, designated VP44, was used to inject fuel through two-spring five-hole nozzles. A 74 kW TCI version and a 2.2 litre 88 kW TCI derivative followed (Vauxhall News Release, 1996). This was the first application of the Bosch VP44 high-pressure rotary fuel injection pump, which was one of a new breed of solenoid valve spill pumps specifically designed for electronic control.

Table 1.1 lists the early high-speed DI diesel engines. It is interesting to note that a number of the traditional diesel passenger car manufacturers were absent from the list of those producing first-generation HSDI diesel engines during the mid-1980s to mid-1990s. Notably BMW, Peugeot and Renault were late in the market with high-speed DI diesel engines for passenger cars, and while Ford was the first company to produce an HSDI engine for the Transit commercial van and bus, a similar type of engine was not offered for passenger cars until 1999, when the 1.8 litre Endura DI engine was released in

Table 1.1 Early high-speed DI diesel engines

Year of introduction	Manufacturer	Layout	Capacity (litres)	Power (kW)	Torque (Nm)	Aspiration	Reference
1984	Ford	I-4	2.5	52	143	2-valve N/A	Bird, 1985
1985	Isuzu	I-4	2.5	50	152	2-valve N/A	Takeuchi *et al.*, 1985
1985	Isuzu	I-4	2.8	57	172	2-valve N/A	Takeuchi *et al.*, 1985
1985	Iveco	I-4	2.45	68	216	2-valve T/C	Knecht *et al.*, 1988, 1991
1985	Iveco	I-4	2.5	76	225	2-valve T/C	Knecht *et al.*, 1988, 1991
1986	Perkins/Rover	I-4	2.0	46	122	2-valve N/A	Perkins Tech. Info., 1988
1988	Fiat	I-4	1.9	68	182	2-valve TCI	*Ward's Engine Update*, 1988
1989	Perkins	I-4	2.0	60	154	2-valve TCI	Stephenson and Hood, 1988
1989	Audi	I-5	2.5	88	265	2-valve TCI	Basshuysen *et al.*, 1989; Stock and Bauder, 1990
1989	Ford	I-4	2.5	52	146	2-valve N/A	Bird *et al.*, 1989
1989	Land Rover	I-4	2.5	82	260	2-valve TCI	*High Speed Diesels & Drives*, 1989
1992	Ford	I-4	2.5	74	224	2-valve T/C	Bostock and Cooper, 1992
1992	VW-Audi	I-4	1.9	66	182	2-valve TCI	Rhode *et al.*, 1991
1995	Perkins/Rover	I-4	2.0	77	210	2-valve TCI	Rover External Affairs, 1995
1995	Mercedes	I-5	2.9	95	300	2-valve TCI	Krause and Saltzer, 1995; Peters and Pütz, 1995
1996	Iveco	I-4	2.8	76	240	2-valve T/C	Iveco Daily Press Pack, 1996
1996	Iveco	I-4	2.8	90	285	2-valve TCI	Iveco Daily Press Pack, 1996
1996	Opel/Vauxhall	I-4	2.0	60	185	4-valve TCI	Vauxhall News Release, 1996

the new Focus car. The major reason for this delay was the level of refinement of this new technology; it will be noted that the first engines on the market were for commercial vehicles, and refinement in terms of noise, vibration and harshness (NVH) was not at the same level as in the indirect injection (IDI) engines of the period. It was not until the introduction of 'two-spring' injectors that combustion noise, caused by the high initial rate of cylinder pressure rise, could be modulated to give competitive NVH levels.

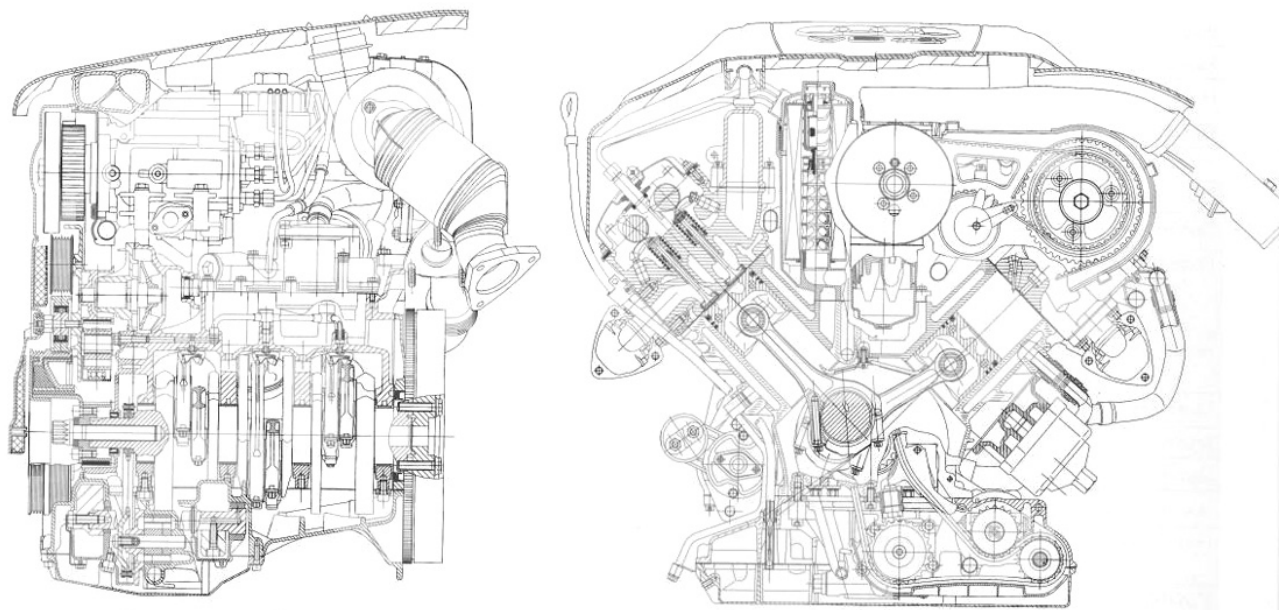
1.3 Recent trends in high-speed direct injection (HSDI) diesel engine design

1.3.1 More recent developments of the HSDI diesel engine

During the late 1990s and early 2000s most of the major automobile manufacturers developed second-generation four-valve high-speed DI diesel engines. The move to four valves per cylinder, utilising two intake and two exhaust, was principally to allow the installation of a central vertical injector to give symmetrical fuel spray plumes for improved air–fuel mixing and air–fuel ratio distribution in the combustion chamber. There were also some additional benefits, such as variable swirl levels by port deactivation and a more uniform temperature distribution around the cylinder head flame face, since it is possible to cool the bridges between the exhaust ports. So a new breed of high-performance, fuel-efficient diesel engines came onto the market.

In 1997 Audi launched its V6 four-valve TDI, the first six-cylinder DI diesel engine designed specifically for the passenger car. This was a 90° V6 with 30° offset crankpins and a single counter-rotating balance shaft. This bank angle was obviously chosen with a V8 derivative planned. The four vertical valves, two intake and two exhaust, were laid out obliquely to the engine axis around the central vertical injector. A tangential and a helical port were used to generate in-cylinder swirl. This engine used a six-cylinder version of the Bosch VP44 radial piston distributor pump and an Allied Signal variable geometry turbocharger. The engine produced 110 kW at 4000 rpm and 310 Nm between 1500 and 3200 rpm (Bauder *et al.*, 1997a,b), the most powerful TDI engine of its day. Figure 1.3 shows the Audi 2.5 litre V6 diesel engine.

BMW launched a 2.0 litre 16-valve four-cylinder engine for the 3-Series in the spring of 1998. This engine produced 100 kW at 4000 rpm, and had a maximum torque of 280 Nm at 1750 rpm. The valves were operated by two overhead camshafts via roller finger followers, pivoted by hydraulic lash adjusters. The cylinder head layout was arranged to give one intake downdraught helical port located between the camshafts and a tangential



1.3 Audi 2.5 litre V6 diesel engine (courtesy of *MTZ*).

port to generate in-cylinder swirl to support combustion. Fuel was injected by a Bosch VP44 electronically controlled radial-piston distributor pump through central vertical six-hole injectors. The intake charge was boosted by a variable geometry turbocharger. European Stage III emissions were met with the assistance of a cooled EGR system and a close coupled oxidation catalyst together with an underfloor oxidation catalyst. At a specific power of 51.3 kW/litre, this was the highest power density diesel engine of its day (Anisits *et al*., Special Edition, *ATZ/MTZ*). A new in-line six-cylinder version followed later the same year, the major difference being that this engine had a Bosch common rail fuel injection system. Peak power was 135 kW at 4000 rpm, giving a lower specific power of 46.2 kW/litre, and a peak torque of 410 Nm between 2000 and 3000 rpm (Anisits *et al*., 1998).

With the advent of common rail fuel injection technology, Daimler-Benz introduced the first common rail diesel engine for the C-Class in 1997 and subsequently for the E-Class. Following the success of this engine, Daimler-Benz went on to develop and introduce a completely new range of direct injection diesel engines during the late 1990s. This new family of engines had a common bore of 88 mm and a stroke of 88.34 mm, with a cylinder spacing of 97 mm, and was produced in four-, five- and six-cylinder configurations having displacements of 2.2, 2.7 and 3.2 litres respectively. These engines all featured four valves per cylinder with a central vertical injector and were turbocharged with a VNT turbocharger and charge cooled. To meet EU III and USA Tier 1 emissions the engines were equipped with exhaust gas recirculation. A novel feature of this system was feeding exhaust gas through the cylinder head, where it received a certain amount of cooling before flowing through an EGR cooler to the intake manifold via an EGR valve (Klingmann and Brüggemann, 1997; Peters and Pütz, 1997).

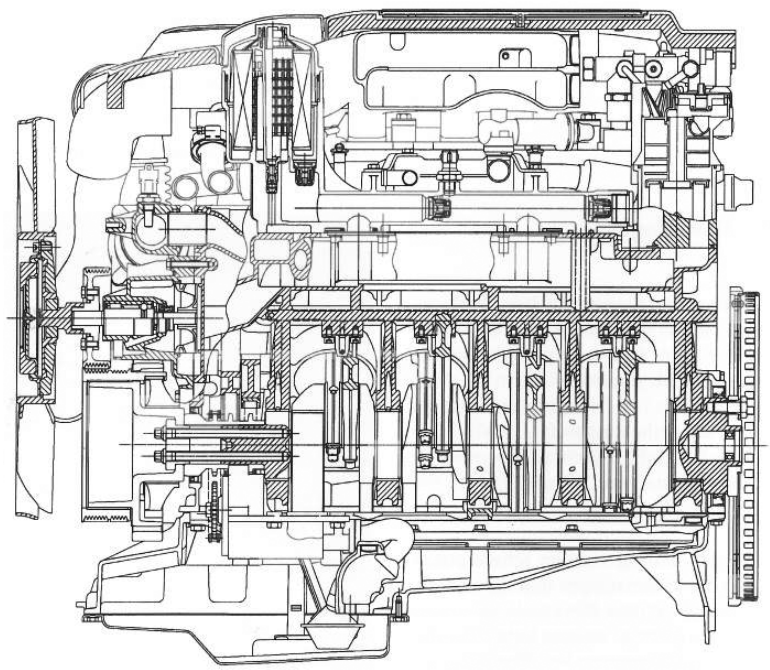
The following year Mercedes-Benz introduced the in-line four-cylinder 1.7 litre diesel engine for the A-Class. When introduced this was the smallest-displacement high-speed DI engine for automotive use. It had a completely new lightweight design specifically for installation in the A-Class, having a diecast aluminium cylinder crankcase and the cylinder axis installed at 30° to the horizontal (Brüggemann and Wamser, 1998).

In the same year Fiat introduced what they referred to as third-generation HSDI diesel engines; these were an in-line four-cylinder 1.9 litre and five-cylinder 2.4 litre TCI engines, which formed the JTD family. They were two-valve engines that featured the new UNIJET common rail fuel system operating up to a maximum pressure of 1350 bar, which was developed by Fiat and put into production by Bosch (see Chapter 2 for more details). The 2.4 litre engine also featured a variable geometry turbocharger. Both engines were installed in the Alfa Romeo 156 car (Piccone and Rinolfi, 1997).

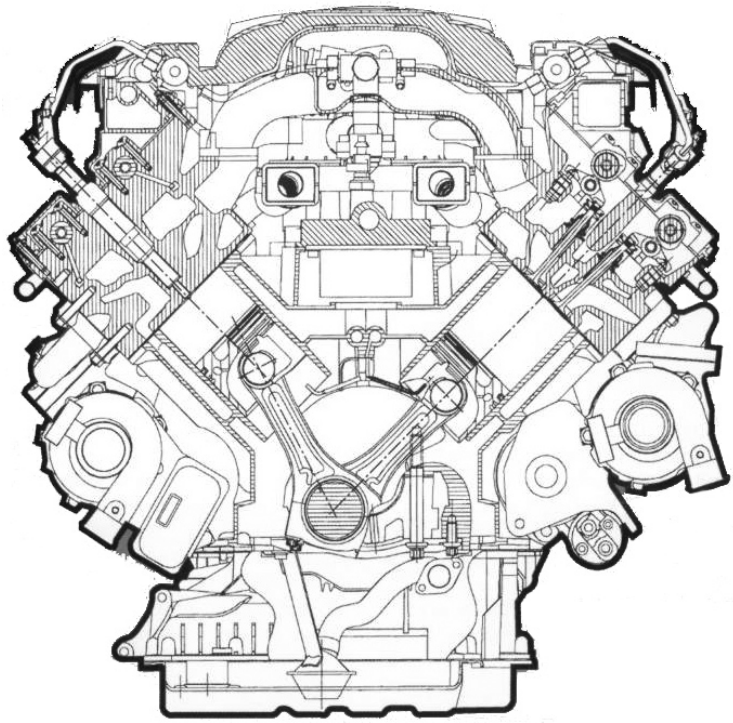
BMW was the first manufacturer to produce a V8 high-speed DI diesel engine specifically for luxury cars in 1999. This 3.9 litre engine had a bank

angle of 90° in the vermicular, or compacted graphite, cast iron cylinder block, the first time this material had been used in low-volume production. Another notable and unique feature was fracture splitting of the main bearing caps. The cylinder layout was basically the same as the in-line engines, with bore and stroke of 84 and 88 mm respectively. Like the six-cylinder engine, the V8 used the Bosch 1350 bar common rail fuel system with a rail on each bank supplying four injectors; a distributor rail fed by the high-pressure pump supplied each bank rail. Two exhaust gas turbochargers were used, one on each bank. These were controlled electronically by the engine management system. The engine produced 175 kW at 4000 rpm and 560 Nm at 1750–2500 rpm (Anisits *et al.*, 1999). Figures 1.4 and 1.5 show the BMW V8 engine in longitudinal and transverse sections.

Mercedes-Benz was the second premium brand manufacturer to introduce a V8 turbo-diesel that incorporated all the latest technologies: four valves per cylinder, swirl control, bi-turbocharging with VNT and intercooling, cooled EGR and common rail fuel injection. Following their earlier smaller engines, the V8 had an aluminium crankcase with banks at 75° rather than the normal 90°, to reduce the package envelope, but this necessitated a balance shaft. Centrifugally cast grey iron liners were surrounded by coolant on the upper portion. The bottom end had a traditional bedplate, which had



1.4 BMW V8 engine longitudinal cross-section (courtesy of *MTZ*).

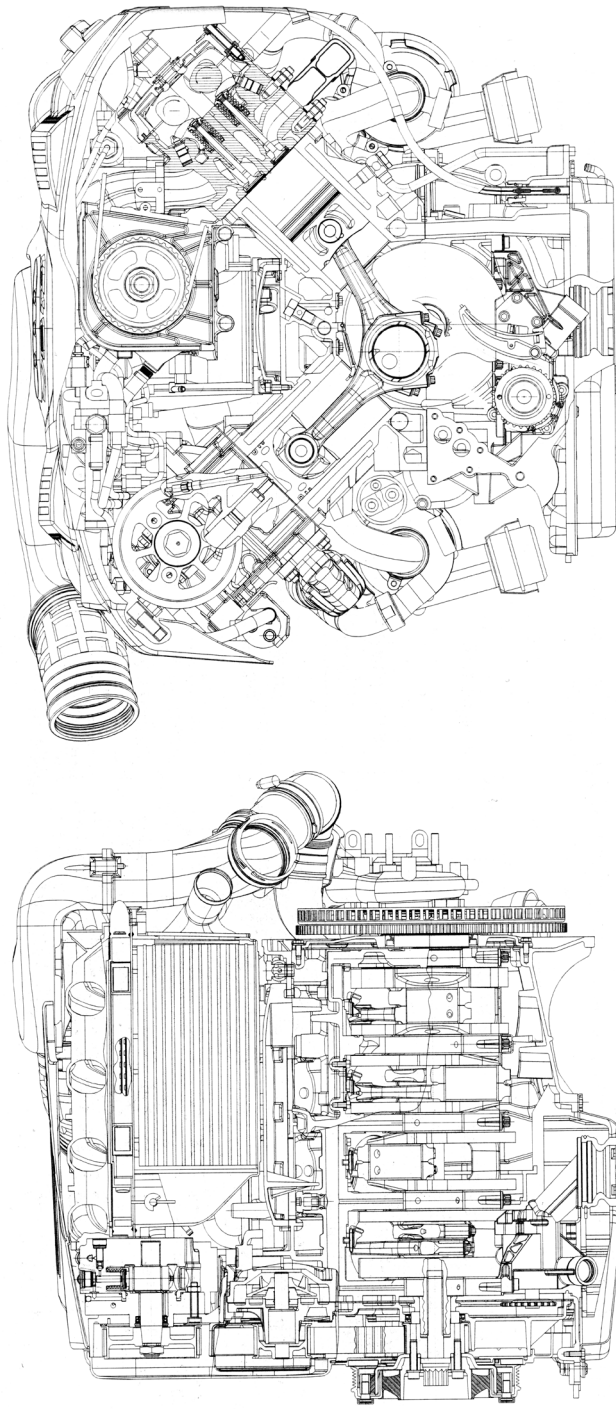


1.5 BMW V8 engine transverse cross-section (courtesy of *MTZ*).

cast-in nodular iron bearing brackets. Fuel was injected through a seven-hole nozzle by a first-generation Bosch common rail system. The 4-litre diesel produced 184 kW at 4000 rpm with a peak torque of 560 Nm from 1700 to 2600 rpm. At the time of introduction the engine met Euro III emission standards (Brüggemann *et al.*, 2000).

Audi was the third manufacturer to introduce a state-of-the-art V8 diesel in 1999. It was notably smaller than the premium diesels announced by BMW and Mercedes, at 3.3 litres displacement, with a bore and stroke of 78.3 and 86.4 mm respectively. With a conventional bank angle of 90°, for a V8, the cylinder block was manufactured from vermicular or compacted graphite cast iron to give a weight saving of 10% over grey iron. Like its contemporaries, the Audi V8 used the first-generation Bosch 1350 bar common rail fuel injection system. Peak power of 165 kW was developed at 4000 rpm and the maximum torque was 480 Nm at 1800 rpm (Bach *et al.*, 1999a, 1999b, 1999c, 1999d). Figure 1.6 shows the Audi V8 diesel engine.

Table 1.2 lists the main second-generation high-speed DI diesel engines, which are all four-valve, except the Alfa Romeo four- and five-cylinder engines.



1.6 Audi 3.3 litre V8 diesel engine (courtesy of *MTZ*).

Table 1.2 Second-generation four-valve high-speed DI diesel engines

Year of introduction	Manufacturer	Layout	Capacity (litres)	Power (kW)	Speed (rpm)	Torque (Nm)	Speed (rpm)	Reference
1997	Audi	V-6	2.5	110	4000	310	1500–3200	Bauder *et al.*, 1997b
1997	Mercedes-Benz	I-4	2.2	92	4200	300	1800–2600	Klingmann & Brüggemann, 1997
1998	Alfa Romeo	I-4	1.9	77	4000	255	2000–2500	Piccone and Rinolfi, 1997
1998	Alfa Romeo	I-5	2.4	100	4000	304	2000–2500	
1998	BMW	I-4	2.0	100	4000	280	1750	Anisits *et al.*, 1998
1998	Mercedes-Benz	I-4	1.7	44	3600	160	1500–2400	Brüggemann & Wamser, 1998
1998	Mercedes-Benz	I-4	1.7	66	4200	180	1600–3200	*Autocar*, 1996
1998	Opel/Vauxhall	I-4	2.2	86		260		Vauxhall News Release, 1996
1999	BMW	V-8	3.9	180	4000	560	1750–2500	Anisits *et al.*, 1999
1999	Mercedes-Benz	I-3	0.8	30	4000	100	2000	Thiemann *et al.*, 1999
1999	Mercedes-Benz	I-4	2.2	85	4200	250	1350–2800	Klingmann *et al.*, 1999
1999	Mercedes-Benz	I-4	2.2	105	4200	315	1800–2600	
1999	Mercedes-Benz	I-5	2.7	125	4200	400	1800–2600	
1999	Mercedes-Benz	I-6	3.2	145	4200	470	1800–2600	
1999	Mercedes-Benz	V-8	4.0	184	4000	560	1700–2600	Brüggeman *et al.*, 2000
1999	Audi	V-8	3.3	165	4000	480	1800	Bach *et al.*, 1999b

1.3.2 Base engine architecture

Cylinder block material

To reduce engine weight, there has been a recent trend to manufacture the cylinder block from aluminium, examples being the Mercedes-Benz 4.0 litre V8, the Volvo D5 2.5 litre in-line five-cylinder and the more recent Peugeot/Ford 1.4 and 1.6 litre in-line four-cylinder diesel engine. However, higher engine performance will be accompanied by an increase in cylinder pressures and the engine structure will have to cope with higher forces. Critical sections in aluminium such as the main bulkheads can be made thicker, but ultimately a stronger material will be required for cylinder pressures of around 180 bar and above. Compacted graphite iron (CGI) is a material that offers superior tensile strength and fatigue properties and was used in low-volume production by Audi for the 3.3 litre V8 diesel. Table 1.3 lists the properties of grey and CG iron.

To illustrate the benefits of CG iron, it is interesting to compare the statistics of the V8 engines from Audi and Mercedes-Benz, shown in Table 1.4. This illustrates the difference between two very similar engines, one with an aluminium cylinder block and the other using CG iron, and it is very interesting to note that the iron engine has the lower total engine weight.

Table 1.3 Comparison of properties for grey and CG iron

Property	Grey	CGI	Factor
Tensile strength (MPa)	250	450	1.8
Elastic modulus (GPa)	105	150	1.4
Fatigue: push-pull (MPa)	70	150	2.2
Notch sensitivity	1.0–1.1	1.2–1.4	1.1–1.4
Thermal conductivity (W/m.K)	47	37	0.8

Source: Turner and Dawson (2008).

Table 1.4 Comparison of V8 diesel engines with CG iron and aluminium cylinder blocks

Parameter	Audi 4.2 V8 TDI CG iron	Mercedes 4.0 V8 CDI Aluminium
Peak power (kW)	240 (57 kW/litre)	231 (57 kW/litre)
Torque (Nm @ rpm)	650 @ 1600–3500	580 @ 1600, 730 @ 2200
Acceleration (0–100 km/h/s)	5.9	6.1
Bore pitch (mm)	90	97
Overall length (mm)	520	640
Engine weight (kg)	255	259
Power to weight (kW/kg)	0.94	0.89

Source: Turner and Dawson (2008).

No doubt the aluminium cylinder block is lighter, but as shown in the table it is longer, and so all the other engine components, notably the crankshaft, camshafts and cylinder heads, will also be longer, adding more weight to the engine.

CG iron was introduced by Ford and Peugeot in 2004 for the 2.7 litre Lion V6 diesel engine used in Jaguar, Land Rover, Peugeot and Citroën vehicles. Audi also uses this material in high-volume production for its new 3.0 litre V6 diesel engine launched in 2003 (Mortimer, 2002) and the new 4.2 litre V8 and 6.0 litre V12. Ford has used this material again for the cylinder block of the 3.6 litre V8 diesel engine designed and manufactured at Dagenham, England, specifically for Range Rover vehicles. Table 1.5 lists key features of high-speed diesel V-engines.

Table 1.5 High-speed diesel V-engines

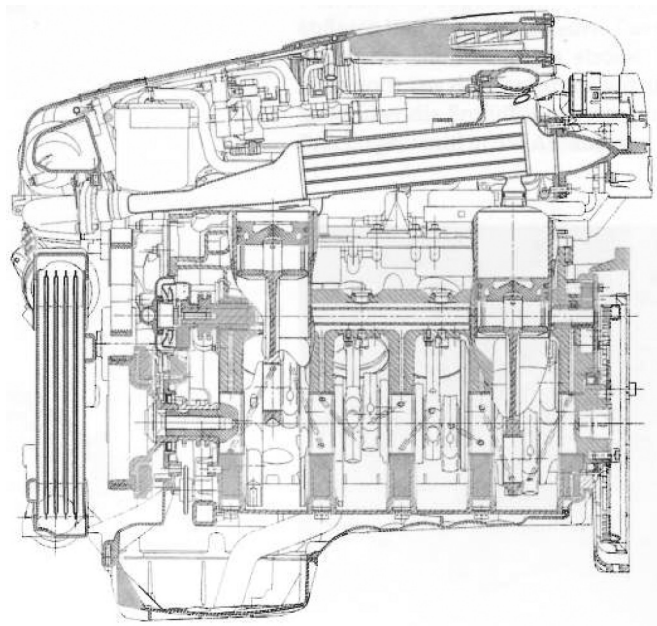
Manufacturer	Type	Capacity (cc)	Bore spacing (mm)	Cylinder block material	Bottom end	Weight, DIN 70020A (kg)	Engine length (mm)
Audi	90°V6	2967	90.0	GJV 450	SG iron, GJS600 main bearing frame	220	444
Audi	90°V8	3328	88.0	Vermicular graphite iron	Main bearing frame	260	
Audi	90°V8	4134	90.0	GJV 450		255	520
Audi	60°V12	5934	90.0	GJV 450	Main bearing frame	329	680
BMW	90°V8	3900	98.0	Vermicular graphite iron (GGV500)	Fracture split bearing caps	273	
Ford/Peugeot	60°V6	2720	93.0	CG iron	Crossbolted bearing caps	202	455
Ford	90°V8	3628	93.0	CG iron	Crossbolted bearing caps	284	688
Mercedes-Benz	75°V8	3996	97.0	Aluminium ($AlSi_7Mg$), grey CI wet liners	Aluminium ($AlSi_7Mg$) bedplate with SG iron inserts		
Mercedes-Benz	72°V6	2987	106	Aluminium ($AlSi_6Cu$), grey CI liners	Aluminium bedplate	208	

V-engine main bearing structure

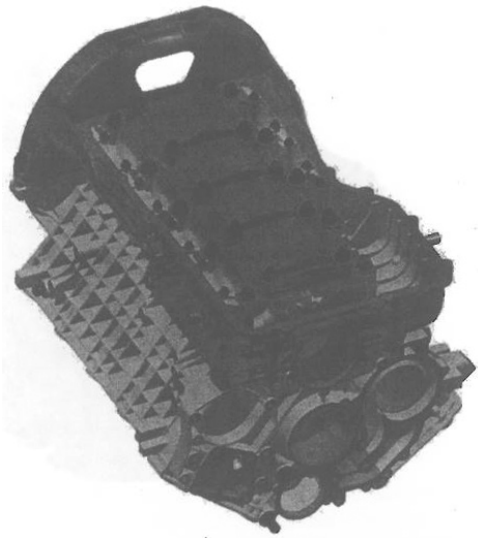
The bottom-end structure of a V-engine is of paramount importance for the overall engine stiffness and good NVH characteristics in the form of structure-borne noise, owing to the alternating oblique nature of the firing loads from each bank, leading to high lateral forces.

The Mercedes-Benz V8 diesel engine, having an aluminium alloy ($AlSi_7Mg$) cylinder block, has been designed with a bedplate of the same material. To provide greater stiffness to the main bearings, cast-in nodular iron bearing 'brackets' are utilised. There are four bolts per main bearing through the nodular iron bearing bracket. As well as increasing the strength of the assembled block bearing area, these also minimise the increase in bearing clearance owing to thermal expansion (Brüggemann *et al.*, 1999, 2000). Figure 1.7 shows a longitudinal section of a Mercedes-Benz V8 diesel engine from Brüggemann *et al.* (2000). Figure 1.8 shows a view of the bottom of a Mercedes-Benz V8 diesel engine (Brüggemann *et al.*, 2000).

The BMW V8 diesel engine was designed with a high-strength compacted graphite cylinder block and BMW has utilised fracture-splitting technology to fracture-split the main bearing caps from the cylinder block casting. This ensures perfect realignment of the bearing cap, prevents micro-movement even with the lateral forces during engine running, and requires only two



1.7 Mercedes-Benz V8 diesel engine longitudinal cross-section (Fig. 2 from Brüggemann *et al.*, 2000).



1.8 View of the bottom of the Mercedes-Benz V8 diesel engine (Fig. 5 from Brüggemann *et al.*, 1999).

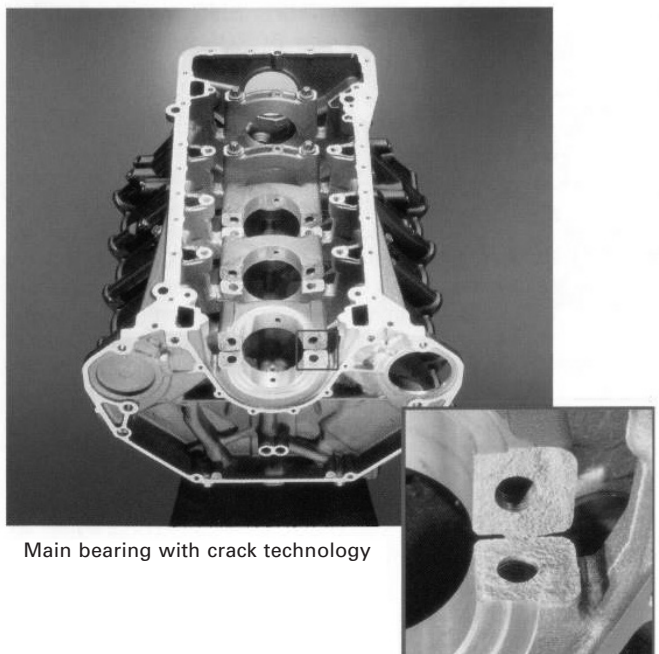
bolts – see Fig. 1.9 showing the BMW V8 cylinder block with fracture-split bearing caps (Anisits *et al.*, 1999).

The Ford/Peugeot 2.7 litre V6 diesel engine has a deep-skirt, high-strength CGI cylinder block for structural rigidity and low noise radiation. A ladder frame is used to give optimum sealing and control of high frequency modes of the bearing caps and skirt. The deep-skirt block incorporates a unique combined lock-width and cross-bolt feature. This design was chosen to reduce fillet stress, which is critical with the higher notch sensitivity found in CGI. This bottom-end concept is shown in Fig. 1.10.

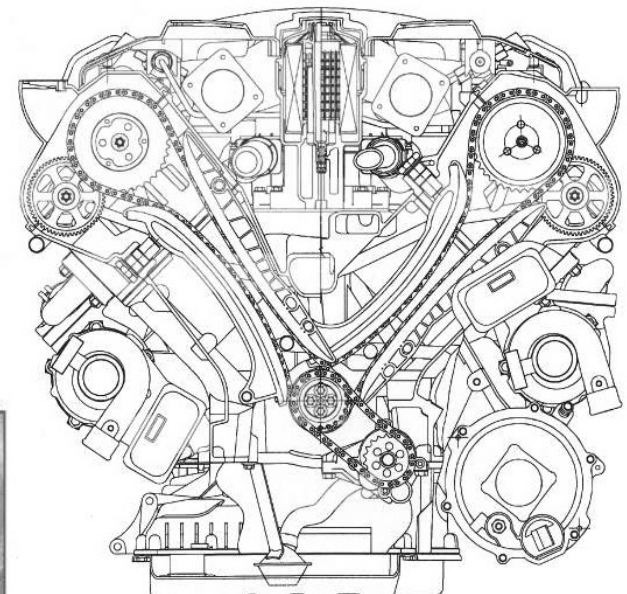
The new Audi family of 'V' diesel engines, the 3.0 litre V6, 4.2 litre V8 and 6.0 litre V12, all have a main bearing beam or 'frame' with four bolts per main bearing manufactured from GJS 600 spheroidal graphite cast iron. Figure 1.11 shows the main bearing beam from the Audi 6.0 V12 (Bauder *et al.*, 2008).

1.3.3 Performance systems

The dramatic increase in performance from light-duty diesel engines over the last 10 years or so has been made possible by three key engine component system developments: first, significant increases in fuel injection system operating pressure, together with greater flexibility of timing and the number of injection events per cycle; second, improvements in turbocharger efficiency with volume production of variable geometry turbochargers, and third, more

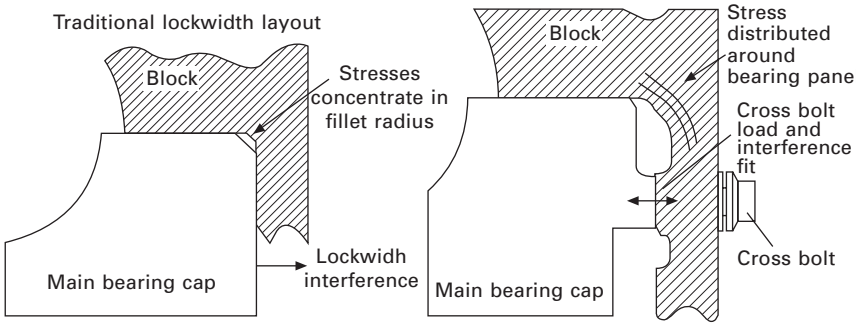


Main bearing with crack technology

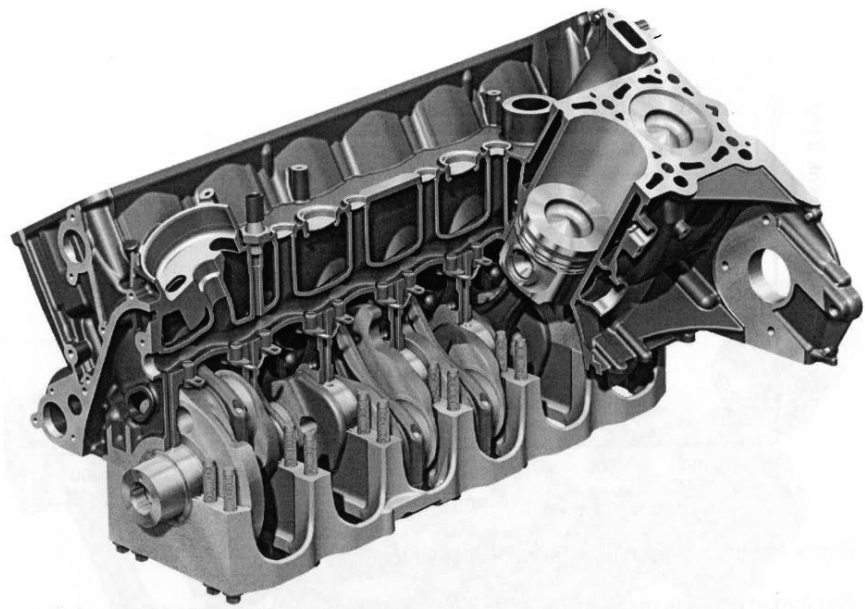


Chain drive

1.9 BMW V8 cylinder block with fracture-split bearing caps (Fig. 4 from Main bearing with crack technology, from Anisits *et al.*, 1999).



1.10 Ford/Peugeot V6 main bearing cap lock-width and cross-bolt feature (courtesy of Ford Motor Company).



1.11 Main bearing beam from Audi 6.0 V12 (Fig. 5 from Bauder *et al.*, 2008).

sophisticated electronic controls for greater flexibility and refinement of the engine systems to provide superior power and response and more acceptable noise levels.

The fuel injection system is key to diesel engine performance, emissions and refinement of combustion noise. Over the last decade common rail injection systems have been developed for automotive high-speed diesel engines. The breakthrough features of this type of system are firstly decoupling

injection pressure from engine speed, thus allowing injection pressure to be an independent variable; and secondly enabling multiple injections over the speed–load range combined with flexible injection timing. The latter feature provides the opportunity for a pilot injection to control combustion noise over the engine speed range where combustion noise dominates overall engine sound pressure levels.

Robert Bosch's first-generation common rail was introduced in 1997 for the Mercedes C-Class (Peters and Pütz, 1997). This was a solenoid-actuated injector operating at a peak rail pressure of 1350 bar. This was followed by similar systems from the Japanese manufacturer Denso, for Toyota products; and in Europe from Delphi (formally Lucas Diesel Systems) for Renault and Ford applications. All these first-generation systems used solenoid actuators and operated at peak pressures of between 1300 and 1400 bar.

SiemensVDO (now Continental) of Germany was the first company to manufacture in volume production a common rail injector incorporating a piezo actuator. The piezo actuator has a faster response time, about four times quicker than a solenoid, thus enabling the use of smaller pilot injections and at least five injections per cycle (Christoffel, 2002). Small pilot injections are a major enabler for the combustion noise/emissions trade-off required to meet more stringent emissions standards. This fuel injection system was introduced for the Peugeot/Ford joint venture 2.0 litre diesel and was followed in 2004 by the Ford/Peugeot Lion 2.7 litre V6 engine, at 1650 bar, which is still in use to the present day. Further derivatives of this system are used at 1700 and 1750 bar for the Lion 3.6 litre V8 engine in the Range Rover and the Euro 4 light-duty truck version of the Lion V6 engine in the Land Rover Discovery and Range Rover Sport.

Diesel fuel injection systems will be dealt with in more detail in Chapter 2.

Since its first introduction by Garrett Turbochargers in 1991 for the Fiat Croma, the variable nozzle turbine (VNT) turbocharger has been progressively developed for smaller frame sizes, higher efficiency and volume production. Today the VNT turbocharger is standard equipment for high-power-density diesel engines and all manufacturers of diesel passenger cars offer high-power output engines using VNT turbochargers. The most notable are the new premium V8 engines from Audi, BMW Mercedes and Ford, which produce power in the range of 165–240 kW, and VW's recently announced 230 kW V10. These engines are fitted with twin VNT Garrett turbochargers that have electric actuators to enable the electronic engine management system to directly control the turbine vane position. Garrett Turbochargers has led the field in this technology and the demand for VNT turbochargers has risen dramatically over the last 10 years. Garrett produced over 1.8 million VNT turbochargers in 2000. Other manufacturers such as 3K Warner Turbosystems, Mitsubishi and IHI have all developed similar VNT units.

The latest development in turbocharging is the use of sequential twin turbochargers, as developed by BMW and BorgWarner Turbo Systems for the BMW 3.0 litre six-cylinder in-line diesel engine in 2004. This system utilises a small and a larger turbocharger operating in series and in parallel, by means of a turbine control valve actuated by the engine management system. Using two different-sized turbochargers overcomes the usual compromise between low engine speed responsiveness and high engine speed air flow requirements. The variable twin turbo (VVT) technology, as BMW calls it, operates in essentially three different modes. At low engine speeds, the intake air flows through the larger compressor and is compressed by the smaller turbocharger. For the BMW 3.0 litre engine this provides compressed air to support a torque of 530 Nm at 1500 rpm. With increasing engine speed, the larger turbocharger becomes active, initially as a pre-compressor for the smaller unit, which completes the boosting to support the maximum torque of 560 Nm at 2000 rpm. The turbine control valve splits exhaust gas between both turbochargers and thus regulates the work done by each. At high engine speeds the large turbocharger takes over and provides all the boost air to support the engine's peak rating of 200 kW at 4400 rpm. The VVT system provided a 20% increase in performance and at the time of introduction the BMW 3.0 litre engine had the highest specific power of any production diesel engine (Cover Story, 2004; Steinparzer *et al.*, 2005). Other manufacturers have since applied twin turbochargers to in-line engines, Peugeot has applied this technology to their 2.2 litre four-cylinder diesel and Fiat has applied it to their 1.9 litre engine. The Fiat engine also uses BorgWarner twin turbochargers to push engine peak power to 190 bhp and peak torque to 400 Nm (Fortune, 2007). BMW has since extended the VVT system to the 2.0 litre four-cylinder engine (*Ricardo Quarterly Review*, 2007; Challen, 2007).

Exhaust gas recirculation (EGR) is currently the most effective method of reducing emissions of nitrogen oxides (NO_x) from light-duty diesel engines, since it is particularly beneficial at part load conditions. These conditions characterise the duty cycle of these types of engines and form the prevalent part of the emissions test drive cycle. At part load a diesel engine is operating at a high air to fuel ratio and therefore a large proportion of the intake air charge can be replaced with exhaust gases, up to around 60% by volume for a high-speed DI. EGR reduces the oxygen concentration and increases the heat-absorbing capacity of the inlet charge, thus reducing the peak flame temperatures to lower the formation and emissions of NO_x. EGR involves, in effect, the replacement of a small quantity of oxygen and nitrogen in the inlet air to the engine with carbon dioxide and water vapour from the exhaust. Since the specific heat capacity of both CO_2 and water vapour is greater than that for oxygen, the gas temperatures within the engine cylinder during combustion are reduced (Ladommatos *et al.*, 1996a,b,c). Furthermore, by

definition, EGR reduces the exhaust gas mass flow and so lowers the mass of NO_x emitted per unit time or distance.

Diesel engine EGR systems comprise a number of different components, each with a different function, which connect the exhaust to the intake system. These may include:

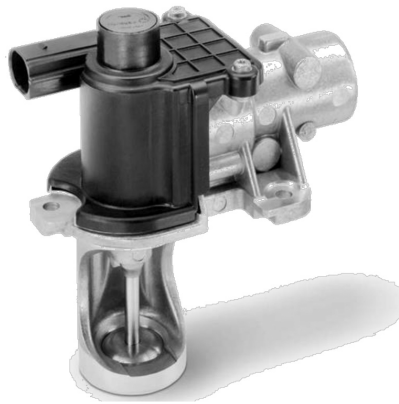
- EGR valve
- Throttle valve
- Venturi
- EGR cooler
- EGR cooler bypass
- EGR tube.

The primary role of the EGR valve is to regulate the flow of recirculated exhaust gas. The vast majority of valves in production up until Euro III emissions standards had an inward opening poppet valve operated by a vacuum actuator. Figure 1.12 shows a Pierburg pneumatic EGR valve from the 1980s. Electric actuators have now become the standard owing to faster, more precise control for the stricter emissions standards. These may have inward- or outward-opening poppet valves, depending on the type of actuator. Linear solenoids, stepper motors, torque motors and DC motors are types of electric actuators being used and developed by various component suppliers. These offer the advantage of faster and more precise operation compared to a conventional vacuum motor system. Figure 1.13 shows a direct-drive DC motor-actuated EGR valve.

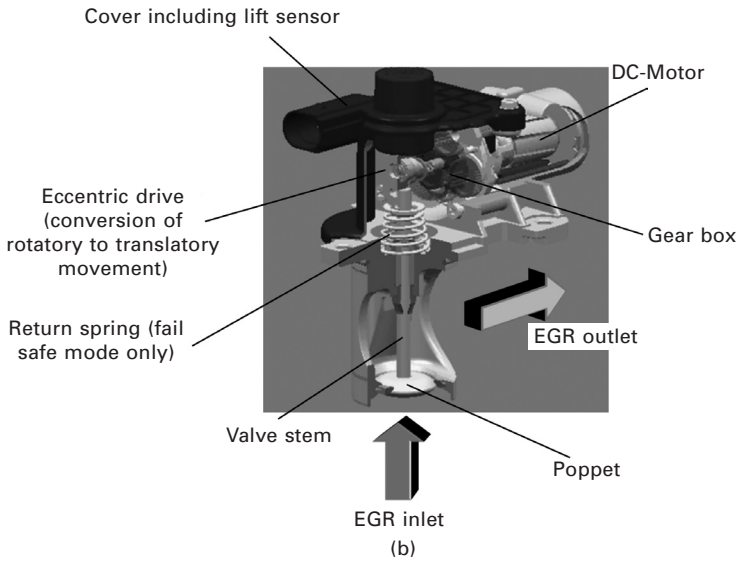
Throttle valves are used in the intake system, upstream of the EGR entry point, to provide a greater pressure difference between the exhaust and intake manifold, to increase the flow of EGR when the EGR valve is already fully



1.12 Early pneumatic single-poppet EGR valve (1980) (courtesy of Pierburg GmbH).



(a)



1.13 Direct drive DC-motor actuated single/dual-poppet EGR valve: (a) photograph, (b) cross-section diagram (courtesy of Pierburg GmbH).

open. These valves are traditional 'butterfly' valves, similar to petrol engine throttles.

A venturi is sometimes used to provide a higher pressure differential between exhaust and intake manifolds, to assist the flow of EGR into the air charge. A venturi is normally used instead of a throttle valve, in order to get better pressure recovery.

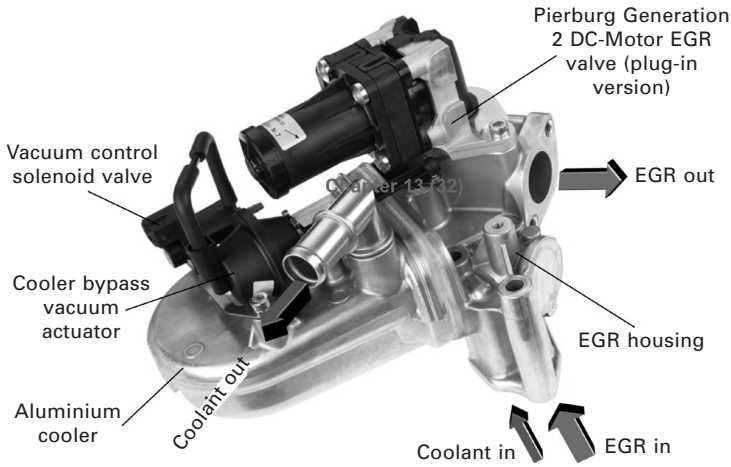
The EGR cooler cools the exhaust gas before it is introduced into the air charge stream. The majority are of tube and plate construction in stainless

steel, generally vacuum brazed together. Engine coolant is passed through the EGR cooler to provide the cooling medium. Figure 1.14 shows typical early EGR coolers. Figure 1.15 shows a state-of-the-art EGR module with an aluminium EGR valve and cooler.

The full potential of EGR in reducing NO_x emissions will not be realised unless the EGR is cooled. This is because the EGR is at high temperature, hotter than the intake air it replaces, which results in an increase in the overall intake charge temperature. Ford introduced the concept of cooled EGR in 1993 for the 2.5 litre TDI Transit. The use of cooled EGR enabled further reductions in NO_x and particulates compared to the previous hot EGR system. Cooling the EGR prior to mixing with the intake air lowers the combustion temperatures and increases the oxygen to fuel ratio. The higher flow of CO_2 and H_2O into the engine with cooled EGR increases the heat-absorbing capacity of the inlet charge; the lower inlet charge temperature generally reduces the combustion temperatures. The slight increase in O_2 availability may raise the flame temperature (Wilson *et al.*, 1974) but is beneficial for soot control. Because the bulk intake charge density is higher with cooled EGR, the engine's volumetric efficiency is increased compared



1.14 Typical EGR coolers (courtesy of Serck Heat Transfer Ltd).



1.15 EGR module with aluminium EGR valve and cooler (courtesy of Pierburg GmbH).

to the case with hot EGR. This reduction in pumping work translates to an improvement in fuel consumption, up to moderate levels of EGR.

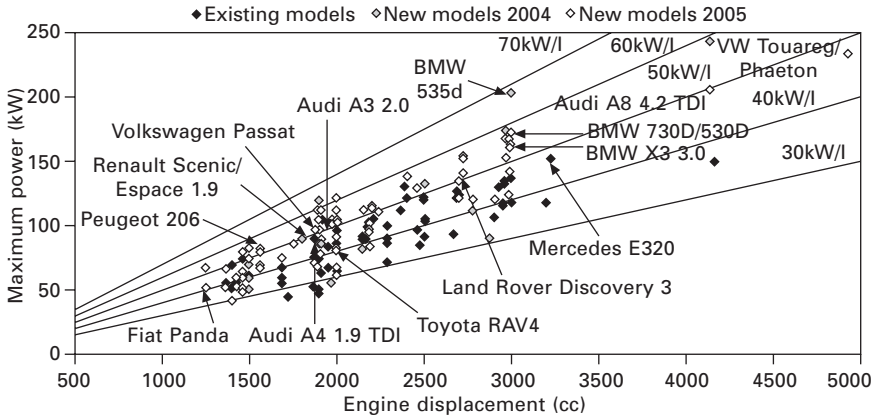
The EGR cooler bypass is used during engine warm-up to eliminate the cooler from the EGR circuit, to prevent cooling of the exhaust gas being fed back into the intake system while the combustion chambers are below their normal operating temperatures and to improve the light-off times of the exhaust after-treatment. The EGR tube is a thin-walled stainless steel tube that is used to connect the various system components together, to allow flow from the exhaust to intake manifolds. Connections are usually by two-bolt flanges or V-band clamps.

EGR systems in production at present connect the exhaust gas from upstream of the turbocharger turbine to the intake system downstream of the turbocharger compressor and are known as high-pressure systems. Looking ahead to Euro 6 emissions standards and beyond, engineers are investigating the options of 'low-pressure' systems, whereby the exhaust gas is taken from downstream of the turbocharger and fed into the intake charge upstream of the compressor (Paffrath and Sari, 2008).

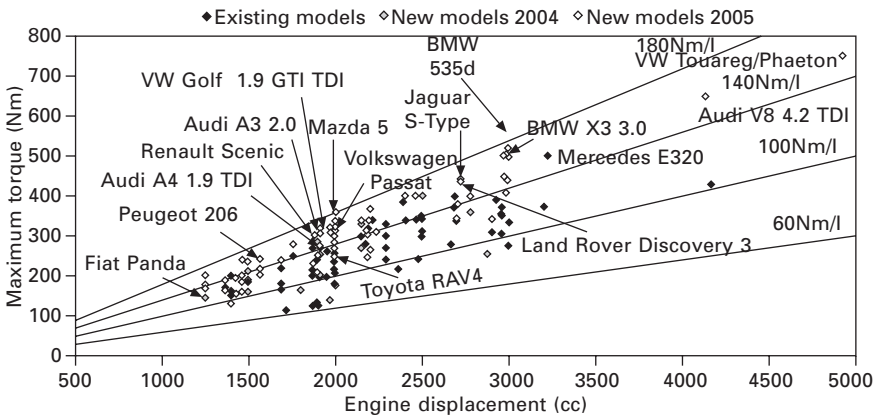
1.3.4 Engine performance and emissions

Duggleby and Johnson (2006) plotted the movements in engine performance in their survey of diesel passenger cars and light commercial vehicles in Western Europe, and the figures presented here are reproduced with kind permission from Ricardo UK Ltd from their publication.

Figure 1.16 shows maximum power plotted against engine displacement,



1.16 Maximum power plotted against engine displacement (courtesy of Ricardo plc).



1.17 Maximum torque plotted against engine displacement (courtesy of Ricardo plc).

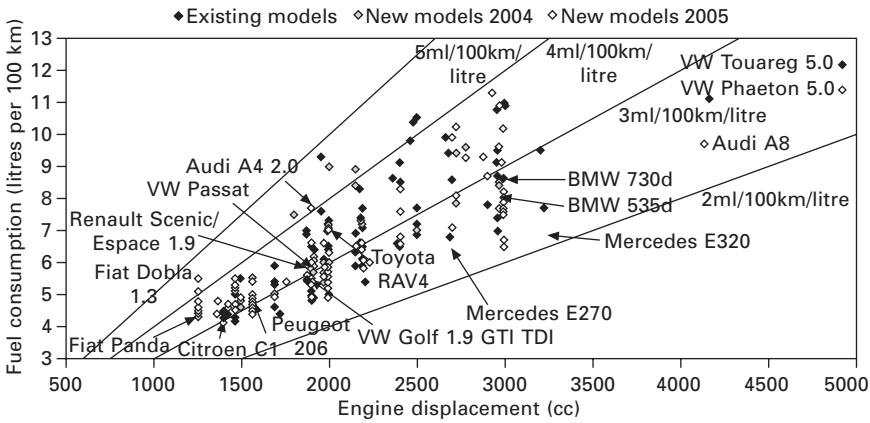
with superimposed lines of constant specific power for 30, 40, 50, 60 and 70 kW/l. It can be seen that there is a wide spread of specific power, particularly around the popular displacement of 2 litres, where the range is from 30 to 60 kW/l. The newer BMW 2.0 litre engine described earlier, but not shown on this figure, has the highest specific power of 74.6 kW/l (100 bhp/l). In the larger range of engines, the BMW 3.0 litre engine has the highest specific power of 66.8 kW/l.

Figure 1.17 shows maximum torque plotted against engine displacement, with superimposed lines of constant specific torque for 60, 100, 140 and 180 Nm/l. It can be seen that the majority of new engines lie within the 140 to

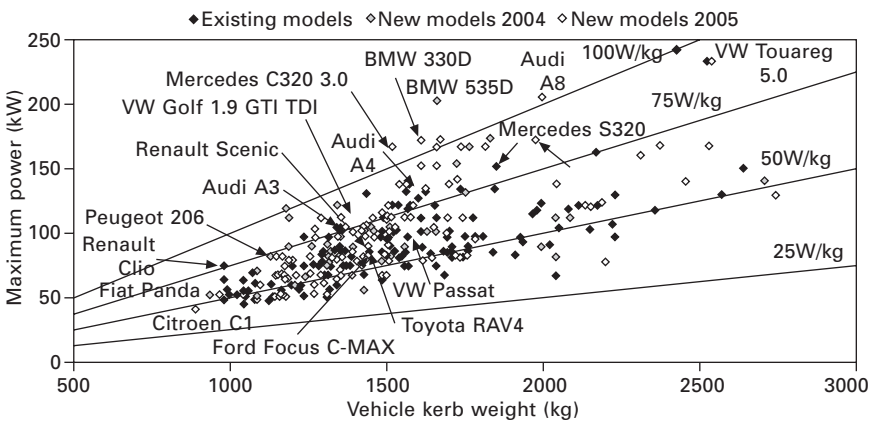
180 Nm/l range, with the BMW 3.0 litre engine in the 535d vehicle having the highest specific torque at 187 Nm/l.

Fuel consumption versus engine displacement is shown in Fig. 1.18. In this figure, lines of specific fuel consumption per litre are expressed in ml per 100 km per litre. It is interesting to note that some of the higher specific powered premium engines are in the lower sector for fuel consumption, such as the Audi A8 and BMW 535d.

Maximum power versus vehicle kerb weight is plotted in Fig. 1.19, illustrating vehicle specific power in W/kg, and demonstrates the huge range from below 50 W/kg to over 100 W/kg for some of the premium offerings from the likes of Audi and BMW.



1.18 Fuel consumption versus engine displacement (courtesy of Ricardo plc).



1.19 Maximum power versus vehicle kerb weight (courtesy of Ricardo plc).

1.4 A survey of some of today's engines

1.4.1 Audi

Audi introduced a new V-diesel engine family, initially with a 4.0 litre V8, in 2003. This was followed by a new 3.0 litre V6 diesel engine in 2004. To achieve the increased displacement of the V6, the bore was increased to 83 mm and the cylinder spacing from 88 to 90 mm. The V8 engine had a bore of 81 mm and a stroke of 95.5 mm and like the earlier 3.3 litre engine used a cylinder block manufactured from vermicular, or compacted graphite, cast iron. It had four valves per cylinder but these were operated by roller followers rather than sliding followers of the earlier engine. Fuel was injected by a second-generation 1600 bar common rail system and the engine developed 202 kW and 650 Nm torque. The A4 4.0 V8 TDI offered best-in-class performance and 'combined' fuel consumption of 9.6 litres per 100 km (29.4 mpg) with a CO_2 rating of 259 g/km (Slavnich, 2003).

The 3.0 litre V6 was a major development, sharing only a few components from the earlier 2.5 litre engine. The increased bore spacing meant an entirely new cylinder block and heads, with larger valves. To support the larger displacement and increased performance, the con-rod bearing sizes were increased as well. The 90° bank angle is retained, so a first-order balance shaft is located in the 'V'. A novel feature of this engine is the innovative four-chain timing drive at the flywheel end of the engine. An intermediate chain drive gives the necessary 1:2 reduction ratio. From this there are two 1:1 chain drives to the inner intake camshafts, one for each bank. This arrangement allows a small camshaft sprocket. Exhaust camshafts are driven from the intake by gears at the front of the engine. Fuel is injected by a third-generation Bosch piezo common rail system operating up to 1600 bar. Peak power of 171 kW at 4000 rpm is developed with a maximum torque of 450 Nm at 1400 rpm (Anton *et al*., 2004).

In 2005 Audio revised the V8 bore spacing from 88 to 90 mm and increased the bore diameter by 2 mm to give a capacity of 4134 cc, designating the engine '4.2 l TDI V8'. This engine uses Bosch's third-generation piezo common rail system, utilising a maximum rail pressure of 1600 bar, and two Garrett 'step-3' variable geometry exhaust turbochargers. Peak power has been increased to 240 kW, and while the peak torque remains the same at 650 Nm, the speed range at this torque is widened to between 1600 and 3500 rpm (Bach *et al*., 2005; Bauder *et al*., 2005).

In 2007, following their success at Le Mans with the R10 TDI, Audi presented the V12 TDI diesel for the Q7 vehicle. A high level of transfer from race to road engine followed, according to Wolfgang Ullrich, Audi's Head of Motorsport: 'The combustion and injection system of this engine are nearly identical with that of the R10 TDI', said Ullrich (Christoffel, 2007). The V12 engine has the same bore of 83.0 mm and stroke of 91.4 mm as the

new 3.0 litre V6, to give a displacement of 5934 cc. It also shares the same bore spacing of 90 mm, but not the 90° bank angle; the V12 has the typical 60° bank angle. Peak power is 368 kW at 3750 rpm and a maximum torque of 1000 Nm is available from 1750 to 3250 rpm. A notable feature of this engine is the flywheel-end timing drive. A split camshaft drive is utilised, whereby a pair of 'acoustically optimised' helical gears take the drive above the crankshaft, from the driven gear two simplex chains rearward of the gears drive each outer exhaust camshaft in each cylinder head. To the rear of the crankshaft gear are two more simplex chain drives from the crankshaft to drive each of the two high-pressure fuel pumps at three-quarters crankshaft speed. The intake camshafts are driven by spur gears at the opposite end and the driven shaft has a scissor-gear to eliminate backlash. Two Bosch 2000 bar piezo common rail fuel injection systems are used, one for each bank, together with variable intake swirl, a sophisticated EGR system with three-stage cooling, twin oxidation catalysts and particulate filters, enabling Euro V emissions standards to be achieved (Bauder *et al*., 2008). Table 1.6 lists the main features and dimensions of Audi's latest diesel V-engines.

From Table 1.6 it is interesting to note the trend of reducing the compression ratio with each later design, which supports the increase in specific power and torque and is made possible by common rail injection strategies and improved glow plugs for cold starting at the lower compression ratios. It is also noteworthy that the increased injection pressure for the V12 has led to a bigger uplift in specific power and torque.

1.4.2 BMW

Virtually every car produced today is available with a diesel engine option. The new Mini, now owned by the BMW Group, has a diesel option that was introduced in 2003. The Mini One D features a four-cylinder diesel engine of 1.4 litres, having a bore and stroke of 73 mm by 81.5 mm respectively and a compression ratio of 18.5:1. With a second-generation common rail fuel injection system it develops a peak output of 56 kW and a maximum torque of 180 Nm. The engine was developed with Toyota and is manufactured at Toyota's engine plant in Kamigo, Japan (Wilson, 2003).

BMW was the first manufacturer to apply two-stage turbocharging to an automotive diesel engine. The BMW 3.0 litre in-line six-cylinder engine was introduced with twin turbochargers in the autumn of 2004 for the 535d passenger car. The two-stage system was developed with BorgWarner Turbo Systems. A small turbocharger provides the low-speed boost response for clutch engagement and moving off from rest; then the two turbochargers work in series for the mid-range speed. As the engine speed increases the small turbocharger is bypassed and the large turbocharger operates on its own for the high engine speed operation. Steinparzer *et al*. (2005) describe in detail

Table 1.6 Main features and dimensions of Audi's latest diesel engines

Feature	Unit	3.0V6	4.2V8	6.0V12
Bank angle	Degrees	90	90	60
Displacement	cc	2967	4134	5934
Bore	mm	83.0	83.0	83.0
Stroke	mm	91.4	95.5	91.4
Stroke/bore		1.10	1.15	1.10
Compression ratio		17:1	16.5:1	16:0:1
Bore spacing	mm	90	90	90
Main bearing diameter	mm	65	65	65
Cylinder block material		Vermicular (CGI) cast iron GJV 450	Vermicular (CGI) cast iron GJV 450	Vermicular (CGI) cast iron GJV 450
Crank pin diameter	mm	60	60	60
Con-rod length	mm	160.5	158	155
Valve diameter:				
Inlet	mm	28.7	28.7	28.7
Exhaust	mm	26.8	26.8	26.8
Fuel injection		Bosch 3rd generation piezo, 1600 bar	Bosch 3rd generation piezo, 1600 bar	Bosch 3rd generation piezo, 2000 bar
Turbocharger		Single Borg Warner VGT BV50	Two water-cooled VGT Garrett GT17	Two water-cooled, latest generation (Step 3) VGT Garrett GT22
Firing order		1,4,3,6,2,5	1,5,4,8,6,3,7,2	1,7,5,11,3,9,6,12, 2,8,4,10
Power	kW	171 at 4000 rpm	240 at 3750 rpm	368 at 3750 rpm
Specific power	kW/litre	57.6	58.1	62.0
Torque	Nm	450	650	1000
Specific torque	Nm/litre	151.7	157.2	168.5
Emissions level		Euro IV	Euro IV	Euro V
Weight	kg	220	255	329
Length	mm	444	520	680

Source: Anton *et al.* (2004), Bach *et al.* (2005), Bauder *et al.* (2004, 2005, 2008).

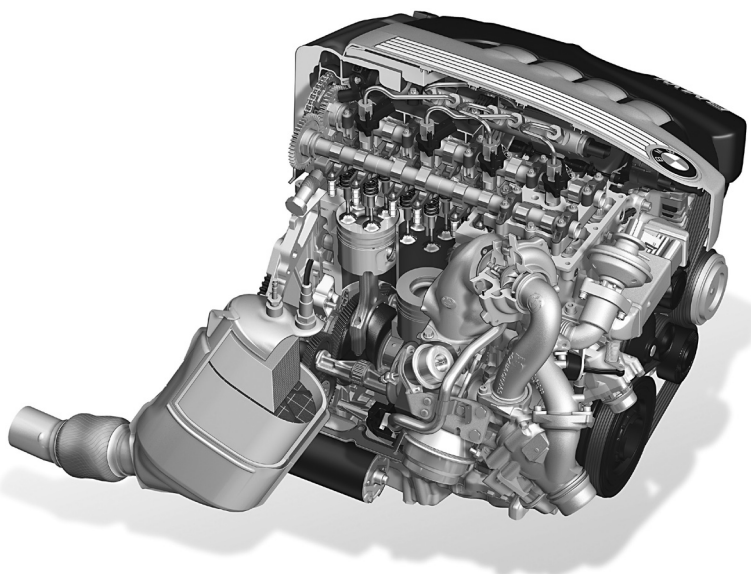
the packaging and layout of the turbochargers, and control of the flow and boost pressure. The compression ratio was reduced from 17:1 to 16.5:1 and the injector flow rate was increased by 20% to support the increase in peak power from 160 to 200 kW and in maximum torque from 500 to 560 Nm. In addition the rated speed has been increased from 4000 to 4500 rpm, giving the engine more 'gasoline-like' driveability (Steinparzer *et al.*, 2005).

From September 2006 the 2 litre four-cylinder diesel for the new coupé version of the 1-Series has an-aluminium cylinder block, making it an all-

aluminium unit, and uses twin turbochargers to boost the output to 152 kW (204 bhp), which made it the first diesel engine to achieve greater than 75 kW/litre (100 bhp/litre). The twin-turbo arrangement also provided an increase in peak torque to 400 Nm from 2000 rpm (*Ricardo Quarterly Review*, 2007). This engine is shown in Fig. 1.20.

The latest versions of BMW diesel engines use Bosch third-generation piezo 1600 bar common rail fuel injection systems. The 2.0 litre for the 320d and 520d M Sport models produces 130 kW at 4000 rpm and 350 Nm of torque at 1750 rpm. The six-cylinder engine produces 170 kW at 4000 rpm and a torque of 520 Nm from 2000 to 2750 rpm for the 5- and 7- Series, but performance is enhanced to 210 kW at the higher rated speed of 4400 rpm and 580 Nm of torque from 1750 to 2250 rpm for the 535d M and X3, X5 and X6 xDrive 35d M Sports models. Interestingly, the flagship V8 engine is not available in the UK (source: BMW UK website).

Specifically for the new 7-Series Sedan, the in-line six-cylinder and V8 engines have been developed with aluminium crankcases. This new six-cylinder engine for the 7-Series produces 180 kW with a peak torque of 540 Nm. The new V8 diesel engine, which is 30 kg lighter than the previous model, produces a peak power of 242 kW at 3800 rpm and a maximum torque of 750 Nm at 1900 rpm (source: bmw.com, the international BMW website).



1.20 BMW 2.0 litre four-cylinder diesel with aluminium crankcase and variable twin turbocharger (courtesy of BMW AG).

1.4.3 Fiat

The latest technology developed at Fiat Powertrain Technologies (FPT) is the application of two-stage turbocharging, which has been applied to their 1.9 litre 16-valve JTD engine. This takes the power from 112 kW (150 bhp) to 134 kW (180 bhp) for external customers such as GM, and 142 kW (190 bhp) for Fiat Group products such as the Grande Punto, Alfa 159 and the new 166 replacement, as well as other Fiat and Lancia products. The twin-turbo arrangement has allowed torque to be increased from 320 Nm to 400 Nm, at 209 Nm/litre an industry best. To meet Euro 5 emissions standards the twin-turbo assists in providing higher EGR levels for the water-cooled system that also has a bypass for low temperature operation. In addition, exhaust catalyst and particulate filter are fitted. The two-stage turbochargers are sourced from BorgWarner and supplied as a sub-assembly to the Pratola Serra plant in Avellino province, Italy (Fortune, 2007). Table 1.7 lists Fiat Powertrain Technologies' light-duty diesel engines.

1.4.4 Ford

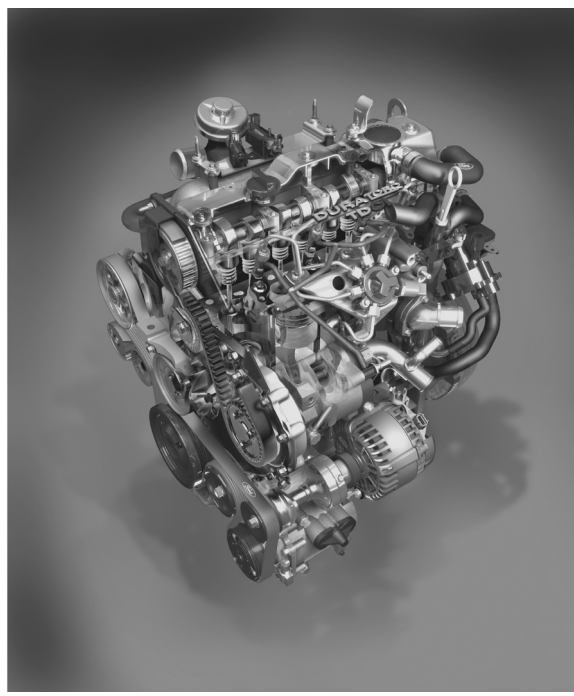
The Ford 1.8 litre diesel engine, known affectionately as 'Lynx' internally but marketed as 'Endura DI', was introduced in direct injection form for the introduction of the new Focus car in 1998. The engine retained its cast iron eight-valve, single overhead camshaft layout of cylinder head from

Table 1.7 Fiat Powertrain Technologies' light diesel engines

Capacity	Family	Type	Power range (kW)	Torque range (Nm)	Emissions
1.3	SDE	I-4 16v FGT	56	190	Euro 5
1.3	SDE	I-4 16v VGT	71	200	Euro 5
1.3	SDE	I-4 16v VGT	78	200	Euro 4
1.6	JTD	I-4 16v FGT	78	290	Euro 5
1.6	JTD	I-4 16v VGT	90	305	Euro 5
1.9	JTD	I-4 8v FGT	75	260	Euro 4
1.9	JTD	I-4 8v VGT	90	280	Euro 4
1.9	JTD	I-4 16v VGT	112	320	Euro 4
1.9	JTD	I-4 16v 2-stage VGT	134–142	400	Euro 5
2.3	F1A	I-4 16v VGT	97–138	240–320	Euro 4
2.4	JTD	I-5 20v VGT	138	400	Euro 4
2.4	JTD	I-5 20v VGT	149	410	Euro 4
2.4	JTD	I-5 20v VGT	157	410	Euro 4
2.8	8140	I-4 8v	67–109	209–320	Euro 3
3.0	F1C	I-4 16v	108–131	350–400	Euro 4

Source: Special supplement to *Diesel Progress*, Diesel Progress International, Jan–Feb 2008, Vol. 27, No. 1.

the earlier engine, but it incorporated a new helical intake port to create a swirl ratio in excess of 2, to support the direct injection, bowl-in-piston combustion system. The re-entrant combustion bowl gave a compression ratio of 19.4:1. The engine initially went into production with the Bosch solenoid-valve controlled, axial-piston distributor pump VP30 with Lucas two-spring injectors incorporating valve covered orifice (VCO) nozzles to inject the fuel. Peak power of 66 kW at 4000 rpm was produced with 200 Nm of torque at 2000 rpm. To meet Euro III emissions standards a new EGR system with a cooler and vacuum-actuated EGR valve, with closed-loop control of the valve position, was operated by the engine management system (Gray *et al.*, 1999). In 2001 this engine was released as the Ford Duratorq TDCi with Delphi second-generation common rail technology. Engine performance was increased by more than 25%, giving a peak power of 115 ps combined with 250 Nm of steady-state torque and 280 Nm of transient over-torque. The fuel system also incorporated a novel combustion 'knock' sensor, an accelerometer attached to the cylinder block, to control pilot injection and thus combustion noise levels. Figure 1.21 shows the Ford 1.8 litre Duratorq TDCi engine.



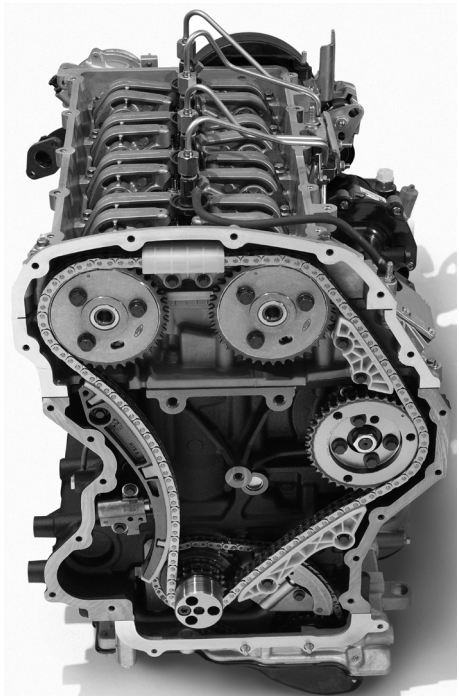
1.21 Ford 1.8 litre Duratorq diesel engine (courtesy of Ford Motor Company).

To meet Euro 4 emissions standards, the 1.8 litre engine was equipped with the Siemens (now Continental) 1600 bar 'piezo' common rail fuel system in conjunction with an enhanced EGR system and revised turbocharger matching. This engine is currently fitted in the Ford Focus, C-Max, Mondeo, S-Max and Galaxy vehicles with a rating of 92 kW at 3700 rpm and 320 Nm torque at 1800 rpm with a transient overboost of 340 Nm.

In 2000, to mark the introduction of the new Transit, Ford introduced a brand new diesel engine to replace the well-known 2.5 DI engine, which was the first production high-speed DI diesel. The 2.5 litre engine had been in production for 16 years with more than 3 million produced in naturally aspirated and, since 1992, also turbocharged form. The new engine was launched under the name Duratorq, but known internally and throughout the component industry as 'Puma'. Like the outgoing engine it was an in-line four-cylinder engine but was produced in two capacities, 2.0 and 2.4 litres, although during development a 2.2 litre version was also manufactured and tested. This engine was the first of the new breed of 'four-valve per cylinder' diesel engines for Ford. The engine had a deep-skirt grey cast iron cylinder block, with an aluminium ladder-frame to improve powertrain stiffness. The diecast aluminium cylinder head housed the four vertical valves (two intake and two exhaust) and the central vertical injector. A cam carrier formed the upper half of the camshaft bearing caps, for the intake and exhaust camshafts, which were located low in the cylinder head, to keep the height of the engine lower than with a more conventional roller finger follower valve-train design. The valves were located in a skewed orientation to the crankshaft centre-line to facilitate twin helical intake ports. The two exhaust valves were connected by a short Siamese exhaust port to the exhaust flange and via an integrated manifold to the turbocharger turbine. The engine was introduced with fixed-geometry waste-gated turbochargers from Mitsubishi and Allied Signal (Garrett). Fuel was injected with two-stage lift injectors and Bosch electronically controlled rotary pumps, VP44 and VP30, depending on power output. An EGR system was fitted to control NO_x emissions. The 2.4 litre engine went into production in the new Transit with power ranging from 55 to 88 kW and corresponding peak torque of 185 to 240 Nm (Lawrence *et al.*, 2000). Figure 1.22 shows the Ford 2.0 litre Duratorq diesel engine.

The following year, the same engine was launched in the new Mondeo at two power ratings, 66 or 85 kW at 4000 rpm, and 245 or 280 Nm at 1900 rpm. For 2002 the engine was equipped with a Delphi common rail fuel injection system that enabled the peak power to be increased to 96 kW at 3800 rpm with peak torque of 330 Nm at 1800 rpm.

In 2005 a 2.2 litre version of the Duratorq diesel was released for the Mondeo ST TDCi and Jaguar X-Type. This variant had a longer stroke of 94.6 mm to give a displacement of 2198 cc. Fuel was injected by a Delphi



(a)



(b)

1.22 Ford 2.0 litre Duratorq diesel engine: (a) end view, (b) top view (courtesy of Ford Motor Company).

1600 bar common rail system with solenoid injectors. Power was increased to 114 kW at 4000 rpm with a peak torque of 360 Nm at 1800 rpm.

In 2006 this engine was upgraded and a five-cylinder variant added for use in the Transit light commercial vehicle. Key features and performance attributes are shown in Table 1.8 (van den Heuvel *et al.*, 2006). Table 1.8 lists the main dimensions and attributes for the Duratorq range of diesel engines for the Ford Transit.

Under the Ford–Peugeot agreement for the joint development of diesel engines, Ford took the lead in the design of a completely new V6 engine. Known within the Ford group as the Lion V6 diesel, it has a 60° bank angle and bore and stroke of 81 mm by 88 mm respectively, giving a displacement of 2720 cc. It was introduced in 2004 with two twin-turbocharged variants: a 'north-south' version for the rear-wheel-drive Jaguar S-Type and an 'east-west' version for the front-wheel-drive Peugeot 604, 806 and Citroën C5 vehicles, and lastly a single turbocharger 'north-south' variant for the Land Rover Discovery and Range Rover Sport. These engines were developed and went into production with the Siemens 1650 bar 'piezo' common rail fuel system. This system was chosen for the fast operation of the piezo-activated

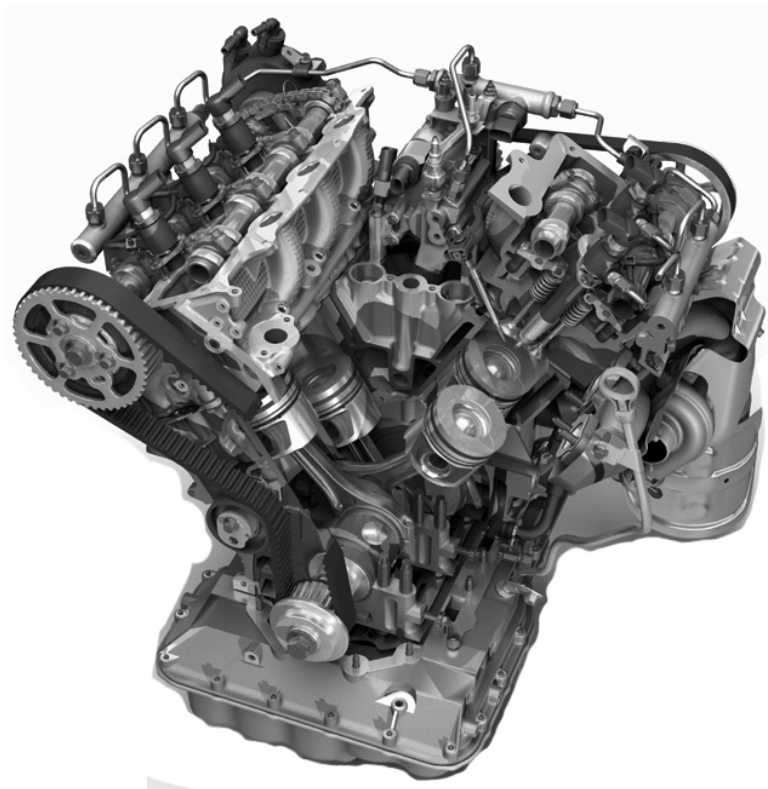
Table 1.8 Ford Duratorq diesel for Transit

Feature	Unit	2.2 litre	2.4 litre	3.2 litre
Configuration		Inline 4 cylinder	Inline 4 cylinder	Inline 5 cylinder
Displacement	cc	2198	2402	3199
Bore	mm	86.0	89.9	89.9
Stroke	mm	94.6	94.6	100.8
Stroke/bore		1.10	1.05	1.12
Compression ratio		17.5:1	17.5:1	15:8:1
Bore spacing	mm	89.9	89.9	89.9
Main bearing diameter	mm	65	65	65
Crank pin diameter	mm	60	60	60
Con-rod length	mm	160.0	149.8	152.0
Fuel injection		Denso solenoid common rail, 1600 bar	Denso solenoid common rail, 1600 bar	Denso solenoid common rail, 1600 bar
Turbocharger		Mitsubishi FGT (63–81 kW) Garrett GT17 VNT (96–103 kW)	Mitsubishi FGT (74–85 kW) Garrett GT20 VNT (103 kW)	Garrett GT22 VNT
Firing order		1,3,4,2	1,3,4,2	1,2,4,5,3
Power	kW	63–103	74–103	150
Torque	Nm	50–350	285–375	470
Emissions level		Euro IV LDT	Euro IV LDT	Euro IV LDT

injector, allowing small pilot injections of 1 mm^3 to control the rate of cylinder pressure rise and hence combustion noise. The initial version for Jaguar was released at Euro 3 emissions level and the Land Rover version achieved Euro 3 light-duty truck standards in the two 4 × 4 vehicles. The slightly later introduction of the engine for Peugeot enabled it to be developed to meet Euro 4 in combination with the Peugeot exhaust particulate trap system (Gill *et al.*, 2004). A Euro 4 version was subsequently developed for Jaguar S-Type and XK models with the application of a catalysed particulate filter. Figure 1.23 shows the Ford/Peugeot Lion 2.7 litre V6 diesel engine.

To achieve Euro 4 light-duty truck emissions standards for the Land Rover Discovery and Range Rover Sport vehicles, a further development of the V6 was conducted using a 1750 bar Siemens piezo common rail system and a more sophisticated EGR system. This variant went into production for the 2007 model year.

A 3.6 litre V8 derivative of the Lion 2.7 litre V6 engine was developed specifically for Land Rover, to be used in the Range Rover and Range

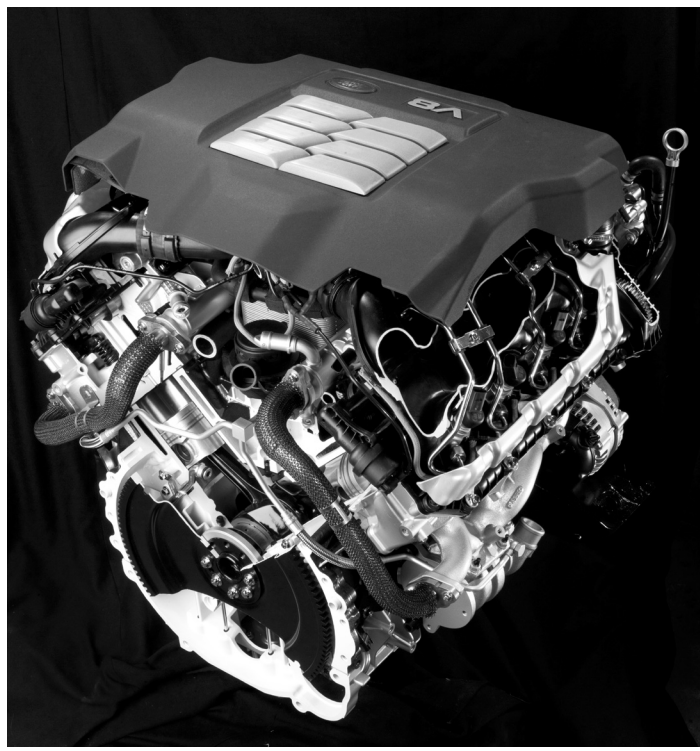


1.23 Ford/Peugeot 2.7 litre V6 diesel engine (courtesy of Ford Motor Company).

Rover Sport models. As a modular extension of the V6 engine, the V8 has the same bore and stroke, enabling use of the common components. For optimum refinement of the V8 configuration the cylinder block has a 90° bank angle and, like the V6, the cylinder block is cast in compacted graphite cast iron to save weight and provide excellent stiffness and refinement. The engine uses a similar Siemens piezo common rail fuel injection system, with a slightly larger displacement pump for the extra cylinders, and peak rail pressure is limited to 1700 bar for this application. Twin variable-geometry turbochargers boost the engine to give 200 kW at 4000 rpm and 640 Nm of torque at 2000 rpm (Family affair, 2006; Ernst *et al.*, 2007). Figure 1.24 shows the Ford Lion 3.6 litre V8 diesel engine.

1.4.5 Honda

A new entrant to diesel engine design and manufacture, Honda was one of the last volume car manufacturers to produce its own diesel engine in 2005. The result was a 2.2 litre in-line four-cylinder engine utilising aluminium for the



1.24 Ford 3.6 litre V8 diesel engine (courtesy of Land Rover).

block and head castings. A distinctive feature of this engine was the 6.5 mm crankshaft offset to the cylinders, whereby the cylinders were 'ahead' of the crankshaft; this had been known historically as the 'Desaxe' crankshaft setting. This layout thus reduces con-rod obliquity during the firing stroke, which Honda said reduces noise and improves fuel consumption. For performance and emissions control the engine had a swirl control valve and an EGR system, fuel was injected by a Bosch second-generation 1600 bar common rail system, and intake boost up to 1.3 bar was generated by a turbocharger. A stamped stainless steel exhaust manifold facilitated rapid warm-up for the close-coupled oxidation catalyst. Additional NO_x control was achieved with an under-floor zeolite selective catalytic reduction catalyst (Abe *et al.*, 2004, Hara *et al.*, 2005). Honda later developed a diesel particulate filter (DPF) system, which was added to the exhaust after-treatment.

In 2008, Honda presented its second-generation 2.2 litre diesel engine, which has been developed to give significantly more performance and lower exhaust emissions as well as reduced noise and vibration. Fuel is injected by a third-generation Bosch piezo common rail fuel injection system operating up to 180 MPa which, with a new variable nozzle turbocharger and higher combustion pressures, gives an increased peak power of 132 kW with a maximum torque of 380 Nm. The variable swirl control valve is electrically operated to provide more precise control and the EGR system has been upgraded to incorporate a cooler bypass to stabilise combustion at lower exhaust gas temperatures. Exhaust after-treatment includes a typical oxidation catalyst and an upgraded DPF (Fritz, 2008). Table 1.9 lists the main dimensions and performance for the Honda diesel engines (Matsui *et al.*, 2008).

Table 1.9 Honda engine specifications

Feature	Unit	Specification i-CTDi	Specification New i-DTEC
Displacement	cc	2204	2197
Bore	mm	85.0	85.0
Stroke	mm	97.1	96.8
Bore pitch	mm	94	94
Compression ratio		16.7:1	16.3:1
Fuel injection system	–	Bosch 2nd generation 1600 bar solenoid injectors	Bosch 3rd generation 1800 bar piezo injectors
Maximum power	kW	103 at 4000 rpm	132 at 4000 rpm
Maximum torque	Nm	340 at 2000 rpm	380 at 2000 rpm

Ref: Abe *et al.* (2004), Matsui *et al.* (2008)

1.4.6 Mercedes

In a break from tradition, in 2005 Mercedes-Benz introduced a 3.0 litre V6 (OM642) to replace the previous in-line five- and six-cylinder engines. Owing to its more compact package, this enabled a six-cylinder engine to be offered in the C- and M-Class cars for the first time. Like the earlier V8 engine, the new V6 has an aluminium alloy ($AlSi_6Cu$) crankcase with cast-in grey cast iron liners. A 72° bank angle was chosen as the best compromise between package space and component design and loading. A 48° crank pin offset angle is used with a primary order balance shaft located in the V of the crankcase. A bore of 83 mm and a stroke of 92 mm, the same as for the in-line four-cylinder 2 litre engine, are used for the V6, to give a displacement of 2987 cc. Having an aluminium cylinder block with cast-in liners, the bore spacing is longer at 106 mm compared to the inline engines with cast iron blocks. A single variable geometry turbocharger is packaged in the 'V' of the crankcase at the rear, with exhaust ducting round the back of the engine from each manifold. A single EGR valve feeds exhaust gas via a water-cooled EGR cooler to the intake system to achieve Euro 4 NO_x levels. Fuel is injected through eight hole nozzles by third-generation piezo common rail injectors working to a maximum pressure of 1600 bar. Engine performance is 165 kW at 3800 rpm and 510 Nm torque between 1600 and 2800 rpm for the C320CDI, and ML320CDI and 173 kW at 3600 rpm with 540 Nm between 1600 and 2400 rpm for the S320CDI (Doll *et al.*, 2005). The four-cylinder 2.0 and 2.2 litre engines remain in production for the lower-power variants of the Mercedes range, as does the 4.0 litre V8 for the high-power premium segment.

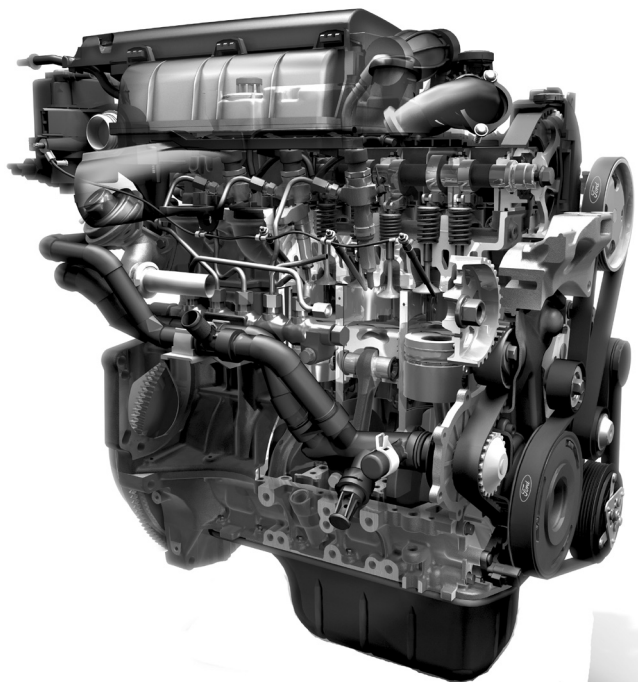
1.4.7 Opel

Opel produces five families of diesel engines; the smallest, a 1248 cc four-cylinder in-line engine having a bore of 69.6 mm and a stroke of 82.0 mm, produces 55–66 kW at 4000 rpm and 190–200 Nm of torque at 2000 rpm. The next size up is a 1.7 litre four-cylinder in-line engine, with bore of 79.0 mm and stroke of 86.0 mm, which has power ratings of 74, 81 and 92 kW and peak torque of 240, 260 and 280 Nm at 2300 rpm. The next four-cylinder engine has a capacity of 1.9 litres with a bore of 82.0 mm and stroke of 90.4 mm. This engine has power ratings of 74, 88 and 110 kW with peak torques of 260, 280 and 320 Nm. The largest four-cylinder engine has a bore of 83.0 mm with a stroke of 92.0 mm to displace 2.0 litres. This engine has power ranging from 93 to 110 kW and peak torque of 295 to 320 Nm. The largest capacity diesel from Opel is an all-aluminium 3.0 litre 60° V6 having a bore of 87.5 mm with a stroke of 82.0 mm to give a peak power of 135 kW and 400 Nm of torque at 1900 rpm (*Automobil Revue*, 2008).

1.4.8 Peugeot

Peugeot is the second largest producer of diesel passenger cars in Western Europe. PSA produces two families of four-cylinder diesel engines in collaboration with Ford. The smaller 'DV' range comes in two capacities of 1.4 and 1.6 litres displacement, and the larger engine family, known as 'DW', has 2.0 and 2.2 litres displacement. The DV family is an in-line four-cylinder engine with aluminium cylinder head and block. The 1.4 litre has two valves per cylinder. A bore of 73.7 mm and a stroke of 82.0 mm give a displacement of 1398 cc. Performance ranges from 40 to 50 kW at 4000 rpm and from 130 to 160 Nm at 1750 rpm. The 1.6 litre variant has a bore of 75.0 mm and a stroke of 88.3 mm to displace 1560 cc. This engine has four valves per cylinder and peak power ranges from 66 to 80 kW at 4000 rpm with a peak torque of 215 to 240 Nm at 1750 rpm. Both engines use second-generation common rail fuel injection systems. Figure 1.25 shows the Peugeot/Ford 1.4 litre diesel engine.

The DW family is an in-line four-cylinder engine with grey cast iron cylinder block and aluminium cylinder head with four valves per cylinder.



1.25 Ford/Peugeot 1.4 litre diesel engine (courtesy of Ford Motor Company).

The 2.0 litre has a bore of 85.0 mm and a stroke of 88.0 mm giving a displacement of 1997 cc. It is rated at 100 kW at 4000 rpm with 320 Nm at 2000 rpm. The 2.2 litre variant has the same bore with an increased stroke of 96.0 mm to displace 2179 cc. This engine has a peak power of 125 kW at 4000 rpm with a peak torque of 370 Nm at 1750 rpm. These engines also use second-generation common rail fuel injection systems.

A new premium version of the 2.2 litre engine has been developed by Peugeot. This unit uses twin turbochargers, supplied by Honeywell, to provide better response at low engine speeds, where the lower inertia turbo operates, and improved peak power. The engine also uses Bosch's third-generation 1800 bar common rail with piezo injectors and seven-hole nozzles. Known as the HDi 170 the engine develops 170 bhp (127 kW) at 4000 rpm and 376 Nm at 1500 rpm and was first introduced in the Peugeot 407 model (*Engine Technology International*, 2006).

1.4.9 Renault

Renault produces three I-4 in-line engine architectures: a 1.5 litre with bore of 76.0 mm and stroke of 80.5 mm with turbocharged and intercooled power ratings of 50, 63 and 78 kW with corresponding torque of 160, 200 and 240 Nm; a 1.9 litre with bore of 80.0 and stroke of 93.0mm having power ratings of 85 and 96 kW with peak torque of 300 Nm, and finally a 2.0 litre having bore of 84 mm and stroke of 90 mm, giving power of 110 and 127 kW and torque of 340 and 380 Nm. The top of the range is a 3.0 litre 66° V6 of 87.5 mm bore and 82.0 mm stroke giving a power of 130 kW and a peak torque of 400 Nm at 1800 rpm (*Automobil Revue*, 2008).

1.4.10 Subaru

Subaru is a new entrant in the diesel market and this is notable because this company has introduced the first 'flat-four' HSDI diesel engine for passenger cars. This follows Subaru's normal petrol engine design practice since 1966. The 'boxer' diesel engine has been developed to complement their range and fall in line with their vehicle weight distribution and all-wheel drive transmission strategies for the Legacy and Outback models (cross-sectional drawings of this engine can be found in Harima (2008)). It was launched in March 2008 for the European market. Technically, apart from being horizontally opposed, the engine follows modern practice, with a bore and stroke of 86 mm, a compression ratio of 16.3:1, four-valve aluminium cylinder heads with central vertical injector, Denso 1800 bar common rail fuel system with solenoid injectors, a variable geometry turbocharger and a high flow EGR system with a cooler. Another notable feature is that the cylinder block is cast in aluminium and features a metal matrix composite

Table 1.10 Subaru engine specifications

Feature	Unit	Specification
Displacement	cc	1998
Bore	mm	86.0
Stroke	mm	86.0
Compression ratio		16.3:1
Bank offset	mm	46.8
Deck height	mm	220
Main bearing journal diameter	mm	67.0
Crank pin diameter	mm	55.0
Con-rod length	mm	134
Piston pin diameter	mm	31.0
Piston compression height	mm	43.0
Maximum power	kW	110 at 3600 rpm
Maximum torque	Nm	350 at 1800 rpm
Engine length	mm	353.5

for the five main bearings, which are inserted during the casting process. The engine develops 110 kW at 3600 rpm with a peak torque of 350 Nm from 1800–2300 rpm (Harima, 2008; Cover Story, 2008a). Table 1.10 shows the main engine specifications for the Subaru diesel engine.

1.4.11 Toyota

Toyota upgraded their small DI diesel with a newly designed 1.4 litre engine in 2004. This engine has an all-aluminium construction. With a bore diameter of 73.0 mm it has a two-valve cylinder head. The stroke is 81.5 mm to give a displacement of 1364 cc and it has a compression ratio of 18.5:1. A notable feature is an integrated intake manifold with the cylinder head. Otherwise the engine features follow current practice, having a Bosch second-generation 1600 bar common rail fuel injection system and being turbocharged and intercooled to give a specific power of 40 kW/litre (Hashimoto *et al*., 2004). Table 1.11 lists the key dimensions and performance of the Toyota 1.4 litre engine. The mainstay 2.2 litre engine remains in production and with

Table 1.11 Toyota 1.4 litre engine specifications

Feature	Unit	Specification
Displacement	cc	1364
Bore	mm	73.0
Stroke	mm	81.5
Compression ratio		18.5:1
Maximum power	kW	55 at 4000 rpm
Maximum torque	Nm	170 at 2000–2800 rpm
Engine length	mm	353.5

a new 4.5 litre V8 engine, which is essentially two 2.2 engines but with a lightweight aluminium cylinder block with cast-in iron liners. The V8 is rated at 210 kW with a peak torque of 650 Nm for the Land Cruiser 100 (Yamaguchi, 2008).

1.4.12 Volvo

Volvo Car Corporation introduced its own in-house automotive diesel engine in 2001. It was a state-of-the-art 2.4 litre all-aluminium in-line five-cylinder engine having four valves per cylinder operated by twin overhead camshafts. It was turbocharged with a Garrett VNT turbocharger also equipped with a waste-gate, and intercooled. Fuel was injected by a Bosch second-generation 1600 bar common rail system to give a peak power of 120 kW (50 kW/litre) and a maximum torque of 340 Nm. It was upgraded in 2005 with major changes being revised intake and exhaust ports, a reduced compression ratio from 18 to 17.3:1, and a water-cooled VNT turbocharger with a bigger compressor and electronic actuator. To meet Euro IV emissions an improved EGR system and a Bosch 1800 bar common rail system was installed. Three power ratings are used with the highest being 136 kW at 4000 rpm and 400 Nm at 1750 rpm.

1.4.13 VW

Volkswagen introduced its well-known 1.9 litre diesel engine with direct injection in 1992 and since then it has been produced in a number of forms with an increase in performance at each stage. The first stage was in 1995 when a variable geometry turbocharger was added, which coupled with higher flow rate injector nozzles and a higher rate of injection from the pump enabled the power to be increased to 81 kW at 4150 rpm, with a maximum torque of 235 Nm at 1900 rpm (Willman *et al.*, 1995). In 2000 the performance was stretched further with the use of '*pumpedüse*' or unit injectors to provide up to 2050 bar maximum injection pressure to boost peak power to 110 kW with 320 Nm of torque at 1900 rpm (Bartsch, 2000). This engine retains the two-valve per cylinder layout with '*pumpedüse*' or unit injector fuel injection system. The current peak performance of the 1.9 litre engine is 96 kW with 310 Nm for the Polo car.

A three-cylinder version of the previously discussed 1.9 litre four-cylinder engine was developed by Volkswagen and introduced in 1998 for the small Lupo car. This engine had the same bore and stroke as its bigger cousin, giving a displacement of 1422 cc. With the '*pumpedüse*' or unit injector fuel injection system and a Garrett GT12 turbocharger, the engine produced 55 kW at 4000 rpm and 195 Nm of torque at 2200 rpm. To improve the refinement of the three-cylinder configuration, a primary balance shaft was

incorporated in the engine (*MOT*, 1998). In the same year, VW announced a smaller 1.2 litre three-cylinder engine, with an aluminium cylinder block specially developed to achieve 2.99 litres per 100 km fuel consumption over the European drive cycle.

The newer 2.0 litre in-line four-cylinder engine was upgraded at the end of 2007 with a new cylinder head featuring four valves per cylinder, actuated by roller finger followers driven from twin overhead camshafts. The exhaust camshaft is driven by a 30 mm wide timing belt that also drives the Bosch CP 4.1 common rail high pressure pump at crankshaft speed to provide one pumping event per cylinder firing stroke. The intake camshaft is driven by spur gears from the rear of the exhaust camshaft. To support performance and emissions, variable swirl is achieved by electrically operated flaps in the intake manifold. Intake boost is supplied by a variable turbine geometry exhaust turbocharger. The Bosch CRS 3.2 common rail system delivers up to 1800 bar pressure and fuel is injected by Bosch CRI 3.2 injectors with eight holes. Peak power of 103 kW is developed at 4200 rpm with peak torque of 320 Nm between 1750 and 2500 rpm. Euro V emissions standards are achieved with oxidation catalyst and particulate filter exhaust after-treatment (Hadler *et al*., 2007, Rudolph *et al*., 2007).

The other engine of interest from the VW camp is the 5.0 litre V10 used in the Touareg. This has the same bore and stroke, 81.0 and 95.5 mm, as the in-line 2.5 litre five-cylinder and 2.0 litre four-cylinder engines. This common rail two-valve-per-cylinder engine develops 230 kW at 3750 rpm and provides a peak torque of 750 Nm from 2000 rpm (*Automobil Revue*, 2008).

Table 1.12 lists the performance of the major high-speed diesel V-engines and Table 1.13 lists current passenger car diesel engines.

1.5 Future trends

What of the future? The diesel engine remains the most efficient prime mover and so it will have a significant role to play for many years to come, while there is a suitable hydrocarbon fuel, whether it is mineral or vegetable or a combination of both. Intensive research continues into improved combustion systems, and further refinement of fuel injection systems, coupled with injection pressures reaching 2000 to 2200 bar, will enable the high-speed diesel engine to meet Euro 6 and the tighter US standards, in combination with the appropriate exhaust after-treatment. For the CO_2 challenge, the advanced diesel engine, with smaller displacement and higher specific power, will form part of a strategy together with advanced transmissions, reduced vehicle weight and drag, and lower parasitic losses, to achieve better real-world vehicle fuel economy.

A potential emerging role is likely to be as the primary source of propulsion

Table 1.12 High-speed diesel V-engines performance.

Manufacturer	Type	Bore (mm)	Stroke (mm)	Capacity (cc)	CR	Peak (power) (kW)	Speed (rpm)	Peak torque (Nm)	Speed (rpm)
Audi	90°V6	83.0	91.4	2967	17.0	171	4000	450	1400
Audi	90°V8	78.3	86.4	3328	18.5	165	4000	480	1800–3000
Audi	90°V8	81.0	95.5	3936	16.5	202	3750	650	1600–3500
Audi	90°V8	83.0	95.5	4134	16.5	240	3750	650	1600–3500
Audi	60°V12	83.0	91.4	5934	16.0	368	3750	1000	1750–3250
BMW	90°V8	84.0	88.0	3900	18.0	180	4000	560	1750–2500
Ford/Peugeot	60°V6	81.0	88.0	2720	17.3	152	4000	440	1900
Ford	90°V8	81.0	88.0	3628	17.3	200	4000	640	2000
Mercedes-Benz	75°V8	86.0	86.0	3996	18.5	184	4000	560	1700–2600
Mercedes-Benz (C320CDI, ML320CDI)	72°V6	83.0	92.0	2987	18.0	165	3800	510	1600–2800
Mercedes-Benz (S320CDI)	72°V6	83.0	92.0	2987	18.0	173	3600	540	1600–2400

Table 1.13 Current passenger car diesel engines

Manufacturer	Layout	Bore (mm)	Stroke (mm)	Capacity (cc)	CR	Power (kW)	Speed (rpm)	Torque (Nm)	Speed (rpm)
Audi	I-4	79.5	95.5	1896	18.5:1	77	4000	250	1900
	I-4	81.0	95.5	1968	18.0:1	103	4000	320	1750–2500
	I-4	81.0	95.5	1968	18.0:1	125	4200	350	1750–2500
	V6	83.0	83.1	2698	16.8:1	140	3500	400	1400–3250
	V6	83.0	91.4	2967	16.8:1	176	4000	500	1500–3000
	V8	83.0	95.5	4134	16.5:1	240	3750	760	1800–2500
	V12	83.0	91.4	5934	16.0:1	368	3750	1000	1750–3250
Alfa Romeo	I-4	82.0	90.4	1910	18.0:1	88	4000	280	2000
	I-4	82.0	90.4	1910	17.5:1	110	4000	320	2000
	I-5	82.0	90.4	2387	17.9:1	154	4000	400	1500
BMW	I-4	84.0	90.0	1995	16.0:1	130	4000	350	1750–3000
	I-4	84.0	90.0	1995	16.0:1	150	4400	400	2000–2250
	I-6	84.0	90.0	2993	17.0:1	145	4000	400	1300–3250
	I-6	84.0	90.0	2993	17.0:1	170	4000	500	1750–3000
	I-6	84.0	90.0	2993	17.0:1	210	4400	580	1750–2250
	V8	87.0	93.0	4423	17.0:1	242	3800	750	1900–2500
Fiat	I-4	69.6	82.0	1248	17.6:1	55	4000	145	1500
	I-4	69.6	82.0	1248	17.6:1	66	4000	200	1750
	I-4	82.0	90.4	1910	18.0:1	96	4000	280	2000
	I-4	82.0	90.4	1910	17.5:1	110	4000	320	2000
	I-4	85.0	88.0	1997	17.6:1	88	4000	300	2000
	I-4	85.0	88.0	1997	17.1:1	100	4000	320	2000
Ford	I-4	73.7	82.0	1399	17.9:1	50	4000	160	2000
	I-4	75.0	88.3	1560	18.3:1	66	4000	204	1750
	I-4	82.5	82.0	1753	18.5:1	74	3850	280	1800
	I-4	85.0	88.0	1997	17.9:1	103	4000	320	1750–2240

(Jaguar)	I-4	86.0	86.0	1998	18.2:1	96	3800	330	1800
(Jaguar)	I-4	86.0	94.6	2198	17.5:1	107	3500	360	1800
(Land Rover)	I-4	89.9	94.6	2402	17.5:1	90	3500	360	2000
(Land Rover)	V6	81.0	88.0	2721	17.3:1	140	4000	440	1900
(Jaguar)	V6	81.0	88.0	2721	17.3:1	152	4000	435	1900
(Land Rover)	V8	81.0	88.0	3628	17.3:1	200	4000	640	2000
Honda	I-4	85.0	97.1	2204	16.7:1	103	4000	340	2000
Hyundai	I-4	77.2	84.5	1582	17.3:1	85	4000	255	1900–2750
	I-4	83.0	92.0	1991	17.5:1	103	3800	304	1800
Mazda	I-4	86.0	86.0	1998	16.7:1	105	3500	360	2000
Mercedes-Benz	I-4	83.0	92.0	1991	18.0:1	60	4200	180	1400–2600
	I-4	83.0	92.0	1991	18.0:1	80	4200	250	1600–2600
	I-4	83.0	92.0	1991	18.0:1	103	4200	300	1600–3000
	I-4	88.0	88.3	2148	18.0:1	90/100	4200	270	1600–2800
	I-4	88.0	88.3	2148	18.0:1	110/125	4200	340/400	2000
	V6	83.0	92.0	2987	17.7:1	165	3800	415	1400–3800
	V8	86.0	86.0	3996	16.7:1	231/235	3600	730	2200
Mitsubishi	I-4	81.0	95.5	1968	18.0:1	103	4000	310	1750
Nissan	I-4	76.0	80.5	1461	18.8:1	50/63	3750	160/200	1900
	I-4	76.0	80.5	1461	15.3:1	78	3750	240	1900
	I-4	84.0	90.0	1994	15.6:1	110	4000	320	2000
	I-4	84.0	90.0	1994	15.6:1	127	3750	360	2000
Opel (GM)	I-4	79.0	86.0	1686	18.4:1	74	4400	240	2300
	I-4	79.0	86.0	1686	18.4:1	81/92	3800	260/280	2300
	I-4	82.0	90.4	1910	17.5:1	110	4000	320	2000
	I-4	83.0	92.0	1991	17.5:1	93/110	4000	295/320	1800–2000
	V6	87.5	82.0	2958	18.5:1	135	4000	400	1900
Peugeot	I-4	73.7	82.0	1398	17.9:1	40/50	4000	130/160	1750
	I-4	75.0	88.3	1560	17.6:1	66/80	4000	215/240	1750

Table 1.13 Continued

Manufacturer	Layout	Bore (mm)	Stroke (mm)	Capacity (cc)	CR	Power (kW)	Speed (rpm)	Torque (Nm)	Speed (rpm)
	I-4	85.0	88.0	1997	17.6:1	100	4000	320	2000
	I-4	85.0	96.0	2179	18.0:1	115/125	4000	380/370	1750
	V6	81.0	88.0	2721	17.3:1	150	4000	440	1900
Renault	I-4	76.0	80.5	1461	17.9:1	50	4000	160	1700
	I-4	76.0	80.5	1461	17.9:1	63	3750	200	1900
	I-4	76.0	80.5	1461	15.6:1	78	4000	240	2000
	I-4	80.0	93.0	1870	17.1:1	85/96/110	4000	300/340	2000
	I-4	84.0	90.0	1995	15.7:1	110/127	4000	340/380	2000
	V6	87.5	82.0	2958	18.5:1	130	4000	350/400	1800
Subaru	Boxer 4	86.0	86.0	1998	16.3:1	110	3600	350	1800
Toyota	I-4	73.0	81.5	1364	17.9:1	66	3800	190	1800–3000
	I-4	86.0	86.0	1998	16.8:1	93	3600	300	1800–2400
	I-4	86.0	96.0	2231	15.8:1	130	3600	400	2000–2600
	I-4	96.0	103.0	2982	17.9:1	127	3400	410	1600–2800
	V8	86.0	96.0	4461	16.8:1	210	3600	650	1600–2800
Volkswagen	I-3	79.5	95.5	1422	19.5:1	51	4000	155	1600–2800
	I-3	79.5	95.5	1422	19.5:1	59	4000	195	2200
	I-4	79.5	95.5	1896	19.0:1	74	4000	240	1800–2400
	I-4	79.5	95.5	1896	18.5:1	77	4000	250	1900
	I-4	79.5	95.5	1896	18.0:1	85	4000	310	1900
	I-4	79.5	95.5	1896	19.0:1	96	4000	310	1900
	I-4	81.0	95.9	1968	19.0:1	55	4200	140	2200–2400
	I-4	81.0	95.9	1968	18.5:1	103	4000	320	1750–2500
	I-4	81.0	95.9	1968	18.5:1	125	4200	350	1750–2500
	I-5	81.0	95.5	2461	18.0:1	128	3500	400	2000

(Audi)	V6	83.0	91.4	2967	16.4:1	171	4000	450	1400–3500
(Audi)	V6	83.0	91.4	2967	16.4:1	176	4000	550	2000–2250
	V10	81.0	95.5	4921	18.5:1	230	3750	750	2000
Volvo	I-4	75.0	88.3	1560	18.3:1	80	4000	240	1750
	I-4	85.0	88.0	1997	18.5:1	100	4000	320	2000
	I-5	81.0	93.2	2400	18.0:1	93	4000	300	1750–2250
	I-5	81.0	93.2	2400	17.3:1	132	4000	350	1750–3250
	I-5	81.0	93.2	2400	17.3:1	136	4000	400	2000–2750

Source: *Automobil Revue* (2008).

for a hybrid system. Small diesel engines, such as the Peugeot 1.4 litre I-4 engine or the Volkswagen 1.2 litre I-3 engines, would be ideally suited for this type of application. Indeed VW has made public information on a concept Golf TDI Hybrid, using their 1.2 litre TDI engine, which delivers 55 kW (74 bhp) at 4000 rpm and 180 Nm of torque at 2200 rpm with common rail fuel injection and a variable geometry turbocharger. The electric motor is mounted behind the diesel engine's flywheel, in series, and a seven-speed dual clutch transmission completes the powertrain. Nickel metal hydride batteries supply 202 V for the electric motor, which can operate in drive or generator mode, depending on the energy management system. Fuel consumption of 3.4 litres per 100 km and 89 g/km CO_2 is claimed for the hybrid over the European 'combined' drive cycle (Cover Story, 2008b).

Mercedes-Benz demonstrated a technically interesting V8 diesel hybrid, the concept Vision Grand Sports Tourer at the 2004 Detroit show. It used some S-class and next-generation M-class elements and is expected to return 30 mpg (US). On the European driving cycle the car uses 20% less fuel than a comparable diesel model. It has permanent all-wheel drive and regenerative braking; the latter contributes between 5% and 7% to fuel economy. The standard S-class 4.0 litre 184 kW V8 turbo-diesel was linked to a 50 kW electric motor, which together could produce an impressive torque of 860 Nm. Electrical energy was provided by a nickel/metal-hydride battery having 1.5 kWh storage capacity and providing 270 V. The electric motor would be used for standing-start acceleration, low-speed parking manoeuvres, city traffic conditions or when the car is being driven slowly with only a small power demand. The diesel engine had an automatic stop–start strategy whereby the engine stops after a few seconds idling (Birch, 2004).

General Motors showed a new V6 clean diesel engine intended for Cadillac, at the 2007 Geneva Motor Show. The 2.9 litre unit will develop 184 kW and 550 Nm of torque and is expected to be in production for 2009 to help raise Cadillac's profile in Europe, and is also likely to be used by Saab and Opel/Vauxhall. The compact V6 will use a 2000 bar common rail fuel system with closed-loop combustion control designed to meet future emissions requirements. Development is being conducted by GM Europe and VM Motori (Birch, 2007).

Looking at North America, GM has also announced a brand new Duramax 4.5 litre V8 diesel for 2010 to power its full-size pickup trucks and utilities. This engine is unique compared to European 'V' diesels in having the exhaust ports facing inboard, with the EGR system, single VNT turbocharger and close-coupled oxidation catalyst in the valley between the banks. The cylinders are angled at 72° for packaging, which necessitates a balance shaft, and the cylinder block is cast from CGI following Audi and Ford 'V' engine practice. The engine is packed with the latest state-of-the-art technologies including a 2000 bar piezo common rail fuel injection system and a urea-

based selective catalytic reduction system for reducing NO_x to meet Tier 2 Bin 5 and California LEV2 emissions regulations. The engine is rated at 231 kW with 705 Nm peak torque (Brooke, 2007).

Diesel engines could account for up to one in five light vehicle sales in the US by 2020, according to experts at the SAE World Congress in Detroit in April 2008. At the 2008 Vienna Motor Symposium, Volkswagen unveiled its latest low-emission diesel aimed at the US market. The new 2.0 litre four-valve TDI is able to meet the very tough Bin 5/LEV2 standards, especially the stringent 0.05 g/mile NO_x requirement, through a dual high/low pressure EGR system, a NO_x trap and use of cylinder pressure sensors enabling cylinder-specific combustion control. The 103 kW engine consumes 3.77 litres per 100 km on the highway in the Jetta car (Hadler *et al*., 2008). The challenge for diesel engineers is to ensure that fuel efficiency is improved, or at least maintained, while meeting future emissions legislation, and the cost of the technologies required will not cause it to lose its attraction as a fuel-efficient engine for the vehicle purchaser.

Audi made racing history in 2006 by winning the Le Mans 24-hour race with diesel power. The Audi team designed and developed a 485 kW (650 bhp) 5.5 litre V12 bi-turbo diesel engine specifically for this race. Aluminium was used for the major castings, turbochargers were supplied by Garrett and the 2000 bar common rail injection system came from Bosch (Diesel glory, 2006).

Peugeot has also entered endurance racing with the diesel-powered 908 HDi FAP sports car. This is powered by a 5.5 litre V12 diesel engine, with twin turbochargers and fuel injected by a Bosch piezo common rail fuel injection system; the engine develops 522 kW (700 bhp) and a peak torque of 1200 Nm. Peugeot won the 2007 Le Mans Series, but suffered disappointment in 2008 after coming so close to winning the Le Mans 24-hour race, with four wins from five races in the 2008 Le Mans Series (Gehm, 2007; Peugeot website, 2009).

Finally, while not a light-duty engine, it is interesting to note that there has been sufficient interest in the land speed record for a diesel-powered automobile for JCB and Ricardo to develop the JCB in-house engine for this task. This has served to illustrate the performance potential of the diesel engine as it continues to break new ground. In August 2006 the JCB 'Dieselmax' vehicle powered by two 5.0 litre JCB444-LSR diesel engines each developing 559 kW and 1500 Nm of torque went into the record books with a speed of 350 mph (*Ricardo Quarterly Review*, 2006).

1.6 Sources of further information and advice

ATZ Autotechnology (official publication of FISITA), Springer Automotive Media, GWV Fachverlage GmbH, PO Box 1546 D-65173 Wiesbaden, Germany.

Automobil Revue 2008, Büchler Grafino SA, Dammweg 9, case postale, CH-3001 Berne, ISBN 978-3-905386-08-0

Diesel Progress, International Edition, Diesel and Gas Turbine Publications, 20855 Watertown Road, Waukesha, WI 53186-1873, USA.

Engine Technology International, published by UKIP Media & Events Ltd, Abinger House, Church Street, Dorking, Surrey RH4 1DF, UK.

MTZ and *MTZ Worldwide*, Vieweg Verlag, GWV Fachverlage GmbH, PO Box 1546, D-65173 Wiesbaden, Germany.

Ward's Engine Update & Vehicle Technology, Ward's Communications Inc., 3000 Town Center, ste 2750, Southfield, MI 48075, USA.

1.7 References

Abe T, Nagahiro K, Aoki T, Minami H, Kikuchi M and Hosogai S (2004), Development of new 2.2-litre turbocharged diesel engine for the Euro-IV Standards, SAE paper 2004-01-1316, March 2004.

Anisits F, Borgmann K, Kratochwill H and Steinparzer F (1998), The new BMW six-cylinder diesel engine, Special Edition, *MTZ* November 1998.

Anisits F, Borgmann K, Kratochwill H and Steinparzer F (1999), The first direct-injection eight-cylinder diesel engine from BMW, *MTZ Motortechnische Zeitschrift* 60(6) (1999).

Anton C, Bach M, Bauder R, Franzke G, Hatz W, Hoffmann H and Ribes-Navarro S (2004), The new Audi 3L V6-TDI engine, *MTZ Worldwide* 65(7–8) (2004).

Autocar (1996), 26–31, December 1996.

Automobil Revue (2008), 103. Jahrgang der 'Automobil Revue', 6 March 2008.

Automotive Engineer (2007), BMW boosts diesel development ahead of US launches next year, 32(3) (2007) 5.

Bach M, Bikker S, Henning H, Kutschera I and Pölzl H-W (1999a), Der neue V8-TDI-Motor von Audi, Teil 1: Vorentwicklung und Berechnung, 10 Jahre TDI-Motor von Audi, *ATZ/MTZ-Sonderausgabe*, September 1999.

Bach M, Jablonski J, Bauder R, Hoffmann H, Endres H and Pölzl H-W (1999b), Der neue V8-TDI-Motor von Audi, Teil 2: Konstruktion und Mechanik, 10 Jahre TDI-Motor von Audi, *ATZ/MTZ-Sonderausgabe*, September 1999.

Bach M, Bauder R, Endres H, Pölzl H-W and Wimmer W (1999c), Der neue V8-TDI-Motor von Audi, Teil 3: Thermodynamik, 10 Jahre TDI-Motor von Audi, *ATZ/MTZ-Sonderausgabe*, September 1999.

Bach M, Bauder R, Endres H and Pölzl H-W (1999d), A consistent continuation of Audi's tradition in diesel engine development after 10 years – the new Audi V8 diesel engine, *20th International Vienna Motor Symposium*, 6–7 May 1999.

Bach M, Bauder R, Froehlich A, Hoffman H, Muth S and Seifried G (2005), The new 4.2 L TDI-V8 engine from Audi, Part 1: Design and mechanics, *MTZ* 66(10) (2005).

Bartsch C (2000), Der neue VW-Vierzylinder-TDI mit 150PS, *mot* 11 (2000) 71–73.

Basshuysen R V, Steinwart J, Stahle H and Bauder A (1989), Audi Turbodiesel-motor mit Direkt-einspritzung, *MTZ Motortechnische Zeitschrift* 50 (1989) 12.

Bauder R, Dursch N, Pölzl H-W and Mikulic L (1997a), The new Audi V6 turb-diesel engine with direct injection and four valves per cylinder, Part 1: General concept and thermodynamics, *18th International Vienna Motor Symposium*, Vol. 1, 48–69.

Bauder R, Hoffmann H, Stahle H and Pölzl H-W (1997b), The new Audi V6 turbo-diesel engine with direct injection and four valves per cylinder, Part 2: Engine design and mechanical components, *18th International Vienna Motor Symposium*, Vol. 1, 70–87.

Bauder R, Brucker D, Hatz W, Lörch H, Macher A, Giovanni Z, Reuss T, Riegger R and Schiffgens H-J (2004), Der neue 3.0L V6-TDI Motor von Audi, Teil 2: Thermodynamik, Applikation und Abgasnach-behandlung, *MTZ* 65(9) (2004) 684–694.

Bauder R, Gruber M, Michels E, Pamio Z-G, Schiffgens H-J and Wimmer W (2005), The new Audi 4.2 l V8 TDI-engine, Part 2: Thermodynamics, application and exhaust after-treatment, *MTZ* 66(11) (2005).

Bauder R, Froehlich A, Hatz W, Marckwardt H and Michels E (2008), The new Audi 6.0 l V12 TDI, the ultimate performance diesel, *29th International Vienna Motor Symposium*, 2008.

Birch S (2002), High-technology VW Phaeton, *Automotive Engineering International* 110(5), May 2002.

Birch S (2004), Diesel-hybrid from Mercedes-Benz, *Automotive Engineering International* 112(9), September 2004.

Birch S (2007), Diesel for a caddy, *Automotive Engineering International* 115(5), May 2007, 14.

Bird G L (1985), The Ford 2.5 litre high speed direct injection diesel engine – its performance and future possibilities, SAE paper 850262.

Bird G L, Duffy K A and Tolan L E (1989), Development and application of the Stanadyne new slim tip pencil injector, *I. Mech. E. Seminar on Diesel Fuel Injection Systems*, 10–11 October 1989, 133.

Bostock P G and Cooper L (1992), Turbocharging the Ford 2.5 HSDI diesel engine, *I. Mech. E. Seminar on Diesel Fuel Injection Systems*, 14–15 April 1992.

Brooke L (2007), GM's surprising new V8 diesel has no manifolds, *Automotive Engineering International* 115(10), October 2007, 20.

Brüggemann H and Wamser M (1998), The new OM668 diesel engines with common-rail-direct injection for the Mercedes-Benz A-Class, Part 1: Engine design, *Sonderausgabe ATZ und MTZ.*

Brüggemann H, Arbeiter E and Reifenrath H-P (1999), The new V8 CDI, lightweight design by Daimterchrysler: diesel engines with common rail injection – state of development and forecast, 8th Aachen Colloquium: Automobile and Engine Technology, 4–6 October 1999.

Brüggemann H, Arbeiter E, Fausten H, Reifenrath H-P, Roth H and Weisbarth M (2000), The new Mercedes-Benz V-8 passenger car diesel engine, *MTZ Worldwide*, *MTZ Mototechnische Zeitschrift*, 61(6) (2000) 362–375.

Challen J (2007), Set of twins, *Engine Technology International*, September 2007, 14.

Christoffel J (2002), Ceramic muscle, *Automotive Engineer* 28(1), January 2002, 52–54.

Christoffel J (2007), Technology transfer goes both ways, *Automotive Engineering International* 115(3), March 2007.

Cover story (2004), BMW's variable twin turbo technology, *Auto Technology* 4, December 2004, 44–47.

Cover Story (2008a), Subaru Boxer diesel, *Engine Technology International*, March 2008, 6–7.

Cover Story (2008b), Volkswagen TDI hybrid, *Engine Technology International*, June 2008, 6–7.

Diesel glory (2006), Developing the world's first Le Mans winning diesel engine, *Engine Technology International*, June 2006.

Doll G, Fausten H, Noell R, Schommers J, Spengel C and Werner P (2005), The new V6 diesel engine of Mercedes-Benz, *MTZ* 66(9) (2005).

Duggleby P and Johnson A (2006), Diesel passenger car and light commercial vehicles in Western Europe, Ricardo UK Limited, July 2006.

Engine Technology International (2006), Bi-diesel, September 2006, 10.

Ernst R, Gruenert T and Turner P (2007), The new V8 diesel engine for Land Rover, *MTZ* 68(4) (2007).

Family affair (2006), *Engine Technology International*, September 2006

Fortune, K (2007), Twin peaks, *Engine Technology International*, September 2007, 8.

Fritz D (2008), A new generation of engine efficiency – Honda's next-generation clean diesel, *Automotive Engineering International* 116(7), July 2008, 52–54.

Gehm R (2007), Peugeot 908 sports Bosch, Dow diesel technology, *Automotive Engineering International* 115(5) May 2007, 66.

Gill S, Griffiths B, Regent L (2004), The all new Ford / PSA 2.7l V6 diesel engine, 2004.

Gray M, Hösterey J and Wölfle M (1999), The new 1.8L Endura – DI diesel engine for the Ford Focus, The new Ford Focus, *Special Edition ATZ/MTZ.*

Hadler J, Rudolph F, Engler H-J, Röpke S (2007), The new 2.0 L 4V TDI engine with common rail, *MTZ* 68(11) (2007).

Hadler J, Rudolph F, Dorenkamp R, Stehr H, Dueesterdiek T, Hilzendeger J, Mannigel D, Kranzusch S, Veldten B, Koesters M and Specht A (2008), Volkswagens's new 2.0l TDI engine fulfils the most stringent emissions standards, *29th International Vienna Symposium*, Vienna, 2008.

Hara I, Kaneko I, Fujiki K and Ohshima M (2005), Honda 2.2 litre diesel engine for passenger cars, *Auto Technology* 4 (2005), 44–47.

Harima K (2008), Subaru Boxer diesel first four-cylinder horizontally-opposed diesel engine, *ATZ Autotechnology* 8(11–12) (2008) 18–25.

Hashimoto H, Sato T, Takeda M, Kibe K and Aiba T (2004), The Toyota 1.4 litre direct injection diesel engine, *Auto Technology* 4 (2004), 52–55.

High Speed Diesels and Drives (1989), Rover RV market improves with 2.5 L diesel, VIII(6), Nov–Dec 1989, 16.

High Speed Diesels and Drives (1991), Variable turbo boosts car diesel performance, X(6), July–August 1991.

Iveco Daily Press Pack (1996), July 1996.

Jelden H and Willman M (1995), Possibilities for increasing the power of the Volkswagen four-cylinder TDI engine, *5th Aachen Symposium, Vehicle and Engine Technology*, Aachen, October 1995.

Klingmann R and Brüggemann H (1997), Der neue Vierzylinder-Dieselmotor OM 611 mit Common-Rail-Einspritzung, Teil 1: Motorkonstruktion und mechanischer Aufbau, *MTZ Motortechnische Zeitschrift* 58(11) (1997) 652–659.

Klingmann R, Fick W and Brueggemann H (1999), The new common rail direct injection diesel engines for the updated E-Class, Part 1: Engine design and mechanical layout, *MTZ Worldwide* Jul/Aug 1999, 2–5 (MTZ 7-8/99 p426–438).

Knecht W, Isik T and Tardi R (1988), Development of small high speed diesel engines with direct injection for low emissions, SAE paper 885152, *XXII Fisita Congress 'Automotive Systems – The Future'*, September 1988.

Knecht W, Maul G and Schoni A (1991), Development of a low emission small high-speed turbocharged diesel engine with direct injection, I. Mech. E. Conference '*Worldwide Engine Emissions Standards and How to Meet Them*', September 1991.

Krause R and Saltzer W (1995), A new turbo diesel engine with direct injection for the Mercedes-Benz E-Class. Part 1: Design and mechanics, *MTZ Motortechnische Zeitschrift* 56 (1995) 6.

Ladommatos N, Abdelhalim S M, Zhao H and Hu Z (1996a), The dilution, chemical and thermal effects of exhaust gas recirculation on diesel engine emissions – Part 1: Effect of reducing inlet charge oxygen, SAE paper 961165, May 1996.

Ladommatos N, Abdelhalim S M, Zhao H and Hu Z (1996b), The dilution, chemical and thermal effects of exhaust gas recirculation on diesel engine emissions – Part 2: Effect of carbon dioxide, SAE paper 961167, May 1996.

Ladommatos N, Abdelhalim S M, Zhao H and Hu Z (1996c), The effects of carbon dioxide in EGR on diesel engine emissions, *Proceedings of International Seminar on Application of Powertrain and Fuel Technologies to Meet Emissions Standards*, Institution of Mechanical Engineers, 1996, 157–174.

Lawrence P, Lake P, Turtle D, Taylor T, Carnochan W, Finch J, Gellett, T and Woelfle M (2000), The all new Duratorq direct injection diesel engines in the Ford Transit, *MTZ Motortechnische Zeitschrift* 61(1) (2000), 8–17.

Love M (1997), Diesel passenger car and light commercial vehicle markets in Western Europe, Ricardo Consulting Engineers Ltd, February 1997.

Love M (2002), Diesel passenger car and light commercial vehicle markets in Western Europe, Ricardo Consulting Engineers Ltd, 2002.

Matsui R, Shimoyama K, Nonaka S, Chiba I and Hidaka S (2008), Development of high-performance diesel engine compliant with Euro-V, SAE paper 2008-01-1198, April 2008.

Mortimer J (2002), Can Audi knock Ford's block off? *Automotive Engineer* 28(1), January 2002, 56–57.

MOT (1998) Die TDI-Offensive, December 1998, 6–7.

Paffrath H and Sari O (2008), Exhaust gas recirculation and secondary air injection – systems and components for combustion engine emission reduction, *Engine Design Seminar*, I. Mech. E., April 2008.

Perkins Technical Information (1988).

Peters A and Pütz W (1995), A new turbo diesel engine with direct injection for the Mercedes-Benz E-Class. Part 2: Combustion and engine management, *MTZ Motortechnische Zeitschrift* 56(7/8) (1995).

Peters A and Pütz W (1997), Der neue Vierzylinder-Dieselmotor OM 611 mit Common-Rail-Einspritzung, Teil 2: Verbrennung und Motormanagement, *MTZ Motortechnische Zeitschrift* 58(12) (1997) 760–767.

Peugeot website (2009), http://www.peugeot.com/media/770082/peugeot-908-2009-en.pdf Object: Le Mans, 9 February 2009.

Piccone A and Rinolfi R (1997), Fiat third generation DI diesel engines, *I. Mech. E. Seminar Publication paper* S490/004/97, from *Future Engine and System Technologies, The Euro IV Challenge*, 47–63.

Rhode W, Gokesme S, Liang JR and Schmitt JL (1991), Der neue direkteinspritzende 1.9 l Dieselmotor von Volkswagen, *3rd Aachen Colloquium, Fahrzeug- und Motorentechnik '91*, 1991.

Ricardo Quarterly Review (2006), Ricardo partners JCB on land speed record engine development, Q2, 2006.

Ricardo Quarterly Review (2007), BMW pushes diesel power, Q3, 2007, 4.

Rover External Affairs (1995), Rover's new 'L' series the 'best practice' diesel, January 1995.

Rudolph F, Hadler J, Engler H-J, Röpke S (2007), The new 2.0L 4V TDI with common rail – state-of-the-art diesel technology from Volkswagen, *16th Aachen Colloquium, Fahrzeug- und Motorentechnik*, 2007.

Slavnich D (2003), Turning dreams into reality, *Automotive Engineer*, June 2003.

Steinparzer F, Stütz W, Kratoch H and Mattes W (2005), Der neue BMW-Sechszylinder-Dieselmotor mit Stufenaufladung, *MTZ* 66(5) (2005) 334–344.

Stephenson J A and Hood BA (1988), A high-speed direct injection diesel engine for passenger cars, *Proc. Instn Mech. Engrs, Part A*, 202(A3) (1988) 171–181.

Stock D and Bauder R (1990), The Audi 5-cylinder turbo diesel engine: the first passenger car diesel engine with second generation direct injection, SAE paper 900648, February 1990.

Takeuchi K, Kubota K, Konagai M, Watanabe M and Kihara R (1985), The new Isuzu 2.5 litre and 2.8 litre 4-cylinder direct injection diesel engine, SAE paper 850261, 1985.

Thiemann W, Finkbeiner H and Brueggemann H (1999), The new common-rail direct-injection diesel engine for the smart, Part 1: Engine design and mechanical construction, *MTZ Worldwide*, Nov 1999, 2–5 +24 (MTZ 11/99 p722–733).

TurboDaily Iveco Information (1985).

Turner P and Dawson S (2008), Compacted graphite iron for cylinder blocks, *Engine Design Seminar, I. Mech. E.* 16 April 2008.

Van den Heuvel B, Willems W, Krämer F, Morris T and Karvounis E (2006), Brennverfahrens-Entwicklung für die neuen Dieselmotoren in leichten Nutzfahrzeugen von Ford und PSA, *MTZ* 67(9) (2006) 606–614.

Vauxhall News Release (1996), New Vauxhall direct injection Ecotec engines open a new chapter in the history of the diesel, July 1996.

Volkswagen Press Information (1996), Volkswagen, Wolfsburg, March 1996.

Ward's Engine Update (1988), Fiat brings world's first DI car diesel to market in Italy, 14(13), 1 July 1988.

Willman M, Jelden H, Pohle J, Roost G and Kracke A (1995), The new 81 kW-TDI engine from Volkswagen, *MTZ* December 1995, 722–727.

Wilson R (2003), Diesel option for Minimobile, *Automotive Industries*, December 2003.

Wilson R P, Muir E B and Pellicciotti F A (1974), Emissions study of a single-cylinder diesel engine, SAE paper 740123.

Yamaguchi J K (2008), Back to the high-power future, *Automotive Engineering International*, 116(8), August 2008.

2

Fuel injection systems for high-speed direct injection diesel engines

R. W. HORROCKS, R. LAWTHER, and L. HATFIELD,
Ford Motor Company Limited, UK

Abstract: This chapter reviews development of HSDI diesel engine fuel injection equipment, from pump-line-nozzle systems of the 1980s, to the latest high pressure common rail systems in production today. The Bosch VE distributor pump was widely used until the 1990s. The next development was addition of electro-mechanical actuators and electronic controls, with the Lucas EPIC (Electronically Programmed Injection Control) fuel injection system in1992 and Bosch VP44 pump introduced in 1996. The first generation of common rail was introduced by Bosch in 1997. This was followed by similar systems from Denso and Lucas (now Delphi). All these first generation systems used solenoid actuators and operated at peak pressures between 1300 and 1400 bar. Further generations with solenoid and piezo actuators and increasing pressure up to 2000 bar are reviewed for each manufacturer. Common rail operating principles are explained, as well as electronic control systems, covering ECU hardware, sensors, actuators and software. Finally future trends are discussed.

Key words: direct-injection, high speed, diesel, engine, perfomance, fuel injection, common rail, high-pressure, pump, injector, actuator, electronic, control, software.

2.1 Introduction

The fuel injection system was one of the key enabling technologies, with helical intake ports to develop in-cylinder swirl for high-speed combustion, that made possible development of the high-speed direct injection diesel (HSDI) engine in the late 1970s. This led to the introduction of production in the 1980s and to the situation today where approximately 50% of all passenger cars and 90% of light-duty truck engines are high-speed DI diesels in Europe. Development of the rotary distributor fuel pump with increased pressure capability over previous versions for pre-chamber engines, and more precise timing control, were the breakthrough features to support high-speed diesel combustion. Pressure build-up in the pump had to more than double from indirect injection levels, reaching 800 to 1000 bar in the pump and 1200 to 1400 bar at the injector. This, combined with timing advance, advancing injection timing with engine speed, and torque control to vary fuel delivery with engine speed to match the full load characteristic of the engine, facilitated the development of the combustion systems that led to

acceptable HSDI engine attributes of power, torque, smoke and noise levels and feasible production designs for the automotive industry to invest in for light-duty vehicles.

As stricter gaseous and particulate exhaust emissions limits were enforced and further engine refinement was demanded by vehicle engineers and the customers, and since the fuel injection system is key to diesel engine performance, emissions and refinement of combustion noise, further developments of the fuel system were required. These focused on greater flexibility of injection rate control. This was achieved with some success by two-spring injectors and pump cam profiles. But the pump–line–injector fuel system was limited by the distributor pump having to be driven at half engine speed, for a four-stroke engine, and the injector receiving effectively a single pressure pulse, even if there was a dwell in the case of a 'stepped' cam, from the pump. Solenoid valve-controlled distributor pumps were developed that enabled a pilot injection ahead of the main injection, but fuel pressure was still linked to pump speed and hence crankshaft speed.

Over the last decade common rail injection systems have been developed for automotive high-speed diesel engines. The breakthrough features of this type of system are firstly decoupling injection pressure from engine speed, thus allowing injection pressure to be an independent variable, and secondly enabling multiple injections over the speed–load range combined with flexible injection timing. The latter feature provides the opportunity for a pilot injection to control combustion noise over the engine speed range where combustion noise dominates overall engine sound pressure levels.

Robert Bosch's first-generation common rail was introduced in 1997 for the Mercedes C-Class (Peters and Pütz 1997). This was a solenoid-actuated injector operating at a peak rail pressure of 1350 bar. This was followed by similar systems from the Japanese manufacturer Denso, for Toyota products; and in Europe from Delphi (formally Lucas Diesel Systems) for Renault and Ford applications. All these first-generation systems used solenoid actuators and operated at peak pressures of between 1300 and 1400 bar.

Siemens (now Continental) of Germany was the first company to manufacture in volume production a common rail injector incorporating a piezo actuator. The piezo actuator has a faster response time, about four times quicker than a solenoid, thus enabling smaller pilot injections to be used and at least five injections per cycle (Christoffel 2002). Small pilot injections are a major enabler for the combustion noise/emissions trade-off required to meet more stringent emissions standards. This fuel injection first went into production for the Peugeot 2.0 DW10 engine in 2001 at 1500 bar and later in the Ford/Peugeot 2.7 litre V6 at 1650 bar in 2004. It has more recently been introduced for the Peugeot/Ford joint venture 1.4 diesel, which is used in the company's small cars such as the Citroën C3 and the Ford Fiesta.

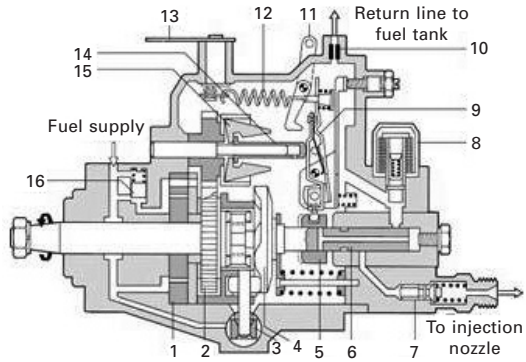
It is noteworthy that VW did not follow the common rail fuel system

trend for many years, but instead opted to use the unit injector, supplied by Bosch and latterly by Siemens (now Continental). This had an advantage of higher peak injection pressure at maximum power engine speed, of just over 2000 bar, but did not offer the same flexibility of injection pressure control at other engine speeds, nor did it have the capability of multiple injections compared to a common rail system. More recently VW has moved to the latest state-of-the-art Bosch 1800 bar common rail with piezo injectors for its 2.0 litre 4-valve TDI engine (Hadler *et al*. 2008) and 4.9 litre V10 for the Touarag (*Automobil Revue* 2008).

2.2 Early high-speed direct injection (HSDI) diesel fuel systems

Although early prototype engines were run with small inline pumps, the first fuel injection systems used for early production HSDI diesel engines were developments of the previous generation of pre-chamber or indirect injection (IDI) engine fuel systems. These were rotary distributor pumps with HP pipes from the HP pump outlet to each injector, known as pump–line–nozzle systems. Thus the pump had to be designed for the number of cylinders on the engine so that there was a HP outlet to connect to an injector for each cylinder. Owing to the physical constraints of the plunger design, these pumps were limited to a maximum of six cylinders. For a four-stroke engine, the pump would be driven at half engine crankshaft speed, to provide an injection on the firing stroke of each cylinder. The pump therefore had to generate fuel pressure, displace the correct volume of fuel and deliver it to the correct cylinder at the desired crankshaft angle, or more exactly the correct piston position. Initially, this was all carried out mechanically; later, with the advent of electronic controls, electro-mechanical actuators were utilised.

The Bosch VE pump was widely used by a number of engine manufacturers from the mid-1980s to the late 1990s, namely Ford, Iveco, Rover and VW. This was an axial-single plunger distributor pump with a mechanical governor. The high-pressure plunger was rotated by the drive shaft, via a yoke, and a face cam plate attached to the plunger and acting against rollers caused it to move axially to give the pumping stroke. The number of strokes per pump revolution equalled the number of engine cylinders; owing to mechanical limitations with the design of the plunger, the maximum number of cylinders for the VE pump was six. A vane-type fuel supply pump was located on the shaft at the front of the pump and provided fuel pressure via a regulator to the interior of the pump body. The pump delivered high-pressure fuel to the injectors, while the plunger moved axially due to the cam profile. Delivery ended when the spill port was uncovered by the control collar. The governor determined the position of the control collar and hence the quantity of fuel delivered. Timing advance as engine speed increased was



1 Vane-type supply pump
2 Governor drive
3 Timing device
4 Cam plate
5 Control collar
6 Distributor plunger
7 Delivery valve
8 Solenoid-actuated shutoff
9 Governor lever mechanism
10 Overflow throttle
11 Mechanical shutoff device
12 Governor spring
13 Speed-control lever
14 Control sleeve
15 Flyweight
16 Pressure-control valve

2.1 Bosch VE distributor-type fuel injection pump, basic version (courtesy of Robert Bosch GmbH).

provided by rotation of the roller ring in the opposite direction to the pump shaft rotation. The roller ring was rotated by a spring-loaded plunger being acted upon by speed-dependent fuel pressure from the internal supply pump. More detailed descriptions are available in the references (Tschöke 1999, Bosch 1999, 2007). The Bosch VE distributor pump is shown in Fig. 2.1.

The other rotary distributor pump used in the early days of HSDI diesel was the Lucas DPS pump, which was a development of the earlier CAV DPA pump that had its origins from a 1939 distributor pump design by V Roosa of Hartford, Connecticut (Smith 1959). This pump is quite different in design and operation from the Bosch VE. To develop injection pressure, it had four opposing radial plungers whose inward stroke was controlled by roller and shoe followers acting on an internal cam ring. The cam ring had a pair of lobes for each cylinder. The plungers were located in the pump rotor that also had the charging ports, which were used to fill the cavity with the correct quantity of fuel, and the distribution port that connects the rotor to the desired outlet for injection at the cylinder due to fire. An inlet metering valve controlled the fuel flow to the plungers by throttling the supply, to give the desired injection quantity. A sliding vane transfer pump incorporated at the end of the rotor maintained fuel pressure to the metering valve and plungers, but also provided hydraulic pressure for the advance mechanism. Advancing the injection timing with engine speed was achieved by rotating the cam ring in the opposite direction to the rotation.

The next stage in the development of fuel systems to meet the increasing demands of the HSDI engine was the addition of electro-mechanical actuators and electronic controls to rotary distributor pumps. The Bosch VP34 was such a pump, basically a VE with electro-mechanical actuators for controlling

fuel quantity, replacing the mechanical governor, and timing, replacing the spring-loaded hydraulic piston. To operate this system, an ECU contained a number of pre-calibrated three-dimensional maps of fuel mass versus air mass flow and engine speed, start of injection versus fuel mass and engine speed, and for EGR flow, air flow mass versus fuel flow and engine speed. To support the control strategies in the ECU, there were a number of input signals from additional sensors, namely accelerator pedal position, engine speed, temperatures of intake air, charge air, water and fuel, ambient and charge pressures, and air mass flow. Electronic control clearly gave the engine developers more flexibility compared to simple mechanical control and also reduced the level of variability. This system was first used by Fiat in 1987 for its Croma model but it became better known when used by Audi for its 2.5 litre I-5 HSDI engine for the Audi car. This system was applied to VW's new 1.9 litre DI engine in 1992 (Rhode *et al*. 1991).

The Lucas EPIC (Electronically Programmed Injection Control) fuel injection system was based around an electronically controlled rotary distributor pump managed by an electronic control unit with input from a number of sensors. It also controlled the EGR system by activating the air throttle and EGR valve. It was applied to the 1992 Ford 2.5 DI turbocharged diesel in the Transit and was the first light-duty commercial van with 'drive-by-wire' technology (Bostock and Cooper 1992). The pumping principle of the EPIC was similar to that of the DPA and DPS family of pumps, in that it used a stationary internal cam ring with four roller and shoe followers acting on four pumping plungers. Fuel was admitted in and pumped out by the plungers via ports in the rotor. Fuel quantity control was achieved by restricting the outward movement of the plungers by tapered ramps on the followers and on the rotor guides. The rotor was moved axially by hydraulic pressure, to adjust the stroke of the plungers, thus controlling fuel delivery. Injection timing was adjusted by rotation of the cam ring via a spring-loaded hydraulic piston. A transfer pump with spring-loaded vanes supplied fuel to the high-pressure plungers and for the hydraulic actuation of rotor and cam ring positions, both of which had position sensors for feedback (Lewis 1992). This system remained in production on the Ford 2.5 litre engine until it was replaced by the new 'Puma' or Duratorq diesel in 2000, which was introduced with the Bosch VP30 and VP44 electronically controlled pumps. From a performance aspect, the EPIC system met all the engine requirements of that time, but not having a 'spill' sharp cut-off for the end of injection limited its ultimate low emissions potential.

The Bosch VP44 high-pressure electronically controlled distributor pump was the final development of rotary fuel injection pumps and was introduced in 1996 at the twilight of this technology, shortly before the introduction of common rail fuel systems for automotive diesel engines. It was a complete change from the 'VE' concept of a face cam, using instead the V Roosa

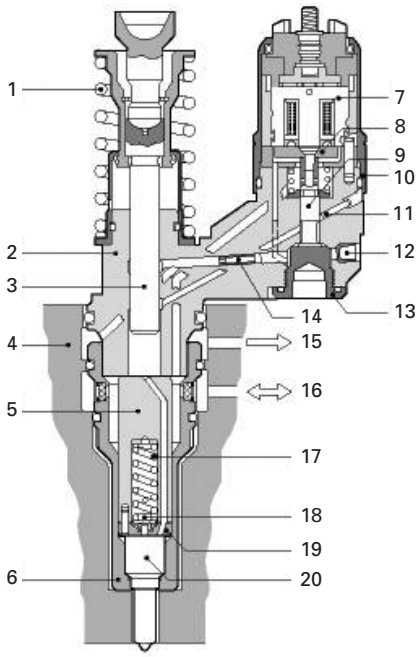
principle of radial plungers with an internal cam ring. The pump shaft rotated with two, three or four radial plungers operated via roller shoes by the lobes on the internal cam ring. For a four-cylinder engine there were two or four plungers and the cam had four lobes symmetrically spaced around the cam ring circumference. At the front of the pump a sliding vane supply pump with a pressure control valve provided fuel pressure to the high-pressure stage. A single solenoid operating a needle valve, located at the delivery end of the rotor, controlled the filling of the high-pressure cylinders and, by closing, the start of delivery. At that time, the rotor distribution slot was connected to the appropriate high-pressure outlet. The end of injection occurred when the solenoid opened the needle valve and fuel was spilled into a diaphragm chamber within the pump body. Those pressure pulses were damped by the accumulator diaphragm. Injection timing was controlled by rotation of the cam ring by a spring-loaded hydraulic piston and servo-valve, the fuel pressure being set by the timing device solenoid (Krieger 1999, Bosch 1999). A more detailed description may be found in the references.

The electronic unit injector (EUI) was developed for truck heavy-duty engine applications in the second half of the 1980s by Bosch and Lucas, and has been a dominant fuel system since then (see Chapter 9 for more details). Bosch developed jointly with VW a smaller unit injector for HSDI engines and this went into production for the VW 1.9 litre inline four-cylinder engine in 1998. The increased peak injection pressure of 2050 bar provided a 4.5% increase in maximum power, to 85 kW, and a 21% increase in peak torque to 285 Nm. The EUI is effectively a unit high-pressure pump fitted directly onto an electronically controlled injector. On the VW engine it is operated by an additional rocker and cam lobe on the overhead camshaft (Kendall 1998). Figure 2.2 shows a sectioned view of a Bosch EUI. Fuel is supplied to the EUI by a lift pump. A high-speed solenoid valve controls the start and end of injection by closing off and opening, respectively, a passage connected to the high-pressure cylinder. The solenoid valve is triggered by the ECU, so the start and end of injection are programmable from a calibrated map contained within the control unit (Bosch 1999). Siemens (now Continental) also manufactured EUIs for VW.

2.3 Common rail fuel injection systems

2.3.1 Background and a brief history of common rail fuel injection systems

With the advent of the high-speed direct injection (HSDI) diesel engine during the 1980s, all the major high-volume fuel injection system suppliers were investigating improved systems to provide better control of the fuel injection process, particularly a means to have a consistent and reliable small



1 Return spring
2 Pump body
3 Pump plunger
4 Cylinder head
5 Spring retainer
6 Tension nut
7 Stator
8 Armature plate
9 Solenoid-valve needle
10 Solenoid-valve tension nut
11 High-pressure plug
12 Low-pressure plug
13 Solenoid travel stop
14 Restriction
15 Fuel return
16 Fuel supply
17 Injector spring
18 Pressure pin
19 Shim
20 Injector

2.2 Sectioned view of a Bosch EUI (courtesy of Robert Bosch GmbH).

pilot injection to modulate the rate of cylinder pressure rise at the start of combustion, in order to reduce or ideally eliminate diesel combustion knock, which was typical of the early HSDI engines. While electronically controlled distributor pumps, like the Bosch VP30 and VP44 and the Lucas EPIC systems, provided improved control of injection timing and quantity over the engine speed and load range, injection pressure remained a function of engine speed. Additionally injection rate and pressure were still controlled by cam rate.

The Fiat Group initiated a strategic project at Magneti Marelli in the mid-1980s to develop an innovative fuel injection system for high-speed DI engines. Various concepts and architectures were examined that resulted in the decision to pursue a 'common rail' strategy. In 1989 a consortium for research and technology development called ELASIS was formed. Magneti Marelli joined this consortium and transferred the project for the common rail system, called 'Unijet', to ELASIS. A research centre for fuel injection equipment was established in Bari, Italy. The ELASIS consortium worked closely with the Fiat Research Centre and by the end of 1991 second-generation Unijet system hardware was demonstrating functional potential. Two years later a pre-industrialisation version was available. In the spring of 1994 the Fiat Group signed an agreement with Robert Bosch for the industrialisation and further development of the system (Riolfi *et al.* 1995).

In North America, Caterpillar were developing a new and unique fuel injection system that provided injection pressure control completely independent from engine speed or load. Moreover, it did not require any mechanical actuation or mechanical control devices. It was a novel electronic unit injector with hydraulic actuation. This system used engine oil hydraulic pressure with a pressure intensifier to create the injection pressure. The desired injection pressure was controlled by modulating the oil pressure, which had a separate high-pressure circuit from the normal engine lubrication system. Start and end of injection were controlled by a solenoid valve that connected high-pressure oil to the intensifier plunger. Thus injection timing and pressure were independent of engine speed and load (Glassey *et al*. 1993). This system was first applied to the Navistar T 44E 7.3 litre V8 DI diesel engine, which went into production in 1994 (Hower *et al*. 1993). Developments of this hydraulic electronic unit injector (HEUI) system are in use today; however, by its very nature the injector is rather large and it has never been used for a small-bore HSDI engine, despite a programme to develop a design iteration for light-duty automotive application (Glassey *et al*. 1995).

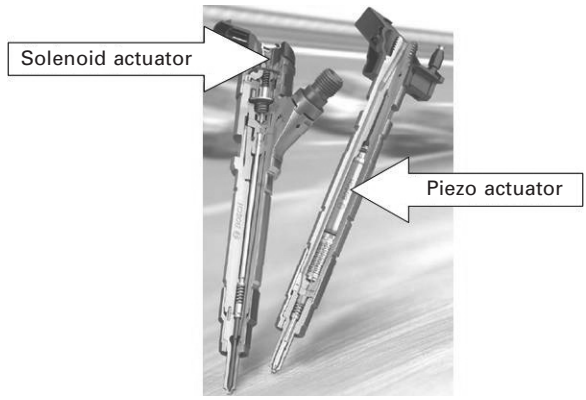
2.3.2 Common rail operating principles

The FIE systems described below refer to systems from suppliers Bosch and Continental. Denso and Delphi manufacture similar systems and, although the designs vary, the general operating principles are the same.

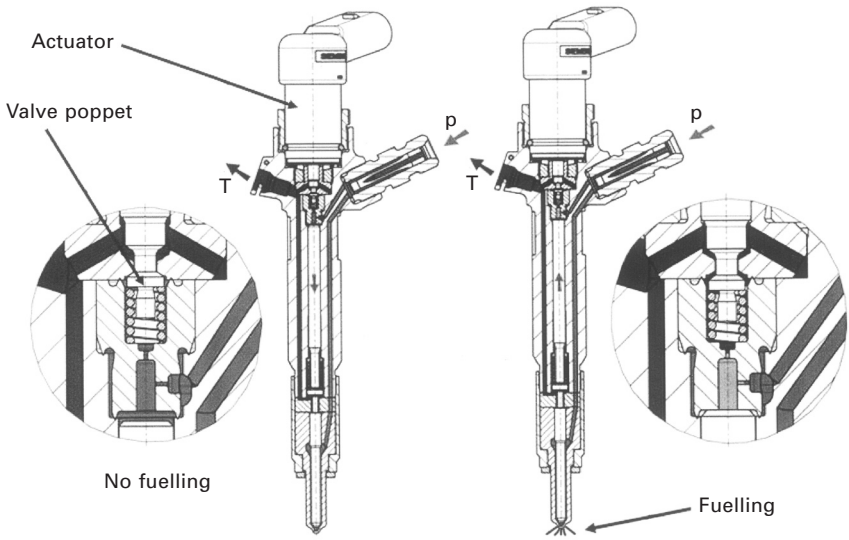
Injector

Current-generation diesel common rail injectors operate on a similar principle. Hydraulically they are connected via HP fuel pipes to the HP fuel rail; electrically they are connected to the Engine Control unit (ECU) via the engine wiring harness. Regardless of the amount of fuel pressure in the HP fuel rail, the injector will not operate (not inject fuel into the engine cylinder) until there is a voltage supply from the ECU to the injector actuator. The duration of the voltage supply is proportional to the amount of fuel demanded to be injected into the engine cylinders. Figure 2.3 shows examples of diesel common rail injectors; the HP fuel inlet and actuators are identified. Although different in design, the operating principle is the same.

The operating principle of the Continental PCR2.x injector is shown in Fig. 2.4. An exploded diagram of the injector is shown in Fig. 2.5 with the names of all parts identified. When there is a HP fuel supply to the injector but no voltage supply, the injector needle is closed and the injector does not fuel. The force due to HP fuel trying to lift the nozzle needle from its seat is overcome by the force due to HP fuel acting on the top of the control



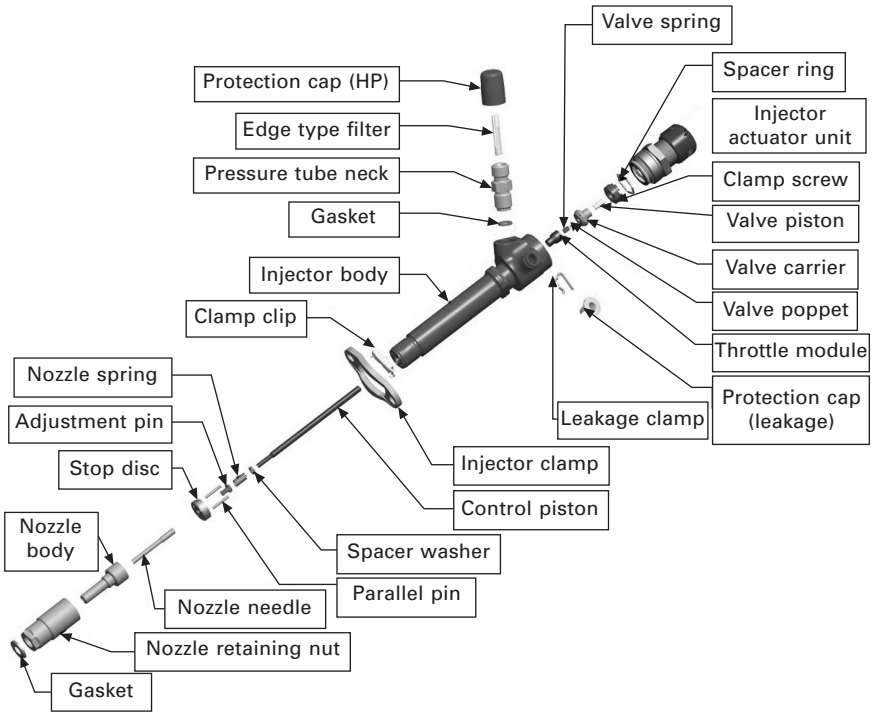
2.3 Examples of diesel common rail injectors (courtesy of Robert Bosch GmbH).



2.4 Operating principle of the Continental PCR2.x injector (courtesy of Continental).

piston. When voltage is supplied to the actuator (located on the top of this injector) this moves the poppet valve off its seat and the HP fuel (dark grey in Fig. 2.4) in the control volume beneath the valve poppet is released to the LP circuit (black). The drop in pressure in the control volume reduces the downward force applied by the HP fuel on top of the control piston significantly to allow the needle and control piston to move upwards.

When the supply voltage is removed, the poppet valve spring moves the valve back onto its seat, the pressure in the control volume rises to match



2.5 Exploded diagram of the Continental PCR2.x injector with all parts identified (courtesy of Continental).

the rail pressure, the downward force at the control volume overcomes the upward force on the needle, and the needle closes. There are two throttles connected to the control volume. The inlet throttle (connecting the control volume to the HP fuel supply from the HP fuel rail) defines the rate at which the control volume fills with HP fuel, and therefore controls the injector closing speed. The outlet throttle (connecting the control volume to the injector leak-off circuit, T, in Fig. 2.4) defines the rate at which fuel exits the control volume, and therefore the injector opening speed. The throttle diameters (typically 0.6–0.8 mm) and control volume (typically 20 mm^3) are designed small to act as a restriction and minimise the HP fuel leakage to the LP circuit when the injector is operated.

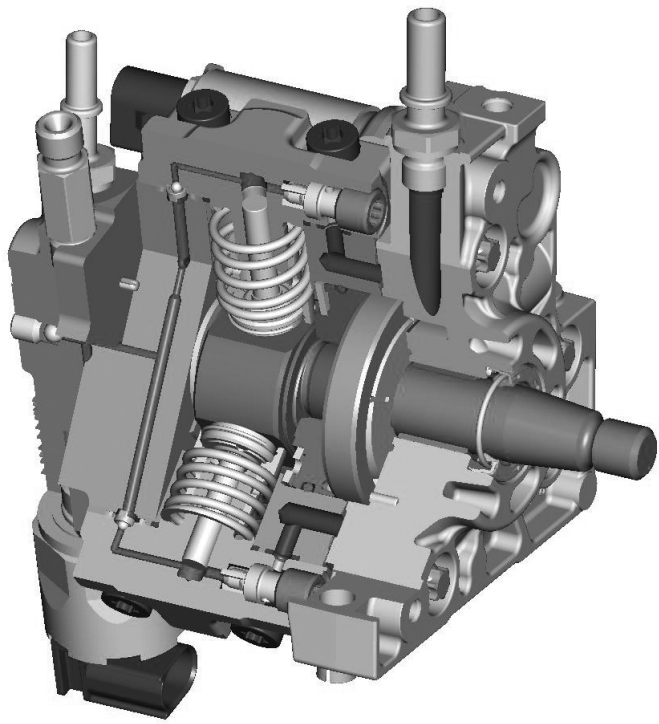
There are two types of leakage from this diesel injector: continuous and switch. Continuous leakage occurs regardless of an injection event. Leakage quantity is a function of fuel rail pressure. On the Continental PCR2.x injector, continuous leakage occurs when fuel seeps from the control volume along the control rod guidance, and from the nozzle body along the needle guidance; both these quantities return through the injector leak-off. Switch leakage occurs as discussed above when the injector is fuelling and there is a direct

leak path between the HP fuel rail and the injector leak-off. From the engine measurements with standard (non-modified) injectors, it is not possible to differentiate switch and continuous leakage measurements; however, Fig. 2.21 shows an example of analytical data for an engine using a Continental PCR2.x injector. This shows the split between the leakages and shows that total leakage is of a similar quantity to the injection quantity.

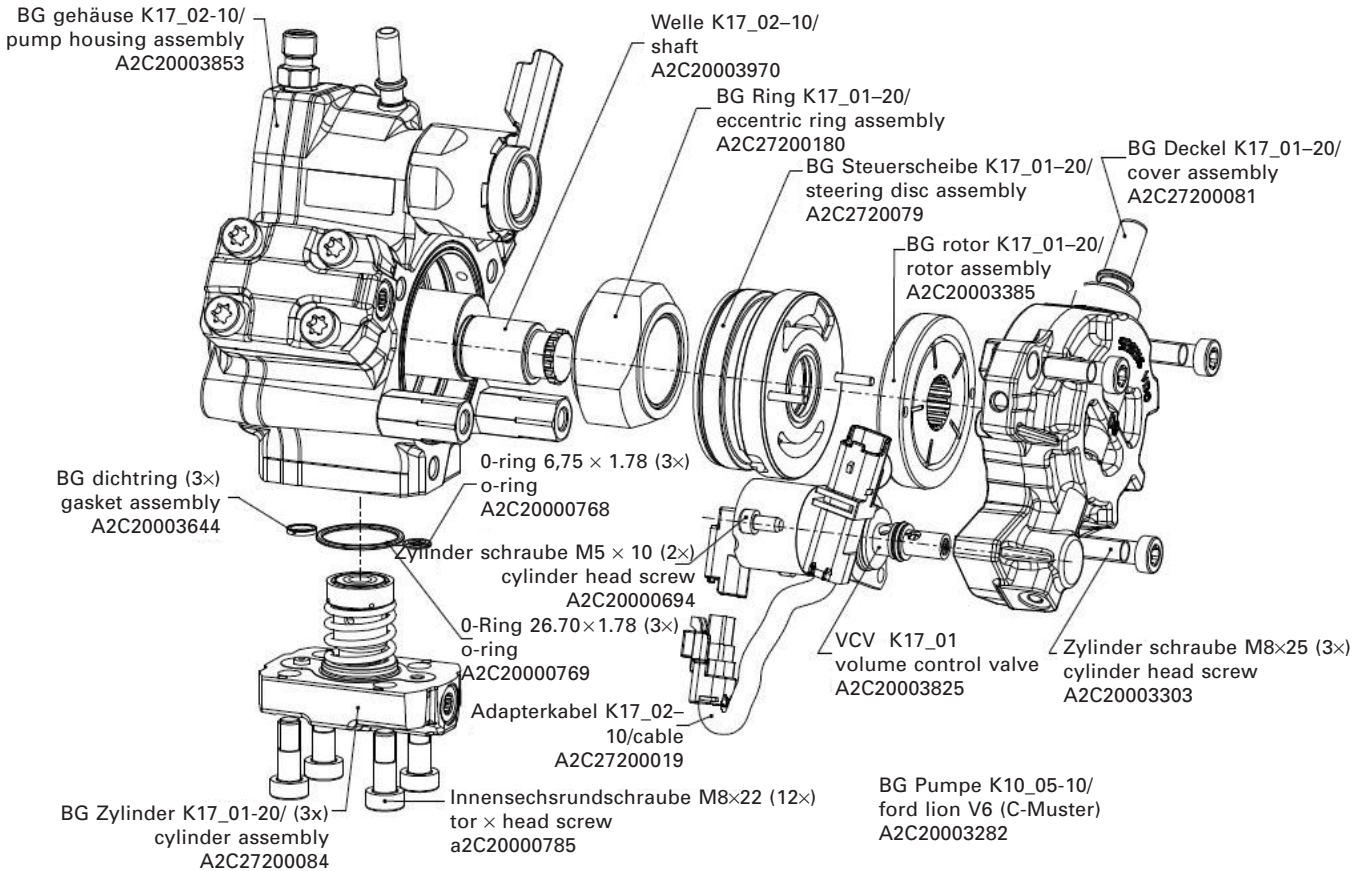
Alternative design injectors exist to prevent continuous leakage. An example is the Bosch third-generation CRI3.x piezo injector, shown in Fig. 2.3. This injector has the actuator mounted deep in the injector body. As the control valve is mounted close to the nozzle needle, this eliminates the separate control piston; therefore leakage occurs only when the control valve is moved off its seat by an energised actuator.

HP pump

Figure 2.6 shows the cross-sections of the Continental HP pump. This is based on a Rexroth design. The individual components are shown in Fig. 2.7. This shows an exploded view and identifies some of the major components.



2.6 Cross-section of the Continental HP pump (courtesy of Continental).

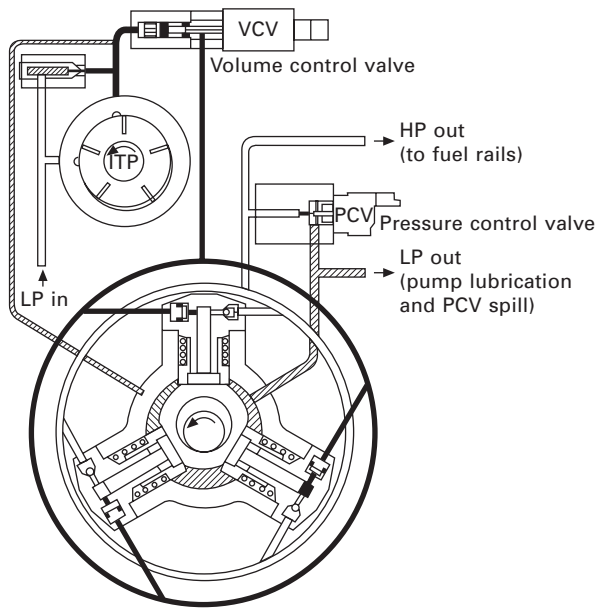


2.7 Exploded view of the Continental HP pump and identification of some of the major components (courtesy of Continental).

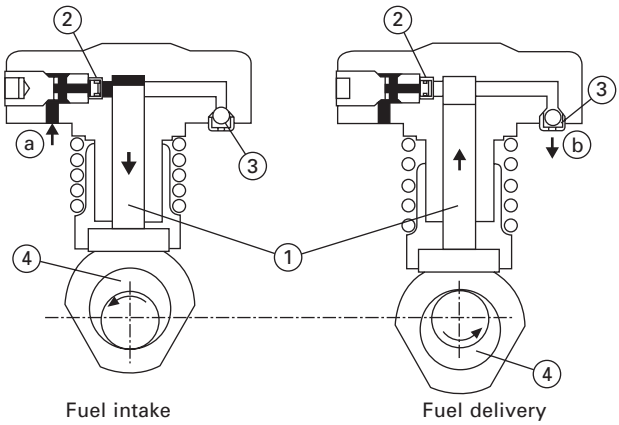
The hydraulic flow schematic to help understand the operating principle of the HP pump is shown in Fig. 2.8. The LP fuel circuit is shown in black, the HP circuit in white and the LP lubrication circuit is shown as hatched. Fuel enters the HP pump (at LP in) as it is drawn past the internal transfer pump (ITP), which is a mechanical pump (vane or gerotor type). The output pressure of the ITP is regulated. The volume control valve (VCV) is an electonic solenoid valve controlled by the ECU to regulate the amount of flow that will be delivered to each HP pumping element and ultimately to the HP fuel rail. The operating principle of the HP pumping elements is shown in Fig. 2.9. The lubrication flow quantity is controlled by flow-restricting throttles. As the ITP outlet pressure is regulated, the lubrication flow should be constant; however, the HP pump LP return flow (at LP out) includes pressure control valve (PCV) fuel spill. PCV is an electric solenoid that is connected to the HP pump HP outlet and regulates the pressure in the HP rail, mostly during transient vehicle decelerations where fuel is spilled from the rail to decay HP fuel rail pressure.

Referring to Fig. 2.9 again, the operating principle of the HP pumping elements can be split into two functions as it operates on a two-stroke cycle principle.

1. Fuel intake. The downward movement of the piston (1) produces a vacuum in the pump cylinder which opens the inlet valve (2) against



2.8 Hydraulic flow diagram of the Continental HP pump (courtesy of Continental).



2.9 The operating principle of the Continental HP pumping elements (courtesy of Continental).

the spring force. The fuel (a) supplied from the VCV is drawn in. At the same time, the outlet valve (3) is closed by the difference in pressure between the pump cylinder and the fuel pressure in the HP fuel rail.

2 Fuel delivery. The eccentric cam (4) on the HP pump shaft presses the piston (1) up. The inlet valve (2) is closed by the spring force and the pressure building up in the pump cylinder. The outlet valve (3) opens when the pressure in the pump cylinder exceeds the fuel pressure in the HP fuel rail (b).

2.4 Common rail systems

Common rail fuel injection systems are often referred to as a generation level. Although there are discrepancies within the automotive industry between the definition of FIE generations, it can be loosely clasified by the maximum rail pressure at which the system operates. Table 2.1 represents the most widely used definitions.

In reality, rather than maximum rail pressure, what is most important for engine performance is the pressure in the nozzle during injection, as well as the injector performance in terms of operating speed to allow short and multiple injections and injection repeatability, for example shot-to-shot tolerances. Injection spray momentum is regarded as an ideal measurement to compare systems for good air–fuel mixing and efficient combustion. Alternatively, Needham and Whelan (1994) used mean effective injection pressure (MEIP) which they reported gave a reliable measure of average injection pressure and hence injection energy:

Table 2.1 Definitions of fuel injection engine (FIE) generations

FIE generation	System definition (maximum rail pressure)
First	<1600 bar
Second	≥ 1600 bar, injectors with continuous leakage
Third	≥ 1800 bar, injectors with no continuous leakage
Fourth	≥ 1800 bar, direct acting piezo stack

$$\text{MEIP (bar)} = \left(\frac{0.0426Qn}{\theta h d^2} \right)^2 \qquad 2.1$$

where:

Q = fuelling (mm^3/injection)
N = engine speed (rev/min)
θ = injection period (deg crank)
h = number of injector nozzle holes
d = hole diameter (mm)
0.0426 is a constant which includes the discharge coefficient of a typical nozzle hole.

2.4.1 Bosch

First-generation Bosch common rail system

As described in the background, Bosch had signed an agreement with Fiat for the industrialisation and further development of the 'Unijet' system in 1994 (Riolfi *et al*. 1995). Stumpp and Ricco (1996) of Bosch reported on the development of this system at the 1996 SAE Congress. The system consisted of the major components that we know of typical common rail systems today: a high-pressure pump, a high-pressure rail or accumulator, solenoid injectors, one for each engine cylinder, and the ECU. The pump, rail and injectors were, as today, connected by HP pipes. The pump was based on the Rexroth hydraulic pump principle, whereby an eccentric, on the pump shaft, displaced three radial pistons in succession, each with an inlet and HP outlet valves. The outlet valves were connected via a pressure regulator and HP pipe to the rail. The pressure regulator consisted of a solenoid acting on a ball and seat; thus increased current to the solenoid increased the force acting on the ball and increased fuel pressure, and vice versa. The inlet valve of one of the pistons could be opened by a solenoid to

reduce the displacement by one third, so that the delivery could be adapted closer to demand. The injector was a classic common rail configuration, with a solenoid operating a servo-valve to activate opening and closing of the nozzle needle. High-pressure fuel from the rail is connected via a small orifice to a volume above the control piston, causing a downward force to act on the nozzle needle to keep it closed on its seat. High-pressure fuel is also connected to the nozzle and acts on the smaller diameter of the needle guide. When the solenoid valve is activated, to start injection, it opens another small orifice above the control piston, thus reducing the pressure above the control piston, and rail pressure lifts the needle to inject fuel through the holes in the nozzle. When the needle was fully open, the control piston almost covered the bleed orifice, thus reducing the return fuel flow. When the electrical voltage to the solenoid is switched off, the bleed orifice above the control piston is closed by spring force and fuel pressure builds up again via the feed orifice, so that the force acting on the control piston closes the needle to end injection. The rail was a steel forging with a central drilling to provide the accumulator volume, with smaller side drillings for the feed and each injector connection. There was also a connection for a silicon piezo-resistive strain gauge pressure sensor.

The ECU takes signals from all the sensors and contains all the functions for controlling the fuel injection system as well as other engine systems such as the EGR and turbocharger. Input signals are processed and output signals for rail pressure, injection timing, pilot injection, injection quantity, boost pressure and EGR are sent to the respective system actuators to give the desired output response.

Second-generation Bosch common rail system

Bosch enhanced the operating pressure from 1350 to 1600 bar for the next evolution of their common rail system. This was achieved with further refinement of materials and manufacturing processes.

Third-generation Bosch common rail system

Bosch, the market leader for diesel fuel injection systems, offers so-called third-generation common rail systems for passenger car and light-duty truck applications. There are two solutions for injector actuator, as well as two concepts of HP pump (discussed later).

Injector

Historically, higher-pressure FIE systems utilise a piezo actuator. The fast actuation speed of the piezo actuator along with higher rail pressures allows

this to be marketed as a premium system for high power density engines and/or engines with stringent emission targets. This can be compared to solenoid actuator systems where the technology is more widely used, and therefore a lower-cost solution. At any given time, the latest generation Solenoid actuated injectors do not have the same performance as piezo injectors, such as lower maximum rail pressure capability and increased fuelling tolerances; however, for high volume, lower power density/lower engine emissions applications, this is the favoured choice.

Lower FIE cost targets from automotive manufacturers to make diesel vehicle ownership affordable, especially due to the high cost of diesel fuel, diesel after-treatment and the threat from rapidly advancing gasoline GDI technology, have prevented the expiration of the solenoid injector, so much so that many of the FIE manufacturers have continued to develop solenoid injectors in parallel with their piezo counterpart, and it is being observed that they are being marketed separately. This is summarised in Table 2.2.

Actuator location

The actuator location has performance benefits for the injector, and is located either on the top of the unit or in-body. The actuator is located above the injector's control valve that controls the injection event. When the actuator is energised by the ECU, the control valve is moved off its seat and the HP fuel within the control volume that applies a force to keep the injector needle on its seat is leaked to the LP fuel system. This reduces the force acting on the needle and the needle lifts off its seat due to HP fuel acting around the needle seat. When the needle is lifted, the injector injects.

In-body actuators have the control volume directly above the needle, whereas top-mounted actuators require a control piston to connect the control volume to the needle. The addition of the control piston causes two main problems: continuous leakage and increased moving mass, or inertia. A path is required to carry fuel that seeps past the needle guidance and up into the injector, away from the top of the needle, otherwise the needle will not lift off its seat when the injector is actuated due to fuel pressure forcing the needle on its seat. In theory, the control piston and continuous leakage exit path could simply be eliminated; however, the significant increase in

Table 2.2 Comparison of solenoid and piezo injectors

Injector actuator	Volume production	Engine power density	Engine emissions requirement	Cost premium
Solenoid	Very high	Low/average	Low/average	No
Piezo	Low/medium	High	Stringent	Yes

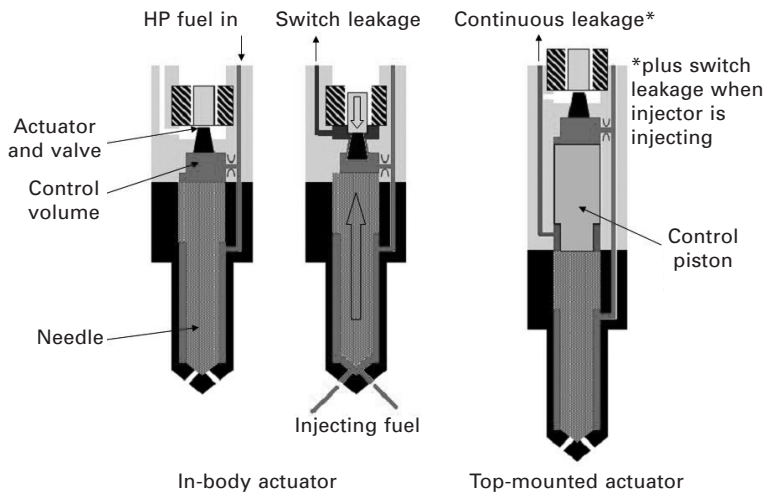
the control volume would change the injector operating speed and increase switch leakage quantity. This is shown in Fig. 2.10.

The benefit of reduced inertia due to in-body actuators not requiring a control piston leads to faster and more direct control of the injector needle, leading to improved injection quantity and tolerance control.

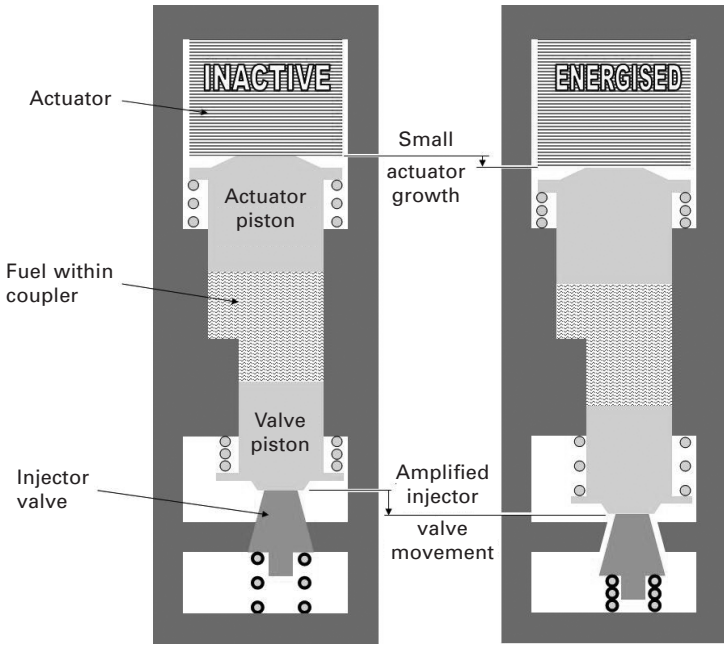
Piezo actuators

Piezo actuators, comprising a stack of crystals that elongate when a current is applied, have a relatively small movement when compared to solenoids, typically 0.1% (or 1 μm per mm stack length). This small movement requires tight component and assembly tolerances within the injector as well as movement compensation due to effects of ageing and temperature, for example.

The Bosch CRI3 piezo injector incorporates a combined hydraulic amplifier/gap compensator. The operating principle is that the actuator remains in contact with the injector valve at all times and the movement of the actuator is amplified via differential diameters in the hydraulic amplifier. A spring maintains the actuator pistons in contact with the actuator, and two additional springs keep the valve piston and injector valve in contact with each other; however, the injector valve spring has a higher spring force to ensure that the valve remains closed when the actuator is inactive. The piston springs ensure that there is no gap between the actuator and the injector valve, as well as ensuring that any leaked fuel from within the coupler is drawn back in. This is shown in Fig. 2.11.



2.10 Diagram showing injector function versus actuator position.



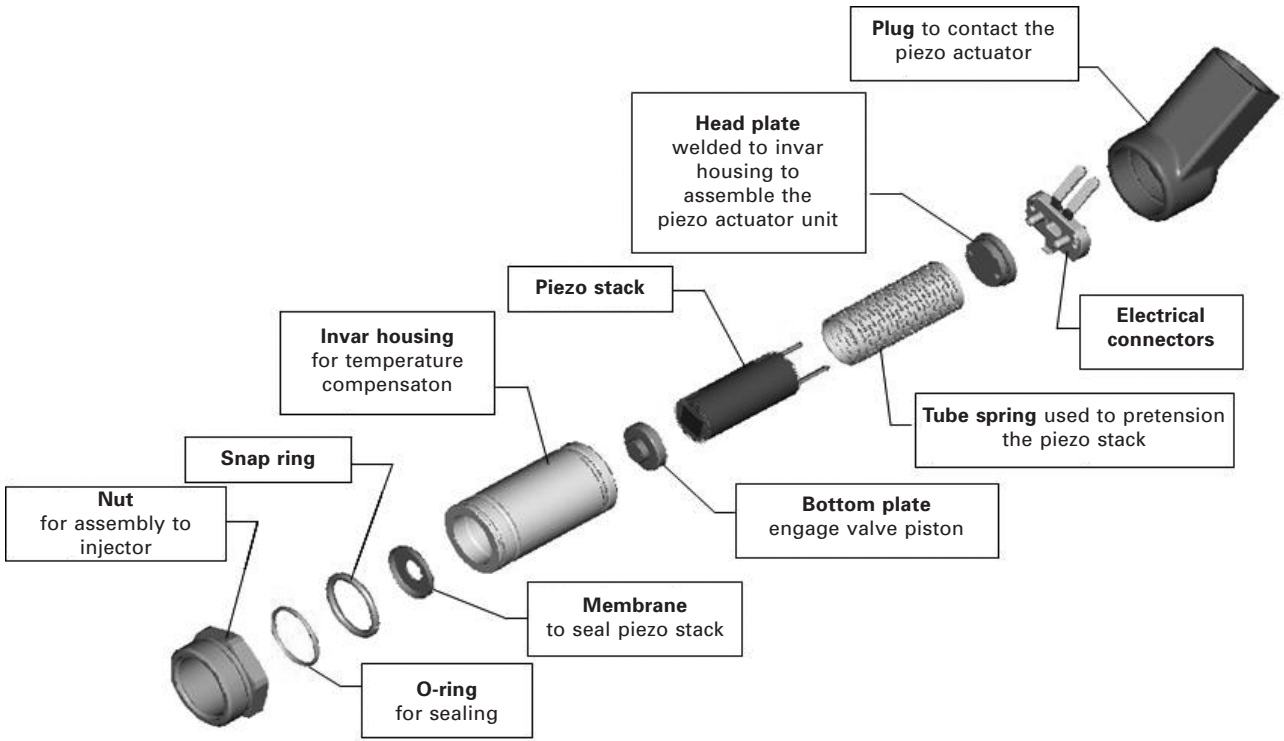
2.11 Function of injector hydraulic amplifier.

2.4.2 Continental (Siemens)

SiemensVDO of Germany, now Continental, made a strategic decision to enter the diesel fuel injection market and developed a second-generation 1500 bar common rail system utilising an innovative piezo actuator for their injector. Piezo actuators have a four times faster response time than conventional solenoids, thus enabling smaller pilot injections to be used and at least five injections per cycle (Christoffel 2002). Initially introduced for the Peugeot DW10 2.0 litre engine in 2001, it was the first volume production of a piezo common rail injector. The system was further refined with detailed changes to achieve 1650 bar and introduced for the Ford/Peugeot 2.7 litre V6 engine in 2004.

In principle, the injector is typical of traditional common rail injectors with the piezo actuator positioned high on the injector body to trigger the servo-valve, which allows pressure to build up or decay, above a control rod acting on the nozzle needle, as described above in Section 2.3.2. Figure 2.12 shows the Continental piezo actuator details and construction.

Small pilot injections are a major enabler for the combustion noise/emissions trade-off required to meet more stringent emissions standards. This fuel injection system has recently been introduced for the Peugeot/Ford joint venture 1.4 diesel, which is used in the Citroën C3 and the Ford Fiesta.



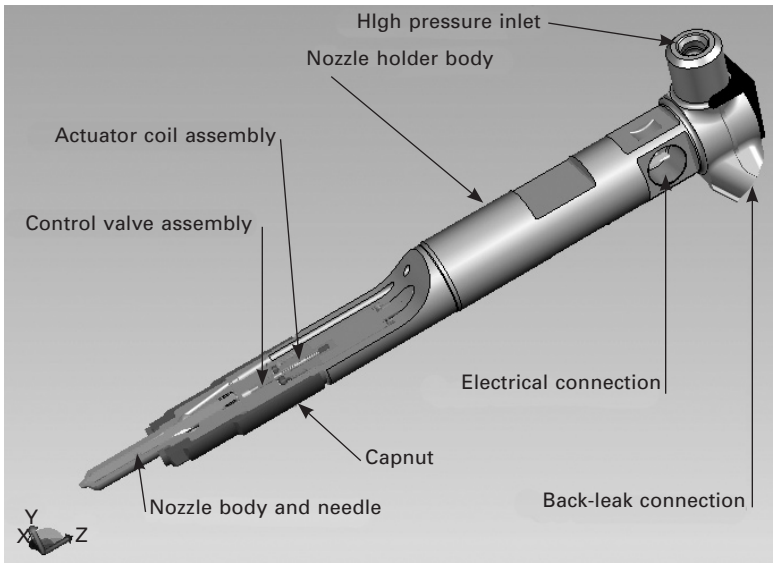
2.12 Continental piezo actuator details and construction (courtesy of Continental).

2.4.3 Delphi

Lucas Diesel Systems, now under the Delphi company and trade name, reported on its design of a diesel common rail fuel system at the 1998 SAE Congress. Guerrassi and Dupraz (1998) described this company's new addition to the fuel injection system market. This system had a number of novel features associated with the pump and injectors. The pump operated on the same principle as the company's rotary distributor pumps, using the concept of an internal cam ring and radial plungers, like the DPC and EPIC pumps, but in this case there were two separate pairs of plungers, phased at 90° and spaced axially along the pump. The cam ring had four lobes giving eight filling and pumping strokes per revolution. This arrangement gave a large delivery capability, reduced the magnitude of the pressure pulses and resulted in a more even drive torque. The plungers were operated by roller shoes, as in the earlier pumps. A pair of inlet and high-pressure outlet valves was located in the hydraulic head for each pair of plungers. An inlet metering solenoid valve was mounted at the inlet to the pump to control delivery. A pressure-regulating valve was mounted adjacent to the high-pressure outlet. The ECU-controlled rail pressure was by modulating these two valves, depending on the mapped fuel delivery and demanded rail pressure.

The injector was a very clever design, because unlike the other manufacturers, Lucas designed the electro-hydraulic common rail injector within the envelope of a traditional 17 mm diameter injector. This meant there were no installation changes for the engine manufacturer to move from a pump-line-injector to a common rail injector. The injector operated in the same way as other common rail injectors, in that a solenoid operated servo-valve controlled hydraulic pressure to cause a force to act on the nozzle needle to hold it closed, or when activated, to cause it to open, providing an injection. The solenoid and small balanced two-way control valve were located at the nozzle end of the injector body. To cause an injection, the ECU energised the solenoid, which lifted the control valve, allowing fuel to flow to the low-pressure return, thus reducing the pressure in the control chamber above the needle. With rail pressure acting on the opposing surfaces of the needle causing the net force on the needle to be in the opposite direction, the needle opened, causing an injection (Guerrassi and Dupraz, 1998). Figure 2.13 shows a Delphi common rail injector.

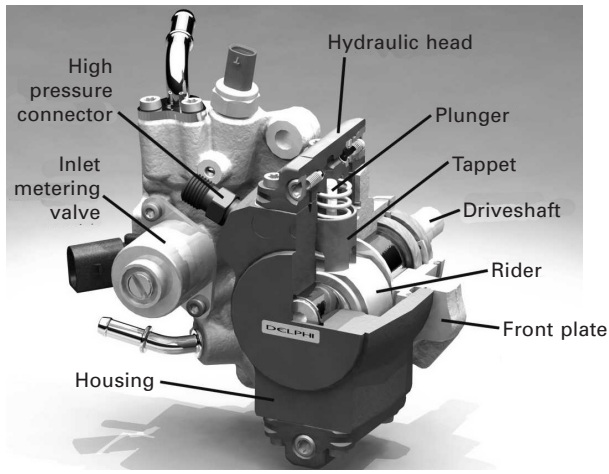
In 2005 Delphi launched their second-generation 2000 bar Multec™ diesel common rail system. The major change from the earlier first-generation system was the introduction of a completely new family of high-pressure pumps covering capacities from 0.5 to 1.5 cc/rev. This has been achieved with two and three plunger pumps with 6.5 mm and 7.5 mm diameter plungers. This pump operates on the same basic principle as the Bosch CP1, the Continental and Denso pumps with a single eccentric on the pump shaft,



2.13 A Delphi common rail injector (courtesy of Delphi Diesel Systems Ltd).

onto which runs a ring or rider that has two or three flats depending on the number of cylinders. A slipper tappet for each cylinder rests on the flat of the rider. As the shaft is rotated the eccentric causes each tappet to move outwards, pushing its plunger up the cylinder to compress the fuel, which is pressurised and flows out of the high pressure outlet valve to the rail. As the eccentric continues to rotate, the tappet and plunger move inwards and fuel is drawn through the inlet valve into the cylinder for the next stroke. Delivery control is by an inlet metering valve, which throttles the flow into the high-pressure cylinders and ensures that only the fuel quantity demanded is pressurised. A low-pressure transfer pump and pressure-limiting valve to feed the high-pressure stage is offered as an option (Jorach *et al*. 2007). Figure 2.14 shows a Delphi common rail HP pump.

Delphi's latest technology offering is its Direct Acting Diesel Common Rail (DADCR), whereby the injector needle movement is controlled directly by a piezo actuator, thus also enabling proportion control of the needle lift. The injector is capable of injecting at pressures up to 2000 bar with seven or more injection events per engine cycle. Apart from the enhanced injector performance attributes, one of the key advantages for vehicle manufacturers is the fact that there is no return, or back-leak flow, from this injector. This reduces the parasitic losses of the system and enables a smaller-capacity high-pressure pump to be selected. It also eliminates the need for the leak-off tubes and reduces the heat rejection from the fuel system, which would probably eliminate the need for a fuel cooler (Birch 2008).

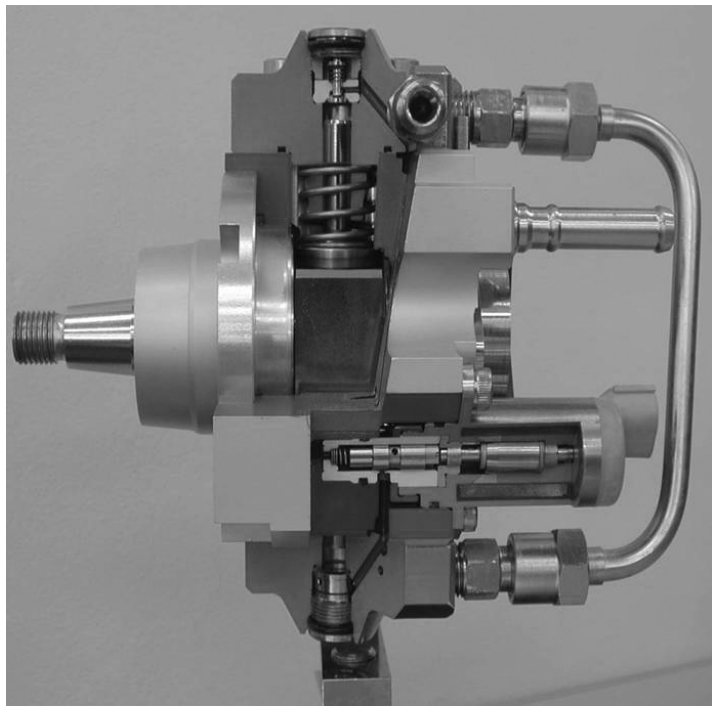


2.14 A Delphi common rail HP pump (courtesy of Delphi Diesel Systems Ltd).

2.4.4 Denso

Denso introduced their first common rail fuel injection system for passenger cars at 1450 bar in 1999. The Denso common rail system was further developed to achieve a peak rail pressure of 1800 bar in 2002, the highest common rail system pressure in the world at that time, and was applied to the Mazda MPV the following year. Takeuchi and Toyao (2003) described Denso's second-generation 1800 bar system; the injector was an evolution of the earlier unit. For the higher pressure, strength and sealing were improved and leakage was reduced, and the command piston diameter was reduced from 5.0 to 4.3 mm to reduce the force on the seat and seat wear. To improve the response time the solenoid was improved and the weight of the moving parts reduced. New high-pressure pumps were developed for the 1800 bar system; a twin plunger pump with cylinders at 180° for automotive use and a three-cylinder for medium-sized truck engines. Figure 2.15 shows a sectioned Denso automotive twin cylinder HP pump. A plant was set up in Hungary to manufacture the system for European applications with production starting in 2003 and then in Thailand for 2004.

It was a typical diesel common rail fuel injection system with a high-pressure pump supplying a rail and injectors connected to the rail by high-pressure pipes. This system used Denso's advanced solenoid injectors, capable of up to five injections per engine cycle. Figure 2.16 shows a sectioned Denso common rail solenoid injector. Lubrication flow from the pump and back-leak from each of the injectors returned back to the fuel tank. An engine control unit (ECU) contained the electronic injector driver unit and took input from



2.15 A sectioned Denso automotive twin cylinder HP pump (courtesy of Denso).



2.16 A sectioned Denso common rail solenoid injector (courtesy of Denso).

the various sensors. Rail pressure was set via pump inlet control valve with feedback from the rail pressure sensor.

The Denso injector is a traditional common rail type with a high-mounted solenoid operating a servo-valve to trigger injection via a control rod acting on the needle in the nozzle. Continuous refinement of the specification has enabled the same basic design to be operated at up to 1800 bar.

In striving to improve the response of the system, Denso developed jointly with Toyota a piezo injector, which the company started manufacturing for the 1800 bar system in 2005 and which went into production on various Toyota vehicles. The injector configuration was quite different from the conventional solenoid unit that had been in production since 1999. The piezo-electric stack was located in the injector body, rather than on top of the body as in the case of the solenoid actuator. As with other piezo injectors, the expansion of the stack when an electric charge is applied was used to trigger an injection. The small displacement of the piezo stack is transmitted via a hydraulic amplifier, which magnifies the motion while also absorbing any tiny movement caused by differential thermal expansion between the piezo stack and the injector body. Instead of a traditional servo-valve, this injector has a pressure balanced control valve, which is capable of opening and closing a large port area with a small displacement from the piezo stack via the hydraulic amplifier. This control valve regulates the pressure acting on the end of the nozzle needle, from rail pressure to the much lower return pressure when the piezo is actuated by an electric charge, thus causing the needle to lift and injection to start. The piezo injector can deliver five injections per engine combustion cycle with a minimum interval between a pilot and main injection of 0.1 ms (Oki *et al.* 2006, Tomishima *et al.* 2008).

In response to the requirements of the diesel engine manufacturers to meet ever tightening emissions regulations, CO_2 targets and higher specific power demands, Denso is developing a third-generation 2000 bar solenoid common rail system. Compared to the second generation, the third generation has the following improved features according to Tomishima *et al.* (2008):

- A finer atomised spray achieved by the higher injection pressure (2000 bar)
- Reduced fuel leakage and higher efficiency due to the optimised design of the moving parts
- A quicker response by employing a faster solenoid.

To operate at the higher pressure each part of the third-generation injector, known as the G3S, has been enhanced, although the external dimensions of the injector have been kept the same as the second generation to provide interchangeability for the engine manufacturer. The leakage from the two-way servo-valve has been reduced and the magnetic circuit of the solenoid

valve has been improved to provide faster valve opening and closing speeds (Tomishima *et al*. 2008).

2.5 Nozzle technology

The nozzle is an extremely important part of the injector, since it creates the fuel spray and the level of atomisation and spray penetration is critical for the combustion process. Nozzle designs for HSDI engines fall into two broad categories, nozzles with a sac and those without a sac. The sac is a small volume that is located below the needle seat, from which the holes radiate. Current common rail injectors have conical sac nozzles for reasons of strength and to minimise the sac volume. The sac volume needs to be minimised for current low emissions engines because the fuel left in the sac after the injections escapes late in the combustion cycle and causes hydrocarbon emissions. To avoid this, nozzles were developed without a sac volume; these are known as 'valve covered orifice' (VCO) or seat-hole nozzles by Bosch. With this type of nozzle the holes radiate from just below the needle seat. However, while this type of nozzle minimises the hydrocarbon emissions due to late dribbling of fuel into the combustion chamber, their spray quality is not as good as with a sac nozzle because of the throttling effect of the needle at low lift from its seat. It is therefore now more common to have micro-sac type nozzles, where the holes radiate from a very small sac.

Nozzle technology and feature specification has enhanced dramatically since the early days of the HSDI diesel engine, when nozzles were simply specified by the number of holes, hole diameter, cone angle and an offset or side angle, because the injectors were installed at an angle to suit two-valve per cylinder head designs. Sac volumes had not been optimised for low emissions at that time and were huge in comparison with modern state-of-the-art nozzles. Nozzle hole diameters were large in comparison to today, because emissions were not a strong consideration and the fuel systems did not have the high pressures that are available today. The holes were also parallel, since the fuel system suppliers had not developed the technology to offer conical or rounded entry holes.

Today, nominal hole diameters are feasible down to around 100 microns diameter using electrical discharge machining (EDM) methods, and nozzles can be manufactured with a conical cross-sectional shape, having a smaller diameter at the outlet compared to the diameter inside the nozzle, and the entry at the nozzle end can be rounded by a 'hydro-eroding' process. Both these processes improve the flow efficiency or the discharge coefficient of the holes and increase the spray momentum. Caprotti *et al*. (2006) showed by CFD modelling that by increasing the hydraulic efficiency with a conical spray hole, the areas of high vapour fraction are reduced. Conical holes and hydro-eroding are used today so that advantage can be taken of small

holes for better atomisation, while the higher efficiency gives better flow rates. Up to 10 of these small holes can now be produced in a nozzle for an automotive injector.

Two alternative equations are used in the industry to define the conic section of the hole:

$$\text{Cone-factor} = \frac{D_i - D_o}{10} \tag{2.2}$$

where:

D_i = inner hole diameter (μm)

D_o = outer hole diameter (μm).

or

$$\text{Cone-factor} = \frac{D_i - D_o}{10\,L} \tag{2.3}$$

where L = hole length (mm).

$$\text{Hydro-eroding (\%)} = \frac{F_a - F_b}{F_b} \times 100 \tag{2.4}$$

where:

F_a = nozzle flow after hydro-eroding

F_b = nozzle flow before hydro-eroding.

2.5.1 Nozzle deposits

Injector nozzle deposits are not new; indirect injection pintle nozzles were prone to carbon deposit build-up that affected the shape of the rate of discharge curve and hence the combustion characteristics, often leading to noisy combustion. Early DI engines seemed relatively immune to this phenomenon. However, to meet the stricter emissions requirements and provide competitive specific power, diesel engine development is demanding higher efficiency nozzles with a larger number of small holes operating at temperatures up to around 300°C. This harsh environment coupled with the small hole diameter with lower levels of cavitation within the hole, due to the improved design for higher flow efficiency, means that current nozzles are much more susceptible to formation of deposits within and/or around the holes. This is generally known as ‘coking’ within the industry. The effect of deposits in the holes is a reduction in the hydraulic diameter and a consequent loss of flow. Since all current common rail systems use time-based control for the injection period, a reduction in the hydraulic diameter results in a lower injection quantity than demanded; this will, for example, lead to a reduction in power. As a result of this phenomenon, diesel engine manufacturers and the petroleum industry have developed coking tests, which

will generally include periods at high load and maximum power to promote the highest injector nozzle temperature conditions.

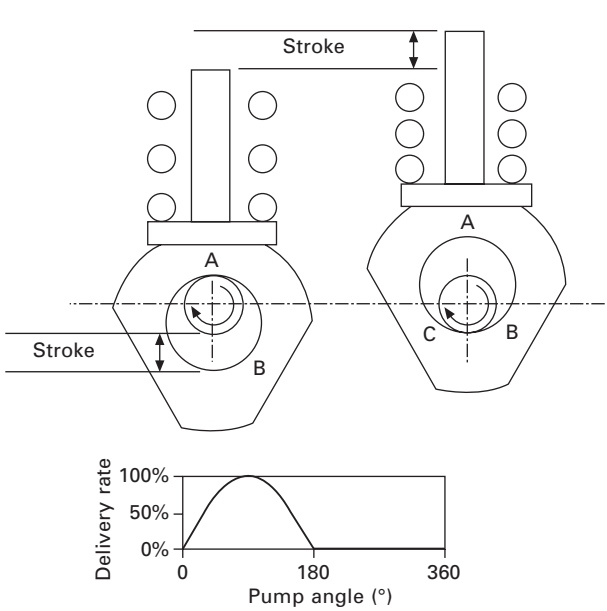
Birgel *et al*. (2008) review published literature on injector hole deposit formation and confirm that the three main influences are temperature, fuel composition and nozzle geometry. They conclude that at nozzle temperatures around 300°C fouling occurs through thermal condensation and cracking reactions, but the chemical and physical processes that lead to deposit formation are not known or well understood owing to their complexity. The sensitivity to coking is influenced by the design of the holes through cavitation; implosion of cavitation bubbles limits the level of deposits.

It has been well reported (Barbour *et al*. 2007, Birgel *et al*. 2008, Caprotti *et al*. 2004, 2005, 2006, Ullmann *et al*. 2008) and experimentation at Ford has also confirmed that contamination of diesel fuel with trace levels of metals such as copper and zinc, even at very small concentrations in the order of one part per million (ppm), will have the effect of increasing the rate of deposit formation. Caprotti *et al*. (2006) demonstrated that the initial rate of deposition was much higher with 3 ppm level of zinc present in the fuel, compared to 1 ppm, but the deposit reached an equilibrium level earlier than with a 1 ppm contamination level. Barbour *et al*. (2007) showed that the fouling tendency of the fuel dropped off sharply below 0.6 ppm zinc contamination. It has not been proven in the literature, but it is possible that zinc is having a catalytic effect, accelerating the rate of deposit formation.

Finally, Barbour *et al*. (2007) conclude that recent developments in fuel detergent design have produced new detergents that are capable of providing exceptional performance in all the engine designs that they tested, but further comment on fuel additives is beyond the scope of this chapter.

2.6 High pressure (HP) pump technology

In recent times, the trend of diesel HP pumps offered from suppliers has changed from an eccentric cam type to a cam-and-roller type. The main reason for this change is to increase pumping efficiency which is achieved by increasing the velocity of the pumping pistons. On an eccentric cam type pump, a pump piston travels from the bottom of its stroke to the top of its stoke in half a pump revolution, as shown below, and its velocity can be determined. This is shown in Fig. 2.17. On a cam-roller type pump, the rotation angle of the pump required for the piston to travel its stroke is defined by the profile of the cam, and this is typically 90° (or a quarter of a pump revolution). Compared to an eccentric cam type pump, the piston on a cam-roller type pump travels at twice the mean velocity. Added to this, it is possible to modify the cam so that an additional lobe is added. This allows the cam-roller type pump to give two high-efficiency deliveries per pump revolution. This is shown in Fig. 2.18. By allowing the plunger to pump



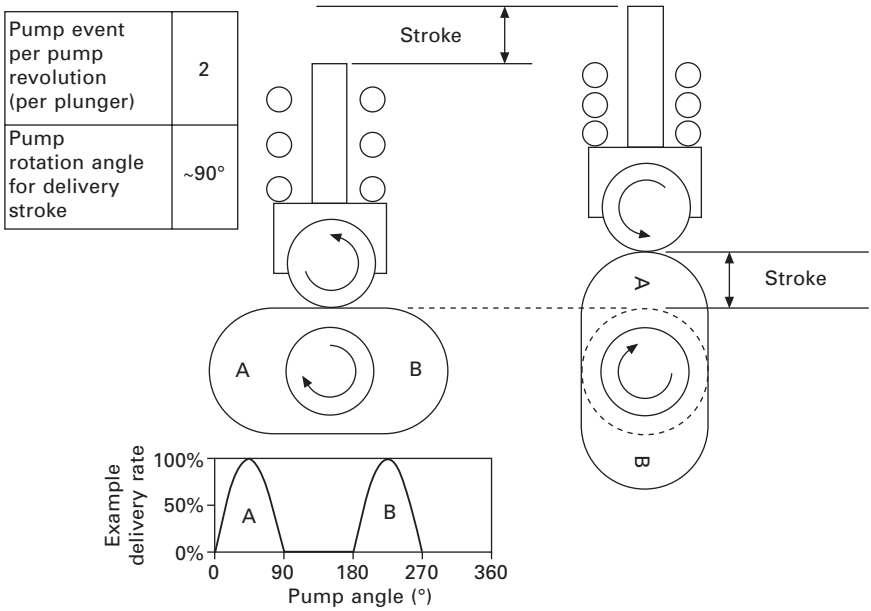
Pump event per pump revolution (per plunger)	1
Pump rotation angle for delivery stroke	180°

2.17 Eccentric cam delivery characteristics.

twice per pump revolution, this allows the HP pump to be 'downsized' by using fewer and smaller-capacity plungers.

Multi-plunger HP pumps allow additional capacity, but introduce delivery variations. A single-plunger single-lobe cam pump has a consistent HP delivery – this is optimum. For the cam-roller type pump the addition of the second cam lobe introduces a small variation between cam profiles. Multi-piston pumps, however, have larger variation, or introduce considerable cost at the HP pump assembly plant. The one-way valves that each HP plunger requires, which control flow direction in and out of the HP units, have a tolerance which leads to variation. The impact of this variation leads to increased rail pressure variation between engine firing events.

To minimise injector fuelling variation the HP pump has an important contribution. Every time the engine has a combustion event, the fuelling variation can be minimised if the rail pressure in the HP rail is consistent. To achieve this, synchronous delivery from the HP pump is important. Ideally, the HP pump should deliver once per firing event, ideally from the same plunger as mentioned above. To achieve synchronous delivery, the HP pump drive ratio and the number of HP plungers can be tuned – for example, the HP pump on a six-cylinder engine needs to deliver three times per revolution, achieved by a three-piston eccentric cam pump running at



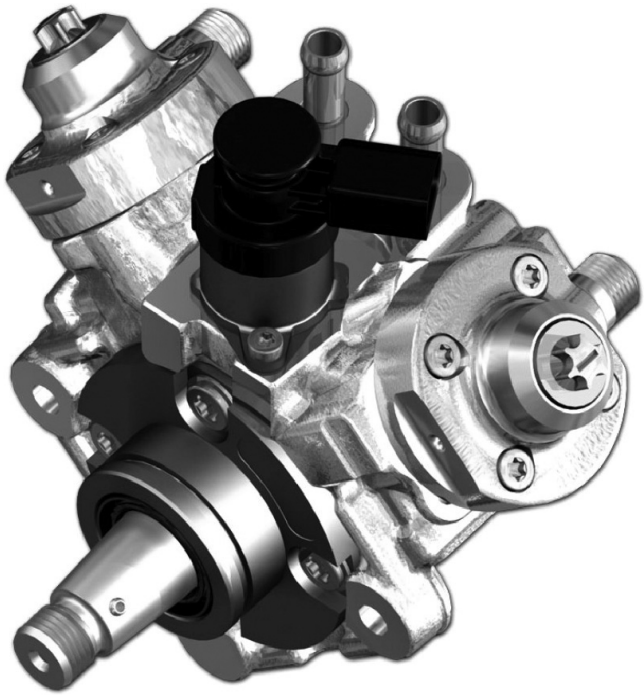
2.18 Cam roller delivery characteristics.

engine speed, or a two-plunger twin-cam cam-roller type pump running at 0.75 times engine speed.

The series production Bosch CP4.2 two-plunger cam-roller type pump is shown in Fig. 2.19. HP pumps require an input torque to rotate the drive shaft. The drive torque profile is a function of the delivery rate; high delivery rates require high drive torque. As individual pumping events produce individual pumping spikes in the drive torque profile, this can be minimised by overlapping the delivery stroke, achievable with multi-plunger pumps. HP pump delivery variation and drive torque profile have to be traded off against each other.

To assist in low CO_2 vehicles, the weight of new-generation HP pumps is reduced. This is achieved by reducing the number of pumping plungers as mentioned above and the adoption of lower weight materials for the housing, such as aluminium in lieu of cast iron or forged steel as used on some earlier designs. This allows the HP pump to achieve half the weight, typically 3.5 kg, when compared to ferrous-bodied units. Plungers on multi-plunger pumps need to be connected together, either via internal drillings on cast iron or forged steel-bodied pumps, or via HP pipes connecting the plunger units together on the pump, or separate HP pipe connections to the HP rail network. The internal drillings solution for connecting multi-plunger pumps is simple in package and design, but has a weight penalty.

A summary of HP pump attributes is given in Table 2.3.



2.19 Series production Bosch CP4.2 two-plunger cam-roller type pump.

Table 2.3 Summary of HP pump attributes

Attribute	Feature	Eccentric cam	Conventional cam and roller
Pump efficiency	Plunger speed	Limited by pump speed	High due to aggressive cam profile
Smooth drive torque	Smooth and continuous pumping	Achievable with 3+ plungers	As Eccentric, but no design exists. Non-smooth pumping due to aggressive cam profile
Low weight	Aluminium housing	Available, but requires HP pipes to connect plungers rather than internal drilling in steel housings	
Low cost	Single plunger	Requires high pump drive ratio (e.g. 1:1)	
		In development; efficiency to be verified	Conventional cam pump allows plungers to deliver twice per revolution
Stop–start ability	Rapid rail pressure rise	Possible, with sufficiently high drive ratio; especially for single plunger pumps	
Engine cylinder phasing	Aligned pumping/ firing events	Optimised pump cylinders and pump drive ratio, e.g. one pump event per firing event	

2.7 Diesel fuel injection equipment heat rejection

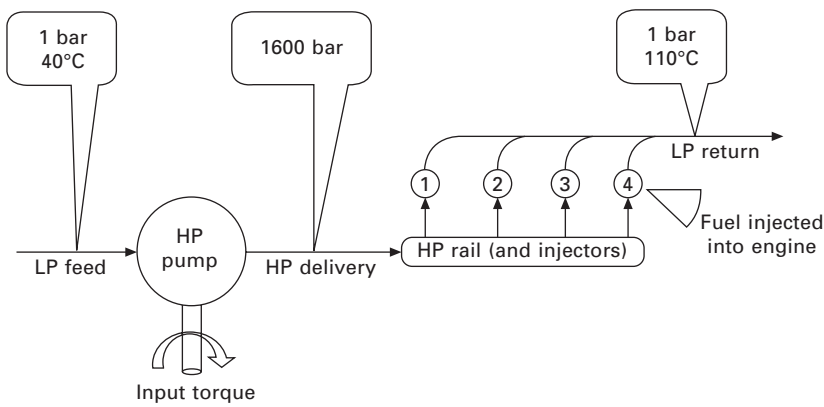
Fuel system heat rejection occurs due to internal high pressure (HP) fuel leakage from the fuel injection equipment (FIE). Energy within HP fuel is returned to the low pressure (LP) system in terms of heat, i.e. hot fuel. Fuel temperatures must be managed to avoid component temperature limits, set by their manufacturer, being exceeded, as well as to limit energy loss, which has a direct relationship with fuel consumption and therefore CO_2 emissions.

Customer usage of a vehicle can be demanding, such as operating under full engine load in hot ambient conditions. Vehicles must operate without noticeable performance degradation. Fuel system heat that has been rejected to the vehicle has to be managed, otherwise, as a last resort, the engine performance has to be de-rated (engine torque limited) to prevent excess fuel temperatures within the system.

Figure 2.20 shows typical temperatures and pressures across the HP fuel system circuit. The feed and return temperatures are where the engine fuel system interfaces with the vehicle.

A trend observed for stricter future engine emissions requirements is that the injected fuel spray into the combustion chamber needs to be atomised into ever smaller droplet sizes; this drives the development of smaller spray holes in the injector nozzle. Unfortunately for heat rejection, in order to achieve equal if not increased engine power density targets, the maximum HP fuel rail pressure has to be increased.

- Biodiesel (e.g. B10) degradation (reduction in oxidation stability) is accelerated exponentially when the fuel is hot, therefore the vehicle LP fuel system must be engineered to ensure maximum fuel temperature



2.20 Typical temperatures and pressures across the HP fuel system circuit.

limits are not exceeded, with an emphasis on reducing temperature levels.
- Heat loss from the engine results in a loss of engine efficiency and thus a negative fuel economy and CO_2 impact, therefore the engine should be optimised to minimise heat rejected to fuel.

2.7.1 System overview and sources of heat

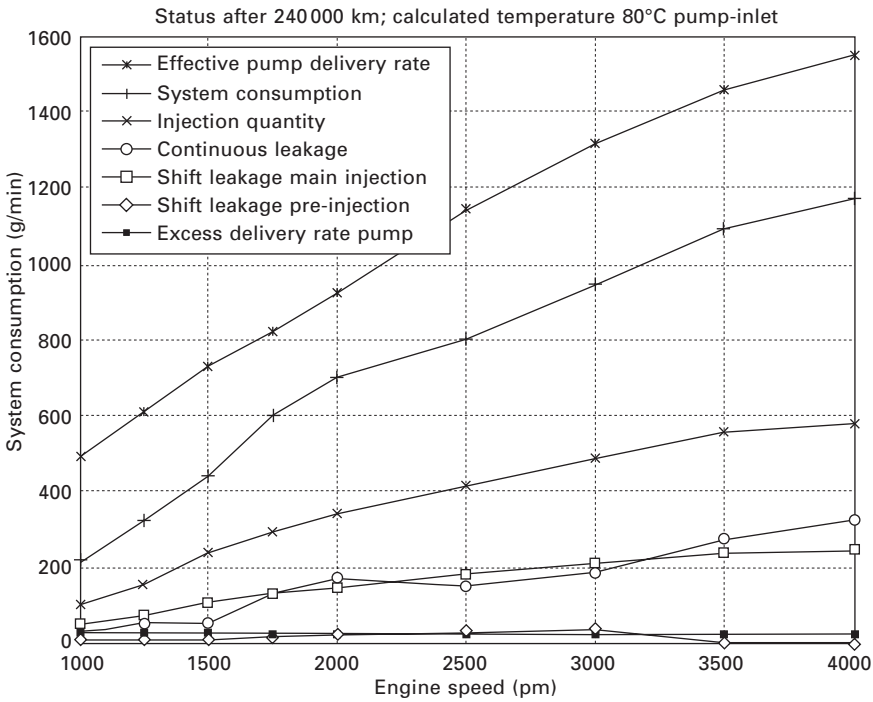
On certain injectors, continuous leakage occurs regardless of an injection event. Continuous leakage quantity is a function of fuel rail pressure and occurs as fuel seeps along clearances in the injector. Switch leakage occurs on servo-assisted injectors where HP fuel that acts on the needle nozzle to prevent the injector from injecting fuel is released to allow the needle to lift and the injector to inject.

In addition to the fuel required for engine operaton, the HP pump requires a quantity of fuel for lubrication of internal components where heat is generated by friction within the pump (sliding surfaces create heat; this friction increases the HP pump drive torque). Hot fuel is also generated by HP fuel leaking past the plungers (due to clearance between plunger and bore) and pressure control valve (PCV) leakage; this is a solenoid valve that is hydraulically connected to the HP rail and, when requested, can drop rail pressure by spilling HP fuel back to the LP circuit, which occurs during transient rail pressure reductions during customer drive cycles. A typical system consumption graph for the various component flows at end of life after 240 000 km is shown in Fig. 2.21.

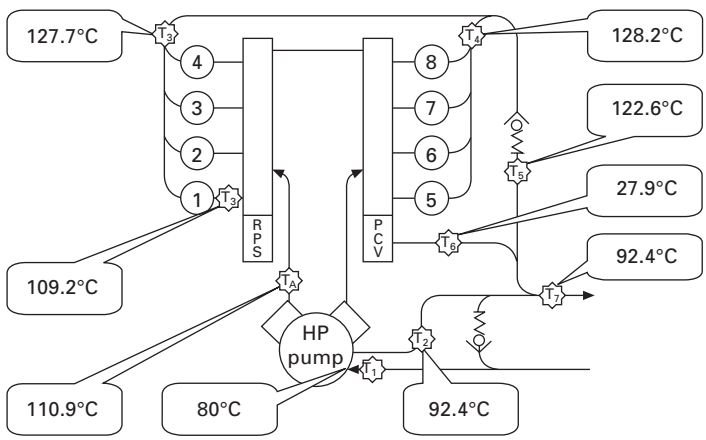
2.7.2 Engine testing

HP fuel system heat rejection measurements on a V8 4.4L Eu5 emission engine were completed. Maximum observed fuel temperatures around the fuel system are shown in Fig. 2.22. These occurred at 4000 rpm 100% engine load.

- The greatest rise in fuel temperature across the system was at the HP pipe surface measurement. Here the fuel had increased in pressure up to 2000 bar.
- The fuel temperature increases further when spilled from the injector, measured at the injector leak-off.
- A temperature drop was observed along straight tubing, indicating a radiated cooling effect from the colder test cell air temperature.
- The low PCV spill temperature confirms that there is no flow past the PCV during steady-state operation; the thermocouple was checked for calibration.



2.21 Typical system consumption graph for the various component flows at end of life after 240 000 km.



2.22 Maximum observed fuel temperatures around the fuel system.

2.7.3 Opportunities to reduce heat

The heat rejection equation (Lawther 2008) derived is:

$$Q = \dot{V}\rho C_{\mathrm{p}}\Delta T \qquad 2.5$$

where:

Q = heat (kW)
$\dot{V}$ = volume flow rate (m^3/s)
ρ = fuel density ~ 835 kg/m^3
C_p ~ 2005 J/kg.K
ΔT = fuel temperature change (K).

The fuel is heated due to energy transfer within the FIE system, therefore reducing the energy will lower the temperature. The rail pressure, or load, on the system is the engine calibration demand required to meet engine emission, so cannot be changed. Friction of moving components can be reduced where possible to reduce heat. The quantity of heat is determined by the flow, which can be reduced by measures such as lower leakage injectors, and improving the piston to plunger clearances in the HP pump to reduce leakage. As density and specific heat capacity are considered constant and not directly controllable, and as temperature has a direct relationship with rail pressure (an engine calibration requirement), the only variable is flow rate which is reduced in the latest-generation state-of-the-art systems.

2.7.4 Managing rejected heat

Fuel coolers (or heat exchangers) perform when the fuel temperature is higher than the surrounding coolant/air temperature. In order to increase fuel cooling performance, higher fuel temperatures are required. The data from Fig. 2.22 shows that fuel temperatures from the injector are higher than those from the HP pump return. The PCV spill temperature is high when the PCV is activated. There is a benefit in cooling only injector and PCV spill flows if necessary to maximise fuel cooler performance.

To reduce biodiesel fuel degradation (maintain oxidation stability), fuel temperatures should be kept to a minimum. Recommended engine design focuses on optimising temperatures, not just heat. This could involve circulating cold fuel around the leak-off rail to dilute the hot fuel.

2.7.5 Conclusions

- Diesel engines reject heat into diesel fuel that is being returned by the HP fuel system to the LP fuel system in terms of hot fuel.
- Heat rejection results in a loss of engine efficiency, a negative fuel economy and CO_2 impact.
- Reduction of heat rejection is possible with new-generation technology FIE, but this has a cost premium and therefore total vehicle system cost vs. performance gain is to be considered.

2.8 Electronic control of fuel systems

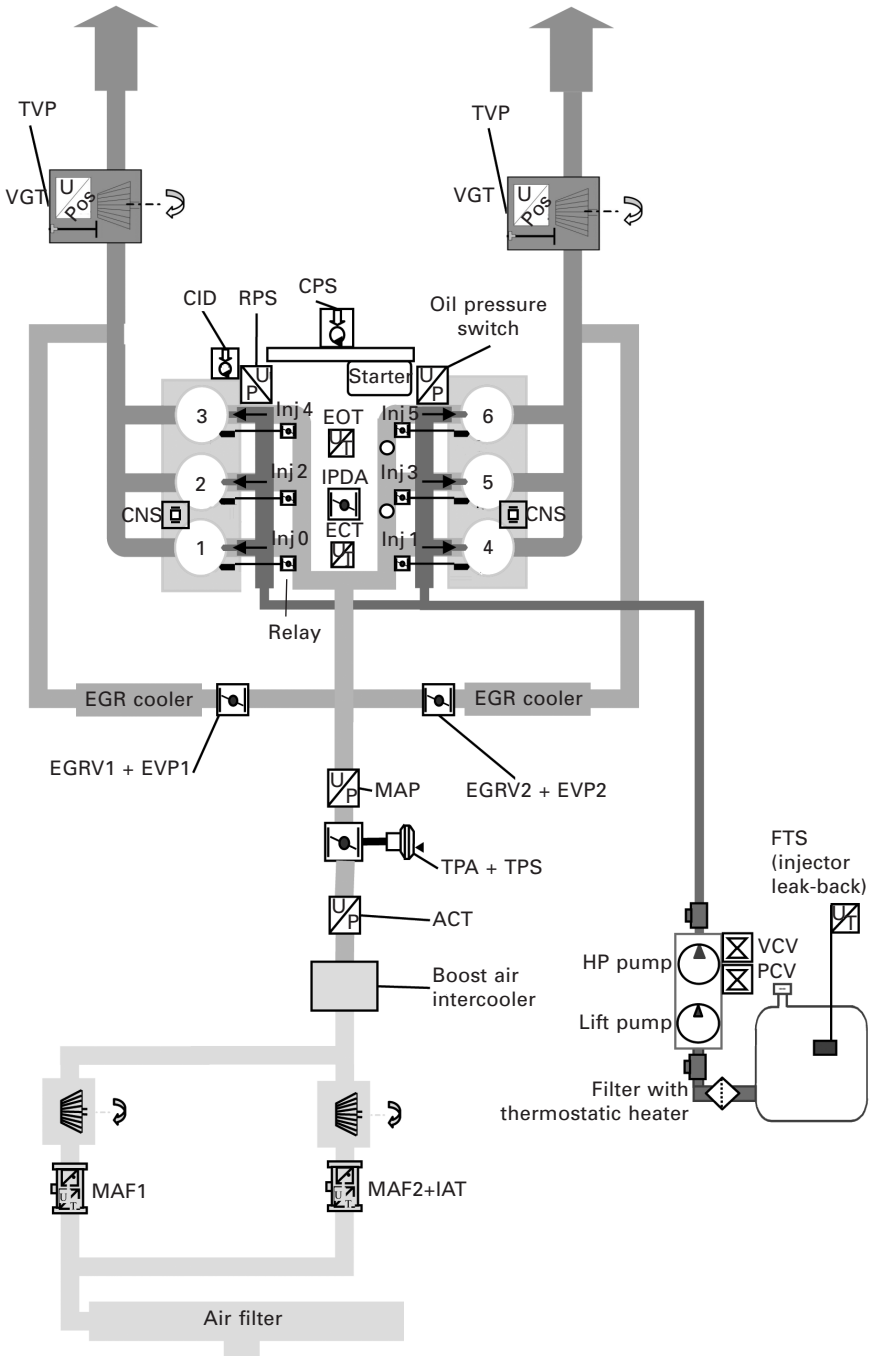
2.8.1 Power-train controls introduction

All automotive diesel fuel systems are now controlled by a micro-processor based electronic control unit (ECU). In most cases, the whole engine or even the whole power-train (including the transmission) are controlled by a single ECU and the diesel fuel system is just one of about 10–15 sub-systems which are managed by the ECU. All modern high-speed diesel engines utilise some form of common rail fuel system and these are all controlled electronically. The key inputs for the fuel system control are the engine crankshaft speed and position, the desired fuel injection parameters and the desired/achieved pressure of the fuel delivered to the injectors by the common rail. The key outputs control the duration of opening of the injector (and sometimes lift or rate of movement) and the pressure in the common rail. A typical system diagram for a V6 diesel is shown in Fig. 2.23.

2.8.2 Control system history

The first petrol engine controls went into production in around 1968 using very simple discrete analogue electronic control circuits. By the early 1980s simple micro-processor based control systems had been introduced on some petrol engines and the first engine control software was developed. The first diesel passenger car electronic control system was released to production by Bosch in the late 1980s (VP34-IDI-BMW323) and another system was released by Lucas in 1992 (EPIC80-DI-Ford Transit). These first systems were developed from the mechanically controlled rotary-distributor pumps commonly used at that time. The Bosch VP34 used an electric actuator to control the pumps' fuel delivery and an electro-hydraulic actuator to control injection timing. Other engine systems were also controlled, such as exhaust gas recirculation (EGR), and these systems were also the first drive-by-wire systems released (petrol engines at the time usually still had a direct mechanical linkage between the accelerator pedal and the throttle). Drive-by-wire systems are considered more safety critical, as a software or electronic error could lead to a vehicle run-away and so all such systems include some level of independent watchdog monitor, to ensure all failures can be safely managed.

During the 1990s all light-duty diesel engines migrated from indirect injection (IDI) to direct injection (DI) and electronic control became standard. By the early 2000s, almost all DI diesel engines had migrated to use common rail systems and electronic control was a key enabler for such systems. The complexity of electronic controls has grown exponentially since the first systems were introduced in the late 1980s. The Lucas EPIC EP5 ECU for the 92MY Ford Transit used a Motorola 68HC11 micro-processor with a 2



2.23 Typical V6 system diagram.

MHz clock speed, 384 bytes of RAM and 32 KB of ROM. The latest Bosch EDC17 ECUs use an Infineon Tri-Core TC1797 micro-processor with a 180 MHz clock speed, 128 KB of RAM and 4 MB of ROM.

Control software was usually written directly in assembly language on the first production power-train control systems. This enabled very simple but efficient code to be used, providing quite complex control, with very cheap and simple micro-processors. During the 1990s most ECU code developers moved to ANSI-C code for all but the low-level code development. The trend now is for a large amount of the code to be developed using model-based coding techniques. Typically new functions are now developed in a graphical modelling tool, such as Matlab/Simulink/Stateflow or ETAS ASCET, and these models can then be tested offline on a workstation or online using rapid-prototype techniques. These models can then be used to produce production auto-coded using tools such as Matlab RTW-EC, dSpace TargetLink or ETAS ASCET. Fixed-point maths and data types are often still used to reduce memory consumption but there is an increasing trend towards floating-point code and most ECUs now provide 32-bit micro-processors, with hardware floating-point capability.

2.8.3 ECU hardware

Most ECUs are built to a cost and so tend to use mature high-volume electronic production techniques. ECUs are usually chassis mounted, as this provides a less harsh environment, although some higher cost ECUs are engine or even fuel system mounted. A single fibreglass printed circuit board (FR4/5-PCB) is often used to provide both digital and analogue control circuits. Most ECUs use multi-layer PCBs, to enable the components to be fitted into the space available. Packaged surface-mounted components are typically used, although bare die chips are sometimes used for high temperature/vibration environments on-engine. Usually, as much of the required functionality as possible is implemented in software or with custom digital hardware, integrated into a single micro-processor chip. This generally gives the most flexible and lowest cost solution. Various other custom application-specific integrated circuits (ASICs) are used to provide input/output and other circuits. Power devices are usually surface mounted, with copper heat-pipes through the circuit board to conduct waste heat to the ECU case. The main connector is an important part of the ECU, because as many as 220 wires may need to be connected to various parts of the power-train or vehicle. Custom automotive connectors, with multiple pockets, are usually used to enable independent connections to several parts of the vehicle or power-train wiring harness. All current ECUs use flash ROM to store the program code and data and these can usually be reprogrammed at a service dealer or during vehicle assembly, enabling new control software or calibration to be distributed to a vehicle

fleet in the field. This provides the option to improve engine operation, if specific problems come to light after the initial launch of a vehicle. Various forms of network are used to exchange data between ECUs in a vehicle, with the most widely used being the controller area network (CAN), which was originally developed by Bosch and Intel.

2.8.4 Key fuel system control sensors

The most important sensor for CR diesel controls is the engine crankshaft speed and position sensor. Most CR systems use a 60-2 toothed-wheel system on the crankshaft and most also have a second sensor on the engine camshaft, whose main purpose is to provide phase information on a four-stroke engine. Such toothed-wheel systems provide a digital pulse to the ECU at regular angular intervals (usually 360/60 = 6 degrees). This pulse can then be compared to a free-running timer in the ECU and the time period between these pulses can be measured. This gives the average speed over the 6° interval and also provides a regular sync pulse which can be used to schedule injection events at the desired crank angles. Interpolation is used to provide continuous angular scheduling of injections. A synchronisation gap is usually provided at a single point, so that absolute crank position can be determined by counting teeth following the gap. The angular acceleration of the crankshaft is directly related to the rotating inertia of the engine and the cylinder pressure and so this signal can also be used for many other purposes, such as monitoring the combustion process and adapting the injected fuel mass, to correct for injector drift over lifetime.

The next most important sensor in a CR system is the fuel rail pressure sensor. This is used to provide feedback on the pressure applied to the injectors. The rail pressure can be varied, independent of engine speed, according to a desired schedule. The measured pressure is also used to determine how long the injectors should be pulsed-open for, to achieve the desired injection mass.

2.8.5 Key fuel system actuators

The most important actuator in a CR system is the injector actuator. Two main types of actuator are used: solenoid and piezo. Solenoid actuators are generally cheaper and simpler to control but piezo can offer more control over the actuator. In a solenoid, the current applied is proportional to the force derived. The force is also a function of the position of the actuator (size of the air-gap), and this effect is usually quite non-linear. For this reason it is not easy to control the position or velocity of a solenoid actuator and they tend to be controlled as on/off or open/closed devices. In a piezo actuator the voltage applied is proportional to the force derived and/or the

displacement and this relationship is relatively linear. In practice, this means that the displacement and velocity of a piezo actuator can be controlled with much more precision than with a solenoid. Most CR injectors use an electro-hydraulic servo actuation mechanism, where the solenoid or piezo actuator controls a valve, which in turn controls the pressure/flow of fuel around the injector needle, providing a variable force balance, which can either open or close the injector needle valve. In some cases (such as the Delhi DCR3 system) the injector needle can be directly actuated by a piezo actuator, which leads to the possibility of variable lift and rate of lift control, as well as injection duration. The electronics required in an ECU to control piezo actuators are generally more expensive and complex than those required for solenoids.

Many CR systems utilise two solenoid actuators to control the pressure of fuel in the rail. The first type is used to control the volume of fuel passing into the high-pressure pump inlet (often known as an inlet metering valve, IMV, or volume control valve, VCV). This valve varies the volumetric flow as a function of the current applied by the ECU. The second type is used to control the pressure of the fuel delivered by the pump to the common rail, by 'spilling' excess fuel back to the fuel return system (often known as a pressure control valve, PCV). This valve varies the pressure in the rail, as a function of the current applied by the ECU. Some systems utilise only one of these actuators, but this can lead to various problems with system efficiency and transient control. If an inlet valve is not available, then the HP pump will always pump at its maximum capacity and any excess fuel that is not required by the injectors will have to be 'spilled' back to low-pressure by the PCV (this leads to increased heat rejection and higher pump drive torques, thus reducing the efficiency of the engine and increasing fuel consumption). If a PCV is not available, then all control of pressure must be achieved utilising the IMV/VCV. This can be difficult due to the increased control lag introduced by working on the pump inlet. It is also generally necessary to find an alternative 'spill' path to enable rapid reduction in fuel pressure during periods of engine over-run, when the injectors are shut off. This is often achieved by sending a series of short pulses to the injector actuators, which are sufficient to provide some dynamic leakage to the fuel return system but are not long enough to open the injectors.

2.8.6 Diesel fuel system control software

The software in a typical engine or powertrain control ECU can be divided up into about 10–15 sub-systems, of which one is dedicated to the control of the diesel fuel system. Other sub-systems control other engine systems, such as the air-path, exhaust after-treatment, engine torque, combustion, and various vehicle and possibly transmission control functions. The diesel

fuel control sub-system can be divided into several software features, each dedicated to a particular control aspect. Some of the software tasks associated with control of the fuel system can be scheduled by an operating system at regular time intervals, but many of the tasks associated with the injection system have to be scheduled at variable time intervals, which are synchronised to the angular rotation of the engine. There are typically more such angle scheduled tasks associated with the fuel injection control system than in any other control sub-system. For this reason, the software used to process angular events generated by the crankshaft position sensor is very tightly linked to the injection control software. As the crankshaft rotates, the crankshaft position sensor provides a signal to the ECU at regular intervals (typically every 6 degrees for a 60-2 tooth wheel). A gap in this profile is usually used to provide initial synchronisation and then a counter in the microprocessor hardware is used to count the teeth and keep track of the angular position. Software tasks which have to be executed at specific angles can then be triggered at specific event counts. Some of these tasks are executed once for each compression cycle (e.g., every 180 degrees of crank rotation for a four-cylinder engine) and some are executed for each injection pulse (e.g., up to five or more times per compression cycle, depending on the number of multiple injections) or at other angular intervals as required to provide synchronous control of the actuators. The scheduling of the injector drive pulses is usually carried out by a specific microprocessor hardware timer function, to provide the necessary accuracy to provide stable fuel injection mass and timing control.

The common rail pressure can generally be varied independently of the engine speed and load, which provides great flexibility, in conjunction with the multiple injection capabilities of a common rail system. This pressure control is usually achieved using a closed-loop PID controller, often with various open-loop pre-control terms and various calibratable correction factors. Adaptive control is also often used, where the part–part or lifetime component variability can be learned and corrected by the control software. Such adaptation terms are generally stored in an ECU's non-volatile memory, so that they are not lost when the engine is shut down and the ECU is powered off.

Various algorithms are often used to improve the open-loop performance of the fuel system actuators, particular in respect of the injectors. The crankshaft speed fluctuations relating to the firing of specific cylinders can be used to vary the relative fuel mass demanded from each injector (without varying the mean demanded fuel value, etc.), thus correcting for any variations in actual fuel delivery from the injectors or in the combustion performance of each cylinder. This improves the smooth running of the engine, particularly at low engine speeds. Another correction can be applied to individual injector pulses to correct for the pressure waves induced in the high-pressure system

each time an injector is actuated. Typically the high-pressure system has a resonant frequency of roughly 1 kHz and this knowledge can be used to determine the effect of each injection pulse on subsequent pulses. A correction factor can then be computed, which can be used to vary the length of pulse applied, thus compensating for the fact that the average pressure applied during the pulse is not equal to the demanded average rail pressure.

2.9 Future trends

Clearly there has been a trend of increasing maximum rail pressure as common rail fuel systems have been developed and evolved from the first systems that had a peak pressure of 1350 bar to the 2000 bar of the latest equipment available for automotive use in production today. This trend has been driven by the requirement to meet more stringent emissions legislation and the desire for higher specific power, whether for premium performance cars or for engine downsizing to improve fuel economy and CO_2 emissions. This trend will continue, but at a slower rate, since the physics of achieving higher pressures requires more sophisticated designs, materials and processes in order to withstand the stresses involved and minimise the leakage and parasitic losses. Nevertheless, 2200 bar is on the horizon and further increases are likely, but the cost versus benefit equation may limit these very high-pressure systems to the premium end of the market.

An area where fuel system improvements will have to continue to be made is in increased accuracy of injection delivery, particularly for pilot injections, where deviations from the very small quantities demanded have a disproportionate effect on engine attributes, such as combustion noise and emissions. Hence improved basic injector control and reduced variation, coupled with enhanced feedback control strategies, will be required to meet more stringent emissions standards and customer expected attributes.

With the faster response of the piezo actuator, it is likely that more use will be made of this type of injector in the future, to take advantage of its quicker actuation. All the major manufacturers have piezo injectors either in production or near to production. However, this comes at a cost and it is likely that volume engines will remain with improved solenoid injectors.

To reduce high pressure pump displacement, minimise parasitic losses, avoid fuel coolers and reduce installation costs, the ultimate target for future injectors is to have no return flow. The Bosch CRI3 series of piezo injectors have only ‘switch’ leakage, in other words return flow during injection. This greatly reduces both the return flow and heat rejection from the fuel system. The new Delphi Direct Acting piezo injector is the first of a new generation of injectors which are completely leak free (Schöppe *et al*. 2008), thus meeting the above target.

Finally, with the rising costs of more sophistication fuel injection equipment

there will inevitably be a cost trade-off with exhaust after-treatment, which may in future be biased in favour of more effective downstream catalysis. There is also another threat: that of GDI gasoline engines for passenger cars, especially with stratified injection technology avoiding throttled pumping losses, and the commercial benefit that this brings compared with the cost of diesel fuel injection systems. Fuel consumption and torque of these products is good, and with lower cost fuel (petrol vs diesel) and lower cost vehicles, the balance may well swing away from diesel.

2.10 References

Automobil Revue (2008), 103, Jahrgang der 'Automobil Revue', 6 March 2008.

Barbour R, Arters D, Dietz J, Macduff M, Panesar A and Quigley R (2007), Diesel detergent additive response in modern, high-speed, direct-injection, light-duty engines, JSAE paper 20077144, SAE paper 2007-01-2001.

Birch S (2008), Delphi claims world-first for direct-acting diesel injector, *Automotive Engineering International*, 116(10), October 2008, 33.

Birgel A, Ladommatos N, Aleiferis P, Zülch S, Milovanovic N, Lafon V, Orlovic A, Lacey P and Richards P (2008), Deposit formation in the holes of diesel injector nozzles: a critical review, SAE paper 2008-01-2383.

Bosch (1999), *Diesel-engine Management*, 2nd edition, Robert Bosch GmbH, Stuttgart.

Bosch (2007), *Automotive Handbook*, 7th edition, July 2007, Robert Bosch GmbH, Stuttgart.

Bostock P G and Cooper L (1992), Turbocharging the Ford 2.5 HSDI diesel engine, I. Mech. E. Seminar on Diesel Fuel Injection Systems, 14–15 April 1992.

Caprotti R, Leedham A, Graupner O and Klaua T (2004), Impact of fuel additives on diesel injector deposits, SAE paper 2004-01-2935.

Caprotti R, Breakspear A, Graupner O and Klaua T (2005), Detergency requirements of future diesel injection systems, SAE paper 2005-01-3901.

Caprotti R, Breakspear A,Graupner O, Klaua T and Kohnen O (2006), Diesel injector deposits potential in future fueling systems, SAE paper 2006-01-3359.

Christoffel J (2002), Ceramic Muscle, Automotive Energy, 28(1), January 2002, 52–54.

Glassey S F, Stockner A R and Flinn M A (1993), HEUI – a new direction for diesel engine fuel systems, SAE paper 930270, March 1993.

Glassey S F, Holtman R H and Smith III, P E (1995), Development of HEUI fuel system for 2-3L automotive diesels, I. Mech. E. Seminar, September 1995.

Guerrassi N and Dupraz P (1998), A common rail injection system for high speed direct injection diesel engines, SAE paper 980803, reprinted from *Diesel Fuel Injection and Sprays* SP-1316, pp. 13–20, International Congress & Exposition, February 1998.

Hadler J, Rudolph F, Dorenkamp R, Stehr H, Dueesterdiek T, Hilzendeger J, Mannigel D, Krauzusch S, Veldten B, Koeters M and Specht A '(2008), Volkswagens's new 2.01 TDI engine fulfils the most stringent emissions standards, 29th International Vienna Symposium in Vienna, 2008.

Hower M J, Mueller R A, Oehlerking D A and Zielke M R (1993), The new Navistar T 44E direct-injection turbocharged diesel engine, SAE paper 930269, March 1993.

Jorach R W, Schoeppe D, Nevard R T, Thornthwaite I R and Wilson N D (2007), Delphi's 2000 bar common rail development for the Multec™ diesel common rail system, paper C660/015/07 presented at the I. Mech. E. Conference, Internal Combustion Engines: Performance, Fuel Economy and Emissions, London, 11–12 December 2007, published by Chandos, Oxford, 2008.

Kendall J (1998), VW Passat TDI 115, *Diesel Car*, September 1998.

Krieger K (1999), Diesel injection technology for passenger cars – a survey of procedures and results, *MTZ Worldwide*, May 1999, 6–8.

Lawther R (2008) Fuel system heat rejection, MSc thesis, June 2008.

Lewis G R (1992), The development of the Lucas EPIC system for HSDI diesel engines, I. Mech. E. Seminar on Diesel Fuel Injection Systems, 14–15 April 1992.

Needham J R and Whelan S (1994), Meeting the challenge of low emissions and fuel economy with the Ricardo 4-valve HSDI, *Proc I Mech E Part D*, D3, 208, 181–190.

Oki M, Matsumoto S, Toyoshima Y, Ishisaka K and Tsuzuki N (2006), 180 MPa piezo common rail system, SAE paper 2006-01-0274; Emission: new diesel engines and components and CI engine performance for use with alternative fuels (SP-2014), 2006 World Congress, Detroit, MI, 3–6 April 2006.

Peters A and Pütz W (1997), Der neue Vierzylinder-Dieselmotor OM 611 mit Common-Rail-Einspritzung, Teil 2: Verbrennung und Motormanagement, *MTZ Motortechnische Zeitschrift* 58(12) (1997) 760–767.

Rhode W, Gökesme S, Liang J R and Schmitt J L (1991), Volkswagen's new direct-injection 1.9 litre diesel engine, 3rd Aachen Colloquium, Vehicle and Engine Technology.

Riolfi R, Imarisio R and Buratti R (1995), The potential of a new common rail diesel fuel injection system for the next generation of DI diesel engines, 16th International Vienna Motor Symposium, May 1995.

Schöppe D, Zülch S, Hardy M, Geurts D, Jorach R W and Baker N (2008), Delphi common rail system with direct acting injector, *MTZ*, 69(10), 2008.

Smith D (1959), *The Modern Diesel, Automotive Oil Engines for Transport, Marine and Industrial Use*, Iliffe & Sons, pp. 69–71.

Stumpp G and Ricco M (1996), Common rail – an attractive fuel injection system for passenger car DI diesel engines, SAE paper 960870, reprinted from *Fuel Spray Technology and Applications*, International Congress and Exposition, February 1996.

Takeuochi K and Toyao T (2003), Development of 2nd generation common rail system, I Mech E C610/013/2003.

Tomishima H, Matsumoto T, Oki M and Nagata K (2008), The advanced diesel common rail system for achieving a good balance between ecology and economy, SAE paper 2008-28-0017.

Tschöke H (1999), Mechanically controlled (governed) axial-piston distributor fuel-injection pumps VE, in *Diesel-engine Management*, Robert Bosch GmbH, Stuttgart.

Ullmann J, Geduldig M, Stutzenberger H, Caprotti R and Balfour G (2008), Investigation into the formation and prevention of internal diesel injector deposits, SAE paper 2008-01-0926, from *Diesel Fuel Injection and Sprays*, 2008 (SP-2183).

3

Mixture formation, combustion and pollutant emissions in high-speed direct-injection diesel engines

A. VELJI, M. LÜFT and S. MERKEL, Universität Karlsruhe (TH), Germany

Abstract: This chapter deals with mixture formation, combustion and pollutant emissions in high-speed direct injection (HSDI) diesel engines. In the first part of the chapter the fundamentals of mixture preparation are covered. The physics of spray formation, spray propagation and their characterisation by global values like spray angle and penetration are described in detail. It is shown that fuel atomisation, characterised by droplet diameter, plays a fundamental role in mixture formation. Further, air entrainment as a second important factor governing mixture preparation is discussed in combination with air-distributed and fuel-distributed mixture preparation, combustion chamber design, in-cylinder flow (swirl, turbulence, etc.) and injection rate. It is shown that there is a clear relationship between injection pressure, swirl number, combustion chamber design, number of nozzle holes and nozzle hole diameter.

The combustion part of the chapter includes description of ignition delay, different combustion modes, pressure progress, pressure rise rate and heat release. Low temperature combustion as part of homogeneous charge compression ignition (HCCI) is also covered.

The final part of the chapter deals with mechanisms governing pollutant formation, especially oxides of nitrogen and soot. Engine internal measures, including exhaust gas recirculation and water injection to reduce engine-out pollutant emissions, are described. The chapter concludes with an outlook on future trends for HSDI diesel engines.

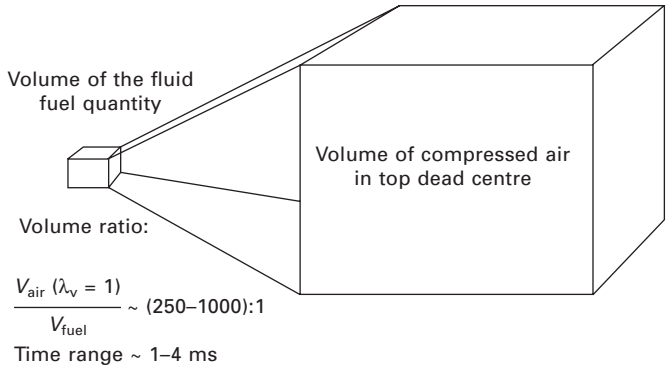
Key words: HSDI diesel engines, mixture formation, combustion, pollutant emissions, HCCI.

3.1 Mixture preparation

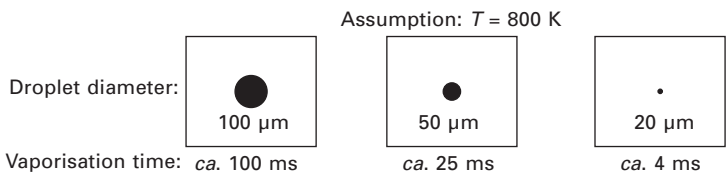
3.1.1 Fundamentals

The combustion process in diesel engines influences thermal efficiency and pollutant levels, particularly nitrogen oxide (NO_x) and soot/particle emissions. The quality of combustion, on the other hand, is largely influenced by mixture preparation. Figure 3.1 illustrates the problems associated with mixture preparation.

If the volume of liquid fuel to be introduced into the combustion chamber is compared to the air volume at an air–fuel ratio of $\lambda_V = 1$, the fuel must



3.1 Illustration of problems associated with mixture preparation.



3.2 Fuel vaporisation in static air.

be dispersed throughout a volume that is 250–1000 times larger than the volume of the liquid fuel, in a time between 1 and 4 ms. Additionally, it is necessary to evaporate the liquid fuel in order to prepare an ignitable mixture. Figure 3.2 shows the vaporisation time as a function of the fuel droplet size in static air conditions at a temperature of T = 800 K.

It is evident from the illustrations provided so far that the mixture preparation is not an automatic process and some assistance or intervention is required. In this context, this is energy that is required to prepare the mixture, which is defined as follows (Velji *et al.*, 1997):

> Mixture preparation energy = injection energy (injection pressure, injection time, etc.) + air energy (swirl, turbulence, etc.)

A number of factors that influence the mixture preparation can be derived from this definition for mixture preparation energy. These are listed below:

- Fuel atomisation
- Air entrainment:
  - fuel distribution
  - type and duration of fuel delivery (injection rate, injection time)
  - movement of air in combustion chamber (swirl, turbulence)
  - shape of combustion chamber, also referred to as combustion bowl.

For the purposes of analysing the above influencing factors on mixture preparation it is necessary to examine the fuel spray and its propagation in the combustion chamber.

3.1.2 Fuel spray

High-pressure fuel injection is used in all diesel engines today. The injection pressures range up to 2200 bar in common-rail fuel injection systems (with pressure transmission up to 2500 bar) and up to 2200 bar in unit injector systems. The fuel is injected via a nozzle into the combustion chamber at the corresponding injection pressure. Forces in the compressed air in the combustion chamber, nozzle hole and downstream of the nozzle outlet act on the fuel spray thus causing it to deform and ultimately to break up. In this case, the inert force, viscosity force and surface force are relevant to the fuel and only the inert force is relevant to air. Even today, the mechanisms that lead to breakup of the jet through removal or shearing off of individual fluid ligaments and the formation and subsequent evaporation, etc., of droplets that leads to breakup of the spray are still not fully understood. However, a qualitative description of the atomisation process as the spray spreads out can be obtained from a wide range of experimental and theoretical studies carried out during the last few years, as shown in Fig. 3.3.

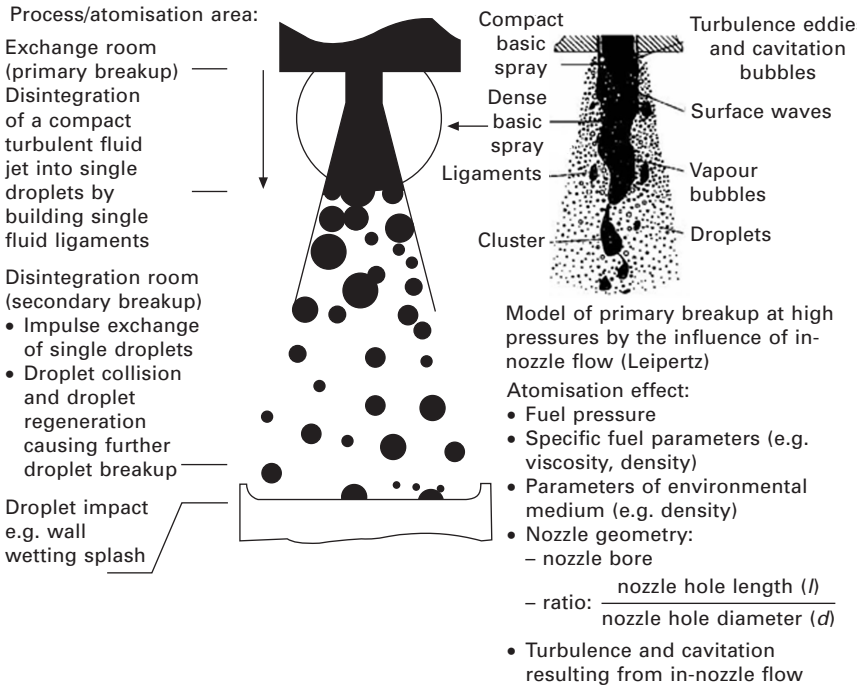
Spray breakup can be subdivided into the following phases according to the model shown in Fig. 3.3.

- *Primary breakup*. During this phase the turbulent and still compact spray (mainly liquid) disintegrates into single droplets through the formation of individual ligaments. Although the processes occurring in the nozzle (such as cavitation) play an important role in this regard, these are phenomena that cannot be quantified.
- *Secondary breakup*. Secondary breakup comprises:
  - impulse exchange of individual droplets with air
  - collision and new formation and/or further breakup of droplets.

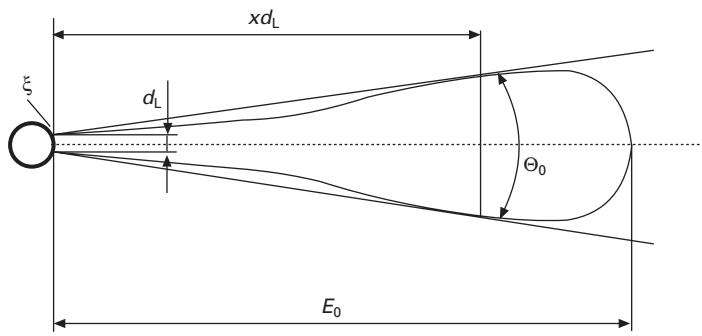
  The actual evaporation of the fuel and mixing with air takes place during secondary breakup.
- *Droplet impact*. Backspraying may occur during this phase in addition to stratification. Droplet impact plays a decisive role in small combustion chambers where fuel is likely to make contact with the wall of the combustion chamber.

3.1.3 Spray propagation

Spray propagation refers to the temporal and spatial propagation of fuel in the combustion chamber. As previously mentioned, an analytical description



3.3 Illustration of various phases of spray breakup and parameters influencing the atomisation process.



3.4 Spray parameters: penetration depth and spray angle without swirl.

of spray propagation is not possible. For the purposes of quantifying this process, however, global spray parameters have been defined and corresponding empirical models have been developed using experimental data. Figure 3.4 shows the most important spray parameters – spray angle Θ_0 and spray penetration E_0.

Spray angle

The full spray angle Θ_0 (Fig. 3.4) follows according to an analysis by Arai *et al.* (1984) from:

$$\Theta_0 = 0.05 \sqrt{\frac{d_L}{v_G \rho_G} \cdot \sqrt{\rho_G \Delta p_m}} \tag{3.1}$$

where:

d_L = nozzle hole diameter
v_G = kinematic viscosity of gas (air)
ρ_G = density of gas (air)
Δp_m = average pressure difference.

Other authors also take the shape of the nozzle hole into account, i.e. the diameter and length of the nozzle hole and the diameter of the sac hole:

$$\Theta_0 = 83.5 \left(\frac{\rho_G}{\rho_K} \right)^{0.26} \frac{d_L^{0.37}}{d_{SL}^{0.15} l_L^{0.22}} \tag{3.2}$$

where:

ρ_K = density of fuel
d_{SL} = diameter of sac hole
l_L = length of nozzle hole

On the other hand, according to Wakuri *et al.* (1990), it is only the density ratio of air and fuel that influences the opening angle:

$$\Theta_0 = 2 \arctan \left[0.427 \left(\frac{\rho_G}{\rho_K} \right)^{0.35} \right] \tag{3.3}$$

Spray penetration

A 'breakup' time t_v is defined in the formulas of Arai *et al.* (1984), which is the time for the spray core to become fully developed. The behaviour of the spray as a function of time changes after this point. According to this, for swirl-free flow in the combustion chamber the following apply in the interval $0 < t < \Delta t_E$:

$$t_v = 28.65 \frac{\rho_K d_L}{\sqrt{\rho_G \Delta p_m}} \tag{3.4}$$

$$E_0(t) = 0.39 t v_K^0 \tag{3.5}$$

$$E_0(t) = 2.95\sqrt{t\,d_L\sqrt{\frac{\Delta p_m}{\rho_G}}} \qquad 3.6$$

where:

Δt_E = injection time
E_0 = spray penetration
t = time
v_K^0 = initial velocity of spray.

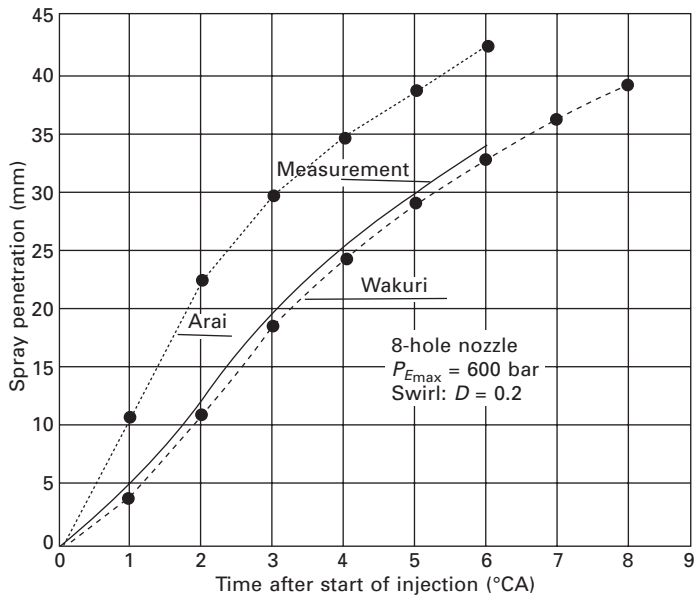
An improved formula for penetration which is in good agreement with experimental results from Binder (1992) is offered by Wakuri *et al*. (1990). This is documented in Fig. 3.5.

$$E_0(t) = \sqrt{\frac{1}{\tan(\Theta/2)}\,t\,d_L\sqrt{\frac{2\xi\,\Delta\,p_m}{\rho_G}}} \qquad 3.7$$

where ξ = flow coefficient.

The spray angle characterises the cross-sectional area of the spray to be taken into consideration for impulse exchange between air and fuel. The flow coefficient ξ identifies the effect of friction during injection.

The values for cone angle and penetration depth must be adjusted if the



3.5 Spray penetration without swirl: comparison of various model approaches, with measured values.

flow is subject to swirl. This adjustment is made via the air angle velocity ω_D (Fig. 3.6).

$$\Theta_D = \Theta_0 \left(1 + \frac{-\omega_D E_0}{V_K^0}\right)^2 \quad 3.8$$

$$E_D = E_0 \left(1 + \frac{\omega_D E_0}{V_K^0}\right)^{-1} \quad 3.9$$

where:

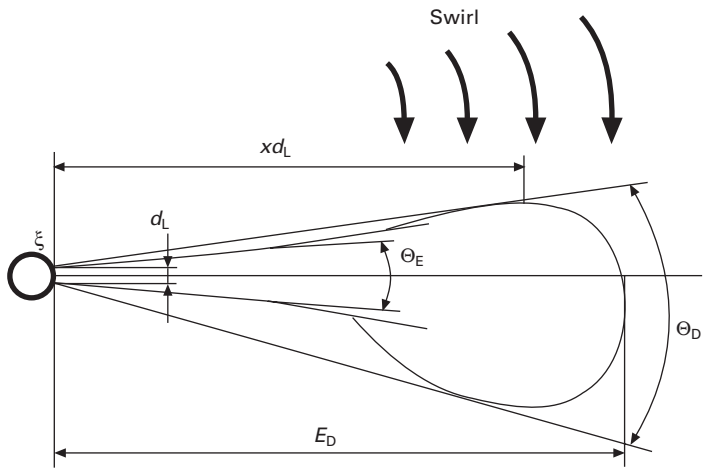
Θ_D = spray angle with swirl
E_D = spray penetration depth with swirl
ω_D = air angle velocity.

3.1.4 Spray atomisation

The atomisation quality of the fuel is influenced by the injection pressure and the injection nozzle, whereby in the latter case other parameters are also of relevance in addition to the diameter of the nozzle hole:

- Ratio between length and diameter of nozzle hole
- Degree of rounding/properties of injection orifice
- Turbulence of flow inside nozzle.

The most reliable means of representing the atomisation quality is by measuring fuel droplet diameter. As the diesel jet contains a host of different



3.6 Spray parameters: penetration depth and opening angle with swirl.

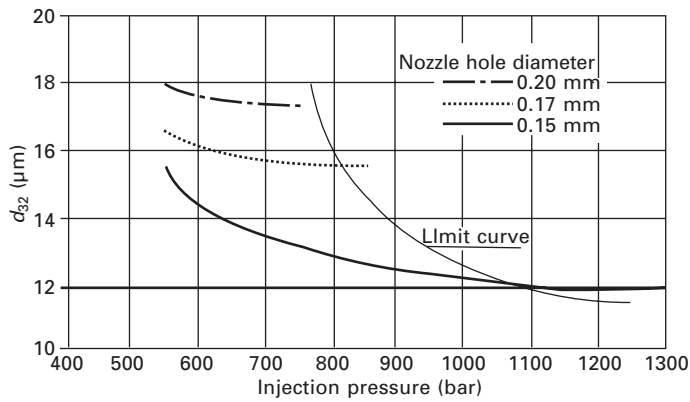
droplet sizes and the spatial and temporal distribution of droplet sizes is a stochastic process, the average droplet size is specified. In this case (mixture preparation and combustion) the Sauter approach, also referred to as 'Sauter Mean Diameter (SMD)', has proven to be an effective practical method of determining the average diameter. The SMD d_{32} specifies the droplet size, where the ratio of droplet volume to surface area is equal to that of the entire spray. In this case the index '32' provides an indication of the volume to surface area.

Figure 3.7 shows the effect of injection pressure and nozzle hole diameter on the average droplet diameter d_{32} (Velji *et al.*, 1997). The following important relationships can be derived from the result presented here:

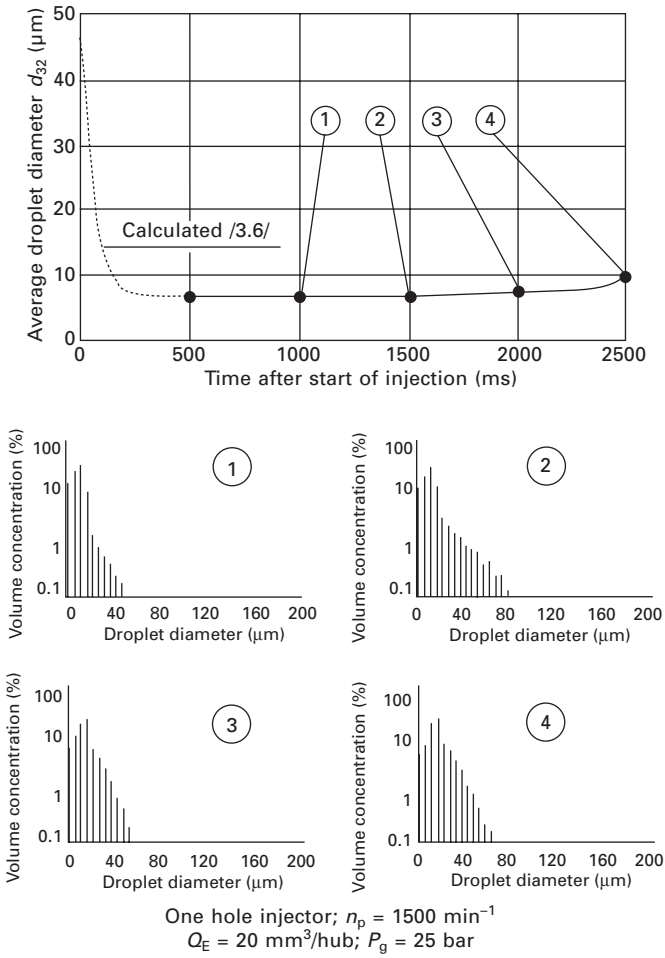
- With a constant nozzle hole diameter, the droplet diameter initially reduces as the injection pressure rises and then remains constant as the injection pressure continues to rise.
- With a constant injection pressure, the droplet diameter reduces as the nozzle hole diameter reduces.

It can be concluded in summary that every nozzle hole diameter has a maximum injection pressure above which an increase in injection pressure is no longer effective. A reduction in droplet diameter and therefore an improved atomisation quality can only be achieved by increasing the injection pressure whilst at the same time reducing the diameter of the nozzle hole. The atomisation quality also remains constant in other areas having high injection pressures and smaller hole diameters. This situation is reflected by the limiting curve in Fig. 3.7.

Figure 3.8 shows the diameter and size distribution of droplets at various points in time following the start of injection. The experiments were carried out in a so-called combustion bomb. During this process, the fuel (testing



3.7 Effect of the injection pressure and nozzle hole diameter on droplet diameter (Velji *et al.*, 1997).



3.8 Average droplet diameter and droplet size distributions at different times following injection start according to Renner (1994).

oil in this example) is injected into a chamber via a single-orifice nozzle containing an inert gas (normally nitrogen) at a specific pressure.

The upper diagram in Fig. 3.8 shows that, following a short start-up phase, the average droplet diameter remains more or less constant. The lower diagrams show the development of droplet size distributions over time. Whereas mainly smaller droplets are present at the start of injection, larger droplets are present in the middle (due to breakup of the liquid core and coalescence of smaller droplets) and a greater number of smaller droplets can be observed again at the end of the injection (droplet breakup and evaporation).

3.1.5 Air entrainment

A further significant factor that influences the preparation of the mixture is the spatial and temporal air entrainment inside the combustion chamber. Air entrainment refers to the supply, evaporation, distribution and mixing of fuel with the air. It is influenced by the following factors:

- Fuel distribution
- Type and duration of fuel delivery (injection rate, start of injection, injection duration)
- Movement of air in the combustion chamber (swirl, turbulence)
- Shape of the combustion chamber.

Fuel is dispersed through the compressed air or is sprayed on the wall of the combustion chamber, depending on the size of the combustion chamber and type of fuel injection used. Two different methods exist for preparing the mixture:

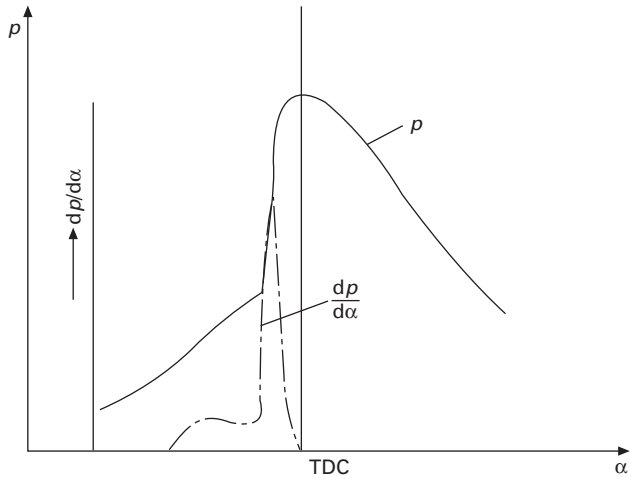
- Air-distributed mixture preparation
- Wall-distributed mixture preparation.

Today, air-distributed mixture preparation is particularly important in engines with direct fuel injection for producing a combustible air–fuel (A/F) mixture in the cylinder. Wall-distributed mixture preparation is used in the MAN-M procedure, for example, and plays a relatively insignificant role in modern diesel engines.

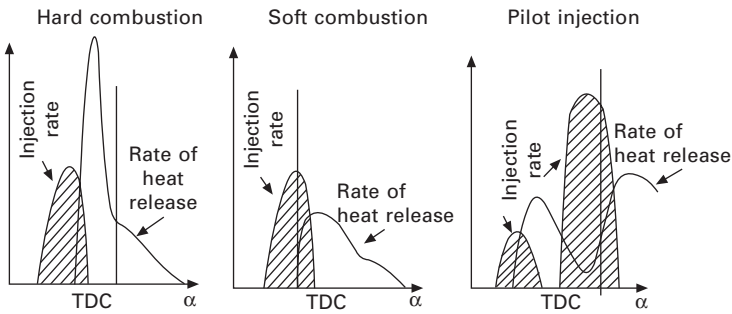
The air-distributed method is mainly used in engines with larger cylinder bores. The basic feature of this principle is that fuel is directed to the air, which means that the fuel performs most of the work involved in preparing the mixture. The slower the air movement, the more finely the fuel atomisation via the injection nozzle (micromixing) and corresponding higher injection and nozzle-opening pressures need to be. A further significant factor is the uniform distribution of fuel in the combustion chamber (macromixing) for which multihole nozzles are required.

The finer the atomisation and the more even the distribution of fuel in the combustion chamber, the more favourable the conditions for high ignition and burnout speed will be (formation of ignition cores). However, this is generally accompanied by extremely high combustion pressures (p_{max}) and rapid increases in pressure ($dp/d\alpha$) that have particularly negative effects on the drive train (Fig. 3.9).

The rate of pressure rise can be reduced by ensuring that only a small amount of fuel is prepared during ignition delay. This means that the start of injection and the injection rate (Fig. 3.10) are particularly important. The rate of pressure rise can also be reduced considerably by pre-injection during which a small quantity of fuel is initially injected and the main injection only starts following ignition of this fuel.



3.9 Qualitative pressure and rate of pressure increase characteristic in engine with air-distributed mixture preparation.



3.10 Injection and combustion characteristics with hard (left, advanced injection start), with soft (centre, retarded injection start) and with pre-injection (right) combustion.

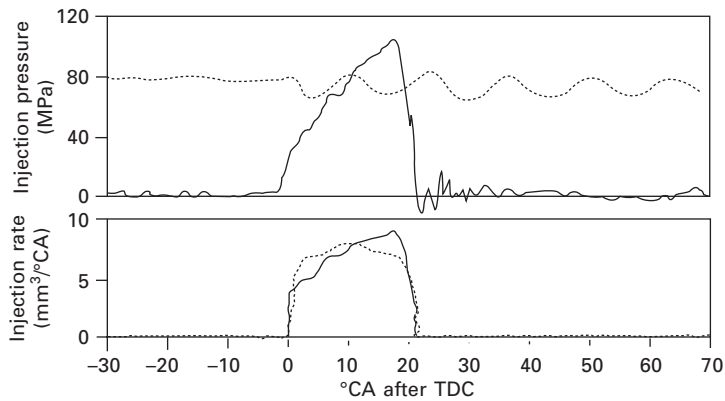
Another way of limiting the rate of pressure rise is to reduce ignition delay by designing the combustion chamber to reduce the amount of heat dissipated via the walls.

3.1.6 Injection rate

The injection rate describes the progression of the fuel mass flow injected into the combustion chamber as a function of time. With cam-controlled injection systems a pump piston steadily increases the pressure during injection. In this case the speed of the piston directly influences the delivery speed and therefore also the injection pressure. In unit-injector systems (UIS),

a mechanically–hydraulically controlled pre-injection is realised that can be controlled only for a limited period of time. It is necessary to inject a small fuel mass prior to the main injection to ensure low combustion noise and low peak pressures (Robert Bosch GmbH, 2004). The injection rate in cam-controlled injection systems is ramp shaped (Fig. 3.11). This ramp-shaped injection rate effectively supports combustion during part-load operation in the lower engine speed range by producing a gentler increase in pressure and therefore low combustion noise but is less beneficial during full-load operation, since a square injection rate with high injection rates is required to utilise the air more effectively.

In common rail systems, the injection pressure is generated by a high-pressure pump independently of the crankshaft position and is delivered in a rail, in which it is permanently available for injection. This means that parameters such as start of injection, injection rate and injection pressure can be freely defined for the various operating points of the engine with the engine application via an electronic control system. The quantity of fuel injected at a given pressure is proportional to the activation time of the valve in the injector and is independent of the engine speed (time-controlled fuel injection). This produces a more or less square injection rate (Fig. 3.11) that intensifies the utilisation of air at full load due to short injection times and more or less constant spray velocities, thus facilitating higher specific power outputs. As far as combustion noise is concerned, the results are less favourable, since a large quantity of fuel is injected into the combustion chamber during the ignition delay due to the high injection rate at the start of fuel injection which causes a considerable buildup of pressure during premixed combustion. Up to two pre-injections are possible using solenoid-valve injectors, which means that the combustion chamber can be preconditioned



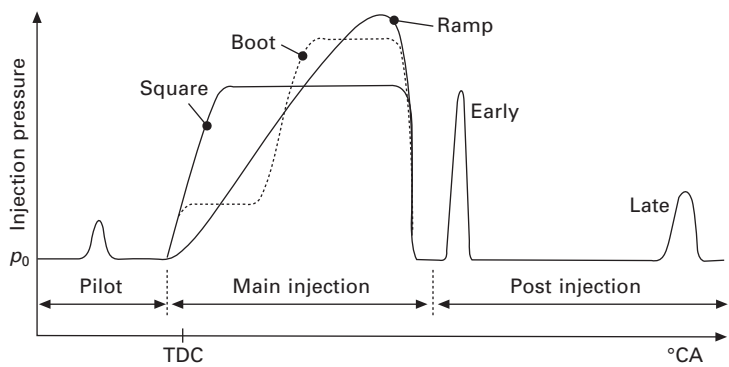
3.11 Injection pressure and injection rate with cam-controlled and common rail injection systems (Chmela *et al.*, 1999; Seebode, 2004).

and the ignition delay can be reduced, thus achieving extremely low noise levels. Up to five injection operations are possible in modern piezo-actuated common rail injection systems during one operating cycle.

Owing to the general problem of coordinating the charge movement, in future applications attempts will be made to transfer the energy required to prepare the mixture to the injection spray impulse. This could be carried out, for example, by shaping the injection rate. Injection rate shaping refers collectively to all measures that effect a change in the shape or quantity of the specific injection rate. These include pre-, multiple and post-injection, opening and closing edge variations as well as modulation of the injection pressure or limitation via needle lift (needle seat throttling) during injection (Fig. 3.12). Due to the varying requirements at the operating points of the engine, it must be possible to control the injection rate depending on the operating point. This can be achieved by using hydraulic pressure transmission (pressure modulation) in the injector, for example.

3.1.7 Combustion chamber design

In the method that uses direct fuel injection, the combustion chamber has a compact design and the fuel enters directly through an injection nozzle that protrudes into it. The combustion chamber itself is formed as a recess located in the piston base that can accommodate up to 80% of the compression volume (Van Basshuysen *et al.*, 2005; Tschöke *et al.*, 2005). According to the versions shown in Section 3.1.5 one can differentiate between mixture preparation processes with low air movement and processes with high air movement (e.g. MAN-M method). Diesel engines with cylinder diameters greater than 300 mm can normally operate efficiently without additional air movement in the combustion chamber and the mixture is essentially

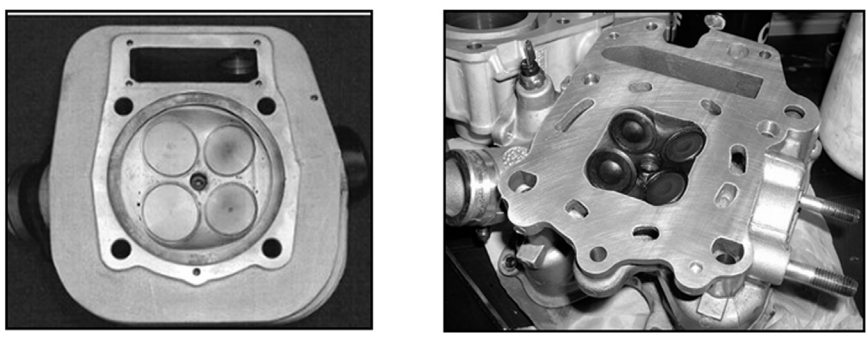


3.12 Injection rate shaping, here indicated by injection pressure (Baumgarten, 2005).

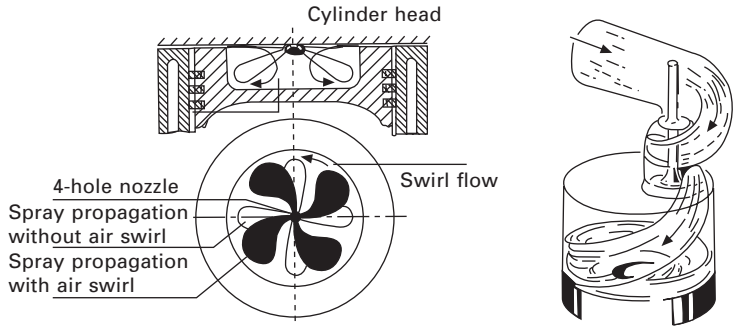
prepared by atomising the fuel as it emerges from the injection nozzle. The injection nozzles used are multihole nozzles containing up to 12 holes. In an engine version with four valves (as in Fig. 3.13) it is possible, due to the central alignment of the injection nozzle on the cylinder axis, to achieve an advantageous symmetrical design of the combustion chamber in terms of mixture preparation and thermal loading.

With smaller engines and therefore higher engine speeds, the charge movement that normally occurs as a result of the intake process, injection of fuel and piston motion is no longer sufficient to prepare the mixture effectively. Special measures are required to increase the relative speed of fuel and air in the combustion chamber. As the inlet ports are designed as swirl and/or tangential ports, an intensive rotational movement of air occurs around the cylinder axis (swirl) when air enters the combustion chamber. This is superimposed on the turbulence that already exists in the combustion chamber and has the effect of distributing and mixing the fuel vapour that immediately forms in the area around the injection jet when fuel is injected with the air already in the combustion chamber (macro mixture preparation) (Mollenhauer, 1997). A further way of increasing the speed of the fuel relative to the air in the combustion chamber is to form a constriction at the opening of the piston crown bowl in the piston base. This leads to the air above the piston base being displaced towards the piston crown bowl during the compression stroke. When air flows into the recess it produces a swirling movement, referred to as squish turbulence (Fig. 3.14).

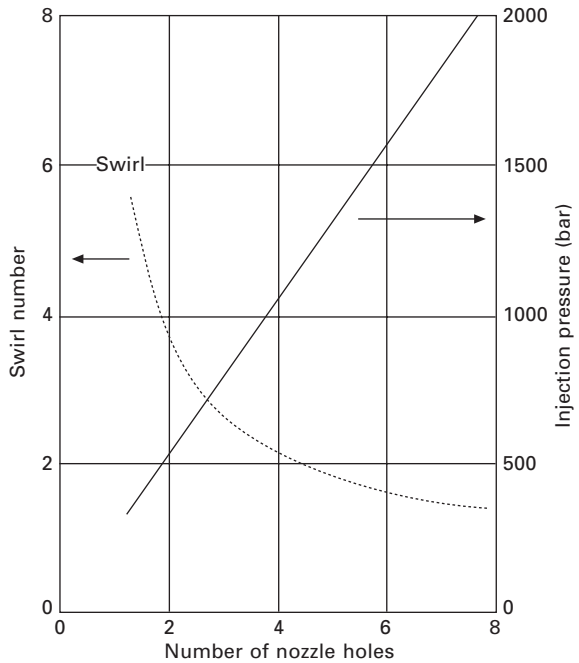
The advantage of squish turbulence over swirl is that its intensity increases as it approaches the piston at TDC (fuel injection phase) whereas swirl generated during the intake process begins to subside at this point. A combination of both methods is applied as the high running speed capability of engines increases. In order to achieve best values for fuel consumption and exhaust emissions, the design of the combustion chamber geometry and fuel injection system must be optimised and matched to each other (Fig. 3.15).



3.13 Combustion chamber arrangement with four-valve technology.



3.14 Flow process in the combustion chamber of a diesel engine with direct fuel injection (Mollenhauer, 1997).



3.15 Typical relationship between injection pressure, swirl number and nozzle hole number (Dietrich, 1999).

The swirl must be increased where the number of nozzle holes is reduced and vice versa. If the swirl is too high, the fuel in the individual fuel jets gets blown together. This leads to spatial 'over-enrichment' of the mixture which results in poor air utilisation and high exhaust emissions. To ensure optimum engine operation, the swirl must be adapted to suit the load and engine speed. High-speed engines require compression ratios between 15:1 and 19:1 and

reach speeds of up to 4500 rpm. With exhaust-gas turbocharging, they can reach an effective efficiency of up to 43% at the best point (Van Basshuysen *et al.*, 2005; Tschöke *et al.*, 2005). The relationship between engine speed (engine size), air movement and the shape of the combustion chamber can be clearly seen by comparing typical shapes of the combustion chamber in engines with direct fuel injection with increasing engine speed.

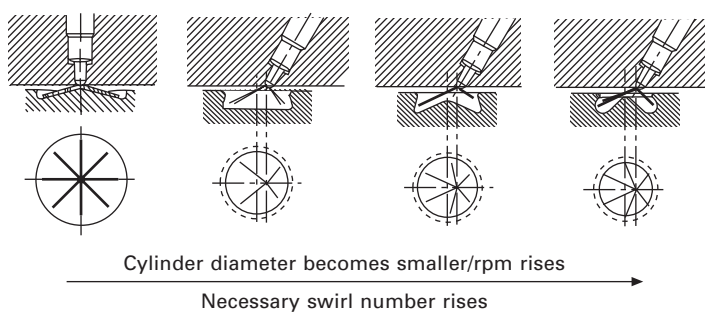
The typical combustion chamber of a medium high-speed engine (e.g. in commercial vehicles) and a passenger car engine are shown on the left and right respectively in Fig. 3.16. The illustration clearly shows that, as the engine speed increases, the constriction and depth of recess in the piston crown bowl increases. This increases the squish effect and the swirl is maintained up to the expansion stroke. The relevance of the necessary swirl number is shown in Fig. 3.17.

A tendency towards a reduction in the number of nozzle holes is also evident. As the engine speed increases, it becomes more difficult to adjust the combustion operation as the system is more sensitive to the combustion chamber geometry. In the case of passenger car combustion chambers, particular attention must be paid to the detailed profiling of the edge of the bowl (turbulence ring) (Thiemann, 2000). Use of the version with four valves and a central injection nozzle is also becoming more widespread in small cylinder sizes.

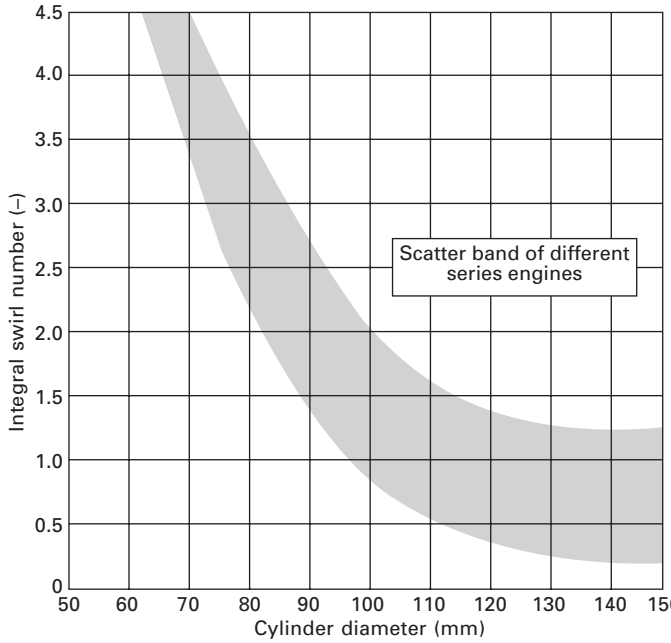
3.2 Combustion

3.2.1 Fundamentals

Engine combustion is a complex process that depends on many engineering design, fuel-specific and atmospheric factors. It is not possible to fully quantify the reciprocal dependency of these factors, let alone take them fully into account when configuring an engine.



3.16 Influence of engine size (engine speed) on shape of combustion chamber recess and required air movement in diesel engines with fuel injection (Mollenhauer, 1997).

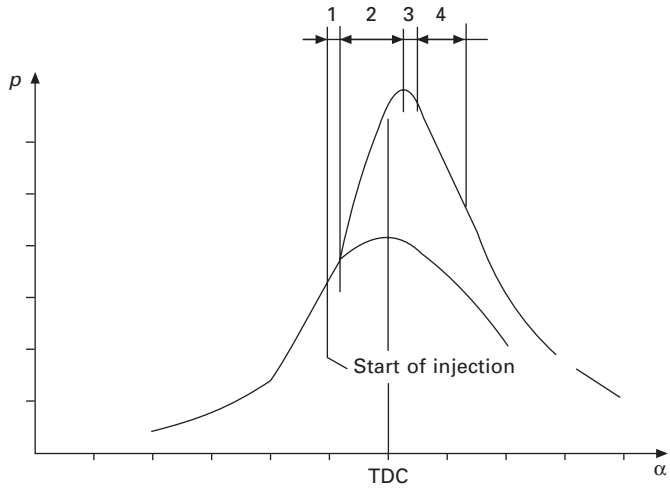


3.17 Typical relationship between required swirl number and cylinder diameter (Thiemann, 2000).

However, to use an engine correctly it is necessary to identify the effects the most important factors have. It has been possible in recent years to demonstrate and also correct many detailed aspects of combustion that previously were only suspected with the assistance of measurement and recording technology, the use of which has become more widespread. Using this approach, it has been possible to analyse the combustion process with increasing accuracy.

Based on the new insights gained, the combustion process is subdivided into four phases (Fig. 3.18):

- *Ignition delay phase*. This is generally defined as the time from the start of injection to the first identifiable increase in pressure in the indicator diagram.
- *Sudden pressure increase phase*. This covers the time period starting with thermal ignition – this can be regarded as the point identified in the indicator diagram at which the pressure increases – and ends when the maximum pressure is reached.
- *Main combustion phase*. This refers to the period that starts when the maximum pressure is reached and ends when the maximum temperature is reached.



3.18 The combustion phases according to Sitkei (1964).

- *Delayed post-combustion phase*. In high-speed diesel engines, this phase can last for approximately 50% of the entire combustion time.

The first phase, the ignition delay phase, has a decisive impact on the conversion of fuel. A great deal of importance is therefore assigned to analysis of this phase.

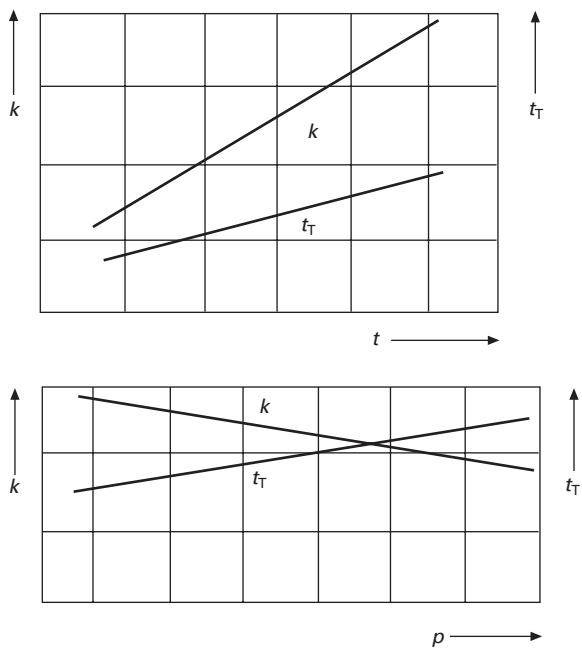
The main combustion phase has recently only come to light as an independent phase in high-speed diesel engines. It is therefore dealt with in conjunction with the second phase. The influence of parameters occurring in both phases can therefore be more clearly seen. The quality of the mixture preparation decisively influences the post-combustion phases and quantity of fuel converted during this phase. The quantity of fuel used during post-combustion contributes to the power generated only to a limited extent. In modern combustion systems attempts are therefore made to end the combustion process as quickly as possible after TDC, and this approach has met with a great deal of success in some cases.

In the diesel engine the ignition of fuel occurs as a result of internal processes in the fuel that take place at relatively low temperatures. The factors influencing this process are both physical and chemical in nature and determine the time required to prepare the fuel for ignition as well as the quantity of fuel prepared during firing. This means that important operating characteristics such as fuel consumption, load, combustion noise and low fuel sensitivity are influenced by the ignition process in the diesel engine. This explains why a great deal of attention is paid to research on ignition processes. From a physical point of view, the preparation of fuel prior to ignition comprises breakup of the fuel jet, evaporation of the fuel droplets and mixing of droplets/fuel vapour with the necessary quantity of

air. In physical terms, the ignition delay largely depends on the fuel jet and mixture preparation (cp. Section 3.1).

At this point, the subject of fuel evaporation merits some special attention as vaporisation is one of the most important preconditions for combustion. Heat must be applied in order to evaporate the fuel droplet and this heat is obtained from the compressed air in the combustion chamber. This means, however, that the air immediately surrounding the droplet is continuously cooled down to the fuel temperature until the droplet changes from the liquid to vaporised state as a result of heat exchange. The time required for this exchange of heat is a component of ignition delay and depends (amongst others) on the vaporising capability of the fuel, the droplet size and temperature, and the pressure in the combustion chamber.

The relationships between droplet temperature t_T and vaporisation rate k and also pressure p and temperature t are shown in Fig. 3.19. While the influence of the air temperature is clearly evident, the influence of pressure varies depending on the droplet temperature and vaporisation rate. The vaporisation rate reduces as the pressure increases (with t constant) – this is logical when viewed in the context of the laws of physics. In the context of practical engine applications this situation will not occur, as a pressure increase in the engine cylinder is associated with an increase in temperature.



3.19 Temperature of droplets (t_T) and evaporation rate (k) as a function of air temperature (t) and air pressure (p).

The negative effect of the pressure is therefore compensated for. (The variable k that characterises the evaporation rate refers only to the evaporating surface, and not the quantity of fuel that evaporates during a specific unit of time. In this respect the curves can be used only for qualitative comparisons.)

Chemical ignition delay also occurs in addition to physical ignition delay. During this time, the molecular structure of the fuel changes until it reaches a favourable composition for combustion. Based on the knowledge acquired to date, the chemical ignition delay can be subdivided into three phases (Fig. 3.20).

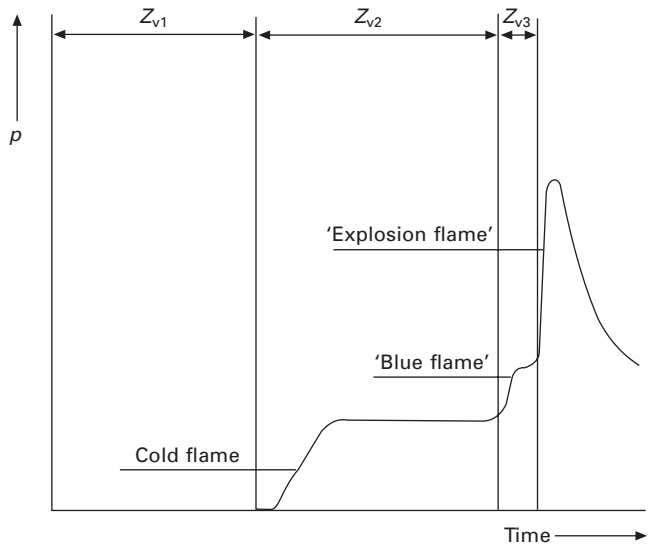
- *First phase*. Centres are created due to the effects of compression pressure and compression temperature in which fuel molecules are heavily enriched with oxygen. This results in the formation of what are known as peroxides and aldehydes. For example:

$$\text{RH (hydrocarbon molecules)} + O_2 \rightarrow 2H_2O + 4\text{R (hydrocarbon radicals)} \quad 3.10$$

$$\text{R} + O_2 \rightarrow \text{ROO (peroxide radicals)} \quad 3.11$$

$$\text{ROO} + \text{RH} \rightarrow \text{ROOH (hydroperoxide)} + \text{R} \quad 3.12$$

- *Second phase*. The enriched molecules break down again and energy is released to perpetuate the reaction (5–10% of fuel energy). The process is accompanied by the formation of a 'cold flame' together with a slight increase in pressure and temperature.



3.20 Illustration showing chemical ignition delay phase of low-temperature ignition process.

- *Third phase*. A further compound is formed between the broken-down products of the reaction and oxygen. CO mixtures are created accompanied by the formation of a 'blue flame'. Energy is released during this chemical reaction that leads to an 'explosion flame' that ignites the fuel–air mixture that was part of the pre-reaction by bonding the remaining oxygen with the CO mixtures,
  e.g.

$$4HCHO + O_2 \rightarrow 4HCO + 2H_2O \quad 3.13$$

$$4HCO + O_2 \rightarrow 4CO + 2H_2O \quad 3.14$$

$$2CO + O_2 \rightarrow 2CO_2 \quad 3.15$$

According to Sitkei (1964) the overall ignition delay is the sum of the physical and chemical ignition delays:

$$\tau_v = \tau_{vphys} + \tau_{v1} + \tau_{v2} + \tau_{v3} \quad 3.16$$

The duration of the ignition delay depends on many different factors and cannot be precisely calculated at present. Attempts have been made to establish suitable formulas for ignition delay. These are normally empirical in character and are valid only for specific test conditions.

Analysis has shown that chemical breakdown of the fuel does not always occur after the fuel has evaporated. Particularly in the case of soot-forming combustion reactions, it has been established that this is caused partly by a molecular breakdown of the liquid droplet.

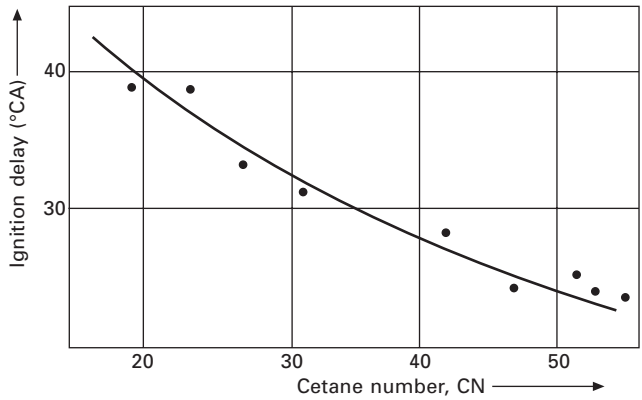
As previously shown, ignition delay is influenced by the pressure and temperature process variables and properties of the fuel. It follows that the ignition delay of fuels with a high self-ignition temperature and/or low volatility is longer. The long physical ignition delay of diesel fuel due to its high viscosity and boiling temperature is reduced by atomising the fuel. Providing that certain conditions are met, ignition delay can be referred to as the fuel quality, expressed as the cetane number. These relationships are shown graphically in Fig. 3.21, as determined by Meurer (1966) in engine tests.

Another way to reduce ignition delay is to increase the compression ratio. However, the reduction in ignition delay is not only due to the improved transfer of heat between air and fuel due to the higher compression temperature.

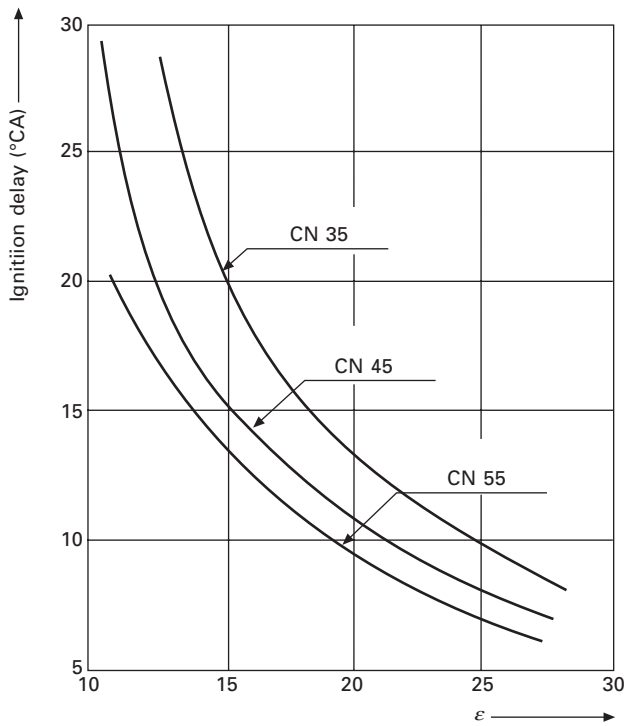
Tests have shown that the auto-ignition temperature of most fuels drops as the pressure increases (Fig. 3.22). This phenomenon obviously has a significant impact on the change in ignition delay.

An increase in the charge pressure of turbocharged engines produces a similar effect to an increase in compression.

It is possible to reduce the ignition delay using the measures described



3.21 Ignition delay of fuels with varying ignition quality versus cetane number.



3.22 Ignition delay as a function of compression ratios for various cetane numbers.

but the objective of this is not to eliminate ignition delay completely. If the ignition delay is too small this leads to insufficient fuel/air mixing and also flame formation directly at the injection nozzle. This causes coking at the

injection nozzle in addition to incomplete combustion and soot buildup. The ignition delay must therefore be long enough to allow the quantity of fuel required for ignition to mix with the air. In this case, the ignition source should be far enough away from the injection nozzle to ensure that fuel components subsequently injected are mixed with sufficient quantities of air before they reach the ignition flame.

3.2.2 Heat release

The second phase of combustion (cp. Section 3.2.1) is characterised by a sudden increase in pressure. This is shown in the indicator diagram as a deviation from the compression line. The pressure increase $dp/d\alpha$ can be used as the yardstick for the rise in pressure. This is frequently used as a measure for assessing the combustion noise of the engine.

The pressure increase $dp/d\alpha$ is the first diversion from the pressure indexed according to the crankshaft angle. This is obtained in increments through formation of the quotient from $\Delta p/\Delta\alpha$. A sufficient level of accuracy can be obtained by using a correspondingly small interval $\Delta\alpha$.

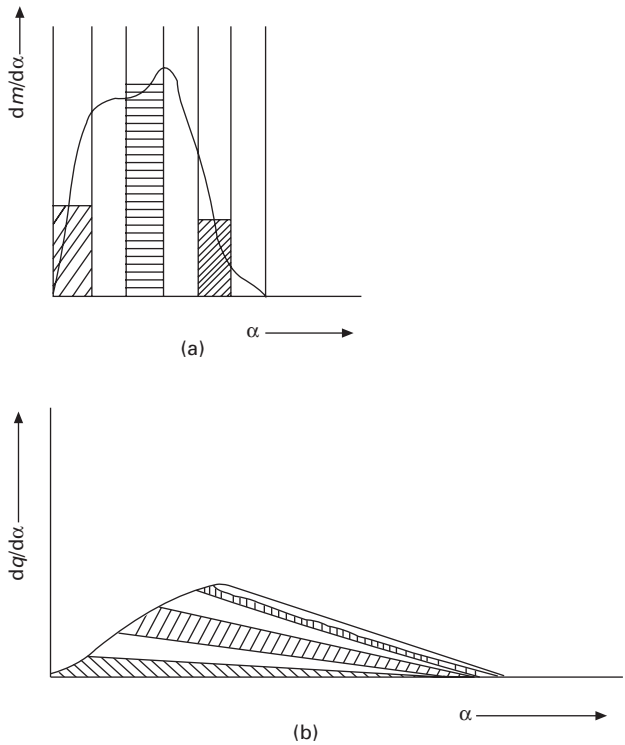
Pressure increases $dp/d\alpha$ of 20–50 N/cm^2 per °CA are anticipated in quiet running engines. These values are achieved by petrol engines and quiet running diesel engines. Many older types of diesel engines do not achieve these favourable values.

From previous analyses it follows that the more fuel that is prepared for ignition during ignition delay, the greater the pressure increase will be. This quantity of fuel should be small in order to maximise fuel combustion efficiency during the main combustion phase and to avoid overloading the power unit and bearing.

The purpose of the following is to illustrate the effect that the injection rate and ignition delay have on the combustion characteristics.

The specified injection rate has the shape shown in Fig. 3.23. To maintain clarity throughout the process, the total injection quantity is split into six volume sections. It is assumed that a time of 40 °CA is required to convert each of the volume sections. Based on this assumption, a corresponding diagram for conversion of the fuel is shown in Fig. 3.23(b).

The size of both areas below the injection rate and conversion characteristic curve is the same in terms of energy content. If no ignition delay was present, the forms of the diagrams for the combustion characteristic curve and conversion characteristic curve would be identical. However, following a specific ignition delay, the quantity of fuel prepared up to the point at which ignition occurs suddenly burns and causes a deviation between the shape of the combustion characteristic curve and the shape of the conversion characteristic curve. Assuming that combustion subsequently takes place without interference and without significant ignition delay, this produces the



3.23 (a) Injection rate and (b) schematic conversion characteristic curve for direct injection, showing the six volume sections (see text).

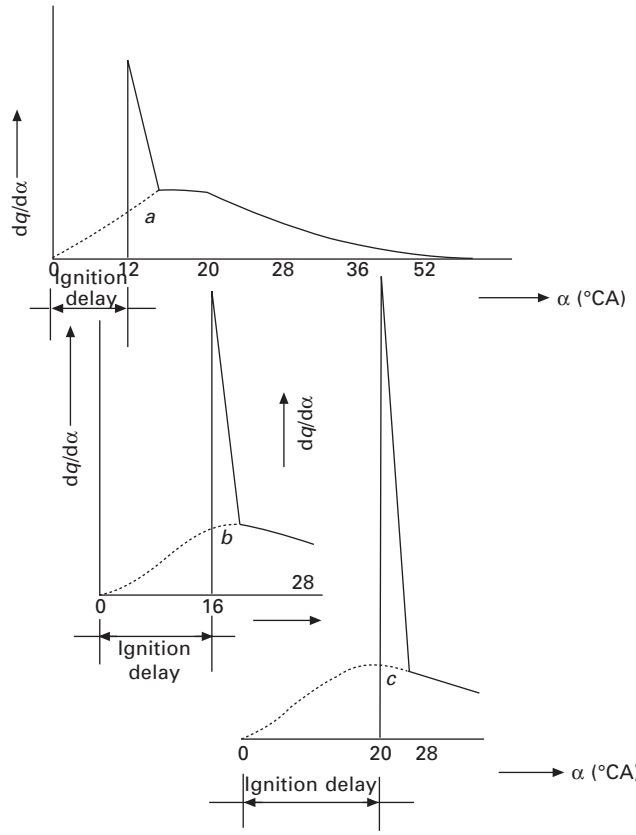
combustion characteristic curves shown in Fig. 3.24 for various durations of ignition delay.

The conversion peak superimposed on the combustion characteristic curve corresponds in terms of surface area to the quantity of fuel prepared during ignition delay.

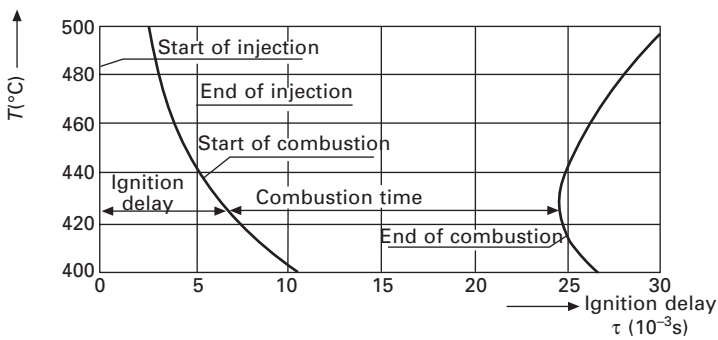
The compression temperature in the combustion chamber can be increased in an endeavour to shorten the ignition procedure for the purposes of achieving a softer combustion process (Blume, 1940). Blume (1940) carried out corresponding tests in a combustion bomb and the temperature–time diagram (Fig. 3.25) was established based on this result.

The ignition delay decreases as the air temperature increases over a uniform injection period. The burnout period, on the other hand, increases as the temperature increases. It may therefore be concluded that the longer the fuel preparation time prior to ignition the shorter the burnout period will be.

On the other hand, the work of Meurer (1966), in particular, has shown that at high temperatures the combustion that occurs following ignition delay



3.24 Schematic combustion characteristic curves for direct injection according to Fig. 3.23 with varying durations of ignition delay.



3.25 Ignition delay and burnout duration as a function of combustion chamber temperature (bomb tests) according to Blume (1940).

is inhibited. The following explanation exists for this apparent contradiction, which has remained unanswered for a long time.

During the tests by Blume (1940) fuel was injected into static air, which means that fuel fed in after ignition was injected into the flame or the combustion residues. The fuel quickly passes through the chemical ignition delay phase but has little or no opportunity to mix with fresh air. The fuel components break down (cracking). Although fast-oxidising hydrogen components still react, soot is formed from the carbon components. This requires a relatively long combustion time that is normally not available in the engine. For this reason it is often not considered appropriate to try to achieve a smooth combustion characteristic by setting a retarded injection start.

The events described above occur due to the higher prevailing temperatures and pressures in the combustion chamber at injection start. The softer combustion characteristic is obtained at the expense of higher soot buildup.

The conclusions drawn from observation of these relationships were formulated by Meurer (1966) as follows:

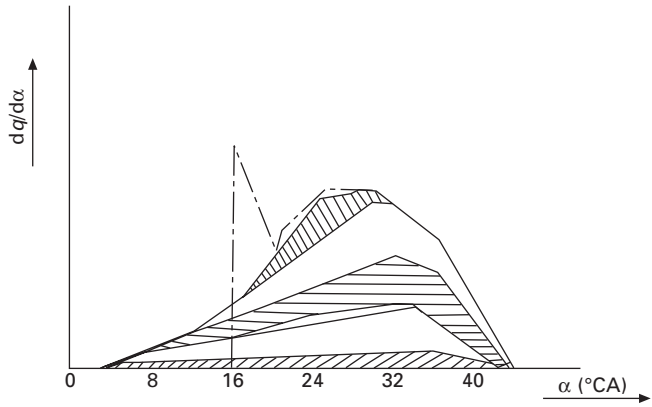
1. Keep the fuel component determined by the auto-ignition to a minimum.
2. Allow the fuel to oxidise slowly and warm the fuel up together with the air as far as possible.
3. Mix the fuel with the hot air quickly enough to ensure that at least one stoichiometric mixing ratio is produced prior to ignition of the fuel. Do not mix more fuel with air than should be produced taking the increase in pressure into consideration.

The preparation sequence and combustion process must take on a different form in order to meet these requirements. Figure 3.26 shows such a fuel preparation sequence and combustion process, assuming an injection rate similar to that shown in Fig. 3.23(a). The small conversion peak is not due to ignition delay, as comparison with Fig. 3.24 shows.

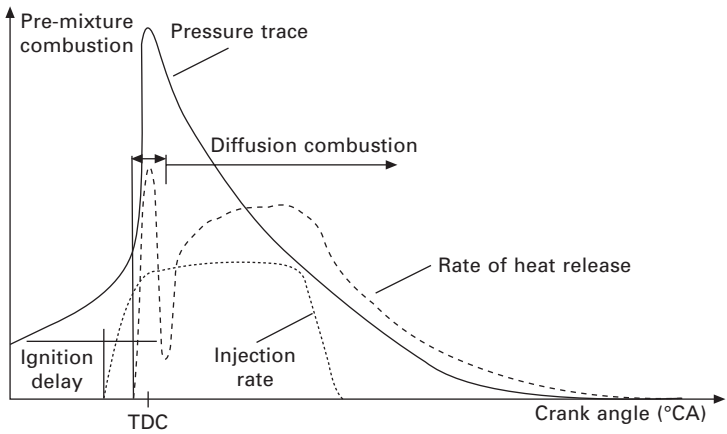
The type of fuel preparation is decisive and this in turn depends on the fuel injection, the shape of the combustion chamber and the process used to mix the fuel with the air. In summary, the characteristic curves for injection, pressure and combustion are shown in Fig. 3.27.

3.2.3 Low temperature combustion

A detailed description of pollutant formation will be given in Section 3.3.1. This section deals with different possible combustion modes to avoid formation of nitrogen oxides (NO_x) and soot. The main parameters controlling formation of NO_x and soot are the local temperature (T) and local air–fuel ratio (λ), as shown in Fig. 3.28.



3.26 Schematic preparation and combustion characteristic curve for practical implementation of mixture preparation proposed by Meurer.

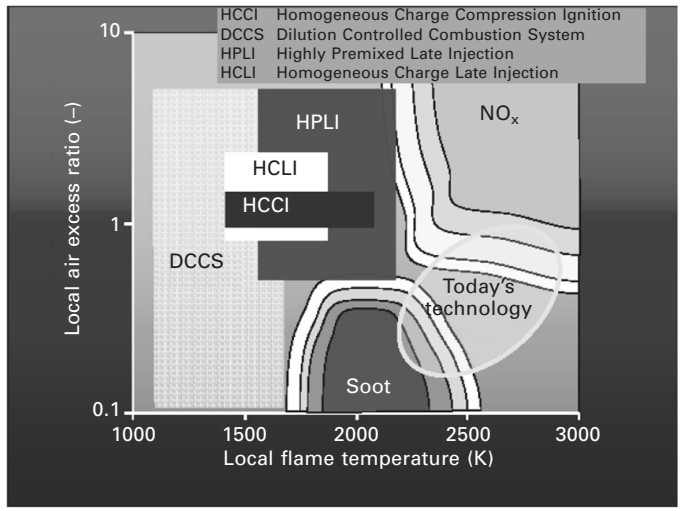


3.27 Pressure and combustion characteristic curve.

Conventional heterogeneous diesel combustion occurs in ranges where both NO_x and soot are formed. The idea of a low temperature combustion is to create modes where combustion takes place in areas outside the critical λ–T ranges (Fig. 3.28). The best known modes are:

- Homogeneous Charge Compression Ignition (HCCI)
- Dilution Controlled Combustion System (DCCS)
- Highly Premixed Late Injection (HPLI)
- Homogeneous Charge Late Injection (HCLI).

All these modes are at present only applicable in part load (<50%). Further features characterising these modes are:



3.28 Soot and NO_x formation regions as a function of local temperature and local air–fuel ratio (Johnson, 2005).

- Pre-mixed combustion
- Very high rates of pressure rise
- Lack of reliable combustion control
- High HC and CO emissions
- Very low PM and NO_x
- No or small fuel penalties.

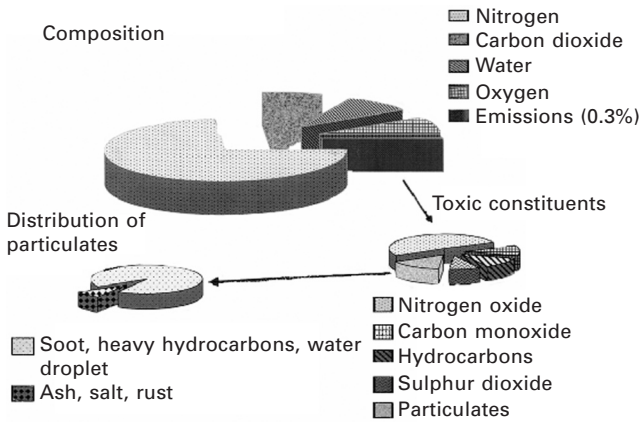
3.3 Pollutant emissions

Figure 3.29 shows the typical composition of exhaust gas from a modern DI diesel engine at full load. The part of pollutant emissions is only 0.3 vol%. The highest part of this 0.3 vol% is formed by nitrogen oxide and particulates.

3.3.1 Formation

The pollutants produced during the engine combustion process can be classified as follows, depending on their cause:

- Pollutants caused by incomplete combustion (soot, carbon monoxide, hydrocarbons)
- Pollutants produced as a result of undesirable secondary reactions (NO_x)
- Pollutants that are the products of reactions with impurities in the fuel (SO_2).



3.29 Exhaust-gas composition of diesel engines.

To reduce the level of pollutants in exhaust gas, the mechanisms that lead to their formation must be identified.

NO_x formation

The term nitrogen oxide (NO_x) refers to a group of nitrogen and oxygen based chemical compounds with varying atom-to-atom relationships. NO is the main component of NO_x (>90%). Nitrogen monoxide (NO) is essentially produced in three different ways during combustion processes (Kremer, 1986; Leuckel, 1985; Kolar, 1990; de Soete, 1981):

- 'Thermal NO' is formed at high temperatures ($T > 2200$ K) in the burnt component of the working medium (post-flame range) from molecular nitrogen in the combustion air. This process is initiated by oxygen radicals and assisted by OH radicals (significant for $\lambda_V < 1$). The reaction kinetics that form the basis of 'thermal NO formation' can be described using the extended 'Zeldovich mechanism' (Heywood, 1988; Zeldovich, 1946).
- 'Prompt NO' is also formed from molecular atmospheric nitrogen, but inside the radical-enriched main reaction zone of hydrocarbon combustion (flame zone) according to the reaction mechanism investigated by Fenimore (1971). The temperatures reached at this point are practically the same as the temperatures present under adiabatic combustion conditions and achieve maximum values of up to around 2800 K with $\lambda_{Vi} = 1$ in the diesel engine, depending on the air–fuel mixture and localised air–fuel ratio (λ_{Vi}). The necessary reaction times for the formation of 'prompt-NO' are in the millisecond range (Sutton and Flemming, 2008).
- 'Fuel NO' is formed by the oxidation of the nitrogen chemically bound

within the fuel. Before entering the combustion zone, nitrogen within the fuel is converted to radicals or compounds of the CN group (cyan compounds) that partially oxidise to form NO in the flame zone (Kolb, 1990). However, the nitrogen content of standard diesel fuels is so low that the 'fuel NO' formation can be disregarded.

Investigations carried out to date (removal of exhaust gas from the combustion chamber and/or exhaust-gas testing at end of combustion combined with simulation calculations) indicate that in diesel engine combustion processes – in analogy to combustion in natural gas or light oil operated industrial firing systems – NO is essentially formed via the formation mechanism of 'thermal NO' (Heywood, 1988; Lavoi *et al.*, 1970; Kleinschmidt, 1974).

The extended 'Zeldovich mechanism' forms the basis of 'thermal NO formation' and encompasses the following reactions:

$$N_2 + O \rightarrow NO + N \qquad 3.17$$

$$O_2 + N \rightarrow NO + O \qquad 3.18$$

$$OH + N \rightarrow NO + H \qquad 3.19$$

In this case reactions 3.17 and 3.18 with 'lean' mixtures ($\lambda_V \geq 1$) and also reaction 3.19 with near stoichiometric and 'rich' mixtures ($\lambda_V \leq 1$) are significant. In the diesel engine operating environment, the progression of the reaction mechanism is kinetically controlled, which means that, for the given residence times of the gas mixture in the combustion chamber, chemical equilibrium is not reached at the locally prevailing temperatures during combustion in the diesel engine with localised air–fuel ratio! As a consequence, the NO concentration measured in the exhaust gas of the diesel engine is considerably higher than the corresponding equilibrium concentration for the temperature and air–fuel ratio of the exhaust gas. This is referred to as the 'freeze effect' of NO formation and breakup reaction and takes effect at temperatures below roughly 2200 K.

The change in nitrogen oxide concentration (c_{NO}) in a localised area 'i' in the combustion chamber during the combustion process can be expressed in a simplified form using the following functional relationship:

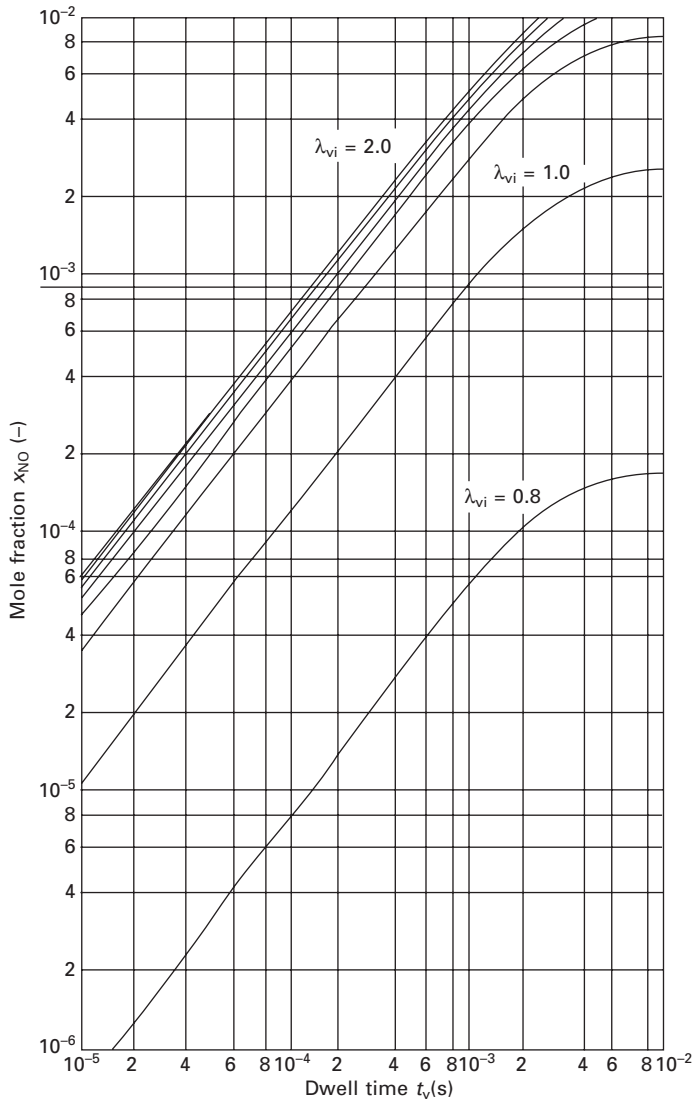
$$d(c_{NO})/dt = f(T, c_{N_2}, c_{O_2}, c_{NO}, c_N, c_O, c_{OH}, c_H) \qquad 3.20$$

The main influencing variables of thermal NO formation can be derived directly from the above relationship:

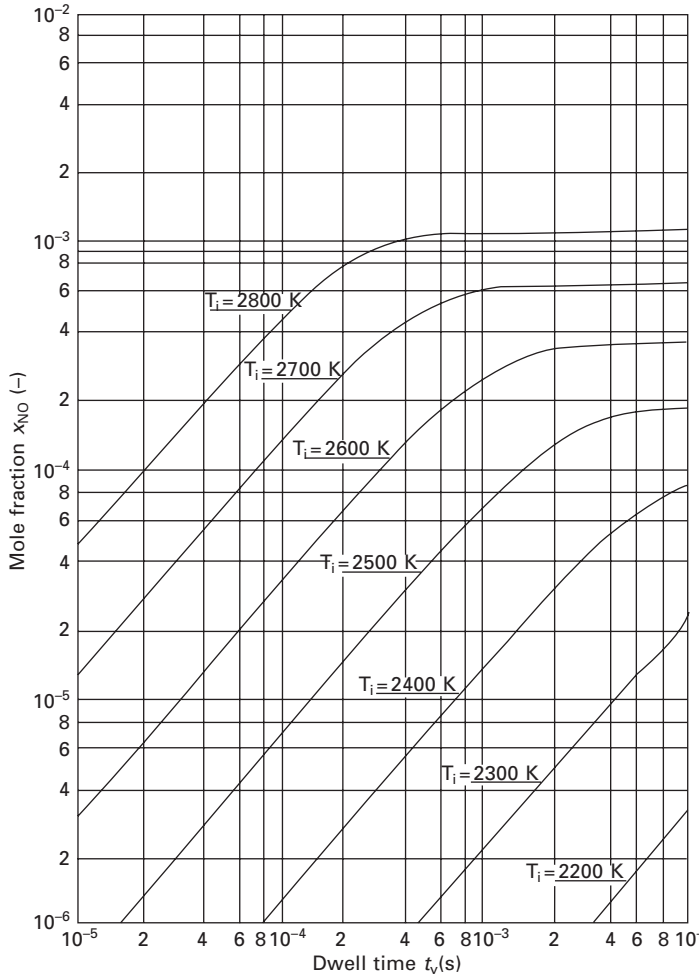
- Locally prevailing temperature T_i
- Localised air–fuel ratio λ_{Vi} as indication of the concentration of components involved (N_2, O_2, NO, N, O, OH and H)
- Residence times t_v of mass element under consideration in area 'i' with T_i, λ_{Vi}.

The influence of these variables on thermal NO formation can be shown quantitatively based on the result of a simulation calculation.

Figures 3.30 and 3.31 show the time characteristic of nitrogen monoxide NO concentration in a discrete volume range with constant marginal conditions (pressure, temperature, air–fuel ratio), assuming a starting condition c_{NO} = 0 for t = 0. To make the influence of localised air–fuel ratio and localised



3.30 Thermal NO formation for p_{max} = 140 bar, T_i = 2500 K and λ_{Vi} = 0.8–1.6 (initial concentration x_{NO} (t = 0) = 0).



3.31 Thermal NO formation for p_{max} = 140 bar, T_i = 2200–2800 K and λ_{Vi} = 0.8.

temperature clear, the localised air–fuel ratio is varied at a constant temperature in Fig. 3.30. The localised temperature with constant air–fuel ratio is shown in Fig. 3.31.

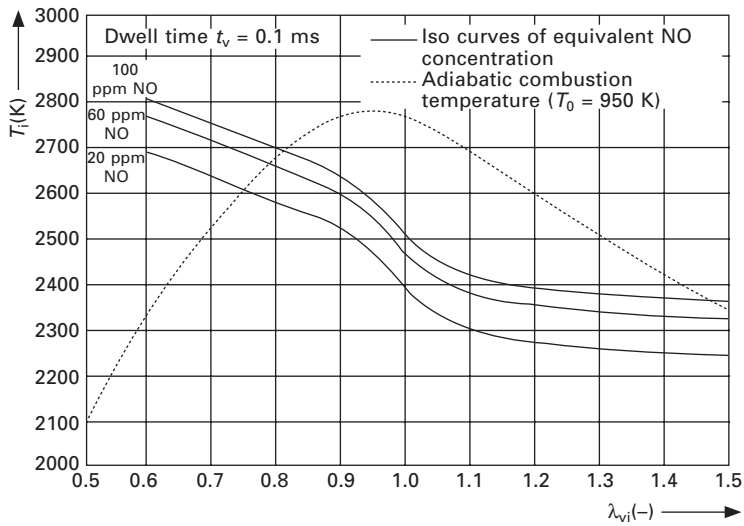
The marginal conditions (p, T_i, λ_{Vi}) are selected with reference to real values for diesel engine combustion processes. It is evident that if the localised temperature and/or localised air–fuel ratio are increased in equal measure, this leads to an increase in the formation rate of NO and equilibrium concentration of NO. As an example, chemical equilibrium is only reached after 10 ms under marginal conditions T_i = 2500 K, λ_{Vi} = 0.8 (for comparison: 1 ms = 9 °CA with n = 1500/min, combustion duration at full load approx. 80

°CA ≈ 9 ms). This demonstrates that under real combustion conditions with high-speed diesel engines the chemical equilibrium is not achieved within the available residence time, which means the process of NO formation is kinetically controlled.

The influencing variables referred to above (localised temperature and localised air–fuel ratio) are to be clearly differentiated from the variables energetically averaged process temperature and global combustion air–fuel ratio (determined using a cycle calculation, for example), as the conditions at the corresponding localised points of origin, and not the integral average values, are decisive.

The combined effect of the influencing variables localised process temperature, localised air–fuel ratio and residence time on the reaction kinetics of thermal NO formation is shown in Fig. 3.32 in a T_i–λ_{Vi} diagram. The curves with solid lines represent equivalent conditions (T_i, λ_{Vi}) for thermal NO formation. These curves connect value pairs (T_i, λ_{Vi}) for which an equal amount of NO forms during the same residence time t_v (here x_{NO} = 100 ppm, 60 ppm and 20 ppm in t_v = 0.1 ms, x_{NO} (t = 0) = 0).

More NO forms under conditions above these curves and less NO forms under conditions below these curves. Under real conditions, the localised process temperature T_i and localised air–fuel ratio λ_{Vi} are coupled due to the process conditions in the flame front (≈ adiabatic) in the post-flame area and cannot therefore be selected independently of one another. The adiabatic combustion temperature characteristic curve (dotted line) is superimposed



3.32 Relationship between thermal NO formation and conditions in flame front during adiabatic combustion.

over via the localised air–fuel ratio λ_{Vi} in Fig. 3.32 and represents this characteristic, assuming a temperature T_0 = 950 K of unburnt compressed mixture.

It can be concluded from the characteristic curve of the difference between adiabatic combustion temperature and lines with the same NO formation that an increasing quantity of thermal NO forms as the localised air–fuel ratio approaches the value $\lambda_{Vi} \approx 1.1$. The reason for this is an increasing combustion temperature and increasing O_2 concentration. If the localised air–fuel ratio increases further, the NO formation falls again due to a reduction in the adiabatic combustion temperature, despite a continued increase in O_2 concentration. This means that under adiabatic combustion conditions the highest amount of nitrogen monoxide forms in the air–fuel ratio range $\lambda_{Vi} \approx 1$. This characteristic is exploited during what is referred to as 'incremental combustion' in gas-fired combustion systems during which appropriate combustion control methods (primary stage $\lambda_{Vi} < 1$; mixture cooling, i.e. reduction of T_0 via supply of cold fresh air; secondary stage $\lambda_{Vi} > 1$) are used to prevent near stoichiometric combustion in the range $\lambda_{Vi} \approx 1$.

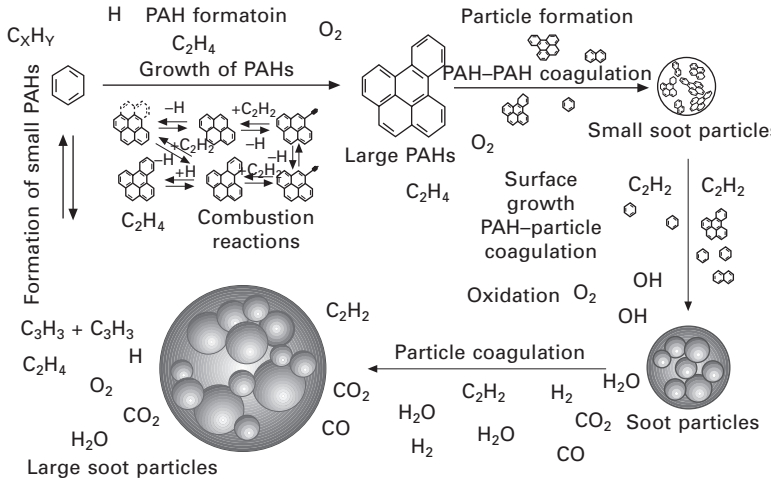
Soot formation

Soot is an exhaust-gas component that can be collected via a filter in fluid or solid form (with the exception of water). Depending on the formation process, one differentiates between flame soot and soot coke (Leuckel, 1985).

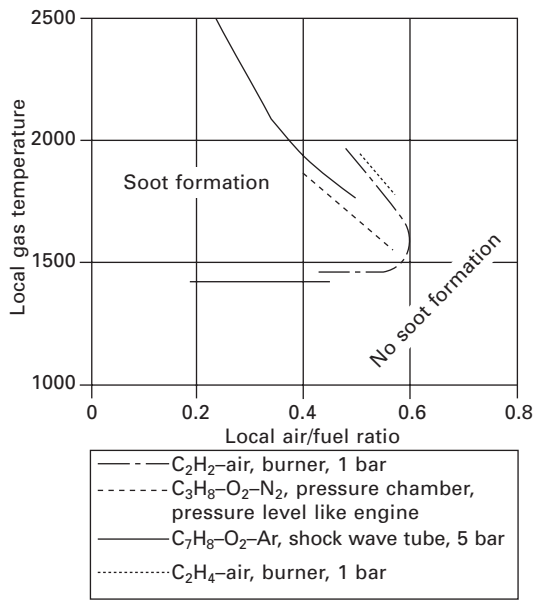
Flame soot is a potential intermediate product of combustion processes that occurs directly in the flame or combustion chamber when insufficient oxygen is available at sufficiently high temperatures. This process is initiated by the decomposition of fuel molecules at temperatures above 1000 K to form unsaturated intermediate products such as acetylene (if sufficient oxygen is available, it is possible to fully oxidise the small hydrocarbon compounds). In the case of oxygen deficiency, large unsaturated hydrocarbons are formed due to agglomeration and dehydration processes that contain mainly carbon and also, to a lesser extent, hydrogen. The first soot particles form at this stage. These rapidly grow into large spherical particles as a result of agglomeration and coagulation (Fig. 3.33).

The formation of soot is assisted by carbon-rich and unsaturated starting components. Additionally, cyclical hydrocarbons produce more soot than chain compounds. The soot formation limits determined on the basis of fundamental analyses in flame and shock-wave discharge tubes according to localised air–fuel ratio and localised temperature are shown in Fig. 3.34 (Pischinger *et al.*, 1988)

Inside the soot formation limits the soot yield (= soot mass/overall carbon mass) increases as the localised air–fuel ratio decreases. However, the formation of soot is a complex matter the details of which are not yet fully



3.33 Soot formation and soot oxidation mechanism (Bockhorn, 1994).



3.34 Soot formation limits as a function of localised temperature and localised air–fuel ratio according to Pischinger *et al.* (1988).

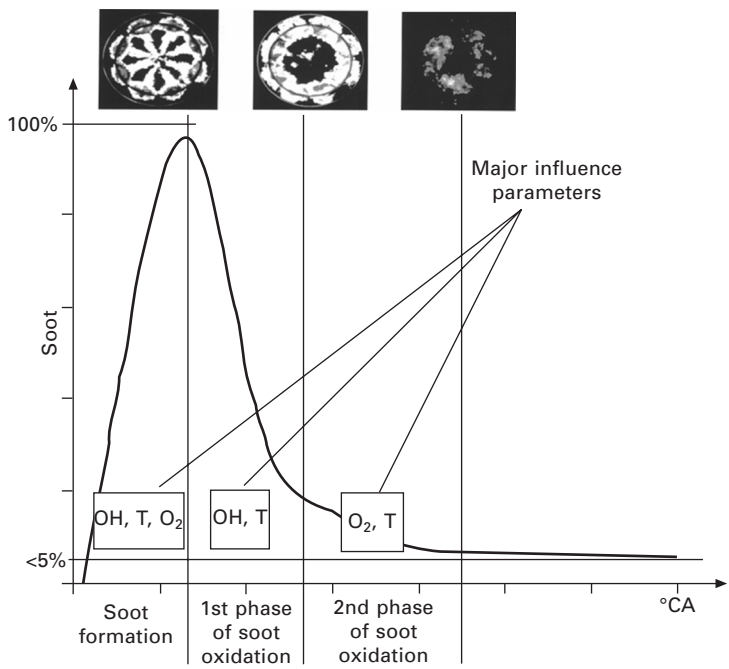
understood, which means that a quantitative calculation is not possible. The diameter of typical flame soot particles is in the region of 0.02–0.08 μm and soot is formed in less than 1 millisecond, whereby up to 50% of the carbon in the fuel can be converted to soot. However, in general 95% of the soot

formed in the combustion chamber is post-oxidised. Figure 3.35 illustrates the formation and oxidation of soot in qualitative terms over the course of time.

In contrast to flame soot, soot coke is formed in the droplet phase during the combustion of liquid fuel by injecting it into the flame (in the case of fuel oil combustion, for example). Components of diesel fuel with high boiling points, especially naphthene content, are decisive in the formation of soot coke. These 'crack' in the liquid phase before reaching their evaporation temperature as a result of radiation from the flame and form a hollow cone-shaped C-skeleton ('cenospheres'). The diameter of the cenospheres is roughly the same as the initial diameter of the injected fuel droplet (5–50 μm).

CO formation

Carbon monoxide is an intermediate product of the oxidation of hydrocarbons in the combustion chamber. Further oxidation of CO to CO_2 (complete combustion, $CO + OH\square \leftrightarrow CO_2 + H\square$) is particularly impeded in areas where air is locally insufficient (incomplete fine mixing) as a result of 'flame quenching' on cold walls and if the residence time in the combustion chamber



3.35 Formation and oxidation of soot in qualitative terms over time (Source: D Bertsch, PhD thesis, University of Karlsruhe (TH), 1999).

is too low. At the start of combustion the first carbon monoxide molecules form at the edges of the injection jet where the prevailing temperatures are insufficiently high to allow further oxidation to carbon dioxide. Carbon monoxide also forms near the wall and in the core area of the injection jet where low concentrations of oxygen are present, and whether further oxidation occurs depends mainly on the mixing process (air entry).

Formation of hydrocarbons

The causes of unburned hydrocarbon emissions are practically the same as these of pollutant component carbon monoxide. The molecular bonds of heavy fuel components break down at high temperatures in the combustion chamber, forming a variety of hydrocarbons with smaller C-atom chains (thermal cracking). They are surrounded by the flame during subsequent combustion. However, the flame cannot propagate further in certain areas of the spray as the necessary preconditions (oxygen concentration and temperature) do not exist (quenching effect). Hydrocarbons cannot be oxidised further in these areas and remain unburned until the end of combustion unless they reach areas with more favourable oxidisation conditions by suitable flow characteristics. The zones next to walls and the spray core and periphery are critical in this regard.

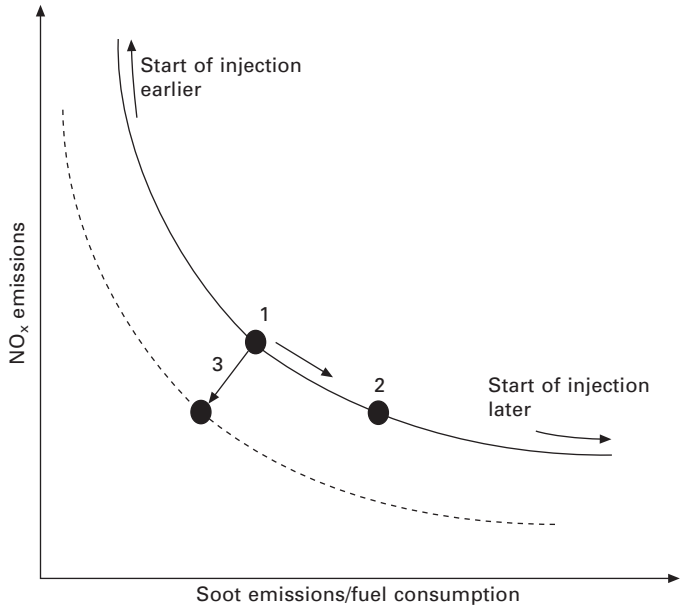
SO_2 formation

Sulphur dioxide is formed from sulphur contained in the fuel through direct oxidation with molecular oxygen in the flame front and 'post-flame' area. During this process nearly all of the sulphur in the fuel (as organic sulphide amongst others) is converted to SO_2. SO_2 emissions can therefore be quantitatively determined by the sulphur content of the fuels used.

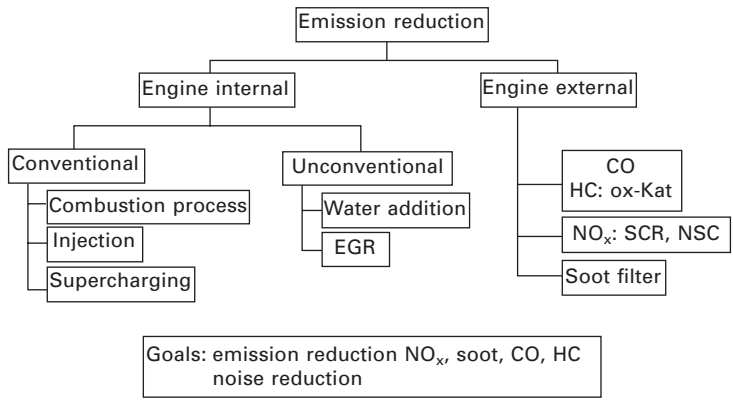
3.3.2 Measures to reduce pollutant emissions

The mechanisms of pollutant formation were dealt with in detail in Section 3.3.1. Critical diesel engine exhaust emissions are nitrogen oxide (NO_x) and particles consisting mainly of soot. A special aspect in this case is the opposing behaviours of these pollutants, i.e. combustion conditions that favour the reduction of NO_x often increase soot emissions and fuel consumption b_e. This is referred to as a NO_x–soot or NO_x–BSFC trade-off (Fig. 3.36). Measures taken to reduce pollutants must therefore aim to avoid operating within this trade-off zone (from 1 to 2 in Fig. 3.36) but to ease this conflict of interests instead (from 1 to 3 in Fig. 3.36).

There is a wide range of engine-internal measures available for reducing the emission levels of diesel engines. The measures used in practice nowadays



3.36 NO_x–soot or NO_x–fuel consumption trade-off.



3.37 Possibilities of emission reduction.

to reduce pollutants can be classified as conventional and unconventional measures (Fig. 3.37).

Conventional measures are all measures that modify combustion by influencing the geometry of the combustion chamber, air movement including supercharging, fuel injection, etc., to the extent that the formation of pollutants is partly or completely eliminated. The composition of the air and fuel is not changed in this case.

Unconventional measures are measures taken to purposefully influence the air–fuel composition. These include water injection and exhaust-gas recirculation. Strictly speaking, unconventional measures also modify the combustion process and partly or completely eliminate the formation of pollutants. However, for practical reasons this differentiation makes sense as the effects of conventional and unconventional measures on design features and associated time/effort and costs vary greatly.

The objective of conventional measures is to influence combustion to the extent that peak temperatures in the combustion chamber are reduced. As explained in detail in Section 3.3.1, the formation of NO is reduced by lowering the peak temperature. At the same time a corresponding increase in particle emissions and fuel consumption should be kept within acceptable limits (cp. Fig. 3.36).

All important parameters (referred to as influencing parameters) that can assist in influencing combustion are listed below:

- Number of inlet and exhaust valves
- Combustion chamber:
  - shape
  - compression ratio
- Air:
  - swirl
  - turbulence
  - compression ratio
- Fuel injection:
  - location of injection nozzle
  - injection pressure
  - injection start
  - injection duration
  - injection rate
  - number of injection orifices
  - size and geometry of nozzle geometry
  - free spray length.

The combustion process to be modified using the above parameters is characterised by the following variables:

- Proportion of premixed combustion
- Level of homogenisation
- Localised air–fuel ratio λ_v
- Combustion duration
- Maximum compression pressure
- Compression focal point.

The following serve as parameters of success:

- NO_x emission
- Particle emission
- Specific fuel consumption, BSFC.

The above parameters influence one another mutually to a greater or lesser extent and also bring about partially opposing effects. It is therefore extremely difficult to categorically state the effects of individual parameters. However, a qualitative statement can be provided that gives an impression of the effects of individual parameters on pollutant emissions and efficiency (Fig. 3.38).

The lines highlighted in grey show parameter variations that basically tend to lead to a reduction in particle emissions and fuel consumption. This includes increasing the injection pressure, the number of nozzle holes (associated with nozzle hole diameter reduction) and the free spray length. Typical measures in relation to mixture formation and combustion are:

- High proportion of premixed combustion
- High level of homogenisation due to efficient air entrainment
- Relatively lean combustion with high localised air–fuel ratio
- Short combustion duration
- Shifting of combustion centre to advance.

The shaded lines indicate measures that reduce NO_x including retarded

Engine procedure	Fuel mixture generation/combustion						Engine results		
					Combustion				
	Premixed combustion	Homogeni-sation	Local λ_v	Combustion duration	Maximum pressure	Balance points	NO_x	PM	BFSC
Injection pressure (high)	↑	↑	↑	↓	↑	←	↑	↓	↓
Start of injection (late)	↓	↓	↓	↑	↓	→	↓	↑	↑
Hole diameter (small)	↓	↑	↑	↑	↓	→	↓	↓	↑
Hole number (large)	↑	↑	=	↓	↑	←	↑	↓	↓
Swirl (small)	↓	↓	↓	↑	↓	→	↓	↑	↑
Free spray length (large)	↑	↑	↑	↓	↑	←	↑	↓	↓
Compression ratio (high)	↓	↓	↓	↓	↑	←	↓	↑	↓
Goal	↓	↑	↑	↓	↑	Optimal	↓	↓	↓

3.38 Influence of individual parameters on emissions and efficiency (Bach *et al.,* 1997).

injection start, low swirl and a high compression ratio. Decisive factors in this behaviour are reduction of premixed combustion and reduction in localised air–fuel ratio.

The only way to reduce both types of pollutant is to reduce the diameter of the nozzle hole (hatched pattern). When used in isolation this measure produces a higher fuel consumption due to the longer injection time.

The individual measures listed in Figure 3.39 show the typical behaviour for the NO_x–particle or NO_x–fuel consumption trade-off (cp. Fig. 3.36). An overall improvement, i.e. reduction in pollutant emissions accompanied by no or only slight reduction in efficiency, is only possible by logically combining individual measures.

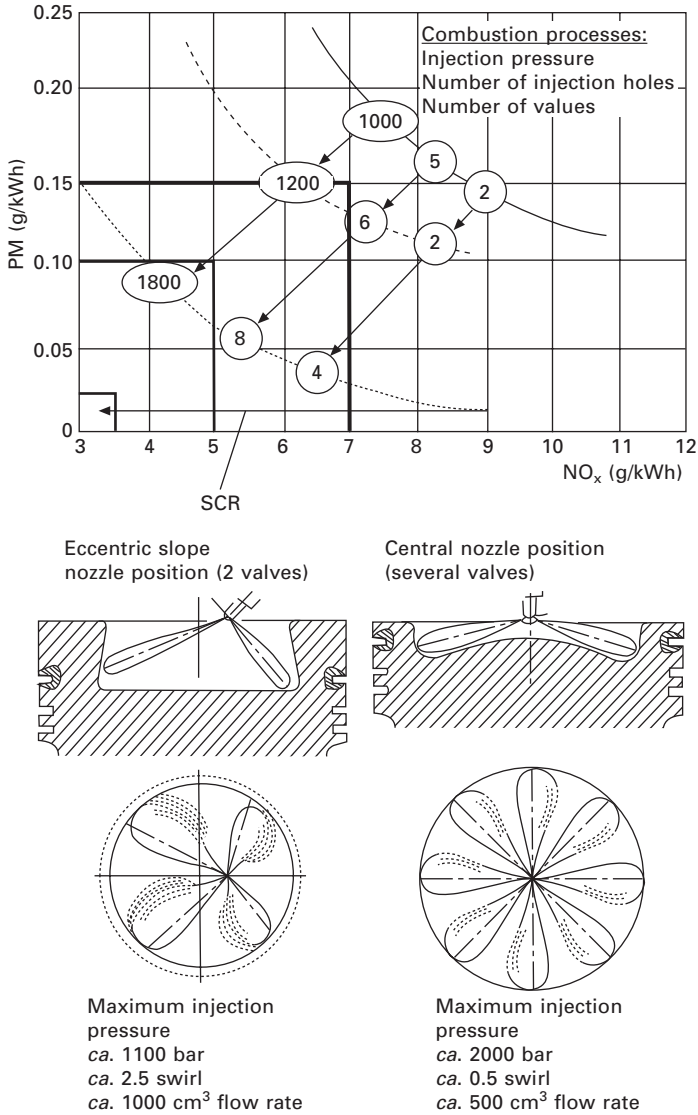
Figure 3.39 (top) shows developments in this regard using commercial vehicle engines as an example based on appropriate EURO I to III limit values for NO_x and particle (PM) emission. The corresponding combustion chamber shapes, nozzle position, etc., are shown in the lower section of the figure. In general, the current situation as regards engine-internal reduction of pollutants is based on shifting the energy used for mixture preparation from the air to the fuel side. The most important aspects to consider during implementation are an increased number of nozzle holes combined with a reduced diameter of nozzle hole and low swirl. The limits of this procedure are determined by the justifiable injection pressure level and corresponding minimum nozzle hole diameters.

The most important unconventional measures are water injection and exhaust-gas recirculation.

Water injection

The water introduced into the combustion chamber reduces the temperature in the combustion chamber and therefore also reduces NO formation due to the evaporation enthalpy required to evaporate the water. There are many ways in which water can be introduced into the combustion chamber. The four most important methods are shown in Fig. 3.40.

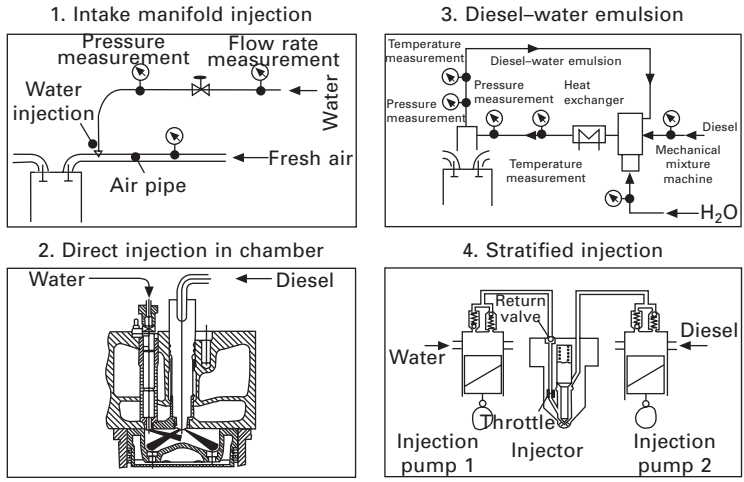
In the first method, the water is injected continuously into the inlet port. In the second, the water is injected directly into the combustion chamber via an additional injection nozzle in the cylinder head. In this case a complete separate injection system is required. In the third method, a diesel–water emulsion is generated directly in front of the fuel injection pump and is injected into the combustion chamber without further modification to the injection system. In the fourth method, a layer of water is deposited at the nozzle needle during the charge cycle phase. The stratification is structured in such a way that a small quantity of fuel is injected first. The water is then injected, followed by the remaining quantity of fuel.



3.39 Current situation as regards technology in relation to NO_x–PM trade-off using EURO limit values for commercial vehicle engines (Binder, 1997).

NO_x and soot emissions

Figure 3.41 shows the relative change in NO_x and soot emission as a function of water content for a constant injection start. The water content is therefore defined as follows.



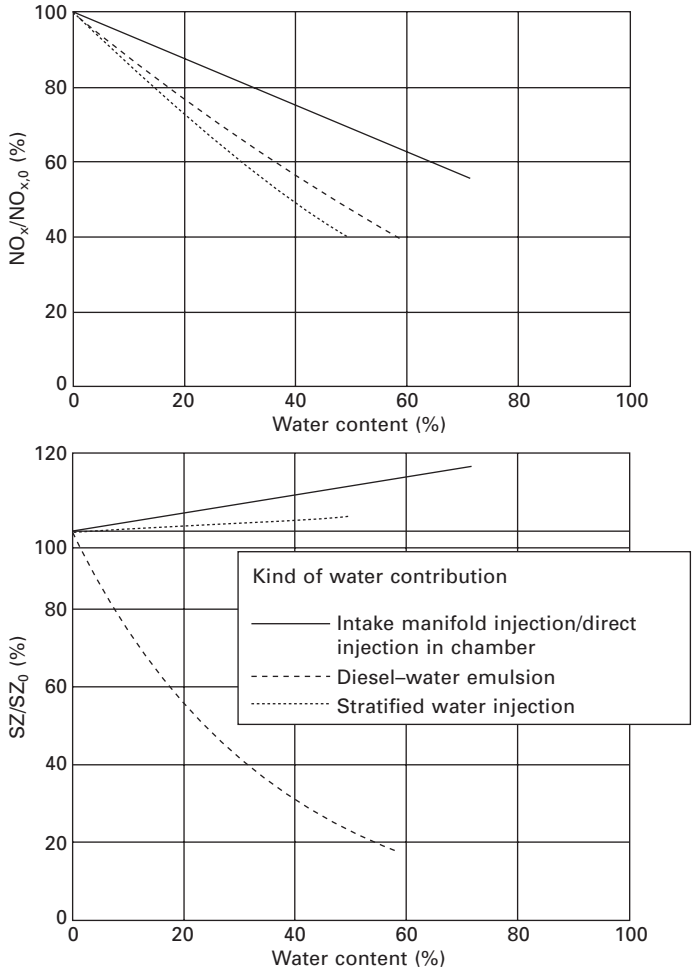
3.40 Schematic representation of the four water introduction methods (Velji *et al.,* 1996).

The respective behaviours for water introduction via the inlet port and direct injection into the combustion chamber are shown in a combined presentation, as their effect on emissions is more or less identical. The following conclusions can be drawn from Fig. 3.41:

- To achieve the same relative NO_x reduction, less water is required with diesel–water emulsion and stratified injection than with injection via inlet port or directly into the combustion chamber.
- Soot emission with diesel–water emulsion reduces by 80% for a water content of 50%.
- With stratified injection the addition of water barely influences the emission of soot.
- A slight rise in soot emissions is evident with other methods of water addition. This is roughly 10% at a water content of 50%.

The biggest NO_x reduction can be achieved where the following conditions are met:

- Water is in the correct location. Water should be present only at the point where combustion takes place. This can be achieved only if the fuel and water are injected together through the same nozzle into the combustion chamber. The diesel–water emulsion and stratified injection method satisfy this requirement.
- Correct timing of water introduction. The highest amount of NO is formed at the point where the highest temperatures occur locally. This is the case during diffusion combustion, so it is not necessary to introduce water



3.41 Relative change in NO_x (g/m^3, 5% O_2, standard conditions, deg and soot emission SZ (Bosch units) as a function of water content (Velji *et al.*, 1996).

for the entire fuel injection time. In fact, it is sufficient to start injecting water once the ignition delay period has elapsed and to maintain this until midway through diffusion combustion.

The 'right place at the right time' conditions referred to above can be satisfied only using stratified injection. Diesel–water emulsion fulfils the 'right place' condition but not the 'right time' condition as the water enters throughout the entire injection time. If the 'right place' condition is not satisfied, as is the case with the other two water injection methods, the 'right time' condition is irrelevant.

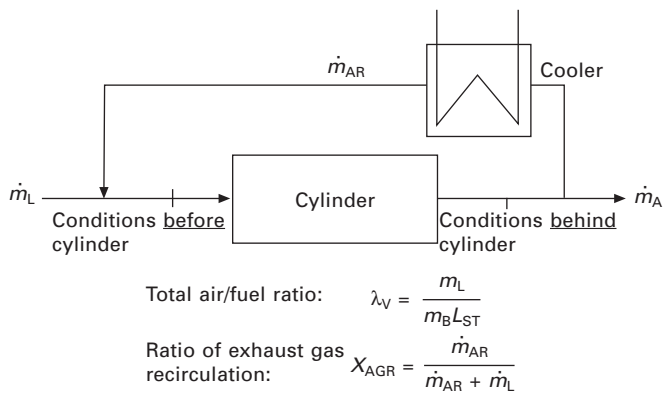
It can be determined, by analysing the influence of water on soot emission, that water effectively reduces soot only in the case of diesel–water emulsion (80% reduction with 50% water content, Fig. 3.41). Soot emission is either not affected or made worse with all other water addition methods including stratified fuel injection (roughly 10% increase with 50% water content, Fig. 3.41). The mechanisms leading to significant soot reduction in the diesel–water emulsion method cannot be explained in every detail at present. It is feasible that improved mixture preparation as a result of an extremely effective fuel atomisation process could cause water in the fuel to break down the spray. An additional cause could be more frequent post-oxidation of soot that has already formed. The post-oxidation of soot is known to be assisted by OH radicals which in turn are formed by means of water dissociation (Velji *et al.*, 1995)

If the highest possible NO_x reduction rates and also soot reduction are to be achieved with acceptable rates of increase in pressure, the advantages of stratified fuel injection and diesel–water emulsion must be combined. This could be achieved by initially injecting a small amount of fuel to overcome the ignition delay and then injecting a diesel–water emulsion for the optimum period. The remaining fuel is then injected (Velji *et al.*, 1995).

It can finally be concluded that when devising a standard solution for water injection not only the effectiveness of the various water addition methods in reducing pollution but also the level of expenditure required for the relevant application must be taken into account.

Exhaust-gas recirculation

With exhaust-gas recirculation (EGR), part of the exhaust gas flow is fed back to the combustion chamber, uncooled or cooled (Fig. 3.42). However,

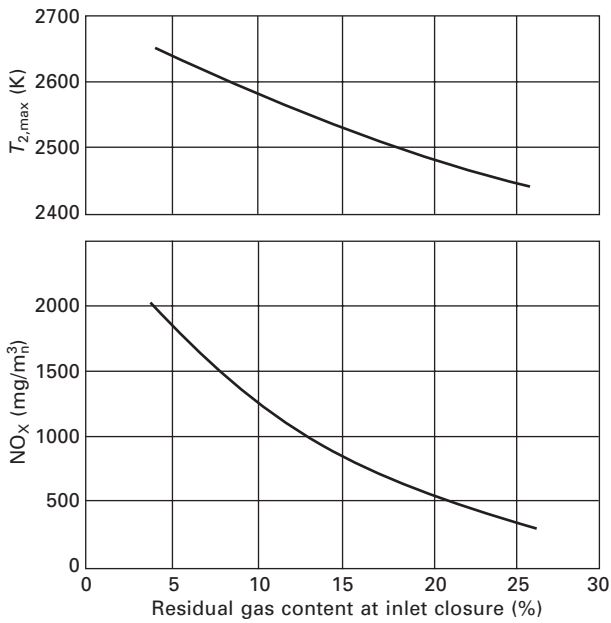


3.42 Schematic representation of exhaust-gas recirculation.

a particle filter is necessary in the case of the diesel engine when cooling the recirculated exhaust-gas flow as otherwise the exhaust-gas cooler quickly becomes blocked with soot particles. As the volume of exhaust gas recirculated depends on power and speed, use of a variable turbine geometry (VTG) is expedient to achieve the highest possible reduction in pollutants. The operating principle of the EGR is based on increased cylinder charge residual gas content (Fig. 3.43). It is evident that if the content of residual gas is roughly 20%, this reduces the NO_x mass originally formed by around a quarter.

The EGR lowers the temperature in the post-flame area and reduces the time interval during which the temperature threshold of 2200 K is exceeded. As an exponential relationship exists between the formation of NO and temperature, this drastically reduces the rate at which NO is formed. The temperature in the post-flame area is reduced for the following two reasons:

- The partial pressure of O_2, i.e. the oxygen content of the cylinder charge, decreases. However, the quantity of oxygen required locally for combustion of the fuel is constant. It is therefore necessary to transport a higher gas mass through the flame front than if the engine were operated without EGR. With EGR the increased mass throughput leads to a higher mass in the post-flame area. Low temperatures are therefore produced



3.43 Influence of EGR rate on maximum temperature and nitrogen oxide formation.

in the post-flame area with the same amount of heat being supplied and practically the same combustion characteristic curve.

- The specific heat capacity of the recirculated exhaust gas is greater than that of the air. Up to 90% of the temperature-reducing effect of the EGR is due to the reduction in oxygen content of the cylinder charge. The oxygen content is reduced by the recirculated exhaust-gas mass flow and is therefore a function of the EGR rate and air–fuel ratio. This means that the reduction in NO_x emissions is a function of the EGR rate and air–fuel ratio.

The following observations can be made:

- The relative effect of the EGR on NO_x reduction becomes weaker as the EGR rate increases.
- Engine operating points with small λ_{V0} have the greatest potential for NO_x reduction.
- NO_x reduction rates of between 40% ($\lambda_{V0} = 4.0$) and 80% ($\lambda_{V0} = 1.6$) can be achieved with an EGR rate of 20%.

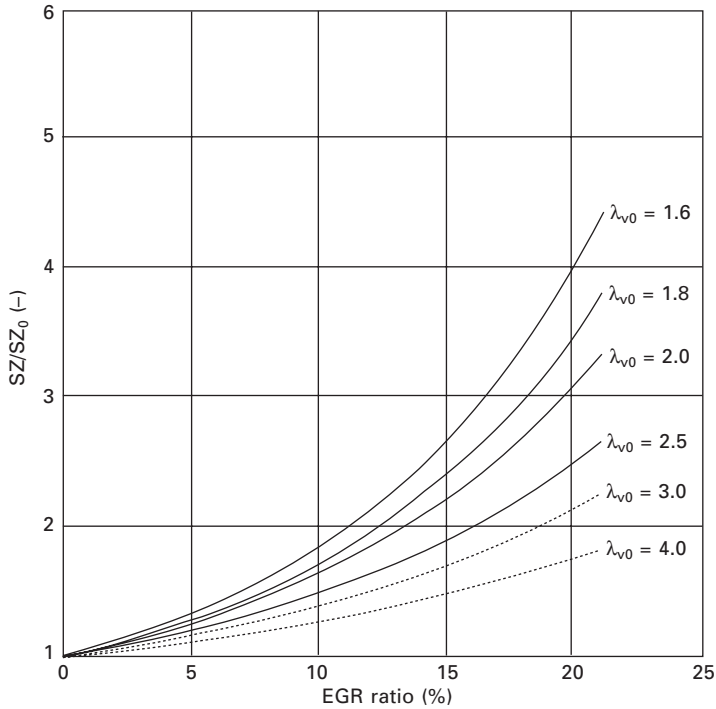
The emission of soot is encouraged by the EGR as this reduces oxygen content and temperature, particularly in the post-flame area (Fig. 3.44). The following conclusions can be drawn from the above:

- The effect of the EGR on the relative change in soot emission becomes stronger as the EGR rate increases.
- The smallest increase in relative smoke emission occurs at engine operating points with high λ_{V0}.
- The absolute increase in smoke emission depends on the level of smoke emission without EGR. The smoke emission increases by a factor of 4.0 with an EGR rate of 20% and $\lambda_{V0} = 1.6$.

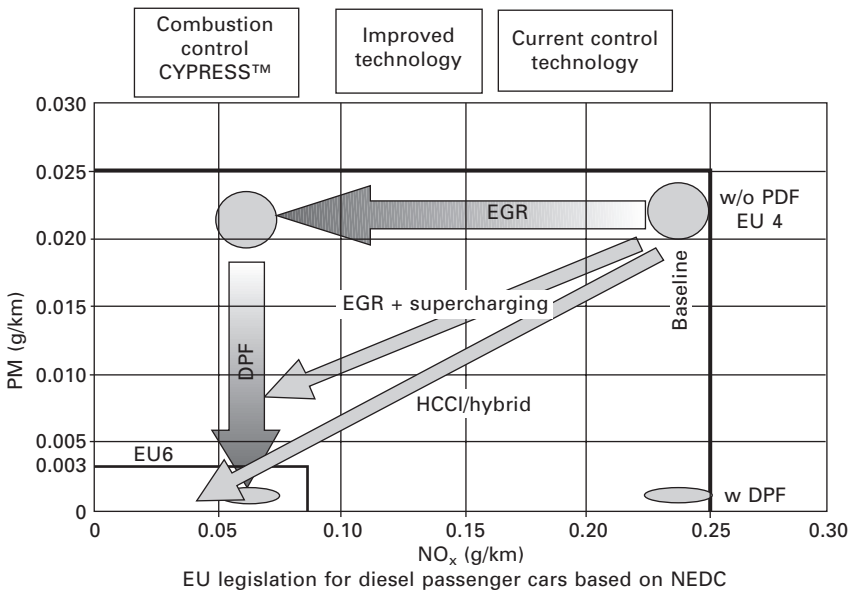
3.4 Future trends

In this section the future trends of HSDI diesel engines will be outlined. The starting point is the state of the art, represented by the baseline in Fig. 3.45. This figure shows the current and future emission legislation of the European Union (EU4, EU5 and EU6 for passenger cars) for the emission components oxides of nitrogen (NO_x) and particulate matter (PM). The test cycle is the New European Driving Cycle (NEDC).

By just applying a diesel particle filter (DPF) it is possible to meet the EU6-PM limit. Combining current control technology, improved control technology and in the near future in-cylinder pressure-based combustion control (CYPRESS™) together with exhaust gas recirculation (EGR), the EU6-NO_x limit can be met. DPF will still be needed to meet the PM limit. Depending on the engine size, correlating with vehicle weight, a DENOX aftertreatment might be necessary (not shown in Fig. 3.45).



3.44 Relative changes in soot emissions as a function of EGR rate and air–fuel ratio λ_{V0} (Remmels *et al.*, 1997).



3.45 Future trends to meet future emission legislation.

Future trends will include EGR combined with supercharging and HCCI combined with hybrid.

There will be not a single technology in the future. Rather a variety of technologies will be offered depending on the market and vehicle size. A decisive factor will be additional costs for the new technologies, which will include:

- High injection pressures
- Supercharging
- Nozzle design, rate shaping, etc.
- Combustion control
- HCCI/hybrid
- New fuels.

3.5 References and further reading

Arai M. *et al*. (1984), Disintegrating process and spray characterization of fuel jet injected by a diesel nozzle, SAE paper 840275

Bach E. *et al*. (1997), Gemischbildungsseitige Einflüsse auf die Reduzierung der NO_x-Emission bei Nutzfahrzeug-Dieselmotoren, 2nd Dresdner Motorenkolloquium

Baumgarten C. (2005), Berechnung der innermotorischen Gemischbildung – heutiger Stand und Herausforderungen bei der Auslegung zukünftiger Brennverfahren, Habilitation, Universität Hannover

Binder K. (1992), Einfluss des Einspritzdrucks auf Strahlausbreitung, Gemischbildung und Motorenkennwerte eines direkteinspritzenden Dieselmotors, Dissertation, TU München

Binder K. (1997), Maßnahmen zur innermotorischen NO_x-Senkung, 2nd Dresdner Motorenkolloquium

Blume K. (1940), *Gemischbildung und Verbrennung in der Bombe*, Deutsche Kraftfahrtforschung, Zwischenbericht No. 91, Dresden

Bockhorn H. (1994), *Soot Formation in Combustion – Mechanisms and Models*, Berlin, Heidelberg: Springer Verlag

Chmela F. *et al*. (1999), Emissionsverbesserung an Dieselmotoren mit Direkteinspritzung mittels Einspritzverlaufsformung, *MTZ* 60, 552–558

De Soete G. (1981), Physical–chemical mechanisms during nitrogen oxide formation in industrial flames, *Gas Wärme International* 30 (1981), No. 1

Dietrich W.R. (1999), Die Gemischbildung bei Gas- und Dieselmotoren sowie ihr Einfluss auf die Schadstoffemissionen – Rückblick und Ausblick, Part 1, *MTZ* 60(1), 28–38; Part 2, *MTZ* 60(2), 126–134.

Fenimore C.P. (1971), Formation of nitric oxide in premixed hydrocarbon flames, *Proc. Combust. Inst.* 13, 373–380.

Heywood J.B. (1988), *Internal Combustion Engine Fundamentals*, NewYork: McGraw-Hill

Houben M. *et al*. (1990), Untersuchungen zur Rußbildung während der dieselmotorischen Verbrennung, *MTZ* 51, 7/8

Johnson T. (2005), The effect of mixed mode combustion on diesel emission control systems, 9th International Conference on Present and Future Engines for Automobiles

Kleinschmidt W. (1974), Untersuchung des Arbeitsprozesses und der NO-, NO_2- und CO-Bildung in Ottomotoren, Dissertation, RWTH Aachen

Kolar J. (1990), *Stickstoffoxide und Luftreinhaltung*, Springer-Verlag.

Kolb T. (1990), Experimentelle und theoretische Untersuchungen zur Minderung der NO_x-Emission technischer Feuerungen durch gestufte Verbrennungsführung, Dissertation, Universität Karlsruhe (TH)

Kremer H. (1986), Grundlagen der NO_x-Entstehung und -Minderung, *Gas Wärme International* 35 (1986), No. 4

Lavoie G.A. *et al*. (1970), Experimental and theoretical investigation of nitric oxide formation in internal combustion engines, *Combustion Science and Technology* 1, 313–326

Leuckel W. (1985), Schadstoffbildung bei industriellen Verbrennungsanlagen und primäre Minderungsmaßnahmen, 1st TECFLAM-Seminar, 15, May 1985, Heidelberg

Meurer S. (1966), Der Wandel in der Vorstellung vom Ablauf der Gemischbildung und Verbrennung im Dieselmotor, *MTZ Motortechnische Zeitschrift* 27 (1966), 4

Mollenhauer K. (1997), *Handbuch Dieselmotoren*, 1st edition, Berlin: Springer

Pischinger F. *et al*. (1988), Grundlagen und Entwicklungslinien der dieselmotorischen Brennverfahren, *VDI Berichte* No. 1988

Remmels R. *et al*. (1997), Grundsatzstudie: Einfluss der Abgasrückführung auf Emission und Wirkungsgrad, 2nd Dresdner Motorenkolloquium

Renner G. (1994), Experimentelle und rechnerische Untersuchungen über die Struktur technischer Dieseleinspritzstrahlen, Fortschritt-Berichte VDI, Series 12, No. 216, VDI-Verlag, Düsseldorf

Robert Bosch GmbH (2004), *Dieselmotor-Management*, Vieweg Verlag, 4th revised edition

Seebode J. (2004), Dieselmotorische Einspritzratenformung unter dem Einfluss von Druckmodulation und Nadelsitzdrosselung, Dissertation, Universität Hannover

Sitkei G. (1964), *Kraftstoffaufbereitung und Verbrennung bei Dieselmotoren*, Berlin/Göttingen/Heidelberg: Springer-Verlag

Sutton J.A. and Fleming J.W. (2008), Towards accurate Kinetic modelling of prompt NO formation in hydrocarbon flames via the NCN pathways, Combust. Flame. Vol. 154. pp. 630–636.

Thiemann W. (2000), Schwerpunkte bei der Entwicklung des Smartdieselmotors, in Bargende M. and Essers U. (eds), *Dieselmotorentechnik 2000*, Renningen-Malmsheim: Expert-verlag

Tschöke H. *et al*. (2005), Verbrennungsverfahren für Dieselmotoren, in *Handbuch Verbrennungsmotoren*, 3rd edition, Vieweg Verlag, Chapter 15.1

Van Basshuysen R. *et al*. (2005), *Handbuch Verbrennungsmotoren*, 3rd edition, Vieweg Verlag

Velji A. *et al*. (1995), Water to reduce NO_x emissions in diesel engines, a basic study, *CIMAC* (D46)

Velji A. *et al*. (1996), Dieselmotoren erfüllen mit Wassereinspritzung zukünftige NO_x- und Rußgrenzwerte, *MTZ Motorentechnische Zeitschrift* 57, 7/8

Velji A. *et al*. (1997), Verbrennungsentwicklung mit einem Common-Rail-Einspritzsystem, *Sonderausgabe der Motortechnischen Zeitschrift MTZ*, Die neuen Motorbaureihen 2000 und 4000 von MTU und DDC

Wakuri Y. *et al*. (1990), Studies on the fuel spray combustion characteristics in a diesel engine by the aid of photographic visualization, *ASME ICE*, Vol. 10, Fuel and Injection

Zeldovich Y.B. (1946), The oxidation of nitrogen in combustion and explosions, *Acta Physicochimica*, *USSR* 21, 577–628

4

Multiple injection diesel combustion process in the high-speed direct injection diesel engine

B. M. VAGLIECO, Istituto Motori-CNR, Italy

Abstract: In the diesel engine, the fuel injection system is the heart and it has become one of the critical emissions control technologies with the advance of electronically controlled fuel injection. It is one of the important keys to fulfil the stringent exhaust emissions standards, even if incorrect injection can cause reduced efficiency. In recent years, new injection systems with electronic control have been promoted as the future standard in fuel injection systems for diesel engines, maintaining fuel economy which is directly correlated to the reduction of CO_2. Among the new injection systems, the advantages claimed of the common rail ones have been the injection rate shaping, the variable timing and the duration of the injection, in addition to variable injection pressure, enabling high injection pressure even at low engine loads and mainly the split of total fuel amount. The split of injection or, better, the use of multiple injection can be considered as the most important aspect of modern diesel injection systems development. With the application of multiple injection technology, improved injection scheme design and better control of engine combustion have been achieved. Moreover, they have been effective in reducing not only NO_x and particulate matter but also diesel combustion noise. This chapter presents a few examples of researches carried out on both production and optical engines in combination in order to evaluate the effect of pilot, post- and multiple fuel injection strategies on engine performance and emissions.

Key words: multi injection, common rail, optical diagnostics.

4.1 Introduction

In recent years, manufacturers have greatly improved the power and efficiency of internal combustion engines. In particular, they have focused their attention on compression ignition direct injection (CIDI) engines because of their superior fuel economy over spark ignition engines. As a result, today's best diesel cars are over 35% more efficient than their gasoline counterparts. This higher efficiency translates directly into 20–25% savings of CO_2 emissions. However, emissions of nitrogen oxides (NO_x) and particulate matter (PM) from diesel engines are of major concern.

In order to overcome and reduce these pollutants, diesel engines are equipped with a high-pressure injection system, exhaust gas recirculation (EGR) and after-treatment devices. In particular, the new generation of high

speed direct injection (HSDI) engines is equipped mostly with a high pressure common rail (CR) system (30 to 180 MPa) capable of multiple injections [1–8].

The use of multiple injection was pioneered on larger engines and involved injection modulation and/or split injection as a good means to reduce NO_x and particulate emissions [9–13]. The CR injection system permits multiple injection. The common rail was the result of the pioneering work made at Centro Ricerche Fiat and Fiat Auto in Turin in the 1990s. The potential of the new CR system, named UNIJET™, was fully demonstrated and the reliability tests on a pre-production version were entirely successful [13]. In the spring of 1994, Fiat signed an agreement with Bosch for the commercialisation of the system. The availability of this new technology allowed the development and the production of the new generation DI diesel engines. The injection duration, fuel pressure and flow area of the nozzles determined the injected fuel quantity. In the same engine cycle the injectors could be electrically actuated many times and therefore multiple injection could be realised in a very simple and efficient way. A very small quantity of fuel down to 1 mm^3 per stroke could be managed in each injection.

The new technology was first introduced by Bosch on passenger car DI diesel engines in 1997. The first vehicles to feature the technology were the Alfa Romeo 156 JTD and the Mercedes-Benz 220 CDI. The major differences of the CR system compared with the standard diesel injection equipment are the free choice of the injection pressure and timing as well as the benefit of the available pilot injection at almost all operating points. As a result, a drastic reduction of the engine-out emissions, both gaseous and particulate, and of combustion noise was obtained thanks to the flexible management of the injection pressure and the shape during transient operation as a function of engine operating parameters [14–17]. Since the end of the 1990s, the evolution in the development of CR systems has continued to meet the ever-stringent emission standards.

The use of multiple injection strategy with the new CR injection system has enabled noticeable improvements in the emissions and performances of the DI diesel engine. In particular, the number of injections, the duration of a single injection and the dwell time between consecutive injections have offered the opportunity to meet emissions regulation using the faster electronic drivers for the pressure regulator valve and the solenoid injectors and the new generation of electronic control units (ECUs) [2, 3, 13–19]. At the same time, further efforts in the development of the combustion chamber geometry and the intake systems have contributed to optimising the in-cylinder thermo-fluid-dynamic processes [20].

Many papers have been published to demonstrate the potential of splitting the injection in diesel engines. First-generation HSDI engines were equipped with CR injection systems of the maximum rail pressure, 1350 bar. The CR

system was limited to two consecutive injections (pilot + main) due to the intrinsic limitation of the minimum dwell time of 1800 μs between two consecutive injections, imposed by the technology available at the time [1–3, 5]. Pilot injection was primarily used for combustion noise control. However, the engine experiments showed that with high pressure multiple injection (two or more injection pulses per power cycle) the soot–NO_x trade-off curves of a diesel engine could be shifted closer to the origin than with conventional single-pulse injections, reducing both soot and NO_x emissions simultaneously. Further improvements were no longer limited by the lack of more flexible injectors, and it was thus helpful to simulate the engine processes with the use of computational models, which could provide detailed and precise temporal and spatial information concerning parameter-controlled injection and combustion processes [18–20].

Next, faster electronic drivers for solenoid injectors were developed [2, 3, 6, 14, 15, 17]. The flexibility of the injection system allowed the split of the main injection in a sequence of three very closely coupled stages (pre–main–after), while maintaining the possibility of managing the present pilot and post-injection stages [16, 21]. The duration of the main injection process could therefore be managed independently from the injection pressure. Pre-injection offered possibility of controlling the combustion rate of the premixed charge. Post-injection contributed to oxidising the soot previously generated during the regeneration of particulate filters over the entire driving range. The cyclic regeneration of the trap, i.e. burning the particulate trapped in the filter, dispensed with the use of complex and expensive systems for increasing the exhaust gas temperature [22].

Moreover, in order to further improve the diesel combustion, basic and advanced experiments were made in order to better understand the physical and chemical processes involved in CR diesel engines. Transparent engines comparable with production engines have allowed investigation of the interaction between the air motion and the jet, the fuel spray distribution and evaporation, mixture preparation, autoignition, spatial distribution of key transient species and, finally, pollutant formation. These results have allowed the calibration and evaluation of the numerical data [20–30].

The recently developed piezo-actuated CR fuel injector is capable of delivering up to five injection events per combustion cycle at high pressure. These can reduce NO_x emissions down to a level of 0.15–0.20 g/km depending on the vehicle weight and rolling resistance. Despite these significant improvements, more research is in progress [31, 32].

For the diesel engine the goal remains of simultaneously reducing NO_x and PM emissions further while keeping unburned gaseous emissions (HCs and CO) at low values. In future diesel engines NO_x and PM reduction will occur by decreasing the local and overall temperatures in the cylinder and achieving a leaner and more homogeneous mixing level among air, EGR and

injected fuel. Again, multiple injection can be used to obtain the so-called 'premixed combustion' with early or late injections, though it presents a complex control issue because each mode can only operate over a limited speed–load range [4, 22, 33–36].

4.2 Double injection or pilot + main

Injection modulation and/or split injection were evaluated as a good means to reduce NO_x and particulate emissions. It is known that a small amount of fuel as well as a sufficient fuel–air mixture is necessary to reduce soot formation, and an intensified mixture of residual air and combustion gases can help oxidise the soot. To begin with, these requests were partially fulfilled using pilot injection. The experiments were carried out in a direct injection turbocharged diesel engine equipped with an experimental mechanical injection system. The pilot injection allowed control of the rate of heat release in the first stage of the combustion process and realised a smoother increase of the cylinder pressure with a reduction of combustion noise and NO_x. Although this injection system did not have the capability of a fully flexible electronic system, it demonstrated the effectiveness of pilot injection [9].

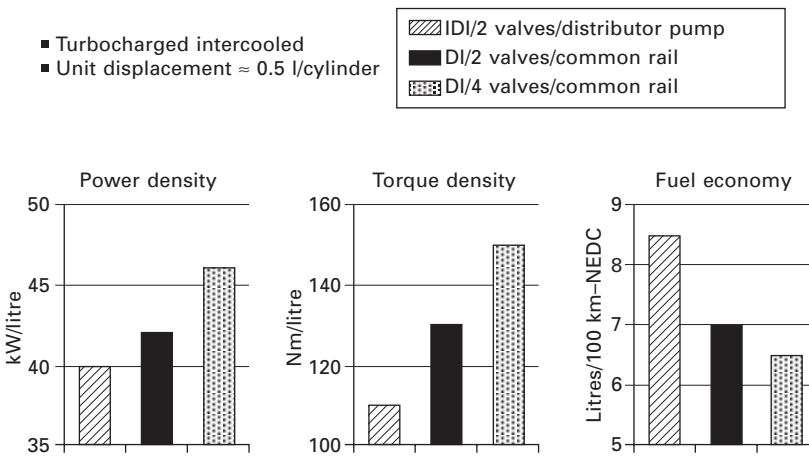
The main part of the experiments based on splitting injection was carried out on larger engines, although at first it was not always possible to achieve the simultaneous reduction of NO_x and particulate emissions, as demonstrated by contradictory results in the open literature. Nehmer and Reitz [10] experimentally studied the NO_x and soot trade-off in a large single-cylinder Caterpillar engine, showing that the double-pulse split injection provided a reduction of NO_x emissions with a limited increase in the soot emissions. They varied the amount of the fuel injected in the first injection pulse from 10 to 75% of the total amount of fuel and found that split injection affected the soot–NO_x trade-off. In general, their split-injection schemes reduced NO_x with only a minimal increase in soot emissions and did not extend the combustion duration. Tow *et al*. [37] continued the study of Nehmer and Reitz [10] using the same engine, and included different dwells between injection pulses. They found that at high engine load, particulates could be reduced by a factor of three with no increase in NO_x and only a few percentage points increase in the specific fuel consumption compared to a single injection, using a double injection with a relatively long dwell between the injections. Another important conclusion of Tow *et al*. [37] was that the dwell between injection pulses was very important in controlling soot production, and that there existed an optimum dwell.

Pierpont *et al*. [11] confirmed that the amount of fuel injected in the first pulse affected the particulate formed whereas the NO_x emission level was held constant. They found that the amount of fuel injected during each pulse represented a key parameter in achieving good control of emissions. Moreover,

the best double injections were found to also depend on the spray nozzle included angle. They observed that using an injector with a 125° included angle, which resulted in significant wall impingement on the piston bowl, the best double injections were found to be those with 50–60% of the fuel injected in the first pulse.

Han *et al.* [12] performed multidimensional calculations in order to investigate the NO_x and soot reduction mechanisms. They found that the split injection provided significant soot reductions without NO_x penalty. Moreover, they also showed that it had the same NO_x reduction mechanism as a single injection with retarded injection timing. Fuchs and Rutland [38] performed an analysis of the impact of swirl motions on emissions: they found that high swirl ratios might distribute the fuel such that it remained in the bowl, depleting almost the whole bowl of oxygen during combustion. Moreover, the split injection cases with high swirl showed slower initial combustion than the single injection case because of the temporary fuel cut-off. This resulted in poor second injection combustion. In this case the split injection failed to reduce soot emission because a large amount of soot was formed during the diffusive burning phase.

In the meantime, the introduction of common rail (CR) fuel injection systems for passenger cars made possible the consideration of advanced fuel-injection techniques, such as rate modulation and the use of split and pilot-injection strategies. The advantage of the CR fuel injection system on full load performance, in comparison with other injection technologies, is clearly shown in Fig. 4.1. The high injection pressure levels, available at all engine speeds, allowed substantial improvements in the engine torque (20–30%). The engine operating range could be further extended to higher

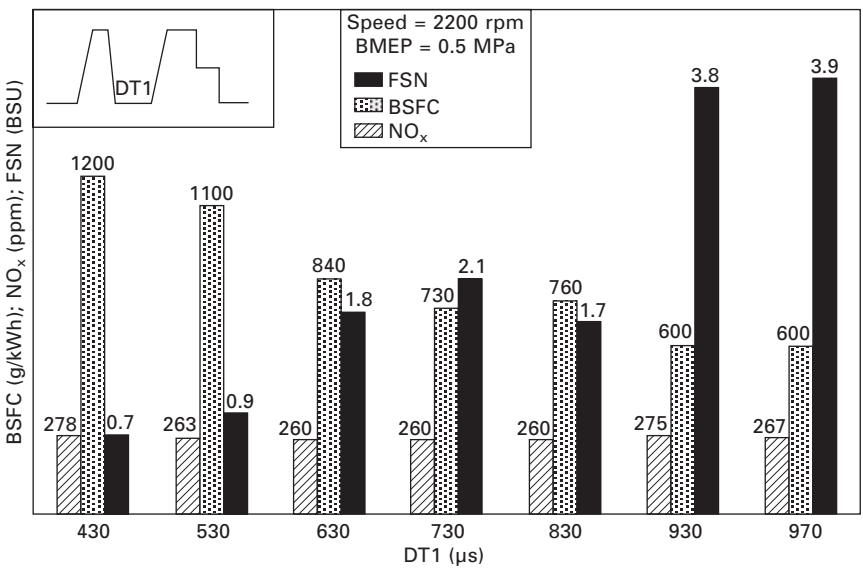


4.1 Comparison among different diesel engine technologies [14].

speed, since the mechanical and hydraulic limitations of the conventional distributor pumps were removed. A higher torque at low speed and an extended speed range offered great potential for vehicle fuel economy improvements, through the adoption of longer transmission ratios, without performance penalties. Driveability and comfort were for the first time getting closer to those of a gasoline engine powered vehicle. The injection strategies were based on the split of the total fuel amount in a pilot and a main. The pilot injection allowed the control of the rate of heat release in the first stage of the combustion process and the realisation of a smoother increase of the cylinder pressure. In this way a large reduction in combustion noise could be achieved in the most critical part-load operating conditions [13, 15].

Figure 4.2 shows the influence of the dwell time on smoke and NO_x emissions as well as on specific fuel consumption for the double injection strategy applied on a small single-cylinder research engine [39]. It can be noted that the reduction of the dwell time DT1 is very effective on the smoke even if NO_x increases, and that it was possible to find a good compromise between smoke and NO_x with low fuel consumption [39, 40].

Simultaneously, these mechanisms were fully analysed by many research groups both by CFD code and by advanced diagnostics in an optical engine [20, 23, 26, 28, 29, 41]. CFD simulations of light-duty engines and experimental measurements carried out by several groups [18, 19, 20, 41–46] helped to analyse the highly transient in-cylinder processes in detail. These methods



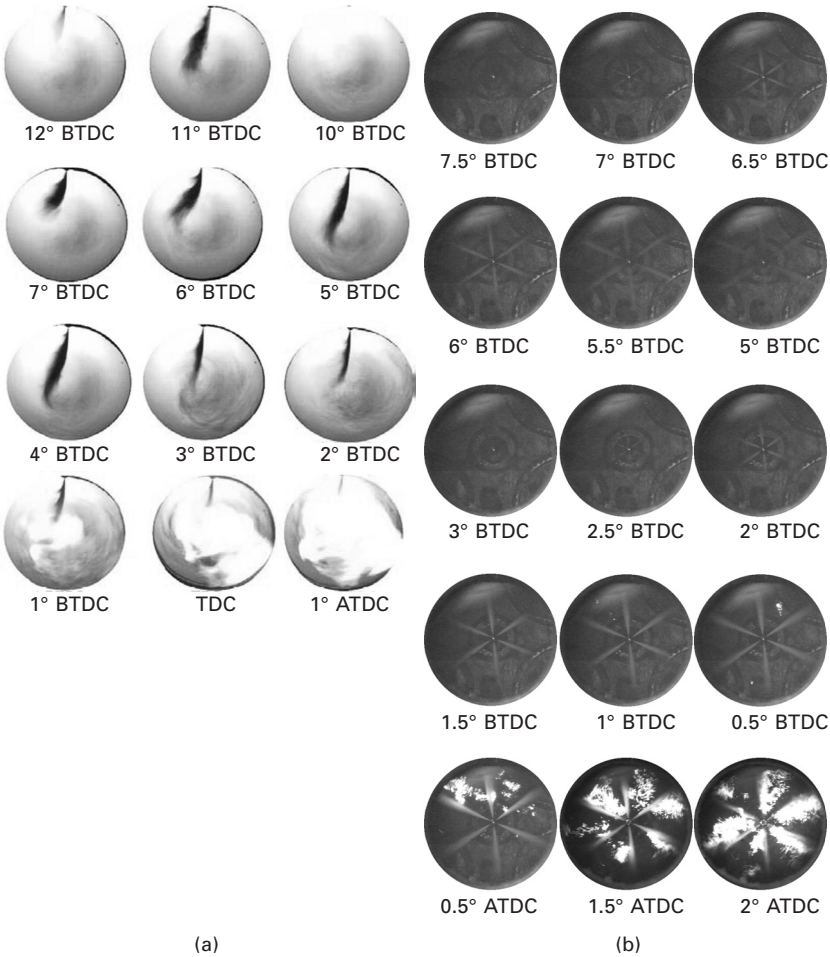
4.2 Smoke and NO_x emissions and fuel consumption with double injection vs dwell time [39].

provided essential insight into understanding the complicated physical and chemical interactions and underlying mechanisms during mixture formation, combustion and pollutant formation as well as the function of components of the system [43]. Optical diagnostics with high spatial and temporal resolution allowed the phenomena for different injection strategies to be investigated [24–27], The results were used for calibrating and evaluating the numerical simulation [20, 30].

Combined measurements, based on digital imaging and spectroscopic techniques, helped to follow the evolution of combustion processes from the start to the exhaust phase. While the direct imaging allowed one to see what happened inside the engine, the spectroscopic techniques helped in understanding the chemical reactions involved in combustion processes and pollutant formation mechanisms. Amongst the several studies carried by many groups, Mancaruso and colleagues evaluated the air–fuel mixing and the combustion process of the multi-injection strategy from both a single hole nozzle and multiple holes at the same engine operating condition [23–25, 43]. Figure 4.3 reports the effect of the pre + main strategy on the spray and combustion evolution of a single and a six-hole injector, respectively. The air–fuel mixing and its evolution can be observed in good detail for the single jet and for the interactions between multiple jets in the case of multiple holes. Both injector systems show the same behaviour up to the first luminous flame. During the fuel injection phase, the single-hole jet was influenced by the swirl motion charge and was lightly distorted with respect to the other one. A good jet atomisation due to the CR high fuel injection pressure was observed. In 1 CAD, the pre-injection spray vaporised rapidly and disappeared before the start of main injection. However, due to the low local temperature and pressure, the visible combustion did not appear. During the main injection, the liquid jet penetrated almost linearly, reaching the maximum length in approximately 3 CAD. The strong aerodynamic resistance broke up the fuel drops and reduced their size. As injection proceeded, fuel vaporisation took place, the liquid spray became thin and the impingement of the wall was avoided.

As observed by Schmid and Leipertz [24] in an optical engine, single injection led to deeper penetration into the combustion chamber and nearly reached the wall of the combustion bowl with a fast and nearly complete combustion of the cylinder charge. The additional pre-injection could lead to a decrease of the ignition delay and the main injection penetrated into an existing flame. This caused a larger amount of soot, and although the combustion was longer, this was not sufficient for complete oxidation of more soot.

On the other hand, Koyanagi *et al.* [41] carried out the investigation in a CR optical engine, maintaining all production-type details of the combustion chamber geometry, and analysed all the phases of injection and combustion



4.3 Comparison between (a) the images of spray of one hole and (b) six-hole nozzle for the pre + main strategy at engine speed of 1000 rpm and P_{inj} = 800 bar.

under virtually real engine conditions. This optical engine was used along with 2D optical diagnostics for evaluation of the temperature, soot and OH as well as spray shadowgraphy. By using the special prototype CR injectors, the effects of engine design and operation strategies on ignition, combustion and pollutant formation were studied and the controlling parameters were isolated. Special emphasis was devoted to the effects of injector stability, spray symmetry, nozzle geometry, injection rate, pilot injection and swirl effects. In particular, the authors observed that the pilot + main injection strategy was characterised by a complete premixed combustion of the fuel fraction injected during the pilot injection (about 10% of the total mass).

The resulting increase of cylinder pressure and temperature, as well as the presence of active radicals, substantially reduced the auto-ignition delay time of the fuel injected during the subsequent main injection. In these conditions the mixing of the main injected fuel deteriorated, promoting soot formation. The increased sooting tendency of the main combustion due to the presence of the pilot combustion could be controlled by increasing the rail pressure and with a proper choice of the dwell angle between pilot and main.

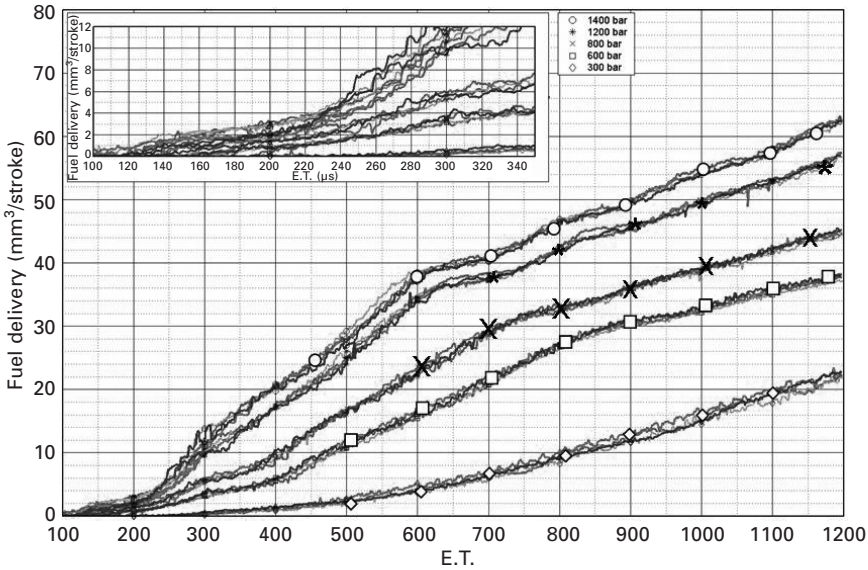
Studies have shown that performance became increasingly unfavourable as the number of pilot injection phases increased and that the most satisfactory level of emissions is obtained without pilot injection. Diesel engines without pilot fuel injection are unacceptable on account of their poor combustion noise. Pilot injection close to the main injection achieved the best acoustics but poorer particulate emissions; whereas a longer interval between the pilot and main injection phases reduces the particulate emission but worsens the noise pattern. A larger pilot-injected fuel volume improved the acoustics but increased particulate emissions, but it should be noted that the volumetric tolerance demand increased if pilot injection occurred only shortly before the main injection stroke. Analogous results were obtained even with piezo-injectors [31, 32].

4.3 Multiple injection technology

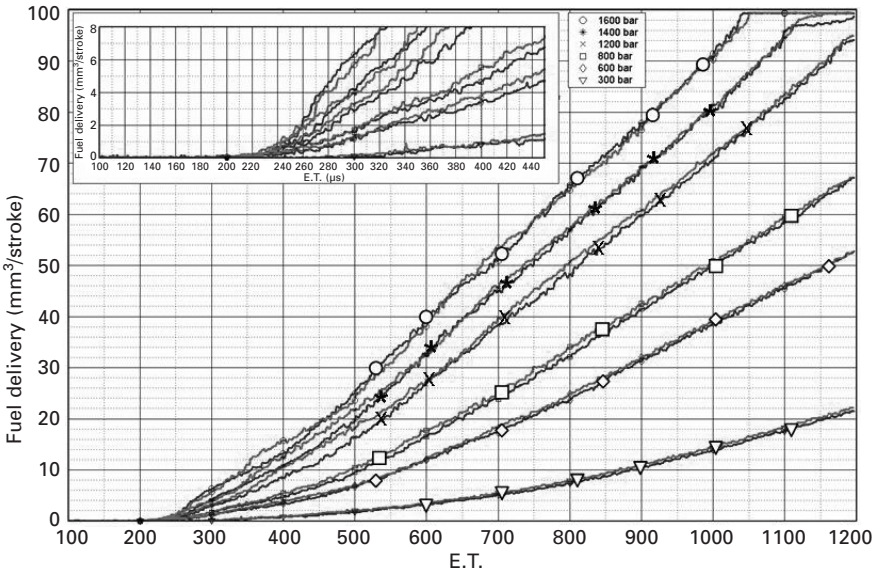
Multiple injection technology was considered very attractive for the HSDI diesel engine based on the results of heavy-duty engines [10, 32]. It went beyond the standard 'pilot–main' strategy and was not restricted by the long minimum dwell time (around 1.8 ms). Multiple injection involves minor modifications of the present CR system components and, therefore, is not accompanied by a significant cost increase [21, 29, 36, 37]. However, due to design limitations, the first generation of CR injection systems could not handle sequential injections with reduced dwell times between one injection and the following one. It was necessary to design a new injector, capable of actuating multiple injections.

The application of multi-injection strategies was obtained with the second-generation common-rail, solenoid fuel-injection system. Figure 4.4 reports the behaviour of the fuel delivery versus time of the first and second generation of CR systems. The second generation was a better system in terms of performance and robustness and vastly improved the linear behaviour, without a plateau in the fuel delivery. This last feature allowed the improvement of the fuel metering accuracy in all of the injection pulses, with further reductions in the engine noise and emissions. This was obtained with creative control algorithms.

Experimental measurements carried out by several groups [16, 17, 42] showed that with the new generation of solenoid injector and ECU the number



(a)

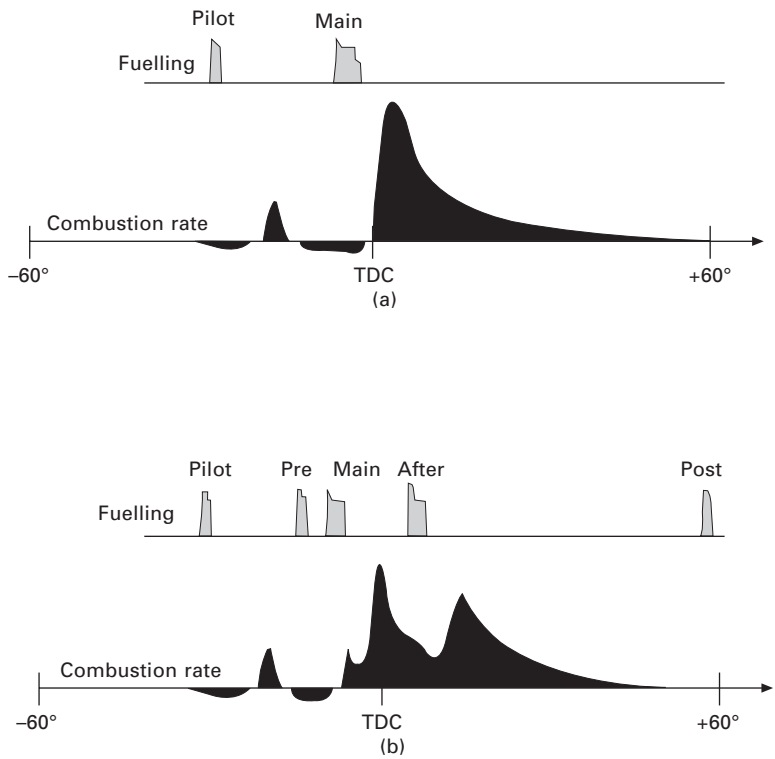


(b)

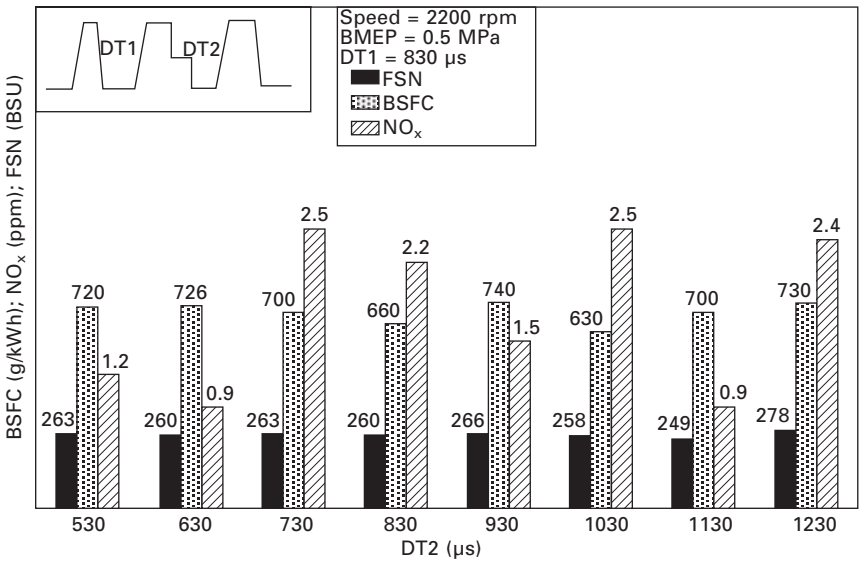
4.4 Comparison between the fuel deliveries of (a) the first and (b) the second generation of CR injection systems for different injection pressures.

of consecutive injections and the balance of fuel amount per injection can be controlled accurately, as well as the reduction of the dwell time between consecutive injections (Fig. 4.5).

Three consecutive injections (pilot + main + after) were found to be particularly effective in reducing smoke. This strategy was investigated for different dwell times. It was demonstrated that, for constant DT1 of 830 μs, a post-injection after the main is very effective to further reduce smoke from 1.7 to 0.9 BSU with a simultaneous positive effect on NO_x as shown in Fig. 4.6, in which the history of combustion pressures and the rate of heat release for this strategy are shown. It can be seen that the after-injection locally increases the soot oxidation activity, resulting in lower smoke emission without a penalty on NO_x. The amount of fuel in the main injection was split in a sequence of very closely coupled stages (usually up to three). The flexibility of the system also allowed managing, if needed, the injection stages at a longer dwell time with respect to the main injection The optimal multiple injection strategy was characterised by a first injection



4.5 Comparison between (a) pilot injection and (b) multiple injections.



4.6 Smoke and NO_x emissions and fuel consumption with triple injection vs dwell time [39].

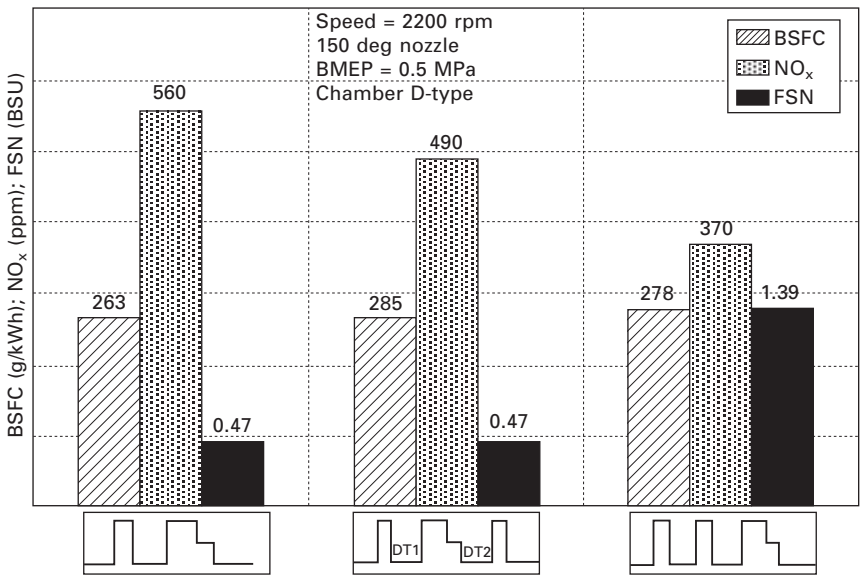
(called 'preinjection') very near to the main injection and by an injection following the main one (called 'after-injection') [22].

The choice of the optimal injection strategy required much experimental work in order to evaluate the effect of each single parameter. A large number of single injection parameters were considered, as well as the complicated interactions among them. Split injections have been shown to be effective in simultaneously reducing soot and NO_x emissions when the injection timing is optimised. However, they can also result in worse soot emissions when either the injection timing is too retarded or the injection dwell is not optimised. In comparison, as reported in Fig. 4.6, the three injections strategy allowed managing more appropriately the compromise between NO_x and smoke. In particular, the third injection, made late after the TDC, could contribute to oxidising the soot formed previously without increasing the NO_x emissions [39, 40, 47]. This conclusion was confirmed from the combustion pressure cycle that shows a slight peak during the expansion stroke and by the flame evolution detected in optical engines. Plate I (between pages 364 and 365) shows the UV–visible flame and OH distribution evolution of the triple injection strategy. In order to shorten the description, the first phase is not included because it is comparable with the pre + main strategy previously reported in Fig. 4.3, even though there is a small shift in the crank angles. It can be noted that the first evidence of after-injection was around 13.5 CAD ATDC, from which time the jets penetrated quickly in the high temperature and pressure environment of the chamber and this contributed to a short ignition

delay (less than 1 CAD). At this time the start of post-combustion occurred. This combustion had a less intense premixed phase and was comparable with the diffusive phase. It can be noted that, after the auto-ignition phase due to the last fuel injection and until 15 CAD ATDC, fast reduction of OH radicals was observed [26]. OH radicals, produced by the exothermic reactions of the post-injection combustion, spread in the chamber during the oxidation process of the soot produced by the main injection combustion. The persistence and high concentration of OH radicals, at the same time, could induce good burning of soot leading to a lower level of soot at the exhaust with respect to the other strategies, but it promoted a small increase in NO_x emission.

On the other hand, the soot–NO_x trade-off obtained by splitting the main injections of various dwell times in a single-cylinder engine did not always show a relevant effect on both the emissions and BSFC. Figure 4.7 shows the emissions and fuel consumption for the optimised dwell times in a small single-cylinder diesel engine. Similar results were obtained for a multi-cylinder engine [39, 40, 44].

The experimental analyses carried out by Badami *et al*. [21] allowed better understanding of the effect of the pilot–pilot–main and the pilot–main–after for a light-duty engine. These authors investigated performance and emissions at three engine operating points that are typical of a driving cycle, with different pilot injection advances, after-injection quantities and positions. They observed that the pilot–pilot–main strategy could be more effective in



4.7 Smoke, NO_x emissions and BSFC for three different injection strategies with optimised dwell times DT1 and DT2 [40].

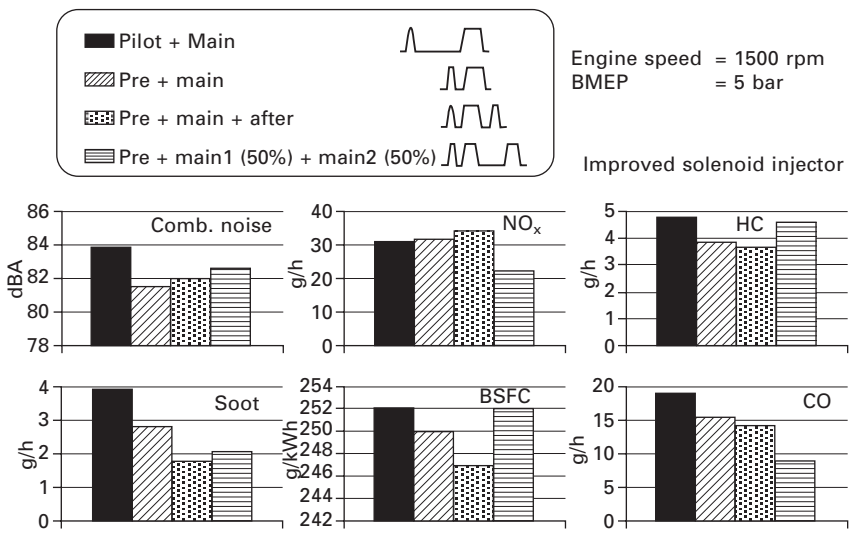
decreasing combustion noise and fuel consumption than the corresponding double injection strategy, but higher values of emissions had to be faced. The pilot–main–after injection strategy was very effective in lowering the soot but the timing had to be carefully selected. Finally, they detected that particular values of the dwell time created pressure waves in the rail and in the pipes. These hydraulic phenomena could change the characteristics of the injection and could produce some unpredictable situations, modifying the positive effect of the pilot or after-injections.

Figure 4.8 reports the performances and emissions at 1500 rpm and 5 bar BMEP for a typical CR engine operating with select injection parameters. It can be noted that the use of up to three injection pulses per cycle allowed combustion noise reduction and also reduced emissions of HC and CO [15].

As observed by Schmid *et al*. [24] in the condition of post-injection the situation was even worse. Here, the additionally injected fuel which was considered to increase the combustion duration in order to improve the soot oxidation had the opposite effect and produced an additional amount of soot, mainly close to the nozzle.

4.4 Other diesel combustion technologies

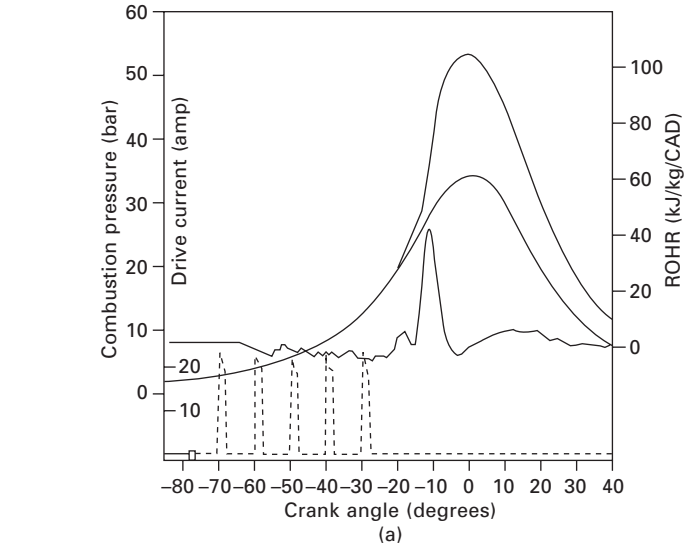
One of the most recent advances in fuel injection technology has been systems that use multiple injections with the rate being controlled (or 'shaped') to

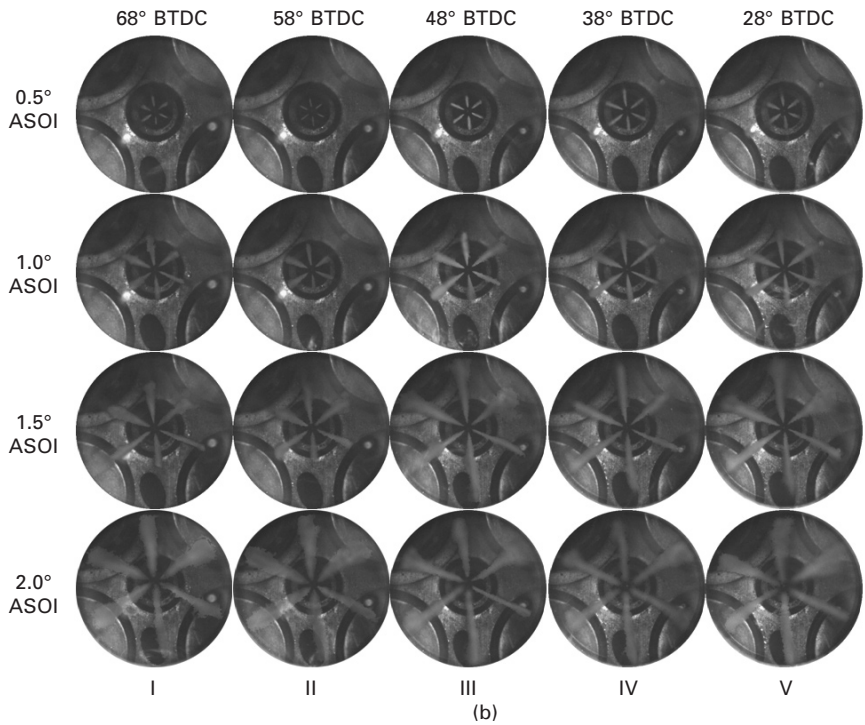


4.8 Effect of multiple injection on the performance and emissions of an HSDI passenger car [15].

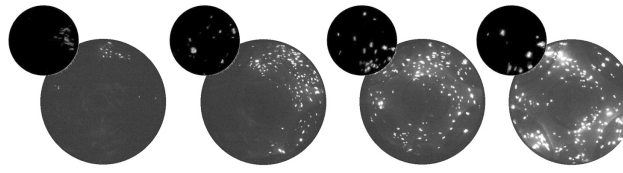
vary the delivery of fuel over the course of a single combustion event. These systems are beginning to be used extensively on light-, medium- and heavy-duty diesel trucks, a class of engines commonly carried over to off-road engine applications. This allows the ignition of a small quantity of fuel in order to initially limit the characteristic rapid increase in pressure and temperature that leads to high levels of NO_x formation. Most of the fuel is then injected into a higher temperature charge, leading to a shorter ignition delay and hence less premixed high-temperature high-NO_x combustion. Rate shaping may be done either mechanically or electronically. In electronically controlled engines, multiple injections may be used to shape the rate of fuel injection into the combustion chamber. Recent advances in fuel system technology have allowed high-pressure multiple injections to be used to reduce NO_x by 50% with no significant penalty in PM. Two or three bursts of fuel can come from a single injector during the injection event. The most important variables for achieving maximum emission reductions with optimal fuel economy using multiple injections are the delay preceding the final pulse and the duration of the final pulse [47].

The new CR systems offer multiple injections up to seven events per cycle, but the minimum hydraulic dwell time between consecutive injections is limited. The challenge is to develop an enhanced solenoid or piezo-actuated CR injector able to merge injections for the shape of the injection profile and thus of the combustion process. In conventional combustion mode, this feature means that a pre- and a main injection could become a nearly continuous injection process, with a smoother starting phase followed by a stronger main phase. Experimental results have demonstrated that with this strategy of injection modulation it is possible to control both soot and noise with higher benefits at medium to high loads. Moreover, if an after-injection could be placed very close to the main one, further soot reduction is achievable without a fuel consumption penalty. Finally, a new area of applications could be foreseen in which premixed combustion is adopted. The next step will be to alter the combustion process itself by applying the new concepts of so-called premixed combustion, even though this presents a complex control issue, since each mode can only operate over a limited speed–load range. In particular, the use of early injection enables the premixed combustion of a portion of the charge [22]. Thanks to the multiple-injection CR injection system, HCCI combustion based on five early injections per cycle at high pressure as previously used by Denbratt and Helmantel [33] was applied to an optically accessible diesel engine equipped with high pressure. Combined measurements, based on digital imaging and spectroscopic techniques, allowed the observation of the evolution of air–fuel mixing and the combustion process and better understanding of the effect on emissions reduction [34] (Fig. 4.9). The early fuel injection reaches a near-homogeneous state and thus with a proper air–fuel ratio and temperature control can produce very





4.9 (a) History of the in-cylinder pressure, rate of heat release and driven injector current, (b) some images of the spray, and (c) combustion evolution obtained from the quartz windows located in the piston and in the valve site at 1000 rpm and P_{inj} = 700 bar for five injection strategies [34].



4.9 Continued

low NO_x levels when it burns. However, as one increases the amount of fuel in this early pulse, eventually the amount of energy released becomes too great and one moves back into a regime of higher NO_x and high noise. Thus, premixed combustion with early injection can only be used at low loads and speeds.

The second strategy proposed is the use of late fuel injection and relying on high EGR rates to delay the ignition process until the fuel is well mixed with the air and EGR in the combustion chamber [15, 22]. In addition to slowing down the ignition chemistry, the high EGR rates of well-cooled gases also slow down the chemistry during the main combustion event. This process can also produce very low NO_x emission levels but at the expense of some engine efficiency, as the phasing of the combustion process gets shifted from the ideal location. Again, as in the early injection mode, there is a limit as to how much fuel can be injected and thus this mode is limited within the operating range of the engine to levels of around 8 bar BMEP. The potential of injection rate shaping for enhancing the mixing process in this combustion mode is under investigation. Furthermore, it has already been confirmed that it can significantly help in optimising the transition between conventional and premixed combustions.

Recently, it has been shown that a piezo-actuated injector energises quicker than its solenoid counterpart and is able to reduce the transition time for the start and end of the fuel injection event. In particular, it reduces the minimum injection interval delay from electronic activation to mechanical delivery from 0.4 ms with the conventional solenoid-actuated fuel injector to 0.1 ms. This reduced response time has led to achieving precise injection quantity and timing control, and finer spray atomisation [31, 32].

4.5 Conclusions

Intensive research on multi-injection strategies has been carried out in engine research laboratories throughout the world, as we are approaching the introduction of more strict emission legislation, and as the commitment to CO_2 reduction becomes imperative. This chapter has presented a few

examples of relevant research performed on both production and optical engines. The multiple injection capability is an effective technology used in modern diesel engines because it can be realised with minor modifications of the injection system components, without a relevant increase of cost, and therefore it should be considered a must for all future generation CR-DDI engines.

4.6 Acknowledgements

The author would like to acknowledge the contributions of present and former students, colleagues who co-authored the referenced papers and, in particular, Dr Carlo Beatrice and Ezio Mancaruso for useful discussions in the preparation of this paper. The author is grateful to Mr Carlo Rossi and Mr Bruno Sgammato for their support in the experimental activities carried out in the years reported in the referenced papers.

4.7 References

1. Ganser, MA (2000), 'Common rail injectors for 2000 and beyond', SAE paper 2000-01-706.
2. *Proceedings of International Symposium – The Future of Diesel Engine Technology for Passenger Cars*, Porto Cervo, Italy, 2000.
3. Schommers, J, Duvinage, F, Stotz, M, Peters, A, Ellwanger, S, Koyanagy, K, Gilden, H (2000), 'Potential of CR injection system for passenger car DI diesel engines', SAE paper 2000-01-0944.
4. *Proceedings of International Symposium – Towards Neutral Standards Diesel vs Gasoline Engine*, Ortigia, Italy, 2006.
5. Flaig, U, Polach, W, Ziegler, G (1999), 'Common rail injection system for passenger car DI diesel engines; experience with applications for series production projects', SAE paper 1999-01-0191.
6. Imarisio, R, Rinolfi, R (1999), 'The third generation direct injection diesel engine for passengers cars', *ATA Journal*, Vol. 52, No. 8/9.
7. Stumpp, G, Ricco, M (1996), 'Common rail – an attractive fuel injection system for passenger car DI diesel engines', SAE paper 1996-08-70.
8. Boehner, W, Hummel, K (1997), 'Common rail system (CR-system) for commercial diesel vehicle', SAE paper 1997-03-45.
9. Durnholz, M, Endres, H, Frisse, P (1994), 'Preinjection: a measure to optimize emission behavior of DI diesel engines', SAE paper 940674.
10. Nehmer, DA, Reitz, RD (1994), 'Measurement of the effect of injection rate and split injections on diesel engine soot and NO_x emissions', SAE paper 940668.
11. Pierpont, DA, Montgomery, DT, Reitz, RD (1995), 'Reducing particulate and NO_x using multiple injections and EGR in a D.I. diesel engine', SAE paper 950217.
12. Han, Z, Uludogan, A, Hampson, GJ, Reitz, RD (1996), 'Mechanism and NO_x emissions reduction using multiple injection in a diesel engine', SAE paper 960633.
13. Rinolfi, R, Imarisio, R, Buratti, R (1995), 'The potential of a new common rail diesel fuel injection system for the next generation of DI diesel engines', 16th International Vienna Motor Symposium, VDI – Verlag Reihe 12, no. 239.

14. Rinolfi, R, Piccone, A (1999), 'Future engine technologies', in *Internal Combustion Engines: Experiments and Modeling* (ICE99), Capri, Italy, pp. 33–40.
15. Imarisio, R, Rossi, GM (2000), 'Potential of future common rail DI diesel engines', paper 20A2004, *Proc. Int. Symp.: The Future of Diesel Engine Technology for Passenger Cars*, Porto Cervo, Italy.
16. Imarisio, R, Ricco, M, Rossi Sebastiano, GM (2000), 'Multiple injection, a cost effective solution for emission reduction of common rail DI diesel engines', *Proc. Aachen Colloquium*, Aachen, Germany.
17. Hummel, K, Krieger, K, Hansen, N (2000), 'Evolution of the Bosch common rail system for passenger cars', paper 20A2012, *Proc. Int. Symp.: The Future of Diesel Engine Technology for Passenger Cars*, Porto Cervo, Italy.
18 Bianchi, GM, Pelloni, P, Filicori, F, Vannini, G (2000), 'Optimization of the solenoid valve behavior in common rail injection systems', SAE paper 2000-01-2042.
19. Bianchi, GM, Corcione, FE, Pelloni, P, Luppino, F (2001), 'Numerical analysis of passenger car HSDI diesel engines with the 2nd generation of CR injection systems: the effect of multiple injections on emissions', SAE paper 2001-01-1068, *SAE Trans. Journal of Engines*, Vol. 110, pp. 1099–1117.
20. Beatrice, C, Belardini, P, Bertoli, C, Lisbona, MG, Migliaccio, M. (2001), 'Combustion patterns in CR D.I. engines inferred by experiments and C.F.D. computations', *Comb. Sci. Tech.*, Vol. 162, pp. 235–261.
21. Badami, M, Mallamo, F, Millo, F, Rossi, EE (2003), 'Experimental investigation on the effect of multiple injection strategies on emissions, noise and brake specific fuel consumption of an automotive direct injection CR diesel engine', *Int. J. Engine Research*, Vol. 4, No. 4, pp. 299–314.
22. Imarisio, R, Peters, B, Rossi Sebastiano GM, Pinson, J, Boretto, G, Buratti, R (2004), 'Diesel strategies towards fuel neutral European emission standards', paper 04A5010, ATA Symposium, Bari, Italy.
23. Corcione, FE, Formisano, G, Merola, SS, Vaglieco, BM (2002), 'Spectral analysis of combustion process of CR diesel engine', SAE paper 2002-01-1634.
24. Schmid, M, Leipertz, A, Fettes, C (2002), 'Influence of nozzle hole geometry, rail pressure and pre-injection on injection, vaporisation and combustion in a single-cylinder transparent passenger car engine', SAE paper 2002-01-2665.
25. Merola, SS, Vaglieco, BM, Mancaruso, E, Corcione, FE (2003), 'In-cylinder combustion analysis by flame emission spectroscopy of transparent CR diesel engine', SAE paper 2003-01-1112.
26. Hasse, C, Peters, N (2005), 'Modelling of ignition mechanisms and pollutant formation in direct-injection diesel engines with multiple injections', *Int. J. Engine Research*, Vol. 6, No. 3, pp. 231–246.
27. Mancaruso, E, Merola, SS, Vaglieco, BM, Di Iorio, S (2003), 'Soot temperature and concentration in a transparent CR DI diesel engine', SAE paper 2003-01-70.
28. Schmid, M, Leipertz, A (2003), 'Investigation on mixture formation and combustion inside diesel engines using modern optical diagnostics', SAE paper 2003-01-69.
29. Gill, K, Zhao, H, Sison, K, Marriner, C (2005), 'In-cylinder studies of multiple diesel fuel injection in a single cylinder optical engine', SAE paper 2005-01-0915.
30. Costa, M, Corcione, EF, Vaglieco, BM, Omote, H (2007), 'Multidimensional modeling of diesel combustion by a detailed kinetic scheme and comparison with in-cylinder optical measurements', *Int. J. Vehicle Design*, Vol. 45, Nos 1/2, pp. 100–127.
31. Shuichi, M, Toyoshima, M, Ishisaka, K, Tsuzuki, N (2006), '180MPa piezo common rail system', SAE paper 2006-01-0274.

32. Bach, M, Bauder, R, Hatz, W, Hoffmann, H, Pamio, ZG, Schiffgens, HJ (2004), 'The new Audi 3.0 V6 diesel engine with piezo injectors and catalysed soot filter', Paper 04A5009, ATA Symposium, Bari, Italy.
33. Denbratt, I, Helmantel, A (2004), 'HCCI operation of a passenger car common rail di diesel engine with early injection of conventional diesel fuel', SAE paper 2004-01-0935.
34. Mancaruso, E, Merola, SS, Vaglieco, BM (2007), 'Extinction and chemiluminescence measurements in CR DI diesel engine operating in HCCI mode', SAE paper 2007-01-0192.
35. Zhao, H (2007), *HCCI and CAI Engines for the Automotive Industry*, Woodhead Publishing, Cambridge.
36. Bertoli, C, Beatrice, C, Di Lorenzo, A (2006), 'The evolution of the diesel combustion system toward the near zero emission goal', *Int. J. Vehicle Design*, Vol. 41, Nos 1–4, pp. 3–17.
37. Tow, T, Pierpont, A, Reitz, RD (1994), 'Reducing particulates and NO_x emissions by using multiple injections in a heavy duty D.I. diesel engine', SAE paper 940897.
38. Fuchs, TR, Rutland, CJ (1998), 'Intake flow effects on combustion and emissions in a diesel engine', SAE paper 980508.
39. Corcione, FE, Vaglieco, BM, Corcione, EG, Lavorgna M, Lanzafame, R (2003), 'Study of the combustion of a new small DI diesel engine with advanced common rail injection system', JSAE/SAE International Spring Fuels & Lubricants Meeting,Yokohama, Japan, 2003, SAE paper 2003-01-1782.
40. Corcione, FE, Vaglieco, BM, Corcione, EG, Vitale, G, Carpentieri, F (2003), 'Multiple injection strategies for low emissions of a new small common rail D.I. diesel engine', *Proc. 4th Congress Engine Combustion Processes: Current Problems and Modern Techniques*, München, Germany, pp. 143–156.
41. Koyanagi, K, Oing, H, Renner, G, Maly, R (1999), 'Optimizing common rail-injection by optical diagnostics in a transparent production type diesel engine', SAE paper 1999-01-3646.
42. Corcione, EF, Vaglieco, BM, Corcione, EG, Lavorgna, M (2002), 'Potential of multiple injection strategy for low emission diesel engines', SAE paper 2002-01-1150, *SAE Trans. J. Engines* Vol. III, pp. 2021–2027.
43. Liu, Y, Reitz, RD (2005), 'Optimizing HSDI diesel combustion and emissions using multiple injection strategies', SAE paper 2005-01-0212.
44. Merola, SS, Vaglieco, BM, Mancaruso, E (2003), 'Analysis of combustion process in a transparent common rail diesel engine by 2D digital imaging and flame emission spectroscopy', paper ICES2003-644, *Proc. ASME-ICED 2003 Spring Technical Conf.*, Salzburg, Austria.
45. Merola, SS, Vaglieco, BM, Mancaruso, E (2003), 'Soot formation analysis by multiwavelength spectroscopy in an external chamber diesel engine equipped with a CR injection system', SAE paper 2003-01-1111.
46. Molina, S, Payri, F, Benajes, J, Pastor, JV (2002), 'Influence of the post-injection pattern on performance, soot and NO_x emissions in a HD diesel engine', SAE paper 2002-01-0502.
47. Imarisio, R, Ivaldi, D, Lisbona, MG, Tonetti, M (2006), 'Technologies towards Euro6 passenger car diesel emissions standards', *Proc. Int. Symp. – Towards Neutral Standards Diesel vs Gasoline Engine*, Ortigia, Italy.

5

Turbocharging and air-path management for light-duty diesel engines

K. TUFAIL, Ford Motor Company Limited, UK

Abstract: Current diesel air-path and combustion performance is mainly influenced by two factors: first the optimisation of stand-alone hardware design and response, and secondly system performance, i.e. compatibility with other engine hardware and their management through the engine control unit (ECU). The chapter begins with a review of recent advances made in exhaust gas recirculation (EGR) and boosting technologies. It then presents a review of air-path management strategies currently utilised in production, together with the potential of air-path performance management through the use of model based control (MBC).

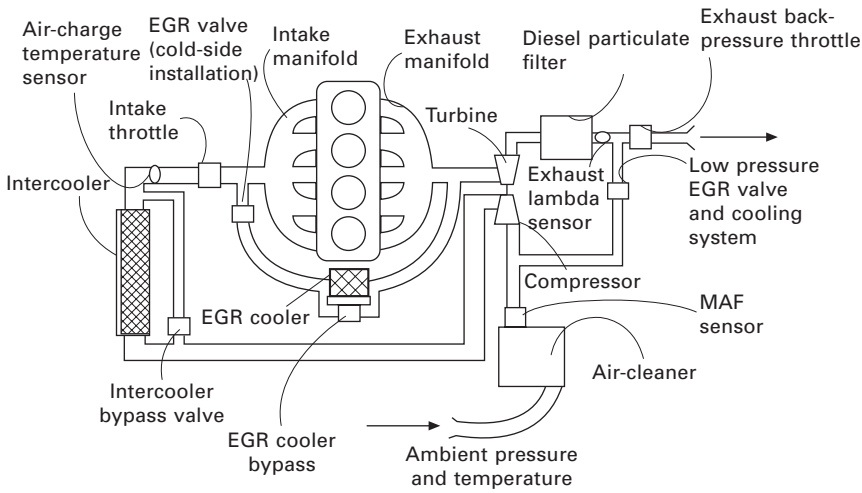
Key words: engine control unit (ECU), exhaust gas recirculation (EGR), high pressure common rail (HPCR), model based control (MBC), variable geometry turbocharger (VGT).

5.1 Introduction: air-path challenges and acceptance criteria

The increase in power requirements with stringency on noise, emissions, fuel consumption (market-driven attributes) and statutory emission legislation requirements has spurred rapid advances in air-path and combustion technology. Current diesel air-path and combustion performance is mainly influenced by two factors, first the optimisation of stand-alone hardware design and response, e.g. turbocharging, exhaust gas recirculation (EGR), intake throttling (ITHR), high pressure common rail (HPCR), fuel injection equipment (FIE), etc., and secondly, system performance, i.e. compatibility with other engine hardware and their management through the engine control unit (ECU). Figure 5.1 illustrates a schematic of a typical modern turbocharged diesel engine (discussed later), together with the main components and sensors that affect air-path flow and control.

The two main questions that air-path management tries to address are: How does a diesel engine (for global production and thus widely varying environmental conditions) achieve:

- the intake manifold conditions, namely through EGR and boosting, for 'optimum' combustion (i.e., reduce simultaneously NO_x, soot, etc.)?
- 'robust' intake manifold (air-path) conditions, during steady and transient



5.1 Diesel engine schematic and its air-path related components (reproduced and modified from van Nieuwstadt, 2003).

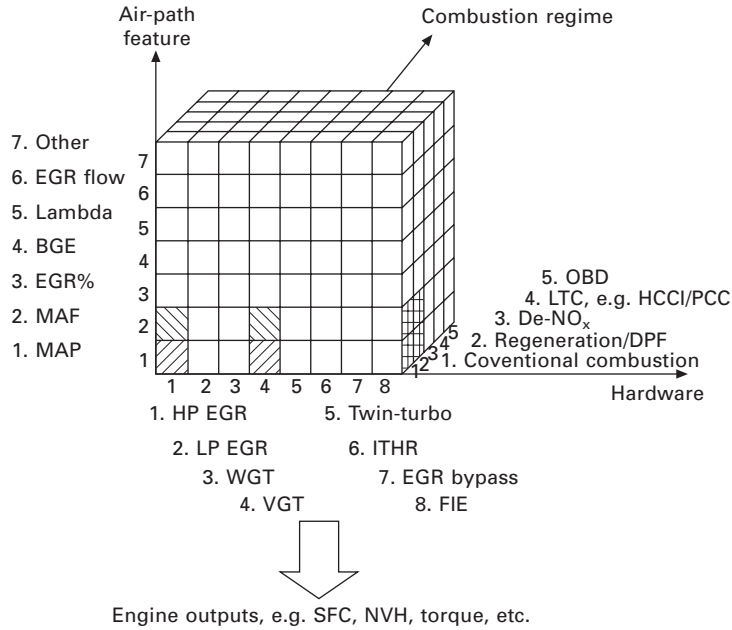
operation, for 'optimum' combustion (i.e. maintain the reduction of NO_x and soot emissions after 100 000 miles across production engines)?

The main question that combustion management tries to address is: How does a diesel engine achieve robust operation against production component tolerances with simultaneous reduction in NO_x and soot without degrading specific fuel consumption (SFC) and noise vibration and harshness (NVH)?

The challenge lies in optimising hardware performance, e.g. EGR valve, turbocharger, ITHR, etc., with air-path control features, e.g. mass air flow (MAF), manifold air pressure (MAP), etc., to support, or in some cases create, an optimised combustion regime, e.g. conventional combustion, low temperature combustion (LTC), soot regeneration conditions in the diesel particulate filter (DPF) and de-NO_x combustion conditions.

Figure 5.2 illustrates a system-complexity diagram, with axes considering typical combustion regimes, air-path feature and related hardware, to demonstrate the management interactions that may arise as engine outputs such as torque, SFC, NVH, etc., when several pieces of hardware are required to work together (i.e. 'system compatibility'). The shaded boxes in Fig. 5.2 illustrate a typical current diesel engine employing variable geometry turbocharger (VGT) and high pressure (HP) EGR set-up.

It can be seen from Fig. 5.2 that the current turbocharged diesel engine covers a small area of the full complexity diagram; and future hardware, with a variety of air-path features employing different combustion regimes, may result in a larger operational area. Clearly as the operational area in



5.2 Diesel engine system complexity: air-path – combustion – hardware – system performance (nomenclature section explains the abbreviations used in this diagram).

Fig. 5.2 increases, the ability of air-path feature and hardware management to deliver engine outputs (e.g. NO_x, soot, NVH, etc.) becomes of paramount importance.

A typical engine output list that can be affected by air-path performance can be summarised as below:

- Steady- and transient-power output (function of ambient pressure and temperature conditions), e.g. torque, maximum pressures and temperatures
- Exhaust emissions, e.g. nitrogen oxide (NO_x), soot, carbon monoxide (CO), carbon dioxide (CO_2), hydrocarbon (HC), etc.
- Combustion NVH
- Fuel economy (FE)
- On-board-diagnostic (OBD) detection and resolution
- Other, e.g. engine warm-up performance, oil dilution, driveability, etc.

A series-production engine for the global market also requires the manufacturing costs to be minimised and, hence, it is often required that one type of engine, i.e. engine capacity, be installed across a variety of vehicle inertia classes, i.e. vehicle weights. This can result in variable air-path and

combustion demands for a given vehicle speed due to differences in engine speed and load conditions.

Manufacturing an engine for series production must permit component-to-component variations, which thus introduces variability in engine outputs, i.e. deviation from the optimised performance and emissions. In order to keep this variation to a minimum, robustness to production tolerances must also be addressed by component (air-path and combustion related) management.

Integrated in-cylinder closed-loop control with a desired output (Schten *et al*. 2007; Husted *et al*. 2007), including reduction of emissions/NVH/SFC, would partly provide for simultaneous reduction of emissions and engine robustness. In a conventional diesel engine (for production), in-cylinder events are not monitored by the ECU and therefore no direct online connection between inputs and outputs (including emissions) is offered. Air-path control therefore assumes, before inlet valve closure (IVC), that intake manifold conditions contain similar charge conditions to the in-cylinder events. Thus, the main objective of air-path management is to produce in a controlled manner (observing design limitations), for any given steady- or transient-operating point, the intake manifold charge conditions which are necessary for 'optimum' combustion. The key ingredients of the air-path system are fresh air (boosted air), EGR (burnt gas fraction, BGF) and the corresponding intake manifold temperature (as will be discussed later).

The subsequent sections present a review of the open literature on recent advances made in EGR and boosting technologies. This entails a brief discussion on design of engine components, the aim being to describe the intake manifold conditions, namely EGR and boosting, for 'optimum' combustion. A review of air-path management strategies currently utilised in production, together with their acceptance and performance criteria, is presented. The potential of air-path performance management through the use of model based control (MBC) is briefly discussed. Finally, future trends in air-path management for passenger car and light-duty truck applications are summarised.

5.2 Air-path technologies, part 1: exhaust gas recirculation (EGR)

Key ingredients of the air-path system are fresh air (boosted air), EGR (i.e. BGF) and the corresponding intake manifold temperature. This section reviews development in air-path technologies (EGR) for optimum engine performance. Management and control of air-path technologies for steady- and transient engine operation are discussed later (Section 5.3).

The main motivation for introducing EGR into the intake manifold is to minimise emissions of NO_x (Ladommatos *et al*. 2000). However, this degrades soot emissions and SFC (Mito *et al*. 2003). In addition EGR lowers

combustion noise and therefore potentially introduces, during activation and de-activation of EGR, a step change in combustion NVH (Ahlinder *et al*. 2007).

Conventional methods of regulating EGR involve the introduction of partial exhaust manifold gas, controlled by an EGR valve, back into the intake manifold. The hot exhaust gas introduced in the intake manifold, typically manufactured by injection-moulded thermo-plastic material (Kolbenschmidt Pierburg 2007), is limited to an upper temperature limit due to the manifold's melting properties. In order to cool exhaust temperatures, before introduction into the intake manifold the exhaust gas is routed through an EGR cooler. Introduction of EGR lowers the fresh MAF, as measured by the compressor inlet MAF sensor, and cooled EGR further increases EGR density. Thus it is common practice, in conventional diesel engine control, to infer EGR flow rate from the MAF sensor signal (van Nieuwstadt *et al*. 2000).

The principal constituents of EGR are N_2, CO_2, H_2O and O_2 (Ladommatos *et al*. 1998a, 1998b) during lean operation (Olsson *et al*. 2003). The three main effects of cooled EGR on the inlet charge composition of a diesel engine (Ladommatos *et al*. 1997; Maiboom *et al*. 2008; Olsson *et al*. 2003) are as follows: (i) reduction of O_2 concentration resulting in a lower flame temperature (dilution effect), (ii) CO_2 and H_2O have higher specific heat capacities as compared with O_2 and N_2 (at constant boost pressure) resulting in lower gas temperatures during combustion (thermal effect), and (iii) CO_2 and H_2O can potentially dissociate at the high temperatures prevailing during combustion and the products of dissociation participate in the combustion process (chemical effect). In addition, hot EGR will increase the inlet charge temperature.

In the case when CO_2 or H_2O displaces O_2 in the inlet charge, both the chemical and thermal effects on exhaust emissions are small. Increased inlet charge temperature (which reduces charge density and hence the mass of inlet charge) increases NO_x, soot and reduces unburned-HC (uHC) and engine volumetric efficiency. However, the dilution effects are substantial and result in large reductions in NO_x, even if at the expense of higher soot and uHC.

The ECU utilises a set of optimised (typically for emissions and fuel economy) and calibrated steady-state MAF demand maps (2- or 3-D maps function of engine speed and load) to regulate EGR. For transient operation, the ECU interpolates between maps, together with closed-loop control, e.g. PID, to ensure a successful feedback (with the controlled variable being MAF). This use of interpolation, during a transient, may expose limitations in the control system as the nature of transients varies, e.g. engine cylinder head temperature, ambient pressure and temperature, etc. (Rakopoulos *et al*. 2004a, 2004b). Therefore, it is important to consider the type of controlled variable, e.g. MAF, intake manifold O_2, BGF, EGR, etc., that accurately

represents steady-state and transient engine conditions (van Nieuwstadt *et al*. 2000).

The above literature review indicates that the different constituents of EGR can affect the NO_x–soot trade-off curve in varying degrees. The control aspect primarily considers the selection of control variable, i.e. set-point, and its related electrical control system, such as PID or neural network control, etc.; whereas 'EGR management' is used here as a generic term that includes hardware and sensor compatibility with engine performance. As NO_x emission levels become more stringent, two main motivations for further improvement in EGR management emerge: (i) simultaneous reduction of NO_x and soot emissions without deterioration of other attributes, e.g. SFC/NVH/power-torque, and (ii) improving robustness, due to production tolerance in components, to maintain optimum levels of emissions performance, e.g. NO_x vs. soot, and NO_x vs. SFC trade-off.

This section reviews two main types of EGR system technologies that are typically used in production and are actively being researched, namely high and low pressure.

5.2.1 High pressure (HP) EGR

Conventional EGR is driven by high (relative to the intake manifold) pressure in the exhaust pre-turbine region, via an EGR valve, back into the intake manifold (Fig. 5.1) (Langridge and Fessler 2002). This increases the intake manifold charge temperature and reduces the mass of the charge drawn into the cylinder. Consequently, heat capacity is reduced and higher in-cylinder temperatures are observed (Ladommatos *et al*. 2000). EGR coolers are employed to cool (super-cooled EGR can typically exceed 80% cooler efficiencies) the exhaust gas before it mixes with fresh air in the intake manifold (Fraser *et al*. 2005). EGR coolers typically comprise shell-and-tube type heat exchangers, where the exhaust gas passes through the tubes and the coolant passes over the shells. The main factors influencing the EGR cooler efficiency, at least in the non-fouled state, are coolant temperature and exhaust mass flow rate (Fraser *et al*. 2005). Under certain cold environmental conditions, e.g. sub-freezing ambient conditions, hot EGR may be desirable (lasting for a short duration) and therefore EGR coolers are also equipped with a bypass valve.

Depending on the engine packaging requirements, the EGR valve is installed on either hot- or cold-side locations, i.e. pre- or post-EGR cooler. It is desirable to install the EGR valve on the cold side (as indicated in Fig. 5.1), since it results in faster (compared to the hot side) intake manifold response times. However, this raises soot build-up on the EGR valve stem due to cold-side EGR valve mounting and brings contamination that may result in valve performance deterioration (from new). Conversely, hot-side

installation with reduced volume between the EGR valve and turbine inlet may improve EGR response and resolve contamination issues. Under certain high-speed and load-transient conditions, when pre-turbine pressure is lower than in the intake manifold, ITHR is added to reduce intake pressure and consequently restrict the incoming fresh charge, thereby extending the EGR operation range. As a consequence of activating ITHR (for driving the EGR into the intake manifold) the SFC is further deteriorated (from optimised steady-state value) due to potential increases in pumping losses.

A variation on the above EGR system (Lundqvist *et al*. 2000) extracts exhaust gas at a location upstream of the DPF and introduces it downstream of the intercooler. A large portion of the operating region may experience post-intercooler pressures that exceed those experienced in the exhaust. To avoid low EGR flow rates under these conditions a venturi is installed (Lundqvist *et al*. 2000) to draw the charge into the intake manifold. The disadvantage of this system is that if the venturi is designed to enable EGR at every point of the speed–load envelope, the flow resistance of the venturi may give rise to an excessively high pressure drop across the venturi at high load and speed.

Lundqvist *et al*. (2000) propose a variable venturi, where a variable proportion of the airflow bypasses the venturi, to reduce pumping losses. Although the venturi itself has fixed dimensions, axial displacement of the EGR-injector facilitates variation of the critical area, defined as that lying between the EGR-injector and the venturi wall. For example, at an engine load point with high air flow and low pressure difference between the inlet and exhaust manifold, the EGR-injector is drawn away from the throat of the venturi to make the critical flow area sufficiently large to control EGR. Conversely, at an engine load point with low airflow and high pressure difference between intake and exhaust manifold, the EGR-injector is pushed towards the throat to make the critical area sufficiently small to control EGR. By adjusting the EGR-injector position relative to the throat of the venturi, the EGR-rate can be optimised for each driving condition.

The performance of the EGR system, and thus delivery of the desired setpoint (optimised under steady-state operation), is degraded mainly by the following durability-related issues:

- Reduced thermal efficiency of the EGR cooler (EGR cooler fouling, etc.; Bravo *et al*. 2005)
- Increased pressure losses in the EGR system (Zhang *et al*. 2004)
- EGR inhomogeneous distribution in the intake manifold (Partridge *et al*. 2002; Siewert *et al*. 2001; Green 2000)
- Drift of electronically controlled EGR valve and sensor
- Contamination of the EGR system (e.g., soot contamination in the valve/cooler).

Accurate and robust feedback systems are required to minimise the effect of the above factors on engine outputs, e.g. power and torque (due to high intake temperatures caused by EGR), emissions (due to variation in the operating region of the NO_x–soot trade-off curve caused by varying levels of EGR), fuel consumption (Jacobs *et al*. 2003) (due to long ignition delays caused by EGR and high pumping losses caused by ITHR) and engine durability, e.g. lubricating oil quality (Tokura *et al*. 1982; Nagai *et al*. 1983; Cadman and Johnson 1986) (due to oil viscosity and component wear issues caused by excessive cooled EGR).

The distinction between accurate and robust feedback is made where, in the absence of a fouled component, an accurate-feedback method distinguishes between sensor fault, e.g. sensor component drifts measured as corresponding signal response, compared with a genuine fault (i.e., a signal response due to a fouled component). Robust feedback ensures that the sensor management takes appropriate action: for example, in the case of a fouled EGR cooler it either offsets the sensor transfer function accordingly (in the case of a sensor drift) or alerts the user to an OBD error (in the case of a blocked EGR cooler).

Lastly, recent developments in materials have aided manufacturers' performance and packaging requirements by introducing die-cast aluminium for the manufacture of EGR coolers. The thermal conductivity (compared with steel) of aluminium is high and thus it allows higher heat exchanger effectiveness in the limited available installation space. The low density and anti-corrosive properties of aluminium have improved the strength to weight ratio and have introduced flexibility in integrated (i.e. one-piece EGR valve and cooler assembly) design that minimises soot build-up in EGR systems, consequently improving the system durability.

5.2.2 Low pressure (LP) EGR

Low pressure (LP) EGR (Fig. 5.1; Chatterjee *et al*. 2003) is another approach to achieve high rates of EGR, simultaneously bestowing improved durability and minimum SFC deterioration. The most common example of this arrangement is where exhaust is extracted downstream of a DPF and then introduced to the compressor inlet (Chatterjee *et al*. 2003). The main reasons (and thus advantages) for post-DPF EGR extraction are that, by the time the air–exhaust mixture is introduced into the intake manifold, it is clean, cooler and fully homogenised (compared with HP EGR). The compressor inlet operates at conditions where intake depression usually arises (relative to ambient pressure and due to compressor inlet suction) and thus a drawing-path for EGR exists. The EGR cooler and the exhaust throttle are installed (similar to HP EGR, explained earlier) respectively for further cooling and to increase the exhaust pressure for driving EGR into the intake

system. Potential improvement in turbine efficiency may also exist as all of the exhaust manifold gas is used to drive the turbine, rather than some being bled off for HP EGR.

There are three main disadvantages in employing a LP EGR system: (i) component fouling, e.g. compressor (due to hotter compressor inlet gas from EGR) and intercooler/sensor contamination, e.g. by sulphuric acid, soot, HC and nitrogen exhaust gas compounds; (ii) transient delays resulting from the time delay for EGR to reach the intake manifold due to the relatively long route; and (iii) increase in pumping losses, compared with conventional LP EGR, due to increase in the number of throttles.

All of these disadvantages affect delivery and compromise accurate and robust feedback management of EGR. Applications of LP EGR have been reported in heavy-duty trucks, and the following paragraphs attempt to summarise installation solutions to cater for the above fouling and transient control issues. However, due to the nature of heavy-duty applications, it should be noted that transient control and pumping loss issues may not be major limitations in that application.

The LP EGR employed by Langridge and Fessler (2002) draws the EGR from a location downstream of the DPF and introduces it upstream of the compressor via an EGR cooler. A throttle (mounted downstream of the DPF) is used to control the backpressure to ensure an adequate EGR driving pressure ratio. With high-pressure systems the EGR cooler needs to be more effective, whereas with low-pressure systems the increase in compressor inlet temperature increases the work that the compressor must perform per unit mass of air delivered. The installation of a second EGR cooler (downstream of the DPF and upstream of the compressor inlet) ensures that an additional benefit (with LP EGR) is provided where the EGR is cooled twice. However, two EGR cooler installations can result in a higher pressure drop in the exhaust system compared with a conventional single cooler.

Another type of LP EGR system for heavy-duty trucks (Chatterjee *et al*. 2003) demonstrates a 50–60% reduction in NO_x. The EGR throttle valve is located between the inlet air filter and the turbocharger (compressor). The system has two electrically controlled butterfly valves mounted on two concentric shafts, which can move independently of each other. One valve controls EGR gas flow and the other the intake air flow.

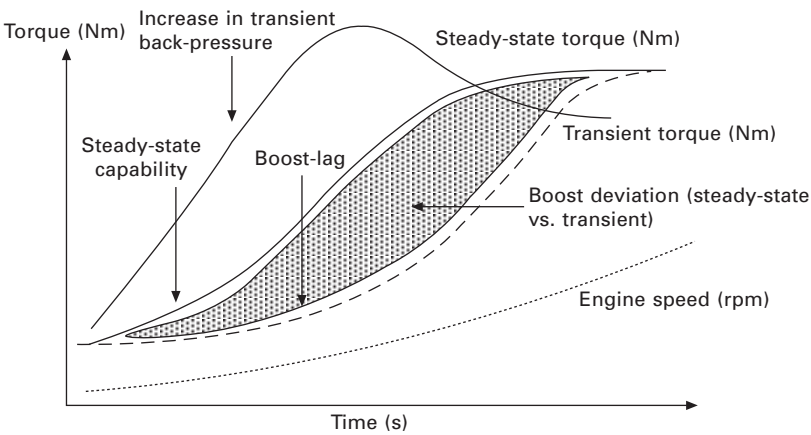
A comparison between high and low pressure EGR systems applied to heavy-duty diesels is presented in Kohketsu *et al*. (1997). It is necessary to increase boost pressure in order to maintain sufficient fresh air and a high excess air ratio, even when operating with EGR. Low pressure EGR can be applied in the high-load region, although durability and reliability problems with the compressor, and fouling of the intercooler, are encountered.

5.3 Air-path technologies, part 2: boosting systems

The main driver behind boosting a diesel engine is to increase performance, whilst retaining economical fuel consumption. This section reviews development in air-path technologies (boosting systems) for optimum engine performance. Management and control of air-path technologies for steady- and transient engine operation are discussed later (Section 5.4).

Figure 5.3 illustrates a schematic that describes vehicle acceleration from low to middle engine speed. The schematic highlights the typical boost-lag area (relative to steady-state boost pressure) at low engine speeds, whilst pre-turbine pressure is rising to overcome the turbocharger inertia. This increase in pre-turbine pressure can potentially give rise to high pumping loss and therefore increase fuel consumption with respect to steady-state driving conditions that do not suffer from turbocharger inertia 'loss'.

This scenario translates into a steady-state operation requirement for high power and torque and, during transients, for minimum boost-lag. A turbocharger utilises energy in the exhaust manifold to drive a turbine via a compressor, to create higher density (boosted) air for the intake manifold. This allows for more fuel to be used and hence increases power output per unit displacement of an engine. However, the turbocharger is a continuous flow machine and the diesel engine is a reciprocating, intermittent machine so that there is a major technical challenge of compatibility or 'turbocharger matching', in which there is a high- and a low-end speed and power trade-off. Any attempt to improve the gas-flow dynamics of the turbocharger at low speed either reduces compressor efficiency or increases engine backpressure at high exhaust flow rates, and thus reduces top-speed engine volumetric efficiency. Conversely, any effort in reducing backpressure at high exhaust



5.3 Turbo-lag – vehicle low speed 'pick-up'; the boost vs exhaust pressure trade-off.

flow rates through turbocharger breathing will cause a deterioration in gas-flow dynamics at low speed.

In order to strike an acceptable compromise between low- and top-speed engine performance, whilst retaining economical fuel consumption, there exist a number of variations in boosting options (e.g., turbocharging, supercharging, turbo-compounding, etc.) and installation layouts. This sub-section commences by briefly reviewing turbocharger hardware advances (related to engine performance) and reviews implementation opportunities and limitations on a variety of boosting arrangements currently being applied, or under consideration, for passenger car and light-duty truck applications.

5.3.1 Turbocharging

Turbochargers in the automotive industry consist of radial compressors and turbines, contained in dedicated housings, connected through a common spindle in the bearing housing. Hot gases from the engine exhaust manifold are received by the turbine inlet duct and volute, where the gas stream is modified to obtain a uniform angular momentum distribution before it is introduced to the impeller tip. Some turbines, e.g. VGT, adjust a set of nozzles to optimise the angle of incidence in order to accommodate a wider range of operating flow conditions (Kawamoto *et al.* 2001). As the flow accelerates radially inwards (through turbine entry), the impeller rapidly extracts work from the high exhaust pressure, whilst turning its flow to the axial direction. As a consequence, cooler gas (compared with the turbine entry) is released, at approximately ambient pressure, to the exhaust pipe. Air enters the compressor impeller (typically constructed of an aluminium alloy), ideally in an axial direction, where its pressure and kinetic energy rise (from the turbine work which is transferred to the compressor by a shaft). A diffuser recovers some of the kinetic energy and collects, radially, the boosted air into a scroll with one exit port, before releasing it, via a series of ducts and an intercooler, to the intake manifold. As the compressor raises the density of air it also raises its temperature. In order to obtain further increase in density, an intercooler between the compressor outlet and the intake manifold is employed. Furthermore, to retain pressure at the compressor outlet, it is desirable to keep the pressure drop between the compressor outlet and the intake manifold to a minimum.

Historically, engine performance enhancement has been sought from improvements in turbomachinery design. However, the competitive nature of the diesel automotive industry and global production philosophies have recently driven the research thrust into turbomachinery and engine components as ‘compatibility optimisation’. In this manner a performance enhancement from the turbocharger is required and judged relative to engine performance enhancement.

This sub-section briefly reviews turbomachinery component improvements, namely compressors and turbines, together with various types of turbochargers relative to engine performance (as opposed to stand-alone turbomachinery aerodynamics) and gives examples, wherever appropriate, of practical passenger car/light-duty truck applications.

Turbomachinery components: compressors

The main requirement of an automotive turbocharger compressor is to provide boost, by achieving a high compressor pressure ratio, e.g. ~3.5 (Watson and Janota 1982), under all engine speed and load conditions (i.e., it must operate efficiently over a large range of flow rates) with minimum transient lag. In addition, the unit should not exceed specified design limits, e.g. compressor-out temperature, turbocharger speed, compressor surge, turbine inlet and outlet temperature, engine SFC, etc.

The requirements for high pressure ratio and minimum transient lag have led to the development of impellers with small dimensions with thinner blades; however, these imply high impeller rotational speeds. Consequently, these high rotational speeds cause high temperatures near the exducer of the wheel, together with high stresses. The impeller wheels, conventionally made from aluminium alloys, operate close to the design limits of the material and thus may creep, resulting in fouling against the compressor housing, ultimately causing impeller failures (Mukherjee and Baker 2002).

A major limitation in establishing a large operating flow range for stable engine operation is *surge* (Theotokatos and Kyrtatos 2001; Guo *et al*. 2007). Several studies on compressor surge have been reported in the open literature, detailing surge operation and its transition from low to high frequency (deep to mild surge respectively) (Theotokatos and Kyrtatos 2001). Below are some findings.

Surge

During surge (Guo *et al*. 2007) mass flow through the compressor is reduced; the flow in the compressor stagnates due to stalled blades and is partially reversed. This often leads to periodically reversed flow, or a surge of the entire compressor system, limiting the compressor's operating range and increasing compressor noise, resulting in mechanical failure of the compressor wheel. It should also be noted that surge is not just critical for compressor durability but also causes instability in engine torque and thus vehicle performance.

Stall is conventionally characterised by two types of instability: (i) a distinct pressure and mass flow fluctuation (sinusoidal) exists at the onset of instability; the oscillations have a wavelength of approximately four times that of the volute circumferential length; and (ii) as the mass flow

rate is reduced, the amplitude and speed of rotation of the pressure pattern increase.

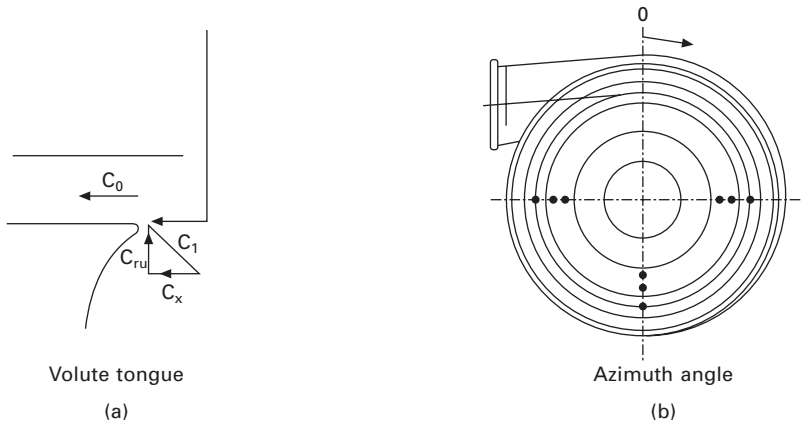
Results from Galindo *et al*. (2006a) indicate that, during stall, pockets of rotating air cells exist which are functions of air mass flow-rate. The volute, under these circumstances, acts like a tuned pipe, amplifying flow unsteadiness into a standing wave. This wave modifies the flow exit boundary condition and leads to periodic local backflows at the volute exit. This reversed flow occurs only after the compressor stage stalls. Thus, surge can be detected through a frequency-based criterion, e.g. at 5–15 Hz depending on compressor size, installation arrangement and operating conditions.

Volute design

A spiral-shaped volute collects the flow from the diffuser and passes it to a single exit port, whilst raising the static pressure and flow kinetic energy through the compressor impeller (Pan *et al*. 1999). The design objective of the volute is to achieve a uniform flow at the volute exit. This is usually attained at the design flow-rate only, so that at off-design conditions the volute is either too small or too large, and a pressure distortion develops circumferentially around the volute passage. At low flow-rates the pressure increases with azimuth angle, while at high flow-rates the pressure decreases (Eynon and Whitfield 2000). These circumferential pressure distortions are transmitted back to the impeller discharge and have been observed at the impeller inlet. The pressure distortions reduce the stage's performance and have a direct impact on diffuser and impeller flow stability. The computational fluid dynamics (CFD) investigation in Eynon and Whitfield (2000) showed that the internal flow distribution could be improved by enlarging the flow area near the tongue (Fig. 5.4, reproduced from Eynon and Whitfield 2000). This led to reduced pressure and flow inhomogeneities with azimuth angle (as indicated in Fig. 5.4, reproduced from Eynon Whitfield 2000) and a predicted improvement in the performance of the vaneless diffuser upstream of the volute.

Variable geometry compressor (VGC)

Variable geometry in compressors (Arnold 2004), i.e. variable vanes incorporated into the diffuser passage, are used to extend compressor flow range and thus engine torque capability which is otherwise limited due to surge (Tange *et al*. 2003; Arnold 2004). At low speeds the engine operating line may be too close to the surge line at the nominal angle setting. Closing the vanes causes the surge line to rise, thereby increasing the margin for safe operation. Results from Tange *et al*. (2003) showed that a 3.0 litre IDI diesel gained, compared with a vaneless compressor, 4.8% higher boost pressure and 3.2% improvements in SFC when using VGC.



5.4 (a) Turbocharger volute tongue and (b) azimuth angle schematic (reproduced and modified from Eynon and Whitfield, 2000).

Inlet guide vanes (IGV) and swirl generation device (SGD)

Packaging constraints often dictate that upstream of the compressor inlet duct there is a 90° bend. This generates a non-uniform entry flow (radial and circumferential) to the inducer (Kindl *et al*. 2004). Thus, a swirl generation device (SGD) (Galindo *et al*. 2007) and inlet guide vanes (IGV) (Uchida *et al*. 2006) are proposed to be installed in the inlet to improve flow uniformity. The study conducted by Galindo *et al*. (2007) shows that at low mass flow-rates, a potential for increasing the surge margin also exists. Improving low-end flow may, however, create restrictions at high flows, e.g. high engine speeds. The long-term durability of devices such as the above also needs to be assessed.

Variable inlet guide vanes (VIGVs) (Arnold *et al*. 2005a) can significantly extend the stable operating range of industrial centrifugal compressors as a result of imparting swirl to the inlet flow. An undesirable consequence of the large setting angles required by the vanes is a pressure loss, leading to a decrease in the overall stage efficiency. An ideal inlet guide vane system will therefore induce large swirl angles in the inlet flow with a low associated pressure loss.

Two-stage compressor

A low speed turbocharger (LST) (Arnold *et al*. 2005b), with two back-to-back compressor wheels in a two-stage compressor, mounted on a single shaft, was used to obtain high pressure ratios (5:1), wide flow range and efficiency. Two-stage compressor turbocharging offers performance advantages but presents disadvantages in terms of cost, complexity, thermal inertia and packaging.

Fatigue failures

The trend to higher compressor rotational speeds and the corresponding fatigue failures have generated an interest in vibration analysis. The design of compressors from the point of view of vibration should take into account the following considerations: (i) the determination of amplitude and frequencies of the aerodynamic forces acting on the blades; (ii) the determination of the damping values; and (iii) the investigation of the eigenfrequencies and mode shapes.

The excitation of the impeller blades is caused by the following phenomena:

- Excitation of blade vibration caused by aerodynamic non-uniformity of flow at inlet or exit of the compressor
- Self-excited vibrations by operating the turbochargers in the flutter region of the compressor
- Blade excitation by cells of rotating stalls
- Blade excitation by operation near the surge zone
- Multiple blade-pass frequency.

It is recommended that the compressor should operate away from the excitation frequencies that may cause excessive stresses and reduce the fatigue life.

Turbomachinery components: turbines

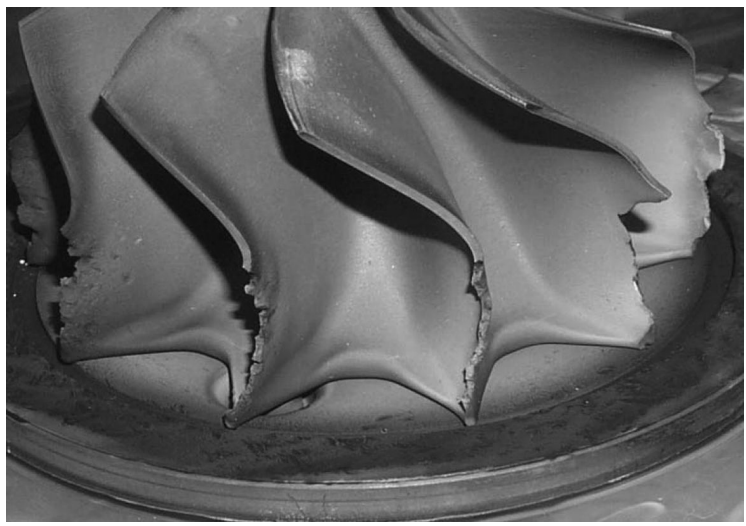
Turbine rotor geometry is optimised, at the design operating condition, to minimise incidence losses and achieve a desired rotor inlet flow angle. At this operating condition the flow through a turbine enters the rotor perfectly aligned (parallel) with the blades, at least on average. During normal operation of the turbine, flow conditions vary and therefore deviations from the optimised design point in the rotor inlet flow angle occur. As the angle at the rotor inlet deviates from that of optimum (parallel) alignment, additional incidence losses occur and this reduces turbine efficiency (Coppinger and Swain 2000). In order to accommodate varying degrees of turbine inlet flow conditions, the angle of incidence can be varied and thus controlled using a VGT.

Variable geometry turbines (VGT)

Variable geometry turbines (Arnold *et al*. 2005c) are used on diesel vehicles to improve engine performance by changing the *flow* capacity of the turbine, i.e. increasing boost, with a variable geometry mechanism (Chen 2006). The boost is achieved by closing the flow guide vanes (typically nozzles) upstream of the turbine rotor, resulting in an increase of the turbine inlet pressure. This increases the pressure in the engine's exhaust manifold, i.e. engine

backpressure. At low engine speeds and loads, the increase in backpressure is relatively low and can even be desirable to drive the EGR into the intake manifold. However, as the engine speed and load are increased, and with the nozzles in the closed position, a high mass flow-rate through a highly restricted flow passage (nozzles) increases engine backpressure. This may result in increasing engine pumping losses (Black *et al*. 2007a) and therefore introduce deterioration in engine SFC. Reducing boost pressure under these operating conditions, by reducing exhaust mass flow-rate, i.e. with the nozzles in a more open position, the flexibility (utilising VGT) of optimising boost pressure with engine backpressure offers a potential reduction in engine pumping losses (Bringhenti and Barbosa 2004).

Under certain driving conditions, such as so-called 'over-run', i.e. high engine speed with no-load conditions, an increase in backpressure is beneficial to slow down the engine for vehicle braking (engine braking arising from high pumping losses). However, under the engine braking condition, nozzles operate in choked conditions as the flow accelerates downstream along the pressure side of the nozzles. This can often generate shockwaves from the nozzle exit, i.e. the pressure side after the throat. These shockwaves impinge on the turbine wheels, creating an excitation force at the blade passing frequency (BPF). This force and its higher-order harmonics can destroy a turbine wheel (Fig. 5.5, reproduced from Chen 2006). A high blade number increases the frequency of this noise, making it less audible to humans.



5.5 Turbocharger durability and turbine wheel damage (reproduced from Chen 2006).

Nozzle performance

Optimisation of nozzle shape, to minimise incidence losses, can improve the relationship between the nozzle incidence- and vane angle (at a design point) and thus improve engine SFC. Analysis of two types of nozzle shapes, namely curved and straight, indicates (Spence and Artt 1998) that curved nozzle vanes introduce an area of 'slow-down', otherwise known as diffusion, at the nozzle exit, whereas straight-line shapes are used for smooth flow-area variation. Results from Spence and Artt (1998) show that with straight-line shaped nozzles the area of diffusion is absent and the flow between nozzles accelerates smoothly. Thus the straight-line shaped nozzle has an advantage of 3% (at small flow range) and 1% (at middle flow range) in efficiency over the curved-line shaped nozzle.

Resonance of turbine rotor

The relationship between natural frequency and harmonics with the aim of avoiding resonance is studied in Spence and Artt (1998). In the case of VGT, in addition to resonance of the first natural frequency, the nozzle-passing frequency should also be considered. Results show that when turbine impeller and nozzles are designed, not only does the number of the nozzle vanes have to be considered to avoid resonance but so also does the nozzle wake, i.e. the domain of low total pressure behind the nozzles.

Nozzle driving link mechanisms

Three main types of nozzle driving link mechanisms for moving vane nozzle mechanisms are compared in Spence and Artt (1998) and are summarised as (i) the slide-joint system, (ii) the unison-ring system, and (iii) the chain link type system. It is indicated from Spence and Artt (1998) that the unison ring satisfies most design criteria and hence forms an attractive solution for production use. It is also desirable for the materials of the nozzle-drive mechanism to have high-temperature, low-friction and low-oxidation (under high temperature) characteristics, including low cost. Once the mechanism for driving the vanes is established, the actuator control takes a leading role in linking with the engine management system.

Actuator control and hysteresis

The purpose of the actuator is to control (through either a vacuum-controlled duty solenoid valve or an electronic control valve) the nozzle movements that control turbine flow capacity. An additional requirement for nozzle control is repeatability in its performance, and thus minimum hysteresis is desirable for

production robustness. Hysteresis within the actuator components is caused by aerodynamic force and friction. If the hysteresis is large, accurate boost control may not be achieved. Increasing the size of the actuator decreases hysteresis since it can yield a large operating power for the same control pressure. A change of spring rate for the actuator also improves control performance, since with lower constants a smaller change in pressure is given to the actuator: this means a smaller power requirement to move the nozzles. Higher spring rates help fine adjustments of nozzle position. A rotary electric actuator (REA) implementation offers a more expensive option (over pneumatic actuators) to reduce hysteresis.

Materials (turbines)

The simplest way to improve turbocharger response is to manufacture the turbine rotor with lighter materials that exhibit high-temperature resistance properties. Additional requirements are endurance against centrifugal stress and oxidation resistance (Toshimitsu 2002). Above all these requirements is the extra cost that should be kept to a minimum.

These requirements restrict the use of conventional lightweight metallic materials, e.g. aluminium (Al) or titanium (Ti) based alloys due to their low heat-resistantce properties. Ceramic materials, which are both lightweight and heat-resistant, being used for turbine wheels (Loria 2000; Noda 1998), have limited flexibility in optimum shape design and are costly. A new high-performance titanium–aluminium (TiAl) alloy has been developed, reported in Yamaguchi *et al*. (2000) and Toshimitsu (1999); and a new high-response turbocharger using this TiAl for its turbine wheel has been developed (Loria 2000). This turbocharger has been used in a production vehicle, in which 5000 units have been sold to date (Toshimitsu 2002).

5.3.2 Wastegate and variable geometry turbochargers (VGT)

In order to improve the gas exchange performance, compared with a fixed geometry turbocharger (FGT), at low and high engine speeds, (i.e., to increase turbine flow capacity, a bypass valve, i.e. wastegate, is installed on turbine entry linking it to turbine exit. Most designs commonly have the wastegate valve closed at low engine speeds for increasing transient response, with opening restricted to high-engine speeds, also known as a two-stage wastegate, for controlling the exhaust flow. More recently, variable valves known as smart wastegates have been introduced, where the wastegate valve varies continuously according to mass flow (as a function of engine speed), thus allowing a greater degree of freedom in its operation, together with a potential improvement in engine SFC.

In order to improve the gas exchange performance requirements (compared with wastegate turbochargers) at low and high engine speeds, a VGT varies the incidence of exhaust flow to the turbine rotor, and thus changes the flow capacity of the turbine. A key factor that determines the choice of mechanism employed in the variable geometry is control of engine backpressure through a restriction in the exhaust mass flow-rate. A popular solution, in passenger car/light-duty truck applications, makes use of varying nozzles to control incidence angles for turbine rotor entry and optimises backpressure for engine breathing. VGT thus provides optimum boost with respect to emissions (controlling backpressure for EGR) and SFC (controlling pumping losses), whilst controlling, under all operating conditions, the vanes.

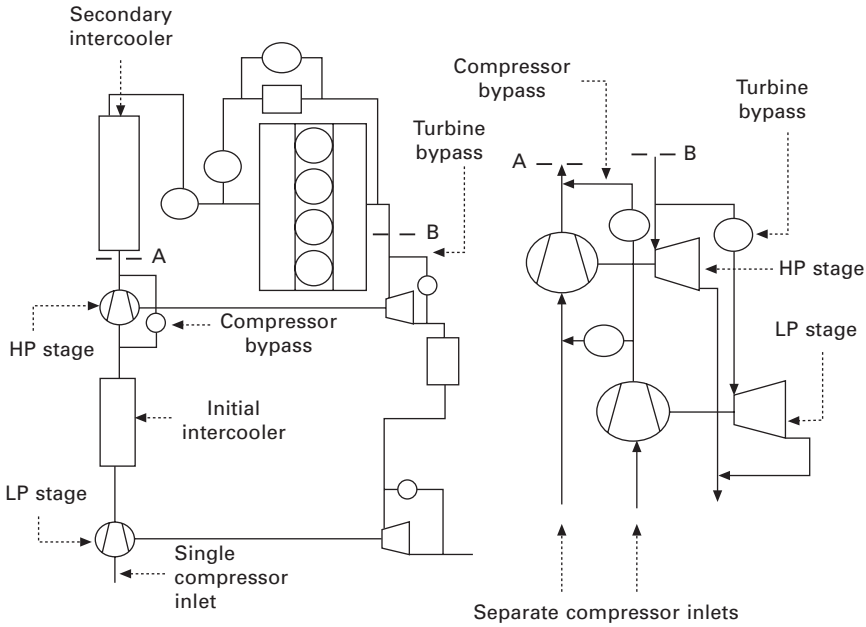
5.3.3 Two-stage turbocharging

Engine downsizing offers an attractive solution for reducing CO_2 emissions but also presents an undesired reduction in maximum power. Some of the loss in power due to downsizing can be potentially regained through optimising the turbocharging matching process. Two-stage turbocharging technology (Cantemir 2001; Choi *et al*. 2006) employed by Saulnier and Guilain (2004) indicates that a 2.0 litre engine's transient performance passenger car acceptance criterion (e.g., 1000–4000 rpm full load in third gear and 80–120 kph in fifth gear) could be achieved with a 1.5 litre (downsized) engine. Results from a computational study showed that a steady-state matched turbocharging system does not guarantee acceptable transient performance. Hence it can be seen that two-stage turbocharging attempts to address two main challenges, namely power loss and transient performance loss due to downsizing of the diesel engine.

Serial vs parallel sequential two-stage turbocharging installations

Two-stage turbocharging is commonly offered as one of two different installations, namely serial or parallel sequential two-stage turbocharging (Figs 5.6(a) and (b):

- *Serial* (Fig. 5.6(a)). This system utilises two turbochargers of different sizes, i.e. a large (low-pressure stage) and a small (high-pressure stage) turbocharger, to cater for the low engine speeds and transients respectively, with a bypass option of the high-pressure stage for high engine speeds and rated power (Portalier *et al*. 2006). This system operates by utilising one compressor inlet and employs one turbocharger at any given time.
- *Parallel* (Fig. 5.6(b)). This system utilises two turbochargers of almost the same size as a function of engine mass air flow, so that the turbochargers always operate in the optimum flow range. This system operates by utilising two compressor inlets and employs two modes of operation.



5.6 Schematics of typical two-stage turbocharging: (a) serial and (b) parallel sequential turbocharging.

The first mode is activated at low speed and torque (with the second turbocharger isolated) to cater for low-speed requirements and transients, while both turbochargers are activated in the second mode at high engine speeds. Since a large engine operating area is associated with two modes of operation, a transition mode is required (Catania *et al*. 2002; Mario 2000) to avoid steps in torque/boost, i.e. switching between modes 1 and 2 and vice versa. A variety of installation configurations (Portalier *et al*. 2006) could be applied to avoid the aforementioned torque steps by utilising a number of valves installed in the ducting. The challenge, however, is to avoid any increase in associated pumping losses and in control complexity whilst satisfying vehicle installation/packaging requirements.

5.3.4 Supercharging

Conventional turbocharging demand at low speed for high torque utilises a significant proportion of the exhaust gas to overcome turbocharger inertia, and

this is associated with boost-lag. This can potentially generate undesired smoke if transient fuelling is not carefully matched. Deterioration in performance is thus achieved initially due to poor utilisation of exhaust energy to drive the compressor and subsequently due to smoke-limited restriction in the fuel flow-rate. Furthermore, the recent drive to reduce engine capacity for improvement in SFC ('downsizing'), and longer gear ratios for improvement in emissions, have *increased* boost-lag. An ideal solution would offer an ample amount of intake air volume flow-rate, thus reducing the emissions and SFC penalty associated with boost-lag.

A supercharger, driven by the crankshaft, de-couples the production of boost pressure with respect to engine load (Catania *et al*. 2002; Schmitz *et al*. 1994). Consequently, the supercharger accelerates simultaneously with the increase in engine exhaust gas flow. Therefore, during any lean operation the supercharger offers the choice of adding fuel to increase torque. However, the challenge in matching the supercharger to the engine exacerbates the parasitic loss which increase with engine speed. It is for this reason that superchargers are utilised for low-speed performance enhancements (George *et al*. 2004).

5.3.5 Turbo-compounding

As engine downsizing becomes more attractive to meet future CO_2 targets, turbo-compounding, i.e. mechanical and electrical as explained below, attempts to address associated low-end transient boost-lag (Yamashita *et al*. 2006). In doing so it also offers a compounded turbocharger tuned for high-speed performance for a particular powertrain application. This section gives a brief overview of various heavy-duty turbo-compounding installations, mechanical and electrical, that can be applied to light-duty.

The simplest form of mechanical turbo-compounding can be seen in Brands *et al*. (1981) where the power turbine, mounted downstream of the conventional turbocharger, is mechanically coupled, via a gear train, to the engine crankshaft. In the case where mechanical losses are high, an electric generator (discussed later) can be used to replace the mechanical coupling. Comparison between mechanical and electrical compounding shows that the electrical system has no mechanical connection to the diesel engine, i.e. recovery of energy from the engine exhaust is performed electronically (Hopmann and Algrain 2003).

Electrical turbo-compounding (Hountalas *et al*. 2007) recuperates part of the exhaust gas heat energy directly from the turbocharger, using a high-speed generator. In this case the turbine produces more power compared to that required to drive the compressor. This excess power is converted to electric power using a high-speed generator incorporated into the turbocharger casing. The application of this on an 11-litre six-cylinder turbocharged diesel engine

resulted in a 5% improvement in bSFC at full load (Hountalas *et al*. 2007). Other examples of electrical turbo-compounding can be found in Hopmann and Algrain (2003) on a 14.6-litre diesel and with a reported average bSFC reduction of about 4.7% (for a 50 000 miles extra-urban driving test in the US).

Millo *et al*. (2006) investigated a variation on electrical turbo-compounding that used an electric motor, connected to the turbocharger shaft, to accelerate the impeller during transients and showed that this configuration reduced the boost-lag. In this case an electric motor/generator was integrated into the turbocharger shaft. The generator extracted surplus power at the turbine, and the electricity it produced was used to run a motor mounted on the engine crankshaft, recovering otherwise wasted energy in the exhaust gases. This electric turbo-compound system also provided more control flexibility in that the amount of power extracted could be varied. This allowed for control of engine boost and thus air–fuel–ratio (AFR). Thus, the principal mode of operation was with the electric machine on the turbocharger shaft acting as a generator, and the electric machine on the engine crankshaft working as a motor. Performance predictions in Hopmann and Algrain (2003) indicate a 5–10% improvement in fuel consumption. System capability offers the potential for reduced emissions and improved driveability through improved air-system response using the turbocharger assist capability. Here, the challenges lie in the design of the electric motor to accommodate vehicle packaging constraints, e.g. to fit into the central section of the turbocharger housing and to tolerate, due to high revolution speeds, the resulting high operating temperatures.

Another example of turbo-compounding, known as assisted turbocharging, is *e-Turbo*. Designated a 'Light Hybrid' (Shahed 2006), this describes a system that has an integrated starter motor/generator (alternator) system and enables automatic engine start/stop function (i.e., features engine fuel cut-off strategy during deceleration/coasting). This system may provide limited launch assist capability, due to having low energy storage capacity.

An application of electric turbo-compounding to a heavy-duty engine replaces current VGT with FGT connecting an electric machine which can be operated as an electric motor and as an electric generator to the turbocharger shaft (Millo *et al*. 2006). The electric motor can be used to speed up the turbocharger during acceleration transients and reduce the boost-lag, while the generator can be used to recover the excess exhaust energy when the engine is operated near the rated speed, in order to produce electrical power that can be used to drive engine auxiliaries.

Yamashita *et al*. (2006) researched an example of a hybrid turbocharger for heavy-duty application with the purpose of eliminating boost-lag and increasing engine torque. An ultra-high-speed motor (a permanent magnet synchronous motor, driven by an inverter) drove the compressor electrically.

Motor torque was in both directions and thus it aided not only low-speed torque but also braking at high speed. Results show that the torque could be increased by 17% at 1000 and 1200 rpm. Transient simulation results indicate that a 1.3 kW motor would shorten the boost-lag by approximately 50% and a 2.0 kW motor by 70%.

5.4 Air-path management

Diesel engine combustion and air-path controls are separated through engine hardware components, e.g. FIE, VGT, EGR, etc. However, in order to achieve a desired engine output, e.g. SFC, emissions, etc., their management is coordinated through the ECU and a set of precalibrated maps (engine calibration). Recent development in the field of MBC is trying to manage the combustion and air-path as one intelligent system with a direct feedback control on desired outputs (discussed later). This section reviews, related to air-path, engine management strategies and highlights potential areas where further work may be required.

5.4.1 Air-path strategies

Air-path management can be broadly discussed under two headings, namely partial and full load. During partial-load operation, the intake manifold composition consists of EGR as well as boosted air, whereas during full load it is only the latter. The targets for the above two conditions also are different, with part-load encompassing minimisation of emissions, e.g. NO_x–soot; and with high loads it is performance in accordance with design limits and SFC, as well as soot.

This section reviews engine control strategies, initially for part-load and emissions problems, followed by specific strategies for full-load operation and reduction of fuel consumption. Finally, transient engine response and control are reviewed, highlighting areas for further study.

Engine control strategies and their limitations

Two ‘air-path’ control features are the focus of this sub-section. The first, EGR (Serrano *et al*. 2005; Ladommatos *et al*. 1996a, 1996b), the purpose of which is to decrease emissions of NO_x, has the well-known drawbacks of poorer fuel economy and increased emissions of soot (Zheng *et al*. 2004; Zhu *et al*. 2003; Tanin *et al*. 1999). The second, the VNT, decreases the emissions of soot by supplying more air to the charge (‘boost pressure’) than is possible by natural aspiration – as controlled by adjusting the vanes, and thereby adjusting also the exhaust mass flow and the exhaust pressure at turbine entry. One of the main drawbacks of employing a VNT is the

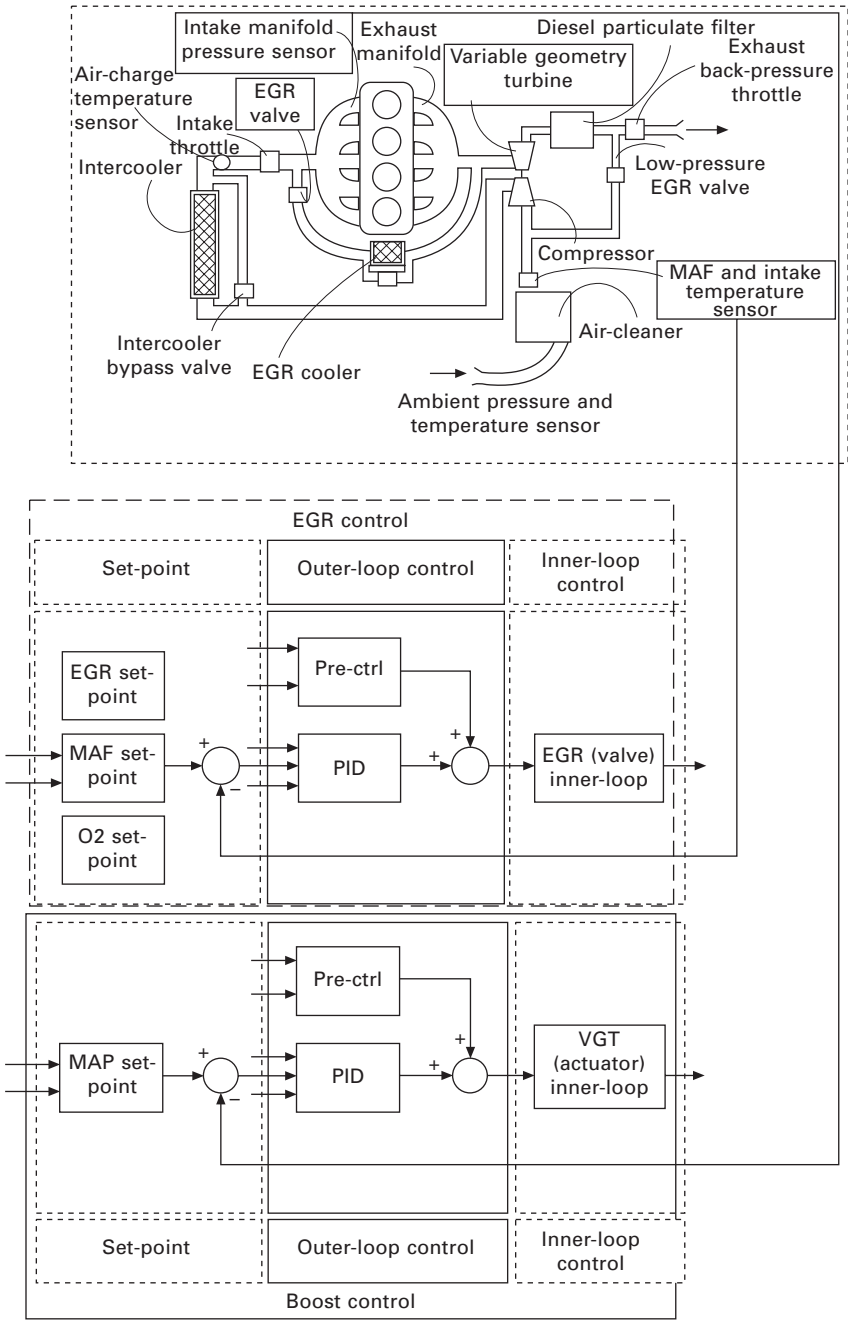
increased pumping loss associated with vane closure, leading to poorer fuel economy. The dynamic behaviour introduced in the exhaust flow, as a result of movement in the EGR (valve) and the VNT (vanes), defines the state and composition of the air charge entering the engine. Hence, much attention is paid to the development of the control of EGR and VNT to improve exhaust emissions, fuel economy, NVH and engine performance.

From the above description of diesel engine operation, the immediate challenge of simultaneously reducing emissions of NO_x and soot emerges. In order to rise to the above challenge, conventional engine control systems, as illustrated by Fig. 5.7, (i) regulate EGR by controlling to a steady-state optimum MAF demand, as measured at the compressor inlet, and (ii) boost pressure by controlling to a steady-state optimum MAP demand, as measured in the intake manifold. A problem may arise during engine transients (measured as rate of change of load on the engine: Jain 1990) because, during these transients, inherent lags (mechanical, fluid dynamic and thermal: Benajes *et al*. 2002; Galindo *et al*. 2006b) associated with turbocharger inertia, exhaust manifold volume (Rakopoulos *et al*. 2004a) and cylinder wall temperatures (Rakopoulos *et al*. 2004b), to name a few, may lead to undesired emission 'spikes' which may exceed those produced in steady-state operation (Kang and Farell 2005).

Transient engine response and its management

Transient manoeuvres such as load-steps, speed-steps, and simultaneous load- and speed-steps (Jain 1990) can induce three main types of transient (Benajes *et al*. 2002): (i) mechanical, e.g. mechanical friction, mechanical turbocharger inertia, other rotating elements of an engine, etc.; (ii) thermal (mass and energy transfer) (Rakopoulos and Giakoumis 2006), e.g. pressure pulses, gas friction, flow inertia, heat transfer, etc.; and (iii) fluid dynamics, e.g. mismatch of injection system during transients.

During a transient from low speed and low load to full load, the performance of the engine is heavily dependent on AFR control for limiting smoke opacity. One method of achieving this is by limiting the (steady-state derived) fuel demand during transient full-load operation. This in turn takes some energy out of the exhaust gas stream that drives the turbocharger and hence increases the boost-lag in the system (Galindo *et al*. 2006b; Rakopoulos *et al*. 2004a). Boost-lag causes sluggish vehicle response during full-load acceleration. In order to mitigate this boost-lag, the turbocharger during the transient responds to a (steady-state derived) MAP demand with alternative VGT vane settings (more closed in the case of a boost-lag and more open in the case of an over-boost relative to steady-state operation). Closure of the VGT vanes during the early part of the 'bottom-end' acceleration, such as idle to full load, can potentially raise engine backpressure. The increase in backpressure on the



5.7 Conventional EGR and VGT control.

engine may then raise, concomitantly, the pumping mean effective pressure (PMEP) of the engine, and thus may also increase its fuel consumption. The penalty in fuel consumption can be ameliorated through design modifications to turbocharger components (Osaka *et al*. 2002; Martinez-Botas 2001) or by applying alternative methods of boosting (Jain 1990).

The constraints to engine operation illustrated above, e.g. part-load emissions and full-load smoke, can be summarised within the air-path management pass-off criteria. These can be categorised in several operating regions as illustrated in Fig. 5.8(a) (based on and modified from the diagram in Guzzella and Amstutz 1998). It can be seen from Fig. 5.8(a) that engine speed and load regions can be prioritised in terms of feature trade-offs and they are accordingly adjusted as a function of engine coolant temperature (z-axis). The above objectives may also be adjusted with respect to ambient pressure and temperature regions that correspond to various geographical locations. Figure 5.8(b) categorises a grid of ambient pressure and temperature conditions and hence environmental conditions. Figure 5.8(a) objectives can then be superimposed in each grid of Fig. 5.8(b), creating a comprehensive control acceptance matrix for a global product. In this manner control objectives and their acceptance are identified *before* optimisation, thus highlighting where manufacturing components can be commonised, and showing where a potential manufacturing cost-saving can be achieved through control commonality.

5.4.2 Advanced air-path management

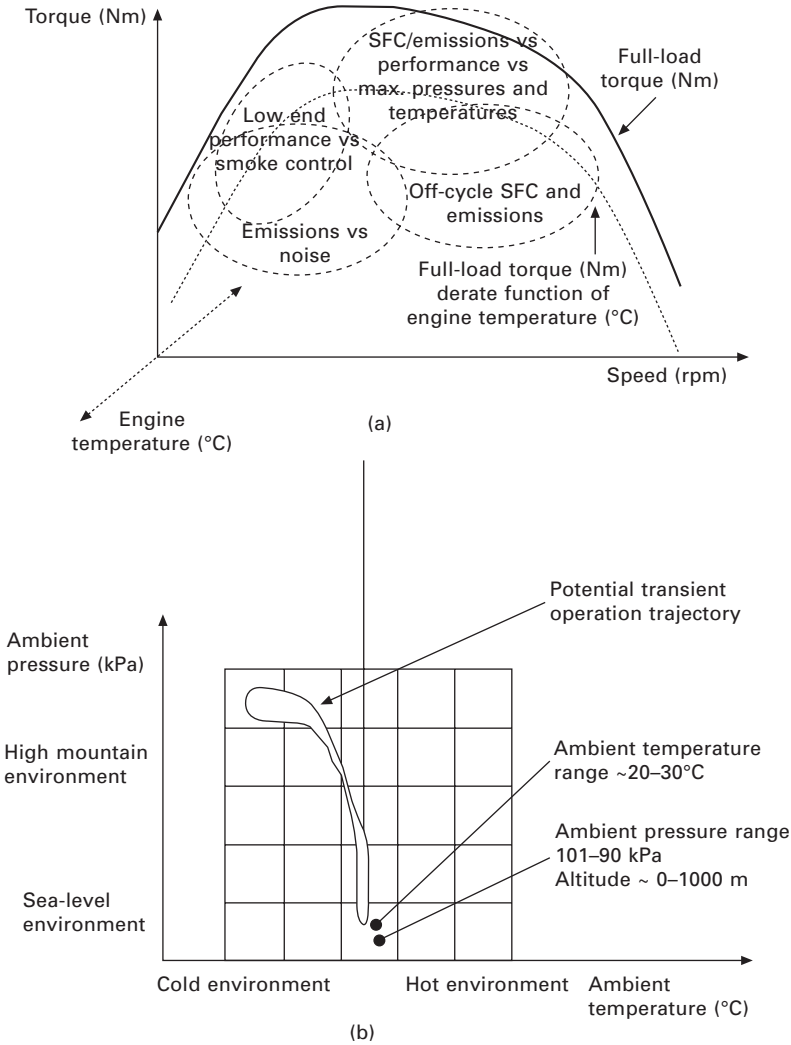
Various approaches have been adopted to handle the close-coupled relationship between MAP and MAF, and to ameliorate the trade-off between NO_x and soot, especially during transient operation (Black *et al*. 2007b; Ford *et al*. 2002; Onder and Geering 1995). A few of the activities currently being researched are reviewed below.

Anticipation logic control

'Anticipation logic' is a function of driver pedal-demand that sends a signal to the VNT control algorithm in order to predict future MAP demands (Jain 1990). Most approaches being researched in this field do not consider VNT and EGR interactions, and consider only high-load transients, operating outside the emissions drive-cycle.

MBC and coordinated control

MBC is used to improve performance through accurate representation of system dynamics (Brace *et al*. 1999), e.g. air excess ratio (lambda



5.8 Diesel operating range and priorities: (a) diesel full-load operating condition and engine control priorities; (b) diesel engine environmental operation.

control). Here, the EGR valve is closed momentarily during accelerations (Yokomura *et al*. 2004). Some coordinated control theories suggest areas of operation where saturation of VNT and EGR control should be avoided (van Nieuwstadt 2003); others use an intake air mass observer to cater for transient AFR control in a turbocharged diesel engine (Bai and Yang 2002). Another type of cooperative control/feed-forward method, based on a system dynamics model, shows that significant improvements are achieved, relative

to conventional methods, in reducing transient NO_x emissions (Shirakawa *et al*. 2001). Gasoline engines have also taken the cooperative control approach for the intake air quantity, EGR and fuel injection quantity (Yasuoka *et al*. 1998). However, the benefits reported generally in the open literature may not always be commercially relevant, because comparisons are not always made against fully emissions-optimised conventional calibrations.

Oxygen sensors and MBC

An exhaust backpressure sensor, in conjunction with the MAP sensor, can be used to estimate air-charge, thus removing the need to use a MAF sensor. The removal of MAF sensor may be desirable to eliminate production component variation associated with the MAF sensor component, thus eliminating the corresponding emission variation. Although Wijetunge *et al*. (2004) discuss high loads, neither NO_x measurements nor drive cycle results are presented.

Nakayama *et al*. (2003) and Roettger *et al*. (2006) present a new control method based on estimated oxygen concentration of charge gas and excess air ratio. The oxygen concentration in the charge is estimated from EGR, and the air mass flow-rate is estimated from the pressure and temperature in the intake manifold. These papers highlight that a discrepancy can arise in emissions between steady-state and transient operation, due to boost-lag. The effects of boost-lag can be met using new control methodology, and thus improvements in NO_x emissions are made during transients. However, the details of the steady-state operation used in conducting the above comparison with transients are not discussed in Nakayama *et al*. (2003), neither is the cost of implementation of the new method for production use.

Neural network approach

Neural networks have also been considered for optimal control of EGR and boost levels (Brahma and Rutland 2003; Galindo *et al*. 2005). An adaptive air-charge estimator for a turbocharged diesel engine, using MAP, air charge temperature (ACT) and engine speed measurements, is applied with no EGR. The design scheme cannot estimate fast transients, and its performance deteriorates due to temperature sensor lags (Stefanopoulou *et al*. 2004).

Lastly, a detailed study of various conventional control systems is presented by van Nieuwstadt *et al*. (2000), who conclude that determining the setpoints is more crucial to the control problem, rather than the controller used to achieve these.

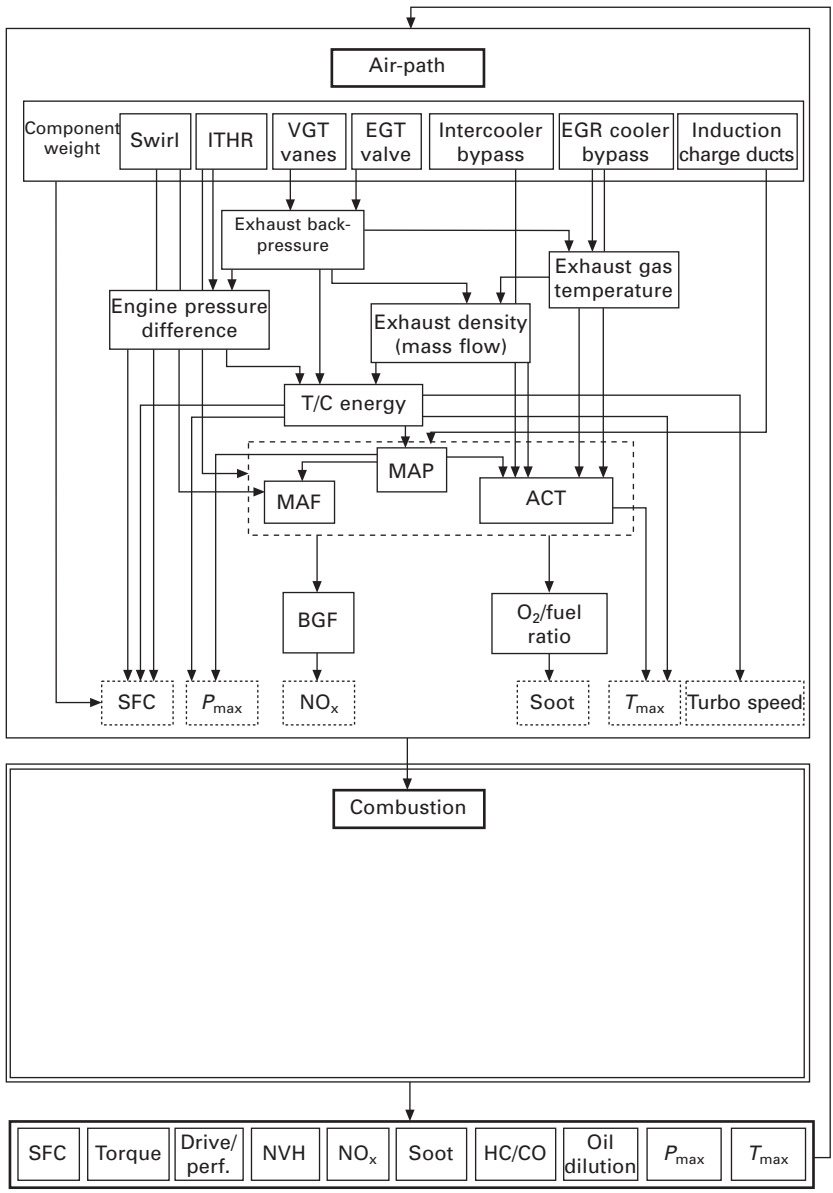
Full-load transients

Optimisation techniques for full-load transients are explained in detail in Arcoumanis *et al*. (1990), Benajes *et al*. (2000), Bizari (1990), Lee and Choi (2002), Galindo *et al*. (2001) and Theotokatos and Kyrtatos (2001). The main objectives are control of full-load transients to maintain high levels of performance with minimum visible smoke.

As indicated in the above review, the main goal of all of the above strategies is to manipulate the thermodynamic properties and oxygen concentration of the cylinder charge, whilst keeping deterioration in power and SFC, under steady-state and transient operating conditions, to a minimum (Zheng *et al*. 2004). It should be noted that the control strategies that are being researched (discussed above) do not take into account integration and implementation aspects for production (vehicle) use in their solution, i.e. level of complexity in control system vs. cost and overall benefits. Furthermore, as engine hardware offers greater flexibility to cater for market demands, e.g. stringent emission standards, higher performance, etc., the control and optimisation management becomes a greater challenge. Thus a solution, potentially through MBC, that merges the two aspects, i.e. control and optimisation, to obtain real-time optimisation becomes the new challenge.

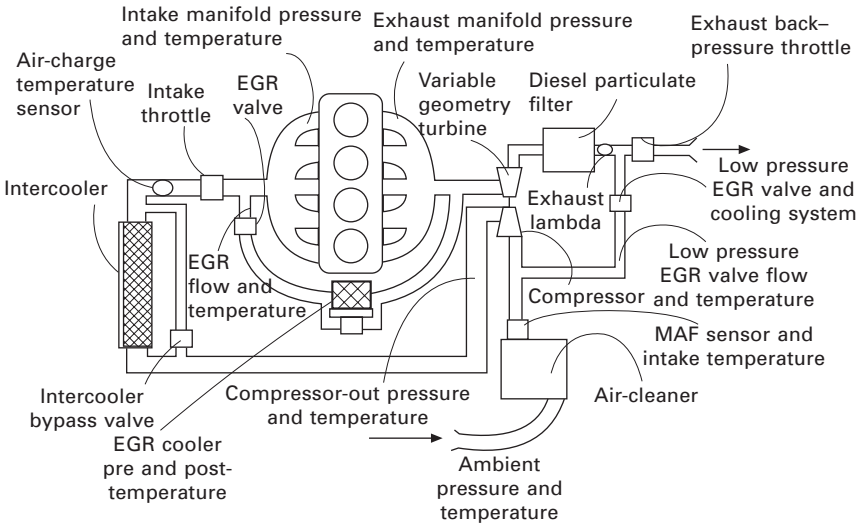
5.4.3 Model based control (MBC) and the engine control unit (ECU)

As engine operation targets, e.g. emissions, full-load performance, etc., become more challenging, and increasingly 'flexible' hardware becomes available, e.g. HPCR, twin-turbocharging, HP- and LP-EGR, etc., engine management requirements become more complex (as illustrated by Fig. 5.8). Figure 5.9 (based on and modified from Guzzella and Amstutz 1998) is a schematic of the events that lead through air-path and combustion processes to emissions on a typical production engine (more information available in Guzzella and Onder 2004). The key engine components that influence the air-path in a diesel engine are listed at the top of the diagram (as inputs) and the final outputs such as emissions are listed at the bottom. Figure 5.9 shows that the modern diesel engine is a complex machine where more than one component can influence each output. Analysis of Fig. 5.9 can help to identify the main factors that contribute towards a particular output, and hence a better control (over conventional methods) can be offered. However, in order to achieve the above, a comprehensive monitoring scheme may be required. Engine behaviour can be monitored by implementing sensors that detect each output. However, implementing a sensor also introduces errors due to the sensor itself and hence an alternative could be supplied by a virtual sensor, through



5.9 Diesel engine input and output diagram (reproduced and modified from Guzzella and Amstutz 1998).

MBC. Figure 5.10 illustrates a schematic of a diesel engine with virtual monitoring of engine conditions through MBC. In applying this air-path management philosophy, the MBC aids engine management robustness in two steps: (i) improvement in outputs, compared with conventional engine



5.10 Diesel engine schematic and its air-path related components for model based control.

control, by modelling and controlling local level influences, e.g. hardware/sensors, etc; and (ii) improvement in outputs, compared with conventional engine control, by modelling and controlling directly to engine outputs.

All of the above themes have been researched individually, e.g. by Darlington (2006). However, little work has been reported in the open literature on joining all of the above themes together. The current, conventional approach in ECU management structure reflects the independent approach, where control strategies are developed for individual features and then joined together through complex interactions for management. The challenge lies in encapsulating complex engine dynamic behaviour (transient- and steady-state) through MBC, and easing the complexity of the management strategy in the ECU, thus potentially minimising room for error and reducing effort in engine development and calibration (including OBD) tasks. However, major challenges lie in the design of accurate engine characterisation models, encompassing transients, and the quality of data generation on which these models are based (Cary 2003; Sens *et al*. 2006).

Traditionally the model-based mapping technique acts as a single multi-objective optimisation tool. One aim of using such a tool would be to optimise for a given engine configuration; the second would be to utilise response models, as developed for optimal exhaust emissions, across a variety of different vehicle inertia classes. A novel approach would extend the above capabilities to implement and utilise these response models in the ECU (Guzzella 2007). This would potentially enable the ECU strategy to have access to stored engine characteristics, in transient- and steady-state

environment. Any deviation from the steady-state operation/optimised state could be predicted/quantified, e.g. emissions, SFC and NVH deficit. Online characterisation and monitoring of the engine under transient or steady-state operation in the above manner could potentially introduce a novel approach to engine air-path and control management for passenger car/light-duty truck applications.

5.5 Future trends

The three main areas of focus in this chapter have been exhaust gas recirculation (EGR), boosting and air-path management. This section briefly recapitulates each one, and further suggests their future implementation trends in passenger cars and light-duty trucks.

EGR

Stringent NO_x emission standards require higher (compared with conventional systems) EGR, engine durability requires a significant reduction in component fouling; and on-board-diagnostics (OBD) requires detection and proper resolution of failed states. These requirements have motivated the further development of EGR technology. The control variable (set-point demand), delivery and accurate and robust feedback are set as pass-off criteria to evaluate these developments.

Developments in the field of materials applied for manufacturing of EGR coolers, e.g. aluminium and magnesium, as opposed to conventional steel, have given manufacturers an opportunity to improve heat exchanger efficiency. Changes in design (in addition to materials) have reduced soot build-up and contamination/corrosion issues, with improvement in durability. High strength/weight ratio has presented an opportunity to create a more compact and integrated EGR valve, cooler and bypass arrangement, allowing more freedom for vehicle installation.

One further challenge that remains is to implement and manage the above advanced techniques for production in the car/light-duty truck market. The introduction of LP EGR in heavy-duty applications gives some production implementation confidence; however, the combination of fast transients (associated with passenger cars) with LP EGR – and their consequence on emissions – still remain to be quantified. The complexity of introducing two EGR systems (HP and LP) with extra bypass valves and throttles, to control exhaust and intake pressures and temperatures, requires delicate coordination and extra calibration effort. The cost–benefit analysis (relating to emissions, specific fuel consumption (SFC) and performance in general) is another item that needs to be explored.

Boosting systems

Providing greater boost to improve performance, whilst downsizing and increasing gear ratios, offers reduction in emissions and improvements in SFC. Turbocharging technology is rapidly developing to cater for fast transient response and thus provide minimum boost-lags (for varying environmental conditions). This is done by either two-stage turbocharging or supercharging and turbo-compounding concepts. The potential increase in weight, cost and installation complexity (including control management) have introduced further key development stages for passenger car/light-duty truck applications. For the near future it is envisaged that advances (e.g., light weight/low inertia, high temperature resistant materials) made in wastegate and VGT two-stage turbocharging may lead the implementation for passenger cars and light-duty truck applications.

Air-path management

Increased expectations in engine performance requirements, e.g. emissions/power/SFC, have spurred rapid advances in control and system compatibilities with engine component technology, e.g. combustion, EGR, FIE, turbocharging, etc. Consequently, surplus activity in offering solutions, through engine component and control advancements, has introduced system complexity. The literature review indicates that simultaneous reduction of emissions, together with improvements in NVH and SFC, may not always be possible without further attention to hardware design and management strategies. A key approach, therefore, to setting up a coherent engine management strategy, lies in specification of the *question* being addressed, i.e. do we seek lower emissions, or improved SFC, or transient 'performance', etc., by using the specific engine management strategy? It was also demonstrated that developments in engine optimisation techniques are linked to engine control strategies that may provide an efficient solution by circumventing compromises in meeting the above outputs.

5.6 Acknowledgements

The author would like to express his gratitude to Ford Motor Company in allowing him to write this chapter. He is also grateful for the invaluable technical input that was provided by Professor A M K P Taylor, Dr Y Hardalupas (Imperial College, London), Mr T Winstanley, Dr P Eastwood and Mr J Black (Ford Motor Company, Dunton, UK) during the writing of this chapter.

5.7 References

Ahlinder, S., Fredriksson, K. and Kropp, W. (2007) 'A study of parameters affecting noise on a heavy duty DI engine', JSAE paper 20077085, SAE paper 2007-01-2081

Arcoumanis, C., Chan, S.H. and Bizari, Z. (1990) 'Optimisation of the transient performance of a turbocharged diesel engine using turbocharging and fuel injection controls', *Imeche Seminar: Engine Transient Performance*, pp. 13–26

Arnold, S. (2004) '19th Cliff Garrett Turbomachinery Engineering Award lecture, Garrett engine boosting systems', SAE paper 2004-01-1359

Arnold, S., Balis, C., Barthelet, P., Poix, E., Samad, T., Hampson, G and Shahed, S.M. (2005a) 'Garrett Electric Boosting Systems (EBS) program', Federal Grant DE-FC05-00OR22809, Final Report, Honeywell Turbo Technologies, 22 June, 2005

Arnold, S., Calta, D., Dullack, K., Judd, C. and Thompson, G. (2005b) 'Development of an ultra-high pressure ratio turbocharger', SAE paper 2005-01-1546

Arnold, S., Balis, C., Jeckel, D., Larcher, S., Uhl, P. and Shahed, S.M. (2005c) 'Advances in turbocharging technology and its impact on meeting proposed California GHG emission regulations', SAE paper 2005-01-1852

Bai, L. and Yang, M. (2002) 'Coordinated control of EGR and VNT in turbocharged diesel engine based on intake air mass observer', SAE paper 2002-01-1292

Benajes, J., Lujan, J.M. and Serrano, J.R. (2000) 'Predictive modeling study of the transient load response in heavy duty turbocharged diesel engine', SAE paper 2000-01-0583

Benajes, J., Lujan, J.M., Bermudez, V. and Serrano, J.R. (2002) 'Modelling of turbocharged diesel engines in transient operation. Part 1: Insight into the relevant physical phenomena', *Proc. IMechE Part D: J. Automotive Engineering* **216**(4), pp. 431–441

Bizari, Z. (1990) 'The transient performance analysis of a turbocharged vehicle diesel engine with electronic fuelling control', SAE paper 900236

Black, J., Eastwood, P.G., Tufail, K., Winstanley, T., Hardalupas, Y. and Taylor, A.M.K.P. (2007a) 'The effect of VGT vane control on pumping losses during full-load transient operation of a common-rail diesel engine', SAE paper 2007-24-0063

Black, J., Eastwood, P.G., Tufail, K., Winstanley, T., Hardalupas, Y. and Taylor, A.M.K.P. (2007b) 'Diesel engine transient control and emissions response during a European Extra-Urban Drive Cycle (EUDC)', JSAE paper 20077291, SAE paper 2007-01-1938

Brace, C.J., Cox, A., Hawley, J.G., Vaughan, N.D., Wallace, F.W., Horrocks, R.W. and Bird, G.L. (1999) 'Transient investigation of two variable geometry turbochargers for passenger vehicle diesel engines', SAE paper 1999-01-1241

Brahma, I. and Rutland, C.J. (2003) 'Optimisation of diesel engine operating parameters using neural networks', SAE paper 2003-01-3228

Brands, M.C., Werner, J. and Hoehne, J.L. (1981) 'Vehicle testing of Cummins turbocompound diesel engine', SAE paper 810073

Bravo, Y., Lázaro, Y.L. and García-Bernad, J.J. (2005) 'Study of fouling phenomena on EGR coolers due to soot deposits. Development of a representative test method', SAE paper 2005-01-1143

Bringhenti, C. and Barbosa, J.R. (2004) 'Methodology for gas turbine performance improvement using variable-geometry compressors and turbines', *Proc. IMechE Part A: J. Power and Energy* **218**, pp. 541–549

Cadman, W. and Johnson, J.H. (1986) 'The study of the effect of exhaust gas recirculation on engine wear in a heavy-duty diesel engine using analytical ferrography', SAE paper 860378

Cantemir, C.-G. (2001) 'Twin turbo strategy operation', SAE paper 2001-01-0666

Cary, M. (2003) 'A model based engine calibration methodology for a port fuel injection, spark-ignition engine', PhD thesis, University of Bradford

Catania, A.E., d'Ambrosio, S., Misul, D., Mittica, A. and Spessa, E. (2002) 'High-boost C.R. diesel engine: a feasibility study of performance enhancement and exhaust-gas power cogeneration' SAE paper 2002-01-2814

Chatterjee, S., Conway, R., Viswanathan, S., Blomquist, M., Klüsener, B. and Andersson, S. (2003) 'NO_x and PM control from heavy duty diesel engines using a combination of low pressure EGR and continuously regenerating diesel particulate filter', SAE paper 2003-01-0048

Chen, H. (2006) 'Turbine wheel design for Garrett advanced variable geometry turbines for commercial vehicle applications', 8th International Conference on Turbochargers and Turbocharging, IMECHE

Choi, C., Kwon, S. and Cho, S. (2006) 'Development of fuel consumption of passenger diesel engine with 2 stage turbocharger', SAE paper 2006-01-0021

Coppinger, M. and Swain, E. (2000) 'Performance prediction of an industrial centrifugal compressor inlet guide vane system', *Proc. I MechE Part A: J. Power and Energy* **214**, pp. 153–164

Darlington, A. (2006) 'Diesel air-path mean-value modelling and charge properties under transient conditions', PhD thesis, Department of Engineering, University of Cambridge

Eynon, P.A. and Whitfield, A. (2000) 'Pressure recovery in a turbocharger compressor volute', *Proc. IMechE Part A: J. Power and Energy*, **214**, pp. 599–610

Ford, R., Glover, K., Collings, N., Christen, U. and Watts, M. (2002) 'Parameterization and transient validation of a variable geometry turbocharger for mean-value modelling at low and medium speed-load points', SAE paper 2002-01-2729

Fraser, L.R.C., Ewing, D., Becard, J., Chang, J.-S. and Cotton, J.S. (2005) 'Optimization of the exhaust mass flow rate and coolant temperature for exhaust gas recirculation (EGR) cooling devices used in diesel engines', SAE Paper 2005-01-0654

Galindo, J., Bermudez, V., Serrano, J.R. and Lopez, J.J. (2001) 'Cycle to cycle diesel combustion characterisation during engine transient operation', SAE paper 2001-01-3262

Galindo, J., Lujan, J.M., Serrano, J.R. and Hernandez, L. (2005) 'Combustion simulation of turbocharger HSDI diesel engines during transient operation using neural networks', *Applied Thermal Engineering* **25**(5–6), pp. 877–898

Galindo, J., Serrano, J.R., Guardiola, C. and Cervello, C. (2006a) 'Surge limit definition in a specific test bench for the characterization of automotive turbochargers', *Experimental Thermal and Fluid Science* **30**, pp. 449–462

Galindo, J., Lujan, J.M., Serrano, J.R., Dolz, V. and Guilain, S. (2006b) 'Description of a heat transfer model suitable to calculate transient processes of turbocharged diesel engines with one-dimensional gas dynamics codes', *Applied Thermal Engineering* **26**(1), pp. 66–76

Galindo, J., Serrano, J.R., Margot, X., Tiseira, A., Schorn, N. and Kindl, H. (2007) 'Potential of flow pre-whirl at the compressor inlet of automotive engine turbochargers to enlarge surge margin and overcome packaging limitations' *Int. J. Heat and Fluid Flow* **28**(3), pp. 374–387

George, S., Morris, G., Dixon, J., Pearce, D. and Heslop, G. (2004) 'Optimal boost control for an electrical supercharging application', SAE paper 2004-01-0523

Green, R.M. (2000) 'Measuring the cylinder-to-cylinder EGR distribution in the intake of a diesel engine during transient operation', SAE paper 2000-01-2866

Guo, Q., Chen, H., Zhu, X.-C., Du, Z.-H. and Zhao, Y. (2007) 'Numerical simulations of stall inside a centrifugal compressor', *Proc. IMechE Part A: J. Power and Energy* **221**, pp. 683–693

Guzzella, L. (2007) 'Control of IC engine systems', *8th Int. Conf. on Engines for Automobiles*, *ICE2007*, SAE, Naples, 16–20 September 2007, SAE International

Guzzella, L. and Amstutz, A. (1998) 'Control of diesel engines', *IEEE Control Systems*, 0272-1708/98, pp. 53–71

Guzzella, L. and Onder, C. (2004) *Introduction to Modelling and Control of Internal Combustion Engine Systems*', Springer-Verlag, Berlin and Heidelberg.

Hopmann, U. and Algrain, M.C. (2003) 'Diesel engine electric turbo compound technology', SAE paper 2003-01-2294

Hountalas, D.T., Katsanos, C.O. and Lamaris, V.T. (2007) 'Recovering energy from the diesel engine exhaust using mechanical and electrical turbocompounding', SAE paper 2007-01-1563

Husted, H., Kruger, D., Fattic, G., Ripley, G. and Kelly, E. (2007) 'Cylinder pressure-based control of pre-mixed diesel combustion', SAE paper 2007-01-0773

Jacobs, T., Assanis, D. and Filipi, Z. (2003) 'The impact of exhaust gas recirculation on performance and emissions of a heavy-duty diesel engine', SAE paper 2003-01-1068

Jain, D. (1990) 'Using an electronically controlled VNT to improve engine transient performance', *IMECHE Seminar: Engine Transient Performance*, pp. 27–30

Kang, H. and Farell, P.V. (2005) 'Experimental investigation of transient emissions (HC and NO_x) in a high speed direct injection (HSDI) diesel engine', SAE paper 2005-01-3883

Kawamoto, A., Takahashi, Y., Koike, T. and Nakamura, F. (2001) 'Variable geometry system turbocharger for passenger car diesel engine', SAE paper 2001-01-0273

Kindl, H., Schorn, N., Schulte, H., Serrano, J.R., Margot, X. and Donayre, J.C. (2004) 'Influence of various compressor inlet designs on compressor performance', SAE paper 2004-30-0008

Kohketsu, S., Mori, K., Sakai, K. and Hakozaki, T. (1997) 'EGR technologies for a turbocharged and intercooled heavy-duty diesel engine', SAE paper 970340

Kolbenschmidt Pierburg Group (2007) 'Intake manifolds – smart intake systems with low weight and multiple functions', commercial sales literature, report pb08_intake_manifold.pdf, (www.kspg-ag.de)

Ladommatos, N., Abdelhalim, S.M., Zhao, H. and Hu, Z. (1996a) 'The dilution, chemical, and thermal effects of exhaust gas recirculation on diesel engine emissions – Part 1: Effect of reducing inlet charge oxygen', SAE paper 961165

Ladommatos, N., Abdelhalim, S.M., Zhao, H. and Hu, Z. (1996b) 'The dilution, chemical, and thermal effects of exhaust gas recirculation on diesel engine emissions – Part 2: Effects of carbon dioxide', SAE paper 961167

Ladommatos, N., Abdelhalim, S.M., Zhao, H. and Hu, Z. (1997) 'The dilution, chemical, and thermal effects of exhaust gas recirculation on diesel engine emissions – Part 4: Effects of carbon dioxide and water vapor', SAE paper 971660

Ladommatos, N., Abdelhalim, S. and Zhao, H. (1998a) 'Control of oxides of nitrogen from diesel engines using diluents while minimising the impact on particulate pollutants', *Applied Thermal Engineering* **18**, pp. 963–980

Ladommatos, N., Abdelhalim, S.M., Zhao, H. and Hu, Z. (1998b) 'Effects of EGR on heat release in diesel combustion', SAE paper 980184

Ladommatos, N., Abdelhalim, S.M. and Zhao, H. (2000) 'Effects of exhaust gas

recirculation temperature on diesel engine combustion and emissions', *Int. J. Engine Research* **1**(1), pp. 107–126

Langridge, S. and Fessler, H. (2002) 'Strategies for high EGR rates in a diesel engine', SAE paper 2002-01-0961

Lee, C.S. and Choi, N.J. (2002) 'Effect of air injection on the characteristics of transient response in a turbocharged diesel engine', *Int. J. Thermal Sciences* **41**(1), pp. 63–71

Loria, E.A. (2000) 'Gamma titanium aluminides as prospective structural materials', *Intermetallics* **8**, pp. 1339–1345

Lundqvist, U., Smedler, G. and Stålhammar, P. (2000) 'A comparison between different EGR systems for HD diesel engines and their effect on performance, fuel consumption and emissions', SAE paper 2000-01-0226

Maiboom, A., Tauzia, X. and Hetet, J.-F. (2008) 'Experimental study of various effects of exhaust gas recirculation (EGR) on combustion and emissions of an automotive direct injection diesel engine', *Energy* **33**, pp. 22–34

Mario, M. (2000) 'Some problems of sequential turbocharging of diesel engines for racing boats', SAE paper 2000-01-0528

Martinez-Botas, R.F. (2001) 'Mixed-flow turbine: steady and unsteady performance with detailed flow measurements', in *Thermofluid Dynamic Processes in Diesel Engines* (ed. Whitelaw, J.H., Payri, F. and Desantes, J), Springer-Verlag, pp. 239–263

Millo, F., Mallamo, F., Pautasso, E. and Mego, G.G. (2006) 'The potential of electric exhaust gas turbocharging for HD diesel engines, SAE paper 2006-01-0437

Mito, Y., Tanaka, D., Wock Lee, S., Daisho, Y. and Kusaka, J. (2003) 'The effect of intake, injection parameters and fuel properties on diesel combustion and emissions', JSAE paper 20030161, SAE paper 2003-01-1793

Mukherjee, S. and Baker, D. (2002) 'Thermal design of high pressure ratio turbocharger compressor wheels', SAE paper 2002-01-0162

Nagai, I., Endo, H., Nakamura, H. and Yano, H. (1983) 'Soot and valve train wear in passenger car diesel engine', SAE paper 831757

Nakayama, S., Fukuma, T., Matsunaga, A., Miyake, T. and Wakimoto, T. (2003) 'A new dynamic combustion control method based on charge oxygen concentration for diesel engines', SAE paper 2003-01-3181

Noda, T. (1998) 'Application of cast gamma TiAl for automobiles', *Intermetallics* **6**, pp. 709–713

Olsson, J.O., Tunestål, P., Ulfvik, J. and Johansson, B. (2003) 'The effect of cooled EGR on emissions and performance of a turbocharged HCCI engine', SAE paper 2003-01-0743

Onder, C. and Geering, H.P. (1995) 'Model-based engine calibration for best fuel efficiency', SAE paper 950983

Osaka, K., Higashimori, H. and Mikogami, T. (2002) 'Study on the internal flow of radial turbine rotating blades for automotive turbocharging', SAE paper 2002-01-0856

Pan, D., Whitfield, A. and Wilson, M. (1999) 'Design considerations for the volutes of centrifugal fans and compressors', *Proc. IMechE Part C*, **213**, pp. 401–410

Partridge, W.P., Lewis, S.A., Ruth, M.J., Muntean, G.G., Smith, R.C. and Stang, J.H. (2002) 'Resolving EGR distribution and mixing', SAE paper 2002-01-2882

Portalier, J., Blanc, J.C., Garnier, F., Hoffmann, N., Schorn, N., Kindl, H., Galindo, J., Jeckel, D., Uhl, P. and Laissus, J.-J. (2006) 'Twin turbo boosting system design for the new generation of PSA 2.2 litre HDI diesel engines', *THIESEL 2006 Conference on Thermo- and Fluid Dynamic Processes in Diesel Engines*

Rakopoulos, C.D. and Giakoumis, E.G. (2006) 'Review of thermodynamic diesel engine simulations under transient operating conditions', SAE paper 2006-01-0884

Rakopoulos, C.D., Giakoumis, E.G., Hountalas, D.T. and Rakopoulas, D.C. (2004a) 'The effect of various dynamic, thermodynamic and design parameters on the performance of a turbocharged diesel engine operating under transient load conditions', SAE paper 2004-01-0926

Rakopoulos, C.D., Giakoumis, E.G. and Rakopoulos, D.C. (2004b) 'Cylinder wall temperature effects on the transient performance of a turbocharged diesel engine', *Energy Conversion and Management* **45**(17), pp. 2627–2638

Roettger, D., Vigild, C. and Calendini, P.O. (2006) 'A model based approach for diesel combustion control', *Aachener Kolloquium Fahrzeug- und Motorentechnik* **15**, pp. 439–459

Saulnier, S. and Guilain, S. (2004) 'Computational study of diesel engine downsizing using two-stage turbocharging', SAE paper 2004-01-0929

Schmitz, T.N., Holloh, K.D., Juergens, R. and Fleckenstein, G. (1994) 'Potential of additional mechanical supercharging for commercial vehicle engines', SAE paper 942268

Schten, K., Ripley, G., Punater, A. and Erickson, C. (2007) 'Design of an automotive grade controller for in-cylinder pressure based engine control development', SAE paper 2007-01-0774

Sens, M., Nickel, J., Grigoriadis P. and Pucher, H. (2006) 'Influence of sensors and measurement system configuration on mapping and the use of turbochargers in the vehicle', SAE paper 2006-01-3391

Serrano, J.R., Climent, H., Arnau, F.J. and Traumat, G. (2005) 'Global analysis of the EGR circuit in a HSDI diesel engine in transient operation', SAE paper 2005-01-0699

Shahed, S.M. (2006) 'An analysis of assisted turbocharging with light hybrid powertrain', SAE paper 2006-01-0019

Shirakawa, T., Itoyama, H. and Miwa, H. (2001) 'Study of strategy for model based cooperative control of EGR and VNT in a diesel engine', *JSAE Review* **22**, pp. 3–8

Siewert, R.M., Krieger, R.B., Huebler, M.S., Baruah, P.C., Khalighi, B. and Wesslau, M. (2001) 'Modifying an intake manifold to improve cylinder-to-cylinder distribution in a DI diesel engine using combined CFD and engine experiments', SAE paper 2001-01-3685

Spence, S.W.T. and Artt, D.W. (1998) 'An experimental assessment of incidence losses in a radial inflow turbine rotor', *Proc IMechE Part A: J. Power and Energy* **212**, pp. 43–53.

Stefanopoulou, G., Storset, O.F. and Smith, R. (2004) 'Pressure and temperature based adaptive observer of air charge for turbocharged diesel engines', *Int. J. Robust and Nonlinear Control*, **14**, pp. 543–560

Tange, H., Ikeya, N., Takanashi, M. and Hokari, T. (2003) 'Variable geometry diffuser of turbocharger compressor for passenger vehicles', SAE paper 2003-01-0051

Tanin, K.V., Wickman, D.D., Montgomery, D.T., Das, S. and Reitz, R.D. (1999) 'The influence of boost pressure on emissions and fuel consumption of a heavy-duty single-cylinder D.I. diesel engine', SAE paper 1999-01-0840

Theotokatos, G. and Kyrtatos, N.P. (2001) 'Diesel engine transient operation with turbocharger compressor surging', SAE paper 2001-01-1241

Tokura, N., Terasaka, K. and Yasuhara, S. (1982) 'Process through which soot intermixes into lubricating oil of a diesel engine with exhaust gas recirculation', SAE paper 820082

Toshimitsu, T. (1999) 'Gamma Ti aluminides for non-aerospace applications', *Current Opinion in Solid State and Materials Science* **4**, pp. 243–248

Toshimitsu, T. (2002) 'Development of a TiAl turbocharger for passenger vehicles', *Mater. Sci. Eng.* **A329–331**, pp. 582–588

Uchida, H., Kashimoto, A. and Iwakiri, Y. (2006) 'Development of wide range compressor with variable inlet guide vane', Special Issue Turbocharging Technologies, Research Report, R&D Review of Toyota CRDL Vol. 41, No. 3

van Nieuwstadt, M. (2003) 'Coordinated control of EGR valve and intake throttle for better fuel economy in diesel engines', SAE paper 2003-01-0362

van Nieuwstadt, M.J., Kolmanovsky, I.V. and Moraal, P.E. (2000) 'Coordinated EGR-VNT control for diesel engines: an experimental comparison', SAE paper 2000-01-0266

Watson, N. and Janota, M.S. (1982) *Turbocharging the Internal Combustion Engine*', Macmillan, London

Wijetunge, R.S., Hawley, J.G. and Vaughan, N.D. (2004) 'Application of alternative EGR and VNT strategies to a diesel engine', SAE paper 2004-01-0899

Yamaguchi, M., Inui, H. and Ito, K. (2000) 'High-temperature structural intermetallics', *Acta Mater.* **48**, pp. 307–322

Yamashita, Y., Ibaraki, S. and Ogita, H. (2006) *Development of Electrically Assisted Turbocharger for Diesel Engine*', Mitsubishi Heavy Industries, Tokyo

Yasuoka, M., Uchida, M., Iwona, H. and Yoshino, T. (1998) 'A study of a torque control algorithm for direct injection gasoline engines', *JSAE Review* **19**, pp. 235–241

Yokomura, H., Kouketsu, S., Kotooka, S. and Akao, Y. (2004) 'Transient EGR control for a turbocharged heavy duty diesel engine', SAE paper 2004-01-0120

Zhang, R., Charles, F., Ewing, D., Chang, J.S. and Cotton, J.S. (2004) 'Effect of diesel soot deposition on the performance of exhaust gas recirculation cooling devices', SAE paper 2004-01-0122

Zheng, M., Reader, G.T. and Hawley, J.G. (2004) 'Diesel engine exhaust gas recirculation – A review on advanced and novel concepts', *Energy Conversion and Management* **45**(6), pp. 883–900

Zhu, Y., Zhao, H. and Ladommatos, N. (2003) 'Computational study of the effects of injection timing, EGR and swirl ratio on a HSDI multi-injection diesel engine emission and performance', SAE paper 2003-01-0346

5.8 Appendix: Acronyms

ACT Air Charge Temperature
AFR Air Fuel Ratio
BGF Burned Gas Fraction
BPF Blade Passing Frequency
bSFC brake Specific Fuel Consumption
CFD Computational Fluid Dynamics
CR Common Rail
DPF Diesel Particulate Filter
ECU Engine Control Unit
EGR Exhaust Gas Recirculation
FE Fuel Economy
FGT Fixed Geometry Turbocharger

FIE	Fuel Injection Equipment
HC	Hydrocarbon
HCCI	Homogeneous Charge Compression Ignition
HP	High Pressure
IDI	Indirect Injection
IGV	Inlet Guide Vanes
ITHR	Intake Throttling
IVC	Inlet Valve Closure
LP	Low Pressure
LST	Low Speed Turbocharger
LTC	Low Temperature Combustion
MAF	Mass Air Flow
MAP	Manifold Air Pressure
MBC	Model Based Control
NVH	Noise Vibration and Harshness
OBD	On-Board-Diagnostic
PCCI	Premixed Charge Compression Ignition
PID	Proportional, Integral, Derivative
P_{max}	Maximum pressure (e.g. in-cylinder pressure)
PMEP	Pumping Mean Effective Pressure
REA	Rotary Electric Actuator
SFC	Specific Fuel Consumption
SGD	Swirl Generation Device
T/C	Turbocharger
T_{max}	Maximum temperature (e.g. intake manifold, in-cylinder)
VGC	Variable Geometry Compressor
VGT	Variable Geometry Turbocharger
VIGV	Variable Inlet Guide Vanes
VNT	Variable Nozzle Turbine
WGT	Waste-Gate Turbocharger

6

Advanced concepts for future light-duty diesel engines

I. DENBRATT, Chalmers University of Technology, Sweden

Abstract: Future diesel engines for passenger cars will have to meet increasingly stringent exhaust emissions legislation and be more efficient in order to reduce CO_2 emissions. The most difficult challenges are to meet US Tier 2 regulations, which will impose limits of 0.07 g/m NO_x and 0.01 g/m PM, and the requirements of the US06 Supplemental Federal Test Procedure for low NO_x emissions at high load. To cope with the increasingly stringent emissions legislation new technologies must be introduced. The chapter describes possible new technologies, such as new combustion concepts, future fuel injection systems, advanced charging and EGR systems and after-treatment systems needed for meeting the future requirements.

Key words: emissions legislation, combustion systems, injection systems, charging, EGR systems and after-treatment systems.

6.1 Introduction

Diesel-powered vehicles are steadily increasing in popularity, especially in Western Europe, where the diesel share of the car market increased from 13.8% in 1990 to 50.8% in 2006 (the first time that it surpassed gasoline engines in this respect). Furthermore, its market share is still increasing (ACEA 2007) and predictions indicate that it might approach 80% by 2020. The increase in diesel sales can be partly explained by the rapid recent increases in fuel prices (which have prompted increasing consumer demands for fuel efficiency) and partly by developments in engine technology, such as new fuel injection systems, turbochargers and engine control systems that have provided substantial improvements in performance and reductions in NVH (noise, vibrations and harshness). However, in other parts of the world the situation is quite different. In the USA the market share of diesel engines is still only about 3%, because they acquired a very undesirable reputation during the 1970s and 1980s for being noisy, emitting black smoke and performing poorly. Nevertheless, increasing fuel prices and technical developments have led to increased interest in diesel engines in the USA too, and predictions indicate (J.D. Power 2008) that sales of light-duty diesels will grow in the USA and are expected to account for 14% of the total by 2017. More light-duty diesel vehicles were actually sold in the USA during 2007 than hybrids. A problem to overcome is that currently only 42% of

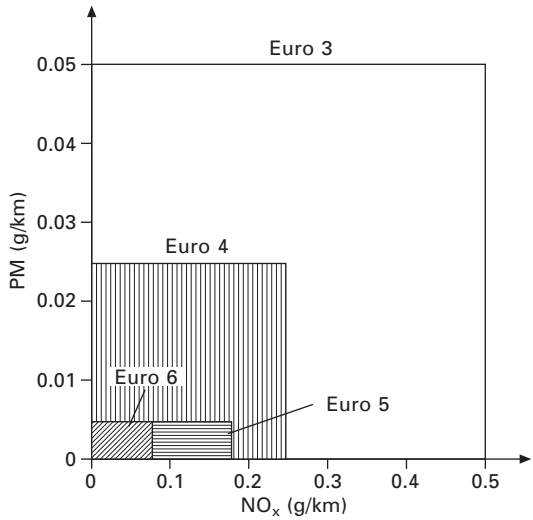
American filling stations sell diesel. In Japan diesel sales are currently very low, but Japanese diesel sales are also predicted to increase, following the trend in the United States.

However, future diesel engines for passenger cars will have to meet increasingly stringent exhaust emissions legislation and be more efficient in order to reduce CO_2 emissions. The most difficult challenges are to meet US Tier 2 regulations, which will impose limits of 0.07 g/mile NO_x and 0.01 g/mile PM, and the requirements of the US06 Supplemental Federal Test Procedure for low NO_x emissions at high load. To cope with the increasingly stringent emissions legislation new technologies must be introduced. New combustion concepts, like partly premixed combustion (pPCCI) and low temperature (LTC) combustion, must be launched. Fuel injection systems must be further refined, with features such as rate shaping, variable geometry and injection pressures in the range 2000–2500 bar (fourth generation). Advanced charging and EGR systems must be applied, and after-treatment systems containing particulate filters and SCR/NO_x-traps will have to be used. In addition, various technical problems associated with these developments still remain to be solved, for instance the high cylinder pressures rises and noise generated by combustion systems in which high injection pressures and long ignition delays are used.

6.2 Legislative exhaust emission standards

6.2.1 European Union

Previous, current and proposed EU emission limits for NO_x and PM, as stipulated by Euro 3, 4, 5 (Regulation (EC) 715/2007, European Commission, 2007) and 6, are shown in Fig. 6.1. The Euro 5 and 6 particulate standards are likely to be reduced from 0.005 to 0.003 g/km driven distance, as determined using a new method for measuring particulates that takes the number of particles into consideration as well as their mass (the Euro 5/6 requirements were to be finally decided in July 2008). The change in the PM mass limit is designed to compensate for the differences in measurements obtained using the old and new methods. The proposal is to introduce a particle number emission limit, based on measurements obtained using the so-called PMP method (Andersson *et al*. 2007), in addition to the mass-based limits, to prevent the use of filters that can meet the PM mass limit but allow large numbers of ultra-fine particles to be released. The draft suggests a particle number limit of 5×10^{11}/km. Euro 5 will start to be implemented in 2009 and Euro 6 in 2014. The in-service conformity will be 100 000 km or 5 years (whichever comes first) as for Euro 4, but for type approval durability testing for 160 000 km is necessary from Euro 5. Emissions are tested using the New European Driving Cycle (NEDC). EU Member States are allowed to introduce

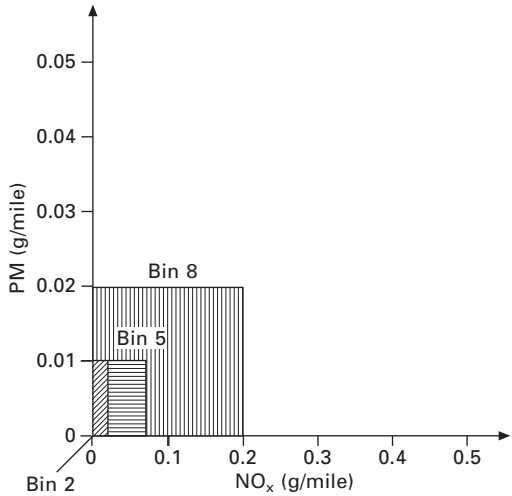


6.1 European emissions standards for NO_x and PM (EURO 5 and 6 limits have not yet been finally decided).

tax incentives to encourage early introduction of vehicles that comply with future emissions standards earlier than required by legislation.

6.2.2 United States

The federal (49 state) Tier 2 emissions standard (Federal Register 2000) is to be implemented in stages between 2004 and 2009. When fully implemented in 2009, the average NO_x emissions of the entire light-duty vehicle fleet sold by each manufacturer will have to meet the average NO_x standard of 0.07 g/mile. Light Duty Vehicles (LDV) and Light Duty Trucks (LLDT) had to meet the standards from 2007, while Heavy Light Duty Trucks (HLDT) and Medium Duty Passenger Vehicles (MDPV) must comply from 2009. The same emissions standards apply to all vehicles up to a weight of 10 000 lb GVWR (Gross Vehicle Weight Ratio: the maximum allowable weight of a vehicle, including the vehicle, passengers, cargo and fuel) that are used for passenger transportation. The same standards also apply to both gasoline and diesel vehicles. There are eight 'certification bins', and vehicle manufacturers can choose to certify a particular model according to any of these bins, as long as its average NO_x emissions meet the 0.07 g/mile NO_x standard. Figure 6.2 illustrates three of the different certification bins. Bin 5 is equal to the Tier 2 standard. Emissions are measured in tests using the FTP (Federal Test Procedure) cycle. There is also a supplementary emissions standard (SFTP) based on two different driving cycles: the US06, representing high speed/high acceleration conditions, in which the maximum speed is close to 130



6.2 US emissions standards.

km/h (80.3 mph); and the SC03 cycle, a low speed cycle representing the use of air conditioning.

The emissions limits depend on the bin chosen for the vehicle's certification. For a vehicle certified in bin 5 the SFTP standard for non-methane hydrocarbons (NMHC) + NO_x is 1.41 g/mile and the PM standard 0.08 g/mile. The SFTP result is calculated as the sum of the results from the different test cycles:

$$SFTP = 0.35 * (FTP) + 0.28 * (US06) + 0.37 * (SC03)$$

For diesel vehicles, meeting US06 limits represents a real challenge. The in-service conformity requirement is 120 000 miles or 10 years, whichever occurs first for LDV and LLDT, while for HLDT and MDPV it is 11 years instead of 10. A manufacturer can also choose to certify for 150 000 miles or 15 years to gain NO_x credits. Manufacturers can obtain Tier 2 credits if their fleet-average NO_x emissions are less than the fleet-average standard. Credits can be banked for future use or traded with other manufacturers. The bin system also covers the California LEVII standards for vehicles having a GVWR less than 8500 lb. Bin 5 and Bin 2 correspond to ULEV (Ultra Low Emission Vehicle) and SULEV (Super-Ultra Low Emission Vehicle) standards, respectively.

6.2.3 Japan

The Japanese emission standards are currently divided into two weight classes: lower and greater than 1250 kg equivalent vehicle weight (1265 kg vehicle weight). However, from 2009 the emissions standards will be the

same for both classes. The NO_x and PM standards from 2009 will be equal to the Euro 6 standards: 0.08 g/km NO_x and 0.005 g/km PM. The testing cycle currently used is the 10–15 mode cycle, but this will be replaced by the JC08 cycle, in which the average speed is higher than in the 10–15 mode cycle. The JC08 cycle will be gradually phased in between 2008 and 2011. During the interim period the emissions will be calculated using weighted averages obtained in the two cycles.

6.2.4 CO_2 emissions/fuel consumption standards

For passenger cars the voluntary European Automobile Manufacturers' Association (ACEA) agreement of 1998 to reduce carbon dioxide emissions to a fleet average of 140 g/km by 2008 will not be met and the EU is now considering more mandatory limits. In December 2007 the European Commission proposed legislation (Regulation (EC) 715/2007, European Commission 2007) to reduce average CO_2 emissions to 130 g/km by means of developments in vehicle technology by 2012, with a further 10 g/km reduction from developments in fuel, tyres, etc., which will apply to vehicles with a reference mass not exceeding 2610 kg. In December 2008 the European Parliament approved the legislation, proposed in 2007. However, the agreed text delays implementation of the CO_2 limits by introducing a phase-in period from 2012 to 2015, setting interim targets for manufacturers intended to ensure that these CO_2 emission limits are met by, on average, 65% of their fleets in January 2012, 75% in January 2013, 80% in January 2014 and 100% from 2015. The approved text also differs from the Commission's proposals in that manufacturers may apply for 'eco-innovation' credits of up to 7 g CO_2/km for using innovative CO_2-reducing technologies, such as energy-efficient lights, etc., which are not currently considered in the normal test cycle. The legislation defines a limit value curve of permitted emissions of CO_2 for new vehicles according to the mass of the vehicle. The curve is set in such a way that a fleet average for all new cars of 130 g of CO_2 per kilometre should be met. For individual vehicles the permitted specific CO_2 emissions will be a function of vehicle weight, and will be calculated using the following formula:

$$CO_2 = 130 + a \times (M - M_0)$$

where

M = mass of the vehicle in kilograms (kg)
$M_0 = 1289.0 \times f$
$f = (1 + \text{AMI})^6$
AMI = autonomous mass increase (= 0%)
$a = 0.0457$

The average CO_2 emissions from new cars sold throughout the EU (all 27 member countries) should then decline to the 120 g CO_2/km target by 2015, which is equivalent to fuel consumption of 4.5 litres per 100 km (48 mpg). Penalties proposed for exceeding the limits (€20 per g/km in 2012 increasing to €95 by 2015) were also modified, so that from 2012 to 2018 the fines will be €5 for the first gram of CO_2, €15 for the second gram, €25 for the third gram and €95 from the fourth gram onwards. From 2019, manufacturers will pay €95 for each gram exceeding the target. The proposal means that the level of CO_2 emissions from heavier cars will have to be improved proportionately more, compared to today's levels, than those from lighter cars. Further ahead, the Commission is aiming to reduce emissions from new cars to an average of 95 g CO_2/km by 2020. For 2025 the European Parliament (European Parliament and Council 2007) has suggested a future possible limit of 70 g CO_2/km or less.

In the US the CAFE (Corporate Average Fuel Consumption) requirement has been 27.5 mpg for light-duty vehicles since 1990. The light-duty truck standard, set by the Department of Transportation, is currently 22.2 mpg (2007) rising to 23.5 mpg by 2011. In December 2007 the US Congress passed an energy bill that will lead to a new combined CAFE requirement (for light-duty vehicles and light-duty trucks) of 35 mpg by 2020. As in Europe, the requirement will be in the form of a mathematical expression. Further reductions will be made between 2021 and 2030.

6.3 Current developments

Diesel engines are known to have the highest efficiency of all internal combustion engines. They are also known to be able to deliver high torque (BMEP); the best contemporary engines deliver about 75 kW/litre maximum power and 25 bar BMEP. Maximum cylinder pressures are increasing and engines are now being developed for 180 bar peak pressure. However, exhaust emissions present problems, especially the 'diesel dilemma', i.e. the difficulties involved in simultaneously reducing particulate and nitrogen-oxide emissions from diesel engines (see below for further details). Furthermore, it is not possible to operate diesel engines stoichiometrically, so cheap, simple NO_x after-treatment devices like three-way catalysts cannot be used in conjunction with them. Instead, engine-out emissions must be reduced as far as possible and for future emissions standards more complex and expensive after-treatment devices will have to be used, like selective catalytic reduction (SCR) systems, with urea as a reducing agent, or lean NO_x traps (LNT) in addition to diesel particulate filters (DPF).

The requirements for future diesel engines can be summarized as needs to:

- reduce emissions
- reduce fuel consumption
- increase specific power, to >80 kW/litre
- improve transient responses, NVH and cold start ability.

No single technological advance will lead to the fulfilment of these future requirements for diesel engines. Instead, multiple measures must be taken and advanced systems introduced in a highly integrated fashion. Notable features of future engines are likely to include low NO_x- and soot-generating combustion modes, advanced injection systems, charging systems including EGR and exhaust after-treatment systems with diesel oxidation catalysts, diesel particulate filters and NO_x-reducing catalysts.

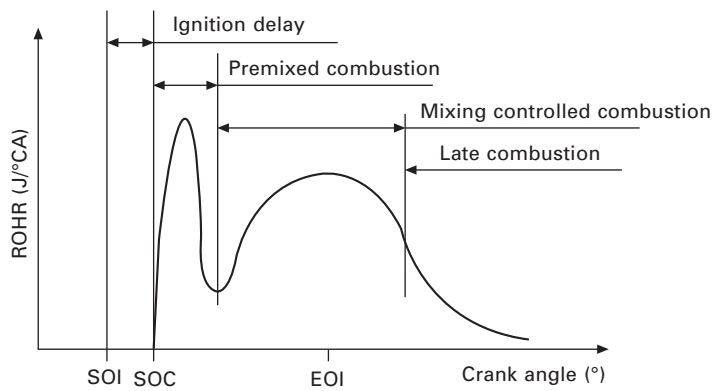
6.4 Low emissions concepts: key aspects

In order to reduce engine-out exhaust emissions some of the key aspects that must be considered include:

- The combustion system (Section 6.5)
- The fuel injection system (Section 6.6)
- Charge induction (Section 6.7)
- The combustion chamber (bowl) geometry (Section 6.8)

6.4.1 Combustion and emissions formation

Diesel combustion can be divided into four phases: ignition delay, premixed combustion, mixing-controlled combustion and burn-out, as illustrated in Fig. 6.3.



6.3 Combustion phases in a diesel engine. ROHR refers to rate of heat release (in joules per crank angle degree).

During the ignition delay period, from start of injection (SOI) until start of combustion (SOC), the injected fuel is atomized, evaporated and mixed with air. The fuel also undergoes chemical (preflame) reactions before it ignites. When ignition occurs (at SOC) a flame rapidly propagates from the ignition site, consuming most of the fuel that has been injected during the ignition delay period, except for the fuel that has not evaporated and mixed within the flammability limits of the fuel. Fuel that has been mixed leaner than the flammability limit will leave the engine as HC emissions. The very fast combustion leads to a rapid increase in cylinder pressure, which is one of the main causes of combustion-generated noise. To suppress noise and avoid premixed combustion accounting for a large proportion of total combustion, a pilot injection is often used.

After the premixed fuel has been consumed during the premixed combustion phase, burning is controlled by the speed at which the remaining fuel mixes with air in combustible ratios. Since the temperature at this stage is high, chemical kinetics are fast. This phase is also referred to as diffusion-controlled combustion.

The spray produces very high turbulence, but after the end of injection (EOI) turbulence declines, the mixing velocity decreases and the in-cylinder temperature decreases during the expansion stroke, thereby reducing the velocity of the chemical kinetics. In this phase fuel that burned in regions with rich conditions is mixed with air and further oxidized ($CO \rightarrow CO_2$) and soot that has been formed in rich conditions is now oxidized. In order to improve mixing and increase the reaction velocity to enhance soot oxidation, a post-injection can be used.

Combustion and emissions formation in diesel engines are very complex processes, involving many phenomena and mechanisms that are not yet understood in detail. However, a conceptual model for diesel combustion was presented by Dec in 1997 (see Plate II between pages 364 and 365) The model is based on information obtained from various types of optical measurements.

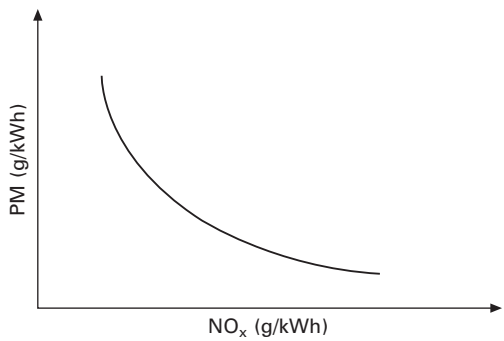
All diesel flames are so-called lifted flames, i.e. flames that do not propagate all the way back to the nozzle but stabilize at some distance from it, due to high cooling losses (from the evaporating fuel) and flame stretching due to high shear forces generated by the high spray velocity (which causes quenching). The distance between the nozzle and flame stabilization point is called the lift-off distance and influences emissions formation. The lift-off distance depends on the injection rate, injection pressure, oxygen concentration (EGR) and temperature (lift-off is larger at lower loads).

At the lift-off point air is entrained into the spray, which helps to evaporate the fuel and dilutes the inner region of the flame. The initial oxidation of the fuel takes place at the centre of the jet under fuel-rich conditions, leading to soot formation. The combustion products formed during this partial oxidation are transported towards the periphery of the spray where they are mixed with

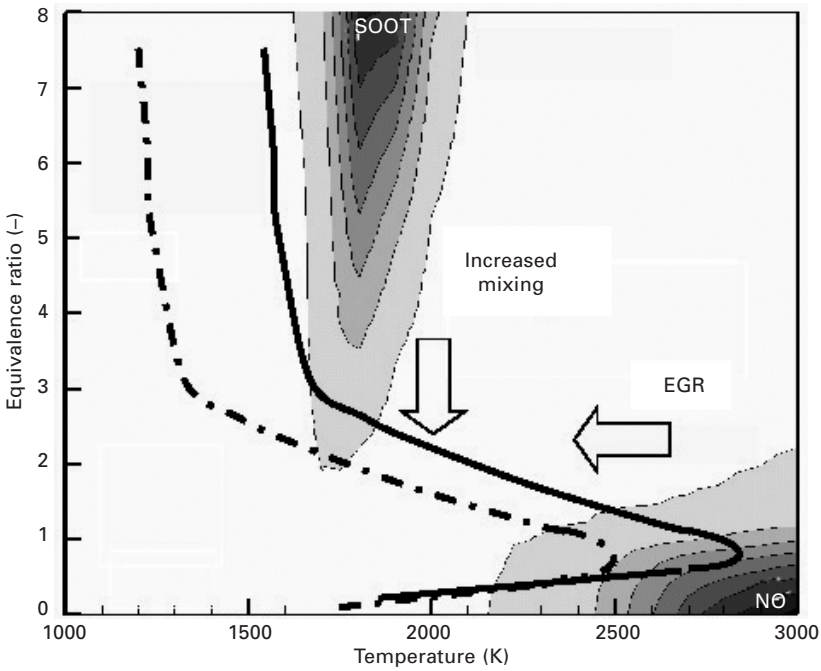
air and further oxidized. This oxidation takes place at high temperatures, which is why NO_x formation occurs at the periphery of the spray. Diesel combustion can thus be regarded as a two-stage process, in terms of soot and NO_x formation, in which soot is formed at points with rich conditions at the centre of the jet and NO_x is formed later at the periphery of the jet at the same time that soot is oxidized. This is the reason for the phenomenon known as the 'diesel dilemma' (Fig. 6.4). When measures are taken that increase the combustion temperature (such as earlier injection) NO_x increases and PM decreases, while the opposite occurs if the combustion temperature is lowered (by retarding injection or adding EGR).

The emissions formation in a diesel engine can be visualized using a so-called equivalence ratio–temperature map (see Fig. 6.5). This type of map was first used by Kamimoto and Bae (1988). From Fig. 6.5 it can be seen that soot is formed in rich conditions, with equivalence ratios >2, and at intermediate temperatures. At high temperatures the polycyclic aromatic hydrocarbons (PAH, which are soot precursors) are oxidized instead of forming soot, while at low temperatures the temperature is too low to transform PAH into soot (Akihama *et al*. 2001). NO is formed at high temperatures in lean conditions due to the high activation energy of the $O + N_2 \rightarrow NO + N$ reaction of the Zeldovich mechanism (Zeldovich 1947) and its dependence on the O_2 concentration. Soot oxidation takes place at high temperatures and in lean conditions, so the soot oxidation zone to a large extent overlaps the NO formation area.

Figure 6.5 also shows lines indicating the adiabatic flame temperature (at constant volume); this is the highest temperature that can be obtained if all chemical energy is converted to thermal energy in an adiabatic system. The figure indicates that the local combustion temperature should be kept below approximately 2200 K to avoid high NO formation at low equivalence ratios. At high equivalence ratios (>2) it becomes necessary to further decrease



6.4 Schematic diagram of the 'diesel dilemma' or PM (soot)–NO_x trade-off.



6.5 Emissions map for soot and NO_x as a function of equivalence ratio and temperature.

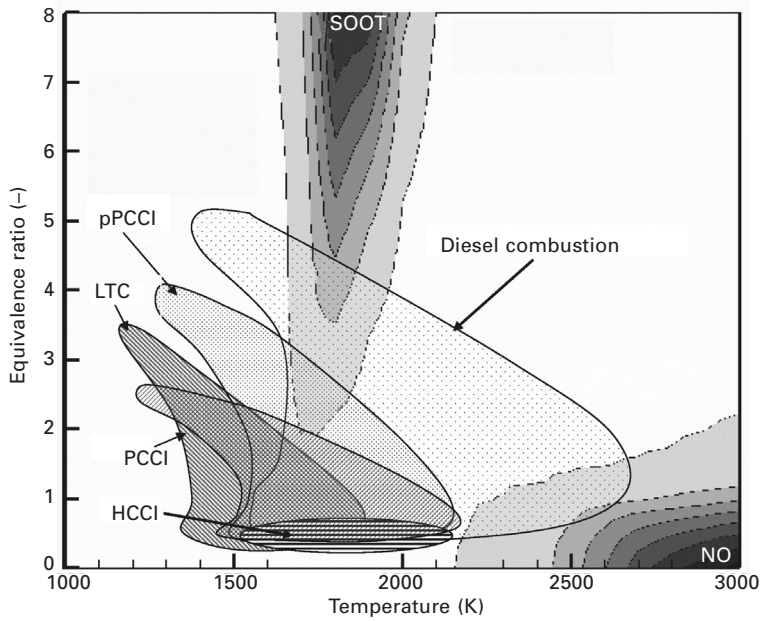
the maximum allowable temperature to completely avoid soot formation. If the local flame temperature is kept below approximately 1650 K, both the NO and soot formation areas are completely avoided, regardless of the equivalence ratio. Also, rapidly mixing fuel and air to local equivalence ratios >2 prevents soot formation. As indicated by Figure 6.5 there are essentially two kinds of measures for reducing soot and NO emissions:

- Measures that lower the local flame temperature such as EGR and reductions in the initial temperature or compression ratio
- Measures that increase the mixing velocity, such as raising the injection pressure, reducing the orifice size and increasing swirl.

In most cases a combination of increasing the mixing and reducing the temperature is used.

Several different combustion regimes can be defined depending on the local in-cylinder conditions during combustion (see Fig. 6.6).

- *Diesel combustion*. This is the 'classical' combustion mode, as illustrated in Figs 6.3 and Plate II. Ignition delay is relatively short, only a small proportion of the fuel is burned in premixed conditions and most of the



6.6 Illustrative equivalence ratio–temperature maps for 'classical' diesel combustion and several alternative modes (see text for details).

burning is controlled by diffusion (mixing). Small or limited amounts of EGR are used in order to reduce temperature and NO_x formation.

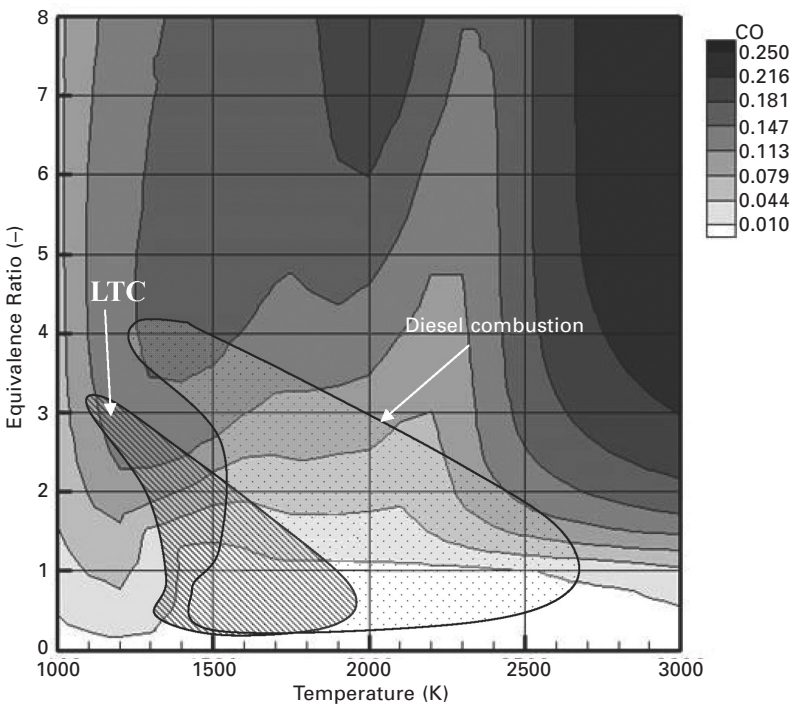
- *HCCI, homogeneous charge compression ignition*. In this mode there are very long ignition delays, often extended by using high rates of EGR and low compression ratios. All fuel is burned in premixed, almost homogeneous conditions. To ensure there is sufficient time for mixing, fuel is injected early during the compression stroke. It is not possible to operate in HCCI mode at high engine loads with conventional diesel fuel.
- *PCCI, premixed charge compression ignition*. In PCCI, large amounts of EGR are used to increase the ignition delay in combination with measures to increase mixing, such as high injection pressure. Ignition delay must exceed injection duration.
- *LTC, low temperature combustion*. Very high levels of EGR are used in this mode to increase the ignition delay sufficiently for it to exceed the injection duration. All fuel is burned in premixed, low-temperature conditions. However, the mixture is not homogeneous. CO emissions and fuel consumption tend to be high due to the low combustion temperature, and LTC can not be used at high engine loads.
- *pPCCI, partially premixed charge compression ignition.* In pPCCI

large amounts of EGR are used to increase ignition delays and reduce NO formation. In addition, measures to increase mixing velocity are often applied, like high injection pressure. This combustion regime is characterized by long ignition delays, leading to a large proportion of the fuel being burned in premixed conditions. Injection schedules including several early pilot injections followed by a late main injection are also used in this regime. Also low cetane fuels can be used to promote this combustion regime.

Other factors must also be taken into consideration when selecting a combustion system. Figure 6.7 shows a map of CO emissions as functions of equivalence ratio and temperature. CO conversion occurs via the reaction:

$$CO + OH \rightarrow CO_2 + H$$

This reaction is slow and at low temperatures it can deviate substantially from equilibrium. From Fig. 6.7 it can be seen that CO emissions increase substantially at temperatures <1400 K. This is due to a rapid decrease in OH radical production at these temperatures.



6.7 CO emissions map as functions of equivalence ratio and temperature.

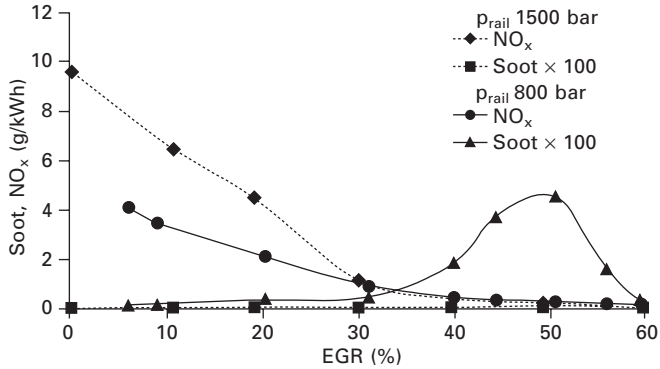
6.5 Combustion systems

6.5.1 Homogeneous charge compression ignition (HCCI)

HCCI refers to the combustion of a nearly homogeneous air/fuel mixture. To leave sufficient time for mixing, fuel has to be injected early during the compression stroke. In 1999 New Ace presented a premixed combustion process called PREDIC (Shimazaki *et al*. 1999), in which fuel is injected in a low-density, low-temperature environment, leading to long fuel penetration and the risk of cylinder wall impingement. One way of preventing liner wetting is to use an injector with a reduced umbrella angle, like the so-called NADI (narrow angle diesel injection) system developed by IFP (Walter and Gatellier 2002). The injector is combined with a shallow, 'W-shaped' piston bowl, EGR is used to control the ignition delay, and emissions of soot and NO_x are virtually zero. The major drawback of HCCI is that it can only be used at loads up to *ca* 50% (10 bar IMEP) when using normal diesel fuel. At higher loads normal diesel (diffusion-controlled) combustion has to be employed, since the small included injector angle causes wetting of the piston, leading to excessive soot formation. An alternative way of reducing spray penetration at low in-cylinder densities is to use a conventional nozzle and multiple injections (Helmantel *et al*. 2005). A difficulty associated with HCCI combustion is that it is very difficult to control the ignition timing during transients, since the ignition delay is very long and EGR cannot easily be adjusted from cycle to cycle. An alternative is to use a combination of EGR and variable valve timing (Helmantel and Denbratt 2006). Since it is difficult to position the combustion perfectly, the fuel consumption is also slightly higher in HCCI mode than in traditional diesel combustion.

6.5.2 Premixed charge compression ignition (PCCI) and low temperature combustion (LTC)

If EGR is gradually increased from zero to a high level in an operating engine, the NO_x and soot responses are generally as illustrated in Fig. 6.8, which shows emissions obtained from a single-cylinder engine in tests with injection pressures of 800 and 1500 bar. With an injection pressure of 800 bar it can be seen that NO_x emissions decrease with increasing EGR and approach zero for EGR values higher than about 50%, at which the maximum combustion temperature has shifted away from the NO formation area shown in Fig. 6.5. In contrast, soot levels are extremely low at zero or low EGR rates, since temperatures are high enough to oxidize most of the soot formed. As EGR rates increase the temperature decreases, and despite associated reductions in soot formation, engine-out soot emissions increase

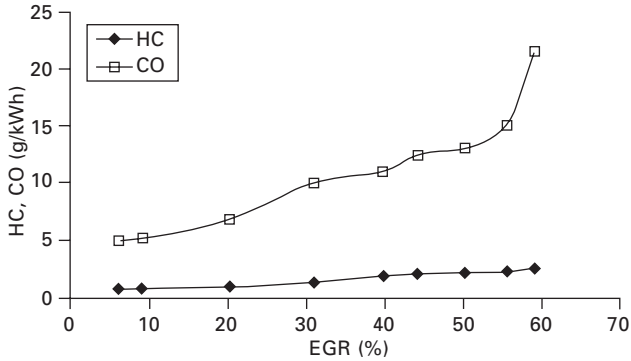


6.8 Soot and NO_x emissions from a single-cylinder engine in tests with injection pressures of 800 and 1500 bar at IMEP = 5 bar and 2000 rpm (note that soot is magnified by a factor of 100). A pilot and a main injection were used and injection timing was adjusted so CA50 remained constant at 7° ATDC. The compression ratio used was 16.

since the soot oxidation rates decline even more sharply. At about 50% EGR engine-out soot emissions are maximal in these operating conditions, and if EGR levels are further increased soot emissions rapidly fall and finally approach zero at 60% EGR. At this operational point the local in-cylinder conditions do not cross the soot formation peninsula shown in Fig. 6.5 and the engine is operating in low temperature combustion (LTC) mode and almost stoichiometric conditions. Low temperature combustion was first presented by Toyota in 2000 (Sasaki *et al*. 2000). Nissan had previously developed the Mk-concept (modulated kinetics) approach, which has some similarities, where late injection, EGR and swirl are used to extend the ignition delay and promote mixing (Kimura *et al*. 1999).

At the higher injection pressure of 1500 bar there are two important differences: the mixing velocity is increased and the injection duration is reduced. The mixing is improved so locally rich areas with equivalence ratios >2 are avoided, thus soot is no longer formed but there are still substantial variations in the charge. An effective way to improve mixing is to use smaller orifices (Bergstrand and Denbratt 2001; Minato *et al*. 2005). As can be seen in Fig. 6.8, the increased injection rate leads to higher NO_x emissions at low EGR due to more rapid combustion. A problem with low temperature combustion is the increase in emissions of unburned hydrocarbons and especially carbon monoxide (see Fig. 6.9), due to the reduced reaction rates.

Low temperature combustion leads to higher fuel consumption due to the lower combustion efficiency, and it is difficult to achieve satisfactory combustion stability at light load, although this can be improved by using



6.9 Indicated specific carbon monoxide and hydrocarbon (ISCO and ISHC) emissions observed at various EGR rates from a single-cylinder engine. Operating conditions: 2000 rpm, 5 bar IMEP.

hot EGR, via bypassing the EGR cooler (Neely *et al*. 2005). In addition, both low temperature combustion and premixed charge compression ignition are limited to the low/medium load ranges. At higher loads the injection duration increases and the ignition delay can no longer be extended sufficiently without substantially reducing the compression ratio. One way of extending the premixed operation to higher loads is to use late intake valve closing (LIVC) and thus reduce the effective compression ratio. A further feature of low temperature combustion that is worth noting is that it can be effectively used for regenerating a lean NO_x trap (LNT).

6.5.3 Partially premixed charge compression ignition (pPCCI)

This combustion mode, sometimes called premixed controlled compression ignition or partial HCCI (pHCCI), can be regarded as an intermediate between PCCI and conventional diesel combustion. If the ignition delay is long, leading to a large proportion of the fuel being combusted in premixed conditions, exhaust emissions and fuel consumption parameters are close to those of PCCI combustion, but if the ignition delay is short the combustion behaviour is more similar to that of a diffusion-controlled combustion process. There are several ways of creating a pPCCI engine. In 1997 the Japanese Traffic Safety and Nuisance Research Institute presented a homogeneous charge compression strategy called HCDC (homogeneous charge diesel combustion) (Suzuki *et al*. 1997) in which most of the fuel was supplied in the intake manifold, so-called fumigation, while a small proportion was directly injected and used for ignition control. In addition, Toyota presented a new combustion system with split injections called Unibus in 1996 (Yanagihara *et al*. 1996; Hasegawa and Yanagihara 2003); New Ace presented a two-

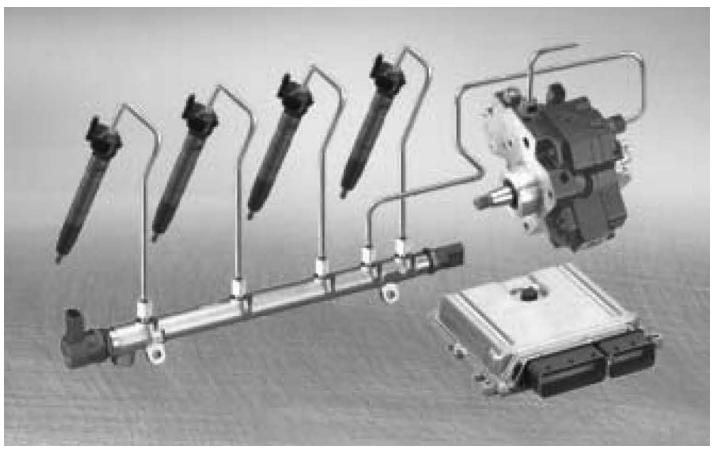
stage combustion system with early and late injections, the Muldic system in 1998 (Hashizume *et al*. 1998), and in studies described by Husberg *et al*. (2008) multiple pilot injections were used together with a main injection. A general problem with premixed combustion modes at higher loads is the noise caused by the rapid pressure rises.

To summarize, the fully homogeneous combustion process is difficult to control, especially during transients, and can only be used at low or moderate engine loads. Thus, it is not regarded as the best candidate for meeting the challenges facing diesel engines. The premixed charge compression ignition and partially premixed charge compression ignition concepts show much greater potential for meeting these challenges at higher loads, and stoichiometric low temperature combustion is a viable candidate for regenerating NO_x traps.

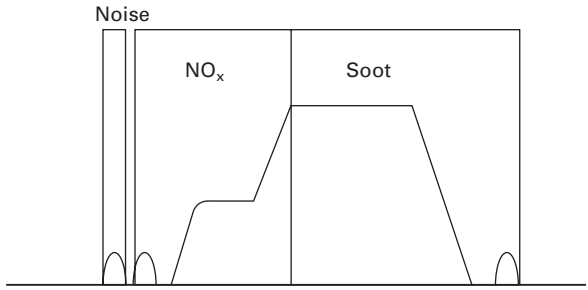
6.6 Fuel injection

Developments in fuel injection equipment are playing leading roles in attempts to develop future diesel combustion systems that will help meet emissions standards. For passenger cars the common rail system dominates (Fig. 6.10).

Figure 6.11 shows a schematic diagram of the injection rates, as a function of crank angle, generated by an advanced diesel injection system with capacities for performing multiple injections and rate shaping. The variations in the injection rate are achieved by varying the injection pressure. Ideally, the injection rate should be relatively low during early parts of the injection to ensure that NO_x emissions are low, while later during combustion the rate should be as high as possible to improve mixing and thus reduce soot formation. However, the ideal injection rate profile is speed- and



6.10 Common rail system (courtesy of Robert Bosch).



6.11 Schematic diagram showing an injection rate versus crank angle profile provided by an advanced injection system. The main injection has a so-called 'boot' shape.

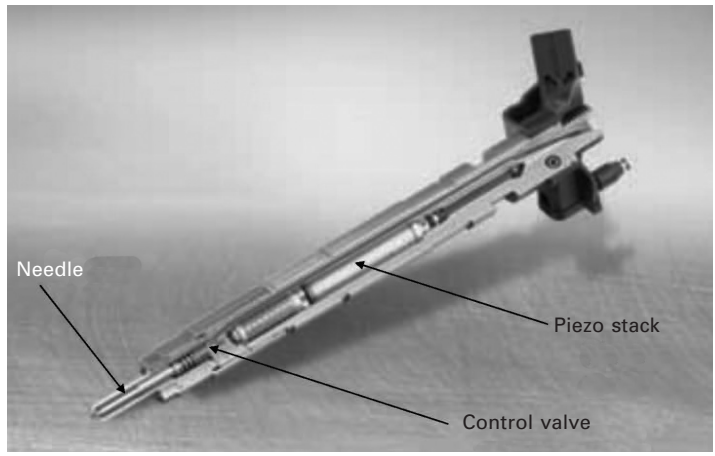
load-dependent. A shape such as the one shown in Fig. 6.11 is preferred in conditions with low or zero EGR rates and high loads. At higher EGR rates NO_x emissions are already low, and thus from an emissions perspective it is better to use a rate shape in the form of a square. A small pilot injection is usually used to reduce the amount of premixed fuel and thus the noise generated during the premixed combustion phase, and a post-injection, from 10 to 20°CA after EOI, is sometimes used to improve mixing and increase the oxidation temperature in order to improve soot oxidation.

To allow the injection rate to be varied in practice, variable nozzles can be used. In a variable nozzle injector a sleeve and the needle control the injections from either the lower row of orifices or both rows. However, there are also other designs that allow the operation of either the upper or the lower row, or both rows, of orifices. These types of nozzles are often called fourth generation nozzles.

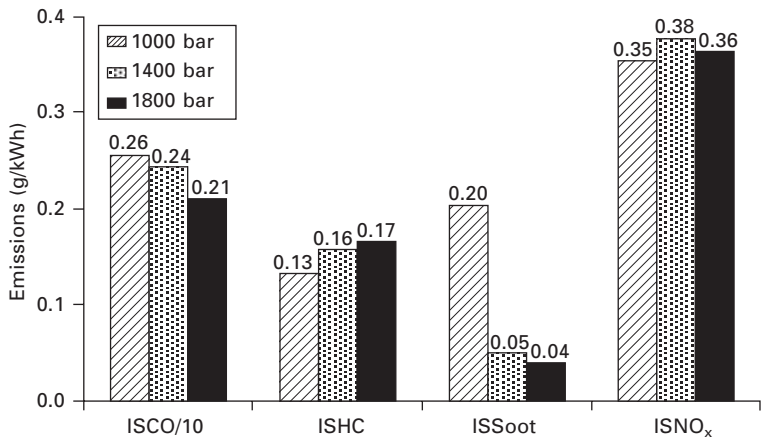
Important features of injectors for low emissions include the capacities to provide flexible and high injection pressures (and thus high and variable injection rates), to allow rapid needle opening and closing, and to inject small quantities of fuel (for pilot and post-injections).

The needs for rapid opening and closing of the nozzle and the ability to inject small quantities of fuel have led to the development of piezo-controlled injectors, in which a piezo stack controls the opening and closing of the control valve instead of a solenoid. The needle can be opened and closed approximately twice as rapidly in a piezo injector than in a solenoid controlled injector, leading to reductions in emissions, noise and fuel consumption (see Fig. 6.12).

Injection pressure has a major impact on emissions formation as illustrated in Fig. 6.13, which shows emissions obtained in tests using a single-cylinder engine, a piezo injector and three different rail pressures: 1000, 1400 and 1800 bar. The strong influence of injection pressure on soot emissions can be clearly seen in the figure.



6.12 Piezo-controlled injector (third generation) (courtesy of Robert Bosch).



6.13 ISCO, ISHC, $ISNO_x$ and ISSoot emissions obtained in tests using a single-cylinder engine, a piezo injector and three different rail pressures: 1000, 1400 and 1800 bar. Note that the ISCO values are divided by 10, for display reasons. Operating conditions: 2000 rpm, 10 bar IMEP, p_{in} 120 kPa, EGR 50% (reprinted with permission from SAE paper 2008-04-14, © 2008 SAE International).

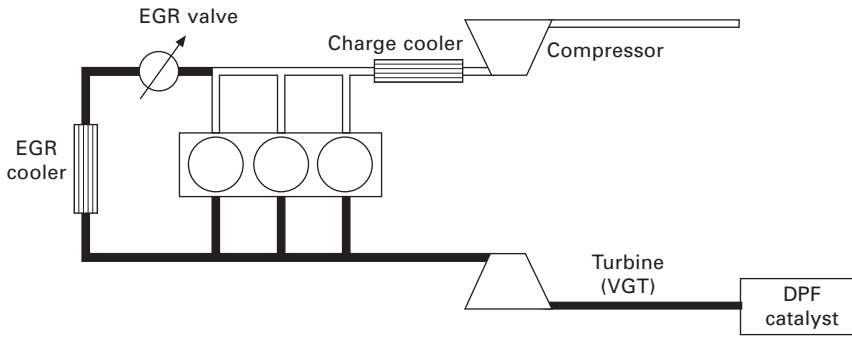
The maximum injection pressure used today is about 1800 bar, but this is expected to increase to a new maximum of *ca* 2500 bar in the future. It should be noted that a drawback of increasing the injection pressure is that parasitic losses increase, leading to higher fuel consumption, although this is partly offset by the shorter combustion duration.

An example of injectors that can provide high and variable injection pressures, thus allowing the injection pressures of pilot and post injections to be substantially lower than those of the main injections, are hydraulically amplified diesel injectors.

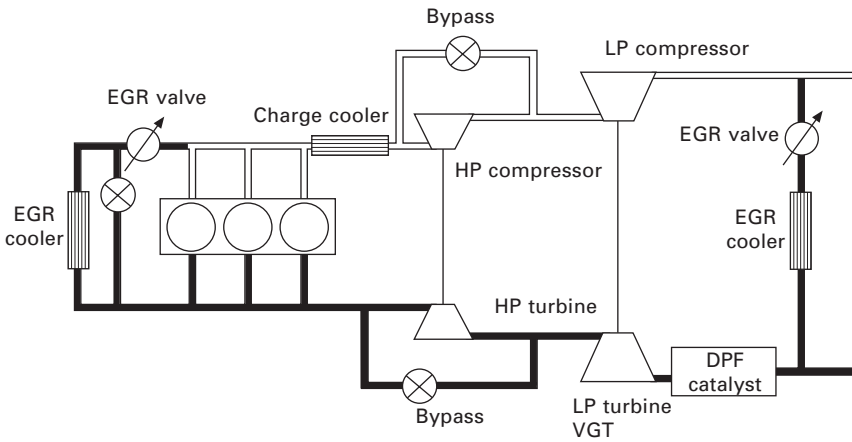
6.7 Charge induction

An inducted charge is composed of fresh air and recirculated exhaust gas (EGR). The requirements for the charging system are that it should be able to deliver high charging pressures at low engine speeds, have fast transient responses, and provide sufficient boost pressure at rated speed to allow high engine power. The high power requirement can be met by using a large compressor/turbine. However, a challenge for turbocharging internal combustion engines is matching the turbocharger to the engine over its speed and load range. For a diesel engine the air requirement is directly proportional to the actual engine power, but the turbocharger air delivery depends exponentially on engine power. For most engines this problem is solved by using a so-called waste gate, i.e. bypassing some of the exhaust at high speed and load to allow a smaller turbine wheel to be used in order to deliver high charging pressures at low engine speeds as well as high speeds. However, bypassing part of the exhaust at high engine speeds/loads inevitably means a loss of efficiency. Therefore, to improve the charging system a variable geometry turbine is often used for today's light-duty diesel engines. In low energy exhaust conditions, the variable vanes reduce the flow area of the nozzle and thus increase the kinetic energy of the exhaust gases, which increases the efficiency of the turbine. In high flow conditions the nozzle area is increased. However, a VGT turbocharger has no significant potential to increase the steady-state charging pressure level, since this is limited by the compressor map.

To reduce NO_x formation EGR is often used. A schematic diagram of a typical charging and EGR system for a contemporary production vehicle is shown in Fig. 6.14. However, future diesel engines will have to meet increasing demands for reductions in exhaust emissions and fuel consumption. To reduce exhaust emissions large amounts of EGR are needed, and to reduce fuel consumption engine downsizing is a powerful tool. However, downsizing must allow engines to operate at much higher specific loads than conventionally sized engines, especially those intended to meet US06 supplementary driving cycle rather than NEDC (New European Driving Cycle) requirements. To ensure emissions are sufficiently low, large amounts of EGR will also have to be used to control NO_x formation and ignition delays (to allow premixed or partially premixed combustion) at higher than currently possible loads. The charge temperature must also be low to ensure NO_x and soot emissions are low. These adjustments will increase the demands for high



6.14 Schematic diagram of a conventional charging system with a variable geometry turbine and short-route EGR (high-pressure EGR).



6.15 Schematic diagram of a two-stage turbocharging system with long-route (low-pressure) and short-route (high-pressure) EGR.

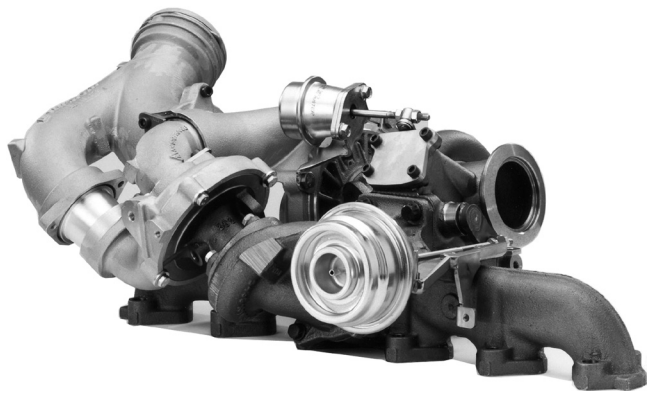
charging pressure, and for further enhancement of the transient behaviour of the charging system. A conventional charging system, as depicted in Fig. 6.14, cannot be used since it will not allow high amounts of EGR to be used during transient changes, and the maximum load with 60% EGR will probably not be much more than 4–5 bar IMEP, only half of what is needed for the US06 cycle. To significantly increase the charging pressure a two-stage charging system could be used (Fig. 6.15), the main advantage of which is that two differently sized compressors can be connected in series so that two optimized maps can be used, one for high flow and one for low flow conditions, thereby greatly expanding the usable compressor map and allowing higher charging pressures.

At the low exhaust flows associated with low engine speeds the exhaust bypass is closed and the whole flow passes through the high pressure turbine.

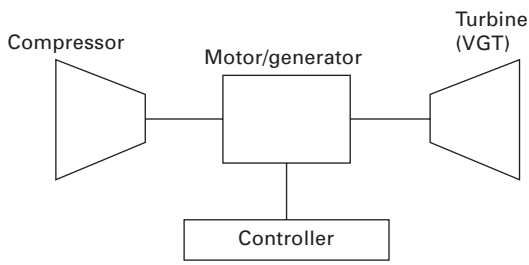
When the exhaust flow increases at higher engine speeds the bypass starts to open and increasingly large proportions of the exhaust gasses are expanded solely in the low pressure turbine. A two-stage turbo charging system, produced by BorgWarner, can be found in the BMW 535d (Fig. 6.16).

The more a diesel engine is downsized, the more the differences between its steady state and transient mean effective pressures grow. In order to both increase the low-end torque and improve the transient characteristics of the engine when insufficient energy is available in the exhaust, a combination of a turbocharger and a high speed motor/generator can be used. Figure 6.17 shows a schematic arrangement of an electrically assisted turbocharger. An advantage of this arrangement is that the turbocharger generates electricity when the exhaust energy exceeds the energy needed for driving the compressor (heat recovery). Other arrangements are also possible.

In Fig. 6.15 two EGR systems are schematically shown: a so-called long route, and a short route system. To maintain sufficiently high EGR flows at low engine speeds, when the backpressure from the silencer is low, long-route EGR also often requires an exhaust throttle. Long-route EGR offers better



6.16 Regulated two-stage turbocharging (R2S) system for the BMW 535d (courtesy of BorgWarner).



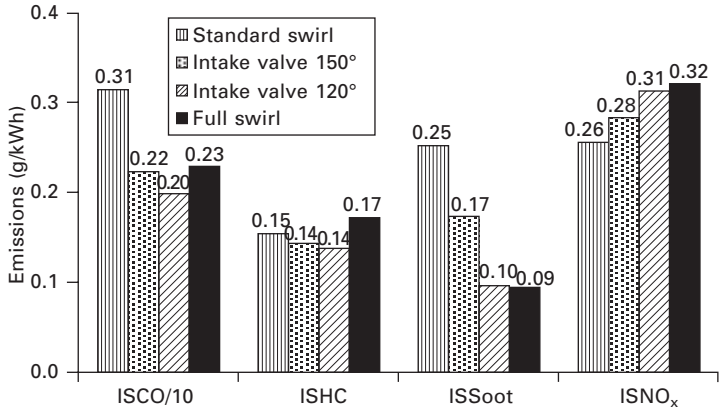
6.17 Schematic diagram of an electrically assisted turbocharger.

mixing with the fresh air and better EGR distribution between cylinders than short-route EGR. At low engine loads short-route EGR is often used, and at very light loads the EGR cooler is also sometimes bypassed to increase the intake temperature and reduce cyclic variations, especially when using low temperature combustion. At medium and high load conditions low pressure EGR is mainly used but the control strategy depends on the specific system architecture. The EGR route that provides the lowest backpressure at a given EGR level should be chosen.

Swirl (rotational motion around the cylinder axis) is often used in small-bore diesel engines to enhance the mixing between fuel and air. The kinetic energy stored in this large-scale motion is used to generate turbulence, which can be further enhanced by the shape of the combustion chamber (bowl). The swirling motion is established during the induction process by the shape of the intake ports. The need for swirl is highest at low engine speeds and decreases at higher speeds. In four-valve combustion systems a combination is often used of a helical (swirling) port and a neutral port (which can be deactivated to strengthen the swirl at low engine speeds, thereby providing variable swirl). The deactivation is often accomplished with a throttle, but valve deactivation can also be used. Swirl leads to reductions in soot formation, but also to lower volumetric efficiency and increased heat transfer, so excessive swirl should be avoided. The influence of swirl on engine-out emissions from a single-cylinder HSDI engine with 0.5 litre swept volume can be seen in Fig. 6.18. For this experiment the duration of the intake valve opening period of the neutral port was reduced by using a fully flexible valve train (full swirl means closed valve).

6.7.1 Variable valve timing

Historically the compression ratio of diesel engines has been largely determined by the cold start ability of the engine. However, the possibility to use variable valve timings allows a high compression ratio to be used during cold starts and low effective compression ratios in normal operation conditions through the use of late or early intake valve closing (LIVC or EIVC) strategies. Reducing the compression ratio leads to lower temperatures and consequently lower NO_x emissions and longer ignition delays, which also increases the scope to operate in PCCI mode. If the timing of the intake valve closure is used to lower the effective compression ratio, the expansion ratio remains the same and thus the fuel conversion efficiency remains unchanged. A supercharged engine cycle in which late intake valve closing is used is often called a Miller cycle (Miller 1947). Various types of systems can be used to control the closure of the inlet valve, including phase shifting mechanisms, cam profile switching with two different but fixed cam profiles, variable event timing with flexible duration (lost motion) systems,



6.18 ISCO, ISHC, $ISNO_x$ and ISSoot emissions obtained from a single-cylinder HSDI engine with 0.5 litre swept volume using four different swirl strategies. Note that the ISCO values are divided by 10, for display reasons. Operating conditions: 2000 rpm, 10 bar IMEP, p_{in} 100 kPa, p_{fuel} 1400 bar, EGR 50% (reprinted with permission from SAE paper 2008-04-14, © 2008 SAE International).

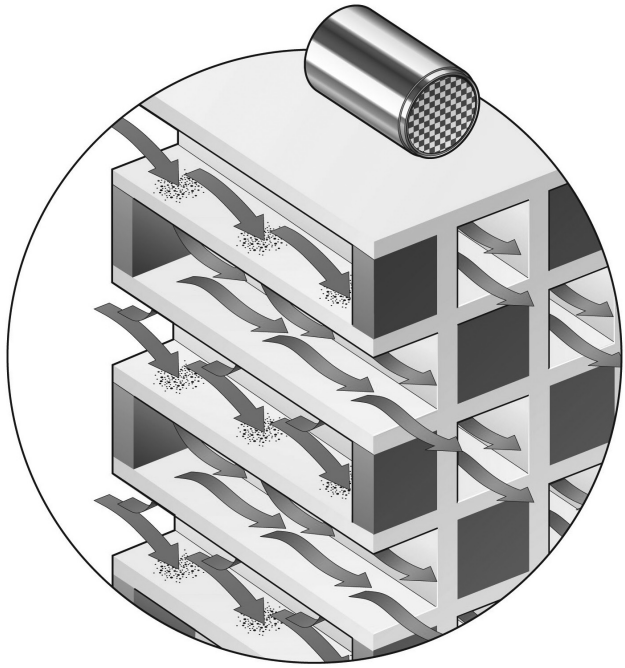
and fully flexible systems with flexible timing and duration (electro-magnetic and hydraulic valve systems).

6.8 Combustion chamber shape

The current trends are towards more open chambers, greater numbers of nozzle orifices and reduced compression ratios. The bowl shape will probably still be of the re-entrant type, partly because of the possibility it provides to maintain and enhance the swirl flow, and partly because of its desirable interaction with the squish motion.

6.9 Exhaust gas after-treatment

Anticipated exhaust emissions standards clearly cannot be met solely by applying advanced combustion modes and injection strategies to reduce engine-out emissions. In addition, improved after-treatment systems will be required. Many engines in production today already use diesel oxidation catalysts (DOC) for the oxidation of unburned hydrocarbons and carbon monoxide, and a diesel particulate filter (DPF) for the removal of particulates (see Fig. 6.19). This figure illustrates the operational principles of a particulate filter, which consists of a ceramic structure with many channels, plugged at alternate ends in order to force the exhaust gas through the wall of the ceramic monolith and thus filter the gas. The ceramic structure has a highly



6.19 Sketch illustrating the operation of a wall-flow diesel particulate filter (courtesy of Johnson Matthey, © Johnson Matthey Plc 2007).

controlled porosity and the filter (trap) needs to be regenerated on a regular basis. This can be done either continuously using NO_2, after oxidizing NO to NO_2 with a catalyst upstream of the filter, or by heat management, i.e. increasing the temperature of the DPF (by throttling, injecting fuel, etc.). Thermal regeneration generally requires high temperatures (>500°C), although the regeneration temperature can be lowered by using an appropriate fuel additive (Salvat *et al*. 2000).

6.9.1 NO_x reduction

Since the diesel exhaust is lean, a three-way catalyst cannot be used to reduce NO_x emissions. However, they can be reduced either by selective catalytic reduction (SCR) or by using NO_x traps.

Selective catalytic reduction (SCR)

In an SCR system ammonia is used to reduce NO_x. Several reactions occur in such systems (Schnelle and Brown 2001); here just two of them are displayed:

$$4NO + 4NH_3 + O_2 \rightarrow 4N_2 + 6H_2O$$

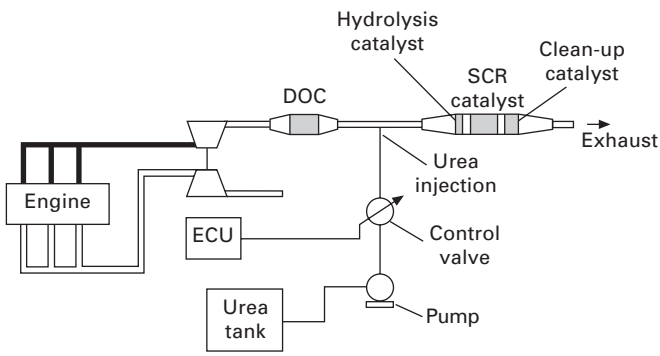
$$NO + NO_2 + 2NH_3 \rightarrow 2N_2 + 3H_2O$$

The first reaction is generally the most important, while the second is important for low temperature SCR.

Since use of ammonia solutions is associated with significant handling and toxicity problems, a safer and more convenient source of the compound is used in SCR systems, i.e. urea – $CO(NH_2)_2$ – which readily decomposes in the presence of water into ammonia and carbon dioxide in the SCR catalyst. Pure urea is a solid at room temperature and is commercially available as an aqueous 32.5% solution, at which the crystallization temperature is lowest. Nevertheless, even at this concentration the freezing point is not sufficiently low (–11°C) for heating of the urea tank to be avoided during the winter in cold climates. In Europe urea solutions are marketed under the name AdBlue. Due to the risk of the SCR catalyst fouling due to incomplete decomposition of urea at low temperatures, a separate catalyst for urea decomposition is often placed in front of the SCR catalyst, a so-called hydrolysis catalyst.

As a catalyst for SCR there are three possibilities: platinum (Pt), vanadium pentoxide (V_2O_5) with a titanium dioxide (TiO_2) carrier, or a zeolite-based catalyst. Platinum is not of practical use in vehicle applications since it loses its activity at temperatures above 250°C. V_2O_5/TiO_2 is most efficient at temperatures ranging from slightly higher than 300°C to 450°C (90%). For temperatures around 250°C the conversion efficiency is only about 50%, so the reduction of NO_x at light loads can be rather low. Alternative reducing agents that can be used in SCR catalysis are hydrocarbons (HC-SCR). To prevent ammonia slip a clean-up catalyst is needed after the SCR. A problem with SCR catalysts is the oxidation of SO_2 to SO_3 (from the sulphur in the fuel).

A typical SCR system can be seen in Fig. 6.20. If the system contains a diesel particulate filter it will be placed between the DOC and the SCR catalyst (before the urea injection point).



6.20 Schematic diagram of an SCR system.

In 2008 Mercedes introduced a urea-based system that will comply with Tier 2 bin 5 regulations even for heavier vehicles. The system is claimed to give 80% reductions in NO_x emissions.

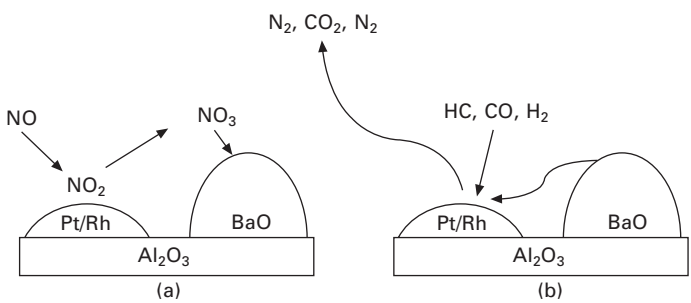
LNT – lean NO_x trap (NO_x storage)

In a lean NO_x trap, NO_x is stored during operation in lean conditions and released during rich operation (Epling *et al*. 2004). The process involves the following four steps (as illustrated in Fig. 6.21):

1. Oxidation of NO to NO_2
2. Formation of nitrates (NO_3) and storage as $Ba(NO_3)_2$
3. Nitrate decomposition and release (in rich conditions)
4. NO reduction to N_2.

By shifting between lean (storage) and stoichiometric (release) phases, NO_x can be stored and subsequently reduced. The release (regeneration) period is considerably shorter than the storage period. For a diesel engine there are three ways of obtaining a stoichiometric or rich mixture without excessively compromising other desirable features: injecting fuel in the exhaust manifold, post-injection (in combination with throttling), or by use of a combustion mode that allows stoichiometric combustion without excessive soot formation (low temperature combustion).

NO_x traps are sensitive to sulphur since sulphur is oxidized to sulphur trioxide (SO_3), which reacts with the trap's barium oxide (BaO) forming barium sulphate ($BaSO_4$) which deactivates the catalyst. However, the catalyst can be regenerated (desulphated) using high temperatures generated by post-injection in combination with a closely coupled catalyst (for heating) (Geckler *et al*. 2001), or (preferably) by using a sulphur trap before the catalyst. NO_x traps have a fairly wide operational temperature range, from slightly above 200°C to about 450°C with conversion efficiencies >50%, and maximum



6.21 Lean NO_x trap, during operation in (a) lean conditions and (b) rich or stoichiometric conditions.

efficiencies >90% for aged catalysts. A NO_x absorber system is similar to the SCR system depicted in Fig. 6.21 but the SCR part is changed to a LNT catalyst (and of course there is no urea system).

Combined and alternative systems

A system that combines a DPF and LNT was developed by Toyota (Nakatani *et al*. 2002). The catalyst consists of a porous monolithic ceramic structure plugged at alternate ends like a conventional DPF. The monolith is coated with platinum and a 'storage material' that can store nitrates like a conventional LNT. During lean operation NO_x is stored while particulates are being oxidized by the oxygen radicals formed when NO and O_2 react to form NO_2. During rich operation the nitrates are released and reduced to N_2 using HC, CO and H_2, this process also generates oxygen radicals, which oxidize the soot during rich operation. Toyota has further developed the system by adding a sulphur trap consisting of an oxidizing catalyst (Pt) and storing SO_x in alkali metals (Yoshida *et al*. 2007). The system was found to deliver a large improvement in NO_x conversion efficiency.

SWRI (Roecker *et al*. 2007) has investigated a system consisting of a lean NO_x trap (LNT) followed by a selective catalytic reduction catalyst (SCR, but without urea injection). The process exploits the substantial (unwanted) amounts of NH_3 that are produced in the LNT when NO_x is released from the trap during rich operation. In the cited system this ammonia is used in the SCR to reduce NO_x. The overall conversion efficiency was found to be higher than that achieved solely with the LNT. Honda (Morita *et al*. 2007) has also used NH_3 formed during rich periods, in a process in which the ammonia produced is stored in zeolite and then used during lean periods to reduce NO_x, as in an SCR catalyst. In addition, Honda has developed a cerium-based material for NO_x absorption that has better low temperature performance than the alkaline metal (barium) previously used. Further developments related to exhaust after-treatment will include the introduction of new materials, improved low-temperature performance and increased sulphur tolerance.

6.10 Heat recovery

Although diesel engines have the highest efficiency of all internal combustion engines, increasing fuel prices and CO_2 legislation due to come into force have necessitated further reductions in their fuel consumption. Most of the chemical energy supplied to internal combustion engines is lost as heat. Thus, one way to increase their efficiency is to recover some of the wasted heat. There are basically three ways in which this can be done:

- Thermoelectric power generation
- Turbo-compounding
- The Rankine cycle.

The last of these options, exploiting Rankine cycles using an organic working fluid, seems to have the highest potential for efficiency improvements.

Future diesel engines will be equipped with two-stage charging systems using high charge air pressures in combination with high EGR. However, a low intake temperature is essential to prevent NO_x formation and increase the ignition delay, so a considerable amount of heat must be discharged. Large amounts of heat can thus be recovered from the charge air- and EGR-cooler for use in a Rankine cycle. This will also be beneficial from a combustion perspective, since an air–liquid heat exchanger is more efficient than an air–air heat exchanger (conventional charge air cooler). The exhaust energy is often too low to be recovered, since it would generally have to be recovered downstream of the exhaust after-treatment devices, but at some stages (during the particulate regeneration period, for example) the temperature is high enough to recover some additional energy from it.

6.11 Engine control

To meet the increasingly stringent emissions legislation new technologies must be introduced, including novel combustion concepts, advanced charging and sophisticated exhaust after-treatment systems. However, emissions levels are becoming so low that production tolerances and ageing will have a significant influence on emissions, especially if the gap between the development targets and emissions standards must be decreased. Closed loop and model-based control systems, using some form of feedback signals from a combustion sensor, will therefore be essential for future engines. Several types of sensors have been suggested for such purposes, including direct and indirect cylinder pressure, ion-current, accelerometers and torque sensors. All of these sensors have pros and cons, but for the moment the direct sensing cylinder pressure sensor (Fussey *et al*. 2006) seems to be the most promising candidate.

6.12 Future fuels

Securing an independent fuel supply that is sustainable in the long term is a strategic goal for Europe. Current goals are for the amounts of such fuels used in the EU to account for 5.75% of total consumption by the end of 2010, and 20% by 2020 (European Parliament and Council 2003). Currently, the two most important biofuels are biodiesel (fatty acid methyl ester, FAME), produced by the transesterification of vegetable oils such as rapeseed or soybean oil, and ethanol, which is produced by the fermentation

of appropriate crops such as sugar beet, wheat, sugar cane, corn or potatoes followed by distillation. Significantly increasing the production of these so-called 'first-generation' biofuels will not be possible, and the amounts of greenhouse gases emitted in complete 'well-to-wheel' cycles of these fuels can be almost as high as those emitted in corresponding fossil fuel cycles, so the future of these first-generation fuels is doubtful.

In order to increase alternative fuel production, second-generation biofuels from biomass or fossil gas-to-liquid (GTL) fuels must be developed and commercialized. It will be very difficult or even impossible in the short to medium term to replace crude-oil based fuels solely by biofuels, so large proportions of the alternative fuels used will have to be GTL fuels. For CI engines, fuels like dimethyl ether (DME), Fischer–Tropsch diesel and diesel–alcohol blends will be viable candidates.

6.13 References and further reading

ACEA (2007). Trends in new car characteristics – diesel/petrol. European Automobile Manufactures' Association, Brussels.

Akihama K, Takatori Y, Inagaki K, Sasaki S and Dean A (2001). Mechanism of the smokeless rich diesel combustion by reducing temperature. SAE paper 2001-01-0655

Andersson J, Giechaskiel B, Muñoz-Bueno R, Sandbach E and Dilara P (2007). Particle Measurement Programme (PMP) Light-duty Inter-laboratory Correlation Exercise (ILCE_LD) Final Report, Institute for Environment and Sustainability.

Bergstrand P and Denbratt I (2001). Diesel combustion with reduced nozzle orifice diameter. SAE paper 2001-01-2010.

Dec JE (1997). A conceptual model of DI diesel combustion based on laser-sheet imaging. SAE paper 970873.

Dohle U, Duernholz M, Kampmann S, Hammer J and Hinrichsen C (2004). 4th generation diesel common rail injection system for future emission legislation. FISITA F2004V271.

Epling WS, Campbell LE, Yezerets A, Currier NW and Parks JE (2004). Overview of the fundamental reactions and degradation mechanisms of NO_x storage/reduction catalysts. *Catalysis Reviews* **46**(2): 163–245.

European Commission (2007). Regulation (EC) 715/2007 on Type approval of motor vehicles with respect to emissions from light passenger and commercial vehicles (Euro 5 & Euro 6) and on access to vehicle repair and maintenance information. *Official Journal of the European Union*.

European Parliament and Council (2003). On the promotion of the use of biofuels or other renewable fuels for transport. Directive 2003/30/EC.

European Parliament and Council (2007). MEPs back cuts in cars' CO_2 emissions. Publication 20071023IPR12110.

Federal Register (2000). Control of Air Pollution from Motor Vehicles: Tier 2 Motor Vehicle Emissions Standards and Gasoline Sulphur Control Requirements; Final Rule 65.

Flynn P, Durrett R, Hunter G, zur Loye A, Akinyemi O, Dec J and Westbrook C (1999). Diesel combustion: An integrated view combining laser diagnostics, chemical kinetics, and empirical validation. SAE paper 1999-01-0509.

Fussey P *et al*. (2006). Reducing diesel emissions dispersion by coordinated combustion feedback control. SAE paper 2006-01-0186.

Geckler S, Tomazic D, Sholtz V, Whalen M, McKinnon D, Gorse R, Baily O and Hoelzer J (2001). Development of a desulfurization strategy for a NO_x adsorber catalyst system. SAE paper 2001-01-0510.

Hasegawa R and Yanagihara H (2003). HCCI combustion in DI diesel engine. SAE paper 2003-01-0745.

Hashizume T, Miyamoto T, Akagawa H and Tsujimura K (1998). Combustion and emission characteristics of multiple stage diesel combustion. SAE paper 980505.

Helmantel A and Denbratt I (2006). HCCI operation of a passenger car DI diesel engine with an adjustable valve train. SAE paper 2006-01-0029.

Helmantel A, Gustavsson J and Denbratt I (2005). Operation of a DI diesel engine with variable effective compression ratio in HCCI and conventional diesel mode. SAE paper 2005-01-0177.

Husberg T, Denbratt I and Karlsson A (2008). Analysis of advanced multiple injection strategies in a heavy-duty diesel engine using optical measurements and CFD-simulations. SAE paper 2008-01-1328.

Kamimoto T and Bae M (1988). High combustion temperature for the reduction of particulate in diesel engines. SAE paper 880423.

Kimura S, Aoki O, Ogawa H, Muranaka S and Enomoto Y (1999). New combustion concept for ultra-clean high-efficiency DI. SAE paper 1990-01-3681.

Miller RH (1947). Supercharging and internal cooling cycle for high output. *Trans. ASME* 69.

Minato A, Tanaka T and Nishimura T (2005). Investigation of premixed lean diesel combustion with ultra high pressure injection. SAE paper 2005-01-0914.

Morita T, Suzuki M, Satoh N, Wada K and Ohno H (2007). Study on low NO_x emission control using newly developed lean NO_x catalyst for diesel engines. SAE paper 2007-01-0239.

Nakatani K, Hirota S, Takeshima S, Itoh K, Tanaka K and Dohmae K (2002). Simultaneous PM and NO_x reduction system for diesel engines. SAE paper 2002-01-0957.

Neely G, Sasaki S, Huang Y, Leet J and Stewart DW (2005). New diesel emission control strategy to meet US Tier 2 emissions regulations. SAE paper 2005-01-1091.

Power JD (2008). Annual Growth of Diesel Light Vehicle Demand. J.D. Power and Associates, Westlake Village, CA.

Roecker R, Zhan R and Stranglmaier R (2007). Feasibility investigation of a high efficiency NO_x aftertreatment system for diesel engines. SAE paper 2007-01-3983.

Salvat O, Marez P and Belot G (2000). Passenger car serial application of a particulate filter system on a common-rail, direct-injection diesel engine. SAE paper 2000-01-0473.

Sasaki S, Ito T and Igushi S (2000). Smokeless rich combustion by low temperature oxidation in diesel engines. 9th Aachen Colloquium.

Schnelle KB and Brown CA (eds) (2001). *Air Pollution Control Technology Handbook*. CRC Press, Boca Raton, FL.

Shimazaki N, Akagawa H, and Tsujimura K (1999). An experimental study of premixed lean diesel combustion process. SAE paper 1999-01-0181.

Suzuki H Koike N, Ishii H and Odaka M (1997). Exhaust purification of diesel engines by homogeneous charge with compression ignition. Part 1: Experimental investigation of combustion and exhaust emission behaviour. SAE paper 970313.

Walter B and Gatellier B (2002). Development of the high-power NADI^{TM} concept using dual-mode diesel combustion to achieve zero NO_x and particulate emissions. SAE paper 2002-01-1744.

Yanagihara H, Satou Y and Mizuta J (1996). Simultaneous reduction of NO_x and soot in diesel engines under a new combustion system. 17th Vienna Motor Symposium.

Yoshida K, Asanuma T, Nishioka H, Hayashi K and Hirota S (2007). Development of NO_x reduction system for diesel aftertreatment with sulphur trap catalyst. SAE paper 2007-01-0237.

Zeldovich YA (1947). *Oxidation of Nitrogen in Combustion*. Academy of Sciences of the USSR. Moscow–Leningrad, Institute of Chemical Physics.

7

Advanced control and engine management for future light-duty diesel engines

L GUZZELLA, Swiss Federal Institute of Technology (ETH), Switzerland

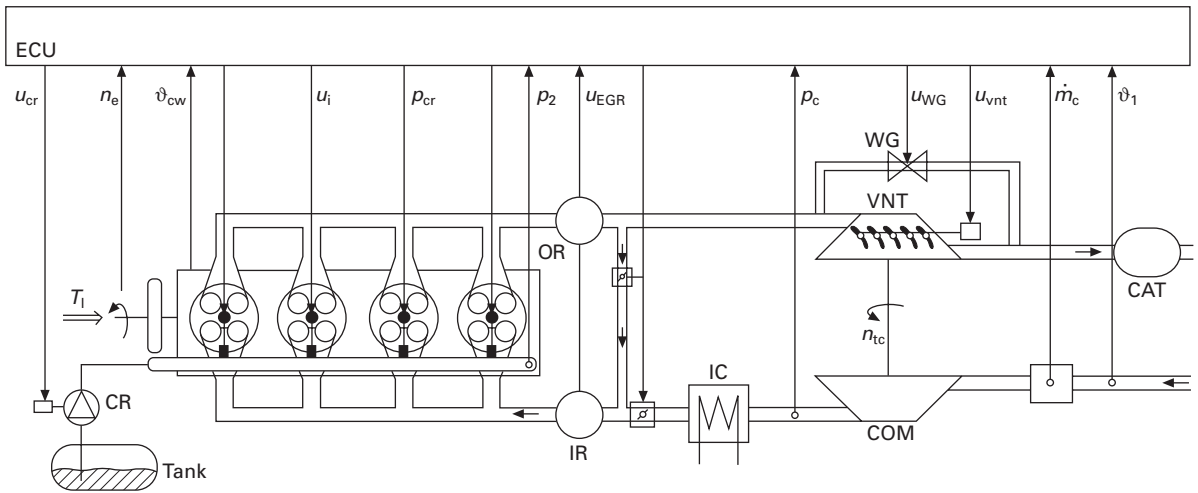
Abstract: This chapter provides an overview of current and future control systems for light-duty diesel engine systems. The role of the several ancillary components and the most important control loops present in modern diesel engines are discussed. Mathematical models of complex engine systems are proposed, which can be used to optimise future control systems which will include additional exhaust gas purification systems, new sensors and actuators.

Key words: diesel engine control systems, modelling and optimisation of diesel engine systems.

7.1 Main control objectives

A modern diesel engine is a complex system that includes many devices in order to guarantee its clean, fuel-efficient and safe operation. Figure 7.1 provides an overview of the most important components and signals present in a typical diesel engine system.

A complex system such as the one illustrated in Fig. 7.1 can only work properly if all of its components are operated in a well-coordinated way. For this purpose, modern diesel engine systems include several feedforward and feedback control loops which are implemented in one or more electronic control units (ECU) running the corresponding software. The two most important engine input variables controlled by such systems are the boost pressure p_2, which strongly determines the torque produced by the engine, and the exhaust gas recirculation (EGR) rate x_{EGR}, which strongly influences the pollutant emissions of the engine. These two loops are feedforward, i.e., only the engine input variables are set (the amount of fresh air and the amount of exhaust gas *entering* the engine), but not the actual target values, namely the NO_x and the particulate matter (PM) emissions. In addition to these two feedforward loops, all engines include a speed control loop, which at least controls the minimum and maximum speeds by varying the quantity



CAT	oxidation catalytic converter	u_{EGR}	EGR valve(s) command	p_c	pressure after COM
COM	compressor	u_{cr}	CR pump command	p_2	intake pressure
CR	common-rail system	u_i	injection command	p_{cr}	CR injection pressure
IR/OR	intake/outlet receiver	u_{vnt}	turbine nozzle command	$\dot{m}_c$	intake air mass-flow
IC	intercooler	u_{WG}	WG command	ϑ_l	intake air temperature
VNT	variable nozzle turbing	T_l	load torque at the flywheel	ϑ_{cw}	cooling water temperature
WG	waste-gate (alternative to VNT)	u_{tc}	turbocharger speed	n_e	engine speed

7.1 The most important diesel engine system components and signals.

of the fuel injected.[1] Figure 7.2 shows a block diagram that illustrates the interconnection structure of these three control loops.

Traditionally, diesel engines have been designed with a minimum number of electronic control systems because ruggedness and simple maintenance were placed very high on the list of priorities. However, stringent pollutant emission limits and fuel economy requirements, and higher comfort levels (noise and vibration), can only be reached with more complex engine systems and sophisticated electronic control loops. In addition, system monitoring and on-board diagnosis are challenges that must be addressed in the future, and these additional functions can only be realised using electronic devices and appropriate software.

Besides the enormous cost reductions of electronic systems (sensors, computers, power electronics, etc.) achieved in recent years, two engineering breakthroughs were responsible for the huge progress in diesel engines. The first was the advent of high performance turbocharger devices, which offer a new and very powerful degree of controllability (turbines with either variable guiding vanes or variable nozzle diameters). The second was the enormous step forward represented by electronically controllable high-pressure[2] common-rail injection systems. These systems have now replaced almost completely the standard mechanical injection systems and soon will be the dominant injection systems in all diesel engines.

The benefits offered by the new degrees of freedom can only be fully achieved by controlling the engine system such that it reaches its optimum performance in all operating conditions. Interestingly, feedback control loops, if well designed, can also contribute to the reduction of manufacturing costs. For instance, the specifications for the manufacturing tolerances of common-rail injectors can be relaxed if appropriate feedback loops are used to achieve the desired performance levels.

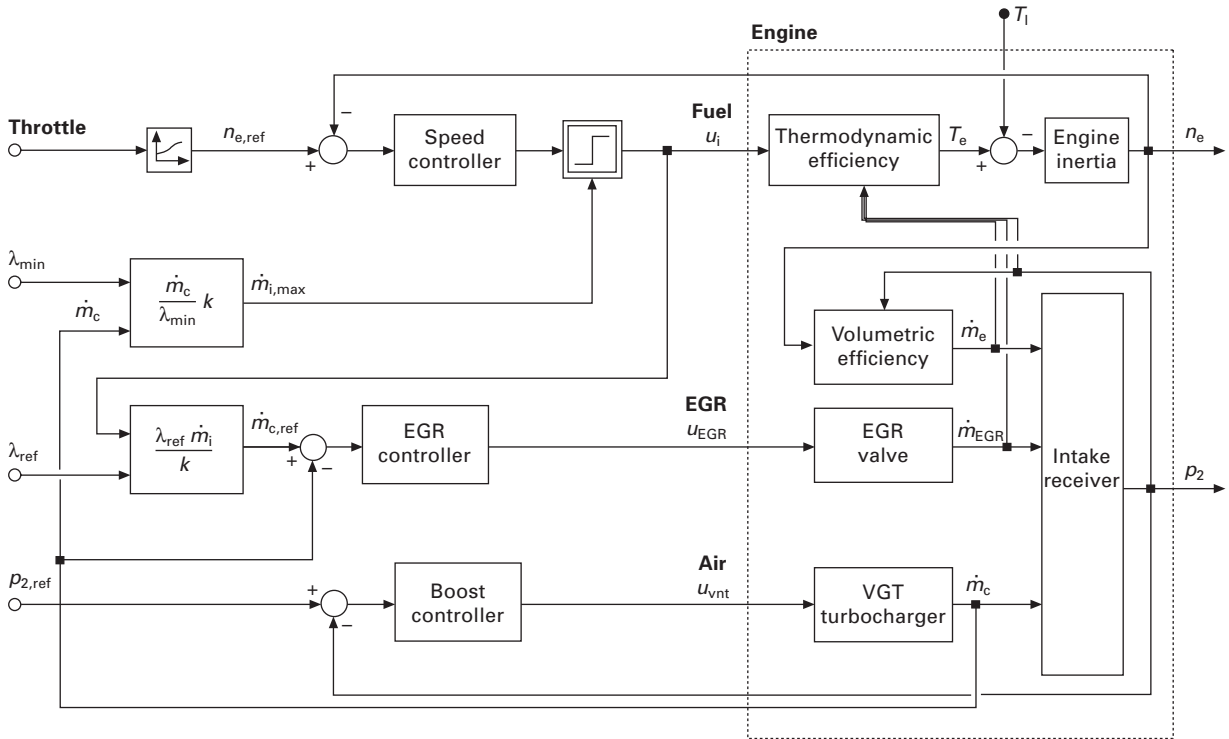
7.2 Standard control loops

This section provides an overview of the most important control loops present in standard diesel engines. More information on that topic can be found in Guzzella and Amstutz (1998) and Guzzella and Onder (2004). Trends for the future are discussed in Section 7.4.

The most important control system is the fuel-injection loop. It determines the amount of fuel injected into the engine, generally as a function of the

[1]To a large extent, the torque produced by the engine is almost proportional to the amount of fuel injected. The timing of the injection, the air/fuel ratio, and the EGR rate have an influence, but these variables affect the torque only weakly.

[2]Injection pressures of up to 2000 bar and more than six individual injections in one single engine cycle are feasible today.



7.2 Main control loops in diesel engines (simplified representation). Most variables are defined in Fig. 7.1, while λ is the air/fuel ratio ('ref' = reference and 'min' = minimum), k is the stoichiometric constant, and m represents mass flows (flowing through 'c' the compressor, 'egr' the EGR valve, and 'e' the engine).

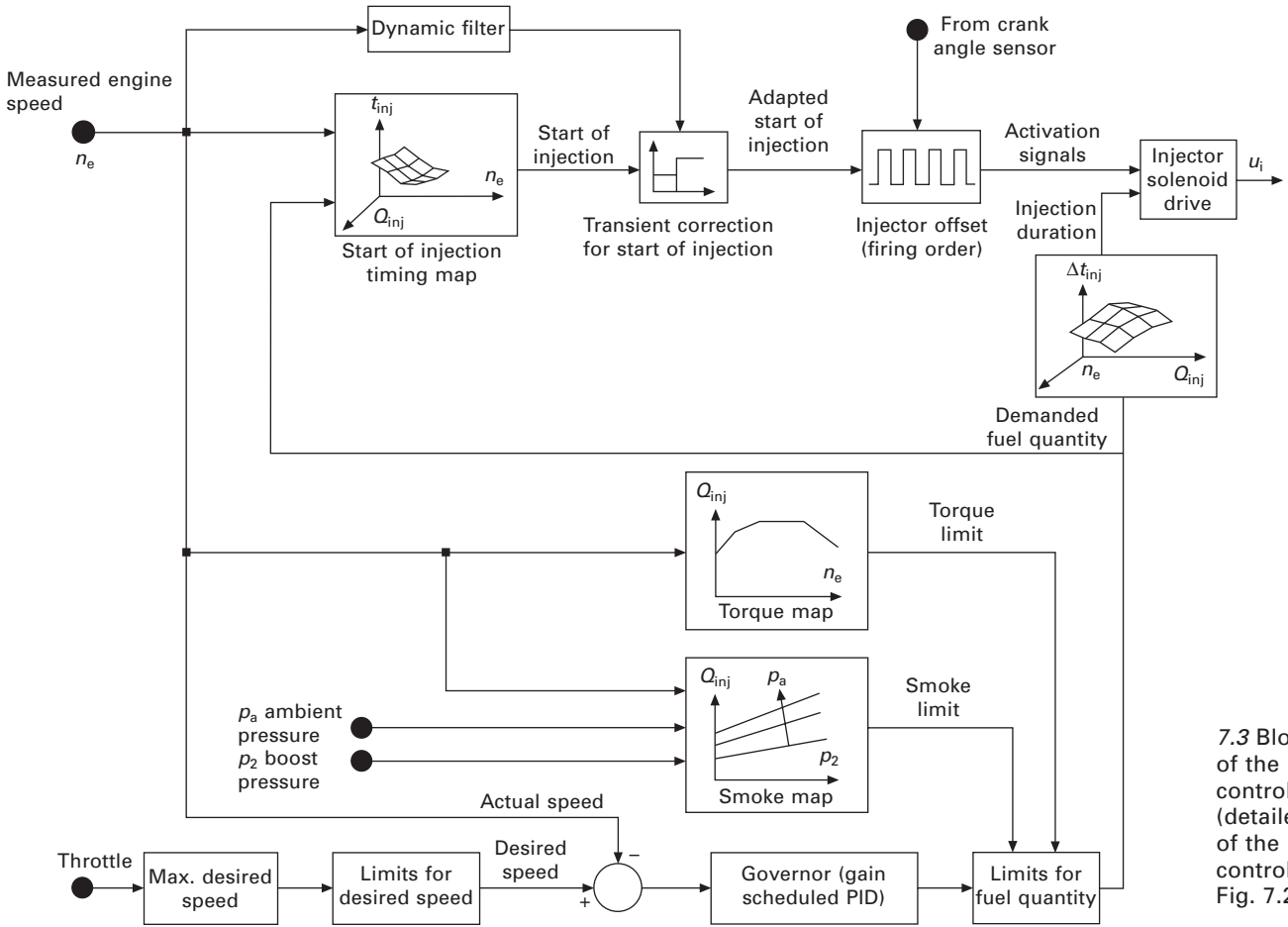
desired torque or speed. Figure 7.3 shows a detailed representation of the block diagram of such a control loop. Traditionally, the driver's input is referred to as 'throttle', although no throttling takes place in diesel engines. The engine speed sensor is a magnetic pick-up sensor mounted on the engine block which measures the field variations produced by a toothed rim of the engine flywheel. The actuator is the solenoid of the common-rail injector. Depending on the error between the commanded and the actual engine speed, a PI(D) controller determines the amount of fuel to be injected. Traditionally, this controller is referred to as the 'governor'. The amount of fuel injected is usually limited in order to prevent the generation of excess PM during transients ('smoke limit' block in Fig. 7.3) and to prevent excess torques that could damage the engine ('torque limit' block in Fig. 7.3).

The control signal u_i is further modified by additional fuel injection control systems not shown in Fig. 7.3. The most important modifications are the control of pilot injections (used, for instance, to reduce the noise and pollutant emission of the engine) and the control of post-injections (used, for instance, to regenerate the particulate filter; see Section 7.4 for more details on this point). Of course, the common-rail pressure control loop (also not shown in Fig. 7.3) has an influence as well. The injection pressure is an additional degree of freedom that is chosen such that pollutant emission, noise and fuel consumption are minimised according to specific trade-off choices. The set-point values of this variable are stored in appropriate speed–load maps, and the parameters of the feedback controller (usually a PI-type system) are scheduled using optimum settings, which are also stored in speed–load maps.

All modern diesel engines are turbocharged, otherwise their power density would be unacceptably low. In such engines, the actuator in the boost control loop is the turbine, which is equipped with either a variable nozzle or adjustable guiding vanes.[3] The pressure sensor of the boost control loop is usually mounted in the intake manifold and some care has to be taken to avoid spurious pressure ringing. In actual diesel engines the controller itself (represented by the 'boost controller' box in Fig. 7.2) is typically a gain-scheduled PI controller. Future systems will be more complex 'model-based' controllers (see the remarks made at the beginning of Section 7.4).

The EGR loop utilises an EGR valve as its main actuator. This valve determines the amount of (usually cooled) burnt gases that are recirculated to the intake manifold. In some systems an additional throttle valve is placed between the compressor and the intake manifold to allow for EGR in all relevant engine-operating points. The sensor of the EGR loop is an air mass flow sensor placed in the engine's intake (usually a hot film sensor, but simpler

[3]Older systems used controllable waste gates, but these systems have been superseded by variable nozzle or geometry systems because of the better driveability and fuel economy of the latter systems.



7.3 Block diagram of the speed control system (detailed view of the 'Speed controller' block in Fig. 7.2).

approaches are possible). Again, the controller (represented by the 'EGR controller' box in Fig. 7.2) is typically a gain-scheduled PI controller.

Several other control loops are usually present in modern diesel engines. Most of them are implemented to improve safety and comfort or to reduce pollutant emissions. Some of these loops will be discussed below.

7.3 System modelling

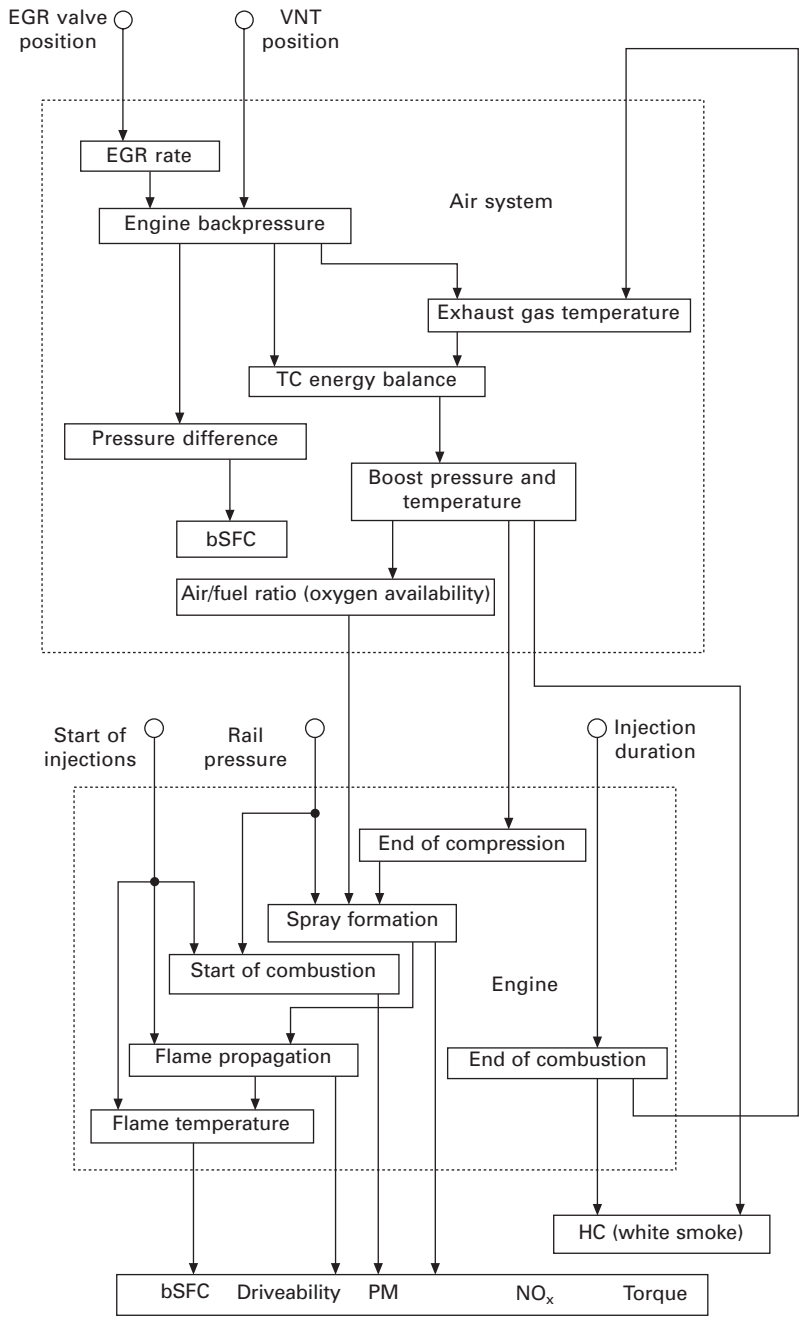
The design of diesel engine control systems is quite a difficult task. The available control inputs influence the engine behaviour in a multitude of ways (see Fig. 7.4). Important engine parameters, such as fuel consumption and pollutant emission, are determined even in steady-state conditions by many input parameters in a complex way that is not yet fully understood. Moreover, internal (physical) feedback loops, mainly caused by the turbocharger and the EGR systems, produce complex and unexpected dynamic effects. Last, but not least, engine wear and changing environmental conditions can substantially alter the engine behaviour. The control system designer must cope with all of these difficulties.

Traditionally, diesel engine controllers have been synthesised experimentally, i.e., the controller structure was chosen using qualitative arguments and previous experience, while the controller parameters were tuned experimentally on appropriate engine test benches (static or dynamic, depending on the control loop to be tuned). This calibration process is tedious, and it becomes even more cumbersome with the increasing number of control loops present in modern engine systems, such that alternatives to this approach have been investigated for many years.

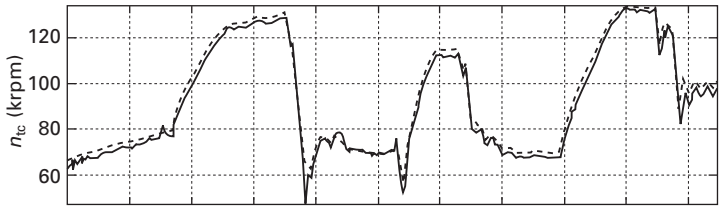
Automated calibration is one possibility for coping with this ever-increasing complexity. The human test bench operators are supported by appropriate software systems that help reducing the total calibration time (systematic optimisation and 'design of experiment' methods).

Another approach is first to produce mathematical models that predict some aspects of the engine behaviour and later to use these models to synthesise the control loops. Early attempts (Streit and Borman, 1971) focused on simple engine structures. Nowadays, rather detailed emulations of the engine dynamics are possible (Kao and Moskwa, 1995; Guzzella and Onder, 2004).

Of course, the modelling approach works well only if the model synthesis process is not too time-consuming and if the prediction power of the models is sufficient for the subsequent control system synthesis. Figure 7.5 shows an example of an engine variable (the turbocharger speed dynamics) that can be predicted well using mathematical models of modest complexity. A typical example of an engine-out variable that is much harder to predict with low-order ('control-oriented') models is the PM emissions.



7.4 Cause–effect relations for the most important subsystems in a diesel engine.



7.5 Experiment result (black) and simulation (grey) of the turbocharger speed in a transient test for a modern passenger car diesel engine (Ammann *et al.,* 2003).

The synthesis of a 'full engine model', i.e., a mathematical description of the input–output behaviour of the complete engine operating in arbitrary conditions, is quite demanding. Figure 7.6 illustrates the various blocks and their interconnections needed to fully model a modern diesel engine. Most variable names have been introduced in Figs 7.1 and 7.2; those not yet defined are listed in the caption of Fig. 7.6.

Each individual block represents a dynamic or a static subsystem. In Fig. 7.6, dynamic blocks have a black background, purely static blocks have no background, and blocks representing time delays have a grey background. All of the blocks shown in Fig. 7.6 are briefly described below. For more details readers are referred to the introductory text (Guzzella and Onder, 2004) and to the references to the original publications listed in that monograph.

7.3.1 Injection system

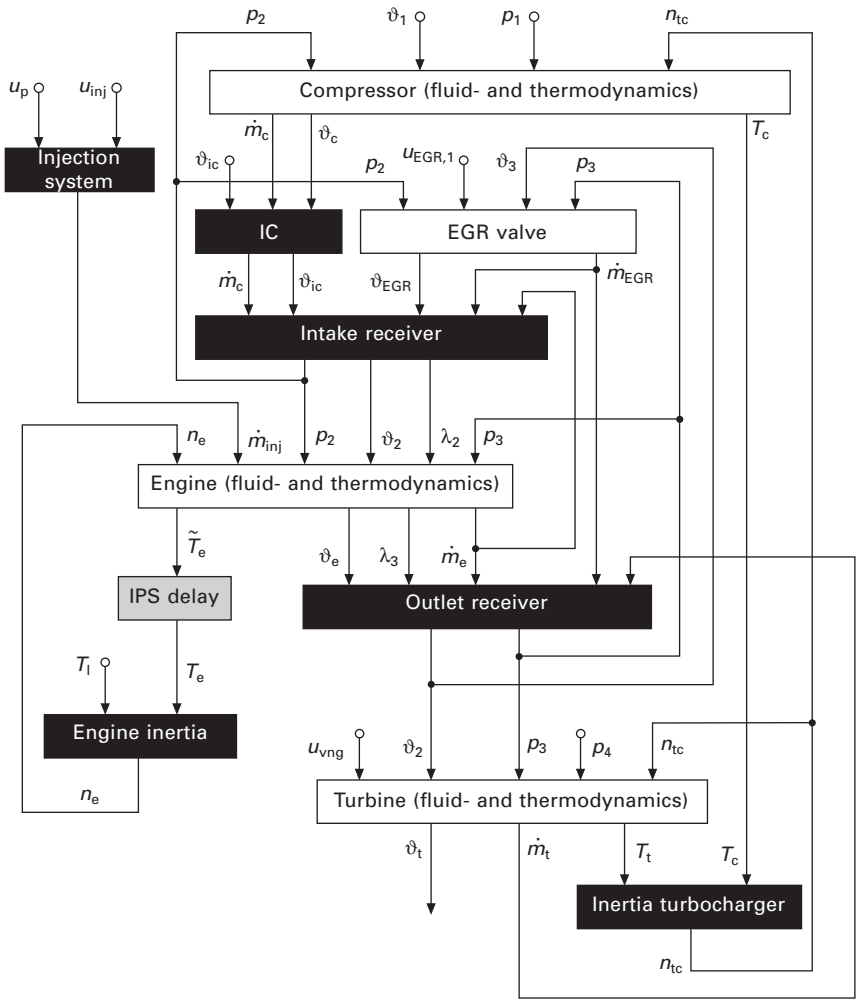
Very complex models are available to describe the injection system (Lino *et al.*, 2007). Such models take into consideration the compressibility of the fuel, the dynamics of the injector, and the spray-formation phenomena in the cylinder. Because of their complexity, such models are not applicable to full-engine control problems, where simpler approaches must be used. The simplest approach is to use a static map $m_{ij} = f(u_{ij}, p_i, \ldots)$ to describe the relationship between the input u_{ij} and the injected fuel quantity m_{ij}. The command signal u_p influences the rail pressure p_r, whose dynamics can be modelled by

$$\tau_\mathrm{r} \cdot \frac{\mathrm{d}}{\mathrm{d}t} p_\mathrm{r}(t) = - p_\mathrm{r}(t) + u_\mathrm{p}(t)$$

where τ_r is the time constant of the fuel rail dynamics.

7.3.2 EGR valve

The 'EGR-valve' block in Fig. 7.6 approximates the exhaust gas mass flow that is recirculated back into the intake manifold using the relation



7.6 Model structure: the shaded blocks represent subsystems that include some dynamic effects; the block 'IPS delay' models the 'induction-to-power stroke' delay (Guzzella and Onder, 2004); the plain boxes include static input/output functions.

$$\dot{m}_{EGR}(t) = \begin{cases} c_d u_{EGR,1}(t) \dfrac{p_3(t)}{\sqrt{R\vartheta_3(t)}} \dfrac{1}{\sqrt{2}} & \text{for } \dfrac{p_2(t)}{p_3(t)} < 0.5 \\ c_d u_{EGR,1}(t) \dfrac{p_3(t)}{\sqrt{R\vartheta_3(t)}} \sqrt{2\dfrac{p_2(t)}{p_3(t)}\left[1 - \left(\dfrac{p_2(t)}{p_3(t)}\right)\right]} & \text{for } \dfrac{p_2(t)}{p_3} \geq 0.5 \end{cases}$$

where the parameter c_d must be determined experimentally (it can depend on

the engine operating point). This approximation is 'static', i.e., the outputs of the 'EGR-valve' block are instantaneous functions of the inputs.

7.3.3 Intake and outlet receivers

In control-oriented engine models, only receivers are considered as storage systems for all of the gases flowing in and out of the engine. With such lumped-parameter reservoirs, pressure-wave phenomena, which are important to model the full-load torque and power of engines, cannot be represented correctly. Receivers can be modelled as adiabatic (thermally insulated) or isothermal (fast heat exchange with the environment and, thus, with constant temperature). Neither of these extreme cases is encountered in practice, but either can be useful to approximate a more complex situation where a limited heat exchange with the environment is present. Below, the more complex adiabatic case is discussed for the example of the intake receiver; formulating the equations for the outlet receiver or simplifying them to the isothermal case is straightforward.

Adiabatic receivers store mass and internal energy. While the balance equation for the mass of gas m_{ir} stored in this receiver is trivial:

$$\frac{\mathrm{d}}{\mathrm{d}t} m_{\mathrm{ir}}(t) = \dot{m}_{\mathrm{c}}(t) + \dot{m}_{\mathrm{EGR}}(t) - \dot{m}_{\mathrm{e}}(t)$$

the balance equation for the internal energy

$$\frac{\mathrm{d}}{\mathrm{d}t} U_{\mathrm{ir}}(t) = \dot{H}_{\mathrm{c}}(t) + \dot{H}_{\mathrm{EGR}}(t) - \dot{H}_{e}(t)$$

requires the additional information regarding the enthalpy flows. For perfect gases, these enthalpy flows can be formulated as indicated below:

$$\dot{H}_{\mathrm{c}} = \dot{m}_{\mathrm{c}} c_{\mathrm{p,air}} \vartheta_{\mathrm{ic}},\ \dot{H}_{\mathrm{EGR}} = \dot{m}_{\mathrm{EGR}} c_{\mathrm{p,egr}} \vartheta_{\mathrm{EGR}},\ \dot{H}_{\mathrm{e}} = \dot{m}_{\mathrm{e}} c_{\mathrm{p,ir}} \vartheta_{\mathrm{ir}}$$

Combining the last two equations with the caloric law

$$U_{\mathrm{ir}}(t) = m_{\mathrm{ir}}(t) \cdot c_{\mathrm{p,ir}} \vartheta_{\mathrm{ir}}(t)$$

and the ideal-gas law

$$p_{\mathrm{ir}}(t) \cdot V_{\mathrm{ir}} = m_{\mathrm{ir}}(t) \cdot R_{\mathrm{ir}} \vartheta_{\mathrm{ir}}(t)$$

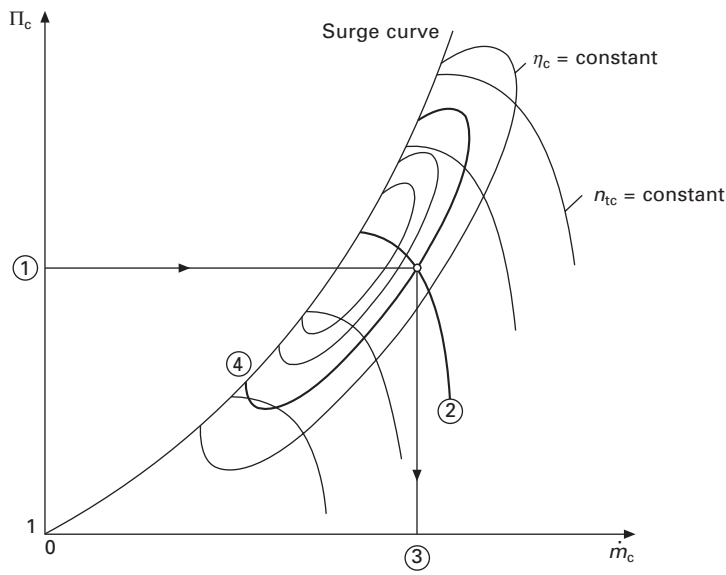
yields the necessary system equations. Since the gas constants of fresh air and exhaust gases are quite similar, the gas constant R_{ir} of the mixture in the intake receiver can be assumed to be independent of the composition of the gas in the intake receiver (approximately 280 J/kg K).

7.3.4 Compressor and turbine

Precise models of these devices require the use of sophisticated concepts of fluid dynamics, and advanced numerical software must be used to solve the resulting system equations. For control purposes this is not feasible and much simpler models must be used instead. The key idea is to describe compressors and turbines by appropriate 'maps' which permit the computation of the mass flows and the efficiencies. These variables depend in an algebraic ('memory-less') way on the input variables that are indicated in the causality diagram in Fig. 7.6.

For instance, compressors can be represented by a map similar to the one shown in Fig. 7.7 (such maps, measured in burner test benches, are usually provided by the turbocharger suppliers). The mass flow is obtained by first computing the pressure ratio $\Pi_c = p_2/p_1$ and second by intersecting that value with the curve that represents the actual rotational speed n_{tc}. The efficiency of the compressor can be found at the intersection point analysing the corresponding contour plot of constant efficiencies. Once the mass flow and the efficiency are known the remaining two output variables, compressor torque T_c and compressor outlet air temperature θ_2, can be computed easily as follows:

$$T_c = \frac{\dot{m}_c c_{p,air} \vartheta_1}{\eta_c \cdot 2\pi n_{tc}/60}\left[\Pi_c^{(\kappa-1)/\kappa} - 1\right]$$



7.7 Schematic representation of a compressor map. Interfaces as illustrated in Fig. 7.6.

$$\vartheta_2 = \vartheta_1 + \left[\Pi_c^{(\kappa-1)/\kappa} - 1\right]\frac{\vartheta_1}{\eta_c}$$

where $c_{p,air}$ is the specific heat of air at constant pressure, ϑ_1 is the inlet air temperature, and κ is the ratio $c_{p,air}/c_{v,air} \approx 1.4$ of the specific heats of air. *Mutatis mutandis*, the behaviour of turbines can be described in the same way.

The 'inertia turbocharger' block is an example of a dynamic block. Its output does not depend instantaneously on the two input signals, only the time derivative of the output has this property:

$$\Theta_{tc}\frac{d\omega_{tc}}{dt} = T_t - T_c,\ n_{tc} = 60\omega_{tc}/(2\pi)$$

7.3.5 Engine fluid and thermodynamics and engine inertia

As before, very simple models of these extremely complex systems are needed for the design and optimisation of control systems. The main effect is the torque generated by the engine. Here either a map-based approach similar to the one shown above, or an even simpler description, which approximates the engine behaviour surprisingly well in most cases, can be used. The latter approach is sometimes referred to as the Willans approach in which the engine torque $\tilde{T}_e$ is assumed to be an affine function of the fuel mass burned:

$$\tilde{T}_e(t) = e(n_e, \lambda_2, \ldots)\dot{m}_{ij}(t) - T_f(n_e, \vartheta_2, p_2, p_3, \ldots)$$

where $e(\ldots)$ is the indicated efficiency and $T_f(\ldots)$ a torque that includes all mechanical friction and other losses. Both of these variables can be determined experimentally (for simulations of higher precision) or be assumed to be constant (for a preliminary analysis).

To model all other delays present in a reciprocating engine, the 'induction-to-powerstroke' (IPS) delay block is usually added:

$$T_e(t) = \tilde{T}_e(t - \tau_{IPS})$$

where the delay τ_{IPS} depends mainly on the engine speed n_e. The latter is determined by the flywheel dynamics

$$\Theta_e\frac{d\omega_e(t)}{dt} = T_e(t) - T_l(t),\ n_e = 60\omega_e/(2\pi)$$

where T_l is the load torque acting on the engine flywheel with inertia Θ_e. In a vehicle, the load torque T_l is determined by the clutch or the torque

converter dynamics. On a test bench, this variable is an additional control input that can be used to verify the quality of the various control loops (EGR, idle speed, cruise control, etc.).

Obviously, those signals that are measured in the engine to be controlled need not be modelled, i.e., the blocks that produce those signals can be omitted. This simplification can substantially increase the model fidelity and streamline the modelling task, which can then focus on those subsystems that yield unmeasurable (intermediate) signals.

Once reliable models are available,[4] they can be used to design and optimise the corresponding control loops in a systematic way. Powerful software exists that supports this step. Typically the high-order and high-fidelity nonlinear models obtained in the modelling process must be further simplified (for instance linearised) for the controller synthesis step. For system simulations, i.e., subsequent model verification, the full-order nonlinear model can be used.

Usually, the resulting control systems are close to the achievable optimum, and only a few final validation and tuning experiments are sufficient to achieve the goals set in the specifications. Many control loops can be handled with such an approach (for instance, the engine torque and speed dynamics). As mentioned above, there are important effects that are not yet sufficiently well understood (for instance the PM formation) such that experiments cannot be completely eliminated in an engine calibration project.

Obviously, mathematical models can be quite useful not only for the synthesis of the control systems but also for other tasks. One notable example is the design of a set of signal processing algorithms needed to continuously monitor the 'health' of the engine system and detect faults as soon as they appear. For many reasons, such a detection of component degradation and subsystem malfunction will become much more important in the future. For instance, on-board diagnosis of some critical parts will be imposed by legislation, and OEMs will be forced to adopt such systems simply to be able to provide meaningful information to the vehicle maintenance people.

7.4 Advanced control systems

The most urgent problem in the development process of modern diesel engines is the requirement to meet the expected future emission limits. Table 7.1 summarises the main parameters of the European legislation; similar trends are followed in all other parts of the world.

[4]Once a library of well-designed and experimentally validated models is readily available, subsequent design projects can be handled in a more efficient way by adapting the existing models to the new engine system parameters. Notice that such a model library represents an efficient way to store in a reusable way the intellectual property of a company.

Table 7.1 Actual and future European emission limits for diesel passenger cars; the units of all emission limits are g/km (MVEG-95 test cycle)

Limit	Date	CO	HC + NO_x	NO_x	PM
Euro 4	2005	0.50	0.30	0.25	0.025
Euro 5	2009	0.50	0.23	0.18	0.005
Euro 6	2014	0.50	0.17	0.08	0.005

The huge progress made in the optimisation of the combustion in diesel engines was sufficient to satisfy the Euro 4 levels without the need to introduce sophisticated exhaust gas purification systems. In fact, most OEMs just added an oxidation catalyst to reduce hydrocarbon (HC) emissions and to reduce the negatively perceived smells of the exhaust gases. Sophisticated feedback control strategies have been proposed for this engine generation, as exemplified in the works of Kolmanovsky *et al*. (1999), Jankovic *et al*. (2000), van Nieuwstadt *et al*. (2000) and Shirakawa *et al*. (2001). However, in series production engines more traditional feedback loops are used, such as speed and load gain-scheduled PI controllers, which are combined with carefully tuned feedforward controls.

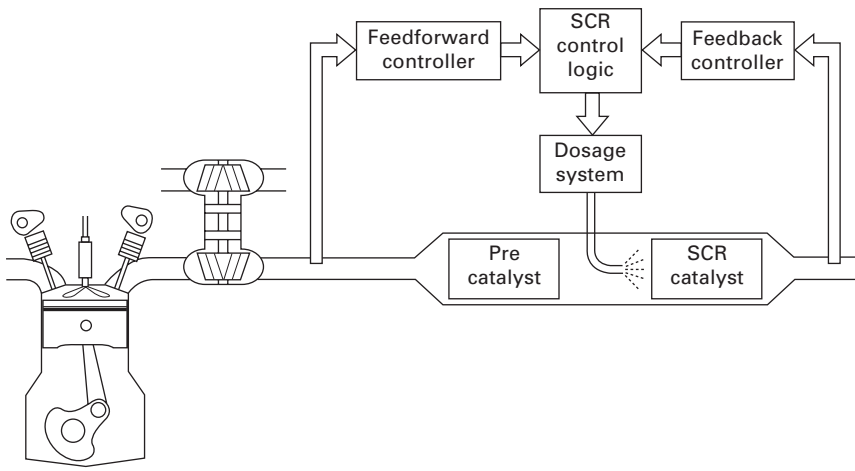
While this approach worked well in the past, it is clear that the Euro 5 level can only be met with the addition of PM filters and that the Euro 6 level will require a dedicated system to reduce the NO_x emissions in the exhaust gases.

The main problem of diesel particulate filters is that their regeneration becomes necessary once the amount of PM captured and stored in these filters reaches their capacity limits. One approach is to continuously regenerate the filter by adding iron-based substances to the fuel (CRT systems). However, in light-duty applications a solution that does not rely on additives is highly desirable. Unfortunately, without continuous regeneration the accumulated mass of PM starts to clog the filter. This is typically the case after approximately 1000 km driven, although this figure strongly varies with the driving profile. For this reason and to protect the filter from excessive temperatures during the regeneration phase, a PM filter monitoring system is usually needed. The pressure difference over the filter is the main information used by such filter-loading control systems. PM filter load models, temperature sensors, etc., complement such systems. Once a critical loading has been detected, the regeneration itself is initiated by a series of late fuel injections, which raise the exhaust gas temperatures above a certain threshold such that the PM stored in the filter starts burning. It goes without saying that this process also must be carefully controlled and monitored to avoid filter damage.

As mentioned above, the Euro 6 limits will require a system that is able to reduce the NO_x concentration of the exhaust gases. For light-duty systems it is not yet completely clear which alternative will prevail. In heavy-duty

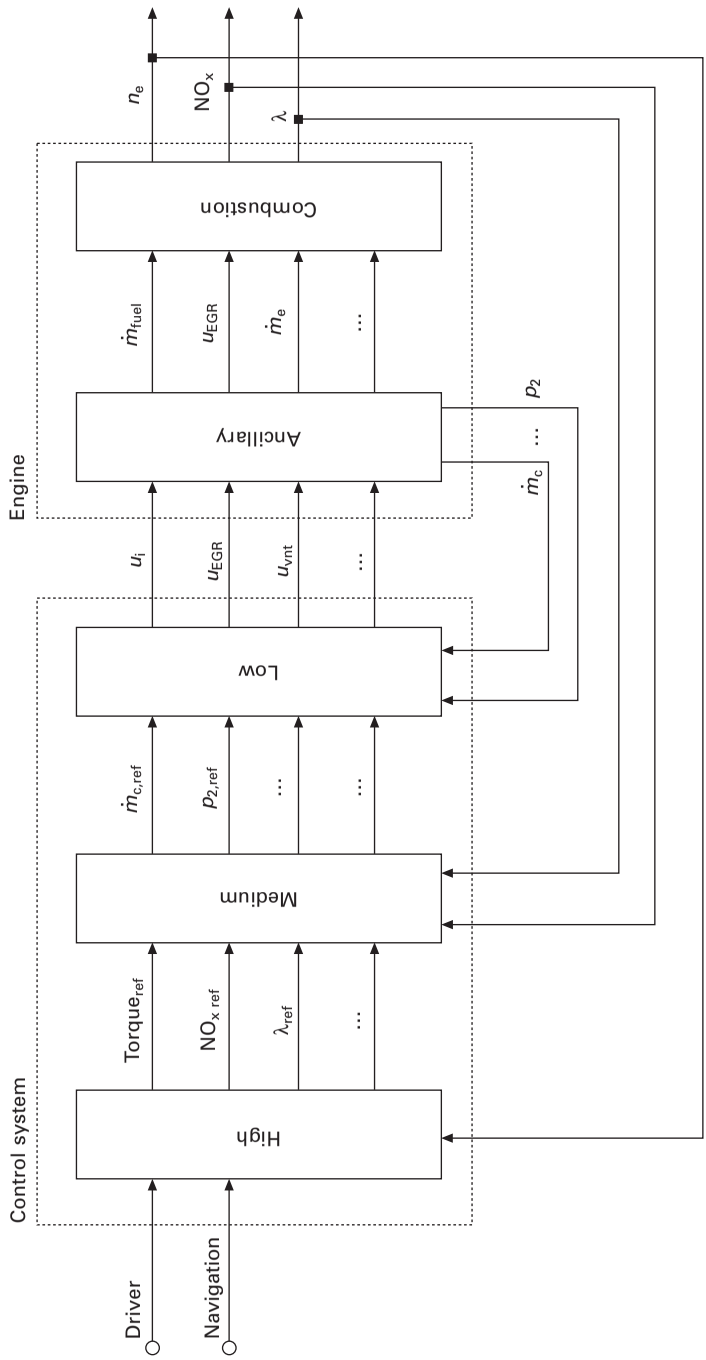
engines urea-based selective catalytic reaction (SCR) systems are the most likely solution.[5] Storage catalyst may be used in smaller light-duty engines, although some OEMs favour SCR systems there as well. Whatever option is chosen, all of these exhaust gas purification systems require additional control systems to work properly. In fact, one key problem of SCR systems is to assure that sufficient reducing agent (ammonia) is stored in the catalyst without allowing any substantial slip of that substance. This requires sophisticated feedforward and feedback control systems as illustrated in Fig. 7.8. The corresponding control problem is quite similar to the oxygen storage problem in three-way catalytic converters used for gasoline engines. Not surprisingly, similar ideas have been proposed to control the ammonia level in SCR converters (Schär *et al.*, 2006).

PM filters and SCR catalysts can be combined with standard diesel engine control systems such as those introduced in the previous section. However, the increasing complexity of such systems and the demand for added functionality leads to the development of 'physics-based' or 'torque-oriented' control system structures. Figure 7.9 illustrates the structure of a simplified version of such a control system using a block diagram representation. The main input variables, i.e., the driver commands and the information provided by the navigation and communication modules, are transformed by a top-level controller into corresponding reference values for the main engine-out physical variables (torque, NO_x concentrations, etc.). These reference values and the corresponding measured signals are then used by an intermediate control system to produce the reference values for the engine-in variables



7.8 Block diagram of a SCR catalyst control system.

[5]The SCR catalysts require ammonia as a reducing agent. Urea is simply a safe and efficient way to store ammonia on board.



7.9 Block diagram of a 'physics-based' control system structure.

(aspirated mass flow, manifold pressure, etc.). The lowest control layer uses the available actuators to force the actual engine-in variables to follow these reference values.

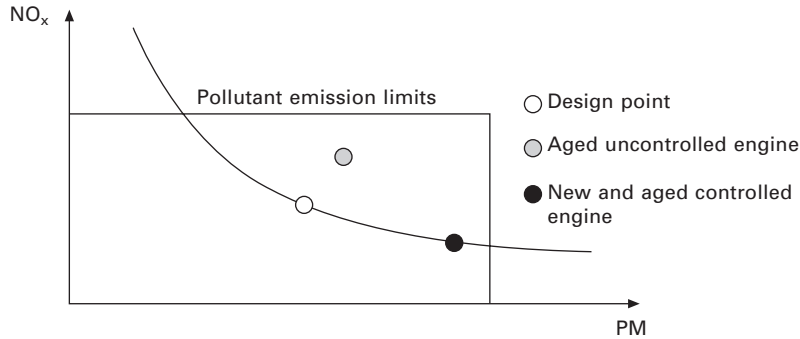
A key point is the fact that not just the engine speed signal is fed back, but also other important engine-out data such as measured pollutant emission concentration (Alfieri *et al.*, 2006). Some variables are directly measurable (for instance NO_x concentrations), some are not (for instance PM concentration). The missing information must be estimated using 'virtual' sensors, i.e. software algorithms that fuse the information coming from several sensors (engine temperature, EGR rate, NO_x concentration, air/fuel ratio, etc., in the case of PM). The basis for these software algorithms is a mathematical model of the corresponding engine processes, which is usually based on physical first principles. Some parameter identification is always necessary to achieve a sufficient prediction capability.

It is obvious that additional sensors will improve the overall system performance. While PM sensors are quite far from being available for series production engines, in-cylinder pressure sensors might be found in standard engines quite soon. For non-standard combustion systems (HCCI and similar approaches) such sensors seem to be a must to guarantee a stable combustion even in transient operating conditions. But also standard engines can benefit from such sensors. Control of combustion timing and the estimation of in-cylinder EGR (Mladek *et al.,* 2000) and engine-out NO_x (Brand *et al.*, 2007) are just a few examples of the benefits that can be expected.

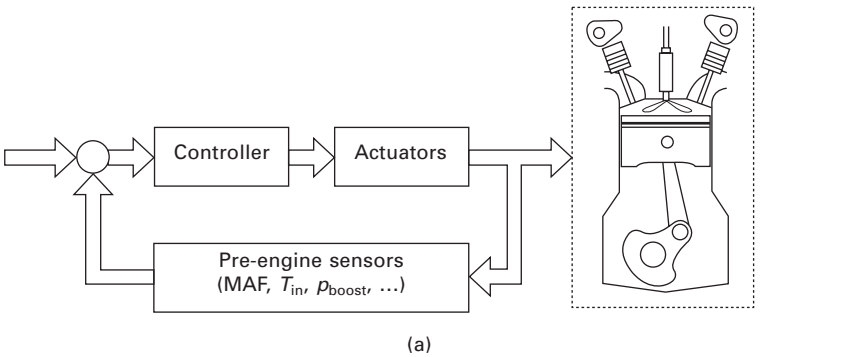
As mentioned above, measuring the actual engine-out variables allows for substantial cost savings because manufacturing tolerances can be relaxed. As an example, if the engine-out air/fuel ratio and NO_x concentration are available, the unavoidable differences in the fuel injector behaviour can be identified during the regular operation. Once this is known, each injector can be 'calibrated' on-line to inject exactly the desired amount of fuel and thus cylinder torque imbalances, higher-than-necessary pollutant emissions and noise problems can be alleviated. Such adaptive control schemes offer great potential, but must be used with great care, because the resulting nonlinear control system can cause unexpected system instabilities.

Another example of using engine-out information is as follows. In the design of all diesel engines the control system designer is faced with the fundamental trade-off problem illustrated in Fig. 7.10. No matter what pollutant emission limits must be met, with diesel combustion systems lower NO_x emissions come at the expense of higher PM emissions and vice versa.[6] In Euro 4 and 5 engines the designer usually chooses a 'safe' calibration (hollow circle

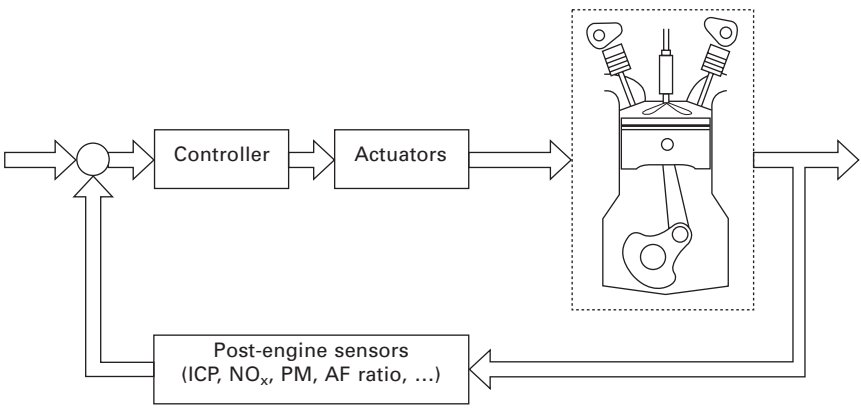
[6]This correlation is not necessarily present in non-standard combustion systems. Low-temperature homogeneous charge compression ignition combustion systems, for instance, are expected to yield lower NO_x *and* lower PM with increasing charge dilution.



7.10 NO_x and PM trade-off curve with possible engine performance points.



(a)



(b)

7.11 (a) Schematic representation of a standard diesel engine control structure (MAF = mass air flow, T_{in} = inlet temperature, p_{boost} = boost pressure, etc.). (b) Novel control structure using engine-out information (ICP = in-cylinder pressure, PM = particulate matter, AF ratio = air-to-fuel ratio, etc.).

in Fig. 7.10 such that manufacturing tolerances and ageing of components cannot cause the engine to leave the emission limit area (grey circle in Fig. 7.10). With new exhaust gas purification systems and engine-out *feedback* control systems in place (see Fig. 7.11), however, new approaches might prove to be advantageous. For instance, the NO_x feedback loop can be used to keep the NO_x emissions during the complete lifetime of the engine close to their maximum values (black circle in Fig. 7.10). Minimum PM engine-out emissions are thus obtained (reducing the need for regeneration of the PM filter) and the fuel economy is also maximised (higher NO_x emission levels are caused by higher combustion temperatures, which improve the thermodynamic efficiency of the engine).

This chapter closes with a discussion of the role of navigation and communication systems, which will increase in future applications. Of course the primary benefits of such systems will be improved vehicle safety (collision avoidance, broadcast of road conditions, etc.) and reduced fuel consumption, in particular in hybrid engines (Guzzella and Sciarretta, 2007), but also the pollutant emissions can be reduced using this information. If the top-level controller in the diagram shown in Fig. 7.9 receives information about the future behaviour of the preceding vehicles, of the velocity limits and of the road inclination, just to name a few, it can much better plan the future reference trajectory for the engine. Smoother accelerations, better gear shifting points and earlier braking manoeuvres all contribute to a safer, more fuel-efficient and less polluting engine operation.

7.5 References

Alfieri E, Amstutz A, Onder C and Guzzella L (2006), 'Model-based feedback control of the air-to-fuel ratio in diesel engines based on an empirical model', *Proceedings of the 2006 IEEE International Conference on Control Applications*, Munich.

Ammann M, Fekete N, Guzzella L and Glattfelder a (2003), 'Model-based control of the VGT and EGR in a turbocharged common-rail diesel engine: Theory and Passenger Car Implementation', *SAE Transactions, Journal of Engines*, vol. 112, no. 3, pp. 527–538.

Brand D, Onder C and Guzzella L (2007), 'Virtual NO sensor for spark-ignited engines', *International Journal on Engine Research*, vol. 8, no. 2, pp. 221–240.

Guzzella L and Amstutz A (1998), 'Control of diesel engines', *IEEE Control System Magazine*, vol. 18, no. 5, pp. 53–71.

Guzzella L and Onder C (2004), *Introduction to Modeling and Control of Internal Combustion Engine Systems*, Springer Verlag.

Guzzella L and Sciarretta A (2007), *Vehicle Propulsion Systems, Introduction to Modeling and Optimization*, 2nd edition, Springer Verlag.

Jankovic M, Jankovic M and Kolmanovsky I (2000), 'Constructive Lyapunov control design for turbocharged diesel engines', *IEEE Transactions on Control Systems Technology*, vol. 8, no. 2, pp. 288–299.

Kao M and Moskwa J (1995), 'Turbocharged diesel engine modeling for nonlinear

engine control and estimation', *ASME Journal of Dynamic Systems, Measurement and Control*, vol. 117, no. 1, pp. 20–30.

Kolmanovsky I, van Nieuwstadt M and Moraal P (1999), 'Optimal control of variable geometry turbocharged diesel engines with exhaust gas recirculation', *Proceedings of the ASME Dynamics*, DSC, vol. 67, pp. 265–273.

Lino P, Maione B and Rizzo A (2007), 'Nonlinear modelling and control of a common rail injection system for diesel engines', *Applied Mathematical Modelling*, vol. 31, no. 9, pp. 1770–1784.

Mladek M, Onder C and Guzzella L (2000), 'A model for the estimation of inducted air mass and the residual gas fraction using cylinder pressure measurements', SAE paper 2000-01-0958.

Schär C, Onder C and Geering H (2006), 'Control of an SCR catalytic converter system for a mobile heavy-duty application', *IEEE Transactions on Control Systems Technology*, vol. 14, pp. 641–653.

Shirakawa T, Itoyama H and Miwa H (2001), 'Study of strategy for model-based cooperative control of EGR and VGT in a diesel engine', *SAE Review*, vol. 22, pp. 3–8.

Streit E and Borman G (1971), 'Mathematical simulation of a large turbocharged two-stroke diesel engine', SAE paper 710177.

van Nieuwstadt M, Kolmanovsky I, Moraal P, Stefanopoulou S and Jankovic M (2000), 'EGR-VGT control schemes: experimental comparison for a high-speed diesel engine', *IEEE Control Systems Magazine*, vol. 20, no. 3, pp. 73–79.

8

Overview of heavy-duty diesel engines

Z. LIU, Navistar Inc., USA

Abstract: Heavy-duty diesel engines are defined, and the emissions standards used and to be used for heavy-duty diesel engines in different countries are presented and discussed. The main features of the latest heavy-duty diesel engines in the United States and Europe are overviewed, including the cylinder head design and the development of combustion system, turbocharger system, EGR system, diesel fuel injection system, electronic control and on-board diagnostics, and NO_x and PM emissions after-treatment systems. Future trends in the development of technology to meet strategies for NO_x, PM, and CO_2 emissions reductions are prospected in heavy-duty diesel engines throughout the world.

Key words: emissions, diesel engine, heavy-duty.

8.1 Introduction

In general, a diesel engine can be defined as a heavy-duty or a light-duty engine, mainly by its application to vehicles. If it is used in a heavy-duty vehicle, the diesel engine is certified as a heavy-duty diesel engine, whereas if it is used in a light-duty vehicle, it is called a light-duty diesel engine. Heavy-duty diesel engines are used around the world to haul commercial vehicles and deliver consumer goods, due to their unique combination of fuel economy, durability, reliability and affordability, which drive the lowest total cost of ownership [1].

8.1.1 Definition and application

A vehicle is defined as heavy-duty if its gross vehicle weight rating (GVWR) is greater than 8500 pounds (3856 kg) or its curb weight is greater than 6000 pounds (2721 kg). However, people use GVWR to define a vehicle type for most cases. The GVWR is the maximum allowable total weight of a road vehicle or trailer that is loaded, including the weight of the vehicle itself plus fuel, passengers, cargo, and trailer tongue weight. The curb weight is the weight of the vehicle with no passengers or cargo. The difference between gross weight and curb weight is the total passenger and cargo weight capacity of the vehicle. For example, a pickup truck with a curb weight of 2000 kg might have a cargo capacity of 3000 kg, meaning it can have a gross weight of 5000 kg when fully loaded.

In the United States, heavy-duty diesel engine classification is based on its primary intended service application, and is further classified as follows.

Light heavy-duty diesel engines

Light heavy-duty diesel engines usually are non-sleeved and not designed for rebuild. Their rated horsepower generally ranges from 70 to 170 pounds (52.2 to 126.8 kW). Vehicle body types in this group might include any heavy-duty vehicle built for a light-duty truck chassis, van trucks, multi-stop vans, recreational vehicles, and some single-axle straight trucks. Typical applications would include personal transportation, light-load commercial hauling and delivery, passenger service, agriculture, and construction. The GVWR of these vehicles is normally less than 19 500 pounds (14 541 kg).

Medium heavy-duty diesel engines

Medium heavy-duty diesel engines may be sleeved or non-sleeved and may be designed for rebuild. Rated horsepower generally ranges from 170 to 250 pounds (126.8 to 186.4 kW). Vehicle body types in this group would typically include school buses, tandem axle straight trucks, city tractors, and a variety of special-purpose vehicles such as small dump trucks and trash compactor trucks. Typical applications would include commercial short-haul and intra-city delivery and pickup. Engines in this group are normally used in vehicles whose GVWR varies from 19 500 to 33 000 pounds (14 541 to 24 608 kg).

Heavy heavy-duty diesel engines

Heavy heavy-duty diesel engines are sleeved and designed for multiple rebuilds. Their rated horsepower generally exceeds 250 pounds (186.4 kW). Vehicles in this group are normally tractors, trucks, and buses used in inter-city, long-haul applications. These vehicles normally exceed 33 000 pounds (24 608 kg) GVWR.

8.1.2 Emission regulation for heavy-duty diesel engines

The emissions standards are quite different throughout the world. The following mainly describes the most challenging emissions standards in the United States, Europe, and Japan.

Emission standards in the United States

Table 8.1 lists the emission standards of oxides of nitrogen (NO_x) and particulate matter (PM) for heavy-duty diesel engines in the United States [2].

Table 8.1 Emission standards of NO_x and PM for heavy-duty diesel engines in the USA

Model year	NO_x, g/bhp.hr (g/kWh)	PM, g/bhp.hr (g/kWh)
1988	10.7 (7.98)	0.60 (0.45)
1990	6.0 (4.47)	0.60 (0.45)
1991	5.0 (3.73)	0.25 (0.19)
1994	5.0 (3.73)	0.10 (0.075)
1998	4.0 (2.98)	0.10 (0.075)
2004	2.5 (NMHC + NO_x) (1.86)	0.10 (0.075)
2007	1.1–1.2 (0.8–0.9)	0.01 (0.0075)
2010	0.2 (0.15)	0.01 (0.0075)

It should be pointed out that the federal emission standards for model year (MY) 1998 heavy-duty diesel engines also require HC = 1.3 g/bhp.hr (0.97 g/kWh) and CO = 15.5 g/bhp.hr (11.56 g/kWh), where HC is hydrocarbon and CO is carbon monoxide. In addition, for urban bus PM the standard is 0.05 g/bhp.hr (0.037 g/kWh). The federal NO_x emission standards for MY 2004 heavy-duty diesel engines have two options. One is NMHC + NO_x = 2.4 g/bhp.hr (1.79 g/kWh), and the other is NMHC + NO_x = 2.5 g/bhp.hr (1.86 g/kWh) and NMHC = 0.5 g/bhp.hr (0.37 g/kWh), where NMHC represents non-methane hydrocarbon. The goal of the standard, per Environmental Protection Agency (EPA), California Air Resources Board (CARB) and heavy-duty diesel manufacturer agreement, is to reduce heavy-duty highway NO_x emissions to about 2.0 g/bhp.hr (1.49 g/kWh). Manufacturers can certify their engines under each option. Emission standards other than NMHC and NO_x continue at their 1998 levels.

Per the EPA, ultra-low-sulfur diesel fuel is viewed as a technology enabler to allow use of advanced, sulfur-intolerant exhaust emission control technologies such as diesel particulate filter and NO_x catalysts. Therefore, since June 2006, diesel fuel in the United States has had 15 ppm by weight sulfur content.

The new and more stringent requirements for NO_x, PM, and NMHC for heavy-duty diesel engines began to apply in MY 2007, but alternative certification using the family emission limit (FEL) is allowed. The new standards are as follows:

- NO_x = 0.2 g/bhp.hr (0.149 g/kWh), FEL cap of 2.0 g/bhp.hr (1.49 g/kWh)
- NMHC = 0.14 g/bhp.hr (0.104 g/kWh)
- PM = 0.01 g/bhp.hr (0.0075 g/kWh)
- CO = 15.5 g/bhp.hr (11.56 g/kWh)
- Formaldehyde = 0.016 g/bhp.hr (0.012 g/kWh).

The MY 2007 rule establishes a 50/50/50/100% phase-in program for

NO_x and NMHC that applies from 2007 to 2010, i.e., the phase-in schedule is that the new standards require 50% NO_x and NMHC FEL from 2007 through 2009, and 100% NO_x and NMHC FEL in 2010. However, 100% FEL is required for PM, CO, and formaldehyde from 2007 through 2010. The NO_x FEL cap is 2.0 g/bhp.hr (1.49 g/kWh) for MY 2007–2009 heavy-duty diesel engines, and 0.5 g/bhp.hr (0.37 g/kWh) for MY 2010 and later heavy-duty diesel engines. The FEL cap of PM and NMHC is 0.02 g/bhp.hr (0.015 g/kWh), applying from MY 2007.

Emissions standards in Europe and Japan

Table 8.2 lists the emission standards of NO_x and PM for heavy-duty diesel engines in the European Union.

Japan requires emission standards of NO_x = 4.5 g/kWh, PM = 0.25 g/kWh, HC = 2.9 g/kWh, and CO = 7.4 g/kWh for heavy-duty diesel engines for 1997, and emissions of NO_x = 3.38 g/kWh, PM = 0.18 g/kWh, HC = 0.87 g/kWh, and CO = 2.22 g/kWh, beginning to apply for heavy-duty trucks and buses greater than 2.5 t GVWR and equal to or less than 12.0 t GVWR in MY 2003, and for heavy-duty trucks and buses greater than 12.0 t GVWR in MY 2004. The 2005 emission limits were NO_x = 2.0 g/kWh, PM = 0.027 g/kWh, NMHC = 0.17 g/kWh, and CO = 2.22 g/kWh. Emission limits of NO_x = 0.7 g/kWh, PM = 0.01 g/kWh, NMHC = 0.17 g/kWh, and CO = 2.22 g/kWh will apply to 3.5 t < GVWR < 12 t vehicles for 2009, and to GVWR > 12 t vehicles for 2010.

The above examples show the most stringent current legislation in the world. In fact, ever tightening standards that restrict the levels of pollutant emissions emitted from heavy-duty diesel engines have been introduced by governments around the world. The ultimate target of emissions legislation is to push technology to the point where a practical and affordable zero-emission heavy-duty diesel engine with acceptable performance can come true.

Table 8.2 Emission standards of NO_x and PM for heavy-duty diesel engines in Europe

Tier	Date and category	NO_x, (g/kWh)	PM (g/kWh)
Euro I	1992, <85 kW	8.0	0.612
	1992, >85 kW	8.0	0.36
Euro II	1996.10	7.0	0.25
	1998.10	7.0	0.15
Euro III	2000.10	5.0	0.1(ESC)/0.16(ETC)
Euro IV	2005.10	3.5	0.02(ESC)/0.03(ETC)
Euro V	2008.10	2.0	0.02(ESC)/0.03(ETC)

8.2 A survey of current heavy-duty diesel engines

Various advanced technologies have been used in current heavy-duty diesel engines by major diesel engine manufacturers in the United States, Europe, and Japan to meet increasingly stringent emissions legislation and ever increasing customer requirements for superior fuel economy, performance, sociability, and reliability. It is important to select the right technology and system architecture for a particular application, execute the design of hardware and control software, and optimize the performance, fuel economy, and emissions through calibration controls using the best available tools.

Current heavy-duty diesel engines are turbocharged and use air-to-air charge air cooling to increase charge air density and reduce NO_x emissions. They feature advanced fuel injection equipment (FIE) with high injection pressure from 1600 to 2400 bar, and full-authority electronic control. These engines typically have cooled exhaust gas recirculation (EGR) technology to further control NO_x emissions. The electronic control system typically features several sensors to enable control of engine performance and emissions under a wide range of operational and ambient conditions. In order to reduce PM emissions drastically, a diesel particulate filter (DPF) has been used in heavy-duty diesel engines in the United States, Europe, and Japan in recent years.

8.2.1 Cylinder head design

Most current heavy-duty diesel engines use the four-valve head. The intake and exhaust valve sizes are optimized for maximum flow area, while maintaining the injector location at the center of the cylinder to improve fuel distribution and air/fuel mixing. In general, in-cylinder swirl is generated using a standard swirl port design for one intake valve location, and a tangential swirl port for the other. The valve seats are parent metal and induction hardened for wear resistance.

In general for cold starting, each cylinder contains a glow plug, located between an intake and exhaust valve, and an protruding into the piston bowl. The other end of the glow plug protrudes to the outboard side of the engine, where it is connected to a wiring harness. The glow plugs can be serviced from outside the engine without removing the valve covers [3].

8.2.2 Turbocharger system

The maximum power that a given diesel engine can deliver is limited by the amount of fuel that can be burned efficiently inside the engine cylinder. The fuel that can be injected into the engine cylinder is limited by the amount of

air that is introduced into the engine cylinder [4]. It is known from theory that the engine power, torque, and mean effective pressure are proportional to the inlet air density. If the inducted air is compressed to a higher density than the ambient, prior to entry into the engine cylinder, the maximum power which the engine can deliver will be increased. A turbocharger, consisting of a compressor and a turbine on a single shaft, is widely used in heavy-duty diesel engines to boost the inlet air density. Energy from the engine exhaust is used to drive the turbocharger turbine which drives the turbocharger compressor which increases the inlet air density prior to entering the engine cylinders.

Matching a turbocharger to a given heavy-duty diesel engine in vehicles is considerably more difficult due to the wide speed and load variations encountered. If a big turbocharger with a fixed geometry turbine (FGT) is used to match a diesel engine well at high speed, the engine can obtain good performance at high speeds, with high torque and power output, low fuel consumption, and low smoke emissions, but the engine performance will deteriorate at low speeds, with high fuel consumption and high smoke, and perhaps there would be a surge. If a small turbocharger is used to match the diesel engine well at low speed, the engine can get good performance and low smoke at low speeds, but the expansion ratio across the turbine will be very high at the maximum engine speed when air flow is greatest. Thus the piston must pump the exhaust gases out against a high backpressure, resulting in poor net power output and fuel consumption. In addition, the engine will exceed the allowable limits of maximum cylinder pressure and turbocharger speed. Clearly the turbocharger should not match heavy-duty diesel engines at one high or low speed and a compromise must be reached in the engine speed range. It is obvious that the turbocharger cannot work at its optimization condition in most of the engine operation range.

A simple method of avoiding the above problem of turbocharger over-speed and cylinder pressure over-limit is to use a waste-gate valve through bypassing some of the exhaust gas around the turbine at high speeds. Thus when a small turbine is fitted to achieve good low-speed boost, the massive increase in specific available energy at the turbine at high speed is alleviated by increasing the effective flow area out of the exhaust manifold. This has two effects. Firstly, only part of the exhaust gas flow goes through the turbine. Secondly, the increase in flow area reduces the exhaust pressure that would otherwise build up. Both measures reduce turbine work and hence boost pressure. In addition, the second factor reduces pumping work during the exhaust stroke and would moderate the loss in brake mean effective pressure (BMEP) and deterioration in fuel consumption at high speeds [5]. Therefore, this technology has been applied to many heavy-duty diesel engines due to its simplicity and low cost.

Ideally the best method to solve the above problem is to use a variable

geometry turbine (VGT). So far, VGT technology has found wide use in current heavy-duty diesel engines to achieve the desired diesel engine performance [6]. The turbochargers have variable nozzle turbines, which are controlled electronically. The VGT feature enables the turbocharger boost to be controlled across the engine speed and load range. In VGT turbochargers the turbine housing contains movable vanes that control the effective size of the housing, and direct the flow of the exhaust gas to the turbine wheel. When the vanes are closed, the exhaust gas is accelerated between the vanes and across the turbine wheel, producing higher turbine speeds and higher boost at low engine speeds. In effect, this shows that the engine uses a smaller turbocharger at these conditions, which means that the turbocharger works at high-efficiency status. At higher speeds and loads, the vanes are opened to control the amount of boost desired, and prevent over-speeding of the turbocharger. This shows that the engine uses a large turbocharger. Thus, the turbocharger still works under high-efficiency conditions. Overall, the VGT turbocharger provides a much wider range of high-efficiency operation and a higher boost level compared with a standard FGT turbocharger with a waste-gate valve.

8.2.3 Fuel system

The fuel system used in modern heavy-duty diesel engines is required to provide not only extremely high injection pressures, but also multiple injections, with each injection having an optimized rate to accomplish a specific purpose [7, 8]. In addition, it is also required that the fuel system not only is satisfied with fulfilling the traditional functions of injection timing and metering control, but also provides flexibility in controlling injection pressure.

Advanced electronically controlled, hydraulically driven high-pressure fuel systems with multiple injection capability have been used in current heavy-duty diesel engines, greatly improving the engine performance. The high injection pressure improves air and fuel mixing for better emissions and brake specific fuel consumption (BSFC). The pilot injection can improve noise and vibration harshness (NVH). The post-injection may reduce soot emissions effectively.

Two types of advanced electronically-controlled high-pressure fuel systems are used in current heavy-duty diesel engines. One is the common rail high-pressure fuel system with maximum injection pressure of 2000 bar, and the other is the intensifying type of high-pressure fuel system with maximum injection pressure of 2400 bar. Both of the two advanced fuel injection systems can control the injection of the diesel fuel at the right time, in the right amount, and with the correct injection pressure in heavy-duty diesel engines. In general, the intensifying type of high-pressure fuel system can provide even higher fuel injection pressure, whereas the common rail

high-pressure fuel system can offer more injection events per engine firing cycle.

The intensifying type of high-pressure fuel system uses high-pressure oil rails, which serve as accumulator volumes feeding the injectors. The rails are located as close to the injectors as possible in order to minimize the oil pressure dynamics that result from elevated hydraulic pressure waves generated by rapid starts and stops in the oil flow. The intensifying type of high-pressure fuel injector uses solenoid coils to control a fast-acting spool valve or poppet valve, which controls the flow of oil to the top of an intensifier piston inside the injector. The intensifier piston acts on the fuel injection plunger with an area ratio of such as 7 to 1, amplifying the fuel pressure over the oil supply pressure by the same ratio. In this manner, varying the oil supply pressure to the injector can control the fuel injection pressure. This can be accomplished independently of engine speed and load. This kind of fuel system can provide a high injection pressure of up to approximately 2400 bar at the present time [6].

Common rail fuel injection systems can provide diesel engines with considerably high flexibility in the adaptation of the injection system to the engine. This kind of fuel system can supply a high injection pressure of up to approximately 2000 bar currently, variable injection timing, the possibility of pilot injection, main injection, and post-injection, and variable injection pressure to match different engine speeds and loads [7]. Pressure generation and fuel injection are completely decoupled in the common rail fuel system. The injection pressure is generated independently of engine speed and load. The fuel is stored under pressure in the high-pressure rail used as the accumulator ready for injection. Based on the engine speed and torque, the injected fuel quantity, the injection timing, and the injection pressure are calculated by the engine control unit (ECU), which sends the command signals to the injector, triggering the fuel injection events.

It is hoped that the fuel quantity injected during the ignition delay period is as small as possible in diesel engines. Common rail fuel systems can meet this requirement easily through a small pilot injection. When this fuel is injected into the combustion chamber, the combustion pressure rises, the peak combustion pressure can be reduced, and the main injection ignition delay can be shortened. This can reduce the combustion noise and the fuel consumption as well as soot emissions in many cases. On the other hand, after-treatment system regeneration also requires diesel fuel post-injection either to increase the exhaust gas temperature for diesel particulate filters or to increase CO for NO_x catalytic converters. It is evident that the advanced common rail fuel system will find more and more applications in heavy-duty diesel engines in the future.

8.2.4 Combustion system

In-cylinder emissions control through combustion optimization is the key technology to meet the emissions legislation and ever increasing customer requirements for superior fuel economy and performance. The strategies used in advanced combustion system in heavy-duty diesel engines include inhibiting the NO_x formation by lowering the mixture temperature at the ignition point and the flame temperature, and intensifying soot oxidation by improving the spatial and temporal fuel distribution and increasing the mixing energy during the late stages of the combustion process.

It is known that NO_x is formed in the high-temperature diffusion flame region, and that NO_x formation is an exponential function of the flame temperature [9]. Therefore, it is obvious that in-cylinder control of NO_x formation can be accomplished through controlling the factors that directly affect the flame temperature.

The temperature of fresh air out of the compressor of a turbocharger is much higher than the ambient temperature which would increase the flame temperature, and hence NO_x emissions. Therefore, air-to-air charge cooling has found wide use in current heavy-duty diesel engines to reduce the compressed fresh air temperatures drastically. A good charge air cooler (CAC) can reduce the compressed air temperature almost to the ambient temperature, resulting in NO_x reduction of about 50%, compared to the unregulated levels. In addition, the CAC can increase fresh air density, resulting in increase in engine torque and power. The CAC is installed between the turbocharger compressor and the intake manifold, usually located at the front of the vehicle and in front of the engine radiator. Thus, it is cooled by the ambient air either by natural ram air from the forward motion of the vehicle or by cooling fan assistance.

EGR is the principal technique used to control diesel engine NO_x emissions [10]. EGR works by returning a fraction of a diesel engine's exhaust gas back to the engine cylinders. An EGR valve is used to meter the EGR percentage needed. The recycled exhaust gas is usually mixed with fresh air before entering the intake manifold. The EGR gas can reduce the amount of excess oxygen, and increase the specific heat capacity of the mixture, thereby lowering the peak burned gas temperatures and NO_x formation rates. NO_x is primarily formed when a mixture of nitrogen and oxygen is subjected to high temperatures. Because NO_x formation progresses much faster at high temperatures, EGR serves to limit the generation of NO_x.

In modern heavy-duty diesel engines, the EGR gas is cooled through one big or two smaller EGR coolers to reduce the intake manifold temperatures, resulting in low combustion temperatures. Therefore, in most heavy-duty diesel engines, the cooled EGR strategy has been used to inhibit NO_x formation. It is found that the cooled EGR is a highly effective NO_x control strategy,

capable of almost total elimination of NO_x when used at high levels. The effectiveness of an EGR cooler is the ratio of the temperature difference between incoming and outgoing EGR gas to the difference of the incoming EGR gas temperature minus the cooler coolant temperature, which represents the EGR cooler performance. It is clear that the EGR cooler design and selection also influence the NO_x emissions.

Other strategies used in heavy-duty diesel engines include using high fuel injection pressure to provide more turbulence energy for mixing and soot oxidation during late combustion. The combustion bowl is deliberately designed to have an optimal match with the fuel spray and the intake swirl, and to maintain the swirl and turbulence intensity in late combustion. The fuel injector is centrally located in the cylinder, and the vertical nozzle arrangement can give a more uniform fuel spatial distribution, resulting in an improved local air and fuel ratio. By using the VGT turbocharger, the required air/fuel ratio and EGR rate can be obtained over the entire operating region.

8.2.5 After-treatment system

The emissions from a diesel engine consist of three phases: solids, liquids, and gases [11]. The combined solids and liquids are called particulate matter (PM), and are composed of dry carbon (soot), inorganic oxides primarily as sulfates, and liquids. The liquids are a combination of unburned diesel fuel and lubricating oils, called the soluble organic fraction (SOF), which form discrete aerosols and/or are adsorbed within the dry carbon particles [12]. Gases include gaseous hydrocarbon, carbon monoxide, nitrogen oxide, and sulfur dioxide.

The incomplete combustion in the cylinders of heavy-duty diesel engines and the lubricating oil entered into the cylinders may produce unburned hydrocarbons that usually make up 10–30% of the total particulates. A diesel oxidation catalyst (DOC) is a passive device installed in the engine exhaust system through which all of the engine exhaust flows [13]. It consists of a metal outer casing which contains a substrate (usually a ceramic honeycomb) that forms a matrix of flow passages parallel to the flow direction. The object of the cellular matrix is to expose a large surface area to the exhaust gases and increase the probability of contact and reaction between exhaust components. The substrate is coated with a washcoat consisting of base metal oxides and a small amount of precious metals. The combination of the base metals and precious metals acts as the catalyst. Thus, DOC can be used to oxidize unburned hydrocarbons emitted from diesel engines and reduce total particulate. A well-designed DOC can reduce 80–90% of the unburned hydrocarbons. In addition, DOC can also reduce CO and oxidize a portion of SOF. Therefore, DOC has been used to control the total particulate as a

part of the PM after-treatment system in all heavy-duty diesel engines. A side-effect of DOC is that it also oxidizes sulfur dioxide to sulfur trioxide which is emitted from the exhaust gas as particulate. It is obvious that DOC operation needs low-sulfur diesel fuel to maintain its good performance.

After the introduction of EGR, the NO_x emission is reduced drastically. However, this results in the increase in PM emissions that corresponds to an increase in EGR. PM that is not burned in the power stroke is the wasted energy. Stricter regulations on PM require further emission controls to be introduced to compensate for the PM emissions introduced by EGR. The most common device is active DPF in the exhaust stream, which can remove about 90% of exhaust carbon particles [11]. They have been commercially applied in passenger cars in Europe for more than eight years, but need to be installed on all heavy-duty diesel engines to meet current stringent particulate emission standards.

The filter medium consists of porous materials, such as ceramic, used to trap the soot in the exhaust gas stream. When the particle accumulation reaches a certain extent, it has to be removed from the filter. This process is called regeneration. In DPF regeneration, methods available to increase the oxidation rates include heating the soot directly, heating the catalyst bed directly, and increasing the exhaust gas temperature. For convenience, the heat from the exhaust gas is usually used to oxidize the carbon from the exhaust gas in the filter with the help of a precious metal catalyst coated on the substrate located on the inside surface of the filter. The heat used for DPF regeneration usually comes from the extra post-fuel injection, which results in a reduction in fuel efficiency.

Another type of after-treatment system can be used for control of NO_x emissions. It includes an NO_x adsorber catalyst (NAC) and selective catalytic reduction (SCR), which will be discussed later in this chapter.

Sulfur is present in diesel fuel, and is recognized to be potentially harmful to diesel engines and after-treatment devices. The performance of oxidation catalysts used in many applications is impaired by the presence of sulfur. Sulfur can form a barrier on the surface of the catalyst and reduce its performance significantly, especially at low catalyst bed temperatures. The sulfur in the diesel fuel will lead to the emission of sulfates which contribute to total particulate emissions. In addition, NAC can be poisoned by sulfur. The NO_x adsorber contains base metal oxides designed to store nitrogen dioxide, an acid gas. However, the storage mechanism also applies to sulfur dioxide in the exhaust stream. The base metal oxide sites will be occupied by sulfates, resulting in a loss of NO_x conversion efficiency. Sulfur is emitted as sulfur dioxide which can lead to the formation of acid rain. Sulfur dioxide is a colorless acidic gas produced in the combustion process within the engine. For the past 10 years, sulfur levels in diesel fuel have been reduced drastically, from 2000–3000 ppm to below 15 ppm now. It is

found from many engine experiments that low sulfur diesel fuel can reduce combustion emissions directly, and the removal of sulfur from diesel fuel is a key enabler for ultra-low emissions engine systems with after-treatment systems such as DPF and NO_x converter.

8.2.6 Control system

In order to make all the above-mentioned systems, such as the fuel system, the EGR system, and the turbocharger system, work well, the control system plays a key role in heavy-duty diesel engines, that is, the control system in diesel engines is responsible for maintaining their performance at the optimum level while at the same time keeping engines from exceeding the emissions limits required by government [14]. In addition, electronic control is also used to diagnose problems with the engine, provide protection under extreme operating conditions, and support on-board diagnostics (OBD).

The control system can provide accurate control of all critical functions of engines under a wide range of conditions, and perform the required functions using three groups of components: sensors, a processor, and actuators. Sensors are used to obtain a measurement of a physical variable through direct measurement or a combination of measurement and calculation. These sensors should be able to measure a range of physical and chemical quantities in a time short enough to meet the control requirements of high speed diesel engines. In addition, sensors have to survive the environment in which they are to perform their functions. At the same time, they need to be produced at reasonable cost and with automotive-type durability.

Electrical signals produced by the sensors are relayed to the second major component of the control system, the processor. The processor is often described as the ECU, in which control actions are determined on the basis of computations, in order to keep the system performing at the required level. The third major component of the control system is the actuator that receives orders from the processor to perform certain functions or required control actions. For example, the solenoid in the fuel injection system of diesel engines controls fuel spray into each cylinder at the required fuel quantity and timing, based on ECU commands.

The basic control system configurations used in heavy-duty diesel engines are open- and closed-loop systems. In open-loop control systems, the measured values of speed and torque are used to construct a control table of values such as injection timing. At any speed and load condition, the corresponding injection timing is calculated using an interpolation algorithm and translated into the output values to set the injection timing. Current heavy-duty diesel engines use a large number of lookup tables and need substantial calibration to fill in the values in those lookup tables in open-loop control systems.

In closed-loop control systems, a measurement of the quantity being

controlled is explicitly compared with the desired value. The difference is often referred to as error. The necessary calculations are made based on the error or the difference between a desired signal and the value measured from the system. Then, a modified control action is performed. This process could be repeated many times until the required value is reached. This process is also called feedback control. Keeping diesel engines at a constant speed and torque is a common example of such a feedback control system.

First-generation controllers are mainly used for fuel system control. They use relatively few sensors and actuators, and feature relatively simple algorithms that make extensive use of a limited number of lookup tables to produce outputs. Second-generation controllers are used to control the fuel system, the EGR system, and the turbocharger system. They use many sensors and a number of actuators. They also use multiple lookup tables and limited closed-loop control, and make some compensations and corrections to control outputs based on ambient temperature or altitude. Currently, third-generation controllers are used to control not only the fuel system, the EGR system, and the turbocharger system, but also after-treatment systems, such as DPF or SCR systems. They use many more sensors and actuators, including virtual sensors and smart actuators to better control engine performance and emissions. They use multiple lookup tables and feature closed-loop control of most critical variables. They can make extensive compensations and corrections for a lot of inputs directly from engine and vehicle sensors and indirectly from virtual sensors, to optimize the engine control.

8.3 Approaches to meet future emissions legislation and CO_2 targets

There is a continuous demand to increase engine torque and rated power, and to reduce engine fuel consumption, which directly helps reduce CO_2 emissions. The United States and Europe are currently establishing CO_2 targets to control vehicle CO_2 emissions. It is also beneficial to further develop the diesel engine combustion system to provide further reductions in engine-out NO_x and PM emissions, even when exhaust after-treatment systems have been used, since in-cylinder combustion improvements can help reduce the urea consumption needed for SCR systems and the required regeneration frequency for DPF or to reduce the sizes of SCR and PDF systems.

8.3.1 Advanced combustion

In order to meet increasingly stringent emissions standards, alternative combustion methods have to be developed and used in heavy-duty diesel engines, instead of the conventional combustion process. A typical alternative combustion process, i.e. homogeneous charge compression ignition (HCCI)

combustion, is receiving a lot of attention, and many people are concentrating their efforts on its research and development in heavy-duty diesel engines [15].

HCCI combustion is the process in which a homogeneous mixture is auto-ignited through compression. This combustion has the potential to significantly reduce NO_x and PM emissions, while achieving high thermal efficiency and having the capability of operating with a variety of fuels. Similar to a spark ignition (SI) engine using gasoline fuel, the diesel fuel and fresh air are mixed to obtain a homogeneous mixture, which can eliminate fuel-rich diffusion combustion and can thus drastically reduce the PM emissions that are usually associated with conventional diesel combustion processes. The HCCI engine undergoes an auto-ignition process through the entire combustion chamber that can eliminate the high-temperature flames of conventional diesel combustion. Therefore, the NO_x emissions from HCCI engines can be very low, compared to those of conventional engine combustion processes.

Since HCCI combustion is achieved through the auto-ignition of the homogeneous mixture around the top dead center (TDC) as it is compressed via the piston, it becomes more challenging to control the start of combustion and the rate of heat release for this combustion process over a wide range of engine operating conditions, as compared to conventional engines that have direct control of combustion initiation such as a fuel injection timing. Other technical challenges include extension of HCCI operation to high loads, operation during transients, excess HC and CO emissions, and cold start.

Over the last decade, many studies have been performed to explore the potential of HCCI technology and numerous innovative strategies for mixture preparation, combustion control, load extension, and emissions reduction have been proposed. Two strategies have already been successfully incorporated into production vehicles. However, they work on HCCI combustion at low speeds and loads. In the future, if full-load HCCI combustion can be realized, diesel engines can get rid of both PM and NO_x after-treatment devices.

8.3.2 Advanced diesel fuel injection system

It is well known that the diesel fuel system is a key factor in controlling the combustion process in heavy-duty diesel engines. For example, in order to expand the HCCI combustion range and control its combustion process, it is required that more fuel is injected into the cylinders before auto-ignition, resulting in an increase in injection pressure and a decrease in injection duration. The high fuel injection pressure can directly reduce both soot emissions and fuel consumption. Therefore, in the future the most important trend in the development of heavy-duty diesel engine fuel systems will be to increase the fuel injection pressure. For common rail fuel systems, the fuel

injection pressure will approach 2400 bar, and for the intensifier fuel system it will approach 3000 bar. With higher injection pressures, the injection rate increases. More fuel is injected earlier and the injection duration shortens, which is helpful in reducing fuel consumption. At the same time the soot formed can experience a longer time at higher temperatures, oxidizing more of the soot. Combinations of the common rail fuel system and the intensifying type of fuel system are also under development, so that the new generation of diesel fuel injection systems should have the advantages of both the injection flexibility of the common rail fuel system and the higher injection pressure of the intensifying type of fuel system.

The strategy of multiple fuel injections is another important measure to control the combustion process [16]. Numerous experiments and computer simulations have shown that pilot injection can reduce the combustion noise and help prepare the HCCI combustion mixture. Near post-injection can reduce soot emissions effectively, since it can increase the temperature in the cylinder in the late combustion phase, which enhances the oxidation of the soot formed [17]. In addition, late post-injection is also used for the regeneration of after-treatment devices. Therefore, future advanced fuel injection systems will provide more injection events to optimize engine combustion and after-treatment as a whole.

With the fuel injection pressure increase, the number of orifices in the injector nozzle will increase, and the orifice diameter will reduce. The increase in nozzle orifice number can improve the fuel distribution, which helps improve fuel/air mixture formation, whereas the reduction in nozzle orifice diameter reduces the fuel spray atomization time, which also helps improve the fuel/air mixture formation. Both of the above can reduce soot formation.

The fuel returned from the injectors brings some engine heat to the fuel tank. If the returned fuel quantity is high, fuel cooling has to be considered. On the other hand, returned fuel wastes engine energy. Therefore, another task for the future is to reduce the fuel returned from the fuel injection process, thus helping increase the engine effective efficiency.

8.3.3 Advanced air management

Air management in heavy-duty diesel engines includes the turbocharger system and the EGR system. It is well known that EGR technology can reduce NO_x emissions effectively, and this has been used widely in heavy-duty diesel engines. In the future, a higher and higher proportion of EGR will be used to meet the increasingly stringent NO_x emissions standards [10]. However, EGR cooling systems are under continuous development to further improve the combustion process for better engine performance and lower pollutant emissions. To reduce the intake manifold temperature, the EGR cooler size is

gradually being increased; two EGR coolers have also been used. A parallel arrangement of two EGR coolers will be used to reduce the EGR gas flow pressure drop over EGR coolers, resulting in a decrease of engine BSFC. At the same time, a large EGR valve will be used for the same purpose.

The turbocharger system will be optimized continuously to increase its efficiency. The compound turbocharger system will find more applications in heavy-duty diesel engines in the future. It combines a turbocharger system and a supercharger system to increase the whole engine efficiency. A two-stage turbocharger system is another solution to improve combustion and transient response in heavy-duty diesel engines. This technology can increase the intake air pressure to increase the air/fuel ratio. Through an optimized design with the bypass feature, it can cover the high and low load operations without using a costly VGT system.

8.3.4 Advanced after-treatment

With increasingly stringent emissions legislation, cleaner and more efficient after-treatment devices have been under development. To meet the PM emission demand in the United States for MY 2010 and beyond, the DPF system has to be used in heavy-duty diesel engines. However, in order to reduce NO_x emissions, NO_x catalytic converters will be required in heavy-duty diesel engines in the future.

Selective catalytic reduction (SCR) technology uses the reactions between ammonia and NO_x by means of a catalyst to form nitrogen and water vapor. If ammonia is kept at the stoichiometric ratio and the ammonia supplied is entirely reacted with the NO_x under ideal steady-state conditions, the NO_x can be eliminated completely, which means that the NO_x conversion efficiency of SCR is 100%. If the diesel engine operations depart from the ideal conditions, the NO_x conversion efficiency will fall, and either NO_x will be slipped through the catalyst, or ammonia will be slipped. However, in real-world heavy-duty diesel engines, the engine operations change all the time, causing sharp changes in exhaust flow, exhaust gas temperature, and exhaust NO_x flow rate, which causes the SCR control to become extremely complicated [18–21]. A further problem is the dynamic storage of ammonia within the SCR system. The storage ability is highest at low bed temperatures, and the ammonia is released when the bed temperature rises with load increase. All the issues mentioned above affect negatively the ability of the SCR system to achieve high conversion efficiency. Therefore, the maximum NO_x conversion efficiency of practical SCR systems is limited to between 80–90%, depending on the performance of the control system.

SCR technology has been used for stationary applications in power plants and other industrial process plants for many years, deployed by a number of engine and truck manufacturers in Europe as part of an integrated emission

control strategy, combined with other technologies aimed at meeting Euro III and Euro IV, and applied to heavy-duty diesel engines in Japan and Europe only in recent years [22, 23]. In the future it will be used for most heavy-duty diesel engines in the world to meet more stringent NO_x emissions standards. For example, Volvo and Daimler truck manufacturers will use the SCR technology to meet Euro V and US MY 2010 emissions standards in the European and US markets, respectively.

Another effective means to remove NO_x from exhaust gases is NAC [24] or the lean NO_x trap (LNT) [25]. It works in a cycle, in which NO_x is stored for a period of time on the catalyst surface as a nitrate, and is later released from the catalyst surface under locally rich conditions, and reduced to nitrogen. The first process is called the lean operation, which converts nitrogen oxide (NO) to nitrogen dioxide (NO_2) over a precious metal catalyst. Then the nitrogen dioxide reacts with the base metal oxide components of the catalyst to form a stable nitrate compound on the surface, until all available base metal storage sites are occupied by nitrates, and NO_x will start to slip through the catalyst, leading to excess emissions. When this point is reached, the second process, called the rich operation, starts and the exhaust is enriched either by control of engine parameters or by enrichment in the exhaust through fuel dosing. This period of enrichment causes the nitrates to become unstable and to be released into the exhaust as nitrogen dioxide. Under these rich conditions a set of three-way reactions take place over the precious metal catalyst among the hydrocarbon, the carbon monoxide, and nitrogen dioxide, producing nitrogen, carbon dioxide, and water vapor.

Since the LNT uses precious metal as catalyst, and its size is proportional to the engine size, large LNT uses more precious metal. Due to the high price of precious metals and complicated combustion requirements, LNT is not practical in heavy-duty diesel engine application. On the other hand, the SCR system does not use precious metal as catalyst. As a result, the SCR technology is the best option for heavy-duty diesel engine application, and will find wide use in heavy-duty diesel engines in the future.

8.3.5 Advanced controls

Using traditional control methods, it has been found that the limits of steady-state emissions calibration capacities are reached rapidly. In lookup table controls, the desired control behavior is represented as values that correspond to any speed and load condition. For example, in an EGR control system, the lookup table may have EGR valve positions that correspond to each speed and load condition under the full load curve of a diesel engine. A new control approach – the model-based control method – should be used for modeling each component of the EGR system that may include exhaust

manifold, EGR cooler, EGR valve, air filter, turbocharger compressor, mixing chamber for fresh air and EGR gas, air-to-air charge air cooler, intake plenum and manifold, intake and exhaust valves, and the dynamics for each of these control elements. The integrated model could provide a rich development environment in which control strategies can be developed and tested. This could provide much better control than a conventional control method [26, 27]. Therefore, it is clear that model-based control methods can improve heavy-duty diesel engine performance and emissions, and will find more and more applications in the future.

8.3.6 On-board diagnosis

The OBD system can quickly detect malfunctions in the emission control system to reduce the time over which increased emissions are produced prior to repair. The OBD regulations in the United States and Europe are used to monitor the emissions control systems for gasoline, diesel and alternative-fueled engines for passenger cars, light-duty trucks and medium-duty vehicles. Although the OBD regulations do not apply to heavy-duty diesel engines at the present time, they will find more and more applications in the future [28, 29]. Even today, some component monitoring sensors, such as coolant and intake manifold temperature diagnosis, are needed to control engine performance and emissions.

8.3.7 CO_2 reduction

In order to help fight climate change, the United States and the European Union are establishing CO_2 emissions regulations for heavy-duty diesel engines. For the reduction of CO_2 emissions, the principal strategy is to reduce fuel consumption through improvements in engine performance, since the carbon content in the fuel is the main source of CO_2 production.

Biodiesel fuel has attracted much attention as a carbon-neutral fuel, and it is desirable to use it for CO_2 reduction [30]. Therefore, another method of reducing CO_2 emissions is through the increased use of biodiesel fuel, which is a biodegradable, non-toxic, clean-burning fuel made from algae, vegetable oils, animal fats, and recycled restaurant greases [31]. These resources are abundant and renewable. Compared to conventional diesel fuel, the fuel-borne oxygen in biodiesel fuels, which could be over 10% by mass, is capable of reducing engine-out emissions of PM, CO, and unburned HC in modern heavy-duty diesel engines [32].

Improvements in the efficiency of vehicle components, such as tires and air-conditioning systems, can also reduce CO_2 emissions [1]. In addition, LNT is an HC type of NO_x adsorber. In general, it needs a late post-fuel injection to obtain HC and CO as reductant during rich mode operation. In

comparison with the LNT system, the SCR system uses urea as reductant, which reduces fuel consumption and hence CO_2 emissions.

8.4 Summary

In this chapter, different stringent emissions standards used and to be used for heavy-duty diesel engines in different countries have been discussed. The main features of the latest heavy-duty diesel engines in the United States and Europe are overviewed, including cylinder head design, and the development of the combustion system, turbocharger system, EGR system, diesel fuel injection system, electronic control, and after-treatment systems. Future technological trends for NO_x, PM, and CO_2 emissions reduction strategies are prospected in heavy-duty diesel engines throughout the world.

8.5 References

1. Charlton, S.J., 'Developing diesel engines to meet ultra-low emission standards', SAE paper 2005-01-3628, 2005.
2. US EPA, 'Code of federal regulations (CFR)', Title 40, Part 86, Section 86.1 to 86.599-99, Protection of Environment, Office of Federal Register, 2007.
3. Hower, M.J. and Yan, J., 'Design and development of International® 6.0 liter V8 modern diesel engine', International Symposium on IC Engine, Shanghai, 2004.
4. Heywood, J.B., *Internal Combustion Engine Fundamentals*, McGraw-Hill, New York, 1988.
5. Watson, N. and Janota, M.S., *Turbocharging the Internal Combustion Engine*, Macmillan, London, 1982.
6. Zhu, Y. *et al.*, 'Combustion development of the new International® 6.0L V8 diesel engine', SAE paper 2004-01-1404, 2004.
7. Bauer, H., Diesel Engine Management, Robert Bosch GmbH, Stuttgart, 1999.
8. Bergstrand, P., 'The effects of orifice shape on diesel combustion', SAE paper 2004-01-2920, 2004.
9. Genzale, C.L., *et al.*, 'A computational investigation into the effects of spray targeting, bowl geometry and swirl ratio for low-temperature combustion in a heavy-duty diesel engine', SAE paper 2007-01-0119, 2007.
10. Alriksson, M., *et al.*, 'The effect of charge air and fuel injection parameters on combustion with high levels of EGR in a HDDI single cylinder diesel engine', SAE paper 2007-01-0914, 2007.
11. Heck, R.M. and Farrauto, R.J., *Catalytic Air Pollution Control*, Wiley, New York, 2002.
12. Zelenka, P., *et al.*, 'Ways toward the clean heavy-duty diesel', SAE paper 900602, 1990.
13. Floerchinger, P., *et al.*, 'Comparative analysis of different heavy-duty diesel oxidation catalysts configurations', SAE paper 2004-01-1419, 2004.
14. Eilyan, Y., *et al.*, 'Model for control of combustion in a piston engine', SAE paper 2006-01-0401, 2006.
15. Zhao, F., *Homogeneous Charge Compression Ignition (HCCI) Engines*, SAE International, 2003.

16. Ehleskog, R., *et al.*, 'Effects of multiple injections on engine-out emission level including particulate mass from an HSDI diesel engine', SAE paper 2007-01-0910, 2007.
17. Desantes, J.M., 'A comprehensive study of diesel combustion and emissions with post-injection', SAE paper 2007-01-0915, 2007.
18. Walker, A.P., *et al.*, 'The development and performance of the compact SCR-trap system: a 4-way diesel emission control system', SAE paper 2003-01-0778, 2003.
19. Havenith, C. and Verbeek, R.P., 'Transient performance of a urea DeNO$_x$ catalyst for low emissions heavy-duty diesel engines', SAE paper 970185, 1997.
20. Miller, W.R., *et al.*, 'The development of urea-SCR technology for US heavy-duty trucks', SAE paper 2000-01-0190, 2000.
21. Block, M.C., *et al.*, 'An investigation into the emissions reduction performance of an SCR system over two years' in-use heavy-duty vehicle operation', SAE paper 2005-01-1861, 2005.
22. Cobb, D., *et al.*, 'Application of selective catalytic reduction (SCR) technology for NO$_x$ reduction from refinery combustion sources', *Environmental Progress*, Vol. 10, pp. 49–59, 1991.
23. Hirata, K., Masaki, N., Ueno, H. and Akagawa, H., 'Development of urea-SCR system for a heavy-duty commercial vehicle', SAE paper 2005-01-1960, 2005.
24. Hinz, A., *et al.*, 'The application of a NO$_x$ absorber catalyst system on a heavy-duty diesel engine', SAE paper 2005-01-1084, 2005.
25. Huff, S., *et al.*, 'In-cylinder regeneration of lean NO$_x$ trap catalysts using low temperature combustion', SAE paper 2006-01-1416, 2006.
26. Ammann, M., *et al.*, 'Model-based control of the VGT and EGR in a turbocharged common-rail diesel engine: theory and passenger car implementation', SAE paper 2003-01-0357, 2003.
27. Park, S., *et al.*, 'Model-based development of engine control system from concept to vehicle', SAE eaper 2006-01-0856, 2006.
28. Peyton-Jones, J.C., *et al.*, 'A novel approach to catalyst OBD', SAE paper 2005-01-0024, 2005.
29. Song, G., *et al.*, 'Real-time diagnosis system development of common rail diesel based on expert system', SAE paper 2005-01-0031, 2005.
30. Shiotani, H., *et al.*, 'Studies of fuel properties and oxidation stability of biodiesel fuel', SAE paper 2007-01-0073, 2007.
31. Li, G., *et al.*, 'Experimental study of biodiesel spray and combustion characteristics', SAE paper 2006-01-3250, 2006.
32. Zheng, M., *et al.*, 'Influence of biosiesel fuel on diesel engine performance and emissions in low-temperature combustion', SAE paper 2006-01-3281, 2006.

9

Fuel injection systems for heavy-duty diesel engines

P. J. G. DINGLE, Delphi Diesel Systems, USA

Abstract: Currently, several different fuel injection systems are available in the heavy duty sector. Perspective is therefore provided on the industry drivers that each system must address, and a full discussion of the differentiating features between the systems is given. Industry trends are reviewed including the prevailing shift toward high-pressure common rail systems of either the conventional block pump or the distributed pump architecture. Some discussion of the future trends with respect to advanced combustion strategies, alternative fuels, and FIE trends in general is provided.

Key words: diesel engine, heavy-duty, fuel injection, common rail, unit injector.

9.1 Introduction

We should start by providing a working definition of heavy-duty in this context, since there are variations on a global basis depending on geographic region. Here, we are discussing fuel systems for engines that are generally used in commercial applications, both on-road and off-road, are heavier than 3500 kg, and are tested on an engine rather than a chassis dynamometer. Today, there are several different test cycles which may be applied regionally, but as we look forward through the twenty-first century, efforts to arrive at a common set of 'world harmonized' test cycles are beginning to find global acceptance. Examples are the World Harmonized Transient Cycle (WHTC), and the World Harmonized Steady-state Cycle (WHSC), both for on-road vehicles [1].

Within the broad category of heavy-duty engines, a further breakdown recognizes the sub-set of medium duty engines and these too are homologated on an engine dynamometer. In very general terms, medium duty engines occupy the cylinder displacement range from 0.75 to 1.5 L/cylinder, and heavy-heavy duty engines cover the range from 1.5 to 3 L/cylinder. A significant aspect is that heavy-duty engines are subject to a 435 000 mile (700 000 km) emissions warranty period, even though the time-between-overhaul (TBO) for heavy-duty engines in on-highway service is typically in excess of 750 000 miles (1 200 000 km). Note however that the impending On-Board Diagnostic (OBD) regulations will require such watchdog systems to be

functional for the actual effective life of the engine, not just the emissions warranty period.

9.2 History of heavy-duty fuel injection equipment (FIE)

9.2.1 Mechanical fuel systems

The widespread introduction of 'solid injection', that is to say liquid-only injection systems, during the 1920s opened up the heavy-duty market to the compression ignition engine. Prior to that time, the prevailing air-blast injection systems resulted in engines that were unsuitable for automotive application on the grounds of bulk, weight, and low power density. So-called pump-line-nozzle (PLN) systems, which had an individual pumping element, high-pressure line, and injector per cylinder, quickly became the convention by the 1930s, albeit with some unit injectors particularly in North America, and this technology survived until well into the 1980s. Peak injection pressures slowly escalated from *ca* 300 bar in the 1920s up to 1200 bar in the 1980s, but for most of this period, efficient and reliable operation was the prime objective, not low emissions. A good perspective on this history is given in ref. [2].

9.2.2 Electronic fuel systems

Development progress in fast-acting solenoid actuators during the early 1980s made electronically controlled fuel injection systems possible; earlier actuators had neither the speed nor the precision to displace mechanical fueling systems in automotive applications. However, the impending requirement to reduce emissions from mobile sources gave impetus to actuator and associated control system development, since the flexibility and precision that electronic control afforded was highly desired. For example, injection timing control over the speed and load range has a strong effect upon exhaust emissions, and yet most heavy duty mechanical FIE (Fuel Injection Equipment) could not offer this feature until the introduction of electronic controls. Early adopters of such controls include Detroit Diesel on the Series 60 engine in 1987, and Caterpillar on the 3176 in 1988, in both cases applied to unit injector FIE.

9.3 Current choices of fuel injection equipment (FIE)

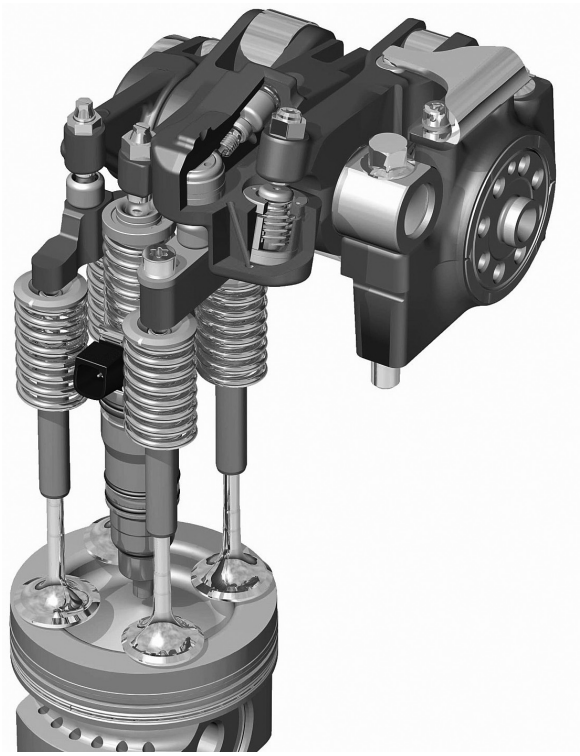
In this section, a brief discussion of the presently available types of FIE is given, to be followed later by a more detailed examination of each. First,

though, we should look at the industry imperatives that have dictated the type and form of FIE that is common in this market sector.

9.3.1 Drivers

Multiple factors influence the choice and functionality of heavy-duty FIE, but they may be summarized as follows:

- Functionality that makes it possible for the engine to meet the legislated emissions. These include factors such as peak injection pressure, mean effective injection pressure, flexible control of injection timing, ability to deliver multiple injections per cycle, control over the rate of injection, and the precision and consistency with which all of these features may be commanded.
- Features that permit attainment of highest fuel efficiency from the engine. In large measure, this comes down to the mechanical and hydraulic efficiency of the system. However, features that enable engine emission targets to be met without compromise will avoid the need for excessive injection timing retard and therefore the concomitant SFC penalty.
- Features that allow attainment of durability and reliability targets, which typically resolve from design, material, and manufacturing process aspects.
- Features that make the FIE conveniently adaptable to typical heavy-duty engine architectures. Today, those architectural variations involve either overhead cam or cam-in-block designs but in the future camless engines can be anticipated. Here it should be noted that the current paradigm for direct injection combustion systems, which has changed little since its introduction in the mid-1930s, comprises a vertically mounted injector on the cylinder axis with a multi-hole nozzle having a *ca* 150° included angle spray pattern cooperating with a central toroidal re-entrant bowl in the piston crown. The injector, being closely surrounded by four gas-exchange valves, typically results in a cylinder head design packaging challenge due to the need to also accommodate free-breathing ports and adequate coolant flow in an area subject to particularly high thermal loading and fatigue stresses (see Fig. 9.1).
- A supply channel that is not only quality and cost competitive, but forward-looking too. Once a supplier's FIE product has been homologated onto an engine, it becomes extremely expensive and inconvenient to homologate a new product or supplier if the superseded system does not have a logical successor. Additionally, in this age of the so-called 'global' engine which may be manufactured in many geographic regions, it is necessary for the injection system supplier to have a global scope to support their product worldwide.



9.1 Injector packaging in modern heavy duty diesel engine (from http://icp.llr.se/CumulusE_Z/VTC_ImageGallery/ image T2007_1748.tif).

9.3.2 Summary of FIE types

Of the mechanical FIE previously found on heavy-duty engines, the near ubiquitous in-line mono-block pump has essentially disappeared, and only electronically controlled versions of the cam-driven unit injector and unit pump have survived. The reasons for this outcome are due to inherent robustness and durability of the EUI architecture, high injection pressure capability, and ease of adaptation to electronic control. Additionally, the mechanical efficiency is quite high, and this resolves to good fuel economy which is a prime requirement of the end user.

The so-called HEUI (Hydraulic Electronic Unit Injector), while retaining some similarity to the unit injector, is also significantly different in that it is not 'cam-driven' in the conventional sense. First developed to production status by the Caterpillar Fuel Systems Group in the early 1990s, the concept of hydraulic intensification internal to the injector brought high-pressure injection capability to medium and heavy-duty engines without requiring extensive redesign to the camshaft and its drive mechanism. Providing an

engine-driven hydraulic pump and a *ca* 240 bar gallery in the cylinder head to feed the injectors is an easier and lower-cost solution for medium-duty on-highway and heavy-duty non-road engines than is an engine redesign for EUI [3].

The second non-cam-driven injection system which is rapidly gaining ground in the heavy-duty field is the high-pressure common rail system (HPCR). Here we are referring to a heavy-duty version of the system architecture that has become dominant in the light-duty automotive market, specifically one in which an engine-driven pump raises the fuel pressure up to the desired level for injection, and accumulates this fuel in a common gallery from which the individual injectors may draw. A pressure intensifier may or may not be featured in the injector.

9.4 Detailed fuel injection equipment (FIE) descriptions

9.4.1 The electronic unit injector (EUI)

At this time, the EUI may be considered the dominant fuel injection system in the heavy-duty sector, in large part due to its ability to address the industry imperatives listed above. It is a logical development of the earlier mechanical unit injector and thus has a well-respected pedigree within the industry. The fundamental feature of the unit injector, as its name implies, is that the essential aspects of any fuel injection system, that is to say the pressure generation, the quantity metering, the injection timing control, and the fuel dispersion into the combustion chamber, are all embodied in a single module (see Fig. 9.2) as opposed to three of the previous PLN systems or even the common rail. This single-module-per-cylinder approach offers distinct advantages particularly with respect to service diagnostics, but also means that the unit injector is more closely integrated into the base engine design than in any other system, which arguably makes it less of a commodity than other less integrated injectors.

By virtue of its compact construction, the unit injector has low internal hydraulic dead volumes relative to other systems, and this makes it both easier and more efficient to generate very high injection pressures. This ability is of course an attribute that is highly prized among the technologies used to reduce exhaust emissions, especially particulate matter (PM). Generation of high injection pressure in a ‘jerk’ type system requires a stiff drive, and for this reason the unit injector is typically applied to an overhead cam (OHC) engine (see Fig. 9.3), wherein a dedicated cam lobe per cylinder actuates a rocker that displaces the pumping plunger. The resulting hydraulic pressure generated below the plunger is reacted through the injector as an impulsive load into the cylinder head fire deck and thus back to the camshaft. A

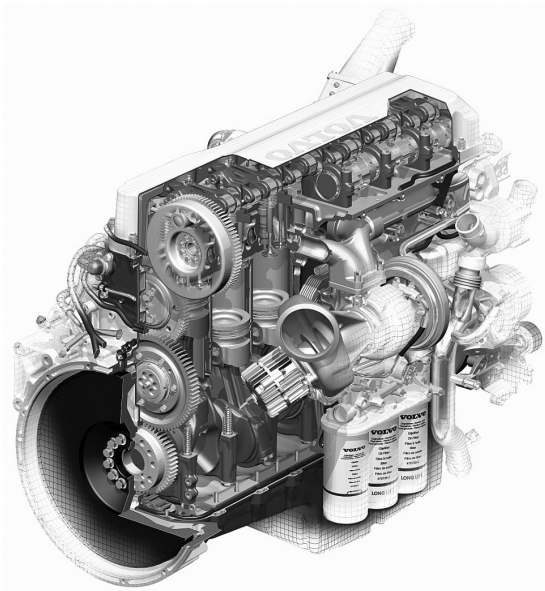


9.2 Electronic unit injector – Delphi E3 (Delphi image # IDC0507-19118).

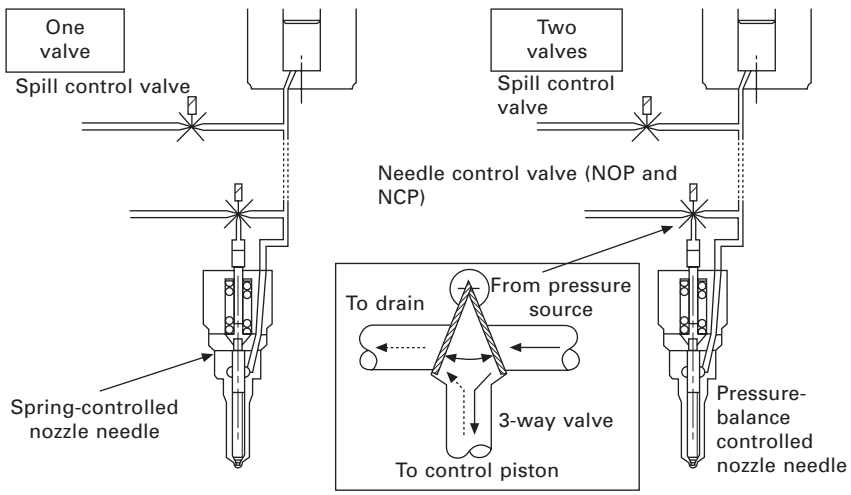
representative value for mechanical stiffness of this drive arrangement may be taken to be *ca* 19000 N/mm.

The unit injector may be characterized in several ways, for example it is a cam-driven positive-displacement pumping system in which the fuel delivery from the nozzle is closely related to the plunger displacement during the injection period. This is so because of the high degree of system stiffness, and as a result, cam rotational angle in conjunction with a constant velocity cam profile is normally used to calculate the delivered fuel quantity, since the plunger displacement will be known from the crankshaft position signal. This control technique works well with the conventional 'single-valve' EUI, but more sophistication is required for metering control of the 'two-valve' EUI systems to be described shortly.

Figure 9.4 schematically illustrates that EUI technology may be subdivided into single-valve or two-valve designs, referring to the number of control valves that are incorporated. Single-valve systems were prevalent from 1987



9.3 Overhead cam timing drive (courtesy of Volvo Powertrain from http://icp.llr.se/CumulusE_Z/VTC_ImageGallery/ image T2008_1564.tif).



9.4 Comparison schematics for mono and two-valve FIE.

through 2006, but the stringency of the on-highway emission requirements dictated the use of the more sophisticated two-valve FIE thereafter.

Although well known, a brief description of single-valve EUI operation will be given here. The three main modules of the EUI are the pumping

plunger, the normally open spill valve (SV), and the spring-controlled nozzle. Displacement of the pumping plunger is immutably driven by the cam and rocker mechanism and the fuel thus displaced is discharged at low-pressure back to the tank through the normally open spill valve. When an injection event is required, the spill valve actuator, commanded by the ECU (electronic control unit), closes the valve, thus terminating the spill so that the high-pressure volume within the injector is now subject to a rapid pressure ramp-up. Nozzle spring preload is typically set to give nozzle opening at *ca* 300 bar, at which pressure the injection event commences. It will be appreciated that the point at which the spill valve is energized controls the timing of the start of injection, and the duration of valve closure determines the delivered fuel quantity, this being essentially a function of plunger displacement during that time period. At the end of injection, the SV actuator is de-energized and a rapid depressurization occurs, allowing the nozzle spring to re-seat the needle. It is the disturbances caused by the depressurization that make close-coupled multiple injections problematic with single-valve systems, since the filling pressure stability upon which consistent operation depends is not present under these circumstances.

Owing to the high mechanical and hydraulic stiffness of the single-valve EUI, the characteristic injection pressure and injection rate profile is triangular, in which it gradually rises to a peak followed by a rapid pressure decay when the spill valve opens. This rising rate profile has been shown to be a good match with the requirements of conventional diffusion diesel combustion, wherein the objective has been to initiate combustion with a minimal premixed portion, followed by an injection rate that is as high as the resulting mixing-controlled conflagration can support. This optimized combustion coupled with the inherently high mechanical efficiency resulted in particularly good thermal and therefore fuel efficiency for the engines thus equipped.

9.4.2 Two-valve systems

As emission standards tightened, it became necessary to lower peak combustion flame temperatures through the addition of a diluent, principally EGR, to bring NO_x emissions into compliance. Given the imperative of maintaining or increasing engine power density, the addition of EGR over and above the necessary oxygen for complete combustion will result in the need for higher boost pressures and therefore higher in-cylinder air densities at the point of injection. Moreover, the effect of a diluent is to slow down the rate of burning, and these two factors require a re-optimization of the combustion system. To counter the effects of EGR, higher injection pressures are required, and square injection rate profiles are necessary to increase the fuel/air mixing rate while still keeping within the typical 30 crank degrees injection duration window at full load. Additionally, pilot injection would

be helpful to mitigate the high combustion pressure rise rates that the new strategies bring.

Increasing injection pressure ratings of FIE is largely an extension of the design, materials and process developments that the system suppliers have faced for several decades now, but changing the injection rate profile and enabling multiple injections requires a more fundamental change. Now it so happens that so-called pressure/time metered injection systems such as common rail naturally provide square injection rate diagrams, and so adapting aspects of that technology becomes a logical path to follow for the EUI.

As observed in Fig. 9.4, for two-valve systems, a nozzle needle control valve (NCV) is added in conjunction with a pressure-backing piston located above the needle in a manner very similar to some common rail injectors. The NCV may be either a two-way valve, or a three-way valve in which case, in its deactivated default position, internal system pressure after the spill valve has closed will act on both the backing piston, to assist loading the needle onto its seat, as well as the needle differential area, attempting to lift the needle from its seat. However, the resulting force balance resolves in favor of the nozzle preload spring (if fitted) plus the backing pressure to thus hold the needle closed against its seat. When energized, the NCV changes state by isolating the pressure backing chamber from the system pressure and connecting it to drain. The force balance is now changed such that the system pressure acting on the needle differential area exceeds the spring preload, resulting in needle lift and an injection event. Because of the close proximity of the NCV to the nozzle and the small hydraulic volumes involved, the switching time for this servo mechanism is very fast, permitting the adoption of multiple injection strategies, as is the case for common rail systems.

By adding this feature to the EUI, its functionality is enhanced over the previous single-valve version in multiple ways:

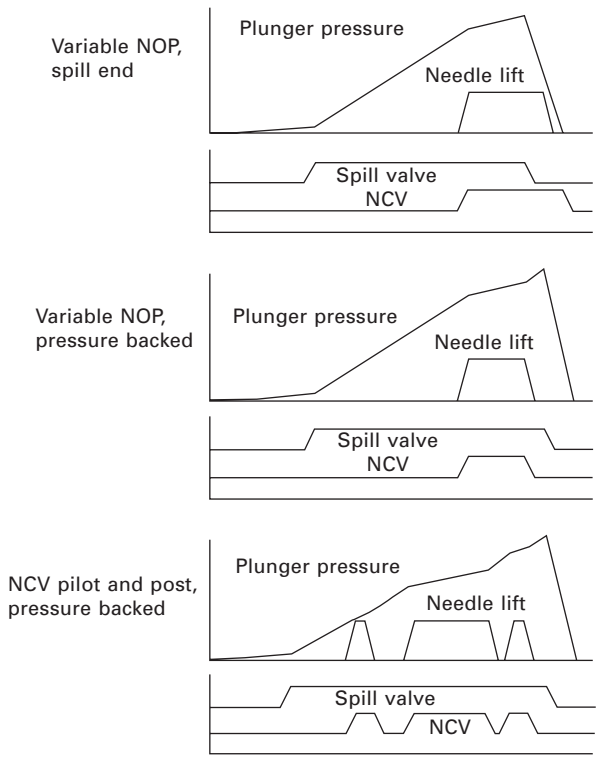
- It enables multiple injections within a single cycle.
- It enables control over the nozzle opening pressure (NOP) and nozzle closing pressure (NCP).
- It provides this pressure control on a shot-to-shot and cycle-to-cycle basis.
- It provides flexibility in injection rate profile, square or triangular.
- It provides flexibility in injection rate amplitude, low to high.
- It enables control over nozzle opening and closing velocity.

This broad combination of attributes provides great flexibility to the calibration process in current engines, enabling different combustion strategies to be adopted in different regions of the speed and load map, as appropriate. Some of these strategies are discussed in refs [4] and [5], in both cases applied to the Delphi E3 injector. Note, however, that the injection schedule can only

occupy the crank angle window where a cam lobe exists, and ideally only during that constant velocity portion around mid-lift. In practice, such systems are limited to a maximum of three injections, typically pilot, main and close post (see Fig. 9.5), unless a multi-lobe profile is used. This represents a distinct limitation where late post-injections or advanced premixed combustion cycles are contemplated, since these require injection events outside this narrow range around TDC. Further, the drive system loadings incurred in generating the high injection pressures, and the unloading that occurs upon spill, create strong perturbations in the cam drive, leading to issues of high NVH (noise, vibration, harshness) which can require expensive countermeasures.

9.4.3 The electronic unit pump (EUP)

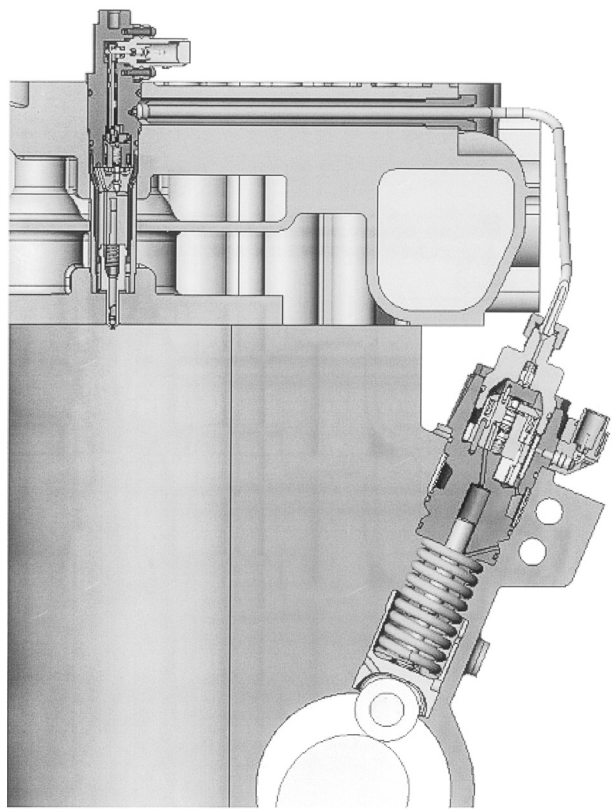
The EUP is a close cousin of the EUI in that it, too, is a cam-driven injection system sharing several common features but packaged in a different way. Whereas EUI requires an overhead camshaft with an expensive and robust drive train extending from crankshaft to cylinder head, the EUP is applied to engines of more conventional construction with the camshaft in the



9.5 Schematic illustration of two-valve injection flexibility.

cylinder block. In this paradigm, the EUP pumping plunger and spill valve assembly are in one module that bolts to the cylinder block with a roller tappet interposed between the cam and plunger as seen in Fig. 9.6. This makes for a very stiff load path, but it will be recognized that because of its direct acting nature, the cam lift and the pumping stroke must perforce be identical, whereas with EUI the rocker ratio permits a smaller cam lift and thus camshaft diameter. With EUP, a relatively short high-pressure pipe connects the pump module to the injector, which is conventionally mounted in the cylinder head (see Fig. 9.7).

As for EUI, the EUP may also be configured as a single-valve or a two-valve system. For the same emissions-driven reasons as given above, heavy-duty on-highway engines with EUP technology moved to the two-valve construction for the 2007 model year. For these engines, the legacy spring-controlled mechanical injector is replaced with one incorporating the NCV servo mechanism. While functionally similar to a common rail injector, these so-called 'smart' injectors (Fig. 9.8) are validated for the higher injection



9.6 Electronic unit pump with roller tappet (Delphi image).



9.7 Electronic unit pump installation (Delphi image IDC0808-29936).



9.8 Electronically controlled ‘smart’ injector (Delphi image IDC0507-19114).

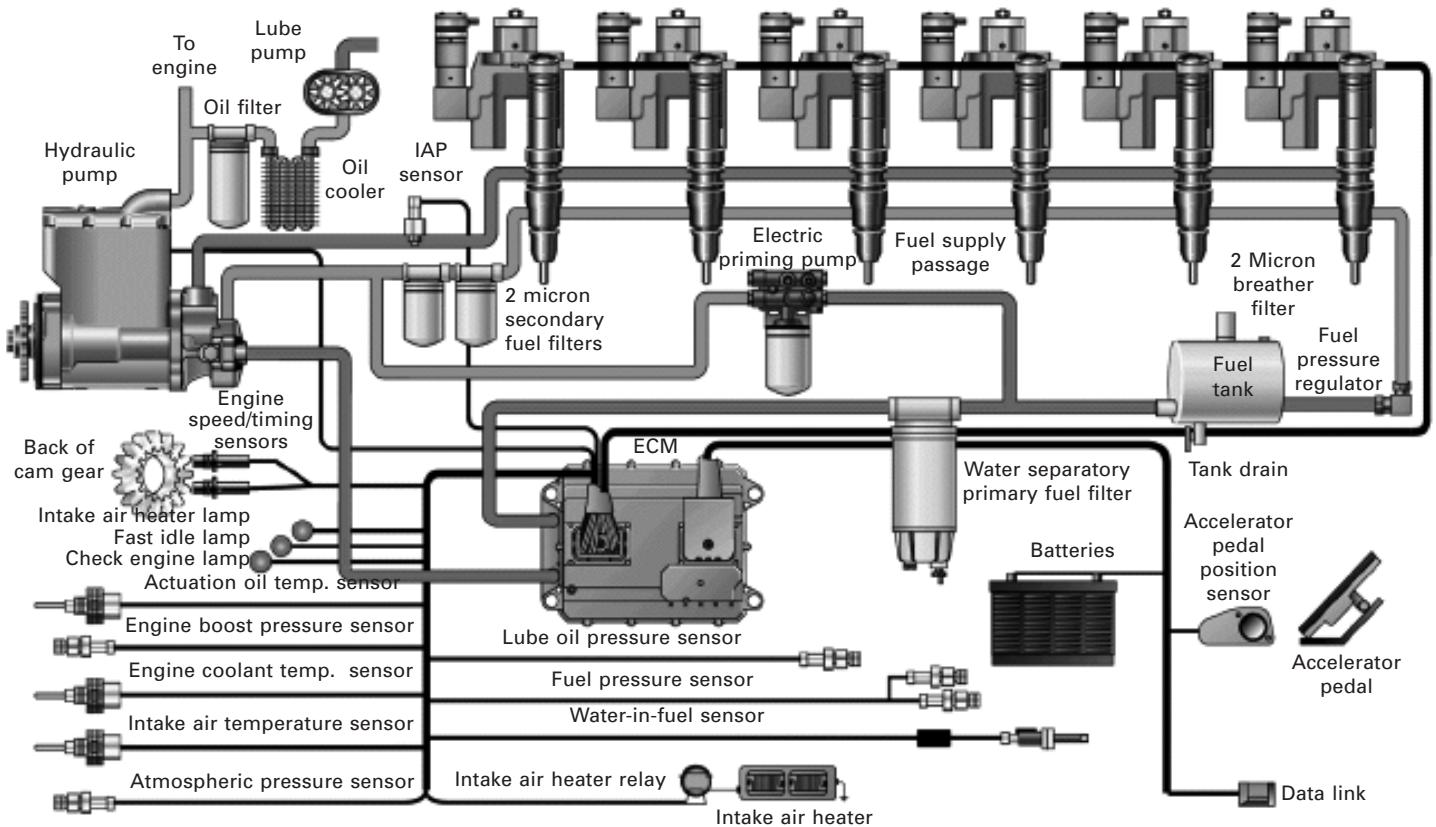
pressures of which the EUP is capable, typically on the order of 2200 bar or greater.

9.4.4 The hydraulic electronic unit injector (HEUI)

The HEUI may be viewed as a hybrid between the unit injector as its name implies in that the pumping element is in unit with the nozzle, and the common rail system in that it too is not directly cam driven and the control element is located at the injector. In this architecture, hydraulic pressure in which the fluid may be lubricating oil, hydraulic oil, or fuel is raised to an intermediate pressure of *ca* 240 bar by an engine-driven pump and is supplied to a gallery that is adjacent to the injectors in the cylinder head (see Fig. 9.9). Here, jumper pipes convey the fluid to a solenoid-actuated, normally closed control valve in the injector and also to a pressure-backing piston above the nozzle needle; thus in the default condition between injections, the needle is held on its seat by both NOP spring load and the backing pressure.

Both single and two-actuator versions of the HEUI architecture are possible, but in this description we will assume a two-actuator (two-valve) embodiment. Immediately prior to an injection event, the intensifier control valve is opened, which admits rail pressure to the intensifier piston. This large-diameter piston is directly linked in series to the smaller pumping plunger, and thus the rail pressure acting on the intensifier piston generates a force that is transmitted directly to the pumping plunger, which in turn produces a greater pressure on the nozzle side that is in exact proportion to the area ratio between them. Thus, for example, an area ratio of 10:1 between the two pistons will in theory produce an injection pressure of 2000 bar when the rail pressure is ~200 bar. Irrespective of the fluid type that is employed on the low-pressure side of the intensifier, fuel will be used on the high-pressure side, and this volume between pumping chamber and nozzle will now be pressurized to a multiple of rail pressure. While single-stage intensification has appeared in several production systems, the feasibility of multi-stage intensification as disclosed in ref. [6] has been demonstrated.

As for the two-valve EUI described above, and given a sufficiently responsive NCV, multiple injections are available until such time as the pumping plunger has exhausted its stroke. It will be appreciated that with this system, injection pressure and therefore rate are controlled by modulating the rail pressure, and injection timing and multiple injections from operation of the NCV. Since over the duration of a combustion cycle the injection pressure is substantially constant, the behavior of the system is similar to that of the high-pressure common rail in which fuel quantity control is derived on a pressure/time basis, even though constructionally it has greater similarity to a unit injector; in the latter case, however, the plunger moves at a constant velocity and not under a constant pressure as for HEUI.



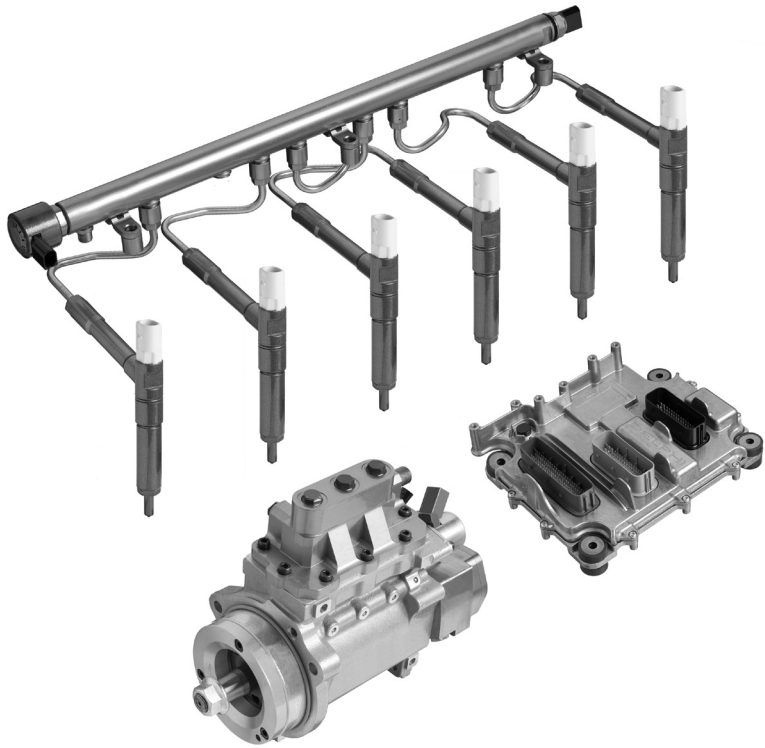
9.9 HEUI system architecture (Caterpillar image).

In 2008, Bosch introduced an injection system for heavy-duty engines originally termed APCRS (for accumulator piston common rail system) but now identified as CRSN4.2. This system may be considered a hybrid between HEUI and HPCRS in that there is amplification within the injector while the HP pump and rail operate in the range of 300 to 900 bar, but on fuel, not on engine lubricating oil. As well as a needle control valve in the injector, there is also a control valve that activates or deactivates the amplifier piston. With this arrangement it is possible to make low-pressure injections direct from the rail, followed by high-pressure injections up to *ca* 2100 bar with the amplifier activated [7]. Growth in these pressure ratings is anticipated in the future as higher diluent levels are used to combat the higher NO_x reduction targets for Euro VI.

9.4.5 High-pressure common rail (HPCR)

Although typically referred to as simply 'common rail', it is necessary to prepend the descriptor 'high pressure' to differentiate the system from gasoline port fuel injection (PFI) operating with a rail pressure of *ca* 3 bar, from gasoline direct injection (GDI) operating at *ca* 200 bar pressure, or even from HEUI as described above with its intermediate pressure rail. Architecturally, diesel common rail is similar to GDI in that there is an engine-driven pump that raises the fuel pressure in a single stage up to the desired value for direct injection into the cylinder, a fuel rail in which that pressure is accumulated, and an injector having control over the injection timing and duration and therefore the delivered fuel quantity. One, or in some cases two, high-pressure pipes connect the pump to the rail (or rails in a multi-bank engine) which is usually mounted adjacent to the cylinder head, and then individual jumper pipes connect the rail to the injectors, as may be observed in Fig. 9.10.

How does common rail FIE address the requirements of the modern heavy duty engine? The fundamental injection rate profile is essentially square, which as noted before is favorable for combustion systems employing high EGR as most future systems are expected to do. Fuel metering is achieved on a pressure versus time basis in which a known rail pressure is exposed to a known nozzle orifice flow area for a known duration as determined by the ECU for the particular operating condition. This results in a robust control of fuel delivery, although variation in fuel viscosity will have effects that are not normally compensated for. Rail pressure stability is an important issue for pressure/time metered systems and this is relatively easy to achieve under single shot-per-cycle operation, but it can be problematic to attain during a train of multiple injections. Flexibility of injection rate through rail pressure control is important, as is the ability to deliver multiple injections on demand and particularly well-controlled small pilot and early injections for advanced combustion strategies.



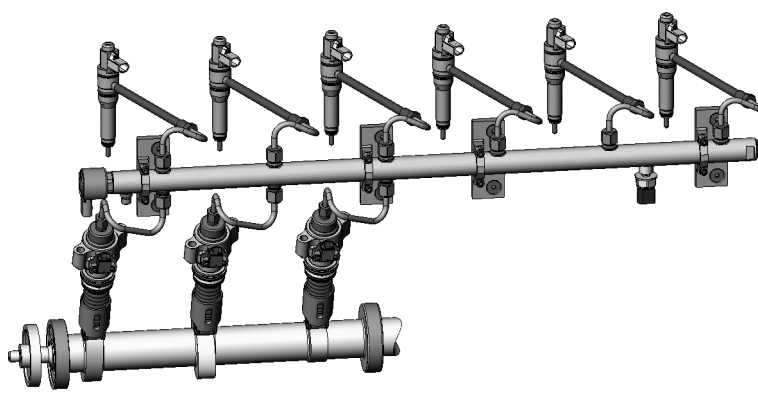
9.10 High-pressure common rail system for heavy duty applications (Delphi image IDC0808-29942).

In the light-duty arena, common rail system architecture is well established and relatively stable, but the priorities for heavy-duty are different and thus the solutions may be different too. The concept of a fuel lubricated multi-plunger high-pressure pump to charge the rail may carry over from light duty to medium and light heavy-duty engines, but other solutions may be more appropriate for *ca* 2-liter/cylinder engines. Quite apart from the fundamental difference in greatly enhanced durability expectations for the HD engine, there is also the fact that it is not unusual for such engines to remain in production for 20 or 30 years during which time two or three different fuel injection systems may be specified. Thus a neat packaging solution must be found to adapt common rail to an engine originally designed for perhaps EUI or EUP, and such systems are in fact available from Delphi who have adapted their previous generation systems to provide a seamless transition.

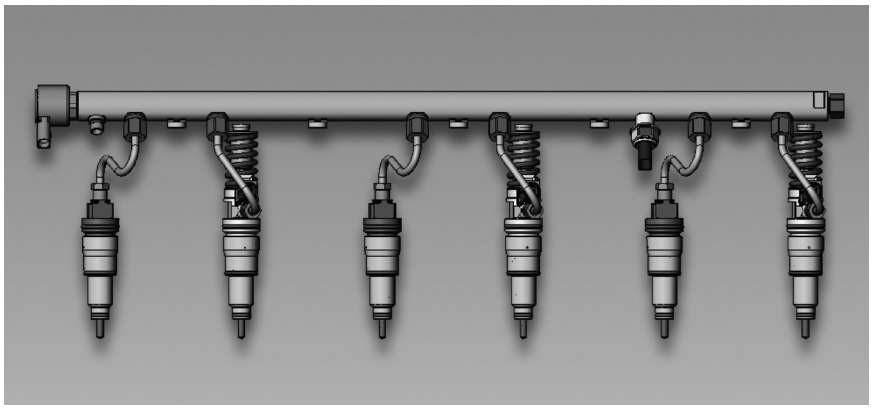
In such an adaptation on, for example, an EUP engine, instead of one electronic unit pump per cylinder, there may be only three in all, but each of these pumps charges the rail with pressurized fuel. Individual jumper

pipes conduct this fuel to the electronically controlled injectors in the normal manner. Beyond the addition of the fuel accumulation rail adjacent to the cylinder head, the other change to the base engine is that the injection cam is changed from a single high-velocity 'jerk' profile that is timed to the combustion event to a two- or three-lobe cam with a lower velocity profile in which the whole of the cam lift may be used with the exception of the nose radius. Relative to the limited effective stroke of current jerk-type pumps, this new arrangement allows greater pumping efficiency which, along with potentially more pumping events per engine revolution, enables the use of plungers with a smaller diameter to deliver the required fuel demand. In turn, the smaller diameter plunger allows higher pressures to be developed while keeping within the Hertzian stress limits of the cam and roller interface than previously was the case. Thus rail pressures of 3000 bar or greater can now be contemplated for the future. Rail pressure managed by closed-loop control between the rail pressure sensor and the unit pump spill valve, which is arranged to prevent over-the-nose pumping, coupled with the lower cam velocity, results in improved mechanical NVH characteristics for this system (see Fig. 9.11).

A very similar architecture is available for engines previously equipped with EUI, but in this case while every cylinder has an injector, only alternate cylinders have a combined pump and injector in which the integrated cam-driven pump supplies the rail which then feeds all the injectors (see Fig. 9.12). The generic name for such systems having multiple high-pressure unit pumps is 'distributed common rail'. It will be recognized that in such systems the Hertzian stress-limited interface, which normally will occur between the cam and the roller, is located within the crankcase oil-lubricated zone and thus operates under favorable conditions. This may be compared with conventional fuel-lubricated high-pressure pumps in which the tribology-



9.11 Distributed unit pump common rail system (Delphi image).



9.12 Distributed unit injector common rail system (Delphi image IDC0808-29943).

Table 9.1 Summary of current heavy duty FIE

Manufacturer	Designation	Type	P_{max} (bar)	Application
Bosch	CRSN-4.2	Amplified common rail	2100	Daimler
Cummins	XPI	HPCRS	2400	Scania
Delphi	E3P	2-valve EUP	2200	DAF
Delphi	E3	2-valve EUI	2500	Volvo

limited interface has to be designed to accommodate the lower and wider variation in lubricity of current and future fuels.

Table 9.1 provides a summary of several representative heavy-duty fuel injection systems that are currently available. Distributed pump-type systems as discussed above have not been included since they are not yet widely available.

9.5 Nozzle developments

Direct injection combustion systems today invariably use multi-hole nozzles of the type illustrated in Fig. 9.13, although that has not always been the case in the past. The atomizing nozzle is the one aspect of all the foregoing injection systems that remains essentially common; there may be subtle differences between the nozzles from different manufacturers, but the function remains the same. It is responsible for the presentation of the fuel to the air in the combustion chamber, and as such it arguably plays the most important role of any aspect of the whole injection system.

It is necessary for the nozzle spray geometry to cooperate with the combustion chamber shape and the induced air motion at the time of injection,



9.13 Multi-hole nozzle (sectioned) (Delphi image).

and in achieving this match there are several application variables that may be manipulated. Among these are the number of spray holes, their angle relative to the nozzle axis, their hydraulic flow characteristics, and the sac type. In general terms, a quiescent chamber will require more spray holes than a medium or high swirl chamber, the included spray cone angle for a conventional combustion system is around 150°, and the steady-state flow value for a typical 2-liter cylinder will be approximately 1.5 L/minute under the ISO conditions of 100 bar supply pressure.

A feature of the DI nozzle is that the primary needle guide is remote from the valve seat and therefore the spray sac, and even though manufactured to extremely close tolerances, the valve end of the needle can unintentionally move laterally, giving rise to undesirable effects. Particularly noticeable with VCO nozzles, this lateral motion can obscure fuel flow to one or more of the spray orifices, leading to preferential flow to the other holes and thus an uneven distribution of fuel into the combustion chamber. Since modern chambers are symmetrical in layout, this maldistribution can result in emission problems. For this reason, modern nozzles frequently have a double or extended guide geometry to minimize this lateral motion.

Driven by more stringent emission legislation and by continued growth in engine durability expectations, there have been significant developments in nozzle manufacture and particularly in the area of the orifice geometry. In

the 1990s, some engines, particularly urban buses, used valve-covers-orifice (VCO) nozzles in which the drillings emanated from the valve seat area, and by so doing residual fuel from the sac was inhibited from weeping into the combustion chamber during the exhaust stroke, which otherwise would result in high HC and aldehyde emissions. As the sophistication of nozzle manufacture improved, the mini-sac nozzle was able to demonstrate very low HC emissions also, and superior engine performance due to the better flow regime in the sac resulted in well-formed sprays with higher momentum. As engine boost levels increase, spray momentum and liquid core penetration assume greater importance, since competitive power density requires high air utilization, while atomization remains important in achieving uniform fuel/air mixing, particularly under high diluent conditions or where premixed combustion is adopted [8].

Problems of cavitation erosion internal to the nozzle spray orifices have been largely overcome by manufacturing techniques such as abrasive paste honing that modify the hole entry condition through the formation of a radius internal to the sac and by creating a hole that is larger at the entry than at the exit. This tapered hole geometry is categorized by a *K*-factor value in which $K = D_1 - D_2/10$, where D_1 is the hole entry diameter and D_2 is the exit diameter (μm), thus a *K*-factor of 1.5 indicates that the entry diameter is 15 μm larger than the exit. The combination of tapered hole geometry with rounded entry conditions can be expected to provide enhanced coefficient of discharge (CD) values that deliver a better match of spray performance to the requirements of modern high-diluent combustion systems. Additionally, the abrasive machining used to form the radiused hole entry conditions also polishes the internal passages subject to high pressure and in so doing raises the peak pressure capability of the nozzle by removing stress risers.

9.6 Synergies with light-duty fuel injection equipment (FIE)

Diesel engines and therefore diesel FIE are to be found in almost all modes of transportation including all forms of marine, rail traction, on and off highway, and many industrial applications from base load generating capacity down to small sub-10 kW single cylinder units. However, the sophistication of the FIE technologies employed in each product segment is closely related to the stringency of the emissions targets that have to be met, and the prevailing NVH or sociability targets. This being the case, then it can be seen that, although there are significant differences between the two, both light-duty and heavy-duty engines have challenging emission and NVH targets that are currently well beyond those of the other sectors. Thus it is between these two groups that any synergies are likely to exist, and this subject has been examined in ref. [9]. Nevertheless, in the non-road sector, EPA Tier 4 Final

emission regulations scheduled to take effect in 2014 will bring near parity to on-road emissions, if not NVH expectations.

9.7 Future trends

In general, FIE developments follow the engine technology trends, but they in turn are largely driven by legislation and end-user requirements. There are different pathways and solutions for achieving these requirements in a manner that offers the lowest total cost of ownership (TCO) for the engine, in part because calculating the TCO is an inexact science. By way of example, heavy-duty engine manufacturers have not coalesced around a common strategy for meeting future legislated emissions, whereas a simple economic model would suggest that they should. Some manufacturers plan to meet future emission standards using very high levels of cooled EGR in conjunction with commensurately high levels of boost and injection pressures, while other manufacturers intend to employ exhaust aftertreatment in the form of SCR but with less aggressive levels of EGR, boost and injection pressure. Note, however, that the FIE manufacturer will be obliged to develop systems that are appropriate for all OEM customer demands.

9.7.1 Drivers for the future

The challenge of exhaust emissions reduction remains with us, and homologating to the legislated levels that are in force both temporally and geographically remains the price of entry into any given market. However, as we move further into the twenty-first century, it is apparent that energy efficiency and 'greenhouse' gas emissions, primarily CO_2, must also receive highly prioritized attention. CO_2 targets for light-duty vehicles in 2020 have been published and proposals for heavy-duty vehicles are presently under discussion. Normal market pressures within the heavy-duty sector already give preference to the most energy-efficient powertrain solution, but with global attention now focused on CO_2 reduction it can be expected that the level of capital funding and effort applied to efficiency improvement will deliver results that could not be funded from within the industry alone.

Without a doubt, FIE will have a role to play in this endeavor. The three obvious areas of focus are mechanical efficiency of the injection system, the ability to enable advanced combustion strategies, and the flexibility to handle alternative fuels. We shall now look at each of these features in turn.

Mechanical efficiency

Based on what we know today, the long-term trend for escalating peak injection pressure from the current 2500 bar benchmark will continue with

likely step increases to 2750 bar in 2010 and perhaps 3000 bar in 2014. The mechanical shaft power to generate these pressures is significant and thus the incentive to minimize fuel leakage from any source is intense. Already, several injection systems have specified so-called 'zero backleak nozzles' that by eliminating the conventional needle guide are able to avoid leakage from that source. Additionally, current injection systems utilize hydraulic servo mechanisms which, by their very function, depend on a hydraulic force imbalance acting upon the nozzle needle that, when switched, requires the control volume to be connected to a drain or return line. Thus for every injection event there is a release of pressurized fuel that represents a waste of energy. Additionally, this fuel, being hot, will need to be cooled prior to re-entrainment back into the low-pressure fuel circuit, and this places an unwelcome burden on the vehicle heat rejection system. Efforts are likely to be directed toward minimizing or eliminating this discharge, by for instance adopting an alternative nozzle valve actuation mechanism: see, for instance, ref. [10].

While ref. [10] discloses an advanced injector actuation approach that has eliminated the servo mechanism entirely and thus the need for backleak plumbing, for those systems that remain with a bipolar hydraulic servo mechanism the goal is to devise a system offering zero static leak. That is to say, for the long duration between injections there should be essentially no internal leakage at all because the system pressure is retained preferably only by one or more positive sealing valve seats with no reliance on a close clearance piston-in-bore for this function. This arrangement is now available in certain designs, as for instance in the Cummins XPI injector (Fig. 9.14) and the Ganser injector [11].

Advanced injection strategies

Conventional diffusion diesel combustion as exploited by the heavy-duty engine has demonstrably proved itself to be an efficient and durable energy conversion mechanism, but reaching extremely low engine-out exhaust emission levels has been challenging. Most engines today have adopted some level of exhaust aftertreatment, typically an oxidation catalyst for HC and CO, a diesel particulate filter (DPF), and increasingly an NO_x reduction strategy such as EGR, LNT or SCR. Very few emission reduction strategies, real-time water injection being a possible exception [12], avoid imposing a negative impact on fuel consumption and so there remains a strong incentive to refine the combustion process to achieve the engine-out emissions goal. This incentive will only be enhanced by the impending CO_2 reduction goals.

That some form of premixed combustion can provide very low levels of PM and NO_x engine-out emissions has been well established by many researchers (see, for example, ref. [13]). Manipulation of the combustion



9.14 Low leakage heavy-duty common rail injector (from http://imagebank.scania.com/indexie.jsp image 06718-001).

process to so steer the oxidizing fuel parcels through the relatively low temperature regions of the well-known local equivalence ratio/temperature map that they avoid the PM and NO_x islands is the generally recognized goal, and this objective is heavily mixing-dependant with reliance on FIE capability (as discussed below).

In achieving premixed combustion, there are two fundamental strategies. They may be characterized at a high level as early injection and late injection, and which one of the two is chosen can have a profound impact on the FIE.

If we ignore for the moment the apparent inability of conventional engines to tolerate premixed combustion at high BMEP, say greater than *ca* 10 bar, then early injection in the range of 180° to say 60° BTDC can provide a more nearly homogeneous mixture and potentially can operate at a relatively low injection pressure, since the time available for fuel/air mixing is extended. Conversely, late injection strategies in which the fuel is introduced around TDC require very high injection pressures, since the concept assumes that the fuel charge is injected and mixed during the ignition delay period of the first fuel parcel to enter the chamber. Reducing one or both of these concepts to a viable production strategy is still within the realm of advanced engineering groups at present, and the near-term practical solution is likely to be a form of multiple-mode combustion in which one or more premixed strategies is used at light loads, transitioning to diffusion combustion at high load.

Over the years, diesel fuel injection systems have been intensively developed to optimize diffusion combustion across the speed and load range. If we now introduce distinctly different strategies such as variants of premixed combustion at specific points in that speed and load range, we find that each strategy requires a different nozzle spray pattern and that it is difficult to provide the optimum characteristics for diffusion and premixed combustion in a single nozzle. Specifically, it will be appreciated that late injection near TDC into a dense high-pressure charge environment requires a highly penetrating spray that is able to approach the outer edge of the combustion bowl, whereas for an early injection the challenge is to avoid over-penetration which will result in wall wetting and lube oil dilution. Nevertheless, some low-level industry activity is being directed toward variable spray nozzles; see, for instance, ref. [14] due to Ricardo.

Additionally, so-called grouped-hole nozzles in which the total flow area is divided between two rows of injection holes are being actively studied; such nozzles offer a broader range of spray characteristics than are available from single-row nozzles. For instance, the interaction between adjacent spray plumes may be influenced by the position, spacing, and orientation of the holes. In general terms, dividing the total flow area between a greater number of smaller holes will improve the atomization, which is beneficial for rapid mixing but will also reduce the liquid core penetration of the individual plumes. However, the latter may be recovered without substantially degrading the former if top and bottom row plumes can be arranged to merge [15].

Some industry activity is also being directed toward development of variable flow area nozzles (VAN, or alternatively VON) in the quest for improved engine-out emissions from future high power density engines. For a traditional DI nozzle, the total orifice flow area will be sized to give a full load injection duration of around 30 crank degrees at the rated speed. This means that at part load the flow area is bigger than necessary and thus the atomization characteristics are sub-optimum. Therefore, a nozzle which

can be configured to dynamically match flow area to fuel flow in two or more discrete steps is expected to deliver an incremental emissions benefit. Achieving this functionality in a robust and cost-effective manner is an extremely challenging task which has occupied the industry for several decades now.

In exploiting advanced injection strategies, flexibility in terms of multiple injections, separation between injections, rate of injection profile, control over velocity of nozzle needle opening and closing, transient response to commanded injection pressure, and shot-to-shot consistency are highly valued. The advent of cylinder pressure-based engine management will permit closed-loop control of the combustion event which in turn will demand highly responsive injection systems. Design of the injection control valve and its actuator can have a critical impact on many of these parameters, particularly as system pressures rise, and a general move away from the widely used unbalanced valve toward the pressure-balanced control valve can be anticipated. This comment applies equally whether a two-way valve or a three-way valve is employed.

A further factor which will have a critical impact on future injection system selection is the anticipated advent of camless engines in which perhaps outward-opening gas exchange valves [16] are actuated by electro-hydraulic means alone. The incentive for this development is that several of the advanced combustion strategies being contemplated by the industry require flexibility of valve timing events that parallel the flexibility of injection events that have been enabled by common rail fuel systems. Thus it can be seen that an engine that has no need for a conventional camshaft must be specified with a non-cam-driven injection system.

Alternative fuels

In comparison to the second half of the twentieth century during which mineral-based diesel fuel emerged as the predominant transport fuel, the twenty-first century is likely to see a number of alternative fuels become popular in specific geographical regions as surging demand exceeds ready supply of conventional diesel fuel. Whereas in the past, world specifications coalesced around a relatively universal fuel for automotive compression ignition engines, the future availability of such fuel and indeed its appropriateness on carbon emission grounds is no longer assured. With the emergence of biofuels, including biodiesel, biomass to liquids (BTL), gas to liquids (GTL) and synthetic fuels including a resurgent Fischer–Tropsch, and the acceptance of mineral oil feedstocks that in the recent past would have been considered unsuitable, it is not clear that the future CI engine will have the luxury of operating over its whole life on fuels as narrowly specified as EN590 (Europe) and ASTM D975 (USA).

The implications of fuel variability on FIE design are many and varied but it should be recognized that several aspects of injection system performance are critically dependent on known values for parameters such as lubricity, viscosity, cetane number, heating value and CFPP (cold filter plugging point) [17]. As these values depart from the specified values around which the injection system was designed, issues arise that may cause customer complaint, reduced life expectancy or an in-use emissions compliance infraction. For example, the heating value for biodiesel is approximately 10% less than that of crude-derived diesel fuel, so depending on the blend ratio a loss of power may be detectable unless appropriate compensation is made. Further, the viscosity is significantly higher too and this can lead to a different NO_x emissions response, higher or lower, depending upon the type of FIE and other factors, and may result in over-penetration of the fuel spray, leading to undesirable wall impingement and lube oil dilution. Additionally, depending on the base feedstock, of which there is a wide variety [18], biodiesel blends generally exhibit a higher temperature for the CFPP point, which is likely to result in field service problems.

Today, engines are designed to use and are calibrated for one specific fuel, whereby a reference fuel normally exists for the emissions homologation tests. As alternative boutique fuels and blends proliferate, it becomes conceivable that engines may require more than one calibration stored in the ECU so that emissions compliance is maintained as far as possible as the available fuel varies.

These problems notwithstanding, the acceptance and approval by the engine OEMs of low biodiesel blends demonstrate that existing FIE can be adapted to operate on fuels that are not entirely compliant with EN590 or D975, though some future fuels will have characteristics that are beyond the scope of conventional FIE. Dimethyl ether (DME) would be an example of just such a fuel that is sufficiently different that a unique fuel system is required. The properties of DME are given in Table 9.2 where it will be seen that although its cetane rating and auto-ignition temperature make it a very good compression ignition fuel, there are other properties that require special handling and design features to make a practical system. Specifically, un-additized DME has very low lubricity (~1000 μm on the modified HFRR (high frequency reciprocating rig) test versus <460 μm for EN590) and low viscosity (~0.185 cSt versus ~3 cSt for EN590). Either of these properties makes DME incompatible with conventional FIE design and manufacturing norms, particularly with respect to meeting current durability targets. Additionally, the lower energy content requires larger fuel flow passages and nozzle orifices, and while common rail may be more appropriate than a cam-driven fuel system due to the low bulk modulus, the high flammability and low viscosity put a premium on low-leakage injector designs.

In the same way that mineral oil-based diesel engine fuels may be blended

Table 9.2 Fuel property comparison

Properties	Diesel	DME	LPG	CNG
Formula	C_{10}–C_{20}	CH_3OCH_3	C_3H_8	CH_4
Boiling point (°C)	180–360	–25	–43	–162
Vapor pressure (bar)	–	6	9.3	246
Density	0.84	0.67	0.5	–
Bulk modulus	$1.49 \times 10_9$	$6.37 \times 10_8$	–	–
Auto-ignition temperature (°C)	250	235	470	650
Cetane number	40–55	55–60	<10	<10
Stoichiometric A/F ratio	14.6	9	15.6	17.2
Lower heating value (MJ/kg)	42.5	28.8	46.3	50
Explosion limits (%)	6–6.5	3.4–17	2.1–9.4	5–15

with fatty acid methyl ester (FAME) fuels to form biodiesel blends, e.g. B20, so the same approach may be taken with the gaseous fuels to extend their use and permit local supply to meet demand, for example low blends of LPG (butane) in DME for CI engines. However, materials compatibility issues are but one consideration on any occasion that a fuel system designed for one fuel is exposed to blends with another fuel, particularly if that blend has not been approved by the engine or fuel system manufacturer. It is necessary that each of the component fuels is produced to an industry standard and that the resulting blend also meets a standard so that the fuel system and the engine performance may be validated for durability and emissions compliance. By way of example, DME has strong solvent properties against which the normal elastomers used in FIE are ineffective, thus only a very few specialized elastomer seal materials are compatible.

Countermeasures to make future FIE more robust to the wider range of fuels that may be encountered across the world in future are likely to include the use of dissimilar materials in highly loaded areas, such as the use of ceramic on steel to avoid the scuffing and galling failures that can afflict steel-on-steel components.

9.7.2 Other trends

With the undoubted focus in the twenty-first century on fuel efficiency and low GHG (greenhouse gas) emissions, alternative propulsion technologies will receive renewed scrutiny. Presently, several of the heavy-duty manufacturers are developing hybrid powertrains primarily for urban vehicle applications. Hybrid electric powertrains are in the forefront of this development, but at a lower level some parallel research activity is being conducted on hydraulic and also air hybrids. At this stage, it is not clear what the implications for the FIE will be, but the ability to switch seamlessly between operating modes is likely to require sophisticated control strategies.

Additionally, significant growth in control system capability and sophistication can be anticipated. As emission standards are driven to lower levels, the tolerance on variation in terms of engine-to-engine, cylinder-to-cylinder, and shot-to-shot must also be held to tighter standards than are possible today. We are already well beyond the point of achieving the necessary standards through wet-side manufacturing precision alone and so the bulk of the responsibility will fall to the control system, requiring further development in responsiveness and resolution. Moreover, this comes at a time of rapid growth in engine complexity, with new features beyond that of just the FIE such as advanced air management, including VVA, hybrid EGR systems, series boosting, and aftertreatment management. The unprecedented level of complexity thus created has resulted in a widespread move toward the adoption of model-based control, auto-coding of software, and auto-calibration strategies of engines on test beds.

Compliance with OBD requirements brings a further level of complication to the HD engine development and homologation process from 2010 onwards. Multiple emission-related engine parameters, including sensors and actuators, must be closely monitored across the speed and load range and over the life of the engine. In the case of the injection system, these parameters at a minimum include fuel quantity, injection timing and injection pressure, and others may be added in the future, depending on the specifics of the system. Continuous monitoring of these parameters is required, not just for base functionality but also for close conformance to the intended calibration within the mandated threshold constraints under all engine and vehicle operating conditions. Current projections suggest that OBD compliance will require a significant increase in product development budget and resource, particularly in the areas of algorithmic code generation, new diagnostic direct or indirect measurement techniques, and validation testing.

9.8 References

1. Schulte, L.-E. *et al.*, 'Heavy-duty engine validation of world harmonised duty cycle (WHDC)', Final Report, May 2004, RWTUV Fahrzeug GmbH.
2. Mardell, J.E., 'Getting fun out of diesel', Institution of Mechanical Engineers, Automotive Division, London, Chairman's Address, 2003/04.
3. Coldren, D.R. *et al.*, 'Hydraulic electronic unit injector with rate-shaping capability', SAE paper 2003-01-1384, 2003.
4. Greeves, G. *et al.*, 'Advanced two-actuator EUI and emission reduction for heavy-duty diesel engines', SAE paper 2003-01-0698, 2003.
5. Rente, T. *et al.*, 'Experimental investigation of the effect of needle opening pressure (NOP) on combustion and emissions formation in a heavy duty DI diesel engine', SAE paper 2004-01-2921, 2004.
6. Sturman, O.E., 'Fuel injectors and methods of fuel injection', US Patent 7,108,200, 19 September 2006.

7. Parche, M. and Becher, S., 'Common rail systems for commercial vehicles from Euro 3 to US EPA 2010 and from Tier 3 to Tier 4 Final', ICPC 2007-2.5.
8. Soteriou, C. *et al.*, 'The flow characteristics of high efficiency diesel nozzles with enhanced geometry holes', Thiesel 2006 Conference on Thermo and Fluid Dynamic Processes in Diesel Engines.
9. Schoeppe, D. *et al.*, 'Challenges and Synergies of Light and Heavy Duty Diesel Systems', 7th Dresden Engine Colloquium, Dresden, 2007.
10. Schoeppe, D. *et al.*, 'Exceeding customer expectations with the innovative direct acting diesel fuel injection system: Unique advantages of a breakthrough technology', 29th International Vienna Motor Symposium, 2008.
11. Ganser, M. *et al.*, 'Fuel injection valve for internal combustion engines', International Patent WO2008/046238 A2, 2008.
12. Chadwell, C. and Dingle, P., 'Effect of diesel and water co-injection with real-time control on diesel engine performance and emissions', SAE paper 2008-01-1190, 2008.
13. Klingbeil, A.E. *et al.*, 'Premixed diesel combustion analysis in a heavy-duty diesel engine', SAE paper 2003-01-0341, 2003.
14. Best, C.H., 'Dual mode fuel injector', US Patent 7,086,377, 8 August 2006.
15. Dohle, U. *et al.*, 'Results of combustion optimization by use of multihole nozzles in modern passenger car diesel engines', 27th International Vienna Motor Symposium, 2006.
16. Dingle, P.J.G., 'Outward-opening gas-exchange valve system for an internal combustion engine', US Patent 7,377,249, 27 May 2007.
17. Schoeppe, D. *et al.*, 'The challenges of worldwide fuels on modern diesel common rail systems', 16th Aachen Colloquium, on Automobile and Engine Technology, 2007.
18. McCormick, R.L. *et al.*, 'Effects of biodiesel blends on vehicle emissions', National Renewable Energy Laboratory, Milestone Report NREL/MP-540-40554, October 2006.

10

Turbocharging technologies for heavy-duty diesel engines

J. CARTER, N. K. SHARP and H. TENNANT,
Cummins Turbo Technologies UK

Abstract: This chapter discusses the application of turbochargers to heavy-duty diesel engines. The emissions legislation background is reviewed, and the effect this has on the turbocharger match is noted. Aerodynamic design principles of the compressor and turbine stages, including compressor flow range improvement and the variable geometry turbine, are explained with reference to wastegates, two-stage turbochargers and turbocompound systems. Design for durability is discussed, including the causes of low- and high-cycle fatigue and thermo-mechanical fatigue. Finally, mechatronic actuation design methods for variable geometry and other air handling devices are proposed.

Key words: turbocharging systems, compressor design, variable geometry turbine, durability, turbocharger actuation.

10.1 Scope

This chapter describes turbocharging technology suitable for heavy-duty commercial diesel engines. Heavy duty (HD) means engines used for commercial vehicles, off-highway applications and stationary generating set applications. Generally these applications are characterised by high load factors and requirement for long life, significantly more than the acceptable norm in light duty/passenger car applications.

Typical design life is now 1 million km. Development of component design tools and manufacturing processes has had to stay ahead of increasing life cycle requirements. This is in addition to the ever present desire for reduced cost.

Most of these applications have to meet emission legislation targets, especially for NO_x and particulates, which have become increasingly stringent in recent years, for example the European legislation series Euro I to Euro VI in a 21-year period from 1992 to 2013. Over this period heavy duty turbochargers have evolved from the relatively simple all-mechanical fixed-geometry turbocharger. Actuation was first applied in the form of the wastegate, then more recently (1998) to variable geometry turbochargers and latterly to bypass valves. This evolution has been accompanied by increasingly sophisticated electronic turbocharger controls linked with widespread use of electronic controls in engine and fuel system management.

Aerodynamic design capability and materials development have enabled the turbocharger compressor and turbine to meet the demand of pressure ratio and flow range without loss of efficiency. In some cases more complex arrangements of two turbochargers have been used where a single unit cannot meet these requirements.

The topics mentioned above will be covered in more detail in the following sections:

- Turbocharger technology state of the art
- Engine performance requirements and operating characteristics
- Turbocharger architectures and aerodynamic design considerations
- Durability
- Actuation
- Future trends.

10.2 Turbocharger technology state of the art

10.2.1 Turbocharger development for heavy-duty engines

Turbocharger development during the early part of the twentieth century was predominantly based on large stationary or marine engines using constant pressure exhaust systems. Alfred Büchi, the pioneer of turbocharging, realised the importance of preserving the exhaust pulse as a means of transferring energy to the turbine and ensuring good cylinder scavenging [1]. Pulse turbocharging has been the basis of all turbocharged automotive engines from the late 1930s to the present day. Good overall turbocharger efficiency and the ability to respond quickly to engine load changes are key factors for vehicle applications.

The first production automotive turbochargers were based on the design of the larger industrial units, but in the 1950s the lightweight bearing systems and vaneless compressor and turbine stages were developed. These formed the basis of the current, fixed geometry turbocharger, albeit much developed in terms of rotation speeds and performance.

10.2.2 Influence of emissions legislation

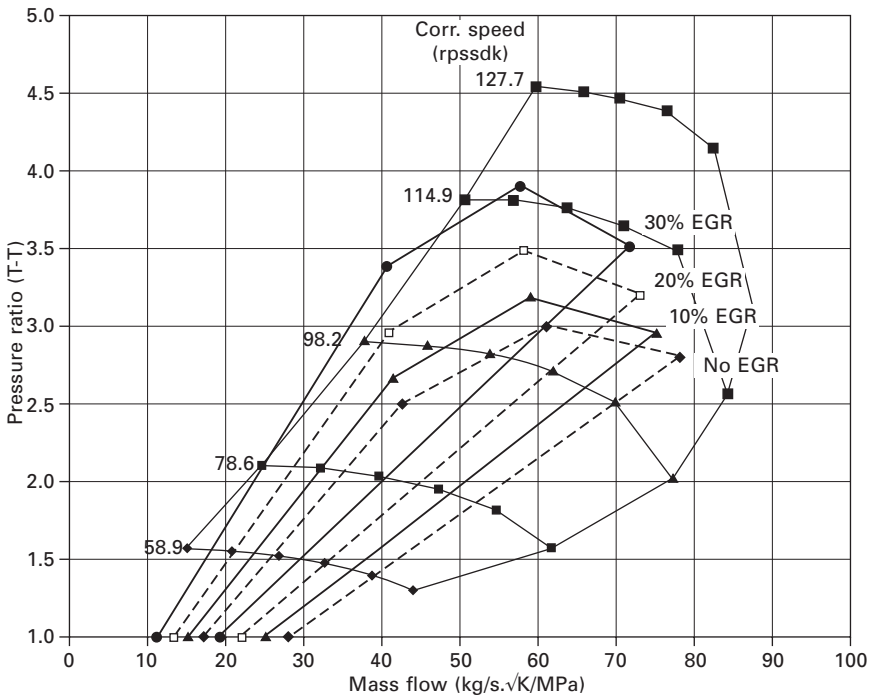
In Europe, the US and Japan there has been a succession of emissions legislation affecting heavy duty engines. Elsewhere in the world the European legislation has been adopted, although often introduced with a time delay from the parent legislation. The legislation and the developments in fuel injection systems and emission reduction technology have had a significant effect on turbocharger development. Most notable has been the increase in pressure ratio needed with exhaust gas recirculation systems.

Exhaust gas recirculation is used to reduce the formation of NO_x in the

combustion chamber. In heavy-duty engine emissions certification this process has to occur at a range of engine loads but especially along the full-load torque curve. Most commonly a quantity of exhaust gas is taken from the exhaust manifold, passed through a cooler and returned to the cylinders via the inlet manifold. The EGR fraction reduces the external airflow through the compressor and the turbine.

In order to compensate for the loss of fresh air flow, the boost pressure has to be increased to give the correct air mass in the cylinder for combustion. There is a residual oxygen content in the recirculated exhaust gas so not all the displaced fresh air has to be replaced. The result of EGR rates rising to levels of 30% or more at full load is to downsize the compressor, but to operate at a significantly higher boost pressure ratio. Figure 10.1 shows this trend.

At the turbine side the flow is similarly reduced, and the expansion ratio has to be increased to provide the necessary work to the compressor. However, it is also necessary to provide sufficient exhaust manifold pressure to drive the EGR flow through the cooler circuit and control valve to mix with incoming air in the inlet manifold. If too much exhaust manifold pressure is produced, the EGR control valve has to be partly closed and the engine



10.1 Effect of EGR rate on boost pressure.

fuel consumption will suffer due to high pumping work losses. If too little manifold pressure is obtained, then insufficient EGR will be produced and the emissions target not met.

Examination of the work balance equations for the compressor and turbine shows that for optimum pressure differential across the engine a specific turbine efficiency is required. Whilst it is possible to generate this efficiency at a single operating point with a fixed geometry turbine, to obtain the required efficiency over a wide range of engine speeds it is necessary to have a controllable turbine characteristic.

Wastegated, modulated wastegate and variable geometry turbochargers have all been used. As EGR rates become high and additionally other aftertreatment systems such as particulate filter or SCR catalyst are employed, the variable geometry turbine gives the widest level of EGR control with best fuel consumption.

10.3 Engine performance requirements and operating characteristics

10.3.1 Matching a turbocharger to a heavy-duty diesel engine

The turbocharger is a continuous flow device, akin to a gas turbine. The four-stroke diesel engine is a reciprocating machine with positive displacement related to its swept volume and rotational speed. How can the characteristics of these two machines be combined in order to select a suitable compressor and turbine?

Turbocharger matching calculations can be made at any engine operating condition, but the two most useful calculation points to make an initial hardware selection are the steady-state rated speed and load, and the peak-torque engine speed. Further calculations will be necessary at very low speeds, part loads and at high idle speed when confirming the suitability of the match. Transient engine and turbocharger modelling calculations are becoming the norm in the face of the more complex test cycles required for emissions compliance.

The power output of the engine at any given speed depends primarily on the quantity of fuel which can be burned in a given time. In a diesel engine injection process an excess air quantity is required because the fuel is not pre-mixed. Thus an air mass flow requirement can be established. To provide this air mass flow, the volumetric flow through the engine cylinders (the product of the swept volume per cycle and the rotational speed) has to be supplied from the inlet manifold at a suitable density. The volumetric efficiency of the engine is taken into account at this stage.

The density in the manifold is determined by the temperature and the pressure according to the equation:

$$M/V = P/RT$$

where

M = mass flow rate (kg/s)
V = volume flow rate (m^3/s)
P = pressure (Pa)
T = temperature (K)
R = gas constant (kJ/kg · K).

The turbocharger compressor needs to supply the airflow at a pressure ratio which ensures this inlet manifold density requirement is met. The temperature in the inlet manifold is nowadays usually controlled by the aftercooler. In most applications this is an air to air cooler with efficiencies of around 90% giving typical manifold temperatures approximately 20°C above the cooling air flow. Thus the mass flow rate and the pressure ratio can be defined for the compressor.

The compressor work under these conditions can be calculated by the well-known steady flow energy equation

$$W_c = m_c C_p T_{in}(PR^{(\gamma-1/\gamma)} - 1)/\eta_c$$

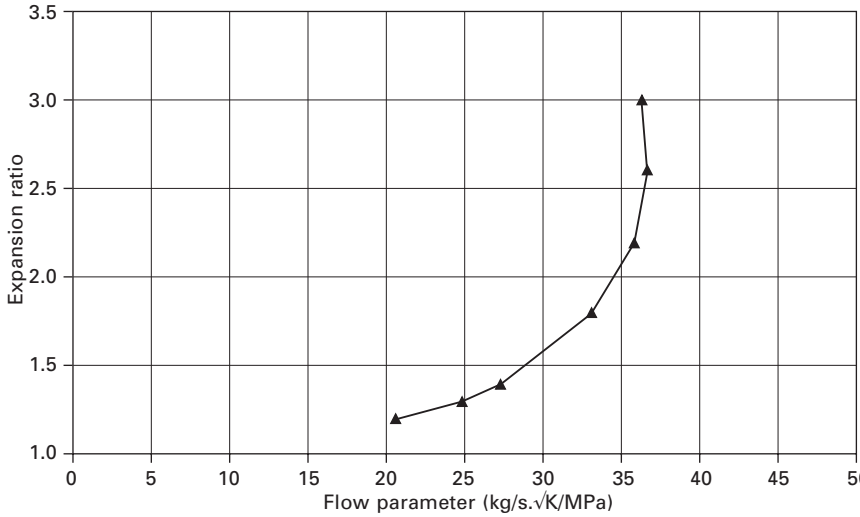
For the turbine the prime requirement is to produce sufficient power to drive the compressor at the required operating point. The turbine expands the exhaust gas from manifold pressure down to exhaust system back-pressure and in doing so produces power given again by the steady flow energy equation

$$W_t = m_t C_p T_{in}(1 - 1/ER^{(\gamma-1/\gamma)})\eta_t\eta_m$$

At a given steady state operating point the turbine work must be sufficient to meet the requirements of the compressor and to overcome the relatively small additional bearing losses.

The turbine inlet temperature is dependent on the fuelling rate and air flow rate through the engine, and on other variables such as the power taken from the engine crankshaft, and the heat lost to coolant and to radiation from the exhaust manifold. This temperature may be estimated accurately enough to give an initial calculation of the expansion ratio required. Computer-based engine simulation models can calculate the temperature extremely accurately taking into account combustion effects and, for example, the effects of exhaust gas recirculation.

Equating the energy calculations enables a required expansion ratio and thus the exhaust manifold pressure. A mass flow parameter $M\sqrt{T}/P$ can then be calculated which, with the expansion ratio, enables the physical flow size of the turbine stage to be determined from the measured turbine characteristics. See Fig. 10.2 for a typical turbine flow characteristic.



10.2 Turbine flow characteristic.

10.3.2 Modifying the boost curve

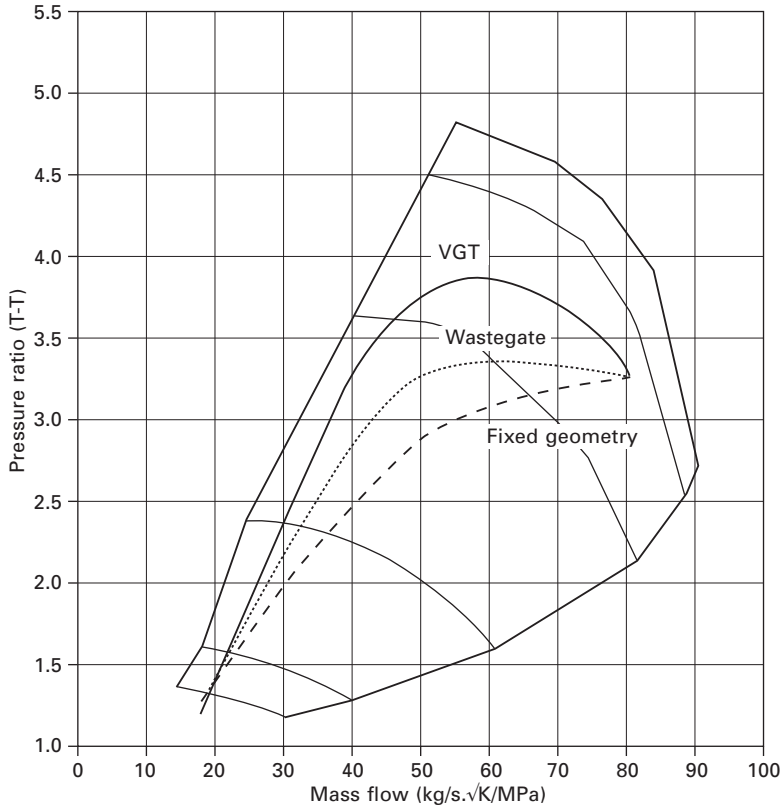
Typically a high torque at low engine speeds is required to give a good vehicle response and ease of accelerating from rest and in each gear. A rising torque curve with reducing speed ('torque back-up') also gives a powerful feel to the engine as the vehicle encounters a gradient and the engine 'lugs down' prior to a gear change.

The natural characteristic of the fixed geometry turbine, when matched to give the correct boost pressure at rated speed, means that at low engine speed and thus airflow, the expansion ratio is also low. The turbine work produced may then not give sufficient boost pressure for the desired engine torque curve. More boost pressure and airflow can be obtained by fitting a smaller turbine, but then at high engine speeds and airflows the turbine becomes choked, the exhaust manifold pressure is high and the turbocharger speed limit may be exceeded.

What is needed is a means of adjusting the turbine flow size so that the energy produced can be better controlled and matched to the engine requirement. The most common means of doing this are the wastegate and the variable geometry turbine. Figure 10.3 shows the effects of these systems.

10.3.3 Wastegate turbines

The wastegate is a bypass valve situated in the turbine casing which, when open, bypasses exhaust gas around the turbine wheel, thus limiting the turbine work produced in the wheel itself. A relatively small flow turbine housing



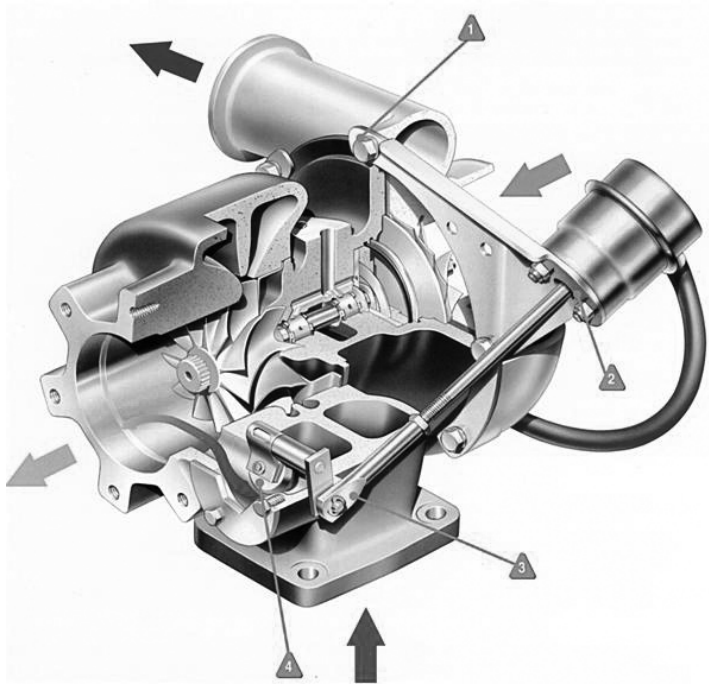
10.3 Compressor map showing effect of different turbocharger systems.

and wheel combination are chosen to give high boost pressure at low engine speeds. The bypass valve is then progressively opened in order to limit the turbine work, boost pressure and turbocharger shaft speed at high airflows and engine speeds.

Most commonly the boost pressure is fed to a spring loaded-diaphragm and used to control the wastegate valve opening. When the force due to boost pressure on the diaphragm exceeds the spring load the valve will open. Combinations of spring rate and pre-load can give different boost characteristics.

A development of this is to modulate the boost pressure fed to the diaphragm by means of a vent channel controlled by an electronically actuated valve. This allows the opening of the wastegate to be delayed, thus keeping the wastegate closed and allowing a higher boost pressure. When the electronic valve is closed there is no venting and the unit functions as a conventional wastegate.

Figure 10.4 shows a typical wastegated turbocharger.



10.4 Turbocharger with wastegate.

10.3.4 Variable geometry turbines

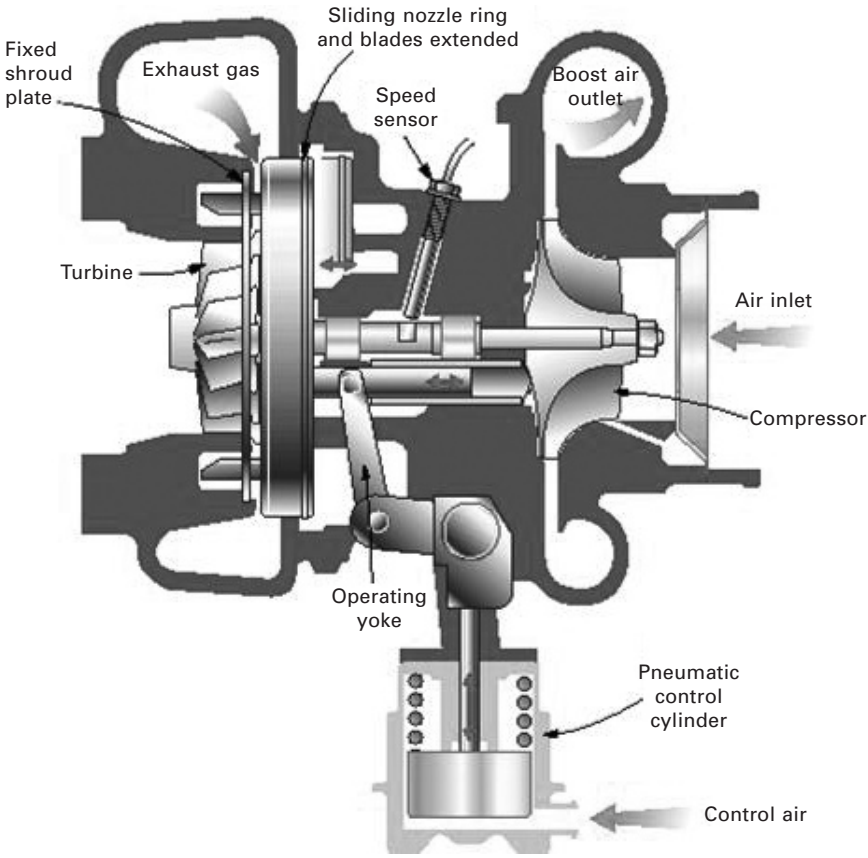
A means of controlling the turbine work over a wider range of air flows is to be found in the variable geometry turbine [2]. This device allows a variation of the controlling gas flow area in a nozzle guide vane array ahead of the turbine wheel. By this method a range of turbine flow sizes is presented to the engine exhaust flow and the energy supplied to the compressor can be varied for each engine operating point.

The effect of the variable geometry is to allow boost pressure generation at low engine speeds and during transients, whilst at the same time enabling a good rated speed turbine match without excessive back-pressure or turbine speed. The variable geometry turbine can also be used for engine braking purposes by creating a high back-pressure and where necessary boost pressure when the engine is in overrun or a decompression brake is in operation.

Figure 10.5 shows the arrangement of a HD VGT.

10.3.5 Turbocompound systems

Foreseen by Büchi but not introduced in production on-highway engines until 1991, the turbocompound engine is a means to increase the overall thermal

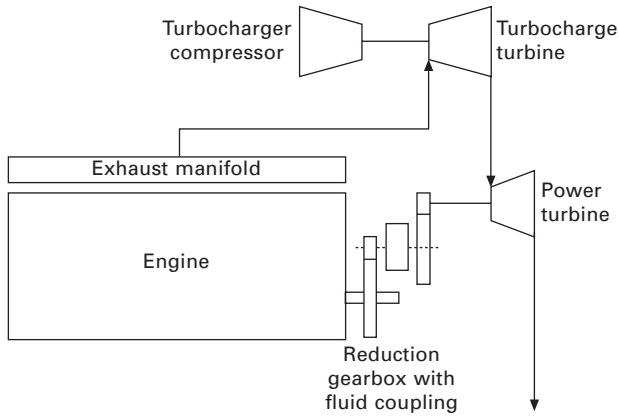


10.5 VGT turbocharger.

efficiency of the diesel engine. The energy available in the conventional turbocharger turbine exhaust is sufficient to make the addition of a second turbine downstream of the turbocharger turbine worthwhile, despite the additional back-pressure this brings to the engine exhaust manifold.

The turbine power is transmitted into the engine crankshaft via a fluid coupling and a suitable reduction gear train, shown in Fig. 10.6. If there is to be a net gain to the engine system, the power turbine contribution must exceed the additional pumping loop work due to the high manifold pressure. The power turbine transmission losses associated must also be considered. Typically in the engines so far seen in production a thermal efficiency gain of about 5% is obtained. As exhaust system back-pressures increase due to aftertreatment systems for low emissions it becomes more difficult to ensure that the basic system benefit is kept positive.

The overall air flow and pressure ratio requirements into the engine inlet manifold are not substantially changed by the turbocompound turbine system,



10.6 Turbocompound schematic diagram.

the compressor is the same as or similar to that used on the conventional engine.

10.3.6 Two-stage turbochargers

Improved design, materials (such as machined from solid aluminium and cast titanium) and process developments for the single-stage compressor allow higher speeds and pressure ratios, but for significantly higher pressure ratio requirements it is necessary to use two-stage (series) turbocharging.

Sequential turbocharging is the use of two turbochargers in parallel, with a means of switching one of the units on or off. The overall pressure ratio capability is not greater than either of the single-stage units. However, the effect of a significant turbine flow change can give a much higher pressure ratio at lower engine speeds than a larger single-stage unit.

In a series two-stage system interstage cooling can be used. In this case the high-pressure compressor material can remain in aluminium. An additional benefit is the high overall apparent compressor efficiency given by this arrangement. If no interstage cooling is employed, then at high overall pressure ratios the high-pressure compressor outlet temperature is likely to exceed conventional cast aluminium material limits, and will require higher-temperature material such as titanium.

Installation of two turbochargers and their associated interconnecting ducting is a major challenge for any vehicle designer. Other considerations are the weight and vibration characteristics of the system, the thermal compliance of the hot and cold gas connections to the engine block-mounted turbocharger and the aerodynamic design of the ducting to avoid high pressure losses.

Greater levels of bypass for the high-pressure turbocharger allow extremely

small high-pressure stages with benefits to air flow at very low engine speeds and to transient response. In these systems the larger low pressure unit operates as a single-stage system at high engine speeds. These have been introduced on several light- and medium-duty applications, but have yet to appear on larger heavy-duty engines.

10.4 Turbocharger architectures and aerodynamic design considerations

Single-stage turbochargers are the most popular choice due to their packaging simplicity. For reasons of cost and simplicity, radial outflow compressors are used exclusively, since to achieve typical HD boost requirements from an axial stage (having a maximum pressure ratio of ~1.25:1) would need more than four stages. Turbines can be either axial or radial inflow depending on size or application. For larger machines where space claim is less of a concern (e.g., marine or power generation) there can be performance advantages to using an axial flow turbine due to its low exit kinetic energy related losses. There is a practical limit to the largest-size radial turbine possible, with appropriate material properties, if it is to be investment cast. This is of much smaller concern with an axial flow machine as it can use individual blades attached to a common disk or hub.

Figure 10.7 shows the flow path arrangement of axial and radial flow machines.

10.4.1 Compressor – single-stage

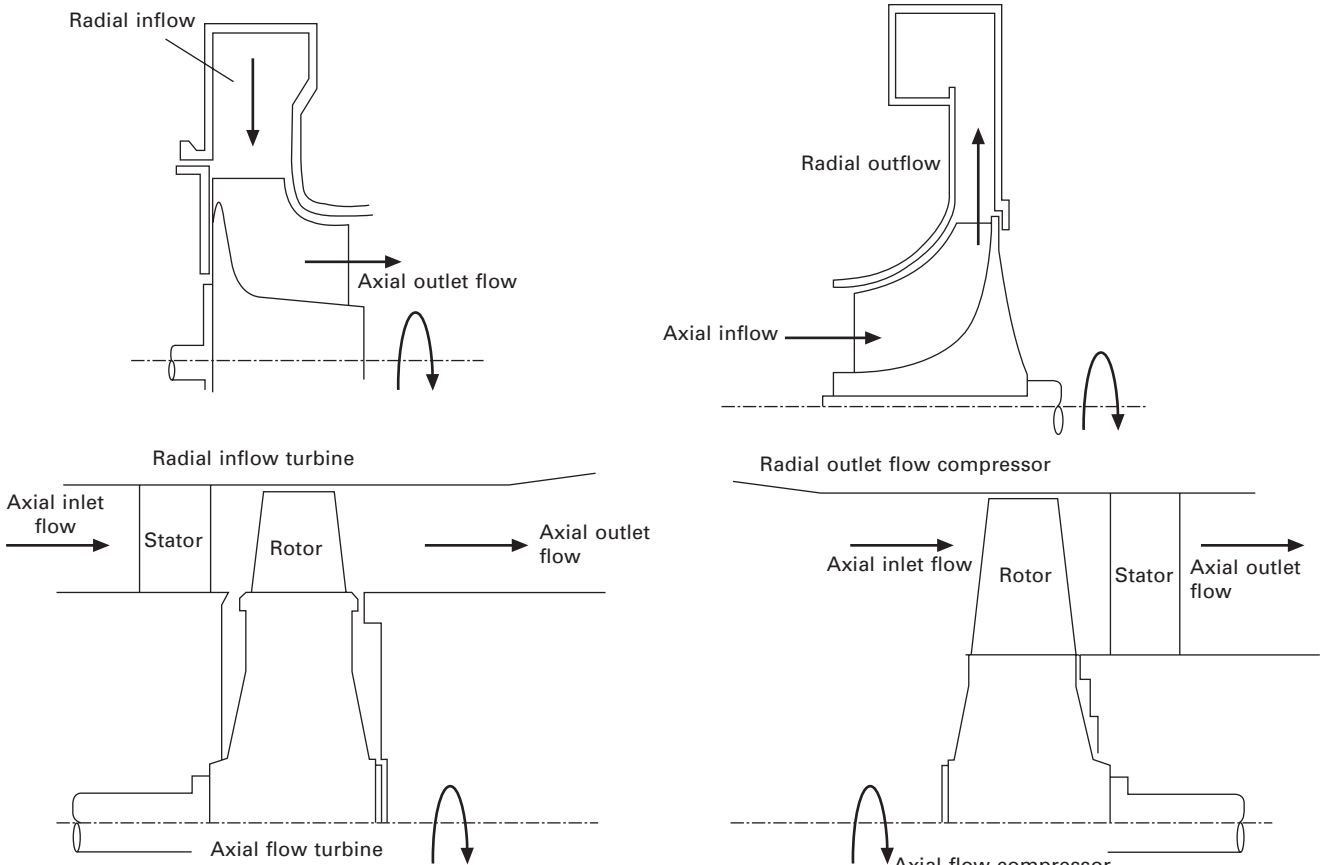
Maximum achievable sea-level pressure ratios are a function of impeller design, application and materials. As will be discussed in Section 10.5, a highly cyclic engine duty cycle results in a highly cyclic turbocharger speed cycle and hence increases the rate at which the impeller sustains fatigue damage. In such cases, the maximum allowable sea-level speed needs careful consideration so as to ensure an acceptable product life.

For a non-cyclic duty the maximum allowable sea-level pressure ratio is largely a function of the material stress levels of the impeller when it is subjected to high centrifugal loads. The pressure ratio can be expressed as a function of impeller geometry, efficiency and speed as shown in the following equation:

$$\left(P_{\text{out}}/P_{\text{in}}\right)^{\frac{\gamma-1}{\gamma}} = 1 + \eta_{\text{c}}\,\sigma\,(\gamma - 1)\left(\frac{U_2}{a_{0_1}}\right)^2$$

where

P_{out} = compressor outlet total pressure



10.7 Axial and radial flow paths.

P_{in} = compressor inlet total pressure
γ = ratio of principal specific heat capacities
η_c = compressor isentropic efficiency
σ = slip factor = C_θ/U_2
U_2 = compressor outlet tip speed
a_{0_1} = local speed of sound.

For a given impeller geometry, the high stress levels in regions such as the impeller blade hub fillet radius are also largely a function of $r\omega^2$, hence using a bigger impeller or higher rotational speed is good for pressure ratio but bad for stress. Typically, modern HD compressors achieve a peripheral blade tip speed of around 550 m/s. As will be discussed, the majority of modern compressor wheels have some level of 'blade backsweep' which is essential for controlling flow angle/quality into the diffuser and the aerodynamic loading on the blade. The level of backsweep thus significantly influences both operating range and isentropic efficiency. Generally speaking, as backsweep is increased to around 50°, efficiency and operating range increase but, in accordance with Euler's work equation, the amount of work done on the gas decreases and so does the pressure ratio. Efficiency is also a function of the machine geometry such that greater efficiency can be achieved at the expense of space claim; selection of specific speed can determine maximum efficiency level.

Consequently, for a given material stress limit, to achieve the best possible sea-level pressure ratio requires careful mechanical design of blade geometry to minimise stress in high stress regions, simultaneous selection of a backsweep level that ensures good pressure coefficient without compromising stress or operating range, and aerodynamic design to ensure optimal performance for the given level of backsweep.

To further improve pressure ratio capability and efficiency from a given impeller design (although generally done in unison), the compressor volute and diffusing element architecture can be selected and optimised. The majority of HD compressor stages utilise a vaneless diffuser as this gives the best compromise between pressure ratio, efficiency and operating range. Additional bladed elements or flow channels can be arranged circumferentially around the outlet of the centrifugal impeller. The ratio of the vane or channel area to the outlet area of the impeller gives a measure of the solidity of the elements. A high solidity diffuser has a distinct aerodynamic throat area between adjacent vanes and controls both flow angles of impeller exit flow and diffusion rate. A low solidity diffuser has no distinct aerodynamic throat, hence mainly controls the flow angles.

In each case, the pressure recovery relative to the vaneless is improved and hence the pressure ratio and efficiency. The disadvantage relative to the vaneless diffuser is operating range. Incidence onto the vane leading edges

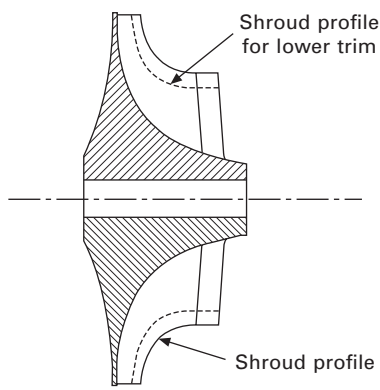
causes flow instability, pressure loss and hence operating range reduction. As with backsweep, a compromise needs to be made between operating range, efficiency and pressure ratio: vaneless gives best range but lowest efficiency; high solidity gives best pressure ratio and efficiency but lowest range; low solidity is a compromise between the two.

In all cases, the vane setting angle and the compressor volute critical area can be selected to achieve peak efficiency at the desired pressure ratio. Typically, a large volute critical area gives good efficiency at low pressure ratio and vice versa. Vane number and overall diffuser geometry are optimised to give good efficiency. Typically, high solidity vaned diffusers use wedge-shaped vanes and low solidity diffusers use airfoil profile vanes.

Generally, having defined the architecture and design flow geometry, for reasons of economy, manufactures will produce flow variants to allow better matching to a wider range of engine flows. Flow variants are created by using different 'trims' (changing the inducer size of the impeller), different setting angles for vaned diffusers or both. Figure 10.8 shows how the impeller flow is changed for a given design.

10.4.2 Compressor – two-stage

As pressure ratio requirements increase above those achievable with the best possible single stage (highest tip speed, optimal efficiency and backsweep) then it becomes necessary to consider multiple compressor stages. As with aero gas turbines, coaxial multi-spool turbocharger and multi-stage radial turbochargers have been proposed and tested. To date, few if any exist in the HD marketplace, possibly due to their extra cost, weight size and complexity. Radial flow turbochargers with an extra coaxial axial machine have been proposed but have yet to be seen in the marketplace. In such



10.8 Impeller flow trims.

machine proposals, the cost, package size and bearing technology most likely limit the machine to one axial stage to augment the radial. In this respect, the maximum achievable pressure ratio will never be as good as the current state-of-the-art multi-stage turbo architecture.

Typically, two stages of turbocharging are enough to deal with current engine air requirements. The aerodynamics design requirements are identical to single-stage except for additional flexibility in mechanical design due to not needing individual stages to achieve the same peak tip speed or pressure ratio. As will be covered later, this lower pressure ratio and speed can thus allow a thinner blade to achieve the associated lower blade natural frequency or a larger blade inlet tip diameter to give more flow for the same impeller tip diameter. Assuming that existing single-stage hardware can be selected or easily modified to the correct flow specifications, the majority of the aerodynamic work in optimisation of the two-stage series turbocharger system is associated with inter-stage duct and package design. Typical package design work can involve modifications to the compressor volute to allow better flow paths, or resizing the volute critical area to target improved efficiency at a lower pressure ratio.

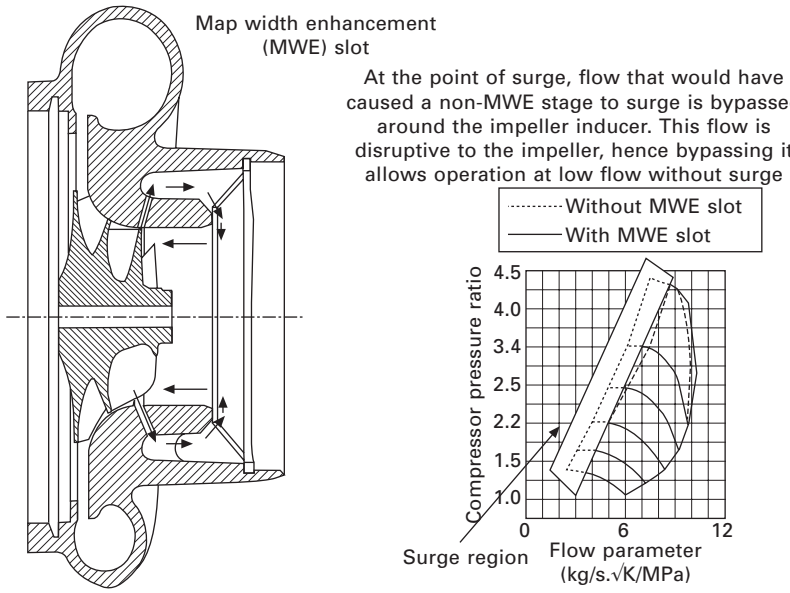
For some engine systems, additional boost pressure assistance devices are used to transiently improve the pressure ratio capability at low engine speeds. Existing systems have utilised separate superchargers in series but allow the additional supercharger to be bypassed.

10.4.3 Compressor – operating range

Engine operating speed and torque backup requirements have driven the need for wide operating characteristics from the compressor stage. Operating range is defined as the distance between the compressor surge and the choke region. Choke is defined as a region in which the compressor efficiency drops below a usable 60%. Surge is a region of unstable operation dominated by a combination of inducer blade or diffuser stall due to the mismatch of gas flow angles with the blade angles, i.e. the flow incidence. Engine speed and flow determine the required compressor flow range. It may also be desirable to improve the high efficiency region so that the so-called ‘off-design’ levels are acceptable.

The simplest and most common approach to improving HD compressor operating range is to utilise some form of inlet casing modification that allows recirculation of inducer flow [3]. An annular chamber connects the inlet flow duct to a region on the impeller shroud downstream of the minimum blade passage area or throat, thus allowing flow to bypass the choked inducer when in surge. Figure 10.9 shows the arrangement of a typical inlet casing geometry used to improve range.

Other systems to improve range have been proposed but few if any are in



10.9 Compressor stage flow improvement.

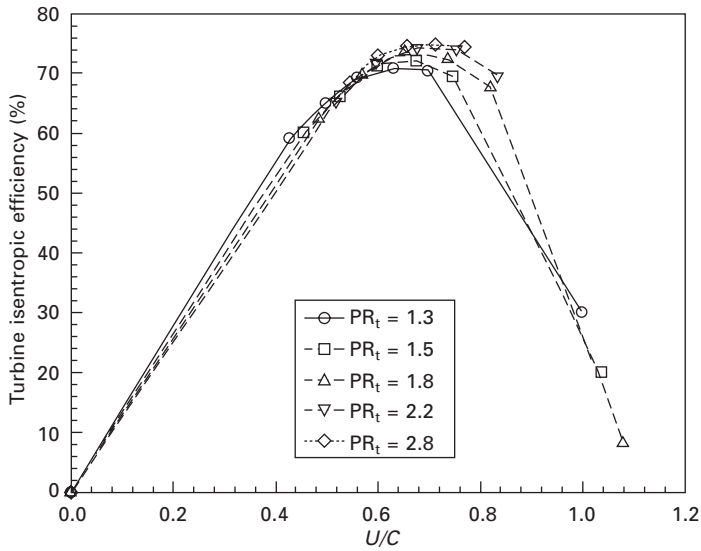
production. Variable inlet guide vanes, positioned axially or radially in front of the impeller can be used to control the flow angle onto the impeller, and hence delay the onset of blade stall and hence surge. Euler's work equation again indicates that any inlet tangential velocity used to improve incidence will decrease the pressure ratio capability at that speed.

Variable diffuser vanes that allow angle or area changes through rotation of the vane about some fixed axis will potentially give a larger operating range than a variable inlet guide vane system but are arguably more difficult to implement and more sensitive to clearance-related losses. As the vanes need clearance to allow movement and thermal expansion, this clearance can allow internal and external leakage flows. External leakage needs to be minimised; internal leakage needs controlling to minimise efficiency loss.

10.4.4 Turbine stage

Space claim and cost limitations normally drive the use of high specific speed designs that, for a given wheel geometry, are used in a variety of FG and WG turbine housing with different critical areas. By also using turbine wheel profile 'trims' it is possible to combine wheel and housing areas to give the desired flow against pressure ratio characteristic, or swallowing capacity. In this way, a larger range of individual engine flows can be accommodated with fewer individual turbine wheels.

Turbine peak efficiency is greatly influenced by its one-dimensional design and selection of blade angle distribution. Manufacturing simplicity and mechanical stresses dictate the need for radial fibred turbine blades in nearly all cases. For these turbines, the inlet blade angles are generally ~90° to the tangential direction and have inlet tip diameters set to ensure good efficiency at the most relevant compressor operating point. Blade speed ratio allows the designer to set the inlet diameter to ensure a good balance between rated point and peak torque turbine efficiency. Generally, as engine speed reduces so does blade speed ratio and hence efficiency. Sacrificing blade speed ratio at high engine speed to ensure good low engine speed efficiency is limited by the maximum allowable tip speed of the turbine. Figure 10.10 shows a typical blade speed ratio plot for radial inflow turbine.



$$U = N_{\text{physical}} \times \pi \times D$$

where:

U = blade tip velocity (length/time)
N_{physical} = actual turbine rotor speed (rev/min)
D = diameter at the inlet of the turbine rotor (length)

$$C = \sqrt{2C_p T_{0,\text{in}} \left[1 - \left(\frac{1}{PR_t}\right)^{\left(\frac{\gamma-1}{\gamma}\right)}\right]}$$

where:

C = spouting velocity (length/time)
$T_{o,\text{in}}$ = turbine inlet total temperature (K)
PR_t = turbine pressure ratio (dimensionless)
C_p = specific heat at constant pressure [(force*length)/(mass*temperature)]

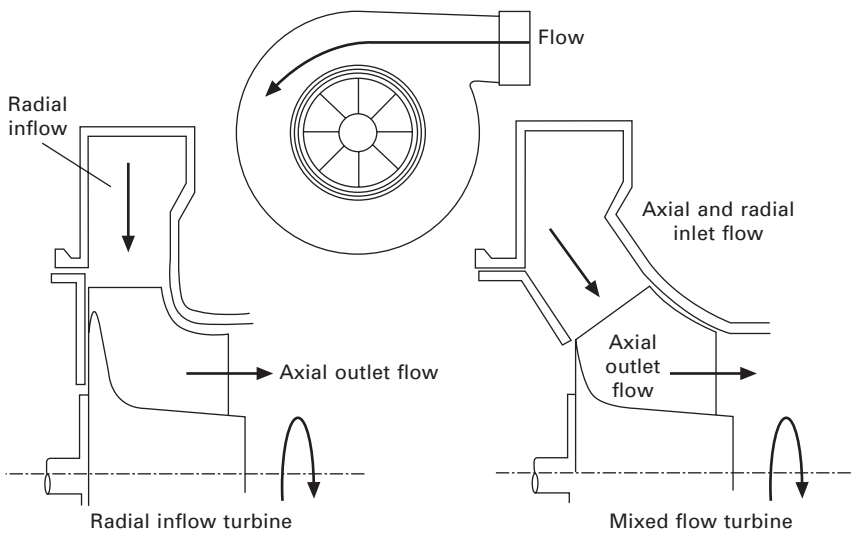
10.10 Blade speed ratio.

The desire to reduce package size generally means maximising the turbine exit area so as to achieve maximum flow for a given wheel inducer diameter. Other than the impact on the mechanical stresses associated with a large blade span and potential efficiency loss due to the thicknesses required to give a suitable natural frequency, this trend is good for efficiency as it minimises exit kinetic energy loss.

Housing and wheel combinations can give the desired swallowing capacity, but as the ratio between wheel and housing varies there is an impact on efficiency. For a given turbine wheel diameter there will be an optimum combination of wheel and housing area in terms of efficiency, and this pairing will have a fixed swallowing capacity. If this swallowing capacity does not match the engine requirements, it is usual to change the housing area provided the efficiency variation is acceptable.

10.4.5 Turbine – mixed flow

Based on market penetration, it could be argued that mixed flow turbines have had limited success. In principle, the mixed flow turbine allows selection of inlet blade angles to improve off-design performance, particularly low speed, whilst maintaining predominantly radial blade fibres. Additionally, as the desired blade angles can be set with a smaller wheel diameter, the space claim is better than for a conventional radial inflow turbine. The smaller diameter may help inertia and transient response but the design and manufacture is arguably more involved due to the more complex blade shape. Figure 10.11



10.11 Comparison of mixed flow turbine with radial flow turbine.

shows a comparison of the flow path through a mixed flow turbine with that of the radial flow turbine.

10.4.6 Turbine – wastegate

For a WGT, once the housing is chosen, the wastegate bypass port size is selected to allow sufficient flow bypass at high engine speeds to avoid excess turbine work and hence boost pressure. The position of the wastegate valve, seat angle and downstream pipework is optimised to ensure maximum flow and minimum influence of the bypassed flow on the 'core' flow from the turbine exit [4]. If the bypassed flow mixes poorly with the turbine exit flow, it can limit the maximum bypass flow rate and increase the back-pressure directly behind the turbine, thus influencing the wheel efficiency.

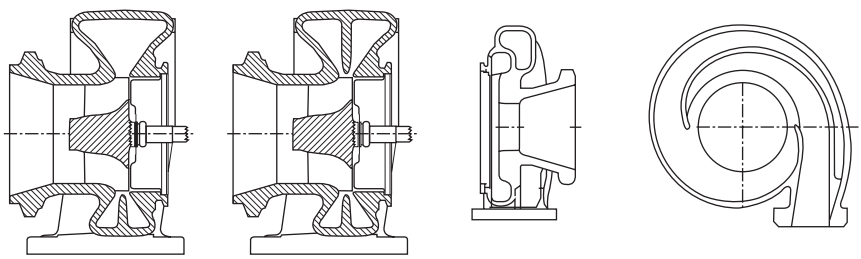
To better utilise exhaust pulse energy, the majority of FG/WG turbines have an axially divided cross-sectional area, effectively producing two critical areas. Typically, these housings are called 'twin entry' or 'twin flow' housings. In most cases each area is half the total volute critical area, but some systems claim improved EGR transport when using different areas such that the EGR take-off is connected to the smaller volute.

Axially divided inlets will not work with a moving nozzle VGT in which case a housing with two ('double entry') or more 'tongues' can be used. As will be discussed in Sections 10.4.8 and 10.4.9, a twin-entry volute is not always desirable as its dividing wall increases skin friction and hence pressure loss.

Figure 10.12 shows single entry, axially divided twin flow and double entry volutes.

10.4.7 Turbine – variable geometry

The variable throat area in the turbine nozzle ring enables the turbine work extracted from the exhaust gas to be increased or decreased at any given engine speed and airflow rate by changing the expansion ratio. At low engine



10.12 Single, twin flow and double entry turbine housings.

speeds and airflow rates the throat area can be reduced so that the expansion ratio is increased; at high flow rates the increased throat area can be used to reduce expansion ratio and back-pressure on the engine.

For simplicity and robustness variable geometry turbines for HD are exclusively radial inflow. The main variants are turbines whose vaned stator areas are varied by either

- changing the vane setting angle and hence the circumferential pitch between adjacent vanes of a fixed axial height, thus giving a different throat area, or
- changing the vane axial height for a fixed setting angle.

The former are often called swing vane VGT and the latter moving nozzle. Swing vane designs should in theory offer some performance advantage over moving nozzle due to the vanes' ability to provide more optimum gas angles off-design. However, in practice, for an equivalent size the two performance characteristics are similar, due in part to the extra clearance-related losses associated with the swing vane mechanism. Figure 10.13(a) shows a moving nozzle VG and Fig. 10.13(b) shows a swing vane VG.

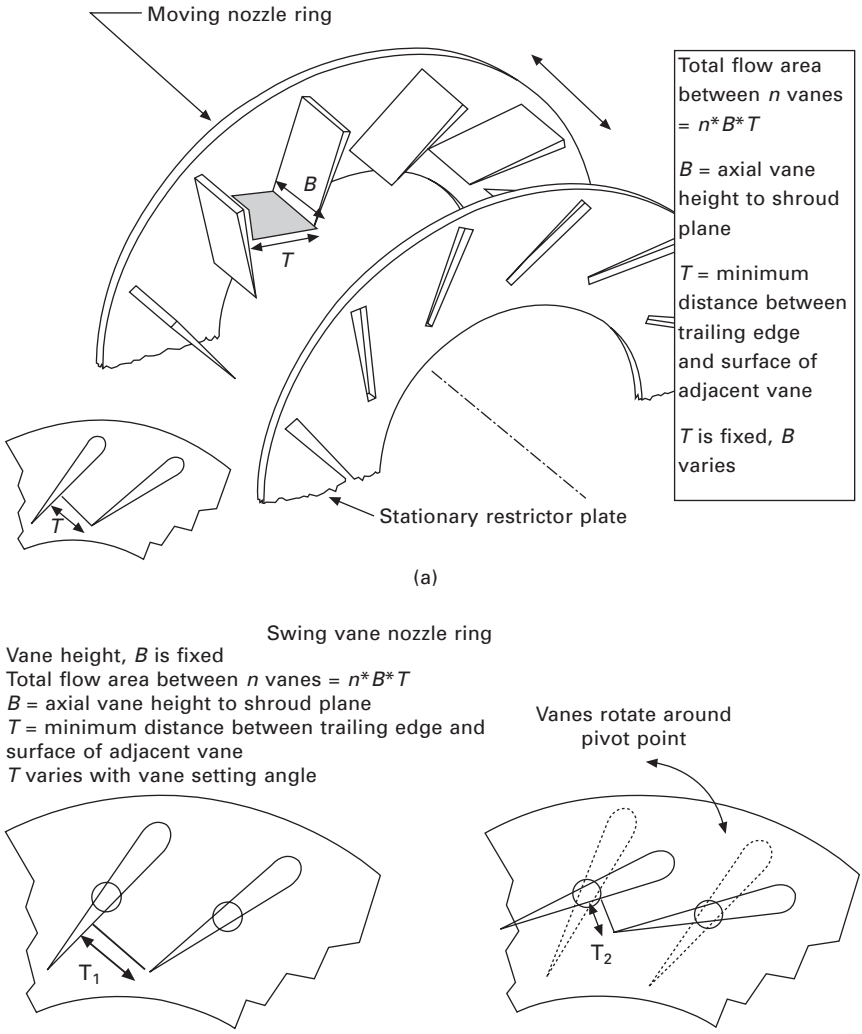
Pivot points and the vane aerodynamic profile on the swing vane machine need careful selection to avoid self-closing or opening off-design. The vane carrier on the moving nozzle design will see a high mean pressure, hence the actuation forces to move the nozzle axially will be higher than that to rotate the swing vanes around their pivot axis. The higher actuation forces will influence actuator design and space claim. Figure 10.14 shows how efficiency varies with flow or VGT setting for a typical swing vane and moving nozzle turbine.

Other systems for variable geometry turbines have been proposed, such as modular moving nozzle and swing vane mechanisms mounted in the turbine housing to allow the addition of VGT to existing product lines. These are less common in HD, most likely due to their design and materials being better suited to light duty applications. Schemes using variable geometry volutes exist but generally only on LD and passenger car applications.

10.4.8 Turbine – two-stage

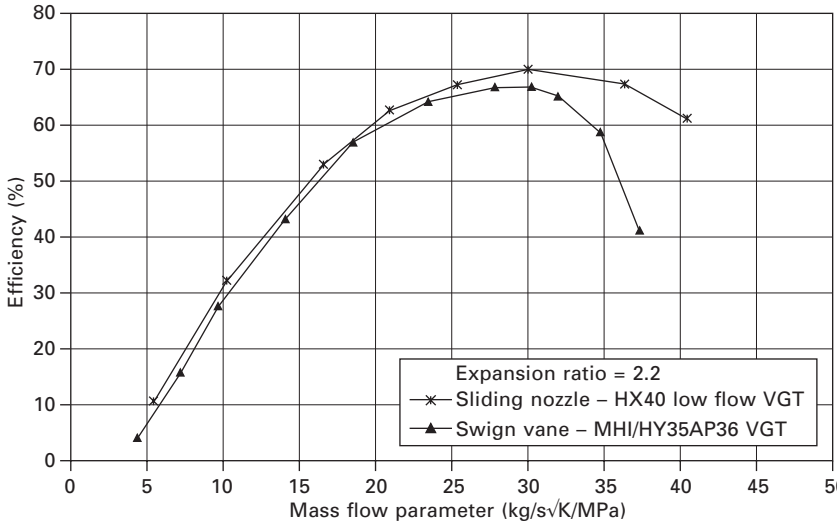
In terms of aerodynamic design, there is little difference between turbines used in single-stage to those used in two-stage systems other than that driven by flow and pressure ratio changes.

An undivided or single-entry turbine housing is used to ensure best efficiency (minimised skin friction related pressure loss) because there is no benefit in pulse capture on the downstream turbine. As with the compressor, the lower rotor speed could lead to some possibility of improving performance through blade thickness change.



10.13 (a) Moving nozzle VG, (b) swing vane VG.

Two-stage turbines may need a variable flow component, especially when used in an EGR system. This is provided by a wastegate or variable geometry turbine incorporated into the high-pressure turbine. The work balance between the two turbochargers is altered by these arrangements, and can be used to benefit transient response and airflow at low engine speeds whilst avoiding excessive boost pressure at high engine speeds. Most automotive systems



10.14 VGT efficiency variation with flow.

appear to be radial inflow, but there could be some packaging advantage to using an axial LP turbine, since it can be positioned on the same axis as the HP turbocharger.

10.4.9 Turbine – turbocompound

The turbocompound system leads to specific design differences for both the turbocharger turbine and the power turbine.

The flow parameter defining the first, turbocharger, turbine is significantly reduced from that used in the conventional turbocharged system as a result of the high turbine inlet pressure. Up to a point the low flow requirement can be achieved with a reducing turbine casing size, but as the match between the casing and the wheel itself changes, eventually a purpose-designed wheel and housing is required to avoid efficiency loss.

The turbocharger turbine wheel design can be optimised to suit the small flow size by reducing its flow area relative to the standard turbocharger, thus giving a good degree of reaction. As the exit kinetic energy can arguably be recovered by the power turbine, some advantage could be gained in rotor total-total efficiency by setting exit blade angles to allow some exit swirl and thus decrease blade-related pressure losses. As with the radial inflow LP turbine, an undivided or single-entry turbine housing is used. A vaned stator to accelerate the flow could further improve efficiency by allowing the use of a very large, low loss housing, though this would affect cost and space claims.

An axial power turbine can give packaging and efficiency benefits but at

the expense of cost (more components relative to vane less radial inflow) and space claim. Freedom with blade angle selection, whilst staying within manufacturing constraints, means more flexibility than the radial in terms of setting wheel design speed for optimum blade speed ratio. However, performance characteristics of the axial, generally having constant or increasing flow with increasing speed, will give a different power contribution against engine speed/load characteristic relative to the radial inflow turbine.

Figure 10.15 shows a comparison of an axial and a radial flow power turbine characteristic.

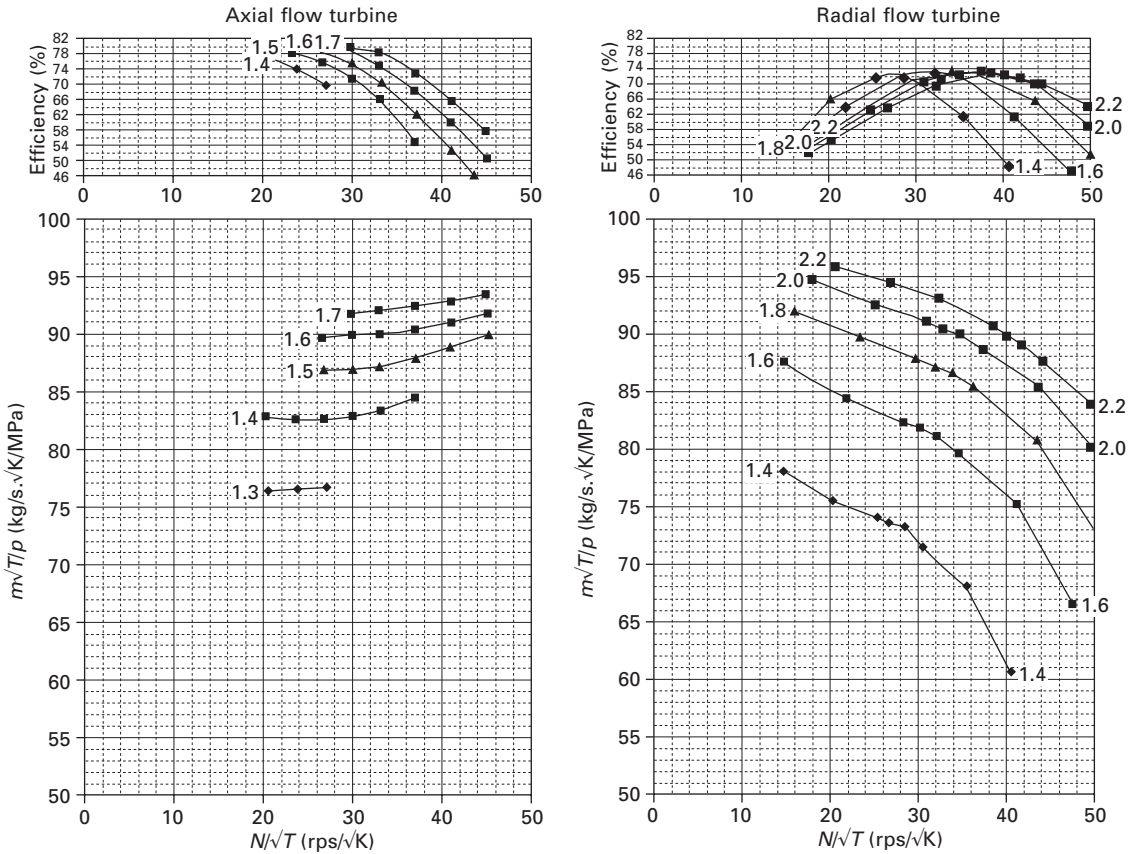
10.4.10 Component design – tools and processes

The high efficiency demands of HD product necessitate using computational fluid dynamics to optimise the rotor blade, stator blade and volute geometry. In most cases, initial design iterations can be done using simplified models, having profiled blade leading and trailing edges but no fillet radii between blade and hub surface. The simplified blade to blade models are first used in calculations that only consider the wheel. As the design progresses, a more time-consuming calculation involving the wheel and volute is done to ensure a good match between the two. Various schemes exist to handle the relative movement of the wheel and housing computational grids; the simpler the scheme, the faster but less accurate is the solution. When the coupling between the rotor and the stator is weak, i.e. the stator blades are a long way from the wheel, simpler schemes should be sufficient. As the components become closely coupled it becomes more necessary to use the more complicated methods, leading ultimately to a full time-unsteady calculation where the relative motion of rotor and stator are fully captured.

Integrated design environments allow better integration between mechanical and aerodynamic analysis essential to a good design solution. An example of such a tool is ANSYS blademodeller as it integrates FEA capabilities of ANSYS workbench with the blade geometry generating tools and links to the CFX CFD code.

Modern optimisation software tools are being employed to investigate and define better design options, especially with respect to optimised mechanical and aerodynamic design. Generally, the geometry is directly modified via the optimisation software according to a strategy that is developed from the knowledge of how each iteration performs according to the analysis tools used. In the case of turbocharger blading, simultaneous optimisation of aerodynamic performance, blade stress levels and blade frequencies can be performed.

For the aerodynamic designs, so-called inverse design techniques are becoming more popular. Here, rather than use CFD to analyse a variety of conventional design iterations until a suitable flow field or efficiency is



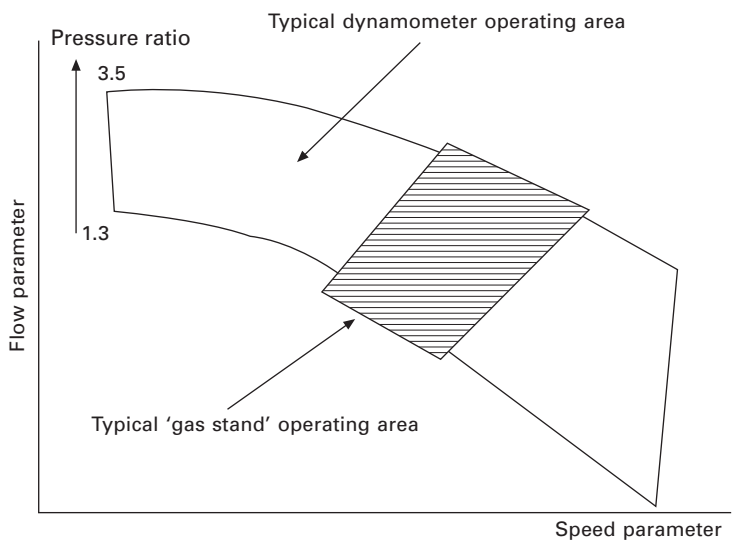
10.15 Axial and radial turbine characteristics.

achieved, CFD-type calculations are used to calculate what blade geometry is necessary to give a prescribed flow distribution. The rational for flow field specification is based on minimising the pressure distributions that drive leakage and secondary flows.

The now commonplace usage of engine cycle simulation tools places demands on the turbocharger manufacturers to provide compressor and turbine performance 'maps'. Very early in the design cycle, initial cycle calculations can be made with basic map estimates. As the engine and turbocharger design progress, increasing use is being made of full CFD predicted maps. Ideally, the turbocharger development cycle will be in advance of the engine so the performance maps, initially from prototype hardware, will be available for key engine simulations.

Compressor performance test cells are commonplace and some turbine information can also be taken using this arrangement, though the speed range of the data is limited by where the compressor can reliably operate. As the simulations often need a wide range of turbine operating speeds, to allow for movement within the map during transient, the data must be either extrapolated or taken directly using a high-speed dynamometer. Figure 10.16 shows the operating range of different testing methods.

To produce the prototype test hardware it is common practice to use rapid prototyping techniques. Five-axis machining for the complex 3D blade geometries is perhaps the most useful and certainly contributes greatly to the rapid development cycle of new high-performance machinery.



10.16 Turbine dynamometer test range.

10.4.11 Efficiency improvements

Manufacturing method plays a large part in the efficiency of a given machine. A perfect aerodynamic design on paper can soon be reduced to one of mediocre performance if it is made with large running clearances or poor surface finish. Clearance control is essential for flow leakage-related loss within the blade passages. Surface finish has a very significant effect on skin friction-related losses especially in the cast stators. The HD market demands high efficiency but, unlike aerospace turbomachinery which utilises abradable materials and brush seals to control leakage flows, it appears currently to be very cost-sensitive. As the need for efficiency increases and on the assumption that there is a practical limit to manufacturing tolerances, the cost–benefit trade-off will doubtless see the increasing use of abradable materials for clearance control and a move away from very basic sandcasting processes to others that allow better surface finish control.

In systems that utilise closed crankcase ventilation, the blowby gases, if fed into the compressor inlet, can leave deposits which will significantly reduce compressor performance. Over time, this could reduce efficiency levels enough to affect engine emissions. If the reduction in efficiency with time cannot be tolerated, wash systems, special coatings or servicing will be required.

10.5 Durability

10.5.1 Turbocharger durability requirements

With increasing vehicle warranty periods and the reducing tolerable failure rates within this period, there is a continuing need to improve engine sub-system component durability. Target design lives for HD applications are typically 1 million km.

10.5.2 Component mechanical design issues

The high speeds, high temperatures and cyclic duty cycles associated with HD application have the following impact:

- The turbocharger rotors are prone to low and high cycle fatigue damage.
- The housings can suffer thermo-mechanical fatigue.
- The compressor impeller and cover, generally being made from aluminium, are susceptible to creep damage.

Having discussed some common durability issues for rotors and end housings, we will now briefly consider the rotor/bearing system. The turbocharger bearing system must be tolerant of:

- High thrust loading caused by high boost pressure and the ability of a VGT to drive the compressor to higher boost at low flows. A low flow in the VGT usually means a small nozzle setting and hence low static pressure behind the turbine wheel to offset the corresponding compressor thrust.
- Oil quality. Longer service intervals and high soot loading due to engine emission controls lead to oil contamination. Additionally, oil contamination can lead to bearing surface corrosion issues.
- Oil delay. Low ambient temperature and large oil feed pipe lengths can increase the time it takes for lubrication to reach the turbocharger on start-up. On start-up, even at low idle the turbocharger speed will be relatively high after a very short period of time, giving rise to potential problems with bearing system wear.
- Hot shutdown. Continuous operation at high temperature followed by rapid engine shutdown without idle leads to localised burning of the oil in the bearing housing and subsequent damage to bearing surfaces.

Generally, hydrodynamic floating ring journal bearings are used in HD turbochargers for their simplicity and tolerance to oil contamination. Ball-bearing systems can be used without a separate thrust bearing, which helps achieve a lower overall bearing loss and hence improved transient response. This would be beneficial for the engine transient performance but the ball-bearing systems' tolerance to oil contamination is less good and this is why such systems are rearely seen mainly on HD applications.

To prevent high temperatures damaging the bearings, water-cooling the housing may be necessary, but arguably less so than for gasoline engines where turbine inlet temperatures are very high.

Other bearing systems have been demonstrated and already exist in other non-automotive turbomachinery applications. Air bearings, tilting pad journal and magnetic bearings all offer performance benefits over conventional hydrodynamic systems, but tolerance to operating environment or cost currently precludes their common use.

10.5.3 Low cycle fatigue (LCF)

The HD turbocharger has to accommodate a wide range of potential applications. Of all applications, the HD city bus, with its stop–start duty cycle, results in large and frequent turbocharger speed cycles. These cycles result in fatigue events in the high stress regions of the impeller. Typical FEA design techniques using test specimen fatigue life properties may need to be augmented with component fatigue life testing to ensure adequate knowledge of fatigue stress intensity factors. FEA and component-specific fatigue information can then be used with application-specific duty cycle knowledge

to give a more accurate life prediction. Life improvement through stress or speed reduction is not an option for HD as both limit engine ratings.

Improved materials, such as wrought aluminium for the compressor wheel, can both improve fatigue properties and reduce the influence of casting defect-related fatigue failures. Post-manufacture inspection techniques, such as eddy-current inspection, can also help reduce defects in supplied product. Additional inspection processes and different materials, with their different processing requirements such as machining from solid, can increase cost.

10.5.4 High cycle fatigue (HCF)

High durability requirements and more time spent at high turbocharger speeds increase the need to produce a turbine stage that is not susceptible to high cycle fatigue. Primarily, the blade's natural frequency must be set to avoid specific excitation orders but the wheel's responsiveness to the forcing function supplied by the stator must be considered.

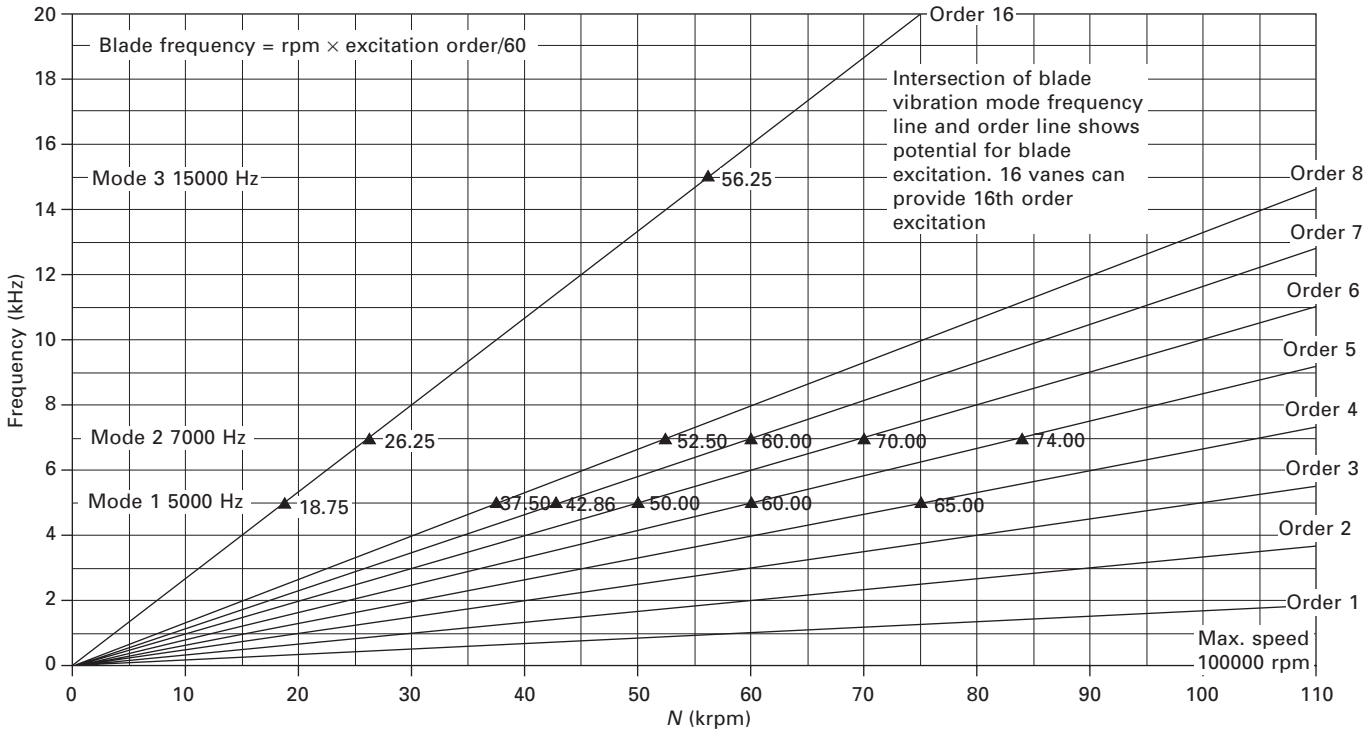
Figure 10.17 shows a Campbell diagram for fixed geometry (FG) and variable geometry (VG). The vaned or vaneless stator will provide a circumferentially varying static pressure field which can force resonance at certain blade excitation orders. As can be seen from the Campbell diagram, a vaned stator introduces many more opportunities for blade resonance. Coupled CFD and FEA techniques exist to optimise the blade shape in order to minimise its responsiveness, but they are time-consuming. Essentially, CFD can be used to calculate the time-varying static pressure field and FEA can use this field in a subsequent harmonic response analysis in which the blade stresses can be calculated. CFD analysis for only the stator can give information about the circumferential variation in exit static pressure. Fourier analysis of this pressure against angle variation can be used to gain valuable insight into the influence of the stator on the wheel at the relevant excitation order [5].

Figure 10.18 shows pressure variation against circumferential position. As most HD applications have high map width requirements, their compressor stages are likely to have some kind of range extension inlet geometry on the compressor cover. This arrangement allows interaction of the blade-generated rotating pressure fields with the stationary parts of the cover and hence a potential source of blade excitation.

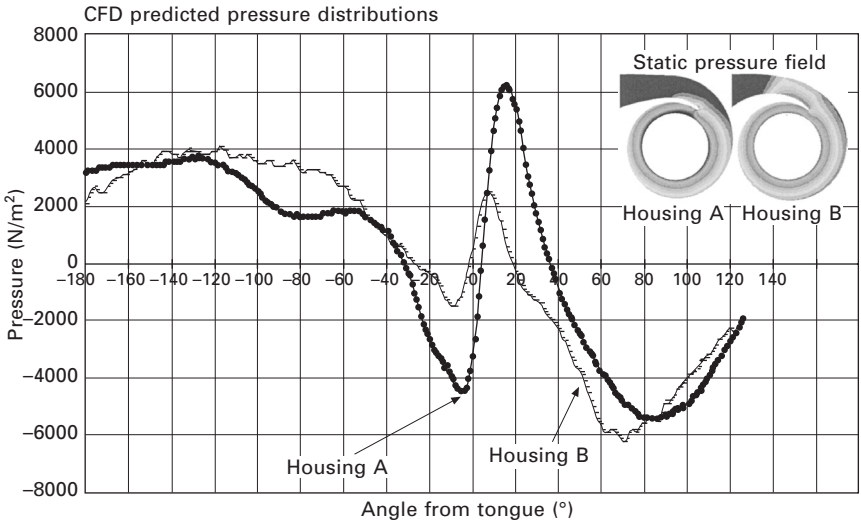
10.5.5 Creep

The high boost pressures associated with HD applications can, in combination with duty cycle, result in sustained high compressor outlet temperatures. Figure 10.19 shows how compressor outlet temperature is influenced by pressure ratio, inlet temperature and efficiency.

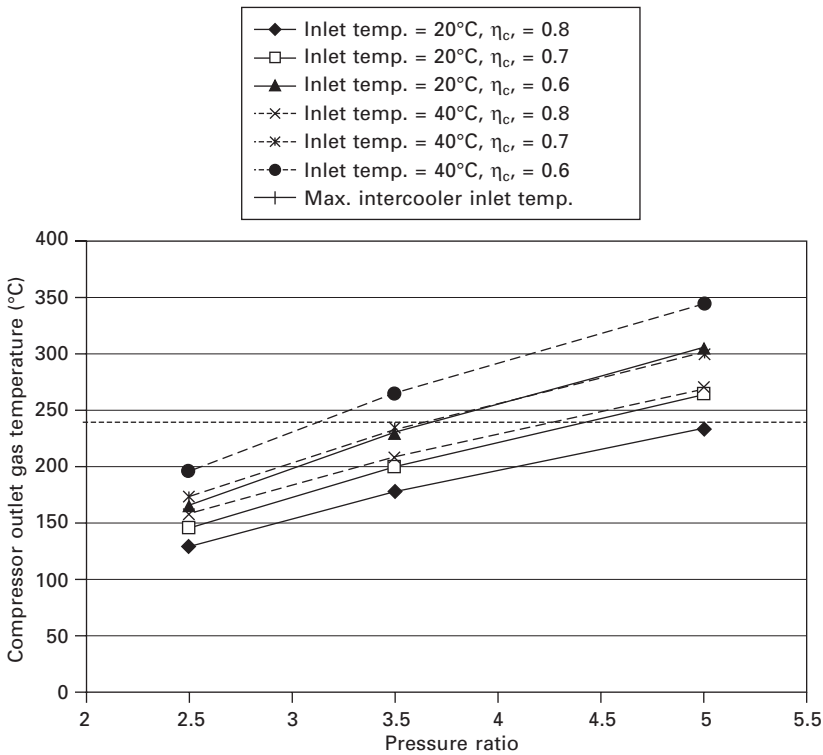
Under steady-state conditions metal temperature, though a function of



10.17 16-Vane VGT Campbell diagram.



10.18 Housing circumferential variation.



10.19 Compressor outlet temperature.

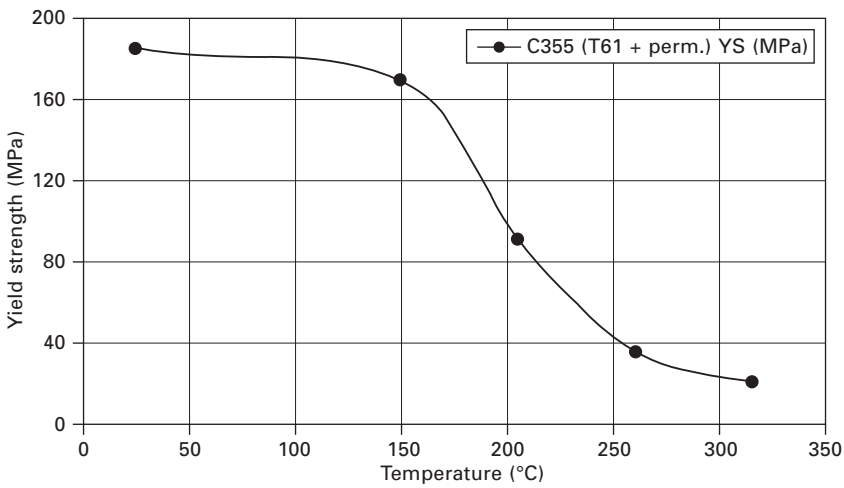
flow velocity, can approach the compressor outlet flow temperature. Hence at high boost and for high inlet temperatures, metal temperatures can soon reach high enough levels to affect the creep rate of the impeller and cover. Wheel creep will ultimately result in rupture but prior to this may cause rubbing and hence balance-related failures. Cover creep will result, at best, in performance degradation. Figure 10.20 shows how impeller material strength varies with temperature. The use of stronger forged aluminium alloys or titanium allows the impeller to tolerate higher mean outlet temperatures. Stronger aluminium casting alloys or cast iron alloys are used for the same reasons on the compressor cover.

10.5.6 Thermo-mechanical fatigue (TMF)

High exhaust temperatures in combination with a cyclic duty cycle result in a significant thermal cycle of the turbine housing. Careful control of housing geometry is essential to prevent thermal fatigue cracks causing failure due to cracking which in some cases can result in external gas leakage or complete flange failure.

10.5.7 Tools and processes for mechanical design

Finite element analysis methods are relied upon heavily for predicting and analysing all the mechanical stresses within the turbocharger, for example centrifugal and vibratory stresses within the rotors, stresses in non-rotating components such as actuator, bracketry and thrust bearings, and stresses



10.20 Impeller material strength variation (compressor impeller material C355 ASM, Handbook data for separately cast test bars).

due to the harmonic response of entire turbocharger assemblies to engine vibration levels. The same tools can also be used for transient and steady-state thermal stress calculations.

Once complete, designs are produced and verified with processes such as low cycle fatigue testing using turbocharger test cells, individual component fatigue tests using tensile test machines, shaker rig testing of brackets/actuators, and blade strain measurements using strain gauges with slip rings or telemetry (depending on rotational speed). Blade tip displacement-based strain measurement techniques are also used as these eliminate the need for strain gauges on the rotor blades.

Detailed reverse engineering techniques, in particular X-ray computed tomography, can be used to capture internal air passage geometry and this along with CFD analysis can be used to understand the actual influence of the geometries on blade strain. Similarly, coordinate measurement machine data is used to capture rotor geometry for comparison against design and FEA calculations for the production geometry. On-vehicle duty cycle data logging is used to provide actual operating conditions and duty cycle information.

In addition to predicting pressure fields for harmonic response analysis, CFD is used to give heat transfer predictions for thermo-mechanical analysis and can be used for the hydrodynamic bearing calculations. The complexity of the hydrodynamic bearing calculations within CFD means that it is common practice to employ empirical journal and thrust-bearing design codes.

10.6 Actuation

10.6.1 Today's applications

Today the turbocharging system may feature actuators for the variable geometry turbine, turbine bypass valve, compressor bypass valve, variable inlet guide vanes, or some combination of these. There are also actuator devices which are not part of the turbocharger, but are certainly part of the air-handling system: intake throttle, EGR control valve, cooler bypass valve and exhaust brake valve.

The rapid increase in the number of actuated components on and around the turbocharger has been driven by the desire to increase engine performance whilst conforming to ever-tightening engine emission limits. Therefore turbocharger actuators are critical components in terms of customer satisfaction and regulatory compliance. Well-executed actuation can provide significant value and differentiation.

10.6.2 Typical requirements for HD actuation

Compared with many other actuated devices on the engine, the turbocharger presents some severe requirements on the actuator in terms of temperature,

vibration, applied load, transient response and duty cycle. The turbocharger actuator may be a relatively high-current device, usually on the opposite side of the engine to the engine control module, requiring a lengthy wiring harness, which can increase the challenge of ensuring electromagnetic compatibility. Heavy-duty turbocharger product can be characterised relative to other market segments as demanding the highest reliability and the longest lifetimes. These requirements drive an actuator architecture which emphasises high performance and high component reliability.

10.6.3 Actuator architecture

The optimum architecture of a turbocharger actuator is a function of performance requirements, environmental requirements, reliability and durability expectation, cost, material capability and technology availability Pneumatic, hydraulic and electric actuators may be considered and each of these options has its own advantages and disadvantages. Pneumatic actuation is a mature technology and very widely used for wastegate control. It is typically applied in more cost-sensitive, lower performance applications. Hydraulic actuation has the potential for high power density, although this usually requires a higher-pressure hydraulic circuit separate from the engine lubrication oil circuit. This separate oil circuit may also be required to provide the oil cleanliness required by the hydraulic control valve. From these considerations it would appear that hydraulic turbocharger actuation is most suited to marine or industrial-vehicle applications where a high-pressure oil circuit can be provided.

Electric turbocharger actuation was introduced on HD turbochargers in 2002 and its application has greatly widened in model year 2007 in the US. Compared to pneumatic and hydraulic actuation, electric actuation promises simpler vehicle installation and lower system cost (no need for pneumatic or hydraulic pipework, control valve, accumulator, etc.). Electric actuation is obviously part of the industry ‘mega-trend’ of the more-electric vehicle or x-by wire, but is a relatively immature and hence rapidly developing technology, at least as applied to turbochargers. Given these factors, only electric actuators will be discussed further.

The first architectural decision for an electric actuation system is the type of motor to use. At the power levels required permanent-magnet motors are generally specified, but these can be sub-divided in rotary or linear, brushed or brushless, limited-angle or continuously rotating types. Solenoids are very common linear actuators for short-stroke on–off operations such as door locks. For turbocharger applications (continuous modulation of nozzle or valve position over a relatively long stroke) the highly non-linear force–stroke characteristic of a solenoid is unsuitable. Torque motors may be used for limited angle, lower torque positioning (up to 90° and 0.5 Nm) and are cost-

effective devices requiring only a simple drive circuit. If higher torque is required it is normal to use a continually revolving motor in combination with gearing. As mentioned above, these motors may be brushed or brushless.

Brushed motors are a mature technology and are manufactured in very large quantities leading to low cost. However, brush arcing can lead to poor electromagnetic compatibility, brush wear limits lifetime and maintaining good contact between the brushes and the commutator can be difficult in high-vibration applications. The brush-wear and brush-bounce problems are particularly relevant in heavy-duty applications. Premium brushed motors may typically be specified to 7000-hour life whereas the lifetime requirement for heavy-duty applications is typically 20 000 hours. Furthermore, for turbine-side actuators, exhaust gas pulsation means that 'dither' cycles seen by the actuator are on the order of 10^9 cycles during life. This is very problematic for sliding-contact interfaces. Brushless motors have no such sliding contact, and a further advantage is the reduced rotational inertia due to the absence of the commutator. This results in a higher torque/inertia ratio which is an advantage in highly dynamic applications.

Brush motors typically carry the windings on the rotor and the magnets on the stator whereas the opposite is true of the brushless motor. The windings are the main source of self-generated heat and also the most temperature-sensitive component. Consequently, another advantage of the brushless motor configuration is that the windings, located on the stator, may be directly cooled. However, winding onto the external diameter of a rotor is easier than winding onto the internal diameter of a stator and so this helps to give the brushed motor a cost advantage. This problem may be resolved by designing the stator with open slots to allow the winding to be wound round a former, then placed into the stator [6, 7] or by using a segmented stator. This may be made of pressed magnetic composite rather than the usual steel laminations to further reduce cost [8, 9].

Given that the bill of materials for a brushless motor is less than for a brushed motor (no brushes, no commutator) it seems likely that as the manufacturing volumes of brushless motors increase they will equal or better the cost of brushed motors. Of course, the brushless motor also requires electronic commutation, which has to be taken into account when considering costs. Drive circuits for brushless motors are being made available at increasing levels of integration. Indeed, for low current applications it is possible to obtain a 'drive on a chip' [10–12]. At higher current levels the switching FETs are packaged separately from the microprocessor but are available in full-bridge and half-bridge modules. This increasing level of integration is helping to reduce the cost of the drive circuit.

If a brushless motor is used, the next architectural decision is whether to locate the drive electronics with the actuator ('smart' actuator) or in the engine control unit ('dumb' actuator). The advantages of smart actuation are:

- Better electromagnetic compatibility (EMC) – no switched voltage in the harness; logic-level commutator switch signals stay within the actuator
- Reduced number of harness wires (typically four vs. eight) so reduced engine control module (ECM) pin count
- Reduced heat dissipation in ECM
- Dedicated controller for relatively high-bandwidth control loop
- Easier repeated application (new turbo on a different engine with different ECM)
- Clearer warranty responsibility: the supplier of actuator supplies both motor and drive electronics.

The advantages of dumb actuation are:

- Better environment for the electronics (heat, vibration)
- Reduced cost of electronics through improved environment and shared circuit board.

The general automotive industry trend is towards distributed electronics. This trend is less clear in the heavy-duty market, where the reliability requirements and long lifetimes tend to favour location of the electronics in the well-protected ECM. It seems that today, the question of smart vs. dumb needs to be evaluated for each engine/turbo development. In the longer term, it seems likely that as electronics integration increases and costs decrease, and with the greater availability of higher-temperature semiconductor devices (such as those based on silicon-on-insulator (SOI) processes), smart actuation will dominate even in the heavy-duty market. Nearer-term there are opportunities to create an environment which can be tolerated by 'standard' automotive electronics even if they are local to the turbocharger. This can be achieved through collaborative design of the turbocharger together with the actuator, focusing on heat transmission and isolation techniques. This is one example of many actuator–turbocharger interaction challenges which are considered further in the following section.

10.6.4 Design process challenges

The challenges of an electric actuation system can be divided into two groups: the technological challenge and the cycle-time challenge. These are described below and then ways to meet these challenges are outlined.

10.6.5 Technological challenge

The technological challenge of actuator development arises from the multi-disciplinary nature of the product and the multiple interfaces that it supports, as summarised below.

Multi-disciplinary

The sub-components that form electromechanical product are 'owned' by a variety of engineering disciplines:

- Mechanical: structures, gears, bearings, linkages
- Electrical and electronic: analogue and digital circuit design, simulation, layout, component selection
- Motor design
- Electromagnetic compatibility
- Dynamic modelling and control system design
- Software: requirements capture, algorithm development, coding, testing
- Materials: metals, composites, thermoplastics, elastomers.

Multiple interfaces

A smart actuator has various interfaces with the turbocharger and engine system:

1. A mechanical interface with the turbocharger, having the same issues as a traditional turbocharger, and perhaps also some new issues (e.g., gear design and alignment requirements).
2. An interface with the engine control unit, which has three aspects:
   - Mechanical: connector housing, contact terminal and wiring harness reliability and durability need to be proven in the environment.
   - Electrical and electromagnetic: voltage and current levels need to be compatible, electromagnetic emissions and immunity need to be acceptable.
   - Software and communications protocol. Protocols need to be agreed to ensure correct communication, software releases need to be coordinated and tested prior to implementation to ensure compatibility.
3. A performance interface with the turbocharger and engine system. The dynamic characteristics of the component can influence engine performance and emissions. These characteristics can be influenced both by component design (motor torque, mechanism stiffness, backlash) and by control system design and implementation.
4. A diagnostic interface with the engine control unit and perhaps also the service tool. Diagnostic design needs to be carefully considered in order to provide relevant information to meet diagnostic legislated requirements and service technician troubleshooting. Similar routines may also be designed to record product duty cycle information. This can be used in reliability analysis and to support future product design.

10.6.6 Cycle-time challenge

One challenge of actuator development is that one needs the turbo hardware running on the engine to get the data to define first the turbo design and then the actuator design. The pressure to reduce development cycle-time makes this increasingly difficult. This challenge is compounded by development times which may be as long for the actuator as for the turbocharger, and as electric replaces pneumatic actuation there is less historical data or experience on which to base the design.

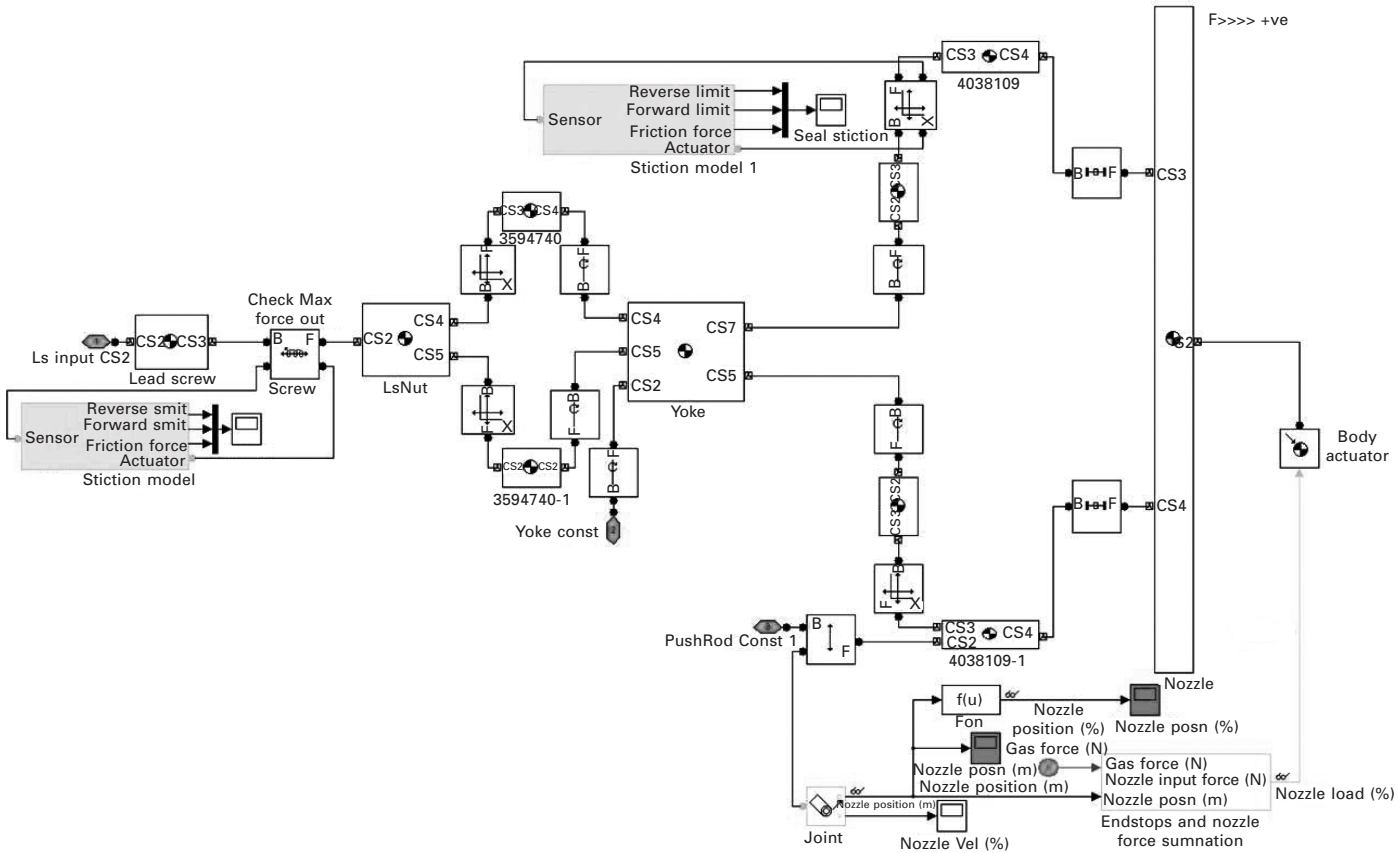
In the case of an electric actuator, basic design inputs and requirements include stroke, applied force (mean and at engine firing frequency), speed of response, position accuracy and resolution, packaging envelope, mounting arrangement, and environmental requirements (temperature, vibration, EMC). As the engine development programme progresses these requirements may change.

10.6.7 Design process solution: analysis-led, multi-domain design

It is clear that methods to manage the complexity of design within acceptable cycle time are required. Analysis-led (also known as model-based) design methods can be used to help meet this challenge. Various tools are now available which support system simulation, with multiple engineering domains (mechanical, electrical, control, etc.) being included together in one simulation. These include Easy5 [13] and Saber [14].

It is also possible to perform multi-domain simulations by connecting existing design and simulation tools. For example, engine cycle simulation in GT Power may be run within a dynamic system simulation in Matlab/Simulink. Furthermore, mechanism models suitable for dynamic simulation may be automatically generated from 3D-CAD by linking Pro-Engineer to Simulink via SimMechanics, another toolbox from The MathWorks [15]. With this approach the CAD models of the turbo and actuator mechanism can be imported automatically into the Mathworks environment for simulation of the dynamics, design of the control system and development of the software. The corresponding SimMechanics representation of a mechanism design can be seen in Fig. 10.21.

One significant success of this approach has been the ability to optimise motor torque, inertia and gear ratio in the model before making parts. Plate III (between pages 364 and 365) shows a plot of response time vs. gear ratio and applied load. For low loads, response time increases as the gear ratio between motor and load increases, as might be expected. However, at high loads the opposite is generally true. This observation allows the design of a gear ratio which minimises both the average response time and the variation of response



10.21 SimMechanics diagram.

time with load. In future this development environment may be further extended to automatically generate real-time code for downloading to the prototype hardware. Figure 10.22 shows schematically these software connections.

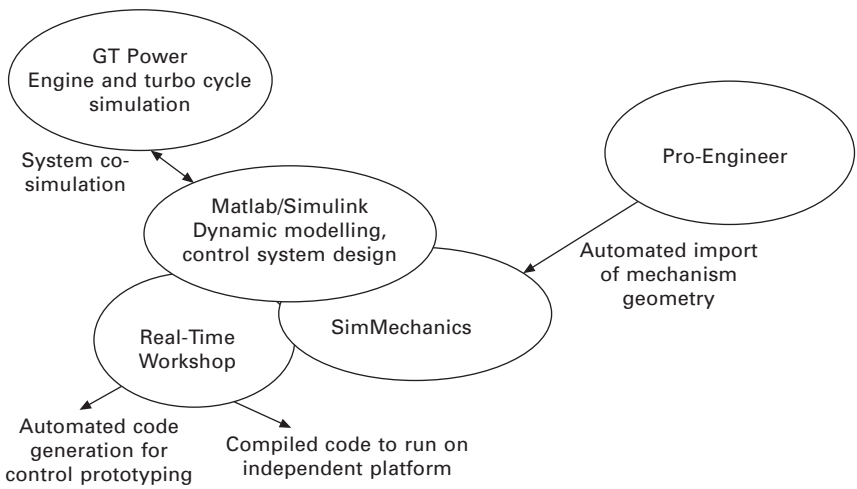
Regardless of the specific software tools used, the benefits of analysis-led design in a connected software environment include:

- Automated creation of a dynamic model from CAD, reducing the time and potential for errors in describing the mechanism in the dynamic simulation domain
- A means of specifying performance requirements and also validating designs against those requirements
- A means of defining and validating software
- Parallel design (concurrent engineering) of turbocharger and actuator.

These advantages will be essential in meeting the future requirements of better performing, more durable, smaller, cheaper, more rapidly developed actuation systems for heavy duty turbochargers.

10.7 Future trends

It is likely that the legislated levels of NO_x and PM emissions will stabilise in future years, and the focus of new, progressively stricter emissions legislation will be CO_2 (or fuel economy in the US). Advanced combustion systems, variable valve timing and more complex test procedures will ensure a continuing need for more precise control of the air delivered by the turbocharger. This will help to reduce NO_x and PM emissions, allowing the fuel system to be controlled in a more fuel-efficient regime.



10.22 Analysis software connectivity.

Downsizing and higher engine power density will require higher pressure turbochargers. Two-stage systems may become more prevalent. However, the desire for a smaller space claim is also evident. Attention will focus on customer specific compact installations. This in turn leads to increased problems of high temperatures and heat dissipation within the turbocharger components. These challenges will have to be met with increased reliability and durability, and improved serviceability.

10.8 Sources of further information and advice

Turbocharging the Internal Combustion Engine, by N. Watson M.S. Janota. Macmillan, 1982 (no longer in print)

Fundamentals of Turbocharging, by N.C. Baines. Concepts NREC, 1998

Turbomachines: A Guide to Design, Selection and Theory, by O.E. Balje. John Wiley & Sons, 1981

Permanent Magnet Motor Technology: Design and Applications, by J.F. Gieras and M. Wing. Marcel Dekker, New York, second edition, 2002

10.9 References

1. Büchi A.J., *Exhaust Turbocharging of Internal Combustion Engines*, Franklin Institute, 1953
2. McKean P.S. *et al*., 'Variable turbine', European patent EP0884453
3. Fisher F.B. and Langdon P., 'Improvements in compressors', European patent EP0229519
4. McEwen J.A., 'Turbocharger with annular bypass', European patent EP0627550
5. Kitson S.T. *et al*., 'Improving analysis capability in order to reduce turbine HCF', 8th International Conference on Turbochargers, I.Mech.E, London, 2006
6. Krawczyk A. (ed.), 'An efficient BLDC with gearbox for EGR', in *Electromagnetic Fields in Mechatronics, Electrical and Electronic Engineering*, IOS Press, 2006
7. Prudham D., 'Polyphase motor in particular for driving the hand of a display', European patent EP 0949747
8. Jack A.G. *et al*., 'Permanent-magnet machines with powdered iron cores and prepressed windings', *IEEE Trans. Ind. Appl*., vol. 36, no. 4, July/August 2000, pp. 1077–1084
9. Jack G., Mecrow B.C. and Evans S.A., 'Low cost SMC brushless DC motors for high volume applications in the automotive sector', Second IEE International Conference on Power Electronics, Machines and Drives, p. v1-356, 31 March–2 April 2004
10. http://www.toshiba-components.com/applications/HomeAppliances/PowerProducts/SinglechipInverter/SingleChipInverter.html
11. http://www.toshiba-components.com/applications/Automotive/MotorControl.htm
12. http://www.atmel.com/dyn/corporate/view_detail.asp?FileName=ATA6824_27_32_10_16.html
13. http://www.mscsoftware.com/products/easy5.cfm
14. http://www.synopsys.com/products/mixedsignal/saber/auto/saber_auto.html
15. http://www.mathworks.com/products/matlab/

11

Alternative combustion system for heavy-duty diesel engines

W. SU, Tianjin University, China

Abstract: An alternative combustion technology for HD diesel engines has been developed to operate the engine with PCCI (premixed charge compression ignition) combustion at low load, and combined PCCI and so-called lean diffusion combustion (LDC) at medium and higher loads, through development of technologies of multi-pulse injections and combustion chamber designs. The LDC combustion process covers the early phase mixing process, the rich premixed combustion process and the later phase mixing process. Enhancement of mixing is essential and critical to the LDC combustion. Countermeasures to enhance the mixing rate are discussed in relation to multi-pulse injection and combustion chamber design.

Key words: alternative combustion of internal combustion (IC) engines; strategy of multiple-pulse injection, high mixing rate combustion chamber, lean diffusion combustion, compound combustion in IC engines.

11.1 Introduction

11.1.1 Background and themes

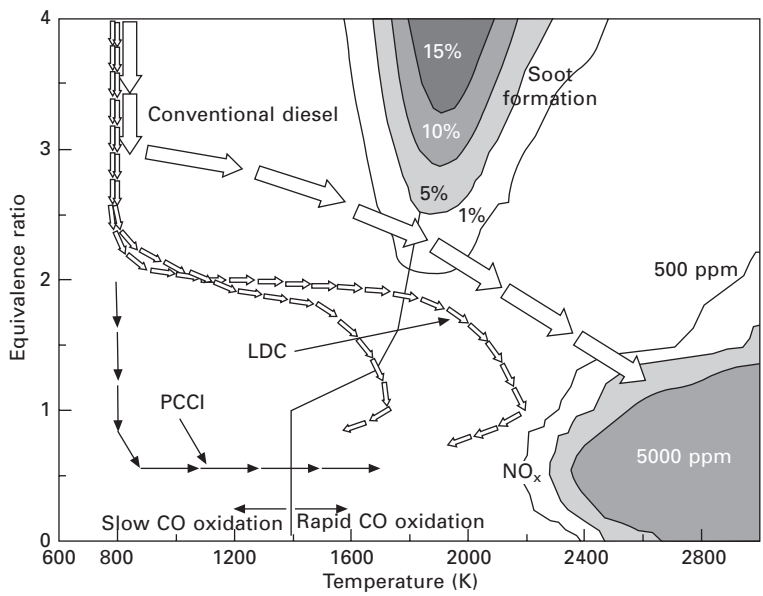
A lot of research and development work on HCCI (homogeneous charge compression ignition) or PHCCI (partial HCCI) has been reported for heavy-duty (HD) diesel engines (Zhao *et al.*, 2003). However, HCCI combustion is normally limited to low and medium load operations by the excessive rate of the pressure rise due to simultaneous burning of the whole charge in the cylinder. An alternative combustion technology, termed compound combustion for HD diesel engines, has been developed to operate the engine with PCCI (premixed charge compression ignition) combustion at low load, and combined PCCI and so-called lean diffusion combustion (LDC) at medium and higher loads, through development of technologies of multi-pulse injections and novel combustion chamber designs. The LDC is defined as a combustion process of diesel spray diffusion combustion, starting to burn with a quite homogeneous mixture and with an overall fuel/air equivalence ratio equal to or less than 2.0, which is the critical value for soot formation. The burning can continue to proceed and complete only under conditions of a suitable mixing rate. The rate of heat release (ROHR), the combustion temperature and the combustion completeness depend strongly on the mixing process.

In this chapter, the compound combustion technology will be described

both in fundamental terms and in terms of the application aspects of the technology.

11.1.2 Theoretical analysis on Φ–T plane

The combustion process in a HD diesel engine starts with fuel injection, and then a fuel spray is formed by going through spray formation stages such as break-up, atomization, evaporation and air-entrainment. In the meantime the fuel is heated by the entrained air. A very slow chemical reaction of molecules of fuel with oxygen starts, when a molecule of fuel meets a molecule of oxygen. However, only when the charge temperature rises to over 800 K, which is the low reaction temperature for diesel fuel, does the reaction rate reach a higher level, accompanied by more apparent heat release. If the temperature of the mixture of fuel with air rises to over 1000 K, the reaction rate rises quickly with a higher rate of heat release, which is termed the high temperature reactions of diesel fuel with oxygen. The high temperature reaction rates strongly depend on the mixture equivalence ratio and the ambient temperature. Therefore, the in-cylinder mixture conditions can be represented by the fuel/air equivalence ratio Φ and the combustion temperature T, as shown in Fig. 11.1, which illustrates what is called the Φ–T plane, proposed by Kamimoto and Bae (1988) and Kitamura *et al.* (2002). The formation zones for soot and NO_x are included on the Φ–T plane.



11.1 The Φ–T plane.

Although a qualitative analysis, the diagram is effective for understanding of a combustion concept. But for alternative combustion in HD diesel engines, various amount of EGR (exhaust gas recycle) are employed and the oxygen concentration can be adjusted by adjusting boost pressure. This must be taken into account in calculating the equivalence ratio Φ.

The combustion path of a conventional HD diesel engine is qualitatively represented on the Φ–T plane (Fig. 11.1) by hollow arrows. The path starts from fuel injection. As the fuel spray develops, the mixture equivalence ratio drops quickly. But the mixture temperature changes slightly, because of slow heating up by air-entrainment and very weak chemical reaction. By the end of the ignition delay period, some points in the periphery of the fuel spray start high temperature reactions and then trigger auto-ignition of the premixed mixture, resulting in a rapid increase of the mixture temperature. Just as shown by the arrows, an almost 90° turn is observed, showing a rapid rise of temperature. Then the subsequent combustion process is dominated by the diffusion rate of the fuel spray. The interaction of the rate of heat release and the rate of mixing decides the slope of the combustion path, decreasing the mixture equivalence ratio and increasing the mixture temperature. Unfortunately the combustion path goes through first the soot formation zone and then the NO_x formation zone. This is essentially the source of engine-out emissions.

The objectives of research on alternative combustion of HD diesel engines are to seek new combustion paths and their realizing technology, so as to avoid the soot and NO_x formation zones. Figure 11.1 shows two such possible paths that do not go through soot and NO_x formation zones. One of the paths is the PCCI path, which can be organized by early direct ignition. For this path, the diesel fuel is injected at a relatively early stage of the compression stroke, when the in-cylinder pressure and temperature are quite low, resulting in a very low chemical reaction rate. Therefore the fuel by early direct injection has enough time to complete homogeneous mixing before ignition. The PCCI combustion can reach very low soot and NO_x emissions, but it is limited in operational range by a series of technical obstacles, which include:

- Impingement of injected fuel on the cylinder wall due to lower in-cylinder pressure and temperature during early fuel injection. This will dilute lubrication oil and increase fuel consumption.
- Knock combustion caused by early ignition timing of the premixed mixture. This often occurs at 200°CA BTDC (before top dead center) and results in a sharp heat release rate. As engine load increases, the rising rate of in-cylinder pressure increases and the engine-out NO_x emissions increase.

The other combustion path to prevent going into the soot and NO_x

formation zones is the LDC path as indicated in Fig. 11.1. The LDC path is organized by a main fuel injection at the injection timing around the engine top dead center (TDC). To realize the LDC path, significant effort must be made to enhance the mixing process of the main injection fuel so that the equivalence ratio of the mixture will fall to about 2.0, the critical value for soot formation. Then a premixed combustion breaks out, accompanied by a rapid increase of mixture temperature. But the heat release is greatly limited by lack of oxygen, resulting in the formation of incomplete combustion products. The following combustion is again controlled by mixing, by which the incomplete combustion products meet with oxygen and complete the combustion at a certain in-cylinder temperature. In fact, the mixing rate decides, to a large extent, the combustion efficiency (completeness) and the engine cycle thermal efficiency. Section 11.3 will discuss this in detail.

11.2 Premixed charge compression ignition (PCCI) combustion organized by early direct injection

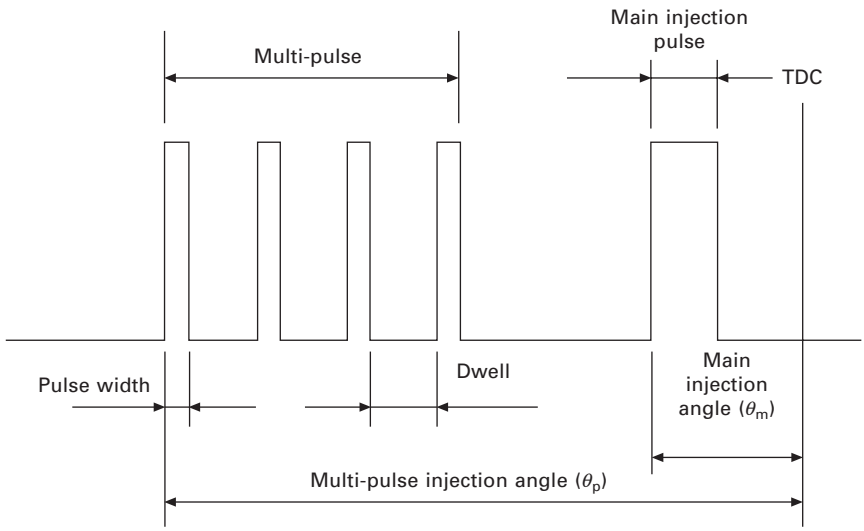
11.2.1 Strategies of early fuel injections

Early direction injection has been the most commonly investigated approach to achieve diesel-fueled alternative combustion based on the concept of the HCCI. But there still exist obstacles due to the diesel fuel's properties of low volatility and high cetane number. Furthermore, HD diesel engines are equipped with only one fuel handling system with high fuel injection pressure, which tends to cause wall wetting due to the low in-cylinder gas density, resulting in increased unburned hydrocarbons (uHC) emissions and dilution of lubrication oil. A fuel injection technology for these engines that can help homogeneous mixture formation without wall wetting is in active demand.

To reduce spray–wall impingement, enhance fuel/air mixing, and improve engine performance, different injection strategies were proposed by many researchers. Takeda *et al*. (1996) and Nakagome *et al*. (1997) designed their diesel early injection DI HCCI combustion by using two colliding sprays in their premixed lean diesel combustion (PREDIC) system, in which three injectors were installed on the cylinder head. Sun and Reitz (2007) proposed a fuel injection strategy named AIS, which used low-pressure (5–20 MPa) narrow-angle sprays in early injections to prepare a homogeneous mixture for HCCI-like combustion, and to use conventional high-pressure (>100 MPa) wide-angle injections for conventional diesel diffusion combustion. One purpose of using AIS was to control spray penetration (using different injection pressures) and to match spray targeting with the piston position (using different included angles) so that spray–wall impingement can be avoided or reduced. The above two schemes have a common future of using separated fuel systems for early fuel injection and second-stage fuel injection.

The complexity of the fuel system poses serial obstacles in their engineering applications. Kobori *et al*. (1996) showed that fuel/air mixing can be enhanced by using micro-hole nozzles (orifice diameter as small as 0.06 mm), in order to reduce wall wetting. Walter and Gatellier (2002) developed a narrow angle direct injection (NADI) combustion system applied to homogeneous charge compression ignition at part load and switches to conventional diesel combustion to reach full-load requirements. Lechner *et al*. (2005) presented their study results using injectors with different included angles. It was shown that a low flow rate, 60° spray cone angle injector nozzle, optimized EGR rate and split injection strategy can reduce engine-out NO_x by 82% and PM by 39%, at the expense of a modest increase (4.5%) in fuel consumption, having the potential for meeting upcoming stringent fuel specific NO_x emission levels of less than 1.0 g/kg-fuel and fuel-specific PM levels less than 0.25 g/kg-fuel. But as the authors pointed out: 'the narrow cone angles may prove particularly effective at low load PCCI conditions, but may inhibit performance at high load, conventional combustion conditions.'

The author has presented a HCCI combustion technology termed compound combustion (Su *et al*., 2003, 2005a), which operated the engine with PCCI combustion at low loads and combined the PCCI combustion and the LDC combustion at medium and high loads. The compound combustion process is basically organized by the multi-pulse fuel injection strategy. Through multi-pulse injection mode modulations the PCCI combustion could reach near-zero NO_x and soot emissions at low load. Adding the LDC combustion to the compound combustion could produce very low NO_x and soot emissions at middle loads. Figure 11.2 shows the control time sequence of the technology



11.2 Schematic of the time sequence of multi-pulse injections.

of multi-pulse injection, which features flexible control of the width of each pulse injection, the dwell time between injections, and the start and end of the multi-pulse injections. Such control enables more fuel injected with reduced spray penetration, avoiding impact of fuel on the cylinder liner. A CFD simulation study (Su *et al*., 2004) also showed that the dwell time between injection pulses could be controlled to produce disturbed fuel parcels separate from each other, hence enhancing the turbulent mixing of fuel with air.

Helmantel and Denbratt (2004) carried out a study on HCCI combustion organized by five short injections in a single-cylinder test engine. The results showed that the NO_x and soot emissions were reduced by 98% and 95% respectively compared to those of conventional diesel operation, while the uHC and CO emissions increased dramatically. Buchwald *et al*. (2004) studied the multi-injection HCCI on a direct injection passenger-car diesel engine equipped with a turbocharger and a common rail injection system. Comparing the test results with those of engine operation of the Euro III mode and the minimum BSFC mode, the HCCI mode resulted in a dramatic decrease in NO_x and soot emissions. However, the uHC and CO emissions were 3.0 and 8.5 times those of the Euro III mode respectively. Beatrice *et al*. (2002) found that the Euro IV emission limits can be approached without advanced after-treatment systems by using multi-pulse injection with the optimized dwell time. Liu and Reitz (2005) performed computational work to investigate the effects of one to five injections on a HSDI diesel engine at part load. In addition, some investigations on fundamental aspects of multi-pulse injection have shown that it has a significant effect on the fuel/air mixing process.

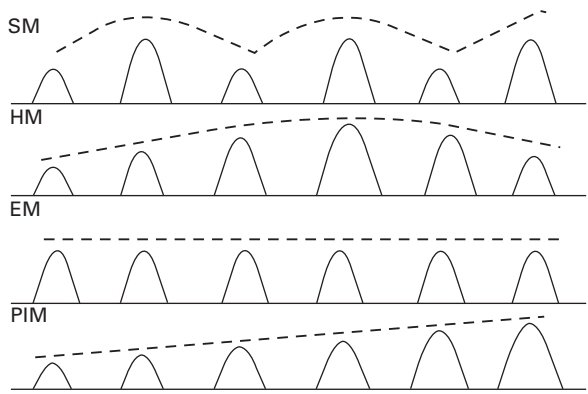
11.2.2 Injection mode modulation and optimization

Recent reports on compound combustion by the multi-pulse fuel injection strategy further confirmed that near-zero engine emissions of NO_x and soot could be achieved in a certain operation range (Su *et al*., 2005b, 2007). But it was found that the engine thermal efficiency of the compound combustion mode dropped by about 3%, compared with that of a conventional DI diesel engine, due to uncompleted combustion and increased heat loss attributed to the advanced combustion phase (Su *et al*., 2004, 2006). Therefore, the mechanism of the mixing process needs to be further investigated, including the effects of multi-pulse injection parameters on spray atomization, evaporation and mixing, so that the injection mode (injection rate pattern) for low engine emissions and potential high thermal efficiency in wider engine operation conditions can be precisely designed. Computational studies showed that the multi-pulse injection timing was of particular importance (Su *et al*., 2006). For earlier injection cases, the pulse width showed a strong impact

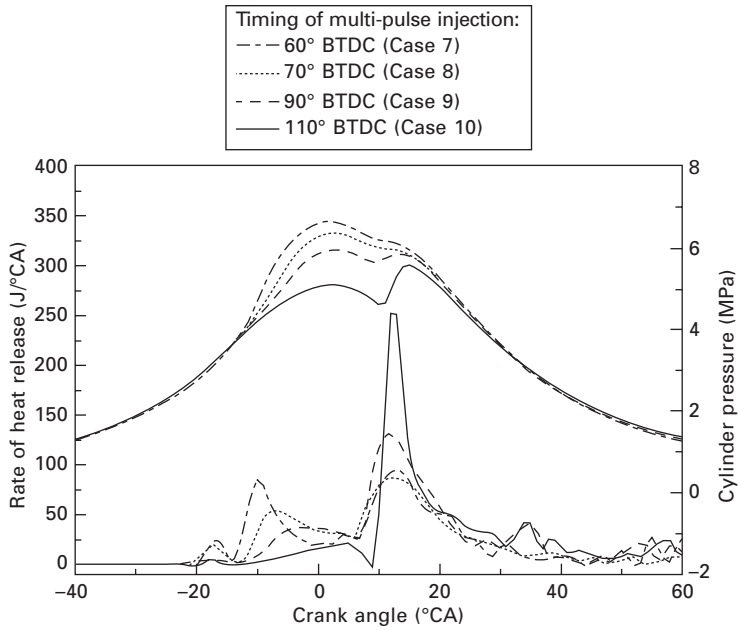
on evaporation and mixing rate. Long width led to over-penetration of fuel sprays, which would result in severe wall wetting. Hence, short pulse widths should be employed for earlier pulse injections. The dwell time was also an important factor, and a short dwell time would result in less stratification of the fuel for later injection cases. In general, it was important to match and optimize the above three injection parameters, and then the engine could operate in a well-premixed mode.

Based on the understanding of the parameters of multi-pulse injection, a series of typical injection modes of four- or five-pulse injections were modulated and named the even mode (EM), hump mode (HM), staggered mode (SM) and progressive increase mode (PIM) respectively, as shown in Fig. 11.3. The experimental engine results for these injection modes showed that the low temperature reaction always started at about 20°CA BTDC and the corresponding in-cylinder temperature was about 800 K, as predicted by chemical kinetics (Su and Huang, 2005). But the ROHR (rate of heat release) and the peak pressure rising rate during high temperature reaction varied with different injection timings and modes. At earlier injection timings such as 110°CA BTDC, lower peaks of ROHR appeared than at later injection timings (70°CA BTDC). This indicated that multi-pulse injection strategies could offer the freedom to adjust the ROHR and the in-cylinder pressure rising rate (see Fig. 11.4). This feature of early multi-pulse injection is extremely important, because it offers the possibility to design and control the entire compound combustion to pursue high thermal efficiency and very low NO_x and PM emissions. Therefore, optimization of injection rate patterns (modes) is crucial to the optimization of the entire compound combustion. The aims of the optimization of multi-pulse injection modes are:

- Avoiding fuel spray impingement on the cylinder liner



11.3 Typical injection rate patterns.

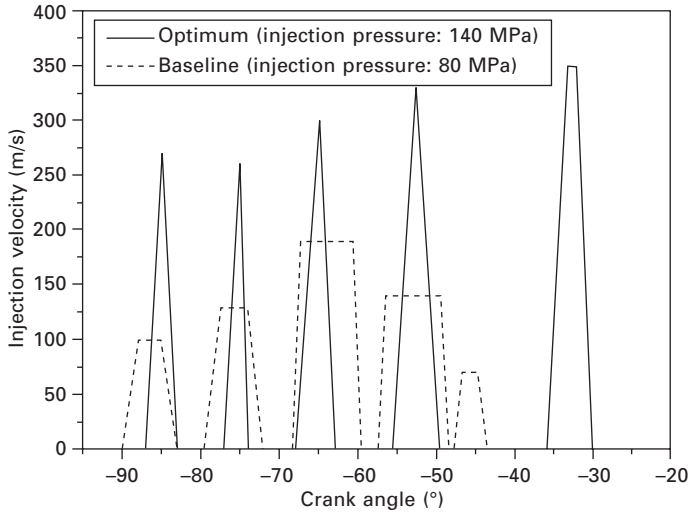


11.4 Adjusting ROHR by adjusting the injection timing and modes (IMEP = 0.67 MPa, case 7–10, P_{cr} = 80 MPa, 1400 rpm).

- Retarding ignition timing and slowing ROHR during PCCI combustion to reduce the heat loss due to heat transfer and the rate of pressure rise
- Reducing the PCCI combustion temperature so as to generate a longer mixing time for the stage of premixed mixture preparation of the LDC combustion.

Optimization for avoiding wall wetting

Huang *et al*. (2008) reported an optimization study by design of a series of multi-pulse injection modes with four or five pulses in each mode. In addition, a micro-genetic algorithm coupled with a modified 3D engine simulation code was utilized to optimize the injection parameters, including the injection pressure, the start-of-first-injection timing (SOI), the fuel mass in each pulse injection and the dwell time between consecutive pulse injections. Figure 11.5 compares the optimized injection profiles with the baseline mode. The optimum mode is characterized by a high injection pressure of up to 140 MPa and an injection rate of progressively increasing shape. The BSFC (brake specific fuel consumption) in the optimum case decreases by 25.4% compared to the baseline case, while the NO_x and soot emissions are acceptable. Plate VI (between pages 364 and 365) shows that



11.5 Comparison of optimized injection mode with the baseline mode (by raising the injection pressure and adjusting pulse timing).

for the optimized case, the droplet size and number decrease dramatically due to the increase of injection velocity. In addition, enhanced fuel/air mixing and reduced spray penetration result in a more homogeneous mixture and less wall impingement. Furthermore, reduced injection duration leads to a reduction of penetration length, resulting in less fuel on the cylinder liner. This is also supported by LIF (laser induced fluorescence) measurements (Su *et al.*, 2008), which showed that the measured spray penetrations of both vapor phase and liquid phase were much shorter.

Optimization for retarding and slowing the ignition process

In order to retard and slow the ignition process of the PCCI combustion for the purpose of reducing the engine heat loss and rate of pressure rise, Yu *et al.* (2008) performed a study on the effect of fuel stratification on the ignition process by developing a mixing and chemical characteristic time-scale model. The model was intended to correlate non-uniformity of mixture with mixing time-scales. It was found in this study that the start of the low temperature reaction, the start of the high temperature reaction (ignition) and the appearance of the highest combustion temperature happened to occur in the same area of the combustion bowl, where the mixture equivalence ratio is close to the mean equivalence ratio of the overall mixture. The ignition process of the PCCI combustion was characterized by low initial ignition temperature (1000–1200 K) and slow enlargement of ignition regions because of its slow chemical kinetics of the lean mixture. The neighboring areas of

the initial ignition region accumulated heat with a finite speed and finally came into auto-ignition after a relatively long delay. Therefore, the ignition process was determined by the propagation of the auto-ignition volume and was affected by the fuel distribution. The more homogeneous the mixture distribution became and the more near-stoichiometric a fuel/air mixture was formed, the more violent auto-ignition process would be observed, and vice versa. A V-type distribution of fuel fraction versus equivalence ratio revealed that the high temperature reaction became weaker due to less fuel taking part at the start of the high temperature reaction, when less heat was released from the ignition area. Consequently, a larger fraction of the mixture in both richer and leaner regions absorbed heat from the ignition, resulting in a delay in the start of the rise of temperature. For optimized compound combustion, the heat released during the PCCI stage should be reduced to benefit the LDC combustion. Therefore, a new target was set to pursue so-called 'no fire' PCCI, where intermediate products are produced from the fuel oxidation reaction with little heat release and temperature rise, consequently providing a longer chemical time-scale for mixing of the fuel injected during the main injection so that much fuel/air mixture may reach the critical value of equivalence ratio of about 2.0. The high combustion temperature produced by the LDC combustion will trigger the burning of the existing intermediate and incomplete products. In addition, the problem of knocking combustion limit (Su WH *et al*. 2005a) with PCCI stage will be consequently solved. In order to reach the target, the control of ambient temperature and EGR are the parameters with the most potential, as well as the suitable stratification of fuel concentration and temperature.

11.3 Lean diffusion combustion

11.3.1 Characteristics

As described above, the concept of compound combustion combines the PCCI path with the LDC path in the Φ–T plane (Fig. 11.1) and is realized by a multiple fuel injection strategy. This includes two injection periods. The first group is a series of early multi-pulse injections with deliberately designed injection rate patterns. This is followed by a group of later injections, starting around the engine top dead center. For some cases the later injection includes only a single main injection, but for reduction of engine-out emissions a split main injection is often employed.

The LDC can be divided into three stages. Stage 1 is for premixed mixture preparation during ignition delay of the main injection. It is the time period from the start of main injection to the start of auto-ignition. This stage is dominated by the fuel mixing, while the chemical time-scale in this period is much longer than the mixing time-scale. If the mixing rate is high enough, the mixing zone becomes more homogeneous and the equivalence ratio of the

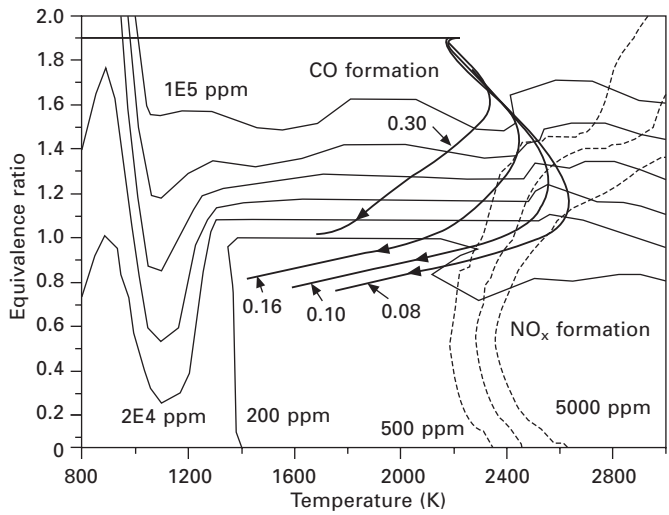
premixed mixture drops quickly and becomes about 2.0, which is the critical value for elimination of the formation of soot. In order to operate the engine in the LDC mode for an operating range of higher loads and speeds, more premixed mixture with an equivalence ratio of about 2.0 must be prepared during the ignition delay. This compels one to develop advanced technologies to control the in-cylinder conditions, including temperature, pressure and gas composition, enlarging the chemical characteristic time-scale and enhancing the mixing rate.

To enlarge the chemical characteristic time-scale of the premixed stage, there are many possible countermeasures to be employed, which include temperature control, variable engine compression ratio, later start of main injection, higher EGR and so on. The EGR may draw down the in-cylinder temperature because of a higher specific heat value than that of air. The effect of dilution of oxygen concentration would slow down the rise of combustion temperature. However, the LDC process follows the PCCI combustion: the control of in-cylinder conditions during the LDC process must be influenced by the PCCI combustion. A comprehensive optimization of in-cylinder conditions is necessary in order to take advantage of the compound combustion in terms of operating range of load and speed with very low NO_x and soot emissions. For instance, the PCCI combustion is intended to be organized as a fuel reforming process so that less chemical heat is released and less rise of in-cylinder temperature is expected. The consumption of oxygen during PCCI combustion results in a decline of oxygen concentration in the stage of LDC. This has two implications for the LDC process. One is the dilution effect of oxygen, enlarging the chemical time-scale; the other is slowing of the mixing rate between fuel and oxygen. Therefore, the countermeasures of control of the chemical time-scale in the path of the LDC are strictly limited because of the existence of PCCI combustion. On the other hand, the control of the PCCI combustion has the potential to improve the entire compound combustion process. In any case, to make as much premixed mixture as possible with $\varphi \leq 2.0$ in stage 1 of the LDC path, enhancement of mixing of the main injection fuel with oxygen during the ignition delay is the deciding technology. For this purpose many technologies of mixing enhancement can be employed, such as raising the injection pressure, reducing the nozzle hole diameter and boosting the intake charge. However, reducing the nozzle hole diameter is limited by the allowed injection duration, the boost pressure is limited by the allowed combustion pressure, and the common rail pressure of the fuel system is limited by parts strength and driving energy consumption. Su *et al*. (2003) and Su and Zhang (2005) put forward a design for the combustion chamber of a heavy-duty diesel engine termed BUMP (Bump-Up Mixing Process). The idea of the design is to better utilize the mixing energy from the fuel injection through the design of the combustion chamber geometry. This will be further discussed in Section 11.3.3.

Stage 2 of the LDC is the premixed combustion at the fuel/air equivalence ratio of about 2.0. It is characterized by first a 'richer premixed combustion', with uncompleted combustion, followed by a rapid heat release and temperature rise, which depend on the mass of the premixed mixture, the mixture fuel/oxygen equivalence ratio and the EGR. Therefore, the combustion can only be completed through further mixing with oxygen in the cylinder. The further mixing process is stage 3 of the LDC, which is a mixing-dominated combustion in the later phase of combustion.

11.3.2 The role of mixing in the later phase of combustion

During late combustion, the cylinder volume expands and oxygen concentration is relatively low. As a result, the peak combustion temperatures at the premixed burning stage usually do not reach the adiabatic flame temperature line from the burning of the mixture with 15% oxygen concentration at 1000 K (see Fig. 11.6). Subsequently, in mixing-controlled combustion, Stage 3 of the LDC departs still further from the adiabatic flame temperature line due to continued cooling by the volume expansion as the piston moves down. Along this path segment, CO, uHC, and other products of the premixed combustion are oxidized as mixing proceeds. The rate of oxidation of the intermediate products produced in stage 2 of the LDC depends on the mixing rate of the products with oxygen. So stage 3 is again mixing-dominated combustion. In order to analyze theoretically the effects of mixing on the LDC, a quantitative



11.6 Effects of mixing rates on low-temperature diesel combustion with 40% EGR rate on the CO–ϕ–T map.

'CO–*Φ*–*T*' map (Fig. 11.6) has been created by the author by performing the same zero-dimensional calculations as in the methods of Kitamura *et al*. (2002) and Akihama *et al*. (2001). The formation of CO as a function of equivalence ratio and combustion temperature prevalent in stages 2 and 3 of the LDC in HD diesel engines is calculated by using detailed kinetics of *n*-heptane (Curran *et al*., 1998). As shown in Fig. 11.6, the calculated CO concentration increases with increasing equivalence ratio, in particular in the area of equivalence ratio higher than 1.0. As the equivalence ratio approaches 1.0, the CO concentration increases dramatically at temperatures below 1400 K. This is due to the low production of OH-radicals at these temperatures, resulting in only partial oxidation of CO to CO_2. As shown in Fig. 11.6, the low emission, high efficiency region is found to be located from approximately 1400 K to 2000 K combustion temperature, and on the lean side of the stoichiometric equivalence ratio.

In order to achieve high efficiency combustion, mixing must be completed before temperatures drop below 1400 K. This requires the mixing rates to be kept high, but this becomes more difficult due to the reduction of mixing energy resulting from volume expansion and the need to mix with a greater volume of ambient fluid under low oxygen conditions. Additionally, the lower flame temperatures of diluted mixtures imply that less time is available before the temperature drops below the critical CO oxidation temperature as the cylinder volume expands. As the mixing time, which is defined as the time to accomplish combustion, is decreased, the mixing rate increases and the combustion paths tend to enter the zones of higher NO_x formation as shown in Fig. 11.6. In the case of 40% EGR, the combustion path with mixing time of $\tau = 0.3$ ends up in the zone of high CO formation due to the relatively lower mixing rate under low O_2 concentrations, resulting in higher incomplete combustion products and lower indicated fuel conversion efficiency. When the mixing time τ is decreased to less than 0.10 (i.e., increasing the mixing rate), the combustion path crosses the zones of higher NO_x formation, leading to the increase of NO_x emissions.

It is concluded from the above analyses that during late phase combustion with a locally rich mixture, a high mixing rate may increase NO_x emissions whilst a low mixing rate increases CO emissions. As the EGR rate increases, the mixing rate must be proportionally increased so as to reduce CO emissions and lower NO_x emissions simultaneously. The results of the calculation also indicate that the employment of EGR causes two opposing influences. One is to increase the chemical time-scale due to the effects of dilution and specific heat capacity; the other is to decrease the mixing rate between fuel and oxygen due to the dilution effects of oxygen. From this point of view, careful optimization of the EGR rate is necessary in organizing compound combustion.

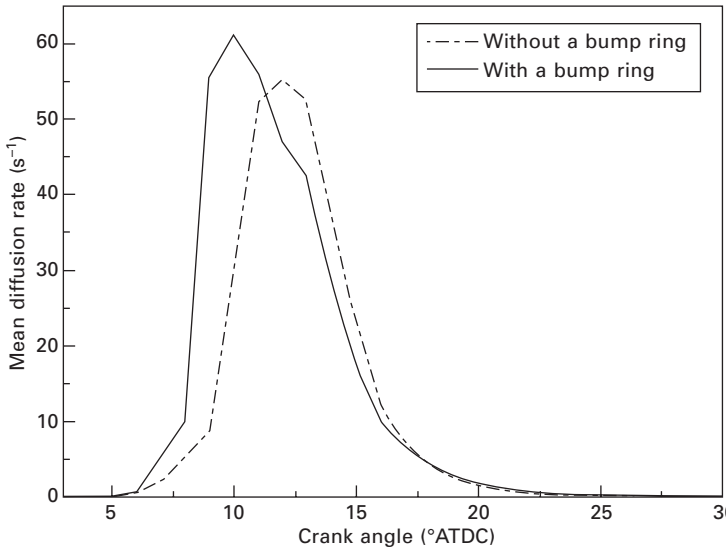
11.3.3 Combustion chamber design and utilization of mixing energy

As mentioned above, the LDC combustion path covers three stages. Two are dominated by mixing. Stage 1 is dominated by mixing at a certain chemical time-scale, which decides how high the fuel mass fraction can reach the equivalence ratio of soot-free combustion. For convenience, this mixing process is termed the early phase mixing. Stage 3 is also dominated by mixing, which decides combustion efficiency, thermal efficiency (combustion temperature) and engine-out emissions. Since stage 3 of the LDC is in the later phase, the corresponding mixing process is termed later phase mixing.

Enhancement of the mixing rate essentially relies on raising the mixing energy through intensification of air motion, increase of injection pressure and improvement of atomization. In this section the utilization of mixing energy will be focused on enhancement of both the early phase and later phase mixing of the LDC.

BUMP (Bump-Up Mixing Process) combustion chamber

Previous studies by the author (Su *et al*., 1996; Su and Lin, 1997) had shown that when even for a gas impinging jet on a plate, a thin and rich wall jet would be formed and the air-entrainment rate of the wall jet was halved compared with that of a space jet. In order to enhance the spray mixing rate, the authors developed a technology to strip off the wall jet and enhance the mixing rate. They found that a bump on the plate located downstream of the impingement point of an impingement jet could strip off the wall jet and form a secondary space jet. The measured scalar (concentration) dissipation rate in the secondary space jet increased by several times for a certain case, in comparison with the case without a bump on the plate. Based on these findings, a combustion chamber termed the BUMP (Bump-Up Mixing Process) combustion chamber was developed and the effectiveness of the enhancement of the spray mixing process was confirmed by LIF (laser induced fluorescence) measurement carried out in an optical engine (Su *et al*., 2003). Engine experiments were also conducted, which confirmed that the engine-out soot and NO_x emissions could be simultaneously reduced by employment of the BUMP combustion chamber. Figure 11.7 is a CFD simulation result, showing the comparison of fuel concentration (scalar) diffusion rate between the BUMP bowl and the original combustion bowl without a bump ring. A great increase of the fuel concentration diffusion rate in the BUMP combustion bowl was clearly observed in the early combustion phase, which was attributed to better utilization of the fuel injection energy. The BUMP bowl transfers the fuel spray momentum into turbulence kinetic energy and consequently produces a high scalar diffusion rate.



11.7 Comparison of the mean diffusion rate of fuel concentration between the BUMP combustion bowl and the conventional bowl.

Vortex induced combustion bowl (VICB)

Stage 3 of the LDC combustion is again controlled by mixing in later-phase combustion as discussed above. The mixing process to a large extent decides the combustion efficiency, which can be measured by less unburned hydrocarbon (uHC) and more complete conversion of CO into CO_2. It also decides the engine cycle thermal efficiency, which can be measured by the combustion temperature and its appearance phase in the crank angle after top dead center. All need a high mixing rate. On the other hand, the combustion path must be inhibited from going into the NO_x formation zone, which is the limit of the highest mixing rate in the later combustion phase. Zhang *et al*. (2008) developed a vortex induced bowl, by which a pair of opposite vortices were created, resulting in a high burning rate in the later combustion phase (see Plates IV and V between pages 364 and 365). Plate IV shows the distributions of 'fuel' (including incomplete combustion products) and oxygen in later-phase combustion. As shown, the fuel zone consists of fuel, uHC, intermediate combustion products, including CO, radicals and other incomplete products, but no oxygen. Oxygen is separated from the mixture zone and distributed either in the central area of the combustion chamber or in the area above the piston. So for the later combustion phase, the function of mixing is to transport fuel, uHC and other uncompleted combustion products to meet with oxygen, forming a wider interface. For this purpose we need to create large-scale air motions, which must be able to transport uncompleted

substances and oxygen, respectively, into the common interface. Plate V shows the transportation process of the fuel (incomplete combustion products) and the oxygen. One of the vortices rotates along the wall of the combustion chamber and then the vortex is divorced from the chamber wall at the point of cut-down of the wall, which causes the formation of the opposite vortex. The former vortex carries fuel into the common interface, while the latter vortex carries oxygen into the common interface. This resulted in a high burning rate in the later combustion phase.

11.4 Summary

Compound combustion is a kind of two-stage combustion process that combines the PCCI combustion with the LDC combustion based on the principle of controlling chemical and mixing characteristic time-scales. The PCCI combustion is organized by the technology of multi-pulse injections, which must be optimized for a suitable injection rate pattern to avoid 'spray wall wetting' and as a new target to pursue a no-fire process of PCCI, beneficial to organization of the LDC.

The LDC combustion process covers three stages: the early-phase mixing process, the rich premixed combustion process and the later-phase mixing process. A longer chemical characteristic time-scale will give a longer mixing time to the early-phase mixing, but sometimes brings obstacles for the fuel to meet with oxygen, for instance in the case with a high EGR rate. Therefore, enhancement of mixing is essential and critical to LDC combustion.

Besides the well-known countermeasures to enhance the mixing rate, such as higher injection pressure, increased boost pressure and smaller nozzle hole diameters, this chapter has focused on better utilization of the mixing energy by optimizing the design of the combustion chambers. As one example, the BUMP chamber has been proved to be effective in enhancing early-phase mixing, resulting in more fuel/air mixture being formed at an equivalence ratio of about 2.0 before auto-ignition appears in the fuel of the main injection. The VICB (vortex induced combustion bowl) chamber then proved to be a good solution to accelerate the transportation of the unburned fuel and oxygen into the common interface. However, further investigation of the mechanism and technology for mixing control in both early and later phases is extremely important for high thermal efficiency and low engine-out emissions in full engine operating conditions.

11.5 References

Akihama K, Takatori Y, Inagaki K, Sasaki S and Dean A M (2001), 'Mechanism of the smokeless rich diesel combustion by reducing temperature', SAE paper 2001-01-0655.

Beatrice C, Belardini P, Bertoli C, Lisbona M G and Rossi Sebastino G M (2002), 'Diesel combustion control in common rail engines by new injection strategies', *Int J Engine Res*, 3(1), 23–36.

Buchwald R, Brauer M, Blechstein A, Sommer A and Kahrstedt J (2004), 'Adaption of injection system parameters to homogeneous diesel combustion', SAE paper 2004-01-0936.

Curran H J, Gaffuri P, Pitz W J and Westbrook C K (1998), 'A comprehensive modeling study of *n*-heptane oxidation', *Combustion and Flame*, 114(1), 149–177.

Helmantel A and Denbratt I (2004), 'HCCI operation of a passenger car common rail DI diesel engine with early injection of conventional diesel fuel', SAE paper, 2004-01-0935.

Huang H, Su W and Pei Y (2008), 'Experimental and numerical study of diesel HCCI combustion by multi-pulse injection', SAE paper 2008-01-0059.

Kamimoto T and Bae M (1988), 'High combustion temperature for the reduction of particulate in diesel engines', SAE paper 880423.

Kitamura T, Ito T, Senda J and Fujimoto H (2002), 'Mechanism of smokeless diesel combustion with oxygenated fuels based on the dependence of the equivalence ratio and temperature on soot particle formation', *Int J Engine Res*, 3(4), 223–248.

Kobori S, Kamimoto T and Kosaka H (1996), 'Ignition, combustion and emissions in a DI diesel engine equipped with a micro-hole nozzle', SAE paper 960321.

Lechner G A, Jacobs T J, Chryssakis C A, Assanis D N and Siewert R M (2005), 'Evaluation of a narrow spray cone angle, advanced injection timing strategy to achieve partially premixed compression ignition combustion in a diesel engine', SAE paper 2005-01-0167.

Liu Y and Reitz R D (2005), 'Optimizing HSDI diesel combustion and emissions using multiple injection strategies', SAE paper 2005-01-0212.

Nakagome K, Shimazaki N, Niimura K and Kobayashi S (1997), 'Combustion and emission characteristics of premixed lean diesel combustion engine', SAE paper 970898.

Su W and Huang H (2005), 'Development and calibration of a reduced chemical kinetic model of *n*-heptane for HCCI engine combustion', *Fuel*, 84(9), 1029–1040.

Su W and Lin R (1997), 'Enhancement of near wall mixing of an impinging jet by means of a bump on the wall', SAE paper 971616.

Su W and Zhang X (2005), 'Study of mixing enhancement by a bump ring in a combustion chamber', *Proc Int Green Energy Conf, 12–16 June 2005*, Canada, paper 068.

Su W, Xie H, Lin R and Shi S (1996), 'Experimental study on the effects of spray impingement and turbulence structure on spray mixing rate by gas jet simulation', SAE paper 960775.

Su W, Lin T and Pei Y (2003), 'A compound technology for HCCI combustion in a DI diesel engine based on the multi-pulse injection and the BUMP combustion chamber', SAE paper 2003-01-0741.

Su W, Zhang X, Lin T, Pei Y and Zhao H (2004), 'Study of pulse spray, heat release, emissions and efficiencies in a compound diesel HCCI combustion engine', *Proc ASME ICE Div 2004 Fall Tech Conf*, ICEF2004-927.

Su W H, Lin T J, Zhao H and Pei Y Q (2005a), 'Research and development of an advanced combustion system for the direct injection diesel engine', *Proc IMechE, Part D: J Automobile Engineering*, 219(2), 241–252.

Su W, Wang H and Liu B (2005b), 'Injection mode modulation for HCCI diesel combustion', SAE paper 2005-01-0117.

Su W, Zhang X, Lin T, Pei Y and Zhao H (2006), 'Effects of heat release mode on

emissions and efficiencies of a compound diesel HCCI combustion engine', *J Eng Gas Turbines Power*, 128(2), 446–454.

Su W, Liu B, Wang H and Huang H (2007), 'Effects of multi-pulse injection mode on diesel homogeneous charge compression ignition combustion', *J Eng Gas Turbines Power*, 129(1), 230–238.

Su W, Guo H and Sun T (2008), 'Effect of injection pressure on spray characteristics and fuel distribution under ultra-high injection pressure by plane lasar induced exiplex fluorescence (PLIEF) technology', *Atomization and Sprays*, 18(8), 761–779.

Sun Y and Reitz R D (2007), 'Adaptive injection strategy (AIS) for diesel engines', *University of Wisconsin WARF Patent Application*, P07342US.

Takeda Y, Nakagome K and Niimura K (1996), 'Emission characteristics of premixed lean diesel combustion with extremely early staged fuel injection', SAE paper 961163.

Walter B and Gatellier B (2002), 'Development of the high-power NADI^{TM} concept using dual-mode diesel combustion to achieve zero NO_x and particulate emissions', SAE paper 2002-01-1744.

Yu Y, Su W and Huang H (2008), 'Study of fuel distribution on diesel PCCI combustion by development of a new characteristic-time combustion model'. SAE paper 2008-01-1605.

Zhang X, Su W and Pei Y (2008), 'Mixing-enhanced combustion in the circumstances of diluted combustion in direct-injection diesel engines', SAE paper 2008-01-0009.

Zhao F, Asmus T W, Assanis D N, Dec J E, Eng J A and Najt P M (2003), *Homogeneous Charge Compression Ignition (HCCI) Engines*, Warrendale, PA, Society of Automotive Engineers.

12
Heavy-duty diesel engine system design

Q. XIN, Navistar, Inc., USA

Abstract: This chapter provides a comprehensive theory and analytical design techniques on engine performance and system integration (EPSI) for diesel engine system design and development. The content is not intended to be all-encompassing to cover all the details of engine design; rather, the objective is to fill the gap between understanding the fundamentals of engine behavior and applying the knowledge to conduct design. It introduces the topics that a system design engineer needs to consider during the process of precise and optimized analytical system design. The critical topics covered include the concept of EPSI; the matching among vehicle, engine, aftertreatment, combustion, EGR and turbocharging systems; the principle of engine air system design; transient performance and engine controls; subsystem interaction; and analytical design of mechanical components to optimize system performance and fuel economy. The chapter discusses the system design requirements and provides examples to illustrate advanced design approaches using engine cycle simulation tools.

Key words: engine performance and system integration (EPSI), diesel engine system design, diesel air system, vehicle matching, cycle simulation.

12.1 Overview of analytical engine design process and system simulation approach

12.1.1 The characteristics and challenges of modern automotive diesel engine design

Compared to its gasoline engine counterpart, the diesel engine is characterized by higher 'well-to-wheel' efficiency, higher thermal efficiency (due to less intake throttle loss or pumping loss, higher compression ratio, leaner mixture of air and fuel, higher brake-mean-effective-pressure resulting from turbocharging, higher thermodynamic cycle efficiency, and lower friction), lower fuel consumption and CO_2 emission, lower unburned hydrocarbons (HC), negligible carbon monoxide (CO), and higher particulate matter (PM) and nitrogen oxides (NO_x, primarily NO and NO_2 with a NO_2/NO ratio approximately 5–25%) at tailpipe compared to gasoline engines equipped with three-way-catalyst. Diesel engines run at lower speeds due to the limitation of the slower diffusion combustion rate. They produce a lower exhaust temperature due to lean-mixture burning. They are also generally noisier and more expensive because of their sophisticated fuel injection system.

Direct injection (DI) diesel engines have approximately 10–15% better

fuel economy than indirect injection (IDI) diesel engines mainly for the following two reasons. First, DI engines do not have a divided combustion chamber and its associated high pumping losses of the flow restriction at the throat in the pre-chamber. Second, DI engines have less heat rejection lost to coolant due to less heat transfer area.

In on-highway applications, heavy-duty engines are used for heavyweight trucks and buses under highly loaded duty cycles with much time spent at full load. On the contrary, automobiles and light trucks usually operate at very light loads and low engine speeds, with high speed and load encountered only at brief transients. The duty cycle difference determines the durability and fuel economy design features. The design of automotive diesel engines has been driven by emissions regulations, fuel economy, noise, vibration and harshness (NVH), durability, drivability and product cost. Usually, engine system design features are measured by power density, vehicle power-to-weight ratio, high-altitude capability without de-rating, cold start capability, adequate cooling capacity at hot ambient temperature, etc.

Modern diesel engines normally use exhaust gas recirculation (EGR) as a very effective technology to reduce NO_x, especially in the US for meeting future stringent emissions regulations. In certain European applications urea-based selective catalytic reduction (SCR) was used instead of EGR to control NO_x. However, there are concerns on SCR's capital and operating costs, weight, packaging space, increased exhaust restriction, complexity of electronic controls, ammonia slip, readiness of infrastructure, maintenance burdens on vehicle customers, and in-use compliance.

EGR reduces NO_x through the mechanisms of reducing in-cylinder oxygen concentration and combustion temperature. Intercooled turbocharging has been used to increase power density and reduce PM emissions. Compared to the old-era turbocharged non-EGR engines, EGR engines have very different design considerations from system to component. For instance, the usual practice in non-EGR engines was to match the turbocharger to make intake manifold pressure higher than exhaust manifold pressure (i.e., creating a negative pressure differential or negative 'engine delta P') because there was no need to drive EGR flow. Such a negative engine delta P not only resulted in a net gain in brake specific fuel consumption (BSFC) due to pumping work instead of pumping loss, but also improved cylinder gas scavenging with large valve overlap and reduced thermal load on the cylinder head, exhaust valves and turbine. Moreover, the air–fuel ratio (A/F ratio) could be designed very high without the problem of exceeding the maximum cylinder pressure limit, thus helping to increase combustion efficiency and decrease soot. However, in EGR engines those advantages disappear because the need for driving EGR flow requires a positive engine delta P (i.e., exhaust manifold pressure higher than intake manifold pressure). Increased exhaust restriction due to the addition of PM and NO_x aftertreatment devices further

complicates turbo matching. Moreover, the larger fluctuation on engine flow and gas temperature requirements (e.g., EGR on and off during transients or aftertreatment regeneration) also demands a careful system design approach in order to optimize all the systems involved, from vehicle-engine-aftertreatment matching to transient engine controls.

In addition to EGR, modern diesel engines are also characterized by innovative combustion and tight integration between the engine and aftertreatment, as well as the advances from fuel formulation (higher cetane number, lower aromatics, ultra low sulfur) to lubricant additives (for ash control and aftertreatment compatibility to avoid poisoning or fouling).

Currently, meeting emissions regulation is the driving factor for developing new engines. In the future, it will be fuel economy, along with greenhouse gases, cost and reliability. The competition in fuel economy will be fiercer in the market for customer satisfaction. The potential government regulations on CO_2 emission or fuel economy will impose another pressure on engine manufacturers. (There is a direct correlation between CO_2 and fuel economy (Steinberg and Goblau, 2004).) Not only will the competition happen among diesel engine manufacturers, it will also occur against the challenges from other advanced powertrain concepts such as direct injection gasoline engines and hybrid electric vehicles. All the challenges require an optimized system approach in diesel engine design, and use of such an approach in technological innovation of each subsystem, as well as a new look at the traditional mechanical design issues such as friction and NVH reduction. The goal is to develop a superior product with minimum cost.

12.1.2 Analytical engine system design process and subsystem interaction

Engine design is one of the most sophisticated industrial design processes due to its complex nature in that the functions of many components affect each other. Inside the engine, air is mixed with fuel to combust to produce power and generate emissions. The function and design of the fuel system are closely related to those of the combustion system, but the details of fuel system integration are outside of the scope of this chapter. The engine system design is largely related to air handling. An engine has several major subsystems related to air delivery and pumping loss: intake manifold, exhaust manifold, cylinder head, valvetrain, turbocharger, EGR circuit, coolers and exhaust aftertreatment. Their performance is affected by certain key parameters such as air and EGR flow rate, exhaust temperature, peak cylinder pressure, boost and back pressures. The optimization among those subsystems needs to be carried out carefully. Modern, electronically controlled engines require an on-target ‘precise’ design to deliver air–fuel ratio, EGR rate and intake manifold temperature at critical operating modes of speed and load in

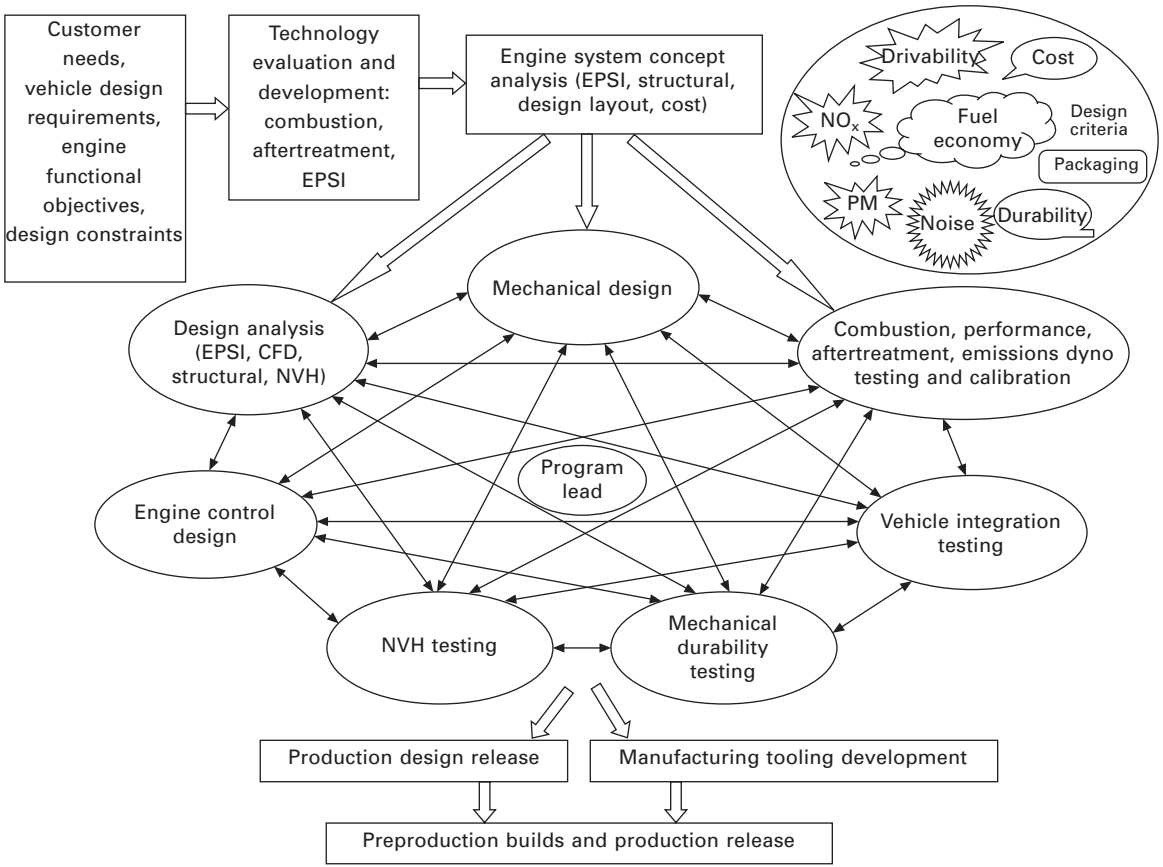
order to push the design to the limit. Neither over-design nor under-design is acceptable. From emissions and performance perspectives, a system design issue can be defined as one that relates to those commonly shared key performance parameters or to fuel economy, and as one whose design change affects the design of other subsystems. For instance, turbo matching is a system design issue because it has a direct impact on air–fuel ratio and EGR circuit restriction design. On the contrary, an exhaust manifold runner design is more like a local component design issue. As system optimization propagates more widely and deeply throughout the whole engine to address the interaction among different components, the boundary between 'system' and 'local component' will become blurred. The purpose of system engineering is to ensure excellent functional interaction with neighboring subsystems.

A workflow process of engine design and development from concept to production is illustrated in Fig. 12.1. The input and output of the functional areas are interactive and affect each other, as shown by the double-headed arrows in the figure. The efficiency of the engine development process depends on how clearly technical specifications or design/development changes are organized and cascaded by the system team and component teams within a given organization. Although the technical communication channels between different functional areas are complex, overall there is an optimum 'top-down' process as shown by the thicker block arrows. In the old era when technical specifications were generated with crude hand-calculations, precise design and optimization were impossible. Today, with the effective use of computer simulations of engine thermodynamic cycle performance, it is feasible to accurately predict air system performance and subsystem interaction. Such a function of analytical system integration needs to be placed at the very top of the development chain. A common objective in engine development is to continue improving the upstream analysis capability while minimizing the costs in the prototype testing stages, as pointed out by Hoag (2006) in his detailed description of the engine development path.

12.1.3 Introduction to engine performance and system integration analysis

Objectives of EPSI analysis

Engine performance and system integration (EPSI, shown in Fig. 12.1) is a specialized technical field of engine system design that analyzes and integrates the performance of various engine subsystems or technologies, and properly matches them with optimization approaches. It conducts large-scale sophisticated computation in the areas related to thermal conditions, fluids, dynamics and controls to derive precise system design solutions by using analytical tools such as engine cycle simulation software or analytical models



12.1 Concurrent engineering of the engine development process with cross-functional teams.

and advanced data processing techniques. The missions of EPSI are: (1) to provide engine system design and analysis; (2) to develop system analysis methodologies and simulation techniques; and (3) to develop core engine technologies with the viewpoint of system integration.

The system design covers a wide range of technical specialties including vehicle-engine-aftertreatment integration, thermodynamic cycle performance, air system design and turbo matching, powertrain dynamics and electronic controls. System design is very important for the integration of simultaneous engineering processes for diesel engine product design, ranging from high-level product strategy planning to detailed production design. The important role of EPSI simulation analysis is illustrated in Fig. 12.1. The techniques used in engine system design and matching analysis are essentially similar, i.e., comparing the characteristic maps of different systems and conducting optimization, although the details can be quite complex (to be addressed in later sections).

The engine system design analysis generates three types of output. They are (1) performance sensitivity data and optimization results; (2) system performance design specifications; (3) the root cause analysis of particular problems. Specifically, the system specification refers to a predicted list of all critical steady-state and transient engine performance and emissions parameters for a given concept configuration in the entire engine speed and load domain (especially at critical modes such as rated power, peak torque and driving part load) at various ambient temperatures and altitudes. The specification also defines the data for turbocharging, EGR circuit design, engine heat rejection and electronic controls to be used in each subsystem design by suppliers and customers, for both specification target (on-target nominal design) and limits/range (robust design for variability). The performance sensitivity and optimization refer to any steady-state and transient simulation data of parameter sweeping or Design-of-Experiments (DoE) optimization for comparing configuration concepts or justifying design specifications of hardware sizing. For example, the sensitivity study may be on the maximum achievable rated power, or the optimum turbine nozzle areas in two-stage turbocharging, or transient vehicle acceleration simulation as a function of time with different vehicle weights. The specification should come out from optimization. The engine system specification needs to cover five aspects: (1) steady-state performance design specification; (2) steady-state virtual calibration; (3) steady-state vehicle in-use simulation (e.g., variations in charge air cooling, exhaust restriction, radiator performance and underhood thermal conditions compared to engine test cell conditions); (4) transient specification simulation; and (5) transient vehicle in-use simulation. The above-mentioned ‘root cause’ analysis refers to a simulation on any particular issue or failure. For example, insufficient EGR flow at engine peak torque is caused by inadequate engine delta P due to an excessively large turbine

nozzle area. Another example is an excessively high exhaust manifold gas temperature caused by cooler failure or low air–fuel ratio. Generally, the need for root cause analysis should be minimized as much as possible through successful up-front specification design with system optimization. The system performance specification is usually the most important of the four system specifications in engine design, namely performance (function), durability, packaging (geometry and weight), and cost.

Theoretical foundation and analysis tools

The foundation of engine system design analysis is built on thermodynamic cycle simulation. In the model, the differential equations describing the instantaneous gas pressure, temperature and flow rate inside each engine subsystem are solved. The in-cylinder process is usually solved with zero-dimensional assumption (i.e., spatially homogeneous). The gas dynamics in engine pipes and manifolds can be solved by either zero-dimensional or one-dimensional assumption. The input of the model includes engine geometry, subsystem characteristics and engine calibration parameters such as fuel injection timing and EGR valve opening. There are two types of output: the crank-angle based instantaneous values (e.g., gas temperature and pressure); and the cycle-average macro system performance parameters (e.g., engine torque, air–fuel ratio and coolant heat rejection). Both steady-state and transient performance can be computed at various ambient conditions. There are several commercial software packages of cycle simulation, such as Gamma Technologies' GT-POWER, Ricardo's WAVE and AVL's BOOST. Figure 12.2 shows an example of an engine cycle simulation model.

In design optimization, the DoE method has been widely used to generate a statistical design matrix to cover various combinations of input 'factors'. Each case in the matrix is run with cycle simulation software, and the output data are called 'responses'. Mathematical models (e.g., polynomials) are built to link each response parameter with factors. Then, optimization is conducted to search the global optima under certain given constraints to minimize or maximize a functional target (e.g., BSFC). It should be noted that engine cycle simulation cannot replace performance and emissions testing, and vice versa. Combining simulation with testing brings mutually reinforced strengths for both.

Technical areas of engine system analysis

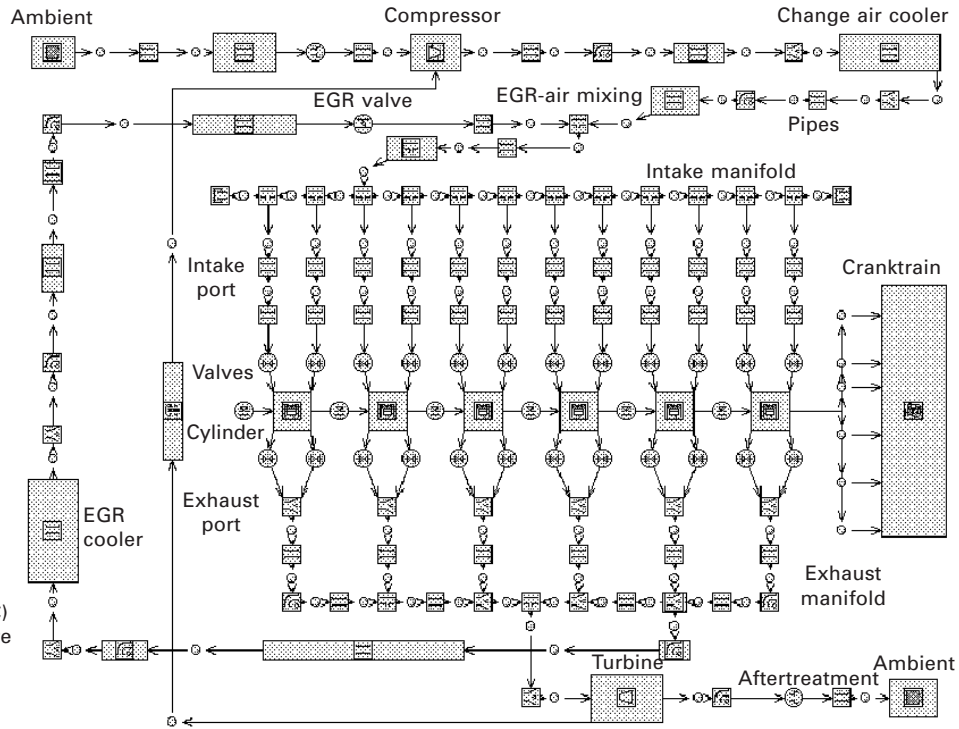
In order to define the system design specifications, engine performance and system integration analysis includes but is not limited to the following functional areas:

Cycle simulation model

Theory of the model
- Engine cycle thermodynamics
- Mass and energy conservation
- In-cylinder gas property changes
- Cylinder and pipe heat transfer
- Turbocharger principle
- Combustion and heat release rate
- 1-dimensional gas wave dynamics
- Acoustics of intake and exhaust
- Piston-assembly dynamics
- Controls linked to Matlab/Simulink

Input of the model
- Engine geometry
- Valve lift profile and port flow C_f
- Turbocharger maps and efficiency
- Base engine heat rejection percent
- Engine mechanical friction
- EGR cooler and CAC characteristics
- Fuel injection or combustion timing

Output of the model
- Cylinder average parameters (e.g. BSFC)
- Instantaneous gas pressure, temperature and mass flow rate inside the engine



12.2 Engine thermodynamic cycle simulation model (GT-POWER).

1. Technical field 1: Engine system thermodynamic cycle performance
   - Engine performance functional objectives, power rating, torque curve, peak cylinder pressure
   - Engine basic configuration (cylinder bore, stroke, compression ratio, engine valve size, etc.)
   - Valve timing, port flow coefficient, cam profile, valvetrain system, valvetrain dynamics
   - Intake and exhaust manifold 1-D flow gas exchange performance
   - Exhaust restriction sensitivity
   - EGR system performance
   - Turbocharging and performance at extreme ambient conditions
   - Engine heat rejection
   - Cooling circuit performance
   - Combustion, fuel injection and emissions modeling
   - Engine friction, piston-assembly lubrication dynamics
   - Fuel economy improvement roadmap
   - Engine brake performance
   - Transient engine performance (load response, turbo lag, warm-up, emissions cycle, etc.).
2. Technical field 2: Vehicle and powertrain performance
   - Engine torque curve, vehicle acceleration, vehicle launch, gradeability and drivability
   - Drivetrain configuration evaluation and drive axle ratio selection
   - Engine–transmission matching
   - Vehicle fuel economy
   - Transient driving cycle performance
   - Powertrain energy management and integration.
3. Technical field 3: Aftertreatment system integration (performance matching, controls and modeling)
4. Technical field 4: Model-based engine performance and emissions calibration and optimization
5. Technical field 5: Engine controls modeling
   - Thermal/fluids performance models for model-based controls
   - Performance models for virtual sensors
   - Evaluation of engine control strategies and algorithms.

In each area above, advanced competitive benchmarking analysis techniques should also be applied to provide valuable insight for design improvement. The advances of industry-wide research on critical but weak areas such as the modeling of emissions, engine transients and aftertreatment integration may tremendously elevate the quality level of engine system design analysis.

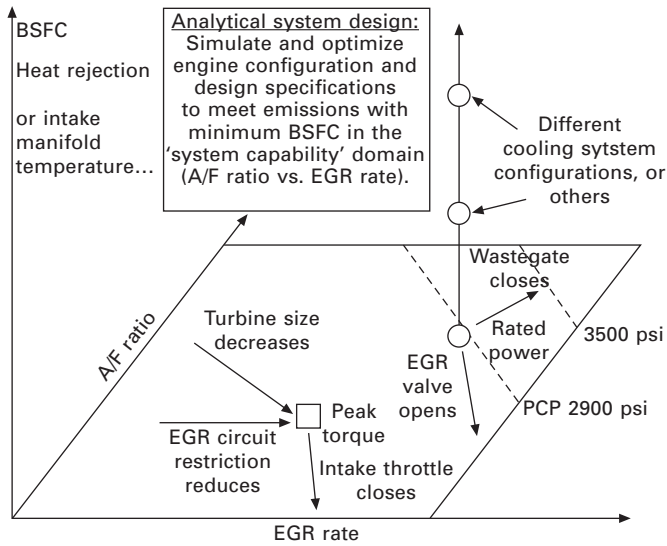
The EPSI process in engine development

Engine system performance analysis is characterized by large-scale complex data handling across a wide range of technical specialties. The following are three key factors for successfully implementing system design analysis in the engine product development process: (1) creating clear and effective technical data communication across different functional areas to ensure central data management and information sharing; (2) establishing analysis task categories within EPSI and their standard analysis procedures to ensure quality and consistency; and (3) building advanced data processing templates to maximize efficiency. The essence of EPSI analysis is to reveal the fundamental parametric dependency among various design and performance parameters in order to derive an optimized system solution. As an example, Fig. 12.3 shows the tasks involved in executing system specification analysis and the role of analytical system design.

12.2 Fundamentals of in-cylinder cycle computation and air system steady-state performance

12.2.1 Theoretical formulae for the engine in-cylinder thermodynamic cycle process

Understanding how to calculate the engine thermodynamic cycle process, which is the core of air system theory, is very important for engine performance and emissions engineers. With today's modern commercial software, an engine system model can be built easily by putting the objects together, and a large amount of performance data can be produced by running the software to solve the differential equations. However, the system analysis engineers need to understand and explain the root causes of the computed results in a simple, intuitive and theoretical way. For example, what are the reasons for pumping loss change after the value of a hardware design parameter is changed? The best way to understand the fundamentals is to look at the governing equations, even if in their simplified form, which describe the system behavior. The parametric dependency can be revealed from the equations mathematically. This section presents the fundamental theory behind cycle simulation software. The performance of the internal combustion engine was introduced in several classical textbooks (Heywood, 1988; Stone, 1999). The design details were provided by Challen and Baranescu (1999) and Basshuysen and Schafer (2004). In this section, both the differential equations of the in-cylinder cycle process and the steady-state equations of the turbocharged EGR engine system will be described. Their links will be discussed. The complementary sub-models of heat transfer, intake and exhaust valve flow and combustion rate will also be provided.



Step 1: Understand the current engine's performance
- List all design constraints
- Analyze performance test data and subsystem characteristics
- Analyze emissions test data. Calculate heat release rate.
- Build well-tuned simulation model
- Identify transient problems by analyzing test data

Step 2: Check sensitivity and define new engine system specification
- Define engine performance functional targets
- Explore parametric performance sensitivity by simulation
- Generate system design specification and obtain consensus
- Issue specification to subsystem teams and suppliers to start design
- Simulate to check proposed design hardware and controls
- Analyze test data of engine hardware and calibration
- Revise functional targets and iterate system specification analysis

12.3 Analytical system design and tasks of engine performance specification analysis.

Model assumptions

The engine in-cylinder cycle process is determined by gas temperature (T), pressure (P) and mass (m). These are solved from two ordinary differential equations (for energy and mass conservation) and the ideal gas law equation. Initial conditions of in-cylinder P, T and m can be estimated from intake manifold parameters, and the computation continues with time-marching numerical integration until cyclic convergence is achieved for all the gas

state parameters inside the entire engine. The assumptions for the in-cylinder model described in this section include the following:

1. The in-cylinder single-zone model (i.e., the burned and unburned mixture has a uniform temperature).
2. Zero-dimensional state parameters (i.e., at each moment, the pressure, temperature or concentration in the cylinder are equal or homogeneous everywhere; no condensed species).
3. Ideal gases (i.e., the gases obey the equation of state $PV = mRT$; specific heat, internal energy and enthalpy of the gases vary with temperature and constituents but not pressure).
4. Quasi-steady-state process for gas flowing into and out of the cylinder (i.e., within a small time step in numerical integration the flow process is treated as steady-state).
5. Ignoring the kinetic energy of intake and exhaust gas flows.

Governing equations of the in-cylinder instantaneous cycle process

The energy conservation equation of the in-cylinder gas can be expressed as

$$\frac{dU}{d\phi} = \frac{dW}{d\phi} + \sum_i \frac{dQ_i}{d\phi} + \sum_j h_j \cdot \frac{dm_j}{d\phi} \tag{12.1}$$

where ϕ is the crank angle (degrees), U is the internal energy of the in-cylinder gas, W is the mechanical work acting on the piston, Q_i is heat exchanged through the system boundary and fuel combustion, h_j is the specific enthalpy, and $h_j m_j$ is the energy brought into and out of the cylinder by intake and exhaust gas flow. The enthalpy can be calculated with datum of zero enthalpy at 0 K or 298.15 K or any other arbitrary datum temperature. Note that a positive value for heat or mass flow means flowing into the cylinder and a negative value means flowing out of the cylinder. Each term in equation 12.1 is further expressed as below:

$$\frac{dU}{d\phi} = \frac{d(m \cdot u)}{d\phi} = u\frac{dm}{d\phi} + m\frac{du}{d\phi}$$

$$\frac{dW}{d\phi} = -P\frac{dV}{d\phi}$$

$$\sum_i \frac{dQ_i}{d\phi} = \frac{dQ_{fuel}}{d\phi} + \frac{dQ_{wall}}{d\phi}$$

where V is the in-cylinder instantaneous volume, m is the in-cylinder mass, Q_{fuel} is the heat energy released from fuel combustion, and Q_{wall} is the heat

transfer through the walls of the cylinder head, piston and liner. The energy of intake and exhaust gas exchange mass flows is given by

$$\sum_j h_j \cdot \frac{dm_j}{d\phi} = h_{in} \cdot \frac{dm_{in}}{d\phi} + h_{ex} \cdot \frac{dm_{ex}}{d\phi}$$

where m_{in} is the intake gas mass flowing into the cylinder, m_{ex} is the exhaust gas mass flowing out of the cylinder, and h_{in} and h_{ex} are specific enthalpies of gases at intake and exhaust valves. Since specific internal energy $u = u(T, \sigma)$ for ideal gases, where σ is the excess air–fuel ratio (defined as actual air–fuel ratio divided by stoichiometric air–fuel ratio, or the reciprocal of 'equivalence ratio'),

$$\frac{du}{d\phi} = \frac{\partial u}{\partial T} \cdot \frac{dT}{d\phi} + \frac{\partial u}{\partial \sigma} \cdot \frac{d\sigma}{d\phi} = c_v \cdot \frac{dT}{d\phi} + \frac{\partial u}{\partial \sigma} \cdot \frac{d\sigma}{d\phi}$$

Substituting these relationships into equation 12.1, the energy conservation equation is converted to the following form for solving the in-cylinder gas temperature T:

$$\frac{dT}{d\phi} = \frac{1}{m \cdot c_v}$$

$$\times \left(\frac{dQ_{fuel}}{d\phi} + \frac{dQ_{wall}}{d\phi} - P\frac{dV}{d\phi} + h_{in}\frac{dm_{in}}{d\phi} + h_{ex}\frac{dm_{ex}}{d\phi} - u\frac{dm}{d\phi} - m\frac{\partial u}{\partial \sigma}\cdot\frac{d\sigma}{d\phi} \right) \qquad 12.2$$

The mass conservation equation can be expressed as

$$\frac{dm}{d\phi} = \frac{dm_{in}}{d\phi} + \frac{dm_{ex}}{d\phi} + \frac{dm_{fuel\,B}}{d\phi}$$

where m_{fuelB} is the fuel mass injected into the cylinder. If the total injected fuel mass per engine cycle is m_{fuelC} and the fraction of fuel burnt is defined as $X = m_{fuelB}/m_{fuelC}$, then

$$\frac{dm_{fuelB}}{d\phi} = m_{fuelC} \cdot \frac{dX}{d\phi}$$

The mass conservation equation is then converted to the following form:

$$\frac{dm}{d\phi} = \frac{dm_{in}}{d\phi} + \frac{dm_{ex}}{d\phi} + m_{fuelC}\frac{dX}{d\phi} \qquad 12.3$$

The heat release rate from burnt fuel in equation 12.2 is

$$\frac{dQ_{fuel}}{d\phi} = \frac{m_{fuelB}}{d\phi} \cdot q_{LHV} \cdot \eta_{com} = m_{fuelC} \cdot \frac{dX}{d\phi} \cdot q_{LHV} \cdot \eta_{com}$$

where q_{LHV} is the lower heating value of the fuel, and η_{com} is combustion efficiency ($\eta_{com} = 1$ means complete combustion).

The ideal gas law applied to in-cylinder gas gives the equation of state:

$$PV = mRT \tag{12.4}$$

where R is the gas constant. In the system of equations 12.2–12.4, $dQ_{wall}/d\phi$, $h_{in}(dm_{in}/d\phi)$ and $h_{ex}(dm_{ex}/d\phi)$ are functions of gas temperature and pressure; $\partial u/\partial\sigma$ and c_v are functions of gas temperature and constituents; $dX/d\phi$, $dV/d\phi$, m_{fuelC}, q_{LHV} and η_{com} are treated as known input. Therefore, the three unknowns, in-cylinder gas pressure P, temperature T and mass m, can be solved by time-marching numerical integration. Equations 12.2 and 12.3 can be further simplified for different stages during an engine cycle.

Simplification of the governing equations for each stage of the cycle process

Compression stage (from intake valve closing to start of combustion)

In this stage, $dm_{in}/d\phi = 0$, $dm_{ex}/d\phi = 0$, $dm_{fuel}/d\phi = 0$, and $d\sigma/d\phi = 0$; therefore, $dm/d\phi = 0$ and $dQ_{fuel}/d\phi = 0$. The energy conservation equation 12.2 becomes

$$\frac{dT}{d\phi} = \frac{1}{m \cdot c_v}\left(\frac{dQ_{wall}}{d\phi} - P\frac{dV}{d\phi}\right)$$

Combustion stage (from start of combustion to end of combustion)

In this stage, $dm_{in}/d\phi = 0$ and $dm_{ex}/d\phi = 0$. Equation 12.3 becomes

$$\frac{dm}{d\phi} = \frac{dm_{fuelB}}{d\phi} = m_{fuelC} \cdot \frac{dX}{d\phi}$$

Ignoring the impact of σ on u, the energy conservation equation 12.2 becomes:

$$\frac{dT}{d\phi} = \frac{1}{m \cdot c_v}\left[m_{fuelC}(\eta_{com} \cdot q_{LHV} - u)\frac{dX}{d\phi} + \frac{dQ_{wall}}{d\phi} - P\frac{dV}{d\phi}\right]$$

Expansion stage (from end of combustion to exhaust valve opening)

In this stage, $dm_{in}/d\phi = 0$, $dm_{ex}/d\phi = 0$, $dm_{fuel\,B}/d\phi = 0$ and $d\sigma/d\phi = 0$; therefore $dm/d\phi = 0$, $dQ_{fuel}/d\phi = 0$ The energy conservation equation 12.2 becomes

$$\frac{dT}{d\phi} = \frac{1}{m \cdot c_v}\left(\frac{dQ_{wall}}{d\phi} - P\frac{dV}{d\phi}\right)$$

Exhaust stage (from exhaust valve opening to intake valve opening)

In this stage, $dm_{in}/d\phi = 0$, $dm_{fuel\,B}/d\phi = 0$ and $d\sigma/d\phi = 0$. Equation 12.3 becomes $dm/d\phi = dm_{ex}/d\phi$. The energy conservation equation 12.2 becomes

$$\frac{dT}{d\phi} = \frac{1}{m \cdot c_v}\left[\frac{dQ_{wall}}{d\phi} - P\frac{dV}{d\phi} + (h_{ex} - u)\frac{dm_{ex}}{d\phi}\right]$$

Intake stage (from exhaust valve closing to intake valve closing)

In this stage, $dm_{ex}/d\phi = 0$ and $dm_{fuel\,B}/d\phi = 0$. Equation 12.3 becomes $dm/d\phi = dm_{in}/d\phi$. Ignoring the impact of α (see below) on u, the energy conservation equation 12.2 becomes:

$$\frac{dT}{d\phi} = \frac{1}{m \cdot c_v}\left[\frac{dQ_{wall}}{d\phi} - P\frac{dV}{d\phi} + (h_{in} - u)\frac{dm_{in}}{d\phi}\right]$$

Valve overlap stage (from intake valve opening to exhaust valve closing)

In this stage, $dm_{fuel\,B}/d\phi = 0$ and $dQ_{fuel}/d\phi = 0$. Equation 12.3 becomes $dm/d\phi = dm_{in}/d\phi + dm_{ex}/d\phi$. Ignoring the impact of σ on u, the energy conservation equation 12.2 becomes:

$$\frac{dT}{d\phi} = \frac{1}{m \cdot c_v}\left[\frac{dQ_{wall}}{d\phi} - P\frac{dV}{d\phi} + (h_{in} - u)\frac{dm_{in}}{d\phi} + (h_{ex} - u)\frac{dm_{ex}}{d\phi}\right]$$

Key sub-models

Instantaneous in-cylinder volume

In equation 12.2, the instantaneous volume $dV/d\phi$ can be derived from engine geometry as

$$V = \frac{\pi B^2}{4}\left\{\frac{S}{\Omega - 1} + \frac{S}{2}\left[\left(1 + \frac{1}{\chi}\right) - \cos\phi - \frac{1}{\chi}\sqrt{1 - \chi^2 \sin^2\phi}\right]\right\}$$

$$\frac{dV}{d\phi} = \frac{\pi B^2 S}{8}\left[\sin\phi + \frac{\chi}{2}\frac{\sin(2\phi)}{\sqrt{1 - \chi^2 \sin^2\phi}}\right]$$

where Ω is engine geometric compression ratio, B is cylinder bore diameter, S is engine stroke, and χ is the ratio between connecting rod length and crank radius.

Heat transfer through cylinder walls

The heat transfer terms in the energy conservation equation 12.2 can be derived in the following:

$$\frac{dQ_{wall}}{d\phi} = \sum_{i=3} \frac{dQ_{wall,i}}{d\phi} = \frac{-1}{6N} \sum_{i=3} \alpha_g A_{wall,i}(T - T_{wall,i})$$

where α_g is the instantaneous spatial-average heat transfer coefficient from in-cylinder gas to cooling medium, N is engine speed (rpm), A_{wall} is heat transfer area, T_{wall} is cylinder wall surface spatial-average temperature, and i = 1, 2, 3 refers to cylinder head, piston and liner, respectively. The cylinder liner heat transfer area is $A_{wall,3} = \pi B[L_{clear} + y(\phi)]$, where L_{clear} is clearance height, and $y(\phi)$ is given by:

$$y(\phi) = \frac{S}{2}\left[\left(1 + \frac{1}{\chi}\right) - \cos\phi - \frac{1}{\chi}\sqrt{1 - \chi^2 \sin^2\phi}\right]$$

The α_g is critical for heat transfer calculation. The development history of engine heat transfer theory has gone through three stages: empirical modeling (pioneered by the Nusselt correlation in 1923); semi-empirical similarity theory (represented by the Woschni correlation); and the multi-zone CFD simulation since the 1980s. To date the widely accepted and successful approach is still the Woschni correlation. It was developed in 1965 and was based on $N_u = 0.035 R_e^{0.8} P_r^{0.333}$ (where N_u is the Nusselt number, R_e is the Reynolds number and P_r is the Prandtl number). It assumed forced convection has a dominant effect on cylinder heat transfer as follows:

$$\alpha_g = K_1 B^{-0.214} (Pc_m)^{0.786} \left(T^{-0.525} + K_2 \frac{T}{T_c}\right)$$

In 1970 an improved formula was given by Woschni as:

$$\alpha_g = 820 B^{-0.2} P^{0.8} T^{-0.53} \left[C_1 c_m + C_2 \frac{T_a V_s}{P_a V_a}(P - P_0)\right]^{0.8}$$

in the unit of W/(m^{2}K).

In the above formula, P is in-cylinder gas pressure (MPa), T is instantaneous in-cylinder bulk gas temperature (K), T_c is in-cylinder gas temperature at the end of compression, B is cylinder diameter (m), c_m is mean piston speed (m/s), P_a, T_a and V_a are in-cylinder pressure, temperature and volume at the beginning of the compression stroke, V_s is cylinder displacement (m^3), P_0 is in-cylinder pressure at motoring condition without combustion, K_1 is a scavenging constant, K_2 is a combustion constant, and C_1 is a gas velocity coefficient. $C_1 = 6.18 + 0.2085\ (B\omega_p/c_m)$ for intake and exhaust strokes, and

$C_1 = 2.28 + 0.154\ (B\omega_p/c_m)$ for compression and expansion strokes, where ω_p is paddle wheel angular velocity (in radians per second) in the steady-flow swirl test. C_2 is a combustion chamber shape coefficient in the expansion stroke. C_2 = 0.00324 m/K.s for direct injection combustion chamber; C_2 = 0.00622 m/K.s for indirect injection combustion chamber; $C_2 = 0$ for intake, exhaust and compression strokes. The last term in the Woschni correlation attempted to reflect the effects of radiation and combustion.

The Woschni correlation has several limitations, for example: (1) zero-dimensional homogeneous heat transfer was assumed; (2) the heat transfer equivalent diameter was treated as a constant B rather than an instantaneous parameter within an engine cycle; and (3) the modeling of radiation heat transfer was primitive. In fact, accurately determining α_g is very difficult, from either theoretical computation or experimental measurement. Fortunately, the impact of heat transfer modeling accuracy on the accuracy of computing engine power and gas flow rate is not extremely critical. For engine system-level cycle simulation, the main objective of accurately computing cylinder heat transfer is to predict the base engine heat rejection for cooling system design and exhaust manifold temperature. It is usually sufficient to apply a multiplier to the Woschni heat transfer coefficient α_g to calculate cylinder heat transfer. The multiplier is tuned based on the energy balance analysis of engine test data in order to capture the engine fundamental characteristics of what percentage of fuel energy is lost to cylinder heat rejection. This topic will be further explained in Section 12.6.

Gas masses flowing into and out of the cylinder through engine valves

With the simplified assumptions of subsonic one-dimensional isentropic flow for intake valves, the intake mass flow rate entering the cylinder is given by:

$$\frac{dm_{in}}{d\phi} = \frac{\mu_{in} A_{in} P_{in}}{6N\sqrt{R_{in} T_{in}}} \cdot \sqrt{\frac{2\gamma_{in}}{\gamma_{in} - 1}\left[\left(\frac{P}{P_{in}}\right)^{\frac{2}{\gamma_{in}}} - \left(\frac{P}{P_{in}}\right)^{\frac{\gamma_{in}+1}{\gamma_{in}}}\right]}$$

where N is engine speed (rpm), μ_{in} is intake valve flow coefficient, A_{in} is intake valve instantaneous flow area, P_{in} and T_{in} are pressure and temperature in the intake port just before the intake valve, R_{in} is the gas constant, γ_{in} is the adiabatic exponent, and P is the in-cylinder pressure.

The exhaust mass flow rate out of the cylinder is given as below. When

$$\frac{P_{ex}}{P} > \left(\frac{2}{\gamma_{ex}+1}\right)^{\frac{\gamma_{ex}}{\gamma_{ex}-1}}$$

the valve gas flow is subsonic and can be described as

$$\frac{dm_{ex}}{d\phi} = \frac{-\mu_{ex} A_{ex} P}{6N\sqrt{R_{ex} T}} \cdot \sqrt{\frac{2\gamma_{ex}}{\gamma_{ex}-1}\left[\left(\frac{P_{ex}}{P}\right)^{\frac{2}{\gamma_{ex}}} - \left(\frac{P_{ex}}{P}\right)^{\frac{\gamma_{ex}+1}{\gamma_{ex}}}\right]}$$

When

$$\frac{P_{ex}}{P} \leq \left(\frac{2}{\gamma_{ex}+1}\right)^{\frac{\gamma_{ex}}{\gamma_{ex}-1}}$$

the valve gas flow is supersonic and can be described as

$$\frac{dm_{ex}}{d\phi} = \frac{-\mu_{ex} A_{ex} P_{ex}}{6N\sqrt{R_{ex} T_{ex}}} \left(\frac{2}{\gamma_{ex}+1}\right)^{\frac{1}{\gamma_{ex}-1}} \cdot \sqrt{\frac{2\gamma_{ex}}{\gamma_{ex}+1}}$$

where μ_{ex} is exhaust valve flow coefficient, A_{ex} is exhaust valve instantaneous flow area, and P_{ex} is the pressure in the exhaust port just behind the exhaust valve.

The valve and port flow coefficients μ_{in} and μ_{ex} are generally acquired from experimental flow bench test of the cylinder head. They are monotonic functions of normalized valve lift (Stone, 1999). The flow coefficients are determined by port design, valve diameter, valve seat angle and flow recirculation effects between the valve and cylinder bore.

Thermodynamic properties of in-cylinder gases

The in-cylinder specific internal energy is a function of temperature and species including combustion products. Its calculation is referred to Stone (1999) for in-depth discussions.

Combustion heat release rate and burn rate

The combustion heat release rate can be calculated by using a known measured cylinder pressure trace and the energy conservation equation as

$$\frac{dQ_{fuel}}{d\phi} = \frac{dU}{d\phi} - \frac{dW}{d\phi} - \frac{dQ_{wall}}{d\phi}$$

where $Q_{fuel} = m_{fuelC}\ Xq_{LHV}\ \eta_{com}$, or the heat release rate may also be specified as input by using an empirical formula. The widely used Wiebe semi-empirical formula (also known as the Wiebe function) was developed based on homogeneous chain reaction theory and gasoline engine test data.

In the Wiebe function, the burned fuel percentage X represents combustion rate as follows:

$$X = 1 - \mathrm{e}^{-C_w\left(\frac{\phi-\phi_{burn}}{\Delta\phi}\right)^{\delta+1}}$$

$$\frac{dX}{d\phi} = C_w \frac{\delta+1}{\Delta\phi}\left(\frac{\phi-\phi_{burn}}{\Delta\phi}\right)^{\delta} \cdot \mathrm{e}^{-C_w\left(\frac{\phi-\phi_{burn}}{\Delta\phi}\right)^{\delta+1}}$$

where δ is a non-dimensional shape factor characterizing the instantaneous change of fuel concentration of effective burning portions during the combustion process. The δ value is a function of engine type and speed, etc., and affects the shape of the heat release rate: a smaller δ produces a faster burning rate, hence the peak of normalized heat release rate occurs earlier. In the formula, $\Delta\phi$ is combustion duration in the unit of degree crank angle, ϕ_{burn} is the crank angle of combustion start, and C_w is a constant. If $X = 0.999$ (i.e., 99.9% of the fuel is burnt at the end of combustion), $C_w = 6.908$. The start of combustion is determined by the start of fuel injection and ignition delay. The start of injection is usually defined as when the injection needle has lifted a specified distance from its seat. Practically, the start of combustion is regarded as when the heat release rate becomes zero or when the accumulated heat release rate is at a minimum, or approximately as when the first derivative of the cylinder pressure reaches a minimum after the start of injection.

Ignition delay consists of physical and chemical processes. In the physical processes, fuel sprays break up, vaporize and mix with air. In the chemical processes, pre-flame oxidation of the premixed fuel occurs and localized ignition in multiple areas within the combustion chamber happens. Ignition delay is dependent upon in-cylinder pressure and temperature, mean piston speed and fuel cetane number. High cetane number reduces ignition delay and may prevent diesel knock. In the empirical modeling of diesel engine combustion, many efforts were made to predict the reaction of the fuel burn rate (split to premixed and diffusion phases) based on ignition delay models or the more fundamental Arrhenius equation of reaction rate. Moreover, there are many models of fuel propagation rate and the diffusion of oxygen into the fuel jet (Stone, 1999).

Bypassing the complex details of the combustion process, the Wiebe function provides a simple, convenient but still effective way to calculate in-cylinder thermodynamic bulk pressure and temperature. The $\Delta\phi$, ϕ_{burn} and δ in the function can be easily determined by an experimental cylinder pressure trace diagram and heat release rate analysis, and can then be used as input data for cycle simulations. The above formula is based on a single Wiebe function, which can generally simulate the heat release rate

of low-speed diesel engines. For a more complex heat release rate which characterizes diesel premixed and diffusion combustion phases, two or three Wiebe functions can be linearly superpositioned together.

Predicting $\Delta\phi$, ϕ_{burn} and δ for other operating conditions based on a set of known $\Delta\phi$, ϕ_{burn} and δ values for a given condition was attempted by previous researchers, but still remains a significant challenge for modern EGR diesel engines equipped with advanced fuel systems. A practical approach is to rely on engine testing to obtain the experimental data for $\Delta\phi$, ϕ_{burn} and δ in the entire speed–load domain or at various ambient conditions, and then empirically interpolate or surface-fit them to obtain the required values. Another approach is to reply on advanced combustion simulation (e.g., KIVA) to deduce certain general trends or phenomenological correlations of heat release rates.

12.2.2 Thermodynamic processes of transient performance of intake and exhaust systems

If the engine cylinder itself is the only subject of study, a simplified approach to solve the above governing equations of the in-cylinder process is to assume the pressures in intake port and exhaust port are known constants. However, a more realistic and complex approach is to model them as instantaneous unknowns by using the equations governing the gases in intake and exhaust systems, coupled with the equations of the in-cylinder process. If the gas properties in intake and exhaust ducts are assumed to change only as functions of time, and their variation along the duct dimension is ignored, then the zero-dimensional 'filling and emptying' method can be used as below. Denoting P_3, T_3, m_3,V_3 and A_{3in} as the gas pressure, temperature, mass, volume and inbound effective flow area in the exhaust port and manifold, P, T and m as the gas pressure, temperature and mass in the cylinder from which the gas is flowing into the exhaust control volume; and P_{3pout}, T_{3out}, m_{3out} and A_{3out} as the gas pressure, temperature, mass and outbound effective flow area at the downstream of the exhaust control volume (e.g., flowing to the turbine), the following equations are obtained:

$$\text{Mass conservation}: \frac{dm_3}{d\phi} = \frac{dm}{d\phi} + \frac{dm_{3out}}{d\phi} \tag{12.5}$$

$$\text{Energy conservation}: \frac{d(m_3u_3)}{d\phi} = \frac{dm}{d\phi}h + \frac{dm_{3out}}{d\phi}h_3 + \frac{dQ_{loss}}{d\phi} \tag{12.6}$$

Substituting equation 12.5 into 12.6 gives

$$\frac{dT_3}{d\phi} = \frac{1}{m_3c_{v3}}\left[\frac{dm}{d\phi}(h-u_3) + \frac{dm_{3out}}{d\phi}R_{ex}T_3 + \frac{dQ_{loss}}{d\phi}\right] \tag{12.7}$$

where

$$\frac{dm_{3out}}{d\varphi} = \frac{-A_{3out}P_3}{6N\sqrt{R_{ex}T_3}} \cdot \sqrt{\frac{2\gamma_{ex}}{\gamma_{ex}-1}\left[\left(\frac{P_{out}}{P_3}\right)^{\frac{2}{\gamma_{ex}}} - \left(\frac{P_{out}}{P_3}\right)^{\frac{\gamma_{ex}+1}{\gamma_{ex}}}\right]}$$

Applying the ideal gas law to the gas in the exhaust control volume (port and manifold) gives:

$$P_3V_3 = m_3R_{ex}T_3 \qquad 12.8$$

The port heat loss can be modeled by forced convective water cooling. The heat transfer of the manifold is modeled by natural convection. T_3, m_3 and P_3 are solved by using the governing equations 12.5, 12.7 and 12.8. The equations describing the gas dynamics in intake port and manifold can be formulated in a similar way.

When the manifold pipe is short, the 'filling and emptying' method may give satisfactory results. If the gas pressure wave propagation and reflection along the intake or exhaust pipe needs to be calculated for manifold tuning design or valve timing analysis, the partial differential equations of one-dimensional wave dynamics must be solved with the method of characteristic lines or finite volume or finite difference numerical methods (Benson, 1982; Horlock and Winterbone, 1986). Comprehensive theories of engine unsteady one-dimensional gas dynamics and applications in manifold design were provided by Winterbone and Pearson (1999, 2000). The more complicated three-dimensional CFD modeling of manifold flows is usually a specialized component-level analysis, and is outside the scope of engine system design analysis.

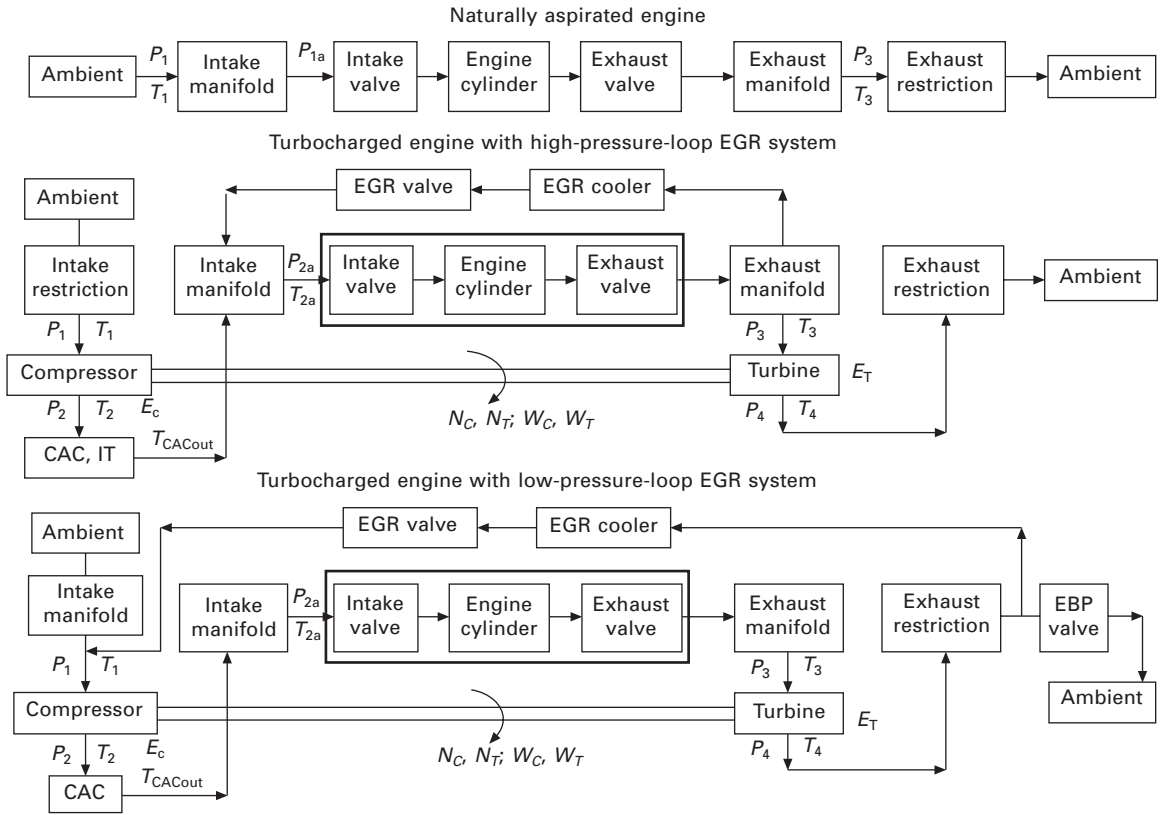
12.2.3 Mathematical formulation of engine system steady-state performance

Theory of math formulation for predicting hardware performance

In order to understand the engine air system design theory and the factors affecting pumping loss, the mathematical formulation of the entire engine gas circuit (Fig. 12.4) needs to be derived in a simple format so that a close-form solution can be analyzed intuitively.

After the instantaneous cylinder pressure P is solved by the cycle process, if mechanical friction work W_{fri} is known, the engine brake work W_E of the total n cylinders can be calculated with the following formula:

$$W_E = \sum_{j=1}^{n} \int P_j \cdot dV_j - W_{fri} \qquad 12.9$$



12.4 Schematic diagrams of engine system layout.

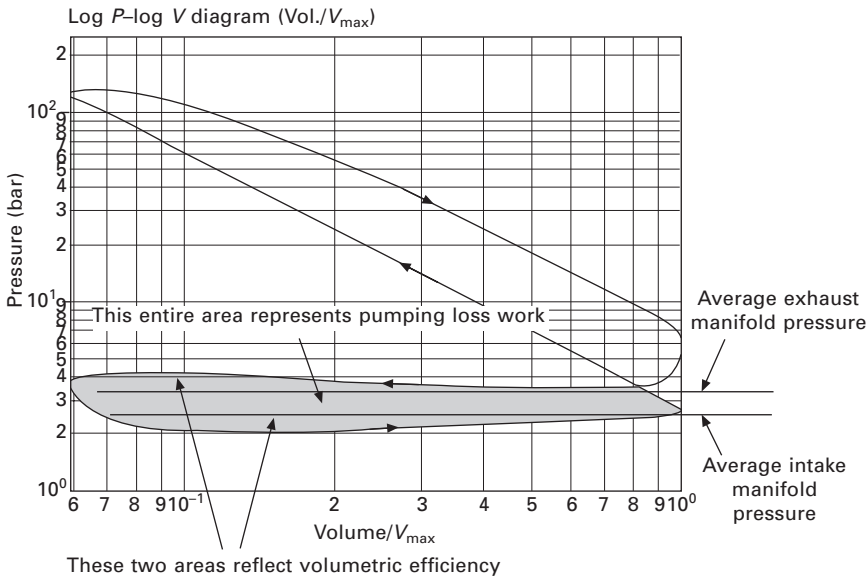
Equation 12.9 is the link between the in-cylinder cycle process and the performance of other subsystems.

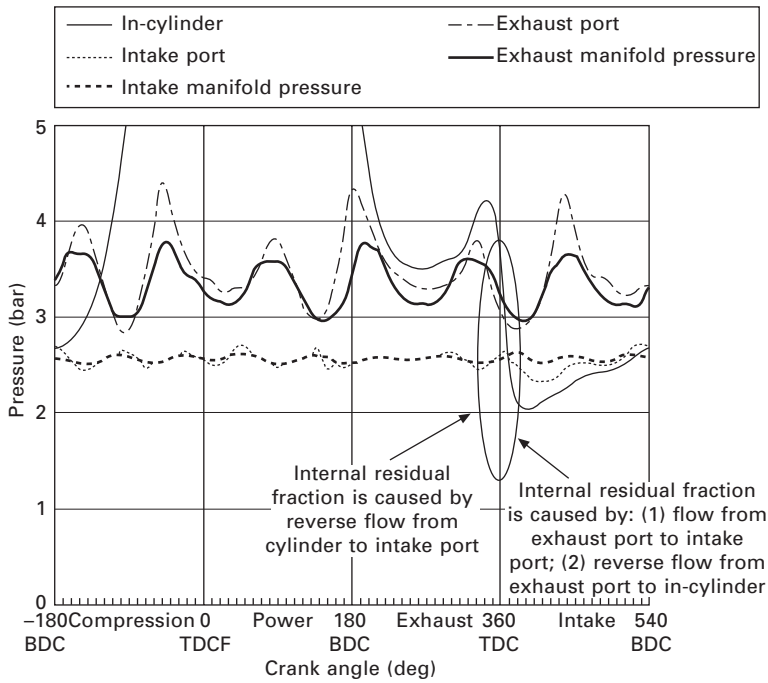
In the *P–V* diagram, the area enveloped by the curve of in-cylinder pressure vs. instantaneous volume during intake and exhaust strokes is pumping loss work (Fig. 12.5). Its characteristic in-cylinder pressure differential is $\Delta P_{cyl} = P_{exhaust} - P_{intake}$ where $P_{intake} = P_{IntakeManifold} - \Delta P_{in}$ and $P_{exhaust} = P_{ExhaustManifold} + \Delta P_{ex}$. The ΔP_{in} is the pressure drop across the flow restrictions of intake manifold, ports and valves. The ΔP_{ex} is the pressure drop across the flow restrictions of exhaust valves, ports and manifold. The pumping loss indicator ΔP_{cyl} can be derived as $\Delta P_{cyl} = (P_{ExhaustManifold} - P_{IntakeManifold}) + (\Delta P_{in} + \Delta P_{ex})$ = (engine delta P) + $(\Delta P_{in} + \Delta P_{ex})$. The engine delta P is defined as exhaust manifold pressure minus intake manifold pressure. It is noted that pumping loss consists of two parts: engine delta P, and the flow restrictions related to volumetric efficiency. Both parts are equally important in engine system design. Engine delta P is related to turbocharger and EGR circuit, while volumetric efficiency is primarily related to the designs of cylinder head, valvetrain and manifolds.

The system of equations governing the steady-state engine performance is derived below. Starting with a simpler example of naturally aspirated non-EGR engine (Fig. 12.4 top), at a given (known) engine speed, fuel rate and brake power, the four unknowns to be solved are engine air flow rate M_{air}, exhaust manifold temperature T_3, inlet pressure P_1 and exhaust manifold pressure P_3. T_3 can be solved based on engine energy balance. M_{air} is solved based on the definition of engine volumetric efficiency (assuming volumetric efficiency is a known value). P_1 is solved by using intake flow restriction characteristics (a curve of pressure drop vs. volume flow rate). P_3 is solved by using exhaust flow restriction characteristics.

For turbocharged EGR engines (Fig. 12.4), the situation is much more complex. At a given engine speed, fuel rate and brake power, assuming turbo characteristics (turbo maps) are known, there are 18 unknowns to be solved: M_{air}, M_{EGR}, T_3, P_4, $T_{1,ROA}$, P_1, P_2, T_2, P_3, T_4, N_C, N_T, E_C, E_T, P_{2a}, T_{2a} (for high-pressure-loop EGR system) or T_1 (for low-pressure-loop EGR system), T_{CACout} and $T_{EGRcoolerGasOut}$. (The detailed explanation of high-pressure-loop and low-pressure-loop EGR systems is provided in Section 12.7 and Fig. 12.38.) The engine delta P is $P_3 - P_{2a}$. In order to understand system performance a set of 18 equations is formed (equations 12.10–12.27) based on the thermal, flow or efficiency characteristics of each element. It should be noted that the formulated equations also serve as a foundation for developing future real-time model-based algorithms in advanced electronic controls.

Unlike the detailed differential equations of the in-cylinder cycle process (equations 12.2–12.4), in the air system circuit the engine is treated as one lumped element in energy balance, so that exhaust enthalpy or exhaust manifold temperature can be calculated by:





12.5 Pumping loss, engine delta P and manifold gas wave dynamics (GT-POWER simulation).

$$\dot{Q}_{fuel} = \dot{W}_E + \Delta\dot{H} + \dot{Q}_{base-cooling} + \dot{Q}_{miscellaneous} \quad 12.10$$

where $\Delta\dot{H}$ is the rise of gas enthalpy rate from intake manifold to exhaust manifold, $\dot{Q}_{base-cooling}$ is base engine heat rejection to coolant (if water cooled) or cooling air (if air cooled), and $\dot{Q}_{miscellaneous}$ is treated as a known quantity here and will be detailed in Section 12.6. Equation 12.10 is used to solve for exhaust manifold temperature T_3 when engine brake power $\dot{W}_E$ is assumed to be known or is calculated from equation 12.9.

The four-stroke engine may also be treated as a lumped element in breathing performance, and is overall characterized by using the definition of intake manifold air–EGR mixture non-trapped volumetric efficiency:

$$\eta_{EV} = \frac{2M_{mixture}}{\rho_{2a} N_E V} = \frac{2(M_{air} + M_{EGR}) T_{2a} R}{P_{2a} N_E V} \quad 12.11$$

where η_{EV} is volumetric efficiency with a reference gas density defined at the intake manifold, N_E is engine crankshaft speed (revolutions per second), V is engine displacement, T_{2a} and P_{2a} are at intake manifold, $P_{2a} = P_2 - \Delta P_{\text{Intake Throttle}} - \Delta P_{CAC}$, M_{air} is engine fresh air flow rate, and M_{EGR} is EGR mass flow rate. The η_{EV} is related to valve size, valve timing, valve lift profile, port flow coefficient and manifold design. The η_{EV} is also affected by intake manifold temperature, engine delta P and the consequent internal residual fraction. The trapped residue is affected by engine delta P and gas scavenging. In fact, it is very difficult to use hand calculation to compute η_{EV}. Note that equations 12.10 and 12.11 describe the engine macro behavior, and they are essentially the lumped simplified forms of the detailed in-cylinder cycle process shown in equation 12.2–12.4.

The lumped intake air flow restriction at compressor inlet is given by:

$$M_{air} = f_1 (C_{d\text{-}intake}, P_{ambient} - P_1, T_{ambient}) \quad 12.12$$

where f_1 is a known function (e.g., second-order polynomial) and $C_{d\text{-}intake}$ is a lumped flow restriction coefficient of the intake system at the compressor inlet, including the restrictions of air filter and any regulating valves (for example, an intake throttle valve used in a low-pressure-loop EGR system). Equation 12.12 is used to solve P_1. It should be noted that the intent here is not to provide a detailed precise form of the function f but is to illustrate how to formulate the air system design problem mathematically to match the number of unknowns with the number of equations, so that the problem does not become over-constrained or under-constrained. Such a mathematical formulation is important for identifying various air system control 'knobs'.

The intake air temperature at the compressor inlet is given by:

$$T_{1,ROA} = T_{ambient} + ROA \tag{12.13}$$

where *ROA* is a 'rise-over-ambient' air temperature difference between compressor inlet and ambient. *ROA* is related to pipe insulation and vehicle underhood thermal management. In a high-pressure-loop EGR system, $T_1 = T_{1,ROA}$. In a low-pressure-EGR system, $T_1 > T_{1,ROA}$ due to EGR mixing.

The following equation of lumped exhaust flow restriction at the turbine outlet is used to solve P_4:

$$M_{exh} = M_C + M_{fuel} + M_{LubeOilCons} = f_2\,(C_{d\text{-}exh},\, P_4 - P_{ambient},\, T_4) \tag{12.14}$$

where M_{exh} is exhaust mass flow rate, M_C is compressor mass flow rate (in a high-pressure-loop EGR system, $M_C = M_{air}$), M_{fuel} is fuel flow rate, and $C_{d\text{-}exh}$ is a lumped exhaust restriction flow coefficient.

The lumped EGR circuit flow restriction is given by:

$$M_{EGR} = f_3\,(C_{d\text{-}EGR},\, P_{EGRin} - P_{EGRout},\, T_{EGRcoolerOut}) \tag{12.15}$$

P_{EGRin} refers to the gas pressure at the EGR circuit inlet, and P_{EGRout} refers to the gas pressure at the EGR circuit outlet. For example, in a high-pressure-loop EGR system, $P_{EGRin} = P_3$, $P_{EGRout} = P_{2a}$, and engine delta P is the EGR driving force. In a low-pressure-loop EGR system, P_{EGRin} is a pressure somewhere between P_4 and $P_{ambient}$, depending on where the EGR flow is picked up between different aftertreatment devices, and P_{EGRin} is a function of $C_{d\text{-}exh}$ and P_4 or a function of $C_{d\text{-}intake}$ and P_1; $P_{EGRout} = P_1$. $C_{d\text{-}EGR}$ is a lumped flow restriction coefficient including low restrictions of both EGR cooler and tubing (fixed restriction) and EGR valve opening (adjustable restriction). For convenience the discussion below is mainly focused on the high-pressure-loop EGR system.

T_2 can be calculated based on the definition of compressor isentropic efficiency (E_C, quoted on a total-to-total basis) as below, assuming a single-stage compressor or a two-stage compressor without inter-stage cooling:

$$E_C = \frac{(P_2/P_1)^{\frac{\gamma_c - 1}{\gamma_c}} - 1}{(T_2/T_1) - 1} \tag{12.16}$$

T_4 can be calculated based on the definition of turbine isentropic efficiency (E_T, quoted on a total-to-static basis) as below:

$$E_T = \frac{1 - (T_4/T_3)}{1 - (P_4/P_3)^{\frac{\gamma_t - 1}{\gamma_t}}} \tag{12.17}$$

Compressor power on a total-to-total basis is given by

$$\dot{W}_C = \frac{M_C c_{p,C} T_1}{E_C}\left[\left(\frac{P_2}{P_1}\right)^{\frac{\gamma_c - 1}{\gamma_c}} - 1\right]$$

Turbine power on a total-to-static basis is given by

$$\dot{W}_T = E_T M_T c_{p,T} T_3 \left[1 - \left(\frac{P_4}{P_3}\right)^{\frac{\gamma_t - 1}{\gamma_t}}\right]$$

Turbocharger power balance is given by $\dot{W}_C = \dot{W}_T E_M$ (where E_M is turbocharger mechanical efficiency if it has not been included in the turbine efficiency), which can be expanded as below:

$$1 - \left(\frac{P_2}{P_1}\right)^{\frac{\gamma_c - 1}{\gamma_c}} + E_C E_T E_M \left(\frac{M_T}{M_C}\right)\left(\frac{c_{p,T}}{c_{p,C}}\right)\left(\frac{T_3}{T_1}\right)\left[1 - \left(\frac{P_4}{P_3}\right)^{\frac{\gamma_t - 1}{\gamma_t}}\right] = 0 \qquad 12.18$$

Note that the measured gas stand turbine efficiency is usually the product of isentropic efficiency E_T multiplied by mechanical efficiency E_M. The overall turbocharger efficiency is defined as $E_{TC} = E_C E_T E_M$. Assuming piston blow-by is neglected, the turbine flow rate and compressor flow rate are related by $M_T = M_C + M_{fuel} - M_{WG}$ where M_{WG} is the turbine wastegate or bypass flow rate.

The compressor speed needs to be equal to the turbine speed, and this relationship is given as:

$$N_C = N_T \qquad 12.19$$

The compressor efficiency map can be described as a function (e.g., a sixth-order polynomial) of corrected compressor flow rate and pressure ratio, as shown in any compressor maps:

$$E_C = f_4\,(M_C,\, P_2/P_1) \qquad 12.20$$

The turbine efficiency map with a given effective area can be described as a function (e.g., a sixth-order polynomial) of corrected turbine flow rate and pressure ratio, as shown in any turbine maps:

$$E_T = f_5\,(M_T,\, P_3/P_4) \qquad 12.21$$

The compressor speed map can also be described as a function of corrected flow rate and pressure ratio:

$$N_C = f_6\,(M_C,\, P_2/P_1) \qquad 12.22$$

The turbine speed map with a given effective area is also a function of flow rate and pressure ratio:

$$N_T = f_7\,(M_T,\, P_3/P_4) \tag{12.23}$$

In fact, the turbine efficiency can also be described as a parabolic function of speed ratio based on its aerodynamics. Different turbine pressure ratios usually form a family of such parabolic curves. Denoting the subscript '*o*' for total state and '*s*' for static, the speed ratio is defined by

$$u_T/C_0 = (\pi d_T N_T)/\sqrt{2(h_{o3} - h_{s4})}$$

The EGR and air mixing in the intake manifold for a high-pressure-loop EGR system can be described by:

$$M_{air}\int_0^{T_{CACout}} c_{p,air}dT + M_{EGR}\int_0^{T_{EGRcoolerGasOut}} c_{p,EGR}dT$$

$$= (M_{air} + M_{EGR})\int_0^{T_{2a}} c_{p,mix}dT \tag{12.24a}$$

The EGR and air mixing at the compressor inlet for a low-pressure-loop EGR system can be described by:

$$M_{air}\int_0^{T_{1,ROA}} c_{p,air}dT + M_{EGR}\int_0^{T_{EGRcoolerGasOut}} c_{p,EGR}dT$$

$$= (M_{air} + M_{EGR})\int_0^{T_1} c_{p,mix}dT \tag{12.24b}$$

The effectiveness of the charge air cooler is defined as

$$E_{CAC} = \frac{T_2 - T_{CACout}}{T_2 - T_{CACcooling}} \tag{12.25}$$

The effectiveness of the EGR cooler is defined as

$$E_{EGRcooler} = \frac{T_3 - T_{EGRcoolerGasOut}}{T_3 - T_{EGRcoolantInlet}} \tag{12.26}$$

A detailed discussion on cooler effectiveness and design parameters is provided in Section 12.6.

The lumped flow restriction of the charge air cooler and its downstream intake throttle valve opening (if any) is characterized by a lumped flow coefficient $C_{d\text{-}CAC\text{-}throttle}$ as:

$$M_{air} = f_8(C_{d-CAC-throttle},\, P_2 - P_{2a},\, T_{CACout}) \tag{12.27}$$

After the turbine flow rate M_T is solved by the above 18 equations, the turbine effective cross-sectional area A_T can be calculated by using equation 12.28 for the compressible flow in an axial flow turbine, as a simplified illustration:

$$M_T = A_T \cdot \frac{P_3}{\sqrt{R_{ex}T_3}} \cdot \sqrt{\frac{2\gamma_t}{\gamma_t - 1}} \cdot \sqrt{\left(\frac{P_4}{P_3}\right)^{\frac{2}{\gamma_t}} - \left(\frac{P_4}{P_3}\right)^{\frac{\gamma_t+1}{\gamma_t}}}$$

(for subsonic flow with P_3 and T_3 in total state) 12.28

The flow equation for a radial flow turbine (as for most automotive diesel engines) is much more complex and there is an enthalpy factor to modify the terms of P_4/P_3. The turbine effective area A_T consists of two parts multiplied together: (1) the turbine physical area (a constant related to nozzle throat area and exducer throat area); and (2) the turbine flow coefficient (a variable, being a function of turbine pressure ratio and turbine speed).

In equations 12.10–12.27, the parameters of gas pressure, temperature and flow rate can be cycle-average steady-state values or instantaneous quantities as functions of crank angle in a quasi-steady-state sense. The earlier equation 12.2 (in transient differential form) is essentially the same as 12.10 (in steady-state form). They are based on energy conservation which can solve for T_3. The earlier equation 12.3 is essentially the same as 12.11. They are based on mass conservation which can solve for M_{air}. It is worth noting that the steady-state cycle-average integral of in-cylinder pressure is essentially the engine power, reflected by equation 12.9. In the formulation of equations 12.10–12.27, engine brake power is assumed to be a known quantity. If the power is unknown, the governing equation 12.4 of the in-cylinder instantaneous cycle process must be used to solve for the in-cylinder pressure, and then its steady-state counterpart 12.9 must be used to integrate over an engine cycle to solve for brake power.

Because equations 12.22 and 12.23 are included to describe particular characteristics of given turbo hardware, the formulation of 12.10–12.27 can only be used to predict engine performance of given hardware. Equations 12.10–12.27 consist of a non-linear system which has to be solved iteratively by assuming an initial value for one of the 18 unknowns and iterating to convergence.

Theory of mathematical formulation for hardware specification design with target performance

In the last section, predicting hardware performance was discussed. Actually, in engine air system specification design, usually the objective is reversed, i.e., to the find required hardware (e.g., turbine effective area) to match a given functional target of air flow rate (or gravimetric air–fuel ratio) and EGR

rate. (The EGR rate here is defined as the ratio between EGR mass flow rate and the total flow rate of EGR and fresh air.) If desirable compressor and turbine efficiencies are assumed as fixed input, a system of 16 equations, 12.10–12.19 and 12.22–12.27, is formed. The 16 unknowns are M_{air}, M_{EGR}, T_3, P_4, $T_{1,ROA}$, P_1, P_2, T_2, P_3, T_4, N_C, N_T, P_{2a}, T_{2a}, T_{CACout} and $T_{EGRcoolerGasOut}$. Turbine speed can still be guaranteed to be equal to compressor speed because equations 12.19, 12.22 and 12.23 are used. However, turbo speed is usually not required in the output of engine system specification calculation. Instead, turbine area is a required specification design parameter. Therefore, by deleting the turbo speed and map equations 12.19–12.23, which describe fixed turbo hardware characteristics, and by adding 12.28, a mathematical system of 14 equations, 12.10–12.18 and 12.24–12.28, is formed for engine system specification design. In fact, this system can be used for two purposes: (1) to calculate the required hardware for a given performance target; or (2) to calculate the performance for given hardware (though in a simplified form of 12.10–12.27). For example, the 14 unknowns can be M_{air} or A_T, M_{EGR}, T_3, P_4, $T_{1,ROA}$, P_1, P_2, T_2, P_3, T_4, P_{2a}, T_{2a}, T_{CACout}, $T_{EGRcoolerGasOut}$ and It should be noted that this set of 14 equations can be reformulated to any smaller sets if the number of unknowns is reduced accordingly. In air system design, it is important to understand the engineering implication behind this mathematical formulation. When M_{air} is known and A_T is unknown, the required turbine area needs to be found to match the given air flow rate. In such a calculation without using turbo speed maps and efficiency maps, the calculation does not guarantee that turbine speed is equal to compressor speed, although it still calculates the flow rate and pressure ratio of the compressor and turbine.

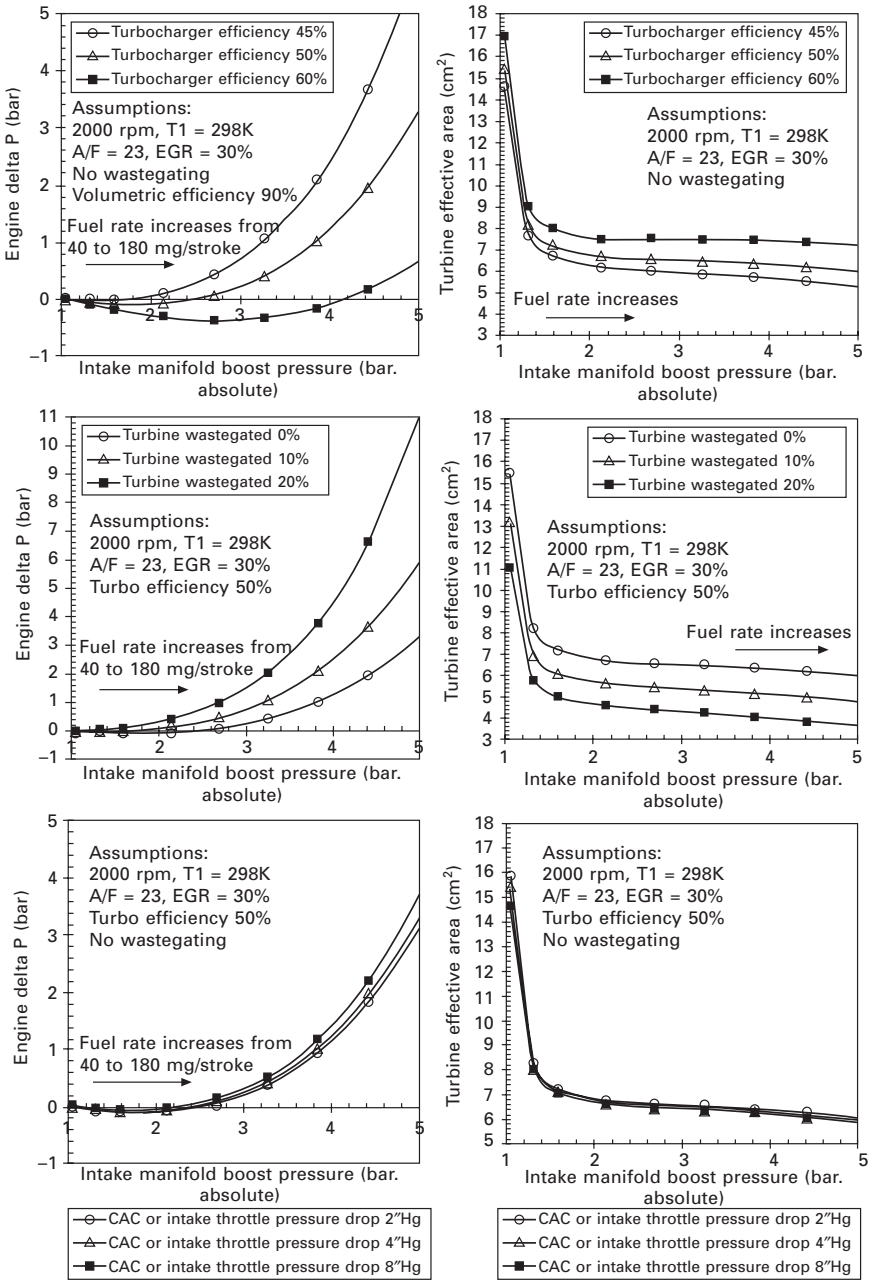
In system specification design analysis, in order to achieve the minimum engine delta P at fixed target of air–fuel ratio and EGR rate, it is often convenient and necessary for the engine manufacturer to start with computing the required turbo efficiency and proposing the desirable turbocharger specification (i.e., turbo flow rate, pressure ratio and 'fixed' required efficiency) to turbo suppliers. It should be noted that the assumption of imposed turbo efficiency sometimes might not be realistic in real turbo hardware, especially when fixed efficiencies are specified at multiple engine speed and load modes. Turbo suppliers have the responsibility to select or design turbochargers to reach the efficiency requirements specified by engine manufacturers. They are also responsible for matching a turbocharger with proper rotating shaft speed to reach the desirable flow rate and pressure ratio specified by the engine manufacturer as closely as possible. After obtaining the proposed real turbocharger maps from turbo suppliers, the engine manufacturer can move to the next step of using computer simulation to check turbo hardware performance (i.e., using the formulation of equations 12.10–12.27) in order to evaluate how much deviation the proposed turbocharger hardware has compared to the original system design specification.

The characteristics of engine delta P

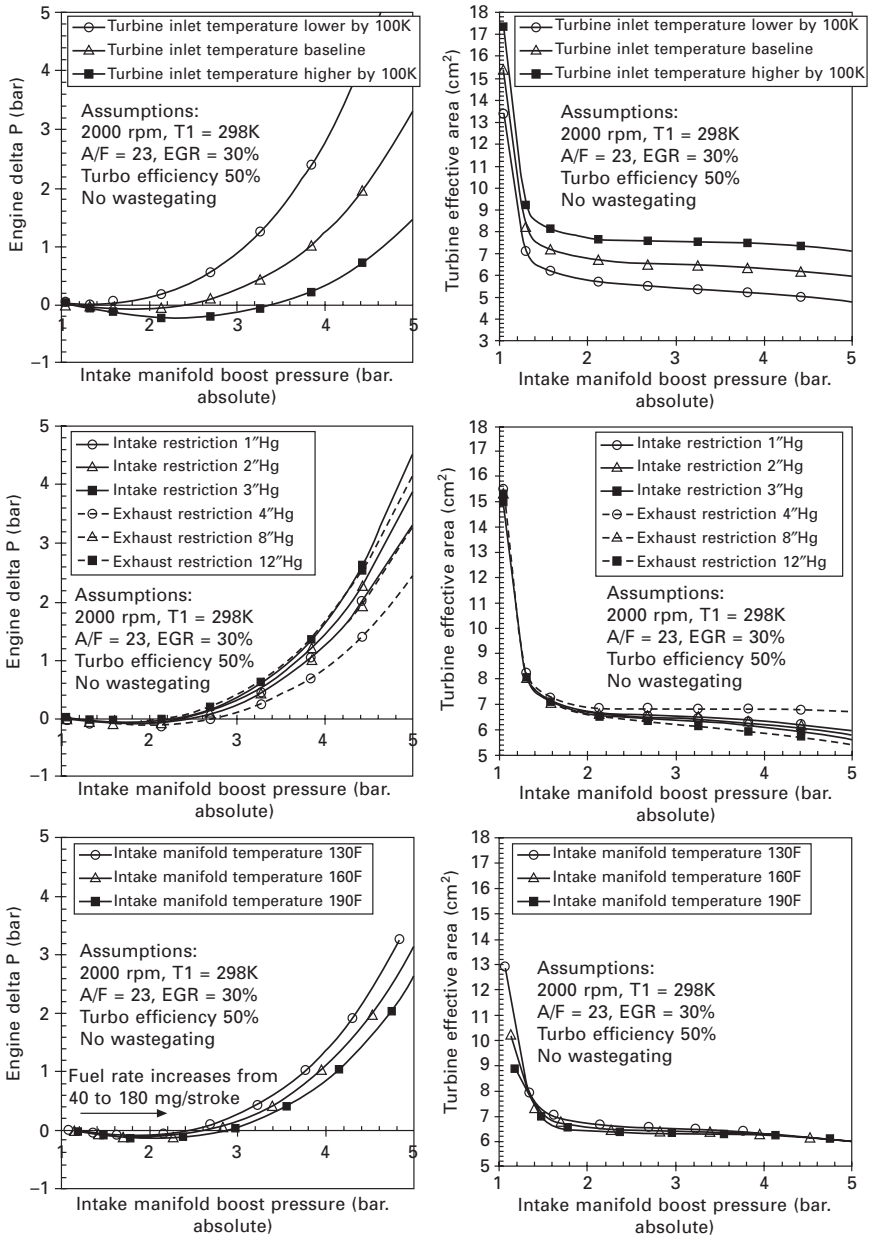
Engine delta P is a critical part of pumping loss. There are four core equations related to air system performance: 12.11 for engine-turbo coupled breathing characteristic, 12.15 for EGR circuit flow restriction, 12.18 for linking intake manifold boost pressure to exhaust manifold back pressure, and 12.28 (or its equivalent counterpart for radial flow turbine) for generating engine air flow by the turbine. Substituting 12.11 into 12.18, the parametric dependence of engine delta P ($P_3 - P_{2a}$) can be reflected by 12.18 and 12.28. With air flow rate and EGR rate as known target input (or equivalently intake manifold pressure P_{2a} and EGR rate as target, according to 12.11), when T_3 and P_4 do not change, if the turbine area A_T changes, the exhaust manifold pressure P_3 will change according to 12.28. Thus, in 12.18 a change in P_2, $E_C E_T E_M (M_T/M_C)(T_3/T_1)$ or P_4 is required in order to balance the equation. Therefore, the parameters which can reduce engine delta P (i.e., minimize P_3 at a given P_{2a}) are shown directly in 12.18 and 12.28. The parameters are P_1, P_2, the term $E_C E_T E_M (M_T/M_C)(T_3/T_1)$, P_4 and A_T. T_1 is affected by *ROA*. P_1 is affected by the degree of flow throttling at the compressor inlet. P_2 is affected by engine speed, volumetric efficiency and intake manifold temperature, as shown in 12.11; and it is also affected by charge air cooler flow restriction and intake throttle as shown in 12.27. T_3 is affected by cylinder cooling and heat losses from the exhaust port and manifold, as shown in 12.10; and it also depends on air–fuel ratio. M_T is affected by turbine wastegate opening. P_4 is affected by aftertreatment exhaust restriction $C_{d\text{-}exh}$ as shown in 12.14. $E_C E_T E_M$ and A_T are turbocharger design parameters.

EGR circuit flow restriction also affects engine delta P and other system design parameters. In a high-pressure-loop EGR system, the EGR circuit flow restriction coefficient $C_{d\text{-}EGR}$ (or lumped EGR valve opening) can be solved with 12.15 when $P_3 - P_{2a}$ and EGR flow rate are known. On the other hand, at fixed air flow rate and EGR rate (or equivalently, at fixed EGR mass flow rate), when EGR circuit flow restriction is also fixed, P_3 must be calculated by 12.15. Then turbine area A_T must change according to 12.28, and simultaneously another change is required in one of the following in order to balance 12.18: P_1, P_2, the term $E_C E_T E_M (M_T/M_C)(T_3/T_1)$ or P_4.

Figure 12.6, obtained by solving equations 12.11, 12.18 and 12.28, supported by an exhaust manifold temperature model of 12.51, shows the factors affecting the cycle-average engine delta P. It illustrates that the following design may reduce engine delta P at a given speed–load mode and fixed target of air–fuel ratio and EGR rate: higher turbocharger efficiency, higher exhaust manifold temperature, less turbine wastegating, lower exhaust restriction, and lower charge air cooler pressure drop. It is also observed that at higher engine load (fuel rate), engine delta P becomes higher. It is worth noting that in some engine designs with reed valve, EGR flow can be



12.6 Theoretical analysis of engine delta P.



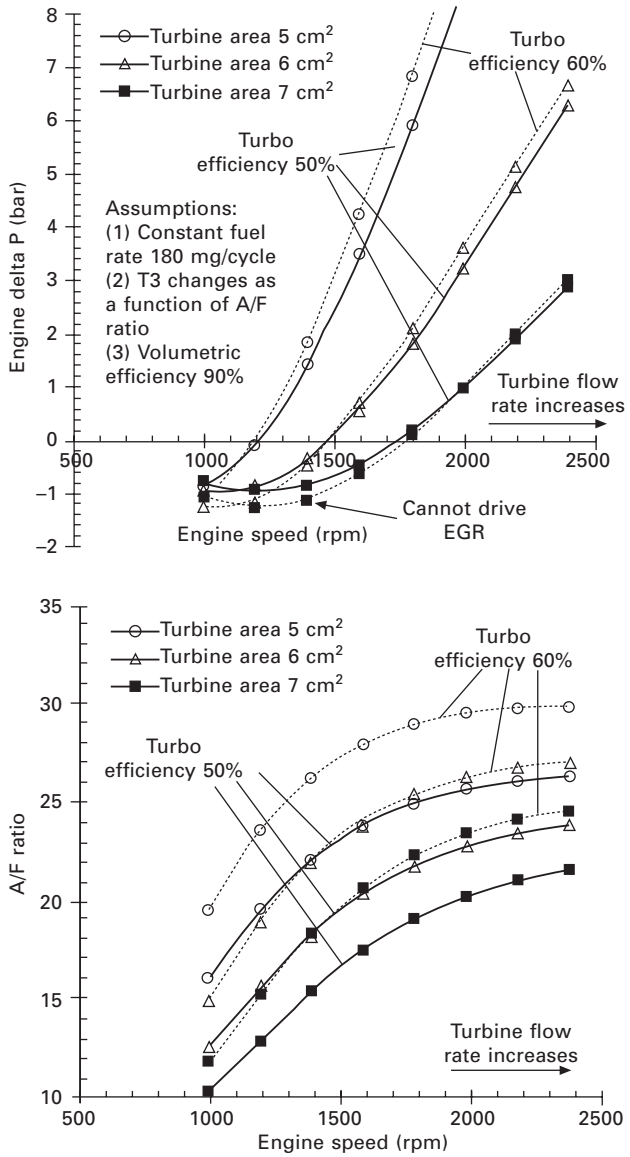
12.6 Continued

harvested into the cylinder with the pulsating pressure differential even if the cycle-average engine delta P becomes slightly negative. The effect of turbine wastegating can be explained as follows. With wastegating the turbine flow loss must be compensated by an increase in turbine pressure ratio in order to maintain sufficient turbine power to deliver a target compressor boost pressure. The larger turbine pressure ratio results in an inevitable increase in exhaust manifold pressure and engine delta P. Variable geometry turbine (VGT) does not have wastegate flow loss, hence it may produce lower pumping loss and brake specific fuel consumption (BSFC) than a wastegate turbine does, provided both turbines have similar efficiency. It should be noted that in some two-stage turbochargers, there is usually a high-pressure-stage turbine bypass valve or wastegate to divert the exhaust flow to the low-pressure-stage turbine inlet. The bypassed exhaust flow in such a two-stage turbo essentially is not all wasted because it is utilized by the low-pressure-stage turbine to deliver certain boost. But some flow throttling loss does occur at the wastegate when the valve is partially open.

In EGR engine design, insufficient engine delta P and inadequate capability to drive EGR flow often occur at low engine speeds, especially at peak torque condition. In a turbocharged engine, the parameter delivering and controlling the exhaust manifold pressure and compressor boost pressure is the turbine effective area. It acts as a restricting orifice and also a power-producing element to drive the compressor. The required turbine area can be determined by using equation 12.28. It is the turbine area that primarily decides the engine delta P relationships depicted above. With a fixed turbine area, engine delta P reduces as engine speed decreases at fixed load, as shown in Fig. 12.7. The figure is obtained by using the four core equations 12.11, 12.15, 12.18 and 12.28. It is observed that a smaller turbine area produces a higher engine delta P to enable EGR driving at low speeds. Figure 12.7 also shows that at a fixed air–fuel ratio target at a given low speed, turbocharger efficiency should not be too high, otherwise the matched large turbine area would produce very low engine delta P or even very negative engine delta P which cannot drive EGR flow (EGR rate 30% here).

Summary of theoretical options of air system design

From the set of 14 equations for engine system specification design (12.10–12.18 and 12.24–12.28) any 14 parameters can be chosen as unknowns to formulate the system in order to evaluate the effects of engine hardware design or operating conditions. Sixteen typical systems are listed in Table 12.1 to cover most air system possibilities with high-pressure-loop EGR. In Table 12.1 the second column lists possible unknowns, either a performance parameter or hardware design. One unknown needs to be chosen from each equation in order to formulate a system. The parameters listed under each



12.7 Effect of engine speed on engine delta P.

system number are the 14 unknowns. The parameters not shown under each system number but shown in the second column are assumed as known input data. The **hardware** or **calibration** parameters are shown as **bold** in Table 12.1. For example, in system 1, E_C (compressor efficiency), $C_{d\text{-}EGR}$ (EGR valve opening), A_T (turbine effective area) and M_T (representing turbine wastegate opening) are assumed to be known fixed hardware or calibration

Table 12.1 Mathematical formulation of HPL-EGR engine air systems at given engine speed, fueling rate and power

Equation	Symbol	Engine system number															
		1	2	3	4	5	6	7	8	9	10	11	12	13	14	15	16
12.10	T_3, $Q_{base\text{-}cooling}$	T_3	T_3	T_3	T_3	T_3	T_3	T_3	T_3	T_3	T_3	T_3	T_3	T_3	T_3	T_3	T_3
12.11	η_{EV}, M_{air}, M_{EGR}, T_{2a}, P_{2a}, V	M_{air}	P_{2a}	P_{2a}	P_{2a}	P_{2a}	P_{2a}	P_{2a}	P_{2a}	P_{2a}	P_{2a}	P_{2a}	P_{2a}	P_{2a}	P_{2a}	P_{2a}	T_{2a}
12.12	M_{air}, $C_{d\text{-}intake}$, P_1, $P_{ambient}$	P_1	P_1	P_1	P_1	P_1	P_1	P_1	P_1	P_1	P_1	P_1	P_1	P_1	P_1	P_1	P_1
12.13	$T_{1,ROA}$, ROA, $T_{ambient}$	$T_{1,ROA}$	$T_{1,ROA}$	$T_{1,ROA}$	$T_{1,ROA}$	$T_{1,ROA}$	$T_{1,ROA}$	$T_{1,ROA}$	$T_{1,ROA}$	$T_{1,ROA}$	$T_{1,ROA}$	$T_{1,ROA}$	$T_{1,ROA}$	$T_{1,ROA}$	$T_{1,ROA}$	$T_{1,ROA}$	$T_{1,ROA}$
12.14	$C_{d\text{-}exh}$, P_4, $P_{ambient}$	P_4	P_4	P_4	**$C_{d\text{-}exh}$**	P_4	P_4	P_4	**$C_{d\text{-}exh}$**	P_4	P_4	**$C_{d\text{-}exh}$**	P_4	P_4	**$C_{d\text{-}exh}$**	**$C_{d\text{-}exh}$**	P_4
12.15	M_{EGR}, $C_{d\text{-}EGR}$, P_3, P_{2a}	M_{EGR}	**$C_{d\text{-}EGR}$**	**$C_{d\text{-}EGR}$**	**$C_{d\text{-}EGR}$**	**$C_{d\text{-}EGR}$**	**$C_{d\text{-}EGR}$**	P_3	P_3	P_3	P_3	P_3	P_3	P_3	P_3	P_3	P_{2a}
12.16	E_C, P_1, P_2, T_1, T_2	T_2	T_2	T_2	T_2	T_2	T_2	T_2	T_2	T_2	T_2	T_2	T_2	T_2	T_2	T_2	P_2
12.17	E_T, P_3, P_4, T_3, T_4	T_4	T_4	T_4	T_4	T_4	T_4	T_4	T_4	T_4	T_4	T_4	T_4	T_4	T_4	T_4	T_4
12.18	P_1, P_2, E_C, E_T, E_M, M_T (turbine wastegate flow), T_1, T_3, P_3, P_4	P_2	P_3	P_3	P_4	P_2	**$E_{T/C}$**	**M_T**	P_4	P_2	**$E_{T/C}$**	P_4	P_2	**$E_{T/C}$**	P_2	**$E_{T/C}$**	**$E_{T/C}$**
12.24a	M_{air}, M_{EGR}, T_{CACout}, $T_{EGRcoolerGasOut}$, T_{2a}	T_{2a}	T_{2a}	T_{2a}	T_{2a}	T_{2a}	T_{2a}	T_{2a}	T_{2a}	T_{2a}	T_{2a}	T_{2a}	T_{2a}	T_{2a}	T_{2a}	T_{2a}	T_{CACout}
12.25	E_{CAC}, T_2, T_{CACout}	T_{CACout}	T_{CACout}	T_{CACout}	T_{CACout}	T_{CACout}	T_{CACout}	T_{CACout}	T_{CACout}	T_{CACout}	T_{CACout}	T_{CACout}	T_{CACout}	T_{CACout}	T_{CACout}	T_{CACout}	T_2
12.26	$E_{EGRcooler}$, T_3, $T_{EGRcoolerGasOut}$ (= T_{EGR})	T_{EGR}	T_{EGR}	T_{EGR}	T_{EGR}	T_{EGR}	T_{EGR}	T_{EGR}	T_{EGR}	T_{EGR}	T_{EGR}	T_{EGR}	T_{EGR}	T_{EGR}	T_{EGR}	T_{EGR}	T_{EGR}
12.27	M_{air}, P_2, P_{2a}, $C_{d\text{-}CAC\text{-}throttle}$ (= $C_{d\text{-}IT}$)	P_{2a}	P_2	P_2	P_2	**$C_{d\text{-}IT}$**	P_2	P_2	P_2	**$C_{d\text{-}IT}$**	P_2	P_2	**$C_{d\text{-}IT}$**	P_2	**$C_{d\text{-}IT}$**	P_2	**$C_{d\text{-}IT}$**
12.28	M_T, A_T, T_3, P_3, P_4	P_3	**A_T**	**M_T**	P_3	P_3	P_3	**A_T**	**A_T**	**A_T**	**A_T**	**M_T**	**M_T**	**M_T**	P_4	P_4	P_3

parameters. System 1 solves 14 performance parameters as unknowns with a given set of hardware and calibration. For a fixed pair of air–fuel ratio and EGR rate target, each of systems 2–16 needs to be solved for two hardware or calibration parameters. The two hardware selections have a certain flexibility of regulating air–fuel ratio and EGR rate within a range. Different systems of hardware formulation provide a different range of controllability. Systems 2–6 have high pumping loss when EGR circuit flow coefficient $C_{d\text{-}EGR}$ is low (i.e., more restrictive). Systems 7–9, 11 and 12 are practical ones with known turbo efficiency and maximum $C_{d\text{-}EGR}$. They can be used to seek hardware to reach a target air–fuel ratio and EGR rate with minimum engine delta P ($P_3 - P_{2a}$). Systems 10 and 13 can be used to compute the required turbo efficiency, turbine area or wastegate opening with given exhaust restriction $C_{d\text{-}exh}$ in order to achieve a target air–fuel ratio and EGR rate. System 14 may have redundancy in functionality because exhaust back pressure valve and intake throttle valve have similar effects on performance. System 15 (or 16) can be used to compute the required turbo efficiency and exhaust (or intake) restriction with a given turbine. The mathematical formulations of low-pressure-loop EGR and hybrid EGR systems can be derived similarly. In low-pressure-loop EGR, although intake air throttling at the compressor inlet may be used to induct EGR flow, it is usually less effective than using an exhaust back pressure valve at the turbine outlet. It is worth noting that the non-EGR engine can be viewed as a simplified form of the above system formulation. The engine applications of Table 12.1 will be elaborated in Section 12.7.

12.2.4 Engine cycle simulation model tuning

In engine cycle simulation, tuning the model is one of the most difficult tasks in EPSI analysis because of the complex interaction among the performance parameters of different subsystems. Model tuning refers to calibrating the model to tune (adjust) the hardware features to match existing (known) engine test data. The key of building a successful model is to identify and tune appropriate model parameters to reflect the true physics embedded in engine performance test data. The theoretical foundation of model tuning can be referred to pages 404–405. Those equations capture many governing hardware design parameters which can be relatively easily tuned in the model (e.g., turbine area and efficiency). However, there are more complex physical processes shown in the test data which cannot be modeled very accurately by the zero-dimensional or one-dimensional cycle simulation software, for example the in-cylinder combustion, BSFC and heat transfer. It should be noted that although the cycle simulation model is the best tool for system design due to its sufficient accuracy on macro engine performance parameters and fast computing time, it has certain limitations on predictability and it requires

careful model tuning with experimental data to handle the uncertainties. Lumping some uncertainties together in subsystem models (e.g., within the boundary of the system of equations formulated earlier) is an effective approach in system-level analysis when detailed accurate experimental data of each component are not available and when certain complex physics cannot be modeled accurately. Over-complicated modeling on minor details or on highly uncertain physical processes (e.g., in-cylinder heat transfer and emissions) slows down system analysis and only provides diminishing return in product design. The effectiveness of system simulation relies on a fine balance between model complexity and simplicity. It is worth noting that the quality of model tuning and model predictability must be judged by comparing with multiple data points, because the model could be 'purposely matched or fudged' to be 100% accurate for a single data point.

Some limitations of the cycle simulation model are as follows. First, the model cannot accurately predict engine in-cylinder processes of heat transfer, combustion and emissions because it is difficult to simulate the three-dimensional distribution of thermodynamic properties and the combustion process as a function of space and time for the in-cylinder heterogeneous mixture of air, fuel and combustion products. The model usually only uses a burn rate derived from a measured cylinder gas pressure trace, or at most it uses zero-dimensional phenomenological combustion models to compute a burn rate. Secondly, the model cannot capture all the micro details of thermal-fluid components such as the soot layer effect in EGR cooler fouling or CFD effects around valves. Instead, the model uses a lumped approximate approach to simulate their global or macro performance characteristics. Thirdly, the input data of hardware characteristics used in the model (e.g., turbocharger efficiency maps) are normally obtained from an off-engine test bench, and might not represent the true behavior of the devices under realistic transient boundary conditions on the engine. All these difficulties cause simulation errors when compared to engine test data.

In the engine cycle simulation model, the following eight key elements characterize the system: intake restriction, exhaust restriction, charge air cooler, inter-stage cooler if any (characterized by cooling capacity and flow restriction), EGR cooler (cooler cooling capacity, flow restriction), compressor (efficiency), turbine (efficiency, effective area), and engine cylinder (mechanical friction, base engine heat rejection, volumetric efficiency). In model tuning at a given engine speed, it is important to match the following three types of system performance parameters with high-quality test data:

1. The five major design targets (brake power, BSFC, air–fuel ratio, EGR rate, and intake manifold temperature).
2. Design constraints (peak cylinder pressure and in-cylinder combustion pressure pattern, exhaust manifold gas temperature, compressor outlet

temperature, exhaust manifold pressure, engine delta P, coolant heat rejection, engine outlet coolant temperature, and turbo speed).

3. All the rest of the 18 parameters mentioned earlier (M_{air}, M_{EGR}, T_3, P_4, $T_{1,ROA}$, P_1, P_2, T_2, P_3, T_4, N_C, N_T, E_C, E_T, P_{2a}, T_{2a} or T_1, T_{CACout} and $T_{EGRcoolerGasOut}$). These parameters are related not only to model tuning, but also essentially to system design for new engines.

The exhaust restriction will be further discussed in the aftertreatment analysis in Section 12.5. The coolers will be further discussed in Section 12.6. Turbochargers will be discussed in Section 12.7. Engine cylinder heat rejection and friction will be discussed in Section 12.6. Volumetric efficiency will be elaborated in Section 12.7. Emissions design targets will be explained in Section 12.4. Design constraints will be addressed in Section 12.9.

Using a PID feedback controller to automatically search and match the data is an important technique to accelerate the tuning process, for example by using constant torque PID control, target air–fuel ratio and EGR rate PID controls. Another challenge encountered in model tuning is to identify the root cause of simulation errors and minimize the errors, especially for multiple speed/load mode points. For example, an error in exhaust manifold temperature may be caused by several factors such as wrong air–fuel ratio, EGR rate, BSFC, injection timing or cylinder heat rejection. A DoE method can be used to speed up the process of error-finding and minimize the uncertainties. Theoretically, there is only one unique set of model tuning results which can match the true physical behavior of the engine on all performance parameters. The challenge is to approximate that unique solution with a minimum weighted simulation error and reasonable adjustment of model tuning parameters of each subsystem.

A guideline for steady-state engine performance model tuning is outlined below in order to illustrate the logic and contents of EPSI simulation.

1. Set up key input data of the model (valve size, valve lift profile, port flow coefficient, cylinder and pipe geometry, pipe heat transfer, turbo maps, etc.).
2. Check the quality of engine performance test data with the energy balance calculation and the turbocharger power balance calculation.
3. Tune volumetric efficiency by using either engine motoring or firing test data.
4. Calculate mechanical friction power by subtracting the calculated pumping loss power from the measured engine motoring power.
5. Tune intake restriction and exhaust restriction by matching simulation data to the test characteristic curve of ‘pressure drop vs. volume flow rate’.
6. Tune charge air cooler flow restriction and effectiveness by matching simulation data to the test curves of ‘charge air cooler pressure drop vs. volume flow rate’ and ‘effectiveness vs. air mass flow rate’.

7. Tune EGR cooler flow restriction and effectiveness by matching simulation data to the test curves of 'EGR cooler pressure drop vs. volume flow rate' and 'effectiveness vs. EGR mass flow rate'.
8. Calculate heat release rates at various speeds and loads by using engine cylinder pressure test data.
9. Set up the model properly to reflect the true heat rejection characteristics of the miscellaneous losses. Tune cylinder heat rejection by adjusting the Woschni heat transfer multiplier and cylinder/head heat transfer coefficients to match simulation data to the computed test data of base engine heat rejection characteristics. Or, equivalently from the basis of energy balance, tune the Woschni multiplier to match the exhaust manifold gas temperature.
10. Plot the engine test points on compressor and turbine maps; look up compressor and turbine efficiencies. Calculate turbo efficiencies with engine firing test data; determine efficiency multipliers.
11. At a given speed and load, use the DoE approach (or a simpler parametric sweeping method) to tune DoE factors (i.e., turbine effective area or VGT/wastegate opening, turbo efficiency multiplier, EGR valve opening, start-of-combustion timing, duration of heat release rate, etc.) to match simulation to engine test data of engine delta P, air–fuel ratio, EGR rate, brake power (or BSFC), exhaust manifold gas temperature, in-cylinder combustion pressure pattern, and other system performance parameters. Use optimization software to process the DoE simulation data to compute the factor values for minimized weighted errors in BSFC, exhaust manifold temperature or engine delta P at target air–fuel ratio and EGR rate.
12. Repeat step 11 at other engine speeds and loads. For transient engine simulation, the tuned engine control modeling parameters need to be smooth functions of the engine speed and load.

12.3 Engine–vehicle matching analysis for powertrain system design in engine firing and braking

Automotive engines are designed for real-world vehicle operating needs. Engine development is focused on improving the engine cycle process and torque shape, reducing parasitic losses and fuel consumption, etc. Drivetrain design is focused on increasing drivetrain efficiency, reducing resistance forces, and selecting proper transmission ratios to match the engine. A close collaboration will lead to optimum system integration for engine–vehicle matching of the diesel powertrain. Among the four major areas of vehicle dynamics (powertrain transmission, braking, suspension, and steering systems), the first two areas are directly related to engine system design.

12.3.1 The theory of vehicle performance analysis

Heavy-duty trucks usually are front-engined and rear-wheel-driven for reasons of engine cooling and good tractive effort for acceleration and upgrade climbing. In order for a vehicle to move, the tractive force provided by the engine and transmission needs to be greater than the total of all static resistance forces. But the maximum tractive force acting on the vehicle driving wheels actually is also limited by the tire–road adhesion force, even if the engine and transmission can produce a higher tractive force.

The vehicle force balance at any steady-state or transient condition can be written as:

$$F_t + F_r + F_{acc} + F_b + F_f + F_a + F_i + F_g + F_o = 0 \qquad 12.29$$

When the vehicle moves at a constant speed, the inertia force $F_i = 0$. If F_i is not equal to zero, the vehicle either accelerates or decelerates in transients. F_t is the tractive force acting on the vehicle wheels and is delivered from the engine firing operation. Note that the tractive force due to engine firing is defined as a positive value, and all resistance forces are defined as negative values. In engine firing, the engine brake retarding force $F_r = 0$. F_{acc} is a vehicle resistance force equivalently acting on the wheels caused by accessory loads such as the cooling fan, air-conditioning and power steering. If the driver does not use the service brake, the wheel brake (service brake) force $F_b = 0$. F_f is the tire–road rolling friction force. F_a the is aerodynamic resistance force. F_g is the gravity force on a grade. F_o is the resistance force of other drivetrain retarders such as hydrodynamic or electromagnetic retarders. At engine firing without wheel braking or drivetrain retarder braking, the tractive force acting on vehicle wheels is $F_t = -(F_{acc} + F_f + F_a + F_i + F_g)$. On the other hand, the maximum allowable tractive force is actually limited by the tire–road adhesion force, which is equal to the normal load multiplied by the road adhesion coefficient. The adhesion force is determined by the axle load, the road surface condition and the tires. For example, an icy road has very low adhesion force, and the vehicle wheels may slip on the ice. It should be noted that each term in the vehicle force balance equation 12.29 is for the entire vehicle mass m_V (including trailers, if any).

The gravity force is given by $F_g = m_V g \sin\theta$ and the road grade is defined as $G = \tan\theta$, where θ is the road slope angle (positive for downhill, negative for uphill) and g is the acceleration due to gravity. The rolling friction resistance is calculated from $F_f = -m_V g \mu_{fri} \cos\theta$ if the aerodynamic lift force is ignored in net normal load. The tire rolling friction coefficient μ_{fri} increases when vehicle speed, tractive force or tire tilting angle increases. The friction coefficient decreases when tire pressure or temperature increases. The tire rolling friction coefficient is also affected by tire structure, tire material and road surface condition. The friction coefficient is independent of vertical

load. Usually, the rolling friction coefficient is in the order of magnitude 0.005–0.01 on a concrete road. Moreover, for a radial-ply truck tire, when $N_V < 100$ km/hour, experimental data gave $\mu_{fri} = 0.006 + 0.23(0.001N_V)^2$, where N_V is vehicle speed; and for a bias-ply truck tire, $\mu_{fri} = 0.007 + 0.45(0.001N_V)^2$ (Wong, 1993).

The aerodynamic resistance force is calculated by $F_a = -0.5\rho C_D A_f N_r^2$ where ρ is the ambient air density, C_D is the aerodynamic resistance coefficient, A_f is the projected frontal area of the vehicle in the direction of travel, and N_r is the vehicle speed relative to the wind.

The transient inertia force is given by $F_i = -\xi m_V a$, where m_V is the total effective vehicle mass including payload, and a is the vehicle's linear acceleration. The ξ is the rotational mass coefficient which is defined as the ratio between the total vehicle inertia force and the linear inertia force. The total refers to the sum of the inertia force caused by linear motion of the vehicle mass and the equivalent inertia force caused by all rotating masses. The ξ can be derived as:

$$\xi = 1 + \frac{I_{drive}}{m_V r^2} + \frac{I_E C_{tr} i_g^2 i_0^2 \eta_t}{m_V r^2} + \frac{I_E C_{tr} i_g i_0^2 \eta_t N_V}{m_V r^2 a}\left(\frac{di_g}{dt}\right) \qquad 12.30$$

where r is the dynamic tire radius, I_{drive} is the total equivalent mass moment of inertia of all driveline components including vehicle wheels, I_E is the engine moment of inertia of engine rotating components connected to the driveline such as the flywheel, i_g is the transmission gear ratio, i_0 is the overall drive axle gear ratio, t is time, and η_t is drivetrain efficiency representing frictional power losses of the entire drivetrain (from engine crankshaft to vehicle wheels, including clutch or torque converter, transmission, universal joints, differential, drive axles, final drive gear, etc.). Note that vehicle accessory power is defined as a resistance power rather than a frictional power loss. The drivetrain efficiency of manual transmission can be around 95% at lower gears and 97–98% at the 1:1 direct transmission top gear. The efficiency of automatic transmission is roughly 10% lower. The overall drivetrain efficiency of heavy-duty trucks and buses usually peaks around 80–90%. The efficiency varies widely at different engine speeds, loads and gear numbers (Kluger and Greenbaum, 1993). C_{tr} is the torque ratio of the torque converter used with automatic transmission (for manual transmission without torque converter, C_{tr} can be set to 1). Torque converter efficiency is $\eta_c = C_{sr}C_{tr}$ where the speed ratio C_{sr} is defined as output speed divided by input speed, and the torque ratio C_{tr} is defined as output torque divided by input torque. When locked up without hydraulic coupling, the torque converter efficiency reaches its highest value. C_{sr} and C_{tr} are obtained from the characteristic chart of the torque converter when the input capacity factor C_{TV} is known ($C_{TV} = N/J^{0.5}$ where N is speed and J is torque). The torque

converter input capacity factor C_{TV} is equal to the engine capacity factor C_E, which is calculated by using $C_E = N_E/J_E^{0.5}$, where N_E is engine speed and J_E is engine torque. In the last term of equation 12.30, the transient gear ratio change di_g/d_t can produce significant resistance inertia force in continuously variable transmissions. The ξ can be approximated by an empirical formula $\xi = 1 + 0.04 + 0.0025 i_g^2 i_0^2$ (Wong, 1993). The ξ in equation 12.30 is a very important parameter which includes the engine moment of inertia. Based on 12.30, the transient powertrain equation 12.40 will be derived later.

The vehicle tractive force acting on the wheels F_t, tractive torque J_t and engine brake torque J_E are related by:

$$F_t = \frac{J_t}{r} = \frac{J_E C_{tr} i_g i_0 \eta_t}{r} \tag{12.31}$$

The engine firing brake torque at the crankshaft can be calculated by:

$$J_E = \frac{-(F_{acc} + F_f + F_a + F_i + F_g) r}{C_{tr} i_g i_0 \eta_t} \tag{12.32}$$

The engine speed can be calculated by:

$$N_E = \frac{N_V i_g i_0}{2\pi r C_{sr} (1 - s)} \tag{12.33}$$

where N_E is engine speed (revolutions per second), s is the slip of the vehicle running gear, s = 2–5% (Wong, 1993), and C_{sr} is the speed ratio of the torque converter used with automatic transmission (for manual transmission without torque converter, C_{sr} can be set to 1). Engine brake power can be calculated by $\dot{W}_E = J_E N_E$. Note that the term 'brake power' derives from the engine dynamometer which absorbs power by a type of brake (e.g., a friction brake). The engine 'brake power' refers to crankshaft net power which is input to the vehicle drivetrain in either firing or braking operation, and it is not the same as the engine 'braking power or retarding power' in engine brake operation. Figure 12.8 illustrates the vehicle tractive force characteristics with a seven-speed transmission.

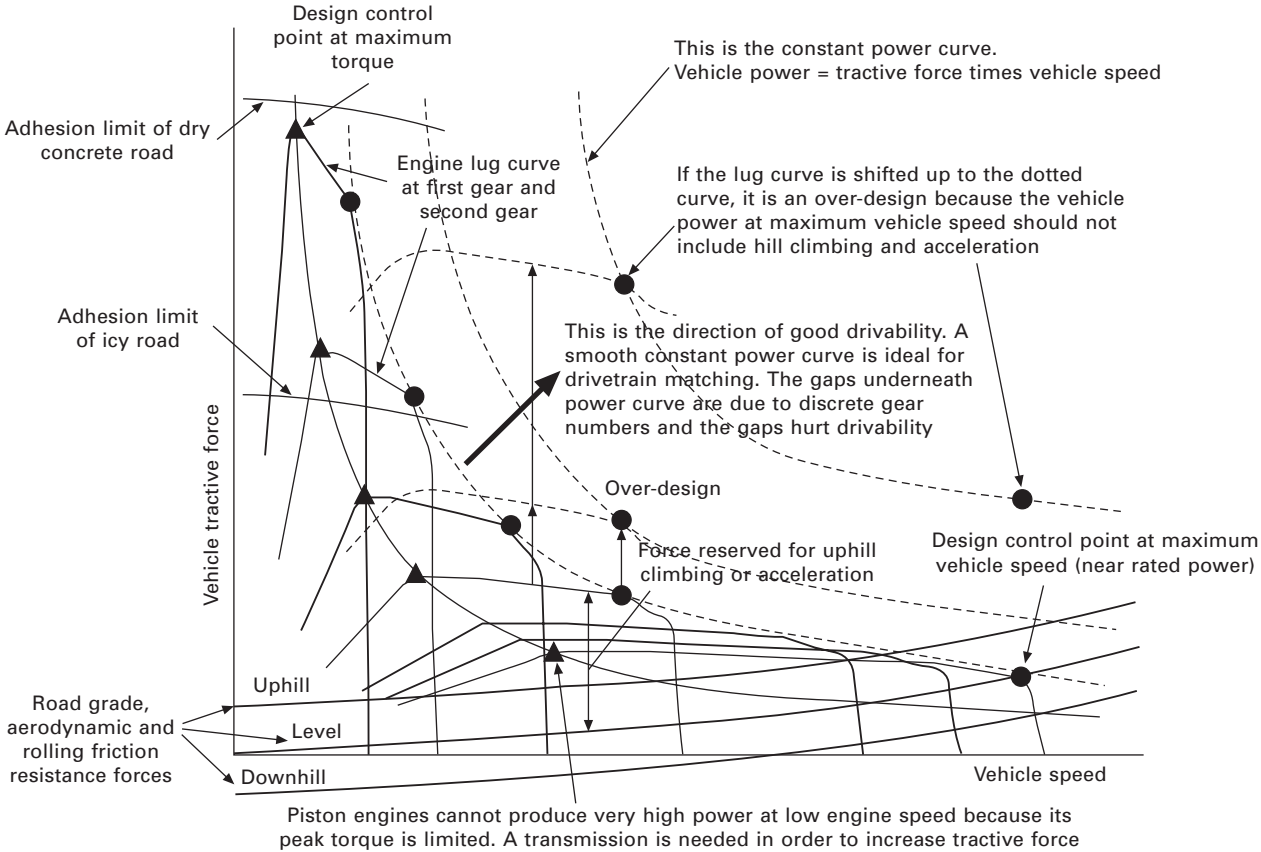
Denoting t as time, vehicle acceleration a is calculated by:

$$a = \frac{dN_V}{dt} = \frac{1}{\xi m_V} (F_{acc} + F_t + F_f + F_a + F_g) \tag{12.34}$$

Vehicle speed is calculated by:

$$N_V^{t2} = N_V^{t1} + \int_{t_1}^{t_2} a \cdot dt$$

Vehicle distance is given by:



12.8 Vehicle tractive force characteristics.

$$L_V^{t_2} = L_V^{t_1} + \int_{t_1}^{t_2} N_V \cdot dt$$

Vehicle acceleration time is calculated by:

$$\Delta t = \int_{t_1}^{t_2} dt = \int_{N_{V1}}^{N_{V2}} \left(\frac{1}{a}\right) dN_V$$

$$= \int_{N_{V1}}^{N_{V2}} \left[\frac{\xi \cdot m_V}{(F_{acc} + F_t + F_f + F_a + F_g)}\right] dN_V \qquad 12.35$$

where F_t is the transient vehicle tractive force resulting from available engine transient torque during acceleration in each gear. It should be noted that under the same fueling rate the transient engine torque is usually lower than the steady-state engine torque due to the losses in combustion, pumping loss, turbo lag and thermal inertia. In some cases transient power can be 5–8% lower than steady-state power. It is observed that the vehicle acceleration time from speed N_{V1} to N_{V2} is actually the area under the curve of the reciprocal of acceleration vs. vehicle speed, plus gear-shifting time (typically 0.2–0.6 s for each gear change). The area under the curve depends on where the transmission gear is shifted. Figure 12.9 shows the vehicle acceleration characteristics with the full load engine torque curve for a seven-speed transmission calculated by using equation 12.34.

Vehicle dynamics can also be expressed by a power balance $\dot{W}_t = -(\dot{W}_{acc} + \dot{W}_f + \dot{W}_a + \dot{W}_i + \dot{W}_g)$, where $\dot{W}_{acc} = \dot{W}_{E,acc}(2 - \eta_t)$ and $\dot{W}_t = \dot{W}_E \eta_t = F_t N_V$. The engine brake power can be calculated by:

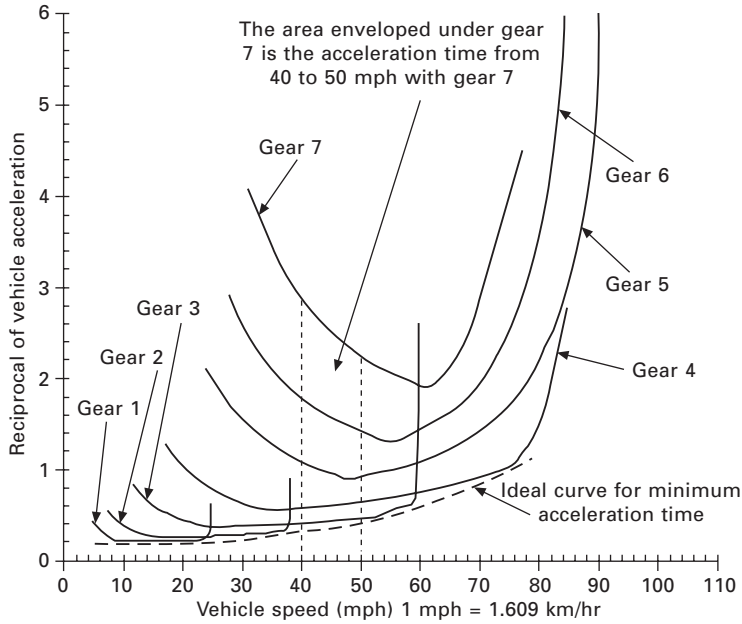
$$\dot{W}_E = \frac{-(F_{acc} + F_f + F_a + F_i + F_g) N_V}{\eta_t} \qquad 12.36$$

It is noted that the calculation of required engine power in 12.36 does not relate to drivetrain transmission ratio, unlike the torque calculation. The difference between engine brake power and vehicle accessory power is the net available power at the inlet of the clutch or torque converter to drive the vehicle to move. Figure 12.10 shows the calculated vehicle power requirements at different running conditions.

12.3.2 Engine–vehicle powertrain matching in engine firing operation

Overview on matching criteria

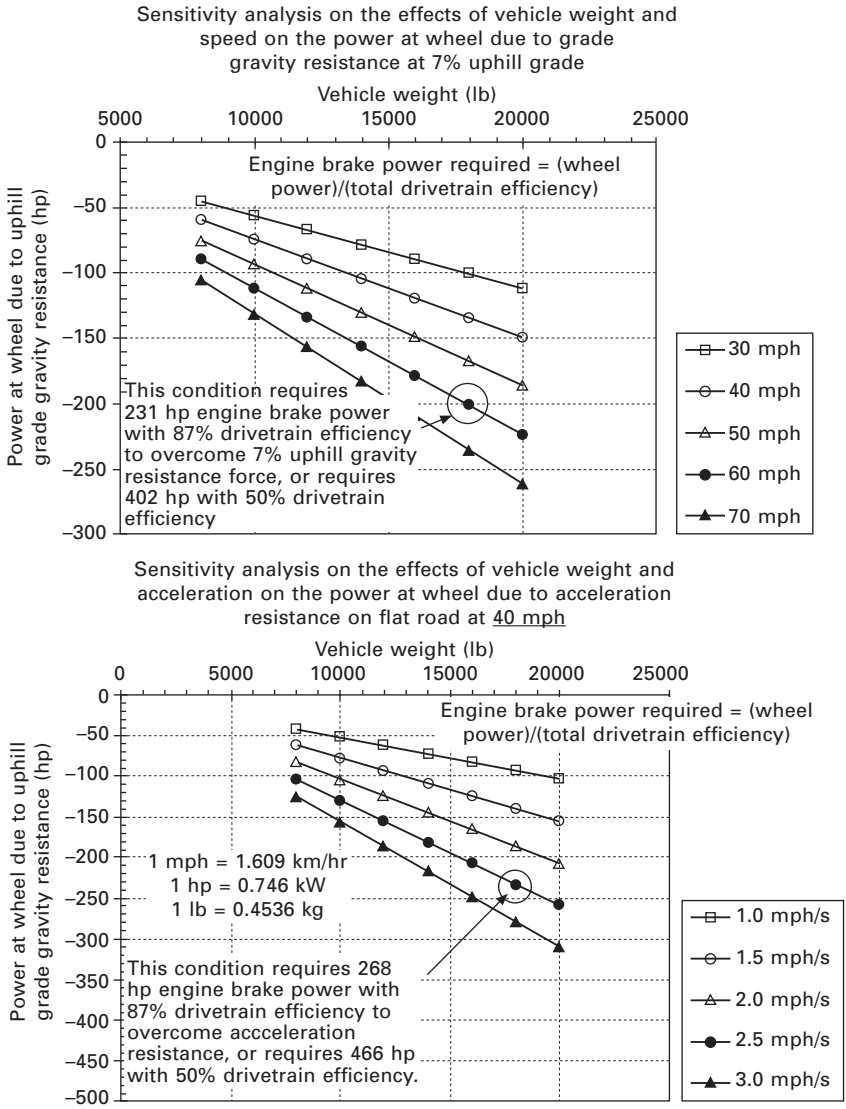
Drivability primarily refers to a wide range of global feeling of driving pleasure including acceleration, deceleration, gradeability, transition between



12.9 Vehicle acceleration characteristics.

engine operating modes and gear shifts, as well as powertrain NVH during the events of tip-in, tip-out, takeoff and gearshift, etc. Drivability evaluation is related to the entire vehicle dynamics engineering and controls, including engine, engine mount stiffness and damping, powertrain command and torque-demand coordination management, gearbox stiffness and inertia, clutch, drivetrain, wheel, tire, suspension, vehicle body, etc. However, in engine system design, the vehicle driving performance is usually narrowed to three aspects: (1) maximum vehicle speed on level ground; (2) acceleration time; and (3) maximum gradeability at combined vehicle weight rating at constant speed in first gear. The overall vehicle transient acceleration performance is usually characterized by the time of 0–60 mph during acceleration from the first gear to near the highest gear, or is characterized by the time spent to achieve 0–400 meters distance. Vehicle launch capability can be measured by the time of 5–35 mph. Vehicle overtaking capability is measured by the time of 35–60 mph or 60–80 mph during acceleration from a high gear. The maximum desirable gradeability is usually less than 8% uphill grade on highway for heavy duty commercial vehicles, and approximately 12–16% in mountains. The maximum gradeability is also related to the vehicle's startability.

Vehicle fuel economy is measured by miles per gallon of fuel (mpg) or liters of fuel per 100 km. Several methods exist to evaluate fuel economy:



12.10 Vehicle power requirements at different operating conditions.

1. A curve of the fuel amount consumed in liters per100 km during cruising at each constant speed vs. vehicle speed;
2. The fuel amount consumed in mpg or liters per 100 km for a specific driving cycle;
3. The weighted average fuel consumption, for example, US EPA's CAFE composite fuel economy indicator $mpg_{composite} = 1/(0.55/E_{urban} + 0.45/E_{highway})$, where E_{urban} is the fuel economy of the city (urban) driving

cycle (mpg), and $E_{highway}$ is the fuel economy of the highway (suburban) driving cycle (mpg).

4. Fuel economy during full-pedal acceleration.

The total fuel mass consumed during a driving cycle can be calculated by:

$$m_{fuel} = \int_{t_1}^{t_2} M_{fuel}\, dt = \int_{t_1}^{t_2} (E_{BSFC} \dot{W}_E) dt \qquad 12.37$$

where M_{fuel} is fuel flow rate and E_{BSFC} is engine BSFC. If treated as a quasi-steady-state approximation, the BSFC at any non-idle condition (i.e., engine brake power greater than zero) can be determined at each engine speed–load point of the driving cycle from the engine BSFC map. The real transient BSFC must be computed by a high-fidelity cycle simulation model that reflects transient combustion efficiency and heat losses, as well as the transient pumping loss during turbo lag which is related to engine controls. A similar approach can be used to compute total emissions over the driving cycle if engine emission maps are available. Engine brake power can be computed by vehicle powertrain transient simulation considering the acceleration inertia effect (12.30). It should be noted that during vehicle deceleration the fuel rate M_{fuel} is either the idle fueling or zero (especially during engine braking), depending on vehicle fueling calibration and whether using the engine brake. If the vehicle cruises at constant speed N_V to travel a distance L_V, the fuel mass consumed can be simplified as:

$$m_{fuel} = E_{BSFC} \dot{W}_E (L_V / N_V) \qquad 12.38$$

Drivability and drivetrain design parameters

The limits of vehicle application determine the design limits of the drivetrain. The vehicle tractive power requirements $(\dot{W}_t = F_t N_V)$ are best explained in Fig. 12.8. The entire domain is formed by a family of constant-power curves. The ideal characteristic is a constant power over the full vehicle speed range because it provides the vehicle with high tractive force at low speed where the demands for grade climbing and acceleration are high. To achieve superior vehicle performance, fuel economy and emissions, the drivetrain parameters must be optimized together with the engine torque curve.

Final drive gears are used in driving axles and transaxles to transmit torque from the gearbox output shaft to the driven wheels through a constant gear reduction in order to keep the wheel size practical. The final drive ratio (also called the drive axle ratio) is given by the ratio between the number of teeth on the crown wheel of the bevel drive and the number of teeth on the bevel pinion. The drive axle ratio is determined based on the best trade-off

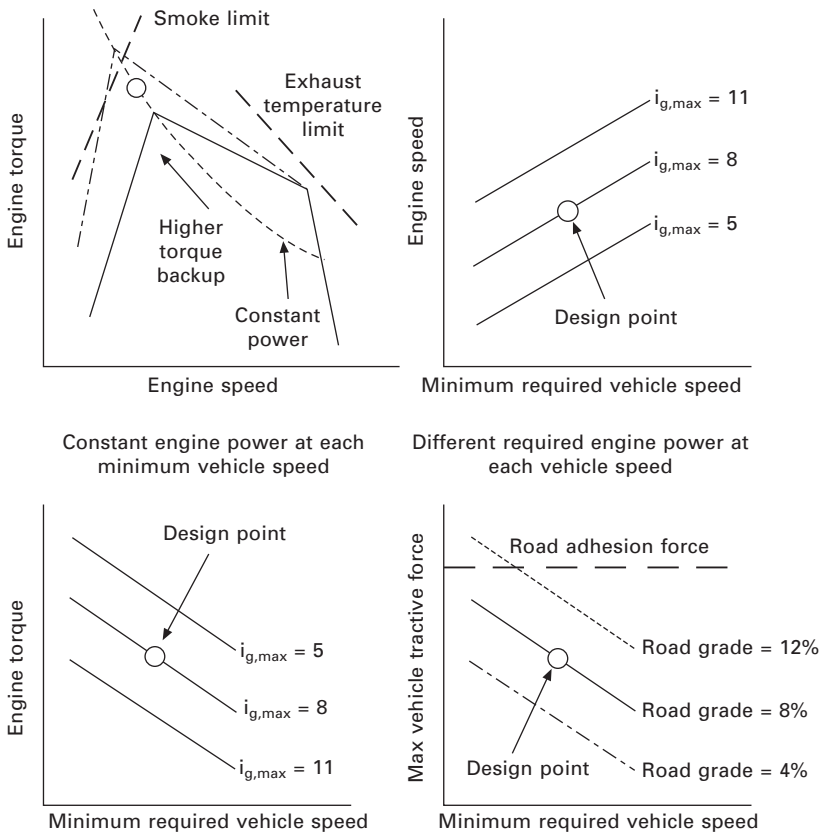
between acceleration time and vehicle fuel economy. The minimum drivetrain transfer ratio $(i_g i_0)_{min}$ at the highest (top) transmission gear and engine torque J_E should be designed together to ensure the combined term $J_E i_g i_0 \eta_t$ can overcome the minimum resistance forces (usually only rolling friction and aerodynamic resistance on level ground) at the maximum vehicle design speed. It is mainly determined by changing drive axle ratio. From a power perspective, once the maximum vehicle speed target is specified, the required engine power can be calculated by 12.36. The selection of the minimum drivetrain ratio is based on an optimum trade-off between engine speed and torque at a fixed power $(\dot{W}_E = J_E N_E)$. The choice of engine speed depends on engine design factors such as mechanical friction and diesel combustion quality at high speed. The maximum vehicle speed target should be high enough to ensure the vehicle can have certain power in reserve to climb an upgrade or accelerate at a lower normal driving speed in the highest gear. Another important analysis in the selection of the rear axle ratio is to conduct a sensitivity calculation to analyze its effect on vehicle fuel economy and acceleration ability, then choose the best trade-off from the 'C shape' curve (Chana *et al*., 1977; Wong and Clemens, 1979).

The engine speed at the maximum vehicle speed depends on the matching strategy. The traditional strategy is to design it at the right side of the engine rated speed (where the maximum power occurs) to favor power reserve and sacrifice fuel consumption. Alternatively it can be designed at the left side of the engine rated speed to reduce fuel consumption but sacrifice power reserve; or it can be designed just at rated speed. Engine rated power is determined from the above drivetrain-matching considerations. The diesel engine maximum speed is determined by three factors: (1) mechanical limitations such as valvetrain no-follow speed and high reciprocating inertia forces of the heavy components; (2) the rapidly increasing friction at high speeds; and (3) the time required to complete the combustion process of the diesel fuel. High-speed governors are used to rapidly reduce fueling to steeply reduce brake torque from a speed slightly above rated speed to high-idle speed.

The maximum drivetrain transfer ratio $(i_g i_0)_{max}$ and engine torque J_E should be selected together to ensure the combined term $J_E i_g i_0 \eta_t$ can overcome the maximum resistance forces (including uphill climbing or acceleration) at a minimum required vehicle speed. It needs to be achieved by combining the final drive ratio and the maximum transmission gear ratio. Again, from a power perspective, once the minimum required vehicle speed target is specified, the required engine power can be calculated by 12.36. The $(i_g i_0)_{max}$ can be calculated by 12.33. The selection of the maximum drivetrain ratio should be based on an optimum trade-off between engine speed and peak torque at a fixed power requirement. The choice of engine peak torque speed depends on the desirable speed range between peak torque and rated power for torque backup and acceleration, and also depends on the engine's

ability to breathe sufficient air to produce a high peak torque. Usually, it is desirable to have a low peak-torque speed and a high torque level for better drivability and faster acceleration (related to the area under the curve of $1/a$ vs. vehicle speed shown in Fig. 12.9). Moreover, the engine peak torque should not exceed the durability limit of the drivetrain. Also note that the maximum tractive force should not exceed the tire–road adhesion force in order to avoid tire spinning or slippage. (The traction control system provides flexible firing or braking torque to prevent the tire from spinning during acceleration or on a slippery road.) A design approach to determine the minimum required vehicle speed, maximum transmission gear ratio, engine speed and torque is illustrated in Fig. 12.11. A proper maximum drivetrain ratio is also required to start the vehicle on a level road or grade to ensure sufficient startability.

Diesel engines are characterized by high torque due to turbocharging. During fast transient acceleration the steady-state full-load curve cannot

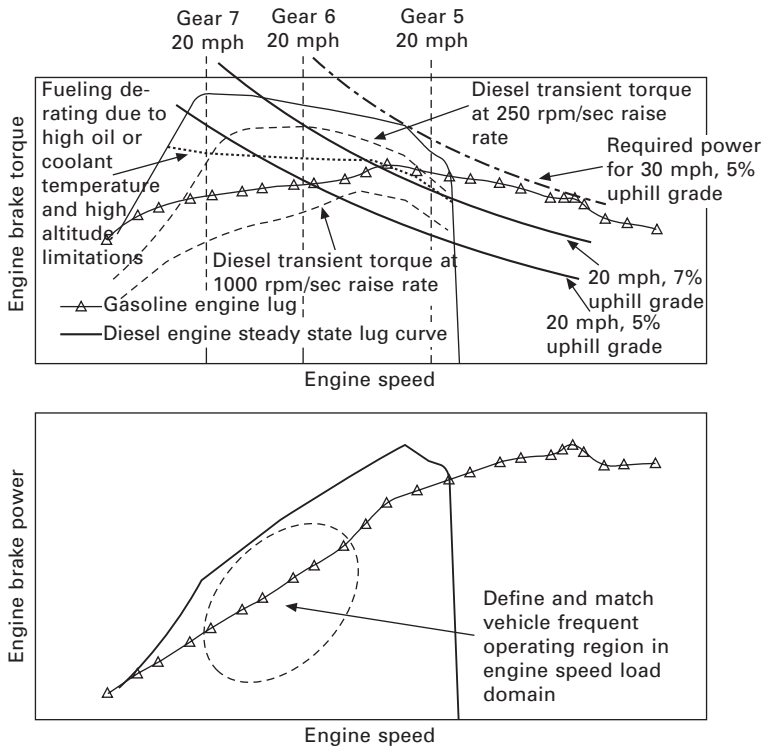


12.11 Integrated design of maximum drivetrain transfer ratio for engine peak torque.

be achieved because of turbo lag and air–fuel ratio smoke limit. Vehicle acceleration is limited by engine transient torque characteristic curves (Fig. 12.12). Figure 12.12 also shows the vehicle driving characteristic curves and engine de-rating curve. It is worth noting that the design decision on the shape of the modern engine torque curve is also affected by how easy or difficult it is to meet heavy-duty emissions certification regulations, the speed setting for declared rated speed and governed speed, the FTP emissions cycle data distribution within the speed range, and fuel economy considerations.

In the earlier discussions, torque curve shape and torque backup were mentioned. The advantages of a large torque backup coefficient, which is defined as the ratio between peak torque and the torque at rated power, are summarized in the following:

1. A high torque backup makes the tractive force vs. vehicle speed curve closer to the ideal constant power curve. It allows the vehicle to accelerate or climb steeply uphill from low speed and high torque, and may reduce the number of gears and gear changes required during driving. High torque backup allows the engine to stably respond to a load increase when running along the full-load curve (e.g., climbing a hill). The higher



12.12 Diesel full-load lug curve and transient torque.

the torque backup, the less rapidly the engine speed will decrease when going uphill. On the contrary, if the engine runs along the lug curve below the peak torque speed where engine torque decreases with falling speed, a sudden load increase will stall the engine. A lower peak torque speed is desirable because the gear-changing speed needs to be higher than the peak torque speed in order to prevent the engine from stalling. When operating in the low engine speed, high brake torque region, a large torque backup lug curve requires no or less gear down-shifting (changing down) when climbing hills or accelerating. This provides driving convenience.

2. A high torque backup reduces vehicle acceleration time as shown by the smaller area under the curve of $1/a$ vs. vehicle speed in Fig. 12.9. This results in a higher overall vehicle speed and associated better fuel economy in driving cycles because of the higher acceleration and faster attainment of the higher speed.
3. As a result of less down-shifting to low gears, there is less chance to operate in the region of high engine speed, low brake torque and high BSFC. This results in better fuel economy.
4. A high coefficient of speed reserve, which is defined as the ratio between rated power speed and peak torque speed, can increase gradeability and defer the required gear downshift. The coefficient of adaptability (defined as torque backup coefficient multiplied by coefficient of speed reserve) and gear ratios determine how often the driver must shift gears.

A variation of drivetrain transfer ratio between the minimum and maximum enables the vehicle to be driven properly at various conditions of load, speed, road surface, etc. The ratio change can be a discrete change in several gear ratios such as in a traditional transmission, or it can be a continuously variable ratio change. The number of transmission gears depends on the ratio span between $(i_g i_0)_{max}$ and $(i_g i_0)_{min}$, and directly affects the vehicle's acceleration performance and fuel economy. A larger number of gears increases the possibility of running the vehicle near maximum power and enhances the acceleration and climbing ability. With an extreme of using a continuously variable transmission, it also increases the possibility of running the vehicle in the low fuel consumption region of the engine speed–load map (i.e., the high load and low speed region) when vehicle power requirements change during driving. The gear ratios are designed based on the usage frequency of each gear and also based on a rule that the engine is operated within a similar speed range in each gear. The ratios, usually less than 1.7–1.8, basically follow a pattern similar to a geometric progression as below:

$$\frac{i_{g1}}{i_{g2}} \geq \frac{i_{g2}}{i_{g3}} \geq \cdots \geq \frac{i_{g(n-1)}}{i_{gn}} \tag{12.39}$$

Properly selecting the transmission gear number and ratios can make the curves of vehicle tractive force close to the ideal constant power shape, hence maximize vehicle acceleration capability. A detailed introduction to drivetrain mechanical structure was provided by Nunney (1998).

Powertrain matching and vehicle fuel economy

The goal of system integration analysis is to provide sensitivity analysis to seek the optimum combination of engine and drivetrain. The optimum is usually the best trade-off between vehicle fuel economy and acceleration time. The design options to improve vehicle fuel economy include the following.

1. Design proper engine displacement and higher BMEP level or load factor for driving cycles, possibly by downsizing the engine. High BMEP operation provides higher thermal efficiency and a lower proportion of mechanical friction. But the requirements for vehicle launch or off-idle responsiveness (basically starting with naturally aspirated) and engine rated power may set limitations on displacement reduction.
2. Reduce engine BSFC and extend the low BSFC region as much as possible in the engine speed–load map. The desirable shape of constant low-BSFC contours associated with engine design features can be determined by matching the frequent vehicle driving cycles depicted on such an engine map.
3. Increase torque backup and coefficient of speed reserve to improve the shape of the engine lug curve.
4. Reduce engine and vehicle weight, aerodynamic resistance, tire rolling friction and accessory power loss. The aerodynamic resistance force is proportional to the square of the vehicle speed. Excessively reducing the rolling friction coefficient in tire design may result in losses in road adhesion and driving smoothness, especially on wet roads. A detailed discussion on fuel consumption and design trade-offs was provided by Steinberg and Goblau (2004).
5. Improve drivetrain efficiency (e.g., torque converter lockup to prevent slip and efficiency loss in automatic transmissions); increase the number of transmission gears to make the engine operate in the low BSFC region more often; identify the frequent operating region of vehicle speed and resistance power, then map the region to the engine speed–load domain to match closely the low BSFC area by adjusting the rear axle ratio, transmission gear ratio and shift schedule.
6. As shown in equation 12.37, the fuel rate consumed depends on the BSFC, engine power and vehicle speed. At low vehicle speed, although the power consumed is low, the BSFC is high. At high vehicle speed, high engine power is needed to overcome fast increasing aerodynamic

resistance, but BSFC is low because of the high BMEP level. In fact, the lowest fuel consumption happens at medium vehicle speed.

7. Steady-state cruising at constant vehicle speed or engine power consumption using a higher gear (with an extreme of using the overdrive gear which has an even smaller gear ratio than the top gear) gives lower engine speed, higher engine torque, higher load factor and lower BSFC, but the torque reserve or power reserve for uphill climbing and acceleration becomes less.

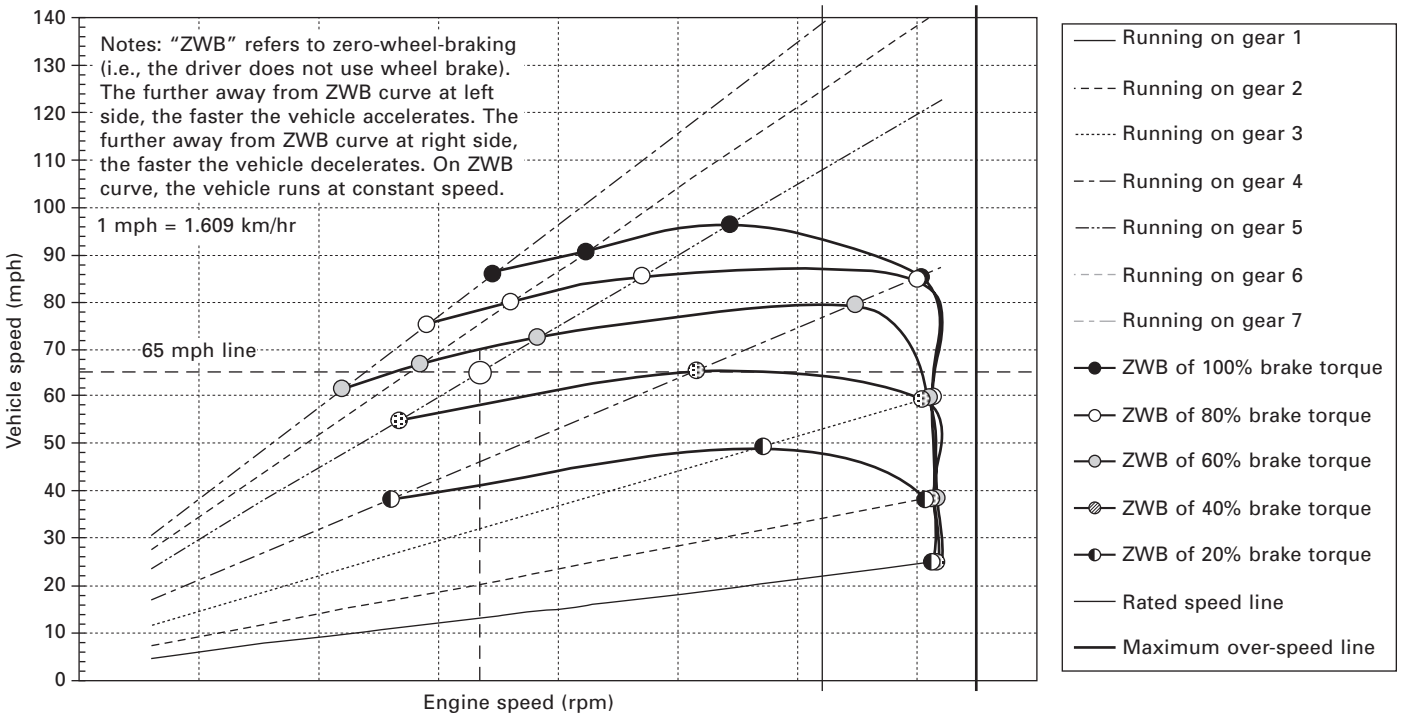
Analytical engine–drivetrain matching with characteristic maps

In analytical engine–vehicle matching, the vehicle characteristics (such as vehicle speed contours, gear lines and typical vehicle acceleration contours) are mapped on engine characteristic maps (such as for the contours of firing power, BSFC, NO_x, soot, air–fuel ratio, EGR rate and transient torque smoke limit). The matching quality and parametric sensitivity can be viewed conveniently, and the best trade-offs between drivability and fuel economy can be selected more easily. The analytical formulas presented earlier are used to construct the vehicle characteristic curves graphically. The scope of the analytical matching approach includes the following:

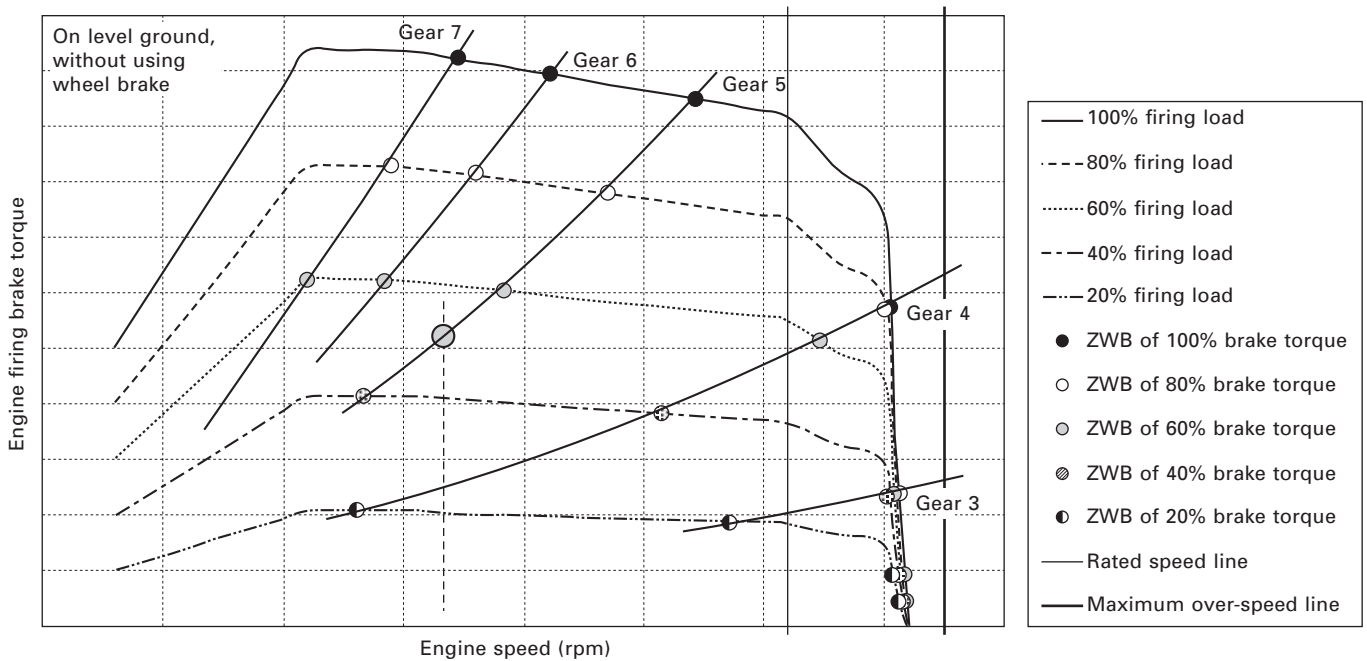
- Conduct a vehicle force balance to predict the engine power required and the load factor for various vehicle operations in order to better design the engine and its air system for real-world driving scenarios.
- Select the drive axle ratio, transmission gear number, gear ratios, and design transmission shift schedule based on the best trade-offs.
- Simulate transient driving cycles and calculate cycle composite fuel economy and emissions.

An analytical matching approach is proposed in Fig. 12.13 to map the vehicle operating point to the engine speed-load domain. A concept of 'ZWB' (zero-wheel-braking) is introduced in the approach. The 'ZWB' points on each gear are calculated by using the vehicle force balance for a given vehicle weight, drivetrain ratio and road condition in both the engine speed–vehicle speed domain and the engine speed–torque domain. The 'ZWB' anchor points are connected to form characteristic curves such as the gear lines in the engine speed–load domain. Then, at a given vehicle speed, the vehicle operating point can be visually selected at a preferred gear, and the corresponding engine speed can be graphically determined. The selected engine speed is used in the speed–load domain to intersect with the selected gear line, so that the intersection point is the mapped condition of the running vehicle on the engine map. It should be noted that when the drivetrain condition changes, the 'ZWB' points also change.

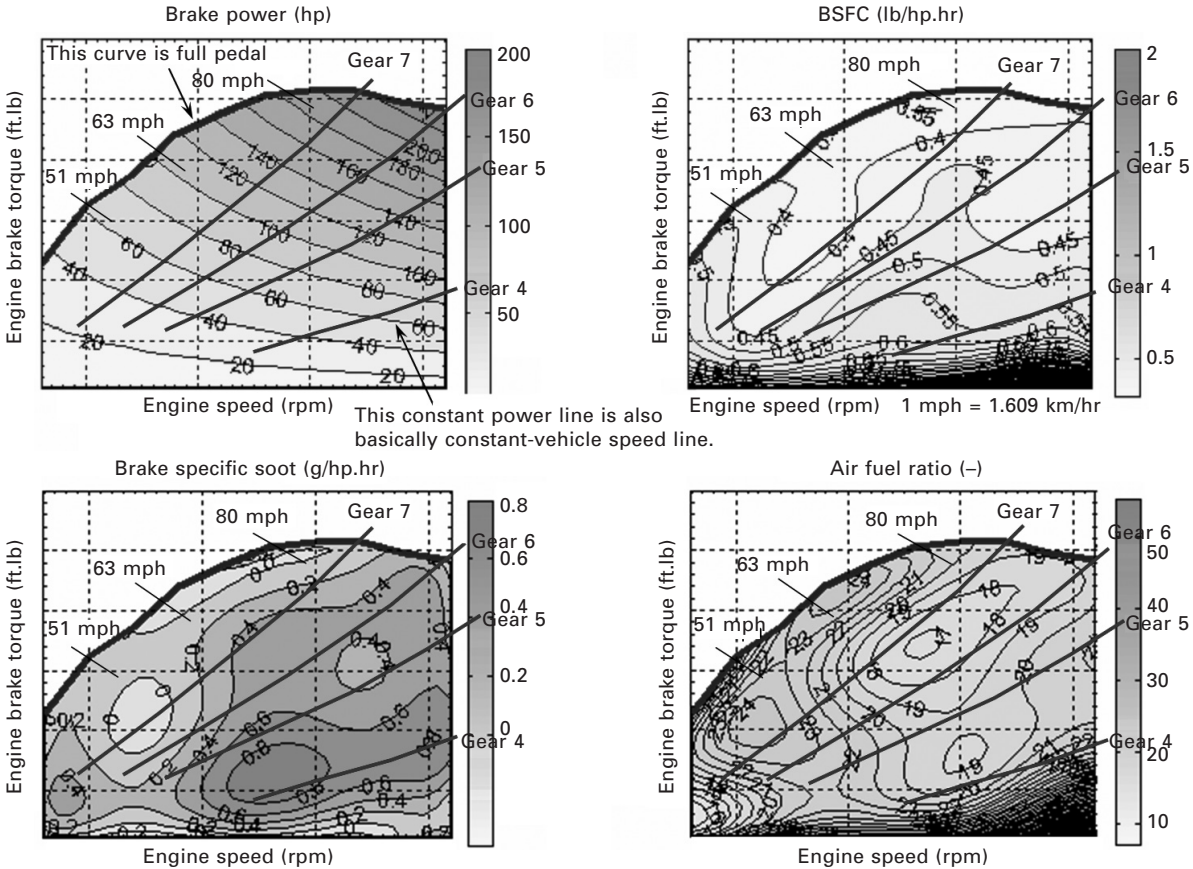
A more powerful matching approach is shown in Fig. 12.14 (in the low



12.13 Illustration of engine–vehicle matching method with the 'ZWB' concept.



12.13 Continued



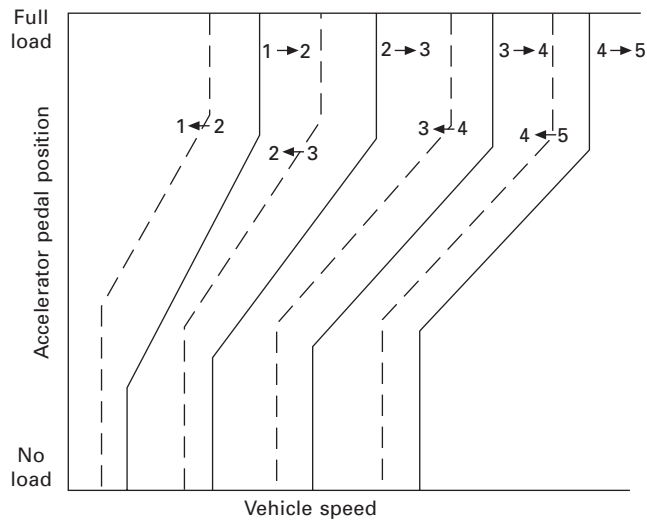
12.14 Engine–vehicle matching method with performance characteristic maps.

to medium speed range as an example) where the vehicle speed curves and gear lines for a selected drivetrain or road condition are computed and superpositioned on various engine characteristic maps. The driving points can be conveniently selected on the engine maps by considering all the features, such as BSFC, air–fuel ratio smoke limit, power reserve for acceleration, emissions, etc. Moreover, it is noted that the engine map domain essentially may be viewed as a 'distorted coordinate' domain of the transmission shift map (i.e., accelerator pedal position vs. vehicle speed in Fig. 12.15, compared to Fig. 12.14). Once the transmission shift schedules are visually located on the engine maps based on all trade-offs, the transmission shift map can be directly 'computed' with mathematical coordinate transformation conveniently. Such an analytical method of engine–transmission matching entirely changes the traditional 'trail-and-error' way of generating the transmission shift map.

With this advanced analytical technique of engine–vehicle matching, drivetrain design parameters and engine–transmission matching can be evaluated as a part of engine system design before the combustion development and calibration happen. The calculated vehicle operating characteristics are mapped on engine maps in order to provide guidance from vehicle driving requirements to engine design and testing.

Transient powertrain performance simulation

Transient powertrain simulation is important for both understanding engine transient behavior and obtaining cycle-composite fuel economy and emissions



12.15 Illustration of transmission shift schedule map.

data during any vehicle driving cycle or engine speed–load certification test cycles. Taking the time derivative of equation 12.33, engine acceleration (i.e., dN_E/dt) can be obtained as a function of vehicle acceleration (i.e., dN_V/dt) and a time derivative of the transient gear ratio (i.e., di_g/dt). In the derivation below, the transient gear ratio effect is neglected for simplicity. By substituting equations 12.30 and 12.34 and the time derivative of 12.33 into 12.29, equation 12.40 is derived as an ordinary differential equation to solve for the transient engine speed N_E when a transient engine tractive torque J_E is produced (see equation 12.31 on how to relate engine brake torque to vehicle tractive torque).

$$I_E \frac{dN_E}{dt} = \frac{r\left(F_t + F_r + F_{acc} + F_b + F_f + F_a + F_g + F_o - m_V a - \frac{I_{drive}}{r^2} a\right)}{2\pi i_g i_0 \eta_t \eta_c (1 - s)} \qquad 12.40$$

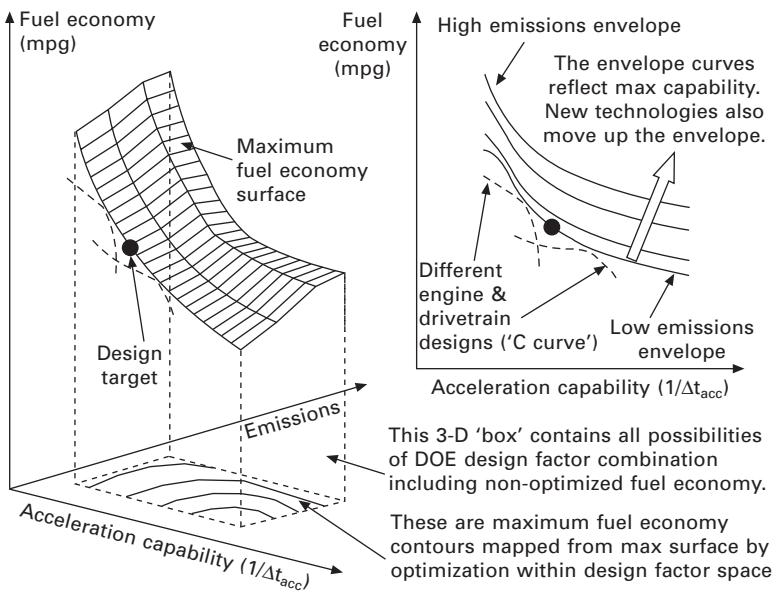
All the terms in 12.40 are in the transient sense and can be modeled in further detail. The tractive force F_t is produced by engine torque. Transient engine torque can be modeled in one of the following ways: empirical formula, model-based formula, mapped engine model, mean-value cylinder model, or high-fidelity crank-angle-resolution detailed cycle simulation model (containing smoke limiter, turbocharger lag effect and transient engine control strategies). Diesel engine transient torque characteristics are shown in Fig. 12.12. The available transient torque level strongly depends on how fast the transient event is.

In vehicle full-pedal acceleration simulation, step-fueling and transmission shift schedule can be imposed as input, and transient engine speed and vehicle speed can be computed as a function of time. In vehicle driving cycle simulation, a vehicle speed schedule as a function of time is imposed as input, and transient engine torque (or retarding torque or vehicle braking torque) and engine speed are computed to try to meet the speed and load requirements implied by the imposed vehicle speed and gear-shifting schedule, unless the imposed vehicle speed transient is not realistic. Once the engine's state (i.e., speed and load) is obtained, fuel consumption and emissions can be calculated either by a high-fidelity cycle simulation model or by looking up the engine BSFC map and emissions maps (used as input, if a mapped engine model is adopted).

Optimization of engine–vehicle powertrain performance

In powertrain concept selection, with a given engine–vehicle–road configuration, the above-mentioned steady-state and transient analyses can be automated by computer simulation or programming, and the final analysis

can be summarized as one data point within a three-dimensional domain of 'fuel economy (e.g. mpg)' vs. 'vehicle acceleration capability (e.g. the reciprocal of 0–60 mph acceleration time)' and 'engine emissions (NO_x, PM, HC or their weighted average)', as illustrated in Fig. 12.16. Different configurations can be repeated in a DoE analysis, including various drive axle ratios, transmission gear ratios, gear number, torque converter, engine rated power and speed, engine displacement, emission control technologies, or any other system-level parameters. Finally, all the summary data points (one from each configuration) are processed with DoE emulator optimization techniques (i.e., building mathematical equations to link the input data to the output summary data: see Section 12.4 for details on DoE). Fuel economy can be compared on a fair basis at fixed acceleration capability and emissions. The calculated trade-off envelope curves are identified as the maximum limit of the system capability. The minimum fuel economy constant-contours and its parametric dependency can be computed. Such an optimization design approach may greatly enhance the quality of powertrain concept selection and cascade the best concept to the lower level of hierarchy of design with a truly 'top-down' system approach.



12.16 Method of powertrain performance optimization.

12.3.3 Engine–vehicle powertrain matching in the engine braking operation

Vehicle braking performance with the engine brake

A lumped model of vehicle longitudinal dynamics during engine braking (no fuel) is provided as below:

$$J_{E,r} + \frac{r}{C_{tr} i_g i_0} (F_{acc} + F_b + F_f + F_a + F_g - \xi m_V a + F_d + F_o) = 0 \quad 12.41$$

where F_b is the service brake force applied on the vehicle wheels, F_d is the drivetrain friction force which can be calculated by using the drivetrain efficiency, and $J_{E,r}$ is the engine retarding torque acting on the crankshaft (including the engine motoring torque).

As in the vehicle tractive situation (engine firing), the maximum vehicle retarding (braking) force that the tire–ground contact can support is determined by the tire–road adhesion force. Above the adhesion limit, the tire will slide or lock up. Locking up rear tires or semitrailer tires in a trailer–semitrailer makes the vehicle completely lose directional stability in yaw motion, and creates the dangerous tractor 'jackknifing' and semitrailer swing, or makes a two-axle vehicle rotate by 180°. The lockup of front tires causes a loss of steering directional control but not yawing instability. Optimum braking force distribution between the front and rear tires ensures the maximum braking forces on the front and rear axles to be developed simultaneously to achieve the maximum deceleration rate and the minimum stopping distance. But the optimum braking force distribution varies with vehicle load, vehicle design and road surface condition. With non-optimum distribution, one of the axles will lock first. To prevent locking, less braking force must be applied, and results in reduced deceleration capability. Braking force distribution also affects brake lining temperatures.

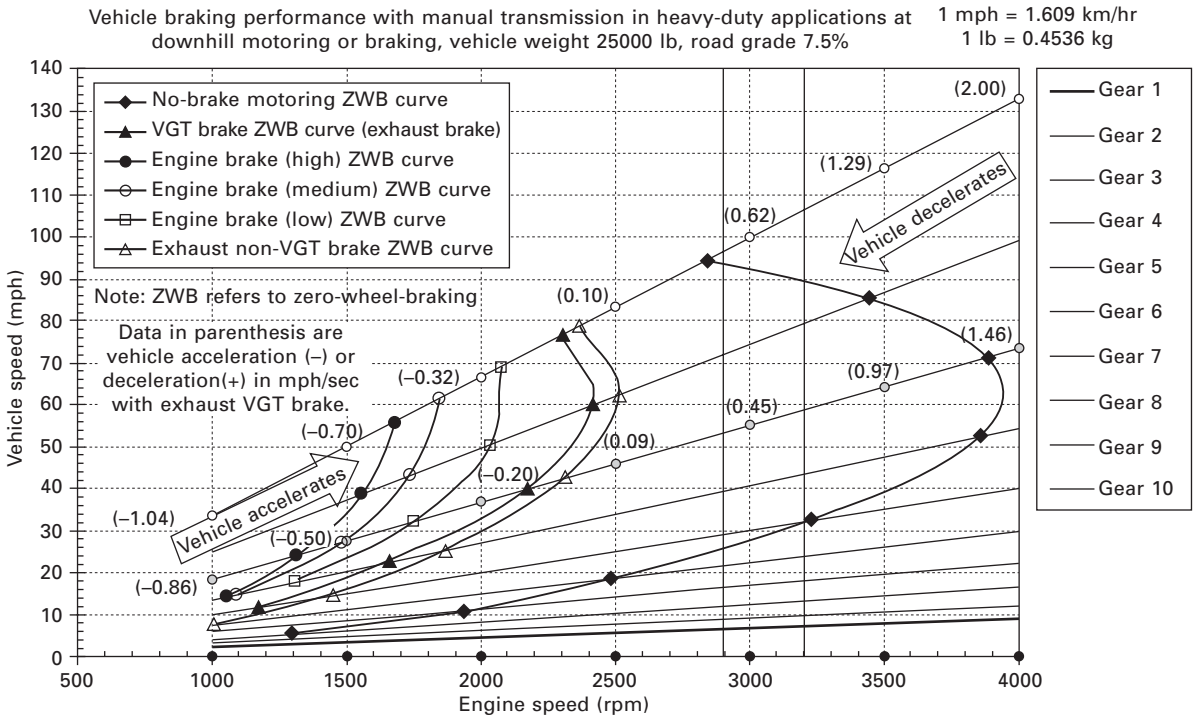
Heavy-duty trucks are usually equipped with engine brakes or other drivetrain retarders in order to enhance vehicle retarding capability and prevent wheel brake pads from overheating during overuse, especially on a long downhill grade. The engine brake retarding force is an important part of the total vehicle braking force. The target of maximum engine retarding power should be carefully determined by checking the tire–road adhesion limit for each wheel of the given vehicle configuration (front-wheel-driven, rear-wheel-driven or four-wheel-driven) and by checking the braking force distribution between the axles under various braking conditions (i.e., different deceleration rate, vehicle weight, road surface, tire lock-up sequence, etc.). The retarding power target should not be over-designed. The force balance analysis of different vehicle configurations was given by Wong (1993). An antilock brake system (ABS) provides flexible adjustment of the braking force to optimize vehicle braking performance. Engine brakes may be disabled by the ABS if wheel slippage is detected.

In order to determine an appropriate design target of engine brake retarding power, its effect on vehicle braking performance can be analyzed with the method proposed in Fig. 12.17. The engine brake 'high, medium, low' in the figure refers to three different design targets for the retarding power of a compression-release engine brake. The VGT exhaust brake refers to an exhaust brake actuated by closing a variable geometry turbine vane opening. The exhaust non-VGT brake refers to a conventional exhaust brake actuated by using an exhaust back-pressure valve installed at the turbine outlet. The 'ZWB' concept again refers to 'zero-wheel-braking', which means that the driver does not need to use the service brake (wheel brake). The ZWB anchor points are calculated by using the retarding power of different engine brakes with the vehicle torque balance equation 12.41. The ZWB curves are characteristic curves on which the vehicle keeps moving at constant speed without the need for using the wheel brake, i.e., an ideal situation without over-engine-braking or under-engine-braking. At different vehicle weights, road grades or tire–road rolling friction coefficients, the ZWB curves will become different. Along each gear line, on the right side of the ZWB point, the vehicle decelerates. On the left side of the ZWB point, the vehicle accelerates. Such an analytical approach can intuitively analyze the vehicle braking power needs and determine an appropriate design target for the engine brake retarding power (for example, for achieving 'ZWB' under certain conditions). The analysis is also useful in determining a wise design target for the valvetrain separation speed (i.e., over-speed limit) based on analyzed real-world no-fuel motoring braking scenarios.

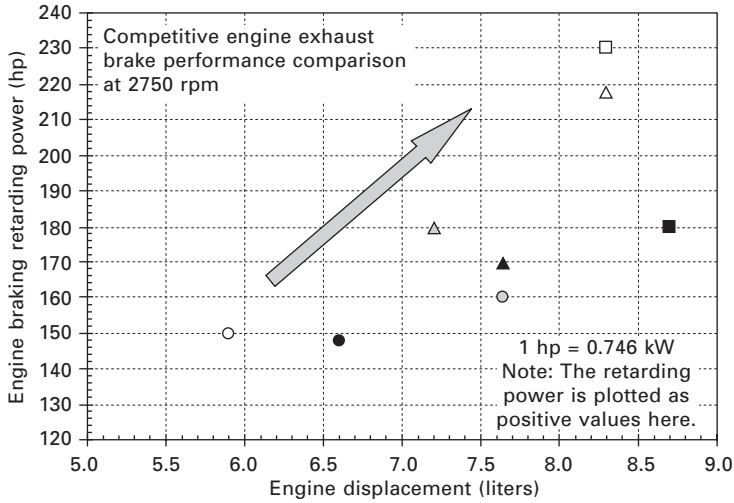
Engine brake performance and design method for enhancing retarding power

There are generally two types of engine brakes: compression-release brakes (e.g., Jake brake, bleeder brake), and exhaust brakes (e.g., conventional exhaust brake using a flap valve installed at the turbine outlet, VGT exhaust brake modulating variable geometry turbine area). Engine retarding power consists of the contributions from mechanical friction power, engine accessory power, the pumping loss power in intake stroke and exhaust stroke, and the indicated power in compression stroke and expansion stroke. Figure 12.18 shows there is a large variation in engine retarding power at a fixed engine displacement due to the variation in brake type and design details.

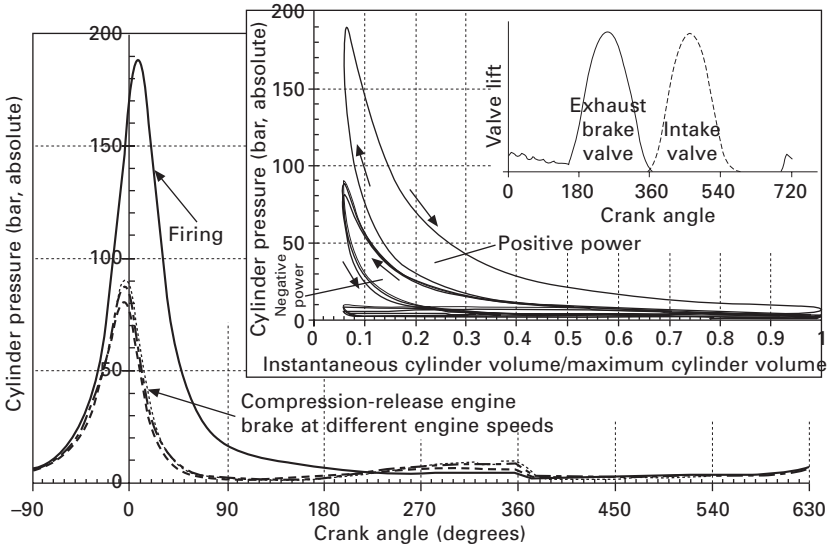
In compression-release brakes, engine indicated power and retarding power can be adjusted by the opening timing and lift profile of an exhaust brake valve, as shown in the simulation curves in Fig. 12.19. Compression-release brakes usually offer higher retarding power than exhaust brakes due to a more effective retarding mechanism in the in-cylinder process. A variable geometry turbine can be used with compression-release brakes to further



12.17 Effect of engine brake retarding power on vehicle braking performance.



12.18 Competitive benchmarking analysis on engine brake retarding power.



12.19 Principle of the compression-release engine brake.

increase retarding power by closing the turbine effective area. When the turbine area is reduced, pumping loss increases, and the compression-release mechanism may also be enhanced with a higher air flow rate. It should be noted that a fixed geometry turbine or wastegate turbine selected for good firing operation is inferior to a VGT in retarding power capability. Therefore,

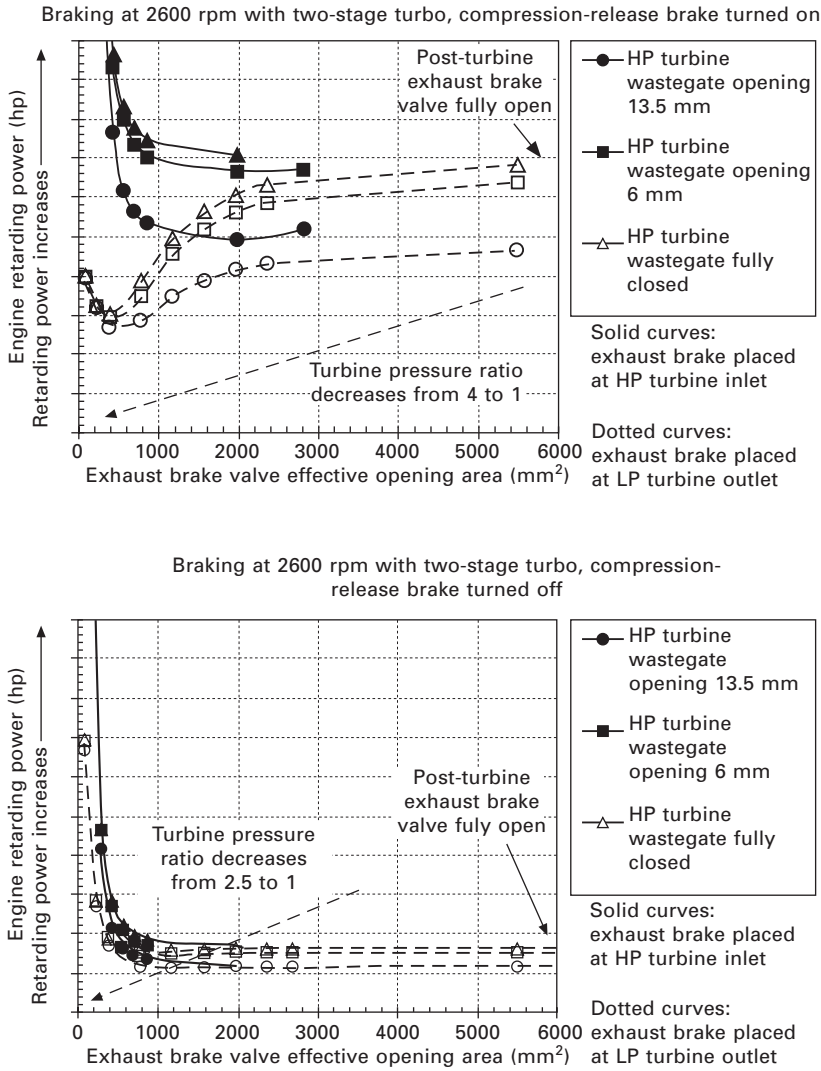
in engine air system design and turbocharger selection, both firing operation and engine retarding need to be considered.

The retarding performance of conventional exhaust brakes is complicated by turbine performance. When the turbine pressure ratio is much larger than 1, when the exhaust brake is used together with a compression-release brake (turned on) at high engine speed, closing the exhaust brake flap valve at the turbine outlet actually results in a reduction in turbine pressure ratio and air flow rate. As a consequence, both engine delta P and retarding power decrease. When the turbine pressure ratio is closer to 1, closing the exhaust brake flap valve leads to a monotonic increase in engine delta P and retarding power. Figure 12.20 shows the simulation of such a complex behavior of the exhaust brake and its interaction with the compression-release brake.

The design of VGT exhaust brake performance is limited by valvetrain capability in terms of the exhaust valve floating off the valve seat (related to engine delta P and exhaust valve spring preload), peak valvetrain force and intake valvetrain no-follow (i.e., valvetrain separation, which is related to high-speed vibration excited by the recompression pressure gas loading at valve overlap TDC). Figure 12.21 shows the design concept of the relationship between engine brake and valvetrain.

In addition to engine delta P, another important durability design constraint in engine brake design is injector nozzle tip temperature. The injector tip temperature during engine braking is very different from that during the firing operation because in firing there is a supply of fuel flow to cool the injector. The injector tip temperature directly depends on the in-cylinder gas temperature, which is affected by engine air flow rate and compressor boost pressure. Turbocharger performance and the exhaust brake flap valve opening at the turbine outlet directly impact engine air flow rate. Moreover, in the powertrain retarding operation (e.g., with a hydrodynamic retarder), the coolant heat rejection may exceed that in the engine firing operation. This needs to be considered in designing the cooling system capability.

Figure 12.22 summarizes the fundamental characteristics of engine brake design to match engine breathing features. The above summary illustrates that, when turbocharger matching and valvetrain design are conducted, the requirements of engine brake performance need to be considered. It emphasizes again that the engine performance design must be integrated as a whole system, not only because of the complex interaction between different subsystems, but also for the purpose of coordinating the needs of different applications.

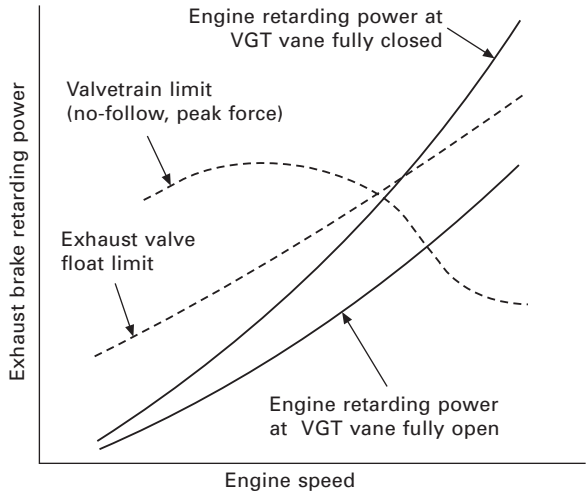


12.20 Interaction between engine compression-release brake and conventional exhaust brake.

12.4 Emissions calibration optimization development and engine performance design target

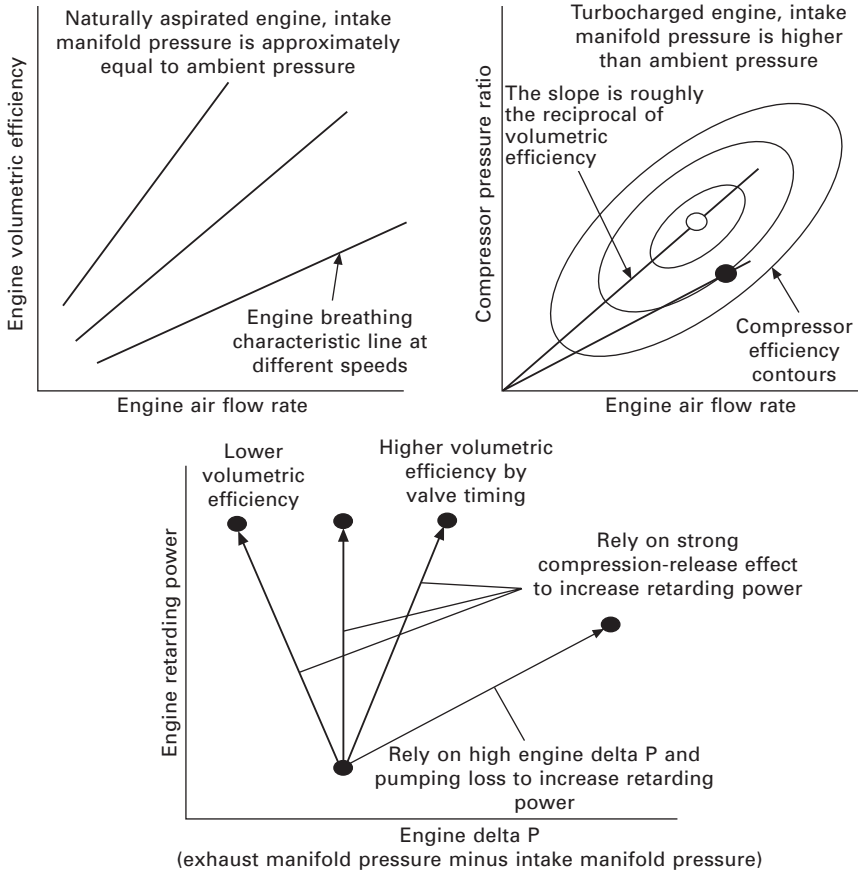
12.4.1 The process from emissions requirements to system design

At the beginning of an engine program, performance simulation can be used extensively during the stage of choosing key technologies (e.g.,



12.21 Engine exhaust brake design constrained by valvetrain limits.

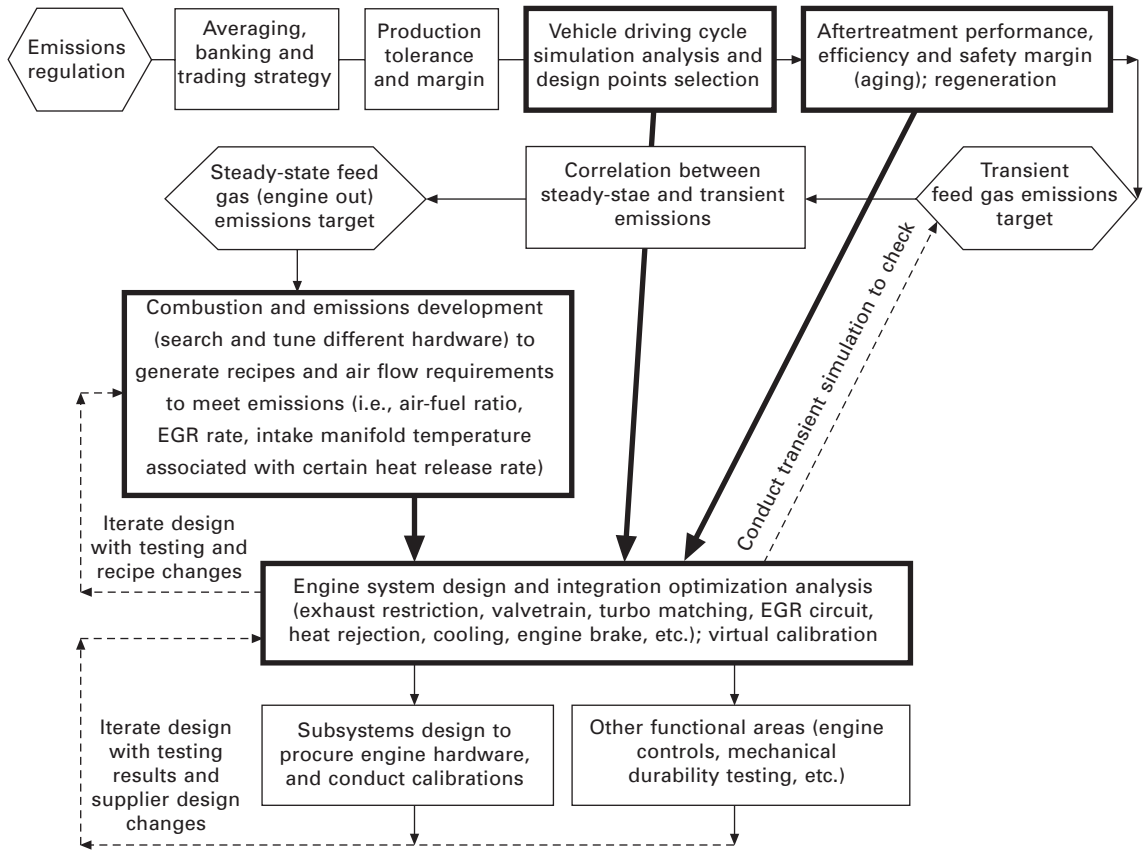
variable valve actuation and cylinder deactivation). Once the technology path is defined, engine air system design can start, with several possible configuration options, for example high-pressure-loop or low-pressure-loop EGR, parallel or series EGR coolers, single-stage or two-stage turbocharger, air-cooled or coolant-cooled charge air cooler, and so on. The required input for system performance design analysis is the established target of air flow requirements to meet emissions, mainly gravimetric air–fuel ratio, EGR rate and intake manifold temperature at each critical speed and load mode. Those requirements are produced by conducting combustion hardware search and tuning. The 'search' means screening different sets of hardware (intake ports, combustion chambers and fuel injection systems) to explore their potential to meet emissions. The 'tuning' (referred to before system design) or 'calibration' (referred to after system design) means any optimization of the tunable parameters with a fixed set of hardware. Some examples include calibrating fuel injection pressure, injection timing, vane opening of variable geometry turbine and EGR valve opening to find the optimum air–fuel ratio, and EGR rate for minimum BSFC while meeting emissions. The 'calibration' links electronic software controls with the selected hardware for production engines. Engine system design resides in the center of this design process and bridges the upstream combustion development and the downstream production calibration (Fig. 12.23). When the combustion–fuel–air system hardware is selected, it is important to foresee and predict what will happen at the engine calibration stage because a late change to inadequate hardware during the calibration stage is extremely expensive. Engine system analysis not only produces a specification for each subsystem design, but also generates



12.22 Engine breathing characteristics and principle of turbocharged engine brake design.

a virtual simulation of engine performance and emissions calibration before calibration testing happens.

From a working technique point of view, actually the optimization techniques used by the three functional areas (combustion hardware screening, system simulation and design, and calibration testing) share the same analysis method, namely design-of-experiments (DoE) combined with the response surface method (RSM). A thorough understanding of hardware screening and calibration processes in the entire engine speed–load domain under various situations (cold and hot ambient, high altitude, aftertreatment regeneration) is critical for properly translating emissions requirements to the airflow functional target, which is needed by engine system design as analysis input. This section will use engine calibration to introduce the DoE optimization method and emissions sensitivity to calibration parameters. The



12.23 The process from vehicle, aftertreatment and combustion emissions to system design.

method of setting the engine system design target of airflow requirements to meet emissions will be discussed. Emissions modeling methodology will be briefly reviewed.

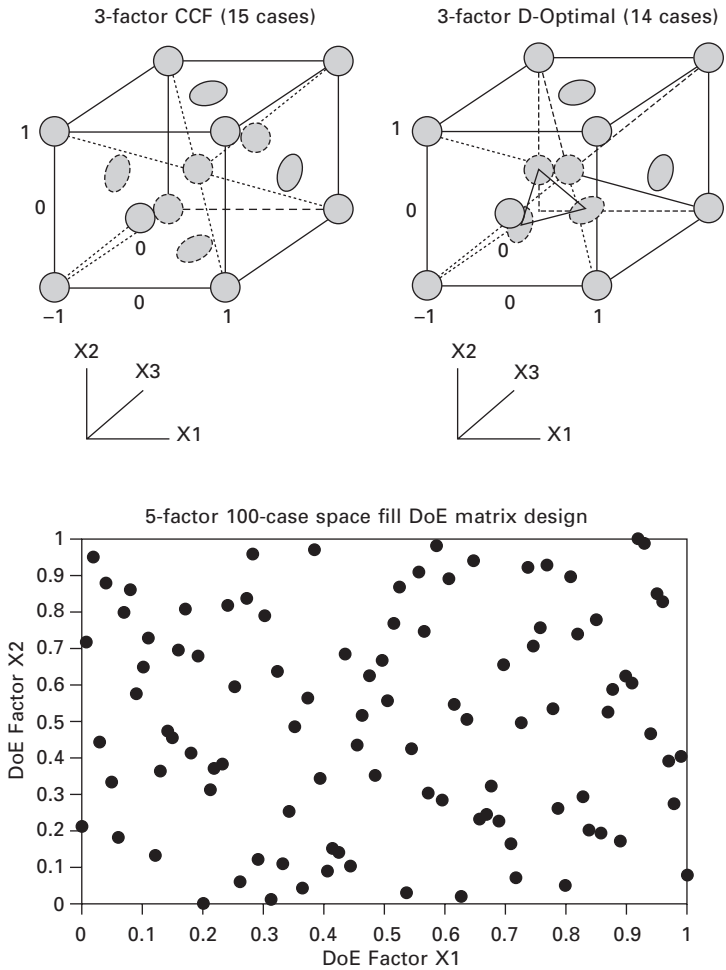
12.4.2 DoE technique for calibration and design optimization

DoE design methods

Strictly speaking, parametric sweeping is not 'optimization'. Rather, it is only a 'comparison'. True optimization requires a mathematical tool to build the equations which link the input (called 'factors') and output (called 'responses', either steady state or transient), and solve them for global optima to minimize or maximize one or more functional targets. The key processes in optimization include five steps:

1. Prepare factors in a statistical DoE design matrix.
2. Generate responses by either experimental testing or numerical simulation (for instance, run engine cycle simulation software to produce performance output data).
3. Build empirical mathematical models to link the factors and the responses by using polynomials or other continuous functions (called 'emulators') with response surface fitting.
4. Validate the emulator models to check surface-fitting accuracy by confirmation runs.
5. Conduct optimization computation to search the global optima under given constraints.

Both single- and multi-objective optimizations are encountered in EPSI work. DoE methods have been used traditionally to identify the main and interaction effects; they can extract maximum information on the relationship between factors and responses with a minimum number of runs in a systematic manner instead of by a trial-and-error method. This advantage is especially prominent when the number of runs of using the one-factor-at-a-time full factorial method increases exponentially with the number of factors. Figure 12.24 shows the DoE statistical designs with the central-composite-face-centered (CCF) method, the D-Optimal method and the space fill method, with X_1, X_2 and X_3 as factors. The factors can be any parameters in engine design, hardware screening and calibration testing, or simulation. The D-Optimal method may tailor the corners of the experimental space, and also provides as much orthogonality as possible between the columns in the design matrix, hence maximizes the output information for a given number of experimental runs or for a given response surface model that one expects to fit the data. The space fill method is another effective



12.24 Examples of input factor space in DoE matrix design.

design for engine applications where highly accurate third-order emulators are needed.

DoE data processing and optimization

After engine testing or cycle simulation data are obtained, a polynomial model of second or third order including interaction terms can be built to link each response (denoted as Y, e.g. NO_x or BSFC) with the factors (denoted as X, e.g. injection timing, EGR valve opening, VGT vane opening), for example in the form

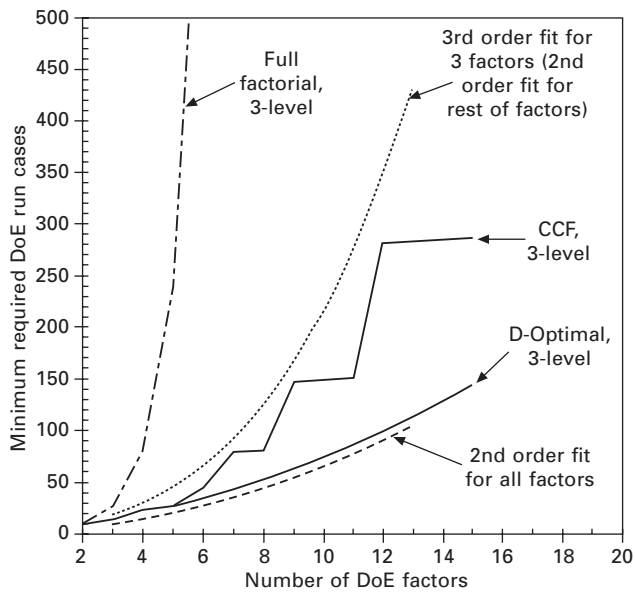
$$Y_1 = C_1 + C_2X_1 + C_3X_1^2 + C_4X_2 + C_5X_2^2 + C_6X_3 + C_7X_3^2 + C_8X_1X_2 + C_9X_1X_3 + C_{10}X_2X_3 + \text{error}$$

The coefficients C_i in the equation are calculated with least-squares fit (e.g., in MATLAB). Radial basis functions or a genetic algorithm may also be used to fit the data. Figure 12.25 shows that the number of runs required in a DoE design depends on the number of factors, the DoE design method and the order of accuracy of the emulator. Three-level factor settings are suitable for second-order surface fitting, while third-order fitting requires a factor level more than three. The third-order fitting may be used for certain highly nonlinear factors such as exhaust restriction flow coefficient, EGR circuit restriction flow coefficient or VGT vane opening. The DoE method is usually good enough to handle steady-state optimization. For transient optimization, the neural network approach often becomes necessary.

12.4.3 Combustion and emissions development and calibration optimization

Introduction to emissions control

Compared with gasoline engines, diesel engines emit a similar amount of NO_x (at engine out), much more PM, and much less CO and HC. Improving air–fuel mixing and combustion processes can reduce PM, but usually result



12.25 DoE matrix size.

in an increase in NO_x. There exists a fundamental trade-off between NO_x and PM in diesel engines. The NO_x emissions from gasoline engines may be reduced by three-way catalyst aftertreatment. But currently it is still very costly to use aftertreatment devices to clean the NO_x from diesel engines, because the NO_x exists in an oxygen-rich exhaust flow and is formed with air–fuel ratios much larger than those in gasoline engines. Reducing engine-out NO_x and PM while still maintaining low fuel consumption poses significant challenges to diesel engine combustion and air system design. NO is largely formed during premixed lean burn combustion with local excess air–fuel ratio 1.0–1.2, and soot is mainly formed in diffusion combustion with insufficient air at local excess air–fuel ratio lower than 0.5–0.6. The heterogeneous local mixing between air and fuel during the combustion process is the root cause of soot emission in diesel engines. Achieving better mixing and preventing high NO_x and soot is the design goal of air–fuel combustion systems.

Fuel system design and matching with combustion and air systems is a highly important and specialized area for low emission diesel engines. Fuel injection pressure, nozzle number, hole size, injection rate shaping and many other design and calibration parameters need to be optimized. The air system (e.g., air–fuel ratio and swirl ratio) is designed to match the capability of the fuel system for a given emissions target.

Emissions control is also closely related to mechanical design. A typical example is lube oil consumption control to reduce the soluble organic fraction (SOF) in PM emissions by using high-tension piston rings or better cylinder bore distortion control with improved cooling jacket design. The high-tension piston rings result in increased friction losses and durability problems. Another example is using retarded fuel injection timing to reduce NO_x. This leads to higher soot emission, and the faster soot accumulation in lube oil would force more frequent oil changes. In fuel system design, the demand of using a higher injection pressure to control PM exerts a higher load on the injector mechanism. The lubricating oil will experience a higher shear rate, and the oil viscosity improver additive will break down more quickly.

Combustion chamber design

In direct injection diesel combustion system design, combustion chamber shape and engine compression ratio are important for in-cylinder air motion and emissions. The compression ratio has a direct impact on system design because it affects unaided cold start, peak cylinder pressure at full load, allowable air–fuel ratio and EGR rate, friction losses and mechanical efficiency, emissions, engine cycle indicated thermodynamic efficiency and BSFC. For low emissions and fuel consumption the heat release rate during premixed combustion needs to be reduced in order to lower the combustion

temperature and reduce NO_x emission (for example, by using pilot injection). The heat release rate during diffusion combustion needs to be raised to keep fast combustion and a proper in-cylinder temperature to reduce HC, CO and PM. The late stage of diffusion combustion needs to be shortened to reduce fuel consumption and exhaust temperature. Key issues of combustion design include the following.

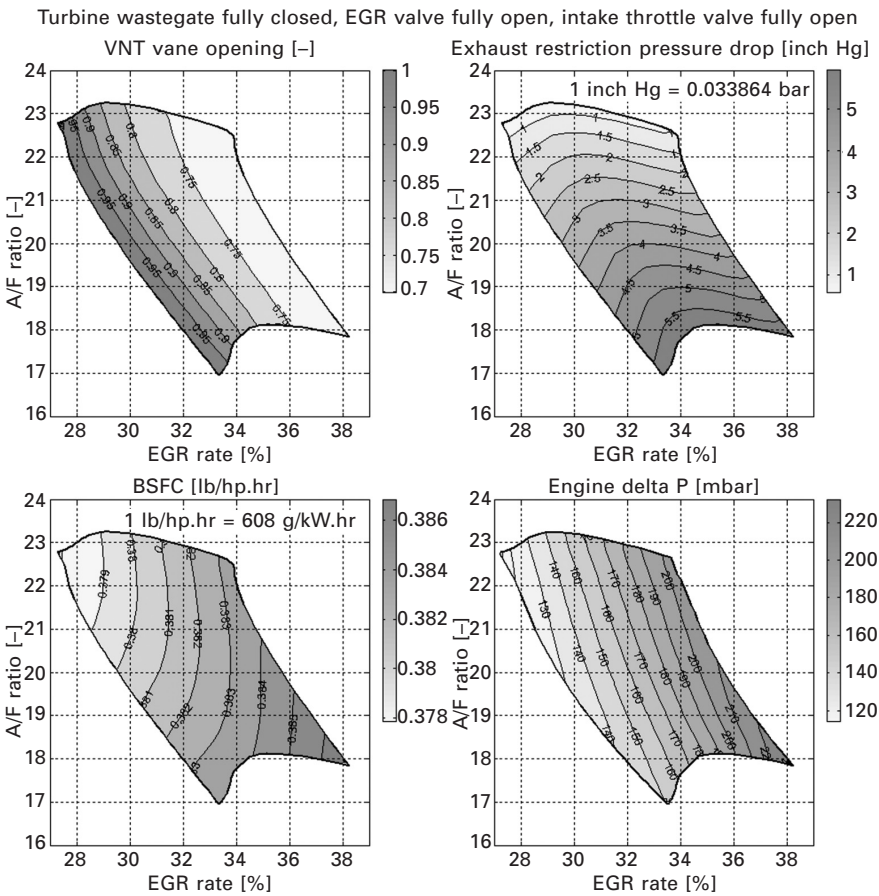
1. The engine compression ratio needs to be selected to ensure acceptable peak cylinder pressure and reliable unaided cold start. During cold start, self-ignition is determined by a combination of sufficient time and temperature required, which are affected by a number of factors, including compression ratio, ambient temperature, fuel injection amount and timing, starting speed, and speed-related gas leakage past piston rings and heat transfer losses, and other starting aids (excess fuel injection, glow plug, heaters, ether, etc.). A low compression ratio causes a reduction in thermodynamic cycle efficiency and possibly an undesirable increase in ignition delay (Note that the indicated fuel conversion efficiency of the constant-volume cycle is $\eta_{th} = 1 - \Omega^{1-\gamma}$ where Ω is the compression ratio and γ is the ratio of specific heats, c_p/c_v.). An excessively high compression ratio results in increased mechanical friction and NO_x emissions. When intake valve closing timing is changed, the 'effective' engine compression ratio actually can be altered, although the effect is not exactly the same as changing the geometric compression ratio.
2. The combustion chamber design needs to match the high-pressure fuel injection system and intake swirl for good mixing. The combustion chamber shape variation along the radial or axial direction controls the swirl, vortex and turbulence of in-cylinder airflow and wall impingement of the fuel spray to achieve better air utilization and reduce the air–fuel ratio required.
3. Optimum swirl intensity has a tendency to decrease to favor more quiescent bowl design with high injection pressure. Low heat rejection combustion chamber design may be adopted through low swirl or no swirl (resulting in low turbulence in the cylinder, hence low heat rejection) with ultra-high fuel injection pressure, without wall impingement of the fuel spray, for low or medium speed engines.
4. Low surface-to-volume ratio is preferred in order to minimize heat rejection losses.
5. The metal temperature at the edge of the combustion bowl is related to the bowl shape. It needs to be optimized for the best trade-off between airflow turbulence enhancement and thermal fatigue life.
6. Combustion noise may be reduced by turbocharging and fuel injection strategies through a reduced rate of increase of the cylinder pressure, and also by the attenuation of structural damping.

Fundamental combustion emissions engine test and air system requirements

Either single-cylinder or multi-cylinder emission experiments can be conducted in order to determine the combustion recipe and air system requirement at minimum engine delta P (pumping loss) and BSFC. At a given speed and torque, the air–fuel ratio and EGR rate required to meet target emissions are contingent upon the BSFC produced in the test. Therefore, the engine delta P and BSFC used in the emissions recipe test need to be as close to the optimum as possible. In the test, EGR circuit hardware needs to be selected with the lowest possible flow restriction for the EGR cooler and EGR valve. Hardware screening with DoE methods is conducted by KIVA simulation and engine testing to select the best compression ratio, combustion bowl design, intake swirl ratio and fuel injector nozzle design. Then, DoE tuning testing may be conducted at the critical speed–load modes used for heavy-duty emissions certification. In the single-cylinder test, the DoE factors are intake manifold temperature (varied by EGR or charge air cooling), intake manifold pressure, exhaust manifold pressure, EGR valve opening, fuel injection timing and pressure. In the multi-cylinder engine test, the DoE factors are the same except for using VGT vane opening or turbine wastegate opening to replace the intake manifold pressure, and using exhaust restriction setting to replace the exhaust manifold pressure. Intake throttle valve opening is an optional DoE factor that may be used near the peak torque region to drive EGR flow or used in the high-speed low-load region to largely reduce the air–fuel ratio in order to reduce NO_x. More DoE factors may be included for more flexible air systems (e.g., variable valve actuation). Those DoE factors are very similar to those used in the production engine calibration stage.

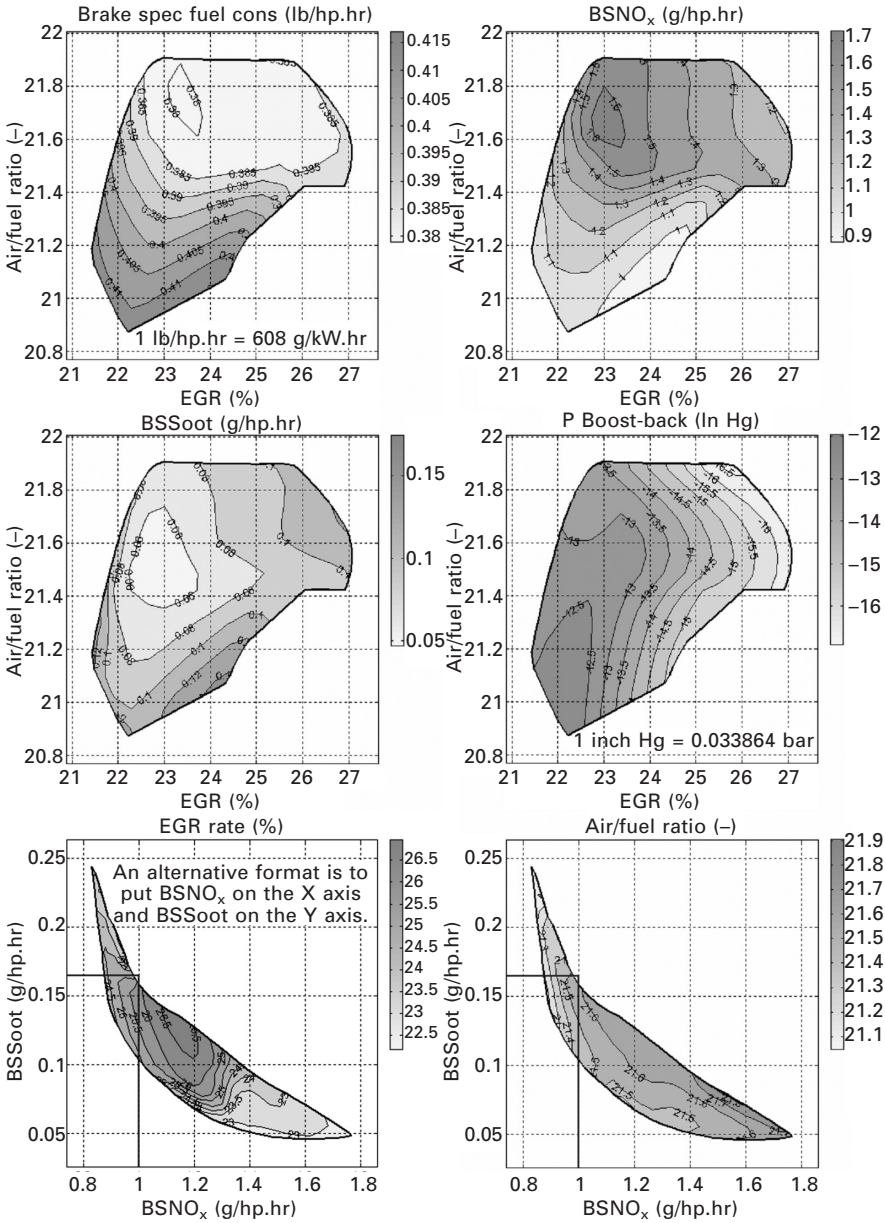
Before running the multi-cylinder engine test, in order to check whether the test can cover a desirable range of EGR rate and air–fuel ratio, the capability of the available turbocharger hardware needs to be checked by an engine cycle simulation through sweeping the VGT vane or turbine wastegate opening, exhaust restriction or intake throttle opening. The simulation data in Fig. 12.26 illustrate how to build a sufficiently wide and controllable range of air–fuel ratio and EGR rate in such a fundamental emissions test. (Each point in the figure can be solved by using the equations in Section 12.2.) If the air–fuel ratio is too low, the exhaust restriction pressure drop can be artificially lowered. If the EGR rate is too high with the VGT (VNT) vane fully open, a turbine wastegate passage can be built in the test cell to reduce engine delta P in order to reduce the EGR rate.

After the test data are obtained, DoE emulators need to be built and optimization needs to be conducted to compute engine performance contour maps (e.g., EGR rate, air–fuel ratio, intake manifold temperature, fuel injection timing and pressure, engine delta P, BSFC, combustion noise, etc. as shown in Fig. 12.27) in the 'PM or soot vs. NO_x' or 'PM vs. NO_x + HC' domain



12.26 Effects of turbine area and exhaust restriction at rated power.

or mapped to the 'air–fuel ratio vs. EGR rate' domain to find the required emissions recipe for a given emissions target of NO_x, PM, HC and CO. In order to cover the possible differences in turbo efficiency and EGR circuit restriction in a future design stage, two sets of contour plotting are useful: (1) in the ideal situation with the EGR valve fully open, which produces minimum engine delta P (pumping loss) and BSFC; (2) with partially open EGR valve, which produces a higher pumping loss. The degree of EGR valve throttling depends on speed, torque, turbine area and efficiency. The above emissions test may also be conducted to mimic high altitude and hot ambient emissions performance for the US NTE (Not-To-Exceed) emissions requirements. The DoE data can be processed using the same approach to obtain the air system requirements for NTE. During the process of determining the combustion emissions recipe, the correlation between steady-state and



12.27 DoE calibration optimization test data analysis of emissions and air/EGR flow.

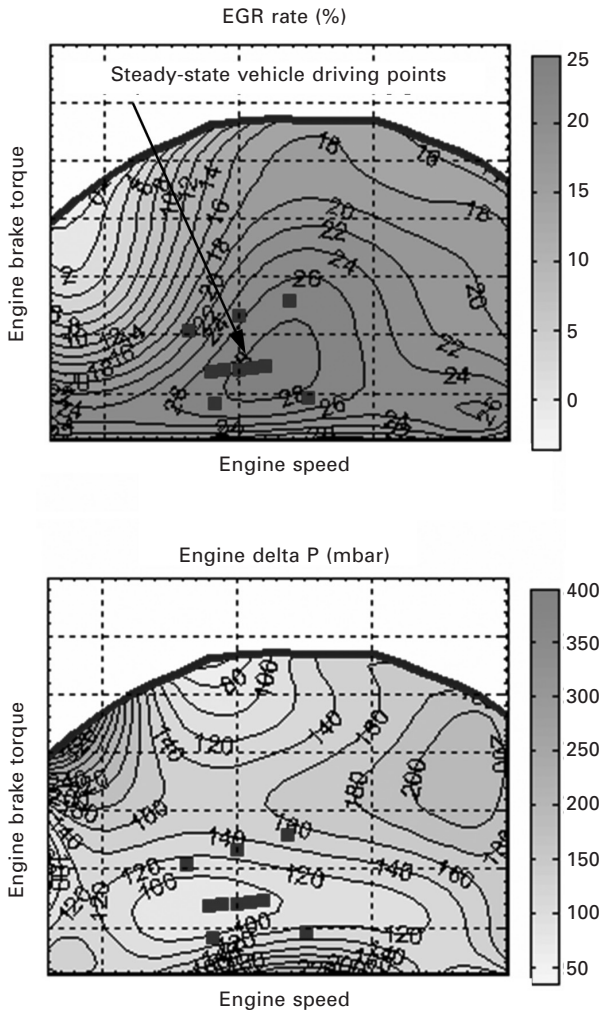
transient emissions with proper engine control strategies should be factored in. These air system functional requirements of air–fuel ratio, EGR rate and intake manifold temperature (associated with a certain heat release rate and start-of-combustion timing, BSFC and combustion-fuel system matching assumptions) are then sent to the system design analysis engineers for computing and optimizing specifications for hardware sizing of turbo, EGR circuit flow restriction and cooler size, etc. The lower the air–fuel ratio and EGR rate required for combustion, the easier the air system design. It should be noted that multiple turbocharger or cooling configurations may reach the same air system functional target, and it is the system analysis engineer who will optimize the hardware selection. An example of combustion development can be found on Navistar's model year 2004 6.0L V8 engine (Zhu *et al.*, 2004).

Engine emissions behavior and calibration optimization

Different combustion hardware gives different ranges of emissions capabilities. Within a fixed set of hardware, electronic controls of tunable actuators such as the EGR valve and common rail fuel injection provide a range of emissions variation as a function of air system parameters. In system design, because the air flow requirement may be an immature moving target, it is important to understand and document the emissions behavior in order to design the system precisely and robustly. Emissions testing or simulation may reveal such sensitivity behavior. In contrast to the traditional trial-and error 'knob-turning' rudimentary tuning or calibration approach, modern automated engine calibration or hardware screening is based on DoE-model emulators. Engine calibration can be so complex in a multi-dimensional factor space that even an experienced calibrator cannot always find the best settings without using optimization. Unlike the 'knob-turning' approach where the data are poorly scattered, the model-based calibration documents the engine sensitivities completely, systematically and concisely with optimization maps and mathematical models to facilitate any future reuse. The model-based approach ensures the minimum BSFC is found by conducting optimization computation. Figure 12.27 shows the NO_x and soot behavior in the 'air–fuel ratio vs. EGR rate' domain at a fixed speed and load with a given set of hardware. Each data point on the maps has the minimum BSFC achievable within the factor range of the DoE. In this example, the maps are bounded by the ranges of the factors (VGT vane opening, EGR valve opening, fuel injection timing and injection pressure here). Different combustion hardware will shift or rotate the map data so that the emissions recipes may approach closer to or depart further away from the emissions regulation 'box' with different levels of BSFC. These optimized contour maps in the sense of minimum BSFC in the domain of emissions or air system parameters are a

powerful and concise tool for the system engineer to judge the sensitivities and determine a precise and robust performance functional target.

The above local optimization needs to be conducted by combustion emissions development at each critical speed–load mode. After the air system functional targets are derived, system simulation will be conducted, often with the DoE optimization method, to produce hardware design specification as well as smooth steady-state performance maps in the global speed–load domain. Such a 'virtual calibration' (e.g., as shown in Fig. 12.28) may be used to identify the problems in combustion emissions recipes or in the calibration optimization of emissions, drivability and fuel consumption.



12.28 Virtual engine calibration simulation in the speed–load domain.

Rapid transient calibration optimization

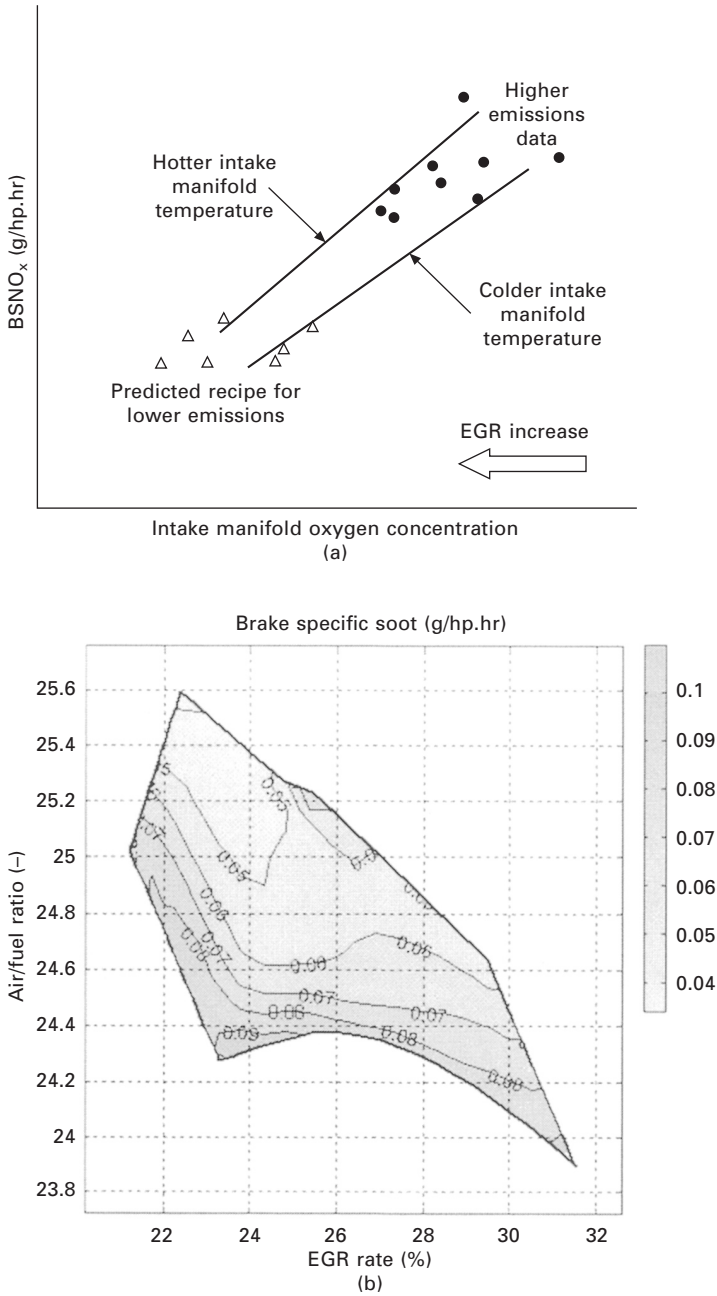
The above-mentioned DoE approach is well suited for steady-state engine emissions calibration, but is cumbersome for transient calibration of emission regulatory cycles due to its difficulty of surface-fitting the highly nonlinear fast-changing time-dependent response data. Transient calibration and control optimization has been a bottleneck in the engine development process and is very time-consuming and expensive. Neural network modeling provides a solution for this problem. A large amount of transient cycle engine test data with a systematic perturbation of all calibrateable parameters (including transient gains) is used to train and build the neural network model. Then, the model can be used to predict transient emissions and BSFC. Optimization can be steered to minimize BSFC subject to the weighted constraints of emissions, drivability and durability. Details of model-based transient calibration were given by Atkinson and Mott (2005). Transient performance analysis will be elaborated in Section 12.8.

12.4.4 Emissions modeling

In addition to the experimental approach to predict the relationship between emissions and air system parameters, emissions simulation is also promising for establishing the airflow functional requirements in a more cost-effective way. Four types of emissions modeling approach are overviewed below.

Empirical approach

A primitive but useful approach used in the engine industry to predict emissions is to build empirical parametric correlations among engine performance test data. There are two types of such models: (1) to directly plot without surface-fitting, for example, plot with Microsoft Excel the curves of NO_x vs. oxygen concentration and intake manifold temperature, soot vs. air–fuel ratio or EGR rate, etc.; and (2) to surface-fit DoE engine test data to build mathematical emulators of emissions as functions of either engine calibration parameters (e.g., EGR valve opening and fuel injection timing) or performance parameters (e.g., air–fuel ratio and EGR rate). Two examples are shown in Fig. 12.29. The advantages of such an approach include the availability of a large amount of engine test data, ease of plotting, regressing or surface-fitting the data trends, and quickly estimating a ballpark value or ‘rule-of-thumb’. The disadvantages include being purely empirical and lacking fundamental or universal physics in the deduced correlations or emulator models; lacking real-time predictability and feasibility to be implemented in future advanced intelligent engine controls; and limited predictability only to the given engine hardware from which the test data were generated.



12.29 Empirical emissions modeling: (a) direct plot; (b) DoE optimization emulator model.

Traditional phenomenological approach

A typical traditional phenomenological combustion and emissions model is the diesel jet model developed from Cummins, Inc. The model simulates the mixing rate of fuel spray and air, and calculates the local temperature, air–fuel ratio and combustion in each zone of spray so that the computed in-cylinder gas properties vary with both space and time. The advantages of such a model include the facts that some combustion physics and chemistry are built into the model, and with proper calibration the model can have certain limited predictability on heat release rate and NO_x. The disadvantages include the following: (1) many simplified assumptions concerning spray penetration, turbulence, swirl, heat transfer, vapor concentration distribution, wall impingement, flame propagation, combustion, and emissions formation; (2) the practical difficulty of obtaining in-cylinder experimental data to justify or calibrate each sub-model for industry use; (3) many model tuning parameters as a result of many detailed sub-models; (4) the difficulty of evaluating many design parameters related to the combustion chamber and air–fuel combustion system matching because many of those factors cannot be built into the model; (5) inability to predict particulate matter and soot accurately; and (6) the fact that it is computationally intensive, and at current computer speeds it is impossible to implement in real-time simulation or intelligent engine controls. It seems that the focus of traditional phenomenological modeling may be directed towards assisting the development of the more practical heuristic macro-parameter-dependent modeling (to be mentioned below), instead of trying to become a stand-alone design tool, at least from an engine system design point of view.

CFD-KIVA modeling

The three-dimensional KIVA is a very complex multi-zone combustion model based on partial differential equations of viscous fluid dynamics, turbulence, chemical reaction, boundary layer, heat transfer, etc. It has demonstrated strong potential and practicality to be used as a design tool to predict emissions and optimize combustion chamber design and air–fuel combustion system matching. The problems with KIVA are the complexity of model tuning and the long computing time required.

Heuristic macro-parameter-dependent approach

Heuristics are the doctrine of obtaining new insights and universally valid design and calculation methods with the law of similarity or partially empirical simplification. It is a counterbalance to the theoretical KIVA method. The heuristics lead to more detailed insights if detailed models are established. The ‘macro’ means global apparent engine performance parameters and zero-

dimensional in-cylinder bulk parameters. Diesel emissions are extremely complex to model in micro detail due to the various mechanisms involved in ignition delay, premixed and diffusion flame combustion processes. For example, the creation of soot is determined by local temperature and oxygen concentration during the events of radical chain reaction in the core of the fuel jet, adsorption of polycyclic aromatic hydrocarbons, polymerization, cyclization, coagulation and agglomeration in soot formation and reoxidation phases. The idea of using a macro-parameter-dependent approach to build emissions models is to try to bypass the difficulties encountered by the traditional phenomenological model. The approach tries to link the emissions to more fundamental engine performance parameters, which are either apparently macro cycle-average parameters such as air–fuel ratio, or macro instantaneous crank-angle based parameters such as in-cylinder bulk temperature, in a relatively simplified combined theoretical form. It still conforms to basic physics of emissions chemistry, for example, by using a similar logic to the successful approach of the Woschni correlation in the engine heat transfer area. (Certainly, emissions modeling is much more complex than heat transfer.) Its theoretical depth is far beyond the empirical emissions data processing, and it is a practical semi-empirical approach, especially suitable for the needs of engine system design and analysis. The advantage of such a model is that it may eliminate many of the disadvantages of the empirical approach and the traditional phenomenological approach. Most importantly, it will be the only feasible emission prediction model that can be used in future advanced intelligent real-time emissions-model-based electronic engine controls to handle both steady-state and transient control needs. The technique of building such a model can also be applied to build macro emissions models for aftertreatment devices, where the technical difficulty is actually less challenging because the variation of gas properties within an engine cycle is not as strong as the in-cylinder processes. This type of macro model will not be intended to predict heat release rate or evaluate combustion chamber design. Heat release rate is used as input in the model. The predictability of the model is limited to the given hardware of combustion and fuel systems. If the effects of different combustion hardware design need to be simulated, KIVA must be used. The heuristic macro models of NO_x and soot were proposed by Zheng and Xin (2009).

The best emissions model is not necessarily the most complicated theoretical model; rather it should be a simple, practical and most efficient model for engineering design applications.

12.5 Diesel aftertreatment integration and matching

Current design and calibration strategies for diesel engine-out emissions reduction are approaching the practical limits. The diesel particulate filter (DPF) is needed for the US 2007 model year and NO_x aftertreatment may

be considered for the future. Diesel aftertreatment devices exhibit several characteristics which influence engine design and operation: performance variation (e.g., the change of DPF pressure drop as soot loads up); the need for regeneration and flexible engine controls; performance closely related to vehicle duty cycle; and the interactive chemistry nature between different aftertreatment devices. There is a large body of literature on aftertreatment performance itself. But there is very little literature on either the approach of engine–aftertreatment matching or the critical analysis topics of aftertreatment integration in engine system design and calibration.

12.5.1 Overview of aftertreatment performance and requirements on engine system design

Diesel exhaust gases exhibit several unique characteristics compared to gasoline engines: lower HC and CO; higher PM; lower exhaust temperature due to higher air–fuel ratio; and oxidizing exhaust gas chemistry suppressing the chemical reduction of NO_x. Modern diesel exhaust aftertreatment devices consist of diesel oxidation catalyst (DOC), diesel particulate filter (DPF) and possibly a NO_x aftertreatment device such as selective catalytic reduction (SCR) or lean NO_x trap (LNT, also known as NO_x adsorber). The muffler usually can be replaced by a wall-flow DPF in commercial vehicles, or it may be used to further reduce exhaust noise. The emissions formation mechanisms and aftertreatment control technologies were provided in detail by Eastwood (2000, 2008), Blakeman *et al*. (2003), and Majewski and Khair (2006).

The DOC reduces HC (including PAH), CO, SOF in PM, and diesel exhaust odor by converting them to H_2O and CO_2. Some small de-NO_x capability with HC inside DOC is possible, but the NO_x is almost unaffected. Nanoparticles are not affected, either. The combustion of high-sulfur diesel fuel produces SO_2, which is converted to SO_3 and a large amount of sulfate particulate in DOC at high engine load under high exhaust temperature. Therefore, the SOF removal ability of DOC may be offset by the addition of sulfate particulate matter. Using low sulfur diesel fuel can reduce sulfate particulate matter and avoid catalyst poisoning. Because NO_2 may assist DPF regeneration, the oxidation of NO to NO_2 by O_2 and the reduction of NO_2 by HC in DOC need to be optimized.

The efficiency of catalytic converters is related to air–fuel ratio, light-off temperature and light-off time (defined at 50% conversion efficiency), space velocity (the ratio between normalized exhaust volume flow rate and aftertreatment component volume), flow restriction characteristics (the curve of pressure drop vs. flow rate), and durability features. The light-off temperatures of HC and CO become lower when the air–fuel ratio is higher. The three-way catalytic converter used in gasoline engines has a high conversion efficiency above 80% simultaneously for CO, HC and NO_x only when the excess

air–fuel ratio stays around 1 (i.e., stoichiomatric) with a slight fluctuation window about 0.01. Diesel engines must run 'lean burn' with a much higher air–fuel ratio because of the heterogeneous nature in diesel combustion and high PM emissions. In the oxidizing exhaust environment the reductants such as HC and CO are more reactive to excess oxygen rather than to the NO_x. Therefore, the three-way catalyst used in gasoline engines cannot be used in diesel. SCR and LNT combined with ultra-low sulfur fuel are two promising technologies for diesel NO_x aftertreatment with up to 80–90%+ NO_x reduction. They both require reductants such as hydrocarbons, ammonia (NH_3) or urea ($CO(NH_2)_2$) to be injected.

Urea-based SCR is believed by many in the industry to be more suitable than LNT for heavy duty applications. In SCR, ammonia is less reactive to oxygen than hydrocarbons are, and NH_3 can be mainly reduced by NO_x rather than the other oxidant, O_2. Therefore, the NO_x conversion efficiency of SCR is higher than the active de-NO_x catalytic reduction of using hydrocarbons. NO_x is reduced to nitrogen and water. The dosing rate must match temperature, exhaust composition and space velocity. Precise dynamic dosage control is required for SCR in order to prevent excessive slip of the toxic ammonia during engine transients in automotive applications. A second DOC may be added downstream of the SCR to convert the slipped ammonia to nitrogen. The freezing point of –11 °C of the aqueous solution of urea could be a problem. The ammonium sulfate accumulated in SCR needs to be purged at high temperature periodically. Moreover, SCR is effective in removing HC and some SOF. SCR modeling and control were detailed by Kim *et al*. (2007) and Willems *et al*. (2007).

LNT adsorbs NO_x when exposed to oxidizing exhaust, through an oxidation catalytic conversion from NO to NO_2 and then adsorbing NO_2 as nitrates on alkaline earth compounds such as $Ba(NO_3)_2$. The LNT is periodically and briefly regenerated to reduce NO_x by using a reductant or electric heating. The working temperature window of the LNT is bounded on the lower side by NO light-off and on the upper side by nitrate instability. The LNT regeneration in diesel engines is more difficult than in their lean-burn GDI gasoline counterparts because it is challenging to use the required rich air–fuel ratio in diesel engines due to high-smoke concerns. LNT performance is very sensitive to sulfur (even at 3 ppm sulfur in the fuel); therefore, desulfation (usually lasting several minutes with rich air–fuel ratio at high temperature) or other sulfur management (e.g., ultra-low sulfur or sulfur-free fuel or sulfur traps) is needed.

In DPF design, achieving high filtration efficiency and low flow restriction with small dimensions and low cost are challenging tasks. The exhaust restriction at the turbine outlet refers to the pressure drop through all the aftertreatment components plus the exhaust pipes. Exhaust restriction depends on hardware design and the flow restriction characteristics of the components. The pressure

drop of the DPF increases as the filter is filled with soot and ash deposits. It also varies when DPF soot loading changes before and after DPF regeneration. Exhaust restriction also can be regulated by using an exhaust back-pressure valve, such as a flap valve installed at the turbine outlet. Closing the back-pressure valve reduces exhaust flow rate or may assist engine braking. Exhaust restriction has a large impact on turbocharged engine performance.

Flexibly controlling exhaust gas temperature and flow rate is another critical air system design topic for engine thermal management and optimum aftertreatment performance. For example, the functions of NO_x adsorber during the adsorption and reduction phases require different exhaust temperatures and oxygen concentrations. In order for the converter more easily to reach the light-off temperature or to achieve aftertreatment regeneration, the following measures can be used to raise the exhaust temperature: (1) minimizing heat losses by either insulating the exhaust pipe or installing the aftertreatment device close to the exhaust manifold or runner; (2) raising the intake manifold temperature by flexible cooling or bypassing coolers; (3) raising the exhaust temperature by bypassing the turbine; (4) retarding fuel injection timing; (5) using in-cylinder post-fuel injection (with engine torque balance) to reduce the air–fuel ratio and provide the reductant needed for the NO_x adsorber or DPF regeneration; (6) using external fuel dosing into the exhaust stream; and (7) reducing engine air flow rate by intake throttling, exhaust throttling or variable valve actuation to raise the exhaust temperature. In some regeneration strategies, the EGR is turned off or reduced during regeneration in order to make the exhaust hotter or to increase the NO_x:C ratio to assist soot burning by raising the concentration of feed-gas NO_x. Hotter exhaust gas at the DOC outlet due to its exothermic reaction and faster light-off also helps to initiate DPF regeneration.

Engine-out and aftertreatment-out emissions during transient cold-start have received much greater attention since the 1990s after the type approval procedures in emissions regulations became more stringent, especially for gasoline engines. Diesel engines are less sensitive in cold-start emissions than gasoline engines, although diesel may have a problem of 'white smoke' (i.e., evaporated fuel droplets). Close-coupled catalysts for cold-start emissions control may affect the HC:NO_x ratio in exhaust flow so that it may influence the aftertreatment recipe. But overall the emissions control at cold-start and in a cold climate is a more local design issue of catalyst warm-up or cold-start aid rather than a system design focus.

12.5.2 Overview of DPF regeneration requirements on engine system design

DPF removes PM including nanoparticles if high filtration efficiency is achieved. Engine–DPF matching requires careful integration. DPF is more

complex than DOC because DOC is entirely passive, reacting continuously, and does not require regeneration, DPF is usually the opposite.

A soot load factor is defined as the ratio between the DPF pressure drop at fully loaded and the pressure drop at clean (no soot accumulated). Regeneration efficiency is defined as the ratio between the pressure drop reduction after regeneration and the pressure drop reduction after an ideal complete cleaning of soot. The soot load factor and DPF size design are determined by the exhaust restriction level allowed for acceptable engine performance, the regeneration frequency, the peak burning temperature and the temperature gradient during the exothermic regeneration process related to DPF thermo-mechanical stress durability, and the regeneration efficiency. The regeneration efficiency is defined by:

$$\eta_{regen} = \frac{\Delta P_{loaded} - \Delta P_{regen}}{\Delta P_{loaded} - \Delta P_{clean}}$$

where ΔP_{loaded} is the pressure drop of a soot-loaded DPF, ΔP_{regen} is the pressure drop after regeneration, and ΔP_{clean} is the pressure drop of a clean DPF associated with certain incombustible ash loading. Filters that are only partially loaded are more difficult to regenerate and maintain self-sustaining soot combustion. When soot loading accumulated in the DPF exceeds a certain level, it is desirable to have regeneration, either passive or active, burn off the soot to reduce exhaust restriction. Uncontrolled burning results from too much accumulation of soot and deposited hydrocarbons. It generates excessively high burning temperature or temperature gradient to melt or crack the filter. The related factors in catalytic soot regeneration mainly include exhaust temperature, the concentrations of O_2 and NO_2 (for C + O_2 and C + NO_2 reactions of carbon burning), the NO_2:NO ratio, and the NO_x:C mass ratio. The following means can assist soot burning: higher temperature and higher O_2 concentration in exhaust flow, more deposited hydrocarbons (SOF) and its exothermic burning reaction to provide energy to ignite soot, lower space velocity or volumetric flow rate, and lower soot loading.

DPF durability is related to filter material and design, regeneration burning temperature, temperature spatial and temporal gradients, and regeneration frequency (fatigue life). The regeneration frequency is affected by the installation position and soot loading, which is related to filter size, soot load-up rate and driving cycle. Small filters located closer to the engine under high-load driving will regenerate more regularly. DPF design and regeneration details were given by Yamaguchi *et al*. (2005), Soeger *et al*. (2005) and Johnson (2007b). DPF analytical models were developed by Konstandopoulos *et al*. (2000, 2005).

In non-catalyzed DPF regeneration, soot burning lasts a few minutes and requires approximately 550–650°C exhaust temperature to start, which actually cannot be reached at most part-load operating conditions. It was

reported that for soot to completely burn, an exhaust temperature of above 600°C with oxygen concentration above 7% is required (Basshuysen and Schafter, 2004). In catalyzed DPF (CDPF) regeneration, in order to reduce the thermal energy required to initiate the regeneration, additives can be added in the fuel or catalytic coating may be applied inside the filter to significantly reduce the soot ignition temperature to the range of 275–450°C. The catalyst, either for SOF or for carbon soot, is usually more effective at higher oxygen concentration in the exhaust flow. The ignition and burning performance of the catalytic regeneration also depends on NO_x, fuel sulfur, SOF and PM composition.

Passive regeneration, also known as self regeneration, usually assisted by catalytic means to lower the soot oxidation temperature, has certain advantages such as not using sensing/control systems and eliminating their durability troubles. In passive catalytic regeneration, because the driving condition can extinguish or initiate the regeneration, there is no control over the soot loading, the pressure drop of the DPF, and the regeneration efficiency before and after the regeneration. Once started, the combustion of soot may become self-sustaining, and thermal runaway could happen. Therefore, low soot loading is preferred in passive regeneration to avoid catastrophic thermal failure.

In active DPF regeneration, when ΔP_{loaded} exceeds a certain preset threshold, regeneration is triggered to occur. In addition to the above mentioned measures of raising the exhaust temperature, other methods may also be adopted, some with additional costs, to precisely control the course of regeneration and regeneration efficiency. The methods include: (1) using a fuel-fed burner; (2) electrical heating; (3) microwave; (4) compressed air; (5) using controlled pre-DOC or post-DOC dosing of hydrocarbons as a catalyst to generate sufficient heat energy to regenerate the DPF; (6) using a transmission to force the engine to operate at high load; and (7) producing oxidants such as NO_2 turnover from the NO in DOC or CDPF in order to oxidize carbon soot (reactions: $NO + 0.5O_2 = NO_2$, $2NO = NO_2 + 0.5N_2$, $C + NO_2 = NO + CO$). It is noted that NO_2 is much more toxic than NO; but after leaving the tailpipe NO will be converted to NO_2 in the atmosphere anyway. For low engine-out NO_x emissions, there is an impact on the NO_2 oxidant available for DPF regeneration.

Dynamic precise control of the DPF regeneration process is needed for several reasons as below. A dangerous phenomenon called ‘hill-cresting’ refers to thermal runaway (meltdown) with uncontrolled, excessively high soot-burning temperature inside the DPF when regeneration occurs immediately before the end of a high load condition, or in other words when engine speed/load decreases during the course of regenerating the DPF. After engine load or EGR rate decreases or speed changes, the air–fuel ratio may increase, the exhaust flow rate may become lower, so that the rate of convective cooling

inside the DPF is reduced, and the temperature may rise unacceptably high to cause durability issues. Moreover, it is important to control the regeneration burn-off rate (i.e. slowed down) and the temperature spatial gradient because they affect the thermal stress and fatigue life of the DPF. The burn-off rate can be slowed down or optimized by either increasing or decreasing the exhaust flow rate. It can also be slowed down by reducing the oxygen concentration via air–fuel ratio reduction or EGR rate increase.

Secondary emissions may occur during regeneration, such as the following: the CO from incomplete soot burning; evaporaton of the adsorbed HC and SOF during a slow exhaust heating phase without being oxidized; the unburned hydrocarbons of post-injection during DPF heating; the NO_x due to shutting off EGR or due to the soot oxidation reaction of $C + NO_2 = CO + CO_2 + NO$; sulfuric acid aerosol nanoparticles created by the catalyst; and organic compounds nucleated downstream of the DPF. Using ultra-low sulfur fuel, low-sulfur lube oil and a sulfur trap may eliminate the aerosol nanoparticles. The effectiveness of DPF regeneration also depends on the sulfur content in the diesel fuel.

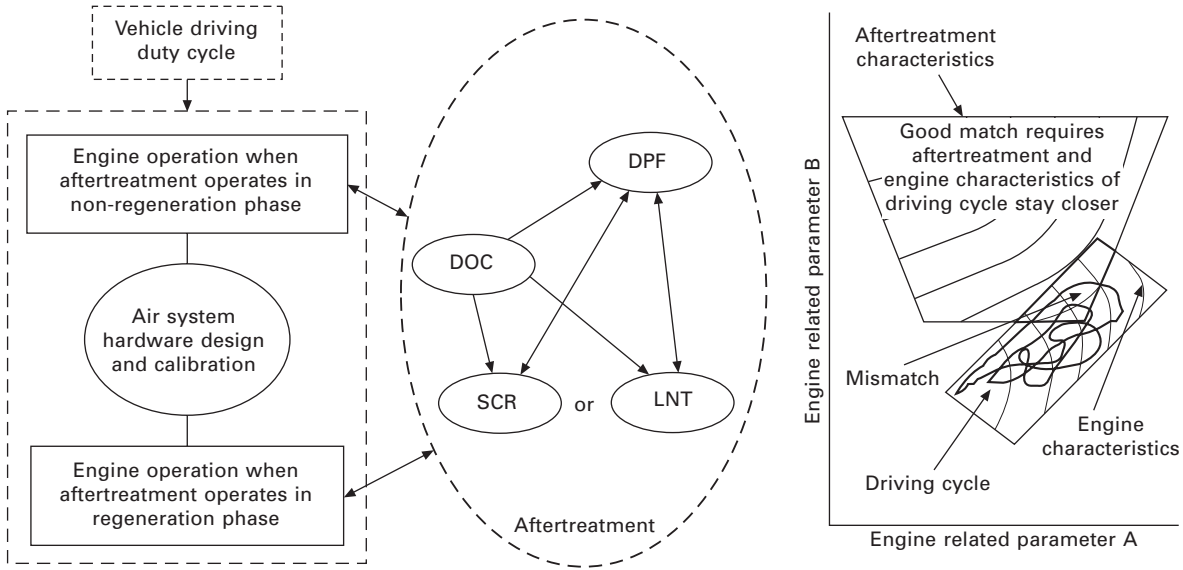
An important goal of engine air system design is to robustly adapt to the varying exhaust restriction caused by DPF soot loading change, and to achieve the capability required for optimum DPF regeneration at all ambient conditions and operating modes. Vehicle driving cycle simulation plays a critical role in analyzing the exhaust temperature windows as functions of time and occurrence frequency for optimized DPF matching and regeneration.

12.5.3 Analytical procedure of engine–aftertreatment integration

The analysis tasks of engine–aftertreatment integration or matching need to start with analyzing the requirements of exhaust temperature, flow rate and constituent concentrations (O_2, HC, CO, NO, etc.) at the inlet of each aftertreatment device (DOC, SCR or LNT, DPF, etc.) for their normal operation and regeneration in the entire engine speed–load domain. The common requirements need to be consolidated and the differences need to be identified. Finally, the optimum air handling system needs to be designed to minimize BSFC and maintain good durability for the whole engine–aftertreatment system. A similar approach of engine–vehicle matching and engine–turbocharger matching may be used in engine–aftertreatment matching, i.e., plotting engine operating data on aftertreatment characteristic maps of the non-regeneration and regeneration phases.

The process of engine–aftertreatment performance matching is proposed to consist of the following five steps (Fig. 12.30):

1. Understand aftertreatment design and operating features for both normal operation and regeneration, and create characteristic maps for each device



12.30 Engine–after treatment matching.

(DOC, DPF, SCR or LNT) where the characteristics need to be presented as functions of engine performance-related parameters (such as flow rate, temperature and gas mass, and certain fundamental combinations of them) and chemical parameters (such as the NO_2:NO_x ratio) in order to facilitate the matching in the next steps. The characteristic responses may be presented in contours, for example the chemical reactions involved, light-off temperature, DPF 'balance point temperature', temperature windows, species conversion efficiency, other efficiencies, size, storage capacity, flow restriction, loading performance (e.g., DPF or LNT load-up rate), heat losses, regeneration energy and temperature, thermal durability, etc. Identifying the fundamental influential parameters and constructing such characteristic maps are the important tasks for aftertreatment suppliers when they cooperate with engine manufacturers.

2. Analyze engine–aftertreatment calibration DoE test data to understand the aftertreatment performance on the engine. Engine manufacturers are responsible for this step.
3. Match engine and each aftertreatment device by plotting engine performance characteristic data (e.g., exhaust gas temperature, flow rate and engine-out emissions in the engine speed–load domain, at various ambient and altitude conditions) on aftertreatment characteristic maps; or vice versa, whichever is more convenient. Engine manufacturers hold a major responsibility for this step.
4. Discover any mismatch in both normal operation and regeneration from the maps; revise engine air system controls and reconstruct the matching maps, or reselect aftertreatment; and finally optimize all the links between different aftertreatment devices and the engine–aftertreatment interface. The supplier and engine manufacturer need to work together to accomplish this step. During the matching, engine air system performance and vehicle transient driving duty cycle simulations will need to be largely adopted. In addition to aftertreatment design and cost, important performance matching topics include the following, especially focused on fuel consumption and aftertreatment durability:
    - Select the optimum location and sequence of each aftertreatment device based on engine and aftertreatment steady-state and transient performance criteria (e.g., during turbo lag).
    - Reduce the mismatch in the temperature windows and space velocity windows.
    - Arrange exhaust thermal management to minimize the thermal energy required (e.g., bypass or in-line regeneration). Turbocharger efficiency, air–fuel ratio and EGR rate all have a direct impact on the turbine outlet exhaust temperature and aftertreatment performance.
    - Select the optimum catalytic or precious metal amount based on the balance between engine and aftertreatment.

- Control back-pressure variations and the pressure drop of aftertreatment for engine performance.
- Optimize DPF regeneration methods (active or passive) and control the regeneration process.
- Minimize the regeneration fuel economy penalty by balancing engine–aftertreatment as a whole.
- Minimize the risk of temperature-induced aftertreatment durability problems.
- Minimize the engine power surge during aftertreatment regeneration for vehicle drivability.

5. Finalize the engine-out emissions target and the requirements from aftertreatment perspectives for the design of the engine air system and electronic controls.

12.6 Engine heat rejection and base engine characteristics

12.6.1 Energy balance analysis

Thermal load and challenges in heat rejection control

Turbocharged diesel engines have a higher thermal load than non-turbocharged engines. The thermal load is typically characterized by a higher intake manifold temperature (caused by the hot compressor outlet air temperature), in-cylinder gas temperature and exhaust manifold gas temperature. The higher thermal load causes many durability problems, such as cracking in the cylinder head and piston, and damage in the turbine rotor. Managing thermal load and reducing the exhaust manifold temperature have been important design issues for turbocharged engines. The successful measures include the following: (1) reducing the intake manifold temperature by using air charge cooling; (2) increasing fresh air scavenging from intake port to exhaust port by increasing the pressure difference between intake manifold and exhaust manifold through turbocharger matching or manifold design; (3) increasing fresh air scavenging by increasing the valve overlap; (4) reducing the compressor outlet air temperature by increasing the compressor efficiency; (5) increasing the air–fuel ratio to reduce the exhaust temperature; (6) enhancing the cooling capacity of the cylinder head; and (7) adjusting the heat release rate shape and injection timing to reduce the exhaust temperature.

However, EGR engines are different. Many of the above measures no longer apply to EGR engines. For example, enhancing fresh air scavenging with a negative engine delta P is impossible due to the need for driving EGR flow with a positive engine delta P. On the other hand, adding cooled EGR actually reduces the in-cylinder gas temperature and NO_x due to the higher heat capacity of the EGR gases, hence the exhaust gas temperature

can be reduced accordingly. But regardless of whether cooled by engine coolant, air or low-temperature radiator coolant, cooling the EGR increases the total engine heat rejection. The heat rejection increases as more EGR is used. A lower intake manifold temperature is desired for meeting more stringent emissions regulations. (There is an effort to recover the large amount of waste heat lost to EGR cooler heat rejection by using the organic Rankine cycle to convert the waste heat to mechanical shaft power so that both BSFC and heat rejection can be reduced.) Moreover, the increasing customer demand on engine power rating results in a directly proportional increase in fuel rate and coolant heat rejection. Sometimes the coolant heat rejection during engine braking may exceed that during full-load firing if the retarding power is very high for heavy-duty commercial vehicles equipped with engine brakes or retarders. The increased total heat rejection imposes a great challenge for vehicle front-end cooling package design in order to bring the engine-out coolant temperature under control. A critical system design task in engine–vehicle thermal management is to predict engine heat rejections at various hot ambient conditions and high altitudes for different cooling system configurations.

Energy balance analysis methods

The measurement of engine coolant heat rejection often contains large experimental errors in coolant flow rate and coolant temperature data. The heat rejection error can range from about 3 to 20 kW and become unacceptably large for precise design. This common error is a difficult problem when trying to measure engine cylinder coolant heat rejection directly. As a solution, an alternative approach needs to be used to calculate the coolant heat rejection by using the engine gas flow rate and gas temperatures in engine energy balance equations. Two methods of calculating the energy balance are proposed below, depending on where the control volume boundary is drawn.

Method 1 sets the control volume boundary for gas flows at the compressor inlet and turbine outlet, and for fuel flow at the fuel tank. If low-pressure-loop EGR is used, the boundary is set after EGR pick-up. For a coolant-cooled turbocharged engine, for example, the energy balance equation is given below:

$$\begin{aligned} & M_{comp}h_{comp\text{-}in} + M_{fuel}h_{fuel\text{-}in} + M_{fuel}q_{LHV} \\ & = \dot{W}_E + \dot{W}_{Eacc} + M_{exh}h_{turb\text{-}out} + \dot{Q}_{base\text{-}coolant} + \dot{Q}_{EGRcooler} \\ & \quad + \dot{Q}_{CAC} + \dot{Q}_{ISC} + \dot{Q}_{FuelCooler} + \dot{Q}_{miscellaneous,1} \end{aligned} \tag{12.42}$$

where M_{comp} is the compressor air or gas flow rate, $h_{comp\text{-}in}$ is the specific enthalpy of the compressor inlet air or gas flow, M_{fuel} is the fuel flow rate,

$h_{fuel\text{-}in}$ is the specific enthalpy of fuel flow at the fuel tank temperature ($M_{fuel}h_{fuel\text{-}in}$ is usually very small compared to the enthalpy of the air flows), q_{LHV} is the lower heating value of the fuel (depending on fuel formulation; note that the enthalpy of vaporization of diesel fuels is usually small compared to their lower heating value), $\dot{W}_E$ is the engine firing brake power, $\dot{W}_{Eacc}$ is a certain engine accessory power including alternator, air compressor and cooling fan, M_{exh} is the exhaust gas flow rate, $h_{turb\text{-}out}$ is the specific enthalpy of the turbine outlet exhaust gas flow, $\dot{Q}_{base\text{-}coolant}$ is defined as base engine coolant heat rejection (to be detailed later), $\dot{Q}_{EGRcooler}$ is EGR cooler heat rejection, $\dot{Q}_{CAC}$ is charge air cooler heat rejection, $\dot{Q}_{ISC}$ is compressor inter-stage cooler heat rejection (if any), $\dot{Q}_{FuelCooler}$ is fuel cooler heat rejection (if any), and finally $\dot{Q}_{miscellaneous,1}$ is miscellaneous energy losses such as the convection and radiation heat transfer from the exhaust manifold, EGR tubing (excluding EGR cooler), engine block and turbocharger surface, and the thermal energy of unburned or incompletely burned fuel (up to 1–2% of fuel energy), etc.

Method 2 sets the control volume boundary for gas flows at the intake manifold and turbine inlet, and for fuel flow at the fuel tank. If high-pressure-loop EGR is used, the boundary is set before EGR pick-up. For example, for a coolant-cooled turbocharged engine the energy balance is given below:

$$\begin{aligned} &M_{air}h_{IMT\text{-}air} + M_{EGR}h_{IMT\text{-}EGR} + M_{fuel}h_{fuel\text{-}in} + M_{fuel}q_{LHV} \\ &= \dot{W}_E + \dot{W}_{Eacc} + \dot{W}_{EGRpump} + \dot{W}_{supercharger} + M_{exh}h_{turb\text{-}in} \\ &+ \dot{Q}_{base\text{-}coolant} + \dot{Q}_{FuelCooler} + \dot{Q}_{miscellaneous,2} \end{aligned} \qquad 12.43$$

where $h_{IMT\text{-}air}$ is the specific enthalpy of the air flow entering the intake manifold, $h_{IMT\text{-}EGR}$ is the specific enthalpy of the EGR flow entering the intake manifold, $h_{turb\text{-}in}$ is the specific enthalpy of the turbine inlet exhaust gas flow, $\dot{W}_{EGRpump}$ is the EGR pump power (if any), and $\dot{W}_{supercharger}$ is the mechanical supercharger power (if any). It should be noted that $\dot{Q}_{miscellaneous,2}$ is lower than $\dot{Q}_{miscellaneous,1}$. Moreover, the heat rejections of the transmission cooler and other small auxiliary coolers are not explicitly included in the above equations. For example, the heat generated inside the transmission comes from the gear or torque converter frictional power losses, which are already a part of the engine output crankshaft power. Similarly, vehicle accessory resistance power such as from the power steering pump and air conditioning compressor needs to be overcome by part of the engine crankshaft power $\dot{W}_E$.

The equivalence between equations 12.42 and 12.43 can be derived and justified by the turbocharger power balance between compressor and turbine. The gas flow enthalpy is calculated by $h = \int_0^T c_p \cdot dT$ where the

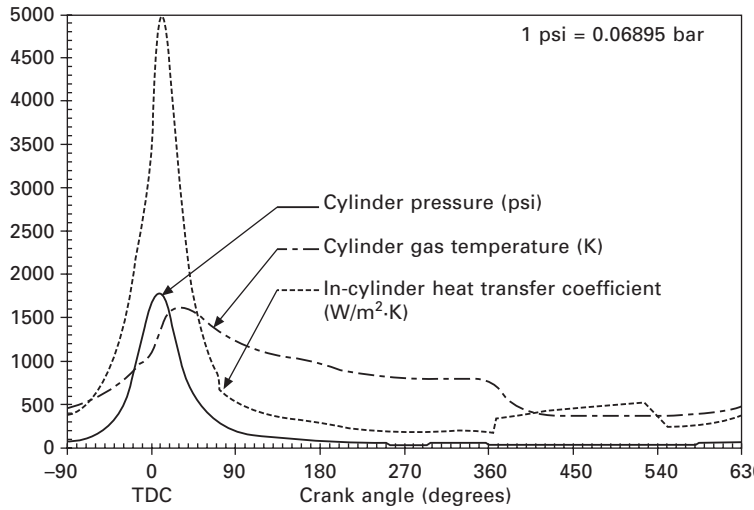
specific heat c_p must be used as a function of temperature and gas species composition here for acceptable accuracy. The cooler heat rejection can be calculated by:

$$\dot{Q}_{cooler} = M_{gas} c_p (T_{CoolerInletGas} - T_{CoolerOutletGas})$$

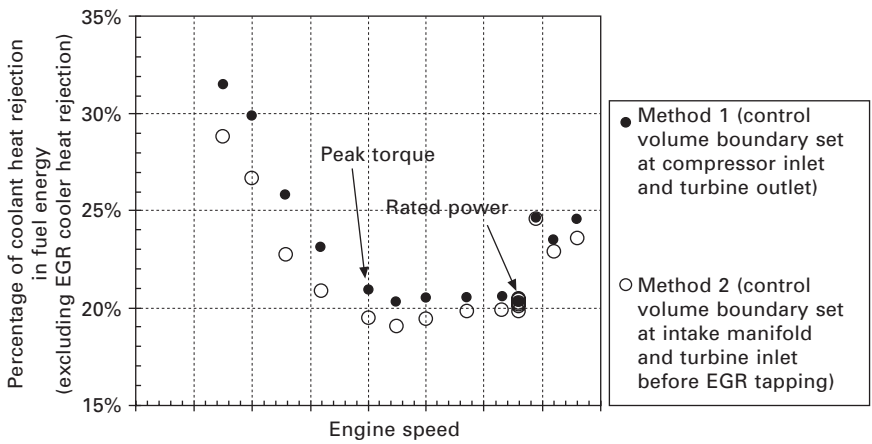
In order to characterize a base engine heat rejection to quantify design quality, it is important to distinguish two types of working fluids: the in-cylinder flows (including air, EGR and fuel) and the outside-cylinder cooling media (including coolant and oil flows). The pressures and temperatures of the gas and fuel flows at the entry of the cylinder are affected by their respective pumping power (e.g., a compressor or supercharger for fresh air, an EGR pump for EGR flow, a fuel pump for fuel flow) and cooler heat rejection (e.g., charge air, EGR or fuel cooler). The in-cylinder gas flows participate in the cycle processes and their energy leaves the cylinder as shaft work, exhaust enthalpy and heat rejection. On the other hand, the water pump power and oil pump power for pumping the outside-cylinder cooling media eventually just dissipate as heat rejection only. Therefore, it is usually convenient to define the base engine coolant heat rejection to include the heat rejections from the cylinders (piston, valves, liner and cylinder head, including exhaust ports) and oil cooler (piston cooling and mechanical rubbing friction), as well as water pump and oil pump power. The base engine heat rejection is a critical parameter which characterizes the fundamental design and operating features of the 'base engine' (i.e., excluding the effect of coolers, except for the oil cooler). Different engines can be compared on the common basis of the percentage of fuel energy entering the base engine coolant heat rejection in order to evaluate their competitiveness. It should be noted that if the cylinder heat transfer is the focus of the study, engine friction and water/oil pump power should be excluded from the definition of base engine coolant heat rejection.

In equations 12.42 and 12.43, the only unknown is $\dot{Q}_{base\text{-}coolant}$. If there were no experimental errors on gas temperature and flow rate measurements, theoretically the same result for base engine coolant heat rejection would be calculated using both methods 1 and 2. If the results from both methods are very different, there must be experimental errors in the test data. Therefore, the above energy balance methods can serve the following five purposes: (1) calculating coolant heat rejection accurately for cooling system design (note that vehicle radiator coolant heat rejection is equal to the sum of heat rejections from base engine, EGR cooler and other coolant-cooled coolers); (2) comparing the calculated coolant heat rejections of methods 1 and 2 with available heat rejection data from direct coolant flow measurement in order to verify the data accuracy for each method; (3) checking the accuracy of engine performance test data for gas temperature and flow rate; (4) revealing

the energy balance distribution and the competitive nature of the base engine design in term of heat losses; and (5) tuning the cylinder heat transfer model in engine cycle simulation to match test data on the percentage of fuel energy entering base engine coolant heat rejection (e.g., the tuned in-cylinder heat transfer coefficient shown in Fig. 12.31). Figure 12.32 shows an example of the energy balance calculations with engine test data at full load. It is observed that the results given by the two methods match well.



12.31 In-cylinder cycle simulation of gas pressure, temperature and heat transfer.



12.32 Energy balance calculation on full-load lug curve.

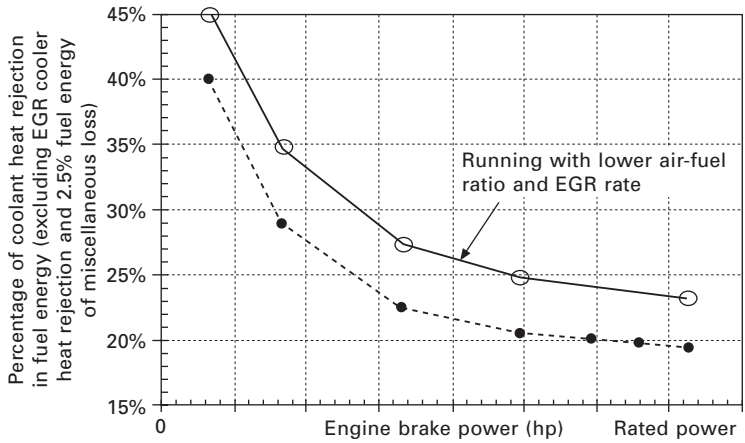
12.6.2 Base engine coolant heat rejection characteristics

Heavy-duty direction injection diesel engines usually have an oil cooler, which uses engine coolant as cooling medium. Consequently, the engine coolant heat rejection includes the heat removed by the oil. Oil cooler heat rejection mainly consists of two parts: piston cooling and engine rubbing friction power loss. For system simulation, the total rubbing friction can be obtained by subtracting the calculated pumping loss and accessory power from the measured engine motoring power. The engine accessories here include water pump, oil pump, fuel pump, alternator, air compressor for service brake, etc. A practical method for estimating motoring power is the Willan's line, where a plot of fuel flow rate vs. BMEP is used to extrapolate to zero fuel flow rate to determine the motoring MEP or power.

A more detailed global friction model (Taraza *et al*., 2000) of individual friction components (e.g., piston assembly, bearings, valvetrain) and auxiliaries is desirable in engine system simulation to enhance accuracy. Such a friction model retains most of the important design parameters of the component and relatively simple physics governing friction. For subsystem or component design analysis, a more detailed friction model is needed. A very complex tribological model of piston-assembly lubrication dynamics is shown in Section 12.10 as an example of an advanced analytical design tool used in mechanical subsystem design.

In addition to being characterized by the brake specific heat rejection, actually the base engine coolant heat rejection is principally characterized by its 'percentage' in fuel energy rate. The percentage is related to everything that affects the cylinder heat transfer area and instantaneous heat transfer coefficient, as well as friction. The relevant design or operating factors are cylinder bore diameter and stroke; volume-to-surface ratio; cylinder liner, piston and exhaust port design, especially the metal surface area exposed to heat transfer; swirl ratio and in-cylinder turbulence; the ratio between in-cylinder charge (air plus EGR) and fuel (note that the larger the ratio, the lower the base engine heat rejection 'percentage'); intake manifold gas temperature; fuel injection timing (note that the more retarded timing, the lower the 'percentage' but the higher the BSFC, Fig. 12.31); engine speed and load; mean piston speed; and water pump and oil pump power, etc. Good engine performance and low heat rejection design require a small percentage of fuel energy entering base engine coolant heat rejection. Figure 12.33 was obtained by cycle simulations and shows that the base engine heat rejection percentage increases when the engine load decreases.

The most critical parameter for engine cooling system design is heat rejection because it affects engine-out coolant temperature, durability and vehicle front-end cooling packaging. Once heat rejection is known, cooling medium flow rates of radiator and charge air cooler, water pump power and



12.33 Base engine coolant heat rejection percentage in fuel energy at constant speed.

cooling fan power can be calculated relatively easily. Heat rejection is directly affected by emissions control technologies such as turbocharging, intercooling, air–fuel ratio, EGR rate, fuel injection timing, combustion chamber design, swirl ratio and in-cylinder turbulence. The coolant temperature, the coolant-side convection heat transfer coefficient and the cylinder head material (cast iron or aluminum alloy) have relatively small impacts on coolant heat rejection. The compression ratio may have an impact on the percentage of fuel energy entering coolant heat rejection due to its effect on the surface-to-volume ratio of the combustion chamber.

Coolant heat rejection is dominated by the large gas-to-wall thermal resistance in the thermal boundary layer of the combustion chamber, rather than by the smaller wall-to-coolant thermal resistance on the coolant side. Despite the fact that ceramics have a much lower thermal conductivity than metals (by one or two orders of magnitude), 'adiabatic' (or so-called Low Heat Rejection or LHR) engines using ceramic materials as cylinder wall insulation do not reduce heat rejection by an order of magnitude. The reason is that the thermal resistance of the gas side plays a major role in the overall thermal resistance. Improving engine thermal efficiency through in-cylinder heat rejection reduction has been the key objective of LHR engines. In LHR research, it was found that there is a reduction in ignition delay and premixed combustion, and there is an increase in diffusion combustion duration compared to conventionally cooled engines. An adverse aspect of LHR engines is that the much hotter cylinder wall temperature heats up the induction air and results in a reduction in volumetric efficiency and an increase in NO_x emission. Overall, the findings and conclusions on LHR engines remain inconsistent and inconclusive. An improvement in LHR

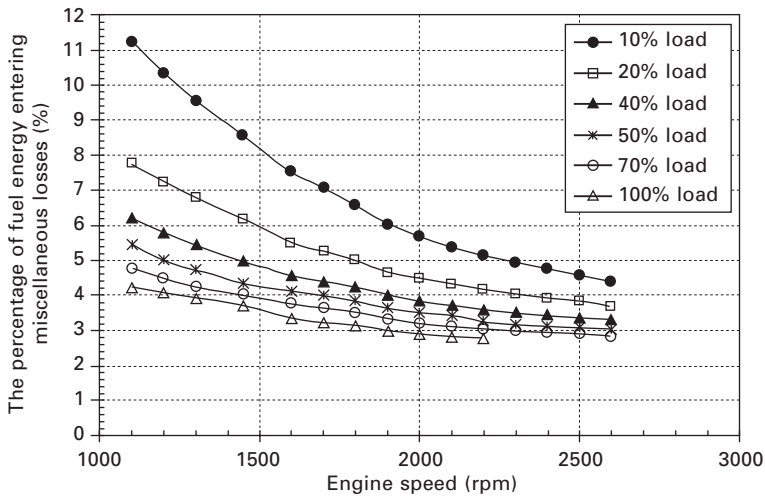
engine fuel consumption has been reported in the range of 4–10% (Jaichandar and Tamilporai, 2003). The in-cylinder heat transfer characteristics of LHR engines and their tribological impact are very complex and still not clearly understood in research.

12.6.3 Miscellaneous energy losses

In the energy balance equations 12.42 and 12.43, the miscellaneous loss is treated as a known quantity. In fact, its analysis is very complex. Its heat transfer part is related to engine speed (i.e., the time scale for heat transfer) and exhaust manifold temperature which depends on engine load. Figure 12.34 shows that the percentage of fuel energy entering the miscellaneous losses increases when engine speed or load decreases. For diesel engines, usually, if the losses due to incomplete combustion are negligible, 2–3% of fuel energy going to the miscellaneous energy losses (in energy balance method 1) is a reasonable estimate at full load from peak torque to rated power. A complete analysis on miscellaneous heat losses was provided by Xin and Zheng (2009).

12.6.4 Cooling system design and calculations

Cooling system performance is important for engine performance. The purpose of cooling is to maintain the engine metal component temperature and temperature gradient at appropriate levels (e.g., about 380°C for cast iron and a lower temperature for aluminum alloys, and 180–200°C for the top piston



12.34 Miscellaneous energy losses as functions of engine speed and load.

ring groove to prevent deterioration of lubricating oil film). Undercooled engines may have the following problems: loss of material strength, high thermal strain, lubricating oil degradation, overheating and scuffing of power cylinder components, heating intake air and lower volumetric efficiency, etc. On the other hand, overcooled engines may exhibit poor combustion and fuel economy, excessive heat rejection, high wear at piston rings and liner, high friction and noise. An excessively low cylinder liner temperature, even below the condensation temperature of burnt gases, may cause liner corrosion. The maximum cooling capacity of heavy-duty diesel engines is usually designed based on an in-vehicle condition running at rated power in summer at high altitude with air-conditioning switched on. At part load or in a cold climate, engine coolant can be excessively cold and can adversely affect engine combustion and performance. Moreover, overcooling in cooler design for certain operating conditions requires additional measures to fix the problem. For example, if the charge air cooler outlet air temperature is lower than the dew temperature, water is condensed in the cooler and requires a device to separate the condensation. Another example is the fouling problem of hydrocarbons and acidic vapor condensate in the EGR cooler when the EGR cooler outlet gas temperature is too low at part load.

To reach a target intake manifold temperature for emission control, there is also a balance between the charge air cooler size (or effectiveness) and the EGR cooler size within their allowable packaging constraints. Overcooling the intake manifold mixture may be detrimental to NO_x control because of the increase in ignition delay for the very cold charge and the resulting increase in the premixed portion of fuel injection and NO_x emissions.

EGR cooler performance deteriorates when a soot layer and sulfate particulates deposit on the cooling tube surface. The mechanism of EGR cooler fouling due to soot deposition is complex and largely depends on operating conditions such as soot amount and composition, exhaust gas temperature and flow rate, and flow pulsation. The most critical condition for soot fouling is at low speed and low load. The fouling resistance changes over time. The rate of change in cooler performance degradation due to fouling is initially quite large, but the cooler effectiveness may asymptotically approach a stabilized constant value after a long time (Zhang *et al.*, 2004). In typical driving conditions the higher exhaust gas velocity may have an abrasive self-cleaning effect to remove certain soot fouling to avoid tube clogging and maintain sufficient performance of heat transfer and pressure drop. In cooler sizing design specification, a sufficient margin of effectiveness and pressure drop should be reserved to account for EGR cooler soot fouling. A cooler soot-fouling model coupled with engine-vehicle driving cycle simulation is desirable to provide valuable insight on predicted deterioration of cooler performance.

In coolant selection, forced convection or sub-cooled boiling should be

maintained, and saturated boiling should be avoided. With saturated boiling, there is a risk of vapor blanket and film boiling which can cause insulation overheating and thermal fatigue of the component.

In cooling system design, various configurations with different cooling media and cooler arrangements may be proposed in order to control heat rejection with vehicle front-end packaging constraints while achieving the same intake manifold temperature target. The hottest engine-out coolant temperature usually occurs at an intermediate speed between peak torque and rated power due to the nature of the matching between engine heat rejection and operating characteristics of the radiator and water pump. Engine system analysis needs to be conducted at the harshest ambient conditions (e.g., sea level, at 38ºC or 100°F hot ambient, 1676 meters or 5500 feet altitude at 38°C, or 10 000 feet on a hot day) in order to cover the worst application scenarios of the highest engine-outlet coolant temperature. The elevated compressor inlet air temperature due to in-vehicle underhood heating should be considered. Moreover, the effects of using air conditioning and hot air recirculation around the radiator and charge air cooler should not be ignored when analyzing cooling medium temperature.

Cooler performance design specifications include effectiveness, heat rejection, and pressure losses at both gas side and cooling medium side. Cooler thermal performance calculations are basically based on two formulas: the definition of cooler effectiveness, and the equation for the heat transfer rate. Taking EGR cooler as an example, its heat transfer calculation is given below. The cooler effectiveness is defined as:

$$E_{cooler} = \frac{M_{gas} c_{p,gas} (T_{gas,in} - T_{gas,out})}{(Mc_p)_{\min} (T_{gas,in} - T_{coolant,in})}$$

$$= \frac{M_{coolant} c_{p,coolant} (T_{coolant,out} - T_{coolant,in})}{(Mc_p)_{\min} (T_{gas,in} - T_{coolant,in})} = \frac{T_{gas,in} - T_{gas,out}}{T_{gas,in} - T_{coolant,in}} \quad 12.44$$

The cooler heat rejection is expressed as:

$$\dot{Q}_{cooler} = K \cdot F \cdot \Delta T_{mean} \quad 12.45$$

where K is the overall heat transfer coefficient, F is the heat transfer area, and the mean temperature difference of the heat exchanger is defined as

$$\Delta T_{mean} = \frac{(T_{gas,in} - T_{coolant,in}) - (T_{gas,out} - T_{coolant,out})}{\ln\left(\frac{T_{gas,in} - T_{coolant,in}}{T_{gas,out} - T_{coolant,out}}\right)}$$

The cooler heat transfer rate can also be expressed as:

$$\dot{Q}_{cooler} = M_{gas} c_{p,gas} (T_{gas,in} - T_{gas,out})$$

$$= M_{coolant} c_{p,coolant} (T_{coolant,out} - T_{coolant,in}) \quad 12.46$$

For parallel flow cooling, the cooler effectiveness can be calculated by:

$$E_{cooler} = \frac{1 - \exp\left[\frac{-K \cdot F}{M_{gas} c_{p,gas}} \left(1 + \frac{M_{gas} c_{p,gas}}{M_{coolant} c_{p,coolant}}\right)\right]}{1 + \frac{M_{gas} c_{p,gas}}{M_{coolant} c_{p,coolant}}} = \frac{1 - e^{-NTU(1+\tau)}}{1+\tau}$$

12.47

For counter-flow cooling, the cooler effectiveness can be calculated by:

$$E_{cooler} = \frac{1 - e^{-NTU(1-\tau)}}{1 - \tau \cdot e^{-NTU(1-\tau)}} \quad 12.48$$

where the number of transfer unit (NTU) is defined as

$$NTU = \frac{KF}{M_{gas} c_{p,gas}}$$

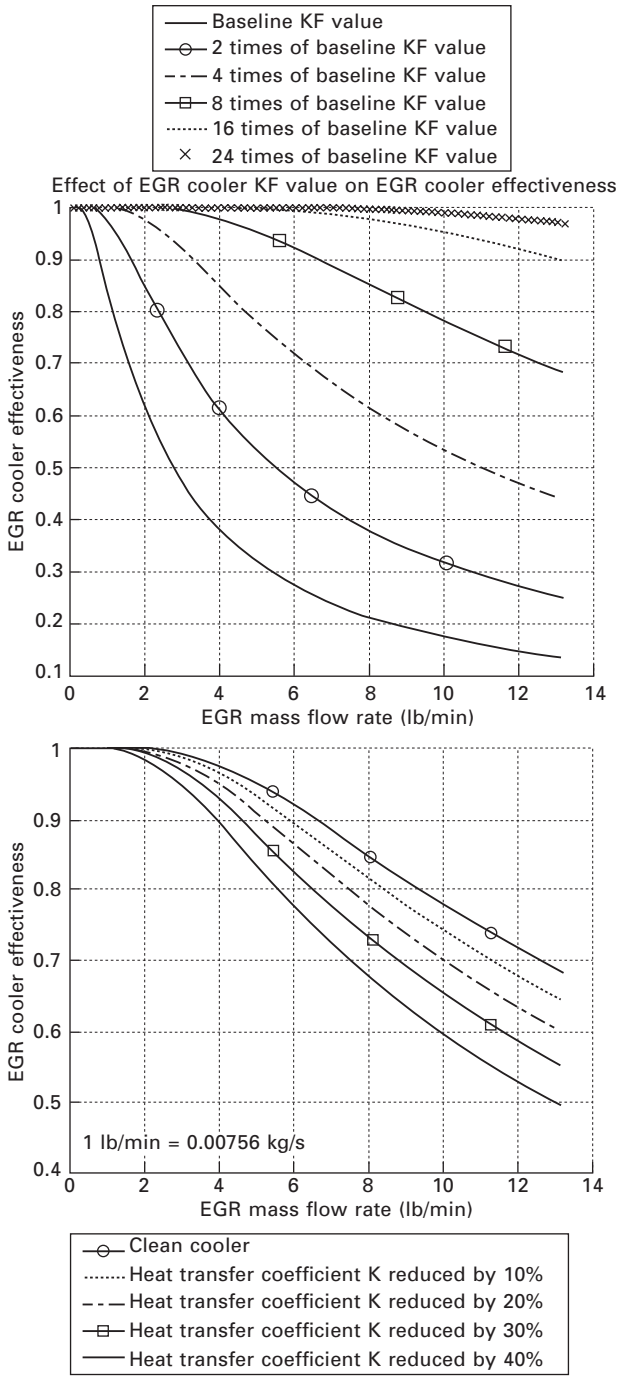
and

$$\tau = \frac{M_{gas} c_{p,gas}}{M_{coolant} c_{p,coolant}}$$

For the EGR cooler, the value of τ is very small (around 0.02). From equation 12.47 or 12.48, it is observed that the EGR cooler effectiveness is a function of the EGR gas mass flow rate and the cooler heat transfer capacity *KF*. The effectiveness does not depend on the cooler cooling medium temperature. Figure 12.35 shows the calculated characteristics of cooler effectiveness. The steady-state performance of the charge air cooler and vehicle radiator can be calculated in a similar way. In engine cycle simulation, the engine coolant temperature and cooler cooling medium temperatures can be calculated by the above equations if coupled with engine coolant heat rejection computation.

As to the transient performance of coolers, Pearson *et al*. (2000) provided a theoretical analysis of the wave-action model of the charge air cooler boundary and a methodology of predicting the instantaneous effectiveness and heat transfer coefficient of the cooler as a function of air mass flow rate. The simulation methodology of EGR and engine cooling systems and their controls was given by Chalgren *et al*. (2002).

Finally, it is worthwhile to notice the importance of cooling sink temperatures



12.35 Cooler effectiveness characteristics.

for engine performance. The sink temperature refers to the cooling medium inlet temperature. For the charge air cooler or radiator, the sink temperature is the cooling air temperature at the front of the cooler or radiator. For the EGR cooler and engine cylinder, the sink temperature is the coolant inlet temperature for the cooler or usually the radiator outlet coolant temperature. The radiator outlet coolant temperature can be calculated after the radiator coolant inlet temperature is calculated, provided the radiator heat rejection and coolant flow rate are known. By using two equations similar to 12.44 and 12.46, the following equation for solving the radiator inlet coolant temperature can be derived:

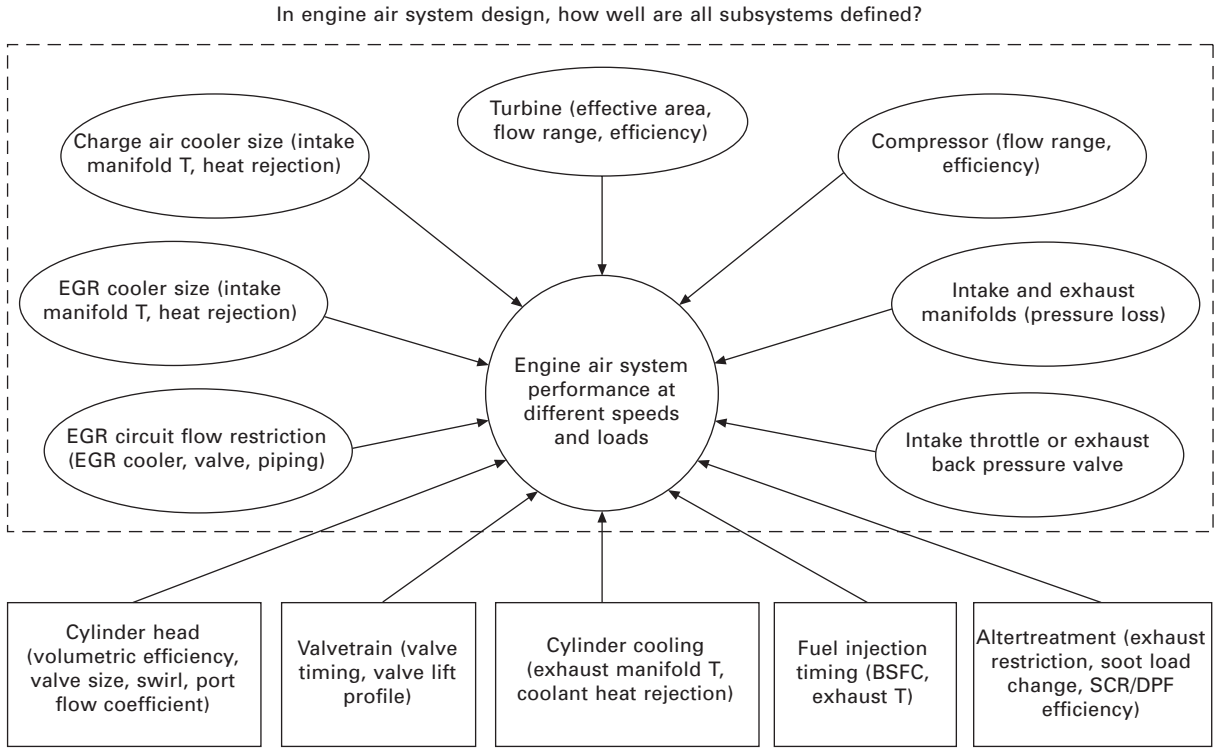
$$T_{RadiatorInletCoolant} = \frac{\dot{Q}_{RadiatorHeatRejection}}{E_{radiator}(Mc_p)_{min}} + T_{sink} \qquad 12.49$$

It is obvious that T_{sink} depends on the vehicle cooling system configuration (e.g., whether the charge air cooler is placed in front of or behind the radiator). Equation 12.49 is not only important for predicting the radiator inlet temperature in cooling system design and heat rejection control, but also necessary to close the loop in the prediction of engine coolant heat rejection by supplying refined or iterated sink temperatures.

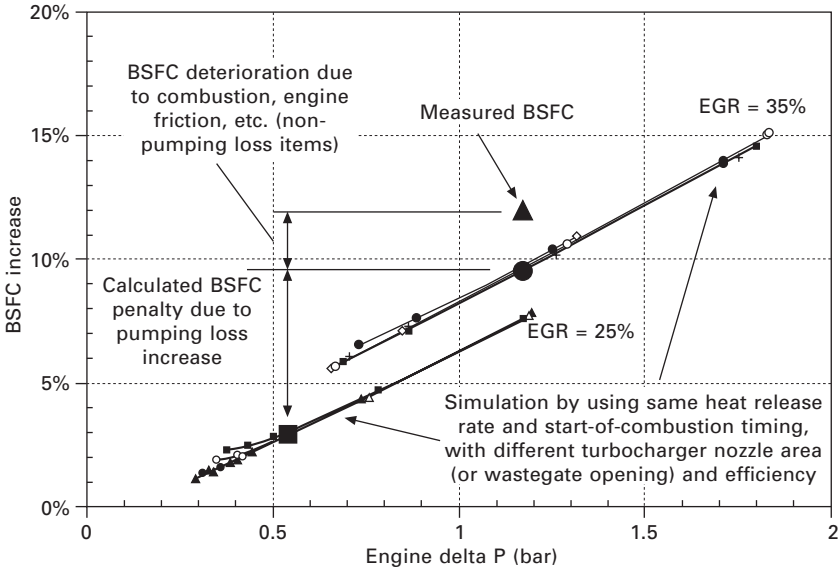
12.7 Pumping loss theory and the principle of engine air system design

12.7.1 The objectives of engine air system design

The diesel engine air system consists mainly of intake and exhaust manifolds, turbocharger, charge air cooler, EGR circuit, intake throttle and exhaust back-pressure valve. Its relationship with other systems is shown in Fig. 12.36. The goal of air system design is to achieve a desirable air–fuel ratio, EGR rate, exhaust gas temperature and oxygen concentration to meet the requirements of both engine-out emissions and aftertreatment operation with minimum pumping loss (high volumetric efficiency and low engine delta P) and low BSFC without violating design constraints in the desirable operating region of engine speed and load at all vehicle driving and ambient conditions. The constraints include the maximum limits of cylinder pressure, exhaust manifold temperature, compressor outlet air temperature and heat rejection, etc. Note that the requirements resulted from aftertreatment devices are new challenges for the air system. Figure 12.37 shows the direct correlation between engine delta P and BSFC. Earlier, Section 12.2 discussed the mathematical formulation behind the air system. This section will focus on its engine applications.



12.36 Boundary of air system design.



12.37 Effect of engine delta P on BSFC at rated power.

12.7.2 Overview of low emissions design and air system requirements

In base engine design with a given displacement, there are five factors directly related to air system performance in terms of volumetric efficiency, heat rejection, pumping loss and mechanical friction. The factors are: (1) number of cylinders; (2) stroke-to-bore (S/B) ratio; (3) valve flow area (number of valves and valve size); (4) valve overlap height; and (5) the 'K-factor' (the ratio between piston bowl volume and total combustion chamber volume at TDC) used to measure the proportion of air available for combustion. The larger the K-factor, the lower the dead volume in the combustion chamber. Fewer cylinders results in fewer parts and lower material cost but increases the reciprocating mass for each cylinder. At high speed, the reciprocating inertia force is high, and using more cylinders is an option to reduce the force. Increasing the number of cylinders increases the surface-to-volume ratio and heat losses. A larger S/B ratio reduces piston ring circumference and potential air leakage during cold start and may also reduce the surface-to-volume ratio for TDC volume and heat losses. A smaller S/B ratio can make the intake or exhaust valve size bigger to achieve higher volumetric efficiency and lower pumping loss. Engine friction and inertia force increase as mean piston speed increases, which is proportional to the S/B ratio. The K-factor affects air system design because it is related not only to the tolerances of piston assembly, cylinder head and gasket, but also to the size of

the valve recess or piston cutout and hence the valve overlap height at TDC. Valve overlap is a key design parameter for engine breathing performance and valvetrain dynamics. Reducing the clearance volume can increase the K-factor, reduce soot emission and improve the smoke limit. Competitive engine data analysis indicates that there seems to be a trend of the K-factor being a function of the S/B ratio. As the S/B ratio increases from 1.0 to 1.2, the K-factor range increases from 0.7 to 0.8 approximately. The optimum system design concept should be based on the best trade-offs among the S/B ratio, the K-factor and the valve overlap height.

In cylinder head design, the four-valve head is the prevailing design in modern diesel engines, with benefits such as higher volumetric efficiency compared with the two-valve head, enabling a centralized vertical fuel injector, the feasibility of shutting off one intake port to regulate swirl, a lower valvetrain weight and better valvetrain dynamics. In intake port design, the appropriate swirl ratio needs to be determined based on the following considerations: matching with fuel injection parameters for good penetration and mixing; matching with the combustion chamber shape for proper air motion and utilization; matching with the cylinder bore size to control wall impingement of the fuel spray and evaporation of the fuel film on the cylinder wall; a good trade-off with port flow discharge coefficient and volumetric efficiency; a proper balance between the swirl levels at low speed and high speed; and an acceptable cylinder coolant heat rejection loss, which is affected by in-cylinder air turbulence level. The current trend in heavy-duty diesel engine design seems to be to lower the intake swirl and to increase the fuel injection pressure, number of nozzle holes and combustion chamber diameter.

Compared to naturally aspirated engines, turbocharging with intercooling can increase the air–fuel ratio and reduce soot. With other means to reduce NO_x (e.g., retarding fuel injection timing), the overall emissions level of NO_x and soot can be reduced. In order to satisfy different air demands in a wide speed range in automotive diesel applications, the fixed geometry turbine has been gradually replaced by wastegate or variable geometry turbines. Turbocharging also enables EGR to be used because the engine delta P can be created by the turbine to drive EGR (in a high-pressure-loop EGR system) or a compressor can be used to pump EGR into the intake manifold (in a low-pressure-loop EGR system). Coordinated joint design of turbocharging, intake port and cam profile to match the EGR system is the key to fulfilling the air flow requirements over a wide speed range. The fundamentals on turbocharged EGR diesel engine air system configurations and performance were provided by Jacobs *et al*. (2003) and Hochegger *et al*. (2002).

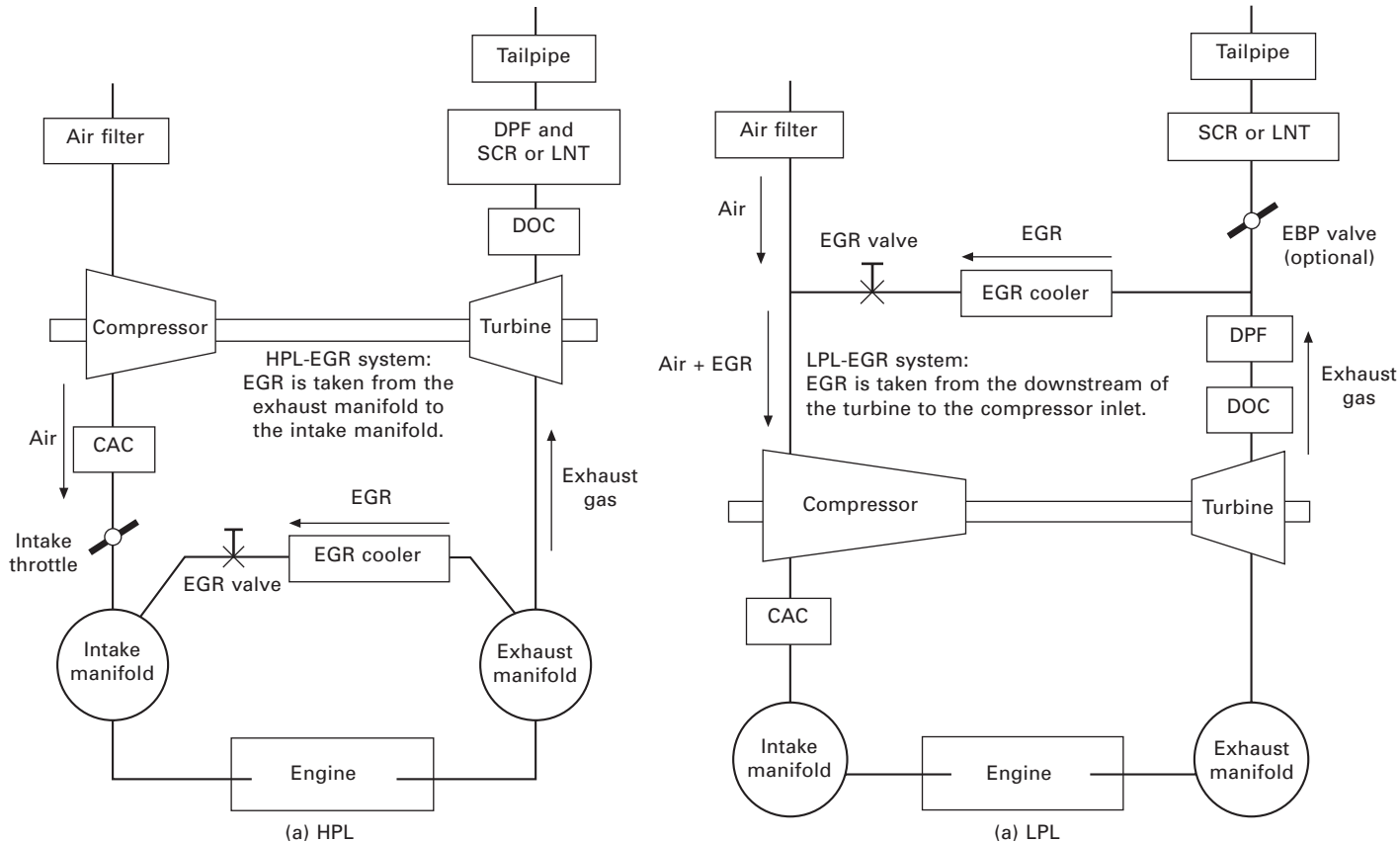
Exhaust manifold gas temperature is a critical parameter in air system design. It affects turbocharger performance and also has been used to judge the thermal loading on engine components. When the in-cylinder gas

temperature increases, the exhaust temperature and heat transfer to power cylinder components also increase. In the old era without an emissions-driven design approach, turbocharging parameters were selected based on a target turbine inlet temperature determined by the requirements of engine reliability and acceptable thermal loading. The required air–fuel ratio and large valve overlap were then calculated to achieve the target exhaust manifold temperature. Finally, the turbine inlet pressure and turbine flow area were determined based on the intake boost pressure and turbocharger efficiency. Now the situations are different due to an emissions-driven approach. The turbo selection criterion is based on air–fuel ratio and EGR rate to meet emissions, with the maximum exhaust manifold temperature as a durability design constraint.

12.7.3 EGR system configurations

Among various EGR systems, external cooled EGR is generally more effective than internal uncooled EGR (in-cylinder residue) for emissions reduction and fuel economy, although the external EGR heat rejection needs to be handled by the cooling system. The external EGR can be classified as high-pressure-loop (HPL) EGR, low-pressure-loop (LPL) EGR, and hybrid EGR systems. The HPL EGR uses the engine delta P created by the turbocharger to drive EGR from the exhaust manifold to the intake manifold. The EGR circuit flow restriction needs to be as low as possible, and the EGR cooler effectiveness needs to be sufficiently high even under fouled conditions. When the engine delta P is insufficient to drive EGR at low speed and high load, the following measures can be considered: reducing flow restriction of the EGR valve and cooler (e.g., using parallel EGR coolers instead of series); using a check valve or a reed valve to harvest pulse EGR flow and prevent EGR backflow loss; using a small turbine area such as VGT to raise engine delta P; using the intake throttle to lower the intake manifold pressure; using a venturi device to locally reduce the static pressure at the EGR merging location in order to induce EGR flow into the intake manifold; or using an EGR pump. Note that pumping loss always increases as engine delta P is raised.

In a clean LPL EGR system (Fig. 12.38) the EGR flow is driven by the pressure difference between the EGR pick-up location (usually downstream of the DPF) and the compressor inlet. EGR cooling is needed to prevent the compressor outlet gas temperature from exceeding allowable limits. EGR circuit flow restriction needs to be minimized because otherwise any artificial increase in the EGR-driving pressure differential beyond the ‘natural available free pressure differential’ provided by the system would lead to a large increase in pumping loss. The increase in LPL EGR circuit pressure differential can be achieved by closing an exhaust back-pressure



12.38 Turbocharged EGR engine systems: (a) high-pressure-loop and (b) low-pressure-loop EGR system mechanisms.

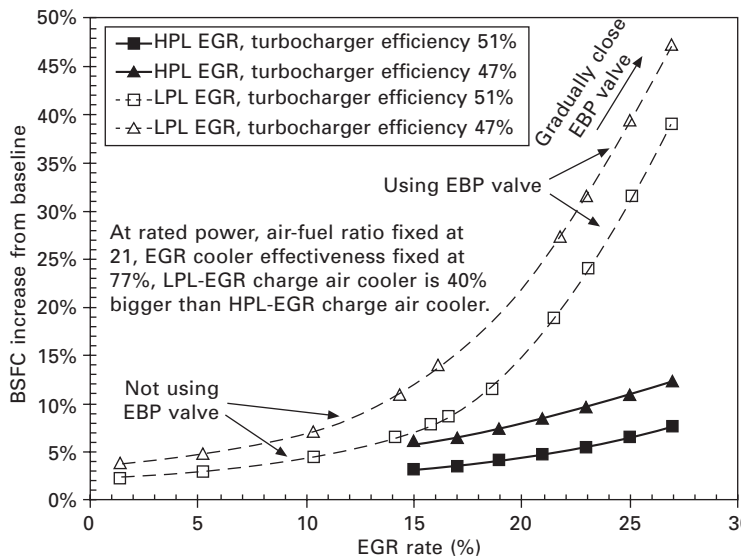
valve installed after DPF or closing an intake throttle valve at the compressor inlet. The latter option usually incurs a larger pumping loss.

At high speed and high load with a large EGR rate, HPL EGR is usually superior to LPL EGR due to its lower turbine power and pumping loss. At low speed and low load or a small EGR rate, LPL EGR may exhibit certain advantages if the compressor is better matched at higher efficiency. Hybrid EGR combines the advantages of HPL and LPL and provides the lowest pumping loss but at the price of increased design complexity and cost. Figure 12.39 shows a simulation comparison between HPL and LPL EGR at a heavy-duty rated power condition. Note that turbocharger efficiency has a significant impact. It shows that the LPL EGR system, if not designed correctly, may incur BSFC penalty.

12.7.4 Turbocharger configurations and matching

Turbocharger configurations

In general, exhaust turbocharging is superior to mechanical supercharging in thermodynamic efficiency. Turbocharging with intercooling may increase intake air density, power and fuel economy, while reducing combustion noise and emissions. Automotive turbocharger design has evolved from the early fixed geometry turbocharger to today's electronically controlled wastegate or variable geometry turbocharger (VGT) with high turbine efficiency of



12.39 Performance interaction between EGR system and turbocharging.

around 80%. The turbine nozzle must be designed to cause the exhaust gas to impinge on the turbine blades at optimum angle and velocity. The compressor diffuser must be designed to maximize the total pressure at the compressor outlet. The efficiency of centrifugal compressors depends on the design of the blade and diffuser. On the compressor map, there is a surge limit line on the upper left side and a choke limit curve on the lower right side. The limit lines represent boundaries between stable and unstable operation. Surge is a self-sustaining but unstable oscillation in flow rate and pressure ratio initiated by a flow reversal within the boundary layers on the compressor blades. Audible coughing and vibration occur when surge happens. Compressor choking happens when air velocity reaches the speed of sound at the inlet of the compressor wheel or diffuser. The flow rate at which choking happens varies with tip speed. The precise position of the choking curve on the compressor map is more difficult to determine than the surge line because it depends on the structure of the internal boundary layers. Sometimes for the purpose of approximation it is assumed that choking happens when compressor efficiency contours reduce to around 55%.

There are two types of turbocharging: pulse and constant pressure. In pulse turbocharging, in order to minimize the pressure wave interference or gap windage in exhaust scavenging between cylinders and to raise average turbine efficiency, the cylinders with a certain firing interval (ideally about 240° crank angles) are grouped together by using a small-volume exhaust manifold to preserve strong exhaust pressure pulses. A pulse converter may be used to eliminate pulse interference. Divided turbine entry may be used to totally separate the pulses of different groups, but may incur a larger pumping loss at high engine speed than an undivided turbine entry. In VGT, sometimes it is difficult to use divided turbine entry because of the extra controlling device. When unsteady energy flow is fed into the turbine, turbine efficiency may decrease. In constant pressure turbocharging, the exhaust flows of all cylinders are collected in one large-volume exhaust manifold to damp out all the pressure pulse fluctuation. A steady energy flow is fed into a single-entry turbine, and the turbine can be matched to better-known peak efficiency on the steady flow test map. The averaged turbine efficiency over an engine cycle with the unsteady flow of pulse turbocharging is usually lower than the peak efficiency matched in constant pressure turbocharging. But the efficiency loss is normally more than offset by the pulse energy available at the turbine. The overall exhaust energy utilization efficiency is actually characterized by the combination of pulse energy and turbine efficiency. Previous experiments indicated that at low compressor pressure ratio (e.g., part load), pulse turbocharging has higher overall efficiency than constant pressure turbocharging. But the situation is reversed at very high compressor pressure ratios because pulsed turbine efficiency is low at very high instantaneous turbine pressure ratios (e.g., above 3:1). During transient

acceleration, pulse turbocharging is superior due to its smaller exhaust manifold volume and faster response of the turbine inlet energy pulse to speed up the turbo. In EGR engines, pulse turbocharging used with a reed valve (check valve) can drive more EGR flow than constant pressure turbocharging with less penalty in engine pumping loss. The detailed theory of turbocharging non-EGR engines was provided by Watson and Janota (1982) and Watson (1999). The technology of turbocharging EGR engines was described by Arnold (2004).

Usually single-stage turbocharging can deliver a compressor pressure ratio around 3.5–4.5, depending upon wheel material and design. Compressor speed is limited by the allowable centrifugal force below the mechanical limit of the compressor wheel. Maximum compressor speed and aerodynamic blade shape limit the pressure ratio capability (Arnold, 2004). Moreover, aluminum alloy compressor wheels and casings are limited in material strength by a compressor discharge temperature of usually about 204–210°C (400–410°F). Titanium impeller wheels can resist much higher temperatures and deliver a very high pressure ratio with simple single-stage turbocharging, but titanium and its manufacturing process are expensive. Another disadvantage of titanium wheels is their heavier weight and larger inertia. Despite the disadvantages in cost, weight, cumbersome piping and packaging space, two-stage turbocharging is superior to single-stage in the following aspects: higher compressor pressure ratio; higher turbo efficiency due to the relatively lower pressure ratio in each stage; feasibility of using inter-stage cooling to reduce compressor discharge temperature and compressor power to improve efficiency; easier matching of turbo for a wider range of engine speeds with high rated power and peak torque; improved altitude capability due to a larger margin of choking; faster transient response due to the small high-pressure-stage turbo and its low rotor inertia; and improved low-cycle-fatigue life of compressor wheels and fewer durability problems associated with excessively high turbo speed. The turbo power split (or turbine sizing) between the two stages should be determined by the best overall BSFC between low speed (e.g., peak torque) and high speed (e.g., rated power), as well as by the resulting turbo efficiency and surge margin for each turbo. In the twin parallel turbo configuration, both turbines can be located very close to the cylinder heads of each bank to minimize the exhaust energy losses caused by manifold volume, pressure drop and heat transfer.

The advantages of VGT over wastegate turbines include the following: no wastegate valve throttling loss; ability to achieve a high air–fuel ratio and high peak torque at low speed as well as fast vehicle acceleration without encountering a large pumping loss penalty at high speed; and a lower engine delta P overall and a wider region of low BSFC in the speed–load domain. The VGT area change can be in either continuous or discrete settings, depending on the requirements of engine performance and reliability. The

maximum efficiency of most variable geometry turbines occurs at a vane opening of around 60–70% . At fully open and fully closed vane openings, the efficiency drops rapidly. The challenges of VGT design include minimizing gas leakage, increasing turbine efficiency, and enhancing reliability.

Compressor matching

The turbocharger is one of the most expensive components in the engine and therefore deserves close commercial attention. The selection of turbocharger size (flow range and pressure ratio) and efficiency is based on the requirements of delivering the best air–fuel ratio and EGR rate as well as transient acceleration performance. The objective of turbo matching is to achieve the best compromise in the engine speed–load range.

The turbocharger test procedure was outlined in SAE J1826 Turbocharger Gas Stand Test Code (1995). In principle, the compressor map can be generated in a flow bench test by regulating two valves, one installed at the inlet of a driving turbine, and the other installed at the compressor outlet. At each turbine valve opening, the compressor outlet valve is gradually closed to obtain a series of compressor flow points from high to low until surge, and the compressor speed remains almost constant. Such a process is repeated at a larger turbine valve opening to obtain another series of compressor flow points at a higher shaft speed.

The focus of engine–compressor matching is to analyze engine operating characteristic points or lines at various speed, load and ambient conditions on the compressor map. Diesel engine characteristic lines include full load (lug curve), constant-speed curve, constant-load curve, etc. The slope of the constant-speed curve on the compressor map, which is the ratio between pressure and mass flow rate, basically reflects the reciprocal of engine volumetric efficiency. Therefore, any factors affecting volumetric efficiency may have an impact on the shape of engine speed characteristic lines. Those factors include valvetrain design (valve size, timing and lift profile), port flow discharge coefficient, intake port heating, engine delta P, intake manifold temperature, etc. Volumetric efficiency will be further discussed in Fig. 12.42 later.

In order to form a cost-effective ‘family’ of designs, different blades with various tip widths and eye diameters are produced for one compressor impeller wheel frame size (or casting). The compressor ‘frame size’ is determined by the engine maximum air flow rate requirement. The design parameters such as the wheel inducer diameter, wheel and shroud contours and diffuser width determine the compressor trim. These ‘trims’ offer different surge and choke flow characteristics as well as efficiency variation. Compressor efficiency and shaft speed characteristic curves on the map can be further fine-tuned by using different trims with changes in impeller splitter blade

outlet angle, diffuser entry angle, diffuser geometry, etc. For example, changing the diffuser entry angle or blade eye diameter can 'rotate' the map curves around the origin of the coordinates so that the compressor surge line moves. It should be noted that changing the aerodynamic design also affects the compressor tip speed and the stress in durability. Turbocharger design details were provided by Rodgers and Rochford (2002), Watson and Janota (1982) and Watson (1999).

Centrifugal compressor matching guidelines are summarized in the following:

1. The matching should suit the normal operating environment of the engine, and should also be conducted at extreme ambient conditions from sea-level cold winter to high-altitude hot summer with minimum fueling de-rating to make sure the matching does not violate all design constraints.
2. Always use a single turbocharger whenever possible to reduce cost, weight and complexity.
3. Provide a proper pressure ratio and air flow rate at all engine speed–load modes, including zero-EGR conditions (fast transient, aftertreatment regeneration, cold climate).
4. There should be no compressor surge along the full-load lug curve, especially below peak torque speed. A proper margin (10–15% of surge flow rate) should be reserved to protect for transients and intake flow variation at various ambient temperature (e.g., cold climate) and high altitude conditions, as well as for the extreme case of high intake restriction caused by air filter blockage.
5. The compressor flow range should be wide enough so that there is no compressor choking and overspeeding at all altitudes and ambient temperatures (i.e., no sonic flow inside the compressor or no operation in the very low-efficiency region such as less than approximately 55%).
6. Provide an acceptable turbine inlet temperature below the limit with a sufficiently high air–fuel ratio and EGR rate. High compressor efficiency is desired to reduce compressor outlet charge temperature.
7. Full-load and typical vehicle driving modes should be matched in the high-efficiency region on the compressor map in order to reduce pumping loss. Minimum fuel consumption in a given driving cycle can be set as the target of matching optimization.
8. The compressor's moment of inertia should be as small as possible to reduce the turbocharger lag for good engine transient acceleration performance.
9. Compressor durability life needs to be acceptable. The turbocharger life is mainly determined by the low-cycle-fatigue (LCF) life of the compressor wheel under cyclic loading at low frequency. The compressor

impeller life is dictated by its maximum tip speed, the difference between the maximum and minimum turbo speed in typical speed–load driving cycles or aftertreatment regeneration cycles, and the cycle frequency. Those factors can be shown in the load cycle diagram of 'turbo speed vs. driving time'. In turbo matching, the maximum turbo speed limit is determined by calculating the compressor fatigue life based on transient vehicle duty cycle, strain, impeller material (aluminum or titanium) and historical warranty data (Ryder *et al.*, 2002). Maximum fueling needs to be restricted at high engine speed in order to limit the maximum turbocharger speed.

10. There should be no oil leakage from the bearing area to the compressor section caused by an improper pressure differential across the compressor with a given sealing design.

Turbine matching

The turbine flow characteristic map shows the turbine corrected flow rate as a strong function of the turbine pressure ratio and a weak function of the turbine speed. The turbine map can be generated on a flow bench by regulating the turbine inlet pressure and the compressor power (load). The process is repeated until each shaft speed line is obtained. Turbine efficiency is a strong function of the blade speed ratio u_T/C_0 and a weak function of the pressure ratio, usually with high efficiency located at a large pressure ratio and a high flow rate. Denoting u_T as the tip speed of a radial turbine rotor ($u_T = \pi d_T N_T$) and C_0 as a theoretical velocity that would be achieved if the gas expanded isentropically from turbine inlet condition to outlet pressure, the C_0 can be calculated as

$$C_0 = \sqrt{2c_p T_{03}\left[1 - (P_4/P_{03})^{\frac{\gamma_t - 1}{\gamma_t}}\right]}$$

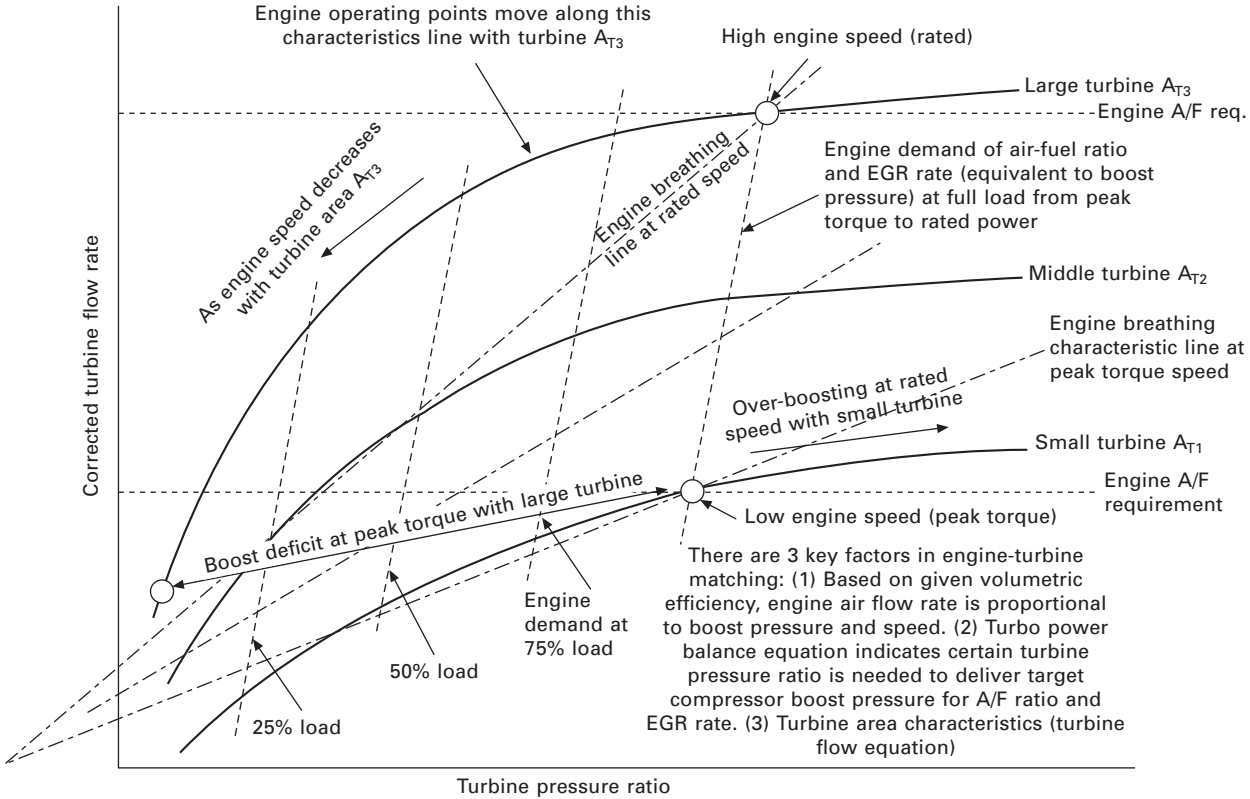
Usually, a larger turbocharger has higher efficiency because of its lower clearance-to-wheel-diameter ratio and associated less leakage. It should be noted that the measured turbine map efficiency is the adiabatic efficiency multiplied by the mechanical efficiency. The efficiency map is significantly affected by the heat transfer from turbine to compressor via the turbocharger housing at a low flow rate. The heat transfer decreases the measured turbine inlet temperature and increases the compressor outlet temperature, which renders the compressor efficiency artificially low and the turbine efficiency artificially high. The turbine efficiencies measured by different turbocharger manufacturers may not be directly comparable because differences in the method of taking the measurement data and gas stand

design (for example, different turbine inlet temperatures causing different heat transfer effects).

The turbine flow range is determined by an 'A/R' ratio, which is the ratio between the smallest area of the turbine housing inlet passage to the radial distance from the shaft centerline to the centroid of the inlet area. A smaller A/R ratio or turbine cross-sectional area produces a higher tangential gas velocity impinging the turbine blades, so that a higher turbine speed, pressure ratio and compressor boost pressure can be achieved. However, a small A/R also increases the exhaust manifold pressure and engine pumping loss. Once the compressor frame size and turbine rotor wheel size are selected, a range of casings with different volute cross-sectional areas or different nozzle stator rings (with various blade angles) can be chosen for the rotor, depending on engine flow requirements. In VGT either the A/R ratio or the nozzle vane is adjustable, discretely or continuously. A VGT may have lower efficiency than a fixed geometry turbine due to larger clearances and flow disturbances. Figure 12.40 illustrates the principle of matching engine and turbine. In the figure, the cross-over point between the engine breathing characteristic line at a given engine speed and the line of the air–fuel ratio requirement determines the required turbine effective area.

The turbine matching guidelines are summarized in the following:

1. The turbine size needs to be small enough to drive EGR flow at low engine speeds (e.g., peak torque), and appropriate to deliver sufficient power to drive the compressor to produce the required air–fuel ratio for peak torque and lower speeds at full load. The turbine effective area, which is controlled by the nozzle ring or volute, needs to be selected to provide the best trade-off between high speed/load and low speed/load. If a small turbine area is sized for peak torque, wastegating is probably needed at the rated power in order to prevent over-boosting so that the peak cylinder pressure is below the structural limit. (Note that peak compression pressure may be calculated approximately by $P_{comp} = P_{boost}\Omega^{1.36}$ where Ω is engine compression ratio.) If the pumping loss penalty associated with a wastegate turbine is not acceptable, the more sophisticated VGT may be considered at higher cost.
2. The necessity of turbine wastegating at various ambient conditions needs to be checked to prevent turbo overspeeding.
3. There should be no turbine choking. In pulse turbocharging, it is necessary to size the turbine frame large enough for the highest instantaneous flow rate.
4. Appropriate turbine efficiency is desired, being neither too high nor too low, to deliver turbine power to match the engine need on the air–fuel ratio and EGR rate. Occasionally, the turbine or compressor is deliberately matched in the low-efficiency region for the purposes of holding down the boost pressure and hence the maximum cylinder pressure at high



12.40 Engine–turbine matching theory.

engine speed below the design limit, or creating a high engine delta P with a small turbine area to flow EGR at low speed. Some special EGR configurations require the turbocharger efficiency to be as high as possible, and in such circumstances the turbocharger may become the limiting factor in engine development.

5. There should be no size mismatch or speed mismatch between compressor and turbine for good aerodynamic performance. Driving a large amount of EGR requires a small turbine area to build up a high engine delta P, and the turbine corrected flow rate may be much lower than the compressor corrected flow rate. Matching a relatively large compressor (driven by a high rated power requirement) with a very small turbine (driven by a high EGR requirement at low engine speed) will give poor turbo performance due to their speed mismatch. If their size difference is too large, the turbine efficiency may decrease and the turbocharger bearings may wear due to excessive axial loading. Possible counteraction includes balancing trim size (turbine exducer or compressor inducer flow area) and impeller size between the turbine and the compressor (Arnold, 2004).
6. For fast transient performance, the turbine size (or A/R ratio) or moment of inertia should be as small as possible to reduce turbocharger lag, for example by using light ceramic turbine wheels.
7. Pulse turbocharging with proper turbine entry may be considered to better use exhaust energy to increase the part-load air–fuel ratio and improve transient acceleration performance.
8. The turbine power split between the stages in two-stage turbocharging needs to be optimized for EGR driving, BSFC, compressor outlet temperature control, and the risk of compressor surge or choking in the two stages. The transition between the two stages at different engine speeds needs to be smooth and should not cause a high engine delta P.
9. Turbine durability life needs to be acceptable. The steel turbine wheel and iron housing must withstand the exhaust manifold gas temperature. The temperature limit is governed by the creep and scaling properties of the turbine wheel and housing materials.

Turbocharger performance at extreme ambient conditions

The turbocharger performance at high altitude can be explained by the four core equations of the air system, 12.11, 12.15, 12.18 and 12.28. As the air density and air mass flow rate reduce, the turbine inlet temperature will rise due to the lower air–fuel ratio. As ambient pressure falls, turbine pressure ratio increases. Therefore, turbo speed and compressor pressure ratio increase so that the inlet air density reduction is partially compensated to alleviate fueling/power de-rating. At hot ambient, the air–fuel ratio decreases, and the operating limits are usually smoke and turbine inlet temperature. At cold

ambient temperature, the maximum cylinder pressure or compressor surge may be the limiting factors. Large variation of ambient temperature or altitude may cause problems in turbocharging such as compressor surge, choking, overboosting, compressor overspeeding, excessively high exhaust manifold temperature, low air–fuel ratio, and engine smoke. The situation is further complicated by the EGR strategy used at various ambient conditions. For example, the compressor may choke when the EGR valve is fully closed at high altitude. Engine power de-rating strategy needs to be assessed at high altitude.

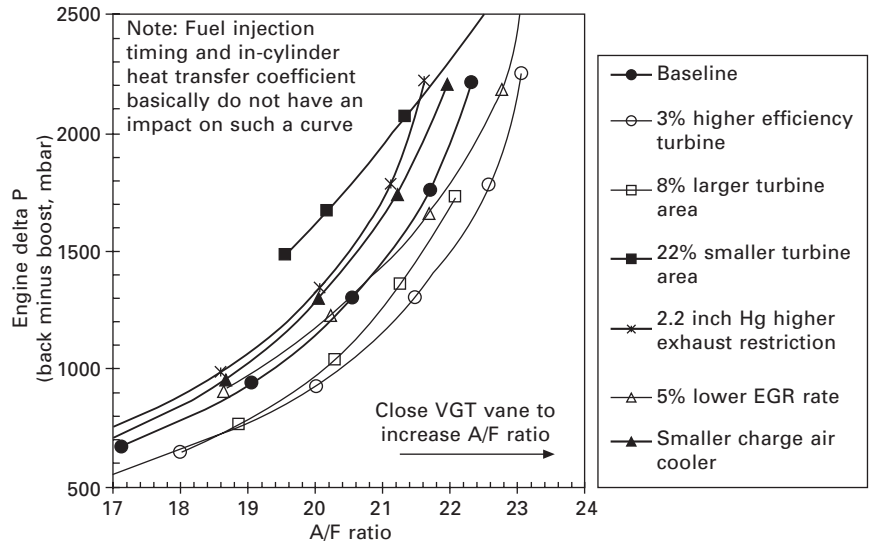
12.7.5 The design of the turbocharged exhaust system

The efficiency of the turbocharging system is characterized by $E_t = E_i E_{TC}$, where E_i is the efficiency of energy transfer from in-cylinder to turbine inlet, and E_{TC} is the turbocharger efficiency, which is equal to $E_C E_T E_M$. Usually, at the same engine speed, E_i decreases as engine load decreases; and at the same engine power, E_i decreases as engine speed decreases. In engine design, a more convenient parameter than E_i is pressure loss. The following factors can increase pulsed energy utilization and E_i:

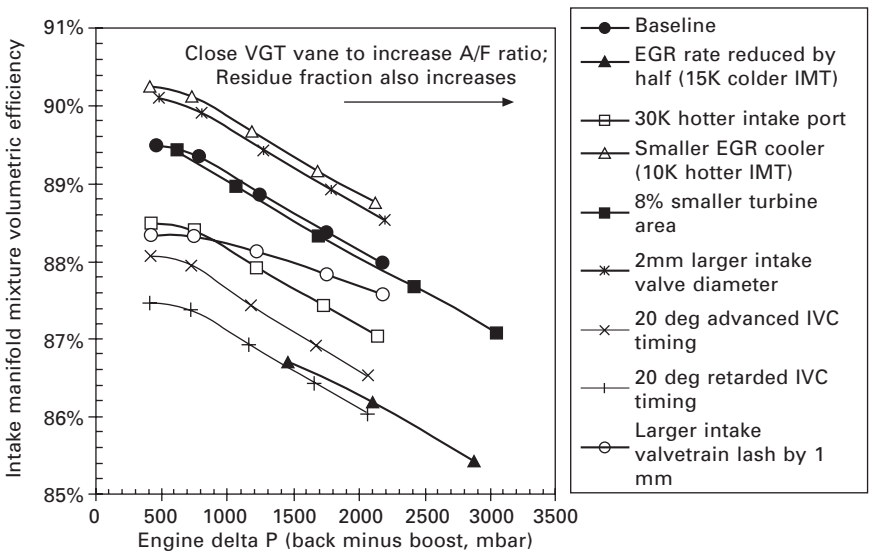
- Fast exhaust valve opening, large exhaust valve diameter and high valve lift. During the exhaust stroke, it is necessary to reduce the throttling loss of exhaust valve supersonic flow, the flow restriction/friction and exhaust manifold pressure in order to reduce pumping loss.
- Proper exhaust runner grouping and turbine entry design (divided or undivided entry).
- Optimum cross-sectional area of the exhaust manifold pipe (affecting pressure wave dynamics).
- A short exhaust runner and manifold piping without sharp turns or abrupt changes in cross-sectional area.

12.7.6 The principle of pumping loss control in turbocharged EGR engines

As discussed in Section 12.2, pumping loss consists of the contributions from engine delta P and intake manifold mixture volumetric efficiency. Figures 12.41 and 12.42 show the simulation data of the design effects on engine delta P and volumetric efficiency, respectively. In the figures, the EGR rate is kept constant (unless especially mentioned) by regulating EGR valve opening. Figure 12.41 shows that engine delta P is largely affected by the air–fuel ratio when VGT vane opening (turbine area) is regulated. In fact, if the air–fuel ratio is varied by changing the turbocharger efficiency without changing the turbine area, engine delta P basically will not be affected.



12.41 Design effects on engine delta P at rated power.



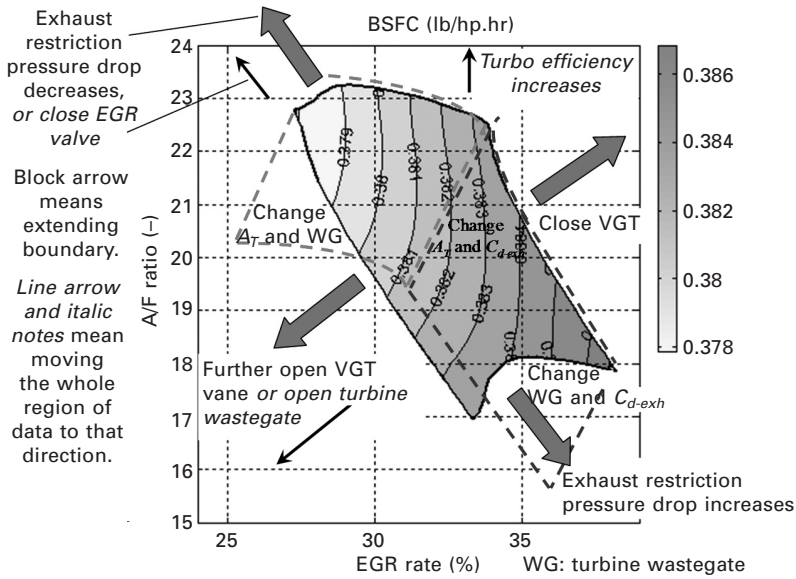
12.42 Design effects on volumetric efficiency at rated power.

From Fig. 12.42 it is observed that with given valvetrain and cylinder head design, volumetric efficiency is strongly affected by engine delta P because the in-cylinder internal residue fraction can be strongly affected by the pressure differential between exhaust port and intake port, depending on the valve

overlap size. As the residue fraction increases, volumetric efficiency decreases. Intake manifold temperature also strongly affects volumetric efficiency. At the same intake manifold mass flow rate, a hotter charge actually results in a higher value of intake manifold volumetric efficiency. The hotter charge can be produced by a smaller EGR cooler or a smaller charge air cooler. Therefore, when comparing the volumetric efficiency values of different engines to try to assess the design effects of cylinder head, valvetrain and manifolds, it is very important to align the values at similar or comparable intake manifold temperatures and engine delta P values in order to avoid misleading conclusions.

At each engine speed and load in steady state, there is a precise design target of air–fuel ratio and EGR rate from combustion and emissions requirements. Ideally, the EGR valve should be set fully open all the time with minimum flow restriction in order to minimize pumping loss. But in reality at some speeds and loads the EGR valve has to be set partially closed for the following reasons: (1) insufficient turbocharger efficiency and the consequent use of a small turbine area and resulting high engine delta P; (2) necessary smooth transition to EGR shut-off; (3) long actuator response time of the EGR valve when the VGT vane is suddenly closed during fast transient. If the turbo efficiency is not high enough, the exhaust manifold pressure must be made high by using a small turbine area to produce a sufficient turbine pressure ratio and turbine power to deliver the target air–fuel ratio. This results in a too-high engine delta P which forces the EGR valve to be partially closed (throttled) undesirably. On the other hand, if the turbo efficiency is too high, the exhaust manifold pressure must be lowered by using a larger turbine area to reduce turbine power to prevent overboosting the air–fuel ratio. In that case, engine delta P may become too low and cannot drive sufficient EGR flow. The root cause of inappropriate engine delta P is the fact that turbo efficiency has its inherent characteristics rooted in turbomachinery design. The efficiency cannot match engine needs flexibly at every speed and load. Generally, closing the EGR valve results in a decrease in the EGR rate and an increase in the air–fuel ratio. Closing the VGT vane or turbine wastegate may result in an increase in both EGR rate and air–fuel ratio. Increasing the turbo efficiency results in an increase in the air–fuel ratio basically without changing the EGR rate. Closing the exhaust back-pressure valve or intake throttle results in a large reduction in air–fuel ratio and a small increase in EGR rate. Figures 12.43 and 12.44 use engine cycle simulation data to illustrate the ability of flexibly controlling the air–fuel ratio and EGR rate with different air system options.

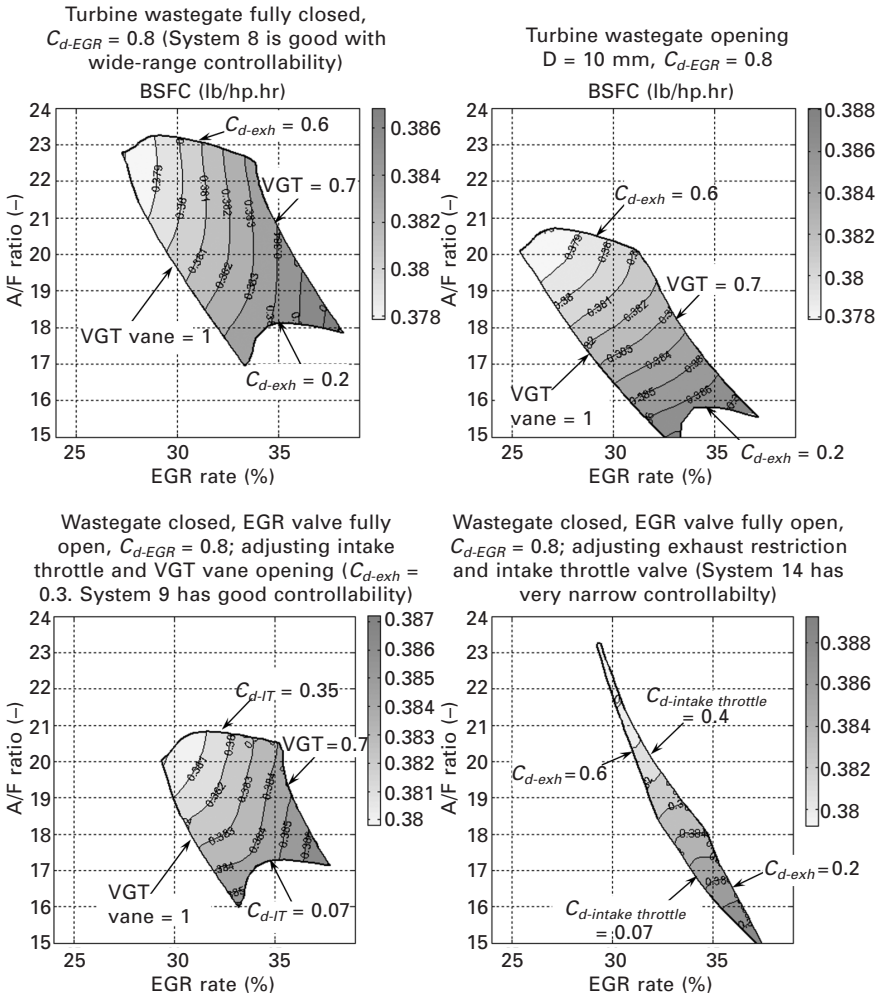
When evaluating how many ‘knobs’ are needed in air system design or how many controls to tune for achieving air and EGR flows, the mathematical systems formulated in Table 12.1 can be used in any flexible combination to count the number of hardware control parameters to match the number of



12.43 The ability to control the air–fuel ratio and EGR rate with different hardware.

unknowns in the system of equations. In this way, the air system control will not become over- or under-constrained. Moreover, the relative effectiveness of each 'knob' can be compared by analyzing the equations in Section 12.2. For example, to reach a given pair of air–fuel ratio and EGR rate values, with a low EGR circuit restriction design (e.g., EGR valve fully open) and turbine wastegate fully closed, the required turbine effective area A_T and turbocharger efficiency E_{TC} can be solved as two unknowns by using the equations in system 10 (i.e., two design 'knobs' are needed: A_T and $E_{T/C}$), but normally turbo efficiency cannot be adjusted freely in the entire engine speed–load domain, due to turbocharger design constraints. Nor can exhaust restriction caused by aftertreatment be freely adjusted. In that case, system 2 has to be used to solve for the required turbine area (e.g., VGT vane opening) and EGR valve opening to reach a pair of target air–fuel ratio and EGR rate values. That is the practice usually encountered by a calibration engineer during the engine calibration stage once the air system hardware has been finalized. It should be noted that closing the EGR valve raises engine delta P and results in a high pumping loss.

There are two reasons for using a turbine wastegate: (1) the required turbine effective area computed with system 10 at low speed is smaller than that at high speed; (2) fast transient response demands low turbo inertia, which requires the turbine not to be sized too large so that at high speed a wastegate may be used to bleed off exhaust. System 3 can be used to solve



12.44 Air system capability and controllability.

for M_T or essentially wastegate opening. In system 13, the turbine area is known, and turbine wastegate opening and turbo efficiency are solved as unknowns for target air–fuel ratio and EGR rate values. If turbine area, turbo efficiency and EGR circuit restriction have to be treated as fixed known input (i.e., input that cannot be changed freely in design), turbine wastegate and exhaust back-pressure valve (or intake throttle) need to be used (systems 11 and 12).

Intake throttle is sometimes used to induce more EGR or reduce the air–fuel ratio. It should be noted that if the intake throttle is the only 'knob' available to adjust performance, either the EGR rate or the air–fuel ratio can

be set as a target, but not both. For example, in system 14, at peak torque condition, the EGR valve is set fully open, the turbine wastegate is fully closed, and the turbine nozzle area and efficiency are fixed known parameters; if exhaust restriction $C_{d\text{-}exh}$ is also fixed then the only adjustable 'knob' will be the intake throttle.

From the above theory, changing any two of the following six parameters can reach a given pair of values of target air–fuel ratio and EGR rate: (1) EGR circuit flow restriction; (2) turbine effective cross-sectional area (or VGT vane opening); (3) turbine wastegate; (4) turbine or compressor efficiency; (5) exhaust restriction or back-pressure valve opening; and (6) intake throttle opening. However, their effects on engine delta P are different.

12.7.7 Entropy analysis of engine air system

While the first law of thermodynamics (i.e., energy balance in 'quantity') has been widely used in engine design and calculation, the second law of thermodynamics (i.e., the 'quality' of usable energy) has not often been used to date. In modern diesel engines with increasingly complex air system and additional energy conversion systems (e.g., hybrid powertrain, waste heat recovery), advanced analysis of engine system thermodynamics should be conducted with second-law entropy analysis in order to compare different design concepts more easily by quantifying the root causes of various losses occurring in the combustion and air systems as well as the effectiveness of turbocharging matched with different EGR systems. The losses include intake throttling, exhaust back-pressure valve throttling, EGR valve throttling, turbine wastegating, and so on. Moreover, the exergy analysis of waste heat recovery for high-EGR engines is very important. Since entropy and availability analyses are not yet a popular design tool in the engine design community, there is plenty of work to be conducted to establish the area. A good review was given by Flynn (2001).

12.8 Transient powertrain performance modeling and engine electronic controls

12.8.1 The roles of engine hardware design and software controls for transient operation

Engine controls fulfill the requirements derived from performance, emissions and durability needs. Moreover, electronic controls make flexible hardware mechanisms feasible in modern engines, such as variable valve timing and high-bandwidth-controlled variable combustion systems, so that the controls start to be a core part of fundamental engine architecture system decision making. When engine hardware design and software calibration are integrated,

two challenges are faced: (1) What hardware should be controlled (i.e., which sensors and controllers should be able to achieve the settings quickly and reliably)? (2) How should the hardware be controlled (i.e., optimum algorithm, and how to seamlessly integrate it in the hierarchical structure of system design with the best trade-offs to minimize transient emission spikes and pumping loss)?

Engine air system hardware needs to be designed to have acceptable transient capability to minimize turbocharger lag, transient pumping loss, fuel consumption and emissions, and ensure fast warm-up. Transient simulation plays a critical role in the development process, from predicting vehicle transients (e.g., load response, launch, acceleration, driving cycle) to evaluating electronic control strategies. Moreover, predicting the transients can also help in analyzing both performance and mechanical durability problems (for example, compressor wheel fatigue life) and reveal their parametric dependency (e.g., the impact of gear shifting during driving cycles on component durability life).

12.8.2 The difference between steady-state and transient performance

The transient acceleration or deceleration process of naturally aspirated diesel engines can be approximated by a continuous series of steady-state operating conditions. However, in turbocharged diesel engines, during transients the turbine power is not equal to the compressor power, and turbocharger speed is affected by turbo inertia and turbo power imbalance. There is a turbo lag during which the compressor boost pressure gradually changes to reach a new steady state. The EGR system has a certain volume and there is a transient dynamic response (in the order of several cycles) of an EGR purging and filling process in the intake manifold. There is also an air–fuel ratio smoke limit for maximum fueling, depending on available air flow. During transients, air–fuel ratio, EGR rate and in-cylinder metal wall temperature (due to thermal inertia) are all different from those in the steady state, and the resulting deteriorated combustion efficiency and pumping loss cause differences in emissions and fuel economy between steady-state and transient. Valve overlap has a large impact on transient acceleration performance, too. With large overlap, at the beginning of fast acceleration, exhaust manifold pressure can be much higher than intake manifold pressure for various reasons (e.g., EGR valve closed), and the high engine delta P results in a large reverse residue flow from exhaust manifold into the cylinder and intake manifold. The increased residue gas fraction reduces the air–fuel ratio and retards vehicle acceleration. On the contrary, a small valve overlap helps transient acceleration for the same reason.

12.8.3 Controlling engine transient performance

Steady-state emissions testing establishes appropriate NO_x, PM, HC and CO throughout the engine speed–load domain by setting the engine calibration parameters, including fuel injection timing and pressure, VGT vane opening, EGR valve opening, and intake throttle valve opening. Coordinated controls of EGR valve and VGT and coordinated controls of EGR valve and intake throttle valve (Nieuwstadt, 2003) have been studied extensively. Boost pressure (or air–fuel ratio) and EGR rate are mapped in the speed–load domain during engine steady-state calibration. But the combined control of VGT and the EGR valve for transient air–fuel ratio and EGR rate is challenging. Steady-state calibration may set VGT and the EGR valve opening positions to establish an air–fuel ratio and EGR rate, but those steady-state air–fuel ratios and EGR rates are not achievable during fast transient due to turbocharger lag, even if transient gains are applied to the steady-state position set-points on lookup table calibration maps. There are three strategies for designing transient emission profile shapes in engine controls, compared to steady-state emission levels: overshoot spike vs. time, undershoot or slow approach vs. time, and a compromise to closely match without too much overshoot or undershoot (depending on how fast the transient fueling rate changes). Each strategy has a different transient NO_x and soot trade-off as well as transient engine delta P and pumping loss. For example, a transient NO_x spike is normally caused by shutting off EGR during fast acceleration. Design for each kind of transient emissions profile with proper combination of hardware and electronic controls is important not only for accurate prediction of the emissions margin (the difference between steady-state and transient emissions) at the early stage of engine development, but also for meeting design objectives of transient emissions and driving cycle fuel economy.

Meeting a composite emissions target in the US supplemental emissions test (SET) 13-mode steady-state does not mean the engine can meet the same emissions target during an FTP transient cycle. In fact, as the NO_x emission regulation becomes more stringent, the difference (or ratio) between FTP transient emissions and steady-state emissions usually becomes larger, and that would translate to an unreasonably low steady-state emissions development target in order to meet the FTP transient emissions target. Therefore, a dynamic high EGR rate and adjustments of fuel injection timing and injection pressure during transients must be used to reduce transient emissions. During transient operation, the purpose of engine air system controls is to calculate and regulate the EGR valve and turbocharger actuator settings to achieve the target of optimum emissions trade-off and maintain drivability. The settings may be obtained from position lookup tables or may be calculated by model-based control algorithms. Various engine control approaches can be used with different effects on engine transients. The conventional approach

uses various gain-based transient controllers to regulate the EGR valve and VGT vane opening. But even with the most sophisticated map-based gain settings, it is still difficult to achieve a prescribed emissions trade-off during speed and load transients. Model-based control is promising in shaping the transient emissions profiles as a function of time.

12.8.4 Transient performance simulation

Transient engine testing is much more difficult and expensive than steady-state testing. Using cycle performance simulation to study transients is a very effective approach, especially for real-time transient modeling. The engine crankshaft lumped model has the governing equation 12.40. In transient engine torque simulation, the 'filling-and-emptying' method is usually used to model zero-dimensional manifold gas dynamics in order to increase computing speed. There are several key issues in transient cycle simulation related to modeling accuracy, as listed below.

1. In a fast acceleration transient when fueling suddenly increases, the rapidly reduced air–fuel ratio may result in incomplete combustion. Combustion efficiency as a function of air–fuel ratio was usually assumed as input in thermodynamic cycle transient simulation. Engine testing or sophisticated combustion simulation that tries to quantify such efficiency change remains challenging.
2. Another difficulty is related to the turbocharger. The instantaneous turbo speed N_{TC} (revolutions per second) is given by $4\pi^2 I_{TC} dN_{TC}/dt = (\dot{W}_T - \dot{W}_C - \dot{W}_{TCfric})/N_{TC}$ where I_{TC} is turbo inertia, $\dot{W}_T$ is turbine power, $\dot{W}_C$ is compressor power, and $\dot{W}_{TCfric}$ is turbocharger bearing friction power. The turbine instantaneous temperature, pressure and efficiency affect N_{TC} and turbo lag. Turbocharging performance transient modeling is usually approximated by a quasi-steady-state approach, which computes the instantaneous turbocharger parameters varying within an engine cycle by looking up steady-state turbo maps. Understanding the difference between steady-state turbine efficiency and transient efficiency remains challenging. There are large discrepancies between the conclusions from different authors (Capobiano *et al.*, 1989; Westin and Angstorm, 2002) who used different measurement methods (pulsating gas stands or on engine in-situ) and CFD simulations. As to turbine flow rate, it was reported that the turbine under unsteady conditions has a 3–6% higher swallowing flow capacity (corrected mass flow rate) than that measured at steady state (Capobiano *et al.*, 1989). The heat losses, volume and thermal inertia of the exhaust manifold also have significant effects on the accuracy of turbo lag and engine transient performance simulation.

3. Transient engine simulation and accurate prediction of driving cycle fuel economy demand fairly accurate engine control models which reflect engine calibration set points in the speed–load domain and actual transient control strategies, as well as the dynamic response of actuators.
4. Accurate simulation of cold start, warm-up and hot start transients are important for simulating transient emission cycles.
5. Transient simulation also requires accurate mechanical loss models of the main friction components (piston-ring-liner assembly, bearings and valvetrain) and accessory parasitic losses (Taraza *et al*., 2007).

Real-time high-fidelity simulation with a detailed instantaneous in-cylinder process and manifold gas wave dynamics is currently available. Before the advent of such a real-time high-fidelity model, mean-value models were used to conduct real-time simulations for engine control design and long vehicle driving cycle analysis. The mean-value models use a simplified map-based cylinder without calculating the crank-angle-resolution in-cylinder cycle process. Typically, volumetric efficiency, indicated efficiency and exhaust energy fraction are built in maps as functions dependent upon certain parameters such as engine speed, fueling rate, intake manifold pressure, air–fuel ratio, etc. The mean-value model has some disadvantages: tremendous efforts need to be spent to run DoE data upfront to build the maps, which are actually too hardware-specific and still too primitive; and the model cannot predict turbocharger lag transient conveniently and accurately. Mean-value models may use a large time step in the order of one engine cycle, while a detailed in-cylinder process model requires 1–5° crank angle resolution. The theory on the mean-value model was provided by Schulten and Stapersma (2003). There is a trend to develop and use the real-time high-fidelity simulation to replace the mean-value models for future transient analysis in order to increase the predictability of the model. Moreover, in engine control simulations software-in-the-loop (SIL) and hardware-in-the-loop (HIL) are used to validate algorithms for both steady state and transient.

12.8.5 Analysis of hardware design for engine transients

Turbocharged diesel engines cannot respond to a sudden change in speed or load as fast as naturally aspirated diesel engines because the change of compressor air flow lags behind the change of fueling rate. The reasons for turbocharger lag include the following: (1) because the manifold has certain volumes, it takes time (usually several cycles) to gradually build up the gas pressure in the exhaust manifold and the intake manifold; (2) during fast acceleration, after the EGR valve is closed it takes time to purge EGR out of the intake manifold; and (3) because the turbocharger rotor assembly has a certain moment of inertia, it takes time for the turbine to gradually accelerate

the compressor to rotate faster under a difference between turbine power and compressor power. For smoke control, fueling rate and engine power are restricted during fast acceleration transients according to the available intake boost pressure. Reducing the volume of the intake manifold and the exhaust manifold can reduce turbocharger lag. For example, pulse turbocharging with a smaller manifold volume has a better transient response than constant-pressure turbocharging. Matching the turbine size with a small flow area for low speed-load conditions can help build up turbine power faster during transients and reduce turbocharger lag. (Note that at high speed and high load, a wastegate or variable geometry turbine needs to be used to prevent over-boosting.) Another way to reduce turbocharger lag is to use low turbo inertia, such as reducing the turbine size, using two smaller turbochargers to replace one big unit, using a low-inertia small high-pressure-stage turbo in a two-stage turbo system, or using a ceramic turbine rotor. Other methods that may reduce turbocharger lag and improve the smoke limit and transient response include locating the EGR valve close to the intake manifold to minimize EGR purging time, reducing heat loss in the cylinder and exhaust manifold, using a small valve overlap, improving transient combustion efficiency, retarding fuel injection timing to increase the turbine inlet exhaust temperature, and using boost-assisting devices such as injecting extra air or mechanical supercharging during fast acceleration.

One important consideration for turbo selection is controlling compressor surge during transients. On the compressor map, the operating trace of a fast speed-increase transient is located an the right side of the steady-state point. The operating trace of the transient of a fast load-increase or fast speed-decrease is located on the left side of the steady-state point, and this possibly results in compressor surge. The compressor surge during fast transients happens when the compressor air flow rate, which responds quickly to engine speed change, decreases much faster than the lagged compressor boost pressure. The boost pressure is affected by the turbocharger shaft speed and turbo inertia. In turbocharger matching there is a need to simulate fast deceleration to check compressor surge.

In addition to the turbocharger, other engine hardware design evaluations for transient acceleration performance usually include the effect of engine inertia, charge air cooler or compressor inter-stage cooler volume and cooling medium temperature, manifold volume and piping, EGR circuit volume and EGR purging time, the location of aftertreatment components, etc.

12.8.6 Analysis of lookup table approach of air system controls for engine transients

In traditional lookup table controls, the set-point is usually either an actuator position (e.g., the EGR valve duty cycle) or a performance parameter, for

example MAF (air flow), MAP (boost pressure), lambda or air–fuel ratio, or intake manifold oxygen concentration. During transients, the air system component actuator (e.g., the EGR valve or VGT turbine vane) can be driven to a preset position, which is obtained from steady-state calibration at a given engine speed and load, superpositioned with transient PID gains and transient algorithms with a feedback PID control (for example, by means of a potentiometer). The moving part within the actuator has transient response characteristics against time (i.e., a delay due to a characteristic time constant, not an instantaneous response to the demand from the engine control unit). In the MAF control, the actuator (e.g., the EGR valve) is modulated to achieve a preset air–fuel ratio through a PI or PID controller fed by the feedback difference between the required MAF and the sensor signal (either the actual measured signal or a virtual-sensor calculated signal).

The lookup table approach is not flexible enough to handle real-world engine variations. One example of the limitations of the lookup table is the aftertreatment dynamic dosage control, e.g., hydrocarbon dosing in active de-NO_x catalyst or urea dosing in SCR. The lookup table approach cannot compensate for interferences from factors such as production variation, component ageing, and engine acceleration or deceleration transients. During transient turbo lag or valve lag, the dosage rate determined from steady-state calibration lookup tables may not be suitable and could result in an unacceptable slip amount.

12.8.7 Analysis of model-based approach of air system controls for engine transients

Traditional engine controls used table-lookup techniques, for which the calibration complexity increased exponentially as new functions and the number of associated control tables (maps) increased with the development of modern turbocharged EGR engines. Electronic controls have been evolving in the direction of mathematical model-based controls (open loop or closed loop), which is an important part of optimal system design or diagnosis. Reviews of engine controls were provided by Osborne and Morris (2002) and Stobart *et al*. (2001). The success of online model-based controls largely relies on the accuracy of the predictive thermodynamic cycle performance models adopted for various operating conditions such as new and aged engines, normal and extreme climates. Model-based air system controls include the sensors and actuators for the gas flows inside and outside the cylinder, for example engine valve actuation, EGR valve, intake throttle valve, exhaust back-pressure valve, and turbine vane actuator. Model-based cooling system controls include the sensors and actuators for coolant flows. For example, the target of future cooling systems is to use more electronic controllers to provide flexible cooling as needed to minimize driving power

consumption and enhance engine performance, beyond today's pump, fan and thermostat. The gas-side data and coolant-side data may be bridged by a model of heat rejection and other engine performance parameters. In coordinated model-based control of the EGR valve and turbine actuator, according to the theory in Section 12.2, the valve opening and actuator setting may be calculated by specifying two performance targets out of the following three parameters: fresh air flow rate, EGR rate, and intake manifold boost pressure. The engine performance parameters used in model-based controls can be either measured signals from real sensors, or simulated data from virtual sensors.

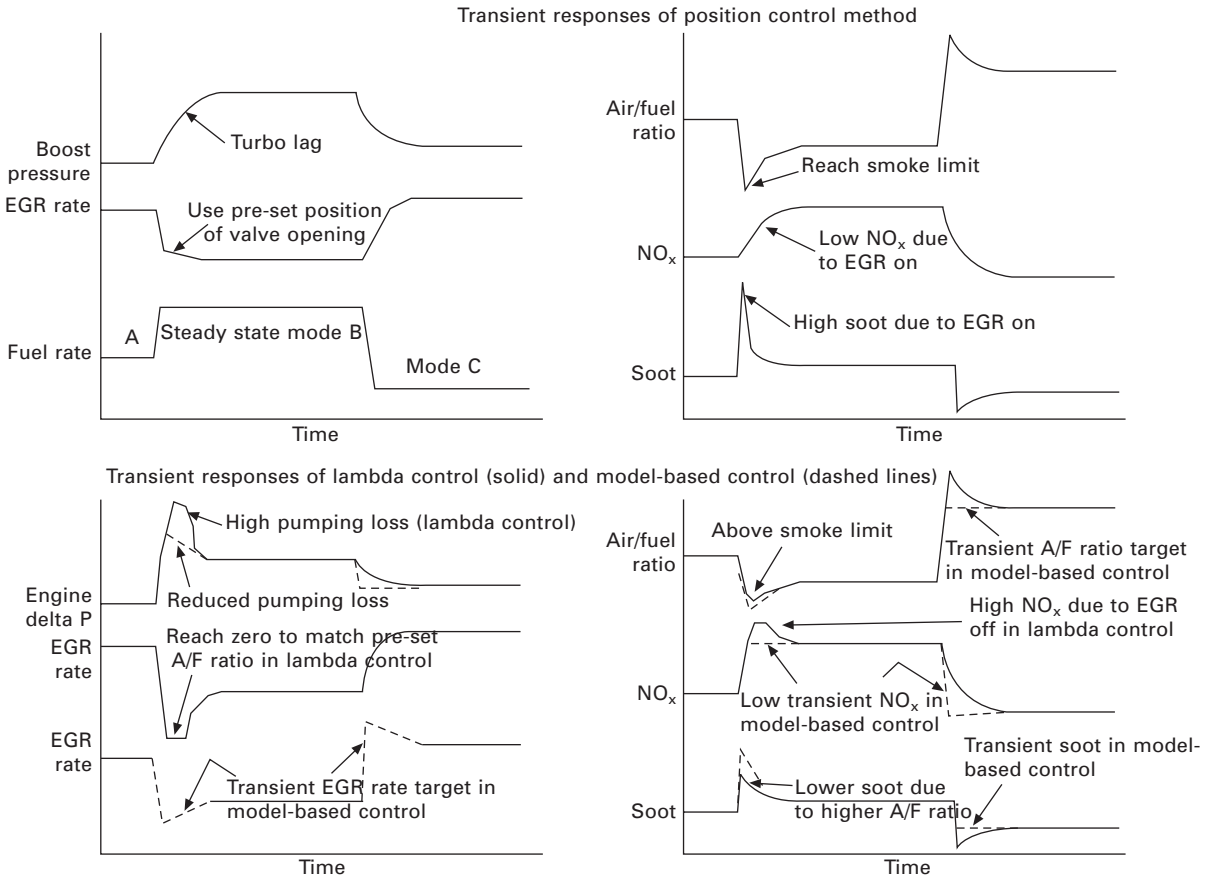
The opening position of valves (EGR valve, intake throttle valve, exhaust back-pressure valve) can be calculated based on target performance parameters. For example, the gas mass flow rate through an EGR valve orifice can be modeled by using the equation of isentropic ideal gas compressible flow as below:

$$M_{EGR} = C_{EGR} \frac{A_{EGR} P_{upstream}}{\sqrt{RT_{upstream}}} \cdot \sqrt{\frac{2\gamma_t}{\gamma_t - 1}}$$

$$\times \sqrt{\left(\frac{P_{downstream}}{P_{upstream}}\right)^{\frac{2}{\gamma_t}} - \left(\frac{P_{downstream}}{P_{upstream}}\right)^{\frac{\gamma_t + 1}{\gamma_t}}} \qquad 12.50$$

where A_{EGR} is the theoretical effective flow area of the valve orifice at a given opening (e.g., obtained from the correlation between valve lift and valve flow area), and C_{EGR} is a variable correction coefficient which is calibrated from measurement at various engine flow conditions and used to correct any errors in the theoretical valve flow area. For solving valve actuator control demand, first the required valve flow area can be calculated from the desired EGR mass flow rate at any given engine speed and load by rearranging equation 12.50. Then, the valve area can be converted to the valve opening position or lift. In model-based controls, in order to achieve a desirable transient EGR rate (not necessarily the minimum deviation from the steady-state EGR rate), a target transient rate profile may be flexibly defined to a certain shape as a function of the rate of transient speed–load change. For example, the target transient EGR rate can be imposed by a fixed EGR percentage multiplied by the measured total engine gas mass flow rate. It is worth noting that in model-based control the component's dynamic behavior can also be modeled.

To illustrate the effect of different engine control methods on transient performance, a step increase of the fueling rate followed by a step decrease is shown in Fig. 12.45. As a result, engine speed and brake torque change through three steady-state modes, named A, B, and C. Such an event is a



12.45 Illustration of transient engine controls and air system performance.

typical snapshot of real-world driving cycles. Due to turbocharger lag, there are inevitable delays in exhaust manifold pressure and intake manifold boost pressure during the fast transient of fueling rate change. The instant fueling increase results in a fast decrease in the air–fuel ratio at the beginning of the transient event, possibly reaching the smoke limit. The level of EGR rate commanded by the engine controls has a direct impact on the air–fuel ratio, NO_x and soot emissions during the transient. For example, in the method of EGR valve position control, the EGR valve opening undergoes sharp changes from the steady-state calibration opening of mode A to those of modes B and C, and the resulting EGR flow reduces the air–fuel ratio and increases transient soot while keeping transient NO_x low. On the other hand, in the method of lambda (air–fuel ratio) control or MAF control, in order to maintain the steady-state air–fuel ratio settings during transients, the EGR valve is commanded to close when the fueling rate suddenly increases, and to open more when the fueling rate suddenly decreases. As a result, during a step load increase, less or even no EGR flow is obtained. Consequently, a higher air–fuel ratio and lower transient soot are achieved, but transient NO_x and pumping loss (due to higher engine delta P) may be higher than in the method of position control.

The transient soot spike is an inevitable phenomenon during fast acceleration due to turbocharger lag. The task of the EGR control is to regulate EGR flow to minimize transient emission spikes or to achieve best NO_x–soot trade-off with the best compromise on drivability. Meanwhile, EGR control needs to be coordinated with turbocharger control for proper intake manifold boost pressure, and to respond to the changes in intake and exhaust restrictions, production variation and ambient conditions. It is difficult for position-based control to accomplish those tasks. MAF or MAP control can accomplish them only partially. A promising approach is model-based control, which may compute the actuator position (e.g., EGR valve or VGT vane) accurately with a calibrated model based on preset desirable engine performance parameters (e.g., desirable transient EGR flow rate profile or dynamic transient fuel injection control parameters, or even ideally desirable NO_x or soot limit if the real-time NO_x or soot model is available). Another advantage of model-based control is that its steady-state engine calibration set-points and transient calibration gains are much less hardware-dependent than in position-based control, because the set-points are more fundamental engine performance parameters, such as air–fuel ratio and EGR rate, rather than the valve opening or vane opening of a particular EGR valve or VGT. Figure 12.45 illustrates the concept of model-based EGR rate control or air-fuel ratio control in order to reduce transient NO_x and pumping loss, as well as to optimize the trade-off between NO_x and soot during load increase and decrease.

The VGT effective area opening or turbine wastegate opening can be

modeled similarly with an orifice flow equation (12.28) and by using the turbine power equation. Model-based turbocharger control may reduce turbocharger lag and prevent transient compressor surge. A detailed theory of model-based VGT and EGR nonlinear controls was outlined by Ammann *et al*. (2003). In summary, hardware design needs to match electronic control strategies so that the inherent transient difficulties (e.g., turbo lag or high transient pumping loss) can be alleviated to the maximum extent.

12.8.8 Model-based virtual sensor modeling

The model-based controls of valves and turbochargers mentioned above are essentially virtual actuators. In their equations, it is noted that the engine temperature, pressure and flow parameters can be from either actual measurement or virtual sensor modeling. Model-based virtual sensors may replace some actual physical sensors in engine and aftertreatment systems in order to reduce cost or to enable flexible controls. For instance, switching combustion mechanisms between different speed–load regions can be achieved by predicting in-cylinder information on the combustion process. The development of virtual sensors largely relies on thermodynamic performance modeling.

Engine sensors usually include the following: (1) crank position sensor and cam position sensor for sensing engine speed, TDC position, fuel injection timing and duration; (2) accelerator pedal position sensor; (3) pressure sensors for manifold absolute air pressure (MAP), barometric ambient, DPF inlet pressure, oil and fuel; (4) temperature sensors for intake manifold air, exhaust manifold gas, DPF inlet and outlet gases, oil, fuel and coolant; (5) mass air flow (MAF) sensor; (6) exhaust oxygen or lambda sensor; (7) NO_x and NH_3 sensors used in aftertreatment; (8) oil and coolant level sensors, etc. There are two types of virtual sensors, steady-state and dynamic transient. They require different computing algorithms. An example of virtual sensors is provided below.

The exhaust manifold temperature virtual sensor is important for engine durability and EGR rate control. Its modeling is based on the thermodynamic first-law energy balance equation 12.43. Assuming

$$\dot{W}_E = \eta_E (q_{LHV} M_{fuel})$$

$$\dot{Q}_{base\text{-}coolant} = \alpha (q_{LHV} M_{fuel})$$

$$\dot{Q}_{miscellaneous,2} = \beta (q_{LHV} M_{fuel})$$

where η_E, α and β are constants or known functions of engine speed, load, air–fuel ratio, and fuel injection timing, etc. The steady-state exhaust manifold

gas temperature can be calculated by using 12.43 as:

$$T_{turbine\text{-}inlet} = \frac{(M_{IM}/M_{fuel})c_{p,in}T_{IM} + q_{LHV}(1 - \eta_E - \alpha - \beta)}{(M_{IM}/M_{fuel} + 1)c_{p,ex}} \qquad 12.51$$

where M_{IM} is the intake manifold mixture flow rate of both air and EGR, and $c_{p,\,ex}$ and $c_{p,in}$ are equivalent average specific heats of exhaust flow and intake manifold flow, respectively. It is observed that the exhaust manifold temperature is a function of the 'mass-to-fuel' ratio (M_{IM}/M_{fuel}). In equation 12.51, one way to estimate engine thermal efficiency η_E is to calculate the engine brake power by using the indicated torque and engine friction obtained in torque-based controls. The prediction of engine indicated torque and brake torque has been used increasingly as a part of coordinated shift control in automotive powertrains. In 12.51, the biggest difficulty arises from an accurate estimate of α. One approach is to use the in-cylinder cycle process equations along with the Woschni heat transfer correlation α_g outlined in Section 12.2 to calculate the transient instantaneous exhaust manifold temperature first, and then average it over an engine cycle to obtain the steady-state exhaust manifold temperature. The other approach is to develop heuristic models for steady-state α to build its sensitivity to engine performance and operating parameters.

There are abundant needs for future virtual sensors in both steady-state and transient for the next generation of 'intelligent' diesel engines. Future development needs include:

- Steady-state virtual MAF and MAP sensors
- Other steady-state virtual sensors for gas flow, pressure and temperature which can be calculated by using the 19 equations 12.10–12.28 governing the engine air system described in Section 12.2
- A virtual engine torque sensor in torque-based controls of powertrain central torque-demand coordination
- Transient virtual sensors for in-cylinder real-time quantities, for example air temperature, pressure and charge equivalence ratio during the compression stroke in HCCI burning control
- Engine-out NO_x, PM/soot and HC virtual sensors based on the in-cylinder cycle process calculation with heuristic macro-parameter-dependent emissions models
- Virtual sensors for aftertreatment flow parameters and outlet emissions based on heuristic models
- Combining all of the above to enable a whole engine model with affordable computational time for virtual sensing everywhere as a fully validated physical model used in real-time predictive algorithms of engine controls.

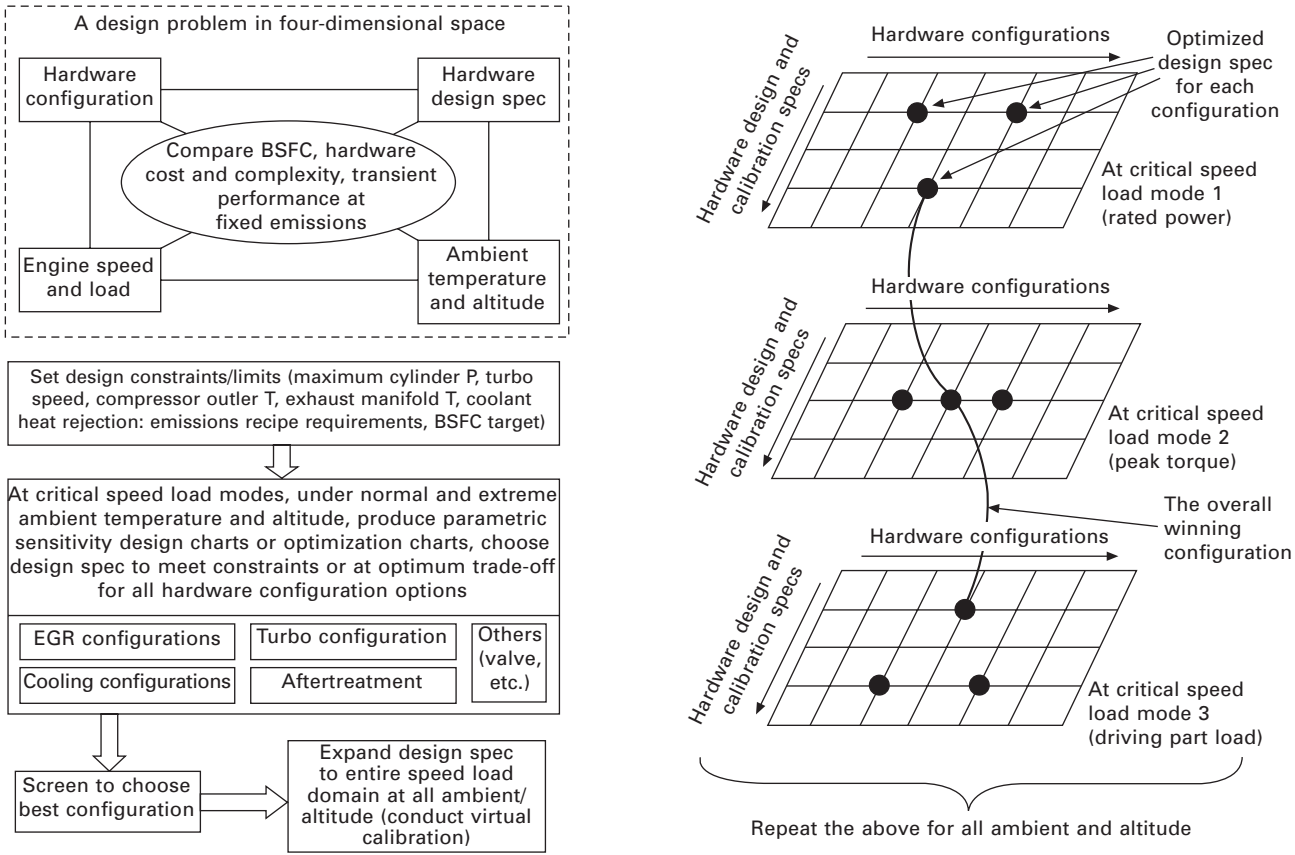
Engine performance and emissions modeling will be the foundation for building those advanced virtual sensors. This area opens many challenges and opportunities for system integration analysis and design.

12.9 Engine system specification design and subsystem interaction optimization

12.9.1 The process of system design analysis

As mentioned in Section 12.1, the main objective of engine system design is to produce system performance design specifications and the justification of optimum design point selection by using sophisticated cycle simulation tools and constructing parametric sensitivity charts or optimization charts. The need for using advanced software is obvious for three reasons: (1) primitive hand calculations of engine air system performance do not meet the requirement of modern precise design to push the hardware capability to the limit; (2) the required nonlinear constrained optimization of DoE emulators for generating parametric design charts can be computed only with specialized software; and (3) the high demand of complex transient analysis in hardware selection cannot be conducted without using simulation software.

Figure 12.46 illustrates the complex process of engine system analysis in a four-dimensional design space as follows: (1) hardware configuration (e.g., single-stage or two-stage turbo); (2) hardware design specification (both steady-state and transient; both normal operation and aftertreatment regeneration; e.g., turbine nozzle area or EGR valve opening); (3) engine speed and load; and (4) ambient temperature and altitude. The process starts with setting design constraints and identifying all possible configuration options to reach the target emissions recipe or its equivalent air system requirements (air–fuel ratio, EGR rate and intake manifold temperature, detailed in Section 12.4). The DoE method is normally used to quickly rule out some options and then to optimize the design specification of each subsystem for minimum BSFC subject to design constraints. The subsystems include turbo, valvetrain, ports, manifolds, EGR circuit, exhaust restriction, cooling, etc. Sensitivity design charts are produced in this stage. At each speed and load, the DoE factors may include some or all of the following: exhaust restriction, charge air cooler size, EGR cooler size, compressor or turbine efficiency (if turbo maps are not used) or efficiency multiplier (if turbo maps are used), turbine effective area, turbine wastegate opening, EGR circuit flow restriction coefficient, certain design factors affecting volumetric efficiency (e.g., valve size, valve timing, port flow discharge coefficient), start-of-combustion or start-of-injection timing, etc. The analysis output includes certain critical instantaneous parameters (in-cylinder details and gas flow pulsation in pipes) and all cycle-average performance parameters describing the entire



12.46 Design process for engine system specification.

system, for instance air–fuel ratio, EGR rate, oxygen mass fraction, BSFC, peak cylinder pressure, peak cylinder bulk gas temperature, pumping loss, engine delta P, volumetric efficiency, manifold pressures and temperatures, heat rejections, cooler effectiveness and flow restriction, turbocharger flow rate, pressure ratio and temperatures, turbo efficiency (if turbo maps are used), etc.

12.9.2 Critical mode design at various ambient conditions for optimum configuration

In system specification design there are two categories of limits (usually occurring at full load): the hardware design limit and a lower limit used for calibration test setting. The necessity for the two limits arises from the fact that there is a statistical distribution on all the variations of hardware tolerances. The 'nominal' engine calibration set-point (e.g., intake manifold pressure or exhaust manifold temperature) in normal ambient conditions should be even lower than the 'calibration limit' by a certain margin. The full-load conditions of the hardware in the system specification need to be designed below the 'design limit' to cover the worst ambient conditions in emissions certification and real-world driving. Different design limits may occur at different ambient conditions or engine speeds, for example:

- The EGR cooler and charge air cooler need to be sized for sea-level altitude and hot ambient (e.g., 38ºC or 100°F) to reach the target of intake manifold gas temperature to meet US EPA NTE emissions.
- The compressor inter-stage cooler in a two-stage turbocharger needs to be sized large enough, with an appropriate cooler sink temperature, to ensure that on a hot day at sea level or high altitude the high-pressure-stage compressor outlet air temperature is below the material limits of the compressor wheel, housing and charge air cooler inlet tube.
- The engine coolant heat rejection and associated EGR strategy need to be designed to ensure that at high altitude (e.g., 1676 meters or 5500 feet – the US EPA NTE limit; or 10 000 feet in practical real-world applications) and hot ambient (e.g., 38°C) the engine outlet or radiator inlet coolant temperature does not exceed the durability limit.
- The turbo control and EGR strategy need to be tailored at high-altitude hot ambient to ensure that with a lower air–fuel ratio the soot emission is still below the smoke limit, and the exhaust manifold temperature is within the limit imposed by the durability of the cylinder head and turbine.
- The compressor needs to be sized large enough to make sure that at high altitude without fueling de-rating, the turbo speed is still below the maximum limit.

- The maximum cylinder gas pressure and temperature as well as the peak heat flux need to be designed below the combination limits of mechanical and thermal stress loading for power cylinder components.
- The turbo and EGR controls need to be designed to ensure that in a cold climate the peak cylinder pressure along the full-load lug curve (e.g., SET modes A100, B100, C100 and peak torque and rated power) does not exceed the structural limit. Moreover, compressor surge at cold ambient should not occur.
- In firing and engine braking operations in both steady state and transient, the exhaust manifold pressure should be below the structural limit, and the engine delta P should be kept below the point at which the exhaust valve floats off the valve seat.
- For high EGR engines in extremely humid climates the intake manifold gas temperature needs to be designed not to exceed the durability limits of condensation control and corrosion resistance.
- All hardware design constraints need to be satisfied during the maximum engine braking operation.

The ambient conditions used in hardware sizing usually include the following: sea-level altitude and normal ambient temperature (e.g., 25ºC or 77°F); the US EPA's heavy-duty emissions NTE limits (sea-level from cold ambient to 38ºC or 100°F hot ambient; 1676 meters or 5500 feet altitude from cold ambient to 30ºC or 86°F, with a humidity range); and real-world driving environments (e.g., 5500 feet on a hot day, a very high altitude such as 8000–10 000 feet on a hot day, and a cold ambient condition at sea level, for example –18ºC or 0ºF). Hot air recirculation, turning on air-conditioning, and the rise-over-ambient elevated compressor inlet air temperature due to in-vehicle underhood heating, should also be considered.

In addition to the variations in ambient conditions, hardware matching is also complicated by large variations in the EGR flow and aftertreatment system. For instance, EGR rate control may vary from zero in very cold conditions or during fast transients to very high in normal ambient. Large fluctuations in exhaust restriction may occur due to soot loading changes in the DPF. The compressor size needs to be large enough to cover all those variations.

In designing the maximum capacity of hardware and in comparing different configuration options, critical speed and load modes are selected, for example rated power and peak torque in heavy-duty applications, as well as typical part-load driving conditions identified by vehicle matching analysis. In light-duty applications, rated power and peak torque conditions are rarely encountered in real-world driving, and usually very little EGR is applied under full-load conditions for light-duty emissions certification. In such light- or medium-duty applications, two practical and frequently used

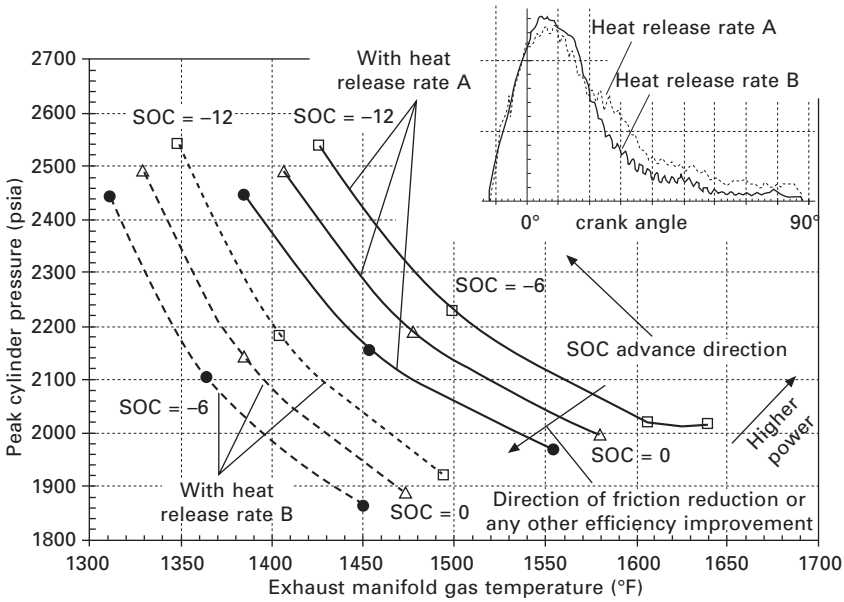
operating modes – high-speed high-load and low-speed high-load with high EGR demand – need to be added to the critical mode analysis in order to size the hardware. It should be emphasized that an important design target is to minimize engine pumping loss and fuel consumption for both steady-state and transient operations in the proper speed–load region. The minimum pumping loss is realized by a low engine delta P design in EGR and turbo systems, and an equally important high volumetric efficiency design in valvetrain, ports and manifolds. For durability design targets, over-speed and over-fueling may be simulated to find out the engine's maximum potential capability and determine the safety margins.

Successful design of the rated power condition is important for heavy-duty engines. All the design constraints mentioned earlier apply to rated power. Moreover, at high speed, the reciprocating inertia force is another constraint for structural strength. The usual methods of designing a series of engines with different power ratings or applications include the following: (1) raising the rated speed; (2) using turbocharging to achieve different levels of air density and corresponding power ratings without changing the engine cylinder bore and stroke; (3) increasing the cylinder bore diameter or stroke to increase the engine displacement and power rating; and (4) increasing or decreasing the number of cylinders to achieve different power ratings. Other methods of increasing the power rating include enhancing volumetric efficiency by valvetrain or port design, reducing mechanical friction, raising the peak cylinder pressure limit, etc.

At a given engine speed, there are trade-offs between the air–fuel ratio, EGR rate and power rating under a fixed constraint of peak cylinder pressure (reflected through equation 12.11). There is also another fundamental trade-off between peak cylinder pressure and exhaust manifold temperature, both being design constraints. The trade-off is affected by the shape of the heat release rate, fuel injection timing and engine friction. The simulation data in Fig. 12.47 shows the measures needed to bring the cylinder pressure and exhaust temperature under control at rated power (i.e., moving the curves in the lower left direction). Reducing the engine compression ratio may reduce the peak cylinder pressure under the penalties of lower indicated thermodynamic efficiency and unaided cold-start capability.

The rated power condition is used to define compressor and turbine maximum flow ranges, cooler size, maximum heat rejection, intake restriction and exhaust restriction. In high-EGR engines, usually the engine delta P at rated power has to be very high due to the small turbine area sized for acceptable EGR rate and air–fuel ratio at peak torque. As a consequence, the EGR valve has to be partially closed in order to prevent excessive EGR. Therefore, the rated power condition should not be used to define the minimum flow restriction of the EGR circuit.

The peak torque condition has the maximum mean effective pressure,



12.47 Engine fundamental trade-offs at a fixed speed and power.

and is prone to compressor surge (especially at high altitude) due to the low engine air flow rate and the relatively high boost pressure. It is also usually the most difficult mode for driving EGR flow due to insufficient engine delta P. The minimum flow restriction of the EGR circuit (with EGR valve fully open, with or without a check valve) and the minimum required turbine area are often determined based on the EGR-driving requirement at peak torque, although the lower speeds at full load also need to be checked to ensure the minimum turbine area. In some vehicle applications, the peak torque or a medium speed between the peak torque and rated power may encounter maximum engine-out coolant temperature due to the matching characteristics of the water pump and radiator, although the coolant heat rejection at peak torque is much lower than at rated power.

At part load, it is important to check pumping loss, fuel economy, the EGR driving capability with the selected turbocharger, and the ability to control the air or cooling system to raise the turbine outlet exhaust temperature for aftertreatment thermal management. Another important mode used in hardware specification design is the peak retarding power during engine/retarder braking.

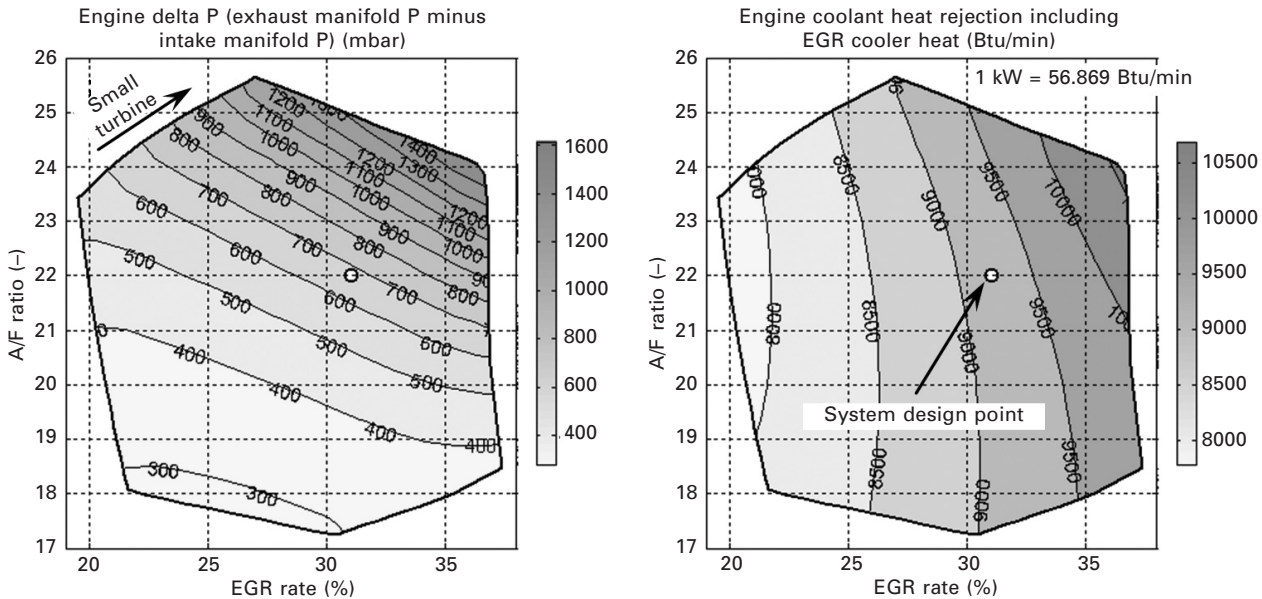
12.9.3 Optimization of each subsystem and their interaction

In parametric sensitivity or optimization analysis, generally there are two types of study: (1) simulation at variable emissions, or at variable air–fuel ratio and EGR rate which are shown in an 'air–fuel ratio vs. EGR rate' domain (note that such a domain represents air system capability, and the reason for this type of simulation is that the emissions recipe or design constraints are uncertain, and the required air or EGR flow can still be a moving target); and (2) simulation at fixed emissions constraints (i.e., NO_x and soot) to compare BSFC and hardware cost. The emissions constraints are usually approximated by one of the following four methods: a pair of fixed air–fuel ratio and EGR rate; a pair of fixed peak cylinder gas temperature and air–fuel ratio; a pair of fixed peak cylinder gas temperature and oxygen mass fraction; or a pair of fixed NO_x and soot predicted by emissions models.

In type (1) analysis, 2-D performance contour charts are used to show the sensitivity of performance to the change of emissions target (Fig. 12.48). Note that the BSFC of each point in such a chart has been minimized or optimized. A design point can be selected based on the best trade-offs between tentative emissions target and design constraints. In type (2) analysis with fixed emissions, subsystem interaction can be analyzed, with a typical example shown in Fig. 12.49. Again, the BSFC of each point in such a chart has been minimized. A hardware design point can be selected based on the best trade-offs between different subsystems supported by sensitivity contours.

In air system design, there are strong dependencies among the following four parameters: exhaust restriction, EGR circuit flow restriction, turbine effective area and turbocharger efficiency. In hardware selection at each speed and load mode for a pair of target air–fuel ratio and EGR rate, when the EGR valve is set fully open to try to minimize engine delta P, the required turbine area and turbocharger efficiency are uniquely determined (Table 12.1). But the reality is that turbocharger efficiency cannot reach all the desirable values computed as such at all speeds and loads. At some modes, if the actual turbo efficiency is too low, the air–fuel ratio would become too low. In order to compensate for that, a smaller turbine area must be used and the EGR valve must be correspondingly partially closed (throttled) to accommodate the increased engine delta P. On the other hand, if the actual turbo efficiency is too high, the air–fuel ratio would become too high. In order to reduce the air–fuel ratio to prevent over-boosting, a larger turbine area or wastegating must be used to slow down the compressor, and the engine delta P would become insufficient to drive enough EGR even if the EGR valve is set fully open.

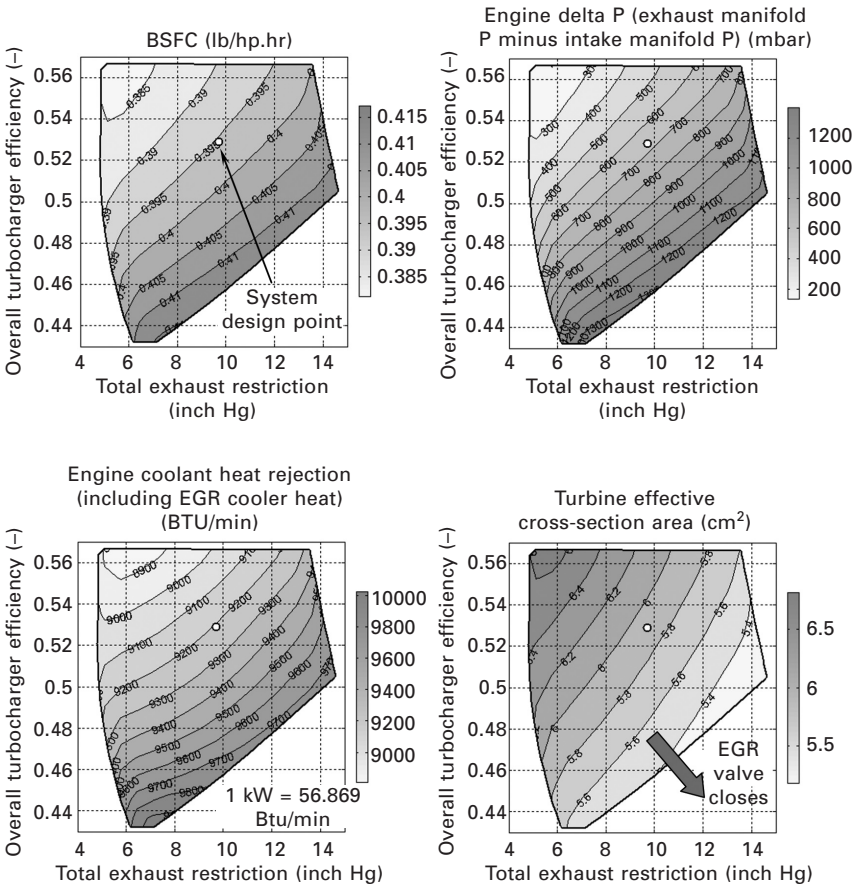
As to the interaction with aftertreatment, for given aftertreatment hardware, its exhaust restriction flow coefficient will change only when DPF soot loading



12.48 Engine delta P and heat rejection at different emissions at rated power (simulation).

changes. When exhaust restriction or turbine outlet pressure increases, the turbine pressure ratio and air–fuel ratio decrease. To compensate for that, a smaller turbine area needs to be used to restore the turbo speed and boost pressure. As a result, the EGR valve has to be more closed; engine delta P and pumping loss will increase. Figure 12.49 shows such an effect.

The cooling system design has an impact on pumping loss through the intake manifold temperature and the flow restriction of the EGR cooler or charge air cooler. Higher cooler effectiveness and lower restriction result in less required engine delta P to drive a target air–fuel ratio and EGR rate, especially at peak torque where the EGR valve is usually fully open. Then, a larger turbine area can be selected to reduce pumping loss. There are trade-offs between cooler effectiveness, cooler flow restriction and packaging size.



12.49 Typical subsystem interaction at approximately fixed emissions (simulation): heavy-duty diesel engine rated power, at fixed air–fuel ratio and EGR rate.

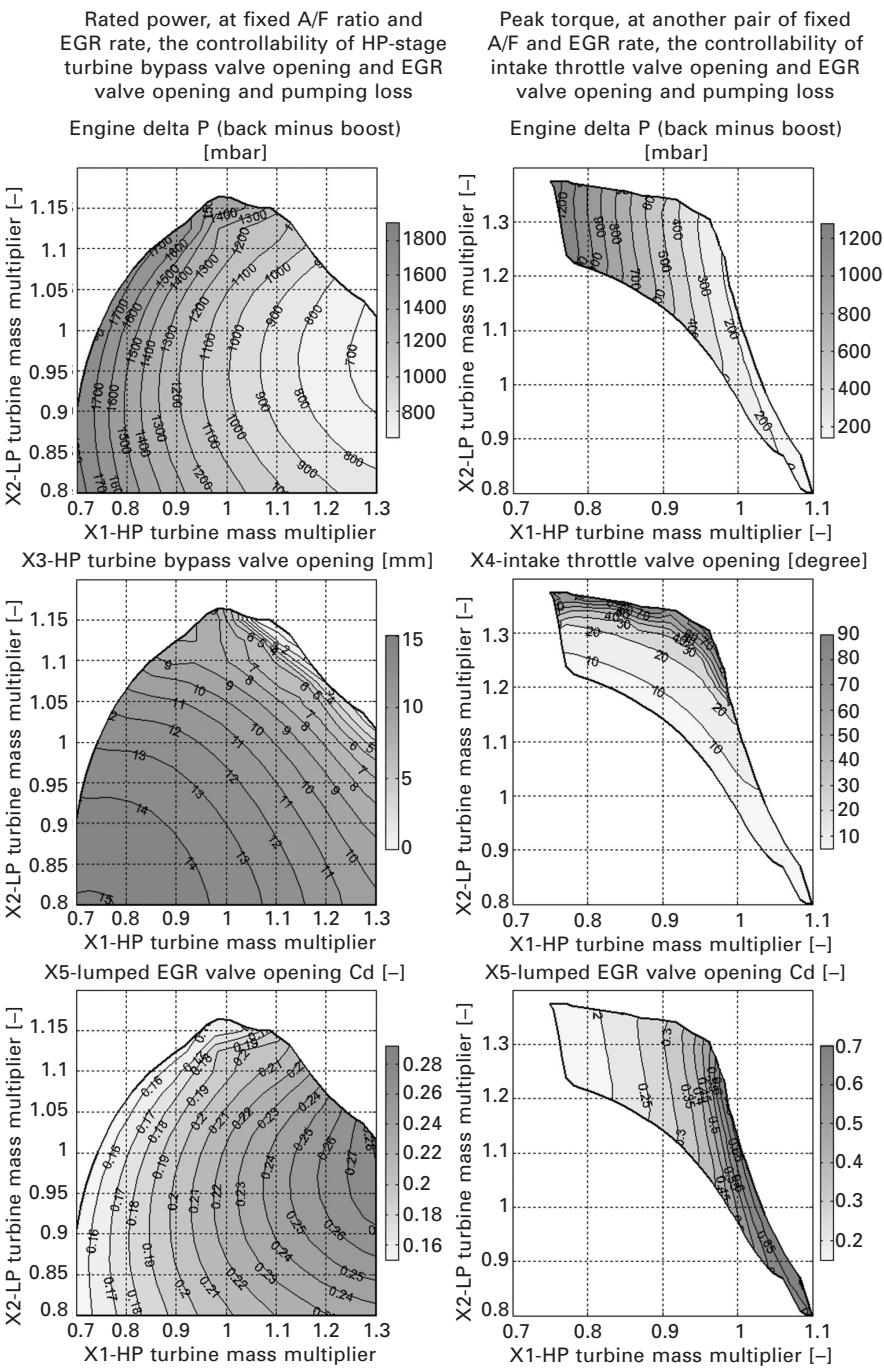
Two-stage turbocharging has been adopted for high power-rating engines with high EGR rate due to the high boost pressure requirement. Generally, a lower pressure at the low-pressure-stage turbine inlet results in an increase in high-pressure-stage turbine power and a decrease in low-pressure-stage turbine power. An advanced approach to analyzing the turbine area sizing of the two stages and the interaction between the two stages is to conduct minimum-BSFC optimization under fixed emissions (or its approximation of fixed air–fuel ratio and EGR rate) at rated power and peak torque conditions, as shown in Fig. 12.50. In the figure, the horizontal axis represents the high-pressure-stage turbine area, and the vertical axis represents the low-pressure-stage turbine area. It is observed that the EGR–turbo hardware capability and the range of controllability are very different at different speed–load modes. A trade-off decision usually needs to be made to select the best turbo sizes for the two stages. A similar dilemma exists between deciding to use a small turbine and to use intake throttle. Using a small turbine may help drive EGR at peak torque but causes higher pumping loss at rated power when the turbine is wastegated or bypassed. On the contrary, using intake throttle at peak torque may increase EGR a little (with a penalty of a large reduction in the air–fuel ratio) so that a larger turbine may be used for peak torque. Although the BSFC at rated power becomes lower due to the larger turbine, using intake throttle results in a BSFC penalty at peak torque. The wider the speed range, the more difficult the trade-off. The best solution is to use a VGT. If a VGT is not used, a wise trade-off decision needs to be made on turbine size based on the vehicle's frequent operating modes (low engine speed vs. high speed) and transient acceleration requirements.

To summarize, although the hardware selection process is interactive between subsystems, the following can be used as a general sequence: (1) exhaust restriction; (2) charge air cooler and EGR cooler capacity; (3) EGR circuit flow restriction; and (4) turbocharger. After the air system hardware has been specified for critical modes in normal and extreme ambient conditions, a simulation of virtual performance and emissions calibration in the entire engine speed-load domain needs to be conducted with proper parameter smoothing over the domain (an example was shown in Fig. 12.28). Transient powertrain simulation also needs to be carried out to evaluate the hardware's transient capability and electronic control algorithms.

12.10 Analytical design of mechanical components for system performance improvement

12.10.1 Roadmap of fuel economy improvement

In the efforts to improve fuel economy, the role of engine performance and system integration is to lead the way in defining a reasonable roadmap and

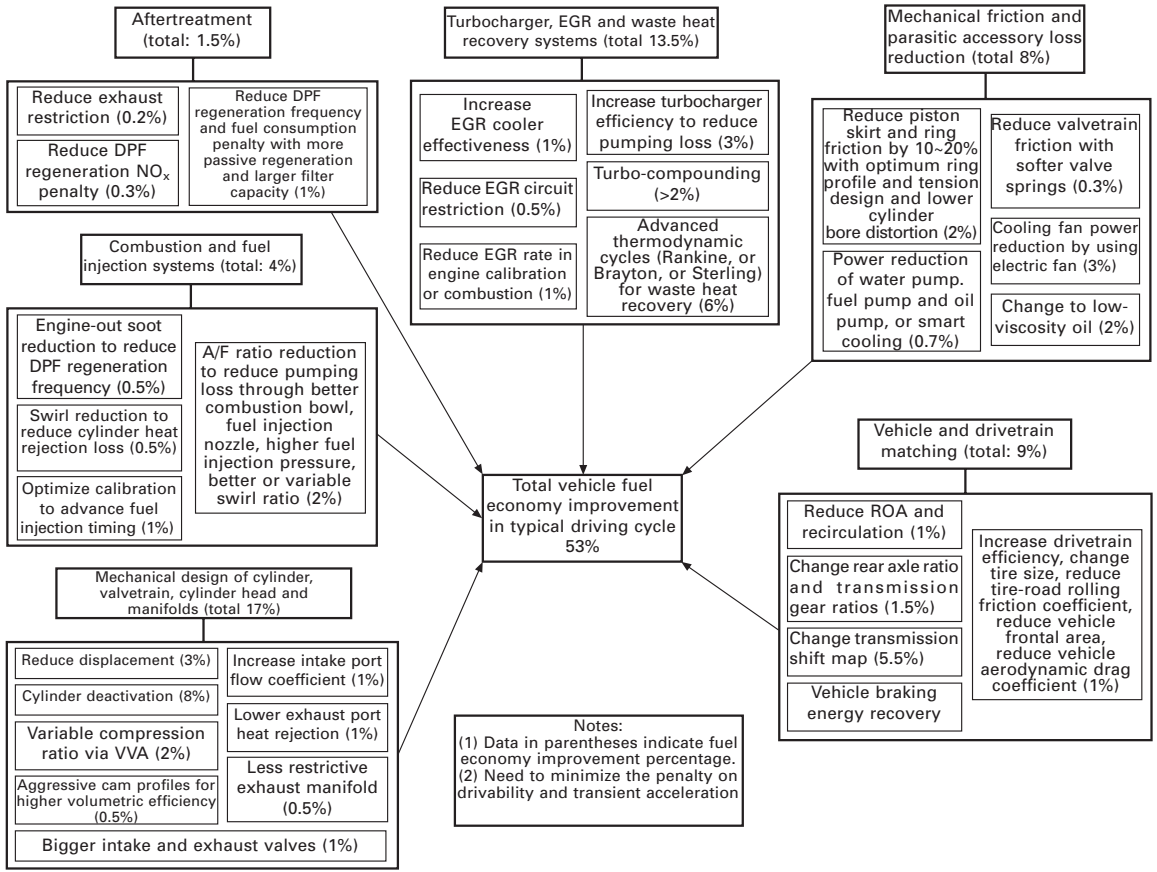


12.50 Optimization of two-stage turbocharging (simulation).

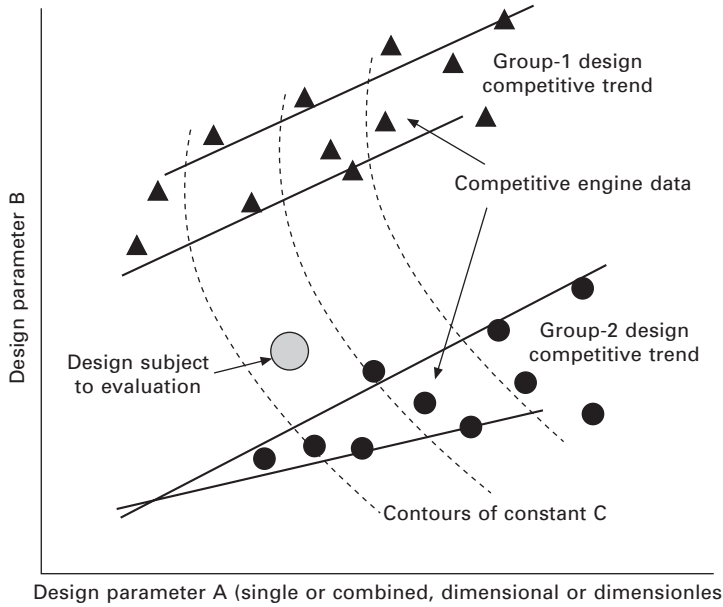
cascade it to each subsystem to implement design changes. The roadmap, as shown in Fig. 12.51 (for improving a non-optimized high pumping loss engine), usually consists of six areas: (1) aftertreatment, (2) combustion and fuel system, (3) mechanical design of cylinder, valvetrain, cylinder head and manifolds, (4) turbocharger, EGR and waste heat recovery systems, (5) mechanical friction and parasitic accessory losses, and (6) vehicle drivetrain matching. Improvements can be made either through incremental changes or by adopting new technologies. In any case, mechanical design and friction reduction are always important areas to address, accounting for 47% of the total improvement potential in the example shown in Fig. 12.51. For modern diesel engines, advanced analytical design has become increasingly critical in the areas of traditional mechanical component design in order to optimize their performance and reduce fuel consumption. The piston assembly tribological system and the valvetrain system are two of the most fascinating fields in the traditional design areas due to their complex nature. Understanding the advances that have been made and applying analytical design methods in these two areas are important for system design engineers. In this section, an overview is first given on the key topics of engine mechanical design and layout, which system design engineers need to know. Then, advanced modeling and design techniques on valvetrain and piston assembly are briefly introduced as examples.

12.10.2 Competitive benchmarking analysis and component design related to system layout

Heavy-duty diesel engine design details can be found in numerous books (for example, the overview by Merrion and Weber, 1999, and the vehicular engine design textbook by Hoag, 2006). These literatures cover empirical design guidelines for engine layout and component details including engine balance, cylinder head, block, water jacket, bearing, gasket, piston, crankshaft, camshaft, etc. Advanced design software and finite element analysis have been widely used in those areas. However, from EPSI's point of view, another way to enhance the quality of analysis in those traditional design areas is to apply a competitive benchmarking design analysis technique. The technique analyzes one fundamental design parameter against another by using a large amount of different engine design data to form empirical trend curves in order to check whether the subject design falls within or outside the range of the trend. The concept is shown in Fig. 12.52. A simple example is to plot stroke-to-bore ratio versus engine displacement for multiple engine power ratings. Such a competitive analysis is very effective for stroke and bore design. In fact, advanced competitive analysis is much more complex than that because it requires heuristic modeling and sometimes similarity theory to extract and group apparent design parameters to reflect the fundamental



12.51 Example of fuel economy improvement roadmap.



12.52 Concept of engine competitive benchmarking design analysis.

physics. Usually, in each complex mechanical system, it is possible to extract one or several fundamental design parameters in a certain combined form that manifests their physical nature of performance or durability in a rather intuitive and simple manner. Through such an analysis, major design problems can be quickly identified for further examination. It is important to identify those characteristic design parameters for each component and system.

Engine block and crankcase design

The design issues concerning the number of cylinders, engine balance, Vee bank angle and uneven firing order were discussed by Hoag (2006). Most diesel engines used for automotive cars and trucks are inline 4-cylinder (I4), inline 6-cylinder (I6), V6 and V8. The reciprocating mass is roughly proportional to the cube of the cylinder diameter. The I4 engine has a shorter block length. Although the secondary reciprocating inertia force of an I4 engine is not balanced, its magnitude is relatively small, being only a fraction of the primary inertia force. For I4 engines having a small cylinder diameter, the engine balance is still satisfactory. Therefore, I4 engines are popular in passenger cars and light trucks that have stringent requirements on engine size. I6 engines have the best engine balance and strong exhaust pulse energy for turbocharging. I6 is the most popular configuration for

commercial truck and bus engines. V8 engines with 90° bank angle are also popular because of their good engine balance and low height. V6 engines are the most compact in length and height, and are used in some passenger cars and light trucks. But the V6 engines with 90° bank angle have an unbalanced secondary reciprocating inertia force, and the V6 engines with 120° bank angle have an unbalanced primary inertia force.

High stiffness and strength, low NVH and low weight are important for engine block design. The potential competitive benchmarking parameters include the following: engine width; the geometric clearances between rotating moving parts and the inner wall of the engine block; engine length; and the 'e/B' ratio, which is the ratio between the cylinder-to-cylinder centerline distance and the cylinder bore diameter. Note that the 'e/B' ratio reflects the compactness of the engine length and is affected by crankshaft length, cylinder head and liner design. Plotting the 'e/B' ratio or typical thicknesses of engine block or head as a function of cylinder diameter for various engines is an example of conducting competitive design analysis.

Cylinder liner design

The following are important design considerations for cylinder liners: low friction and wear occurring on the inner surface between the linear and the piston ring or piston skirt; minimum cavitation occurring on the coolant side caused by piston slap and liner vibration; sufficient cooling at the liner top; proper metal surface temperature across the circumferential and axial directions; minimum bore distortion; and high stiffness for NVH reduction.

Cylinder head design

The subjects of cylinder head design usually include the following: number of valves; valve diameter and seat angle; port flow discharge coefficient and swirl ratio; intake and exhaust port orientation (to avoid intake port heating by exhaust gas); wall thickness; exhaust port length and heat rejection loss; cooling; fire deck temperature control in the area between the valves in the cylinder head (to prevent thermo-mechanical fatigue); cylinder head gasket design, etc. The basic competitive benchmarking parameters include (1) the ratio between port diameter and port length; (2) the ratio between port length and cylinder bore; (3) the swirl ratio vs. port flow coefficient (for the evaluation on the trade-off between in-cylinder turbulence and volumetric efficiency); (4) the number of cylinder head bolts and the head height (for stiffness and sealing evaluation); and (5) the ratio between cylinder head bottom wall thickness and bore diameter (for the evaluation on the trade-off between mechanical load and thermal load).

Connecting rod, crankshaft and engine bearing design

The design guidelines for power conversion components include the following: sufficient mechanical strength and stiffness in compression, stretch, torsional and bending motions under cylinder gas pressure and inertia loading; light weight and light balancing weight; compact geometry; smooth chamfers and low local stress; proper structural design of the lubricating oil feed hole angle; proper setting of bearing clearances; low bearing wear, friction and impact noise, etc. The basic competitive benchmarking parameters include (1) the connecting rod length, which affects engine height, width and piston assembly dynamics; (2) the ratio between connecting rod length and crank radius, which affects secondary reciprocating force and piston side thrust; (3) the crank pin diameter, which affects friction and rotating mass; (4) the main bearing diameter, which needs to satisfy strength and lubrication requirements and helps adjust the design selection of crank web thickness, crank pin diameter and cylinder centerline distance; (5) the overlap between the main bearing journal and the connecting rod crank pin journal, which affects crankshaft strength; and (6) the bearing aspect ratio (i.e., length divided by diameter).

12.10.3 Advanced analytical valvetrain system design

Guidelines for valvetrain design

In valvetrain design, the overspeed target and the valvetrain no-follow (separation) speed design target need to be established first. Engine overspeed may occur during a downshift with too low a gear or due to the vehicle overspeeding the engine in no-fuel motoring on a long downhill grade. The overspeed target needs to be higher than the high-idle speed, with a proper margin. The most important general design guidelines for the valvetrain of turbocharged EGR diesel engines are summarized as follows:

- Low valvetrain weight and high stiffness (i.e., high natural frequency)
- Coordinated design of cam profile and turbocharging to achieve high volumetric efficiency in a wide speed range with proper maximum valve lift, effective valve and port flow area and valve timing
- Relatively small valve overlap for less internal residue fraction and good transient acceleration
- No valve-to-piston contact but designed for tight clearance
- Low recompression pressure at valve overlap TDC achieved by appropriate turbine area and cam profile
- Smooth shape of cam acceleration and jerk; appropriate cam ramp height
- Coordinated design of cam profile, valvetrain dynamics and thermodynamic

cycle performance to achieve an acceptable valvetrain vibration level matched with no-follow speed target for being neither too low nor too high (i.e., on-target precise design for vibration level to maximize cam acceleration)
- Acceptable valve seating velocity and noise through cam design
- Optimized cam base circle, roller size, rocker arm ratio and maximum valve lift
- Acceptable minimum cam radius of curvature for cam machining
- Acceptable maximum pushrod force, cam stress and cam lubrication
- Minimum valve tip scrub achieved by optimum kinematic layout
- Low friction and wear achieved by good kinematics, dynamics and appropriate valve spring load
- No spring surge or coil clash/bind achieved by low cam harmonic amplitudes and proper spring design.

The heart of valvetrain design is the cam profile, which is critical for both engine breathing performance and valvetrain dynamics. It should be noted that the design of the end-pivot finger follower overhead cam is more complex than that of the pushrod cam due to its oscillating cam motion rather than translating motion. The calculations of cam radius of curvature are also different. The fundamentals of valvetrain design were introduced by Wang (2007).

The basic competitive valvetrain benchmarking parameters may include the following: valvetrain natural frequency; a parameter Φ which reflects the aggressiveness of cam acceleration, $\Phi = A_p \nu / N_E$ (where A_p is the duration of cam positive acceleration pulse, ν is valvetrain natural frequency, N_E is engine speed; note that higher Φ results in lower valvetrain vibration); cam base circle radius; valve spring load; valve overlap size; effective valve flow area; the ratio between valve diameter and bore diameter, etc.

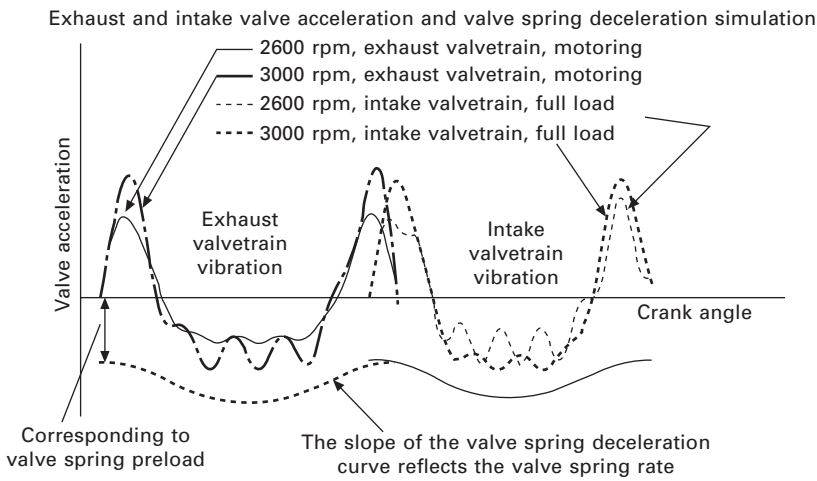
Variable valve actuation (VVA) may enhance diesel engine performance by varying the exhaust and intake valve timing or lift at different engine speeds to change the effective engine compression ratio, air–fuel ratio, BSFC and pumping loss. Intake VVA is an enabler for advanced combustion concepts such as HCCI. VVA can also regulate internal EGR and flexibly actuate cylinder deactivation and compression-release engine brakes.

Analytical system design and valvetrain parameter optimization

Analytical valvetrain design refers to using sophisticated simulation analysis tools in each of the following design steps and optimizing the relationships between the parameters in the valvetrain system:

1. Select an appropriate valvetrain no-follow speed target by vehicle and engine motoring braking analyses.

2. Use engine cycle simulation to determine the cam event duration, valve timing and overlap size together with turbo matching by considering the effect of engine delta P on gas exchange and reverse valve flow. The effect of valve recession on combustion chamber 'K-factor' also needs to be considered.
3. Determine the gas loadings from the cylinder and ports acting on the valvetrain by engine cycle simulation based on the preliminary valve lift profiles produced in step 2.
4. Based on engine firing and braking requirements, preliminarily choose the exhaust valve spring preload. Based on valvetrain dynamic acceleration simulation, select the preliminary spring rate (Fig. 12.53).
5. Determine the effect of gas loading on valvetrain vibration by dynamic simulation.
6. With given valve timing, valvetrain stiffness, weight, valve size and valvetrain lash, optimize a set of design parameters in the valvetrain system by using cam design tools and dynamic simulation to meet all the dynamics criteria (see above). The design parameters to be optimized together include maximum valve lift, rocker arm ratio, cam acceleration shape, base circle size, roller size, cam radius of curvature, and valve spring preload and rate.
7. Conduct valve spring coil design by constructing analytical design charts to examine the parametric dependency among spring diameter, coil diameter, coil clearance, spring natural frequency and stress.
8. Iterate from step 2 to step 7 until satisfactory trade-offs between all the design parameters are obtained.



12.53 Valvetrain dynamics simulation.

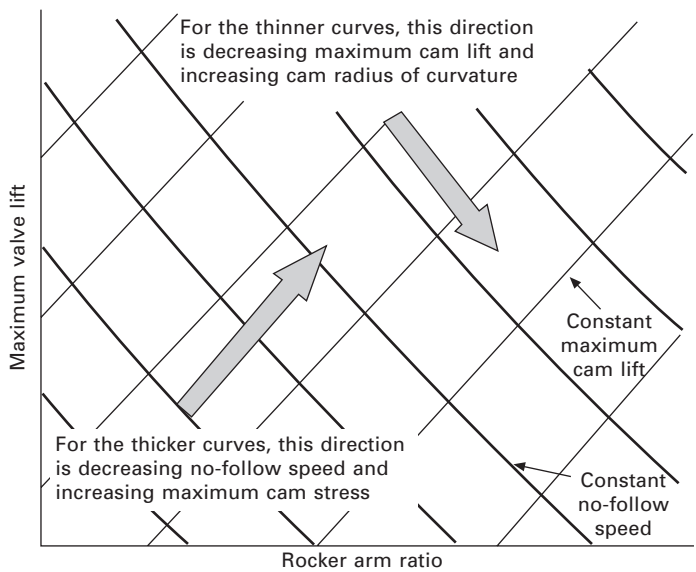
Apparently, valvetrain design is very complex. An iterative process or even DoE optimization is often required. Constructing parametric design charts is very useful in this process, as shown in Fig. 12.54 for cam design.

12.10.4 Piston assembly lubrication dynamics and low-friction analytical design

Overview of piston assembly dynamics

The piston in modern diesel engines needs to have strong thermo-mechanical strength to withstand the peak cylinder pressure and temperature. It also needs to have low friction and wear, low piston slap noise, good control on skirt distortion, proper cooling and lubrication, and light weight (for high-speed operation), and to match with the right combustion chamber shape. Piston rings seal the in-cylinder gas with little blow-by, transfer heat from piston to cylinder liner, and control lube oil consumption. Low-friction piston assembly design is very important for engine fuel consumption. Both analytical and experimental methods play critical roles in piston tribological design.

In heavy-duty diesel engines, piston slap has been identified as the main cause of cylinder liner cavitation due to the high impact energy of the slap. Piston slap can also be the most prominent source of mechanical noise during warm-up. Mechanical noises emitted from the engine surface are caused by impact between the components and the resulting vibration and become



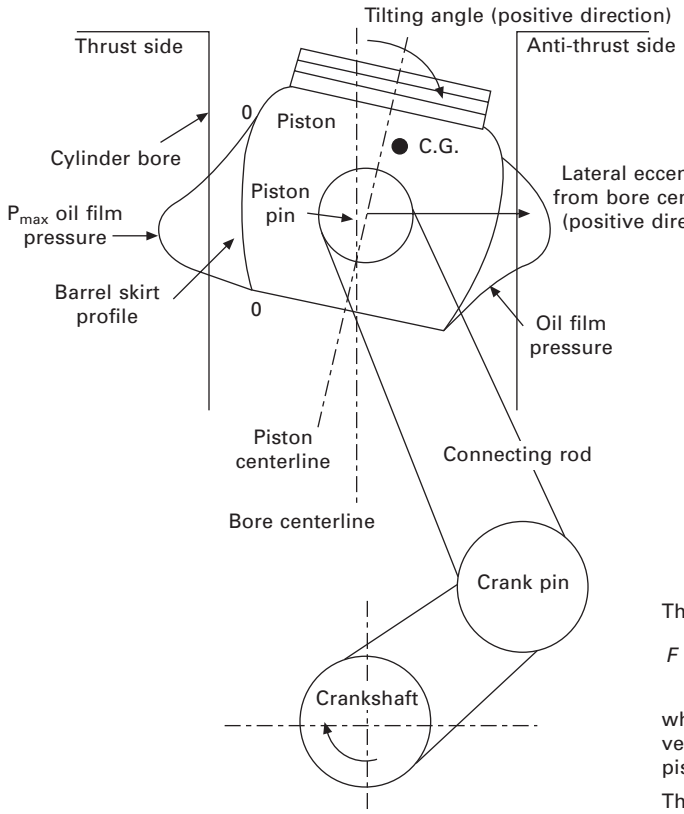
12.54 Parametric design chart for cam design.

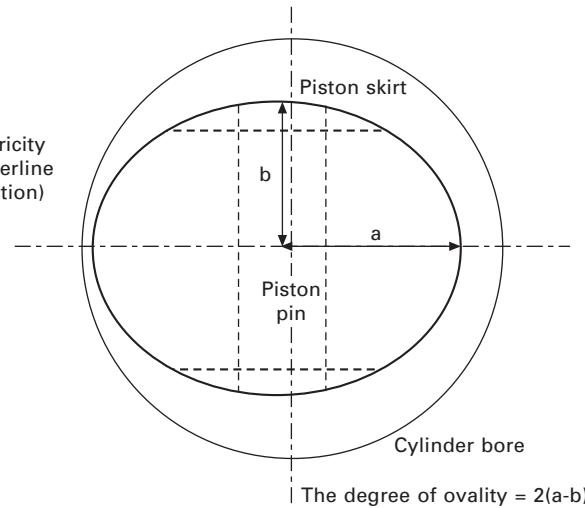
louder as the engine speed increases. The noises are due mainly to piston slap, gear rattling, valve seating, impact within bearings, high-pressure oil pump noise, engine block vibration, etc. In piston tribological design analysis, piston skirt friction power, dynamic minimum lubricating oil film thickness and cold piston slap kinetic energy (or noise) are the three most important performance parameters that should be considered simultaneously. They are interrelated, and analytical simulation plays a critical role in their design optimization.

An analytical model of piston lubrication dynamics is shown in Fig. 12.55. The following design and operating parameters affect piston dynamics: (1) piston mass (including piston pin); (2) connecting rod mass; (3) piston tilting moment of inertia; (4) connecting rod rotating moment of inertia; (5) piston skirt-to-bore clearance; (6) piston center of gravity position (lateral and vertical); (7) piston pin position (lateral and vertical); (8) piston skirt length; (9) piston skirt lubrication wetted arc angle; (10) piston skirt axial profile and ovality; (11) lubricant oil viscosity; (12) engine speed and load, etc. The outputs of the model include piston primary motion (i.e., reciprocating sliding motion) and piston skirt secondary motions (i.e., lateral and tilting motions within the skirt-to-bore clearance), the lubricating oil film thickness and oil film pressure distribution on the piston skirt, frictional forces in the hydrodynamic lubrication regime and metal-to-metal contact scraping regime, and so on.

The analytical model includes piston assembly multi-body dynamics coupled with piston skirt lubrication. The lubrication model is based on the viscous fluid Reynolds equation. This is solved with the finite-difference numerical method for the lubricating oil film pressure distribution after the piston skirt secondary motions are computed at each time step. The three-dimensional oil pressure distribution is then integrated over the skirt surface to obtain the lubricant force and moment, which are used in the dynamics model at each time step. The ordinary differential equations in the multi-body dynamics model must be solved by implicit time-marching integration to obtain the piston secondary motions and primary motion. The motions of the connecting rod and the forces acting on the piston pin, crank pin and crankshaft are also computed. The side thrust (lateral force acting on the piston pin) results from cylinder gas pressure and inertia forces, and induces piston lateral motion. Piston tilting is caused by the moments acting on the piston skirt from various forces (side thrust, vertical force acting on the piston pin, cylinder pressure, lubricant forces, frictional forces between skirt and rings, piston pin friction). The piston skirt friction power is equal to the friction force multiplied by the velocity of piston primary motion.

The piston skirt lubrication model can simulate both a cylindrical skirt and a non-cylindrical skirt, e.g., a barrel shape in the axial direction with ovality in the circumferential direction. Usually, a piston skirt has a barrel profile





Oval piston in cylindrical bore (top view)

The hydrodynamic friction force acting on piston skirt is

$$F = -\int_0^{L_{piston}} \int_0^{2\pi} \left(\frac{h}{2} \frac{\partial P}{\partial y} + \frac{\mu}{h} V \right) R_{piston} \, d\varphi dy$$

where h is oil film thickness, P oil pressure, V piston sliding velocity, μ oil viscosity, L piston length; and y represents piston axial direction, φ piston circumferential direction.

The frictional power loss is given by $\dot{W} = FV$

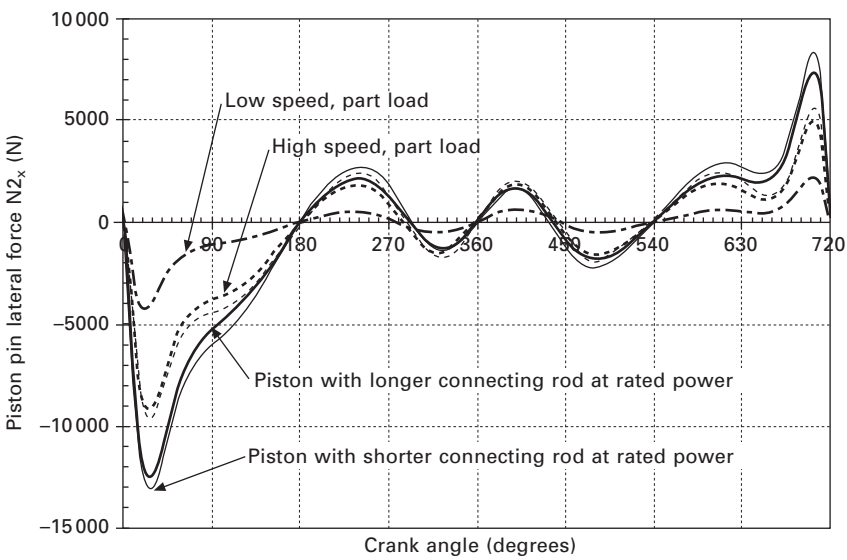
12.55 Illustration of piston-assembly lubrication dynamics model.

at cold. At hot condition the barrel shape and ovality change as the piston expands thermally. As the piston moves laterally and tilts within the clearance between skirt and cylinder bore, the lubricating oil film thickness changes dynamically at each moment during an engine cycle, and the film thickness distribution changes spatially on the piston skirt as well. The piston skirt wear durability can be analytically characterized by the dynamic minimum oil film thickness within an engine cycle at the thrust side and anti-thrust side. When different piston designs are compared, a larger minimum oil film thickness usually reflects better wear durability or a lower risk of wear and scuffing.

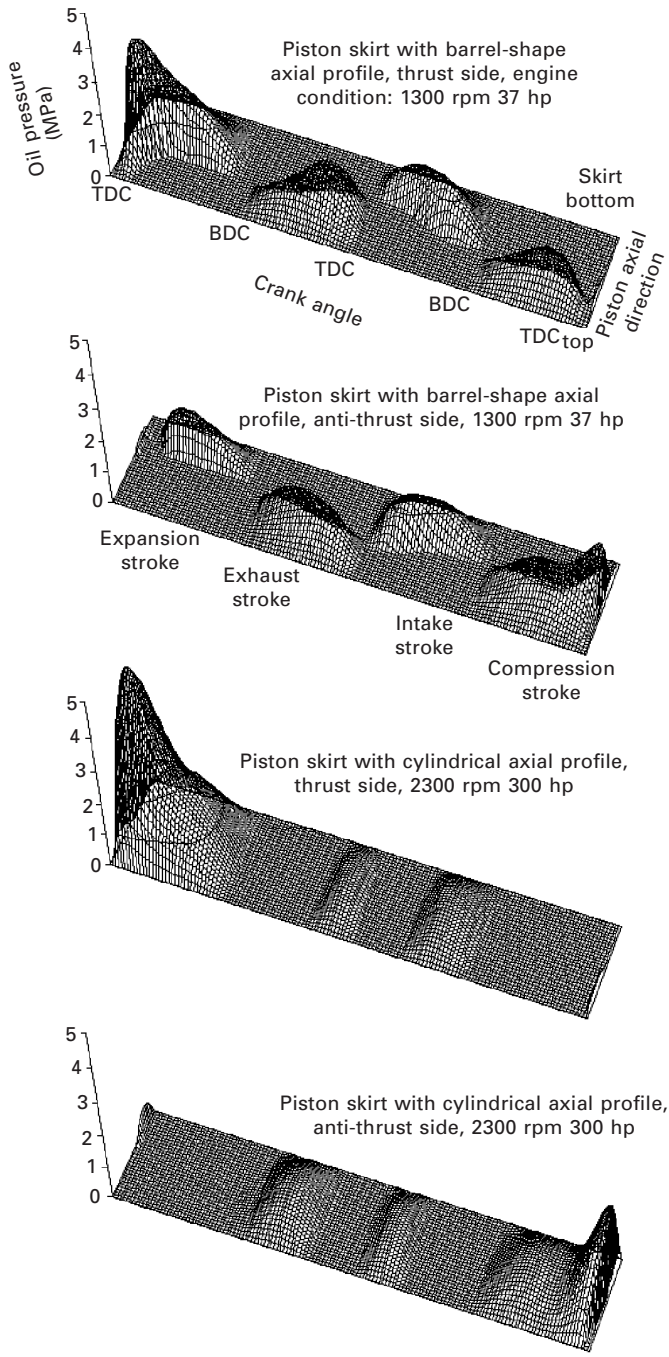
In the design process, the hot piston skirt profile can be optimized by lubrication dynamics simulation, then converted to the corresponding cold profile using finite element thermal contraction analysis to determine the theoretical cold skirt profile design. But a skirt profile experimental test is still needed to cover the complexity and uncertainties caused by cylinder bore distortion and piston deformation in hot dynamic conditions.

The effects of piston design on skirt friction and piston slap

Figure 12.56 shows the computed typical instantaneous variation of piston side thrust within one engine cycle for three speed and load conditions. It is observed that a longer connecting rod reduces piston side thrust. Figure 12.57



12.56 Illustration of piston side thrust at different speeds and loads.



12.57 Lubricating oil pressure distribution on piston skirt.

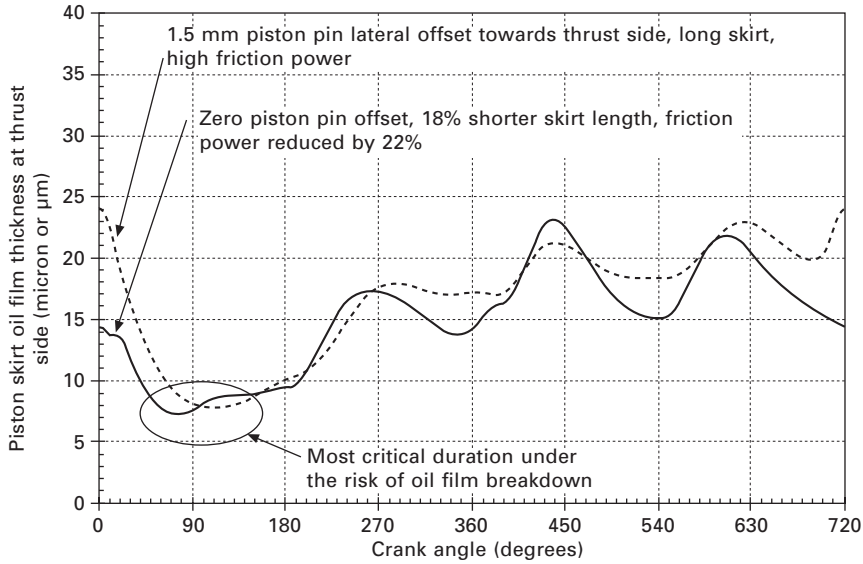
shows the lubricating oil pressure distribution on the piston skirt computed by using the lubrication dynamics model. The oil pressure is generated by a combination of lubrication 'wedge' and 'squeeze' effects caused by piston secondary motions. Zero pressure is caused by oil film cavitation. Note that different skirt profile shapes generate distinct patterns of oil pressure distribution on the thrust side and the anti-thrust side. For example, during the expansion stroke, a cylindrical skirt profile produces oil pressure only at the thrust side, while a barrel profile generates oil pressure at the lower portion of the skirt on both the thrust and anti-thrust sides.

Simulation shows that as long as the piston skirt is designed to operate in the hydrodynamic lubrication regime, at the same engine speed but different loads, piston skirt hydrodynamic lubrication friction power varies in a range of 0.2–2% (depending on skirt profile). However, different piston pin positions can result in up to a 10% difference in the hydrodynamic lubrication friction power of the piston skirt (higher friction corresponding to more violent secondary motions). Piston weight has a very small influence on skirt friction power and a negligible effect on oil film thickness, but piston weight reduction decreases piston slap kinetic energy and noise at cold. An effective way to reduce piston skirt friction power is to reduce the skirt area (i.e., skirt length or lubricating wetted arc angle). Skirt friction power reduction is basically linearly proportional to the reduction of skirt area. Figure 12.58 simulates the complex nature of piston secondary motions within the lubricating oil film clearance at a high engine speed. The motion and friction are affected by piston design parameters.

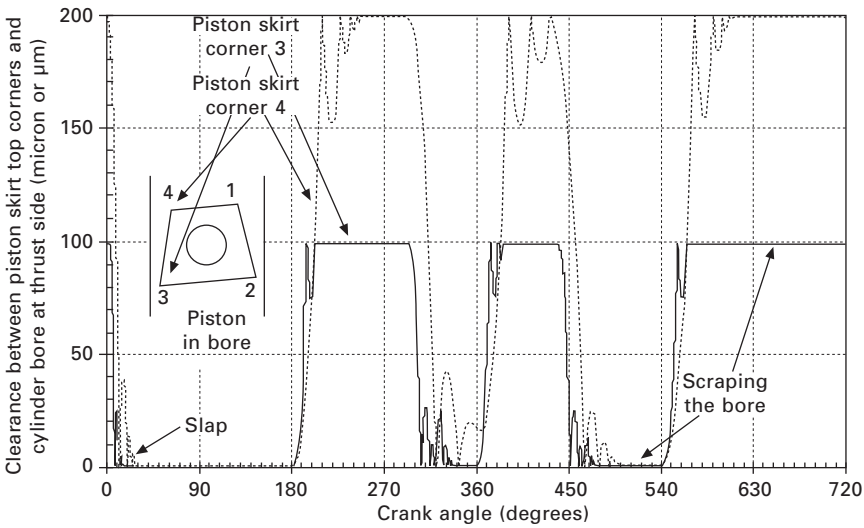
Within an entire engine cycle, piston slap is usually most severe and noisiest during the expansion stroke (0°–180°) due to the high in-cylinder firing pressure in the expansion stroke. Offsetting the piston pin to the thrust side usually reduces the severity of piston slap at the more rigid upper portion of the piston skirt during the expansion stroke. But the piston slap at the less stiff lower portion of the skirt in other strokes might increase. Figure 12.59 shows the simulated piston slap and rebound motions of a cold piston with simplified skirt profile without effective skirt lubrication during one engine cycle (at 2300 rpm engine speed). The simulation provides insights into the complex physical processes that are difficult to measure.

12.11 Future trends

The stringent emission regulations and ever-increasing customer demands on power, fuel economy and NVH will impose greater challenges on future diesel technologies, including direct fuel injection, advanced combustion and air systems, aftertreatment, electronic controls and powertrain integration. Fast-paced optimal engine product development requires a precise emission-driven system design approach to integrate different technical areas in



12.58 Effect of piston design on skirt friction power and oil film thickness.



12.59 Simulation of cold piston slap motion without effective lubrication.

order to reduce development time and cost. Being an emerging technical field, diesel engine system design supported by engine performance and system integration (EPSI) analysis will become increasingly important. The

three cornerstones of EPSI analysis are engine–vehicle matching, engine–aftertreatment matching, and engine–turbocharger matching, surrounded by many boundary conditions such as the requirements from combustion, emissions, cooling, structure, etc.

This chapter summarizes the theory and analytical approaches of diesel engine system design, and elaborates its relationship with other related technical fields. It also provides a new look at the traditional mechanical design areas with the viewpoint of diesel engine system design. As outlined in each earlier section, in order to make simulations more accurate and the system integration process more effective, key research topics in EPSI need to be identified not only within each subsystem itself but also at all the interfaces between vehicle, engine, aftertreatment, combustion, turbocharger and EGR system. Design of Experiments (DoE), neural networks and their mathematical optimization are standard data processing techniques used in EPSI. The fundamental theory presented in Section 12.2 can be used to explore the options of low-pumping-loss engine design and model-based controls. The vehicle integration theory in Section 12.3 can be used to build a truly 'top-down' optimization design approach targeting real-world driving profiles. Challenging research remains in combustion, emissions (Section 12.4) and aftertreatment (Section 12.5) areas to develop heuristic system models that are suitable for EPSI's needs. In the heat transfer area (Section 12.6), further research is required to model EGR cooler soot fouling, transient heat transfer and exhaust manifold temperature. Section 12.7 points out the causes of engine subsystem interaction by applying the mathematical theory of Section 12.2 to engine applications. As to electronic controls, owing to the need to accurately simulate engine load response, vehicle driving cycles and aftertreatment regeneration transients, EPSI and system design will require tremendous effort in transient powertrain performance modeling combined with developing model-based controls, despite the great challenges in transient simulations. All the above-mentioned advances ultimately should lead to a successful engine system specification design and optimization of hardware subsystem interaction as well as virtual engine calibration in a four-dimensional design space (Section 12.9). Moreover, the concept of advanced analytical design and system integration should not be limited to the emerging advanced technologies but should also penetrate all traditional mechanical design areas to enhance the quality of every subsystem design and competitive data comparison (Section 12.10) for continuous improvement of fuel economy.

EPSI not only provides an engine system design approach, it also participates and integrates modern technologies emerging from each subsystem of engine design, for example diesel HCCI, improved thermodynamic cycles, advanced turbocharging, cylinder downsizing or deactivation, hybrid EGR system, variable compression ratio, variable swirl, variable valve actuation,

flexible cooling, hybrid diesel powertrain and energy recovery, closed-loop combustion control, and mapless engine controls. Evaluating the impact of new engine technologies on each other and optimally integrating them is the role of engine system design. The question will be 'To design a good cost-effective system, do we really need to adopt many of these technologies in one engine? If not, how should we simplify the package?' It is very important to use a system integration approach to study engine performance for future powertrains.

12.12 References

Ammann M, Fekete N P, Guzzella L and Glattfelder A H (2003), 'Model-based control of the VGT and EGR in a turbocharged common-rail diesel engine: theory and passenger car implementation', SAE paper 2003-01-0357.

Arnold S D (2004), 'Turbocharging technologies to meet critical performance demands of ultra-low emissions diesel engines', SAE paper 2004-01-1359.

Atkinson C and Mott G (2005), 'Dynamic model-based calibration optimization: an introduction and application to diesel engines', SAE paper 2005-01-0026.

Basshuysen R and Schafer F (2004), *Internal Combustion Engine Handbook*, SAE International, Warrendale, PA.

Benson R S (edited by Horlock J H and Winterbone D E) (1982), *The Thermodynamics and Gas Dynamics of Internal Combustion Engines*, Volume 1, Clarendon Press, Oxford.

Blakeman P G, Chiffey A F, Phillips P R, Twigg M V and Walker A P (2003), 'Development in diesel emissions aftertreatment technology', SAE paper 2003-01-3753.

Capobiano M, Gambarotta A and Cipolla G (1989), 'Influence of the pulsating flow operation on the turbine characteristics of a small internal combustion engine turbocharger', IMechE paper C372/019/1989, *IMechE Conference Transactions of the Seventh International Conference on Turbochargers and Turbocharging*.

Chalgren R D, Parker G G, Arici O and Johnson J (2002), 'A controlled EGR cooling system for heavy duty diesel applications using the vehicle engine cooling system simulation', SAE paper 2002-01-0076.

Challen B and Baranescu R (1999), *Diesel Engine Reference Book*, second edition, SAE International, Warrendale, PA.

Chana H E, Fedewa W L and Mahoney J E (1977), 'An analytical study of transmission modifications as related to vehicle performance and economy', SAE paper 770418.

Eastwood P (2000), *Critical Topics in Exhaust Gas Aftertreatment*, Research Studies Press, Baldock, UK.

Eastwood P (2008), *Particulate Emissions from Vehicles*, Wiley Interscience, New York.

Flynn P F (2001), 'How chemistry controls engine design', *Proceedings of the 2001 Fall Technical Conference of the ASME Internal Combustion Engine Division, Diesel Combustion and Emissions, Fuel Injection and Sprays*, Volume 1, pp. 1–9.

Heywood J B (1988), *Internal Combustion Engine Fundamentals*, McGraw-Hill, New York.

Hoag K L (2006), *Vehicular Engine Design*, SAE International and Springer-Verlag, Vienna.

Hochegger W, Hrauda G, Prenninger P and Seitz H F (2002), 'Effect of various EGR systems on HDT-turbocharging', IMechE paper C602/040/2002.

Horlock J H and Winterbone D E (1986), *The Thermodynamics and Gas Dynamics of Internal Combustion Engines*, Volume 2, Clarendon Press, Oxford.

Jacobs T, Assanis D and Filipi Z (2003), 'The impact of exhaust gas recirculation on performance and emissions of a heavy-duty diesel engine', SAE paper 2003-01-1068.

Jaichandar S and Tamilporai P (2003), 'Low heat rejection engines – an overview', SAE paper 2003-01-0405.

Johnson T V (2007a), 'Diesel emission control in review', SAE paper 2007-01-1233.

Johnson T V (2007b), *Diesel Particulate Filter Technology*, SAE International, Warrendale, PA.

Kim J Y, Cavataio G, Patterson J E, Laing P M and Lambert C K (2007), 'Laboratory studies and mathematical modeling of urea SCR catalyst performance', SAE paper 2007-01-1573.

Kluger M and Greenbaum J J (1993), 'Automatic transmission efficiency characteristics and gearbox torque loss data regression techniques', SAE paper 930907.

Konstandopoulos A G, Kostoglou M, Skaperdas E, Papaioannou E, Zarvalis D and Kladopoulou E (2000), 'Fundamental studies of diesel particulate filters: transient loading, regeneration and aging', SAE paper 2000-01-1016.

Konstandopoulos A G, Kostoglou M, Vlachos N and Kladopoulou E (2005), 'Progress in diesel particulate filter simulation', SAE paper 2005-01-0946.

Majewski W A and Khair M K (2006), *Diesel Emissions and Their Control*, SAE International, Warrendale, PA.

Merrion D and Weber K E (1999), 'Trucks and buses', in Challen B and Baranescu R, *Diesel Engine Reference Book*, second edition, SAE International, Warrendale, PA, pp. 553–585.

Nieuwstadt M (2003), 'Coordinated control of EGR valve and intake throttle for better fuel economy in diesel engines', SAE paper 2003-01-0362.

Nunney M J (1998), *Automotive Technology*, third edition, SAE International, Warrendale, PA.

Osborne R P and Morris T (2002), 'Aspects of EGR control on turbocharged light-duty diesel engines', IMechE paper C602/013/2002.

Pearson R J, Bassett M D, Winterbone D E and Bromnick P A (2000), 'Comprehensive charge-cooler model for simulating gas dynamics in engine manifolds', SAE paper 2000-01-1264.

Rodgers C and Rochford K (2002), 'Small turbocharger turbomachinery', IMechE paper C602/003/2002.

Ryder O, McKenzie D J A and Johnson S (2002), 'Turbo matching techniques for highly cyclic bus applications', IMechE paper C602/006/2002.

Schulten P J M and Stapersma D (2003), 'Mean value modeling of the gas exchange of a 4-stroke diesel engine for use in powertrain applications', SAE paper 2003-01-0219.

Soeger N, *et al*. (2005), 'Impact of aging and NO_x/soot ratio on the performance of a catalyzed particulate filter for heavy duty diesel applications', SAE paper 2005-01-0663.

Steinberg P and Goblau D (2004), 'Fuel consumption', in Basshuysen R and Schafer F, *Internal Combustion Engine Handbook*, SAE International, Warrendale, PA, pp. 737–751.

Stobart R K, Challen B J and Bowyer R (2001), 'Electronic controls – breeding new engines', SAE paper 2001-01-0255.

Stone R (1999), *Introduction to Internal Combustion Engines*, third edition, SAE International, Warrendale, PA.

Taraza D, Henein N and Bryzik W (2000), 'Friction losses in multi-cylinder diesel engines', SAE paper 2000-01-0921.

Taraza D, Henein N, Ceausu R and Bryzik W (2007), 'Engine friction model for transient operation of turbocharged, common rail diesel engines', SAE paper 2007-01-1460.

Wang Y (2007), *Introduction to Engine Valvetrains*, SAE International, Warrendale, PA.

Watson N (1999), 'The theory of turbocharging', in Challen B and Baranescu R, *Diesel Engine Reference Book*, second edition, SAE International, Warrendale, PA, pp. 27–72.

Watson N and Janota M S (1982), *Turbocharging the Internal Combustion Engine*, Macmillan, London.

Westin F and Angstorm H E (2002), 'A method of investigating the on-engine turbine efficiency combining experiments and modeling', IMechE paper C602/029/2002.

Willems F, Cloudt R, Eijnden E, Genderen M, Verbeek R, Jager B, Boomsma W and Heuvel I (2007), 'Is close-loop SCR control required to meet future emission targets?', SAE paper 2007-01-1574.

Winterbone D E and Pearson R J (1999), *Design Techniques for Engine Manifolds*, SAE International, Warrendale, PA.

Winterbone D E and Pearson R J (2000), *Theory of Engine Manifold Design*, Professional Engineering Publishing, London and Burry St Edmunds.

Wong J Y (1993), *Theory of Ground Vehicles*, John Wiley & Sons, New York.

Wong L T and Clemens W J (1979), 'Powertrain matching for better fuel economy', SAE paper 790045.

Xin Q and Zheng J (2009), 'Theoretical analysis of internal combustion engine miscellaneous heat losses', SAE paper 2009-01-2881.

Yamaguchi S, Fujii S, Kai R, Miyazaki M, Miyairi Y, Miwa S and Busch P (2005), 'Design optimization of wall flow type catalyzed cordierite particulate filter for heavy duty diesel', SAE paper 2005-01-0666.

Zhang R, Charles F, Ewing D, Chang J-S and Cotton J S (2004), 'Effect of diesel soot deposition on the performance of exhaust gas recirculation cooling devices', SAE paper 2004-01-0122.

Zheng J and Xin Q (2009), 'Theoretical analysis of diesel engine NO_x and soot with heuristic macro-parameter-dependent approach and virtual multi-zone real-time models', SAE paper 2009-01-2836.

Zhu Y, Ricart-Ugaz L, Wu S, Cigler J, El-Beshbeeshy M, Bulicz T and Yan J (2004), 'Combustion development of the new International 6.0L V8 diesel engine', SAE paper 2004-01-1404.

13
Fuel reforming for diesel engines

A. MEGARITIS, Brunel University, UK, A. TSOLAKIS and M. L. WYSZYNSKI, University of Birmingham, UK and S. E. GOLUNSKI, Johnson Matthey Technology Centre, UK

Abstract: This chapter reviews the application of fuel reforming in diesel engines for on-board generation of hydrogen-rich gas (reformate). The chapter first provides background information about engine fuel reforming applications. It then presents theoretical aspects of hydrogen production by fuel reforming including reforming thermodynamics and modelling, followed by discussion about diesel fuel reforming process parameters and reforming catalyst screening and evaluation. Finally, issues related to different applications of diesel fuel reforming and the corresponding requirements in terms of reforming catalysts and reactor designs are discussed. This discussion includes reforming applications aiming to produce reformate for utilisation as diesel combustion and emissions improver, and as diesel exhaust aftertreatment improver.

Key words: fuel reforming, hydrogen, reforming catalysts, reforming for diesel combustion and emissions, reforming for diesel aftertreatment.

13.1 Why fuel reforming in diesel engines?

13.1.1 Need for hydrogen in diesel engines

It is fair to say that the ongoing global effort to optimise IC engine emissions and performance, by improving fuel injection systems, mixture preparation, combustion chamber design, and exhaust aftertreatment, has resulted in significant advances in modern diesel engine technology. However, despite substantial reduction in engine emissions and improvements in fuel economy, further development is required in order to counterbalance the overall increased production and use of IC engines, and specifically to help reduce not only regulated pollutant emissions such as NO_x and particulate matter (PM) but also greenhouse gases (GHGs) such as CO_2. It is expected that further technological advances will include evolution of combustion systems to reduce engine-out emissions, development of new aftertreatment systems, and improvements in the coupling between engine and aftertreatment system operation (Wallington *et al.*, 2006).

In the longer term, fuel cell technology is expected to bring about a step change in energy efficiency of powertrains, together with the complete eradication of GHG emissions during their use. Progress towards a hydrogen

economy, which is essential for many fuel cell applications, has been picking up pace since the second half of the 1990s. One of the unexpected benefits has been the development of fuel-reforming reactors, which had originally been seen as a transition solution to on-board hydrogen supply, prior to the infrastructure for hydrogen distribution and storage being put in place. Although intended as an enabling technology for fuel cell systems, on-board reforming is now being seriously considered as a means of extending the performance of modern IC engines and advanced aftertreatment units.

Until problems related to hydrogen distribution and on-board storage are resolved, a transition solution to the use of pure hydrogen seems to be the use of hydrogen, produced on-board from hydrocarbon fuels by fuel reforming, as a supplement to the engine main fuel. Increasingly stringent legislation demands engine emission control that is at or beyond the capability of conventional aftertreatment catalysts, and fuel reforming is one of the alternative means of reducing emissions that are under consideration. Attention has been focused on the conversion of more readily available fuels, such as diesel, to hydrogen on board the vehicle. On-board reforming of high-energy density diesel type fuels (Kopasz *et al.*, 2005; Tsolakis and Megaritis, 2004; Abu-Jrai *et al.*, 2006; Tsolakis and Golunski, 2006) including renewable fuels (Tsolakis *et al.*, 2003, 2005b) to produce hydrogen that can be utilised in diesel engines on an as-needed basis is nowadays considered as one of the promising technology routes to improve diesel engine combustion, emissions and aftertreatment performance.

13.1.2 History of engine applications of H_2 addition

The use of hydrogen as fuel for IC engines or as a supplement to the main hydrocarbon (gaseous or liquid) engine fuel was initially researched for spark ignition (SI) engines (e.g. Steban and Parks, 1974; Houseman and Hoehn, 1974; Allenby *et al.*, 2001; Kirwan *et al.*, 2002; Kwon *et al.*, 2006; Verhelst *et al.*, 2006; Bysveen, 2007). In the last decade hydrogen has also been extensively researched as a supplement to the main hydrocarbon fuel for compression ignition engines including standard diesel engines (e.g. Tsolakis *et al.*, 2003, 2005c; Abu-Jrai *et al.*, 2006), and CAI (controlled autoignition) or HCCI (homogeneous charge compression ignition) engines (e.g. Yap *et al.*, 2006), as well as for gas turbines (Juste, 2006).

The use of hydrogen as an addition to the hydrocarbon fuel in SI engines has been reported to extend the lean SI engine operation limits and hence provide higher thermal efficiency and better fuel economy by reducing heat losses and at low load engine operation pumping losses. Benefits in reducing both emissions (especially NO_x) and the tendency of knocking due to leaner engine operation have also been reported (Bysveen, 2007).

Hydrogen enrichment can increase the tolerance of a stoichiometrically

fuelled natural gas (NG) engine to high levels of dilution by exhaust gas recirculation (EGR). This provides significant gains in terms of exhaust emissions without the rapid reduction in combustion stability typically seen when applying EGR to methane and gasoline fuelled engines (Allenby *et al.*, 2001).

In HCCI or CAI engines, hydrogen can extend the engine operating range. For example in the case of NG HCCI operation, it has been reported that hydrogen addition can result in lower intake temperature requirements for a given combustion phasing and that, for a given intake temperature, extension of the lower engine load range can be achieved with hydrogen addition (Yap *et al.*, 2006).

In the case of diesel engines the substitution of part of the main hydrocarbon fuel by hydrogen has been reported to be beneficial mainly in terms of emissions reduction (CO, HC, NO_x, PM) and is regarded primarily as a feasible solution to the so-called PM-NO_x trade-off problem and to a lesser extent as a means of improvements in engine brake power, thermal efficiency and combustion stability (Tsolakis *et al.*, 2003, 2005c; Abu-Jrai *et al.*, 2006).

However, engine operation with hydrogen addition may lead to undesired conditions that are associated with disadvantages of hydrogen as an engine fuel (main fuel). Such hydrogen addition disadvantages can arise from the combination of hydrogen's low activation energy and rapid combustion which can lead to abnormal combustion in forms of knock, pre-ignition and backfire under some operating conditions (Verhelst *et al.*, 2006; Swain *et al.*, 1996; Koyanagi *et al.*, 1994).

In the last years, addition of hydrogen-rich reformate as a means of improving the performance of diesel exhaust aftertreatment processes has also attracted interest. Addition of reformate to aftertreatment systems is beneficial because, as has been shown, hydrogen can improve the performance of catalytic aftertreatment devices by improving emission reduction and regeneration (e.g. NO_x traps, diesel particulate filters) or by expanding the catalyst activity windows towards low temperatures (Houel *et al.*, 2007; Abu-Jrai and Tsolakis, 2007; Abu-Jrai *et al.*, 2007). For this reason, on-board availability of hydrogen produced by fuel reforming will be advantageous for an efficient modern diesel engine aftertreatment system.

13.1.3 Fuel reforming for automotive on-board and stationary applications

On-board fuel reforming for automotive applications is still more marketable than on-board hydrogen storage as long as any added complexity is transparent to the consumer and does not sacrifice any aesthetic or performance characteristics such as fuel economy, acceleration, combustion stability

and in general smooth operation and drivability. The fuel reformer has to be dynamically responsive to the engine demand for reformate (Ahmed and Krumpelt, 2001; Tsolakis *et al*., 2005b; Abu-Jrai *et al*., 2006; Tsolakis and Golunski, 2006), while the catalyst has to be active under a range of operating conditions and durable enough to maintain good performance after several temperature (600–1100°C) and sudden reactant changes that can lead to catalyst deactivation, either short-term (e.g. coking) or everlasting (e.g. sintering, sulphur or silica poisoning).

For stationary power generation that involves internal combustion engines or gas turbines and under engine operation at constant speed–load applications, fuel reforming of liquid fuels is significantly simpler than on-board fuel reforming; however, the advantages compared to hydrogen storage technologies can be significantly reduced. For those types of applications, problems related to hydrogen storage and distribution can be resolved but new costs related to hydrogen distribution and storage will be introduced. On the other hand, reforming reactor and catalyst design complexities and associated costs will be significantly lower compared to on-board applications while the total reformer-catalyst lifetime will be improved.

13.2 Diesel fuel reforming theory

13.2.1 Chemical routes to hydrogen

The oil crisis of the 1970s prompted the earliest attempts at the development of small on-board reforming technology, at a time when the need for substantially improved fuel economy was first becoming apparent on a global scale (Jamal and Wyszynski, 1994, and references therein). In the following decades, much of the development effort was redirected at using reforming as the first step in generating neat hydrogen from a variety of fuels, including alcohols, on fuel cell-powered vehicles (Trimm and Onsan, 2001; Faur Ghenciu, 2002). Over the last few years, however, with a move towards the introduction of stored hydrogen as the primary fuel for mobile fuel cells, the first commercial application of on-board reforming is once more expected to be on IC vehicles (Marsh *et al*., 2000; Kirwan *et al*., 2002; Tsolakis *et al*., 2003).

In developing on-board reforming technology, the available chemical routes are no different from those used for the industrial production of hydrogen (Rostrup-Nielsen T., 2005) or synthesis gas (Wilhelm *et al*., 2001; Rostrup-Nielsen J.R., 2002). This is because, irrespective of scale or the nature of the hydrocarbon fuel, the main reactions involved in producing a hydrogen-rich gas stream are *partial oxidation, steam reforming, direct dissociation* and *dry reforming*. These reactions can be used individually, or combined either in parallel or consecutively. Where the overall route is a combination

of an exothermic reaction (partial or complete oxidation) and one or more endothermic reactions (steam reforming, direct dissociation, dry reforming), it is generally referred to as autothermal reforming.

In partial oxidation, the fuel reacts with a limited amount of oxygen, which is usually supplied as air. In principle, this reaction can generate varying proportions of CO, CO_2 and H_2, depending on the reactant stoichiometry, e.g. for a diesel fuel:

$$C_nH_{1.88n} + (n/2)O_2 \rightarrow nCO + 0.94nH_2 \qquad \Delta H_{298} = -1237 \text{ kJ/mole} \tag{13.1}$$

$$C_nH_{1.88n} + nO_2 \rightarrow nCO_2 + 0.94nH_2 \qquad \Delta H_{298} = -5498 \text{ kJ/mole} \tag{13.2}$$

This approach is frequently the first to be considered for on-board fuel reforming applications, even though the resulting hydrogen-containing gas has a lower calorific value than the original feedstock (Houseman and Hoehn, 1974), which has a detrimental impact on efficiency. Its advantages arise from the overall rate of hydrogen production being relatively high and responding quickly to changes in input (feed composition, space velocity, temperature). A partial oxidation reformer can therefore be compact, containing a small bed of catalyst with low thermal mass, and highly dynamic, i.e. fast starting and having the ability for the hydrogen output to track closely any changes in throughput. In practice, when fuel is made to react with a sub-stoichiometric amount of air, the available O_2 molecules can be consumed by combustion (Trimm *et al.*, 2004; Tsolakis *et al.*, 2005b; Tsolakis and Golunski, 2006), i.e. some of the hydrocarbon molecules burn to form the thermodynamically most stable species ($CO_2 + H_2O$):

$$C_nH_{1.88n} + 1.47nO_2 \rightarrow nCO_2 + 0.94nH_2O \qquad \Delta H = -8903 \text{ kJ/mole} \tag{13.3}$$

The heat of combustion can then enable the remaining hydrocarbon molecules to undergo the slower endothermic reactions that produce hydrogen.

Of the endothermic reactions, the most important is steam reforming, which releases both the hydrogen contained within the hydrocarbon molecules and the hydrogen within the co-reactant steam:

$$C_nH_{1.88n} + nH_2O \rightarrow nCO + 1.94nH_2 \qquad \Delta H_{298} = +2492 \text{ kJ/mole} \tag{13.4}$$

$$C_nH_{1.88n} + 2nH_2O \rightarrow nCO_2 + 2.94nH_2 \qquad \Delta H_{298} = +1749 \text{ kJ/mole} \tag{13.5}$$

The reaction is extremely productive, but it poses a number of problems for on-board vehicle applications: it is energy intensive (Steban and Parks, 1974)

and requires a source of high-temperature steam and, because it is relatively slow, the catalyst volume and temperature need to be high (Tsolakis *et al.*, 2005b; Tsolakis and Golunski, 2006). With well-designed catalysts, steam reforming reactors are typically limited by heat transfer, rather than by reaction kinetics, which means that heat-exchange components are required, adding to the overall system size and weight (Ahmed and Krumpelt, 2001). In the absence of steam and oxygen, these reactors can often function by thermal dissociation (endothermic), in which the fuel molecules are split into their elemental forms:

$$C_nH_{1.88n} \rightarrow nC + 0.94nH_2 \qquad 13.6$$

This reaction has the benefit of not generating CO_2, but creates the practical issue of how to remove the carbon product, which can either condense inside the reactor or emerge as particulate in the hydrogen stream.

As a further alternative to steam reforming, hydrogen can also be formed endothermically by reaction with carbon dioxide. This reaction, known as *dry reforming*, has the notable appeal of consuming carbon dioxide, creating the prospect of a hydrogen-generating process with a negative carbon footprint:

$$C_nH_{1.88n} + nCO_2 \rightarrow 2nCO + 0.9nH_2 \quad \Delta H = +2887 \text{ kJ/mole} \qquad 13.7$$

Although the CO formed can be used to generate more hydrogen by the *water–gas shift reaction*, this can form more CO_2 than is consumed by dry reforming:

$$2nCO + 2nH_2O \rightarrow 2nCO_2 + 2nH_2 \quad \Delta H = -1278 \text{ kJ/mole} \qquad 13.8$$

Furthermore, dry reforming is limited both by its kinetics and by its thermodynamics at low temperatures (Bradford and Vannice, 1999; Rostrup-Nielsen J.R. *et al.*, 2002). A high input of thermal energy is therefore required to achieve measurable rates and to avoid unwanted product formation.

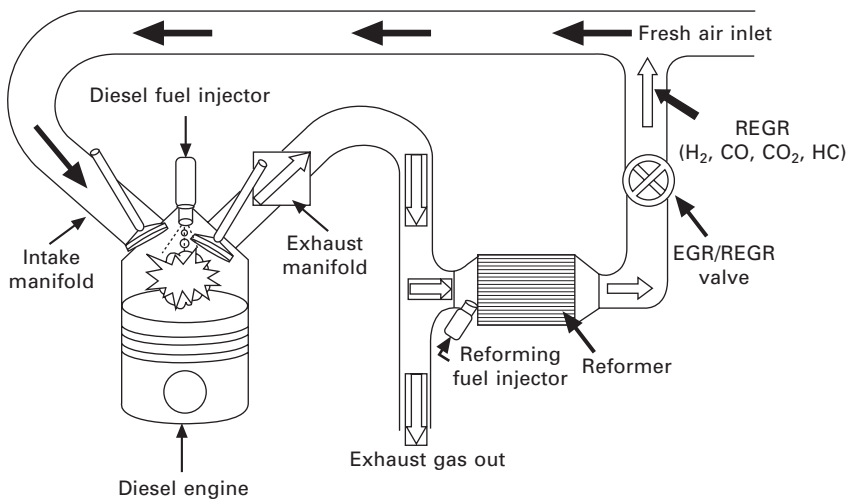
In *Autothermal Reforming* (ATR), several or all of the above reactions can take place in one reactor, but typically the overall process can be represented as a primary reaction between the hydrocarbon fuel and both oxygen (air) and steam to produce a hydrogen-rich gas:

$$C_nH_{1.88n} + [(n-1)/2]O_2 + H_2O \rightarrow nCO + [(1.88n+2)/2]H_2 \qquad 13.9$$

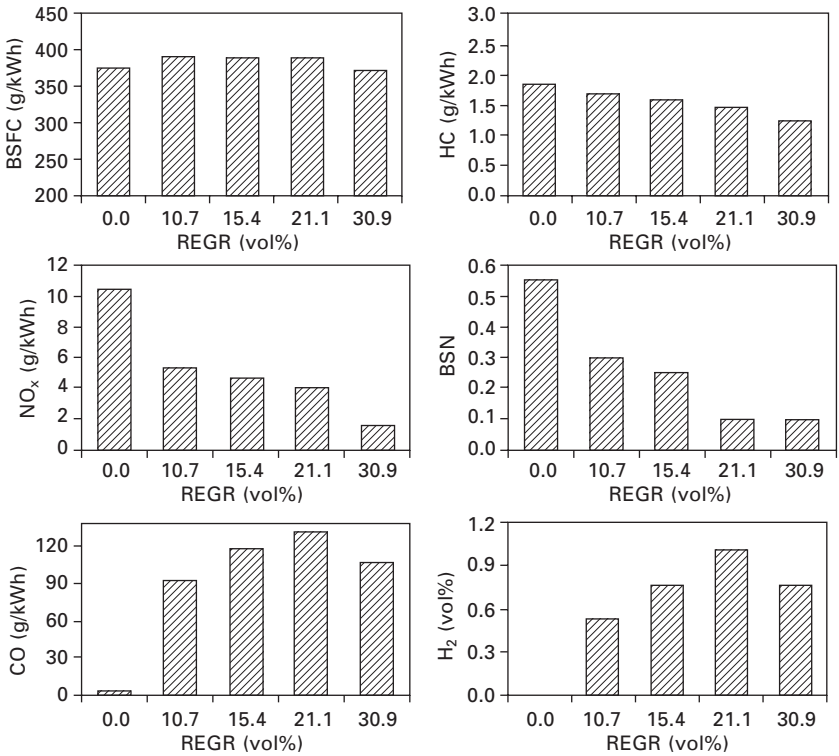
Depending on the temperature profile in the reactor and the composition of the catalyst, the water gas shift (Equation 13.8) can contribute as a secondary reaction, with the effect of changing the relative proportions of CO and H_2 in the product stream. For automotive applications one of the most promising technologies is a combination of autothermal reforming and EGR, referred to as reformed exhaust gas recirculation, REGR, which allows the fuel/air feed to the engine to be enriched with reformate. A schematic of this technique

is shown in Fig. 13.1. This fuel reforming method involves hydrogen-rich gas generation by direct catalytic interaction of hydrocarbon fuels with hot engine exhaust gases. The diesel engine exhaust gases contain considerable amounts of oxygen, steam and carbon dioxide and a hydrogen-rich gas can be produced by using part of the exhaust gas in a catalytic reactor (reformer) fed with fresh hydrocarbon fuel. Hydrogen-rich gas production can be achieved on board by using this process, referred to as *exhaust gas fuel reforming*, without the fuel penalty commonly associated with reforming processes and hence without adverse effects on the overall engine–reformer system fuel efficiency.

When REGR is coupled with a diesel engine, the most notable effect is the simultaneous reduction of NO_x and PM release, which is contrary to the expected trade-off between these emissions (Tsolakis, 2004; Tsolakis *et al.*, 2005c; Abu-Jrai *et al.*, 2006). Typical effects of REGR on engine emissions, as obtained from tests using a single-cylinder DI diesel engine, are shown in Fig. 13.2 (Tsolakis, 2004). The effects of REGR on the levels of hydrogen in the exhaust gas as well as on the total fuel consumption (engine and reformer) are also shown in Fig. 13.2. The reduction of NO_x emissions with REGR was not as high as when standard EGR was used under the same operating conditions. However, in contrast to the increase of smoke occurring with EGR, the use of REGR resulted in substantial reduction of smoke. Thus simultaneous reduction of smoke and NO_x was achieved. Similar substantial reduction of smoke was achieved when hydrogen combined with EGR was added to a modern multi-cylinder direct injection diesel engine with a common-rail injection system (McWilliam *et al.*, 2008). Particulate



13.1 Schematic of REGR system (Abu-Jrai, 2007).

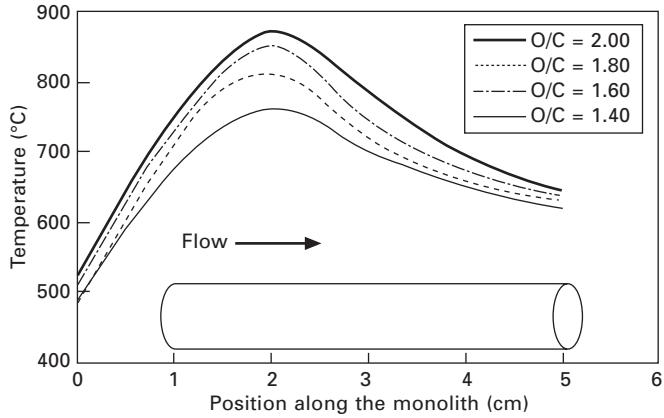


13.2 Effect of REGR on overall fuel economy (engine and reformer) and exhaust emissions (single-cylinder engine, 1500 rpm, 10 Nm, 25% load) (Tsolakis, 2004).

emissions have also been shown to decrease with REGR (Tsolakis *et al.*, 2005a).

In common with conventional autothermal reforming of hydrocarbons (Trimm *et al.*, 2004), the main reactions during exhaust-gas reforming of diesel fuel are combustion (Equation 13.3), steam reforming (Equation 13.4), water gas shift (Equation 13.8) and sometimes dry reforming (Equation 13.7), but as yet there is no conclusive evidence of direct partial oxidation taking place (Tsolakis *et al.*, 2005b) (the steam reforming and water gas shift reaction are sometimes shown as one reaction, Equation 13.5). The different reactions can occur consecutively, resulting in distinctive temperature profiles along the length of the catalyst monolith. Typical reformer temperature profiles for different oxygen-to-carbon atomic ratios (O/C) of the reactants are shown in Fig. 13.3 (Abu-Jrai, 2007).

Compared to steam reforming, the hydrogen content of the reformed product in the ATR and exhaust gas fuel reforming is much lower. This is due to the dilution with nitrogen from the reactant air in ATR or the exhaust gas in exhaust gas fuel reforming.



13.3 Typical reforming reactor temperature profiles (Abu-Jrai, 2007).

13.2.2 Reforming thermodynamics, 1-D and 2-D modelling, kinetics

Thermodynamics of diesel fuel reforming are quite simple if a simple model for the fuel can be assumed. The assumption of a simple model, however, is difficult because of the complex composition of real diesel-type fuels, but can be greatly simplified by adopting single representative molecules for each hydrocarbon group of the main fuel compounds, such as, in the case of fossil-based diesel, *n*-tetradecane representing paraffins (alkanes), L-methyl naphthalene representing aromatics, and decalin representing naphthenes, as exemplified by Berry *et al*. (2003). In such cases, and also where a general abundance of atoms of carbon, hydrogen, oxygen and nitrogen is entering the fuel reformer, the principle of minimisation of the Gibbs function is used to determine the equilibria compositions for an assumed list of chemical species expected to be present in the product. Outlet equilibrium compositions and temperatures can be calculated for a given inlet composition and temperature, i.e. for a given inlet enthalpy into an adiabatic reformer. Such calculations are useful for predicting the theoretically possible compositions and serve well as evaluation tools for experimental results. Because results of thermodynamics-based equilibria calculations do not consider kinetics or any geometry of the system, they are in essence point results which are less useful for the development of 1-D (one-dimensional) and 2-D (two-dimensional) models that involve geometry of the system, and flow and mass transfer characteristics.

On-board fuel reforming reactors are best served by monolithic support, similarly to what has been widely used in automotive exhaust aftertreatment systems. In order to study the monolith reformer's performance, mathematical

models have been developed that are capable of modelling not only a single monolith channel but also its interactions with neighbouring channels. The monolithic reactors are considered as part of complex thermodynamic systems and modelling of these systems aids the development of each component, so that they will be able to cope with the transient demands of the total system. The modelling challenges are twofold: the monolith consists of thousands of channels, each involving heat and mass transfer coupled with complex chemical reactions, yet the systems sub-model needs to be relatively simple. A relatively simple reaction model must be developed and kinetics data need to be provided for the individual reactions taking place on the surface of the catalyst, without interference from the mass transfer phenomena in the channels.

Developments of multi-channel 2-D non-adiabatic models have enabled the study of channel interaction. Two types of non-adiabatic models exist, based on discrete or continuous geometry of the channels. Discrete models are based on the reconfiguration of the monolith geometry to a number of concentric cylindrical rings in order to adopt cylindrical coordinates and axial symmetry. This approach enables a 2-D analysis of a 3-D (three-dimensional) problem and also complex-shaped channels to be represented by simpler ones. The continuous geometry models are based on representing the monolith as a homogeneous medium in which the gas and solid phases are both continuous and coexist in the same space to an extent determined by the volumetric proportion of the two phases in the real monolith. This eliminates the need to consider each channel individually.

The information on kinetics of reactions on a specific catalyst is very limited, particularly in the case of complex multi-component fuels such as refinery diesel or various biodiesels. There are two possible approaches to furnishing information to detailed 1-D and 2-D models outlined above. One method is to study the kinetics of reforming simple single-component fuels assuming a single reaction such as the steam reforming of isobutene (Acharya *et al.*, 2006) or a simple set of reactions (e.g. Phatak, 2006; Creaser, 2006). Reactants can include HCs, O_2 and H_2O while products include H_2, H_2O, CO_2 and CO (Karlovsky *et al.*, 2007). Experiments are performed in order to confirm which reactions occur and determine their rates (calculated directly from data if no more than three reactions are assumed to happen concurrently). Study of kinetic data for an assumed set of reactions has to be performed in such a way as to minimise or fully negate any effect of convective and diffusional flow resistances in mass transfer of the chemical species from the bulk flow to the surface of the catalyst and in the reverse flow of the products. Another approach can be to use the Surface Response Mapping technique, e.g. as presented by Berry *et al.* (2003), where a complex diesel fuel was substituted by single representative fuels for each group of the main fuel compounds. In this case, dominant reaction pathways were

elucidated and a statistical tool was used to map characteristic responses (e.g. selectivity, yield, conversion, carbon build-up, etc.) to input variables (O_2/C, H_2O/C, temperature and hydrocarbon type) over a defined region. This then led to development of kinetic sub-models and validation of kinetic data.

13.3 Diesel fuel reforming process parameters and catalyst screening

13.3.1 Diesel reforming process parameters

Both the ATR and the exhaust gas fuel reforming processes can be carried out with different processing rates but in the case of ATR it is easier to control these rates because of the use of a standard input, i.e., air, steam and fuel. In exhaust gas fuel reforming, the percentages of oxygen and steam in the engine exhaust gas are varying and depend on the engine operating condition (air to fuel ratio), as the diesel engine combustion shows below:

$$C_nH_{1.8n} + \lambda x(O_2 + 79/21N_2) \rightarrow nCO_2 + 0.9nH_2O + (\lambda - 1)xO_2 + \lambda x(79/21)N_2 \quad 13.10$$

where λ is the excess air ratio and x is the number of kmols of air.

The change of the engine exhaust gas composition affects the rates of the reactants (mainly steam and oxygen) in the reforming reactor as can be seen from the idealised diesel exhaust gas fuel reforming given by:

$$C_nH_{1.8n} + y[nCO_2 + 0.9nH_2O + (\lambda - 1)xO_2 + \lambda x(79/21)N_2 \rightarrow zCO_2 + kH_2 + y\lambda x(79/21)N_2 \quad 13.11$$

where y is the number of kmols of exhaust gas required to react stoichiometrically with the fuel, and z and k are the number of kmols of carbon dioxide and hydrogen, respectively, in the reactor product gas.

Since diesel engines operate under lean conditions ($\lambda > 1$), the engine exhaust always contains oxygen as indicated by the diesel combustion reaction equation (Equation 13.10). As the engine operation shifts closer to stoichiometric ($\lambda = 1$) the percentage of steam in the exhaust increases while the percentage of O_2 decreases. In the extreme case of $\lambda = 1$ the exhaust gas contains the maximum percentage of steam (approx. 12% for diesel combustion) and no O_2. In this case the idealised reaction (Equation 13.11) is similar to steam reforming (Equation 13.4) and a high exhaust temperature is required to drive the endothermic reforming. At idle conditions (very lean combustion) the percentage of O_2 in the engine exhaust is approaching that in the air (about 20%) and the percentage of steam is very small. In this case the idealised reaction (Equation 13.11) is very similar to partial or complete oxidation (Equations 13.1–13.3).

The basic process parameters for the exhaust gas fuel reforming reactions are the oxygen-to-fuel molar ratio O_2/F, the steam-to-fuel molar ratio S/F and the oxygen-to-carbon atomic ratio O/C. For the ideal exhaust gas fuel-reforming reaction, Equation 13.11, the three ratios are given by Equations 13.12–13.14 below:

$$O_2(\text{air})/\text{F} = yx(\lambda - 1) \tag{13.12}$$

$$\text{S/F} = 0.9yn \tag{13.13}$$

$$\text{O/C} = \frac{2yn + 0.9yn + 2yx(\lambda - 1)}{n + yn} \tag{13.14}$$

From these equations, the dependence of the basic process parameters on λ is clear. From the idealised reaction (Equation 13.11) it is obvious that the oxygen source is not only in the form of H_2O and O_2 but also in the form of CO_2. Possibly the CO_2 does not affect much the composition of the reformer product gas at low temperatures, but at high temperatures where the dry reforming reaction (Equation 13.7) is favourable, a proportion of fuel added to the feed needs to be allocated for this reaction.

For the reforming processes involving O_2, the *reactor aspect ratio* is a parameter that affects the heat distribution on the catalyst generated by the combustion of part of the fuel and hence the reaction rates of the endothermic hydrogen-producing reactions (Tsolakis *et al.*, 2005b). The reactor space velocity is also an important parameter affecting the reforming process.

13.3.2 Catalysts: screening, evaluation and scale-up

Whichever reforming route is used, a catalyst is required to achieve near-equilibrium yields of products without having to resort to extreme conditions. Non-catalytic techniques, such as *non-thermal plasma* (Petitpas *et al.*, 2007) or *cool-flame partial oxidation* (Naidja *et al.*, 2003) can be used to complement the catalyst in small-scale reforming (Sobacchi *et al.*, 2002) but, used alone, they tend to produce intermediate products rather than principally CO, CO_2 and H_2. The design and operation of catalytic reformers differ across the range of scales and applications, despite the fact that the chemistry is similar. Historically, reformers designed for use on board passenger cars have had much more in common with those developed for mobile and domestic fuel cell systems than with industrial reformers. Whereas large industrial reformers are operated under optimised steady-state conditions using pre-treated feedstocks and carefully activated catalysts, on-board reformers have to be compact, fast-starting and responsive to different throughputs and feed compositions. To minimise the reformer size, highly active catalysts are required, and these tend to contain precious metals rather than the less expensive but also less active base metals. To maximise

efficiency, the catalysts also have to be selective (i.e. they should not form by-products), and they have to tolerate the contaminants, such as sulphur species, that are present in the fuel. Furthermore, on-board heat management has to be designed so that waste energy can be recovered and used to drive the endothermic H_2-producing reactions.

In the early days of reformer development for fuel cell systems, several screening studies were carried out in which catalysts or complete reformers, already known to convert specific compounds (e.g. methanol or methane) to hydrogen, were tested for their ability to reform a range of liquid and gaseous fuels (Carpenter and Golunski, 1998; Ahmed *et al.*, 1998; Harrison, 2000; Siddle *et al.*, 2003). In the development of exhaust-gas reformers for IC vehicles, a different approach has been used. In the first phase, a broad range of potentially active catalyst materials was screened using a simple gaseous hydrocarbon as the model fuel, which was added to a synthetic exhaust gas. Then, having eliminated the least active materials, the complexity of the test procedure was increased (e.g. by adding sulphur species to the gas feed) to mimic more closely the expected operating conditions. In this second phase, the general performance characteristics of the most promising catalysts were established (Peucheret *et al.*, 2006), including (i) light-off temperature as function of exhaust-gas stoichiometry, (ii) sulphur tolerance, and (iii) resistance to deactivation by coking (carbon deposition on the catalyst surface). From these tests, a shortlist of fewer than five catalysts was selected for scale-up and engine testing.

For screening and laboratory evaluation, catalysts are usually in powder or granular form, and are tested in a small packed bed through which the reactants (all in the gas phase) are passed at a constant space velocity. This simple reactor design does not, however, lend itself to scaling. Particularly when subjected to vibration, large beds of powders or granules can become densely packed, resulting in a high pressure drop across the reactor, or the particles can settle unevenly, causing channels to develop through the catalyst bed. Heat management of a large packed bed can also be difficult, particularly where the reforming process is either strongly endothermic or strongly exothermic. Catalyst scale-up, therefore, invariably requires reformulation of the active material so that it can be applied as a thin (75–100 μm) coating to a ceramic or metal monolith, or to the extended metal surfaces (e.g. fins or corrugated foils) of a heat exchanger (Farrauto *et al.*, 2007).

13.4 Diesel fuel reforming applications: trends

13.4.1 Diesel engine combustion and emissions improvement

Currently, the design criteria for fuel reformers are mainly based on the requirements of fuel cell systems (e.g. Ahmed and Krumpelt, 2001; Trimm *et*

al., 2004) which are not entirely appropriate for engines. The application of fuel reforming in engines is rather different from that in fuel cells as the key requirement to achieve emission reduction is the efficient on-demand generation of a reformate with only a relatively low concentration of hydrogen (typically up to 20%) (Steban and Parks, 1974; Kopasz *et al*., 2005). Indeed, diesel engine experimental research with addition of different levels of reformate of various compositions has indicated that the hydrogen concentration does not need to be very high (up to 20% at the reformer outlet), and that it is not always desirable to optimise the hydrogen-generating reactions (Tsolakis *et al*., 2005b).

Unlike fuel-processing in fuel cell systems, there is not necessarily an advantage in converting as much as possible of the produced CO. For example, the water–gas shift reaction (Equation 13.8) increases the H_2 concentration, but at the same time lowers the calorific value of the reformate (as it is an exothermic reaction). Study of diesel engine operation with REGR (i.e. exhaust gas fuel reforming technique) has revealed that the combustion of reformate that contains both H_2 and CO can give better overall fuel economy (engine and reformer fuel consumption), while retaining the emission benefits seen by adding hydrogen alone (Tsolakis *et al*., 2005c). Hence for diesel engine reforming applications aiming to improve combustion and emissions, there will not be a need to optimise the on-board reformer (autothermal or exhaust gas) for maximum H_2 production by promoting the water–gas shift reaction.

For optimum overall fuel economy, the reforming catalyst should be capable of promoting oxidation, steam reforming and dry reforming, but should have low activity for water–gas shift and methanation (Tsolakis *et al*., 2005c). This could lead to improved catalyst durability by eliminating the use of additional material needed in the catalyst to promote the water–gas shift reaction. Thus, avoidance of the promotion of the water–gas shift reaction in the on-board reformer can result in a simplified catalyst design accompanied by improvement of the catalyst durability and reduced catalyst preparation time and cost.

Furthermore, the reactor design will be simplified if there is no need to promote the water–gas shift reaction. This is because, depending on the catalyst, the water–gas shift reaction is favourable at temperatures lower than those present in the reformer and thus to promote this reaction, the reactor size has to be increased due to the requirements of a reactor with good heat exchange and temperature drop upstream of the water–gas shift reaction catalyst. A reformer not optimised to promote the water–gas shift reaction will thus require reactor designs with reduced complexity and cost.

13.4.2 Aftertreatment improvement

The demands of a reformer system aiming to provide reformate that will be fed to the engine cylinder (such as the REGR system) can be quite different

from those required for promoting aftertreatment processes. The reformer and the catalyst design have to be optimised according to the particular engine application as there are different requirements when reformate is to be added to the engine combustion chamber to improve combustion and emissions compared to when reformate is to be utilised as an aftertreatment improver (Burch and Coleman, 2002; Houel *et al.*, 2007; Satokawa *et al.*, 2003). Furthermore, the requirements of different aftertreatment processes may be different in terms of reformate quantity as well as composition.

For example, as has been reported recently, the beneficial effects of H_2 in expanding the hydrocarbon-SCR (selective catalytic reduction of NO_x emissions) activity window of the 1%Pt/Al_2O_3 catalyst toward lower temperatures can be seen when there is only a small concentration of CO (200 ppm) in the catalyst feed gas. Reducing the H_2/CO ratio in the reformate promotes the H_2 preferential oxidation and poisoning of the catalyst active sites in reducing NO_x and the good low temperature activity cannot be seen. Consequently, it is evident that the incorporation of a reformer in the SCR system needs to be optimized in a way that the reformate CO content will be minimum while the H_2 content will be maximum (Abu-Jrai and Tsolakis, 2007). In addition the reformer fuel efficiency will have to be as high as possible. In such a case, the water–gas shift reaction will need to be promoted in contrast to the reforming requirements for combustion improvements discussed in the previous section (Abu-Jrai et al., 2008). However, the demands in terms of reformate quantity will be much lower in the case of reformate generation for hydrocarbon-SCR compared to engine combustion.

In the case of NO_x traps, their regeneration process requires a rich atmosphere, which is currently achieved either by injection of a small amount of fuel or by operation of the engine periodically for short periods at rich conditions. The trap regeneration process can be improved by addition of hydrogen (Kong *et al.*, 2004). In fact, both H_2 and CO are significantly stronger reducing agents than diesel fuel and other hydrocarbons. Furthermore, a potentially more important advantage of using hydrogen-rich reformate instead of diesel as a reductant is the fact that with hydrogen the traps can be regenerated at lower temperatures compared to diesel. As in the case of SCR, the effects of the composition of the reformate on the NO_x trap operation are very important and need to be considered in order to optimise the reforming process accordingly. In the case of the NO_x trap the demand for reformate is periodic and not continuous (i.e. when trap regeneration is required).

The regeneration of diesel particulate filters (DPF) has also been shown to benefit from addition of hydrogen-rich gas (e.g. Bromberg *et al.*, 2005). In this case, again the demand for reformate is periodic. The effects of the composition of the reformate on the filter operation and regeneration have been revealed as very important and are still under investigation.

Regarding the NO_x ammonia–SCR process, the fuel reforming technology has the potential to be utilised as the hydrogen source for on-board ammonia synthesis (instead of following the urea route). The use of reformate for on-board synthesis of ammonia has been investigated in the past (e.g. Nakahira *et al.*, 1992; Bromberg *et al.*, 2002) but more recently it has attracted renewed interest in view of the increasingly stringent emissions standards.

13.5 Summary

Fuel reforming of diesel-type fuels produces a hydrogen-rich gas that can be utilised as a diesel combustion and emissions improver, as well as a diesel exhaust aftertreatment improver. With regard to engine combustion, the application of on-board fuel reforming for diesel automotive applications is beneficial in terms mainly of emissions reduction and to a lesser extent of engine brake power, thermal efficiency and combustion stability. Application of fuel reforming in stationary engines and under constant speed–load engine operation is simpler but the advantages compared to hydrogen storage are reduced. Addition of reformate produced on board by fuel reforming to diesel engine exhaust aftertreatment systems is beneficial in terms of aftertreatment process efficiency and operating window as well as regeneration (e.g. in the case of NO_x traps and particulate filters). The reforming reactor design and catalyst requirements for diesel engine applications are not the same as those of fuel cells. They depend on the particular fuel reforming application and they are different for combustion and aftertreatment processes in terms of reformate quantity and composition as well as in terms of continuous or periodic demand.

13.6 References

Abu-Jrai A. (2007), 'Control of diesel engine NO_x emissions by selective catalytic reduction and exhaust gas-assisted fuel reforming', PhD Thesis, University of Birmingham, UK.

Abu-Jrai A., Tsolakis A. (2007), 'The effect of H_2 and CO on the selective catalytic reduction of NO_x under real diesel engine exhaust conditions over Pt/Al_2O_3', *International Journal of Hydrogen Energy*, 32, 2073–2080.

Abu-Jrai A., Theinnoi K., Tsolakis A., Cracknell R., Megaritis A., Wyszynski M.L., Golunski S.E. (2006), 'Effect of gas-to-liquid diesel fuels on combustion characteristics, engine emissions, and exhaust gas fuel reforming. Comparative study', *Energy & Fuels*, 20(6), 2377–2384.

Abu-Jrai A., Tsolakis A., Megaritis A. (2007), 'The influence of H_2 and CO on diesel engine combustion characteristics, exhaust gas emissions, and aftertreatment selective catalytic NO_x reduction', *International Journal of Hydrogen Energy*, 32, 3565–3571.

Abu-Jrai A., Tsolakis A., Theinnoi K., Megaritis A., Golunski S.E. (2008), 'Diesel exhaust-gas reforming for H_2 addition to an aftertreatment unit', *Chemical Engineering Journal*, 141, 290–297.

Acharya C., Lane A., Krause T. (2006), 'Kinetic study of the steam reforming of isobutane using a Pt–CeO_2–Gd_2O_3 catalyst', *Catalysis Letters*, 106(1–2), 41–48.

Ahmed S., Krumpelt M. (2001), 'Hydrogen from hydrocarbon fuels for fuel cells', *International Journal of Hydrogen Energy*, 26 (4), 291–301.

Ahmed S., Krumpelt M., Kumar R., Lee S.H.D., Carter J.D., Wilkenhoer R., Marshall C. (1998), 'Catalytic partial oxidation of hydrocarbon fuels', DOE Report 96059.

Allenby S., Chang W.C., Megaritis A., Wyszynski M.L. (2001), 'Exhaust gas fuel reforming: a way to maintain combustion stability in a natural gas fuelled engine with EGR', *Proceedings of the IMechE, Part D: Journal of Automobile Engineering*, 215, 405–418.

Berry D.A., Shekhawat D., Gardner T. (2003), 'Development of predictive models for diesel-based fuel processors', National Energy Technology Laboratory Onsite Merit Review, www1.eere.energy.gov/hydrogenandfuelcells/pdfs/merit03/92_netl_dave_berry.pdf.

Bradford M.C.J., Vannice M.A. (1999), 'CO_2 reforming of CH_4', *Catalysis Reviews – Science and Engineering*, 41, 1–42.

Bromberg L., Cohn D.R., Heywood J., Rabinovich A. (2002), 'Onboard plasmatron generation of hydrogen rich gas for diesel engine exhaust aftertreatment and other applications', MIT Plasma Science & Fusion Center Research Report PSFC JA-02-30.

Bromberg L., Cohn D.R., Wong V. (2005), 'Regeneration of diesel particulate filters with hydrogen rich gas', MIT Plasma Science & Fusion Center Research Report PSFC/RR-05-2.

Burch R., Coleman M.D. (2002), 'An investigation of promoter effects in the reduction of NO by H_2 under lean-burn condition', *Journal of Catalysis*, 208, 435–447.

Bysveen M. (2007), 'Engine characteristics of emissions and performance using mixtures of natural gas and hydrogen', *Energy*, 32, 482–489.

Carpenter I.W., Golunski S.E. (1998), 'Alternative feeds for fuel-processing by partial oxidation and autothermal reforming', ETSU Report F/02/00117/REP, Future Energy Solutions, AEA Technology.

Creaser D. (2006), 'Autothermal reforming of a hydrocarbon fuel in a monolithic reactor', *Proceedings of the Nordic COMSOL Conference*, Copenhagen, 2006.

D'Andrea T., Henshaw P.F., Ting D.S.-K. (2004), 'The addition of hydrogen to a gasoline-fuelled SI engine', *International Journal of Hydrogen Energy*, 29, 1541–1552.

Farrauto R.J., Liu Y., Ruettinger W., Illinich O., Shore L., Giroux T. (2007), 'Precious metal catalysts supported on ceramic and monolithic structures for the hydrogen economy', *Catalysis Reviews – Science and Engineering*, 49, 141–196.

Faur Ghenciu A. (2002), 'Review of fuel processing catalysts for hydrogen production in PEM fuel cell systems', *Current Opinion in Solid State and Materials Science*, 6(5), 389–399.

Harrison M.R. (2000), 'Assessment of novel catalyst materials for the extraction of hydrogen from commercial fuel feeds', ETSU Report F/02/00182/REP, www.berr.gov.uk/files/file15207.pdf.

Hawle J.G., Cox A., Horrocks R.W., Bird G. (1999), 'Reduction of steady state NO_x levels from an automotive diesel engine using optimized VGT/EGR schedules', SAE paper 1999-01-0835.

Houel V., Millington P., Rajaram R., Tsolakis A. (2007), 'Promoting functions of H_2 in diesel-SCR over silver catalysts', *Applied Catalysis B: Environmental*, 77, 29–34.

Houseman J., Hoehn F.W. (1974), 'A two-charge engine concept: hydrogen enrichment', SAE paper 741169.

Jamal Y., Wyszynski M.L. (1994), 'On-board generation of hydrogen rich fuels – a review', *International Journal of Hydrogen Energy*, 19(7), 557–572.

Juste G.L. (2006), 'Hydrogen injection as additional fuel in gas turbine combustor. evaluation of effects', *International Journal of Hydrogen Energy*, 31, 2112–2121.

Karlovsky J., Wyszynski M.L., Xu H.M., Tsolakis A., Qiao J. (2007), 'Chemical kinetics and thermodynamic modelling of a fuel reformer for on board hydrogen generation'. *2007 PTNSS Congress*, 20–23 May, Krakow, Poland.

Kirwan J.E., Quader A.A., Grieve M.J. (2002), 'Fast start-up on-board gasoline reformer for near-zero emissions in spark-ignition engine', SAE paper 2002-01-1011.

Kong Y., Crane S., Patel P., Taylor B. (2004), 'NO_x trap regeneration with on-board hydrogen generation device', SAE paper 2004-01-0582.

Kopasz J.P., Applegate D., Miller L., Liao H.K., Ahmed S. (2005), 'Unravelling the maze: understanding of diesel reforming through the use of simplified fuel blends', *International Journal of Hydrogen Energy*, 30, 1243–1250.

Koyanagi K., Hiruma M., Furuhama S. (1994), 'Study on mechanism of backfire in hydrogen engines', SAE Paper 942035.

Kwon J., Sharer P., Rousseau A. (2006), 'Impact of combining hydrogen ICE with fuel cell system using PSAT', SAE paper 2006-01-0037.

Marsh P., Gottberg I., Thorn K., Lundgren M., Acke F., Wirmark G. (2000), 'SULEV emission technologies for a five-cylinder N/A engine', SAE paper 2000-01-0894.

McWilliam L., Megaritis A., Zhao H. (2008), 'Experimental investigation of the effects of combined hydrogen and diesel combustion on the emissions of a HSDI diesel engine', SAE paper 2008-01-1787.

Naidja A., Krishna C.R., Butcher T., Mahajan D. (2003), 'Cool flame partial oxidation and its role in combustion and reforming of fuels for fuel cell systems', *Progress in Energy and Combustion Science*, 29, 155–191.

Nakahira T., Tsujimura K., Kakegawa T., Aika K., Takiguchi M., Ikeda M., Ichihara S. (1992), 'Catalytic engine NO_x reduction of diesel engines with new concept onboard ammonia synthesis system', SAE paper 920469.

Petitpas G., Rollier J.-D., Darmon A., Gonzalez-Aguilar J., Metkemeijer R., Fulcheri L. (2007), 'A comparative study of non-thermal plasma assisted reforming technologies', *International Journal of Hydrogen Energy*, 32, 2848–2867.

Peucheret S., Feaviour M., Golunski S. (2006), 'Exhaust-gas reforming using precious metal catalysts', *Applied Catalysis B: Environmental*, 65, 201–206.

Phatak A.A. (2006), 'Kinetic modeling and first principles study of the water–gas shift and methanation reaction on Group VIII metal catalysts', PhD thesis, Purdue University, West Lafayette, IN.

Rostrup-Nielsen J.R. (2002), 'Syngas in perspective', *Catalysis Today*, 71, 243–247.

Rostrup-Nielsen J.R., Sehested J., Norskov J.K. (2002), 'Hydrogen and synthesis gas by steam- and CO_2-reforming', *Advances in Catalysis*, 47, 65–139.

Rostrup-Nielsen T. (2005), 'Manufacture of hydrogen', *Catalysis Today*, 106, 293–296.

Satokawa S., Shibata J., Shimizu K., Satsuma A., Hattori T. (2003), 'Promotion effect of H_2 on the low temperature activity of the selective reduction of NO by light HCs over Ag/Al_2O_3', *Applied Catalysis B: Environmental*, 43, 179–186.

Siddle A., Pointon K.D., Judd R.W., Jones S.L. (2003), 'Fuel processing for fuel cells – a status review and assessment of prospects', ETSU Report F/03/00252/REP, URN 031644, www.berr.gov.uk/files/file15218.pdf.

Sobacchi M.G., Saveliev A.V., Fridman A.A., Kennedy L.A., Ahmed S., Krause T.

(2002), 'Experimental assessment of a combined plasma/catalytic system for hydrogen production via partial oxidation of hydrocarbon fuels', *International Journal of Hydrogen Energy*, 27, 635–642.

Steban R.F., Parks F.B. (1974), 'Emission control with lean operation using hydrogen supplemented fuel', SAE paper 740187.

Swain M.R., Schade G.J., Swain M.N. (1996), 'Design and testing of a dedicated hydrogen fueled engine', SAE paper 961077.

Trimm D.L., Onsan Z.I. (2001), 'On-board fuel conversion for hydrogen fuel cell driven vehicles', *Catalysis Reviews, Science and Engineering*, 43(1), 31–84.

Trimm D.L., Adesina A.A., Praharso, Cant N.W. (2004), 'The conversion of gasoline to hydrogen for on-board vehicle applications', *Catalysis Today*, 93–95, 17–22.

Tsolakis A. (2004), 'Exhaust gas fuel reforming for compression ignition engines fuelled by diesel and biodiesel', PhD thesis, University of Birmingham, UK.

Tsolakis A., Golunski S. (2006), 'Sensitivity of process efficiency to reaction routes in exhaust-fuel reforming of diesel fuel', *Chemical Engineering Journal*, 117(2), 131–136.

Tsolakis A., Megaritis A. (2004), 'Catalytic exhaust gas fuel reforming for diesel engines – effects of water addition on hydrogen production and fuel conversion efficiency', *International Journal of Hydrogen Energy*, 29, 1409–1419.

Tsolakis A., Megaritis A., Wyszynski M.L. (2003), 'Applications of the exhaust gas fuel reforming in compression ignition engines fuelled by diesel and biodiesel fuel mixtures', *Energy & Fuels*, 17(6), 1464–1473.

Tsolakis A., Hernandez J.J., Megaritis A., Crampton M. (2005a), 'Dual fuel diesel engine operation using H_2 – Effects on particulate emissions', *Energy & Fuels*, 19(2), 418–425.

Tsolakis A., Megaritis A., Golunski S.E. (2005b), 'Reaction profiles during exhaust assisted reforming of diesel engine fuels', *Energy & Fuels*, 19(3), 744–752.

Tsolakis A., Megaritis A., Yap D., Abu-Jrai A. (2005c), 'Combustion characteristics and exhaust gas emissions of a diesel engine supplied with reformed EGR', SAE paper 2005-01-2087.

Verhelst S., Sierens R., Verstraeten S. (2006), 'A critical review of experimental research on hydrogen fuelled SI engines', SAE paper 2006-01-0430.

Wallington T.J., Kaiser E.W., Farrell J.T. (2006), 'Automotive fuels and internal combustion engines: a chemical perspective', *Chemical Society Reviews*, 35(4), 335–347.

Wilhelm D.J., Simbeck D.R., Karp A.D., Dickenson R.L. (2001), 'Syngas production for gas-to-liquids applications: technologies, issues and outlook', *Fuel Processing Technology*, 71, 139–148.

Yap D., Peucheret S.M., Megaritis A., Wyszynski M.L., Xu H. (2006), 'Natural gas HCCI engine operation with exhaust gas fuel reforming', *International Journal of Hydrogen Energy*, 31(5), 587–595.

14

Exhaust gas aftertreatment for light-duty diesel engines

P. EASTWOOD, Ford Motor Company, Limited, UK

Abstract: The chapter reviews the state of the art in various forms of aftertreatment, namely, oxidation catalysts, lean-NO_x traps, particulate filters and selective catalytic reduction. The focus is on practical packaging issues faced by the manufacturer, rather than fundamental research. The constraints on vehicle design unique to the light-duty market are emphasised. It is shown how emissions legislation is 'technology-forcing', and influences the design decisions made by the vehicle manufacturer.

Key words: lean-NO_x trap, oxidation catalyst, diesel particulate filter, selective catalytic reduction, emissions legislation, light-duty diesel.

14.1 Introduction

As the title reveals, this chapter is devoted to *light-duty* aftertreatment. But since the technology of aftertreatment at its fundamental level is common to all diesels – for example, many of the undergirding parameters scale straightforwardly with engine size – the logical question is how any such review is to be instructively demarcated from 'heavy-duty', dealt with in the present volume in another chapter. The answer is that our present aim is not to discuss, other than in passing, fundamental principles or basic research, as particularly practised with bench-top laboratory reactors, test-tube or so-called 'model catalysts', and synthetic exhaust gas. While plenty of worthy research papers of this ilk are evident in the literature, our present focus will be restricted to various *engineering* problems posed by aftertreatment, with particular reference to practical packaging issues, as reported by practitioners in the motor industry. Indeed, it is often remarked that *packaging* engenders greater problems in the light-duty market than in its heavy-duty counterpart, although we shall not belabour this point.

Another distinction should be pointed out: 'light-duty diesel' is a broad-brush term which actually encompasses a formidably wide range of applications, markets or platforms, i.e., not only passengercars or automobiles, but also pick-up trucks, minivans, small commercial or 'tradesman' vans, sport-utility vehicles and so-called 'people-carriers' (not forgetting innumerable off-road platforms). In this market, unlike its parallel, the heavy-duty sector, diesel engines compete directly with gasoline engines, although the extent of dieselisation varies enormously from one country to another. For example,

diesel automobiles in several European countries now outnumber gasoline automobiles, whereas in the USA they have thus far seized only a toehold. This competition engenders further constraints on light-duty aftertreatment not faced in the heavy-duty market.

14.2 Emissions legislation

Exhaust gas is nowadays subject almost universally to some form of statutory regulation, wherever the market; and the four pollutants consistently singled out are unburned hydrocarbons (HC), carbon monoxide (CO), oxides of nitrogen (NO_x) and particulate matter (PM). Before any sale is permitted, representative production-intent vehicles are driven over defined (statutory) driving cycles; following which the total mass of each pollutant is obtained. When divided by the distance driven by the vehicle, this yields a 'mass per unit distance'.

That present-day regulations would seem truly astonishing to engineers of bygone ages is no overstatement: statutory limits within the careers of those still employed in the automotive industry have declined by two orders of magnitude. For example, in the 1970s, emissions of PM from light-duty diesel vehicles were on the order of hundreds of milligrams per kilometre (French and Pike, 1979), whereas today, just a few milligrams per kilometre are permitted. Table 14.1 shows selected emissions standards in Japan, the USA and Europe (Dieselnet, 2007).

In the USA, where 'Tier 2' is currently undergoing a lengthy phase-in (2004 to 2009), the same standards apply to all categories of vehicle weight, up to 10 000 lb (4535 kg). There are 'certification bins' of different stringency, amongst which vehicle manufacturers have freedom to choose. In Japan there are two sets of legislation: for light-commercial vehicles, a division is made at 1700 kg, with less-stringent standards for heavier classes; for passenger cars, a division is made at 1265 kg, but after 2009 identical emissions standards will apply. In the EU, current attention is focused on Stage V, scheduled for 2010, and secondarily Stage VI, scheduled for 2014. Light-duty vehicles are those weighing not more than 2610 kg, although, at the manufacturer's request, this may be extended to 2840 kg (EU Directive, 2007). There are two strands of legislation, for passenger vehicles and goods vehicles. Table 14.1 refers to vehicles with no more than eight seats, in addition to the driver.

The regulatory framework – principally, driving cycle and statutory limit – inevitably influence the *vehicle* technology for emission control selected by the manufacturer. This is another aspect where light-duty and heavy-duty emission control differ: in the latter case, limits are instead laid down in terms of 'mass per unit work' – an index which reflects the preference for engine certification rather than vehicle certification, and which also tends to

Table 14.1 Recently enacted emissions standards for light-duty diesel vehicles (Dieselnet, 2007)

Region	HC*	CO	HC + NO_x	NO_x	PM
USA (g/mile) (Tier 2)					
Bin 8	0.125	4.2	–	0.2	0.02
Bin 7	0.09	4.2	–	0.15	0.02
Bin 6	0.09	4.2	–	0.1	0.01
Bin 5	0.09	4.2	–	0.07	0.01
Bin 4	0.07	2.1	–	0.04	0.01
Bin 3	0.055	2.1	–	0.03	0.01
Bin 2	0.01	2.1	–	0.02	0.01
Bin 1	0	0	–	0	0
Japan (g/km) (2009)					
Passenger cars	0.024	0.63	–	0.08	0.005
Commercial (<1700 kg)	0.024	0.63	–	0.08	0.005
Commercial (>1700 kg)	0.024	0.63	–	0.15	0.007
European Union (g/km)†					
Stage I (1992)	–	2.72	0.97	–	0.14
Stage II (DI, 1996)	–	1	0.9	–	0.1
Stage III (2000)	–	0.64	0.56	0.5	0.05
Stage IV (2005)	–	0.5	0.3	0.25	0.025
Stage V (2009)	–	0.5	0.23	0.18	0.005
Stage VI (2014)	–	0.5	0.17	0.08	0.005

*The standard for HC in Japan and the USA is for NMHC; in the EU, methane is included.
†Vehicles designed to carry passengers rather than goods.

diminish engine capacity and operating point as considerations. For example, one engine may deliver twice the work of another but yet remain on a par from the legislative standpoint.

This leads us to an oft-repeated aphorism: that light-duty emissions legislation is more difficult to satisfy with a large-capacity engine than with a smaller. This is a major simplification, and true only inasmuch as a larger engine generates a greater mass of exhaust gas per unit time, and so concomitantly generates a greater mass of any pollutant per unit time. Emissions legislation is not, however, framed in terms of grams per hour, but grams per kilometre; and it also relates not to the engine in isolation, but to the vehicle taken as a whole. Consequently any factors affecting the relationship between vehicle speed and engine operating point have a hand in deciding the test cycle result. For example, should engine speed double, and vehicle speed also double, then the situation is obviously unchanged in terms of grams per kilometre.

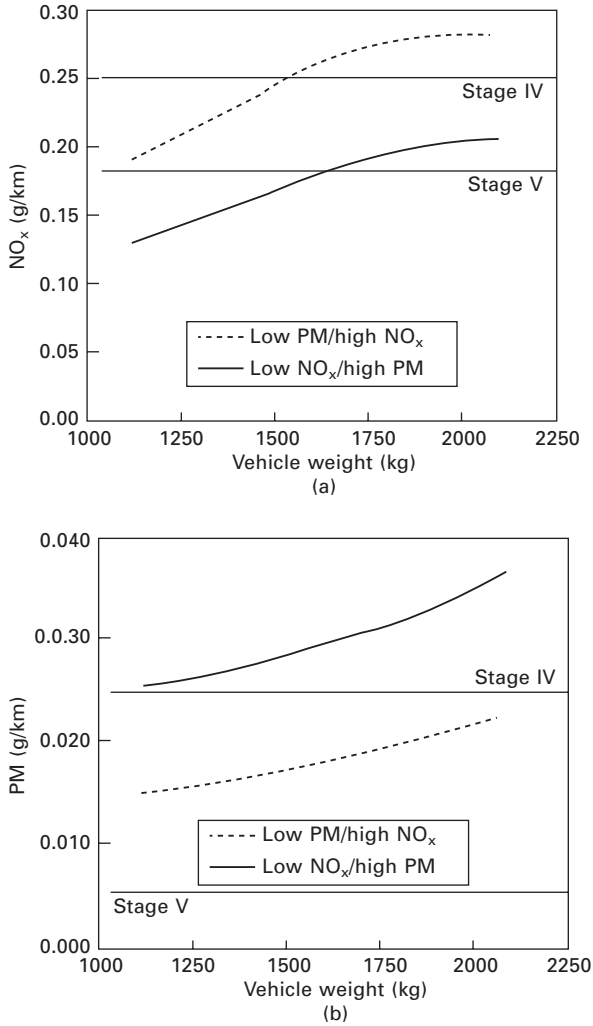
What really counts is engine capacity in relation to vehicle weight. Generally speaking, emission control for NO_x and PM is more problematical for a small engine (say 1.8 litre) in a heavy vehicle (say 1800 kg) than for a large engine

(say 2.2 litre) in a light vehicle (say 1600 kg). It is instructive to reflect on why this should be. To a first approximation, emissions in grams per hour scale with engine load. Thus, if engine capacity is increased, then, all other factors being equal, the same vehicle speed is now realised for lower engine load, so the emission, in grams per hour, is also lower. The inference is that larger exhaust-gas flow-rates, owing to the larger volume swept out by the piston, are offset by other factors. For example, if the mixture is leaner, the cylinder temperatures are lower, so that less NO_x is generated, and oxygen is more available, so that less soot is generated. Obviously, there are many nuances here that cannot be fully explored. The picture is tempered, for example, by gearing, since this modifies the relationship between vehicle speed and engine speed. But generally speaking, NO_x and PM tend to be stronger functions of engine load than of engine speed, for typical ranges traversed by these two parameters. So, the load factor is of major importance in deciding how easy, or (more usually the case) how difficult, is the task of emission control for NO_x and PM.

This logically brings us to aftertreatment. Figure 14.1 gives emissions forecasts for the same-capacity engine when installed in vehicles of different weights, as tested in the New European Drive Cycle (NEDC) and projected onto EU Stage IV and V (after Johnson, 2004, and Krüger *et al.*, 2003). Forecasts are also made for two engine calibrations relating to the well-known trade-off: one biased towards NO_x, the other towards PM. Note that the figure again shows engine-out emissions: for much of the curves, these lie unsatisfactorily above their statutory requirements. If everything conceivably possible has already been done with the engine, then obviously these shortfalls can only be met by aftertreatment. And evidently, the smaller the engine capacity is, in relation to vehicle weight, then the greater the conversion efficiency demanded in the aftertreatment, *in order to reach the same standard*, as already explained. Alternatively, the lightest vehicles carrying large-capacity engines escaped the need for NO_x or PM aftertreatment until relatively recently.

It should be stressed that when aftertreatment devices (to be described) operate *discontinuously*, with periods of storage punctuated by periods of purging or 'regeneration', the engine-out emission is critical in deciding the storage period, since the storage capacity is obviously finite. For example, lower engine-out emissions immediately pay dividends in aftertreatment devices of smaller capacity, thus extending choice in packaging and location. It is also much easier to respect the thermal needs of the aftertreatment, proximity to the engine being paramount in this respect.

It should be admitted that various other design constraints also pertain, but these cannot be fully explored here. For example, even if statutory emissions limits are identical in two markets, the design task still differs if statutory test cycles also differ. This is *inter alia* because the efficiency of



14.1 Powertrain considerations in designing the aftertreatment to control engine-out emissions of (a) NO_x and (b) PM as a function of vehicle weight, with (say) a 2.0-litre engine. Two engine calibrations are portrayed, 'low PM and low NO_x'. Shown also are the Stage IV and Stage V limits in the EU (after Johnson, 2004, and Krüger *et al.*, 2003).

aftertreatment technology is very much test-cycle dependent (Johnson, 2004). Duty cycle, for instance, following a cold-start, controls catalyst light-off: the pollutants emitted prior to this event easily come to dominate the test cycle result. Another example is performance 'off-cycle', especially because the accelerations demanded by many customers are more aggressive, during

which time emissions spikes occur that exceed, by comfortable margins, steady-state emissions.

Returning, however, to Fig. 14.1 and the *statutory* requirement, it is apparent that, following implementation of Stage V, the diesel particulate filter or DPF (Section 14.4) will become essential for all vehicles, by which tailpipe PM emissions are easily cut to below the statutory limit of 5 mg/km. The situation with NO_x is not quite so clear-cut (Johnson, 2007): engine-out emissions of ~0.10–0.15 g/km are known (Johnson, 2006), and a belief exists in some quarters that vehicles of 1600 kg might actually achieve Stage V with no NO_x aftertreatment (Cooper *et al.*, 2006). This scenario, as already explained, to a large extent depends on the configuration of the powertrain: those vehicles to the right of Fig. 14.1(a) will require somewhat greater deNO_x efficiencies, i.e. those available from selective catalytic reduction or SCR (Section 14.5); whereas those to the left of Fig. 14.1(a) are more suited to the lean NO_x trap or LNT (Section 14.6).

Let us not forget HC and CO: generally speaking, these emissions are not an issue insofar as their removal by oxidation catalysts is a well-proven technology. (It should also be said that the LNT, and certain catalytic formulations added to the DPF, can also control HC and CO.) However, for powertrains in which engine capacity is large in relation to vehicle weight, the exhaust gas is relatively cool, thus the catalyst light-off period is embarrassingly protracted. Strictly within this context, countermeasures for NO_x and PM stand in diametrical opposition to those for CO and HC.

Finally, a need is regularly encountered for extra reductant in the exhaust stream, either to promote reducing reactions, or to raise exhaust temperatures, and often both. Depending on the circumstances, this takes place with the engine running on either a rich or a lean air–fuel ratio (AFR). While post-injections into the engine fulfil this purpose to some extent, the universal and unwelcome side-effect is *oil dilution* (Pfahl *et al.*, 2003). Nevertheless, exhaust injection is not in itself without drawbacks, and many advances are still needed (Wu and Hammerle, 2001). Air-assisted injectors (Guo *et al.*, 2003) are less convenient for light-duty powertrains, but liquid-only injectors exacerbate the homogenisation problem (Martin *et al.*, 2006).

Strictly speaking there is some terminological distinction since fuel is not necessarily ‘injected’ as such, but rather encouraged to evaporate from some suitable chamber. Obviously, the exhaust gas must be guaranteed hot enough to rule out subsequent condensation, thus some post-injection, to raise engine-out temperatures, may still be required at exceptionally light loads. Naturally, the injection must occur sufficiently far upstream to allow full homogenisation, otherwise hot and cold spots are generated in the catalyst; this presents an immediate packaging problem insofar as the mandatory mixing length is a major headache, and additional features designed to promote mixing (baffles, etc.) tend to introduce inconvenient back-pressures.

14.3 Oxidation catalysts

Oxidation catalysts were introduced to light-duty powertrains in the 1990s. Since then they have become a well-established technology for the control of HC and CO – so well established that the tendency to take them for granted must be avoided. Although now reported less often in the literature, research nonetheless continues to be published. One reason is that modifications to the engine calibration, undertaken to address NO_x, tend to depress exhaust temperature, and also to raise engine-out HC and CO, rendering control by oxidation catalysts doubly difficult (Spurk *et al.*, 2007). For example, Koltsakis *et al.* (2007a) fabricated an oxidation catalyst by rolling sheets of metal foam around a perforated metal tube, in which the exhaust gas was constrained to flow radially. The reported advantages of this design, compared with conventional honeycomb monoliths, are an order-of-magnitude higher specific surface area, with due relaxation of mass-transfer limitations in the washcoat, and lower thermal inertia, thus shortening light-off time.

A second reason for research into oxidation catalysts is that the introduction of the diesel particulate filter or DPF (Section 14.4) has in effect rewritten the rules: first, because of the laudable desire to integrate the oxidative and filtering functions; second, to ensure sufficient thermal durability, as the oxidative function must withstand high (>600°C) temperatures periodically instigated during the regeneration phase; and third, to oxidise the high concentrations of hydrocarbon needed to force an exotherm and thus regenerate the DPF. For example, Nakane *et al.* (2005) report fuel injection into the exhaust, upstream of a catalyst, during which hydrocarbon concentrations reached 20 000 ppm (C_1) for a 300°C exotherm; they particularly highlight the dangers of coking on the catalyst surface. Makino *et al.* (2006) show how the lifetime thermal durability may be simulated on an accelerated test protocol. Performance was reportedly improved, partly through the formulation (partial replacement of platinum for palladium), and partly through modifications to the geometry of the honeycomb monolith (hexagonal rather than square cells).

An emerging issue in oxidation catalysis is NO_x *speciation* – the two emissions, NO and NO_2, have been taken historically as just one. Now, although engine-out exhaust contains predominantly NO, the introduction of any oxidative aftertreatment naturally tends to convert this to NO_2, which possesses the greater toxicity. Few data exist at this time as to how NO_x speciation shifts with engine operation, although enough is known to say that the two gases respond differently (Richards *et al.*, 2002).

14.4 Particulate filters

The diesel particulate filter (DPF) is a technology that is still relatively new. The first successful serial production is generally believed to relate to European

passenger cars within the last decade (Salvat *et al.*, 2000), since when the device has seen swift implementation, having been introduced to light-duty powertrains virtually without exception. This is certainly no surprise: it is difficult to see how PM emissions of a few milligrams per kilometre could have been realised in any other equally expeditious manner. Thus, in less than one decade (Richards *et al.*, 2000) the technology has transitioned from risky and largely unproven to an acceptable state of development where motor manufacturers are cautiously optimistic, if not yet wholly comfortable. A market for retrofits has also emerged (Richards *et al.*, 2003).

In a DPF, the PM (strictly, its soot component) is captured and stored over several hundred miles; intermittently, for periods of a few minutes, this soot is oxidised. But only in its *primary* function is the DPF unproblematic: filtering efficiencies, expressed in terms of PM *mass*, generally exceed 95% (Jeuland *et al.*, 2002, 2004) and indeed are often undiscernibly close to 100%. The problems, rather, begin with *regeneration*: for most customer duty cycles, exhaust temperatures are far too low for soot oxidation to occur naturally in the DPF, at least with sufficient regularity. The lightly loaded duty cycles of taxis, for example, are a particular problem (Richards *et al.*, 2003). Therefore, some periodic means of intervention is required in order to force up exhaust temperature, e.g. post injection. We shall return to this shortly.

Although the forms of DPF to have been researched are legion, the segmented wall-flow variety, consisting of several silicon carbide (SiC) honeycomb monoliths cemented together, was, in the race to production, left in firm possession of the field. The cordierite monolith, being thermally more vulnerable to melting or cracking during regeneration, is somewhat less favoured (Hiranuma *et al.*, 2003). Other contenders are still being avidly researched. The motivations here are various: for example, to obtain equivalent filtering efficiencies, or to carry more incombustible ash, for less impact on back-pressure. Three examples of ceramic monoliths evaluated on light-duty engines are as follows: (1) silicon nitride (Miyakawa *et al.*, 2003); (2) aluminium titanate (Bardon *et al.*, 2004; Heibel and Bhargava, 2007; Ingram-Ogunwumi *et al.*, 2007); and (3) an unspecified formulation (Li *et al.*, 2007). A recent development is cell geometry that is *asymmetric*, i.e., inlet channels are more voluminous than outlet channels (Ingram-Ogunwumi *et al.*, 2007), the reported advantage being ash-holding capacity. The deep-bed DPF of metal foam is an alternative; its lower filtering efficiency is offset to some extent by lower back-pressure. The filtering efficiency is nevertheless unprovable by electrostatic precipitation (Park *et al.*, 2007). Even so, the chief advantage metal foams appear to hold over ceramics is the facility to fabricate filters more readily according to the available packaging volume (Cho *et al.*, 2007; Koltsakis *et al.*, 2007a). Finally, packaging volume is reducible when DOC and DPF are twin-canned by elimination of the gap

between the two bricks, enabling closer thermal communication (Satoh *et al.*, 2007).

The decision to undertake regeneration requires extremely deft negotiation between two diametrically opposed constraints: too frequent and excessive oil dilution is the inevitable corollary of post injection, yet too infrequent and the excessive soot deposit results in blockage or, when burning, destructive exotherms. Other difficulties are the fuel economy degradation brought by the regeneration methods; the back-pressure imposed on the engine; an inexorable build-up of incombustible ash, by which the useful life is progressively shortened; the high regeneration temperatures, which accelerate thermal ageing in catalysts; and finally the packaging volume – a particular embarrassment with light-duty powertrains (Terry *et al.*, 2002), forcing distant (underbody) locations at which conditions are comparatively cool, thus exacerbating the thermal shortfall and rendering regeneration still more difficult to coerce. In all of these instances, improvements are still avidly sought.

First-generation systems used a fuel–borne catalyst or FBC (Salvat *et al.*, 2000), the chief candidate being cerium (Blanchard *et al.*, 2002), with iron (Caprotti *et al.*, 2003) and strontium (Vincent *et al.*, 2003) as close contenders. Typical design criteria are a 1.5-litre canister to cover a mileage of 120 000 km, with a treat rate of 10 ppm Ce (Blanchard *et al.*, 2002). A few millilitres of additive, at each refuelling event, were introduced automatically to the fuel tank by means of a dosing pump, the design of which was based on the medical syringe (Quigley and Seguelong, 2002; Campenon *et al.*, 2004). An alternative, continuous in-line system metered additive at rates proportional to fuel flow via a solenoid-operated pump; 'multiple dosing', caused by the return of fuel to the tank, was accounted for (Vincent *et al.*, 2003).

But, quite aside from the inconvenience of supplying and accurately metering trace quantities of additive (at ppm levels), the accumulation of spent metal as incombustible ash, within the DPF, made 'fit for life' systems difficult to design (Campenon *et al.*, 2004), i.e., regeneration intervals necessarily became unacceptably shorter (Blanchard *et al.*, 2003). Consequently, many motor manufacturers have transitioned to the catalysed or coated DPF, i.e., CDPF (Yuuki *et al.*, 2003), in which regeneration is forced solely by engine calibrateables–principally by fuel injection schedules; intake and exhaust are also throttled (Kodama *et al.*, 2005). Whether this late-injected fuel burns in the cylinder, raising engine-out temperature, or exits and burns in the oxidation catalyst is a matter of proximity to the main burn. Establishing an *optimal* injection schedule, where the thermal benefit imparted to exhaust gas is maximal, and the oil dilution via impingement of the spray on the cylinder wall is minimal, has attracted the attention of modellers (Belloir *et al.*, 2007). The appropriate injection schedule is very much dependent on operating point, and, to avoid unacceptably cold or hot excursions during

transient driving, post-injections are being increasingly placed under closed-loop control, via exhaust temperature (Hiranuma *et al*., 2003).

Much of the thermal energy swiftly dissipates (i.e., is wasted) prior to the DPF, where it is needed. For this reason, some manufacturers have opted instead, or rather as an adjunct, systems wherein fuel is injected directly into the exhaust stream. In the design reported by Chiew *et al*. (2005), this secondary fuel enters a small pipe and diffuser; heating is via a glow plug. The heating is left on for a short time, following deactivation of the fuel supply, to discourage uncontrolled escape of fuel. In the design reported by Asad *et al*. (2007), the low-pressure injector was mounted 300 mm upstream of a combined DOC–DPF, with vaporisation aided by an electrical heater of 800 W, mounted immediately upstream of the injector. An energy efficiency analysis was conducted to calculate what fuelling strategy gave the best temperature rise, i.e., expressed in °C per unit of energy, and also as fuelling rate with respect to exhaust flow rate.

To reduce the size of the DPF, and thus ease the packaging constraints (or alternatively to widen the intervals between regenerations, and thus ease oil dilution), an obvious strategy is to limit, more effectively, the engine-out PM emission – especially during accelerations, which produce soot spikes. This is possible, indirectly of course, via an oxygen (lambda) sensor, an added benefit of which is surer estimates of soot loading in the DPF (Ootake *et al*., 2007). Another method is exploitation of the reaction between soot and NO_2, the latter serving as an alternative oxidant at comparatively low exhaust temperatures (300–400°C) – the point being that this reaction, on light-duty powertrains, while insufficient to maintain a clean DPF on its own, may render assistance if the appropriate circumstances are contrived (Guo *et al*., 2003).

On the converse side, the size of the DPF is determined by its maximum soot load (MSL), as this determines also the magnitude of the regeneration exotherm. Not only temperature (melting) but also temperature gradients (cracking) are equally important. The greatest temperatures are experienced when regeneration is initiated, and immediately thereon the powertrain is returned to idle (the so-called 'return-to-idle' test). Typical contemporary values for MSL are several grams per litre, and it is no understatement that these are greatly restrictive in powertrain design; indeed, *any* uplift would immediately allow smaller filters (Briot *et al*., 2007) or wider regeneration intervals.

Partly, higher MSL is realisable via engine calibration, but, in order to identify idle calibrations that do not endanger the DPF, and also to avoid the need for expensive and laborious trial-and error, test-to-destruction methodologies, supporting models are advisable (Koltsakis *et al*., 2007b). Restricting the supply of exhaust gas oxygen is key (Brewbaker and van Nieuwstadt, 2002; Flörchinger *et al*., 2004): using a lambda sensor to supply

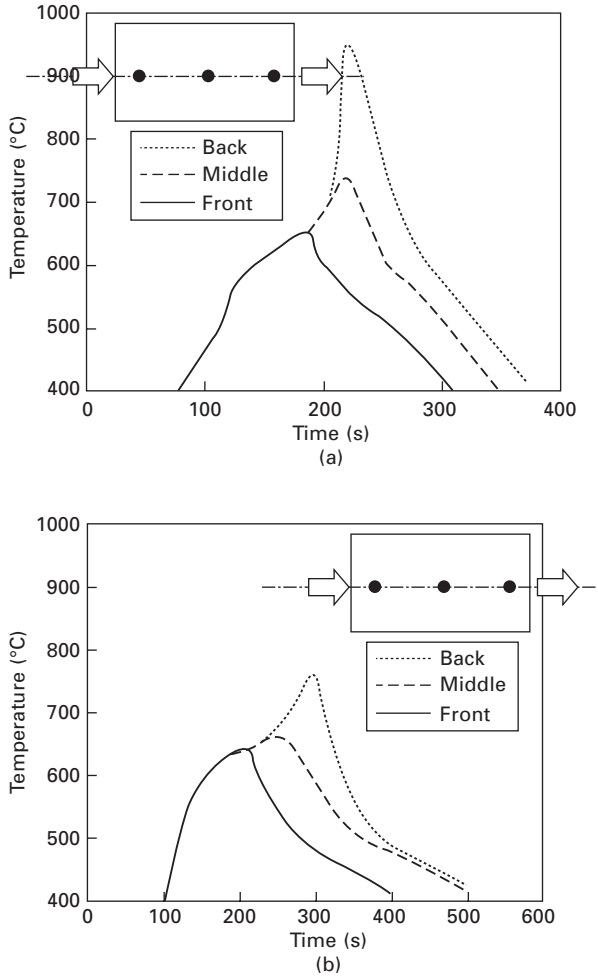
the feedback, engine operation (inlet throttling, injection schedules, EGR and VNT) is automatically adjusted in order to restrict the pace of regeneration (Ootake *et al.*, 2007). Figure 14.2 shows two return-to-idle tests, one using a 'standard' calibration known in production, the other a 'safe' calibration designed to protect the DPF. (The two tests were not precisely back-to-back i.e., the test conditions shifted slightly, but these confounders appear to have been adequately accounted for in the original paper.) It is clear that an appropriate idle calibration is very important in restraining thermal extremities (Koltsakis *et al.*, 2007b).

Higher MSL is also realisable through hardware. Partly, this is a packaging issue: the longer the DPF, the higher the regeneration temperatures for the same soot loading (Mizutani *et al.*, 2006). And partly, this is a material constraint, apparently relaxed using a new form of stress-tolerant cement (Mizutani *et al.*, 2006); or through microstructures which avoid hotspots by encouraging uniform soot deposition (Ichikawa *et al.*, 2004). This observation is instructive on a macro (channel-to-channel) scale: MSL tends to be decided, also, by regions holding the thickest deposits. This makes flow diffusers in the DPF inlet cone an advisable countermeasure, a secondary benefit of which is even distribution, also, of hot exhaust gas during regeneration (Zhan *et al.*, 2007).

14.5 Selective catalytic reduction

In selective catalytic reduction (SCR), some form of exogenous reductant, designedly injected into the exhaust stream, is used to reduce the NO_x over a suitable catalyst, the two chief contenders being metal–zeolite (copper and iron especially) or the traditional formulation still used in non-mobile applications, vanadia–titania. The important distinction, however, is that such reducing reactions operate in exhaust gas that is, in fact, still globally oxidising insofar as air–fuel ratio is still lean. Strictly speaking, the acronym SCR, derived from older, non-mobile applications, identifies no actual reductant as such; but the customary compound is ammonia (NH_3) or at least some lesstoxic precursor that decomposes into ammonia. (For example, an aqueous solution of urea, known under its trade name as 'Adblue', is common.) This practice (NH_3–SCR) is preferable, since it possesses high *selectivity* towards NO_x. The alternative, injection of hydrocarbons (HC–SCR), displays poor selectivity since oxygen readily supplants NO_x as the favoured oxidant.

Unquestionably the largest drawback of SCR – indeed, the sole reason why its adoption by vehicle manufacturers remains so hesitant – is the need to supply NH_3: this rests largely on an (as yet) undeveloped infrastructure. The reductant is supplied to the exhaust stream from a suitable vehicle-mounted receptacle, containing, for example, a eutectic aqueous urea solution of 32.5%. Periodic replenishment is required, since 'fit-for-life' systems are unfeasible:

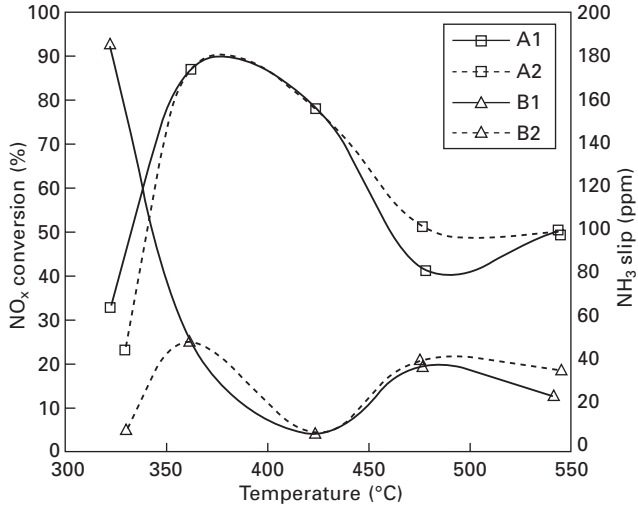


14.2 Experimentally determined temperature profiles within a diesel particulate filter (DPF) during the 'return-to-idle' test. DPF was initially fouled at low load and a rate of ~4 g/hour. At beginning of test, the engine was taken to full load; once DPF entry reached 615°C, and mid-bed reached 600°C, the engine was dropped to idle in 2 s. Two engine calibrations were used: exhaust oxygen concentration, exhaust hydrocarbon concentration, exhaust flow rate, engine speed, exhaust temperature, particulate loading, as follows: (a) 'standard', as typically used in production (16.9%, 81 ppm, 45.4 kg/hour, 800 rpm, 227°C, 6 g/litre); (b) 'safe', as determined to limit exotherm (8.5%, 520 ppm, 30.3 kg/hour, 1400 rpm, 259°C, 5.6 g/litre). Engine details: 2.0-litre, 4-cylinder, common rail, turbocharged. Aftertreatment: 0.7 litre diesel oxidation catalyst (DOC) followed (one metre later) by a catalysed 2.4-litre DPF (cordierite). Temperature readings with 0.75 mm NiCrNi thermocouples, located as sketched in the inset (Koltsakis *et al.*, 2007b).

urea consumption is estimated at 1000 miles/litre for a small passenger car, and ~250 miles/litre for a sport-utility vehicle (Tennison *et al.*, 2004). To reach Tier 2 Bin 5, one assumption is that, for a NO_x conversion of 90%, light-duty powertrains would consume urea at ~700 miles/litre (Lambert *et al.*, 2004). Secondly, there is an issue with low-temperature activity (<~150°C): this is partly an aspect of catalyst light-off, partly an aspect of vaporising and decomposing the urea droplets, and partly an aspect of ammonia storage within the catalyst. Thirdly, the ammonia must be metered carefully according to NO_x speciation (NO/NO_2), and transient operation is a problem, especially as regards storage effects. Fourthly, emissions of unused ammonia, known as 'slip', or of secondary products like isocyanuric acid ($C_3H_3N_3O_3$), formic acid (CH_2O_2), cyanic acid (HNCO) and nitrous oxide (N_2O) (Lambert *et al.*, 2001), must be avoided. Fifthly, current catalysts display insufficient thermal durabilities when exposed to heavily loaded duty cycles (high temperatures).

Much progress has been reported in injection systems. One such system (Wu and Hammerle, 2001) incorporates an air compressor and a miniature solenoid pump, capable of delivery at 5.5 Pa, with an electrical consumption of less than 12 W and possessing a dynamic flow range of 120. In another (Rusch *et al.*, 2006), injection takes place immediately downstream of a delta-wing fixture, protrusion of which into the exhaust stream at an angle of inclination of 20° imparts two counter-rotating vortices with which urea droplets are successfully entrained into the bulk flow, thus avoiding impingement on the wall. A third design (Xu *et al.*, 2007) used an air-assisted injector and mixer, placed respectively 80 cm and 66 cm upstream of the SCR. A distance of a few tens of centimetres between SCR and injector seems typical (Tennison *et al.*, 2004). But not all SCR units are awarded their own individual supplies of urea: in a SCR cascade, those units further downstream may simply consume ammonia slip discharged by earlier ones (Blakeman *et al.*, 2001).

Injection strategy pivots on 'alpha', meaning the ratio of $[NH_3]$ to $[NO_x]$. (As is customary, square brackets denote concentration.) Only in the most general terms is the condition $\alpha = 1$ likely to furnish just sufficient NH_3 for full reduction of NO_x, with none left over to be emitted as slip. The problem here is that highest NO_x conversions are not always coincident with lowest slip. Recent work (Girard *et al.*, 2007) argues for variable α, as a function of temperature. At low temperature (<250°C), conversion is relatively constant, with respect to α, so that slip is avoidable by restricting the supply of NH_3 ($\alpha < 1$), with no detriment to the emission of NO_x. Conversely, at high temperature (>400°C), NH_3 is oversupplied with impunity ($\alpha > 1$), since NO_x conversion is boosted further, while slip is readily oxidised by O_2. Thus, in Fig. 14.3, the *optimised* schedule (varying α) realised higher NO_x conversions across the temperature range than the unoptimised schedule ($\alpha = 1$).



14.3 NO_X conversion realised when NH_3 concentration is varied, with respect to temperature. The concentration ratio is $\alpha = [NH_3]/[NO_x]$. Legend: A, NO_x conversion efficiency; B, ammonia slip; 1, unoptimised α; 2, optimised α. At 230°C, $\alpha = 0.7$; at 450°C, $\alpha = 1.5$. Powertrain: 2.7-litre engine, 1.7-litre DOC and 2.8-litre SCR (Girard *et al.*, 2007).

Low-temperature performance has been particularly addressed. One difficulty is that the expected quantities of ammonia – consistent, that is, with thermal decomposition of injected urea – fail to take effect below 300°C (Xu *et al.*, 2007). At lower temperatures, the catalyst stored undecomposed urea, or partial decomposition products thereof, like cyanuric acid. Above 300°C, decomposition of these species recommenced – albeit this time inside the catalyst rather than in the feed-gas. An arguably extraneous factor is that cold-start hydrocarbon emissions deposit in, and suppress, SCR activity (Tennison *et al.*, 2004). Cold-start countermeasures are engine management strategies that force faster warm-up, and that sustain, in the face of lightly loaded duty cycles, a minimum SCR temperature (Tennison *et al.*, 2004). A platform-specific aspect of low-temperature performance is that, with increasing vehicle weight, test-cycle NO_x conversion efficiency improves significantly. This is because the light-off period is now shorter; this effect is offset, but only in part, by higher concentrations of engine-out NO_x (Pischinger *et al.*, 2007).

On the high-temperature side, release of stored ammonia by the SCR, leads easily to slip and, even in cases where a succeeding oxidation stage is included, this slip is promptly *re-oxidised* to NO_x (Tennison *et al.*, 2004). Not unexpectedly, the exploitable temperature window of the catalyst degrades with thermal ageing. A copper/zeolite catalyst underwent, on a

light-duty powertrain, an accelerated ageing protocol equivalent to 120 000 miles, encompassing intermittent periods (totalling 64 hours) of operation at 600–650°C (Cheng *et al.*, 2007). Based on post-mortem tests of cored samples in a bench-top reactor, mid-temperature (>300°C) deNO_x activity had collapsed in the first 2–3 cm of the brick.

Finally, some work has been reported on HC–SCR. In these systems, the reductant is not necessarily HC but decomposition products thereof. West *et al.* (2006) used inlet throttling and post-injection, albeit their catalyst was not full-size and was exposed only to part of the exhaust flow. For a small three-second period of post-fuelling, appreciable concentrations of H_2 (e.g., 0.1%) were produced, even at lean AFR (e.g., 18). Alternatively, one cylinder ran on a rich AFR for 400 ms, while the others ran lean, all taking turns, in the firing order. This operation produced 0.7% H_2, even with >9% O_2 in the exhaust. It was not, however, proved definitively that hydrogen – a strong reductant – was responsible for the observed deNO_x conversion efficiency of 25%. But without substantial improvement in conversion efficiency, HC–SCR is unlikely to display the required performance (Yu *et al.*, 2002).

14.6 Lean NO_x traps (LNT)

Lean NO_x trap (LNT), NO_x absorber-catalyst (NAC) and NO_x storage catalyst (NSC) are different appellations for essentially the same functionality. This form of deNO_x, already commercialised for direct injection gasoline engines, continues to be the main competitor to SCR with diesel engines. But, in great contrast to SCR, the operating principle is inherently *discontinuous*: periods of storage (tens of seconds) intercalated by periods of regeneration (seconds).

During the storage phase, NO_2 is captured as nitrates of barium and potassium, with assistance from sundry other metals like lithium, sodium and caesium (Nguyen *et al.*, 2007). (A precursive oxidation step converts NO into NO_2.) Storage capacities are generally on the order of a few hundred milligrams of NO_x per litre of LNT (Snow *et al.*, 2007a). In the regeneration phase – during which the deNO_x actually takes place – the LNT is forced to release its NO_x by switching to reducing exhaust gas, possibly with some assistance, from higher temperature. (Engine operation with rich AFR again distinguishes the LNT from SCR.)

Wholesale introduction of the LNT is restricted for two main reasons. First, the implementation of rich AFR is problematical on a diesel engine, in that smoke (soot) emissions are greatly exacerbated. Second, storage sites have far greater affinities for SO_x than for NO_x; this sulphur must be periodically dislodged, i.e., 'deNO_x' cycles are periodically interspersed with 'deSO_x' cycles. Unfortunately, deSO_x necessitates still higher temperatures, and these conditions accelerate thermal ageing. Other difficulties with the

technology are supplying neither too much nor too little reductant; managing the disturbance imparted by transition into, and out of, regeneration; avoiding the conversion of released NO_x into NH_3 or N_2O; and avoiding the conversion of released sulphur into H_2S. Finally, temperature windows are still too narrow to accommodate comfortably the full range of customer duty cycles (Blakeman *et al.*, 2003), although admittedly certain statutory cycles may still be respectively accommodated.

A wide range of calibrateables are manipulated to attain rich AFR (Herrmuth *et al.*, 2004), leading to numerous permutations; methodologies are therefore needed for optimisation (Senatore *et al.*, 2007). One method of attaining this end is as follows (Swartz *et al.*, 2006): partially close the intake throttle, thus reducing AFR from 33 to ~25; allow the airpath to stabilize for 5 s; finally, increase the main injection quantity for a period of 3 s, thereby reducing AFR still further to 13.5. Torque was maintained by retarding the timing of the main injection. In another scheme, rich AFR was achieved solely via post injection, at a timing of 80°ATDC (Swartz *et al.*, 2006).

These are exciting times, since the great flexibility inherent in contemporary fuel injection equipment is facilitating rapid exploration of novel combustion systems. These cannot be comprehensively explored here. Moreover, there are other aims besides regeneration of the LNT; germane is the ability, even at rich AFR, to attain relatively soot-free combustion. This includes, for example, so-called low-temperature combustion (LTC), attained by extremely high (50%) levels of EGR, with assistance from injection scheduling and inlet throttling, reaching a rich AFR of 13.5 (Huff *et al.*, 2006). Other, similar methods are premixed compression ignition (PCI) (Uekusa *et al.*, 2005) and premixed controlled compression ignition (PCCI) (Neely *et al.*, 2005).

Since in-engine methods of realising rich AFR are so problematical on diesel engines, engineers have also turned to exhaust injection. This method is inadvisable insofar as the principal advantage held by the LNT over SCR is discarded; yet this drawback should not be over-emphasised, since *diesel fuel* is injected which, unlike ammonia, is already eminently available on board. There is also an advantage in that the extremity of the engine calibration required for desulphation is relaxed somewhat (Swartz *et al.*, 2006). In-engine and in-exhaust injections can also render mutual assistance, the first method realising stoichiometry, the second nudging the exhaust gas into a reducing condition.

An auxiliary pump must be able to deliver, say, up to 20 or 30 millilitres of fuel per minute (Hackenberg and Ranalli, 2007). Another system delivers fuel at 3.8 bar, using a poppet-type injector with the aim of preventing leakage and nozzle coking (Nam *et al.*, 2007). A valve, mounted between the injector and the low-pressure fuel pump, controlled fuel atomisation and fuel quantity both individually and independently. A prototype system

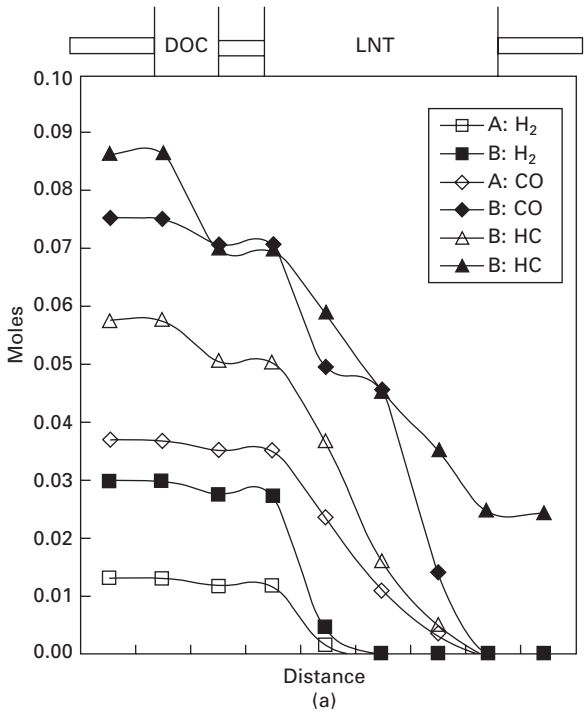
injects fuel into the exhaust ports, under the expectation of turbine-assisted homogenisation (Herrmuth *et al.*, 2004). The injector was that of a direct injection spark-ignition engine, operated with a water-cooled jacket. The fuel pressure was adjustable up to a maximum of 50 bar, but a minimum of 10 bar was used. Critically, as some of these injected hydrocarbons are *recirculated*, in-exhaust injection was synchronised with in-engine injection, *vis-à-vis* the charge preparation. In another system (Herrmuth *et al.*, 2004), the fuel is introduced, via a port-injector at 3 bar, to an evaporation chamber, from which it is evicted at 800°C, courtesy of three glow-plugs. A distance of 300–500 mm upstream of the LNT is recommended, and a vertical mount is preferred, to encourage evaporation in preference to fluid flow.

In *bypass* or dual-bank systems, the lion's share of exhaust gas is diverted to one LNT, so that less reductant is then required to realise reducing conditions in the neighbouring LNT. Thus, a lean AFR is retained for the engine, with all the attendant benefits. There are, however, trade-offs in choosing the relative exhaust flow rates between the two banks, e.g., the NO_x storage rate in one bank and the heating rate in the other (Yu *et al.*, 2002). Alternatively, a rich, premixed diesel-air burner, or 'flame reformer', can be used, rather than the engine, to supply the reducing exhaust gas (Midlam-Mohler and Guezennec, 2007). Fuel and air were injected into the burner housing (a tube) at three locations – tangentially, but in an oppositional swirl. The ignition source was a glow-plug. The tube, about 12.5 cm in length, acted as the combustion chamber. During regeneration, the engine's exhaust gas was rerouted through one LNT, and the flame-reformer gas was directed to the other LNT. An AFR of 11 was attained.

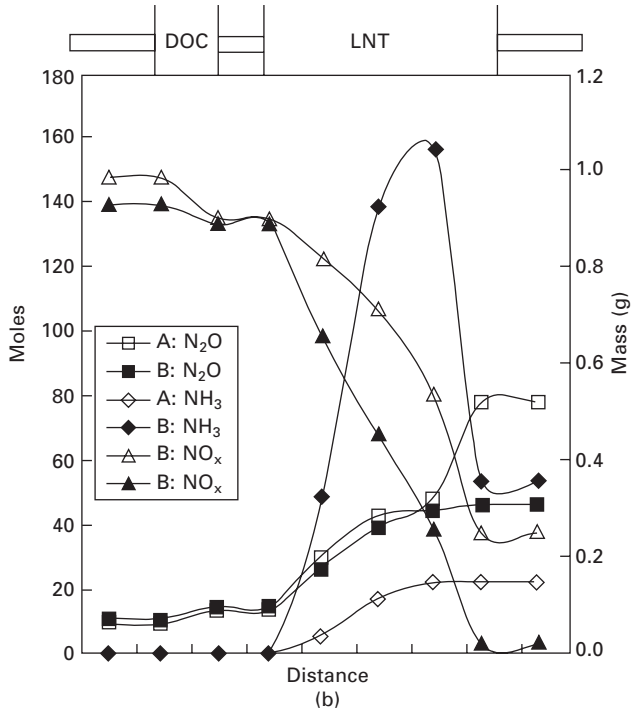
The precise composition of the reductant pool during regeneration, while certainly important, is not prescribed (or indeed easily described) precisely, and varies from one regeneration method to another: fuel hydrocarbons are simply cracked into light hydrocarbons, carbon monoxide and hydrogen. These differences in the reductant pool (of hydrogen content especially) induce significant differences in the reaction pathways. Something of the complexity thereby introduced is evident in Fig. 14.4 (Swartz *et al.*, 2006), which shows how different is the reductant pool for two regeneration methods, one via main injection, the other by post-injection. This, in turn, is responsible for numerous differences in the product pool, as also shown. For example, the main injection method generated significantly more H_2 than the post-injection method, and since this gas is so strongly reducing, regeneration must inevitably be affected (Swartz *et al.*, 2006). Other workers highlight how the most appropriate post-injection timing generated exhaust gas with the lowest oxygen and lowest hydrocarbon content, yet the highest CO content; this operation did not coincide with the worst soot production (Tomazic *et al.*, 2004).

As said, the temperature window of contemporary devices is rather

narrow, but peak conversion efficiency is preferably designed to coincide with peak engine-out NO_x (Uekusa *et al.*, 2005). There are, however, some formulations more active at low temperature and others more tolerant to high temperature, making cascade-LNT systems an obvious design choice, i.e., one close-coupled, the other underfloor. The low-temperature performance is sometimes an embarrassment insofar as storage still takes place; this behaviour confuses the light-off characteristic and, even worse, this NO_X, released inopportunely when higher temperatures return, still requires appropriate reduction. During these moments, the LNT becomes a significant *source* of NO_x, a phenomenon, apparently, that takes place in oxidising conditions – thus pointing to release mechanisms that are purely thermal (Kondo *et al.*, 2005).



14.4 Relevant exhaust species according to spatial position, including inside the LNT: (a) reductant pool (reactants); (b) nitrogen species (products). All quantities are in moles, except for NO_x which is in grams. AFR before LNT: 13.5. Cycle was 57 s lean and 3 s rich. Regeneration schemes: A, by post-injection, 80°ATDC; B, by main injection, timing retarded and quantity increased. Engine: 1.7-litre, 4-cylinder, common rail, model year 1999. Aftertreatment: DOC, followed by LNT (as sketched above graphs). Fuel sulphur: 15 ppm (Swartz *et al.*, 2006).



14.4 Continued

Maintaining optimal performance, via feed-gas temperature and composition, with respect to duty cycle is rather complicated, but understanding is advancing rapidly (Li *et al.*, 2000; Pfahl *et al.*, 2003). Overall performance is vitiated by NO_x spikes emitted on both entering and leaving regeneration (Alimin *et al.*, 2006). These spikes are dominated by NO rather than NO_2, and appear to originate not in the feed-gas but in the LNT. The results suggested that, upon entering regeneration, NO is released at faster rates than CO can consume it. Another need is to restrict emissions of N_2O and NH_3, created by secondary reactions within the LNT, otherwise the perceived deNO_x conversion will be misleading. Ammonia formation is slightly delayed, occurring towards the end of regeneration after most NO_x is consumed (Hackenberg and Ranalli, 2007). In fact, ammonia is even emitted by an ostensibly clean (freshly regenerated) LNT, the solution being not to prolong unnecessarily the period of regeneration: shortening this from 20 s to 5 s nearly halved the total ammonia emitted. Similar conclusions were reached by others (Mital *et al.*, 2003). A paramount distinction should be made between 'total NO_x conversion', or that fraction of feed-gas NO_x converted to some other species (N_2, NH_3, N_2O), and genuine 'NO_x reduction efficiency', or that fraction successfully reduced to N_2. The second (and preferable) reaction pathway

deteriorated at the expense of the former, as regeneration was prolonged from 1 s to 4 s (Parks *et al.*, 2005). Finally, the appropriateness of *pulsed* rather than sustained regeneration in restricting emissions of N_2O and NH_3 is related in some unobvious way to oxygen availability (Parks *et al.*, 2005).

14.7 Integrated systems

Concurrent mitigation of PM and NO_X has spurred integration, in various combinations, of the four basic aftertreatment units (DOC, DPF, LNT and SCR). Such multiple functionality includes discrete devices separated by the intervening exhaust system, occupancy of the same housing or 'can', and intimate combinations on the same brick. But however packaged, the superfluity of possible permutations, in sizes and relative positioning, present significant design optimisation problems (Pischinger *et al.*, 2007). Table 14.2 details several such systems that have been reported.

Nevertheless, exploitable synergies are a plausible aspiration, allowing cost reductions through, for example, precious metal loadings or closer compactedness in packaging. Modelling is an essential tool in designing systems with multiple functionalities. For example, two systems were modelled using MATLAB/Simulink (He, 2007). In one system the DOC was integrated into the same can as the LNT; in the other system, the DOC functionality was split between two separate units. The first system was successfully packaged closer to the engine than the second, but in both systems the DOC carried an identical precious metal loading and catalyst formulation.

Integrated systems are subject to many design conflicts, four of which are as follows. First, the need for proper homogenisation with the exhaust stream, following exhaust injection, *a priori* decides the length of uninterrupted exhaust system between two units. Second, LNT and DPF compete during their respective regenerations for the available HC. Third, a DPF interferes with the NO_x speciation experienced by a subsequent LNT. Fourth, LNT and SCR must withstand high exhaust temperatures generated during regeneration of an upstream DPF. As regards payback, one argument is that since the LNT carries an oxidising component, this replaces in part, or even in whole, the traditional DOC (Rohr *et al.*, 2006). The major synergistical advantage, though, to emerge in recent times is generation of ammonia by the LNT – previously seen as a nuisance – so that subsequent SCR comes into operation in a passive sense, thus obviating the need for exhaust injection of the same compound.

14.7.1 LNT and SCR

Pursuing this recently discovered synergy, the pertinent question is whether LNT–SCR will realise the same deNO_x performance as LNT alone but for

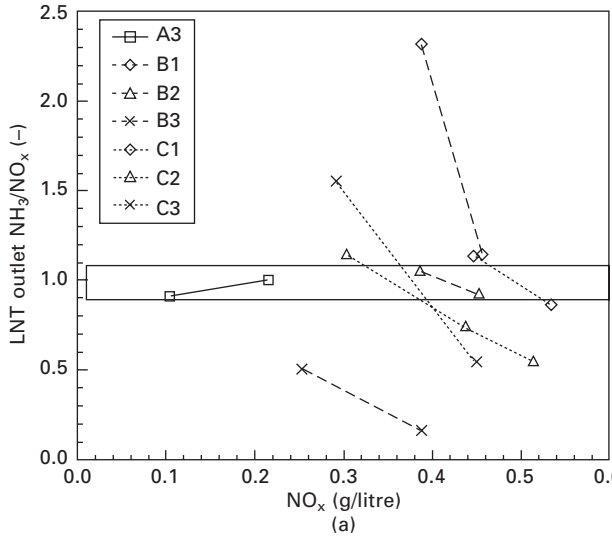
Table 14.2 Integrated aftertreatment systems recently reported in the literature for light-duty diesels

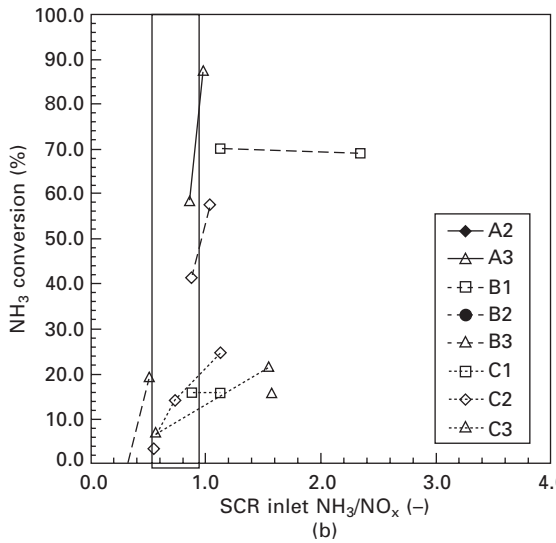
Engine (litre)	Unit 1 (litre)	Unit 2 (litre)	Unit 3 (litre)	Unit 4 (litre)	Reference
2.2	DOC+DPF	LNT+SCR*			Morita *et al.*, 2007
2.2	DOC [1.25]	LNT+SCR			Snow *et al.*, 2007
V	LNT + DPF [1.25V+1.5V]				Pischinger *et al.*, 2007
V	DOC+DPF [1.0V+1.5V]	LNT [1.25V]			Pischinger *et al.*, 2007
V	DOC+DPF [1.0V+1.5V]	SCR [1.8V]			Pischinger *et al.*, 2007
V	DOC [1.0V]	SCR [1.8V]	(DOC+DPF) [1.8V]		Pischinger *et al.*, 2007
3.0	DOC [1.2]	LNT [2.2]	SCR [2.7]		Hackenberg and Ranalli, 2007
2.0	DOC+DPF	DOC+LNT [2.0]			Nam *et al.*, 2007
1.9	LNT [1.34]	LNT [2.5]	DPF [4.1]		Tatur et al., 2005
3.0	DOC	LNT [5.1]	DPF [5.8]	DOC [1.5]	Kondo *et al.*, 2005
1.8	DOC [1.6]	SCR [3.7]	DPF		Tennison *et al.*, 2004
2.0	DOC [1.2]	DPF [2.5]	LNT [1.7]		Neely *et al.*, 2005
1.2	DOC [1.2]	DPF [2.5]	LNT [1.7]		Herrmuth *et al.*, 2004
1.2	LNT [1.7]	DPF [2.5]			Herrmuth *et al.*, 2004
1.2	DPF [2.5]	SCR [2.5]			Lambert *et al.*, 2001

*Using the ammonia generated in LNT as SCR.

less precious metal loading, thus engendering a cost saving. Obviously, this happens if SCR allows sufficient relaxation of LNT conversion efficiency. The key to this system lies in contriving an engine calibration such that, during regeneration of the LNT, an appropriate NH_3/NO_x ratio is realised at the entry of the SCR. As with SCR alone, divergent ratios lead to emission of NH_3 on one side and NO_x on the other. The principle is the same, albeit on a different scale, when both functionalities are integrated on the same brick rather than in different units (Morita *et al.*, 2007).

Figure 14.5(a) shows the NH_3/NO_x ratio at the outlet of the LNT during its regeneration for various space velocities, air–fuel ratios and NO_x retentions (Snow *et al.*, 2007b). The ammonia conversion realised in the subsequent SCR, according to this same ratio, is illustrated in Fig. 14.5(b). Clearly,





14.5 Aftertreatment system consisting of DOC, LNT and SCR, showing interrelation via $[NH_3]/[NO_x]$ ratio (optimal range specified by boxed area): (a) performance of LNT; (b) performance of SCR. Legend: λ, 1, 0.90; 2, 0.92; 3, 0.94; space velocity (hr^{-1}) and engine speed (rpm): A, 36 400 and 1750; B, 43 000 and 2000; C, 68 000 and 2500. Engine: 2.2-litre; LNT: 2.5-litre; SCR: 2.5-litre. Mid-bed temperature: 325°C. Regeneration period: 5 s (Snow *et al.*, 2007b).

many conditions in the LNT fail to realise an appropriate NH_3/NO_x ratio for the SCR. Moreover, the SCR is deactivated (albeit reversibly) if exposed to excessive hydrocarbon concentrations (several thousand ppm) during the rich, NH_3-generating purge of the LNT, thus demonstrating a conflict of interest.

14.7.2 DPF and LNT

One synergy of interest here is concurrent regeneration of the DPF and desulphurisation of the LNT. For example, with DPF followed by LNT, and using LTC and PCCI to manipulate feed-gas composition, reducing and oxidising chemistries were alternately pulsed (Neely *et al.*, 2005). This strategy had the merit of limiting temperature gradients in the LNT. In the converse design, of LNT followed by DPF, the latter was deprived of NO_x as an oxidant, during both the storage phase and the regeneration phase (Pfahl *et al.*, 2003). On the other hand, conditions arose in which the NO_2/NO ratio was higher and the temperature for the carbon–NO_2 reaction more appropriate.

LNT and DPF have been packaged into one convenient unit, called a NO_x-particulate filter or NPF (Ranalli *et al.*, 2004). Regeneration was accomplished through the injection of fuel into the exhaust 300 mm upstream of a preceding DOC. The DPF was regenerated first, using oxidising exhaust, after which reducing conditions were established to regenerate the LNT, including desulphurisation. One difficulty is that regeneration of the DPF causes premature release of NO_x from the LNT by thermal mechanisms. A similar, closely integrated LNT–DPF, called diesel particulate–NO_x reduction or DPNR, was reported (Kasai *et al.*, 2004). This system, in which the DPF is impregnated with the chemical formulation of the LNT (Ohki *et al.*, 2003), has been evaluated in a two-bank configuration (Itabashi *et al.*, 2005).

An aftertreatment system had, first, a SO_x trap, after which the exhaust system was split into two banks, each carrying a LNT, regenerated alternately as described in Section 14.6. Finally, following reuniting of the two paths, there was a DPF (Mital *et al.*, 2003). During regeneration, fuel was injected upstream of a LNT: this was deemed synergistically favourable for regenerating the subsequent DPF, i.e., raising temperature. A system subjected to durability testing consisted of DOC, LNT and DPF (Tatur *et al.*, 2006a, 2006b). During desulphurisation of the LNT, which used temperatures of 700°C and air–fuel ratios of 0.98, the DPF was regenerated through air injection into the exhaust. Two systems were compared: LNT followed by DPF, and DOC followed by DPF and LNT (Herrmuth *et al.*, 2004). The DOC is necessary in the second case in order to force regeneration of the DPF which, in the first case, benefits from the exotherm in the LNT. The DOC did, however, deprive the subsequent LNT of necessary reductants.

During transient operation the large thermal inertia, upstream of the LNT, compromised NO_x conversion at high load: this system was more suited for small-capacity engines in heavy vehicles. The converse system, being more readily close-coupled, is more suited to applications in which the exhaust temperatures are low, i.e., large-capacity engines in light vehicles.

14.8 Summary

In this chapter we have reviewed the recent literature devoted to aftertreatment for light-duty diesel powertrains. The focus mainly (but not exclusively) was on near-market research, as reported principally by practitioners in industry. Particular emphasis was laid on practical packaging problems and design constraints to be overcome.

Emissions legislation

In the USA, today's spotlight falls on 'Tier 2', and in the EU on Stage V. The legislative framework inevitably redounds on the choice of vehicle technology. Pivotally, limits for PM and NO_x tend to be less difficult for a large-capacity engine in a light vehicle: this relates *inter alia* to engine load. For this reason, the lightest vehicles powered by the largest-capacity engines escaped the need for PM and NO_x aftertreatment until relatively recently. As yet there is no convergence on the most suitable aftertreatment choice for NO_x. Again, this choice is co-dependent on the powertrain, as designed for its intended market. Finally, the auxiliary injection of reductants into the exhaust stream is a particular headache, especially as regards packaging.

Diesel oxidation catalyst (DOC)

Oxidation catalysts are a well-proven technology, but research continues nevertheless, because engine calibrations adopted to control NO_x tend to depress exhaust temperatures, thus hampering catalytic oxidation of HC and CO, and also because LNT and DPF intermittently require high temperatures which accelerate thermal ageing. The auxiliary injection of hydrocarbons generates large exotherms in the DOC; these hydrocarbons moreover must be sufficiently oxidised, prior to emission. Recent publications report new formulations resistant to thermal ageing, and non-monolith substrates (metal foam) with shortened light-off periods.

Diesel particulate filter (DPF)

Owing to the DPF, emissions of PM have been reduced to a few milligrams per kilometre. The most popular design is a segmented monolith of silicon

carbide. Other competing designs undergoing swift development are monoliths of silicon nitride or aluminium titanate, and metal foams. Asymmetric cells, or corrugations in the cell walls of the monolith, are a recent development. To avoid the complexity of fuel additives, manufacturers are transitioning to the catalysed DPF (CDPF), but with regeneration still augmented by post injections, coming under increasingly sophisticated closed-loop control (via exhaust temperature). Auxiliary injection of fuel into the exhaust is being avidly researched, to avoid oil dilution. A significant constraint is maximum soot load, needed in order to avoid destructive exotherms. Reported countermeasures are feedback via exhaust gas oxygen, new DPF materials, and identification of the appropriate calibration for 'return to idle'.

Selective catalytic reduction (SCR)

In light-duty applications particularly, the absence of an infrastructure for supplying urea represents a strong disincentive with this technology; the quantity necessary, even for the friendliest powertrains and markets, militates against 'fit-for-life' systems. Research into reductant delivery systems is well reported, however, along with recommended mixing lengths and hardware (baffles, etc.) for exhaust–reductant homogenisation. Enough work has been published to show how the most appropriate NH_3/NO_x ratio is not constant but varies as a function of catalyst operating temperature. The catalyst exhibits storage and release effects with regard to urea or related compounds: these engender a form of operation that is only quasi-continuous, and that must be accommodated in device operation. Rather less work is available on SCR via hydrocarbons: this form of deNO_x is noticeably inferior in the conversion efficiencies it can deliver. It may be possible, however, to crack the fuel into compounds that are more effective reductants.

Lean NO_x trap (LNT)

A considerable body of literature reports methods of realising reducing exhaust gas for the regeneration phase. These are of three types: conventional combustion (e.g., intake throttling and post-injection); novel combustion (e.g., non-traditional, high EGR rates, premixed charge); and third, the injection of fuel into the exhaust. An allied method is to cut the reductant demand by dropping the throughput of exhaust gas with a dual-bank system, each LNT of which is regenerated alternately. The temperature window is still too narrow to accommodate the full operating range, and the current LNT must spend some of its time in a non-optimal condition that is either too hot or too cold. Methods have been reported to limit the emission of NO_x during the transition between regeneration and non-regeneration, and the emission of ammonia.

Integrated systems

Aftertreatment systems containing multiple functionalities are well reported. The major development in recent times is the realisation that ammonia generated in the LNT, formerly cited as a disadvantage, can be used in subsequent SCR, which then operates in a passive sense. The question is whether such systems can realise the same deNO_x efficiency for less cost, i.e., less precious metal loading: the key lies in contriving an optimal NO_x/NH_3 ratio between the two devices. LNT and SCR have been realised on the same brick. The integration of DPF and LNT is also known: desulphurisation of the latter can be integrated to some extent with regeneration of the former. Some research indicates that the most appropriate sequencing of the two devices depends on engine capacity in relation to vehicle weight.

Comparisons and contrasts

The DPF at least has the merit of still filtering at all times, including when cold, and rarely needs heating up. With LNT and SCR, on the other hand, there is an additional consideration of how they should be operated 'off-cycle'. LNT and SCR are to some extent in competition. LNT, like DPF, operates discontinuously, but the cycle or storage regeneration schedule is very much shorter. SCR is only ostensibly a continuous form of aftertreatment: it has storage-release properties that must be accommodated. SCR has been more readily embraced in the heavy-duty sector, because catalyst size scales with engine capacity, whereas the injection system is largely a fixed cost. LNT contains expensive precious metals, whereas SCR uses far cheaper base metals (a significant cost saving): this differential ensures that competition between the two technologies is more evenly balanced in the light-duty sector (Lambert *et al.*, 2004). SCR packaging constraints are more severe than those of LNT on passenger cars, making for more complex systems (Rusch *et al.*, 2006). Unlike DPF and LNT, SCR has little direct impact on fuel consumption: the reductant (urea) must be included as an extra. SCR obtains higher NO_x conversion efficiency than LNT, and throughout a wider range of exhaust temperature. On this basis, it is more suited to powertrains carrying small-capacity engines installed in heavy vehicles. DPF is in a more advanced state of development than LNT and SCR.

14.9 Future trends

The question all industry commentators are asking nowadays is two-stranded, partly involving business or market projections, and partly involving technical hurdles (and of course the interplay of both): will a lucrative market for passenger-car diesels emerge in the USA? The answer from a purely emissions

standpoint would appear to be 'yes'. This is because, owing primarily to aftertreatment, modern light-duty diesels in their toxic emissions (PM, NO_x, HC, CO) show every sign of drawing level with, and indeed of overtaking, gasoline engines, as traditionally conceived. Nor is this picture likely to be changed by direct injection gasoline engines, which are beset by the self-same NO_x and PM emissions problems as diesels.

The business model must consider whether all this extra emission-control hardware is containable in a commercial setting. LNT or SCR should not perhaps be scarified too readily, as their current level of development arguably resembles, say, that of the three-way catalyst 30 years ago. The encircling difficulty is not toxicity but rather emissions of CO_2: with governments keenly promulgating greenhouse gas legislation, a regularly expressed interest is seen in the diesel engine for reasons of its superior fuel economy. Unfortunately, all the elaborate aftertreatment technologies under development, and described herein, unavoidably sap this fuel economy advantage.

If forthcoming aftertreatment technology were to become impracticably complex, unwieldy and cumbersome (and even the most ardent enthusiasts will find it a hard task to argue otherwise), a clear incentive will be created to revisit traditional combustion systems. Indeed, this trend is already firmly established insofar as the LNT requires reducing exhaust gas, and special measures are required to reach rich air–fuel ratios on diesel engines. These alternative combustion systems (e.g., HCCI) eschew, either in part or in whole, diffusion flames (Johnson, 2006); and engine-out emissions of NO_x and PM are remarkably low.

Two aspects of fuel formulation should be mentioned. Unquestionably a major enabler for the LNT is *low-sulphur fuel*, certainly <15 ppm and preferably <5 ppm. It is want of these concentrations in the marketplace which has largely stymied introduction of the LNT. With the DPF, a salient uncertainty is *biodiesel*, on two grounds: first, its ill-described chemical composition insofar as 'biodiesel' is a sweepingly colloquial term; and second, because of variable blend ratios with mineral diesel. There are many implications here for the DPF that cannot be explored in this short note. Biodiesel is to be welcomed from the standpoint of lower engine-out soot and greater catalytic activity in this soot, courtesy, perhaps, of the residual alkali catalyst used in its manufacture (Yamane *et al.*, 2004): both of these shifts will widen regeneration intervals, and so reduce fuel economy impact and post-injection-mediated oil dilution. The difficulty for the motor manufacturer is that contemporary DPF management, *on vehicle*, already depends extensively on control systems that are open-loop, and fuel composition is no exception.

In future years NO and NO_2 may not be legislated as the collective 'NO_x'. This is because NO_2 poses greater risks to public health than NO, and the balance between the two is undoubtedly affected by aftertreatment (Richards

and Kallschewski, 2003). (Usually, NO is oxidised to NO_2.) Moreover, in deNO_x aftertreatment, the conversion of NO or NO_2 to N_2O rather than N_2 – a well-known side-effect – is unlikely to pass muster with environmentalists since N_2O is a powerful greenhouse gas.

Finally, legislation is in preparation for proscription according to particle *number*, especially in the EU. Consequently, the database in this area is growing rapidly in preparation (Andersson *et al.*, 2001). Such legislation will probably take its cue from current light-duty legislation, i.e., 'number of particles per unit distance'. This raises a whole host of issues that cannot be explored here, but one is rather a paradox: the particulate 'cake' which accumulates in a wall-flow filter is a better filter than the wall itself. To simplify somewhat, this is a consequence of the fact that particles of a few hundred nanometres or so, that is, those of the 'accumulation mode', interact only weakly with bulk matter. So, a clean or a recently regenerated filter displays lower filtration efficiency than a fouled one. Should this become an embarrassment, careful consideration will need to be made of flow rate and pore size in relation to particle size (Ohara *et al.*, 2007).

14.10 References

Alimin A.J., Roberts C.A., Benjamin S.F. (2006), 'A NO_x trap study using fast response emission analysers for model validation', SAE paper 2006-01-0685

Andersson J.D., Wedekind B.G.A., Hall D., Stradling R., Wilson G. (2001), 'DETR/SMMT/CONCAWE particulate research programme: light-duty results', SAE paper 2001-01-3577

Asad U., Banerjee S., Reader G.T., Wang M., Zheng M. (2007), 'Energy efficiency analysis between in-cylinder and external supplemental fuel strategies', SAE paper 2007-01-1125

Bardon S., Bouteiller B., Bonnail N., Girot P., Gleize V., Oxarango L., Higelin P., Michelin J., Schuerholz S., Terres F. (2004), 'Asymmetrical channels to increase DPF lifetime', SAE paper 2004-01-0950

Belloir M., Sakushima N., Lahjally H. (2007), 'A CFD study to optimize the injection strategy for diesel particulate filter regeneration', SAE paper 2007-01-0164

Blakeman P.G., Chandler G.R., John G.A., Wilkins A.J.J. (2001), 'Investigations into NO_x aftertreatment with urea scr for light-duty diesel vehicles', SAE paper 2001-01-3624

Blakeman P.G., Andersen P.J., Chen H.-Y., Jonsson J.D., Phillips P.R., Twigg M.V. (2003), 'Performance of NO_x adsorber emissions control systems for diesel engines', SAE paper 2003-01-0045

Blanchard G., Colignon C., Griard C., Rigaudeau C., Salvat O., Seguelong T. (2002), 'Passenger car series application of a new diesel particulate filter system using a new ceria-based fuel-borne catalyst: from the engine test bench to European vehicle certification', SAE paper 2002-01-2781

Blanchard G., Seguelong T., Michelin J., Schuerholz S., Terres F. (2003), 'Ceria-based fuel-borne catalysts for series diesel particulate filter regeneration', SAE paper 2003-01-0378

Brewbaker T., van Nieuwstadt M. (2002), 'Control of oxygen for thernal management of diesel particulate filters', SAE paper 2002-01-0427

Briot A., Carranza F., Girot P., Bardon S. (2007), 'Minimizing filter volume by design optimization', SAE paper 2007-01-0657

Campenon T., Wouters P., Blanchard G., Macaudiere P., Seguelong T. (2004), 'Improvement and simplification of DPF system using a ceria-based fuel-borne catalyst for diesel particulate filter regeneration in serial applications', SAE paper 2004-01-0071

Caprotti R., Field I., Michelin J., Schuerholz S., Terres F. (2003), 'Development of a novel DPF additive', SAE paper 2003-01-3165

Cheng Y., Xu L., Hangas J., Jagner M., Lambert C. (2007), 'Laboratory postmortem analysis of 120k mi engine aged urea SCR catalyst', SAE paper 2007-01-1579

Chiew L., Kroner P., Ranalli M. (2005), 'Diesel vaporizer: an innovative technology for reducing complexity and costs associated with DPF regeneration', SAE paper 2005-01-0671

Cho G., Choi H., Jeong Y., Kim H., An S., Jeong B., Choi Y., Kim D., Yoon C.S., Lee E., Oh K., Han S., Kim K., Park G., Choi S. (2007), 'PM reduction performance and regeneration characteristics of catalyzed metal foam filters for a 3L diesel passenger vehicle', SAE paper 2007-01-3456

Cooper B., Penny I., Beasley M., Greaney A., Crump J. (2006), 'Advanced diesel technology to active tier 2 bin 5 emissions compliance in US light-duty diesel applications', SAE paper 2006-01-1145

Dieselnet (2007), 'Emission standards', www.dieselnet.com, (consulted 4 July 2007)

EU Directive (2007), 'Regulation (EC) No. 715/2007 of the European Parliament and of the Council – On type approval of motor vehicles with respect to emissions from light passenger and commercial vehicles (Euro 5 and Euro 6) and on access to vehicle repair and maintenance function', 20 June

Flörchinger P., Zink U., Cutler W., Tomazic D. (2004), 'DPF regeneration concept to avoid uncontrolled regeneration during idle', SAE paper 2004-01-2657

French C.C.J., Pike D.A. (1979), 'Diesel engined, light duty vehicles for an emission controlled environment', SAE paper 790761

Girard J., Snow R., Cavataio G., Lambert C. (2007), 'The influence of ammonia to NO_x ratio on SCR performance', SAE paper 2007-01-1581

Guo G., Xu N., Laing P.M., Hammerle R.H., Maricq M.M. (2003), 'Performance of a catalyzed diesel particulate filter system during soot accumulation and regeneration', SAE paper 2003-01-0047

Hackenberg S., Ranalli M. (2007), 'Ammonia on a LNT: Avoid the formation or take advantage of it', SAE paper 2007-01-1239

He Y. (2007), 'Development of an integrated diesel exhaust aftertreatment simulation tool with applications in aftertreatment system architecture design', SAE paper 2007-01-1138

Heibel A., Bhargava E. (2007), 'Advanced diesel particulate filter design for lifetime pressure drop solution in light duty applications', SAE paper 2007-01-0042

Herrmuth H., Cartus T., Ducellari R., Derschmidt O. (2004), 'Combined NO_x and PM exhaust gas aftertreatment approaches for HSDI diesel engines', SAE paper 2004-01-1425

Hiranuma S., Yakeda Y., Kawatani T., Doumeki R., Nagasaki K., Ikeda T. (2003), 'Development of DPF system for commercial vehicle – Basic characteristic and active regenerating performance', SAE paper 2003-01-3182

Huff S., West B., Parks J., Swartz M., Green J., Graves R. (2006), 'In-cylinder regeneration of lean NO_x trap catalysts using low temperature combustion', SAE paper 2006-01-1416

Ichikawa S., Uchida Y., Kaneda A., Hamanaka T. (2004), 'Durability study on SiNSiC material for DPF (2)', SAE paper 2004-01-0951

Ingram-Ogunwumi R.S., Dong Q., Murrin T.A., Bhargava R.T., Warkins J.L., Heibel A.K. (2007), 'Performance evaluations of aluminum titanate diesel particulate filters', SAE paper 2007-01-0656

Itabashi S., Niimi K., Kamoshita S., Shoji A., Oda T., Hirota S., Watanabe T. (2005), 'Study of improvements in NO_x reduction performance on simultaneous reduction system of PM and NO_x', SAE paper 2005-01-3884

Jeuland N., Dementhon J.B., Plassat G., Coroller P., Momique J.C., Belot G., Bruchet D. (2002), 'Performances and durability of DPF (diesel particulate filter) tested on a fleet of Peugeot 607 taxis: First and second test phases results', SAE paper 2002-01-2790

Jeuland N., Dementhon J.B., Gagnepain L., Plassat G., Coroller P., Momique J.C., Belot G., Dalili D. (2004), 'Performances and durability of DPF (diesel particulate filter) tested on a fleet of Peugeot 607 taxis: Final results', SAE paper 2004-01-0073

Johnson T.V. (2004), 'Diesel emission control technology – 2003 in review', SAE paper 2004-01-0070

Johnson T.V. (2006), 'Diesel emission control in review', SAE paper 2006-01-0030

Johnson T.V. (2007), 'Diesel emission control in review', SAE paper 2007-01-0233

Kasai Y., Miwa S., Kuki T., Senda K., Ogura Y. (2004), 'New cordierite diesel particulate filter material for the diesel particulate–NO_x reduction system', SAE paper 2004-01-0953

Kodama K., Hiranuma S., Doumeki R., Takeda Y., Ikeda T. (2005), 'Development of DPF system for commercial vehicles (second report) – Active regenerating function in various driving conditions', SAE paper 2005-01-3694

Koltsakis G.C., Katsaounis D.K., Markomanolakis Z.C., Naumann D., Saberi S., Böhm A. (2007a), 'Metal foam substrate for DOC and DPF applications', SAE paper 2007-01-0659

Koltsakis G.C., Haralampous O.A., Samaras Z.C., Kraemer L., Heimrich F., Behnk K. (2007b), 'Control strategies for peak temperature limitation in DPF regeneration supported by validated modeling', SAE paper 2007-01-1127

Kondo N., Takeda Y., Tsutsui Y., Suzuki K., Takahashi Y., Murata M. (2005), 'Development of lean NO_x trap system for commercial vehicle – Application to multi cylinder engine and development issue', SAE paper 2005-01-3875

Krüger M., Wiartalla A., Lichtenberg T., Körfer T. (2003), 'Emission concepts for future passenger car diesel engines', Vienna International Motor Symposium, 15–16 May

Lambert C., Vanderslice J., Hammerle R., Belaire R. (2001), 'Application of urea SCR to light-duty diesel vehicles', SAE paper 2001-01-3623

Lambert C., Hammerle R., McGill R., Khair M., Sharp C. (2004), 'Technical advantages of urea SCR for light-duty and heavy-duty vehicle applications', SAE paper 2004-01-1292

Li C., Mao F., Zhan R., Eakle S. (2007), 'Durability performance of advanced ceramic material DPFs', SAE paper 2007-01-0918

Li Y., Roth S., Yassine M., Beutel T., Dettling J., Sammer C. (2000), 'Study of factors influencing the performance of a NO_x trap in a light-duty vehicle', SAE paper 2000-01-2911

Makino M., Kondo T., Kunz A., Ohara E., Schuetze F.-W., Hoffmann M., Groeger M., Jean E., Ottaviani E., Guertler W., Paule M., Keppeler B., Scharr D. (2006), 'Evaluation of advanced diesel oxidation catalyst concepts: Part 2', SAE paper 2006-01-0032

Martin S., Gehrlein J., Kotrba A., Lacin F. (2006), 'Urea SCR system characterization through unique flow bench testing', SAE paper 2006-01-3471

Midlam-Mohler S., Guezennec Y. (2007), 'Design, modeling, and validation of a flame reformer for LNT external by-pass regeneration', SAE paper 2007-01-1367

Mital R., Li J., Huang S.C., Stroia B.J., Yu R.C., Anderson J.A., Howden K. (2003), 'Diesel exhaust emissions control for light duty vehicles', SAE paper 2003-01-0041

Miyakawa N., Maeno H., Takahashi H. (2003), 'Characteristics and evaluation of porous silicon nitride DPF', SAE paper 2003-01-0386

Mizutani T., Ito M., Masukawa N., Ichikawa S., Yuuki K., Kurachi H., Toyoshima T., Ito T., Lappas I., Schaefer-Sindlinger A., Vogt C.D. (2006), 'The study for structural design of the segmented SiC-DPF', SAE paper 2006-01-1527

Morita T., Suzuki N., Satoh N., Wada K., Ohno H. (2007), 'Study on low NO_x emission control using newly developed lean NO_x catalyst for diesel engines', SAE paper 2007-01-0239

Nakane T., Ikeda M., Hori M., Bailey O., Mussmann L. (2005), 'Investigation of the aging behavior of oxidation catalysts developed for active DPF regeneration systems', SAE paper 2005-01-1759

Nam G.-W., Park J.-W., Lee J.-H., Yeo G.-K. (2007), 'The effect of an external fuel injection on the control of LNT system; the diesel NO_x reduction system', SAE paper 2007-01-1242

Neely G.D., Sasaki S., Hunag Y., Leet J.A., Stewart D.W. (2005), 'New diesel emission control strategy to meet US Tier 2 emissions regulations', SAE paper 2005-01-1091

Nguyen K., Hakyong K., Buntin B.G., Toops T.J., Yoon C.S. (2007), 'Rapid aging of diesel lean NO_x traps by high-temperature thermal cycling', SAE paper 2007-01-0470

Ohara E., Mizuno Y., Miyairi Y., Mizutani T., Yuuki K., Noguchi Y., Hiramatsu T., Makino M., Takahashi A., Sakai H., Tanaka M., Martin A., Fujii S., Busch P., Toyoshima T., Ito T., Lappas I., Vogt C.D. (2007), 'Filtration behavior of diesel particulate filters', SAE paper 2007-01-0921

Ohki H., Ishiyama S., Asano A. (2003), 'Control technology for passenger car diesel engine equipped with the DPNR system', SAE paper 2003-01-1880

Ootake M., Kondou T., Ikeda M., Daigo M., Nakano M., Yokoyama J., Miura M. (2007), 'Development of diesel engine system with DPF for the European market', SAE paper 2007-01-1061

Park S.J., Lee D.G., Cho G., Kim H., Jeong Y., Oh K.O., Lee E.S. (2007), 'A new diesel particulate filter using a metal foam filter combined with electrostatic precipitation mechanism', SAE paper 2007-01-1267

Parks J., Huff S., Pihl J., Choi J.-S., West B. (2005), 'Nitrogen selectivity in lean NO_x trap catalysis with diesel engine in-cylinder regeneration', SAE paper 2005-01-3876

Pfahl U., Hirtler W., Cartus T. (2003), 'Passenger car investigations of NO_x-adsorber and DPF combination to fulfill future diesel emission limits', SAE paper 2003-01-0043

Pischinger S., Körfer T., Wiartalla A., Schnitzler J., Tomazic D., Tatur M. (2007), 'Combined particulate matter and NO_x aftertreatment systems for stringent emission standards', SAE paper 2007-01-1128

Quigley M., Seguelong T. (2002), 'Series application of a diesel particulate filter with a ceria-based fuel-borne catalyst: Preliminary conclusions after one year of service', SAE paper 2002-01-0436

Ranalli M., Schmidt S., Watts L. (2004), 'NO_x-particulate filter (NPF): Evaluation of an aftertreatment concept to meet future diesel emission standards', SAE paper 2004-01-0577

Richards P., Kallschewski W. (2003), 'Retrofitting of diesel particulate filters – Particulate matter and nitrogen dioxide', SAE paper 2003-01-1883

Richards P., Vincent M.W., Cook S.L. (2000), 'Operating experience of diesel vehicles equipped with particulate filters and using fuel additive for regeneration', SAE paper 2000-01-0474

Richards P., Terry B., Pye D. (2002), 'Experience of fitting london black cabs with fuel borne catalyst assisted diesel particulate filters – Part 2 Non-regulated emissions measurements', SAE paper 2002-01-2785

Richards P., Terry B., Pye D. (2003), 'Demonstration of the benefits of DPF/FBC systems on London black cabs', SAE paper 2003-01-0375

Rohr F., Kattwinkel P., Kreuzer T., Müller W., Bailey O.H. (2006), 'NO_x-storage catalyst systems designed to comply with North American legislation for diesel passenger cars', SAE paper 2006-01-1369

Rusch K., Kaiser R., Hackenberg S. (2006), 'DPF SCR combinations integrated systems to meet future LDV emission limits', SAE paper 2006-01-0637

Salvat O., Marez P., Belot G. (2000), 'Passenger car serial application of a particulate filter system on a common rail injection diesel engine', SAE paper 2000-01-0473

Satoh H., Ishizawa T., Sekiguchi K., Matsunami M., Kunishima E., Muramatsu T., Minoshima N., Andoh T., Ozawa J. (2007), 'The IP filter, a DOC-integrated DPF, for an advanced PM aftertreatment system (2): An evaluation of fundamental performance', SAE paper 2007-01-0654

Senatore A., Cardone M., Buono D., Sessa G. (2007), 'Experimental study of lean NO_x trap management', SAE paper 2007-01-3442

Snow R., Dobson D., Hammerle R., Katare S. (2007a), 'Robustness of a LNT–SCR system to aging protocol', SAE paper 2007-01-0469

Snow R., Cavatatio G., Dobson D., Montreul C., Hammerle R. (2007b), 'Calibration of a LNT–SCR diesel aftertreatment system', SAE paper 2007-01-1244

Spurk P.C., Pfeifer M., Schütze F.-W., Kreuzer T. (2007), 'Challenges for the future: diesel engines exhaust gas aftertreatment system', SAE paper 2007-01-0040

Swartz M., Huff S., Parks J., West B. (2006), 'Intra-catalyst reductant chemistry and NO_X conversion of diesel lean NO_x traps at various stages of sulfur loading', SAE paper 2006-01-3423

Tatur M., Tyrer H., Tomazic D., Thornton M., McDonald J. (2005), 'Tier 2 intermediate useful life (50,000 miles) and 4000 mile supplemental federal test procedure (SFTP) exhaust emission results for a NO_x adsorber and diesel particle filter equipped light-duty diesel vehicle', SAE paper 2005-01-1755

Tatur M., Tomazic D., Tyrer H., Thornton M., Kubsh J. (2006a), 'Desulfurization effects on a light-duty diesel vehicle NO_x adsorber exhaust emission control system', SAE paper 2006-01-0423

Tatur M., Tomazic D., Thornton M., Orban J., Slone E. (2006b), 'Tier 2 useful life (120,000) miles) exhaust emission results for a NO_x adsorber and diesel particle filter equipped light-duty diesel vehicle', SAE paper 2006-01-0424

Tennison P., Lambert C., Levin M. (2004), 'NO_x control development with urea SCR on a diesel passenger car', SAE paper 2004-01-1291

Terry B., Richards P., Pye D. (2002), 'Experience of fitting london black cabs with fuel-borne catalyst assisted diesel particulate filters – Part 1: Regulated emissions and regeneration performance', SAE paper 2002-01-2784

Tomazic D., Tatur M., Thornton M. (2004), 'Development of a diesel passenger car meeting Tier 2 emissions levels', SAE paper 2004-01-0581

Uekusa T., Nakada T., Ishikawa N., Ueda T., Fujino R., Brown D.B., Paratore M.J., Ryan D.M. (2005), 'Emission reduction study for meeting new requirements with advanced diesel engine technology', SAE paper 2005-01-2143

Vincent M.W., Richards P.J., Catterson D.J. (2003), 'A novel fuel borne catalyst dosing system for use with a diesel particulate filter', SAE paper 2003-01-0382

West B., Shean H., Parks J., Swartz M., Graves R. (2006), 'In-cylinder production of hydrogen during net-lean diesel operation', SAE paper 2006-01-0212

Wu C.-H., Hammerle R. (2001), 'An on-board reductant delivery system for diesel aftertreatment', SAE paper 2001-01-3622

Xu L., Watkins W., Snow R., Graham G., McCabe R., Lambert C., Carter R.O. (2007), 'Laboratory and engine study of urea-related deposits in diesel urea-SCR after-treatment systems', SAE paper 2007-01-1582

Yamane K., Asakaw T., Numao H., Komori M. (2004), 'Characteristics of DPF for diesel engine fueled with biodiesel – first report: Self regeneration behavior on vehicle road test and engine bench rig test', SAE paper 2004-01-1883

Yu R.C., Cole A.S., Stroia B.J., Huang S.C., Howden K., Chalk S. (2002), 'Development of diesel exhaust aftertreatment system for Tier II emissions', SAE paper 2002-01-1867

Yuuki K., Ito T., Sakamoto H., Matsubara R., Hashimoto S., Hamanaka T. (2003), 'The effect of SiC properties on the performance of catalyzed diesel particulate filter (DPF)', SAE paper 2003-01-0383

Zhan R., Huang Y., Khair M. (2007), 'Methodologies to control DPF uncontrolled regenerations', SAE paper 2007-01-1090

14.11 Appendix: Acronyms

AFR Air–Fuel Ratio
ATDC After Top Dead Centre
BMEP Brake Mean Effective Pressure
DPF Diesel Particulate Filter
EGR Exhaust Gas Recirculation
FTP Federal Test Procedure
MSL Maximum Soot Load
NEDC New European Drive Cycle
NMHC Non-Methane Hydrocarbons
NPF NO_x-Particulate Filter
PM Particulate Matter
SCR Selective Catalytic Reduction
VNT Variable Nozzle Turbine

15

Overview of diesel emissions and control for heavy-duty diesel engines

T. JOHNSON, Corning Incorporated, USA

Abstract: This review covers the exhaust emissions regulations and NO_x and particulate matter (PM) aftertreatment technologies for heavy-duty vehicles. The chapter first discusses recent developments in the regulations, which drive the aftertreatment technologies. NO_x control using selective catalytic reduction and lean NO_x traps is discussed. Finally, the author describes the state of the art in controlling particulates using diesel particulate filters, and summarizes future trends and provides informational sources for staying current.

Key words: diesel emission control, diesel particulate filters, selective catalytic reduction, lean NO_x traps, diesel aftertreatment.

15.1 Introduction

This chapter summarizes the recent developments in diesel regulations and general requirements, and NO_x and PM remediation. Regulatory developments are first summarized with a view towards aftertreatment requirements. Regulatory developments are now focused on Europe, where heavy-duty Euro VI regulations were recently finalized for 2013. The regulations are similar in terms of technology needs to those in the US for 2010. The regulation sets the direction for a particle number (P#) based regulation in addition to the traditional particle mass regulation. Non-road regulations in the US, Europe, and Japan are harmonized. They lag the US truck regulations by about four years, but are closely harmonized regarding technology. All advanced heavy-duty regulations will require either NO_x or particulate aftertreatment control, and most applications will require both.

NO_x control is focusing on selective catalytic reduction (SCR) for diverse applications. Zeolite catalysts will be the mainstay for Japan and the US, followed by Europe to meet the proposed Euro VI regulations somewhat later. The focus is on low temperature performance, secondary emissions and system optimization. Lean NO_x traps (LNTs) are finding applications in light heavy-duty applications, such as in large pick-up trucks, some delivery vehicles, and in several non-road applications. They can deliver up to about 60–70% deNO_x efficiency, and with integrated SCR, which utilizes ammonia generated in the LNT during rich regeneration cycles, deNO_x efficiency can improve to about 80%.

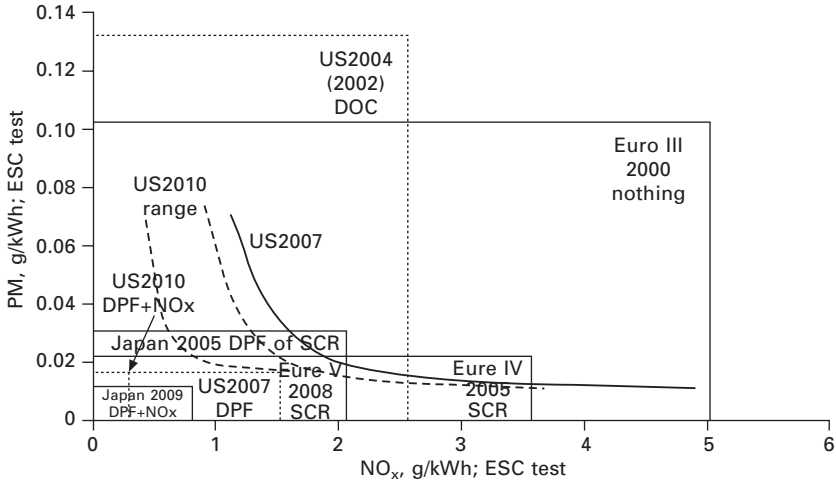
Diesel particulate filter (DPF) technology is in a state of optimization and cost reduction. Very sophisticated management strategies are being utilized, which open up options for new filter materials and alternative system architectures. Secondary emissions issues are emerging and are being addressed.

15.2 Heavy-duty regulatory developments

The on-road heavy-duty diesel (HDD) standards are shown in Fig. 15.1, as are estimates of engine emissions performance. These are unchanged from the author's estimates of 2007 (Johnson 2007b). Japan and the US have finalized their regulations for the next five to ten years, but Europe is just finalizing their regulations for 2013. In that regard, based on industry stakeholder surveys, the European Commission recently proposed (European Commission 2007), and the Parliament approved with Council guidance, NO_x standards of 0.40 g/kWh and PM standards of 0.010 g/kWh as measured on the current European steady state (ESC) and transient (ETC) cycles. Timing for implementation is 2013–14. This is numerically between the US 2010 and Japan 2009 levels, and will generally require similar engine and aftertreatment technologies. As in the final Euro VI light-duty regulations and unique to the European regulations, the Parliament desires that particle numbers be regulated, with the limit value determined later as the test protocol is established.

In 2006 the European Commission adopted the new World Harmonized Transient Cycle (WHTC) as well as the steady-state counterpart. The WHTC is cooler than the European Transient Cycle, with common engines not achieving 200ºC until after 500 seconds starting with a cold engine (Parche 2006). The cold start weighting factor is still to be finalized. In going from the ETC to the WHTC with a 10% cold start weighting factor, the engine industry is recommending a +0.3 g/kWh NO_x adjustment factor (Greening 2007b), as the four engines in their test program using EGR + SCR + DPF (exhaust gas recirculation, selective catalytic reduction, and diesel particulate filters) had WHTC–ETC differences ranging from 0.20 to 0.45 g/kWh NO_x. The difference in NO_x on one engine in another test program (Greening 2007a) using similar technology was about 0.1 g/kWh.

Figure 15.1 can be used to determine general aftertreatment requirements to hit the tightest regulations. In the case of modest incremental changes in engine technology going from US 2007 to US 2010, represented by the right-hand dashed line in Fig. 15.1, cycle-average deNO_x efficiencies in excess of about 60% will be needed. At the 60% deNO_x level, PM reduction efficiencies of >85% are required. If the engine operates at the higher NO_x levels to achieve better fuel efficiencies, required deNO_x efficiency can exceed 85% and the PM standard might be attained without DPFs, although this is highly unlikely (see next paragraph). For cutting-edge engine technology,

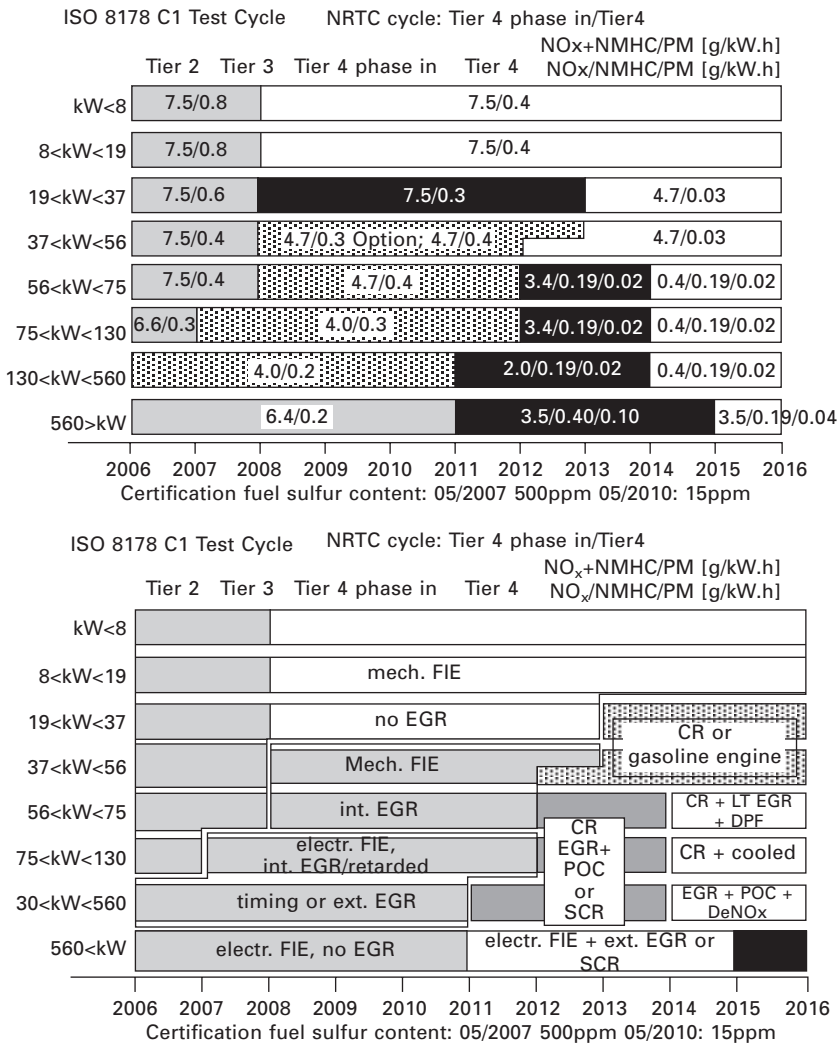


15.1 General comparison of on-road HDD standards in the US, Japan, and Europe. Estimated engine-out emissions for 2007 and 2010 (range) are shown. Steady-state cycle (Johnson 2007b).

represented by the left-hand dashed line in Fig. 15.1, 40% deNO_x levels might suffice, with the same range of PM removal efficiency. To attain the Japan 2009 or the Euro VI standards, considerably less deNO_x, if any, would be needed. No less than 50% PM removal is required due to the tighter PM regulations.

These levels give general guidance on aftertreatment requirements. However, this is much too simple for practical evaluation. For example, deterioration in engine emissions with age and the need for engineering margins will increase aftertreatment requirements. Also, supplementary emissions requirements, such as the US Not-to-Exceed (NTE) requirement, wherein in-use emissions can not exceed 1.5 times the standard (giving 0.4 g/kWh NO_x) in most modes of operation, can dictate requirements. For example, >90% deNO_x and PM efficiencies might be needed to comply with full-load NTE requirements. Finally, as for Euro VI light duty standards, Euro VI particle number (P#) regulations will require the best DPFs. These are used today on all US 2007 and almost all Japanese 2005+ heavy-duty highway vehicles, and will likely remain in future models in these markets.

Figure 15.2 shows the regulations and technology approaches to meet the future European, US, and Japanese non-road requirements, after Dreisbach (2007). Dreisbach describes the technology packages for 56–130 kW and >130 kW engines to hit the interim Tier 4 (2011) and final Tier 4 (2014) standards. The details are beyond the scope of this review. In short, EGR and filters are capable of hitting the interim levels for all engines, but need higher injection pressures (200 bar more), two-stage turbocharging (for the



15.2 Regulations and general technology approaches for future non-road applications (Dreisbach 2007).

higher specific power engines) and better cooling systems than SCR-only options. He chooses SCR because high deNO_x capability (>80%) is desired and the high exhaust temperatures (>250ºC) in the non-road transient cycle (NRTC) fit SCR nicely. Moving into the final Tier 4 engines, EGR, advanced cooling, and SCR are needed in all cases, except the 56 to 75 kW class wherein SCR is not needed. In almost all cases, PM regulations can be reached with partial filters, but DPFs are recommended to meet certain market or political needs. Others (Nishimura 2007; Signer 2007) are showing

only DPFs as the non-road PM-reduction technology solution. In that regard, this author notes that Switzerland is proposing a particle number emission cap for new construction equipment with engines >18 kW of 10^{12} particles per kWh measured on the NRTC.

15.3 NO_x control technologies

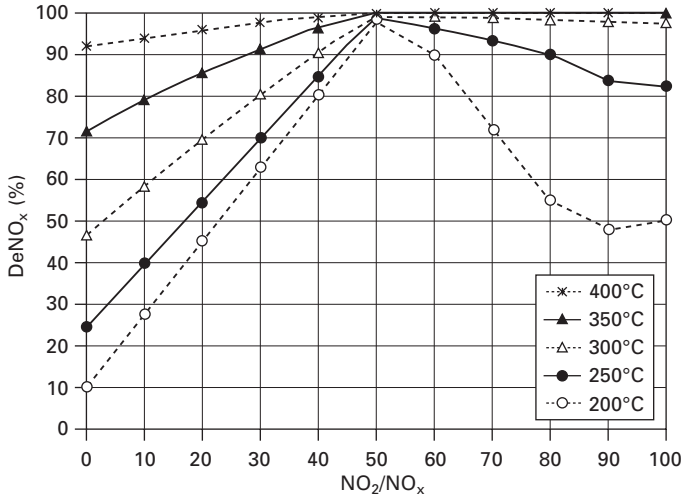
SCR (selective catalytic reduction) is established as the leading NO_x control strategy for heavy-duty applications. The first commercial applications were in 2005 for European and Japanese HD applications, and the technology is expected to be widely used to address the US 2010 regulations. The high NO_x removal efficiency and robust performance allow fuel-sensitive applications to be run at maximum efficiency (high engine-out NO_x, low PM).

For successful application of SCR, the regulators require appropriate measures to ensure the driver keeps urea on board, and that urea be plentiful and readily available. Jackson (2006) estimates that a 1% urea consumption rate (relative to fuel consumption) is expected for US 2010 applications. A 75-liter tankful might last 13 000 to 17 000 miles (21 000 to 27 000 km) for Class 8 and Class 6–7 vehicles respectively. The Class 8 vehicles would need one urea fill between long maintenance intervals (lube oil), while the smaller classes will not. European and Japanese trucks consume up to 5% urea, and the urea infrastructure is well developed.

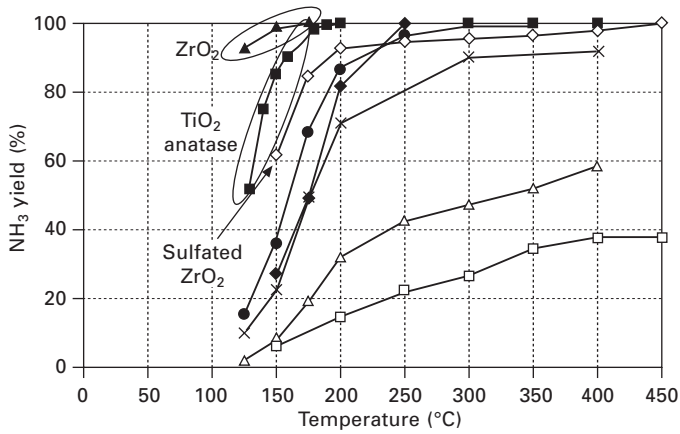
Europe SCR catalysts are based on vanadia, while those in Japan are zeolite-based. Given that zeolites have better high-temperature durability, and that the SCR will be receiving very hot gas from the upstream filter system during regenerations, zeolites are expected to also be used in the US. The new zeolite formulations perform better at the extreme temperatures and are less sensitive to non-ideal NO_2/NO_x ratios (Walker 2005).

There is significant motivation to improve low-temperature SCR performance. Further NO_x reductions in the HD sector are valued, and greater NO_x reductions are desired in urban driving or other low load conditions. Figure 15.3 shows how the efficiency of Fe-zeolites is affected by the proportion of NO_2 in the exhaust gas (Kroecher 2007b). Oxidation catalysts are generally used to oxidize NO to NO_2. SCR efficiency increases as NO_2 is increased to 50%, especially at the lower temperatures. However, increasing NO_2 beyond this level results in lower efficiencies at temperatures less than 250–300ºC. Also, as discussed later excess NO_2 (>50%) will decompose to N_2O, resulting in higher greenhouse gases.

Urea decomposition is a barrier to good low-temperature SCR performance. If urea can be thermally decomposed, for example with a bypass heater, system efficiency can be improved from 75 to 95% (Kowatari, *et al.* 2006). Although this is not a significant issue with vanadia catalysts, wherein urea decomposes faster to ammonia than the catalyst can utilize it at all temperatures, it can



15.3 SCR efficiency goes up markedly as NO_2 increases to 50% at temperatures less than 400°C. Excess NO_2 (>50%) deteriorates SCR performance, especially at the lower temperatures (<250°C) (Kroecher 2007b).



15.4 Efficiency of emerging urea decomposition catalysts (Kroecher 2007a).

limit the performance of zeolite catalysts, according to Kroecher (2007a). Kroecher shows that NO_2 adversely affects the decomposition of urea, in that the decomposition efficiency of a Fe–ZSM5 catalyst dropped from 70 to 40% at 150ºC in the presence of NO_2. Kroecher does show some new urea decomposition catalysts that can help significantly, Fig. 15.4.

Given that urea is decomposed to ammonia, poor low-temperature efficiency of the SCR catalyst itself presents a more fundamental obstacle. In Kroecher's

proposed reduction mechanisms for the SCR reactions over zeolite catalysts (Kroecher 2007a), he shows that with NO_x present only as NO, the oxidation to NO_2 to promote the 'fast SCR reaction' (1:1 = NO_2:NO) is the rate-limiting step. Once NO_2 is present or formed, an important intermediary in the reactor steps is NH_4NO_3 (ammonium nitrate). Ammonium nitrate begins forming with decreasing temperature at about 200ºC, and significantly hampers the reduction reaction after about 15 minutes at 190ºC and 5 minutes at 180ºC. Catalyst performance is restored upon heating to $T > 200$ºC, implying that if used in continuous low-load driving, the SCR catalyst will periodically need to be heated to decompose the ammonium nitrate.

Kroecher also shows (Kroecher 2007a) that excess NO_2 can partially reduce to N_2O over Cu- and Fe-zeolites, beginning in the 150–250ºC temperature range. This is problematic as N_2O is a potent greenhouse gas, and although such emissions are unregulated today, they can account for up to 10–15% of a vehicle's greenhouse gas emission. In his experiments, fresh Cu-zeolites had peak N_2O formation, 110 ppm, at 250ºC, while aged Fe-zeolites peaked at 45 ppm at 300ºC. Fresh Fe-zeolites did not form N_2O. The results illustrate the difficulty in balancing NO_2 concentration to optimize low-temperature SCR performance, catalyst choice, wherein Cu-zeolites have better NO_x conversion at low temperature, and secondary emissions. He shows a new Fe-zeolite catalyst formulation that decreases or eliminates N_2O formation.

In highly efficient SCR systems that run close to NH_3/NO_x stoichiometry, ammonia slip can result, especially in transient conditions. Slip catalysts are generally thought to remove most of the secondary emissions from SCR systems, such as ammonia, isocyanic acid (incomplete urea decomposition), nitrous oxide, and nitro-hydrocarbons (Sluder *et al.*, 2005). New slip catalysts are emerging that will convert ammonia all the way to nitrogen, and will likely go after hydrocarbon based emissions as well (Hamada, *et al.* 2006).

Urea evaporation and decomposition can be strongly dependent on getting good mixing. There are several papers on modeling to improve urea injection and mixing using a variety of devices (Kaiser 2007; Calvo *et al.* 2007; Gruenwald *et al.* 2007). About 10–20% deNO_x efficiency improvements can come from good injection practice, with nominally 5–10% coming from using a variety of mixers.

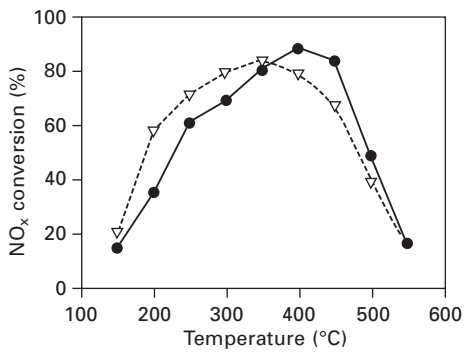
To facilitate OBD (on-board diagnostics) and closed-loop SCR control, aside from the established NO_x sensors (Walde *et al.* 2007), an ammonia sensor was recently introduced (Weisgerber 2007). It has ±5 ppm ammonia detection accuracy up to about 30 ppm ammonia, and has negligible or predictable cross-interference from NO_x, hydrocarbons, or CO.

In other developments, heavy-duty on-board urea systems are now largely being employed with air-assisted injection (Maurer *et al.* 2006; Parche 2005). Urea–exhaust wall interaction modeling shows enhanced mass and heat transfer for better urea distribution when the spray is impinged on the pipe,

but thin films can form if the pipe is at less than about 280ºC (Birkhold *et al*. 2006). There is also much interest in higher-capacity urea systems afforded by using solid urea or $MgCl_2$ storage medium. Solid urea will last more than twice as long as liquid urea for a given volume, but needs to be heated to about 180–200ºC in the presence of water vapor to decompose to ammonia (Mueller 2004). $MgCl_2$ and other chlorides store ammonia, and cartridges can be handled, replaced, recharged, and recycled (Johanssen 2007). It also has three times the volume-specific ammonia content and half the weight of liquid urea.

In some cases, SCR is not the preferred NO_x technology. Some vehicle manufacturers think their customers will resist urea-SCR if other options exist. Short-haul delivery trucks, agricultural equipment, and some non-road applications are some examples. The leading deNO_x approach in these applications is the lean NO_x trap (LNT), sometime referred to as a NO_x adsorber. The principle is to adsorb NOx under lean conditions as a nitrate, and then periodically run rich (a few seconds every minute) to dissociate the nitrate and reduce the NO_x to nitrogen.

One major problem with LNTs has always been related to durability due to sulfur contamination. Sulfates are more stable and block nitrate formation. The sulfur is removed by going rich and hot (700ºC) cumulatively about 10 minutes every 3000 to 6000 miles. Although earlier LNTs lost perhaps 50% of their nitrate capacity af ter about 15–20 desulfation cycles, newer versions now lose only about 25% of the fresh NO_x capacity. Further, in the past it was difficult to control desulfation temperature to within 700 to 800ºC. Newer control strategies now allow this (Wu 2005), and perhaps even better control. Given this, LNTs are good to about 60–70% NO_x efficiency in real-world systems (Rohr 2006), as shown for a heavily aged system in Fig. 15.5.

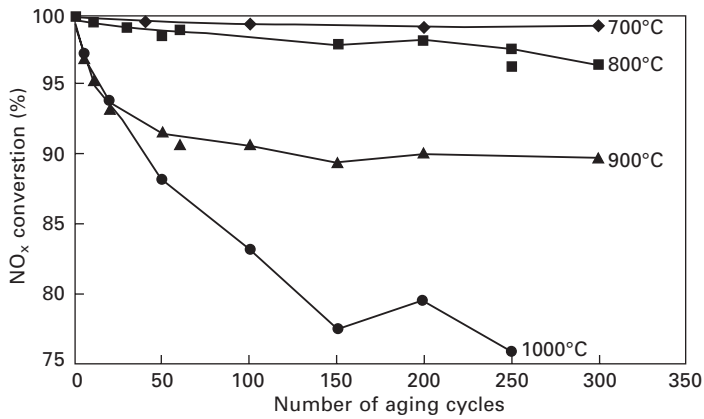


15.5 NO_x performance curves for heavily aged potassium and barium based LNTs. Efficiency is 63%, SVR = 0.94, 3.9 g/liter precious metal loading (Rohr 2006).

High-temperature LNT formulations are stepping up to the challenge of meeting the difficult high-load requirements of the US NTE regulation (Hinz *et al*. 2005). Most use potassium as the NO_x storage component (NO_x stored as a potassium nitrate). The durability of potassium LNTs subjected to aggressive desulfation cycling was recently quantified (Nguyen *et al*. 2007). The decrease in deNO_x efficiency shown in Fig. 15.6 when going from 800 to 900ºC desulfation exposure is mainly caused by potassium migration from the LNT catalyst to the cordierite substrate. Precious metal grain size increased only 15% in this temperature interval. Exposing the LNT to temperatures in excess of 800ºC should be avoided. This might be particularly challenging if the LNT is placed behind a diesel particulate filter, wherein outlet temperatures can exceed this level during soot burning cycles.

Finally, there is much recent interest in combining LNTs with SCR. In this case, a downstream SCR catalyst stores ammonia that is generated in the LNT during rich operation. This ammonia can react with slipped rich NO_x or lean NO_x, increasing system efficiency or decreasing PGM (platinum group metal) cost while maintaining efficiency. The most basic system, with an SCR catalyst following the LNT, is now in series production (DaimlerChrysler 2006) in a light-duty application.

To adapt this system to HD applications, Hu *et al*. (2006) refine this system by adding a fuel reformer in front of the LNT to produce hydrogen during the rich periods. The hydrogen promotes the formation of ammonia in the LNT. In this configuration the SCR adds up to 20% incremental NO_x efficiency to the LNT operating at 60–70% efficiency. Further, the hydrogen



15.6 The significant loss in deNO_x efficiency when going from 800 to 900°C is mainly due to potassium migration out of the LNT catalyst (Nguyen *et al.*, 2007).

which is also produced during the rich desulfation helps remove sulfur, thus helping to extend the minimum desulfation frequency by 30%.

15.4 Particulate matter (PM) control technologies

Diesel particulate filters (DPFs) are now as much a part of the diesel engine as fuel injectors. Virtually all new diesel cars in Europe, the US, and Japan will have DPFs, as do all new trucks in the US and most of them in Japan.

All first-fit DPFs are porous ceramic honeycombs in which the exhaust is forced through the cell walls. Occasionally, the filter needs to be regenerated by burning fuel over a catalyst to generate the high temperatures (generally greater than 550ºC) to burn the soot. For medium-duty applications, system approaches are similar to those for passenger cars in which fuel for periodically regenerating the filter is provided by extra injections in the cylinder. For the larger engines auxiliary injectors or burners in the exhaust are used to impart DPF regeneration. Considerations in this regard are the adverse durability effects of oil dilution by fuel from late in-cylinder injections, and the desire to decouple DPF injection events from engine management requirements.

DPF management is getting quite sophisticated. A catalyzed filter system will 'passively' regenerate from the reaction of NO_2 with carbon under medium- and high-load conditions (Borretto *et al*. 2004). Passive regeneration is limited by temperature and NO_x/C ratios. Successful long-term passive operation of filter systems (Chatterjee *et al*. 2004) has been achieved with exhaust gas temperature profiles of 40% > 210ºC and NO_x/soot > 15. In extended operating conditions in which passive regeneration is not enough to keep the filter clean, 'active' regeneration is needed. Zink *et al*. (2005) reviewed the approaches in the European light-duty sector, and identified common features:

- Estimation of DPF soot loading using engine and back-pressure models, and fuel consumption.
- Preheating of the system to ensure that injected hydrocarbons can ignite and heat up the filter.
- Increase of exhaust hydrocarbon levels via in-cylinder or supplemental fuel injection, for burning on a catalyst.
- Control and monitoring of the regeneration as a function of operating point and conditions.
- Recalculation of pertinent models to account for ash build-up.

Soot loading models have been in development for years. Although contemporary pressure drop models account for filter and catalyst type, ash loading, PM characteristics, and completeness and nature of regeneration, they still generally serve as back-up algorithms to soot loading based on engine operating conditions.

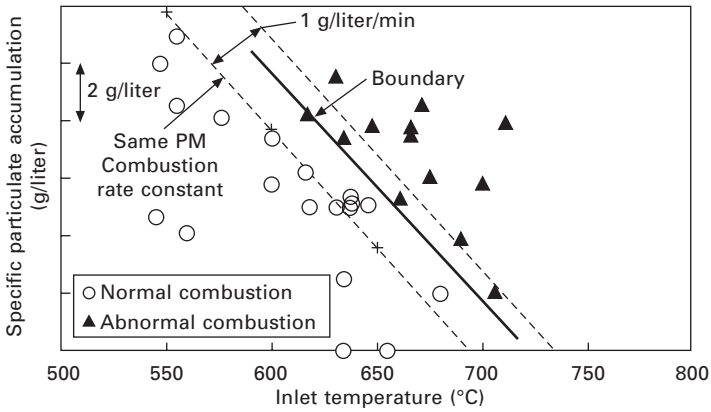
If active regeneration is needed, an oxidation catalyst temperature in the range of 220–250ºC is needed to burn injected hydrocarbons, sometimes requiring active system heat-up strategies. Common approaches are air intake and/or exhaust throttling, as well as appropriate late injection of fuel (Komada *et al*. 2005). These measures enable heat-up at ambient temperatures of –10ºC with the vehicle traveling an average of 14 km/h in a medium-duty vehicle application. Once hot, fuel injection strategies will depend on operating conditions.

To keep lube oil ash from sintering to itself and to protect DPF catalyst, maximum soot burning exotherms need to be controlled. Some parameters to enable this are filter type (material and catalyst), exhaust temperature and flow rate, and soot loading and characteristics. Craig *et al*. (2005) provide an excellent example of how maximum exothermic temperatures under worst-case 'drop-to-idle' conditions (DTI; start soot combustion at high temperature and flow, and then drop to idle) for cordierite filters. Karkkainen *et al*. (2006) show how this information can be incorporated into a safe regeneration strategy, wherein exhaust temperature is gradually increased from 550ºC to 600ºC as soot burns, and if the engine drops to idle, engine idling speed is increased to take heat out of the filter.

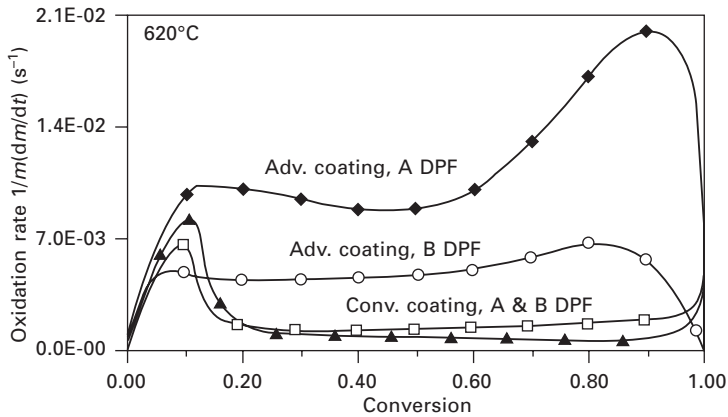
Additionally, managing oxygen through EGR control is being proposed. Ootake *et al*. (2007) describe a DPF regeneration strategy based on oxygen control using a lambda sensor. The method allows better-controlled regenerations, resulting in increased specific soot loadings of about 20%. The strategy is adaptive to account for air flow meter and other input variation. This allows better dynamic control in transient conditions.

An example of the level of sophistication of DPF soot loading models is offered by Muramatsu *et al*. (2006). They found that the primary soot combustion characteristics, namely ignition temperature and oxidation rate, depend on how the soot was produced. They quantified these parameters and incorporated them into their control and monitoring model, part of which is shown in Fig. 15.7.

DPF catalysts and substrates are moving forward with better fundamental understand of how soot, catalyst, and substrates interact. Konstandapolous *et al*. (2007) looked at the combination of DPF substrate porosity and catalyst configuration in the light of a proposed two-layer soot oxidation model. At temperatures of about 450ºC or in the initial stages of oxidation at higher temperatures, the layer of soot in direct contact with the catalyst begins oxidizing. As oxidation proceeds, soot contact is lost and the rate decreases until the higher temperatures when direct gas/soot oxidation begins (~600ºC). In Fig. 15.8, the authors show that these phenomena can be controlled with the use of advanced DPF substrates and an advanced catalyst coating to improve contact. With proper design, good contact can be achieved throughout the oxidation process.

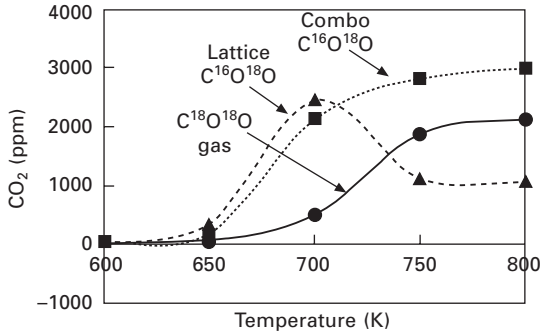


15.7 Relationship between filter soot load and exhaust temperature to impart a normal regeneration event. The boundary changes depend on soot characteristics (Muramatsu *et al.*, 2006).



15.8 DPF porosity and catalyst coating can impact soot oxidation rates. The differences are explained by intimacy of soot/catalyst contact using a two-layer soot model (Konstandapolous *et al.*, 2007).

Concerning soot/catalyst contact Suzuki *et al*. (2007) used isotopic oxygen in the gas to show the soot oxidation mechanisms of oxygen-storage washcoats. Figure 15.9 illustrates the shifting reaction kinetics for a Pr–Ce washcoat. The reaction of soot with only lattice oxygen (^{16}O) begins first (625K, ~350ºC) and peaks at 700K (~430ºC). Reaction with gaseous oxygen (^{18}O) then begins at 650K (~380ºC) with a mixture of the isotopes. With this material, the reaction with purely gaseous oxygen also begins at 650K, but is much slower. This reaction plateaus at 750K (~480ºC) and also likely occurs through the lattice exchange of oxygen.

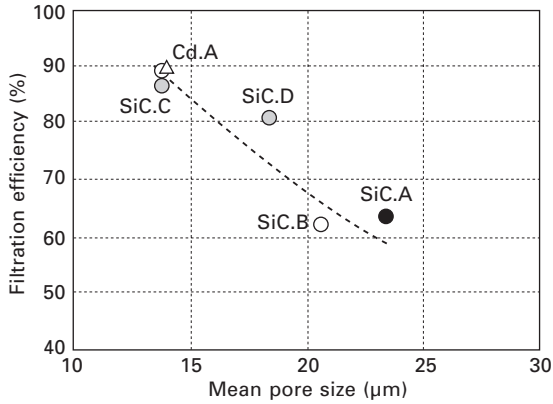


15.9 Using gaseous isotopic oxygen, the soot oxidation mechanism on Ce–Pr based catalyst can be determined (Suzuki *et al.*, 2007). It was shown that all the oxygen transfer at these temperatures occurred through the lattice.

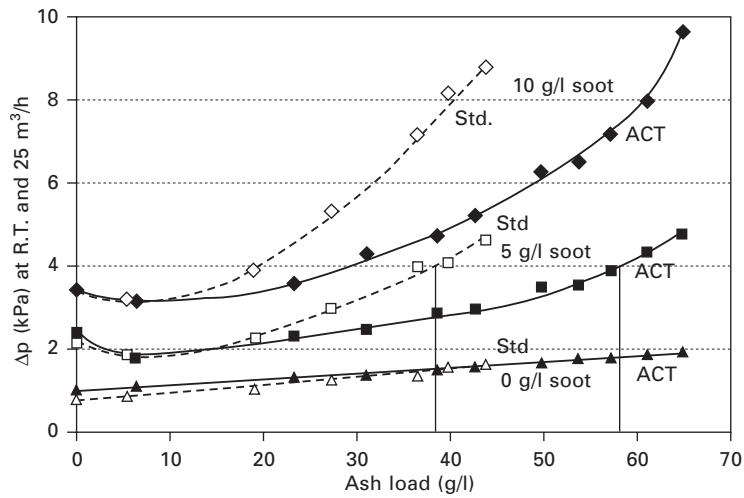
In other DPF catalyst developments, more data are reported on the substitution of palladium for platinum (Pfeifer *et al*. 2007). Pt/Pd formulations have lower light-off temperatures than Pt-only catalysts (240ºC vs. 295ºC) in the aged state, generate as much NO_2 for passive soot oxidation, and are resistant to sulfur contamination. A nominal 3:1 ratio of Pt:Pd is shown to be a good level of substitution. In one investigation, the platinum was completely substituted for palladium with use of a base metal catalyst (Johansen *et al*. 2007). Interestingly, NO_2 emissions were generally lower than from uncoated DPFs and much lower than from DPFs using platinum at the same catalyst loading (1.5 g/liter). Also, the balance point temperature (soot oxidation and accumulation are in equilibrium) was ~25°C lower and HC emissions were lower.

Moving on to substrate materials, advancements in material science are likewise allowing filter materials to advance. For light-duty applications, SiC filters have been the standard. However, aluminum titanate filters are now in series production, and, aided by better engine controls, the light-duty industry is beginning to move to advanced cordierite (Corning Incorporated 2006) filters. Cordierite is the preferred filter material in heavy-duty applications.

Figure 15.10 shows how the initial particle number (P#) filtration efficiency (15 to 500 nm) varies with mean pore size of the DPF substrate (Mizutani *et al*. 2007). All have a similar catalyst coating. Based on these data and other data in the paper, the authors show that initial filtration efficiency drops off dramatically if pores larger than ~20 μm are present. However, as the filter cake builds up, filtration efficiency recovers. This is demonstrated in a sister paper (Ohara *et al*. 2007), wherein the filters with a pore size of 25 μm reached near-parity with 15 μm filters after about 0.5 g/liter soot was captured using a diesel fuel burner rig. In vehicle testing on the NEDC



15.10 Initial P# filtration efficiency drops off significantly as DPF mean pore size approaches 20 μm (Mizutani *et al.*, 2007).



15.11 Asymmetric cell technology (ACT), wherein inlet DPF cells are larger than exit cells, can give 50% more ash capacity while maintaining backpressure (Heibel *et al.*, 2005).

with loaded filters, the larger-pored filters had a filtration efficiency of 94% compared to 98% for the filters with 15 μm pores.

Filter designers are also using creative cell geometry to increase ash storage capacity. By increasing the inlet cell size relative to the exit cell, ash loading can increase 50% while maintaining the same backpressure for soot-loaded filters, as shown in Fig. 15.11 (Heibel *et al*. 2005).

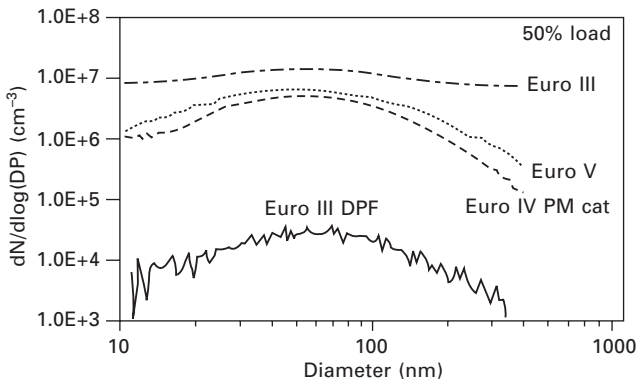
Regarding filtration efficiency and P# emissions, the two leading Euro IV and V HD concepts were compared to Euro III engines with and without

DPFs (Mayer *et al*. 2007). Figure 15.12 shows that the P# emission rates of the Euro IV PM Kat (open filter system) are similar to a Euro V SCR-equipped system without filters. DPFs emitted 99% fewer particles. Similar relationships were shown at lower load points, but at the 100% load point the Euro V engine (SCR) had higher P# emissions than the Euro III (no aftertreatment) or Euro IV engines, which had similar emission levels. The investigators also show that the P# emission rates are higher for the loaded open filters, inverse to that of DPFs, and NO_2 emissions are much higher than for the Euro V SCR system.

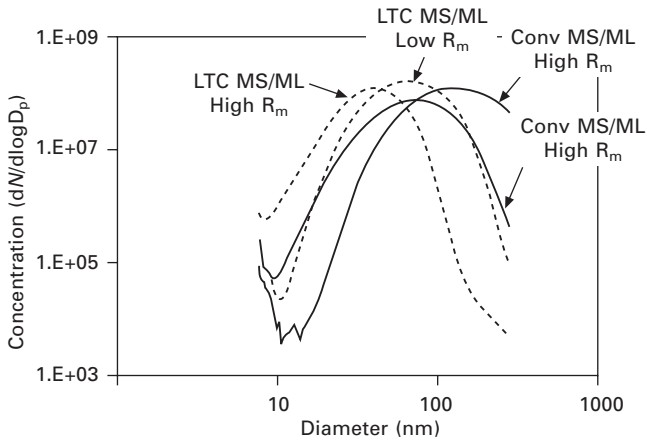
Finally, although a little off the subject of filter catalysts and materials, but still pertinent to P# efficiency, Foster (2007) showed that in two low-temperature combustion modes (LTC, 38º BTDC injection timing, 650 and 1160 bar rail pressure, 60% EGR), the ultrafine particulate emissions are still quite high. Figure 15.13 shows some results, wherein emission levels are similar in magnitude to conventional combustion in medium-speed and medium-load conditions. The results signal that even if low-temperature advanced combustion can be used over the whole engine map, DPFs might still be needed to hit emerging P# emissions standards.

On-board diagnostics (OBD) could emerge as a major issue going into 2013 when California fully phases in their requirements. If emissions exceed 1.5 times the standard, the OBD system needs to detect this. For heavy-duty applications, the OBD system must detect if a DPF has nominally <70% filtration efficiency.

There are a couple of studies worth highlighting concerning the performance of cracked filters. In a light-duty example, Zelenka (2007) showed that SiC filters with a typical ring-off crack, caused by a hot core and relatively cool outer region, lost only 5% P# filtration efficiency at full load, and was



15.12 Particle number emissions for a Euro V engine with SCR, a Euro IV engine with an open filter system, and a Euro III engine with no aftertreatment and with a DPF (Mayer *et al.*, 2007).



15.13 Ultrafine emissions when running in low-temperature combustion mode are similar in level when compared to emissions from conventional combustion (Foster 2007).

still filtering at 99% efficiency at half load, although without the crack the efficiency was 99.999%. PM emissions went from 1 mg/km to 2.5 mg/km, but this is still well under the 5 mg/km standard.

In an attempt to better quantify the effects of damage, Seiler *et al*. (2007) drilled holes in the filter and measured various parameters. Consistent with Zelenka, filtration efficiency showed only minor decreases for partially damaged filters, except in transient conditions (only 50% efficiency), but dropped to 30–50% efficiency for heavily damaged filters. Backpressure changes showed very little reliable and repeatable differences for partially damaged filters, but heavily damaged filters showed changed behavior. The researchers conclude that a PM sensor will likely be needed for OBD. In that regard, Hauser (2007) showed interesting results on a soot sensor. In the sensor, soot transfers charge from one plate to another, the rate of which correlates to soot concentration. In transient testing using a partially cracked filters, the sensor follows the particulate emission very well.

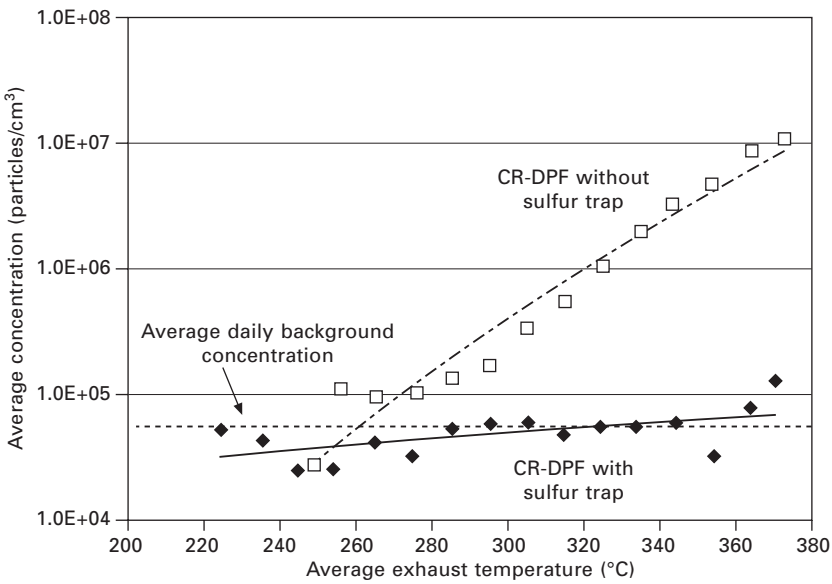
As filter technology evolves and expands, more attention is being paid to secondary emissions. In some European cities, ambient NO_2 levels are increasing despite reduced or constant NO_x levels. Much of this increase is attributed to the large numbers of light-duty diesels that utilize DOCs (Gense *et al*. 2006), but some evidence suggests that catalyzed filter systems are also contributors (Lambrecht *et al*. 2006). Indeed, by 2009 California will require that diesel retrofit systems emit no more than 25% of the NO_x as NO_2. In that regard, Goersmann *et al*. (2006) describe a new system that reduces more than 95% of the NO_2 emissions coming from catalyzed DPFs using a post-catalyst with small amounts of fuel injected to partially reduce the NO_2 back to NO.

Another secondary emission that is being discussed is aerosol nanoparticles. Epidemiological studies have correlated adverse health effects to particulate mass, and some physiological evidence suggests solid ultrafines can cause biological effects. In this regard, filter systems remove 90%+ of PM mass and 99.9%+ of carbon and other solid ultrafine particles. Under some circumstances, aerosol nanoparticles in the <30 nm size range can increase (Kittelson *et al*. 2006) coming from catalyzed filter systems, mainly under high-load conditions and/or low ambient temperatures. Although they are almost all sulfates, use of ultra-low sulfur fuel and low sulfur lube oil has only a minimal impact. However, when a sulfur trap is applied after the catalyzed DPF system (Sawant 2006), the aerosol ultrafine particles drop below ambient levels (Kittelson *et al*. 2006). Figure 15.14 shows some results.

15.5 Integrated NO_x/PM systems

The first integrated heavy-duty NO_x and PM systems are expected in 2009 in the Japan heavy-duty market, formally three months ahead of the US 2010 heavy-duty market.

It is greatly preferred to have the NO_x system after the filter system to allow as much passive NO_2-based regeneration of the filter as possible.



15.14 Sulfur-based aerosol ultrafine particulates can be generated in catalyzed filter systems. Sulfur traps reduce these emissions to below ambient levels (Kittelson *et al.*, 2006).

Using only active regenerations for the filter can result in up to a net 3% fuel penalty, depending on drive cycle. However, for chassis-certified medium-duty applications, fast light-off of the NO_x system is critical, so putting the NO_x system up front is being considered for those applications (Lambert 2006). For most heavy-duty applications, in which passive filter regenerations dominate and low fuel consumption is critical, NO_x systems go behind the filter.

Management of integrated NO_x/PM systems presents a unique set of challenges and synergies. For LNT-based systems, there are synergies, such as coordinating desulfation with active DPF regenerations, and utilizing the periodic rich LNT regenerations to burn soot on catalyzed DPFs that contain oxygen storage washcoats. For both SCR and LNT systems, the upstream DPF might provide NO_2 to facilitate the deNO_x reactions. On the liability side, active DPF regeneration could send hot gas into the NO_x system, raising durability concerns. Also, management of the fuel injection for DPF or LNT management and urea injection events is more difficult.

Moving into the future, we expect to see innovative component and system integration, with plenty of choice between engine, DOC, filter, and deNO_x options.

15.6 Future trends

As the industry moves forward with advanced combustion mixed-mode engines, cold-start hydrocarbon and CO emissions in advanced mode, and/or NO_x emissions in traditional combustion mode, will become very critical. Light-off should be at temperatures less than 175ºC. Further advancements are needed in the LNT + SCR systems, especially in the ammonia formation mechanisms on LNT materials when run in the rich mode. Zeolite SCR catalysts also need improvement in the low-temperature regimes, and better models are needed to understand ammonia storage dynamics. Low-temperature (less than 200ºC) urea decomposition is a limiting factor in many systems, and advanced hydrolysis catalysts might help. However, there is still the fundamental issue of ammonium nitrate condensation that blocks SCR catalyst performance at temperatures less than 200ºC. Lean NO_x catalysts, using fuel instead of ammonia for the SCR reaction, show promise for providing effective, low-cost NO_x reduction. Much more work is needed on these catalyst systems.

For PM control, limiting NO_2 emissions is critical, so modeling, better catalysts and management methods are needed. A better understanding of the catalyst–support–soot–gas interaction might lead to more effective DPF catalysts. Also, there is a glaring need for an OBD approach for PM. We will need to detect nominally 50–70% leakage of PM from a failed DPF system.

15.7 Sources of further information and advice

The Manufacturers of Emission Controls Association website (www.MECA.org) provides excellent primers on diesel emission control technologies. The website is also linked to sister trade associations throughout the world. A recent book by Majewski and Khair (2006) is very comprehensive and covers both diesel engine and aftertreatment technologies. Since 2000 Johnson (2007, 2008) has provided an annual review of key developments in the field of diesel emissions. He also compiled (Johnson 2007a) a collection of key papers on DPF technologies from 2001 through 2006. Regarding newsletters, W.A. Majewski at www.Dieselnet.com provides a monthly newsletter on regulatory and technology developments, and *Diesel Fuel News* (Peckham) provides frequent updates on general diesel fuel, engine, and emissions developments.

Finally, every year, hundreds of papers are presented by leaders in the industry at technical forums. The author recommends the annual Society of Automotive Engineers (SAE) Congress every spring in Detroit, the US Department of Energy Diesel Engine Emissions and Energy Reductions Conference (DEER) every summer, the Japan Society of Automotive Engineers (JSAE) annual conference in the spring, the Vienna Motorsymposium in the spring, the Aachen Colloquium in the fall, the SAE Fuels and Lubricants Conference in the spring, the Car Training Institute conferences throughout the year, and the SAE Commercial Vehicles Conference and the SAE Powertrain and Fluids Conference in the fall.

15.8 References

Birkhold, F., *et al*. (2006) 'Analysis of the injection of urea–water-solution for automotive SCR DeNO$_x$-systems: Modelling of two-phase flow and spray/wall interaction', SAE paper 2006-01-0643

Borretto, G., *et al*. (2004) 'Serial application of a catalyzed particulate filter on common rail DI diesel engines for passenger cars', F2004V068, FISITA 2004, Barcelona, Spain, June 2004

Calvo, S., *et al*. (2007) 'Possibilities of optimizing SCR systems through improved urea preparation', Car Training Institute SCR Forum, Karlsruhe, Germany, May 2007

Chatterjee, S., *et al*. (2004) 'Fuel property, emission test, and operability results from a fleet of class 6 vehicles operating on gas-to-liquid fuel and catalyzed diesel particle filters', SAE paper 2004-01-2959

Corning Incorporated press release, 27 April 2006.

Craig, A., *et al*. (2005) 'Performance aspects of cordierite diesel particulate filters in HD applications', SAE Commercial Vehicles Conference, Chicago, 1–3 November 2005

DaimlerChrysler press release, January 2006

Dreisbach, R. (2007) 'Emission reduction technologies for non-road engines', SAE Heavy Duty Diesel Symposium, Gothenburg, Sweden, September 2007

European Commission (2007), 'Proposal for a Regulation of the Parliament and of the Council on Type-Approval of Motor Vehicles and Engines with Respect to Emissions from Heavy Duty Vehicles (Euro VI) and on Access to Vehicle Repair and Maintenance Information', Brussels, 21 December 2007, COM (2007) 851 Final, 2007/0295 (COD)

Foster, D. (2007) SAE HDE Symposium, Gothenburg, Sweden, September 2007

Gense, R. *et al*. (2006) 'Direct NO_2 emissions from road transport: the current state of knowledge', Environment and Transportation Conference, Reims, France, 12–14 June 2006

Goersmann, C., *et al*. (2006) 'PM control systems with low NO_2 emissions', Dresden Conference 'Emission Control 2006', Technical University – Dresden, May 2006

Greening, P. (2007a) 'Euro VI and the connection to the World Harmonised Duty Cycle – WHDC', Integer Research Diesel Emissions Conference, Frankfurt, Germany, June 2007

Greening, P. (2007b) 'The challenge of emissions compliance – ACEA proposal for Euro VI', SAE Heavy Duty Diesel Symposium, Gothenburg, Sweden, September 2007

Gruenwald, J., *et al*. (2007) 'Design of compact AdBlue evaporation and homogenization zones', IAV MinNOx Conference, Berlin, February 2007

Hamada, I., *et al*. (2006) 'A preliminary evaluation of unregulated emissions during low temperature operation of a small diesel engine with a multi-function SCR catalyst', SAE paper 2006-01-0641

Hauser, G. (2007) 'Possibilities of a soot particle sensor', Car Training Institute DPF Forum, Frankfurt, Germany, July 2007

Heibel, A., *et al*. (2005) 'Performance and durability evaluation of the new Corning DuraTrap® AT diesel particulate filter – Results from engine bench and vehicle tests', Aachen Colloquium, Aachen, Germany, October 2005

Hinz, A., *et al*. (2005) 'NO_x-storage catalyst systems designed to comply with North American emission legislation for diesel passenger cars', SAE paper 2005-01-1084

Hu, H., *et al*. (2006) 'Advanced NO_x aftertreatment system and controls for on-highway heavy duty diesel engines', SAE paper 2006-01-3552

Jackson, M. (2006) 'Distributing urea for the on-road vehicle market', US Department of Energy Diesel Engine Efficiency and Emissions Reduction (DEER) Conference, Detroit, August 2006

Johansen, K., *et al*. (2007) 'Novel base metal–palladium catalytic diesel filter coating with NO_2 reducing properties', SAE paper 2007-01-1921

Johanssen, T. (2007) 'Ammonia storage and delivery systems for automotive SCR-DeNO_x', Car Training Institute SCR Forum, Karlsruhe, Germany, May 2007

Johnson, T.V. (2007, 2008) Annual SAE papers generally titled 'Diesel emissions in review'; latest paper numbers are 2007-01-0233, and 2008-01-0069, www.SAE.org

Johnson, T.V. (2007a) *Diesel Particulate Filter Technology*, Society of Automotive Engineers, Warrendale, PA

Johnson, T.V. (2007b) 'Diesel emission control in review', SAE paper 2007-01-0233

Kaiser, R. (2007) 'Chemical challenges in the development of urea–SCR systems', Car Training Institute SCR Forum, Karlsruhe, Germany, May 2007

Karkkainen, A., *et al*. (2006) 'Development and application of a US-EPA'07 particulate filter system for a 7.6l I-6 medium duty truck engine', Aachen Colloquium, Aachen, Germany, October 2006

Kittelson, D., *et al*. (2006) 'Driving down on-highway particulate emissions', SAE paper 2006-01-0916

Komada, K., *et al*. (2005) 'Development of DPF system for commercial vehicles: (second report) – Active regenerating function in various driving conditions', SAE paper 2005-01-3694

Konstandapolous, A.G., *et al*. (2007) 'Sustained soot oxidation in catalytically coated filters', SAE paper 2007-01-1950

Kowatari, T., *et al*. (2006) 'A study of a new aftertreatment system (1): A new dosing device for enhancing low temperature performance of urea-SCR', SAE paper 2006-01-0642

Kroecher, O. (2007a) 'Chemical challenges in the development of urea–SCR Systems', Car Training Institute SCR Forum, Karlsruhe, Germany, May 2007a

Kroecher, O. (2007b) 'New challenges for urea–SCR systems: from vanadia-based to zeolite-based SCR catalysts', IAV MinNOx conference, Berlin, February 2007b

Lambert, C. (2006) 'Urea SCR and DPF system for Tier 2 diesel light-duty trucks', US Department of Energy Diesel Engine Efficiency and Emissions Reduction (DEER) Conference, Detroit, August 2006

Lambrecht, U., *et al*. (2006) 'High NO_2-concentrations in urban areas of Germany – The influence of traffic emissions and atmospheric chemistry', Environment and Transportation Conference, Reims, France, 12–14 June 2006

Majewski, W.A. and Khair, M.K. (2006) *Diesel Emissions and Their Control*, SAE International, Warrendale, PA

Maurer, B. *et al*. (2006) 'ADS, an airless dosing system for AdBlue® – New dimension for SCR technology', Aachen Colloquium, Aachen, Germany, October 2006

Mayer, A., *et al*. (2007) 'Nanoparticle emission of EURO 4 and EURO 5 HDV compared to EURO 3 with and without DPF', SAE paper 2007-01-1112

Mizutani, T., *et al*. (2007) 'Filtration behavior of diesel particulate filters (2)', SAE paper 2007-01-0923

Mueller, W. (2004) 'SCR using solid urea', 3rd International Exhaust Gas and Particulate Emissions Forum, 2004

Muramatsu, T., *et al*. (2006) 'Development and application of a US-EPA'07 particulate filter system for a 7.6l I-6 medium duty truck engine', SAE paper 2006-01-0878

Nguyen, K., *et al*. (2007) 'Rapid aging of diesel lean NO_x traps by high-temperature thermal cycling', SAE paper 2007-01-0470

Nishimura, A. (2007) 'Construction equipment challenges', SAE Heavy Duty Diesel Symposium, Gothenburg, Sweden, September 2007

Ohara, E., *et al*. (2007) 'Filtration behavior of diesel particulate filters (1)', SAE paper 2007-01-0921

Ootake, M., *et al*. (2007) 'Development of diesel engine system with DPF for the European Market', SAE paper 2007-01-1061

Parche, M. (2005) 'Injection system and engine strategies for advanced emission standards', SAE Heavy Duty Diesel Symposium, Sweden, Gothenburg, September 2005

Parche, M. (2006) Integer Euro V and VI Global Diesel Emission Strategies Conference, Amsterdam, June 2006

Peckham, J., Executive Editor, *Diesel Fuel News*, Hart Energy Newsletters, HartEnergy.com

Pfeifer, M., *et al*. (2007) 'New platinum/palladium-based catalyzed filter technologies for future passenger car applications', SAE paper 2007-01-0234

Rohr, F. (2006) 'NO_x-storage catalyst systems designed to comply with North American emission legislation for diesel passenger cars", SAE paper 2006-01-1369

Sawant, A. (2006) 'Low ultra-fine PM emissions', South Coast Air Quality Management District Ultrafine Particulate Conference, Los Angeles, May 2006

Seiler, V, *et al*. (2007) 'Loading and regeneration behaviour of damaged diesel particulate filters', Car Training Institute DPF Forum, Frankfurt, Germany, July 2007

Signer, M. (2007) 'SCR systems for non-road applications derived from on-road technology', AVL International Commercial Powertrain Conference, Graz, Austria, May 2007

Sluder, C.S., *et al*. (2005) 'Low-temperature urea decomposition and SCR performance', SAE paper 2005-01-1858

Suzuki, K., *et al*. (2007) 'Study on low-temperature oxidation of diesel particulate matters by oxygen storage component for the catalyzed diesel', SAE paper 2007-01-1919

Walde, T., *et al*. (2007) 'Smart NO_x-sensor – Application in diesel systems', Car Training Institute Exhaust Systems Forum, Nuertingen, Germany, January 2007

Walker, A. (2005) 'Heavy-duty emissions control systems – 2010 and beyond', SAE HHD Emission Control Symposium, Gothenburg, Sweden, September 2005.

Weisgerber, V. (2007) 'Delphi NH_3 ammonia sensors', Car Training Institute Exhaust Systems Forum, Nuertingen, Germany, January 2007

Wu, M.-C. (2005) 'Experimental evaluation of reformate-assisted diesel NO_x trap desulfation', SAE paper 2005-01-3878

Zelenka, P. (2007) 'Diesel particulate filter application for EURO 4 – fleet test experiences with HMC/Kia vehicles', Car Training Institute DPF Forum, Frankfurt, Germany, July 2007

Zink, U., *et al*. (2005) 'State-of-the-art filter regeneration management – Concepts realized by LDV companies', US Department of Energy Diesel Engine Emissions Reduction (DEER) Conference, Chicago, August 2005

16

Optical diagnostics in diesel combustion engines

C. SCHULZ, University of Duisburg-Essen, Germany

Abstract: The development of diesel combustion engines depends to a large extent on the use of optical in-cylinder diagnostics. In the diesel process, spray formation, fuel evaporation, fluid flow, ignition chemistry and pollutant formation are coupled in a complicated way. The key challenge for optical diagnostics is to measure processes in the gas phase in the presence of liquid droplets that give rise to light scattering and potentially fluorescence signal that can be significantly stronger than the desired gas-phase signal. The dense sprays used in diesel injection trap and redistribute laser and signal light due to multiple scattering. Later in the combustion process soot is formed in high concentrations that again traps laser and signal light and gives rise to scattering. Strategies to cope with these issues will be reported in this chapter.

Key words: optical diagnostics, diesel combustion, liquid-spray diagnostics, vapour-phase fuel distribution, soot volume fraction laser-induced incandescence.

16.1 Introduction

Diesel combustion engines are of high interest because of their efficient energy conversion. They find an increasing market share especially due to the impressive development over the last decade. This development is based to a large extent on an improved fundamental understanding of the diesel combustion process that has been promoted by optical in-cylinder diagnostics. Conventional diesel combustion is stratified and lean, leading to low CO and HC emissions. NO and soot emissions, however, are of major concern and limiting engine-out emissions in order to prevent the installation of expensive and energy-consuming exhaust gas aftertreatment is of major concern. Moving towards HCCI (homogeneous charge compression ignition) is one of the potential future directions.

16.1.1 Main challenges for in-cylinder optical diagnostics in diesel engines

In the diesel process, spray formation, fuel evaporation, fluid flow, ignition chemistry and pollutant formation are coupled in a complicated way. Optical diagnostics, therefore, face a number of challenges.

In many situations of interest, diagnostics need to cope with multi-phase flows. The injection process with the presence of liquid fuel temporally and spatially overlaps with mixture preparation, ignition and combustion. The challenge is to measure processes in the gas phase in the presence of liquid droplets that give rise to light scattering and potentially a fluorescence signal that can be significantly stronger than the desired gas-phase signal. The dense sprays used in diesel injection trap laser and signal light and redistribute laser and signal light due to multiple scattering. Later in the combustion process soot is formed in high concentrations that again traps laser and signal light and gives rise to scattering. Some strategies to cope with these issues will be reported in this chapter.

High pressure complicates species-selective detection because of line broadening of spectral lines and hence overlapping of spectral features of various species. Additionally, the high density of molecules such as partially burned hydrocarbons and hot CO_2 and H_2O can contribute to the poor optical transmission properties, especially at short wavelengths. High peak pressures also require strong and bulky windows that can cause design problems when inserted into engines with geometries close to production-line engines.

Finally, the diesel combustion can lead to rapid window fouling. Frequent cleaning of the optical ports is therefore required, which limits the data acquisition rate. The advent of high-repetition-rate lasers and high-speed cameras reduces this problem, because now data can be gained within a much shorter time compared to the conventional phase-sampling measurements.

16.1.2 Typical experiments for diesel diagnostics

Despite these challenges a large number of optical diagnostics strategies have been developed and applied over the past years that contributed a lot to the understanding of diesel combustion. Extensive databases set up by different research groups have led to the development of conceptual models and have provided quantitative data for model development and validation.

Diesel-related diagnostics are typically carried out in a variety of experimental setups that are aiming at different aspects of the process. Because of the experimental effort, only a limited number of experiments have been performed in full, continuously running optical engines. Spray formation and the characteristics of injectors are commonly investigated in high-pressure cells. Experiments include the determination of spray angles and the observation of near-nozzle flow. More challenging, but also more realistic data are gained from high-temperature high-pressure cells with pre-combustion. The cell is filled with mixtures of either hydrogen or acetylene and oxygen and nitrogen. Adjusting the time-delay between pre-combustion and diesel injection allows modification of the injection temperature [1,2]. After each experiment the cell must be evacuated and filled with a new

gas mixture, which limits the repetition rate to a few experiments per hour. Alternatively, electrically heated pressurized flow cells have been set up [3,4], though typically they are limited in the temperature and pressure range that can be reached. By adjusting the initial oxygen concentration, reactive or non-reactive conditions are provided during fuel injection. Large windows at right angles that are not hit by the spray allow for a wide variety of diagnostics aiming at spray formation, gas-phase mixture formation, ignition chemistry and pollutant formation.

The ignition process in homogeneously mixed systems in contrast is typically observed in rapid-compression cells [5] or in shock tubes [6]. Here, the ignition delay time and the flame development is observed based on chemiluminescence detection.

The design of optical diesel engines is challenging because of high peak pressures and because of the complicated combustion chamber geometry. Concepts range from windows that replace valves in the cylinder head and limited-sized windows in the piston wall or the piston [7] to full quartz rings and piston windows that have a simplified geometry [8] or an ω-shaped piston bowl similar to the original production engine [9].

Recently, micro-optical laser-based probes using endoscope optics and fibres [10–12] and specific endoscopes [13] have been developed for in-cylinder investigation in IC engines. The further development of these tools might provide improved capabilities for measurements in diesel engines because they simplify the realization of optical access and – due to small diameters – potentially are much more robust and stand higher peak pressures. Further development is expected in the near future.

16.2 Liquid spray diagnostics

16.2.1 Geometrical shape of the spray

Qualitative images of the spatial distribution of sprays can be obtained in a comparably simple manner by Mie scattering. Droplets with diameters significantly larger than the light wavelength $\pi d/\lambda >> 1$ provide strong elastic scattering. Different arrangements with global illumination and with light-sheet illumination have been realized. Measurements include illumination and observation via endoscopes and high-speed imaging [14]. In-cylinder applications are often affected by background scattering, and dense sprays lead to secondary scattering of the laser light. Therefore, algorithms for the determination of the limit of the spray cloud, such as thresholding [15] and more elaborate statistical analysis [16–18] have been presented. This, however, does not influence the determination of geometrical parameters of sprays, such as spray cone angle and liquid tip penetration length, that has been applied in a large number of publications, including the investigation

of fuel jets impinging on surfaces (e.g. [19–22]). The interaction of sprays and the flow field inside the cylinder has been studied with particle image velocimetry, PIV [23].

Laser sheet illumination with a well-defined plane was used to investigate the primary spray break-up close to the nozzle. This allows for high spatial resolution of phenomena such as cavitation and dense core length [24]. Dense regions of the spray, however, cause problems because of laser attenuation and secondary scattering. Recently, ballistic imaging measurements have been presented for these regions that use extremely fast optical shutters and take advantage of the effect that multiply-scattered light reaches the detector later than light that is transmitted on a direct path [25].

16.2.2 Determination of droplet sizes

Droplet sizes have been measured by Phase Doppler Anemometry (PDA) in a crossed-beam setup that provides information not only about droplet sizes but also about velocity [26–28]. The technique relies on the observation of single spherical droplets in the overlap volume of the crossing beams and therefore fails in the dense break-up region of diesel infectors. The data are obtained at a single spot and individual droplets are measured with high repetition rates, It therefore providing droplet particle size distributions for single spots within the spray plume.

Images of droplet sizes and droplet distributions within small segments of the spray have been determined by interferometric Mie scattering where the individual droplets are imaged in a slightly defocused manner. Each droplet then is represented as a bright spot with fringes on top, and the number of fringes gives information about the droplet size [29]. In dense sprays line-of-sight averaged information about droplet sizes has been determined via multiple-laser attenuation [30].

Imaging of the particle-size distribution in cross-sectional areas of full sprays has been aimed at via simultaneous imaging of Mie scattering and laser-induced fluorescence of fluorescing components dissolved in the spray. Based on the zeroth order dependence of the scattering on the overall droplet surface and the fluorescence on the overall droplet volume the ratio of both signals allows the determination of local Sauter mean diameters [31, 32].

16.3 Vapour-phase fuel distribution

For the determination of fuel/air mixing in the gas phase (beyond the liquid jet) different techniques have been applied. Techniques based on fluorescence tracers are similar to those used in gasoline engines. Techniques for the observation of mixture formation are reviewed in [33] and tracer-based LIF

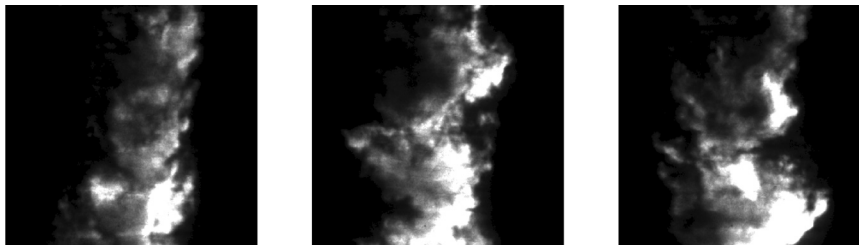
techniques are presented in [34]. The specific challenges that are connected to diesel applications are higher pressure and temperature levels compared to SI engines that can give rise to pre-ignition chemistry that leads to a variation in the chemical composition of the fuel, and hence tracers, in the pre-ignition phase. In the mixing phase, not only fuel concentration but also fuel/air ratio and temperature are of interest.

16.3.1 Fuel concentration measurements

Diesel fuel contains fluorescing components that can be used to quantitatively visualize the distribution of vaporized fuel [35, 36] via laser-induced fluorescence. In several applications, the use of non-fluorescing base fuels and the combination with well-characterized fluorescent tracers is established [34]. The ideal tracer has similar evaporation and transport properties to the parent fuel in order to avoid spatial separation during the fuel evaporation. Therefore, the applicability of tracers such as acetone, 3-pentanone and toluene that are frequently used for mixing diagnostics in gasoline engines is limited. Larger homologues with higher boiling points have been used instead. Recent applications of 5-nonanone, TMPD and α-methylnaphthalene (which is also a component of diesel substitute fuels) as fluorescent tracers have been reported [37, 38]. In all cases, the presence of droplets must be excluded for useful measurements.

Rayleigh scattering can be used as an alternative method for gas-phase measurements of the distribution of large molecular species (i.e. hydrocarbon fuels) in the presence of small molecules (e.g. air). Rayleigh scattering has been frequently used to measure gas density (and hence temperature) in homogeneously mixed systems where the effective cross-section for elastic scattering does not vary spatially [39]. It has also been used to measure relative temperature distributions in the post-flame gases in engines with simplified geometry [40]. Because of its linear dependence on number density and laser intensity, the interpretation of the signal is straightforward. As long as a single component dominates the effective Rayleigh cross-section in a mixing system, Rayleigh scattering allows to measure species number densities. Hydrocarbons have a much larger cross-section for elastic scattering than air. For *n*-decane a factor of $\sigma_{\text{ray, fuel}}/\sigma_{\text{ray, air}} = 120$ applies, which allows are to neglect the contribution of air. Therefore, the local fuel density can be determined from the scattering intensity as long as no background scattering off surfaces and particles is present. With this technique, fuel vapour density has been measured in internal combustion engines [4, 37, 41–43] and in the mixing field of atmospheric pressure natural gas flames [44]: see Fig. 16.1. The cross-sections for elastic scattering can be calculated based on data from [45–47] using dispersion relations from [48, 49].

Rayleigh scattering, however, can be strongly influenced by scattering



16.1 Fuel vapour concentration visualization by Rayleigh scattering (adapted from [37]).

of laser light off walls and particles. It is therefore necessary to assess the background level that results from these additional processes. Strategies to measure and subtract the background, referred to as 'laser flare' have been developed [43]. In environments with strong surface off surfaces or particles (i.e. small enclosed housings, presence of fuel droplets) the standard technique fails. Filtered Rayleigh scattering [50] has been demonstrated under these conditions. Here, a narrowband laser is used for excitation that overlaps with a narrow line filter. Only frequency-shifted signal (Doppler broadening due to the thermal velocity of the scattering molecules) is detected, while signal scattered from surfaces or droplets maintains the laser wavelength and is suppressed.

16.3.2 Fuel/air ratio measurements

The methods mentioned above yield fuel number densities. For the determination of the local equivalence ratio the total number density is required. It can be determined from the pressure once the local temperature is known. This, however, is not trivial in an inhomogeneous system. Approaches have been presented in which the required information was determined by a iterative procedure. The local fuel density is used to calculate the evaporative cooling and hence leads to a correction in signal interpretation. This has been applied to both Rayleigh [41, 51] and LIF-based measurements [52].

A direct measurement for fuel/air ratio can be provided from Raman measurements. As with Rayleigh scattering, the Raman scattering signal scales linearly with pressure. Therefore, despite its low cross-section reasonable signal can be determined for major gas-phase species in high-pressure diesel conditions. It provides multi-species information due to the species-specific frequency shift of the scattered light relative to the laser wavelength. The technique, however, requires high laser intensities and spectrally resolved detection. Demonstrations in engines are limited to 1-D line images [53, 54]. The scattering cross-sections strongly increase with decreasing laser wavelength. On the other hand, UV excitation can cause strong interference

from LIF. Some experiments therefore focused on the suppression of the LIF background by taking advantage of the polarized nature of Raman scattered light [55].

Organic molecules that are frequently used as fluorescent tracers show strong dependences on temperature and oxygen partial pressure. For a quantitative determination of fuel concentration these effects must be corrected for. These cross-sensitivities, however, have been suggested to be suitable for the simultaneous determination of fuel concentration *and* temperature or fuel/air ratio [34, 56]. Here, two signals are detected simultaneously (either using signals from two tracers or detecting the signal from a single tracer in different wavelength ranges). The first measurements for IC engine applications have been presented recently [57–59]. The extension to diesel engines is subject to ongoing research.

16.4 Two-phase flows

The fluorescence and scattering-based techniques mentioned above give signals from both the spray and the vapour phase. Because of the significantly higher density of the liquid, the overall signal is determined predominantly by the contribution from the liquid phase. Therefore, specific techniques have been developed for measurements in two-phase situations.

Laser-induced exciplex fluorescence (LIEF) is similar to tracer-based LIF described above. For LIEF, however, a combination of two tracers is used that form an excited complex in the liquid phase. After exciting one of the two tracers, the exciplex formation causes a loss in energy of the excited state and, thus, a red shift of the fluorescence. In the gas phase the exciplex cannot be formed. Therefore, signals from the gas phase and the liquid phase can be spectrally separated.

Melton [60] compared the fluorobenzene (FB)/triethylamine (TEA) exciplex system with the 4-fluorotoluene (4FT)/*n*-propyl-diethylamine (NPDEA) system in different solvents and recommended 10% TEA and 0.5% FB in *n*-hexane because of the good co-evaporation properties of this particular mixture. Ghandhi *et al*. [61] used 0.5% FB and 9% diethylmethylamine (DEMA) in *n*-hexane for imaging of injection processes. More suitable for the study of diesel sprays or the heavier components of gasoline is the system *N*,*N*,*N*′,*N*′-tetramethyl-*p*-phenylenediamine (TMPD)/naphthalene/ hexadecane that was used amongst other systems by Styron *et al*. [62].

The LIEF technique provides a pragmatic approach to measuring spray formation and evaporation by simultaneously mapping the spatial distribution of liquid and vapour [63, 64]. In the liquid phase, however, the exciplex is in temperature-dependent equilibrium with fluorescing monomers. Because of the much higher density of the liquid compared to the gas phase, even a small fraction of excited monomers in the gas liquid phase can generate a

significant interference for the gas-phase signal. Quantitative interpretation of LIEF measurements, therefore, remains a challenge. Recent approaches for multi-wavelength detection attack these problems by simultaneously measuring liquid-phase temperature [65].

The separation of elastically scattered light off droplets from Rayleigh scattering can be accomplished by filtered Rayleigh scattering mentioned above. Hence, fuel vapour density can also be measured in the presence of spray [50].

When observing sprays with back-illumination from lasers or incoherent light, the combined shadowgraphy/schlieren technique can be used to determine the penetration length and spray cone angles of liquid and gas-phase fuel [66]. While the attenuation of light due to scattering off the spray is strong enough to provide images of the liquid fuel, the gas-phase fuel and the resulting temperature inhomogeneities due to evaporative cooling cause local variations in refractive index that cause beam steering. When imaging the transmitted light with a suitable optical setup that cuts off the directly transmitted light with a knife edge in the optical path, the effect of beam steering becomes clearly visible and thus variations in refractive index. This is a convenient method for qualitative observation of the fuel vapour distribution [19] as long as good optical access to the combustion chamber (typically, parallel, high-quality windows) is available. In some cases measurements have been carried out with single windows in the cylinder head using the polished piston surface as mirror. The development of combustion can also clearly be seen in the images and is often determined along the vapour distribution [2].

16.5 Ignition and combustion

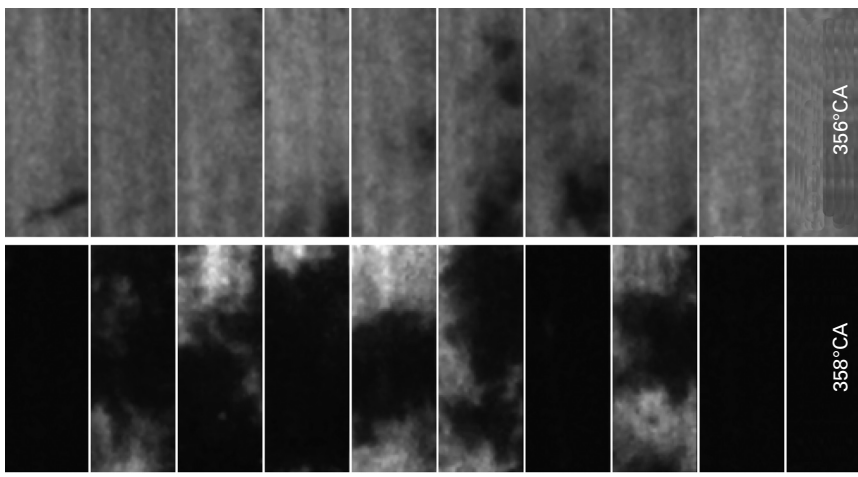
Ignition and combustion can be observed with different strategies. Typically, combustion processes give rise to chemiluminescence from species that are formed in an electronically excited state. This flame luminosity in the UV (OH*) and blue (CH*, C_2*) spectral range is comparatively weak. It appears in the second-stage ignition phase. In the preceding first-stage ignition (cool flame) even weaker emission is observed. In traditional diesel processes by far the strongest emission is caused by hot soot. All measurements of spontaneous emission give information that is integrated along the line of sight.

On the other hand, the occurrence of ignition is connected with the disappearance of fuel. The ignition kernel can therefore be observed in planar fuel images based on LIF or Rayleigh. Finally, in the cool flame period, high concentrations of intermediate, partially oxidized species, such as formaldehyde, CH_2O, are formed. These products can be visualized by LIF [67]. The laser-based measurements yield spatially, resolved information but might overlook the onset of combustion in case this process happens outside the plane illuminated by the laser beam.

16.5.1 Cool flame phase

During ignition delay prior to the onset of the hot combustion, high concentrations of formaldehyde are formed. This effect has been used for the investigation of engine knock in gasoline engines [68]. In auto-igniting engines it was observed that during the cool flame period fuel tracers like acetone or 3-pentanone disappear [69]. Observation of the onset of hot combustion based on tracer-LIF, therefore, was not possible [70]. It was shown, however, that formaldehyde is reaching high concentrations at the same time. CH_2O can be readily visualized with excitation with frequency-tripled Nd:YAG lasers. The high CH_2O concentration under these circumstances compensates for the comparably low absorption cross-section at this convenient laser wavelength of 355 nm. The CH_2O signal then suddenly disappears locally during the onset of the hot reaction phase [70]: see Fig. 16.2. This 'naturally generated tracer' is therefore a good choice to localize ignition sites. During the cool flame phase the base fuel disappears. Investigations of the occurrence of unburned hydrocarbons, therefore, have also chosen CH_2O as their target molecules because their disappearance is directly correlated to hot combustion. In the case of flame quenching, the respective signal remains locally and indicates the emission of incompletely burned fuel [71].

It must be noted that the same process that forms CH_2O in the pre-ignition phase is also responsible for the strong light attenuation at short wavelengths under these conditions. Spectrally resolved transmission measurements show strongly reduced light transmission around top dead centre [72] with fuels that exhibit strong cool-flame behaviour.



16.2 Distribution of CH_2O LIF in an HCCI engine (horizontal plane, 10 individual images for 356 and 348°CA. The dark areas show the region where second-stage ignition has started and thus removed CH_2O (adapted from [70]).

16.5.2 Second-stage ignition

Second-stage ignition can subsequently be determined from the disappearance of CH_2O and the formation of OH. The localization of reactive zones is often based on the determination of hydroxyl radicals by LIF imaging [73]. Simultaneous applications of OH and CH_2O LIF have shown the complementary distribution of both species in HCCI [74]. Similar measurements of these species along with additional data on unspecific, partially burned hydrocarbons that then give rise to soot formation give a more detailed insight into the different phases in diesel combustion and pollutant formation and allow one to improve conceptual models (see Plate VII [75] between pages 364 and 365).

Traditionally, the occurrence of soot luminosity was used as an indicator for the onset of the hot flame [9]. This strong signal enabled the detection of high-speed movies with conventional high-speed cameras. Recent measurements correlated the flame development to the fuel vapour distribution measured by tracer-LIF (see Plate VIII [38] between pages 364 and 365). With the development of non-sooting diesel combustion processes this technique fails. Modern intensified CMOS cameras, however, are sensitive enough to also detect UV chemiluminescence at high repetition rates [76]. OH* chemiluminescence has recently been applied to observe the effects of thermal stratification [77].

The simultaneous measurement of the distribution of OH LIF and soot (via laser-induced incandescence, LII) provided information about the soot burnout and its failure once the flame is quenched at the wall (see Plate IX [8] between pages 364 and 365).

16.6 Pollutant measurements

In diesel combustion the main challenge is to reduce the two main pollutants, NO_x and soot, at the same time. In-cylinder measurements of pollutant formation have significantly contributed to the fundamental understanding of the formation processes of these species.

16.6.1 Nitric oxide LIF measurements

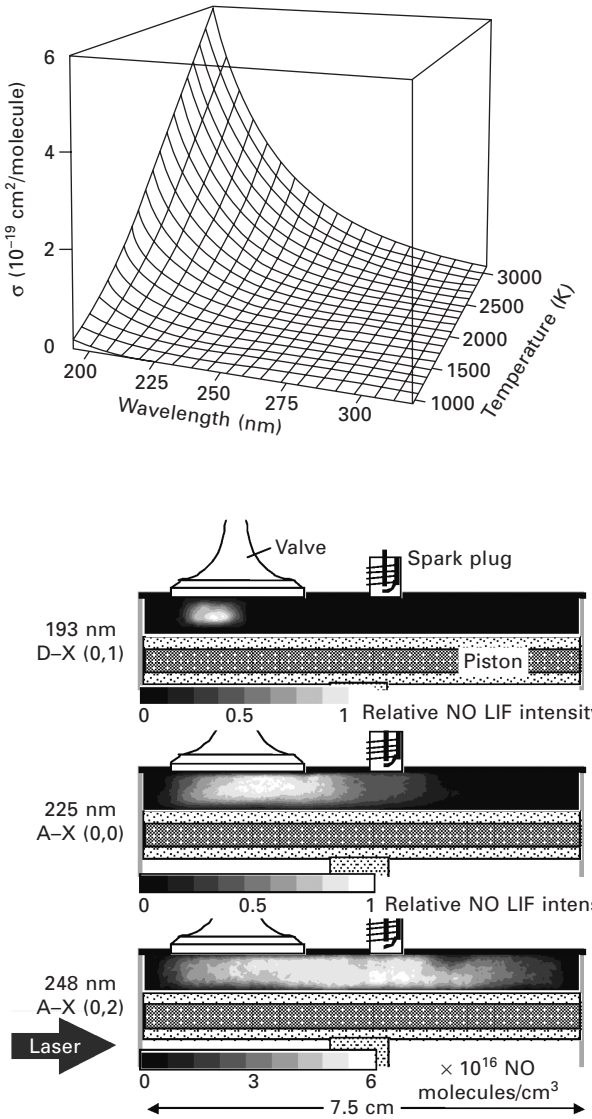
Quantitative measurements of nitric oxide in diesel combustion is a challenge. The signal is inherently weak and high pressure causes increasing levels of interference from other species, namely oxygen and partially burned fuel components. Studies in high-pressure flames have provided the background to choose appropriate detection strategies for the respective situations [78]. In lean mixtures at high temperature interference from O_2 LIF can cause difficulties. The relative signal intensity of NO and O_2 LIF shifts towards O_2 interference with increasing pressure because of strong collisional quenching of NO LIF.

NO LIF requires short UV wavelengths for excitation and detection. Light attenuation in hot combustion gases, however, increases strongly with increasing temperature, increasing pressure and decreasing pressure. Figure 16.3 shows the effect of the strong wavelength dependence of the transmission of laser light in hot combustion gases on NO–LIF diagnostics. In the relevant wavelength range hot CO_2 is a main contributor to light attenuation [79,80]. For H_2O a similar behaviour can be found at short wavelengths. It is, however, negligible at $\lambda > 230$ nm [80]. These effects show that both signal and laser light will be significantly attenuated in engine applications. The wavelength dependence of the attenuation has been measured *in situ* when exciting nearby oxygen lines. O_2 LIF shows a large number of fluorescence emissions that are emitted with known relative intensities. When measuring the actual signal intensity a wavelength-dependent transmission can be determined for the gases in between the measurement region and the detector [81].

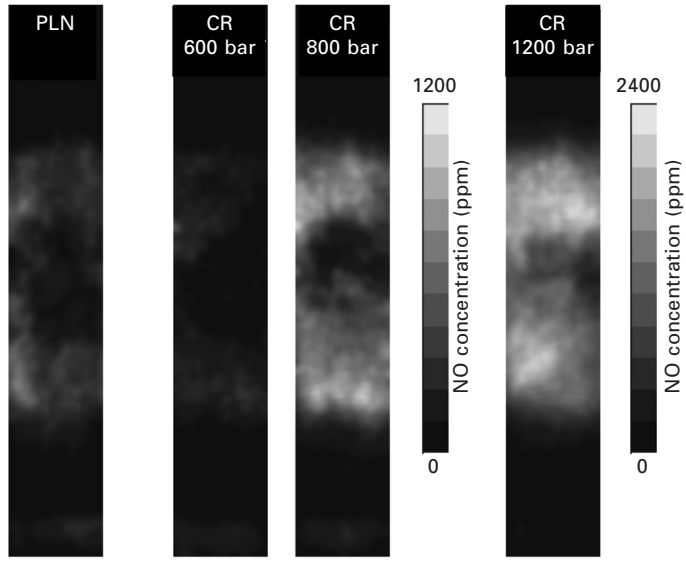
Two-dimensional imaging of NO formation yielded important input about the location of NO formation in diesel combustion. Measurements by Dec and Canaan showed that NO is formed mainly at the periphery of the rich premixed fuel/air cloud, i.e. at the lean side of a supposed diffusion flame [82]. After this initial step NO continuous to be formed in the lean hot post-combustion gases. Dec used laser excitation at 226.035 nm with subsequent LIF signal collection at 237–276 nm. A similar approach was taken by Verbiezen *et al.* who also measured the local laser light intensity variation by measuring the N_2 Raman signal [83]. Schulz and Colleagues used NO excitation in the A-X (0,2) band with a tunable KrF excimer laser at 247.94 nm to reduce laser beam attenuation and subsequent detection of the fluorescence light emitted from the A-X (0,1) transition around 237 nm. This technique allows the effective suppression of interfering LIF signals due to hot O_2 and CO_2 and partially burned hydrocarbons [84–86]. Therefore, selective detection of NO is possible even in inhomogeneous combustion environments such as in direct injecting gasoline [87,88] and diesel engines operated with commercial fuel [89]. Furthermore, with this scheme the influence of laser beam attenuation is minimized [79,90] (*cf.* Fig. 16.4). Based on a calibration, measurements in standard flames as well as spectral simulations (LIFSim [91]) enabled the quantitative determination of NO concentrations [89].

16.6.2 Soot particle size measurements by TiRe-LII

Soot formation has been a major issue in combustion research as soot is emitted by many practical combustion processes. Soot is the result of incomplete combustion of hydrocarbons. Transmission electron microscopy (TEM) shows that flame-generated soot consists of primary particles which have a typical size between 5 and 100 nm. Primary particles form fractal aggregates with up to several hundred primary particles.



16.3 Left: wavelength- and temperature dependence of the absorption cross-section of CO_2. Right: effect of the attenuation of laser light at different wavelengths on NO imaging with 193, 225 and 248 nm excitation. All three frames show measurements from an engine under identical operating conditions. Only with the longest wavelength (248 nm) was the expected symmetrical distribution of NO in the cylinder observed (propane/air flame, ϕ = 1, p = 13 bar) (adapted from [40,79]).



16.4 Quantitative NO–LIF measurements in a heavy-duty diesel engine operated with commercial fuel for different injection systems (adapted from [89]).

Laser-induced incandescence (LII) was observed for the first time by Weeks and Duley in 1973 when they heated aerosols of carbon black and alumina with a CO_2 laser [92]. They set up the first energy balance describing the heating and cooling of particles and suggested that the method could be used for particle sizing. In 1984 Melton set up the first detailed energy and mass balance for LII and suggested using LII as a tool for quantitative measurements of soot volume fractions [93]. Since the early 1990s LII has been used successfully in a variety of systems for measuring volume fractions of soot in laminar diffusion flames [94–98], laminar premixed flames [99–102] and turbulent flames [94,103–105]. Particle sizes have been deduced from the temporal behaviour of the LII signal, taking the ratio of the LII signal at two different delay times after the signal peak [106,107] as well as using the entire decay curve in point measurements [101,108–111]. In exhaust gases particle sizes have been measured with LII as well [112,113]. Particle sizes were obtained assuming mono-disperse particles [101,109,110] as well as considering a poly-disperse log-normal particle-size distribution [108,111]. The status on LII measurements and modelling has been published in recent reviews [114,115]. A web-based tool for calculating the LII signal decay, LIISim, for various conditions and model assumptions has been developed [116].

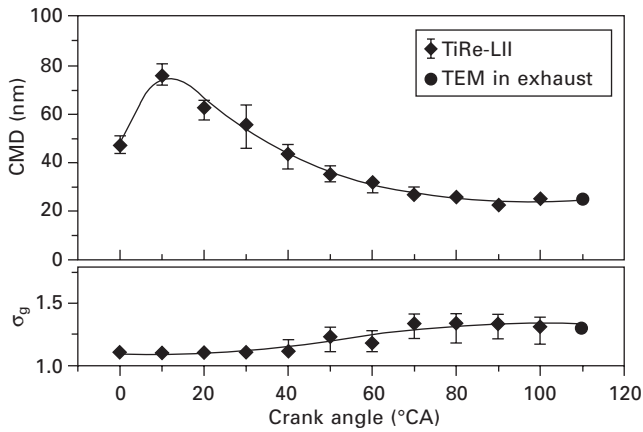
In-cylinder measurements of time-resolved LII for soot particle size measurements have been presented for a diesel engine with 1064 nm excitation.

A two-wavelength time-resolved detection enables a pyrometric determination of the particle heat-up temperature, thus avoiding the need for calculating the particle temperature based on the not well-known absorption properties of soot. Figure 16.5 shows the result of in-cylinder particle-size measurements in a two-stroke diesel engine [117]. An application to measurements in a heavy-duty diesel engine is reported by Bougie *et al*. [118].

16.7 Soot volume fraction laser-induced incandescence (LII)

Soot volume fractions measured with LII are based on the detection of the time-integrated LII signal within a certain detection wavelength range. When expanding the laser beam into a sheet, 2-D images of the soot volume fraction distribution can be obtained. The choice of the temporal detection gate influences the signal. In the initial phase after the laser heat-up smaller particles cool faster than large ones. If long or even delayed (relative to the laser pulse) detection gates are used, the integrated signal will underestimate small particles [94,119]. This effect is amplified at high pressure because with increasing pressure the LII signal decays faster due to increased heat conduction [120]. Hence, short and prompt, i.e. with the start of the laser pulse, detection gates of 50 ns or less should be used.

To obtain absolute soot volume fractions LII signals must be calibrated. Therefore, the accuracy of the measurement is strongly influenced by the accuracy of the calibration method. A common method is the use of light extinction. However, this technique depends on the knowledge of the



16.5 Soot particle size (count median diameter, CMD) and width of the particle-size distribution σ_g from in-cylinder TiRe-LII measurements in a diesel engine (adapted from [117]).

refractive index of soot, for which different values have been reported for this value [121]. A method that is independent of an external calibration is the calibration with absolute light intensity [122].

Spatially resolved measurements of soot distribution have helped researchers to understand the mechanism of soot formation in diesel combustion [123] and have, thus, helped them to develop conceptual models [124]. The simultaneous imaging of soot and OH yielded information about soot burnout (see Plate IX [8] between pages 364 and 365) and showed mainly that soot is left over when the flame extinguishes under dilute conditions or when the flame is quenched at surfaces. Other research groups have used LII imaging to study the influence of injection pressure and timing [20] as well as the influence of pre-injection and nozzle geometry [37] (see Plate X between pages 364 and 365). Quantitative data were used for the validation of soot formation simulations [4].

16.8 Temperature

Temperature is a crucial parameter for many combustion-relevant processes such as fuel evaporation, ignition and flame development. Therefore, despite the complexity of measuring temperature accurately, a large number of diagnostics approaches have been developed for combustion applications. Few, however, have been successfully applied to in-cylinder measurements in diesel engines so far.

16.8.1 Soot pyrometry

Sooting flames exhibit strong light emission because of the high temperature of the solid particles. The thermal emission follows the Planck law. Therefore both the total emission and the spectral distribution of the emitted light are a function of temperature. Once the assumption is justified that the radiating material does not exhibit additional wavelength-dependencies (i.e. the material can be assumed to be a black or grey body), temperature can be determined from an (at least) two-wavelength measurement of the radiation intensity. A review article by Zhao and Ladommatos is devoted to this topic [125]. The method has been applied to high-speed imaging measurements, originally based on an analysis of colour film from high-speed cameras (see Plate XI [9] between pages 364 and 365) and more recently with high-speed CMOS and CCD cameras. Correlations of the pyrometry temperature and the exhaust gas composition, especially the thermal NO_x formation, have been investigated [9]. Endoscopic measurements have been demonstrated [126]. Two-colour pyrometry measurements yield information not only about temperature but also on soot density [125, 127].

Pyrometry measurements, however, must be interpreted with care. As with all emission measurements in a strongly absorbing environment, it is not

obvious from which volume the signal originates. It shifts from the centre of the combustion event as long as the transmission of the environment is good (i.e. low soot concentration or soot confined to a small area) to the surface of the soot cloud once the center of the spray is obscured by soot. Because of the strong increase in total emission with temperature in an environment with variable temperature, the high-temperature regions dominate the total signal, and peak temperatures are determined rather than average temperatures. Additionally, temperature effects in the non- or low-sooting zone are overlooked. Finally, in an oxidizing soot cloud there are some concerns whether soot particles are in thermal equilibrium with the gas phase. Because of the relative simplicity of the technique, despite its limitations it is frequently used and can be considered a standard technique. The development of modern non-sooting diesel processes, however, limits its future applicability.

16.8.2 LIF thermometry

Measuring temperature in diesel engines via laser-based methods is not yet well established because of a number of challenges that arise from the high-pressure, comparably 'dirty' conditions in diesel combustion. The techniques, however, have the potential to provide two-dimensional images and thus provide temperature data with a specific spatial resolution. With small molecules like OH or NO, thermometry typically uses the rotational line structure to address specific quantum states [128]. Line broadening at high pressure, however, complicates selective excitation of well-defined isolated lines. Furthermore, high pressures often cause low fluorescence intensities due to collisional quenching which then give rise to poor signal-to-noise ratios when calculating temperature from a ratio of two individual measurements. Background signal from elastic scattering or interfering fluorescence also causes problems for conventional two-line temperature measurements. In these cases, a third measurement that addresses the background level that is then subtracted from the two other measurements before determining the temperature from the signal ratio might be required. Excitation-wavelength-scanning techniques have been presented that are robust against the previously mentioned effects because they take advantage of the spectral structure rather then the absolute intensity. They, however, are not instantaneous. They have been demonstrated in stationary high-pressure flames and sooting flames [129] as well as for the observation of evaporative cooling in non-stationary sprays when applying phase sampling [130]. First measurements of gas-phase temperature based on atomic LIF have been demonstrated in sooting flames [131].

Alternative strategies use the fluorescence properties of organic molecules to determine temperature. Because of the high density of quantum states in these

larger molecules, broad features with little structure are observed in absorption and emission spectra. While not giving access to isolated individual transition, these features can exhibit significant shifts as a function of temperature that can be used for measuring temperature via ratioing methods. For the gas phase this has been applied to SI engines only. Applications of 3-pentanone [57] and toluene [58] have been demonstrated for the mixing phase prior to ignition. Liquid-phase temperature measurements have been demonstrated using exciplex fluorescence [65,132], organic dyes like rhodamine B [133,134] and added solid micro particles from thermographic phosphors [135].

A general problem for LIF-based thermometry is that temperature is determined from the ratio of two signals that typically arises from two-wavelength excitation. Beam steering due to local variations in density as well as laser and signal attenuation can strongly influence the ratio of local signal intensities. In case of two-wavelength detection with excitation with a single laser, which is possible with some organic tracer molecules that can be applied for the unburned mixture, this effect is reduced. The advantage of ratioing, however, is that the measurement is independent of the spatial distribution of the fluorescing species as long as its concentration exceeds a certain minimum concentration within the field of interest to provide sufficient signal.

Coherent anti-Stokes Raman scattering in principle provides the highest accuracy for temperature measurements in combustion systems. It provides point measurements only. Only a few measurements in a diesel-relevant context have been reported. Recent measurements on evaporative cooling of the gas phase in sprays showed promising results [136].

16.8.3 Absorption

Light attenuation in diesel combustion is a challenge for many diagnostics approaches. It has been observed that the attenuation strongly increases in the UV towards short wavelengths in the burned gases at high temperature. This effect has been attributed to absorption by hot CO_2 (*cf.* Fig. 16.3). Quantifying this wavelength-dependent light attenuation is crucial for diagnostics that apply wavelengths in the 200–300 nm range such as NO LIF. Measurements in optical engines with broadband illumination with D_2 lamps have been used for fundamental studies. Additional measurements have been carried out using O_2 LIF as probe light generated in the same volume as the (originally) desired NO LIF signal [81,83,89]. From a spectrally resolved detection the wavelength-dependent light transmission can then be determined. It has been demonstrated that this information can be used to determine gas-phase temperatures [79] based on the known absorption cross-sections for hot CO_2 [80].

16.9 Future trends

Future diagnostics trends in diesel engines will need to adjust to the change of combustion strategies. While avoiding soot over an increasing part of the operating range is disadvantageous for conventional soot-based pyrometric temperature measurements, a 'cleaner' diesel combustion provides several new opportunities for laser-based techniques that so far have been applied mainly to spark-ignition engines.

The recent development of multi-species measurements, either simultaneously or under identical conditions [4, 37, 67, 75, 137], will provide further insight into the details of the underlying processes. A new challenge will be the determination of the local gas composition with the increasing importance of exhaust gas recirculation. Strategies for tracing the burned gases have been published, e.g. using SO_2 generated from sulfur-containing precursors [138]. The cleaner conditions in modern diesel engines provide opportunities to determine additional species. Recent measurements provide information about CO and unburned hydrocarbons using UV light for two-photon excitation of CO and spectrally resolved detection of the signal [139].

In order to provide optical access to the cylinder of near-production engines, new micro-optical devices are currently being developed. For point measurements approaches based on absorption and fluorescence have been presented. In most cases these devices have been implemented into spark plugs for application in SI engines [140–142], but there is no principal reason for not applying similar concepts to diesel engines. For laser light-sheet-based imaging applications, 10-mm-diameter endoscopes for light-sheet generation and signal imaging have been developed. They significantly facilitate optical access to engines that are close to production. Furthermore, the small diameter of the optics alleviates restrictions in engine speed and load that currently occur with large-scale windows and reduces the influence on the thermal management. High optical throughput and good imaging quality have been reached by specifically designing hybrid optical elements to the geometrical needs for IC engine diagnostics that combine refractive and diffractive optical elements [13].

16.10 Conclusions

The application of optical diagnostics to diesel engines is challenging. Many techniques that are routinely applied in combustion diagnostics need specific adjustments to diesel conditions. Nevertheless, laser-based diagnostics have contributed a tremendous amount of information to the understanding of diesel combustion. The rapid development of diesel engines over the last years would not have been possible without detailed diagnostics of individual processes in generic high-pressure combustion cells and in optical

engines. With the current development of diesel combustion towards non-sooting low-temperature combustion, the diagnostics need to adjust to the new requirements. Cleaner combustion processes, however, provide better conditions for diagnostics. Therefore, significant further developments of diagnostics capabilities in diesel engines are expected for the future.

16.11 References

1. G. Bruneaux, 'A study of mixture formation in direct injection diesel-like conditions using quantitative fuel concentration visualizations in a gaseous fuel jet', SAE paper 2002-01-1632 (2002).
2. D. Verhoeven, J. L. Vanhemelryck, and T. Baritaud, 'Macroscopic and ignition characteristic of high-pressure sprays of single-component fuels', SAE paper 981069 (1998).
3. E. Scheid, F. Pischinger, K. Knoche, H.-J. Daams, E. P. Hassel, and U. Reuter, 'Spray combustion chamber with optical access, ignition zone visualization and first Raman measurements of local air–fuel ratio', SAE paper 861121 (1986).
4. S. Vogel, C. Hasse, J. Gronki, S. Andersson, N. Peters, J. Wolfrum, and C. Schulz, 'Numerical simulation and laser-based imaging of mixture formation, ignition and soot formation in a diesel spray', *Proc. Combust. Inst.* **30**, 2029–2036 (2005).
5. R. Minetti, M. Carlier, M. Ribaucour, E. Therssen, and L. R. Sochet, 'A rapid compression machine investigation of oxidation and auto-ignition of *n*-heptane: measurements and modelling', *Combust. Flame* **102**, 298–309 (1995).
6. J. Herzler, M. Fikri, K. Hitzbleck, C. Schulz, P. Roth, and G. T. Kalghatgi, 'Shock-tube study of the ignition of *n*-heptane/toluene/air mixtures at intermediate temperatures and high pressures', *Combust. Flame* **149**, 25–31 (2007).
7. G. G. M. Stoffels, E.-J. van den Boom, C. M. I. Spaanjaars, N. Dam, W. L. Meerts, J. J. ter Meulen, J. L. C. Duff, and D. J. Rickeard, 'In-cylinder measurements of NO formation in a diesel engine', SAE paper 1999-01-1487 (1999).
8. J. E. Dec and D. R. Tree, 'Diffusion-flame/wall interactions in a heavy-duty DI Diesel Engine', SAE paper 2001-01-1295 (2001).
9. V. Schwarz, G. König, P. Dittrich, and K. Binder, 'Analysis of mixture formation, combustion and pollutant formation in HD diesel engines using modern optical diagnostics and numerical simulation', SAE paper 1999-01-3647 (1999).
10. M. J. Hall, P. Zuzek, and R. W. Anderson, 'Fiber optic sensor for crank angle resolved measurements of burned gas residual fraction in the cylinder of an SI engine', SAE paper 2001-01-1921 (2001).
11. R. Reichle, C. Pruss, W. Osten, H. J. Tiziani, F. Zimmermann, and C. Schulz, 'Acquisition of combustion parameters close to the ignition spark with a fiber optic sensor', in *Optical Measurement Systems for Industrial Inspection IV, Volume 5856* (W. Osten, C. Gorecki, and E.L. Novak, editors), SPIE – The International Society for Optical Engineering, 2005, p. 158–168.
12. M. Richter, B. Axelsson, and M. Aldén, 'Engine diagnostics using laser-induced fluorescence signals collected through an endoscopic detection system', SAE paper 982465 (1998).
13. R. Reichle, C. Pruss, W. Osten, H. Tiziani, F. Zimmermann, and C. Schulz, 'Hybrid excitation and imaging optics for minimal invasive multiple-band UV-LIF-measurements in engines', in *VDI-Berichte 1959,* 223–235 (2006).

14. T. D. Fansler and M. C. Drake, 'Designer diagnostics" for developing direct-injection gasoline engines', *J. Phys: Conf. Series* **45**, 1–17 (2006).
15. R. E. Canaan, J. E. Dec, R. M. Green, and D. T. Daly, 'The influence of fuel volatility on the liquid-phase fuel penetration in a heavy-duty DI Diesel engine', SAE paper 980510 (1998).
16. J. Seneschal, B. Maurin, J. C. Champoussin, and C. Ducottet, 'A fully automatic system for the morphology characterization of high-pressure diesel sprays', SAE paper 2004-01-0025 (2004).
17. J. V. Pastor, J. Arrègle, and A. Palomares, 'Diesel spray image segmentation with a likelihood ratio test', *Appl. Opt.* **40**, 2876–2885 (2001).
18. F. Payri, J. V. Pastor, A. Palomares, and J. E. Juliá, 'Optimal feature extraction for segmentation of diesel spray images', *Appl. Opt.* **43**, 2102–2111 (2004).
19. B. Higgins, D. Siebers, C. Mueller, and A. Aradi, 'Effects of an ignition-enhancing diesel-fuel additive on diesel-spray evaporation, mixing, ignition and combustion', *Proc. Combust. Inst.* **27**, 1873–1880 (1998).
20. G. Bruneaux, D. Verhoeven, and T. Baritaud, 'High-pressure diesel spray and combustion visualization in a transparent model diesel engine', SAE paper 1999-01-3648 (1999).
21. K.-U. Münch and A. Leipertz, 'Investigation of spray penetration and fuel distribution inside the piston bowl of a 1.9l ID diesel engine using 2D Mie scattering', SAE paper 922204 (1992).
22. S. W. Park and C. S. Lee, 'Macroscopic and microscopic characteristics of a fuel spray impinged on the wall', *Exp. Fluids* **37**, 745–762 (2004).
23. P. C. Miles, L. Hildingsson, and A. Hultqvist, 'The influence of fuel injection and heat release on bulk flow structures in a direct-injection, swirl-supported diesel engine', *Exp. Fluids* **43**, 273–283 (2007).
24. C. Heimgärtner and A. Leipertz, 'Investigation of the primary spray breakup close to the nozzle of common-rail high pressure diesel injection system', SAE paper 2000-01-1799 (2000).
25. M. A. Linne, M. Paciaroni, T. Hall, and T. Parker, 'Ballistic imaging of the near field in a diesel spray', *Exp. Fluids* **40**, 836–846 (2006).
26. F. Durst, A. Melling, and J. H. Whitelaw, *Principles and Practice of Laser Doppler Anemometry*, 2nd edn, Academic Press, London, 1981.
27. L. Araneo and C. Tropea, "Improving phase Doppler measurements in a diesel spray', SAE paper 2000-01-2047 (2000).
28. Y. Hardalupas, A. M. K. P. Taylor, and J. H. Whitelaw, 'Characteristics of the spray from a diesel injector', *Int. J. Multiphase Flow* **18**, 159–179 (1992).
29. C. Mounaïm-Rousselle and O. Pajot, 'Droplet sizing by Mie scattering interferometry in a spark ignition engine', *Particle & Particle Systems Characterization* **16**, 160–168 (1999).
30. A. Violi, A. D'Anna, A. D'Alessio, M. Astarita, and B. M. Vaglieco, 'Experimental and modeling study of particulate formation in high-pressure diesel-like conditions', *Proc. Combust. Inst.* **28**, 1241–1247 (2000).
31. I. Düwel, T. Kunzelmann, J. Schorr, C. Schulz, and J. Wolfrum, 'Application of fuel tracers with different volatilities for planar LIF/Mie drop sizing in evaporating systems', in ICLASS-Europe, paper 9-3, Sorrento, 2003.
32. M. C. Jermy and D. Greenhalgh, 'Planar dropsizing by elastic and fluorescence scattering in sprays too dense for phase Doppler measurement', *Appl. Phys. B* **71**, 703–710 (2000).

33. H. Zhao and N. Ladommatos, 'Optical diagnostics for in-cylinder mixture formation measurements in IC engines', *Prog. Energy Combust. Sci.* **24**, 297–336 (1998).
34. C. Schulz and V. Sick, 'Tracer-LIF diagnostics: Quantitative measurement of fuel concentration, temperature and air/fuel ratio in practical combustion situations', *Prog. Energy Combus. Sci.* **31**, 75–121 (2005).
35. A. Arnold, F. Dinkelacker, T. Heitzmann, P. Monkhouse, M. Schäfer, V. Sick, J. Wolfrum, W. Hentschel, and K.-P. Schindler, 'DI diesel engine combustion visualized by combined laser techniques', *Proc. Combust. Inst.* **24**, 1605–1612 (1992).
36. J. V. Pastor, J. J. López, and J. E. Juliá, 'Planar laser-induced fluorescence fuel concentration measurements in isothermal diesel sprays', *Optics Express* **10**, 309–323 (2002).
37. C. Schulz, J. Gronki, and S. Andersson, 'Multi-species laser-based imaging measurements in a diesel spray', SAE paper 2004-01-1917 (2004).
38. G. Bruneaux, 'Study of the correlation between mixing and auto-ignition processes in high-pressure diesel jets', SAE paper 2007-01-0650 (2007).
39. R. W. Dibble and R. E. Hollenbach, 'Laser Rayleigh thermometry in turbulent flames', *Proc. Combust. Inst.* **18**, 1489–1499 (1981).
40. C. Schulz, V. Sick, J. Wolfrum, V. Drewes, M. Zahn, and R. Maly, 'Quantitative 2D single-shot imaging of NO concentrations and temperatures in a transparent SI engine', *Proc. Combust. Inst.* **26**, 2597–2604 (1996).
41. C. Espey, J. E. Dec, T. A. Litzinger, and D. A. Santavicca, 'Planar laser Rayleigh scattering for quantitative vapor-fuel imaging in a diesel jet', *Combust. Flame* **109**, 65–86 (1997).
42. Ö. Andersson, R. Collin, M. Aldén, and R. Egnell, 'Quantitative imaging of equivalence ratios in DME sprays using a chemically preheated combustion vessel', SAE Paper 2000-01-2785 (2000).
43. C. A. Idicheria and L. M. Pickett, 'Quantitative mixing measurements in a vaporizing diesel spray by Rayleigh imaging', SAE paper 2007-01-0647 (2007).
44. T. Landenfeld, A. Kremer, E. P. Hassel, J. Janicka, T. Schäfer, J. Kazenwadel, C. Schulz, and J. Wolfrum, 'Laser diagnostic and numerical studies of strongly swirling natural-gas flames', *Proc. Combust. Inst.* **27**, 1023–1030 (1998).
45. A. I. Vogel, 'Physical properties and chemical constitution of aliphatic hydrocarbons', *J. Chem. Soc.* **9**, 133–142 (1946).
46. R. C. Weast, *Handbook of Chemistry and Physics*, 54th edn, CRC Press, Cleveland, OH, 1973.
47. Landolt-Börnstein, *Eigenschaften der Materie in ihren Aggregatzuständen*, Tabellen, Springer-Verlag, Berlin, 1962.
48. J. R. Partington, *An Advanced Treatise on Physical Chemistry*, Vol. 9, Longmans, Green, London, 1953.
49. W. C. Gardiner, Y. Hidaka, and T. Tanzawa, 'Refractivity of combustion gases', *Combust. Flame* **40**, 213–219 (1981).
50. D. Hoffman, K.-U. Münch, and A. Leipertz, 'Two-dimensional temperature determination in sooting flames by filtered Rayleigh scattering', *Opt. Lett.* **21**, 525–527 (1996).
51. C. Espey, J. E. Dec, T. A. Litzinger, and D. A. Santavicca, 'Quantitative 2D fuel vapor concentration imaging in a firing diesel engine using planar laser-induced Rayleigh scattering', SAE paper 940682 (1994).
52. W. Hwang, J. E. Dec, and M. Sjöberg, 'Fuel stratification for low-load HCCI

combustion: Performance and fuel-PLIF measurements', SAE paper 2007-01-4130 (2007).
53. J. Egermann, M. Taschek, and A. Leipertz, 'Spray/wall interaction influences on the diesel engine mixture formation process investigated by spontaneous Raman scattering', *Proc. Combust. Inst.* **29**, 617–623 (2002).
54. G. Grünefeld, V. Beushausen, P. Andresen, and W. Hentschel, 'Spatially resolved Raman scattering for multi-species and temperature analysis in technically applied combustion systems: Spray flame and four-cylinder in-line engine', *Appl. Phys. B.* **58**, 333-342 (1994).
55. F. Rabenstein, J. Egermann, A. Leipertz, and N. d'Alfonso, 'Vapor-phase structures of diesel-type fuel sprays: An experimental analysis', SAE paper 982543 (1998).
56. W. Koban and C. Schulz, 'Toluene as a tracer for fuel, temperature and oxygen concentrations', SAE paper 2005-01-2091 (2005).
57. S. Einecke, C. Schulz, and V. Sick, 'Measurement of temperature, fuel concentration and equivalence ratio fields using tracer LIF in IC engine combustion', *Appl. Phys. B* **71**, 717–723 (2000).
58. M. Luong, R. Zhang, C. Schulz, and V. Sick, 'Toluene laser-induced fluorescence for in-cylinder temperature imaging', *Appl. Phys. B*, **91**, 669–675 (2008).
59. D. Frieden, V. Sick, J. Gronki, and C. Schulz, 'Quantitative oxygen imaging in an engine', *Appl. Phys. B* **75**, 137–141 (2002).
60. L. A. Melton, 'Exciplex-based vapor/liquid visualization systems appropriate for automotive gasolines', *Applied Spectroscopy* **47**, 782–786 (1993).
61. J. B. Ghandhi, P. G. Felton, B. F. Gajdeczko, and F. V. Bracco, 'Investigation of the fuel distribution in a two-stroke engine with an air-assisted injector', SAE paper 940394 (1994).
62. J. P. Styron, P. L. Kelly-Zion, C. F. Lee, J. E. Peters, and R. A. White, 'Multicomponent liquid and vapor fuel distribution measurements in the cylinder of a port-injected, spark-ignition engine', SAE paper 2000-01-0243 (2000).
63. T. Kim, M. S. Beckman, P. V. Farrell, and J. B. Ghandhi, 'Evaporating spray concentration measurements from small and medium bore diesel injectors', SAE paper 2002-01-0219 (2002).
64. G. Bruneaux, 'Mixing process in high-pressure diesel jets by normalized laser-induced exciplex fluorescence, part I: Free jet', SAE paper 2005-01-2100 (2005).
65. P. Wieske, S. Wissel, G. Grünefeld, and S. Pischinger, 'Improvement of LIEF by wavelength-resolved acquisition of multiple images using a single CCD detector – Simultaneous 2D measurement of air/fuel ratio, temperature distribution of the liquid phase and qualitative distribution of the liquid phase with the Multi-2D technique', *Appl. Phys. B* **83**, 323–329 (2006).
66. G. S. Settles, *Schlieren and Shadowgraph Techniques – Visualizing Phenomena in Transparent Media,* Springer, Heidelberg, 2001.
67. P. C. Miles, R. Collin, L. Hildingsson, A. Hultqvist, and Ö. Andersson, "Combined measurements of flow structure, partially oxidized fuel, and soot in a high-speed, direct-injection diesel engine', *Proc. Combust. Inst.* **31**, 2963–2970 (2007).
68. B. Bäuerle, F. Hoffmann, F. Behrendt, and J. Warnatz, "Detection of hot spots in the endgas of an internal combustion engine using two-dimensional LIF of formaldehyde', *Proc. Combust. Inst.* **25**, 135–141 (1994).
69. J. Nygren, J. Hult, M. Richter, M. Aldén, M. Christensen, A. Hultqvist, and B. Johansson, 'Three-dimensional laser induced fluorescence of fuel distributions in an HCCI engine', *Proc. Combust. Inst.* **29**, 679–685 (2002).

70. N. Graf, J. Gronki, C. Schulz, T. Baritaud, J. Cherel, P. Duret, and J. Lavy, 'In-cylinder combustion visualization in an auto-igniting gasoline engine using fuel tracer- and formaldehyde-LIF imaging', SAE paper 2001-01-1924 (2001).
71. J. T. Kashdan, S. Mendez, and G. Bruneaux, 'On the origin of unburned hydrocarbon emissions in a wall-guided, low-NO_x diesel combustion system', SAE paper 2007-01-1836 (2007).
72. M. Richter, A. Franke, M. Aldén, A. Hultqvist, and M. Johansson, 'Optical diagnostics applied to a naturally aspirated homogeneous charge compression ignition engine', SAE paper 1999-01-3649 (1999).
73. G. Bruneaux, M. Augé, and C. Lemenand, 'A study of combustion structure in high pressure single hole common rail direct diesel injection using laser induced fluorescence of radicals', in *6th International Symposium on Diagnostics and Modeling of Combustion in Internal Combustion Engines, Comodia,* Yokohama, Japan, 2004.
74. R. Collin, J. Nygren, M. Richter, M. Aldén, L. Hildingsson, and B. Johansson, 'Simultaneous OH- and formaldehyde-LIF measurements in an HCCI engine', SAE paper 2003-01-3218 (2003).
75. G. Bruneaux, 'Combustion structure of free and wall-impinging diesel jets by simultaneous laser-induced fluorescence of formaldehyde, PAH and OH', *Int. J. Engine Res.* **9**, 249–265 (2008).
76. J. D. Smith and V. Sick, 'A multi-variable high-speed optical study of ignition instabilities in a spray-guided direct-injected spark-ignition engine', SAE paper 2006-01-1264 (2006).
77. J. E. Dec, W. Hwang, and M. Sjöberg, 'An investigation of thermal stratification in HCCI engines using chemiluminescence imaging', SAE paper 2006-01-1518 (2006).
78. W. G. Bessler, C. Schulz, T. Lee, J. B. Jeffries, and R. K. Hanson, 'Strategies for laser-induced fluorescence detection of nitric oxide in high-pressure flames: III. Comparison of A-X strategies', *Appl. Opt.* **42**, 4922–4936 (2003).
79. C. Schulz, J. B. Jeffries, D. F. Davidson, J. D. Koch, J. Wolfrum, and R. K. Hanson, 'Impact of UV absorption by CO_2 and H_2O on NO LIF in high-pressure combustion applications', *Proc. Combust. Inst.* **29**, 2725–2742 (2002).
80. C. Schulz, J. D. Koch, D. F. Davidson, J. B. Jeffries, and R. K. Hanson, 'Ultraviolet absorption spectra of shock-heated carbon dioxide and water between 900 and 3050 K', *Chem. Phys. Lett.* **355**, 82–88 (2002).
81. F. Hildenbrand, C. Schulz, F. Keller, G. König, and E. Wagner, 'Quantitative laser diagnostic studies of the NO distribution in a DI diesel engine with PLN and CR injection systems', SAE paper 2001-01-3500 (2001).
82. J. E. Dec and R. E. Canaan, 'PLIF imaging of NO formation in a DI diesel engine', SAE paper 980147 (1998).
83. K. Verbiezen, R. J. H. Klein-Douwel, A. P. Van Vliet, A. J. Donkerbroek, W. L. Meerts, N. J. Dam, and J. J. ter Meulen, 'Quantitative laser-induced fluorescence measurements of nitric oxide in a heavy-duty diesel engine', *Proc. Combust. Inst.* **31**, 765–773 (2007).
84. C. Schulz, V. Sick, J. Heinze, and W. Stricker, 'Laser-induced fluorescence detection of nitric oxide in high-pressure flames using A-X(0,2) excitation', *Appl. Opt.* **36**, 3227–3232 (1997).
85. C. Schulz, J. Wolfrum, and V. Sick, 'Comparative study of experimental and numerical NO profiles in SI combustion', *Proc. Combust. Inst.* **27**, 2077–2084 (1998).

86. F. Hildenbrand, C. Schulz, V. Sick, H. Jander, and H. G. Wagner, 'Applicability of KrF excimer laser induced fluorescence in sooting high-pressure flames', in *VDI Flammentag Dresden, VDI Berichte* **1492**, 269–274 (1999).
87. F. Hildenbrand, C. Schulz, M. Hartmann, F. Puchner, and G. Wawrschin, 'In-cylinder NO-LIF imaging in a realistic GDI engine using KrF excimer laser excitation', SAE paper 1999-01-3545 (1999).
88. W. G. Bessler, M. Hofmann, F. Zimmermann, G. Suck, J. Jakobs, S. Nicklitzsch, T. Lee, J. Wolfrum, and C. Schulz, 'Quantitative in-cylinder NO–LIF imaging in a realistic gasoline engine with spray-guided direct injection', *Proc. Combust. Inst.* **30**, 2667–2674 (2005).
89. F. Hildenbrand, C. Schulz, J. Wolfrum, F. Keller, and E. Wagner, 'Laser diagnostic analysis of NO formation in a direct injection diesel engine with pump-line nozzle and common-rail injection systems', *Proc. Combust. Inst.* **28**, 1137–1144 (2000).
90. F. Hildenbrand and C. Schulz, 'Measurements and simulation of in-cylinder UV-absorption in spark ignition and diesel engines', *Appl. Phys. B* **73**, 165–172 (2001).
91. W. G. Bessler, C. Schulz, V. Sick, and J. W. Daily, 'A versatile modeling tool for nitric oxide LIF spectra (www.lifsim.com)', in *3rd Joint Meeting of the US Sections of The Combustion Institute,* (Chicago, 2003, PI05, pp. 1–6.
92. R. W. Weeks and W. W. Duley, 'Aerosol-particle sizes from light emission during excitation by TEA CO_2 laser pulses', *J. Appl. Phys.* **45**, 4661–4662 (1973).
93. L. A. Melton, 'Soot diagnostics based on laser heating', *Appl. Opt.* **23**, 2201–2208 (1984).
94. T. Ni, J. A. Pinson, S. Gupta, and R. J. Santoro, 'Two-dimensional imaging of soot volume fraction by the use of laser-induced incandescence', *Appl. Opt.* **34**, 7083–7091 (1995).
95. D. J. Bryce, N. Ladommatos, and H. Zhao, 'Quantitative investigation of soot distribution by laser-induced incandescence', *Appl. Opt.* **39**, 5012–5022 (2000).
96. C. R. Shaddix and K. C. Smyth, 'Laser-induced incandescence measurements of soot production in steady and flickering methane, propane, and ethylene diffusion flames', *Combust. Flame* **107**, 418–452 (1996).
97. P. O. Witze, S. Hochgreb, D. Kayes, H. A. Michelsen, and C. R. Shaddix, 'Time-resolved laser-induced incandescence and laser elastic-scattering measurements in a propane diffusion flame', *Appl. Opt.* **40**, 2443–2452 (2001).
98. B. Quay, T.-W. Lee, T. Ni, and R. J. Santoro, 'Spatially resolved measurements of soot volume fraction using laser-induced incandescence', *Combust. Flame* **97**, 384–392 (1994).
99. R. L. Vander Wal, 'Laser-induced incandescence: Development and characterization towards a measurement of soot-volume fraction', *Appl. Phys. B* **59**, 445–452 (1994).
100. J. Appel, B. Jungfleisch, M. Marquardt, R. Suntz, and H. Bockhorn, 'Assessment of soot volume fractions from laser-induced incandescence by comparison with extinction measurements in laminar, premixed, flat flames', *Proc. Combust. Inst.* **26**, 2387–2395 (1996).
101. B. Axelsson, R. Collin, and P.-E. Bengtsson, 'Laser-induced incandescence for soot particle size measurements in premixed flat flames', *Appl. Opt.* **39**, 3683–3690 (2000).
102. B. Axelsson, R. Collin, and P.-E. Bengtsson, 'Laser-induced incandescence for

soot particle size and volume fraction measurements using on-line extinction calibration', *Appl. Phys. B* **72**, 367–372 (2001).
103. H. Geitlinger, T. Streibel, R. Suntz, and H. Bockhorn, 'Two-dimensional imaging of soot volume fractions; particle number densities; and particle radii in laminar and turbulent diffusion flames', *Proc. Combust. Inst.* **27**, 1613–1621 (1998).
104. T. R. Meyer, S. Roy, V. M. Belovich, E. Corporan, and J. R. Gord, 'Simultaneous planar laser-induced incandescence, OH planar laser-induced fluorescence, and droplet Mie scattering in swirl-stabilized spray flames', *Appl. Opt.* **44**, 445–454 (2005).
105. H. Bockhorn, H. Geitlinger, B. Jungfleisch, T. Lehre, A. Schön, T. Streibel, and R. Suntz, 'Progress in characterization of soor formation by optical methods', *Phys. Chem. Phys.* **4**, 3780–3793 (2002).
106. S. Will, S. Schraml, and A. Leipertz, 'Comprehensive two-dimensional soot diagnostics based on laser-induced incandescence', *Proc. Combust. Inst.* **26**, 2277–2284 (1996).
107. S. Will, S. Schraml, K. Bader, and A. Leipertz, 'Performance characteristics of soot primary particle size measurements by time-resolved laser-induced incandescence', *Appl. Opt.* **37**, 5647–5658 (1998).
108. T. Lehre, B. Jungfleisch, R. Suntz, and H. Bockhorn, 'Size distributions of nanoscaled particles and gas temperatures from time-resolved laser-induced-incandescence measurements', *Appl. Opt.* **42**, 2021–2030 (2003).
109. D. Woiki, A. Giesen, and P. Roth, 'Time-resolved laser-induced incandescence for soot particle sizing during acetylene pyrolysis behind shock waves', *Proc. Combust. Inst.* **28**, 2531–2537 (2000).
110. R. L. Vander Wal, T. M. Ticich, and A. B. Stephens, 'Can soot primary particle size be determined using laser-induced incandescence?', *Combust. Flame* **116**, 291–296 (1999).
111. B. F. Kock, T. Eckhardt, and P. Roth, 'In-cylinder sizing of diesel particles by time-resolved laser-induced incandescence (TR-LII)', *Proc. Combust. Inst.* **29**, 2775–2781 (2002).
112. D. R. Snelling, G. J. Smallwood, R. A. Sawchuk, W. S. Neill, D. Gareau, D. J. Clavel, W. L. Chippior, F. Liu, and Ö. L. Gülder, 'In-situ real-time characterization of particulate emissions from a Diesel engine exhaust by laser-induced incandescence', SAE paper 2000-01-1994 (2000).
113. S. Schraml, S. Will, and A. Leipertz, 'Performance characteristics of TIRE-LII soot diagnostics in exhaust gases of diesel engines', SAE paper 2000-01-2002 (2000).
114. C. Schulz, B. F. Kock, M. Hofmann, H. A. Michelsen, S. Will, B. Bougie, R. Suntz, and G. J. Smallwood, 'Laser-induced incandescence: recent trends and current questions', *Appl. Phys. B* **83**, 333–354 (2006).
115. H. A. Michelsen, F. Liu, B. F. Kock, H. Bladh, A. Boiarciuc, M. Charwath, T. Dreier, R. Hadef, M. Hofmann, J. Reimann, S. Will, P.-E. Bengtsson, H. Bockhorn, F. Foucher, K.-P. Geigle, C. Mounaïm-Rousselle, C. Schulz, R. Stirn, B. Tribalet, and S. Suntz, 'Modeling laser-induced incandescence of soot: A summary and comparison of LII models', *Appl. Phys. B* **87**, 503–521 (2007).
116. M. Hofmann, B. Kock, and C. Schulz, 'A web-based interface for modeling laser-induced incandescence (LIISim)', in *European Combustion Meeting,* Chania, Greece, 2007, paper 5-11.
117. B. F. Kock, B. Tribalet, C. Schulz, and P. Roth, 'Two-color time-resolved LII

applied to soot particle sizing in the cylinder of a diesel engine', *Combust. Flame* **147**, 79–92 (2006).
118. B. Bougie, L. C. Ganippa, A. P. van Vliet, W. L. Meerts, N. J. Dam, and J. J. ter Meulen, 'Soot particulate size characterization in a heavy-duty diesel engine for different engine loads by laser-induced incandescence', *Proc. Combust. Inst.* **31**, 685–691 (2007).
119. R. L. Vander Wal, 'Laser-induced incandescence: Detection issues', *Appl. Opt.* **35**, 6548–6559 (1996).
120. M. Hofmann, W. G. Bessler, C. Schulz, and H. Jander, 'Laser-induced incandescence (LII) for soot diagnostics at high pressure', *Appl. Opt.* **42**, 2052–2062 (2003).
121. K. C. Smyth and C. R. Shaddix, 'The elusive history of $m = 1.57 - 0.56i$ for the refractive index of soot', *Combust. Flame* **107**, 314–320 (1996).
122. D. R. Snelling, G. J. Smallwood, F. Liu, Ö. L. Gülder, and W. D. Bachalo, 'A calibration-independent LII technique for soot measurement by detecting absolute light intensity', *Appl. Opt.* **44**, 6773–6785 (2005).
123. J. E. Dec and C. Espey, 'Ignition and early soot formation in a DI diesel engine using multiple 2-D imaging diagnostics', SAE paper 950456 (1995).
124. J. E. Dec, 'A conceptual model of DI diesel combustion based on laser-sheet imaging', SAE paper 970873 (1997).
125. H. Zhao and N. Ladommatos, 'Optical diagnostics for soot and temperature measurements in diesel engines', *Prog. Energy Combust. Sci.* **24**, 221–255 (1998).
126. G. J. Hampson and R. D. Reitz, 'Two-color imaging of in-cylinder soot concentration and temperature in a heavy-duty DI diesel engine with comparison to multidimensional modeling for single and split injections', SAE paper 980524 (1998).
127. X. Li and J. S. Wallace, 'In-cylinder measurement of temperature and soot concentration using the two-color method', SAE paper 950848, 147–157 (1995).
128. M. Tamura, J. Luque, J. E. Harrington, P. A. Berg, G. P. Smith, J. B. Jeffries, and D. R. Crosley, 'Laser-induced fluorescence of seeded nitric oxide as a flame thermometer', *Appl. Phys. B* **66**, 503–510 (1998).
129. W. G. Bessler and C. Schulz, 'Quantitative multi-line NO-LIF temperature imaging', *Appl. Phys. B* **78**, 519–533 (2004).
130. H. Kronemayer, K. Omerbegovic, and C. Schulz, 'Quantification of the evaporative cooling in an ethanol spray created by a gasoline direct-injection system measured by NO–LIF gas-temperature imaging', *Appl. Opt.* **46**, 8322–8327 (2007).
131. J. Nygren, J. Engström, J. Walewski, C. F. Kaminski, and M. Aldén, 'Applications and evaluation of two-line atomic LIF thermometry in sooting combustion environments', *Meas. Sci. Technol.* **12**, 1291–1303 (2001).
132. C. Parigger, D. H. Plemmons, R. J. Litchford, and S. M. Jeng, 'Exciplex liquid-phase thermometer using time-resolved laser-induced fluorescence', *Opt. Lett.* **23**, 76–78 (1998).
133. P. Lavieille, F. Lemoine, and M. Lebouché, 'Investigation on temperature of evaporating droplets in linear stream using two-color laser-induced fluorescence', *Combust. Sci. Tech.* **174**, 117–142 (2002).
134. I. Düwel, H.-W. Ge, H. Kronemayer, R. W. Dibble, E. Gutheil, C. Schulz, and J. Wolfrum, 'Experimental and numerical characterization of a turbulent spray flame', *Proc. Combust. Inst.* **31**, 2247–2255 (2007).
135. J. Brübach, A. Patt, and A. Dreizler, 'Spray thermometry using thermographic phosphors', *Appl. Phys. B* **83**, 499–502 (2006).

136. F. Beyrau, A. Bruer, T. Seeger, and A. Leipertz, 'Gas-phase temperature measurement in the vaporizing spray of a gasoline direct-injection injector by use of pure rotational coherent anti-Stokes Raman scattering', *Opt. Lett.* **29**, 247–249 (2004).
137. J. E. Dec and P. L. Kelly-Zion, 'The effects of injection timing and diluent addition on late-combustion soot burnout in a DI Diesel engine based on simultaneous 2-D imaging of OH and soot', SAE paper 2000-01-0238 (2000).
138. V. Sick, 'Exhaust-gas imaging via planar laser-induced fluorescence of sulfur dioxide', *Appl. Phys. B* **74**, 461–463 (2002).
139. D. Kim, I. Ekoto, W. F. Colban, and P. C. Miles, 'In-cylinder imaging of CO and UHC in a light-duty diesel engine operating under PPCI low-temperature combustion', SAE paper 2008-01-1602 (2008).
140. G. B. Rieker, H. Li, X. Liu, J. T. C. Liu, J. A. Jeffries, R. K. Hanson, M. G. Allen, S. D. Wehe, P. A. Mulhall, H. S. Kindle, A. Kakuho, K. R. Sholes, T. Matsuura, and S. Takatani, 'Rapid measurements of temperature and H_2O concentration in IC engines with a spark plug-mounted diode laser sensor', *Proc. Combust. Inst.* **30**, 3041–3049 (2007).
141. R. Reichle, C. Pruss, W. Osten, H. J. Tiziani, F. Zimmermann, and C. Schulz, 'Fiber optic spark plug sensor for UV-LIF-measurements close to the ignition spark', in *Proceedings of SPIE – The International Society for Optical Engineering* (2005), 5856 Part I, 158–168.
142. F. Kallmeyer, S. Dankers, W. Hentschel, G. Grosse, O. Thiele, and C. Schulz, 'Bestimmung des lokalen Lambda-Wertes im FSI®-Motor mittels einer optischen Zündkerze', in *Motorische Verbrennung,* Haus der Technik, Munich, 2007.

17

In-cylinder spray, mixing, combustion, and pollutant-formation processes in conventional and low-temperature-combustion diesel engines

M. P. B. MUSCULUS and L. M. PICKETT,
Sandia National Laboratories, USA

Abstract: This chapter reviews the in-cylinder spray, mixing, combustion and pollutant-formation processes of three characteristic modes of diesel combustion. The first mode is conventional diesel combustion, with fuel injection near top-dead-center of the piston's stroke, and with ignition before the end of injection. The second mode is low-temperature combustion using exhaust gas recirculation, with fuel injection either earlier or later than conventional diesel engines, and with ignition after the end of injection. The third mode is also low-temperature combustion using exhaust gas recirculation, but with ignition typically before the end of injection. The chapter closes with remarks on current research needs.

Key words: optical diagnostics, low-temperature combustion, diesel engine, fuel sprays, pollutant emissions.

17.1 Introduction

Diesel engine performance and pollutant emissions are a result of the chemical and physical processes of the fuel jets in the combustion chamber. Important in-cylinder processes include the spatial and temporal development of liquid-fuel sprays, fuel vaporization, mixing of vaporized fuel with in-cylinder gases, low-temperature autoignition chemistry of fuel components, high-temperature chemical kinetics of combustion and pollutant formation, and late-cycle mixing and burnout processes. This chapter provides an overview of in-cylinder diesel chemical and physical phenomena, based on observations from optical diagnostic techniques like those described in the Chapter 16. Three broad categories of diesel combustion are described. The first category is conventional direct-injection diesel combustion, which is characteristic of late twentieth century production diesel engines. The second category is diesel low-temperature combustion (LTC) using exhaust-gas recirculation (EGR) with fuel injection either earlier or later than conventional diesel engines, and with ignition after the end of fuel injection. The third category is also diesel LTC using EGR, but with ignition before the end of fuel injection,

as with conventional diesel engines. The latter two strategies encompass a wide variety of non-conventional operational strategies designed to reduce pollutant emissions in twenty-first century engines.

17.2 Conventional diesel combustion

The in-cylinder processes that affect combustion and pollutant formation in late twentieth century diesel engines can vary widely across the whole map of operating conditions and engine geometries of conventional diesel combustion. Consequently, a single picture or 'conceptual model' of conventional diesel combustion cannot completely describe all diesel combustion processes in all engines under all conditions. However, in most engine geometries and operating maps, conventional diesel jets share three general features.

1. Significant quasi-steady period. The first distinguishing characteristic is that the combustion event temporally overlaps with much of the fuel injection event. Fuel injection typically begins shortly before top-dead-center (TDC) of the piston's stroke, when the in-cylinder gases are hot and dense. As a result, the time between the start of fuel injection and the start of combustion, or the 'ignition delay,' is relatively short (200–1000 microseconds). After a subsequent premixed combustion phase, the characteristic features of the jet do not change significantly while fuel injection continues. Accordingly, the jets can be characterized as 'quasi-steady'. During this quasi-steady period, combustion is 'mixing controlled' – local rates of mixing are slower than chemical reaction rates, so that the heat-release rate is limited primarily by mixing of vaporized fuel with in-cylinder gases. This typical mode of diesel combustion ranges from moderate- to high-load conditions. Low-load conditions have short injection durations that usually yield little or no quasi-steady combustion.
2. Free jets. Early in the fuel-injection event, diesel jets propagate relatively freely into the combustion chamber as they entrain in-cylinder gases. This 'free jet' period lasts until the jet interacts with in-cylinder surfaces or flows. The duration of the free-jet period therefore depends on engine geometry (e.g., piston bowl shape and size) and operating conditions (e.g., swirl level). Large-bore engines, whose combustion chambers are typically quiescent, generally have a longer free-jet period and less flow and wall interaction than higher-swirl small-bore engines. Even in small-bore engines, however, much of the initial jet development is similar to a free jet. Furthermore, although in-cylinder surfaces and flows can deflect and interact with diesel jets, the general evolution of mixing and combustion is strongly influenced by free-jet processes. Therefore, to provide a simplified framework that is independent of variations in

engine geometry and in-cylinder flows, the diesel jets described in this chapter are treated as free jets.

3. Single fuel injection. Multiple fuel injections per cycle, including pilot, post, and split-main injections, can be beneficial for engine noise, efficiency, emissions, and management of exhaust aftertreatment devices. While these strategies can be advantageous in some conventional diesel engines, the most dominant main injection bears similarities to a single fuel injection and thus additional complexities associated with interactions between multiple fuel injection events are not described here – only single fuel injections per engine cycle are considered.

Several conceptual models have been proposed for conventional quasi-steady diesel combustion [11, 15, 30, 43, 63, 75]. The following sub-sections summarize important physical and chemical processes occurring in free diesel jets, based in large part on the conceptual model of Dec [15]. The discussion begins with the initial jet development, proceeds through autoignition and premixed burning, into the quasi-steady period, and concludes with late-cycle burnout of a single conventional diesel fuel-injection event.

17.2.1 Initial jet penetration

In a direct-injection diesel engine, liquid fuel is sprayed directly into the combustion chamber at high pressure through multiple orifices in the fuel injector tip. The density and pressure of the liquid fuel are each typically 20–40 times greater than the in-cylinder gases at the time of injection, near TDC. Therefore, the in-cylinder jet penetration, gas entrainment, and mixing during most of the injection event are driven by the high-momentum of the fuel spray.

Jet penetration may be measured by various optical techniques, including light attenuation [13, 28] and elastic scattering [4, 7, 9, 13, 25] for non-vaporizing sprays, or by shadowgraphy and Schlieren techniques [1, 9, 21, 36, 51, 73] and laser-induced fluorescence [10, 37] for either non-vaporizing or vaporizing sprays. The penetration rate is effectively governed by exchange of momentum between the high-velocity jet and the relatively stagnant in-cylinder gases. Building on previous works including [79], Naber and Siebers [51] used a simple transient control-volume analysis assuming uniform composition, density, and velocity over the jet cross-section to derive an analytical solution for the velocity at the tip of the jet:

$$U = \frac{\mathrm{d}x}{\mathrm{d}t} = \frac{U_0}{2} \cdot \frac{A_0}{A(x)} \cdot \frac{\rho_\mathrm{f}}{\rho_\mathrm{a}} \cdot \left[\sqrt{1+4\frac{A(x)}{A_0} \cdot \frac{\rho_\mathrm{a}}{\rho_\mathrm{f}}} - 1 \right] \qquad 17.1$$

Equation 17.1 shows that the jet tip velocity U, which is the derivative of the downstream jet penetration x with respect to time t, depends on the jet

velocity at the orifice U_0, the ratio of the fuel density ρ_f to the ambient gas density ρ_a, and the ratio of the effective orifice area A_0 to the adjusted jet cross-sectional area A. (In the development of Eq. 17.1 [13], A was adjusted to 66% of the physical value to compensate for the uniform cross-sectional velocity assumption, so that the model penetration prediction matches measured data.) Naber and Siebers integrated a non-dimensional form of Eq. 17.1 to yield an analytical expression for the penetration *time* as a function of *distance* (an inverse relationship), provided that U_0 is constant. The complete derived expression and non-dimensional relations may be found in [51]. A simplified form of the analytic solution, for which the volume occupied by the liquid fuel is neglected, is

$$t' = \frac{x'}{2U_0} + \frac{x'}{4U_0}\sqrt{1+16\left(\frac{x'}{x^+}\right)^2} + \frac{x^+}{16U_0}\ln\left(4\frac{x'}{x^+} + \sqrt{1+16\left(\frac{x'}{x^+}\right)^2}\right) \qquad 17.2$$

In Eq. 17.2, x' and t' are the penetration distance and time, respectively, referenced from the projected spray origin. The normalization parameter x^+ is

$$x^+ = \frac{d_0\sqrt{\rho_f/\rho_a}}{\tan(\alpha/2)} \qquad 17.3$$

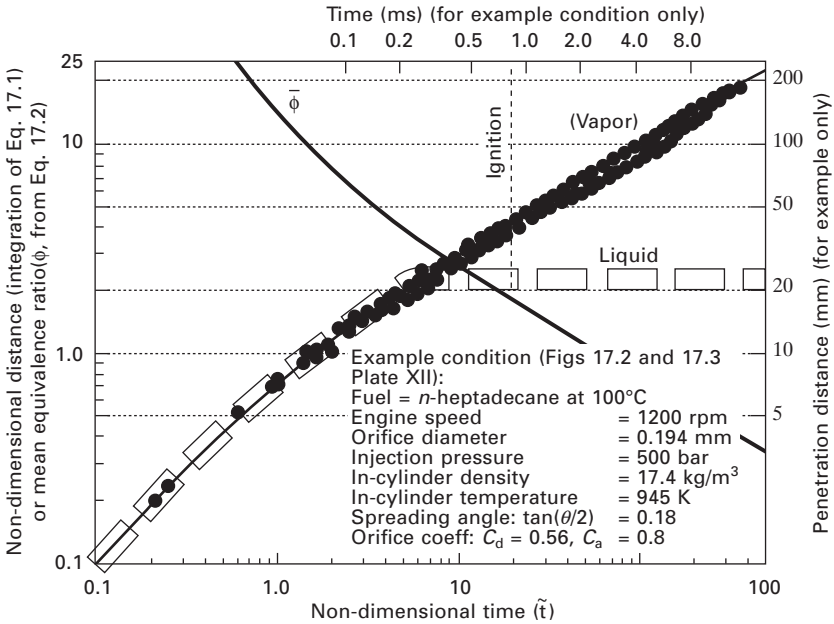
where d_0 is the effective orifice diameter (accounting for area contraction effects) and α is the adjusted jet spreading full-angle (as noted above).

Figure 17.1 shows the predicted penetration from the complete solution of Eq. 17.1, plotted against the non-dimensional space and time coordinates (left and bottom axes, respectively), along with experimentally measured penetration data from high-speed Schlieren photography [51]. As shown in Fig. 17.1, experimental penetration measurements from a wide range of conditions collapse well onto the non-dimensional analytical solution to Eq. 17.1.

Importantly, the analytical solution of Eq. 17.1 also predicts the cross-sectionally averaged equivalence ratio $\bar{\phi}$ in the quasi-steady jet, as a function of the stoichiometric fuel-to-ambient mass ratio $(F/A)_{stoich}$:

$$\bar{\phi}(x) = \frac{(F/A)_{stoich}}{\sqrt{1+16\,\dfrac{A(x)}{A_0}\cdot\dfrac{\rho_a}{\rho_f} - 1}} \qquad 17.4$$

The solution to Eq. 17.4 is also plotted in Fig. 17.1, for mixing with pure air (no exhaust-gas recirculation). Equation 17.4 predicts that $\bar{\phi}$ varies approximately inversely with increasing distance from the injector as more ambient gas is entrained into the jet, which is similar to both theory and



17.1 Measured (circles) and predicted (thin line, integration of Eq. 17.1) diesel-jet penetration, and predicted cross-sectionally averaged equivalence ratio (thick line, Eq. 17.4). Left and bottom axes: non-dimensional penetration $\tilde{S}$ and time $\tilde{t}$. Right and top axes: dimensional penetration and time for a single condition as listed on the figure (corresponds to images in Figs. 17.2 and 17.3 and Plate XII (between pages 364 and 365), including predicted liquid-fuel penetration (thick dashed line).

experiments in fully steady jets [67]. As will be shown in the following sections, the variation of $\overline{\phi}$ along the jet axis is critically important to the evolution of many conventional diesel jet processes. When combustion occurs after the end of injection, as is the case for many LTC jets, the $\overline{\phi}$ distribution is much different than predicted by Eq. 17.4.

17.2.2 Fuel vaporization and liquid length

In addition to becoming less fuel-rich, mixtures farther downstream in the jet have greater sensible thermal energy due to entrainment of hot ambient gases. As a result, the jet temperature increases downstream, and the liquid fuel increasingly vaporizes. The cooling effect of fuel vaporization is offset by the thermal energy of the entrained gases as the local liquid–vapor phase equilibrium shifts toward more vapor at greater downstream distances. During the initial penetration of a diesel jet, the local thermodynamic conditions favor a mixture of both liquid and vapor fuel, and the tip of the liquid fuel

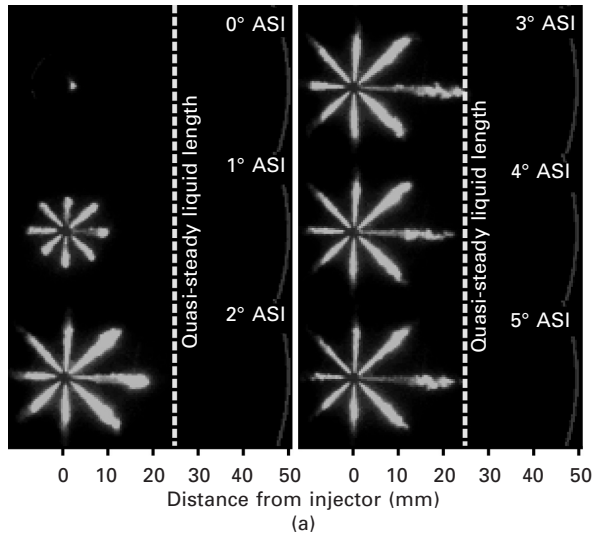
spray penetration increases with time. At some downstream distance, the thermal energy in the jet is sufficient to overcome the total latent vaporization energy of the liquid fuel, so that all of the fuel (locally) enters the vapor state. The downstream distance where the local thermodynamic conditions reach the saturated vapor state and the last bit of liquid fuel survives in the diesel jet is termed the 'liquid length'.

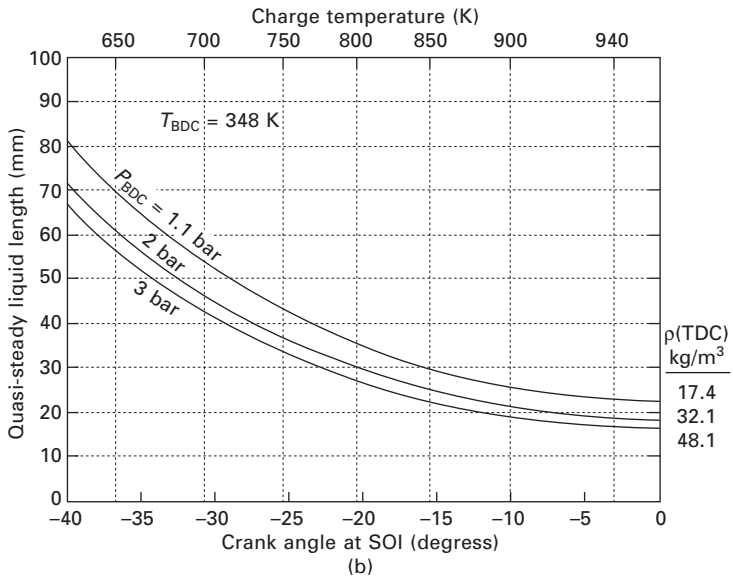
The penetration of liquid fuel may be measured from images of Mie-scattering of light off the liquid-fuel spray [4, 7, 9, 13, 22, 25, 69]. Figure 17.2(a) shows a series of liquid-fuel Mie-scatter images for a typical naturally aspirated operating condition in a heavy-duty engine [22]. The view is through a large piston-crown window. The injector is on the left, at the center of the spray pattern, and the curved line on the right indicates the location of the piston bowl-wall. The specifications for the operating condition are listed in the inset of Fig. 17.1, for which the right and top axes show the dimensional penetration *for this condition only*, using n-heptadecane fuel (a representative diesel fuel surrogate [51]). The left column of images in Fig. 17.2(a) shows that the liquid-fuel penetration initially increases with time. Indeed, measurements of both liquid- and vapor-fuel penetration show that the liquid fuel initially penetrates equally with the overall jet [10, 36, 37, 58], as illustrated by the initial overlap of the liquid- and vapor-fuel penetration in Fig. 17.1. Then, at some time after the start of injection (ASI), the liquid penetration reaches a quasi-steady value, which is the liquid length. The right column of images in Fig. 17.2(a) also illustrates that by 3° (crank angle) ASI, or 0.42 ms at 1200 rotations per minute (rpm), the liquid-fuel penetration length remains nearly constant – the quasi-steady liquid length (vertical dotted line) is established. Note that as illustrated in Fig. 17.1, the vapor jet continues to penetrate after the liquid fuel reaches its quasi-steady liquid length.

Accurate prediction of the quasi-steady liquid length is important because of the potential for liquid-fuel impingement on in-cylinder surfaces, which can inhibit mixing, increase emissions, and cause oil-dilution problems. Using the complete solution to Eq. 17.1 and Eq. 17.4, along with detailed thermodynamic state data for fuel and entrained gases, Siebers derived a scaling law to predict the quasi-steady liquid length L [70]:

$$L = \frac{b}{a} \cdot \sqrt{\frac{\rho_f}{\rho_a}} \cdot \frac{\sqrt{C_a} \cdot d}{\tan(\theta/2)} \sqrt{\left(\frac{2}{B} + 1\right)^2 - 1} \qquad 17.5$$

In Eq. 17.5, b and a are correlation constants with suggested values of 0.41 and 0.66, respectively, C_a is the orifice area contraction coefficient, d is the orifice diameter, θ is the jet spreading full angle, and B is the mass ratio of fuel to ambient gas at the liquid length, i.e., where the enthalpy change in the ambient gases matches the energy required to heat and vaporize the liquid





17.2 (a) Mie-scatter images of liquid fuel from a heavy-duty diesel engine [22] at same conditions as in Fig. 17.3 and Plate XII, and as inset in Fig. 17.1. (b) Quasi-steady liquid-fuel penetration predicted by Eq. 17.5 [70] for diesel fuel as the in-cylinder temperature and density change during compression/expansion for three different boost levels at constant BDC temperature.

fuel at the local liquid–vapor equilibrium temperature. The predictions of Eq. 17.5 agree well with laser-elastic Mie scattering measurements of the liquid length over a wide range of conditions. The success of Eq. 17.5 in predicting the liquid length, along with its independence of injection pressure, implies that for modern high-pressure diesel sprays, fuel vaporization is controlled by mixing, rather than atomization processes [70].

Figure 17.2(b) shows the dependence of the predicted quasi-steady liquid length on the engine crank angle for a typical heavy-duty injector and operating conditions, including several intake boost levels. The liquid length decreases as TDC is approached because the in-cylinder gases become hotter and more dense, so that the jet penetrates shorter distances before sufficient thermal energy is entrained to vaporize the fuel. For conventional, naturally aspirated diesel operating conditions with near-TDC injection, the liquid length is approximately 25 mm, which is well short of distances to in-cylinder surfaces in large-bore engines. Hence, the liquid phase of diesel fuel sprays in conventional large-bore engines does not impinge on in-cylinder surfaces at typical, warmed-up operating conditions. Fuel injectors in small-bore engines typically have smaller nozzle orifices, which give a shorter liquid length (see Eq. 17.5). Also, the swirl flows typical of small-bore engines induce lateral forces that deflect the spray and limit axial liquid penetration, though some liquid impingement may still occur.

Importantly, the plot in Fig. 17.2(b) shows that intake pressure boosting can reduce the liquid length by increasing the density of the entrained gases. Figure 17.2(b) also shows that if fuel injection occurs away from TDC, when the in-cylinder gases are cooler and less dense, the liquid fuel penetration is greater. Thus, the potential for liquid-fuel impingement on in-cylinder surfaces increases with early or late injection, though increasing boost still helps to shorten the liquid length. This behavior has implications for the LTC conditions that are described later in this chapter.

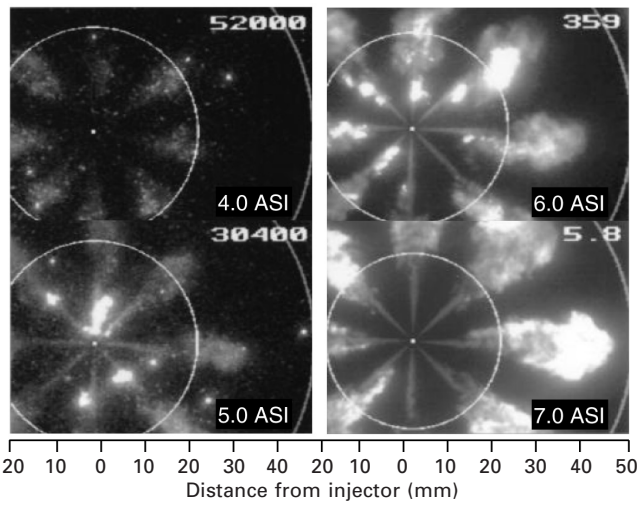
17.2.3 Autoignition and premixed burning

Diesel fuels typically display two-stage ignition chemistry [81]. At lower temperatures (800–1000 K), a pool of ketohydroperoxide radicals builds and then rapidly breaks down at the end of the first stage of ignition, forming another pool of hydrogen peroxide (H_2O_2). The temperature rise associate with the first stage of ignition terminates the pooling of ketohydroperoxides, but the H_2O_2 pool continues to build as the temperature gradually increases. When the temperature reaches approximately 1200 K, the H_2O_2 pool breaks down to release hydroxyl (OH) radicals that promote rapid oxidation during the hotter second-stage ignition and premixed burn.

For homogeneous mixtures of diesel-type fuels, such as in HCCI engines, heat-release rate analysis (derived from measured cylinder pressure) often

shows a distinct separation between the first- and second-stage ignition events. For conventional diesel-jet combustion, however, a distinct separation between the two stages is not typically apparent. At the time of ignition in diesel jets, the mixtures span a wide range of equivalence ratios. First-stage ignition occurs at different times for different equivalence ratios, so the net first-stage heat release is 'smeared out' over many different ignition times. Also, the volume of the jet at ignition is small, so that the heat released by first-stage ignition is comparatively low. Furthermore, mixing with the hot in-cylinder gases can push the mixtures very rapidly through the temperature ranges where first-stage ignition reactions occur. As a result, the radical pools have little time to build, so that the resulting first-stage heat release is small. A clear distinction between first- and second-stage ignition is readily apparent, however, in optical data.

Optical diagnostics show that autoignition in conventional diesel combustion typically occurs when much of the jet is still very fuel-rich. That is, the jet penetration is relatively short at the time of ignition, so the cross-sectionally averaged equivalence ratios, as predicted by Eq. 17.4, are fuel-rich, even at the head of the jet. The spatial location of ignition can be detected using chemiluminescence imaging [18], laser-induced fluorescence [15], or Rayleigh-scattering [23]. Figure 17.3 shows chemiluminescence images from the same



17.3 Chemiluminescence images of diesel autoignition for the same conditions as in Fig. 17.2 and Plate XII, and as listed in Fig. 17.1 (images taken from [18]). The small dot on the middle-left is the injector, the large circle shows the quasi-steady liquid length (see images in Fig. 17.2), and the white arc on the right is the piston bowl-wall. The number in the top right corner is the relative camera gain.

engine and similar conditions as the liquid-fuel images in Fig. 17.2(a). Near 4° (0.56 ms) ASI, the ignition chemiluminescence is first detectable from 10 to 30 mm downstream of the injector. Equation 17.4 (also see Fig. 17.1) predicts mean equivalence ratios in the range from 3 to 10 in this region.

By 6° ASI, the strong second-stage chemiluminescence is between 20 and 40 mm downstream, where Eq. 17.4 predicts mean equivalence ratios from 2 to 4. Rayleigh-scattering measurements confirm that the equivalence ratios at second-stage ignition are indeed in the range of 2 to 4 [23]. Furthermore, the same Rayleigh scattering measurements show that at ignition, fuel molecules are consumed nearly simultaneously throughout the jet cross-section, over a wide range of stoichiometric to fuel-rich mixtures, which is unlike classic flame propagation [23]. The premixed burn increases the temperature in the jet, and the resulting hot, partially oxidized mixtures synthesize PAH soot precursors that go on to form soot.

17.2.4 Quasi-steady period

The period after ignition and premixed burning through to the end of injection is the quasi-steady period, during which significant soot is formed in the hot, fuel-rich core of the jet. A layer of OH forms along the periphery of the jet during the premixed burn, and remains throughout the quasi-steady period. The OH layer at the interface between the fuel-rich jet and the surrounding oxidizing gases indicates that the mixing-controlled combustion occurs largely in a diffusion, or non-premixed, flame.

Evidence of soot formation within the jet can be provided by several optical techniques, as described in [84], including natural soot luminosity imaging, spectroscopic analysis such as the two-color technique, light extinction, and planar laser-induced incandescence (PLII). The location of the diffusion flame may be observed from PLIF images of OH, which is formed in hot diffusion flames [17]. Simultaneous images of soot PLII and OH-PLIF in a plane on the jet axis are shown in Plate XII at various times after the start of injection for a condition similar to Figs. 17.2 and 17.3 [20]. Unlike Figs 17.2 and 17.3, however, the view for the images in Plate XII is through a window in the cylinder head (see figure caption).

Both the soot and the OH typically first appear near the peak heat-release rate of the premixed burn (6° or 0.84 ms ASI). The soot appears and remains throughout the fuel-rich cross-section of the jet as it continues to penetrate during the quasi-steady period. The green OH-PLIF images show that a thin layer of OH surrounds the jet, at the boundary between the fuel-rich jet and the surrounding ambient gases. In typical flames, OH concentrations are greatest in regions of intermediate stoichiometries, in the neighborhood of $\phi = 1$ [49]. The OH therefore marks the location of a relatively thin stoichiometric diffusion flame on the jet periphery, which suggests strong

fuel concentration gradients on the jet periphery. Indeed, Rayleigh-scattering images show that equivalence ratio gradients are steep on the periphery of the jet [23].

Typically, neither the soot nor the diffusion flame extends upstream all the way to the injector. Rather, the diffusion flame stands off a finite distance from the injector, termed the 'lift-off length' [71]. The soot resides throughout the jet cross-section within the envelope of the diffusion flame, starting somewhat downstream of the lift-off length. This description of a soot-filled jet surrounded by a diffusion flame continues throughout the quasi-steady period, until the end of fuel injection.

Soot formation within the jet depends on the local equivalence ratio and temperature in the jet. To illustrate the dependence of soot formation on equivalence ratio and temperature in diesel jets, Kitamura *et al*. [40], Kamimoto and Bae [32], Akihama *et al*. [3] and others plotted contours of soot formation over a range of equivalence ratio and temperature. An example of a chemical kinetics simulation for soot yield using data from Kitamura *et al*. [40] is shown in Fig. 17.4. The soot yields in Fig. 17.4 were calculated for a residence time of 2 ms with temperature, pressure, and equivalence ratio held constant. Figure 17.4 predicts that soot forms at in-cylinder conditions within a peninsula bounded by temperature limits near 1500 and 2600 K, and a lower equivalence ratio limit near $\phi = 2$.

Hypothetical ϕ–T paths of mixing and combustion for diesel jets are also shown in Fig. 17.4(a), both for conventional in-cylinder gases with 21% O_2 and for highly diluted gases with 8% O_2. Prior to ignition, most mixtures in the jet are above the $\phi = 2$ lower equivalence ratio limit for soot formation. However, prior to ignition, the temperature in the jet (<1000 K) is too low for soot formation (i.e., mixtures are outside the plot in Fig. 17.4(a), to the left). After ignition, the premixed burn raises the temperature, as depicted by the horizontal portion of the diesel-jet paths appearing from the left side in Fig. 17.4(a). After ignition, the mixing timescale is typically much longer than the timescale for combustion reactions, so that the hypothetical ϕ–T curve follows a mixing-limited path, at the local flame temperature.

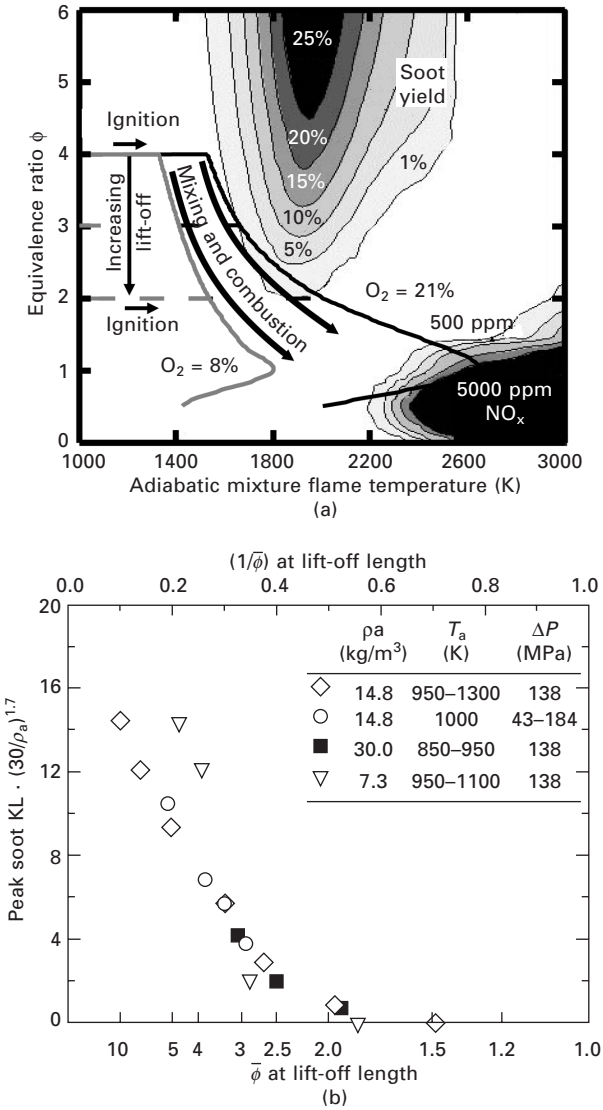
Soot begins to form in conventional diesel combustion (21% O_2 curve) as the mixtures approach the 1% soot-formation threshold. Then, as the jet continues to penetrate, the mixtures follow a path deeper into the soot peninsula in Fig. 17.4(a), leading to formation of more soot during the quasi-steady period. (The 8% O_2 curve for LTC conditions will be discussed in later sections of this chapter.)

The soot typically forms somewhat downstream of the lift-off length [63]. The continued formation of soot after the premixed burn indirectly indicates that during the quasi-steady period, the temperature within the jet must be above the soot formation threshold (approx. 1500 K, Fig. 17.4(a)). Dec hypothesized that oxygen entrained into the jet upstream of the lift-off

length would partially oxidize the fuel in a rich, partially premixed reaction zone downstream of both the liquid length and the lift-off length [15]. Furthermore, entrainment and mixing of hot products from the diffusion flame into the center of the jet also increases the temperature of the fuel-rich, soot-producing core of the jet. Both the premixed reaction zone and the entrainment of hot products occur downstream of the lift-off length. Therefore, the high-temperature diffusion flame lift-off length controls the downstream distance where temperatures are high enough for subsequent soot formation in diesel jets. But, as shown in Fig. 17.4(a), soot formation also depends on ϕ. As shown in Fig. 17.1 and according to Eq. 17.4, the jet cross-sectionally averaged equivalence ratio decreases with downstream distance to the lift-off length. As shown in the ϕ–T plot of Fig. 17.4(a), with increasing lift-off length, the diesel jet mixing path avoids more of the soot-formation peninsula. Optical measurements confirm that soot formation decreases with increasing lift-off length (i.e., decreasing equivalence ratio at the lift-off length). The graph in Fig. 17.4(b) shows the soot optical density, measured by laser extinction [61], plotted versus the jet cross-sectionally averaged equivalence ratio $\overline{\phi}$ (from Eq. 17.4) at the diffusion flame lift-off length, measured by OH chemiluminescence imaging [27]. In Fig. 17.4(b), soot decreases with the equivalence ratio at the lift-off length, reaching essentially zero soot for $\overline{\phi} < 2$, consistent with the ϕ–T concept shown on the left in Fig. 17.4(b). When $\overline{\phi} > 2$, the soot varies approximately linearly with $1/\overline{\phi}$ (see top axis in Fig. 17.4(b)).

While the diffusion flame lift-off length is clearly important for soot formation in the jet, the conditions necessary to completely inhibit soot formation by achieving $\overline{\phi} < 2$ at the lift-off length are extreme compared to conventional diesel combustion. Such conditions require extremely small nozzle orifices, very long ignition delays (low cetane fuels or cool conditions), and/or very high injection pressures [62]. Furthermore, the rate of soot oxidation, as well as soot formation, affects the ultimate exhaust soot emissions of diesel engines. Some of the factors that increase the diffusion flame lift-off length, such as decreasing ambient temperature, also tend to decrease soot oxidation. As a result, exhaust soot may increase even as the soot formation decreases at longer lift-off lengths because soot oxidation may decrease more rapidly than soot formation [29].

The diffusion flame is also important for the other primary pollutant from conventional diesel engines, nitrogen oxides (NO_x). In diesel engines, exhaust NO_x has been shown to vary strongly with the adiabatic flame temperature over a wide range of conditions [65,66], indicating that the thermal NO formation route is dominant over other potential mechanisms (e.g., the prompt NO or the N_2O pathways). The strong temperature dependence means that NO formation should be strongly weighted to regions with the highest temperature, such as the stoichiometric diffusion flame. Figure 17.4 shows



17.4 (a) Soot and NO_x formation in ϕ–T coordinates. The soot yield and NO_x contours are plotted using data from [40]. Jet mixing and combustion pathways are shown for 21% and 8% ambient gas oxygen concentration. (b) Dependence of in-cylinder soot on the equivalence ratio at the flame lift-off length [61].

that NO formation increases rapidly as the diesel jet mixtures approach high temperatures up to 2600 K, in the bottom right corner of the ϕ–T plot where $\phi < 2$. Indeed, planar laser-induced fluorescence imaging of NO shows that the NO initially forms in the diffusion flame, where temperatures are highest [16].

A contrary observation is the correlation of exhaust NOx with the size of the premixed burn, which suggests that the premixed burn is responsible for NO_x formation. However, the optical data show that the premixed burn of conventional diesel combustion is too rich to form significant NO_x, so other factors must be responsible for the correlation. By contrast, large portions of LTC jets with long ignition delays are closer to stoichiometric, so that a larger fraction of the total NO_x may be formed during the premixed burn, as will be shown later in this chapter.

17.2.5 Late-cycle burnout

The quasi-steady period ends with the end of fuel injection, after which the apparent heat-release rate decreases as the remaining fuel, combustion intermediate species, and soot continue to oxidize as they mix with in-cylinder gases. Although the heat-release rate is low compared to the quasi-steady period, oxidation reactions can persist late into the expansion stroke, as evidenced by fluorescence images of strongly oxidizing OH surrounding soot imaged by LII, even after exhaust-valve opening under some conditions [19]. Indeed, the diffusive combustion zone structure of the quasi-steady jet is generally maintained, with OH residing on the perimeter and between the soot pockets. Late in the cycle, the initial large pockets of soot formed by each of the diesel jets break down into smaller pockets, with ever broadening distributions of OH between the pockets. Soot-LII [19] and combustion luminosity measurements [76] show that the persistence of soot very late into the cycle, even after exhaust valve opening, changes significantly with fuel injection timing and duration (i.e., engine load). Combined soot-LII and OH-PLIF imaging [19] shows that soot in the quasi-steady diesel jet may survive into the exhaust gases by two mechanisms. First, if fuel injection is retarded, the time available before exhaust valve opening may be insufficient to complete the oxidation of the soot. Second, if the piston contents cool sufficiently during the expansion stroke to quench the oxidation reactions (i.e., OH is no longer present), soot may survive into the exhaust stroke. This second mechanism typically occurs because of dilution with EGR, and may occur even at modest EGR rates (~10%) [19].

17.3 Positive ignition-dwell low-temperature diesel combustion

As described in the previous section, the mixing and combustion processes of quasi-steady jets in conventional diesel combustion create a hot (>1500 K), fuel-rich, soot-forming core surrounded by an even hotter (~2600 K) NO-forming diffusion flame on the periphery of the jet. Diesel LTC strategies generally seek to reduce combustion temperatures and/or increase

pre-combustion mixing to avoid both the fuel-rich soot formation regions and the high-temperature NO-formation zone. For example, EGR dilution can shift the ϕ–T mixing and combustion path to the left from the 21% O_2 curve toward the 8% O_2 curve in Fig. 17.4(a). As a result, the mixing and combustion processes of low-temperature diesel jets create a very different picture of in-cylinder pollutant formation. A wide variety of engine and fuel delivery concepts have been pursued to achieve these basic goals of LTC. A complete treatment of the whole gamut of reported LTC concepts is beyond the scope of this chapter. Instead, two important subsets of diesel LTC that are currently used in many production early twenty-first century diesel engines will be described. Both of these LTC subsets share the following common three important characteristics:

1. Conventional diesel fuel-injection hardware. Fuel delivery and mixing is critical to the performance of low-temperature diesel engines, and a variety of non-conventional diesel fuel-delivery strategies have been reported, including premixing outside the combustion chamber, as in many homogeneous-charge compression ignition (HCCI) concepts [8], narrow-angle direct injection [33, 80], and impinging jets [2,78]. The mixing processes and jet geometries for these strategies are so different from those of conventional diesel direct injection systems that they preclude a side-by-side comparison with conventional diesel combustion described in the first half of this chapter. Diesel LTC can also be implemented, however, using conventional diesel fuel injection hardware, by injecting fuel either early or late in the cycle to provide extended time for the premixing required to inhibit soot formation. The LTC concept considered here features conventional diesel multi-hole direct-injection systems having a standard, wide included angle between jets.
2. Low-temperature combustion by EGR dilution. The low flame temperatures necessary to reduce NO_x can be achieved either by burning locally fuel-lean throughout the combustion chamber, as in fully premixed HCCI engines [8], or by diluting the intake charge with EGR [45]. While the fuel-lean, fully premixed HCCI approach is promising, it is difficult to create a fully premixed charge for HCCI with conventional diesel fuel-injection hardware. Moreover, the relatively homogeneous in-cylinder mixtures required for HCCI bear little resemblance to the heterogeneous jet structures of conventional diesel combustion, precluding a side-by-side comparison. Instead, EGR-diluted LTC, which is used in many current production diesel LTC engines, is the focus of discussion in this chapter.
3. Single fuel injection. As with conventional diesel combustion, many diesel LTC concepts use multiple fuel injections per cycle to affect the in-cylinder distribution of fuel beyond what can be achieved with a single injection. Many different concepts have been proposed, and it is

beyond the scope of this chapter to describe the in-cylinder processes for multiple injections. Instead, the descriptions of diesel low-temperature combustion are restricted to single fuel-injection events.

With the above characteristics in common, the two LTC subsets differ in whether or not the jets experience significant quasi-steady combustion. The first subset discussed below is for LTC strategies with positive ignition dwell, where ignition occurs after the end of injection. These conditions are typically for low-load operation without a quasi-steady period. The final part of this chapter describes the second subset, quasi-steady LTC, for which fuel injection continues after ignition, which applies to higher loads.

17.3.1 Fuel vaporization and liquid length

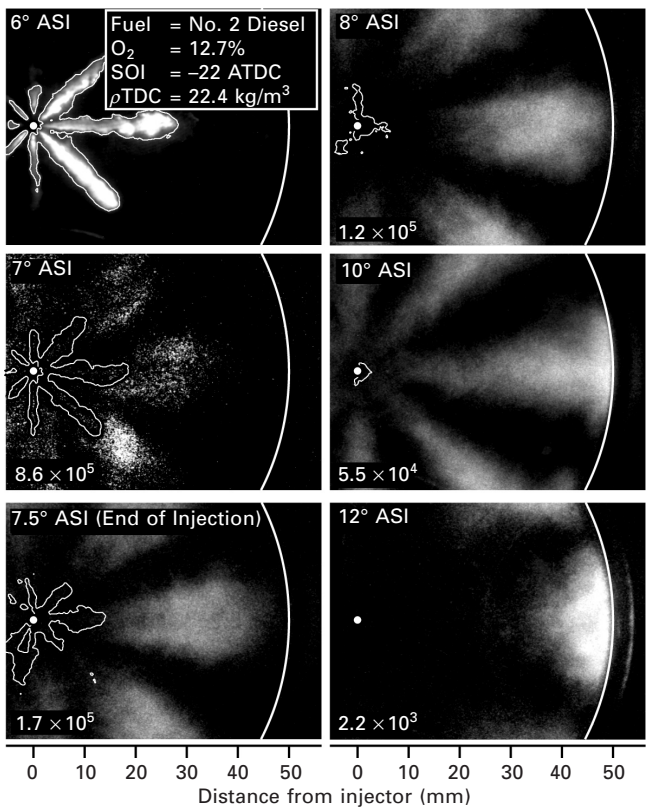
As illustrated in Fig. 17.4, soot formation may be reduced either by increasing the amount of premixing of fuel with the intake charge prior to autoignition and combustion, or by reducing the combustion temperatures. Increased premixing moves the mixtures that react during the premixed burn downward from the soot formation peninsula in Fig. 17.4(a) into lower equivalence ratios, similar to the effect of increasing lift-off length described for conventional diesel combustion. Increased dilution, such as by EGR, moves the combustion temperatures leftward from the soot peninsula, as shown by the 8% O_2 curve in Fig. 17.4(a).

The amount of premixing can be increased by providing more time for mixing. One way to increase the premixing time is by using cooled EGR. Indeed, studies show that with EGR dilution, the ignition delay is approximately inversely proportional to the in-cylinder oxygen concentration [41, 64]. However, the increase in ignition delay with EGR, and the accompanying increase in mixing time prior to combustion, is offset by the lower ambient oxygen concentrations with EGR, for which longer mixing times are required to reach a given equivalence ratio. As a result, the equivalence ratios at ignition remain relatively constant as ambient oxygen concentration is varied.

Another way to increase the ignition delay is to inject fuel when the in-cylinder gases are cooler, so that ignition reactions are slower. As shown in Fig. 17.2(b), the in-cylinder charge temperature decreases when fuel injection occurs farther from TDC, so the ignition delay can be extended by injecting either early [26, 34, 48, 74, 82] or late [38, 39, 47] in the cycle. With fuel injection away from TDC, however, the liquid-fuel penetration tends to increase, as shown in Fig. 17.2(b). Depending on engine geometry, as the injection timing is advanced or retarded from TDC, liquid fuel may impinge on the piston or cylinder wall, causing poor mixing and emissions problems from liquid films [33, 35, 83] or lubrication oil dilution [2, 55, 56]. Figure 17.2(b) shows that boosting the intake to higher pressures can help

to reduce the liquid fuel penetration and associated problems from liquid fuel impingement on in-cylinder surfaces.

In many LTC strategies, both intake-charge dilution and early or late fuel-injection are combined to increase mixing prior to combustion. An example of liquid-fuel penetration and ensemble-averaged ignition chemiluminescence for a low-boost, early-injection LTC condition using EGR dilution is shown in Fig. 17.5, which is taken from Singh *et al*. [72]. Fuel injection starts at –22° ATDC and ends near –14.5° ATDC (7.5° ASI). The intake oxygen concentration is 12.7% (equivalent to 50–60% EGR), and the intake pressure is slightly boosted (22.4 kg/m^3 in-cylinder density at TDC). The top-left image in Fig. 17.5 shows the liquid-fuel Mie-scattering at 6° ASI, with a contour marking the outer edge at 15% of maximum intensity. For all other images in Fig. 17.5, the chemiluminescence is displayed in grayscale, and the outer



17.5 Simultaneous images of liquid fuel contours and ensemble-averaged ignition chemiluminescence (grayscale) for a low-load early-injection LTC condition of [72]. The camera gain for the chemiluminescence images is given on the bottom left of each image.

contour of the liquid fuel is overlaid for comparison. (Chemiluminescence imaging will be described in the next section.)

The initial evolution of the liquid-fuel penetration (not shown here) is very similar to that of conventional diesel combustion (Fig. 17.2). Although the ambient density increases slightly during the injection event, the quasi-steady liquid-length reaches a relatively constant value of approximately 30 mm from 4° to 6° ASI. The liquid length typically varies from cycle to cycle [22], in this case reaching nearly 40 mm on some cycles. Thus, for this particular low-boost condition, the liquid fuel always vaporizes before reaching in-cylinder surfaces (the piston bowl radius is 50 mm in this heavy-duty engine). However, for a similar condition with lower intake-pressure boost (giving 16 kg/m^3 TDC density, rather than 22.4 kg/m^3), some liquid fuel reaches the piston bowl wall (50 mm from the injector) on some engine cycles [49]. Even then, however, the modest energy release from first-stage ignition reactions can raise temperatures in the jet to assist fuel vaporization [49]. Indeed, in Fig. 17.5, the liquid length begins to decrease after 6° ASI, when chemiluminescence emission appears at the beginning of the first-stage ignition heat release [72]. This observation suggests that if first-stage ignition occurs at the proper time, it could help to prevent liquid-fuel impingement on in-cylinder surfaces. Other data also indicate that end-of-injection mixing processes may decrease the liquid fuel penetration near the end of injection, even without first-stage ignition heat release [42].

17.3.2 Autoignition and premixed burning

With longer ignition delay for diluted gases, and with fuel injection farther from TDC, into lower density gases, the diesel jet penetrates farther downstream before ignition. As a result, the autoignition reactions occur farther downstream. For the LTC operating condition in Fig. 17.5, the initial ignition chemiluminescence begins 20 to 40 mm downstream, near 7–7.5° ASI, compared to 15–25 mm downstream and 4–4.5° ASI for conventional diesel combustion (Fig. 17.3). Within 2–3° after its first detectable appearance at 7° ASI, first-stage ignition chemiluminescence occurs throughout the jet, nearly from the injector to the tip of the jet. The indications of ignition spanning the length of the jet are further supported by laser-induced fluorescence images of formaldehyde, which also fills the jet after forming rapidly during the first-stage ignition [24]. Complementary equivalence ratio measurements show that the mixtures where formaldehyde initially appears span from fuel-lean to fuel-rich [24]. During the second-stage ignition and premixed burning, the most intense chemiluminescence is emitted from the downstream regions of the jet, along the piston bowl-wall, as shown in Fig. 17.5 at 12° ASI. The considerable increase in the intensity of the chemiluminescence suggests that second-stage combustion is more intense near the bowl-wall.

Indeed, a few crank angle degrees later in the cycle, near the peak of the premixed burn heat release, OH-PLIF typically first appears in the same downstream area as the brightest chemiluminescence. For example, Plate XIII (between pages 364 and 365) shows simultaneous OH-PLIF (green) and soot luminosity (red) images for a similar early-injection LTC condition as in Fig. 17.5, but with a lower intake boost level, giving a TDC density of 16 kg/m^3 [49]. The view in Plate XIII is similar to Plate XII, though in Plate XIII a portion of the bowl-rim was removed to allow the jet to penetrate as a free jet past the nominal piston bowl-wall (dashed line) all the way to the cylinder wall (white arc on right side of images). OH marks the transition to the hot, second-stage chemistry. Therefore, the appearance of OH downstream, combined with the strong ignition chemiluminescence in Fig. 17.5, indicates that most of the premixed-burn heat release occurs in the downstream region of the jet.

Rather than forming in a thin diffusion flame at the periphery of the jet as in conventional diesel combustion, the OH-PLIF appears in heterogeneous, sometimes ribbon-like structures throughout the downstream region of the jet. The OH-PLIF distribution in the downstream region broadens rapidly after its first appearance, though it still remains heterogeneous with small dark patches distributed throughout the jet cross-section. The appearance of OH in the jet cross-section indicates that the jet is much leaner than a conventional diesel jet. As described in the first half of this chapter, conventional diesel jets are too fuel-rich to accumulate detectable OH in the soot-filled jet cross-section (see Plate XII). With significant OH throughout its cross-section, much of the downstream LTC jet must be of intermediate stoichiometry, in the neighborhood of $\phi = 1$.

Indeed, direct measurements of the equivalence ratio in LTC jets show that mixtures very rapidly become fuel-lean after the end of injection, especially near the injector. Shown in Plate XIV (between pages 364 and 365) are equivalence ratio measurements in an LTC jet at 5° (0.70 ms) after the end of injection (AEI), as measured by fuel-vapor Rayleigh-scattering [50]. The ambient conditions and fuel injection parameters for Plate XIV are similar to the engine conditions for Fig. 17.5 and Plate XIII, though the injector orifice diameter is smaller (0.100 mm in Plate XIV compared to 0.196 mm in Fig. 17.5 and Plate XIII). The equivalence ratio contour map in Plate XIV is a composite of two images, one showing from 2 to 25 mm from the injector, and the other showing from 25 to 60 mm from the injector. Much of the jet downstream of 30 mm, where OH appears in Plate XIII, is near $\phi = 1$, with even leaner mixtures ($\phi < 1$) closer to the injector. Equivalence ratio measurements in the engine at conditions similar to Fig. 17.5 and Plate XIII show similar equivalence ratios of intermediate stoichiometry where OH appears, and with even leaner mixtures upstream [50].

The lean mixtures that form upstream in the LTC jets are certainly a

consequence of the increased premixing time of LTC combustion, but they are also surprising for two reasons. First, the intake charge for the LTC condition is diluted by EGR, so all mixtures in the jet should become richer because of the reduced oxygen concentration. That is, Fig. 17.1 shows that a quasi-steady jet without dilution has $\phi \sim 3$ at 30 mm, with even richer mixtures upstream. With similar dilution as in Fig. 17.5, Plate XIII and Plate XIV, the equivalence ratio 30 mm downstream in Fig. 17.1 would be nearly $\phi = 5$, yet shortly after the end of injection, the LTC jet has near-unity equivalence ratios in the same region.

Second, and more importantly, the LTC jet structure is very similar to that of conventional diesel combustion. That is, the jet is still roughly conical in shape, with nearly the same width. Therefore, at a given downstream location, the jet cross-sectional area, or amount of entrained ambient gases, is similar to that of conventional diesel jets. And yet, in a very short time after the end of injection, the equivalence ratio becomes much lower than in the quasi-steady jet, even with EGR, as indicated by the widespread appearance of OH in the jet cross-section. Consequently, the equivalence ratio distribution shortly after the end of injection must be radically different from the approximately $1/x$ dependence of the equivalence ratio in Fig. 17.1 and Eq. 17.4 that applies to a steady jet. This implies that mixing processes occurring after the end of injection are significantly different than those occurring during injection — mixtures at a given downstream location rapidly become much leaner after the end of injection than they would during the injection.

Consistent with the rapidly leaning jet, and in contrast to conventional diesel combustion, very little soot appears in the jet for the LTC conditions. Furthermore, its appearance is much less repeatable than for conventional diesel combustion, with significant cycle-to-cycle variation in the exact location of the onset of soot. As a result, the location of soot in the jet can be measured more repeatably by soot luminosity imaging (line-of-sight), as shown in Fig. Plate XIII, than by planar laser-induced incandescence. In general, soot does not appear throughout the mid- and downstream portions of the jet as in conventional diesel combustion, but rather only far downstream in the jet and off to the sides of the jet. The downstream region where the soot appears is roughly coincident with the 'roll-up' vortex at the head of the jet, and also with the region where the jet impinges onto and spreads along the cylinder wall in Plate XIII. According to the ϕ–T plot in Fig. 17.4, soot formation is expected only when $\phi > 2$. This implies that after the end of injection, the richest regions of the jet are far downstream, not upstream as in a quasi-steady jet, as shown by the direct measurements in Fig. Plate XIV.

Even late in combustion, OH-PLIF generally remains in the downstream portion of the jet, and it typically does not appear upstream. As shown in Fig. Plate XIII, late in the cycle, the OH-PLIF does not appear upstream

of about 50 mm from the injector. Another study with more optical access to the upstream jet, but with late injection, showed that OH never appears upstream, though strong formaldehyde fluorescence does remain upstream [44]. Chemical kinetics simulations suggest that formaldehyde formed in the main jet during the first-stage ignition would persist late in the cycle if mixtures were too lean for complete combustion, with $\phi < 0.5$ [44]. Indeed, Plate XIV shows that equivalence ratios near the injector do become very low after the end of injection, which may lead to unburned hydrocarbon emissions because of incomplete combustion for conditions with long ignition delays [50].

17.4 Quasi-steady low-temperature diesel combustion

The characterization of LTC described in the previous section applies to a variety of strategies that are typically limited to relatively low-load conditions. In general, these low-load conditions with short injection durations have significant time for mixing between the end of injection and the start of combustion, and thus lower soot emissions. High-load operating conditions, by contrast, typically may have injection durations that exceed the ignition delay, even when in-cylinder gases are diluted with EGR, and especially when injection occurs near TDC. Although significant NO_x-formation is avoided by EGR dilution, the quasi-steady jet may still have significant fuel-rich, soot-forming regions, similar to conventional diesel combustion. Indeed, quasi-steady LTC jets are similar in many ways to conventional quasi-steady jets, but EGR dilution changes several important characteristics of the reacting jets, as discussed below.

17.4.1 Initial jet development

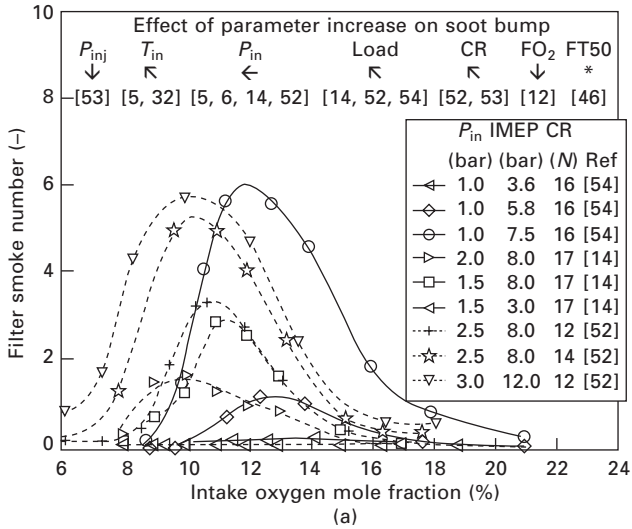
With injection occurring near TDC, the fuel vaporization for quasi-steady LTC fuel jets is controlled by energy entrained with the hot, high-density gases. Therefore, a quasi-steady liquid penetration length is established, as with conventional quasi-steady jets (Fig. 17.2). The ignition processes of quasi-steady LTC fuel jets also follow a two-stage process as with conventional diesel combustion. However, hot, second-stage ignition is delayed because of low in-cylinder oxygen concentrations. The increased ignition delay allows more time for jet penetration. The initial reacting sections of the LTC jet are therefore farther from the injector compared to conventional diesel combustion [31,77], similar to the low-load LTC condition discussed in the previous section. However, once ignited, a structure characterized by a lifted diffusion flame surrounding a fuel-rich jet core is established [60, 68], similar to conventional diesel combustion described in the first part of this chapter.

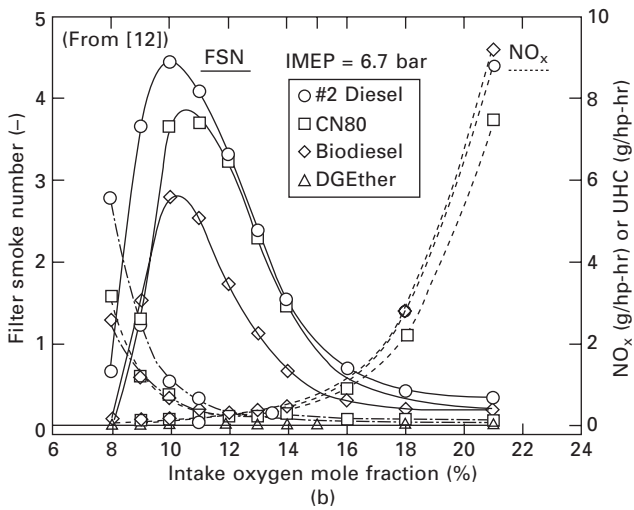
17.4.2 LTC exhaust soot bump

Even though a typical diffusion flame structure is established for quasi-steady LTC, EGR dilution significantly alters the diesel combustion and pollutant-formation processes. Evidence for these changes is provided in Fig. 17.6. Figure 17.6(a) shows exhaust smoke measurements for multiple operating conditions, and Fig. 17.6(b) shows NO_x and UHC emissions for a range of fuels, assembled from multiple studies [3, 5, 6, 12, 14, 46, 52–54]. The emissions data are plotted versus the intake oxygen mole fraction, rather than EGR rate, because the EGR rate required to yield a given intake oxygen mole fraction can vary significantly with engine load and intake pressure. However, in general, as the EGR percentage increases, the exhaust excess oxygen decreases, so that the intake oxygen mole fraction also decreases. The intake pressure (P_{in}), engine load (IMEP, indicated mean-effective pressure), compression ratio (CR), and literature references are provided on the figure to distinguish each operating condition. *Because of fundamental differences between engine facilities, the absolute magnitudes of the emissions should be compared using results from the same facility only.*

Beginning with no EGR (21% O_2), an initial reduction in intake oxygen mole fraction reduces NO_x emissions but increases smoke emissions. The EGR reduces diesel combustion flame temperatures, thereby reducing NO_x emissions, but the lower oxygen concentration and combustion temperature can lead to incomplete oxidation of soot and an increase in exhaust smoke. This behavior is an example of the classic trade-off between NO_x and particulate matter (PM) emissions. However, with further reduction in intake oxygen, the emission measurements show that exhaust smoke reaches a maximum somewhere between 10% and 13% oxygen, and then decreases to almost zero near 6–8% oxygen. This maximum in exhaust smoke with decreasing intake oxygen has been referred to as the ‘soot bump’ [6, 14, 52]. The existence of the soot bump, which indicates a simultaneous reduction of both PM and NO_x emissions with decreasing intake oxygen concentration, is interesting because it represents behavior that is contrary to the classic PM–NO_x tradeoff.

Seeking to mitigate exhaust PM at quasi-steady LTC conditions, researchers have investigated the response of the soot bump over a wide range of engine operating conditions. Their findings are summarized in the top inset in Fig. 17.6(a), with an arrow indicating the change in magnitude and direction of the soot bump with respect to intake oxygen concentration for a given parameter. For example, an increase in engine load corresponds to an arrow pointing up and to the left, which indicates an increase in the soot bump, and a shift of the peak in the soot bump to lower oxygen mole fraction. Note that low-load conditions, with an IMEP of 4 bar or less, which include the positive ignition dwell LTC experimental conditions discussed earlier with





17.6 (a) Exhaust smoke measurements for multiple operating conditions in multiple engines, assembled from references indicated on the graph. Upper legend arrow indicates how the soot bump is affected by an increase in fuel injection pressure (P_{inj}), intake temperature (T_{in}), intake pressure (P_{in}), compression ratio (CR), fuel oxygen mass percent (FO_2), or fuel 50% boiling point temperature (FT50), based on the references cited below the arrow. (b) Exhaust smoke, NOx, and UHC emissions for a range of fuels, taken from [12].

Fig. 17.5 and Plate XIII, produce little PM emissions. Moderate- to high-load conditions, with higher IMEP and more quasi-steady LTC, generally have higher PM emissions. However, low PM emissions remain a possibility even at high load, provided the intake oxygen concentration is below the level at the peak of the soot bump.

17.4.3 LTC in-cylinder soot bump

By themselves, exhaust PM measurements provide limited information about the effects of EGR on soot formation within the reacting diesel fuel spray. For example, *exhaust* PM levels may increase with increasing EGR because of less effective soot oxidation, even as peak *in-cylinder* soot levels decrease because of reduced soot formation. To better understand the effects of EGR soot formation, the in-cylinder soot levels can be directly measured by optical diagnostics. Shown in Plate XV are in-cylinder laser-extinction soot volume fraction measurements from quasi-steady, mixing-controlled diesel fuel jets in a constant-volume vessel, for oxygen concentrations ranging from 21% to 8% [59]. Soot volume fraction (f_v) contours are shown in the left of Plate XV (between pages 364 and 365) for five different EGR levels for an experimental condition with an ambient temperature of 1000 K and an ambient density of 14.8 kg/m^3 (42 bar). The quasi-steady lift-off lengths are shown as dashed vertical lines, along with estimates of $\overline{\phi}$ for each lift-off length (H), from Eq. 17.4.

As shown in Plate XV, left, the quasi-steady lift-off length increases with EGR, but the equivalence ratios at the lift-off length are virtually constant [59, 60, 68]. In other words, the lift-off length increases to compensate for decreasing in-cylinder oxygen concentration, thereby producing similar fuel–oxygen mixtures at the quasi-steady lift-off length. A similar compensating effect applies to the mixture composition at the time of ignition. For a jet at ignition, EGR increases the ignition delay and the time for mixing prior to reaction, but the reduction in oxygen concentration by EGR offsets the increased mixing time. Consequently, the equivalence ratio at ignition remains approximately constant [31]. The net result is that the stoichiometry of incipient soot-forming mixtures in the central core of the jet remains approximately the same, while in-cylinder oxygen concentration is decreased.

The colorbar of Plate XV shows that the peak soot f_v decreases substantially with decreasing oxygen concentration, in agreement with [59]. The soot formation and soot oxidation regions also move farther downstream from the injector. When the oxygen volume fraction is decreased to 8%, the soot f_v decreases to zero throughout the jet (within measurement uncertainty). Although it appears in Plate XV that the sooting region of the jet may have been pushed beyond the measurement volume, further experiments using both laser-induced incandescence of soot near the back wall of the vessel

and luminosity imaging of the entire vessel show that no soot formation is detectable anywhere in the vessel at the 8% O_2 condition [59].

Although the peak f_v decreases with increasing EGR, more important questions are whether the total mass of soot increases or decreases, and whether or not soot formed within the reacting jet escapes oxidation and becomes PM. For example, the 21% O_2 fuel jet appears to have efficient oxidation of soot formed upstream, such that little (if any) soot escapes oxidation at the downstream tip of the flame. To quantify the total mass of soot within the jet as a function of axial distance, the f_v data were integrated over the cross-section of the jet [59]. Soot mass at each axial position is shown for 1-mm 'slices' at the right of Plate XV. For a given in-cylinder oxygen concentration, the soot mass at first increases, then reaches a peak, and finally decreases with increasing axial distance. With decreasing ambient oxygen, the peak soot mass in the axial profile increases to a maximum at 15% O_2 and then decreases to zero at 8% O_2. Note that the soot mass is higher at 15% O_2 compared to 21% O_2, even though the peak f_v is lower, because the sooting region of the jet is wider (greater volume). As a result, the integrated mass is higher despite the generally lower f_v.

These direct measurements of *in-cylinder* soot mass in quasi-steady reacting sprays therefore show that the soot bump occurs at 15% O_2 for these conditions (Plate XV), compared to 10–12% O_2 for exhaust soot (Fig. 17.6). This difference in the location of the in-cylinder and exhaust soot bumps is largely due to differences in the extent of soot oxidation between the constant-volume chamber and an engine. In the quasi-steady reacting spray of Plate XV, the combustion event occurs at constant volume and only a small fraction of the oxygen available in the chamber is consumed by the single, reacting fuel jet (low global equivalence ratio). Consequently, ambient temperatures and pressures remain high, and excess oxygen is very available, so that soot oxidation may proceed to completion as oxygen is mixed into downstream regions of the jet. In an engine, less excess oxygen is available to mix into the reacting jet because of a smaller in-cylinder volume per jet, as well as interactions between neighboring fuel jets. The time available for soot oxidation is also limited by the piston motion. During the expansion stroke of an engine, the in-cylinder contents cool, and soot oxidation reactions slow. Furthermore, as the in-cylinder oxygen concentration is reduced, flame temperatures become lower, so that soot oxidation can be more readily quenched during the expansion stroke. Therefore, expansion should shift the in-cylinder soot bump to lower oxygen concentrations where soot oxidation is quenched. Indeed, one optical engine study with significant expansion after initial soot formation [29], the exhaust soot bump was near 10% O_2, consistent with the data in Fig. 17.6, but the in-cylinder soot bump was near 12% O_2, compared to 15% for the constant-volume combustion chamber [59].

Analysis from [57,59] shows that the cause of the *in-cylinder* soot bump for quasi-steady jets with sufficient time for complete soot oxidation is a tradeoff between residence time in soot-forming regions and the soot formation rates within those regions. The residence time increases with decreasing in-cylinder oxygen concentration because more in-cylinder gas must be mixed into the jet to reach a given equivalence ratio to complete combustion, requiring additional time to accomplish this mixing. On the other hand, decreasing in-cylinder oxygen concentration reduces combustion temperatures, which slows the rate of soot formation. The tradeoff between an increased residence *time* and a reduced *rate* of soot formation essentially determines the in-cylinder oxygen concentration for which the peak in-cylinder soot accumulation is maximum. At high ambient oxygen concentration, a high temperature promotes fast soot formation but rapid oxygen entrainment then quickly impedes soot formation and oxidizes the soot. For very low oxygen concentrations (8% O_2), the soot formation rate is so low that soot does not form despite long residence times. This is illustrated on the ϕ–T diagram of Fig. 17.4, where the 8% O_2 curve shows that the mixing and reaction path of the jet occurs at temperatures far to the left of the soot peninsula, and thus too low for soot formation [3, 62].

While the in-cylinder soot bump occurs at 15% O_2 for the conditions of Plate XV, variation in the in-cylinder pressure or temperature causes the soot bump to shift to different in-cylinder oxygen concentrations, because of temperature and pressure effects on soot formation and oxidation. Increases in temperature and pressure are known to significantly increase soot formation rates in lifted diesel flames [59, 61]. This change to the soot formation rate creates a different tradeoff between oxygen concentration effects on residence time and the increased rate of soot formation, as well as many of the exhaust soot-bump trends depicted in Fig. 17.6. For example, increases in compression ratio, engine load, or intake temperature, result in higher in-cylinder gas temperatures. The increased gas temperature, coupled with higher residence time at low oxygen concentration, causes more soot formation in fuel jets at lower in-cylinder oxygen concentration, thereby shifting the soot bump to lower in-cylinder oxygen concentration [59]. Once again, this shift in *in-cylinder* soot formation is consistent with *exhaust* soot trends for the soot bump shown in Fig. 17.6.

17.5 Closing remarks on low-temperature combustion (LTC) diesel research needs

Current optical diagnostic data have revealed that LTC-jet in-cylinder processes, which are responsible for the performance and emissions of LTC strategies, are significantly different than those of conventional diesel jets. Accordingly, the current understanding of conventional diesel combustion

must be extended and updated to include LTC operating conditions, thereby aiding the development of LTC strategies. The existing conceptual models for conventional diesel combustion have proven very useful, not only as foundations of understanding, but also as springboards for research and development concepts and bases for computer modeling efforts. Extensions of these conceptual models to LTC conditions will promote further development and refinement of LTC strategies. As described in this chapter, many aspects of in-cylinder LTC phenomena have been revealed by optical diagnostic techniques, but further research is still required to fill in missing details needed for the model extensions.

One critical need for further research is improved understanding of mixing processes that occur during the ignition dwell between the end of injection and the start of combustion. Mixture preparation occurring during the ignition dwell, prior to combustion, is critical to the subsequent ignition, combustion, and pollutant formation processes of LTC engines. Although some of the important 'symptoms' of mixing during the ignition dwell have been revealed, the underlying fluid mechanical causes for rapid mixing occurring after the end of injection are not well understood. Another need is for better understanding of post-combustion mixing, including its effects on both formation and oxidation of soot, especially late in the engine cycle. Existing conceptual models describe much of the quasi-steady period of diesel jets, but late-cycle mixing processes have not been explored in as much detail. The reduced soot oxidation rates of diluted, LTC strategies emphasize the importance of late-cycle mixing and soot oxidation, especially at higher loads. Finally, various multiple-injection concepts have demonstrated significant improvements in performance and exhaust emissions for LTC engines. The role of interactions between multiple injections in mixture preparation prior to combustion, as well as in post-combustion mixing, has not been adequately explored by optical diagnostics. Additional insights into the important in-cylinder mechanisms of multiple-injection operating conditions are needed to support further conceptual model extensions to multiple injections for both conventional and LTC diesel combustion.

17.6 References

1 Ahmadi-Befrui B, Wiesler B, and Winklhofer E, 'The propagation of fuel sprays in a research diesel engine – a joint numerical and experimental analysis', *SAE Transactions*, 1991, 100 (3), No. 910181, 209–220.

2 Akagawa H, Miyamoto T, Harada A, Sasaki S, Shimazaki N, Hashizume T, and Tsujimura K, 'Approaches to solve problems of the premixed lean diesel combustion', *SAE Transactions*, 1999, 108 (3), No. 1999-01-0183, 120–132.

3 Akihama K, Takatori Y, Inagaki K, Sasaki S, and Dean A M, 'Mechanism of the smokeless rich diesel combustion by reducing temperature', *SAE Transactions*, 2001, 110 (3), No. 2001-01-0655, 648–662.

4 Alfuso S, Allocca L, Auriemma M, Caputo G, Corcione F E, Montanaro A, and Valentino G (2005), 'Analysis of a high pressure diesel spray at high pressure and temperature environment conditions', SAE paper 2005-01-1239.
5 Alriksson M and Denbratt I (2006), 'Low temperature combustion in a heavy duty diesel engine using high levels of EGR', SAE paper 2006-01-0075.
6 Alriksson M, Gjirja S, and Denbratt I (2007), 'The effect of charge air and fuel injection parameters on combustion with high levels of EGR in a HDDI single-cylinder diesel engine', SAE paper 2007-01-0914.
7 Arrègle J, Pastor J V, and Ruiz S (1999), 'The influence of injection parameters on diesel spray characteristics', SAE paper 1999-01-0200.
8 Assanis D, Najt P M, Dec J E, Eng J A, Asmus T N, and Zhao F, *Homogeneous Charge Compression Ignition (HCCI) Engines – Key Research and Development Issues*, Warrendale, PA, SAE, 2003.
9 Bae C, Yu J, Kang J, Kong J, and Lee K O (2002), 'Effect of nozzle geometry on the common-rail diesel spray', SAE paper 2002-01-1625.
10 Bergstrand P, Persson F, Forsth M, and Denbratt I, 'A study of the influence of nozzle orifice geometries on fuel evaporation using laser-induced exciplex fluorescence', *SAE Transactions*, 2003, 112 (4), No. 2003-01-1836, 1264–1275.
11 Bruneaux G, 'A study of soot cloud structure in high pressure single hole common rail diesel injection using multi-layered laser-induced incandescence', *5th International Symposium on Diagnostics and Modeling of Combustion in Internal Combustion Engines (Comodia)*, Nagoya, Japan, 2001, 622–630.
12 Cheng A S, Upatnieks A, and Mueller C J, 'Investigation of fuel effects on dilute, mixing-controlled combustion in an optical direct-injection diesel engine', *Energy & Fuels*, 2007, 21 (4), 1989–2002.
13 Coghe A, Araneo L, Brunello G, and Cossali G E, 'Experimental investigation of gas density effects on diesel spray penetration and entrainment', *SAE Transactions*, 1999, 108 (3), No. 1999-01-0525, 679–693.
14 Colban W F, Miles P C, and Oh S, 'Effect of intake pressure on emissions from an automotive diesel engine operating in low temperature combustion regimes', *SAE Transactions*, 2007, 116(4), No. 2007-01-4063, (4), 957–977.
15 Dec J E, 'A conceptual model of D.I. diesel combustion based on laser-sheet imaging', *SAE Transactions*, 1997, 106 (3), No. 970873, 1319–1348.
16 Dec J E and Canaan R E, 'PLIF imaging of NO formation in a DI diesel engine', SAE *Transactions*, 1998, 107(3) No. 980147, 176–204.
17 Dec J E and Coy E B, 'OH radical imaging in a DI diesel engine and the structure of the early diffusion flame', *SAE Transactions*, 1996, 105 (3), No. 960831, 1127–1148.
18 Dec J E and Espey C, 'Chemiluminescence imaging of autoignition in a D.I. diesel engine', *SAE Transactions*, 1998, 107 (3), No. 982685, 2230–2254.
19 Dec J E and Kelly-Zion P L (2000), 'The effects of injection riming and diluent addition on late-combustion soot burnout in a DI diesel engine based on simultaneous 2-D imaging of OH and soot', SAE paper 2000-01-0238.
20 Dec J E and Tree D R, 'Diffusion-flame/wall interactions in a heavy-duty DI diesel engine', *SAE Transactions*, 2001, 110 (3), No. 2001-01-1295, 1618–1634.
21 Desantes J M, Payri R, Salvador F J, and Soare V (2005), 'Study of the influence of geometrical and injection parameters on diesel sprays characteristics in isothermal conditions', SAE paper 2005-01-0913.
22 Espey C and Dec J E, 'The effect of TDC temperature and density on the liquid-

phase fuel penetration in a D.I. diesel engine', *SAE Transactions*, 1995, 104 (4), No. 952456, 1400–1416.
23 Espey C, Dec J E, Litzinger T A, and Santavicca D A, 'Planar laser Rayleigh scattering for quantitative vapor-fuel imaging in a diesel jet', *Combust. Flame*, 1997, 109, 65–86.
24 Genzale C L, Reitz R D, and Musculus M P B (2008), 'Effects of piston bowl geometry on mixture development and late-injection low-temperature combustion in a heavy-duty diesel engine', SAE paper 2008-01-1330.
25 Gupta S, Poola R, and Sekar R, 'Effect of injection parameters on diesel spray characteristics', *SAE Transactions*, 2000, 109 (3), No. 2000-01-1600, 1713–1718.
26 Hasegawa R and Yanagihara H, 'HCCI combustion in a DI diesel engine', *SAE Transactions*, 2003, 112 (3), No. 2003-01-0745, 1070–1077.
27 Higgins B and Siebers D, 'Measurement of the flame lift-off location on D.I. diesel sprays using OH chemiluminescence', *SAE Transactions,* 2001, 110 (3), No. 2001-01-0918, 739–753.
28 Hiroyasu H and Arai M, 'Structures of fuel sprays in diesel engines', *SAE Transactions*, 1990, 99 (3), No. 900475, 1050–1061.
29 Huestis E, Erickson P A, and Musculus M P B, 'In-cylinder and exhaust soot in low-temperature combustion using a wide-range of EGR in a heavy-duty diesel engine', *SAE Transactions*, 2007, 116, No. 2007-01-4017.
30 Idicheria C A and Pickett L M, 'Formaldehyde visualization near lift-off location in a diesel jet', *SAE Transactions*, 2006, 115 (4), No. 2006-01-3434, 683–695.
31 Idicheria C A and Pickett L M, 'Effect of EGR on diesel premixed-burn equivalence ratio', *Proc. Combust. Inst.,* 2007, 31, 2931–2938.
32 Kamimoto T and Bae M., 'High combustion temperature for the reduction of particulate in diesel engines', *SAE Transactions*, 1988, 97 (3), No. 880423, 692–701.
33 Kanda T, Hakozaki T, Uchimoto T, Hatano J, Kitayama N, and Sono H (2006), 'PCCI operation with fuel injection timing set close to TDC', SAE paper 2006-01-0920.
34 Kanda T, Hakozaki T, Uchimoto T, Hatano J, Kitayama N, and Sono H, 'PCCI operation with early injection of conventional diesel fuel', *SAE Transactions*, 2005, 114 (3), No. 2005-01-0378, 584–593.
35 Kashdan J T, Mendez S, and Bruneaux G, 'On the origin of unburned hydrocarbon emissions in a wall-guided, low NO_x diesel combustion system', *SAE Transactions,* 2007, 116(4), No. 2007-01-1836, 234–257.
36 Kennaird D A, Crua C, Lacoste J, Heikal M R, Gold M R, and Jackson N S (2002), 'In-cylinder penetration and break-up of diesel sprays using a common-rail injection system', SAE paper 2002-01-1626.
37 Kim T, Beckman M S, Farrell P V, and Ghandhi J B (2002), 'Evaporating spray concentration measurements from small and medium bore diesel injectors', SAE paper 2002-01-0219.
38 Kimura S, Aoki O, Kitahara Y, and Aiyoshizawa E, 'Ultra-clean combustion technology combining a low-temperature and premixed combustion concept for meeting future emission standards', *SAE Transactions*, 2001, 110 (4), No. 2001-01-0200, 239–248.
39 Kimura S, Aoki O, Ogawa H, Muranaka S, and Enomoto Y, 'New combustion concept for ultra-clean and high-efficiency small DI diesel engines', *SAE Transactions*, 1999, 108 (3), No. 1999-01-3681, 2128–2137.
40 Kitamura T, Ito T, Kitamura Y, Ueda M, Senda J, and Fujimoto H, 'Soot kinetic

modeling and empirical validation on smokeless diesel combustion with oxygenated fuels', *SAE Transactions*, 2003, 112 (4), No. 2003-01-1789, 945–963.
41 Kook S, Bae C, Miles P C, Choi D, and Pickett L M, 'The influence of charge dilution and injection timing on low-temperature diesel combustion and emissions', *SAE Transactions*, 2005, 114 (4), No. 2005-01-3837, 1575–1595.
42 Kook S, Pickett L M, Musculus M P B, and Gehmlich R K, 'Liquid-phase diesel spray penetration during end-of-injection transient', *7th International Conference on Modeling and Diagnostics for Advanced Engine Systems (Comodia)*, Sapporo, Japan, 2008 413–420.
43 Kosaka H, Aizawa T, and Kamimoto T, 'Two-dimensional imaging of ignition and soot formation processes in a diesel flame', *Int. J. Engine Res.*, 2005, 6 (1), 21–42.
44 Lachaux T and Musculus M P B, 'In-cylinder unburned hydrocarbon visualization during low-temperature compression-ignition engine combustion using formaldehyde PLIF', *Proc. Combust. Inst.*, 2007, 31, 2921–2929.
45 Ladommatos N, Abdelhalim S M, Zhao H, and Hu Z (1996), 'The dilution, chemical, and thermal effects of exhaust gas recirculation on diesel engine emissions – Part 1: Effect of reducing inlet charge oxygen', SAE paper 961165.
46 Li T, Okabe Y, Izumi H, Shudo T, and Ogawa H (2006), 'Dependence of ultra-high EGR low temperature diesel combustion on fuel properties', SAE paper 2006-01-3387.
47 Miles P C, Choi D, Pickett L M, Singh I P, and Henein N, 'Rate-limiting processes in late-injection, low-temperature diesel combustion regimes', Paper Presented at *Thermo- and Fluid-Dynamic Processes in Diesel Engines: THIESEL 2004*, Valencia, Spain, 2004.
48 Minato A, Tanaka T, and Nishimura T, 'Investigation of premixed lean diesel combustion with ultra high pressure injection', *SAE Transactions*, 2005, 114 (3), No. 2005-01-0914, 756–764.
49 Musculus M P B, 'Multiple simultaneous optical diagnostic imaging of early-injection low-temperature combustion in a heavy-duty diesel engine', *SAE Transactions*, 2006, 115 (3), No. 2006-01-0079, 83–110.
50 Musculus M P B, Lachaux T, Pickett L M, and Idicheria C A, 'End-of-injection over-mixing and unburned hydrocarbon emissions in low-temperature-combustion diesel engines', *SAE Transactions*, 2007, 116, No. 2007-01-0907.
51 Naber J D and Siebers D L, 'Effects of gas density and vaporization on penetration and dispersion of diesel sprays', *SAE Transactions*, 1996, 105 (3), No. 960034, 82–111.
52 Noehre C, Andersson M, Johansson B, and Hultqvist A (2006), 'Characterization of partially premixed combustion', SAE paper 2006-01-3412.
53 Ogawa H, Li T, Miyamoto N, Kido S, and Shimizu H, 'Dependence of ultra-high EGR and low temperature diesel combustion on fuel injection conditions and compression ratio', *SAE Transactions*, 2006, 115, No. 2006-01-3386.
54 Ogawa H, Miyamoto N, Shimizu H, and Kido S (2006), 'Characteristics of diesel combustion in low oxygen mixtures with ultra-high EGR', SAE paper 2006-01-1147.
55 Okude K, Mori K, Shiino S, and Moriya T, 'Premixed compression ignition (PCI) combustion for simultaneous reduction of NO_x and soot in diesel engine', *SAE Transactions,* 2004, 113 (4), No. 2004-01-1907, 1002–1013.
56 Parks J, Partridge B, and Whitcare S (2007), 'Rapid in situ measurement of fuel

dilution of oil in a diesel engine using laser-induced fluorescence spectroscopy', SAE paper 2007-01-4108.
57 Pickett L M, Caton J A, Musculus M P B, and Lutz A E, 'Evaluation of the equivalence ratio–temperature region of diesel soot precursor formation using a two-stage Lagrangian model', *Int. J. Engine Res.,* 2006, 7 , 349–370.
58 Pickett L M and Hoogterp L, 'Fundamental spray and combustion measurements of JP-8 at diesel conditions', SAE *Int. J. Commer. Veh.*, 2009, 1(1), No. 2008-01-1083, 108–118.
59 Pickett L M and Idicheria C A, 'Effects of ambient temperature and density on soot formation under high EGR conditions', paper presented at *Thermo- and Fluid-Dynamic Processes in Diesel Engines: THIESEL 2006*, Valencia, Spain, 2006.
60 Pickett L M and Idicheria C A, 'Soot formation in diesel combustion under high-EGR conditions', *SAE Transactions,* 2005, 114 (4), No. 2005-01-3834, 1559–1574.
61 Pickett L M and Siebers D L, 'Soot in diesel fuel jets: effects of ambient temperature, ambient density, and injection pressure', *Combust. Flame*, 2004, 138, 114–135.
62 Pickett L M and Siebers D L, 'Non-sooting, low flame temperature mixing-controlled DI diesel combustion', *SAE Transactions,* 2004, 113 (4), No. 2004-01-1399, 614–630.
63 Pickett L M and Siebers D L, 'Soot formation in diesel fuel jets near the lift-off length', *Int. J. Engine Res.,* 2006, 6, 103–130.
64 Pickett L M, Siebers D L, and Idicheria C A, 'Relationship between ignition processes and the lift-off length of diesel fuel jets', *SAE Transactions,* 2005, 114 (3), No. 2005-01-3843, 1714–1731.
65 Plee S L, Ahmad T, and Myers J P (1981), 'Flame temperature correlation for the effects of exhaust gas recirculation on diesel particulate and NO_x emissions', SAE Transactions, 1981, 90(4), No. 811195, 3738–3754.
66 Plee S L, Ahmad T, Myers J P, and Faeth G M, 'Diesel NOx emissions - a simple correlation technique for intake air effects', *Proc. Combust. Inst.*, 1982, 19, 1495–1502.
67 Ricou F P and Spalding D B, 'Measurements of entrainment by axisymmetrical turbulent jets', *J. Fluid Mech.*, 1961, 11 (1), 21–32.
68 Siebers D, Higgins B, and Pickett L, 'Flame lift-off on direct-injection diesel fuel jets: oxygen concentration effects', *SAE Transactions,* 2002, 111 (3), No. 2002-01-0890, 1490–1509.
69 Siebers D L, 'Liquid-phase fuel penetration in diesel sprays', *SAE Transactions,* 1998, 107 (3), No. 980809, 1205–1227.
70 Siebers D L, 'Scaling liquid-phase fuel penetration in diesel sprays based on mixing-limited vaporization', *SAE Transactions*, 1999, 108 (3), No. 1999-01-0528, 703–728.
71 Siebers D L and Higgins B S, 'Flame lift-off on direct-injection diesel sprays under quiescent conditions', *SAE Transactions*, 2001, 110 (3), No. 2001-01-0530, 400–421.
72 Singh S S, Reitz R D, Musculus M P, and Lachaux T, 'Validation of engine combustion models using detailed in-cylinder optical diagnostics data for a heavy-duty compression-ignition engine', *Int. J. Engine Res.*, 2006, 8 (1), 97–126.
73 Su T F, Farrell P V, and Nagarajan R T, 'Nozzle effect on high pressure diesel injection', *SAE Transactions*, 1995, 103 (3), No. 950083, 177–188.
74 Takeda Y, Keiichi N, and Keiichi N., 'Emission characteristics of premixed lean

diesel combustion with extremely early staged fuel injection', *SAE Transactions*, 1996, 105 (4), No. 961163, 938–947.

75 Taschek M, Koch P, Egermann J, and Leipertz A (2005), 'Simultaneous optical diagnostics of HSDI diesel combustion processes', SAE paper 2005-01-3845.

76 Upatnieks A and Mueller C J (2004), 'Investigation of the relationship between DI diesel combustion processes and engine-out soot using an oxygenated fuel', SAE paper 2004-01-1400.

77 Upatnieks A, Mueller C J, and Martin G C, 'The influence of charge-gas dilution and temperature on DI diesel combustion processes using a short-ignition-delay, oxygenated fuel', *SAE Transactions*, 2005, 114 (4), No. 2005-01-2088.

78 Wahlin F and Cronhjort A (2004), 'Fuel sprays for premixed compression ignited combustion – characteristics of impinging sprays', SAE paper 2004-01-1776.

79 Wakuri Y F M, Amitani T, and Tsuneya R, 'Studies of the penetration of fuel spray in a diesel engine', *Bulletin of JSME*, 1960, 3 (9).

80 Walter B and Gatellier B, 'Development of the high power NADI concept using dual mode diesel combustion to achieve zero NO_x and particulate emissions', *SAE Transactions*, 2002, 111 (4), No. 2002-01-1744, 779–787.

81 Westbrook C K, 'Chemical kinetics of hydrocarbon ignition in practical combustion systems', *Proc. Combust. Inst.*, 2000, 28, 1563–1577.

82 Yanagihara H, Satou Y, and Mizuta J, A simultaneous reduction of NO_x and soot in diesel engines under a new combustion system (uniform bulky combustion system – UNIBUS), *17th International Vienna Motor Symposium*, Vienna, Austria, 1996.

83 Yang B and Ghandhi J (2007), 'Measurement of diesel spray impingement and fuel film characteristics using refractive index matching method', SAE paper 2007-01-0485.

84 Zhao H and Ladommatos N, 'Optical diagnostics for soot and temperature measurement in diesel engines', *Prog. Energy Combust. Sci.,* 1998, 24 , 221–255.

18

Advanced computational fluid dynamics modeling of direct injection engines

R. D. REITZ, University of Wisconsin-Madison, and
Y. SUN, General Motors Company, USA

Abstract: Multi-dimensional computational fluid dynamics (CFD) is an effective and well-accepted method in engine research, design and development. The focus of this chapter is on engine CFD modeling of in-cylinder phenomena. This chapter reviews various engine CFD models and their application to the research and development of direct injection (DI) engines. These models include turbulence, spray, combustion, emission and other related models and their sub-models.

Key words: computational fluid dynamics (CFD), modeling, direct injection (DI) engine, combustion and emission, numerical simulation.

18.1 Introduction

With the rapid increase of computer processor speed and with continuous improvements to engine numerical models and numerical methods, multi-dimensional computational fluid dynamics (CFD) has become a well-accepted tool in engine research, design and development since its initiation in the late 1970s. It is being used more and more widely in both the automotive industry and academia. In this chapter, the focus is on engine CFD modeling of in-cylinder phenomena. Engine CFD models and their application to the research and development of direct injection (DI) engines are reviewed. The current status and future trends in the field are also discussed.

First, the basic approaches used in engine CFD modeling of DI engines are reviewed.

This is followed by reviews of various currently used models in engine CFD simulations, including turbulence, spray, combustion, emission and other related models. In each category, sub-models which are actively used in engine CFD simulations are reviewed and their application range, advantages and disadvantages are discussed and compared. Instead of giving complete details of each model, the basic ideas are outlined and references to the relevant literature for each model are given. The main emphasis is on combustion models in this chapter. Following this, the most prevalent CFD codes used for engine simulation and their features are introduced and compared. Finally, previous applications of engine CFD modeling, its

current status, and some of the challenges to be faced and future trends are discussed.

18.2 Basic approach

For CFD simulations in DI engine applications the flows can be divided into different categories based on relevant criteria, including two- and three-dimensional flows, single and multi-component flows, single and multi-phase flows, laminar and turbulent flows, compressible and incompressible flows, chemically reactive and non-reactive flows, transient and steady-state flows, and subsonic and supersonic flows.

For example, flows in water jackets, intake manifolds, intake ports, and EGR coolers are single phase, non-reactive flows. Modeling these flows is relatively easy. However, flows in engine cylinders, exhaust ports, exhaust pipes, and aftertreatment devices are usually multi-phase, reactive flows. Modeling these flows requires more complicated numerical models to describe the corresponding physical and chemical processes. The focus of this chapter will be on the latter, in particular modeling the physical and chemical processes in engine cylinders.

In-cylinder flows in IC engines are multi-dimensional, multi-phase, multi-component, turbulent, compressible, reactive flows. The basic governing equations for the fluid are the continuity (mass conservation), momentum (Navier–Stokes equations), energy, and turbulence (normally the k–ε equations) equations, and equations of state (ideal gas law). Assumptions include the use of the ideal gas law, Fick's law of mass diffusion, and others, depending on the details of the model.

Although either Eulerian–Eulerian or Eulerian–Lagrangian (i.e., discrete droplet/particle) methods for the gas–liquid flows, respectively, can be used to solve two-phase flow problems, the Eulerian–Lagrangian approach has been used in most engine CFD simulations. In the Eulerian–Lagrangian approach, the gas phase is treated as continuous and the Eulerian formulation is used to describe the gas phase flow. The liquid phase is treated as consisting of discrete particles and described using the Lagrangian approach, in which liquid droplets are represented as assemblages of particles using the discrete particle method (Dukowicz, 1980). The Lagrangian description of particles avoids numerical diffusion, and allows individual attributes, such as particle size, velocity, position, etc., to be statistically assigned to each particle. Mass, momentum and heat transfer between the gas and liquid phases is accounted for by using source terms.

The governing equations of the Eulerian gas phase are partial differential equations (PDEs). Various numerical methods, such as finite volume, finite difference, and finite element methods, can be used to derive numerical solutions of the PDEs. Finite volume, finite difference and finite element

methods all use a finite-difference mesh or grid to subdivide the computational region into a number of small cells to approximate a continuum problem domain.

Most CFD codes for IC engine simulations employ the finite volume method due to its inherently conservative nature. Irrespective of the errors introduced through various approximations, the discretized equations strictly fulfill global conservation laws. The finite volume method applies the integral form of the governing equations, involving surface integrals (fluxes) and volume integrals (sources and sinks). Rather than using pointwise approximations on a grid, the finite volume method approximates the average integral value on a control volume. This method is also easier to understand than other methods, which are more mathematically involved, because all the terms have clear physical meanings (e.g., flux, force, source, sink, etc.).

Finite-difference approximations to the governing equations are solved in CFD simulations. The equations are discretized in both space and time. Usually, implicit differencing schemes are used to permit large numerical timesteps. Temporal differencing is performed with respect to a sequence of discrete times. Spatial differencing is usually performed by integrating the differential terms in the equations over a control volume (i.e., a computational cell), which largely preserves the local conservation properties of the differential equations.

The in-cylinder dynamics of advanced DI engines involve both complicated physical and chemical processes. Based on the basic approaches described above, numerous engine-related numerical models, which describe the turbulent flow, injection, spray, fuel/air mixing, ignition, combustion, pollutant formation and heat transfer processes in engines, have been developed and used in engine simulations. These models are described next.

18.3 Turbulence modeling

The in-cylinder flows in IC engines are turbulent compressible flows. Many turbulence models with different levels of complexity have been proposed to simulate turbulent flows.

Reynolds Averaged Navier–Stokes (RANS) models are the most prevalent turbulence models in engine applications. RANS models, specifically, the k–ε model and its variants, have been used in engine simulations since CFD was first applied to the engine field. In this case, k is the turbulent kinetic energy and ε is its dissipation rate.

Initially, the standard k–ε model was used in engine simulations with a source term $-\left(\frac{2}{3}C_1 - C_3\right)\rho\varepsilon\nabla\cdot\mathbf{u}$ in the ε equation (see Eq. 18.2 below) to account for length scale changes with velocity dilation, $\nabla\cdot u$, and spray-induced source terms ($\dot{W}^s$) in both the k and ε equations.

Following this, an improved k–ε model, which is based on the re-normalized group (RNG) theory, was first proposed by Yakhot and Orszag (1986). The k equation in the RNG version is the same as in the standard version, but the ε equation is based on a more rigorous mathematical derivation instead of using empirical constants. The RNG k–ε equations are written as:

$$\frac{\partial \rho k}{\partial t} + \nabla \cdot (\rho \mathbf{u} k) = -\frac{2}{3}\rho k \nabla \cdot \mathbf{u} + \tau : \nabla \cdot [\alpha_k \mu \nabla k] - \rho\varepsilon + \dot{W}^s \tag{18.1}$$

$$\begin{aligned}\frac{\partial \rho \varepsilon}{\partial t} &+ \nabla \cdot (\rho \mathbf{u} \varepsilon) \\ &= -\left(\frac{2}{3}C_1 - C_3 + \frac{2}{3}C_\mu C_\eta \frac{k}{\varepsilon}\nabla \cdot \mathbf{u}\right)\rho\varepsilon \nabla \cdot \mathbf{u} + \nabla \cdot [\alpha_\varepsilon \mu \nabla \varepsilon] \\ &+ \frac{\varepsilon}{k}[(C_1 - C_\eta)\ \tau : \nabla \mathbf{u} - C_2 \rho\varepsilon + C_s \dot{W}^s]\end{aligned} \tag{18.2}$$

where τ is the stress tensor and μ is the dynamic viscosity, and α's and C's are model constants.

Han and Reitz (1995) modified the constant C_3 in the RNG k–ε model to take the compressibility effect into account. In their modified RNG k–ε model,

$$C_3 = \frac{-1 + 2C_1 - 3m(n-1) + (-1)^\delta \sqrt{6} C_\mu C_\eta \eta}{3} \tag{18.3}$$

where η is a ratio of turbulence and mean flow time scales, m and n are related gas properties, and C_μ and C_η are constants.

Other details of the modified RNG k–ε turbulence model were given by Han and Reitz (1995), who applied their modified RNG k–ε model to engine simulations and observed improvements in the results compared to the standard k–ε model. It was shown that this model could predict more realistic large-scale flame structures compared with the standard k–ε model. These structures influenced in-cylinder temperature predictions and the modified model was able to quantitatively improve NO_x emission predictions for single-injection combustion cases (Kong *et al.*, 1995).

Large eddy simulation (LES) is a numerical technique for simulating turbulent flows first introduced by Smagorinsky (1963). LES has attracted more and more attention and interest recently. Kolmogorov's theory of self-similarity implies that the large eddies of a turbulent flow are dependent on the device geometry, while smaller eddies are self-similar and have a universal character. Therefore, the basic idea of LES is to solve only for large-scale eddies (i.e., those that can be resolved on the computational mesh) explicitly and to model the more universal small-scale (sub-grid scale) eddies on large meshes through the use of a sub-grid scale (SGS) model. In contrast, in RANS all fluctuations about the local mean are modeled. Therefore, LES

has advantages over RANS in terms of predicting the instantaneous flow characteristics and resolving detailed turbulent flow structures, such as cycle-to-cycle variations in IC engines, as well as the mean flow solution. To capture important dynamic features, LES usually requires a very fine mesh because large cells such as those allowed in RANS simulations would dampen the unsteadiness. Therefore, LES is more computationally expensive than RANS. This is the major reason that has prevented LES from being widely used in engine simulations at this time. However, new LES models such as the dynamic similarity model (Hu *et al*., 2007) have been proposed that give promising results on coarse meshes, too.

Other more complex models are available and can also be used to simulate turbulent engine flows, such as the Reynolds stress model (RSM) (Launder *et al*., 1975). However, RSM does not show apparent advantages over RANS in terms of accuracy and efficiency in engine applications.

Naturally, the direct numerical simulation (DNS) of turbulence is the most satisfying approach to the solution of turbulent flows. In DNS, the Navier-Stokes equations are numerically solved without recourse to any turbulence model, which means that the whole range of spatial and temporal scales of the turbulence must be resolved in the computational mesh. Thus, DNS requires even more computational resources than LES and will likely not be feasible for any realistic engine applications in the foreseeable future.

18.4 Spray modeling

Spray models are very important in engine CFD simulations because they influence the subsequent mixing, ignition, combustion and emission predictions. Spray models include those describing the flows inside injector nozzles (nozzle flow model), atomization of the continuous liquid after the fuel leaves the injector nozzle (primary breakup model), breakup of the formed liquid drops (secondary breakup model), momentum exchange between the liquid and gas phases (i.e., the drag force that liquid droplets experience and the deformation of the droplets), collision between liquid drops and its possible outcomes (collision model), interaction between sprays and walls (e.g., wall–film model), and evaporation of the liquid fuel (evaporation model). Spray modeling is discussed in more detail by Abani *et al*. (2008).

18.5 Combustion modeling

Various combustion models have been developed to simulate a wide variety of combustion phenomena in both spark-ignited (SI) and compression-ignited (CI) engines, including spark and auto ignition, laminar and turbulent combustion, premixed, non-premixed and stratified-charge combustion, kinetics and mixing-controlled combustion, and flame propagation combustion.

For SI engines, the main task of combustion modeling is to describe the spark ignition, flame kernel growth and flame propagation processes. For CI engines, combustion modeling also must resolve two steps: low-temperature chemistry which leads to auto ignition, and the following high-temperature reactions which contribute most of the heat release. Models describing both the ignition and the following combustion processes are reviewed below.

18.5.1 Ignition models

There are two types of ignition processes of interest in DI engines: spark ignition and auto ignition.

Spark ignition

In SI engines, the flame front is initiated by the electrical discharge of the spark plug. Since the typical length and time scales in engine CFD models are usually much larger than those of the developing flame kernels during spark ignition processes, it is not quite feasible to resolve ignition details in engine CFD calculations and a phenomenological description is often used in engine simulations.

Spark ignition can be simulated simply by adding energy to the ignition cells empirically over the spark duration. Other models accounting for different levels of physics can also be used, such as the discrete particle ignition kernel (DPIK) model developed by Fan *et al*. (1999) and later improved by Tan and Reitz (2003). In the DPIK model, the flame kernel is assumed to be spherical during the spark period and marked by many particles suspended in the computational domain. This allows a precise tracking of the growth of the ignition kernel without the need to have a very fine mesh near the spark plug.

Auto ignition

Auto ignition is sensitive to the chemical properties of the fuel and oxidizer and is present in different forms, such as knock in SI (e.g., conventional gasoline) engines and compression ignition in CI (e.g., conventional diesel) engines. The auto ignition processes can be described either by a simple model or by using detailed chemical kinetics mechanisms, which will be discussed later.

The multi-step 'Shell' ignition model (Halstead *et al*., 1977) was developed to predict the auto ignition of hydrocarbon fuels using a simplified reaction mechanism. The premise of the Shell model is that degenerate branching plays an important role in determining the cool flame and two-stage ignition phenomena that are observed during the auto ignition of hydrocarbon fuels.

It was first implemented in the KIVA CFD code and applied in engine simulations by Kong and Reitz (1993). It has been used widely in predicting auto ignition in CI engines.

The Shell model consists of five generic species and eight generic reactions, which represent the initiation, propagation, branching, and termination steps. The five generic species include fuel (RH), oxygen (O_2), radicals (R^*), branching agents (B) and intermediate species (Q). The reactions and species involved in the ignition model are as follows:

$RH + O_2$	$\xrightarrow{K_q}$	2R*	initiation	(a)	
R*	$\xrightarrow{K_p}$	R* + P + heat	propagation cycle	(b)	
R*	$\xrightarrow{f_1 K_p}$	R* + B	propagation forming B	(c)	
R*	$\xrightarrow{f_4 K_p}$	R* + Q	propagation forming Q	(d)	18.4
R* + Q	$\xrightarrow{f_2 K_p}$	R* + B	propagation forming B	(e)	
B	$\xrightarrow{K_b}$	2R*	degenerate branching	(f)	
R*	$\xrightarrow{f_3 K_p}$	termination	linear termination	(g)	
2R	$\xrightarrow{K_t}$	termination	quadratic termination	(h)	

where P represents the oxidized products including CO, CO_2 and H_2O. The original reaction rate constants are given by Halstead *et al*. (1977). However, it has been shown that the ignition delay time is largely controlled by reaction 18.4(d), and its rate constant is often 'tuned' to match experimental data (e.g., Hamosfakidis and Reitz, 2003).

The ignition model is used only for the low-temperature chemistry. After ignition (i.e., when the local gas temperature is greater than ~1000 K), the combustion models described below take over and simulate the subsequent second-stage high-temperature combustion.

18.5.2 Combustion models

Since combustion in DI engines is turbulent, this section is focused on turbulent combustion models. Many turbulent combustion models with different levels of complexity have been proposed for engine applications, including models based on RANS and LES turbulence models. However, since RANS models, specifically the k–ε model and its variants, are the most commonly used turbulence models at present, this section emphasizes combustion models based on the k–ε model.

In general, there are two ways to describe the combustion process in engine cylinders. One is to use a combustion sub-model to describe the overall

combustion characteristics (i.e., flame propagation, reaction rates, and so on) of a combustion process. Combustion models such as mixing-controlled combustion models, flamelet models, and probability density function (PDF) models belong to this category. The other way is to use a detailed reaction mechanism which describes the complex reaction pathways and reaction rates of the important chemical reactions involved in the combustion process and solve for the rate of change of each species in the mechanism. Both methods are discussed below.

Before describing the models, two variables which are used in these models are introduced. The first is the mixture fraction (Z) and the second is the reaction progress variable (c). The mixture fraction quantifies the local mass fraction of materials that originate from the reactant fuel. It is mostly used in the analysis and modeling of non-premixed reacting systems. For premixed combustion systems, a reaction progress variable is used. The progress variable increases from zero in the unburned reactants to unity in the burned products. The calculation of the progress variable can be associated with either the mass fraction of a specific species (combustion products) or temperature.

Arrhenius model

The simplest Arrhenius model assumes a one-step global reaction for conversion of the reactants to the products. The mean chemical reaction rates take the Arrhenius form. Since this model neglects the effects of complex reaction paths and turbulence on the mean chemical reaction rates, it is not surprising that the model can only be used over a narrow range of operating conditions under which the model constants are calibrated against experiments.

Turbulent mixing-controlled models

The underlying premise of turbulent mixing-controlled combustion models is that the burn rate of the mixture is mainly determined by the turbulent mixing rate, instead of by the rate of chemical reactions. In some engine applications, such as diffusion combustion in conventional diesel engines, turbulent mixing occurs relatively slowly compared to chemical reactions (high Damköhler number). In such cases, it is reasonable to expect that turbulent transport of species and enthalpy will be the controlling factor.

For premixed turbulent combustion, the eddy breakup (EBU) model suggested by Spalding (1971) is the first model in this group, where the burnt and unburned gases are assumed to be located in different eddies, and the mean chemical conversion rate is controlled by the eddy's dissipation rate and the fluctuations of the fuel mass fraction or progress variable. In the EBU model, the reaction rate can be expressed as

$$\dot{\bar{\omega}}_{\mathrm{F}} = C_{\mathrm{EBU}}\bar{\rho}(\widetilde{Y_{\mathrm{F}}''^2})^{1/2}/\tau_{\mathrm{t}} \tag{18.5}$$

where $\widetilde{Y_{\mathrm{F}}''^2}$ is the fluctuation of the fuel mass fraction and C_{EBU} is a model constant. When the k–ε turbulence model or its variants are used, the eddy breakup time $\tau_{\mathrm{t}} \propto k/\varepsilon$.

For non-premixed turbulent combustion, Magnussen and Hjertager (1976) modified the EBU model and introduced the modified eddy-dissipation model (EDM). In the EDM model, they suggested that the combustion rate is limited by the deficient species (fuel, oxidizer, or product depending on whether the mixture is lean or rich or on the progress of reaction) instead of fuel. In this model, the fuel burn rate takes the form:

$$\dot{\bar{\omega}}_{\mathrm{F}} = \overline{A\rho}\min\left(\widetilde{Y_{\mathrm{F}}}, \frac{\widetilde{Y_{\mathrm{F}}}}{r}, B\,\frac{\widetilde{Y_{\mathrm{P}}}}{1+r}\right)\Big/\tau_{\mathrm{t}} \tag{18.6}$$

where A and B are model constants, and r is the stoichiometric oxidizer/fuel ratio.

Hybrid models

Hybrid EBU/Arrhenius models have also been proposed. For example, as an extension of the EBU model, Reitz and Bracco (1982) proposed a laminar-and-turbulent characteristic-timescale combustion (CTC) model, which was applied to engine combustion by Abraham *et al*. (1985). The model used the k–ε model for turbulent transport and assumed that the characteristic timescale (τ_{c}) at which all the chemical species approach their equilibrium (indicated by * in Eq. 18.7 below), is the sum of a turbulence characteristic time (τ_{t}) and a laminar or chemical characteristic time (τ_{l}) of Arrhenius form. The rate change of the concentration of species i is given as (Kong *et al*., 1995):

$$\frac{\mathrm{d}Y_i}{\mathrm{d}t} = -\frac{Y_i - Y_t^*}{\tau_{\mathrm{c}}} \tag{18.7}$$

The CTC model has been successfully used to model both premixed (Abraham *et al*., 1985) and non-premixed (Kong *et al*., 1995) turbulent combustion.

In contrast to the Arrhenius model, turbulence mixing-controlled models take the effects of turbulence on combustion into account. However, these models are inadequate under engine operating conditions with low Damköhler number, for example, in low-temperature combustion (LTC) of premixed lean mixtures where chemical kinetics effects dominate, such as homogeneous charge compression ignition (HCCI) engines.

Flamelet models

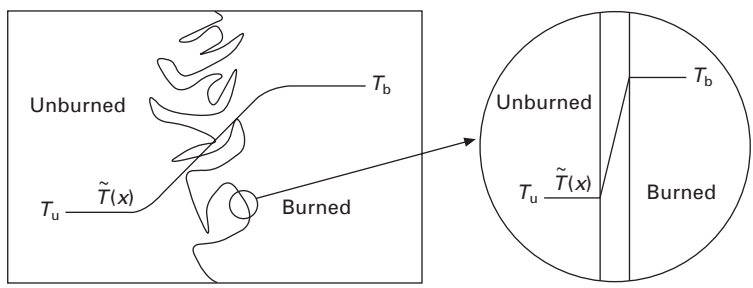
Flamelet models have been developed for both premixed and non-premixed combustion regimes. For premixed combustion with flame propagation, the models are based on tracking a flame front interface defined either by a combustion progress variable, c, or by a non-reacting scalar, G, which divides the flow into burned and unburned portions (Peters, 2000). For non-premixed combustion, the mixture fraction Z is used to determine the dominant effect of turbulent mixing on combustion.

For premixed combustion with flame propagation, such as the combustion of stoichiometric mixtures in conventional SI engines, the premise of flamelet models is that locally, the structure of a turbulent flame is that of a laminar flame subject to the same aero-thermo-chemical conditions. The principal effect of turbulence on combustion is to increase the effective flame surface area, as described by Haworth (2005). A schematic diagram of a turbulent premixed flame is shown in Fig. 18.1.

The Bray–Moss–Libby (BML) model (Bray and Libby 1994) and the coherent flame model (CFM) (Marble and Broadwell 1977) are based on a progress variable, c, which is viewed either as a normalized temperature or as a normalized product mass fraction. These models assume a single-step reaction from unburned reactants to burned products and an infinitely thin flame structure. In the BML model, a PDF of the progress variable is assumed to be a two-delta function distribution. The Favre averaged progress variable is tracked by solving a transport equation.

In a flamelet model the overall burn rate is expressed as the product of the fuel burn rate per unit flame area and the active flame area per unit volume. Therefore, the local mean fuel burning rate can be expressed as the product of the unburned gas density ρ_u, the mass fraction of fuel in the mixture $\tilde{y}_{FR}$, the local laminar flame speed S_L, and the flame surface density (flame surface area per unit volume) Σ:

$$\dot{\bar{\omega}}_F = \rho_u \widetilde{Y_{FR}} S_L \Sigma \qquad 18.8$$



18.1 Flame propagation of a turbulent premixed combustion flame.

The laminar flame speed, S_L, can be computed or stored in a table for use in a CFD program as a function of pressure, temperature, equivalence ratio and strain rate.

Two methods have been proposed for solving for the flame surface density. One approach is to use an algebraic model, such as the one suggested by Bray and Libby (1994). The other more complete approach is to solve a modeled transport equation for Σ. Several modeling strategies have been proposed and these models are called coherent flame models. For example, Trouvé and Poinsot (1994) proposed a formulation based on DNS data.

Flamelet modeling permits chemical kinetics and turbulence to be decoupled while maintaining tight local coupling between chemical kinetics and molecular transport (Haworth, 2005). In cases where flamelet combustion does occur (e.g., flame propagation in a stoichiometric premixed SI engine), flamelet models have been highly successful. Boudier *et al*. (1992) implemented a version of the CFM into a CFD code and validated the model by comparing simulation results with in-cylinder flame front contours in an experimental SI engine.

Recently, flamelet models for flame propagation in premixed combustion systems based on a level set method (Sethian, 1999) are receiving growing attention. The level set method is a numerical technique for tracking interfaces and shapes. With application to combustion, Williams (1985) first suggested a transport equation of a non-reactive scalar, $G(x, t)$, for laminar flame propagation, and this approach is known as the 'G-equation' method in the combustion literature.

The G-equation method is based on the postulate that flame propagation is driven by the bulk fluid velocity, u, of the unburned mixture ahead of the flame front, and the laminar flame speed S_L along the normal direction to the flame, n. Thus, the rate of change of flame position x_f, i.e., the flame propagation velocity, can be written as:

$$\frac{\mathrm{d}x_\mathrm{f}}{\mathrm{d}t} = u + nS_\mathrm{L} \tag{18.9}$$

The flame front is defined by a $G(x, t) = G_0$ iso-surface with G_0 taking an arbitrary but fixed value (normally zero). The normal vector n is defined as

$$n = \frac{\nabla G}{|\nabla G|} = -\frac{\nabla G}{[(\nabla G)^2]^{1/2}} \tag{18.10}$$

and the transport equation for G can be derived by differentiating $G(x, t) = G_0$ with respect to t, as

$$\rho\left(\frac{\partial G}{\partial t} + \mathrm{u} \cdot \nabla G\right) (\rho S_\mathrm{L}) |\nabla G| \tag{18.11}$$

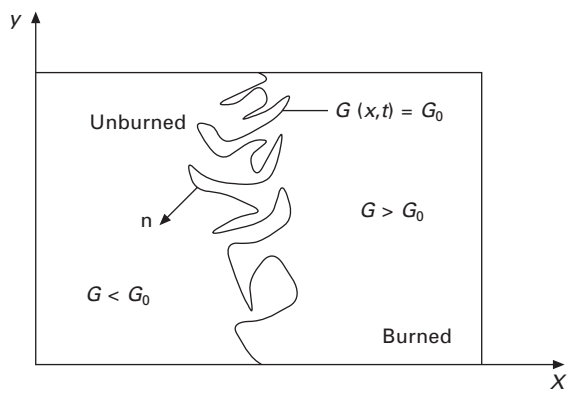
Peters (2000) extended the above equation to turbulent flame regime as

$$\rho\frac{\partial G}{\partial t} + \rho \mathbf{u}\cdot\nabla G = (\rho S_{\mathrm{L}}^{0})\,|\nabla G| - \underbrace{(\rho D_{\mathrm{L}})\kappa\,|\nabla G|}_{\text{flame curvature}} - \underbrace{(\rho L)S\,|\nabla G|}_{\text{strain rate}} \qquad 18.12$$

In his method, the thin turbulent flame front represented by the $G(x, t) = G_0$ iso-surface divides the domain into an unburned region where $G < G_0$, and a burnt region where $G > G_0$, as shown in Fig. 18.2. The turbulent flame front is regarded as an ensemble of local laminar flamelets with considerations of flame stretch effects on the flame speed.

The turbulent G-equation concept has been successfully applied to combustion simulations for SI engines by Dekena and Peters (1999), Tan and Reitz (2003, 2004), Ewald and Peters (2005), and Liang and Reitz (2006). Interestingly, Tan and Reitz (2004) have shown that the G-equation model can also be applied to non-premixed combustion, since in this case the only change is that $S_L = 0$ in Eq. 18.9. This extension forms the basis of Tan and Reitz's so-called GAMUT (G Equation for All Mixtures a Universal Turbulent) combustion model.

For non-premixed (or partially premixed) combustion, such as turbulent diffusion combustion in conventional CI engines, another approach is the representative interactive flamelet (RIF) model. The basic idea of RIF models originates from the flamelet model for turbulent diffusion flames, such as those in counterflow (also called opposed jet) burners and candle flames. The flamelet concept is based on the assumption that the smallest turbulent time and length scales are much larger than the chemical ones, and that there exists a locally undisturbed sheet where the chemical reaction occurs and the reaction zone cannot be intruded by turbulent eddies (Pitsch *et al.*, 1996). This sheet can be treated as an ensemble of counterflow diffusion flames, called flamelets.



18.2 Application of the G-equation to premixed turbulent flames.

The composition, Y_i (mass fraction of each species), is assumed to be dependent only on the mixture fraction Z. Therefore, only the transport equations of the mean and variance of the mixture fraction ($\widetilde{Z}$, $\widetilde{Z''^2}$) are solved, instead of having to solve the transport equations of each species. The composition Y_i as a function of Z is given by laminar flamelet calculations which use detailed fuel chemistry. The flamelet equation for each species is given as

$$\frac{\partial Y_i}{\partial t} = \frac{\chi}{2}\left(\frac{\partial^2 Y_i}{\partial Z^2}\right) + \frac{\dot{\omega}_i W_i}{\rho} \qquad 18.13$$

where χ is the scalar dissipation rate. The scalar dissipation rate is a crucial parameter in flamelet modeling to account for strain effects and has been introduced as:

$$\chi = 2D\left(\frac{\partial Z}{\partial x}\right)^2 \qquad 18.14$$

Note that the diffusivity D is typically taken as the turbulent diffusivity and, thus, Eq. 18.13 can be seen to combine turbulent (first term on right-hand side) and chemistry (second term) timescales, similar to the CTC model. However, a single 'representative' turbulence timescale is used for the entire domain in the RIF model, which limits its accuracy, as discussed by Singh *et al*. (2006).

In simulations the CFD code provides the values of the necessary variables to the flamelet code for solving the flamelet equations, and the species mass fractions obtained from the flamelet code are passed back to the CFD code.

To account for the effects of turbulent fluctuation, a presumed PDF for Z can be used. The PDF is usually a beta PDF, which has two varying parameters determined from the mean and variance of Z ($\widetilde{Z}$, $\widetilde{Z''^2}$). The mean composition is then computed by integrating Z from 0 to 1 with the presumed PDF, $P(Z, (\widetilde{Z}, \widetilde{Z''^2})$:

$$\tilde{Y}_i(\vec{x}) = \int_0^1 P(Z, \tilde{Z}, \widetilde{Z''^2}) Y_i(Z)\mathrm{d}Z \qquad 18.15$$

In the original single flamelet approach (Pitsch *et al*., 1996), the entire domain was represented by one flamelet. Hence, the scalar dissipation rate at stoichiometric mixture χ_{st} is defined as a domain-averaged value rather than being spatially resolved. However, in improved flamelet models for turbulent diffusion flames, the composition Y_i can be computed as a function of both Z and χ, and a global value for the scalar dissipation rate is not assumed. Instead, it must be computed from the local properties of each computational cell. Advanced flamelet models also consider the fluctuation of the dissipation rate, which is usually modeled using a log-normal PDF.

The integration for the mean composition then becomes:

$$\tilde{Y}_i(\vec{x}) = \int_0^x \int_0^1 P(Z)P(\chi)Y_i(Z, \chi)\,\mathrm{d}Z\mathrm{d}\chi \qquad 18.16$$

To apply flamelet models to liquid spray combustion, the effects of liquid vaporization on small-scale turbulent mixing and turbulent combustion should also be considered, such as in the model proposed by Demoulin and Borghi (2000).

Probability density function (PDF) models

PDF models can be used for both premixed and non-premixed turbulent combustion modeling. Other turbulent combustion models also employ the PDF method as discussed above, which normally use a presumed PDF. However, PDF models distinguish themselves from the previous models by determining the PDF by solving its transport equation, instead of specifying a presumed PDF. In PDF models, PDF transport equations for velocity and reactive scalars are solved, usually by using Lagrangian Monte Carlo particle-based methods (Pope, 1985).

A mean chemical source term $\overline{Q}$ can be defined based on a joint PDF of the velocity $u(x, t)$ and the composition variables $\psi(x, t)$ (or a PDF of only the composition variables $\psi(x, t)$):

$$\overline{Q} = \iint Q(V, \psi) f(V, \psi; x, t)\,\mathrm{d}V\mathrm{d}\psi \qquad 18.17$$

where $f(V, \psi; x, t)$ is the velocity-composition joint PDF.

Normally, the gas-phase flow is represented by a large number of particles. Each particle contains information about its position, velocity, temperature, composition, etc., which evolve with time. This treatment is similar to the Lagrangian method used for the liquid spray drops, except that here the gas particles are imaginary while the particles for liquid drops are physical. Therefore, in PDF combustion models, the emphasis is on modeling the molecular mixing processes, which is crucial for PDF models. A number of mixing models for PDF methods in turbulent reacting flows have been developed. Assessment and applications of these methods to premixed combustion can be found in Pope and Anand (1984).

Direct integration of chemical kinetics

Another approach to modeling combustion is to solve the reactions in a chemical kinetics mechanism and to integrate them directly with the CFD as source terms in the energy and species transport equations. The chemical

reactions in a combustion system can be described by a chemical kinetics mechanism, which defines the reaction pathways and the associated reaction rates leading to the change of species concentrations. This usually involves solving a stiff system of ordinary differential equations (ODEs) governing the rate changes of the chemical species involved in the reactions.

The L reversible reactions in a mechanism with N species can be expressed using a compact notation as follows:

$$\sum_{j=1}^{N} \nu'_{ji} X_j \Leftrightarrow \sum_{j=1}^{N} \nu''_{ji} X_j \quad \text{for} \quad i = 1, 2, \ldots, L \tag{18.18}$$

where ν'_{ji} and ν''_{ji} are the stoichiometric coefficients for the reactants and products, respectively.

A system of ODE's which expresses the net production rate of each species in a multi-step mechanism is given as

$$\dot{\omega}_j = \sum_{i=1}^{L} (\nu''_{ji} - \nu'_{fi})(k_{fi} \prod_{j=1}^{N} [X_j]^{\nu_{ji}} - k_{ri} \prod_{j=1}^{N} [X_j]^{\nu_{ji}}) \quad \text{for} \quad j = 1, 2, \ldots, N \tag{18.19}$$

where k_{fi} and k_{ri} are the elementary forward and reverse rate coefficients for the ith reaction. They are usually expressed in Arrhenius form.

The CHEMKIN code (Kee *et al*., 1991) is widely used to solve chemical kinetics problems, and has been directly integrated into CFD codes (e.g., Kong *et al*., 2001).

Various chemical mechanisms have been developed for different fuels. Gasoline and diesel fuels are multi-component fuels. To simplify the problem, iso-octane and n-heptane are usually used as surrogates to describe the reactions of gasoline and diesel fuels because they have similar chemical characteristics to those of gasoline and diesel fuels, respectively. However, the physical properties of the original fuels (e.g., vapor pressure, density, surface tension, etc.) should still be used in modeling the non-chemical processes, such as the fuel sprays.

For turbulent combustion modeling, there are two major tasks. One is to predict how fast the species conversions occur (rate change of each species) and the other is to account for the effects of turbulence on combustion. However, when chemical kinetics is directly integrated into CFD, the effects of turbulence on combustion are only considered at the resolved grid-scale, and each computational cell is treated as a well-stirred reactor. Therefore, sub-grid-scale turbulence-chemistry interactions are not considered. As stated above, each model has its own applicable range. This approach has been shown to be effective in modeling both homogeneous charge compression ignition (HCCI) combustion (Kong *et al*., 2001) and conventional diesel diffusion combustion (Kong *et al*., 2007). Flamelet models such as the G-equation GAMUT model of Tan and Reitz (2004) and Singh *et al*. (2006)

are available for cases where sub-grid-scale turbulence-chemistry interactions are important.

When a detailed fuel chemistry mechanism is used, the computational time is usually much longer than when employing a simple (e.g., one-step) combustion model. Therefore, different approaches or combinations of them are often used to save computer time while maintaining acceptable accuracy.

One way to reduce computer time is to reduce a detailed fuel chemistry mechanism to a skeletal mechanism. The basic idea is to remove species and reactions that are not crucial to capture the major combustion characteristics of interest, and also to combine some reactions to remove unimportant intermediate species and reactions. The reactions rate constants of the remaining reactions usually need adjustment to account for these changes. A detailed mechanism may contain several hundred species and several thousand reactions, which can take months to finish a single cycle in engine simulations with realistic engine geometries. In contrast, a skeletal mechanism only contains tens of species and reactions and only requires days or even hours of run time, which makes its application in engine simulations feasible. Other approaches, such as storage/retrieval-based schemes (Pope, 1997) and parallel computing (Ali *et al.*, 2003), are also used to speed up calculations.

Singh *et al.* (2006) assessed three different approaches (CTC, RIF, and CHEMKIN) for modeling diesel combustion in a heavy-duty DI diesel engine under five different operating modes ranging from conventional high-temperature diesel diffusion combustion regimes to the so-called low-temperature combustion (LTC) regimes. The CHEMKIN method showed superior performance in predicting the LTC behavior and soot emissions as compared to the other two methods.

'Universal' combustion models

Various combustion regimes ranging from locally premixed to partially premixed and non-premixed with and without turbulence-chemistry interaction can occur simultaneously in an engine. This raises the requirement for a 'universal' combustion model which is capable of dealing with all types of combustion phenomena simultaneously. Many researchers have developed hybrid models (Haworth, 2000; Zellat *et al.*, 2003; Tan and Reitz, 2004; Singh *et al.*, 2006, etc.) that combine the methods described above. However, further validation work needs to be done in this direction.

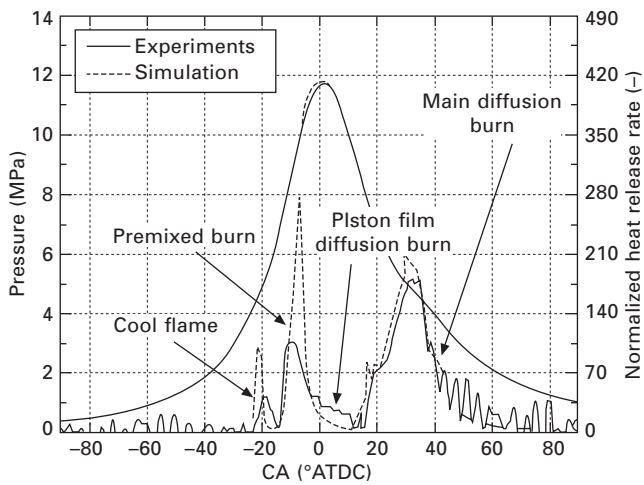
18.5.3 Heavy-duty diesel combustion example

A good example to illustrate the current state of the art in combustion modeling is the simulation of combustion in a heavy-duty diesel engine by Sun and

Reitz (2006). The KIVA-CHEMKIN code was used to model experiments of Hardy and Reitz (2006) on multi-mode combustion with double-injections. The first pulse was injected at –60° ATDC, which led to a well-premixed mixture and caused some wall-impingement by the time of auto ignition. The second pulse was injected at 13° ATDC, which experienced conventional diesel diffusion combustion. These experiments were chosen for model validation because they include various complex combustion phenomena, including cool flames, low-temperature premixed combustion, diffusion combustion of the piston liquid fuel film, and conventional diesel diffusion combustion, as shown in Fig. 18.3. It is a challenge for engine simulation models to capture all of the combustion characteristics.

Figure 18.3 compares Sun and Reitz's simulation with Hardy and Reitz's experimental cylinder pressure and heat release rate. It can be seen that the simulation results match the experiments very well. The simulation was able to reproduce most of the major combustion characteristics of the experiments. The first bump on the normalized heat release rate curve is due to the cool flame phenomena. The second bump is the premixed combustion of the pilot injection. The tail of the second bump is thought to be caused by the diffusion burn of wall-film fuel. The third bump is the diffusion combustion of the main injection.

A slight difference between the simulation and experimental results occurs in the premixed burn part. The simulation results have a faster heat release rate than the experiments, which may be caused by overprediction of fuel–air mixing or by errors associated with the reduced *n*-heptane mechanism when applied to modeling diesel fuel. The simulated heat release curve also does not



18.3 Comparison between the simulation and experimental cylinder pressure and heat release rate (Sun 2007).

have the obvious tail in the premixed burn part, as seen in the experiments. Sun (2007) attributed this to the possibility of underprediction of spray wall-impingement.

Sun and Reitz also simulated Hardy and Reitz's EGR (0% to 30%), pilot (–65° ATDC ~ –50° ATDC) and main (5° ATDC to 20° ATDC) SOI timing sweep cases. Good agreements between the simulation and experiments were achieved under all the conditions tested.

18.6 Emission modeling

The most widely used models for NO_x and soot prediction in multi-dimensional engine simulations are reviewed in this section.

18.6.1 NO_x modeling

The mechanism for NO_x production at high temperatures is well known. NO_x formation is very fast under high-temperature, oxygen-rich conditions. Therefore, NO_x is usually relatively well predicted, especially when the combustion temperature is well predicted.

The extended Zel'dovich mechanism is the most commonly used mechanism that describes NO formation (Heywood, 1988):

$$\begin{aligned} &O + N_2 \Leftrightarrow NO + N && \text{(a)} \\ &N + O_2 \Leftrightarrow NO + O && \text{(b)} \\ &N + OH \Leftrightarrow NO + H && \text{(c)} \end{aligned} \qquad 18.20$$

A factor of 1.533 (the ratio of the molecular weight of NO_2 to NO) is used to convert NO to NO_x to be consistent with ASTM standards. A steady-state assumption for the N species is often employed in engine simulations. Note that the Zel'dovich mechanism only accounts for the thermal NO. A number of other NO_x mechanisms are believed also to be important under different engine operating conditions. For example, an N_2O-intermediate mechanism plays an important role in NO production in fuel-lean low-temperature combustion, and Fenimore or prompt NO is important in fuel-rich combustion.

When a detailed fuel chemistry kinetics mechanism is used in combustion calculations, a detailed NO mechanism can be integrated into the fuel mechanism to better predict NO_x emissions. In such a case, NO_x is given by the sum of NO and NO_2. For example, a detailed NO mechanism has been developed and included in the GRI Mechanism (Bowman et al., 1997) for methane by the Gas Research Institute (GRI). Sun (2007) and colleagues reduced the GRI NO mechanism (containing an additional 22 species and 101 reactions, in addition to the fuel chemistry mechanism) significantly and showed that their reduced ERC NO mechanism (which contains only four

additional species and 12 reactions) behaves almost the same as the original GRI NO mechanism in engine simulations.

18.6.2 Soot modeling

Soot production in engines involves very complicated physical and chemical processes: particle nucleation, surface growth, surface oxidation, and particle coagulation, etc. Since the mechanism of soot production is still not completely understood, developing an accurate soot model is a very challenging task.

Although soot models with detailed descriptions of the physical and chemical processes leading from the fuel molecules to soot particles have been developed (e.g., Kitamura *et al.*, 2002), use of such models in engine applications is still not feasible because solving the soot-related gas-phase chemistry itself takes significant computer time. Therefore, empirical soot models have been widely used in multi-dimensional engine simulations. Among them, two-step soot models have gained wide popularity because of their simplicity and moderate accuracy. In these models, two competing processes are considered, namely soot formation and soot oxidation:

$$\frac{\mathrm{d}M_\mathrm{s}}{\mathrm{d}t} = \frac{\mathrm{d}M_\mathrm{sf}}{\mathrm{d}t} - \frac{\mathrm{d}M_\mathrm{so}}{\mathrm{d}t} \tag{18.21}$$

where M_sf, M_so and M_s are the formed, oxidized and net soot mass in each computational cell at time t.

The Hiroyasu *et al.* (1983) two-step soot model is the best known in this category. In this model, soot formation is linked directly to the concentration of fuel vapor and the oxidation step describes the destruction of soot particles by oxygen. The rates of these two reactions are expressed in Arrhenius form. However, this model has been found to give relatively low peak in-cylinder soot concentrations.

Later, Patterson *et al.* (1994) replaced the original Hiroyasu soot oxidation formulation with the Nagle and Strickland-Constable oxidation model (Nagle and Strickland-Constable, 1962) and achieved more realistic predictions. In their model, carbon oxidation occurs by two mechanisms whose rates depend on surface chemistry involving more-reactive A sites and less-reactive B sites.

Kong *et al.* (2007) pointed out that the concentration of fuel vapor can no longer be associated with soot formation when detailed fuel chemistry is used. This is because fuel molecules decompose to smaller intermediate hydrocarbon molecules very quickly once the low-temperature reactions occur. Another reason is that fuel is not the inception species related to soot formation. They suggested use of acetylene (C_2H_2) to initiate the soot formation. Because acetylene is one of the important precursor species

involved in soot inception, this model has been very successful in predicting sooting tendency.

Fusco *et al*. (1994) questioned the applicability of two-step empirical models for use over a wide range of conditions in engine simulations and suggested relaxing the strong tie between the fuel molecules and soot. They proposed an eight-step phenomenological soot model, in which they included eight global reaction steps to describe fuel pyrolysis, particle inception, surface growth, coagulation and oxidation. In their model, Fusco *et al*. postulated that a generic soot precursor is formed directly from fuel through a single global reaction step. Inspired by Kong *et al*.'s (2007) work, Tao *et al*. (2005) improved Fusco *et al*.'s model by generating soot precursor species from acetylene, rather than directly from fuel molecules. They also added an additional OH-related oxidation step into the eight-step soot model. Since the eight-step models consider more physical processes in soot production, they are physically sounder than two-step models. However, further work on improving the accuracy of eight-step phenomenological soot models is still in progress.

Owing to the complexity of sooting mechanisms and the simplicity of current soot models, soot predictions are in general not as good as NO_x predictions in engine simulations. Further work needs to be done to improve soot models.

18.7 Other models

Other models are used in multi-dimensional engine simulations, such as wall heat transfer models, radiation models, crevice models, and others, depending on the application.

Heat transfer between the fluid in the cylinder and the cylinder walls can significantly affect engine performance, efficiency and emissions. Therefore, accurate modeling of the heat transfer process is also important in successful engine simulations. The heat flux through the chamber walls is mainly due to gas phase convection, liquid fuel film conduction and high-temperature gas and soot radiation. In most SI engines, gas phase convection is the dominant factor for heat transfer. However, in CI engines, radiative heat transfer becomes important (Wiedenhoefer and Reitz, 2003).

In most engine simulations, since the wall boundary layers of the in-cylinder flow are relatively thin compared to computational mesh sizes close to the wall, velocity and temperature wall functions are used to solve for the near-wall shear stress and heat transfer. Traditional temperature wall functions are derived under the assumptions of a steady and incompressible flow, no source terms, constant turbulent Prandtl number and the validity of the Reynolds analogy. However, Han and Reitz (1997) argued that the gas

density varies significantly in IC engines, and unsteadiness and chemical heat release may invalidate the Reynolds analogy. They derived a temperature wall function (temperature profile) formulation from the one-dimensional energy conservation equation and their new function is suitable for variable-density turbulent flows. They applied their new model to gas/wall convective heat transfer predictions in both a premixed charge SI engine and a heavy-duty diesel engine. Satisfactory agreement between the predicted wall heat fluxes and measured data was obtained under both firing and motoring conditions.

When liquid films are present in engine simulations, the heat transfer between the gas phase and the liquid phase, the energy used to vaporize the fuel, and the heat conduction between the liquid film and the wall must all be considered. This is considered in wall–film (spray/wall interaction) models, such as that considered by Amsden (1999).

In most engine CFD simulations, radiation heat transfer effects are not accounted for. However, Musculus (2004) has shown that the radiation heat loss is important, since it can have a measurable effect on in-cylinder temperatures and NO_x emissions. In conventional diesel engines, radiation heat transfer is mainly caused by the continuum emitted by soot particles (Menguc and Viskanta, 1985). However, the radiation emitted by gaseous species should still be considered.

Menguc and Viskanta (1985) were among the first to model radiation effects on diesel engines. In their work, a radiation model based on a P-N method was applied and the cylinder volume was discretized into several axisymmetric, cylindrical enclosures. Though considered accurate, the P-N method is a rather complex method to implement. Therefore, two-zone radiation models were implemented by other researchers (e.g., Morel and Keribar, 1986, etc.). In two-zone radiation models, the combustion region is divided into two zones: burned and unburned zones. Rather than assuming constant wall temperatures, Wiedenhoefer and Reitz (2003) used a discrete ordinate model and accounted for the spatial variation of wall temperatures in a diesel engine. They showed that the non-uniform temperature distribution had a significant effect on heat loss through combustion chamber walls and on NO_x emissions.

The crevice region between the piston, cylinder and piston ring can have significant effects on engine performance. In engine CFD simulations, there are two ways to account for the flow through the piston–cylinder–ring crevice. One is to use an additional crevice grid which is attached to the main computational grid in the crevice region to account for the crevice flow and the additional volume in the crevice region. The other way is to use a phenomenological crevice flow model, such as the one by Namazian and Heywood (1982) extended for use in engine CFD by Reitz and Kuo (1989).

A crevice flow model describes the flow which is pushed into the piston–liner crevice regions due to the high cylinder pressure and then comes back out of the crevice regions during the expansion stroke or leaks into the crankshaft case. One major reason for using a crevice grid or a crevice model is to ensure that the compression ratio in the modeled engine is the same as that in the real engine. Another reason is to model unburned hydrocarbon (HC) emissions more accurately. Unburned fuel in engine cylinder ring crevices is one of the major sources for HC emissions in IC engines.

It should also be mentioned that CFD is also being actively used in aftertreatment system modeling. This requires special models to deal with different types of aftertreatment devices. Usually, models describing both surface and gas phase chemistry are required in such applications. Since aftertreatment system modeling is beyond the scope of this chapter, it will not be further discussed here.

18.8 Computational fluid dynamics (CFD) codes for engine simulations

Many CFD codes, including open source codes (e.g., KIVA), commercial codes (e.g., STAR-CD, FLUENT, FIRE, VECTIS), and in-house codes (e.g., GMTEC, etc.) have been developed and used in IC engine simulations over the past 30 years. The basic approaches and structures of these codes are very similar, with each featuring different physical models and user interfaces.

KIVA (Amsden *et al.*, 1989) is one of the most prevalent open-source CFD codes used in engine applications. It is a transient, three-dimensional, multi-phase, multi-component code for the analysis of chemically reacting flows with sprays for IC engine simulations. It is a large Fortran program developed at the Los Alamos National Laboratory (LANL). This family of codes include KIVA (1985), KIVA-II (1989), KIVA3 (1993), KIVA-3V (1997), and KIVA-3V Release 2 (1999).

The original KIVA program was released in 1985 and was replaced by the improved KIVA-II in 1989, which used a structured mesh. KIVA-3 (1993) was developed to overcome KIVA-2's inefficiency in modeling problems with complex geometries by employing block-structured meshes. This eliminates the necessity of maintaining large regions of deactivated cells and results in a reduction of both storage and computer time for complex geometries. In 1997, an extended version of KIVA-3, KIVA-3V, was released. KIVA-3V can model any number of vertical or canted valves and their motion in IC engines. In 1999, KIVA-3V Release 2 was released, which is the most up-to-date version of KIVA distributed publicly so far. In this version, a variety of new features have been added to enhance the robustness, efficiency, and usefulness of the overall program for engine modeling. A new version of

KIVA, KIVA 4 (Torres and O'Rourke, 2004), is currently under development at LANL. KIVA 4 differentiates itself from the previous versions of KIVA by employing unstructured meshes, which will expedite the grid generation process for complex engine geometries. In KIVA 4, prisms and tetrahedral grids are allowed besides hexahedral grids. More features and improved physical models are also being incorporated into KIVA 4.

Since KIVA is an open-source code, it provides a platform on which researchers have developed many models for engine simulations. Some of the models were then implemented into commercial CFD codes and are being used widely. However, due to its limited mesh generation functionality and lack of a user-friendly interface, KIVA is mostly used in academia and industrial R&D.

Commercial CFD software is being more and more widely used in the design, development, and production processes in the automotive industry. In industry, commercial software is usually preferred to open-source codes for several reasons.

First, commercial software either has its own mesh generation packages or provides interfaces to other well-known mesh generation software (e.g., ICEM CFD, GAMBIT). These mesh generation packages are much more powerful than KIVA's mesh generator (K3PREP), especially when dealing with complex geometries.

Secondly, commercial software usually provides many options for each sub-model. Therefore, users can choose appropriate models based on their problems. Thirdly, the graphic user interface (GUI) that commercial software usually provides makes the software much easier to use than KIVA, especially for new non-expert users. Lastly, commercial CFD software companies also provide training and technical support to their customers.

However, commercial software has its own shortcomings as compared to open-source codes. The codes are much more expensive. They are often 'black boxes' for users and their applications are limited by their functions. Although almost all commercial software provides user functions through which users can add their own models, such work is much easier on an open-source code platform.

In engine CFD applications, the mesh generation process sometimes can take even more than half of the time of the whole CFD process. For example, to simulate an engine cycle in a four-stroke engine, an engine CFD model with valve and piston motion is needed. Usually, a set of meshes is generated at different crank angles (corresponding to different, closely spaced valve lift and piston positions) to avoid too much distortion of the computational cells, and the solutions are interpolated onto the new meshes as the solution proceeds. In some applications, meshes representing special features in the engine geometry may need to be generated, such as the representation of the spark plug and the throttle valve in SI engines, etc. Therefore, mesh

generation technology and the related CFD numerical schemes have been continuously improved.

Initially, structured meshes were used in engine simulations, which only allowed hexahedral cells. Then, block-structured meshes were used for more complex geometries. However, in block-structured meshes, hexahedral cells are still required. Recent codes use hybrid unstructured meshes, which allow hexahedral, tetrahedral, pyramidal and prismatic cells, and these codes are widely used in engine CFD simulations. Hybrid unstructured mesh techniques make it much easier to generate a mesh for a complex geometry, but such meshes can also introduce significant numerical truncation error and numerical diffusion, so they need to be used with caution.

To expedite the mesh generation process, commercial mesh generation software provides automatic mesh generation functions. To deal with the difficulties faced in moving meshes many techniques have been developed, such as mapping between different meshes and using an interface mesh which divides the computational domain into two sub-domains, which do not need to have the same mesh structure and connectivity at the interface (e.g., sliding meshes). However, further improvements to mesh generation techniques are still required.

18.9 Application of engine computational fluid dynamics (CFD) modeling

In the past 30 years, CFD has been increasingly adopted as an adjunct to experimentation in exploring engine designs and in understanding the physics of engine combustion systems. Although laser-based optical diagnostic techniques have been developed to help visualize the flow, spray and combustion processes in optical engines and constant volume combustion vessels, optical diagnostics have their own limitations due to the associated complexity, high cost, low efficiency, and the requirement for optical access. Therefore, CFD has become a good substitute that helps a user to visualize what occurs in engine cylinders and to understand the complex physical and chemical processes occurring in engines. CFD has been widely used in IC engine research, as well as in the design and optimization of engine combustion systems. Even standard engine experiments (non-optical) are relatively more expensive and more time-consuming than CFD analysis. Therefore, CFD is being more and more utilized in engine development efforts to reduce the requirement for experiments, especially in recent years when the accuracy of CFD models and the computational speed of computer hardware have been significantly improved.

When CFD is used in engine research, it can provide a tremendous amount of information about in-cylinder processes, such as all the fluid, thermal, and chemical conditions (velocity, pressure, temperature, species, etc.) and their

spatial distribution and temporal evolution, the evolution of sprays and their interaction with the ambient gas and the combustion chamber walls, and so on.

A good example of the insight afforded by CFD was its successful use in the explanation of soot and NO_x reduction mechanisms using multiple injections in diesel engines (Han *et al.*, 1996). Before it was explained by Han *et al.* in 1996, engine experiments had shown that with multiple injections, the soot-NO_x trade-off curves of a diesel engine could be shifted closer to the origin than with conventional single-pulse injections. Based on their simulations, Han *et al.* found that multiple injections had a similar NO_x reduction mechanism as single injections with retarded injection timings, but that the soot reduction is due to the fact that the soot-producing rich regions at the spray tip are not replenished when the injection is terminated and then restarted. Their work demonstrated the usefulness of multi-dimensional modeling to reveal combustion mechanisms and to provide design insights for low-emission engines.

Similarly, Akihama *et al.* (2001) explained the smoke suppression mechanism of smokeless rich combustion (utilizing large amounts of cooled EGR) also through CFD analysis. In their study, they generated a Φ–T map (equivalence ratio-combustion temperature plot with 'bell shaped' soot and NO_x islands) by performing zero-dimensional calculations using a soot model involving detailed chemical kinetics. They simulated both smokeless rich combustion and conventional high-smoke diesel combustion and plotted and compared their simulation results (in-cylinder equivalence ratio and temperature) on the Φ-T map. Their results showed that the smoke suppression in smokeless rich combustion is realized by reducing the combustion temperature to below that required to generate soot particles, because the chemical reactions leading to soot formation from polycyclic aromatic hydrocarbons (PAHs) do not progress at such low temperatures even in rich combustion situations.

As a further example, using CFD tools, Walter and Gatellier (2002) developed a narrow angle direct injection (NADI) combustion system that applies HCCI combustion at low and medium loads and switches to conventional diesel combustion at high loads. This approach involved a significant amount of work to redesign and optimize the entire combustion system to incorporate HCCI and conventional diesel combustion using the same engine hardware, because HCCI operation requires a relatively narrower spray angle (to reduce spray–wall impingement) while conventional diesel operation requires a wider spray angle (for proper fuel–air mixing). They chose to use a narrow spray angle (less than 100°) to reduce spray–wall impingement for early injection. They redesigned the piston bowl geometry using CFD tools and obtained good performance under both HCCI and conventional diesel operation conditions.

CFD can also be combined with other methods for broader application

or to provide more accurate results. For example, Senecal and Reitz (2000) coupled a genetic algorithm (GA) global optimization code with the KIVA 3V code. Using the KIVA-GA code, they optimized six engine input parameters and achieved an optimum as defined by maximizing a merit function for low emissions and low fuel consumption on a heavy-duty DI diesel engine. They demonstrated that the methodology was efficient in optimizing a large number of parameters in IC engines. Wickman *et al*. (2001) used the KIVA-GA code and optimized a diesel engine's combustion chamber geometry to reduce engine-out emissions and fuel consumption. Similar methodology has also been adopted by other researchers. For example, de Risi *et al*. (2003) optimized the combustion chamber geometry for a DI diesel engine using a multi-objective GA, and their optimized design was adopted by an automotive company. Sun and Reitz (2006, 2008) and Sun (2007) improved the KIVA-GA code used by Senecal and Reitz (2000) and applied the improved code to optimize their so-called two-stage combustion (TSC) at a medium engine load in a DI diesel engine using adaptive injection strategies (AIS). Their AIS involve multiple injections at different injection pressure levels with different spray patterns. Their results suggest that TSC and AIS are very promising techniques to achieve ultra-low emission levels and to meet future stringent emission standards.

CFD simulations can also be integrated with 1-D cycle simulations to achieve more accurate results. In this case, 1-D simulations provide the initial conditions (in-cylinder pressure, temperature and species mass fraction at the time of IVC) for CFD simulations and, in return, the information at the end of the CFD simulation (normally at EVO timing) is passed back to the 1-D simulations to simulate the exhaust process.

CFD can also be dynamically linked with finite element analysis (FEA). Thermal and fluid information can be transferred between CFD and FEA codes to provide more accurate boundary conditions for flow, heat transfer and structural analysis. For example, FEA can be used to solve for wall temperature distribution and provide CFD simulations with more accurate thermal boundary conditions (e.g., Wiedenhoefer and Reitz, 2003). This is believed to be more accurate than assuming constant wall temperatures.

CFD can also be used in engine component design, optimization and analysis, for components such as the intake ports, intake manifolds, water jacket, heat exchanger, turbocharger, injection system, etc. Indeed, CFD analysis has become a standard process in the development process of many component designs in the automotive industry.

18.10 Future trends

Although engine CFD modeling has gained wide recognition and application, it still has several issues which need to be solved.

A major challenge that engine CFD modeling faces is its accuracy, which limits its application. The error in CFD simulations comes from many sources. All models are based on experiments, from which the physics or mechanisms of the related phenomena are understood and used to establish sub-models. The understanding of the physics itself may be inaccurate or incomplete, which introduces errors to the simulations. Models make assumptions and simplifications based on current understanding of the physics. However, not all assumptions are well satisfied under all conditions. No matter how accurate the numerical solver, if the equations to be solved are unknown or are in doubt, this remains the weakest aspect of the simulation. When the governing equations are discretized, the numerical methods themselves cause certain errors. Computers also accumulate round-off error. To match experiments, most models have constants which can be adjusted. However, before a model can be used with confidence, validation should be done against relevant experimental data. It should also be recognized that models may not be accurate when applied outside the applicable range of the model or the scope represented by the experimental data. This is a significant challenge for CFD application, and experts are required to seek methods to reduce these errors and to improve the credibility of the models. As the accuracy of the models is further improved CFD modeling will gain even wider application.

IC engine technologies themselves are growing continuously. With the emergence of new engine technologies, new models/methodologies are required. For example, when HCCI became a hot topic in the late 1990s, engine researchers realized that the auto-ignition processes of HCCI combustion are kinetics controlled and that previous simpler combustion models could not describe the low-temperature chemistry very well. Therefore, CFD simulations using detailed chemistry mechanisms became popular for HCCI simulations. At the present time, alternative fuels (e.g., biodiesel) are becoming an important direction for solving worldwide energy sustainability problems and models describing the features of alternative fuels and their relationships to current fuels are also needed.

As mentioned above, to calculate the full engine cycle, complex moving meshes with resolved intake/exhaust ports and valves are needed. Generating such meshes is still a time-consuming job. Improving mesh generation techniques and making the mesh generation processes highly automatic will significantly reduce the period of CFD analysis. However, it is a big challenge to generate high-quality meshes automatically in a short time.

The applications of models and methods which require more computational resources (e.g., LES and DNS) are also limited by current computer hardware capabilities. With the rapid growth of computer power, more accurate models will be used in engine CFD simulations in the future. At the same

time methods such as parallel computing and storage retrieval are serving as promising solutions to improve computational efficiency.

For turbulence modeling, although LES turbulence models are becoming used in engine simulations, RANS models, especially the k–ε model and its variants, will remain dominant for engine simulations, especially in industrial applications in the near future, due to their significantly lower requirements for computational resources as compared to LES. The Eulerian–Lagrangian method will likely remain the prevalent method for liquid spray droplet modeling. Spray models (most importantly, atomization and droplet breakup models) are unlikely to be significantly improved without new breakthroughs in the understanding of the physics of sprays, and much research is being devoted to this topic. Spray models are still being improved to reduce their dependencies on computational meshes and timesteps (e.g., Sun and Reitz, 2007; Abani *et al*., 2008). RANS-based combustion models will also likely remain dominant. LES-based combustion models are being developed and are expected to have wider application with the growth of LES models. 'Universal' combustion models, which can be applied to describe the combustion regimes of interest in engines, are required and are being developed. As described above, NO_x formation mechanisms are well known and NO_x can be accurately predicted for many combustion processes. However, soot models need to be significantly improved, but this is a difficult undertaking because the soot formation mechanism is very complex and not completely understood.

18.11 References

Abani N, Kokjohn S, Park S W, Bergin M, Munnannur A, Ning W, Sun Y, and Reitz R D (2008), 'An improved spray model for reducing numerical parameter dependencies in diesel engine CFD simulations', SAE paper 2008-01-0970.

Abraham J, Bracco F V and Reitz R D (1985), 'Comparisons of computed and measured premixed charge engine combustion', *Combust. Flame*, 60, 309–322.

Akihama K, Takatori Y, Inagaki K, Sasaki S and Dean A M (2001), 'Mechanism of the smokeless rich diesel combustion by reducing temperature', SAE paper 2001-01-0655.

Ali A, Cazzoli G, Kong S C, Reitz R D and Montgomery C J (2003), 'Improvement in computational efficiency for HCCI engine modeling by using reduced mechanisms and parallel computing', *13th International Multidimensional Engine Modeling User's Group Meeting*, Detroit.

Amsden A A (1999), 'KIVA-3V, Release 2, improvements to KIVA-3V', Los Alamos National Laboratory Report LA-UR-99-915.

Amsden A A, O'Rourke P J and Butler T D (1989), 'KIVA-II – A computer program for chemically reactive flows with sprays', Los Alamos National Laboratory Report LA-11560-MS.

Boudier P, Henriot S, Poinsot T and Baritaud T (1992), 'A model for turbulent flame ignition and propagation in spark ignition engines', *24th Symposium (International) on Combustion,* The Combustion Institute, pp. 503–510.

Bowman C T, Hanson R K, Davidson D F, Gardiner Jr. W C, Lissianski V, Smith G P, Golden D M, Frenklach M and Goldenberg M (1997), GRI-Mech home page http://www.me.berkeley.edu/gri_mech/

Bray K N C and Libby P A (1994), 'Recent developments in the BML model of premixed turbulent combustion', in: Libby P A and Williams F A, editors, *Turbulent Reacting Flow*, Academic Press, London.

De Risi A, Donateo T and Laforgia D (2003), 'Optimization of the combustion chamber of direct injection diesel engines', SAE paper 2003-01-1064

Dekena M and Peters N (1999), 'Combustion modeling with the G-equation', *Oil & Gas Science and Technology-Review*, IFP, 54(2), 265–270.

Demoulin F X and Borghi R (2000), 'Presumed PDF modeling of turbulent spray combustion', *Combust. Sci. Tech.*, 158, 249–271.

Dukowicz J K (1980), 'A particle–fluid numerical model for liquid sprays', *J. Comput. Phys.*, 35, 229–253.

Ewald J and Peters N (2005), 'A level set based flamelet model for the prediction of combustion in spark ignition engines', *15th International Multidimensional Engine Modeling Users' Group Meeting*, Detroit.

Fan L, Li G, Han G and Reitz R D (1999), 'Modeling fuel preparation and stratified combustion in a gasoline direct injection engine', SAE paper 1999-01-0175.

Fusco A, Knox-Kelecy A L and Foster D E (1994), 'Application of a phenomenological soot model to diesel engine combustion', *Comodia 94*, Yokohama, pp. 571–576.

Halstead M, Kirsh L and Quinn C (1977), 'The autoignition of hydrocarbon fuels at high temperatures and pressures – Fitting of a mathematical model', *Combust. Flame*, 30, 45–60.

Hamosfakidis V and Reitz R D (2003), 'Optimization of a hydrocarbon fuel ignition model', *Combust. Flame*, 132(3), 433–450.

Han Z and Reitz R D (1995), 'Turbulence modeling of internal combustion engines using RNG k–ε models', *Comb. Sci. Tech.*, Vol. 106, pp. 267–295

Han Z and Reitz R D (1997), 'A temperature wall function formulation for variable-density turbulence flows with application to engine convective heat transfer modeling', *Int. J. Heat Mass Transfer*, 40(3), 613–625.

Han Z Uludogan A, Hampson G J and Reitz R D (1996), 'Mechanism of soot and NO_x emission reduction using multiple-injection in a diesel engine', SAE paper 960633.

Hardy W L and Reitz R D (2006), 'An experimental investigation of partially premixed combustion strategies using multiple injections in a heavy-duty diesel engine', SAE paper 2006-01-0917

Haworth D C (2000), 'A probability density function/flamelet model for partially premixed turbulent combustion', *Proceedings of the 2000 Summer Program*, Center for Turbulence Research, NASA Ames/Stanford University, pp. 145–156.

Haworth D C (2005), 'A review of turbulent combustion modeling for multidimensional in-cylinder CFD', SAE paper 2005-01-0993.

Heywood J B (1988), *Internal Combustion Engine Fundamentals*, McGraw-Hill, New York.

Hiroyasu H, Kadota T and Arai M (1983), 'Development and use of a spray combustion model to predict diesel engine efficiency and pollutant emission', *Bulletin of the JSME*, 26(24) paper 214-12, 569–575.

Hu B, Jhavar R, Singh S, Reitz R D and Rutland C J (2007), 'Combustion modeling of diesel combustion with partially premixed conditions', SAE paper 2007-01-0163.

Kee R J, Rupley F M and Miller J A (1991), 'CHEMKIN-II: A fortran chemical kinetics

package for the analysis of gas-phase chemical kinetics', Sandia National Laboratories Report SAND89-8009.

Kitamura T, Ito T, Senda J and Fujimoto H (2002), 'Mechanism of smokeless diesel combustion with oxygenated fuels based on the dependence of the equivalence ratio and temperature on soot particle formation', *Int. J. Engine Res.*, 3(4), 223–248.

Kong S C and Reitz R D (1993), 'Multidimensional modeling of diesel ignition and combustion using a multistep kinetics model', paper 93-ICE-22, *ASME Transactions, Journal of Engineering for Gas Turbines and Power*, 115(4), 781–789.

Kong S C, Han Z and Reitz R D (1995), 'The development and application of a diesel ignition and combustion model for multidimensional engine simulation', SAE paper 950278.

Kong S C, Marriott C D, Reitz R D and Christensen M (2001), 'Modeling and experiments of HCCI engine combustion using detailed chemical kinetics with multidimensional CFD', SAE paper 2001-01-1026.

Kong S C, Sun Y and Reitz R D (2007), 'Modeling diesel spray flame lift-off, sooting tendency and NO_x emissions using detailed chemistry with phenomenological soot model', *Journal of Gas Turbines and Power*, 129, 245–251.

Launder B E, Reece G J and Rodi W (1975), 'Progress in the development of a Reynolds-stress turbulent closure', *J. Fluid Mechanics*, 68(3), 537–566.

Liang L and Reitz R D (2006), 'Spark ignition engine combustion modeling using a level set method with detailed chemistry', SAE paper 2006-01-0243.

Magnussen B F and Hjertager H (1976), 'On mathematical modelling of turbulent combustion with special emphasis on soot formation and combustion', *Proceedings of the 16th Symposium (International) on Combustion*, The Combustion Institute, 16, 719–729.

Marble F E and Broadwell J (1977), 'The coherent flame model for turbulent chemical reactions', Project SQUID, Report TRW-9-PU.

Menguc M P and Viskanta R (1985), 'Radiative transfer in three-dimensional rectangular enclosures containing inhomogeneous, anisotropically scattering media', *Journal of Quantitative Spectroscopy & Radiative Transfer*, 33, 533–549.

Morel T and Keribar R (1986), 'Heat radiation in D. I. diesel engines', SAE paper 860445.

Musculus M P B (2004), 'On the correlation between NO_x emissions and the diesel premixed burn', SAE paper 2004-01-1401.

Nagle J and Strickland-Constable R F (1962), 'Oxidation of carbon between 1000–2000 C', *Proceedings of the Fifth Carbon Conference*, Volume 1, 265–325.

Namazian M and Heywood J B (1982), 'Flow in the piston-cylinder-ring crevices of a spark-ignition engine: Effect on hydrocarbon emissions, efficiency and power', SAE paper 820088.

Patterson M A, Kong S C, Hampson G J and Reitz R D (1994), 'Modeling the effects of fuel injection characteristics on diesel engine soot and NO_x emissions', SAE paper 940523.

Peters N (2000), *Turbulent Combustion*, Cambridge University Press, Cambridge.

Pitsch H, Barths H and Peters N (1996), 'Three dimensional modeling of NO_x and soot formation in DI-diesel engines using detailed chemistry based on the interactive flamelet approach', SAE paper 962057.

Pope S B (1985), 'PDF methods for turbulent reactive flows', *Prog. Energy Combust. Sci.*, 11, 119–192.

Pope S B (1997), 'Computationally efficient implementation of combustion chemistry using in situ adaptive tabulation', *Combust. Theory & Modeling*, 1, 41–63.

Pope S B and Anand M S (1984), 'Flamelet and distributed combustion in premixed turbulent flames', *20th Symposium (International) on Combustion*, The Combustion Institute, 403–410.

Reitz R D and Bracco F V (1982), 'Toward the formulation of a global local equilibrium kinetics model for hydrocarbon flames', in: Peters N and Warnatz J, editors *Numerical Methods in Laminar Flame Propagation, Notes on Numerical Fluid Mechanics*, Friedr. Vieweg & Sohn, Braunschweig/Wiesbaden, Vol. 6, p. 13.

Reitz R D and Kuo T W (1989), 'Modeling of HC emissions due to crevice flows in premixed-charge engines', SAE paper 892085.

Senecal P K and Reitz R D (2000), 'Simultaneous reduction of engine emissions and fuel consumption using genetic algorithms and multi-dimensional spray and combustion modeling', SAE paper 2000-01-1890.

Sethian G A (1999), *Level Set Methods and Fast Marching Methods*, Cambridge University Press, Cambridge.

Singh S, Reitz R D and Musculus M P B (2006), 'Comparison of the characteristic time (CTC), representative interactive flamelet (RIF), and direct integration with detailed chemistry combustion models against optical diagnostic data for multi-mode combustion in a heavy-duty DI diesel engine', SAE paper 2006-01-0055.

Smagorinsky J (1963), 'General circulation experiments with the primitive equations: I. The basic experiment', *Monthly Weather Review*, 91(3), 99–164.

Spalding D B (1971), 'Mixing and chemical reaction in steady confined turbulent flames', *Proc. Combust. Institute*, 13, 649–657.

Sun Y (2007), 'Diesel combustion optimization and emissions reduction using adaptive injection strategies (AIS) with improved numerical models', PhD thesis of University of Wisconsin-Madison.

Sun Y and Reitz R D (2006), 'Modeling diesel engine NO_x and soot reduction with optimized two-stage combustion', SAE paper 2006-01-0027.

Sun Y and Reitz R D (2007), 'Modeling low-pressure injections in diesel HCCI engines', *Proceedings ILASS-2007*, Chicago, May 15–18 May 2007.

Sun Y and Reitz R D (2008), 'Adaptive injection strategies (AIS) for ultra-low emissions diesel engines', SAE paper 2008-01-0058.

Tan Z and Reitz R D (2003), 'Modeling ignition and combustion in spark-ignition engines using a level set method', SAE paper 2003-01-0722.

Tan Z and Reitz R D (2004), 'Development of a universal turbulent combustion model for premixed and direct injection spark/compression ignition engines', SAE paper 2004-01-0102.

Tao F, Liu Y, RempelEwert B H, Foster D E, Reitz R D, Choi D and Miles P C (2005), 'Modeling the effects of EGR and injection pressure on soot formation in a high-speed direct-injection (HSDI) diesel engine using a multi-step phenomenological soot model', SAE paper 2005-01-0121.

Torres D J and O'Rourke P J (2004), 'KIVA 4', *14th International Multidimensional Engine Modeling Users' Group Meeting*, Detroit.

Trouvé A and Poinsot T J (1994), 'The evolution equation for the flame surface density in turbulent premixed combustion', *J. Fluid Mech.*, 278, 1–31.

Walter B and Gatellier B (2002), 'Development of the high power NADITM concept using dual mode diesel combustion to achieve zero NO_x and particulate emissions', SAE paper 2002-01-1744.

Wickman D D, Senecal P K and Reitz R D (2001), 'Diesel engine combustion chamber optimization using genetic algorithms and multi-dimensional spray and combustion modeling', SAE paper 2001-01-0547.

Wiedenhoefer J F and Reitz R D (2003), 'Multidimensional modeling of the effects of radiation and soot deposition in heavy-duty diesel engines', SAE paper 2003-01-0560.

Williams F A (1985), *Turbulent Combustion*, SIAM, Philadelphia.

Yakhot V and Orszag S A (1986), 'Renormalization group analysis of turbulence I. Basic theory', *J. Sci. Comput.*, 1, 3–51.

Zellat M, Duranti S, Liang Y, Kralj C, Schmidt G and Duclos J M (2003), 'Towards a universal combustion model in STAR-CD for IC engines: From GDI to HCCI and application to DI diesel combustion optimization', *13th International Multidimensional Engine Modeling Users' Group Meeting*, Detroit.

Index

α-methylnaphthalene, 621
accumulator piston common rail system, 303
acetone, 621, 625
acetylene, 694, 695
actuation, 318
actuator control, 191–2
actuators, 280, *see also* specific actuator
adaptive injection strategies, 701
Adblue, 572
aerodynamic resistance force, 417
aerosol nanoparticles, 611
AFR, *see* air–fuel ratio
after-injection, 166
aftertreatment, 458–67
  analytical procedure of integration, 464–7
    engine-aftertreatment matching, 465
  DPF regeneration requirements, 461–4
  overview of performance and requirements, 459–61
  see also exhaust gas aftertreatment
air charge temperature, 202
air mass flow sensor, 250
air-path management, 197–206
  advanced air-path management, 200–3
    anticipation logic control, 200
    full-load transients, 203
    MBC and coordinated control, 200–2
    neural network approach, 202
    oxygen sensors and MBC, 202
  air-path challenges and acceptance criteria, 175–8
  air-path strategies, 197–200
    engine control strategies and their limitations, 197–8
    transient engine response and its management, 198, 200
  conventional EGR and VGT control, 199
  diesel engine and its air-path related components, 176
  diesel engine system complexity, 177
  diesel input and output diagram, 204
  diesel operating range and priorities, 201
  future trends, 206–7
    air-path management, 207
    boosting systems, 207
    EGR, 206
  key ingredients of air-path system, 178
  MBC and ECU, 203–6
  and turbocharging for light-duty diesel engines, 175–207
air–fuel ratio, 196, 450–1, 453, 567, 582
Alfa 159, 35
Alfa 166, 35
Alfa Romeo 156 JTD, 156
alternative fuels, 702
aluminium titanate, 569, 586, 607
ammonia, 239, 572, 577, 581, 595, 601
  conversion, 582
  storage dynamics, 612
ammonium nitrate, 601
  condensation, 612
analytical engine–vehicle matching, 429–33
  performance characteristic maps, 432
  transmission shift schedule map, 433
  ZWB concept, 430–1
ANSYS blademodeller, 340
ANSYS workbench, 340
anticipation logic, 200
application-specific integrated circuits, 98
Arrhenius model, 683, 684, 690
ASTM D975, 313
ASTM standards, 693

ATR, *see* autothermal reforming
Audi, 31–2
  2.5 litre V6 diesel engine, 11
  main bearing beam from Audi 6.0 V12, 22
  main features and dimensions of latest diesel engines, 33
autothermal reforming, 548
axial power turbine, 339–40

ball-bearing systems, 344
barium oxide, 240
barium sulphate, 240
benchmarking analysis, 522–6
  connecting rod, crankshaft and engine bearing design, 526
  cylinder head design, 525
  cylinder liner design, 525
  engine block and crankcase design, 524–5
  engine competitive benchmarking concept, 524
biodiesel, 313, 702
biofuels, 313
blade backsweep, 330
blade passing frequency, 190
BMW, 32–4
  2.0 litre four-cylinder diesel with aluminium crankcase and variable twin turbocharger, 34
  V8 cylinder block with fracture-split bearing caps, 21
  V8 engine
    3.3 litre diesel engine, 15
    longitudinal cross-section, 13
    transverse cross-section, 14
BOOST, 382
boost-lag, 198
boost pressure, 197
boosting systems, 184–97
  future trends, 207
  supercharging, 194–5
  turbo-compounding, 195–7
  turbo-lag–vehicle low speed pick-up, 184
  turbocharger
    durability and turbine wheel damage, 190
    volute tongue and azimuth angle schematic, 188
  turbocharging, 185–92
  two-stage turbocharging, 193–4
  wastegate and VGT, 192–3
BorgWarner Turbo Systems, 32
Bosch, 75–8
  first-generation common rail system, 75–6
  second-generation common rail system, 76
    1600 bar, 42, 46, 47
  third-generation common rail system, 31, 76–8
    1800 bar, 46, 47
    actuator location, 77–8
    continental piezo actuator details and construction, 80
    function of injector hydraulic amplifier, 79
    injector, 76–7
    injector function vs actuator position, 78
    piezo actuators, 78
    solenoid vs piezo injectors, 77
  VE distributor-type fuel injection pump, 64
Bosch CR13, 102
Bosch CR13 piezo injector, 78
Bosch CRS 3.2 common rail system, 48
Bosch CRS 3.2 injectors, 48
Bosch EDC17 ECU, 98
Bosch EUI, 67
Bosch third-generation CR13.x piezo injector, 71
Bosch VE pump, 63
Bosch VP30, 65, 67
Bosch VP34, 64, 96
Bosch VP44, 65, 67
boxer diesel engine, 45
brake power, 418
brake specific fuel consumption, 275, 377
Bray–Moss–Libby model, 685
BSFC, *see* brake specific fuel consumption
Bump-Up Mixing Process, 368
  BUMP vs conventional bowl mean fuel concentration diffusion rate, 372
burnt gas fraction, 178
butane, 315

CAI, *see* controlled autoignition
California Air Resources Board, 271
caloric law, 256
Campbell diagram, 345, 346
catalysed diesel particulate filter, 570, 586
catalysts, 554–5
Caterpillar Fuel Systems Group, 292
CAV DPA pump, 64

cavitation, 620
cenospheres, 140
Centro Ricerche Fiat and Fiat, 156
ceramic, 279
ceramic monoliths, 569
cerium, 570
CFX CFD code, 160, 340
characteristic-timescale combustion model, 684, 691
chemiluminescence, 660
CHEMKIN code, 690, 691
choke, 332
Citroën C3, 62
coherent anti-Stokes Raman scattering, 633
coherent flame model, 685, 686
coking, 87–8
cold filter plugging point, 314
collision model, 680
combustion
  fundamentals, 120–7
    combustion phases according to Sitkei, 122
    droplet temperature and evaporation rate, 123
    ignition delay as function of compression ratios for various cetane numbers, 126
    ignition delay of fuels with varying ignition quality vs cetane number, 126
    low-temperature ignition process chemical ignition delay phase, 124
  heat release, 127–30
    combustion characteristic curves for DI, 129
    fuel preparation sequence and combustion process, 131
    ignition delay and burnout duration as function of combustion chamber temperature, 129
    injection rate and conversion characteristic curve for DI, 128
    pressure and combustion characteristic curve, 131
  high-speed DI diesel engines, 120–32
  ignition models
    auto ignition, 681–2
    spark ignition, 681
  influencing parameters, 143
  LTC, 130–2
    soot and NO_x formation regions, 132
  measures in relation to mixture formation and combustion, 144
  modelling, 680–93
    flame propagation of turbulent premixed combustion flame, 685
    G-equation to premixed turbulent flames application, 687
    heavy-duty diesel combustion example, 691–3
    ignition models, 680–2
    simulation vs experimental cylinder pressure and heat release rate, 692
  models, 682–91
    Arrhenius model, 683
    chemical kinetics direct integration, 689–91
    flamelet models, 685–9
    hybrid models, 684
    probability density function models, 689
    turbulent mixing-controlled models, 683–4
    universal combustion model, 691
combustion bomb, 112
combustion chamber, 448–9
combustion systems
  different regimes, 224–6
    diesel combustion, 224–5
    HCCI, 225
    LTC, 225
    PCCI, 225
    pPCCI, 225–6
  heavy-duty diesel engines, 277–8, 358–73
    Φ-T plane, 359–61
    lean diffusion combustion, 367–73
    PCCI combustion from early direct injection, 361–7
    summary, 373
  indicated specific carbon monoxide and hydrocarbon emissions, 229
  soot and NO_x emissions from single-cylinder engine, 228
common-rail pressure control loop, 250
common rail systems, 66–86, 230
  background and brief history, 66–8
  Bosch, 75–8
  Continental, 78
  definitions of fuel injection engine generations, 75

Delphi, 81–2
Denso, 83–6
diesel common rail injectors, 69
operating principles, 68–71, 73–4
HP pump, 71–4
injector, 68–71
compatibility optimisation, 185
compression ignition direct injection, 155
compressor, 488–90
architectures and aerodynamic design considerations
operating range, 332–3
single-stage, 328, 330–1
two-stage, 331–2
effect of different turbocharger systems, 324
impeller flow trims, 331
matching guidelines, 489–90
outlet temperature, 347
stage flow improvement, 333
computational fluid dynamics, 187
advanced, modelling of direct injection engines, 676–703
application, 699–701
basic approach, 677–8
codes for engine simulations, 697–9
combustion modelling, 680–93
emission modelling, 693–5
future trends, 701–3
other models, 695–7
spray modelling, 680
turbulence modelling, 678–80
constant pressure turbocharging, 486–7
Continental, 78
HP pump
cross-section, 71
exploded view with major components identification, 72
hydraulic flow diagram, 73
operating principle, 74
PCR2.x injector, 68
exploded diagram with parts identification, 70
operating principle, 69
continuous leakage, 70
control system, heavy-duty diesel engines, 280–1
controlled autoignition, 545
controller area network, 99
conventional diesel combustion
autoignition and premixed burning, 651–3
chemiluminescence images of diesel autoignition, 652
fuel vaporisation and liquid length, 648–51
general features, 645–6
free jets, 645–6
significant quasi-steady period, 645
single fuel injection, 646
in-cylinder spray, mixing, combustion and pollutant-formation processes, 645–57
initial jet penetration, 646–8
late-cycle burnout, 657–8
liquid fuel contours and ensemble-averaged ignition chemiluminescence, 660
measured and predicted diesel-jet penetration, 648
Mie-scatter images of liquid fuel from heavy-duty diesel engine, 650
quasi-steady period, 653–7
simultaneous images of OH-PLIF and soot PLII, Plate XII
for low-boost early-injection LTC condition, Plate XIII
soot and NO_x formation in ϕ-T coordinates, 656
conventional diesel diffusion combustion, 690
cool-flame partial oxidation, 554
coolant heat rejection, 472–4
heat rejection in energy fuel at constant speed, 473
cooling system, design and calculations, 474–9
effectiveness, 478
cordierite, 607
cordierite monolith, 569
Corporate Average Fuel Consumption, 220
cover creep, 348
Croma model, 65
CRSN4.2, 303
Cu-zeolites, 601
Cummins XPI injector, 310
cyan compounds, 134
cyanic acid, 574
cyanuric acid, 575
cycle simulation model, 412–15
guideline, 414–15
cylinder head design
heavy-duty diesel engines, 273

CYPRESS, 151

D975, 314
3D-CAD, 354
D_2 lamps, 633
Damköhler number, 683
Delphi, 81–2
  common rail fuel injection system, 37
  common rail HP pump, 83
  common rail injector, 82
Delphi Direct Acting piezo injector, 102
Delphi E3 injector, 294, 297
DENOX, 151
Denso, 83–6
  automotive twin cylinder HP pump, 84
  common rail solenoid injector, 84
Desaxe crackshaft setting, 42
design-of-experiments, 381
  calibration and design optimisation, 445–7
    design methods, 445–6
    DoE matrix size, 447
    input factor space, 446
    processing and optimisation, 446–7
desulphation, 612
desulphurisation, 587
detailed reverse engineering techniques, 349
diesel combustion engines
  conceptual model, Plate II
  future trends, 634
  ignition and combustion, 624–6
    CH_2O and soot precursors and OH LIF measurement in LTC, Plate VII
    CH_2O LIF distribution in HCCI engine, 625
    cool flame phase, 625
    direct combustion emission visualisation time sequence, Plate VIII
    OH LIF and soot LII simultaneous detection in diesel spray, Plate IX
    second-stage ignition, 626
  in-cylinder spray, mixing, combustion and pollutant-formation processes, 644–70
    closing remarks on LTC diesel research needs, 669–70
    conventional diesel combustion, 645–58
    positive ignition-dwell low-temperature diesel combustion, 657–64
    quasi-steady low-temperature diesel combustion, 664–9
  liquid spray diagnostics, 619–20
    droplet sizes determination, 620
    spray geometrical shape, 619–20
  main challenges for in-cylinder optical diagnostics, 617–18
  optical diagnostics, 617–35
  pollutant measurements, 626–30
    in-cylinder particle-size measurements in two stroke diesel engine, 630
    laser light transmission strong wavelength dependence effect on hot combustion gases, 628
    nitric oxide LIF measurements, 626–7
    quantitative NO-LIF measurements in heavy duty diesel engine, 629
    soot particle size measurements by Tire-LII, 627, 629–30
  soot volume fraction LII, 630–1
  temperature, 631–3
    absorption, 633
    LIF thermometry, 632–3
    soot pyrometry, 631–2
  two-phase flows, 623–4
  typical experiments for diesel diagnostics, 618–19
  vapour-phase fuel distribution, 620–3
    AFR measurements, 622–3
    fuel concentration measurements, 621–2
    fuel vapour concentration visualisation by Rayleigh scattering, 622
diesel dilemma, 220, 223
diesel engine system design, 376–537
  analytical design of mechanical components for system performance improvement, 520–34
    advanced valvetrain system design, 526–9
    benchmarking analysis and component design, 522, 524–6
    fuel economy improvement, 520–2
    Piston assembly lubrication dynamics, 529–34
  analytical engine design process and system simulation, 376–85

characteristics and challenges of modern automotive diesel engine design, 376–8
EPSI analysis, 379, 381–2, 384–5
process and subsystem interaction, 378–9
design specification and subsystem interaction optimisation, 511–20
critical mode design, 513–16
engine delta P and heat rejection, 518
fundamental trade-offs at fixed speed and power, 516
optimisation and interaction of subsystem, 517–20
process analysis, 511–13
process of engine system analysis, 512
two-stage turbocharging, 521
typical subsystem interaction, 519
diesel aftertreatment integration and matching, 458–67
analytical procedure of integration, 464–7
DPF regeneration requirements, 461–4
overview of performance and requirements, 459–61
emissions calibration optimisation development and engine performance design target, 441–58
combustion and emissions development, 447–55
DoE technique for calibration, 445–7
emissions requirements to systems design, 441–5
modelling, 455–8
engine heat rejection and base engine characteristics, 467–79
coolant heat rejection, 472–4
cooling system design and calculations, 474–9
energy balance analysis, 467–71
energy losses, 474
engine–vehicle matching analysis for powertrain system design, 415–40
engine braking operation, 436–40
engine firing operation, 420–35
vehicle performance analysis theory, 416–20
future trends, 534–7
in-cylinder cycle computation and air system steady-state performance, 385–415
engine cycle simulation model tuning, 412–15
mathematical formulation, 396–412
theoretical formulae, 385–95
thermodynamic processes, 395–6
powertrain performance modelling and engine electronic controls, 499–511
analysis of hardware design, 503–4
engine transient performance control, 501–2
hardware design and software controls, 499–500
lookup table approach, 504–5
model-based approach, 505–9
steady-state vs transient performance, 500
transient performance simulation, 502–3
virtual sensor modelling, 509–11
pumping loss theory and engine air system design principle, 479–99
control principle in turbocharged EGR engines, 494–9
design of turbocharged exhaust system, 494
EGR system configurations, 483–5
engine air system design objectives, 479
entropy analysis, 499
low emissions design and air system requirements, 481–3
turbocharger configurations and matching, 485–94
diesel fuel injection equipment heat rejection, 92–5
conclusions, 95
engine testing, 93
managing rejected heat, 95
maximum observed fuel temperatures around the fuel system, 94
opportunities to reduce heat, 94–5
system consumption graph for various component flows, 94
system overview and sources of heat, 93
temperatures and pressures across HP fuel system circuit, 92
diesel fuel reforming, 543–58

applications, 543–6
automotive on-board and stationary applications, 545–6
history of engine applications of H_2 addition, 544–5
need for hydrogen, 543–4
process parameters and catalyst screening, 553–5
catalyst screening, evaluation and scale-up, 554–5
theory, 546–53
chemical routes to hydrogen, 546–50
reforming thermodynamics, 1-D and 2-D modelling, kinetics, 551–3
trends, 555–8
after treatment improvement, 556–8
diesel engine combustion and emissions improvement, 555–6
diesel oxidation catalyst, 237, 278, 568, 585
diesel particle filter, 151, 220, 237, 273, 310, 458–9, 461–4, 557, 568–72, 585–6, 596, 604–11
asymmetric cell technology for improved ash capacity, 608
filter soot load and exhaust temperature relationship, 606
initial particle number filtration efficiency, 608
and LNT, 584–5
porosity and catalyst coating impact on soot oxidation rates, 606
shifting reaction kinetics for a Pr–Ce washcoat, 607
sulfur-based aerosol ultrafine particulates generated in catalysed filter systems, 611
temperature profiles during return-to-idle test, 573
ultrafine emissions when running in LTC mode, 610
diesel particulate–NO_x reduction, 584
diesel–alcohol blends, 243
Dieselmax vehicle, 55
diethylmethylamine, 623
diffusion-controlled combustion, 222
diffusion flame lift-off length, 655
dimethyl ether, 314
Direct Acting Diesel Common Rail, 82
direct injection engines
advanced computational fluid dynamics modelling, 676–703
application, 699–701
basic approach, 677–8
codes for engine simulations, 697–9
future trends, 701–3
other models, 695–7
spray modelling, 680
turbulence modelling, 678–80
combustion modelling, 680–93
combustion models, 682–91
heavy-duty diesel combustion example, 691–3
ignition models, 680–2
emission modelling, 693–5
NO_x modelling, 693–4
soot modelling, 694–5
direct numerical simulation, 680, 703
discrete particle ignition kernel model, 681
distributed common rails, 305
DOC, *see* diesel oxidation catalyst
DPF, *see* diesel particle filter
drive-by-wire, 65, 96
drop-to-idle conditions, 605
dry reforming, 548
dSpace TargetLink, 98
dumb actuator, 351–2
Duramax 4.5 litre V8 diesel, 54
Duratorq, *see* Ford

e-Turbo, 196
early intake value closing, 236
ECU, *see* electronic control unit
eddy breakup model, 683
eddy-current inspection, 345
EGR, *see* exhaust gas recirculation
ELASIS, 67
electrical discharge machining, 86
electromagnetic compatibility, 352
electronic control of fuel systems, 96–102
control system history, 96, 98
diesel fuel system control software, 100–2
ECU hardware, 98–9
key fuel system actuators, 99–100
key fuel system control sensors, 99
powertrain control introduction, 96
typical V6 system diagram, 97
electronic control unit, 68, 96, 156, 246, 296
electronic unit injector, 66, 293–6
electronic unit pump, 298–301
installation, 300
with roller tappet, 299

Electronically Programmed Injection Control, 65
emission calibration
development and optimisation, 447–55
calibration simulation in speed-load domain, 454
combustion chamber design, 448–9
emission behaviour, 453–4
emissions control, 447–8
engine test and air system requirements, 450–1, 453
rapid transient calibration optimisation, 455
test data analysis of emissions and air/EGR flow, 452
turbine area and exhaust restriction, 451
DoE technique for calibration and design optimisation, 445–7
design methods, 445–6
DoE matrix size, 447
input factor space, 446
processing and optimisation, 446–7
modelling, 455–8
CFD-KIVA modelling, 457
empirical approach, 455
Heuristic macro-parameter-dependent approach, 457–8
traditional phenomenological approach, 457
requirements to systems design, 441–5
process from vehicle, aftertreatment and combustion emissions to system design, 444
emission modelling, 455–8, 693–5
CFD-KIVA modelling, 457
empirical approach, 455
direct plot and DoE emulator model, 456
Heuristic macro-parameter-dependent approach, 457–8
NO_x modelling, 693–4
soot modelling, 694–5
traditional phenomenological approach, 457
empty-and-filling method, 502
EN590, 313, 314
Endura DI, 35
energy balance analysis, 467–71
methods, 468–71
calculation on full-load lug curve, 471
gas pressure, temperature and heat transfer simulation, 471
thermal load and heat rejection control, 467–8
energy losses, 474
engine air system
low emissions design and system requirements, 481–3
objectives, 479
design boundary, 480
effect of engine delta P on BSFC, 481
engine control module, 352
engine control unit, 83, 175, 203–6, 276, 280
engine delta P, 398, 406–9
effect of engine speed, 410
theoretical analysis, 407–8
engine in-cylinder cycle
engine cycle simulation model tuning, 412–15
mathematical formulation, 396–412
engine delta P, 406–9
engine speed, fuelling rate and power of HPL-EGR engine air systems, 411
engine system layout, 397
formulation theory for hardware performance prediction, 396–404
formulation theory for hardware specification design with target performance, 404–5
theoretical options of air system design, 409–12
theoretical formula for thermodynamics, 385–95
equations in the cycle process, 387–90
key sub-models, 390–5
model assumptions, 386–7
thermodynamic processes, 395–6
engine performance and system integration, 379–85
EPSI process in engine development, 385
analytical system design and tasks, 386
objectives, 379, 381–2
engine development process with cross-functional teams, 380
technical areas of engine system analysis, 382, 384

theoretical foundation and analysis tool, 382
engine thermodynamic cycle simulation model, 383
entropy, 499
Environmental Protection Agency, 271
EPA, *see* Environmental Protection Agency
EPA Tier 4 Final emissions regulation, 308–9
EPIC, *see* Electronically Programmed Injection Control
EPSI, *see* engine performance and system integration
equivalence ratio–temperature map, 223
error, 281
ETAS ASCET, 98
EU6-NO_x, 151
EU6-PM, 151
EUI, *see* electronic unit injector
Eulerian–Eulerian method, 677
Eulerian–Lagrangian method, 677, 703
Euler's work equation, 330, 333
Euro IV PM Kat, 609
Euro V, 285
Euro V SCR-equipped system without filters, 609
Euro VI, 303
European Automobile Manufacturer's Association, 219
European Steady State Cycle, 596
European Transient Cycle, 596
evaporation model, 680
exciplex fluorescence, 633
excitation-wavelength-scanning techniques, 632
exhaust gas aftertreatment, 237–41
aftertreatment system consisting of DOC, LNT and SCR, 583
emissions legislation, 563–7
future trends, 587–9
integrated systems, 581–5
design conflicts, 581
DPF and LNT, 584–5
LNT and SCR, 581–4
recently reported in the literature for light-duty diesels, 582
for light-duty diesel engines, 562–89
LNT, 576–81
oxidation catalysts, 568
particulate filters, 568–72
recently enacted emissions standards for light-duty diesel vehicles, 564
selective catalytic reduction, 572–6
summary, 585–7
comparisons and contrasts, 587
DOC, 585
DPF, 585–6
emissions legislation, 585
integrated systems, 587
LNT, 586
SCR, 586
exhaust gas recirculation, 96, 155, 175, 178–83, 273, 319, 377, 545
future trends, 206
high pressure EGR, 180–2
influence of rate on maximum temperature and nitrogen oxide formation, 150
low pressure EGR, 182–3
rate, 246
relative changes in soot emissions as function, 152
schematic representation, 149
system configurations, 483–5
performance interaction between EGR system vs turbocharging, 485
turbocharged engine system, 484

Φ-T plane, 359
theoretical analysis, 359–61
fatty acid methyl ester, 242, 315
Favre averaged progress variable, 685
Fe-zeolites, 599, 601
Fe-ZSM5, 600
Federal Test Procedure cycle, 217
feedback control, 281
Fiat Powertrain Technologies, 35
light diesel engines, 35
Fick's law of mass diffusion, 677
FIE, *see* fuel injection equipment
finite element analysis, 348, 701
FIRE, 697
Fischer–Tropsch diesel, 243, 313
fit-for-life systems, 572, 586
fixed geometry turbine, 274
fixed geometry turbocharger, 192
flame soot, 138–40
flamelet concept, 687
flamelet model, 683, 685, 686, 690
flamelets, 687
flat-four HSDI diesel engine, 45
flow coefficient, 110

FLUENT, 697
fluorobenzene/triethylamine exciplex system, 623
4-fluorotoluene/*n*-propyl-diethylamine system, 623
flywheel dynamics, 258
Focus car, 35
Ford, 35–7, 39–41
  1.8 litre Duratorq diesel engine, 36
  2.0 litre Duratorq diesel engine, 37, 38
  2.5 litre turbocharged diesel engine, 7
  3.6 litre V8 diesel engine, 41
  Duratorq, 37
  Duratorq diesel, 65
    for Transit, 39
  Duratorq TDCi, 36
  Ford/Peugeot
    1.4 litre diesel engine, 44
    2.7 litre V6 diesel engine, 40
    V6 main bearing cap lock-width and cross-bolt feature, 22
Ford Fiesta, 62
formaldehyde, 624, 625, 661, 664
formic acid, 574
fourth generation nozzles, 231
freeze effect, 134
fuel burn rate, 684
fuel droplet diameter, 111
fuel economy, 520–2
  improvement roadmap example, 523
fuel injection equipment, 273
  current choices, 290–3
    influencing factors, 291
    injector packaging in modern heavy-duty diesel engine, 292
    summary of types, 292–3
  detailed descriptions, 293–306
    Delphi E3, 293–6
    electronic unit injector, 293–6
    electronic unit pump, 298–301
    electronically controlled smart injector, 300
    high pressure common rail, 303–6
    hydraulic electronic unit injector, 301–3
    mono vs two-valve FIE, 295
    overhead cam timing drive, 295
    two-valve injection flexibility, 298
    two-valve systems, 296–8
  drivers for the future, 309–15
    advanced injection strategies, 310–13
    alternative fuels, 313–15
    fuel property comparison, 315
    mechanical efficiency, 309–10
  future trends, 309–16
  for heavy-duty diesel engines, 289–316
  heavy-duty FIE synergies with light-duty FIE, 308–9
  history of heavy-duty FIE
    electronic fuel systems, 290
    mechanical fuel systems, 290
  low leakage heavy duty common rail injector, 311
  multi-hole nozzle, 307
  nozzle developments, 306–8
  other trends, 315–16
  summary of current heavy duty FIE, 306
fuel-injection loop, 248
fuel return system, 100
fuel system, 275–6
fuel-to-ambient mass ratio, 647
fuel–borne catalysts, 570
fumigation, 229
Fusco model, 695

G Equation for All Mixtures a Universal Turbulent combustion model, 687, 690
G-equation method, 686
GAMUT, *see* G Equation for All Mixtures a Universal Turbulent combustion model
Ganser injector, 310
Garrett GT12 turbocharger, 47
Garrett VNT turbocharger, 47
Gas Research Institute mechanism, 693
gas-to-liquid fuel, 243, 313
gasoline direct injection, 303
Gibbs function, 551
global spray parameters, 108
GMTEC, 697
Golf TDI Hybrid, 54
governor, 250
Grande Punto, 35
gravity force, 416–17
Gross Vehicle Weight Ratio, 217, 269
grouped-hole nozzles, 312
GT-POWER, 382

HCCI, *see* homogeneous charge compression ignition
heat rejection equation, 94
heat transfer, 391

heavy-duty diesel engines
alternative combustion system, 358–73
lean diffusion combustion, 367–73
PCCI combustion from early direct injection, 361–7
approaches to meet future emissions legislation and CO_2 targets, 281–7
aftertreatment, 284–5
air management, 283–4
CO_2 reduction, 286–7
combustion, 281–2
controls, 285–6
diesel fuel injection system, 282–3
on-board diagnosis, 286
summary, 287
comparison of on-road HDD standards in the US, Japan and Europe, 597
definition and application, 269–70
heavy heavy-duty diesel engines, 270
light heavy-duty diesel engines, 270
medium heavy-duty diesel engines, 270
diesel emission and control systems overview, 595–612
future trends, 612
heavy-duty regulatory developments, 596–9
integrated NO_x/PM systems, 611–12
NO_x control technologies, 599–604
particulate matter control technologies, 604–11
emission regulation, 270–2
Europe and Japan, 272
United States, 270–2
emission standards of NO_x and PM
Europe, 272
USA, 271
fuel injection systems, 289–316
overview, 269–87
regulations and technology approaches for future non-road applications, 598
survey of current heavy-duty diesel engines, 273–81
aftertreatment system, 278–80
combustion system, 277–8
control system, 280–1
cylinder head design, 273
fuel system, 275–6
turbocharger system, 273–5
turbocharging technologies, 318–57
actuation, 349–56
architectures and aerodynamic design considerations, 328–43
durability, 343–9
engine performance requirements and operating characteristics, 321–8
future trends, 356–7
scope, 318–19
state of the art, 319–21
heavy heavy-duty diesel engines, 270
Hertzian stress limits, 305
high-frequency reciprocating rig, 314
high pressure common rail, 175, 293, 303–6
distributed unit injector common rail system, 306
distributed unit pump common rail system, 305
heavy duty application, 304
high-pressure pump inlet, 100
high pressure pump technology, 88–90
cam roller delivery characteristics, 90
eccentric cam delivery characteristics, 89
series production Bosch CP4.2 two-plunger cam-roller type pump, 91
summary of HP pump attributes, 91
high-speed direct injection diesel engines, xvii
comparison of V8 diesel engines with CG iron and aluminium cylinder blocks, 17
current passenger car diesel engines, 50–3
direct drive DC-motor actuated single/dual-poppet EGR valve, 26
early development, 4–10
early high-speed DI diesel engines, 9
early pneumatic single-poppet EGR valve, 25
EGR module with aluminium EGR valve and cooler, 28
engine performance and emissions
fuel consumption vs engine displacement, 30
maximum power plotted against engine displacement, 29
maximum power vs vehicle kerb weight, 30

maximum torque plotted against engine displacement, 29
fuel injection systems, 61–103
common rail systems, 66–86
diesel fuel injection equipment heat rejection, 92–5
early fuel systems, 63–6
electronic control of fuel systems, 96–102
future trends, 102–3
high pressure pump technology, 88–90
nozzle technology, 86–8
future trends, 48, 54–5
grey vs CG iron properties, 17
high-speed diesel V engines, 18
performance, 49
influence of swirl on engine-out emissions, 237
mixture formation, combustion and pollutant emissions, 105–53
combustion, 120–32
future trends, 151–3
future trends to meet future legislation, 152
mixture formation, 105–20
pollutant emissions, 132–51
multiple injection diesel combustion process by optical diagnostics, 155–72
double injection or pilot + main, 158–63
multiple injection technology, 163–8
other diesel combustion technologies, 168–71
overview, 3–55
recent trends, 10–30
base engine architecture, 17–20
engine performance and emissions, 28–30
more recent developments, 10, 12–14
performance systems, 20, 22–8
second-generation four-valved engines, 16
survey of today's engines, 31–48
Audi, 31–2
BMW, 32–4
Fiat, 35
Ford, 35–7, 39–41
Honda, 41–2
Mercedes, 43
Opel, 43
Peugeot, 44–5
Renault, 45
Subaru, 45–6
Toyota, 46–7
Volvo, 47
VW, 47–8
typical EGR coolers, 27
high-speed dynamometer, 342
high-speed Schlieren photography, 647
hill-cresting, 463–4
Hiroyasu two-step soot model, 694
homogeneous charge compression ignition, 225, 227, 281–2, 545, 617, 684, 690, 700, 702
homogeneous charge diesel combustion, 229
Honda, 41–2
engine specifications, 42
honeycomb monoliths, 569
hydraulic electronic unit injector, 68, 292, 301–3
system architecture, 302
hydraulic servo mechanisms, 310
hydro-eroding process, 86
hydrocarbons, 239
hydrogen
in diesel engines, 543–4
history of engine applications, 544–5
hydrogen peroxide, 651
hysteresis, 191–2

ideal gas law, 256, 677
ignition delay period, 222
ignition process, 366–7
in-cylinder thermo-fluid dynamic process, 156
incremental combustion, 138
indicated mean-effective pressure, 665
induction-to-powestroke delay block, 258
inertia turbocharger, 258
Infineon Tri-Core TC1797 microprocessor, 98
injection rate shaping, 117
injectors, *see* specific injector
inlet guide vanes, 188
inlet metering valve, 100
inlet valve closure, 178
interferometric Mie scattering, 620
internal combustion engines, xvii
internal transfer pump, 73
inverse design techniques, 340
iron, 570

isentropic ideal gas, 506
iso-octane, 690
isocyanic acid, 601
isocyanuric acid, 574

Japanese Traffic Safety and Nuisance Research Institute, 229
JC08 cycle, 219
Jetta car, 55

κ–ε model, 678, 682, 684
ketohydroperoxide radicals, 651
KIVA, 697
KIVA3, 697
KIVA CFD code, 682
KIVA-CHEMKIN code, 692
KIVA-GA code, 701
KIVA-II, 697
KIVA-3V, 697, 701
KIVA-3V Release 2, 697
Kolmogorov's theory of self-similarity, 679
KrF excimer laser, 627

Lagrangian method, 689
Lagrangian Monte Carlo particle-based methods, 689
lambda sensor, 605
LANL, 698
large eddy simulation, 679, 682, 703
laser flare, 621
laser-induced exciplex fluorescence, 623
laser-induced fluorescence, 652
laser-induced incandescence, 628
  soot volume fraction, 630–1, Plate X
late intake valve closing, 229, 236
lean diffusion combustion, 367–73
  chamber design and mixing energy, 371–3
    BUMP combustion chamber, 371
    vortex induced combustion bowl, 372–3
  characteristics, 367–9
  function of mixing, 369–70
    effect on low-temperature diesel combustion, 369
lean NO_x trap, 220, 229, 240–1, 285, 459–60, 576–81, 586, 595, 602
  bypass or dual-bank systems, 578
  and DPF, 584–5
  effect of potassium migration on deNO_x efficiency, 603
  NO_x performance curves for heavily aged potassium and barium based LNTs, 602
  during operation, 240
  relevant exhaust species according to spatial position, 579–80
  and SCR, 581–4
lean operation, 285
level set methods, 686
lift-off distance, 222
lift-off length, 654
lifted flames, 222
light-duty diesel engines, 562
  advanced concepts, 215–43
    combustion chamber shape, 237
    combustion systems, 227–30
    current development, 220–1
    engine control, 242
    exhaust gas aftertreatment, 237–41
    fuel injection, 230–3
    future fuels, 242–3
    heat recovery, 241–2
    low emissions concepts, 221–6
    variable valve timing, 236–7
    wall-flow diesel particulate filter operation, 238
  advanced control and engine management, 246–65
  advanced control systems, 259–65
    actual and future European emission limits for diesel passenger cars, 260
    NO_x and PM trade-off curve with possible engine performance points, 264
    physics-based control system structure, 262
    SCR catalyst control system, 261
    standard diesel engine control structure, 264
  charge induction, 233–7
    conventional charging system, 234
    electrically assisted turbocharger, 235
  exhaust gas aftertreatment, 562–89
    emissions legislation, 563–7
    future trends, 587–9
    integrated systems, 581–5
    LNT, 576–81
    oxidation catalysts, 568
    particulate filters, 568–72
    selective catalytic reduction, 572–6
    summary, 585–7

influence of rail pressure on engine-out emissions, 232
injection rate vs crank angle profile, 231
legislative exhaust emission standards, 216–20
CO_2 emissions/fuel consumption standards, 219–20
European emissions standards for NO_x and PM, 217
European union, 216–17
Japan, 218–19
United States, 217–18
US emissions standards, 218
low emissions concepts, 221–6
classical diesel combustion and several alternative modes, 225
CO emissions map, 226
combustion and emissions formation, 221–6
combustion phases in diesel engine, 221
diesel dilemma diagram, 223
emissions map for soot and NO_x, 224
main control objectives, 246–8
important diesel engine system components and signals, 247
interconnection structure of the control loops, 249
requirements for future diesel engines, 220–1
standard control loops, 248, 250–2
speed control system, 251
system modelling, 252–9
cause–effect relations for subsystems in diesel engine, 253
compressor and turbine, 257–8
compressor map, 257
EGR valve, 254, 256
engine fluid and thermodynamics and engine inertia, 258–9
injection system, 254
intake and outlet receivers, 256
modern diesel engine model structure, 255
turbocharger speed in transient test for modern passenger car diesel engine, 254
turbocharging and air-path management, 175–207
air-path challenges and acceptance criteria, 175–8
air-path management, 197–206
boosting systems, 184–97
exhaust gas recirculation, 178–83
future trends, 206–7
light extinction, 629
light heavy-duty diesel engines, 270
Light Hybrid, 196
LII, *see* laser-induced incandescence
LIISim, 629
Lion V6 diesel, 39
liquid length, 649
LNT, *see* lean NO_x trap
lookup table, 504–5
low temperature combustion, 216, 225, 227–9, 577, 684, 691
closing remarks on diesel research needs, 669–70
equivalence ratio measurements in an LTC jet at 5°, Plate XIV
exhaust smoke measurements for multiple operating conditions, 666
in-cylinder laser-extinction soot volume fraction measurements, Plate XV
quasi-steady
in-cylinder spray, mixing, combustion and pollutant-formation processes, 664–9
initial jet development, 664
LTC exhaust soot bump, 665–7
LTC in-cylinder soot bump, 667–9
LTC, *see* low temperature combustion
Lucas Diesel Systems, 96
Lucas DPS pump, 64
Lucas EPIC, 65, 67
Lucas EPIC EP5 ECU, 96
Lupo car, 47
Lynx, 35

MAN-M procedure, 114, 117
manifold air pressure, 176
mass air flow, 176
mass conservation, 677
MATLAB, 354, 581
Matlab RTW-EC, 98
Matlab/Simulink/Stateflow, 98
maximum shoot load, 571
Mazda MPV, 83
MBC, *see* model based control
mean effective injection pressure, 74
medium heavy-duty diesel engines, 270
Mercedes-Benz, 43

220 CDI, 156
V8 diesel engine
bottom view, 20
longitudinal cross-section, 19
metal foams, 586
metal–zeolite, 572
$MgCl_2$, 602
Mie scattering, 619, 649, 651, 660
Miller cycle, 236
mixing, 369–70
mixing-controlled combustion models, 683
mixture formation
air entrainment, 114–15
injection and combustion characteristics with hard, with soft, and with preinjection combustion, 115
qualitative pressure and rate of pressure increase, 115
combustion chamber design, 117–20
arrangement with four-valve technology, 118
flow process of diesel engine with direct fuel injection, 119
influence of engine size on shape, 120
relationship between injection pressure, swirl number and nozzle hole number, 119
relationship between required swirl number and cylinder diameter, 121
different preparation methods
air-distributed mixture preparation, 114
wall-distributed mixture preparation, 114
fuel spray, 107
spray angle, 109
spray penetration, 109–11
spray penetration without swirl, 110
various phases of spray breakup, 108
fundamentals, 105–7
fuel vaporisation in static air, 106
problems associated with mixture preparation, 106
high-speed direct-injection diesel engines, 105–20
injection rate, 115–17
cam-controlled and common rail injection systems, 116
shaping, 117
measures in relation to mixture formation and combustion, 144
spray atomisation, 111–13
average droplet diameter and size distributions, 113
effect of injection pressure and nozzle hole diameter on droplet size, 112
spray parameters
penetration depth and opening angle with swirl, 111
penetration depth and spray angle without swirl, 108
spray propagation, 107–11
Mk-concept, 228
model based control, 178, 505–9
and coordinated control, 200–2
diesel engine and its air-path related components for MBC, 205
and ECU, 203–6
and oxygen sensors, 202
transient engine controls and air system performance, 507
model catalysts, 562
model tuning, 412
modified eddy-dissipation model, 684
Motorola 68HC11 microprocessor, 96
moving nozzle, 337
Muldic system, 230
2000 bar Multec diesel common rail system, 81
multiple injection diesel combustion process
air–fuel mixing and combustion process evolution, 170–1
effect on HSDI passenger car performance and emissions, 168
by optical diagnostics, 155–72
comparison among different diesel engine technologies, 159
effect of pre + main strategy on spray and combustion evolution, 162
first vs second generation fuel deliveries, 164
pilot vs multiple injections, 165
smoke and NO_x emissions
and BSFC for three different injection strategies with optimised dwell times, 167
and fuel consumption with triple injection vs dwell time, 166
influence of dwell time, 160

UV-visible flame and OH evolution of triple injection strategy, Plate I
92MY Ford Transit, 96

n-heptadecane fuel, 649
n-heptane, 690
Nagle and Strickland-Constable oxidation model, 694
narrow angle diesel injection, 227, 700
Navier–Stokes equations, 677, 680
Navistar T 44E 7.3 litre V8 DI, 68
Nd:YAG lasers, 625
needle control valve, 297
New European Driving Cycle, 151, 216, 233, 565
NH_3/NO_x ratio, 586
nickel metal hydride batteries, 54
nitro-hydrocarbons, 601
nitrogen oxides, 655
nitrous oxide, 574, 601
*N,N,N′,N′-tetramethyl-p-*phenylenediamine/naphthalene/hexadecane, 623
NO LIF, 626
noise vibration and harshness, 176, 275
non-methane hydrocarbons, 218
non-road transient cycle, 598
non-thermal plasma, 554
5-nonanone, 621
NO_x absorber, *see* lean NO_x trap
NO_x absorber catalyst, 279, 285, 576
NO_x formation, 133–8
  fuel NO, 133–4
  prompt NO, 133
  reduction, 238–41
    combined and alternative systems, 241
    LNT, 240–1
    SCR, 238–40
  thermal NO, 133
NO_x-particulate filter, 584
NO_x reduction efficiency, 580
NO_x retention, 582
NO_x storage catalyst, 576
nozzle closing pressure, 297
nozzle deposits, 87–8
nozzle flow model, 680
nozzle opening pressure, 297

OBD, *see* On-Board Diagnostics
OEM, 259
OH chemiluminescence, 626
OH-PLIF, 653, 657, 662, 663
oil dilution, 567
OM642, 43
On-Board Diagnostics, 259, 280, 286, 289, 601, 609
Opel, 43
open spill valve, 296
operating range, 332
opposed jet, 687
ordinary differential equations, 690
oxidation catalysts, 260, 568
oxygen, 626
  sensor, 571

P-N method, 696
palladium, 607
partial differential equations, 677
partial oxidation, 547
partially premixed charge compression ignition, 225–6, 229–30
partly premixed combustion, 216, 225
passive regeneration, 463
PCCI, *see* premixed charge compression ignition
3-pentanone, 621, 625, 633
pentoxide, 239
Peugeot, 44–5
  1.4 litre I-4, 54
  DW10 2.0 litre engine, 79
  Ford/Peugeot
    1.4 litre diesel engine, 44
    2.7 litre V6 diesel engine, 40
    V6 main bearing cap lock-width and cross-bolt feature, 22
Phase Doppler Anemometry, 620
phenomenological crevice flow model, 696
Pieburg pneumatic EGR valve, 25
piezo-actuated CR fuel injector, 157
piezo actuators, 78, 79, 99–100
  continental details and construction, 80
piezo-controlled injectors, 231, 232
piezo injectors, 46
piston
  effect of design on skirt friction and piston slap, 532–4
    friction power and oil film thickness, 535
    lubricating oil pressure distribution, 533
    side thrust at different speed and loads, 532
    slap motion simulation, 535
  overview of assembly dynamics, 529–32

lubrication dynamics model, 531
planar laser-induced incandescence, 653
Planck law, 631
platinum, 239, 607
platinum group metal, 603
PLII, *see* planar laser-induced incandescence
pollutant emissions
diesel engine exhaust-gas composition, 133
formation, 132–41
CO formation, 140–1
hydrocarbons formation, 141
NO_x formation, 133–8
and oxidation of soot in qualitative terms over time, 140
SO_2 formation, 141
soot formation, 138–40
high-speed direct-injection diesel engines, 132–51
influence of individual parameters on emissions and efficiency, 144
NO_x–soot or NO_x–fuel consumption trade-off, 142
typical behaviour, 146
possibilities of emission reduction, 142
reduction measures, 141–51
conventional measures, 142
EGR, 149–51
NO_x and soot emissions, 146–9
relative change in NO_x and soot emission, 148
representation of water introduction methods, 147
unconventional measures, 143
water injection, 145
thermal NO formation
and conditions in flame front during adiabatic combustion, 137
localised temperature with constant AFR, 136
varied localised AFR at constant temperature, 135
polycyclic aromatic hydrocarbons, 223, 700
positive ignition-dwell low-temperature diesel combustion
autoignition and premixed burning, 661–4
characteristics, 657–9
fuel vaporisation and liquid length, 659–61
in-cylinder spray, mixing, combustion and pollutant-formation processes, 657–64
potassium, 603
powertrain
braking operation, 436–40
benchmarking analysis, 439
compression-release and conventional exhaust brake, 441
effect of brake retarding power, 438
engine brake performance, 436–7
enhanced retarding power, 437–40
principle of compression-release engine brake, 439
turbocharged engine brake design, 443
valvetrain limits in engine exhaust brake design, 442
considerations in aftertreatment to control engine-out emissions, 566
engine firing, 420–35
analytical engine–vehicle matching, 429–33
diesel full-load lug curve and transient torque, 426
drivability and drivetrain design parameters, 423–8
integrated design of maximum drivetrain transfer ratio, 425
optimisation method, 435
overview of criteria, 420–3
performance optimisation, 434–5
transient powertrain simulation, 433–4
vehicle fuel economy, 428–9
performance modelling and engine electronic controls, 499–511
analysis of hardware design, 503–4
engine transient performance control, 501–2
hardware design and software controls, 499–500
lookup table, 504–5
model-based approach, 505–9
steady-state vs transient performance, 500
transient performance simulation, 502–3
virtual sensor modelling, 509–11
pPCCI, *see* partially premixed charge compression ignition
PREDIC, 227
preflame, 222

preinjection, 166
premixed charge compression ignition, 227–9, 361–7, 577
  early fuel injection strategies, 361–3
    time-sequence of multi-pulse injections, 362
  injection mode modulation and optimisation, 363–7
    injection rate patterns, 364
    optimisation for ignition process retardation, 366–7
    optimisation for wall wetting prevention, 365–6
    optimised injection mode vs baseline, 366
    rate of heat release adjustment, 365
    spray vs flow fields in the cylinder for optimised and baseline cases, Plate VI
premixed combustion, 158, 169
premixed compression ignition, 577
pressure control valve, 73, 93, 100
pressure ratio, 328
pressure/time metered injection systems, 297
primary breakup model, 680
Pro-Engineer, 354
probability density function model, 683, 689
processor, 280
pulse turbocharging, 319, 486
Puma, 37, 65
pump-line-nozzle systems, 290
pumpedüse, 47
pumping loss control principle, 494–9
  air system capability and controllability, 498
  control of AFRo and EGR rate, 497
  design effects
    engine delta P, 495
    volumetric efficiency, 495
pumping mean effective pressure, 200
pump–line–nozzle systems, 63

quenching effect, 141

Raman scattering, 622
Rankine cycle, 242, 468
rapid prototyping techniques, 342
Rayleigh scattering, 621, 652, 653, 654, 662
re-normalised group theory, 679
reactor aspect ratio, 554
recirculated exhaust gas, 233
reformate, 545
reformed exhaust gas recirculation, 548–50
  effect on overall fuel economy, 550
  schematics of REGR system, 549
  temperature profiles, 551
regeneration, 279, 584, 587
Renault, 45
representative interactive flamelet model, 687, 691
return-to-idle tests, 571, 572
Rexroth design, 71
Rexroth hydraulic pump principle, 75
Reynolds analogy, 695, 696
Reynolds Averaged Navier–Stokes model, 678, 682, 703
Reynolds equation, 530
Reynolds stress model, 680
rhodamine B, 633
rich operation, 285

SAE J1826 Turbocharger Gas Stand Test Code (1995), 488
Sauter Mean Diameter, 112, 620
Schlieren techniques, 646
SCR, *see* selective catalytic reduction
seat-hole nozzles, 86
secondary breakup model, 680
selective catalytic reduction, 220, 238–40, 241, 279, 284, 460, 557, 572, 574–6, 586, 595
  effect of NO_2 proportion in exhaust gas on Fe-zeolites efficiency, 600
  and LNT, 581–4
  NO_x conversion realised when NH_3 concentration is varied, 575
  particle number emissions for Euro V engine with SCR, 609
  system schematic diagram, 239
  urea decomposition catalysts efficiency, 600
self regeneration, *see* passive regeneration
sensors, 280
sequential turbocharging, 327
series two-stage system, 327
shadowgraphy, 646
shadowgraphy/schlieren technique, 624
Shell ignition model, 681
  reactions and species involved, 682
Siemens, *see* Continental
Siemens 1600 bar piezo common rail system, 37

Siemens 1650 bar piezo common rail system, 39
Siemens 1750 bar piezo common rail system, 40
Siemens piezo common rail fuel injection system, 41
silicon carbide, 569, 585–6
silicon nitride, 569, 586
silicon-on-insulator process, 352
SimMechanics, 354
Simulink, 354, 581
single-cylinder Caterpillar engine, 158
slip, 574
smart actuator, 351–2
  various interfaces with turbocharger and engine system, 353
smart injectors, 299
smoke suppression mechanism, 700
smokeless rich combustion, 700
solenoid actuators, 99
solenoid-controlled injectors, 231
solid urea, 602
solidity diffuser, 330
soluble organic fraction, 278
soot bump, 665
soot coke, 140
soot formation, 138–40, 654
  limits as function of localised temperature and localised AFR, 139
  and NO_x formation regions, 132
  and oxidation
    in qualitative terms over time, 140
  and soot oxidation
    mechanism, 139
soot pyrometry, 631–2
  two-colour, temperature measurement in heavy-duty engine, Plate XI
soot volume fraction, 667
spatial differencing, 678
specific fuel consumption, 176
spray-formation phenomena, 254
spray shadowgraphy, 162
stall, 186–7
STAR-CD, 697
steady flow energy equation, 322
steam reforming, 547–8
stoichiometric diffusion flame, 655
strontium, 570
sub-grid scale model, 679
Subaru, 45–6
  engine specifications, 46
sulphates, 279, 602
sulphur, 279
sulphur trioxide, 240
Super-Ultra Low Emission Vehicle, 218
supercharger system, 284
supercharging, 194–5
supplemental emissions test, 501–2
Surface Response Mapping, 552–3
surge, 332
swing vane VGT, 337
swirl generation device, 188
switch leakage, 70–1

temporal differencing, 678
thermal cracking, 141
thermal load, 467
thermodynamics, 551
thermoelectric power generation, 242
throttle, 250
toluene, 621, 633
torque back-up, 323
torque converter dynamics, 258–9
total NO_x conversion, 580
Touareg, 48
Toyota, 46–7
  1.4 litre engine specifications, 46
Toyota piezo injector, 85
tractive force, 416
transient inertia force, 417
transmission electron microscopy, 627
turbine, 490–3
  architectures and aerodynamic design considerations
    mixed flow, 335–6
    stage, 333–5
    turbocompound, 339–40
    two-stage, 337–9
    variable geometry, 336–7
    wastegate, 336
  axial and radial characteristics, 341
  blade speed ratio, 334
  dynamometer test range, 342
  flow characteristic, 323
  matching guidelines, 491, 493
  mixed flow turbine vs radial flow turbine, 335
  moving nozzle and swing vane VG, 338
  single, twin flow and double entry turbine housings, 336
turbo-compounding, 195–7, 242
turbocharger system, 283–4
  heavy-duty diesel engines, 273–5
turbocharger turbine, 339

turbocharging, 185–92
actuation, 349–56
actuator architecture, 350–2
analysis software connectivity, 356
cycle-time challenge, 354
design process challenges, 352
design process solution, 354–6
response time vs gear ratio, Plate III
SimMechanics diagram, 355
technological challenge, 352–3
today's applications, 349
typical requirements, 349–50
architectures and aerodynamic design considerations, 328–43
component design – tools and processes, 340, 342
compressor, 328–33
efficiency improvements, 343
turbine, 333–40
axial and radial flow paths, 329
configurations and matching, 485–94
compressor matching, 488–90
engine-turbine matching theory, 492
extreme ambient conditions, 493–4
turbine matching, 490–3
durability, 343–9
component mechanical design issues, 343–4
creep, 345, 348
high cycle fatigue, 345
housing circumferential variation, 347
impeller material strength variation, 348
low cycle fatigue, 344–5
requirements, 343
thermo-mechanical fatigue (TMF), 348
tools and processes for mechanical design, 348–9
effect of EGR rate on boost pressure, 320
engine performance requirements and operating characteristics, 321–8
matching turbocharger to heavy duty diesel engine, 321–2
modifying the boost curve, 323
turbocompound systems, 325–7
two-stage turbochargers, 327–8
VGT, 325
wastegate turbines, 323–4
exhaust system design, 494
for heavy-duty diesel engines, 318–57
future trends, 356–7
scope, 318–19
pumping loss control principle, 494–9
state of the art technology, 319–21
effect of EGR on boost pressure, 320
influence of emissions legislation, 319–21
turbocharger development for heavy duty engines, 319
turbocharger with wastegate, 325
turbocompound schematic diagram, 327
turbomachinery components, 186–92
two-stage turbocharging, 193–4
serial and parallel sequential turbocharging, 194
serial vs sequential two-stage turbocharging installations, 193–4
VGT turbocharger, 326
turbomachinery components
compressors, 186–9
fatigue failure, 189
surge, 186–7
two-stage compressor, 188
VGC, 187–8
volute design, 187
turbines, 189–92
actuator control and hysteresis, 191–2
materials (turbines), 192
nozzle driving link mechanisms, 191
nozzle performance, 191
turbine rotor resonance, 191
VGT, 189–90
turbulence mixing-controlled models, 684
twin entry housing, 336
twin flow housing, 336
two-stage ignition phenomena, 681
two-stage turbocharging system, 327–8, 521
with long-route and short-route, 234
regulated system for BMW 535d, 235
serial and parallel sequential turbocharging, 194
serial vs sequential installations, 193–4

Ultra Low Emission Vehicle, 218
Unibus, 229
UNIJET, 67, 75, 156
unit-injector systems, 47, 115

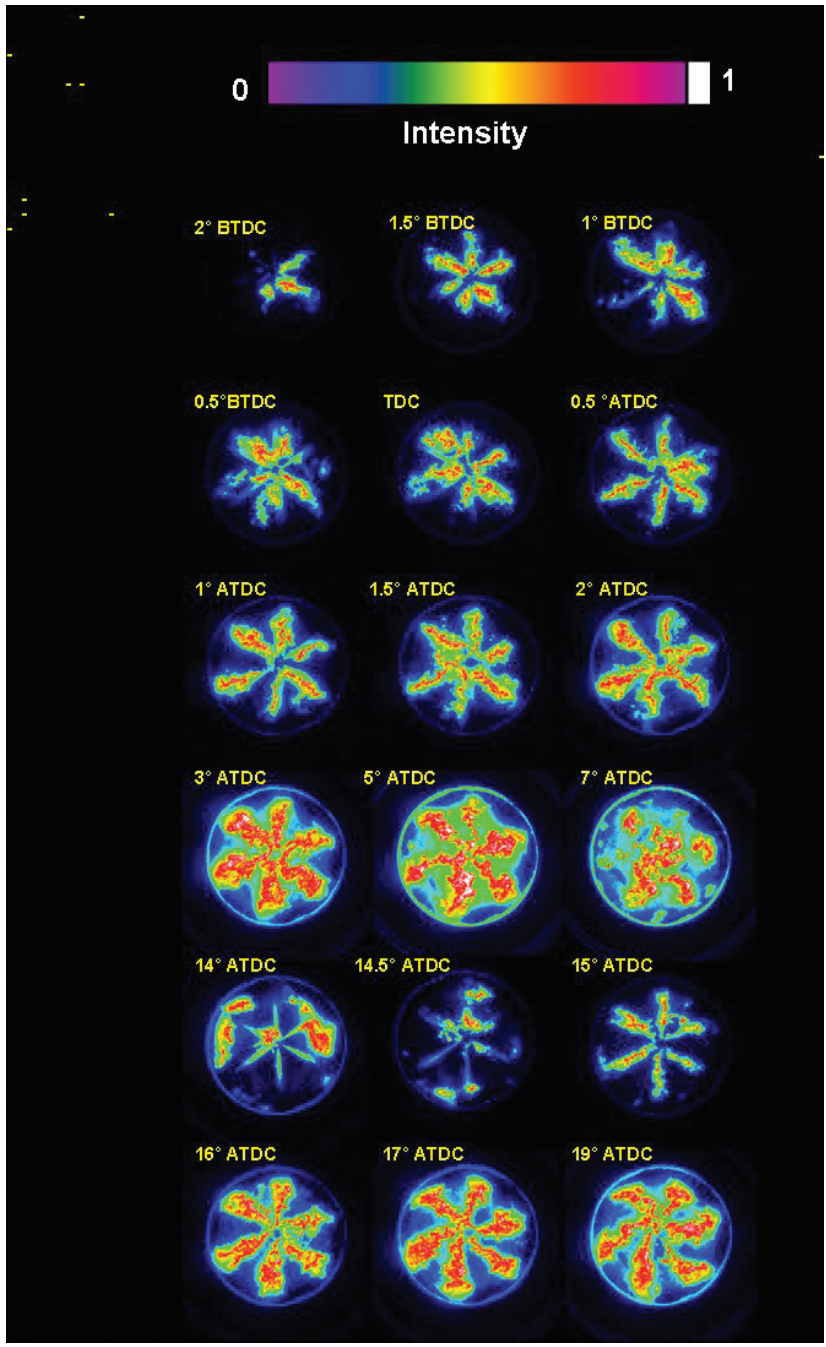
universal combustion model, 691, 703
urea, 239, 287, 572, 574, 586, 600
urea decomposition, 599, 612
US06 cycle, 234
US MY 2010, 284, 285
US Not-to-Exceed requirement, 597
US06 Supplemental Federal Test Procedure, 216
US Tier 2 regulations, 216
UV chemiluminescence, 626

valve covered orifice, 36, 86, 308
valvetrain system design
  design guidelines, 526–9
  dynamics simulation, 528
  parametric design chart, 529
vanadia, 599
vanadia–titania, 572
vanadium, 239
vaneless diffuser, 330
variable flow area nozzles, 312
variable geometry compressor, 187
variable geometry turbine, 409
  16-vane VGT Campbell diagram, 346
  efficiency variation with flow, 339
  see also variable geometry turbochargers
variable geometry turbochargers, 150, 185, 189–90, 192–3, 274–5
variable inletguide vanes, 188
variable turbine geometry (VTG) *see* variable geometry turbochargers
variable valve actuation, 527
VECTIS, 697
vehicle fuel economy, 428–9
vehicle performance analysis, 416–20
  acceleration characteristics, 421
  power requirements at different operating conditions, 422
  tractive force characteristics, 419
venturi, 26
VGT, *see* variable geometry turbine; variable geometry turbochargers
virtual calibration, 454
virtual sensor modelling, 509–11
Vision Grand Sports Tourer, 54
Volkswagen, 47–8
  1.9 litre 81 kW TDI diesel engine, 8
  1.2 litre I-3 engines, 54
volume control valve, 73, 100
Volvo, 47
vortex induced combustion bowl, 372–3
  fuel and O_2 distribution in chamber, Plate IV
  induced vortices and transportation of fuel and oxygen, Plate V

wall–film model, 680
waste gate, 233
water-cooled VNT turbocharger, 47
water-gas shift, 548, 556
WAVE, 382
wheel creep, 348
white smoke, 461
Wiebe function, 393–5
World Harmonised Steady-state Cycle, 289
World Harmonised Transient Cycle, 289, 596
Woschni correlation, 391–2
wrought aluminium, 345

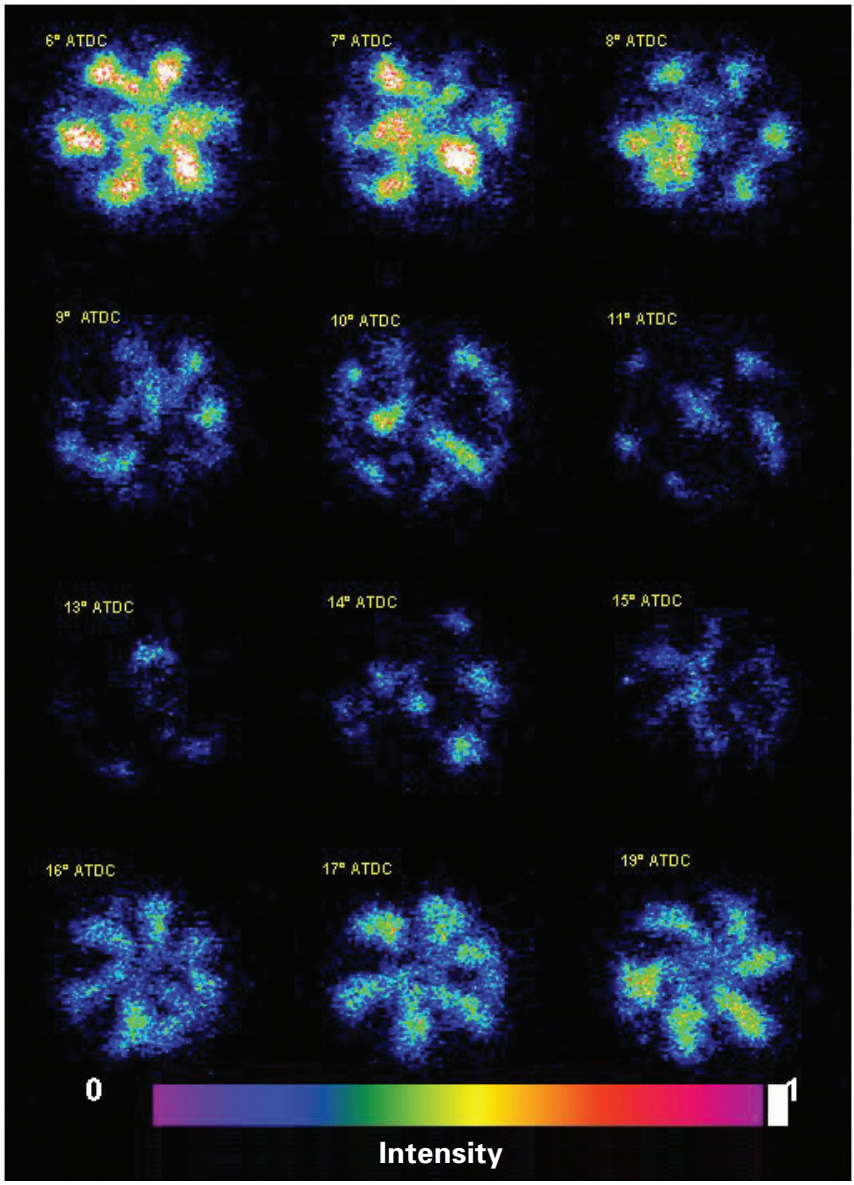
X-ray computed tomography, 349

Zeldovich mechanism, 133, 134, 223, 693
zeolite catalysts, 241, 595, 612
zero backleak nozzles, 310
zero-wheel-braking, 429
zinc, 88
ZWB, *see* zero-wheel-braking



(a)

Plate I (a) UV–visible flame and (b) OH evolution measured at selected crank angles during pre + main + after injection strategy.



(b)

Plate I Continued

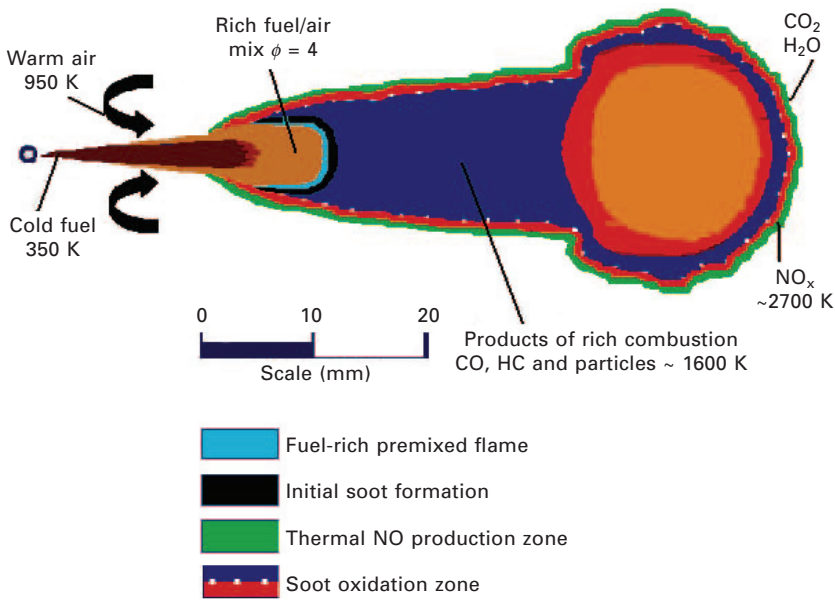


Plate II Conceptual model of diesel combustion (Flynn *et al.*, 1999), reprinted with permission from SAE paper 1999-01-1509, © 1999 SAE International).

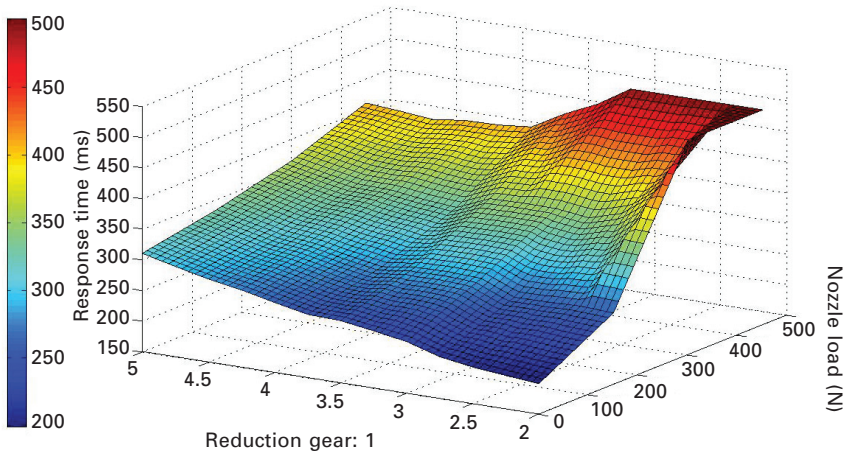


Plate III Response time vs. gear ratio.

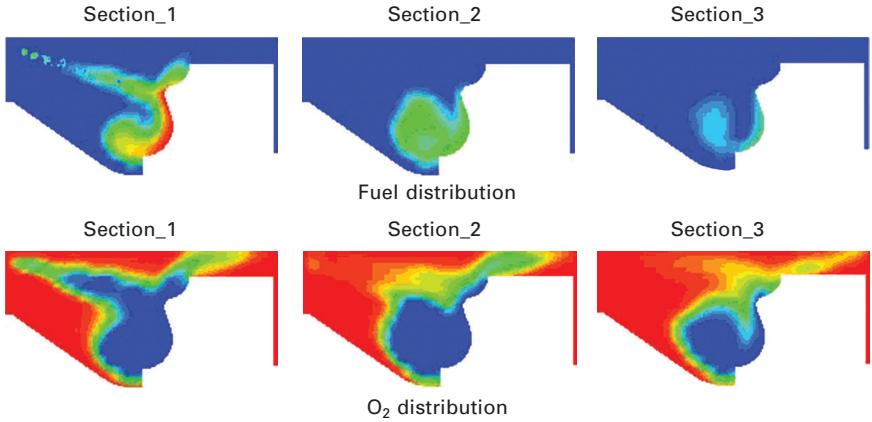


Plate IV Fuel and O_2 distribution in the VICB chamber.

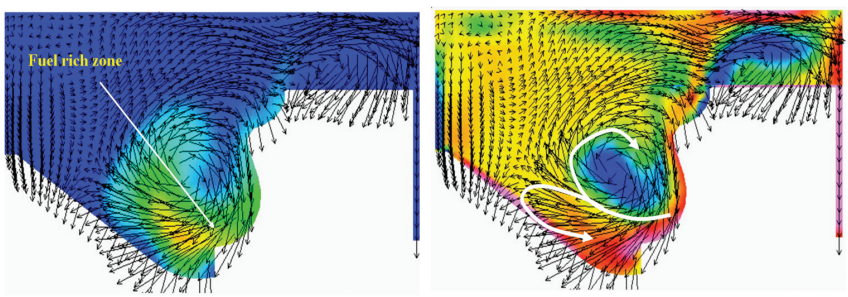


Plate V The induced vortices and the transportation of fuel and oxygen.

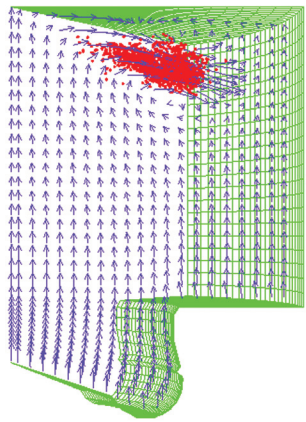
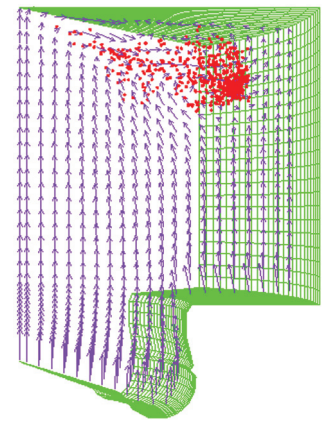
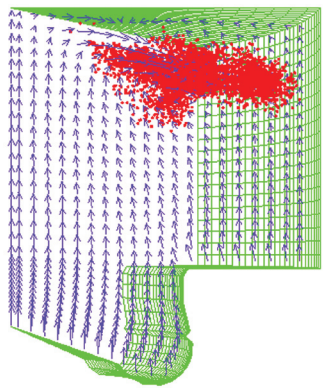
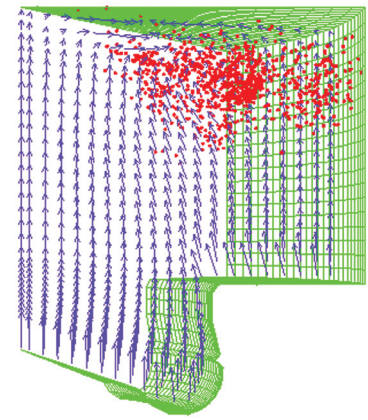
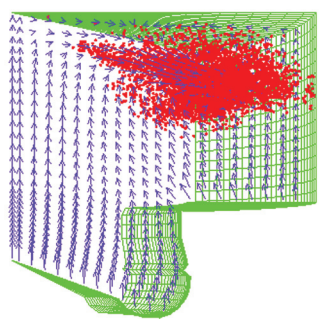
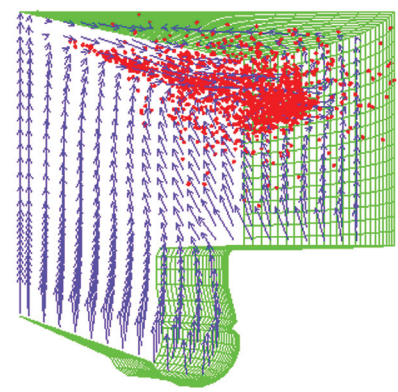
Baseline	Optimized
 (a) 79.976°CA BTDC (first pulse injection)	 (f) 77.922°CA BTDC (first pulse injection)
 (b) 69.914°CA BTDC (second pulse injection)	 (g) 67.952°CA BTDC (second pulse injection)
 (c) 57.998°CA BTDC (third pulse injection)	 (h) 57.928°CA BTDC (third pulse injection)

Plate VI Comparison of spray and flow fields in the cylinder for the optimized and baseline cases.

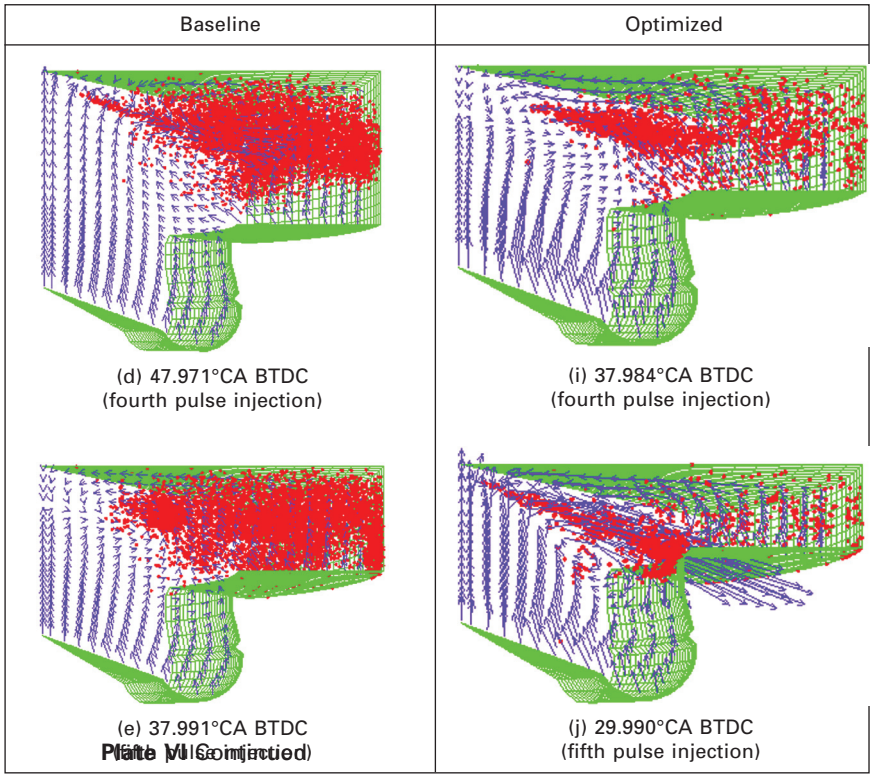


Plate VI Comparison

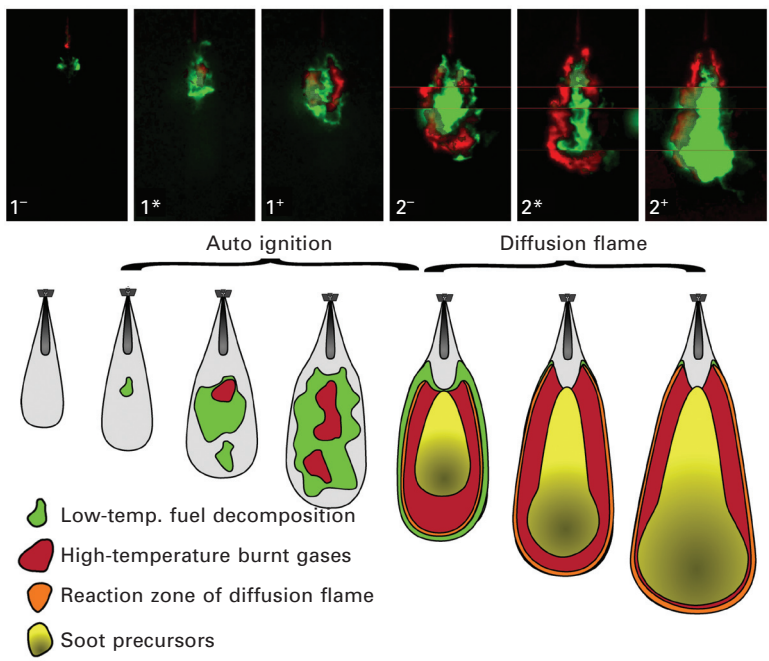


Plate VII Simultaneous measurement of CH_2O and soot precursors (green) and OH (red) LIF in a low-temperature diesel jet combustion. Lower section: schematic of an improved conceptual model based on imaging diagnostics (adapted from [75]).

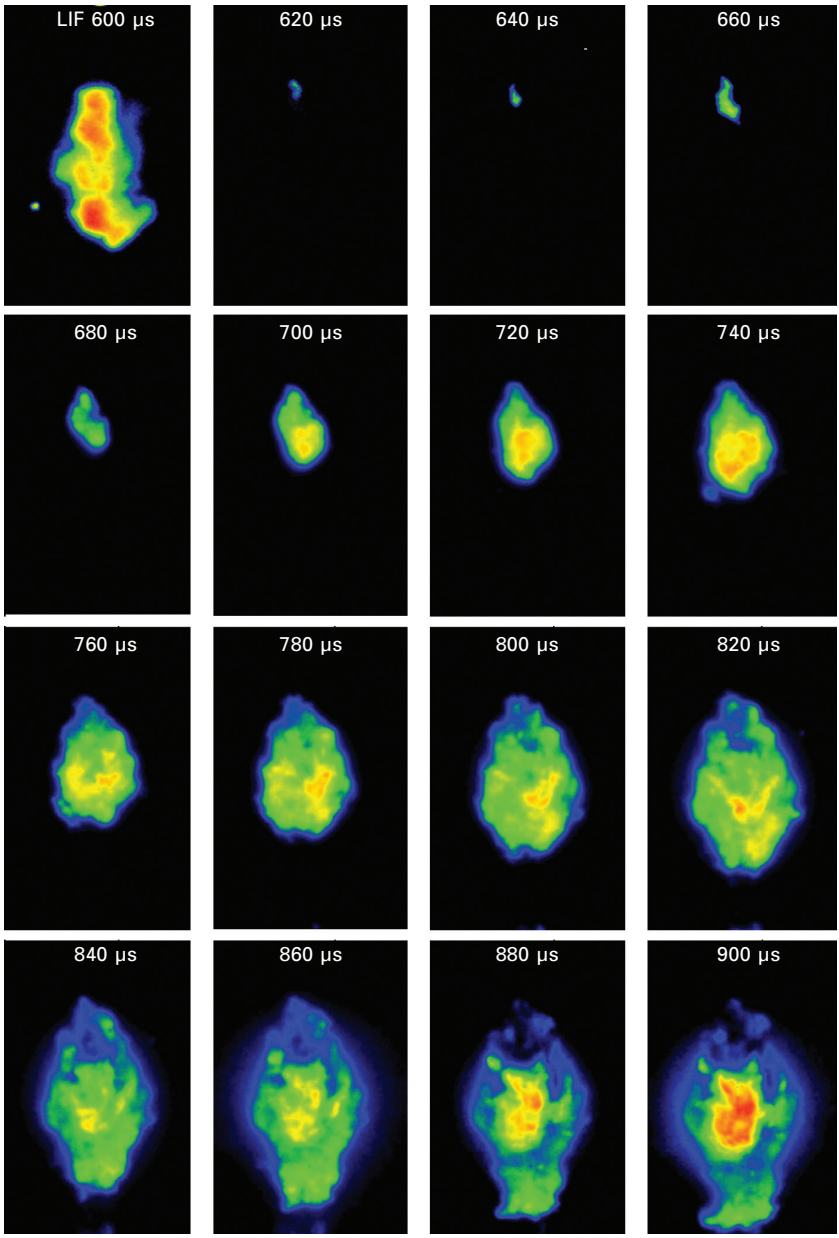


Plate VIII Time sequence of direct combustion emission visualization with a high-speed camera and a single measurement of the fuel-vapour distribution using 5-nonanone as a fluorescent tracer. The image size is 30×45 mm^2 (adapted from [38]).

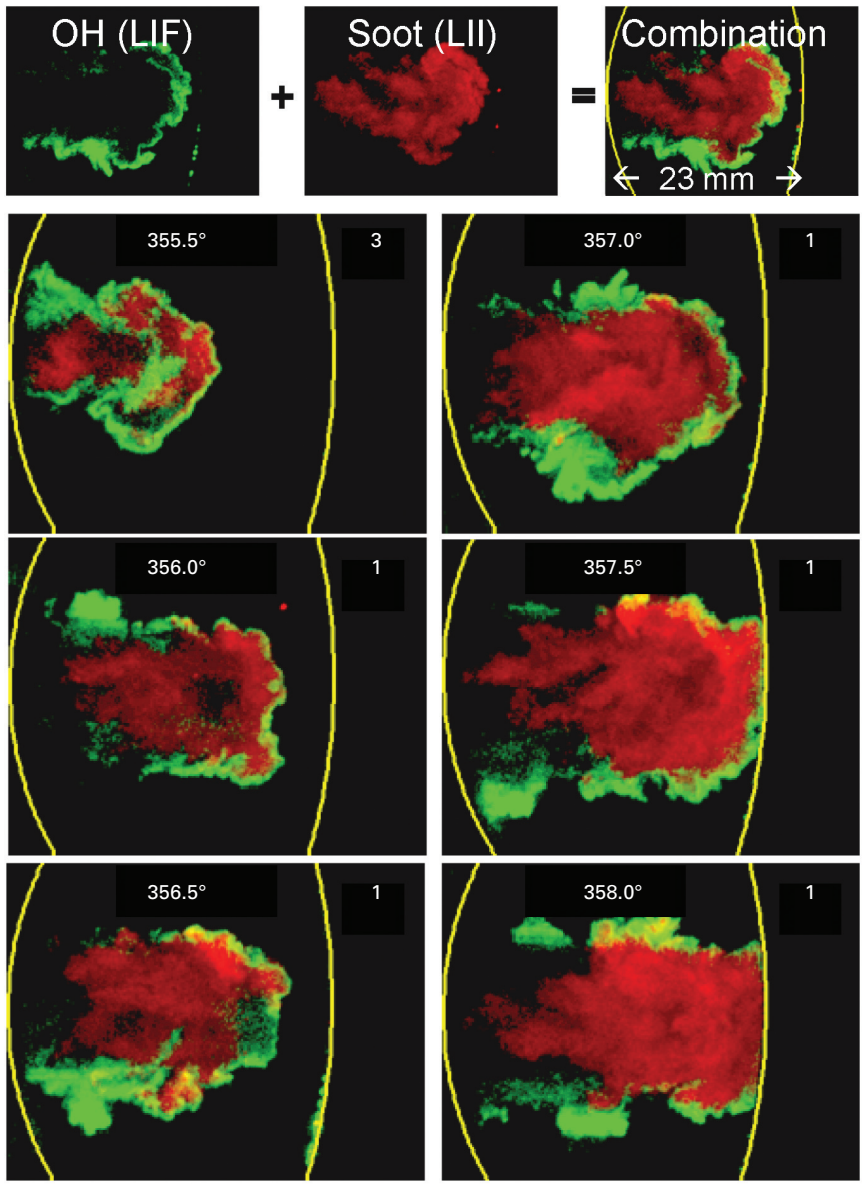


Plate IX Simultaneous detection of OH LIF (green) and soot LII (red) in a diesel spray (adapted from [8]).

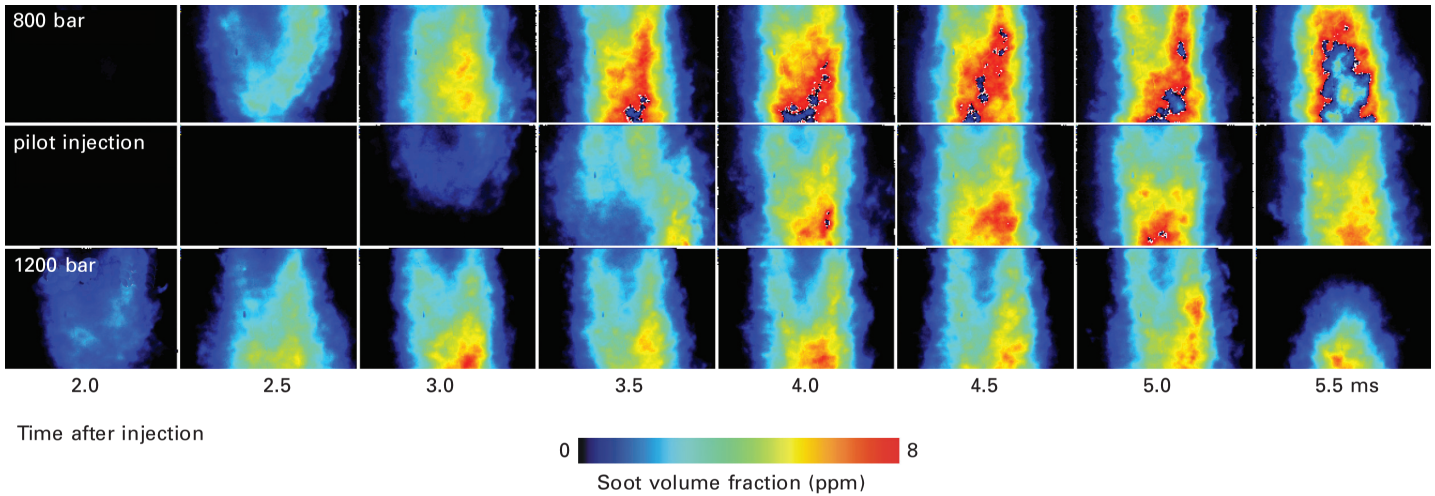


Plate X LII imaging for relative soot volume fractions in a high-pressure high-temperature diesel chamber (p = 73 bar, T = 740 K, t = 2–6 ms after start of injection) with different injection modes: p_{inj} = 800 and 1200 bar single injection and pilot injection (adapted from [37]).

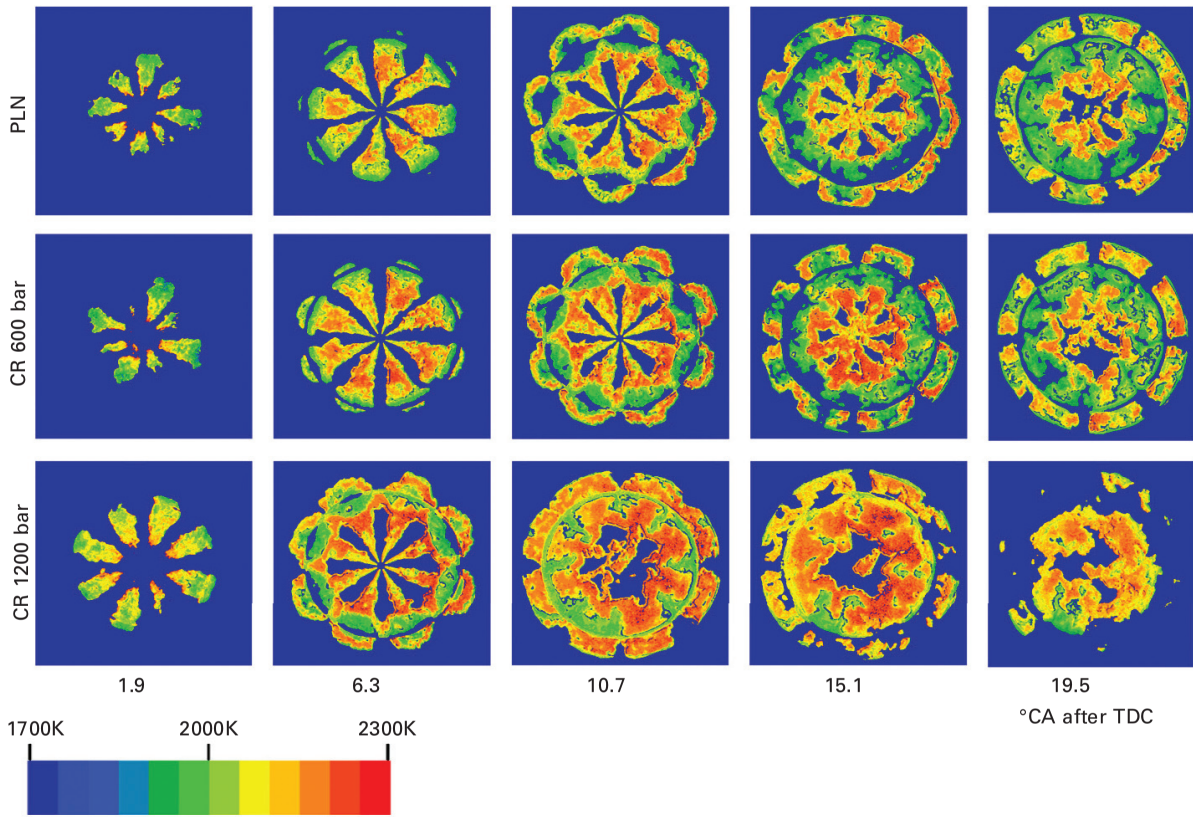


Plate XI Temperature measurements from two-colour soot pyrometry in a heavy-duty engine with pump-line-nozzle (PLN) and common rail (CR) injectors at different injection pressures (50% load, SOI: –3°aTDC) (adapted from [9]).

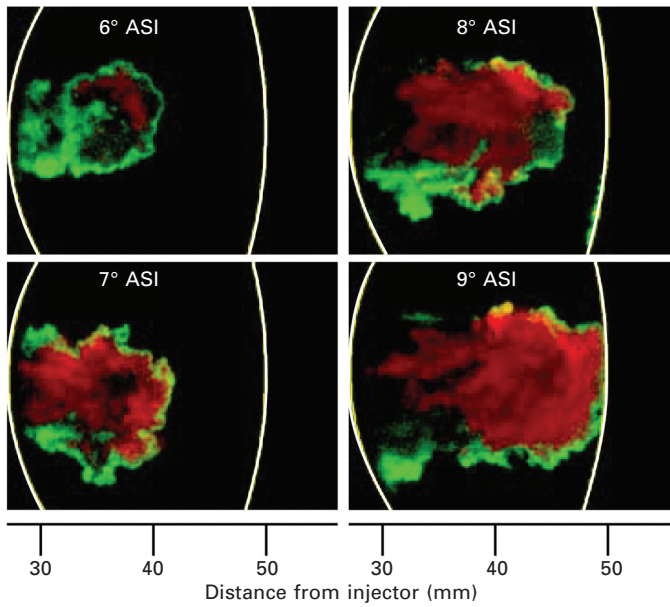


Plate XII Simultaneous images of OH-PLIF (green) and soot-PLII (red) for conditions similar to Figs 17.2 and 17.3 (images taken from [20]). The curved white line on the left is the edge of the cylinder-head window, and the curved white line on the right is the piston bowl-wall. The injector is to the left of the images, outside of the field of view, as indicated by the scale below the images.

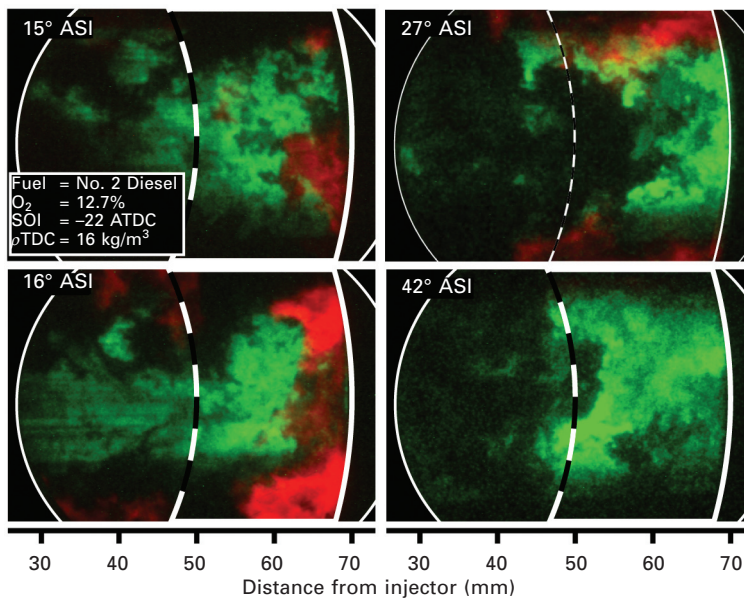


Plate XIII Simultaneous images of OH-PLIF (green) and soot-luminosity (red) for a low-boost early-injection LTC condition [49] (see inset). The curved white line on the left is the edge of the cylinder-head window, the curved dashed line is the usual location of the bowl rim, and the white arc on the right is the piston cylinder wall.

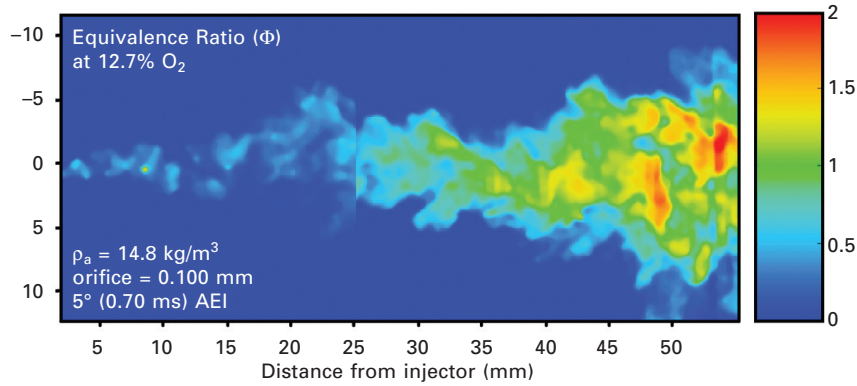


Plate XIV Composite of two Rayleigh scattering images, covering 2 to 25 mm and 25 to 60 mm from the injector, showing contour maps of equivalence ratio 5° (0.70 ms) after the end of injection (AEI) in a single jet, taken from [50].

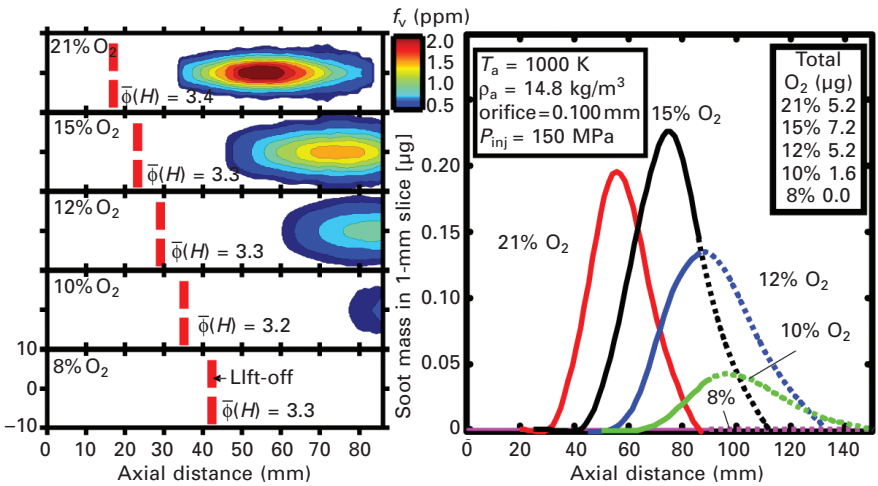


Plate XV In-cylinder laser-extinction soot volume fraction measurements from quasi-steady, mixing-controlled diesel fuel jets in a constant-volume vessel, for oxygen concentrations ranging from 21% to 8% at the conditions listed in the inset [59]. Left: soot volume fraction contours, with equivalence ratios noted at the lift-off lengths (vertical dashed lines). Right: integrated soot mass in one-mm slices, derived from contours on left.